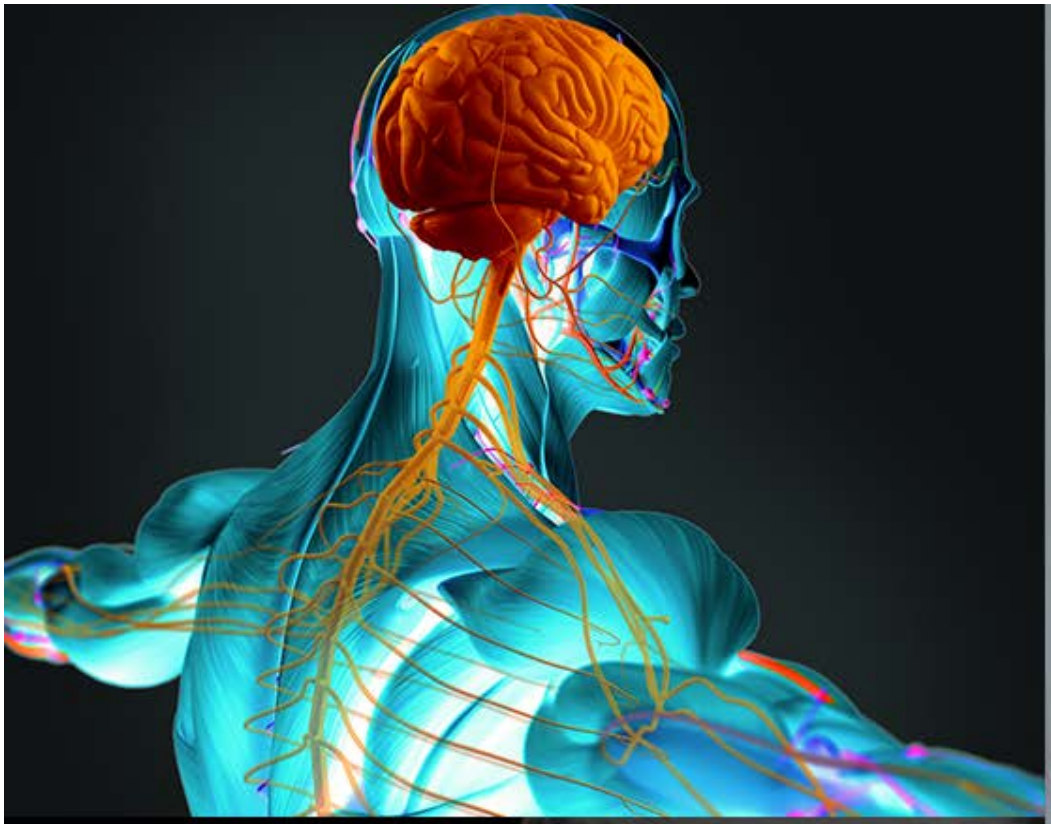

CRYOSTASIS REVIVAL

Robert A. Freitas Jr.

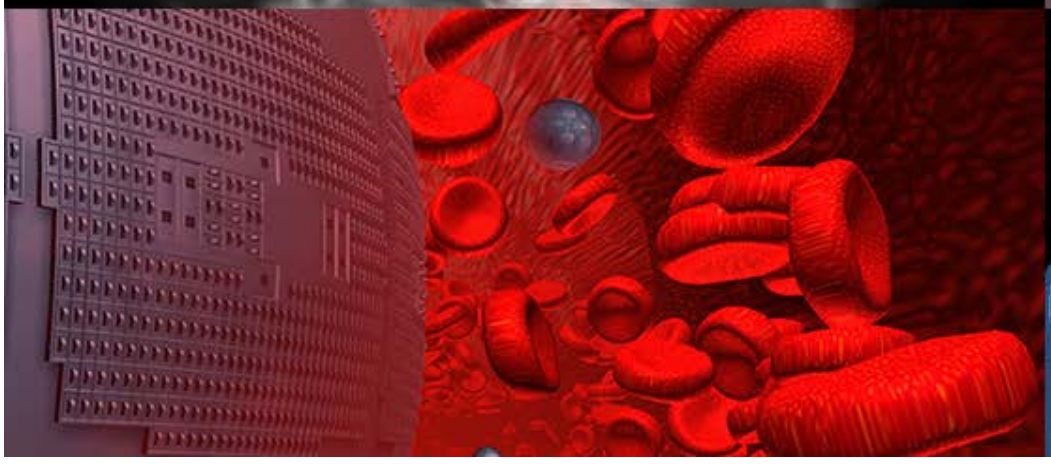

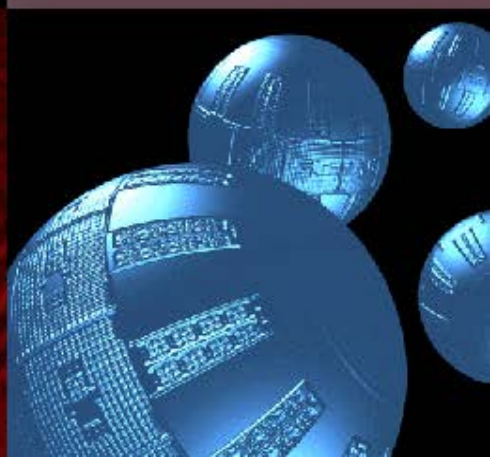

Cryostasis Revival

The Recovery of Cryonics Patients through Nanomedicine

Robert A. Freitas Jr.
Senior Research Fellow
Institute for Molecular Manufacturing
Palo Alto, California USA

Cryostasis Revival

The Recovery of Cryonics Patients through Nanomedicine

Published in the United States by Alcor Life Extension Foundation, 7895 E. Acoma Drive #110, Scottsdale, Arizona, USA

https://www.alcor.org/

Printed by Thomas Group Printing in the United States
ISBN: 000-0-0000000-0-0
First Edition

To all who love life's adventure,
and seek its unbounded continuation

Table of Contents

List of Tables

Foreword by Gregory M. Fahy, Ph.D.

Dr. Greg Fahy is a complex systems cryobiologist and the Executive Director and Chief Scientific Officer of the cryobiological biotechnology company, 21st Century Medicine, Inc. His scientific research has been recognized by the Society for Cryobiology, which made him a Fellow in 2014. [1] *His comments are his own and do not reflect the views of any affiliated organization.*

A Glimpse of the Future

This is a book that is ultimately about the technical feasibility of cryonics. Cryonics is the practice of preserving individuals at cryogenic temperatures today for possible revival in the future. Human cryopreservation could in theory have several uses, ranging from the exploration of the cosmos in the distant future to "medical time travel" in the present. Regarding the latter, if medical conditions that are incurable today, including even the "medical condition" of being preserved by today's imperfect methods under often imperfect circumstances, will become curable in the future, then putting the course of today's fatal illnesses on hold by cryopreservation may provide hope for those who are deemed to be beyond hope by today's medicine.[2]

But "if" is a large word in this context. Without a clear answer, cryonics has been inevitably controversial. In the meantime, in the absence of being able to foretell the future, cryonics has historically been defended on the basis of two fundamental empirical observations.[3]

The first observation is the fact that humans have been creating more and more advanced technology, and a deeper and deeper understanding of the world, since our inception as a species, and that this creative process of discovery and improvement is likely to continue. Carried to its logical conclusion, it seems inevitable that, if the species survives and progress is allowed to continue indefinitely, we will eventually acquire the ability to accomplish any goal that does not violate physical and economic law.

The second observation is that cryobiology, the study of the effects of low temperatures on living systems, teaches us that viable mammalian cells can be stored for very long times at cryogenic temperatures and then revived successfully in a distant future. For example, present estimates suggest that it would take 32,000 years for background radiation to kill 90% of cultured cells after freezing to low temperatures.[4] Neurons in the brain are less sensitive to radiation damage than tissue culture cells and so might last longer, and storage times may also be extended by enhanced post-thawing DNA repair alone and by the presence of very high concentrations of cryoprotective agents, which are used in ice-free cryopreservation by vitrification[5] and may be radioprotective.[6] And even longer survival times have been claimed under natural conditions.[7]

---

[1] https://en.wikipedia.org/wiki/Greg_Fahy.

[2] Ettinger RCW. The Prospect of Immortality. New York: Doubleday; 1964.

[3] *Ibid.*

[4] Ashwood-Smith MJ, Grant E. Genetic stability in cellular systems in the frozen state. In: Elliott K, Whelan J, editors. The Freezing of Mammalian Embryos. Amsterdam: Elsevier / Excepta Medica /North-Holland 1977. p. 251-67.

[5] Fahy GM, Wowk B. Principles of ice-free cryopreservation by vitrification. In: Wolkers WF, Oldenhof H, editors. Cryopreservation and freeze-drying protocols (Methods Mol Biol 2180). New York: Humana Press; 2021. p. 27-97.

[6] Ashwood-Smith MJ. Current concepts concerning radioprotective and cryoprotective properties of dimethyl sulfoxide in cellular systems. Ann N Y Acad Sci. 1975;27:243-6.

Potentially tens of thousands of years is a long time for technological achievements to accumulate. Even today, it seems apparent that advances in all areas of science and technology are proceeding at exponential rates. Some have even projected the arrival of a "singularity",[8] which is a point in time beyond which progress becomes so transformational that it is impossible to imagine what it will mean for our experience of life, just decades from now.

So it does seem relevant to ask: are the tasks that would be required to revive individuals after previous cryogenic storage with present imperfect techniques forbidden by physical law? The answer depends on two factors: how much and what kind of damage must be repaired, and what repair capabilities are possible in principle?

The first question has been addressed experimentally, as reviewed in depth in this book. From the perspective of cryobiology, there are some positive findings, but also still many unknowns and limitations. When conventional ice crystal damage to whole organs was prevented by vitrification, a rabbit kidney was able to support life indefinitely after cooling to -130 °C, rewarming, and transplantation.[9] Regarding the brain in particular, which is of central importance for the proposition of cryonics, it has been found that, as Freitas reviews in this book, partially frozen animal brains have registered coherent electroencephalograms after thawing from -20 °C,[10] frozen hamsters have recovered despite conversion of more than half of their brain water into ice at -1 °C,[11] and both frozen and vitrified worms have retained memories after rewarming that were instilled before cryopreservation.[12] Hippocampal slices, also, have been vitrified and rewarmed with good retention of viability,[13] ultrastructure,[14] electrical responsiveness,[15] and the ability to generate long-term potentiation.[16] The most direct observations that can be made, however, are those that can be made on the brains of actual human cryonics volunteers. Beyond the macroscopic studies reviewed in this book, there has been one study, whose results are presently being analyzed and prepared for publication, on brain fine structural integrity.[17] Preliminary indications are that brain structure was well preserved on both

---

[7] https://www.livescience.com/63187-siberian-permafrost-worms-revive.html?utm_source=notification.

[8] Kurzweil R. The Singularity is Near: When Humans Transcend Biology. New York: Viking; 2005.

[9] Fahy GM, Wowk B, Pagotan R, Chang A, Phan J, Thomson B, *et al*. Physical and biological aspects of renal vitrification. Organogenesis. 2009;5:167-75.

[10] Suda I, Kito K, Adachi C. Viability of long term frozen cat brain in vitro. Nature. 1966;212:268-70. Suda I, Kito K, Adachi C. Bioelectric discharges of isolated cat brain after revival from years of frozen storage. Brain Research. 1974;70:527-31.

[11] Lovelock JE, Smith AU. Studies on golden hamsters during cooling to and rewarming from body temperatures below 0oC. III. Biophysical aspects and general discussion. Proc Roy Soc, B. 1956;145:427-42.

[12] Vita-More N, Barranco D. Persistence of long-term memory in vitrified and revived Caenorhabditis elegans. Rejuvenation Res. 2015;18(5).

[13] Pichugin Y, Fahy GM, Morin R. Cryopreservation of rat hippocampal slices by vitrification. Cryobiology. 2006;52:228-40.

[14] *Ibid.*

[15] Fahy GM, Guan N, De Graaf IAM, Tan Y, Griffin L, Groothuis GMM. Cryopreservation of precision-cut tissue slices. Xenobiotica. 2013;43:113-32.

[16] *Ibid.*

[17] Fahy GM, Wowk B, Vargas V, Hixon H, Graber S, Thomson B, *et al.* Ultrastructural cryopreservation of the mammalian brain. (in preparation).

the histological and electron microscopic level, and was actually preserved much better than in animal brains in past studies. Ice formation was successfully avoided in all brain biopsies examined by differential scanning calorimetry, indicating excellent perfusion of the brain after cardiac arrest and transportation, and whole brain fracturing was not observed after cooling to -146 °C. These results suggest that, when cryonics is carried out under favorable conditions, and when ice formation is prevented by vitrification, it has every appearance of preserving the structure and the molecular inventory of the brain.

However, cryonics is often attempted under poor conditions, and although the effects of disease and ischemia are reviewed in this book in detail, there is no published information on the effects of these pre-cryopreservation factors on the outcomes of preparation for cryopreservation (although some unpublished studies involving 1 hour of warm ischemia followed by 24 hours of cold storage before cryopreservation have been promising[18]). There are also few[19] published studies of human or other mammalian brain viability after vitrification, and past successful studies involving partial brain freezing[20] did not involve cooling to temperatures low enough for long term storage. Factors that may affect brain viability after vitrification (including brain shrinkage, background hypothermic injury, and possibly protein denaturation by cryoprotective agents[21]) have been individually addressed with success in separate model systems, but whole brain viability studies are lacking. The final reality is that, after all, it is still true that today's methods, if applied to the cooling of either a brain or a whole mammal to cryogenic temperatures, even under good conditions, would not be expected to result in spontaneous recovery, and superimposing variable degrees of cardiac arrest prior to such experiments would make failure even more likely. In addition, preserving the brain is far from being the only problem that must be overcome to restore cryopreserved individuals to life.

Therefore, despite several favorable signs, injury induced by present cryonics procedures cannot be repaired without highly advanced future repair technologies that can be applied to cryopreserved systems. Therefore, the second question, pertaining to the ultimate feasibility of these technologies, remains essential for the evaluation of cryonics, and is fortunately the major issue addressed in this book.

Much has been written previously about the general technical feasibility of what K. Eric Drexler named "nanotechnology" (and later, "molecular nanotechnology"), which is the atomically precise engineering and fabrication of molecular machines and molecularly defined materials. Further, the offspring of nanotechnology, "nanomedicine," has been explored in overwhelming detail in previous works by present author Robert Freitas. Ralph Merkle, too, has contributed much to an understanding of the global feasibility of molecular repair of cryopreserved brains, and other scenarios of repair have been suggested and are reviewed in depth in this volume. However, the present book is the only resource that comprehensively puts together the entire picture of nanomedical repair of cryonics patients as only Rob Freitas can do. "Conventional" nanomedicine must confront modifications to a body that is for the most part already maintaining its own viability. It is an entirely different problem to repair patients who are in a solid state at cryogenic temperatures. For that, new tools must be devised, and in this work, Freitas supplies the closest look we have had so far at what these future tools might include.

---

[18] Fahy GM, *et al.* Vitrification of whole rabbits under good and compromised conditions. (unpublished observations)

[19] Pichugin Y, Marchenko VS, Shilo AV, editors. Bioelectric activity of cryopreserved brain pieces of a rabbit. The 14th Conference on Preservation of Genetic Resources; 1996; Pushchino: Academpress.

[20] Suda I, Kito K, Adachi C. Viability of long term frozen cat brain in vitro. Nature. 1966;212:268-70. Suda I, Kito K, Adachi C. Bioelectric discharges of isolated cat brain after revival from years of frozen storage. Brain Research. 1974;70:527-31. Lovelock JE, Smith AU. Studies on golden hamsters during cooling to and rewarming from body temperatures below 0oC. III. Biophysical aspects and general discussion. Proc Roy Soc, B. 1956;145:427-42.

[21] Fahy GM, Wowk B. Principles of ice-free cryopreservation by vitrification. In: Wolkers WF, Oldenhof H, editors. Cryopreservation and freeze-drying protocols (Methods Mol Biol 2180). New York: Humana Press; 2021. p. 27-97.

Freitas' approach to repair proceeds in a logical fashion. First, survey the damage. Second, gain access to what needs to be repaired by tunneling through inconsequential material, particularly in the vascular system and similar conduits. Third, stabilize structures that must be repaired and install structures necessary for later repair and more detailed surveys. Fourth, figure out what needs to be done based on what has been learned. Fifth, start by stabilizing fractures and then warming sufficiently to enable fracture faces to be fused back together again. And sixth, proceed with the rest of the details (of which there are a great many). It is hard to argue with this staging of events.

Even while attempting to describe as many details of the repair process as possible, however, it must be understood that concepts of repair depend on concepts of the damage that requires repair, and, as noted above, the latter remain incomplete. To his credit, Freitas identifies a myriad of topics worthy of future research throughout these scenarios, an acknowledgement that the present work is not and cannot be the final word, but it does not need to be. Extracting and then replacing molecules like glucose and oxygen, attempting to artificially manipulate osmosis, and artificially resealing membranes with altered semipermeability may all be unnecessary. However, if they are technically possible, then it becomes plausible that lesser capabilities will be able to do lesser tasks that actually are necessary. If the real goal is to plumb the depths of the possible, the present volume accomplishes that goal extraordinarily well.

Will the overall possibilities outlined here someday be realized? Will lives be saved? Will new adventures emerge as the people of the present engage with the entities of the future? Only time will tell. The proposals in this book cannot by themselves prove that cryonics will succeed, or define precisely what conditions of preservation will be required for cryonics to succeed. The totality of the arguments presented does, however, elevate the discussion to an unprecedented level of specificity and detail, and must figure prominently in further scientific evaluation of the proposal of cryonics.

Cryonics, uniquely, is a present practice that is largely based on the possibilities of future technology, but the future has always been hard to see. Now, exactly 60 years after cryonics was first proposed in 1962,[22] Freitas has provided a highly concrete glimpse into a future in which a set of definable and technically defensible future technologies could be equal to the task of repairing virtually any degree of biological injury associated with cryonics. His new comprehensive and falsifiable framework for debate and discussion may well lead to less dismissal and more serious consideration of the proposition of cryonics from this point forward. In that sense, just possibly, cryonics itself, if not yet those who have undergone it, may be at the threshold of a new awakening.

Gregory M. Fahy, Ph.D.
Corona, California
January, 2022

[22] Duhring N. Immortality: Physically, Scientifically, Now. Washington, D.C.: 20th Century Books Foundation; 1962.

Acknowledgements

The author would like to thank Ralph Merkle, Aschwin de Wolf, Tad Hogg, Michael Perry, James Ryley, Brian Wowk, and Greg Fahy for reading and commenting on earlier drafts of this manuscript, and for many substantive suggestions that have materially improved the quality and accuracy of the work. Any conceptual or design flaws, mathematical mistakes, or errors of fact that remain are solely the responsibility of the author.

The author also thanks Natasha Vita-More for assembling the cover art, Gina "Nanogirl" Miller for providing several interior illustrations of the nanorobotic vasculoid concept, and Ping Lim for creating an additional interior illustration of the vasculoid at work.

Special thanks must be extended to: (1) Aschwin de Wolf, for initially proposing that the author should undertake a more comprehensive analysis of nanorobotic-based cryonics revival than had ever been attempted before (which turned into this book-length treatment), for constant encouragement throughout 2019-2022 while this book was being written and prepared for publication, and for acting as Alcor's production editor for the project; (2) Brian Wowk, for his particularly extensive technical review; and (3) Greg Fahy, for writing the Foreword and for providing illustrations from his early nanorobotic revival concepts.

Finally, the author thanks Jill Grasse for doing the graphic design and electronic formatting work on the book; Michael Benjamin for assistance securing image permissions; and the Alcor Life Extension Foundation for publishing this book in both print and electronic formats, and for permanently hosting the latter on their website.

1. Introduction

Raising the dead to life is a difficult task. Fortunately for cryonicists, a cryopreserved patient is not actually "dead".[23] Rather, the body or brain of a dying cryonics[24] patient is carefully placed into a condition of cold biological stasis – or "**cryostasis**" – conceptually not unlike hibernating[25] primates[26] and bears,[27] or frozen wood frogs[28] and Siberian salamanders,[29] except that some survival-critical damage exists in the patient's body, requiring repair. Given the right conditions, all of these animals – including the human – can return to normal life. Humans are not natural hibernators, so the cryopreserved person will need technological assistance to accomplish this feat, having previously employed various cryopreservative interventions to enter the state of biological stasis in the first place. It is the goal of this book to describe, in general outline, the technological assistance that may be sufficient to allow human beings to successfully exit the state of cryogenic biological stasis (cryostasis) and resume normal life with their original personal identity intact – and directions for future research that can help bring this technology to fruition.

This book presents the first comprehensive conceptual protocol for revival from human cryopreservation, using medical nanorobots.

The prospect of **revival**[30] is grounded in two grand assumptions: First, that it is possible to cool a human being to cryogenic temperatures "without fundamentally destroying the essential information underlying memory and personality in the brain"; and, second, "that medical and scientific progress will continue until medical resuscitation technology is limited only by physical law." If both these assumptions are correct,

---

[23] Wowk B. The Death of Death in Cryonics. Cryonics 1988 Jun;9(6):30-37; https://www.alcor.org/docs/cryonics-magazine-1988-06.txt. Of course, all cryopreserved patients have been pronounced "legally dead" by the appropriate local medical authorities prior to cryopreservation; https://www.alcor.org/library/the-legal-status-of-cryonics-patients/.

[24] "Cryonics is the practice of preserving life by pausing the dying process using subfreezing temperatures with the intent of restoring good health with medical technology in the future." https://www.alcor.org/.

[25] Hadj-Moussa H, Storey KB. Bringing nature back: using hibernation to reboot organ preservation. FEBS J. 2019 Mar;286(6):1094-1100; https://febs.onlinelibrary.wiley.com/doi/full/10.1111/febs.14683.

[26] Storey KB. The Gray Mouse Lemur: A Model for Studies of Primate Metabolic Rate Depression. Preface. Genomics Proteomics Bioinformatics. 2015 Apr;13(2):77-80; https://www.ncbi.nlm.nih.gov/pmc/articles/PMC4511782/. See also: https://en.wikipedia.org/wiki/Fat-tailed_dwarf_lemur#Hibernation.

[27] https://en.wikipedia.org/wiki/Hibernation#Bears.
[28] https://en.wikipedia.org/wiki/Wood_frog#Cold_tolerance.
[29] https://en.wikipedia.org/wiki/Salamandrella_keyserlingii#Description.

[30] "**Revival**" means the restoration to consciousness or life from a depressed, inactive, or unused state that is generally of indeterminate duration, and best fits the classical intent of direct physical restoration of a human patient from a very-long-term cryopreservation. "**Reanimation**" means to restore to a physically active state and is a close synonym for "revival," but has unfortunate connotations from horror films; also, "reanimate" is 100 times less popular than "revive" in common usage (i.e., 1M hits vs. 100M hits on Google). "**Resuscitation**" also has a similar meaning as "revival" but is generally used in the medical context of a patient who has been inactive for a much shorter period of time, typically hours or days, or occasionally months. "**Reincarnation**" means to be reborn in another body, which would not apply to cryonics cases involving conventional cell repair (Chapter 4) or to molecular reconstruction of the original body (Section 5.3) but could arguably apply to molecular reconstruction of a new body (Section 5.2) or to neuro patients who receive an entirely new body (Chapter 6). "**Resurrection**" means to restore to life a biological entity that was truly "dead," presumably in the information-theoretic sense (Section 2.1.1), e.g., perhaps requiring something like Tipler's far-future "Omega Point" to re-create all lifeforms in the universe that have ever lived since the start of time,[*] and often has religious connotations.

[*] Tipler FJ. The Physics of Immortality. Doubleday, New York, 1994; "Chapter IX. The Physics of Resurrection of the Dead to Eternal Life"; https://www.amazon.com/Physics-Immortality-Modern-Cosmology-Resurrection/dp/0385467990/.

then "the memories and personalities of people preserved by today's methods should be intact after revival by future technology, and medical time travel[31] can be used as a bridge to a time when senescence can be controlled." [32]

In the following pages we will describe exactly how **medical nanotechnology** may be used to restore cryonics patients to the viable physical condition they enjoyed prior to being pronounced legally deceased and prior to being subjected to various cryopreservation procedures. The patient who is revived according to this criterion may still be "sick" by current medical definitions, but they will not be in imminent danger of relapse due to their remaining infirmities. Once alive and stabilized, the revived patient can then receive more conventional nanomedical procedures to restore themselves to full health and youthful vigor, using medical **nanorobots**[33] to correct all commonplace medical disease states such as bacterial infections[34] or genetic defects,[35] up to and including the most challenging ones such as aging[36] and dementia.[37]

It is important to note that "[a]ll cryonics patients in long-term storage are '**cryopreserved**'. Since vitrification is a relatively recent (21st century) procedure in cryonics, not all cryonics patients have been '**vitrified**'. Of the patients that have not been vitrified, some have received some degree of cryoprotection and others have been 'straight frozen'….The best way to think about cryopreservation is to imagine a continuum, ranging from complete freezing without any cryoprotectants, to complete vitrification achieved through the effective use of cryoprotectants. In the case of a **straight freeze**,[38] where cryoprotectants aren't used at all, ice formation is at its maximum. In the case of complete vitrification[39] there is no ice at all. In cryonics, the outcome of a case can theoretically be at either of those extremes, but a more typical

---

[31] Wowk B. Medical Time Travel. In: Immortality Institute. The Scientific Conquest of Death. Libros en Red, 2004, pp. 135-149; https://www.alcor.org/library/medical-time-travel/.

[32] Lemler J, Harris SB, Platt C, Huffman TM. The arrest of biological time as a bridge to engineered negligible senescence. Ann N Y Acad Sci. 2004 Jun;1019:559-63; http://www.alcor.org/Library/pdfs/Lemler-Annals.pdf.

[33] Freitas RA Jr. Nanomedicine, Volume I: Basic Capabilities, Landes Bioscience, Georgetown, TX, 1999; http://www.nanomedicine.com/NMI.htm. Freitas RA Jr. Nanomedicine, Volume IIA: Biocompatibility, Landes Bioscience, Georgetown, TX, 2003; http://www.nanomedicine.com/NMIIA.htm.

[34] Freitas RA Jr. Microbivores: Artificial Mechanical Phagocytes using Digest and Discharge Protocol. J. Evol. Technol. 2005 Apr;14:55-106; http://www.jetpress.org/volume14/freitas.pdf.

[35] Freitas RA Jr. The Ideal Gene Delivery Vector: Chromallocytes, Cell Repair Nanorobots for Chromosome Replacement Therapy. J. Evol. Technol. 2007 Jun;16:1-97; http://jetpress.org/v16/freitas.pdf.

[36] Freitas RA Jr. Chapter 23. Comprehensive Nanorobotic Control of Human Morbidity and Aging. In: Fahy GM, West MD, Coles LS, Harris SB, eds, The Future of Aging: Pathways to Human Life Extension, Springer, New York, 2010, pp. 685-805; http://www.nanomedicine.com/Papers/Aging.pdf.

[37] Freitas RA Jr. The Alzheimer Protocols: A Nanorobotic Cure for Alzheimer's Disease and Related Neurodegenerative Conditions. IMM Report No. 48, June 2016, 433 pp; http://www.imm.org/Reports/rep048.pdf.

[38] According to the official case metrics, Alcor patients received a straight freeze in 14% of all cases during 1967-1999[*] and in 23% of all cases during 2000-2020.[†]
[*] Benjamin M, de Wolf A. Alcor Case Metrics 1967-1999. Cryonics 2021 Qtr III; 42(3):12-18, chart p. 13; https://www.alcor.org/docs/cryonics-magazine-2021-03.pdf.
[†] Benjamin M, de Wolf A. Alcor Case Metrics 2000-2020. Cryonics 2021 Qtr II; 42(2):10-30, chart p. 24; https://www.alcor.org/docs/cryonics-magazine-2021-02.pdf.

[39] https://en.wikipedia.org/wiki/Vitrification#Vitrification_in_cryopreservation and https://en.wikipedia.org/wiki/Cryopreservation#Vitrification.

outcome is some point in between." [40] Most of the nanorobot-based revival procedures described in this book are assumed to be performed on a cryopreserved patient who was well perfused with an appropriate vitrification cryoprotectant[41] such as M22,[42] then cooled all the way to ~77 K (liquid nitrogen or "LN2" cryogenic[43] temperatures; -196 °C) and held continuously at that temperature for some period of time.[44]

We further presume that the patient received a "**good cryopreservation**" with minimal ischemic[45] damage and adequate cryoprotectant saturation of the tissues, especially of the brain: "Patients stabilized immediately post-arrest and perfused under good conditions can enter a state of nearly ice free cryopreservation with very little histological or ultrastructural disruption of the brain." [46] Patients who have been "straight-frozen" without any cryoprotectant or who received grossly inadequate local concentrations of cryoprotectant (Section 7.1.1),[47] or patients who were treated with aldehyde-stabilized cryopreservation (Section 7.1.5),[48] will require somewhat more intensive nanorobotic procedures for successful revival.

The chart below shows the level of cryoprotectant saturation actually achieved in the brains of 37 cryonics patients who were cryopreserved by Alcor[49] during 2000-2020, as directly measured via CT (Computed Tomography) scan. It appears that over the last 20 years, roughly 38% of Alcor neuro patients have received between 50%-100% of the CNV (or "concentration necessary to vitrify" the entire brain), while another 32% of neuros have received 25%-50% of CNV.[50]

---

[40] Phaedra C, de Wolf A. Cryonics Protocols at the Cryonics Institute: Research and Practice. Part 3: Cryoprotection. Long Life 2018 Qtr 2;50(2):13-17; https://immortalistsociety.org/LongLifeV50-02.pdf.

[41] https://en.wikipedia.org/wiki/Cryoprotectant.

[42] Fahy GM, Wowk B, Wu J, Phan J, Rasch C, Chang A, Zendejas E. Cryopreservation of organs by vitrification: perspectives and recent advances. Cryobiology. 2004 Apr;48(2):157-78; http://www.21cm.com/pdfs/cryopreservation_advances.pdf.

[43] https://en.wikipedia.org/wiki/Cryogenics.

[44] https://www.alcor.org/library/alcor-human-cryopreservation-protocol/. See also: "New evidence shows that when human cryopreservation is carried out under favorable conditions, it causes minimal damage that we can reasonably expect to be reversible at some time in the future using molecular nanotechnology." Platt C. Effect of Human Cryopreservation Protocol on the Ultrastructure of the Canine Brain. CryoCare Report #4, Jul 1995; https://www.alcor.org/library/effect-of-human-cryopreservation-protocol-on-the-ultrastructure-of-the-canine-brain-platt/.

[45] https://en.wikipedia.org/wiki/Ischemia.

[46] Darwin M. Cryonics: An Historical Failure Analysis. Part III: Dissociation of Researchers from the Clinical Environment. 2010; https://web.archive.org/web/20140906234205/http://cryoeuro.eu:8080/download/attachments/425990/Cryonics_Failure_Analysis_Part_3v5.4.pdf.

[47] Completely unprotected tissues will experience massive mechanical damage* likely requiring more extensive repairs than those described here.
* Lovelock JE, Smith AU. Studies in Golden Hamsters During Cooling To and Rewarming From Body Temperatures Below 0 degrees C. Part III: Biophysical Aspects and General Discussion. Proc R Soc Lond B Biol Sci. 1956 Jul 24;145(920):427-42; https://www.ncbi.nlm.nih.gov/pubmed/13359396; Fahy GM, Takahashi T, Crane AM. Histological cryoprotection of rat and rabbit brains. CryoLetters 1984;5:33-46.

[48] McIntyre RL, Fahy GM. Aldehyde-stabilized cryopreservation. Cryobiology. 2015 Dec;71(3):448-58; https://www.sciencedirect.com/science/article/pii/S001122401500245X.

[49] Alcor Life Extension Foundation, the leading provider of cryopreservation and long-term cryonics storage services in the world, as of 2021; https://www.alcor.org/.

[50] Benjamin M, de Wolf A. Alcor Case Metrics 2000-2020. Cryonics 2021 Qtr II; 42(2):10-30, chart p. 28; https://www.alcor.org/docs/cryonics-magazine-2021-02.pdf.

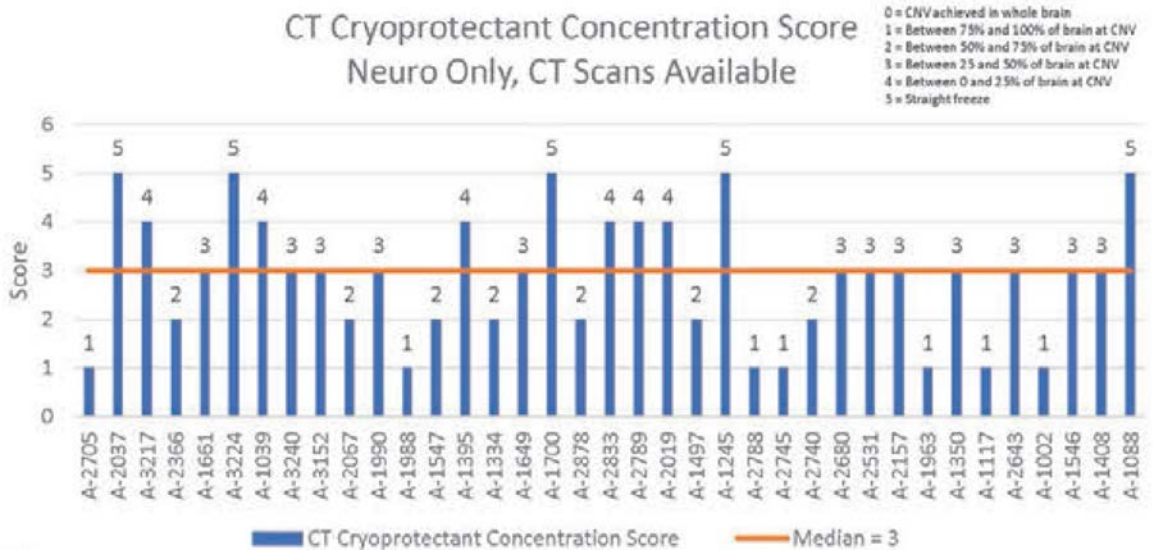

While this book focuses primarily on revival from a "good cryopreservation," methods are also presented for reviving patients who may have received poor cryopreservation with minimal or no prevention of ice formation, possibly including substantial ischemic damage. This is necessary because while the strongest scientific case for the utility of cryonics today can made by assuming ideal cryopreservation conditions immediately following legal death by cardiopulmonary criteria, it has long been an ideological practice of cryonics to cryopreserve people even after very long delays after legal death as an ethical imperative if that was the wish of the person being cryopreserved. Notes Brian Wowk:[51]

> "The word 'cryonics' is actually a name for two different ideas. The first idea is that human cryopreservation under ideal conditions today could be reversible in the future. The second idea is that medicine should never leave patients behind; every patient beyond the capabilities of contemporary care should be cryopreserved instead of destroyed, even if found in poor condition. The distinction is necessary because it is possible to agree with the first idea even while not accepting the second. The first idea is a scientific proposition, while the second is a philosophical imperative."

Cryonics patients may have their entire body cryopreserved (i.e., a "**whole-body**" patient)[52] or may choose for financial and other reasons to cryopreserve only their head (i.e., a "**neuro**" patient)[53] or only an isolated brain. The nanorobotic procedures described in this book are generally presented as being applied to a whole-body patient, thus avoiding the immediate complications of having to rebuild a new trunk that must

---

[51] Wowk B. Ethics of Non-ideal Cryonics Cases. Cryonics 2006 Qtr 4;27(4):10-12; https://www.alcor.org/library/ethics-of-non-ideal-cryonics-cases/.

[52] O'Neal MB, de Wolf A. The Case for Whole-Body. Cryonics 2014 Feb;35(2):16-21; https://www.alcor.org/library/case-for-whole-body/.

[53] Darwin M. But What Will The Neighbors Think? A Discourse On The History And Rationale Of Neurosuspension. Cryonics 1988 Oct;9(10):40-55; https://www.alcor.org/library/but-what-will-the-neighbors-think/. Bridge S. The Neuropreservation Option. Cryonics 1995 Qtr 3;16(3):4-7; https://www.alcor.org/library/neuropreservation-option/. See also: https://www.alcor.org/library/case-for-neuropreservation/ and https://www.alcor.org/library/neuropreservation-faq/.

be seamlessly attached to the fully-repaired previously-cryopreserved head (Chapter 6). Nevertheless, the discussion here often focuses on reparative issues specific to the brain since revival processes for the noncephalic trunk should be technically less challenging and more forgiving of error than for the brain. This is because the nonbrain portions of the body appear to be less important (though not entirely unimportant)[54] for preserving the unique memories and personality of the patient, and could in principle be partially (though inexactly) restored using such prosaic pre-nano technologies as 3D bioprinting,[55] cloning,[56] and conventional surgery.[57]

In brief, the revival methods presented in this book involve three stages: (1) collecting information from preserved structure, (2) computing how to fix damaged structure, and (3) implementing the repair procedure. The first and last of these stages involve sophisticated robots ("nanorobots"; Section 1.2) small enough to pass through blood vessels and other tissue vasculature, as well as a temporary nanorobotic support structure ("vasculoid"; Section 1.2.4) that covers the inside wall of the vessels. The activity in the second stage is primarily computational and takes place outside of the body using an external high-performance computer and specialized software.

How long will the revival process take, and what will it cost? There is considerable uncertainty in the estimates, but it appears that revival may take several months (**Table 16**) using either of the two revival approaches proposed in this book – conventional cell repair ("Plan A"; Chapter 4) or molecular reconstruction ("Plan B"; Chapter 5). The key driver of operating expenses is the price of the energy required to power the nanorobots and computers, with a total revival cost of ~$2 million (**Table 17**) for whole-body patients using Plan A assuming contemporary electricity costs, and similarly using Plan B assuming future energy costs about 100-fold cheaper than today (Appendix G), to be made possible by widespread commercial atomically precise manufacturing (Section 1.3). Implementing either Plan requires considerable development, including designing and building the nanomachines and gaining the biological

---

[54] For example, fingerprints differ between genetic identical twins.[*] Many physical body features such as muscle mass, bone density, body shape and height, microbiome, and other physical characteristics that are significantly determined by environment, parental behaviors, nutrition, exercise patterns, etc. will be unique to a particular individual. See further discussion in Section 2.1.4.

[*] O'Neal MB, de Wolf A. The Case for Whole-Body. Cryonics 2014 Feb;35(2):16-21; https://www.alcor.org/library/case-for-whole-body/.

[55] Mandrycky C, Wang Z, Kim K, Kim DH. 3D bioprinting for engineering complex tissues. Biotechnol Adv. 2016 Jul-Aug;34(4):422-434; https://www.ncbi.nlm.nih.gov/pmc/articles/PMC4879088/. Huang Y, Zhang XF, Gao G, Yonezawa T, Cui X. 3D bioprinting and the current applications in tissue engineering. Biotechnol J. 2017 Aug;12(8); https://www.ncbi.nlm.nih.gov/pubmed/28675678. Ong CS, Yesantharao P, Huang CY, Mattson G, Boktor J, Fukunishi T, Zhang H, Hibino N. 3D bioprinting using stem cells. Pediatr Res. 2018 Jan;83(1-2):223-231; https://www.nature.com/articles/pr2017252.pdf. Francis Collins. Progress Toward 3D Printed Human Organs. NIH Director's Blog, 20 Jun 2019; https://directorsblog.nih.gov/2019/06/20/progress-toward-3d-printed-human-organs/. Organ printing; https://en.wikipedia.org/wiki/Organ_printing. Juliet Childers. How Close are we to 3D Printing Bodies? Edgy, 14 Mar 2018; https://edgy.app/how-close-3d-printing-bodies. Caroline Haskins. 'Marie' Is the First Life-Sized, 3D-Printed Human Body. Motherboard Tech by Vice, 14 Dec 2018; https://www.vice.com/en_us/article/yw7kzv/marie-is-the-first-life-sized-3d-printed-human-body.

[56] Shawlot W, Behringer RR. Requirement for Lim1 in head-organizer function. Nature. 1995 Mar 30;374(6521):425-30; https://www.ncbi.nlm.nih.gov/pubmed/7700351 (headless mice cloned). Shewmon DA, Capron AM, Peacock WJ, Schulman BL. The use of anencephalic infants as organ sources. A critique. JAMA. 1989 Mar 24-31;261(12):1773-81; https://www.ncbi.nlm.nih.gov/pubmed/2645454. Canadian Paediatric Society. Use of anencephalic newborns as organ donors. Paediatr Child Health. 2005 Jul;10(6):335-7; https://www.ncbi.nlm.nih.gov/pmc/articles/PMC2722973/.

[57] Lamba N, Holsgrove D, Broekman ML. The history of head transplantation: a review. Acta Neurochirurgica. 2016 Dec;158(12):2239–2247; https://www.ncbi.nlm.nih.gov/pmc/articles/PMC5116034. Furr A, Hardy MA, Barret JP, Barker JH. Surgical, ethical, and psychosocial considerations in human head transplantation. Int J Surg. 2017 May;41:190-195; https://www.ncbi.nlm.nih.gov/pmc/articles/PMC5490488.

knowledge needed to create the algorithm that determines how to repair the preserved structure. These research questions are described throughout the text and are collected in Appendix R.

1.1 Scientific Rationale for Human Cryopreservation

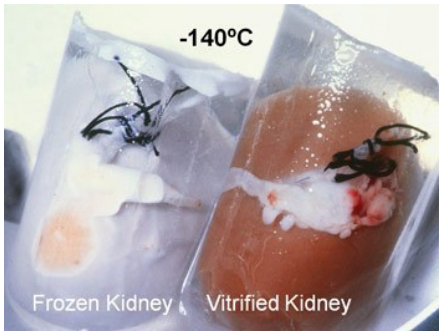

Many biological living materials have been preserved for later use and then restored to full functionality after warming, including human eggs[58] and sperm, embryos and blastocysts, stem cells, testicular tissue, cord blood, histological samples, and plant seeds.[59] Although no whole human or other complex mammal has yet been cryopreserved to liquid nitrogen temperatures and then successfully restored to full functionality at normal body temperature, there have been many experimental successes in cryonics since the first demonstration in 1966 of near normal-appearing brainwave activity in a cat brain that was frozen to -20 °C and then rewarmed.[60] These successes include the first successful vitrification, transplantation, and long-term survival of a vital mammalian whole organ (a rabbit kidney; image, above) after cooling to full cryogenic temperatures,[61] the first demonstration of memory retention in a cryopreserved and revived simple animal,[62] and the first demonstration of whole brain vitrification with perfect preservation of neural connectivity (aka. the "connectome") throughout entire rabbit and pig brains after cooling to cryogenic temperatures.[63] Vitrification is a well-known alternative to cryopreservation by freezing that allows hydrated living cells to be cooled to cryogenic temperatures in the absence of ice.[64]

---

[58] Human embryos have been successfully cryopreserved for up to 24 years. Sabrina Barr, "Longest-frozen embryo is born after being preserved for 24 years," The Independent, 20 Dec 2017; https://www.independent.co.uk/life-style/health-and-families/embryo-24-years-frozen-born-baby-longest-ever-tina-benjamin-gibson-emma-wren-nedc-tennessee-a8119776.html.

[59] https://en.wikipedia.org/wiki/Cryopreservation#Freezable_tissues.

[60] Suda I, Kito K, Adachi C. Viability of long term frozen cat brain *in vitro*. Nature. 1966 Oct 15;212(5059):268-70; https://pubmed.ncbi.nlm.nih.gov/5970120/.

[61] Fahy GM, Wowk B, Pagotan R, Chang A, Phan J, Thomson B, Phan L. Physical and biological aspects of renal vitrification. Organogenesis. 2009 Jul;5(3):167-75; https://www.ncbi.nlm.nih.gov/pmc/articles/pmid/20046680/. After the rabbit received the kidney that had been cryopreserved: "Clinically, the animal regained normal drinking behavior, a normal fecal output score, and a normal urine volume output score by about 1-2 weeks postoperatively, but food consumption and to a lesser extent water consumption and urine output declined on balance after day 24. The rabbit lost about 18% of its body weight by the fifth postoperative day and thereafter maintained this weight....After ensuring that the animal appeared capable of living indefinitely using the vitrified kidney as the sole renal support, it was euthanized for histological follow-up on day 48." Histology revealed some freezing damage in the transplanted organ, which had remained functional nonetheless.

[62] Vita-More N, Barranco D. Persistence of Long-Term Memory in Vitrified and Revived *Caenorhabditis elegans*. Rejuvenation Res. 2015 Oct;18(5):458-63; https://www.ncbi.nlm.nih.gov/pmc/articles/PMC4620520/. The story behind the research project (illustrated): Vita-More N. Persistence of Long-Term Memory in Vitrified and Revived Simple Animals. Cryonics 2015 Sep;36(9):6-11; https://www.alcor.org/docs/cryonics-magazine-2015-09.pdf.

[63] McIntyre RL, Fahy GM. Aldehyde-stabilized cryopreservation. Cryobiology. 2015 Dec;71(3):448-58; https://www.sciencedirect.com/science/article/pii/S001122401500245X.

[64] Fahy GM, Wowk B. Principles of Ice-Free Cryopreservation by Vitrification. Methods Mol Biol. 2021;2180:27-97; https://pubmed.ncbi.nlm.nih.gov/32797408/.

The interested reader can peruse the substantial literature describing the scientific rationale for cryonics[65] and popular arguments favoring the practice,[66] which will not be reviewed here. According to an Open Letter on Cryonics,[67] first signed by 68 scientists in 2004: "Cryonics is a legitimate science-based endeavor that seeks to preserve human beings, especially the human brain, by the best technology available. Future technologies for resuscitation can be envisioned that involve **molecular repair by nanomedicine**, highly advanced computation, detailed control of cell growth, and tissue regeneration. With a view toward these developments, there is a credible possibility that cryonics performed under the best conditions achievable today can preserve sufficient neurological information to permit eventual restoration of a person to full health." There is now an emerging scientific consensus on the feasibility of cryopreserving complex mammalian tissues,[68] and the Society for Cryobiology is no longer openly hostile to cryonicists, though still eschewing cryonics as part of its professional mission (Appendix A).

A review of the scientific rationale for cryonics by Ben Best in 2008[69] explained that "[v]ery low temperatures create conditions that can preserve tissue for centuries, possibly including the neurological basis of the human mind. Through a process called vitrification, brain tissue can be cooled to cryogenic temperatures without ice formation. Damage associated with this process is theoretically reversible in the same sense that rejuvenation is theoretically possible by specific foreseeable technology. Injury to the brain due to stopped blood flow is now known to result from a complex series of processes that take much longer to run to completion than the 6 minute limit of ordinary resuscitation technology. Reperfusion beyond the 6 minute limit primarily damages blood vessels rather than brain tissue. Apoptosis of neurons takes many hours. This creates a window of opportunity between legal death and irretrievable loss of life for human and animal subjects for cryopreservation with possibility of future resuscitation. Under ideal conditions, the time interval between onset of clinical death and beginning of cryonics procedures can be reduced to less than 1 minute, but much longer delays could also be compatible with ultimate survival. Although the evidence that cryonics may work is indirect, the application of indirect evidence is essential in many areas of science. If complex changes due to aging are reversible at some future date, then similarly complex changes due to stopped blood flow and cryopreservation may also be reversible, with life-saving results for anyone with medical needs that exceed current capabilities."

---

[65] Feinberg G. Physics and Life Prolongation. Phys Today 1966;19(11):45; https://www.biostasis.com/physics-and-life-prolongation/. The Cryobiological Case for Cryonics. Cryonics 1988 Mar;9(3):23-36; https://www.alcor.org/library/the-cryobiological-case-for-cryonics/. Merkle RC. The Technical Feasibility of Cryonics. Med Hypotheses 1992 Sep;39(1):6-16; http://www.merkle.com/cryo/TheTechnicalFeasibilityOfCryonics.pdf. Lemler J, Harris SB, Platt C, Huffman TM. The arrest of biological time as a bridge to engineered negligible senescence. Ann N Y Acad Sci. 2004 Jun;1019:559-63; http://www.alcor.org/Library/pdfs/Lemler-Annals.pdf. Best BP. Scientific justification of cryonics practice. Rejuvenation Res. 2008 Apr;11(2):493-503; https://www.ncbi.nlm.nih.gov/pmc/articles/pmid/18321197/. De Wolf A, Platt C. Human Cryopreservation Procedures. Alcor Life Extension Foundation, 2020; https://www.alcor.org/library/human-cryopreservation-procedures/. Scientists' Cryonics FAQ, 2020; https://www.alcor.org/library/faq-scientists-questions/. See dynamic bibliography at https://pubmed.ncbi.nlm.nih.gov/?orig_db=PubMed&cmd=Search&defaultField=Title%20Word&term=cryonics. See also: https://www.alcor.org/library/#scientific.

[66] Urban T. Why Cryonics Makes Sense. Wait But Why, 24 Mar 2016; https://waitbutwhy.com/2016/03/cryonics.html. See also: https://www.alcor.org/library/faq-general-questions/.

[67] https://www.biostasis.com/scientists-open-letter-on-cryonics/.

[68] Lewis JK, Bischof JC, Braslavsky I, Brockbank KG, Fahy GM, Fuller BJ, Rabin Y, Tocchio A, Woods EJ, Wowk BG, Acker JP, Giwa S. The Grand Challenges of Organ Banking: Proceedings from the first global summit on complex tissue cryopreservation. Cryobiology. 2016 Apr;72(2):169-82; https://www.organpreservationalliance.org/s/Lewis-2016-Organ-Banking-Summit-proceedings.pdf.

[69] Best BP. Scientific justification of cryonics practice. Rejuvenation Res. 2008 Apr;11(2):493-503; https://www.ncbi.nlm.nih.gov/pmc/articles/pmid/18321197/.

Lemler *et al.*[70] add that "[t]he ultrastructure of the brain can now be excellently preserved by vitrification, and solutions needed for vitrification can now be distributed through organs with retention of organ viability after transplantation. Current law requires a few minutes of cardiac arrest before cryopreservation of terminal patients, but dogs and cats have recovered excellent brain function after 16-60 minutes of complete cerebral ischemia. The arrest of biological time as a bridge to engineered negligible senescence, therefore, appears consistent with current scientific and medical knowledge."

In 2019, a detailed human Medical Biostasis Protocol was published[71] with the intention of showing how human cryopreservation could be practiced as an elective medical procedure in which the transition between the decline of a terminal patient and the start of cryonics procedures is managed by medical professionals (e.g., in a regular hospital setting). The introduction to the document, which resulted from a collaborative effort between cryobiology researchers and medical professionals, reads as follows:

> "Medical biostasis is an experimental procedure that induces metabolic arrest at cryogenic temperatures to allow terminally ill patients to benefit from future medical advances and restore them to good health. Practiced as a hospital-based, elective medical procedure, medical biostasis consists of three distinct procedures: induction of hypothermic circulatory arrest, cryoprotection, and long-term care at intermediate temperatures (between -120 °C and -130 °C). This document sets out a detailed protocol for medical biostasis, outlines a variation of this protocol for out-of-hospital emergency cases, and outlines research directions to further optimize this protocol."

The Protocol ends with a discussion of the requirements for long-term maintenance of cryopreserved patients, but does not discuss specific methods of revival. According to the Protocol authors, placing a patient in medical biostasis at cryogenic temperatures "prevents any kind of critical condition from advancing and allows science and medicine to catch up to the point where matter can be manipulated at the molecular level and restoration of the patient to good health is feasible.[72]" A few professional organizations are starting to take notice. For instance, EMRA (the Emergency Medicine Residents' Association) recently added a webpage[73] advising hospital staff how to observe proper procedures when confronted with cryonics patients.

To fully understand the technical basis for future revival from medical biostasis using nanotechnology, we must start with a brief description of the nascent field of medical nanorobotics.

1.2 Medical Nanorobotics

The early genesis of the concept of medical nanorobots, manufactured in nanofactories, sprang from the visionary idea that tiny nanomachines could be designed, manufactured, and introduced into the human

---

[70] Lemler J, Harris SB, Platt C, Huffman TM. The arrest of biological time as a bridge to engineered negligible senescence. Ann N Y Acad Sci. 2004 Jun;1019:559-63; http://www.alcor.org/Library/pdfs/Lemler-Annals.pdf.

[71] De Wolf A, Salmensuu V. Medical Biostasis Protocol (V 1.0); https://www.biostasis.com/protocol.pdf. Described in: de Grey ADNJ. Cryonics Takes Another Big Step Toward the Mainstream. Rejuvenation Res. 2020 Jun 16;23(3):191-2; https://www.liebertpub.com/doi/full/10.1089/rej.2020.2356.

[72] Robert A. Freitas Jr., "Chapter 23. Comprehensive Nanorobotic Control of Human Morbidity and Aging," in Gregory M. Fahy, Michael D. West, L. Stephen Coles, and Steven B. Harris, eds, The Future of Aging: Pathways to Human Life Extension, Springer, New York, 2010, pp. 685-805; http://www.nanomedicine.com/Papers/Aging.pdf.

[73] Zald Altawil, MD, "A Different Kind of Therapeutic Hypothermia," EMRA/Clinical, 15 Dec 2018; https://www.emra.org/emresident/article/cryonics/.

body to perform cellular repairs at the molecular level. Although the medical application of nanotechnology was championed in the popular writings of Drexler[74] in the 1980s and 1990s and in the technical writings of Freitas[75] in the 1990s, 2000s, and 2010s, the first scientist to voice the possibility was the late Nobel physicist Richard P. Feynman, who worked on the Manhattan Project at Los Alamos during World War II and later taught at Caltech for most of his professorial career.

In his prescient 1959 talk "There's Plenty of Room at the Bottom," Feynman proposed employing machine tools to make smaller machine tools, these to be used in turn to make still smaller machine tools, and so on all the way down to the atomic level.[76] He prophetically concluded that this is "a development which I think cannot be avoided." After discussing his ideas with a colleague, Feynman offered the first known proposal for a medical nanorobotic procedure of any kind – in this instance, to cure heart disease: "A friend of mine (Albert R. Hibbs) suggests a very interesting possibility for relatively small machines. He says that, although it is a very wild idea, it would be interesting in surgery if you could swallow the surgeon. You put the mechanical surgeon inside the blood vessel and it goes into the heart and looks around. (Of course the information has to be fed out.) It finds out which valve is the faulty one and takes a little knife and slices it out. Other small machines might be permanently incorporated in the body to assist some inadequately functioning organ." Later in his historic 1959 lecture, Feynman urges us to consider the possibility, in connection with microscopic biological cells, "that we can manufacture an object that maneuvers at that level!" The field had progressed far enough by 2007, half a century after Feynman's speculations, to allow Martin Moskovits, Professor of Chemistry and Dean of Physical Science at UC Santa Barbara, to write[77] that "the notion of an ultra-small robot that can, for example, navigate the bloodstream performing microsurgery or activating neurons so as to restore muscular activity, is not an unreasonable goal, and one that may be realized in the near future."

Many questions arise when one first encounters the idea of micron-scale nanorobots, constructed of nanoscale components and operating inside the human body. At the most fundamental level, technical questions about the influence of quantum effects on molecular structures, friction and wear among nanomechanical components, radiation damage, other failure mechanisms, the influence of thermal noise on reliability, and the effects of Brownian bombardment on nanomachines have all been extensively discussed and resolved in the literature.[78] Self-assembled molecular motors consisting of just 50-100 atoms

---

[74] Drexler KE. Engines of Creation: The Coming Era of Nanotechnology. Anchor Press/Doubleday, New York, 1986, Chapter 7 "Engines of Healing"; https://web.archive.org/web/20180722191948/http://e-drexler.com/d/06/00/EOC/EOC_Chapter_7.html. Drexler KE, Peterson C, Pergamit G. Unbounding the Future: The Nanotechnology Revolution. William Morrow/Quill Books, New York, 1991, Chapter 10 "Nanomedicine"; https://web.archive.org/web/20100302193412/http://www.foresight.org/UTF/Unbound_LBW/chapt_10.html.

[75] Freitas RA Jr. Nanomedicine, Volume I: Basic Capabilities. Landes Bioscience, Georgetown, TX, 1999; http://www.nanomedicine.com/NMI.htm. Freitas RA Jr. Nanomedicine, Volume IIA: Biocompatibility. Landes Bioscience, Georgetown, TX, 2003; http://www.nanomedicine.com/NMIIA.htm. Freitas RA Jr. "Technical Analyses of Types of Diamondoid Medical Nanorobots," http://www.nanomedicine.com/#NanorobotAnalyses.

[76] Feynman RP. There's plenty of room at the bottom. Eng Sci (CalTech) 1960;23:22-36; http://www.zyvex.com/nanotech/feynman.html.

[77] Moskovits M. Nanoassemblers: A likely threat? Nanotech. Law & Bus. 2007;4:187-195; https://heinonline.org/hol-cgi-bin/get_pdf.cgi?handle=hein.journals/nantechlb4&section=29.

[78] Drexler KE. Nanosystems: Molecular Machinery, Manufacturing, and Computation. John Wiley & Sons, New York, 1992; https://www.amazon.com/dp/0471575186/. Freitas RA Jr. Nanomedicine, Volume I: Basic Capabilities. Landes Bioscience, Georgetown, TX, 1999; http://www.nanomedicine.com/NMI/2.1.htm.

have been demonstrated experimentally since the late 1990s.[79] Published discussions of technical issues of specific relevance to medical nanorobots include proposed methods for recognizing, sorting and pumping individual molecules;[80] theoretical designs for mechanical nanorobot sensors;[81] flexible nanorobot hull surfaces,[82] power sources,[83] communications[84] and navigation[85] systems, and manipulator mechanisms;[86] nanorobot mobility mechanisms for travel through bloodstream, tissues and cells,[87] and for penetration of the blood-brain barrier;[88] onboard clocks[89] and nanocomputers;[90] and the full panoply of nanorobot biocompatibility issues.[91]

---

[79] Kelly TR, De Silva H, Silva RA. Unidirectional rotary motion in a molecular system. Nature. 1999 Sep 9;401:150-152; https://ww.bostoncollege.org/content/dam/bc1/schools/mcas/Chemistry/news-and-notes/pdf/3.pdf. Koumura N, Zijlstra RW, van Delden RA, Harada N, Feringa BL. Light-driven monodirectional molecular rotor. Nature 1999 Sep 9;401:152-155; https://core.ac.uk/download/pdf/148148838.pdf. Huang TJ, Lu W, Tseng HR, *et al*. Molecular shuttle switching in closely packed Langmuir films, 11th Foresight Conf. Mol. Nanotech., San Francisco CA, 10-12 Oct 2003. Leigh DA, Wong JKY, Dehez F, Zerbetto F. Unidirectional rotation in a mechanically interlocked molecular rotor. Nature. 2003 Jul 10;424(6945):174-179; http://biotheory.phys.cwru.edu/phys414/nature01758.pdf. Browne WR, Feringa BL. Making molecular machines work. Nat Nanotechnol. 2006 Oct;1(1):25-35; https://www.rug.nl/research/portal/files/6702682/2006NatureNanotechBrowne.pdf. Kay ER, Leigh DA, Zerbetto F. Synthetic molecular motors and mechanical machines. Angew Chem Int Ed 2007;46(1-2):72-191; https://pubmed.ncbi.nlm.nih.gov/17133632/.

[80] Drexler KE. Nanosystems: Molecular Machinery, Manufacturing, and Computation. John Wiley & Sons, New York, 1992, Section 13.2; https://www.amazon.com/dp/0471575186/. Freitas RA Jr. Nanomedicine, Volume I: Basic Capabilities. Landes Bioscience, Georgetown, TX, 1999, Chapter 3, "Molecular Transport and Sortation"; http://www.nanomedicine.com/NMI/3.1.htm.

[81] Freitas RA Jr. Nanomedicine, Volume I: Basic Capabilities. Landes Bioscience, Georgetown, TX, 1999, Chapter 4, "Nanosensors and Nanoscale Sensing"; http://www.nanomedicine.com/NMI/4.1.htm.

[82] Freitas RA Jr. Nanomedicine, Volume I: Basic Capabilities. Landes Bioscience, Georgetown, TX, 1999, Chapter 5, "Shapes and Metamorphic Surfaces"; http://www.nanomedicine.com/NMI/5.1.htm. Hogg T. Energy dissipation by metamorphic micro-robots in viscous fluids. J Micro-Bio Robotics 2016; 11(1-4):85-95; https://arxiv.org/pdf/1507.01145.

[83] Freitas RA Jr. Nanomedicine, Volume I: Basic Capabilities. Landes Bioscience, Georgetown, TX, 1999, Chapter 6, "Power"; http://www.nanomedicine.com/NMI/6.1.htm. Hogg T, Freitas RA Jr. Chemical power for microscopic robots in capillaries. Nanomedicine. 2010 Apr;6(2):298-317; https://arxiv.org/pdf/0906.5022.

[84] Freitas RA Jr. Nanomedicine, Volume I: Basic Capabilities. Landes Bioscience, Georgetown, TX, 1999, Chapter 7, "Communication"; http://www.nanomedicine.com/NMI/7.1.htm. Hogg T, Freitas RA Jr. Acoustic communication for medical nanorobots. Nano Commun Networks 2012; 3(2):83-102; https://arxiv.org/pdf/1202.0568.

[85] Freitas RA Jr. Nanomedicine, Volume I: Basic Capabilities. Landes Bioscience, Georgetown, TX, 1999, Chapter 8, "Navigation"; http://www.nanomedicine.com/NMI/8.1.htm.

[86] Freitas RA Jr. Nanomedicine, Volume I: Basic Capabilities. Landes Bioscience, Georgetown, TX, 1999, Section 9.3, "Nanomanipulators"; http://www.nanomedicine.com/NMI/9.3.htm.

[87] Freitas RA Jr. Nanomedicine, Volume I: Basic Capabilities. Landes Bioscience, Georgetown, TX, 1999, Section 9.4, "*In Vivo* Locomotion"; http://www.nanomedicine.com/NMI/9.4.htm. Hogg T. Using surface-motions for locomotion of microscopic robots in viscous fluids. J Micro-Bio Robotics. 2014; 9(3-4):61-77; https://arxiv.org/pdf/1311.0801.

[88] Freitas RA Jr. The Alzheimer Protocols: A Nanorobotic Cure for Alzheimer's Disease and Related Neurodegenerative Conditions. IMM Report No. 48, June 2016, 433 pp; Section 4.3 "Medical Nanorobots: Ingress to, and Egress from, the Brain"; http://www.imm.org/Reports/rep048.pdf. Freitas RA Jr. Nanomedicine, Volume IIA: Biocompatibility. Landes Bioscience, Georgetown, TX, 2003, Section 15.3.6.5, "Biocompatibility with Neural Cells"; http://www.nanomedicine.com/NMIIA/15.3.6.5.htm#p8.

[89] Freitas RA Jr. Nanomedicine, Volume I: Basic Capabilities. Landes Bioscience, Georgetown, TX, 1999, Section 10.1, "Nanochronometry"; http://www.nanomedicine.com/NMI/10.1.htm.

The idea of placing semi-autonomous self-powered nanorobots inside of us might seem a bit odd, but the human body already teems with similar natural nanodevices. More than 40 trillion single-celled microbes swim through our colon, outnumbering our tissue cells almost ten to one.[92] Many bacteria move by whipping around a tiny tail, or flagellum, that is driven by a 30-nanometer biological ionic nanomotor powered by pH differences between the inside and the outside of the bacterium. Our bodies also maintain a population of more than a trillion motile biological nanodevices called fibroblasts and white cells such as neutrophils and lymphocytes, each measuring up to ~10 μm in size.[93] These beneficial natural nanorobots are constantly crawling around inside us, repairing damaged tissues, attacking invading microbes, and gathering up foreign particles and transporting them to various organs for disposal from the body.[94]

The greatest power of nanomedicine will emerge as we learn to design and construct complete artificial nanorobots using nanometer-scale parts and subsystems such as diamondoid bearings and gears, nanomotors and molecular pumps, nanomanipulators, nanosensors, nanobatteries, and nanocomputers.

In the subsections below, we briefly describe four major classes of hypothetical medical nanorobots, listed in order of increasing capacity and sophistication:

(1) **free-floating nonmotile nanorobots** (e.g., respirocytes; Section 1.2.1),

(2) **motile nanorobots** (e.g., microbivores; Section 1.2.2),

(3) **cell repair nanorobots** (e.g., chromallocytes; Section 1.2.3), and

(4) **multidevice nanorobotic systems** (e.g., vasculoid; Section 1.2.4).

We then enumerate some of the major advantages of nanorobots over other medical approaches and instrumentalities (Section 1.2.5).

Much of the following material in Section 1.2 is drawn from a previously published summary.[95]

---

[90] Drexler KE. Nanosystems: Molecular Machinery, Manufacturing, and Computation. John Wiley & Sons, New York, 1992, Chapter 12; https://www.amazon.com/dp/0471575186/. Freitas RA Jr. Nanomedicine, Volume I: Basic Capabilities. Landes Bioscience, Georgetown, TX, 1999, Section 10.2, "Nanocomputers"; http://www.nanomedicine.com/NMI/10.2.htm.

[91] Freitas RA Jr. Nanomedicine, Volume IIA: Biocompatibility. Landes Bioscience, Georgetown, TX, 2003; http://www.nanomedicine.com/NMIIA.htm.

[92] Freitas RA Jr. Nanomedicine, Volume I: Basic Capabilities. Landes Bioscience, Georgetown, TX, 1999, Section 8.5.1, "Cytometrics"; http://www.nanomedicine.com/NMI/8.5.1.htm.

[93] Freitas RA Jr. Nanomedicine, Volume I: Basic Capabilities. Landes Bioscience, Georgetown, TX, 1999, Section 8.5.1, "Cytometrics"; http://www.nanomedicine.com/NMI/8.5.1.htm.

[94] Freitas RA Jr. Nanomedicine, Volume IIA: Biocompatibility. Landes Bioscience, Georgetown, TX, 2003, Section 15.4.3.1, "Phagocytes, Phagocytosis, and the RES"; http://www.nanomedicine.com/NMIIA/15.4.3.1.htm.

[95] Freitas RA Jr. The Alzheimer Protocols: A Nanorobotic Cure for Alzheimer's Disease and Related Neurodegenerative Conditions. IMM Report No. 48, June 2016, 433 pp; Section 4.2 "Medical Nanorobots: Background"; http://www.imm.org/Reports/rep048.pdf.

1.2.1 Respirocyte-Class Nanorobots

The first theoretical design study of a medical nanorobot ever published in a peer-reviewed medical journal (by Freitas in 1998)[96] described an artificial mechanical red blood cell or "respirocyte" to be made of 18 billion precisely arranged atoms. The device was to be a bloodborne spherical 1-μm diameter diamondoid 1000-atmosphere pressure vessel[97] with active pumping[98] powered by the oxidation of endogenous serum glucose,[99] able to deliver 236 times more oxygen to the tissues per unit volume than natural red cells and to manage acidity caused by carbonic acid formation, all controlled by gas concentration sensors[100] and an onboard nanocomputer.[101] The basic operation of respirocytes (image, left; artwork by Forrest Bishop)[102] is straightforward. These nanorobots would mimic the action of the natural hemoglobin(Hb)-filled red blood cells, while operating at 1000 atm vs. only 0.1-0.5 atm equivalent for natural Hb. In the tissues, oxygen will be pumped out of the device by the molecular sorting rotors (Section 4.10.1) on one side. Carbon dioxide will be pumped into the device by molecular sorting rotors on the other side, one molecule at a time. Half a minute later, when the respirocyte reaches the patient's lungs in the normal course of the circulation of the blood, these same rotors reverse their direction of rotation, recharging the device with fresh oxygen and dumping the stored CO_2, which diffuses into the lungs and can then be exhaled by the patient. Each rotor requires very little power, only ~0.03 pW to pump ~10^6 molecules/sec in continuous operation.

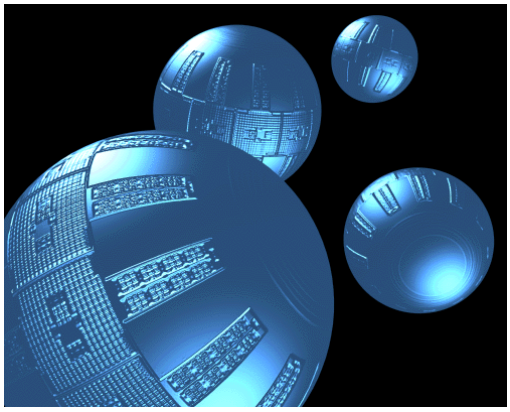

---

[96] Freitas RA Jr. Exploratory design in medical nanotechnology: a mechanical artificial red cell. Artif Cells Blood Substit Immobil Biotechnol. 1998 Jul;26(4):411-30; https://www.tandfonline.com/doi/pdf/10.3109/10731199809117682. A longer version of this paper appears at: https://web.archive.org/web/20100420085137/http://www.foresight.org/Nanomedicine/Respirocytes.html.

[97] Freitas RA Jr. Nanomedicine, Volume I: Basic Capabilities. Landes Bioscience, Georgetown, TX, 1999, Section 10.3, "Pressure Storage and Ballasting"; http://www.nanomedicine.com/NMI/10.3.htm.

[98] Freitas RA Jr. Nanomedicine, Volume I: Basic Capabilities. Landes Bioscience, Georgetown, TX, 1999, Section 3.4.2, "Sorting Rotors"; http://www.nanomedicine.com/NMI/3.4.2.htm.

[99] Freitas RA Jr. Nanomedicine, Volume I: Basic Capabilities. Landes Bioscience, Georgetown, TX, 1999, Section 6.3.4, "Chemical Energy Conversion Processes"; http://www.nanomedicine.com/NMI/6.3.4.htm.

[100] Freitas RA Jr. Nanomedicine, Volume I: Basic Capabilities. Landes Bioscience, Georgetown, TX, 1999, Section 4.2.1, "Broadband Receptor Arrays"; http://www.nanomedicine.com/NMI/4.2.1.htm.

[101] Drexler KE. Nanosystems: Molecular Machinery, Manufacturing, and Computation. John Wiley & Sons, New York, 1992, Chapter 12; https://www.amazon.com/dp/0471575186/. Freitas RA Jr. Nanomedicine, Volume I: Basic Capabilities. Landes Bioscience, Georgetown, TX, 1999, Section 10.2, "Nanocomputers"; http://www.nanomedicine.com/NMI/10.2.htm.

[102] https://web.archive.org/web/20160325053612/https://foresight.org/Nanomedicine/Gallery/Captions/Image139.html.

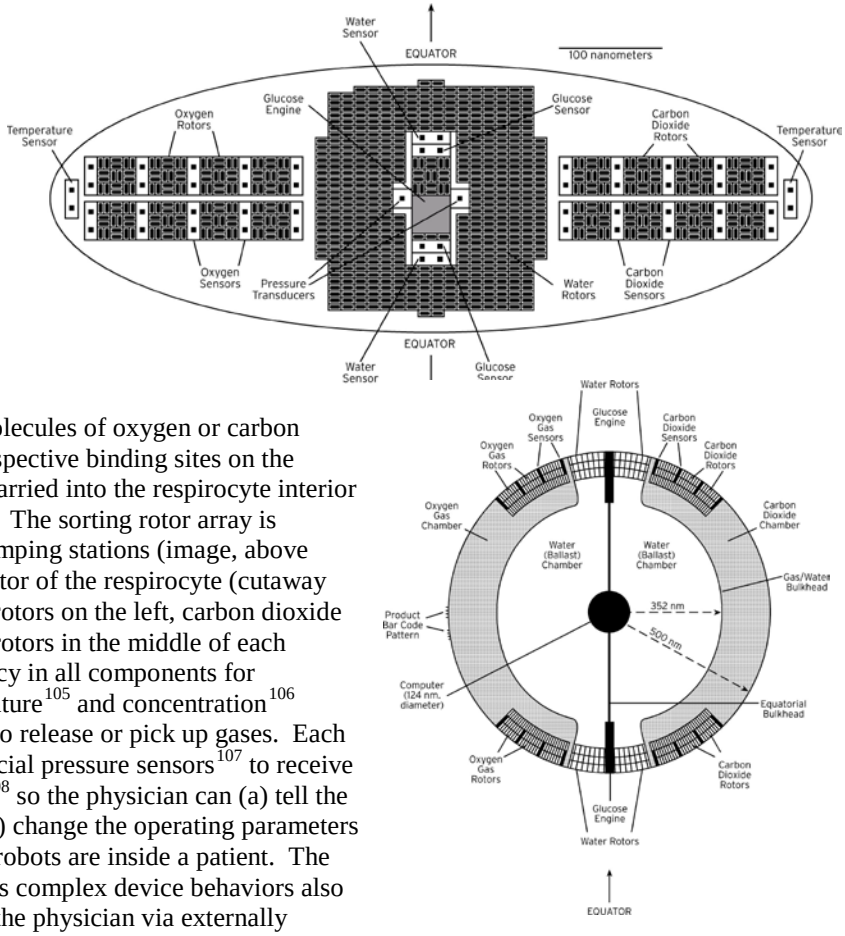

In the exemplar respirocyte design,[103] onboard pressure tanks can hold up to 3 billion oxygen (O_2) or carbon dioxide (CO_2) molecules. Molecular sorting rotors[104] are arranged on the surface to load and unload gases from the pressurized tanks. Tens of thousands of these individual pumps cover a large fraction of the hull surface of the respirocyte. Molecules of oxygen or carbon dioxide may drift into their respective binding sites on the exterior rotor surface and be carried into the respirocyte interior as the rotor turns in its casing. The sorting rotor array is organized into 12 identical pumping stations (image, above right) laid out around the equator of the respirocyte (cutaway image, at right), with oxygen rotors on the left, carbon dioxide rotors on the right, and water rotors in the middle of each station, with tenfold redundancy in all components for enhanced reliability. Temperature[105] and concentration[106] sensors tell the devices when to release or pick up gases. Each pumping station will have special pressure sensors[107] to receive ultrasonic acoustic messages[108] so the physician can (a) tell the devices to turn on or off, or (b) change the operating parameters of the devices, while the nanorobots are inside a patient. The onboard nanocomputer enables complex device behaviors also remotely reprogrammable by the physician via externally applied ultrasound acoustic signals. Internal power will be transmitted mechanically or hydraulically using an appropriate working fluid, and can be distributed as required using rods and gear trains[109] or using pipes

---

[103] Freitas RA Jr. Exploratory design in medical nanotechnology: a mechanical artificial red cell. Artif Cells Blood Substit Immobil Biotechnol. 1998 Jul;26(4):411-30; https://www.tandfonline.com/doi/pdf/10.3109/10731199809117682. A longer version of this paper appears at: https://web.archive.org/web/20100420085137/http://www.foresight.org/Nanomedicine/Respirocytes.html.

[104] Drexler KE. Nanosystems: Molecular Machinery, Manufacturing, and Computation. John Wiley & Sons, New York, 1992, Section 13.2; https://www.amazon.com/dp/0471575186/. Freitas RA Jr. Nanomedicine, Volume I: Basic Capabilities. Landes Bioscience, Georgetown, TX, 1999, Section 3.4.2, "Sorting Rotors"; http://www.nanomedicine.com/NMI/3.4.2.htm.

[105] Freitas RA Jr. Nanomedicine, Volume I: Basic Capabilities. Landes Bioscience, Georgetown, TX, 1999, Section 4.6, "Thermal Nanosensors"; http://www.nanomedicine.com/NMI/4.6.htm.

[106] Freitas RA Jr. Nanomedicine, Volume I: Basic Capabilities. Landes Bioscience, Georgetown, TX, 1999, Section 4.2, "Chemical and Molecular Nanosensors"; http://www.nanomedicine.com/NMI/4.2.htm.

[107] Freitas RA Jr. Nanomedicine, Volume I: Basic Capabilities. Landes Bioscience, Georgetown, TX, 1999, Section 4.5, "Pressure Sensing"; http://www.nanomedicine.com/NMI/4.5.htm.

[108] Freitas RA Jr. Nanomedicine, Volume I: Basic Capabilities. Landes Bioscience, Georgetown, TX, 1999, Section 7.2.2, "Acoustic Broadcast Communication"; http://www.nanomedicine.com/NMI/7.2.2.htm.

[109] Freitas RA Jr. Nanomedicine, Volume I: Basic Capabilities. Landes Bioscience, Georgetown, TX, 1999, Section 6.4.3.4, "Gear Trains and Mechanical Tethers"; http://www.nanomedicine.com/NMI/6.4.3.4.htm.

and mechanically operated valves, controlled by the nanocomputer. There is also a large internal void surrounding the nanocomputer which can be a vacuum, or can be filled with (or emptied of) up to 6 billion molecules of water. This will allow the device to control its buoyancy very precisely and provides a crude but simple method for removing respirocytes from the body using a blood centrifuge (Appendix M), a future procedure now termed "nanapheresis".[110]

A 5 cc therapeutic dose of 50% respirocyte saline suspension containing 5 trillion nanorobots would exactly replace the gas carrying capacity of the patient's entire 5.4 liters of blood. Each device stores enough onboard glucose/O_2 to provide power for at least one circulation time (60 sec), and can also store the CO_2.[111] If up to 1 liter of respirocyte suspension could safely be added to the human bloodstream,[112] this would keep a patient's tissues oxygenated for up to an hour even if a heart attack caused the heart to stop beating, or if there was a complete absence of respiration or no external availability of oxygen. Primary medical applications of respirocytes might include emergency revival of victims of carbon monoxide suffocation at the scene of a fire, rescue of drowning victims, and transfusable pre-oxygenated blood substitution. Respirocytes (image, left; artwork by Forrest Bishop)[113] could serve as "instant blood" at an accident scene with no need for blood typing, and, thanks to the dramatically higher gas-transport efficiency of respirocytes over natural red cells, a mere 1 cm^3 infusion of the devices would provide the oxygen-carrying ability of a full liter of ordinary blood, possibly saving lives even in cases of moderate hypovolemia (lost blood fluid volume) that might otherwise lead to hemorrhagic shock.[114]

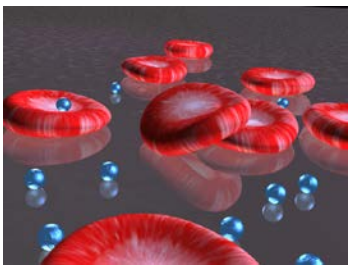

Larger doses of respirocytes could also: (1) be used as a temporary treatment for anemia and various lung and perinatal/neonatal disorders, (2) enhance tumor therapies and diagnostics and improve outcomes for cardiovascular, neurovascular, or other surgical procedures, (3) help prevent asphyxia and permit artificial breathing (e.g., underwater, high altitude, etc.), and (4) have many additional applications in sports, veterinary medicine, military science, and space exploration.

---

[110] Freitas RA Jr. Nanomedicine, Volume I: Basic Capabilities. Landes Bioscience, Georgetown, TX, 1999, Section 10.3.6, "Buoyancy Control and Nanapheresis"; http://www.nanomedicine.com/NMI/10.3.6.htm.

[111] Aqueous conversion of CO_2 to carbonic acid is slow, a significant fraction of a second, while the reverse takes ~300 nsec at neutral pH, hence this equilibrium reaction shouldn't interfere with the respirocyte sorting rotor CO_2 molecule identification and removal process from plasma water. Personal communication from Brian Wowk to Robert Freitas, 30 Sep 2021.

[112] Freitas RA Jr. Nanomedicine Vol. IIA: Biocompatibility. Landes Bioscience, Georgetown, TX, 2003, Section 15.6.2, "Bloodstream Intrusiveness"; http://www.nanomedicine.com/NMI/15.6.2.htm.

[113] https://web.archive.org/web/20210508220644/https://foresight.org/Nanomedicine/Gallery/Captions/Image140.html.

[114] Takasu A, Prueckner S, Tisherman SA, Stezoski SW, Stezoski J, Safar P. Effects of increased oxygen breathing in a volume controlled hemorrhagic shock outcome model in rats. Resuscitation. 2000 Aug 1;45(3):209-20; https://www.sciencedirect.com/science/article/abs/pii/S0300957200001830. Dyson A, Stidwill R, Taylor V, Singer M. The impact of inspired oxygen concentration on tissue oxygenation during progressive haemorrhage. Intensive Care Med. 2009 Oct;35(10):1783-91; https://pubmed.ncbi.nlm.nih.gov/19618165/.

1.2.2 Microbivore-Class Nanorobots

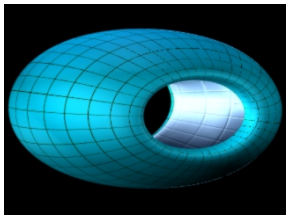

Perhaps the most widely recognized form of disease is an attack on the human body by invading viruses, bacteria, protozoa, or other microscopic parasites. One general class of medical nanorobot could serve as the first-line nanomedical treatment for pathogen-related disease. Called a "microbivore", this artificial nanorobotic white cell substitute, made of diamond and sapphire, would seek out and harmlessly digest unwanted bloodborne pathogens.[115] One main task of natural white cells is to phagocytose and kill microbial invaders in the bloodstream. Microbivore nanorobots would also perform the equivalent of phagocytosis and microbial killing, but would operate much faster, more reliably, and under human control.

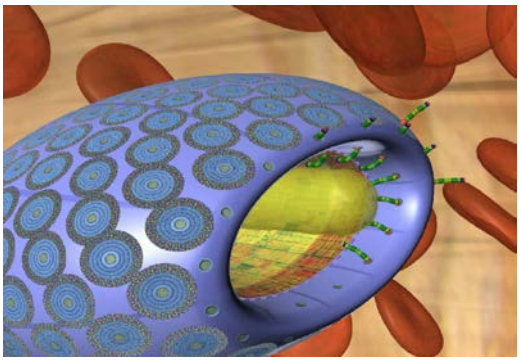

The baseline microbivore (image, left; hull design image, above; all microbivore artwork by Forrest Bishop)[116] is designed as an oblate spheroidal nanomedical device measuring 3.4 μm in diameter along its major axis and 2.0 μm in diameter along its minor axis, consisting of 610 billion precisely arranged structural atoms in a gross geometric volume of 12.1 μm^3 and a dry mass of 12.2 picograms. This size helps to ensure that the nanorobot can safely pass through or avoid even the narrowest of human capillaries and other tight spots in the spleen (e.g., the interendothelial splenofenestral slits)[117] and elsewhere in the human body,[118] given device motility. The microbivore has a mouth with an irising door, called the ingestion port, where microbes are fed in to be digested. This port is large enough to internalize a single microbe from virtually any major bacteremic species in a single gulp. The microbivore also has a rear end, or exhaust port, where the completely digested remains of the pathogen are harmlessly expelled from the device. The rear door opens between the main body of the microbivore and a tail-cone structure. According to the scaling study by Freitas,[119] the device may consume up to 200 pW of continuous power (using bloodstream glucose and oxygen for energy) while completely digesting trapped microbes at a maximum throughput of 2 μm^3 of organic material per 30-second cycle. This "digest and discharge" protocol[120] is conceptually

---

[115] Freitas RA Jr. Microbivores: Artificial mechanical phagocytes using digest and discharge protocol. J Evol Technol 2005;14:1-52; http://www.jetpress.org/volume14/freitas.html.

[116] https://web.archive.org/web/20160827082558/https://foresight.org/Nanomedicine/Gallery/Captions/Image197.html.

[117] Freitas RA Jr. Nanomedicine Vol. IIA: Biocompatibility. Landes Bioscience, Georgetown, TX, 2003, Section 15.4.2.3, "Geometrical Trapping in Spleen Vasculature"; http://www.nanomedicine.com/NMI/15.4.2.3.htm.

[118] Freitas RA Jr. Nanomedicine Vol. IIA: Biocompatibility. Landes Bioscience, Georgetown, TX, 2003, Section 15.4.2, "Geometrical Trapping of Bloodborne Medical Nanorobots"; http://www.nanomedicine.com/NMI/15.4.2.htm.

[119] Freitas RA Jr. Microbivores: Artificial mechanical phagocytes using digest and discharge protocol. J Evol Technol 2005;14:1-52; http://www.jetpress.org/volume14/freitas.html.

[120] Freitas RA Jr. Nanomedicine, Volume I: Basic Capabilities. Landes Bioscience, Georgetown, TX, 1999, Section 10.4.2.4.2, "Digest and Discharge (DD)"; http://www.nanomedicine.com/NMI/10.4.2.4.2.htm.

similar to the internalization and digestion process practiced by natural phagocytes, except that the artificial process should be a hundred-fold faster and also cleaner. For example, it is well-known that macrophages release biologically active compounds during bacteriophagy,[121] whereas well-designed microbivores need only release biologically inactive effluent.

The first task for the bloodborne microbivore is to reliably acquire a pathogen to be digested. If the correct bacterium bumps into the nanorobot surface, reversible species-specific binding sites on the microbivore hull can recognize and weakly bind to the bacterium. A set of 9 distinct antigenic markers should be specific enough,[122] since all 9 must register a positive binding event to confirm that a targeted microbe has been caught. There are 20,000 copies of these 9-marker receptor sets, distributed in 275 disk-shaped regions across the microbivore surface (image, right). Inside each receptor ring are more rotors to absorb ambient glucose and oxygen from the bloodstream to provide nanorobot power.

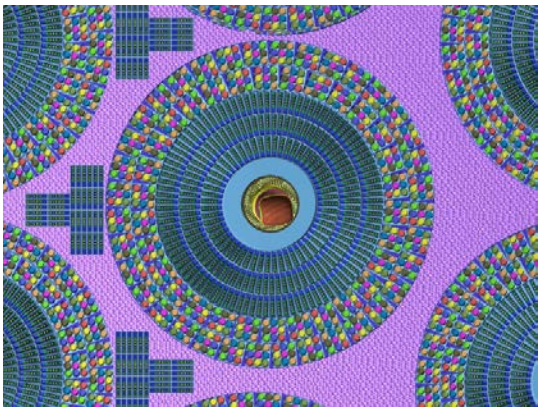

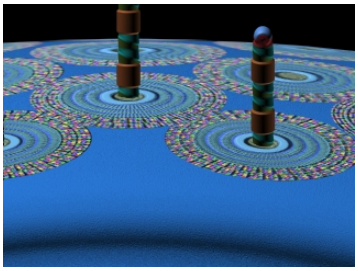

At the center of each 150-nm diameter receptor disk is a grapple silo (image, left). Once a bacterium has been captured by the reversible receptors, telescoping robotic grapples[123] rise up out of the microbivore surface and attach to the trapped bacterium, establishing secure anchorage to the microbe's cell wall, capsid, or plasma membrane. The microbivore grapple arms are about 100 nanometers long and have various rotating and telescoping joints that allow them to change their position, angle, and length. After rising out of its silo, a grapple arm could execute complex twisting motions (image, right), and adjacent grapple arms can physically reach each other, allowing them to hand off bound objects as small as a virus particle. Grapple handoff motions could transport a large rod-shaped bacterium from its original capture site forward to the ingestion port at the front of the device. The captive organism would be rotated into the proper orientation as it approaches the open microbivore mouth. There the pathogen is internalized into a 2 μm^3 morcellation chamber under continuous control of mouth grapples and an internal mooring mechanism.

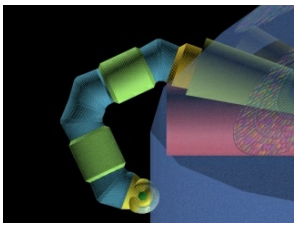

There are two concentric cylinders inside the microbivore. The bacterium will be minced into nanoscale pieces in the morcellation chamber (the smaller inner cylinder),[124] then the remains are pistoned into a

---

[121] Fincher EF 4th, Johannsen L, Kapás L, Takahashi S, Krueger JM. Microglia digest *Staphylococcus aureus* into low molecular weight biologically active compounds. Am J Physiol. 1996 Jul;271(1 Pt 2):R149-56; http://www.ncbi.nlm.nih.gov/pubmed/8760216.

[122] Freitas RA Jr. Nanomedicine, Volume I: Basic Capabilities. Landes Bioscience, Georgetown, TX, 1999, Section 8.5.2.2, "Identification of Cell Type"; http://www.nanomedicine.com/NMI/8.5.2.2.htm.

[123] Freitas RA Jr. Nanomedicine, Volume I: Basic Capabilities. Landes Bioscience, Georgetown, TX, 1999, Section 9.3.1.4, "Telescoping Manipulators"; http://www.nanomedicine.com/NMI/9.3.1.4.htm.

[124] Freitas RA Jr. Nanomedicine, Volume I: Basic Capabilities. Landes Bioscience, Georgetown, TX, 1999, Section 9.3.5.1, "Morcellation and Mincing"; http://www.nanomedicine.com/NMI/9.3.5.1.htm.

separate 2 μm^3 digestion chamber (the larger outer cylinder). In a preprogrammed sequence, ~40 different engineered digestive enzymes will be successively injected and extracted six times during a single digestion cycle, progressively reducing the morcellate to amino acids, mononucleotides, glycerol, free fatty acids and simple sugars, using an appropriate array of molecular sorting rotors. These basic end-product molecules are then harmlessly discharged back into the bloodstream through the exhaust port at the rear of the device, completing the 30-second digestion cycle (images, below; artwork by Forrest Bishop). When treatment is finished, the doctor may transmit an ultrasound signal to tell the circulating microbivores that their work is done. These motile nanorobots may then exit the body through the kidneys by various means[125] and be excreted with the urine in due course.

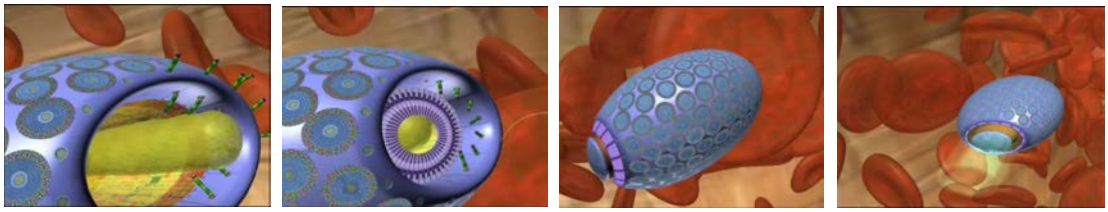

A human neutrophil, the most common type of leukocyte or white cell, can capture and engulf a microbe in a minute or less (images, below), but complete digestion and excretion of the organism's remains can take an hour or longer. Our natural white cells – even when aided by antibiotics – can sometimes take weeks or months to completely clear bacteria from the bloodstream. By comparison, a single terabot (10^{12}-nanorobot) dose of microbivores should be able to fully eliminate bloodborne pathogens in just minutes, or hours in the case of locally dense infections. This is accomplished without increasing the risk of sepsis or septic shock because all bacterial components (including all cell-wall lipopolysaccharide) will be internalized and fully digested into harmless non-antigenic molecules prior to discharge from the microbivore device.

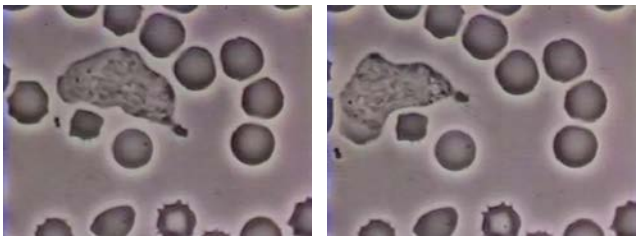

And no matter that a bacterium has acquired multiple drug resistance to antibiotics or to any other traditional treatment – the microbivore will eat it anyway. Microbivores would be up to ~1000 times faster-acting than antibiotic-based cures which often need weeks or months to work. The nanorobots would digest ~100 times more microbial material than an equal volume of natural white cells could digest in any given time period, and would have far greater maximum lifetime capacity for phagocytosis than natural white blood cells.

---

[125] Weatherbee C, Freitas RA Jr. Nanoscale robot navigation of the human kidney. In preparation.

1.2.3 Chromallocyte-Class Nanorobots

The chromallocyte[126] is a mobile cell-repair nanorobot whose primary function is to perform chromosome replacement therapy (CRT). In CRT, the entire chromatin content of the nucleus in a living cell is extracted and promptly replaced with a new set of prefabricated chromosomes that have been artificially manufactured as defect-free copies of the originals.

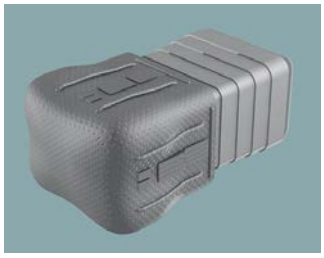

The chromallocyte (images, left; artwork by Stimulacra) will be capable of limited vascular surface travel into the capillary bed of the targeted tissue or organ, followed by diapedesis (exiting a blood vessel into the tissues),[127] histonatation (locomotion through tissues),[128] cytopenetration (entry into the cell interior; see nanorobot images, below, by E-spaces),[129] and complete chromatin replacement in the nucleus of the target cell. The CRT mission ends with a return to the vasculature and subsequent extraction of the nanodevices from the body at the original infusion site.

This ~3 hour chromosome replacement process is expected to involve a 26-step sequence of distinct semi-autonomous sensor-driven activities which are described at length in a comprehensive published technical paper on the subject by Freitas[130] and in summary below, including: (**1**) injection, (**2**) extravasation, (**3**) ECM immigration, (**4**) cytopenetration (image, right), (**5**) inhibition of mechanotransduction (to avoid nanorobot mechanical actions triggering unwanted cell responses), (**6**) nuclear localization, (**7**) nucleopenetration, (**8**) blockade of apoptosis (to prevent misinterpretation of CRT processes as damage demanding cell suicide), (**9**) arrest of DNA repair (to prevent misinterpretation of CRT processes as damage demanding repair), (**10**) blockade of inflammatory signals, (**11**) deactivation of transcription, (**12**) detachment of chromatin from inner nuclear wall lamins (cortex proteins), (**13**) extension of the "Proboscis" into the cell nucleus (image below, left), (**14**) rotation of the Proboscis, (**15**) deployment of the

---

[126] Freitas RA Jr. The ideal gene delivery vector: Chromallocytes, cell repair nanorobots for chromosome replacement therapy. J Evol Technol 2007;16:1-97; http://jetpress.org/v16/freitas.pdf.

[127] Freitas RA Jr. Nanomedicine, Volume I: Basic Capabilities. Landes Bioscience, Georgetown, TX, 1999, Section 9.4.4.1, "Nanorobot Diapedesis"; http://www.nanomedicine.com/NMI/9.4.4.1.htm.

[128] Freitas RA Jr. Nanomedicine, Volume I: Basic Capabilities. Landes Bioscience, Georgetown, TX, 1999, Section 9.4.4, "Histonatation"; http://www.nanomedicine.com/NMI/9.4.4.htm.

[129] Freitas RA Jr. Nanomedicine, Volume I: Basic Capabilities. Landes Bioscience, Georgetown, TX, 1999, Section 9.4.5, "Cytopenetration"; http://www.nanomedicine.com/NMI/9.4.5.htm.

[130] Freitas RA Jr. The ideal gene delivery vector: Chromallocytes, cell repair nanorobots for chromosome replacement therapy. J Evol Technol 2007;16:1-97; http://jetpress.org/v16/freitas.pdf.

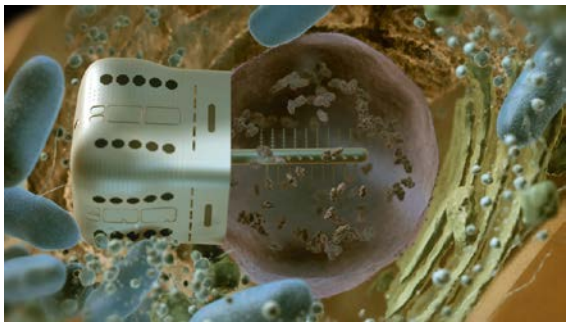

chromosomal collection funnel, (**16**) digestion of stray chromatin, (**17**) dispensation of new chromatin, (**18**) decondensation of the new chromatin, (**19**) re-anchoring of the dispensed chromatin to inner nuclear wall lamins, (**20**) reactivation of transcription, (**21**) reactivation of DNA repair and other DNA-related maintenance and usage processes, (**22**) nuclear emigration, (**23**) cellular emigration, (**24**) ECM emigration, (**25**) return to original point of entry into the body, and (**26**) removal from the body. Treatment of an entire large human organ such as a liver, involving simultaneous CRT on all 250 billion hepatic tissue cells, might require the localized infusion of a ~1 terabot (10^{12} devices) or ~69 cm^3 chromallocyte dose in a 1-liter (7% v/v nanorobots) saline suspension during a ~7 hour course of therapy. This nanodevice population draws 100-200 watts which lies within estimated nanorobot thermogenic limits consistent with maintenance of constant human body temperature.[131]

Replacement chromosome sets would be manufactured[132] in a desktop *ex vivo* chromosome sequencing and manufacturing facility (conceptual image, right; Section D.1.2),[133] then loaded into the nanorobots for delivery to specific targeted cells during CRT. The new DNA is manufactured to incorporate proper methylation for the target cell type and other post-translational modifications constituting the "histone code" used by the cell to encode various chromatin conformations and gene expression states.[134]

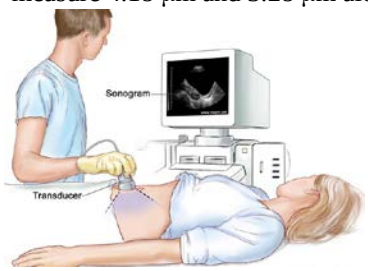

A single fully-loaded lozenge-shaped 69 μm^3 chromallocyte can measure 4.18 μm and 3.28 μm along cross-sectional diameters and 5.05 μm in length, typically consuming 50-200 pW of power in normal operation and a maximum of 1000 pW in bursts during outmessaging, the most energy-intensive task. Onboard power can be provided acoustically from the outside in an operating-table scenario (image, left) in which the patient is well-coupled to a medically-safe 1000 W/m^2 0.5 MHz ultrasound transverse-plane-wave transmitter throughout the procedure. The American Institute of Ultrasound in Medicine (AIUM) deems 10,000-sec exposures to 1000 W/m^2 ultrasound to be safe.[135]

---

[131] Freitas RA Jr. Nanomedicine, Volume I: Basic Capabilities. Landes Bioscience, Georgetown, TX, 1999, Section 6.5.2, "Thermogenic Limits *in vivo*"; http://www.nanomedicine.com/NMI/6.5.2.htm. Freitas RA Jr. The ideal gene delivery vector: Chromallocytes, cell repair nanorobots for chromosome replacement therapy. J Evol Technol 2007;16:1-97, Section 3.6; http://jetpress.org/v16/freitas.pdf.

[132] Strickland E. DNA manufacturing enters the age of mass production. IEEE Spectrum, 23 Dec 2015; http://spectrum.ieee.org/biomedical/devices/dna-manufacturing-enters-the-age-of-mass-production.

[133] Freitas RA Jr. The ideal gene delivery vector: Chromallocytes, cell repair nanorobots for chromosome replacement therapy. J Evol Technol 2007;16:1-97, Section 4; http://jetpress.org/v16/freitas.pdf.

[134] Villar-Garea A, Imhof A. The analysis of histone modifications. Biochim Biophys Acta. 2006 Dec;1764(12):1932-9; http://www.ncbi.nlm.nih.gov/pubmed/17015046.

[135] Freitas RA Jr. Nanomedicine, Volume I: Basic Capabilities. Landes Bioscience, Georgetown, TX, 1999, Section 6.4.1, "Acoustic Power Transmission"; http://www.nanomedicine.com/NMI/6.4.1.htm.

The chromallocyte design includes an extensible primary manipulator 4 μm long and 0.55 μm in diameter called the proboscis that is used to spool up chromatin strands via slow rotation when inserted into the cell nucleus (image sequence, below; images by E-spaces). After spooling (images A and B), a segmented funnel assembly is extended around the spooled bolus of DNA, fully enclosing and sequestering the old genetic material (image C). The new genetic material can then be discharged into the nucleus through the center of the proboscis by pistoning from internal storage vaults (image D), while the old chromatin that is sequestered inside the sealed leakproof funnel assembly is forced into the storage vaults as space is vacated by the new chromatin that is simultaneously being pumped out.

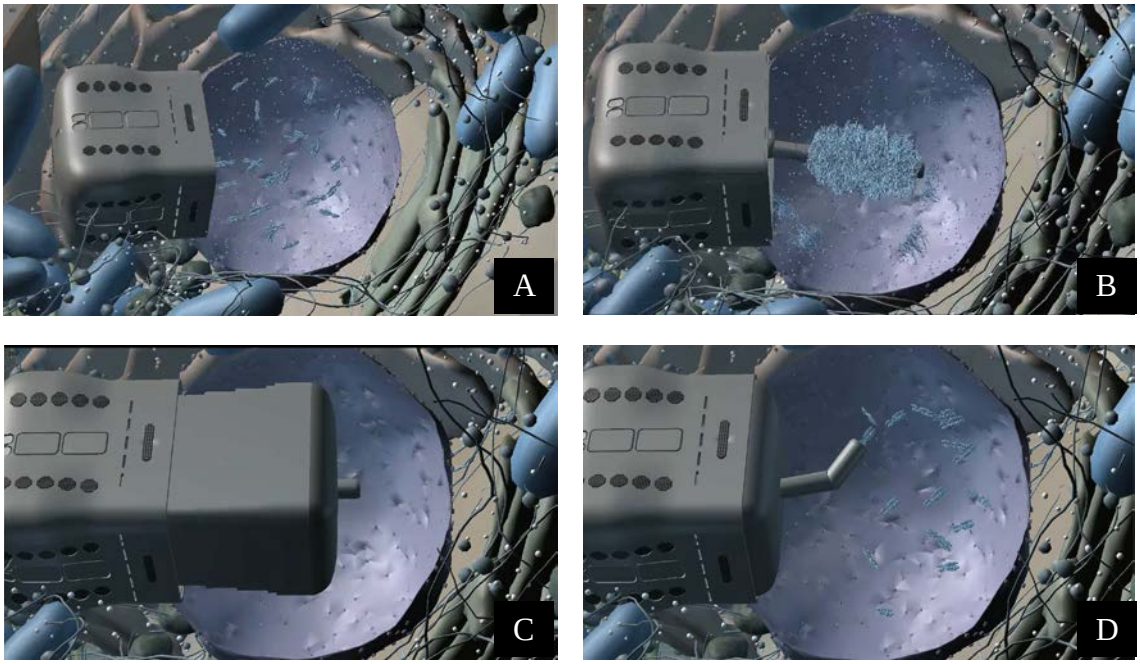

The chromallocyte can employ a mobility system similar to the microbivore grapple system, possibly including a solvation wave drive[136] to help ensure smooth passage through cell plasma membrane and nuclear membrane.

From the cryonics perspective, chromallocytes should be regarded as prototype cell repair machines. They can selectively insert, extract, or replace specific cellular components on a cell-by-cell basis. The devices could perform this function on any cell or tissue that remains in, or has been rewarmed to, a reliquidified state.

---

[136] Freitas RA Jr. Nanomedicine, Volume I: Basic Capabilities. Landes Bioscience, Georgetown, TX, 1999, Section 9.4.5.3, "Solvation Wave Drive"; http://www.nanomedicine.com/NMI/9.4.5.3.htm.

1.2.4 Vasculoid-Class Nanorobots

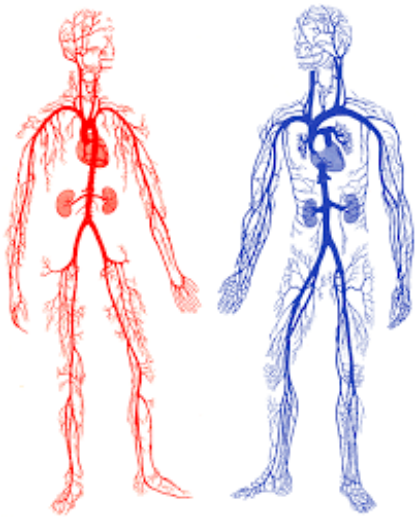

The vasculoid[137] is a single, complex, multisegmented medical nanorobotic system capable of duplicating all essential thermal and biochemical transport functions of the blood, including circulation of respiratory gases, glucose, hormones, cytokines, waste products, and cellular components. This nanorobotic system, a very aggressive and physiologically invasive macroscale nanomedical device comprised of ~500 trillion stored or active individual nanorobots, conforms to the shape of existing blood vessels and serves as a complete replacement for natural blood. In simplest terms, the vasculoid is a watertight coating of nanomachinery distributed across the lumenal surface of the entire human vascular tree (image, right). It uses a ciliary array to transport important nutrients and biological cells to the tissues, containerized either in "tankers" (for molecules) or in "boxcars" (for cells).

The vasculoid appliance is described in greater detail in Section 4.6. It represents a class of medical nanorobotic systems that consist of multiple nanorobot types performing multiple complex medical tasks, often intended for long-term or permanent residence in the human body.

1.2.5 Advantages of Medical Nanorobots

Although biotechnology makes possible a greatly increased range and efficacy of treatment options compared to traditional approaches, with medical nanorobotics the range, efficacy, comfort and speed of possible medical treatments further expands enormously. Medical nanorobots will be essential whenever the damage to the human body is extremely subtle, highly selective (e.g., specific organ, tissue, or cell type), or time-critical (as in head traumas, burns, or fast-spreading diseases), or when the damage is very massive, overwhelming the body's natural defenses and repair mechanisms – pathological conditions from which it is often difficult or impossible to recover at all using current or easily foreseeable biotechnological techniques.

While it is true that many classes of conventional medical problems may be at least partially resolved using existing treatment alternatives,[138] it is also true that as the chosen medical technology becomes more precise, active, and controllable, the range of options broadens and the quality of the options improves. Thus the question is often not whether medical nanorobots are absolutely required to accomplish a given medical objective. In some cases, they are not – though of course there are some things that only biotechnology and nanotechnology can do, and some other things that only nanotechnology can do. Rather, the important question is which approach offers a superior outcome for a given medical problem, using any reasonable metric of treatment efficacy. For virtually every class of medical challenge, a mature

---

[137] Freitas RA Jr., Phoenix CJ. Vasculoid: A personal nanomedical appliance to replace human blood. J Evol Technol. 2002 Apr;11:1-139; http://www.jetpress.org/volume11/vasculoid.pdf.

[138] e.g., https://en.wikipedia.org/wiki/CRISPR#Applications.

medical nanorobotics technology offers a wider and more effective range of treatment options than any other solution. In the case of cryostasis revival, it would appear that only medical nanorobots will be sufficient to meet the challenge (Section 4.17).

A few of the most important advantages of medical nanorobotics over present-day and anticipated future biotechnology-based medical and surgical approaches include:[139]

1. **Speed of Treatment**. Doctors may be surprised by the incredible quickness of nanorobotic action when compared to methods relying on self-repair. Mechanical nanorobotic therapeutic systems should reach their targets up to ~1,000 times faster, all else equal, and treatments which require ~10^5 sec (~days) for biological systems to complete may require only ~10^2 sec (~minutes) using nanorobotic systems.[140]

2. **Control of Treatment**. Present-day biotechnological entities are not very programmable and cannot easily be switched on and off conditionally (while following complex multidecision trees) during task execution. Even assuming that a digital biocomputer[141] could be installed in, for example, a fibroblast, and that appropriate effector mechanisms could be attached, such a biorobotic system would necessarily have slower clock cycles,[142] less capacious memory per unit volume, and longer data access times, implying less diversity of action, poorer control, and less complex executable programs than would be available in diamondoid nanocomputer-controlled nanorobotic systems. The mechanical or electronic nanocomputer approach[143] emphasizes precise control of action,[144] including control of physical placement, timing, strength, structure, and interactions with other (especially biological) entities.

3. **Verification of Treatment**. Nanorobotic-enabled endoscopic nanosurgery[145] will include comprehensive sensory feedback enabling full VR telepresence permitting real-time surgery into cellular

---

[139] Freitas RA Jr. Nanomedicine, Volume I: Basic Capabilities. Landes Bioscience, Georgetown, TX, 1999, Section 1.3.3, "Biotechnology and Molecular Nanotechnology"; http://www.nanomedicine.com/NMI/1.3.3.htm.

[140] Freitas RA Jr. Microbivores: Artificial mechanical phagocytes using digest and discharge protocol. J Evol Technol 2005;14:1-52; http://www.jetpress.org/volume14/freitas.html.

[141] Freitas RA Jr. Nanomedicine, Volume I: Basic Capabilities. Landes Bioscience, Georgetown, TX, 1999, Section 10.2.3, "Biocomputers"; http://www.nanomedicine.com/NMI/10.2.3.htm. Guet CC, Elowitz MB, Hsing W. Combinatorial synthesis of genetic networks. Science. 2002 May 24;296(5572):1466-70; http://science.sciencemag.org/content/sci/296/5572/1466.full.pdf. Yokobayashi Y, Weiss R, Arnold FH. Directed evolution of a genetic circuit. Proc Natl Acad Sci U S A. 2002 Dec 24;99(26):16587-91; http://www.ncbi.nlm.nih.gov/pmc/articles/PMC139187/. Basu S, Mehreja R, Thiberge S, Chen MT, Weiss R. Spatiotemporal control of gene expression with pulse-generating networks. Proc Natl Acad Sci U S A. 2004 Apr 27;101(17):6355-60; http://www.ncbi.nlm.nih.gov/pmc/articles/PMC404049/. Basu S, Gerchman Y, Collins CH, Arnold FH, Weiss R. A synthetic multicellular system for programmed pattern formation. Nature. 2005 Apr 28;434(7037):1130-4; http://macpost.caltech.edu/groups/fha/publications/Basu_Nature2005.pdf.

[142] Basu S, Mehreja R, Thiberge S, Chen MT, Weiss R. Spatiotemporal control of gene expression with pulse-generating networks. Proc Natl Acad Sci U S A. 2004 Apr 27;101(17):6355-60; http://www.ncbi.nlm.nih.gov/pmc/articles/PMC404049/.

[143] Freitas RA Jr. Nanomedicine, Volume I: Basic Capabilities. Landes Bioscience, Georgetown, TX, 1999, Section 10.2, "Nanocomputers"; http://www.nanomedicine.com/NMI/10.2.htm.

[144] Freitas RA Jr. Computational tasks in medical nanorobotics. In: Eshaghian-Wilner MM (ed) Bio-inspired and Nano-scale Integrated Computing. Wiley, New York, 2009; http://www.nanomedicine.com/Papers/NanorobotControl2009.pdf.

[145] Freitas RA Jr. "Chapter 23. Comprehensive Nanorobotic Control of Human Morbidity and Aging," in Gregory M. Fahy, Michael D. West, L. Stephen Coles, and Steven B. Harris, eds, The Future of Aging: Pathways to Human Life Extension, Springer, New York, 2010, Section 6.3.5.3; http://www.nanomedicine.com/Papers/Aging.pdf.

and subcellular tissue volumes. Using a variety of communication modalities,[146] nanorobots will be able to report back to the attending physician, with digital precision and ~MHz bandwidth,[147] a summary of diagnostically- or therapeutically-relevant data describing exactly what was found prior to treatment, what was done during treatment, and what problems were encountered after treatment, in every cell or tissue that was visited and treated by the nanorobot. A comparable biological-based approach relying primarily upon chemical messaging must necessarily be slow with only limited signaling capacity and bandwidth.

4. **Minimal Side Effects**. Almost all drugs have significant side effects, such as conventional cancer chemotherapy which typically causes hair loss and vomiting, although computer-designed drugs can have higher specificity and fewer side effects than earlier drugs. Carefully tailored cancer vaccines under development starting in the late 1990s were expected unavoidably to affect some healthy cells. Even well-targeted drugs are distributed to unintended tissues and organs in low concentrations,[148] although some bacteria can target a few organs fairly reliably without being able to distinguish individual cells. By contrast, mechanical nanorobots may be targeted with virtually 100% accuracy to specific organs, tissues, or even individual cellular addresses within the human body.[149] Such nanorobots should have few if any side effects, and will remain safe even in large dosages because their actions can be digitally self-regulated using rigorous control protocols[150] that affirmatively prohibit device activation unless all necessary preconditions have been met and remain continuously satisfied. Almost three decades ago, Fahy[151] observed that these possibilities could transform "drugs" into "programmable machines with a range of sensory, decision-making, and effector capabilities [that] might avoid side effects and allergic reactions...attaining almost complete specificity of action....Designed smart pharmaceuticals might activate themselves only when, where, and if needed." Additionally, nanorobots may be programmed to harmlessly remove themselves from the site of action, or conveniently excrete themselves from the body, after a treatment is completed. By contrast, spent biorobotic elements containing ingested foreign materials may have more limited post-treatment mobility, thus lingering at the worksite causing inflammation when naturally degraded *in situ* or removed. (It might be possible to design artificial eukaryotic biorobots having an apoptotic pathway[152] that could be activated to permit clean and natural self-destruction, but any indigestible foreign material that had been endocytosed by the biorobot could still cause inflammation in surrounding tissues when released).

5. **Faster and More Precise Diagnosis**. The analytic function of medical diagnosis requires rapid communication between the injected devices and the attending physician. If limited to chemical

---

[146] Freitas RA Jr. Nanomedicine, Volume I: Basic Capabilities. Landes Bioscience, Georgetown, TX, 1999, Chapter 7, "Communication"; http://www.nanomedicine.com/NMI/7.1.htm.

[147] Freitas RA Jr. Nanomedicine, Volume I: Basic Capabilities. Landes Bioscience, Georgetown, TX, 1999, Section 7.3, "Communication Networks"; http://www.nanomedicine.com/NMI/7.3.htm.

[148] Davis S. Chapter 16. Biomedical applications of particle engineering. In: Coombs RRH, Robinson DW (eds) Nanotechnology in Medicine and the Biosciences. Gordon & Breach Publishers, Netherlands, 1996, pp. 243-262.

[149] Freitas RA Jr. Nanomedicine, Volume I: Basic Capabilities. Landes Bioscience, Georgetown, TX, 1999, Chapter 8, "Navigation"; http://www.nanomedicine.com/NMI/8.1.htm. Freitas RA Jr. Pharmacytes: an ideal vehicle for targeted drug delivery. J Nanosci Nanotechnol 2006 Sep-Oct;6(9-10):2769-2775; http://www.nanomedicine.com/Papers/JNNPharm06.pdf.

[150] Freitas RA Jr. Computational tasks in medical nanorobotics. In: Eshaghian-Wilner MM (ed) Bio-inspired and Nano-scale Integrated Computing. Wiley, New York, 2009; http://www.nanomedicine.com/Papers/NanorobotControl2009.pdf.

[151] Fahy GM. Molecular nanotechnology and its possible pharmaceutical implications. In: Bezold C, Halperin JA, Eng JL (eds) 2020 Visions: Health Care Information Standards and Technologies. U.S. Pharmacopeial Convention Inc., Rockville MD, 1993, pp. 152-159.

[152] Freitas RA Jr. Nanomedicine, Volume I: Basic Capabilities. Landes Bioscience, Georgetown, TX, 1999, Section 10.4.1.1, "Apoptosis"; http://www.nanomedicine.com/NMI/10.4.1.1.htm.

messaging, biotechnology-based devices such as biorobots will require minutes or hours to complete each diagnostic loop. Nanomachines, with their more diverse set of input-output mechanisms, will be able to outmessage complete results (both aggregated and individual outliers) of *in vivo* reconnaissance or testing to the physician, literally in seconds.[153] Such nanomachines could also run more complex tests of greater variety in far less time. Nanomechanical nanoinstrumentation will make comprehensive rapid cell mapping and cell interaction analysis possible. For example, new instances of novel bacterial resistance could be assayed at the molecular level in real time, allowing new treatment agents to be quickly composed using an FDA-approved formulary, then manufactured and immediately deployed.

6. **More Sensitive Response Threshold for High-Speed Action**. Unlike natural systems, an entire population of nanorobotic devices could be triggered globally by just a single local detection of the target antigen or pathogen. The natural immune system takes $>10^5$ sec to become fully engaged after exposure to a systemic pathogen or other antigen-presenting intruder.[154] A biotechnologically enhanced immune system that could employ the fastest natural unit replication time ($\sim10^3$ sec for some bacteria) would thus require at least $\sim10^4$ sec for full deployment post-exposure. By contrast, an artificial nanorobotic immune system[155] could probably be fully engaged (though not finished) in at most two blood circulation times, or $\sim10^2$ sec.

7. **More Reliable Operation**. Individual engineered macrophages would almost certainly operate less reliably than individual mechanical nanorobots. For example, many pathogens, such as *Listeria monocytogenes* and *Trypanosoma cruzi*, are known to be able to escape from phagocytic vacuoles into the cytoplasm.[156] While biotech drugs or cell-manufactured proteins could be developed to prevent this (e.g., cold therapy drugs are entry-point blockers), nanorobotic trapping mechanisms could be more secure.[157] Proteins assembled by natural ribosomes typically incorporate one error per $\sim10^4$ amino acids placed;[158] current gene and protein synthesizing machines utilizing biotechnological processes have similar error rates. A molecular nanotechnology approach[159] should decrease these error rates by at least a millionfold (see also Section D.1.2.2). Nanomechanical systems will normally incorporate onboard sensors to determine if and when a particular task needs to be done, or when a task has been completed. Finally, and

---

[153] Freitas RA Jr. Nanomedicine, Volume I: Basic Capabilities. Landes Bioscience, Georgetown, TX, 1999, Chapter 7, "Communication"; http://www.nanomedicine.com/NMI/7.1.htm.

[154] The antigen-independent innate immune system reacts within minutes or hours of encountering an antigen, but adaptive immunity (which is antigen-dependent and antigen-specific) involves a lag time, typically 4-7 days, between antigen exposure and maximal response.[*] Hypersensitivity reactions can take 2-24 hours (Type II) or over 2 days (Type IV) to develop.[†]
[*] https://en.wikipedia.org/wiki/Adaptive_immune_system#Functions.
[†] Warrington R, Watson W, Kim HL, Antonetti FR. An introduction to immunology and immunopathology. Allergy Asthma Clin Immunol. 2011 Nov 10;7 Suppl 1(Suppl 1):S1; https://www.ncbi.nlm.nih.gov/pmc/articles/pmid/22165815/.

[155] Freitas RA Jr. Microbivores: Artificial mechanical phagocytes using digest and discharge protocol. J Evol Technol 2005;14:1-52; http://www.jetpress.org/volume14/freitas.html.

[156] Stenger S, Hanson DA, Teitelbaum R, Dewan P, Niazi KR, Froelich CJ, Ganz T, Thoma-Uszynski S, Melián A, Bogdan C, Porcelli SA, Bloom BR, Krensky AM, Modlin RL. An antimicrobial activity of cytolytic T cells mediated by granulysin. Science. 1998 Oct 2;282(5386):121-5; http://science.sciencemag.org/content/sci/282/5386/121.full.pdf.

[157] Freitas RA Jr. Nanomedicine, Volume I: Basic Capabilities. Landes Bioscience, Georgetown, TX, 1999, Section 10.4.2, "Mechanical Cytocide and Virucide"; http://www.nanomedicine.com/NMI/10.4.2.htm. Freitas RA Jr. Microbivores: Artificial mechanical phagocytes using digest and discharge protocol. J Evol Technol 2005;14:1-52; http://www.jetpress.org/volume14/freitas.html.

[158] https://en.wikipedia.org/wiki/Kinetic_proofreading.

[159] Drexler KE. Nanosystems: Molecular Machinery, Manufacturing, and Computation. John Wiley & Sons, New York, 1992, Section 8.3.4; https://www.amazon.com/dp/0471575186/.

perhaps most importantly, it is highly unlikely that natural microorganisms will be able to infiltrate rigid watertight diamondoid nanorobots or to co-opt their functions. By contrast, a biotech-based biorobot more readily could be diverted or defeated by microbes that would piggyback on its metabolism, interfere with its normal workings, or even incorporate the device wholesale into their own structures, causing the engineered biomachine to perform some new or different – and possibly pathological – function that was not originally intended. There are many examples of such co-option in natural biological systems, including the protozoan mixotrichs found in the termite gut that have assimilated bacteria into their bodies for use as motive engines,[160] and the nudibranch mollusks (marine snails without shells) that steal nematocysts (stinging cells) away from coelenterates such as jellyfish (i.e., a Portuguese man-of-war) and incorporate the stingers as defensive armaments in their own skins[161] – a process which Vogel[162] calls "stealing loaded guns from the army."

8. **Nonbiodegradable Treatment Agents**. Diagnostic and therapeutic agents constructed of biomaterials generally are biodegradable *in vivo*, although there is a major branch of pharmacology devoted to designing drugs that are moderately non-biodegradable – e.g., anti-sense DNA analogs with unusual backbone linkages and peptide nucleic acids (PNAs) that are difficult to break down. An engineered fibroblast may not stimulate an immune response when transplanted into a foreign host, but its biomolecules are subject to chemical attack *in vivo* by free radicals, acids, and enzymes. Even "mirror" biomolecules or "Doppelganger proteins" comprised exclusively of unnatural D-amino acids have a lifetime of only ~5 days inside the human body.[163] In contrast, suitably designed nanorobotic agents constructed of nonbiological materials need not be biodegradable. Nonbiological diamondoid materials are highly resistant to chemical breakdown or leukocytic degradation *in vivo*, and pathogenic biological entities cannot easily evolve useful attack strategies against these materials.[164] This means that medical nanorobots could be recovered intact from the patient and recycled, possibly reducing life-cycle energy consumption and treatment costs.

9. **Superior Materials**. Typical biological materials have tensile failure strengths in the 10^6-10^7 N/m^2 range, with the strongest biological materials such as wet compact bone having a failure strength of ~10^8 N/m^2, all of which compare poorly to ~10^9 N/m^2 for good steel, ~10^{10} N/m^2 for sapphire, and ~10^{11} N/m^2 for diamond and carbon fullerenes,[165] again showing a 10^3-10^5 fold strength advantage for mechanical systems that use nonbiological, and especially diamondoid, materials. Nonbiological materials can be much stiffer, permitting the application of higher forces with greater precision of movement, and

---

[160] Cleveland LR, Grimstone AV. The fine structure of the flagellate *Mixotrich paradoxa* and its associated microorganisms. Proc Roy Soc London B 1964;159:668-686; http://rspb.royalsocietypublishing.org/content/royprsb/159/977/668.full.pdf. Tamm SL. Flagellated ectosymbiotic bacteria propel a eukaryotic cell. J Cell Biol 1982 Sep;94(3):697-709; http://www.ncbi.nlm.nih.gov/pmc/articles/PMC2112208/.

[161] Thompson TE, Bennett I. *Physalia* nematocysts utilized by mollusks for defense. Science 1969 Dec 19;166(3912):1532-3; http://www.ncbi.nlm.nih.gov/pubmed/17742854.

[162] Vogel S. Cats' Paws and Catapults: Mechanical Worlds of Nature and People. W.W. Norton and Company, New York, 1998.

[163] Robson B. Doppelganger proteins as drug leads. Nature Biotechnol 1996 Jul;14(7):892-3; http://www.ncbi.nlm.nih.gov/pubmed/9631018. Robson B, Pseudoproteins: Non-protein protein-like machines. 6th Foresight Conference on Molecular Nanotechnology, Nov 1998; https://web.archive.org/web/20081121153232/http://foresight.org/Conference/MNT6/Abstracts/Robson/index.html.

[164] Freitas RA Jr. Nanomedicine, Volume I: Basic Capabilities. Landes Bioscience, Georgetown, TX, 1999, Section 9.3.5.3.6, "Chemical and Microbial Decomposition"; http://www.nanomedicine.com/NMI/9.3.5.3.6.htm.

[165] Freitas RA Jr. Nanomedicine, Volume I: Basic Capabilities. Landes Bioscience, Georgetown, TX, 1999, Table 9.3; http://www.nanomedicine.com/NMI/Tables/9.3.jpg.

they also tend to remain more stable over a larger range of relevant external conditions including temperature, pressure, salinity and pH. Proteins are heat sensitive in part because much of the functionality of their structure derives from the noncovalent bonds involved in folding, which are broken more easily at higher temperatures. In diamond, sapphire, and many other rigid materials, structural shape is covalently fixed and far more temperature-stable. Most proteins also tend to become dysfunctional at cryogenic temperatures, unlike diamond-based mechanical structures,[166] so diamondoid nanorobots could more easily be used to repair frozen cells and tissues. Biomaterials are not ruled out for all nanomechanical systems, but they represent only a small subset of the full range of materials that can be employed in nanorobots. Nanorobotic systems may take advantage of a wider variety of atom types and molecular structures in their design and construction, making possible novel functional forms that might be difficult to implement in a purely biological-based system (e.g., steam engines[167] or nuclear power[168]). As another example, an application requiring the most effective bulk thermal conduction possible should use diamond, the best conductor available, not some biomaterial having inferior thermal performance.

10. **No Replication.** Contrary to some assertions,[169] revival from cryopreservation does not require the use of self-replicating nanorobots, either inside a nanofactory (Section 1.3.2) that manufactures the robots or inside the body of the cryopatient during the revival process. As noted elsewhere,[170] "it cannot be emphasized too strongly that mechanical medical nanodevices will not self-replicate inside the human body, nor will they have any need for self-replication themselves. Machines that perform medical tasks are fundamentally different from machines that manufacture other machines….[M]echanical medical nanodevices need not be capable of replication. There is no requirement for replication *in vivo*; such replication would be needlessly dangerous, and adding this capability would reduce effectiveness in carrying out the primary medical task." Biological nanorobots or genetically-altered microbes intended to be used in cryonics revival, even if modified to be incapable of replication themselves (as are viral vectors employed in genetic therapies), nevertheless are composed of biological material, parts of which could in theory be co-opted by living microbial organisms and put to ill use as described in item (7) above.

---

[166] Freitas RA Jr. Nanomedicine, Volume I: Basic Capabilities. Landes Bioscience, Georgetown, TX, 1999, Section 10.5, "Temperature Effects on Medical Nanorobots"; http://www.nanomedicine.com/NMI/10.5.htm.

[167] Freitas RA Jr. Nanomedicine, Volume I: Basic Capabilities. Landes Bioscience, Georgetown, TX, 1999, Section 6.3.1, "Thermal Energy Conversion Processes"; http://www.nanomedicine.com/NMI/6.3.1.htm.

[168] Freitas RA Jr. Nanomedicine, Volume I: Basic Capabilities. Landes Bioscience, Georgetown, TX, 1999, Section 6.3.7, "Nuclear Energy Conversion Processes"; http://www.nanomedicine.com/NMI/6.3.7.htm.

[169] Rothblatt M. The Geoethics of Self-Replicating Biomedical Nanotechnology for Cryonic Revival. J Geoethical Nanotechnol. 2007 Qtr 3;2(3):11-20; https://www.terasemjournals.org/pdf/GN_vol3_issue2_whole.pdf.

[170] Freitas RA Jr. Nanomedicine, Volume I: Basic Capabilities. Landes Bioscience, Georgetown, TX, 1999, Section 2.4.2, "Molecular Assemblers"; http://www.nanomedicine.com/NMI/2.4.2.htm#p19. Freitas RA Jr. Nanomedicine, Volume I: Basic Capabilities. Landes Bioscience, Georgetown, TX, 1999, Section 1.3.3, "Biotechnology and Molecular Nanotechnology"; http://www.nanomedicine.com/NMI/1.3.3.htm#p24.

1.3 Atomically Precise Manufacturing of Medical Nanorobots

The nanofactory will be a high quality, extremely low cost, and very flexible manufacturing system in which products such as medical nanorobots are built atom by atom – an atomically precise manufacturing system employing controlled molecular assembly. Nanofactories will enable the creation of fundamentally novel products having the intricate complexity currently found only in biological systems, but operating with greater speed, power, reliability, predictability, and, most importantly, working entirely under human engineering control.

The principal inputs to a nanofactory may be simple hydrocarbon feedstock molecules such as natural gas or propane, along with water and small supplemental amounts of other simple molecules containing trace atoms of a few additional chemical elements needed to make useful products, such as oxygen, nitrogen, sulfur, or silicon. The nanofactory must also be provided with electrical power and a means for cooling the working unit.

The fastest and therefore preferred implementation pathway for this technology will employ scanning probe microscopy (Section F.1.1) and the methods of mechanosynthesis (Section 1.3.1) to build the first nanofactory (Section 1.3.2). Most of the material in Section 1.3 is updated from a previously published summary.[171]

1.3.1 Mechanosynthesis

At the most primitive level of our new manufacturing process, atomically precise objects will be built atom by atom using "mechanosynthesis." Mechanosynthesis, involving molecular positional fabrication, is the formation of covalent chemical bonds using precisely applied mechanical forces to build diamondoid[172] or other structures. Mechanosynthesis employs chemical reactions driven by the mechanically precise positioning of extremely reactive chemical species in an ultra-high vacuum environment. Mechanosynthesis may be automated via computer control, enabling programmable molecular positional fabrication.

Atomically precise fabrication involves holding feedstock atoms or molecules and a growing nanoscale workpiece in the proper relative positions and orientations so that when they touch they will chemically bond in the desired manner. In this process, a mechanosynthetic tool is brought up to the surface of a workpiece. One or more transfer atoms are added to, or removed from, the workpiece by the tool. Then the tool is withdrawn and recharged. This process is repeated until the workpiece (e.g., a growing

---

[171] Freitas RA Jr. The Alzheimer Protocols: A Nanorobotic Cure for Alzheimer's Disease and Related Neurodegenerative Conditions. IMM Report No. 48, June 2016, 433 pp; Section 4.1 "Atomically Precise Manufacturing using Nanofactories"; http://www.imm.org/Reports/rep048.pdf.

[172] Most diamondoids resemble ceramics. First and foremost, diamondoid materials include pure diamond, the crystalline allotrope of carbon. Among other exceptional properties, diamond has extreme hardness, high thermal conductivity, low frictional coefficient, chemical inertness, a wide electronic bandgap, and is the strongest and stiffest material presently known at ordinary pressures. Diamondoid materials also may include any stiff covalent solid that is similar to diamond in strength, chemical inertness, or other important material properties, and that possesses a dense three-dimensional network of bonds, e.g., carbon nanotubes, fullerenes, several strong covalent ceramics such as silicon carbide, silicon nitride, and boron nitride, and a few very stiff ionic ceramics such as sapphire (monocrystalline aluminum oxide) that can be bonded to purely covalent structures such as diamond.

nanopart) is completely fabricated to molecular precision, with each atom in exactly the right place. The sequence of three frames in the images below shows a "DCB6Ge" tooltip[173] depositing two carbon atoms on a diamond surface. The tooltip is attached to a much larger tool handle structure (not shown) which is attached, in turn, to the macroscale tip of a laboratory-scale scanning probe microscope (Section F.1.1). Note that the transfer atoms are under positional control at all times to prevent unwanted side reactions from occurring. Side reactions are also prevented by using proper reaction sequence design so that the interaction energetics help to avoid undesired pathological intermediate structures.

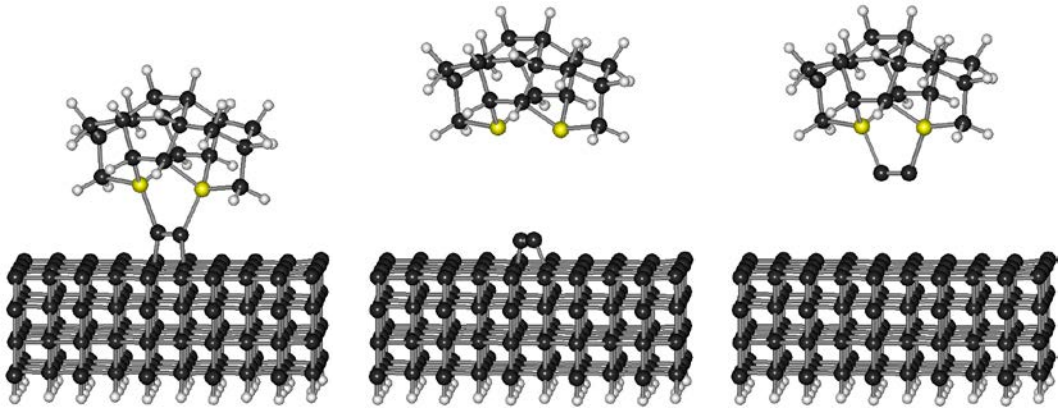

Mechanosynthesis has been extensively discussed in the theoretical literature since 1992,[174] was first demonstrated experimentally in 2003[175] and repeatedly in later years,[176] and the first U.S. patent on mechanosynthesis was issued to Freitas in 2010.[177]

---

[173] Merkle RC, Freitas RA Jr. Theoretical analysis of a carbon-carbon dimer placement tool for diamond mechanosynthesis. J Nanosci Nanotechnol. 2003 Aug;3(4):319-24; http://citeseerx.ist.psu.edu/viewdoc/download?doi=10.1.1.162.2289&rep=rep1&type=pdf.

[174] Drexler KE. Nanosystems: Molecular Machinery, Manufacturing, and Computation, John Wiley & Sons, New York, 1992; https://www.amazon.com/dp/0471575186/. Freitas RA Jr., Merkle RC. A minimal toolset for positional diamond mechanosynthesis. J Comput Theor Nanosci. 2008;5:760-861; http://www.molecularassembler.com/Papers/MinToolset.pdf.

[175] Oyabu N, Custance O, Yi I, Sugawara Y, Morita S. Mechanical vertical manipulation of selected single atoms by soft nanoindentation using near contact atomic force microscopy. Phys Rev Lett. 2003 May 2;90(17):176102; https://link.aps.org/pdf/10.1103/PhysRevLett.90.176102.

[176] Oyabu N, Custance O, Abe M, Moritabe S. Mechanical vertical manipulation of single atoms on the Ge(111)-c(2x8) surface by noncontact atomic force microscopy. Abstracts of Seventh International Conference on Non-Contact Atomic Force Microscopy, Seattle, Washington, USA, 12-15 Sep 2004, p. 34; http://www.engr.washington.edu/epp/afm/abstracts/15Oyabu2.pdf. Sugimoto Y, Pou P, Custance O, Jelinek P, Abe M, Perez R, Morita S. Complex patterning by vertical interchange atom manipulation using atomic force microscopy. Science. 2008;322(5900):413-417; http://www.sciencemag.org/cgi/content/full/322/5900/413. Xie Y, Ma L, Zhang P, Cai X, Zhang W, Gan F, Ning XJ, Zhuang J. Reversible atomic modification of nanostructures on surfaces using direction-depended tip-surface interaction with a trimer-apex tip. Appl Phys Lett. 2009 Aug 18;95:073105; https://aip.scitation.org/doi/abs/10.1063/1.3180814. Chen C, Zhang J, Dong G, Shao H, Ning BY, Zhao L, Ning XJ, Zhuang J. Site-selective substitutional doping with atomic precision on stepped Al(111) surface by single-atom manipulation. Nanoscale Res Lett. 2014 May 13;9(1):235; https://core.ac.uk/download/pdf/81056816.pdf. Kawai S, Foster AS, Canova FF, Onodera H, Kitamura S, Meyer E. Atom manipulation on an insulating surface at room temperature. Nat Commun. 2014 Jul 15;5:4403; http://viesti.physics.aalto.fi/~asf/publications/Nature%20Comm%20manip.pdf. Bamidele J, Lee SH, Kinoshita Y, Turanský R, Naitoh Y, Li YJ, Sugawara Y, Štich I, Kantorovich L. Vertical atomic manipulation with dynamic atomic-force microscopy without tip change via a multi-step mechanism. Nat Commun. 2014 Jul 31;5:4476; https://www.nature.com/articles/ncomms5476. Huff TR, Labidi H, Rashidi M, Koleini M, Achal R, Salomons MH, Wolkow

A scanning probe-based system would enable the fabrication of more precise, more easily rechargeable, and generally much improved mechanosynthetic tools. These more capable tools may include more stable handles of standardized dimensions, such as the rechargeable DCB6Ge dimer placement tool with the more reliable crossbar design (image below, left),[178] or tools with more complex handles incorporating moving components (image below, right).[179]

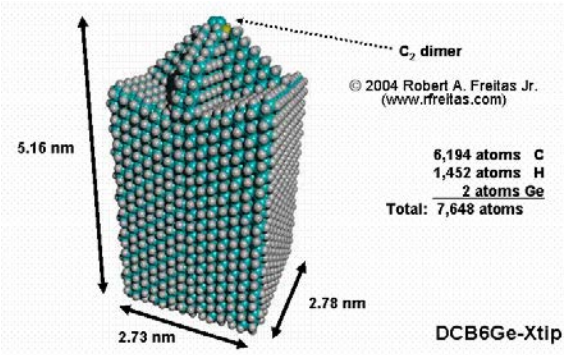

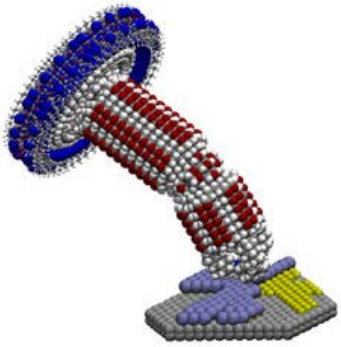

Later systems will incorporate more complex components such as the all-hydrocarbon diamond logic rod (image below, left) for possible use in mechanical nanocomputers, the hydrocarbon bearing (image below, center), the diamond universal joint (image below, right), and related mechanical devices. The end result of this iterative development process will be a mature set of efficient, positionally controlled mechanosynthetic tools that can reliably build molecularly precise diamondoid structures – including more mechanosynthetic tools.

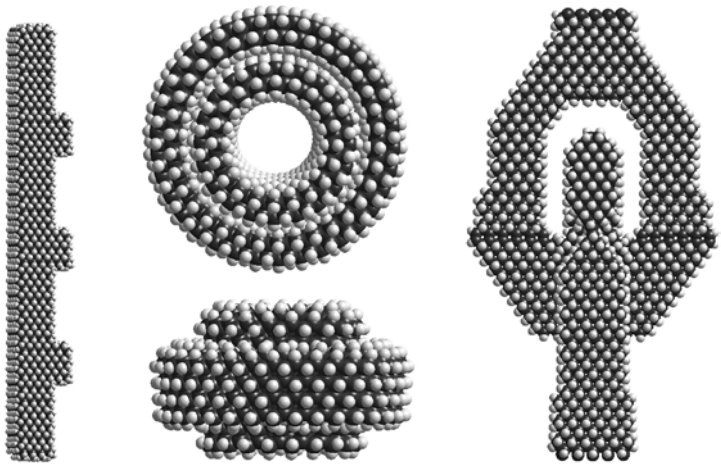

RA. Atomic White-Out: Enabling Atomic Circuitry through Mechanically Induced Bonding of Single Hydrogen Atoms to a Silicon Surface. ACS Nano. 2017 Sep 26;11(9):8636-8642; https://arxiv.org/pdf/1706.05287.

[177] Freitas RA Jr. Simple Tool for Positional Diamond Mechanosynthesis, and its Method of Manufacture. U.S. Patent 7,687,146, 30 Mar 2010; https://patentimages.storage.googleapis.com/a2/f5/54/d2558d5d72aa4a/US7687146.pdf.

[178] Peng J, Freitas RA Jr., Merkle RC, Von Ehr JR, Randall JN, Skidmore GD. Theoretical analysis of diamond mechanosynthesis. Part III. Positional C_2 deposition on diamond C(110) surface using Si/Ge/Sn-based dimer placement tools. J Comput Theor Nanosci. 2006 Feb;3(1):28-41; http://www.MolecularAssembler.com/Papers/JCTNPengFeb06.pdf.

[179] Image and design courtesy of Damian G. Allis.

Once mechanosynthetic tooltips are developed for a few additional element types, a still wider variety of nanomachines may be fabricated incorporating atoms other than hydrogen, carbon and germanium (e.g., silicon, oxygen, nitrogen, and sulfur). Examples of these more varied diamondoid nanomachines include the speed reduction gear (below, left), in which the train of gears reduces the speed from the high-speed one on the left to the half-speed one on the right, and the differential gear (below, center) that smoothly converts mechanical rotation in one direction into mechanical rotation in the opposite direction. The largest publically reported molecular machine model that has been simulated using molecular dynamics is the worm drive assembly (below, pair at right), consisting of 11 separate components and over 25,000 atoms. The two tubular worm gears progress in opposite directions, converting rotary into linear motion.[180]

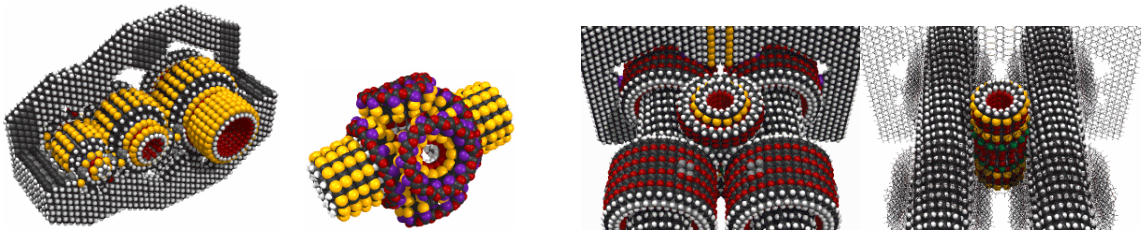

Using computer-automated tooltips performing positionally-controlled mechanosynthesis in lengthy programmed sequences of reaction steps, we will be able to fabricate simple diamondoid nanomechanical parts such as bearings, gears, struts, springs, logic rods and machine casings, to atomic precision. Early tools will rapidly progress from single tools manipulated by laboratory scanning-probe-like mechanisms, to more complex multitip tools and jigs which the simple tools could initially fabricate, one at a time. In a factory production line (image, right), individual mechanosynthetic tooltips can be affixed to rigid moving support structures and guided through repeated contact events with workpieces, recharging stations, and other similarly-affixed opposable tooltips. These "molecular mills" can then perform repetitive fabrication steps using simple, efficient mechanisms in the manner of a production line. Such production lines can, in principle, be operated at very high speeds – with positionally constrained mechanosynthetic encounters possibly occurring at up to megahertz frequencies.[181]

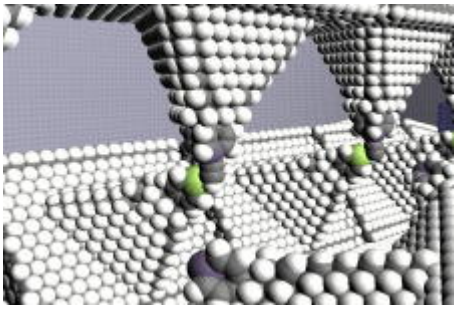

1.3.2 Nanofactories

The goal of molecular nanotechnology is to develop a manufacturing technology able to inexpensively manufacture most arrangements of atoms that can be specified in molecular detail – including complex arrangements involving millions or billions of atoms per product object. This will provide the ultimate manufacturing technology in terms of precision, flexibility, and low cost. To be practical, atomically precise manufacturing must also be able to assemble very large numbers of atomically identical product structures very quickly. Two central technical objectives thus form the core of our current strategy for

---

[180] All images courtesy of Nanorex; https://chem.beloit.edu/classes/nanotech/nanorex/index.html.

[181] Drexler KE. Nanosystems: Molecular Machinery, Manufacturing, and Computation, John Wiley & Sons, New York, 1992; https://www.amazon.com/dp/0471575186/.

atomically precise manufacturing: (1) programmable positional assembly including fabrication of diamondoid structures using molecular feedstock, as discussed above, and (2) massive parallelization of all fabrication and assembly processes, as briefly discussed below.

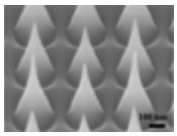

Conceptually, nanofactory systems capable of massively parallel fabrication[182] might employ, at the lowest level, large arrays of mechanosynthesis-enabled scanning probe tips all building similar diamondoid product structures in unison, superficially similar to the highly-uniform, well-aligned ultrasharp silicon nanotips (image, left) fabricated at a surface density of ~10^9 tips/cm^2 in 2012.[183]

Analogous approaches have appeared in microfabricated larger-scale systems. For example, simple mechanical ciliary arrays consisting of 10,000 independent microactuators on a 1 cm^2 chip have been made at the Cornell National Nanofabrication Laboratory for microscale parts transport applications, and similarly at IBM for mechanical data storage applications.[184] Active probe arrays of 10,000 independently-actuated microscope tips were developed by Mirkin's group at Northwestern University for dip-pen nanolithography (DPN) using DNA-based "ink".[185] Almost any desired 2D shape could be drawn with DPN using 10 tips in concert. A million-tip DPN array was later fabricated by the Micro Nano Technology Research Group at the University of Illinois,[186] and another microcantilever array manufactured by

---

[182] Freitas RA Jr., Merkle RC. Kinematic Self-Replicating Machines. Landes Bioscience, Georgetown, TX, 2004, Section 5.7 "Massively Parallel Molecular Manufacturing"; http://www.MolecularAssembler.com/KSRM/5.7.htm.

[183] Wu CC, Ou KL, Tseng CL. Fabrication and characterization of well-aligned and ultra-sharp silicon nanotip array. Nanoscale Res Lett. 2012 Feb 13;7(1):120; http://www.ncbi.nlm.nih.gov/pmc/articles/PMC3292956/.

[184] "1000 Tips for Ultrahigh-Density Data Storage," IBM News, Zurich Research Lab, 11 Oct 1999, http://www.zurich.ibm.com/news/99/millipede.html. IBM Research: Millipede, http://domino.research.ibm.com/Comm/bios.nsf/pages/millipede.html. Vettiger P, Cross G, Despont M, Drechsler U, Durig U, Gotsmann B, Haeberle W, Lantz M, Rothuizen H, Stutz R, Binnig G. The Millipede – nanotechnology entering data storage. Technical Report, IBM Zurich Research Lab; http://domino.research.ibm.com/Comm/bios.nsf/pages/millipede.html/$FILE/pv7201-preprint.pdf; also published in: Vettiger P, Cross G, Despont M, Drechsler U, Durig U, Gotsmann B, Haeberle W, Lantz M, Rothuizen H, Stutz R, Binnig G. The Millipede – nanotechnology entering data storage. IEEE Trans. Nanotechnol. 2002 Mar;1(1):39-55; http://citeseerx.ist.psu.edu/viewdoc/download?doi=10.1.1.159.7003&rep=rep1&type=pdf.

[185] Hong S, Mirkin CA. A nanoplotter with both parallel and serial writing capabilities. Science 2000 Jun 9;288:1808-11; http://www.nanotechnology.northwestern.edu/press/Science%20.Vol288.9june2000.pdf. Zhang M, Bullen D, Ryu KS, Liu C, Hong S, Chung S, Mirkin C. Passive and active probes for dip pen nanolithography. First IEEE Conference on Nanotechnology, 28-30 Oct 2001, Maui, HI; http://mass.micro.uiuc.edu/publications/papers/64.pdf. Bullen D, Zhang M, Liu C. Thermal-mechanical optimization of thermally actuated cantilever arrays. Smart Electronics, MEMS, and Nanotechnology Conference (4700), SPIE's 9th Annual International Symposium on Smart Structures and Materials, 17-21 Mar 2002, San Diego, CA; http://mass.micro.uiuc.edu/publications/papers/70.pdf. Zhang M, Bullen D, Chung SW, Hong S, Ryu KS, Fan Z, Mirkin CA, Liu C. A MEMS nanoplotter with high-density parallel dip-pen nanolithography probe arrays. Nanotechnology 2002 Apr;13:212-217; http://mass.micro.uiuc.edu/publications/papers/72.pdf. Wang X, Bullen D, Zou J, Ryu K, Liu C, Chung SW, Mirkin CA. Linear probe arrays for dip-pen nanolithography. Intl. Conf. on Micro & Nano Systems (ICMNS 2002), 11-14 Aug 2002, Kunming, China; http://mass.micro.uiuc.edu/publications/papers/74.pdf. Bullen D, Chung S, Wang X, Zou J, Liu C, Mirkin C. Development of parallel dip pen nanolithography probe arrays for high throughput nanolithography. (Invited) Symposium LL: Rapid Prototyping Technologies, Materials Research Society Fall Meeting, Boston, MA, Proceedings of the MRS, Vol. 758, 2-6 Dec 2002; http://mass.micro.uiuc.edu/publications/papers/84.pdf. Bullen D, Wang X, Zou J, Hong S, Chung S, Ryu K, Fan Z, Mirkin C, Liu C. Micromachined arrayed dip pen nanolithography probes for sub-100 nm direct chemistry patterning. Proc. 16th IEEE International Micro Electro Mechanical Systems Conference, MEMS 2003, Kyoto, Japan, 19-23 Jan 2003; http://mass.micro.uiuc.edu/publications/papers/86.pdf. Zou J, Bullen D, Wang X, Liu C, Mirkin CA. Conductivity-based contact sensing for probe arrays in dip-pen nanolithography. Appl Phys Lett. 2003 Jul 21;83(3):581-583; https://pdfs.semanticscholar.org/a3cd/c5436f893274a9a6ad81485ae8d54c0ac427.pdf.

[186] "MNTR Research Focus Slide Show: Passive Parallel DPN Array," 2006; http://mass.micro.uiuc.edu/research/current/nanolithography/2006-focus-intro/slide11.html

Protiveris Corp. had millions of interdigitated cantilevers on a single chip.[187] Martel's group at École Polytechnique Montreal investigated using fleets of independently mobile wireless instrumented microrobot manipulators called NanoWalkers to collectively form a nanofactory system potentially to be used for positional manufacturing operations.[188] Almost two decades ago, Zyvex Corp.[189] received a $25 million, five-year, National Institute of Standards and Technology (NIST) contract to develop prototype microscale assemblers using microelectromechanical systems.[190]

At the end of a carefully focused development program, analogous work will lead to the design and fabrication of numerous production lines comprising a nanofactory, both for diamondoid mechanosynthesis and for component assembly operations. Ultimately, atomically precise macroscale products – including components of additional nanofactories – will be manufactured in desktop-size nanofactories efficiently designed for this purpose. The nanofactory system will include a progression of fabrication and assembly lines at several different physical scales, as conceptually illustrated in the images below which show the assembly of nanoparts into larger components and product structures using mechanical manipulators at various size scales (e.g., roughly 0.01 µm, 0.1 µm, 1 µm, and 10 µm in the four images below) on interconnected production lines inside a diamondoid nanofactory.[191]

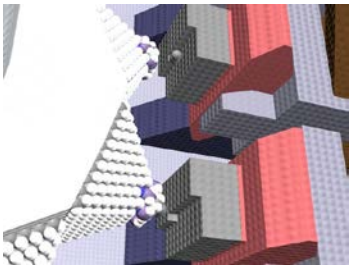
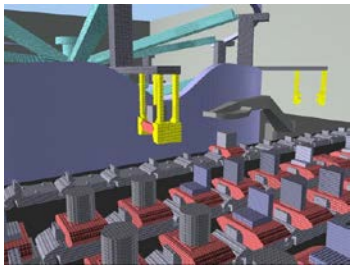
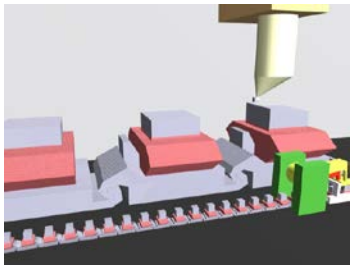
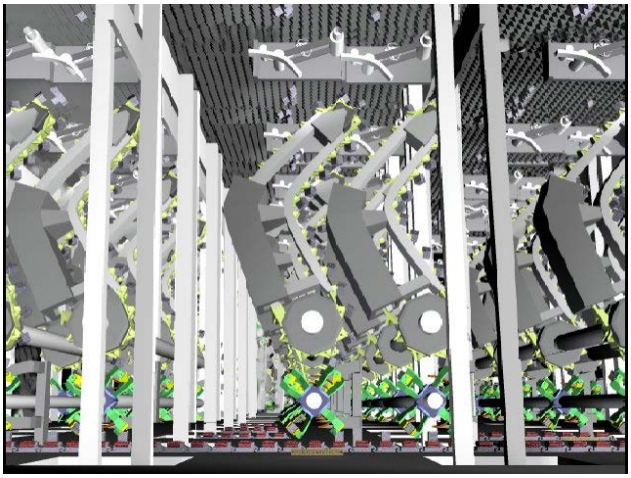

In one conceivable design, at the smallest scale molecular mills would manipulate individual molecules to fabricate successively larger submicron-scale building blocks. These would be passed to larger block assemblers that assemble still larger microblocks, which would themselves be passed to even larger product assemblers that put together the final product. The microblocks could be placed in a specific pattern and sequence following construction blueprints created using modern "Design for Assembly" and "Design for Manufacturability" (DFM) philosophies. As plane after plane is completed, the product slowly extrudes outward through the surface of

[187] "Microcantilever Arrays," Protiveris Corp., 2003; http://www.protiveris.com/cantilever_tech/microcantileverarrays.html

[188] Martel S, Hunter I. Nanofactories based on a fleet of scientific instruments configured as miniature autonomous robots. Proc. 3rd Intl Workshop on Microfactories; 16-18 Sep 2002; Minneapolis MN, pp. 97-100.

[189] http://www.zyvexlabs.com.

[190] Freitas RA Jr., Merkle RC. Kinematic Self-Replicating Machines. Landes Bioscience, Georgetown, TX, 2004, Section 4.20 "Zyvex Microscale Assemblers"; http://www.MolecularAssembler.com/KSRM/4.20.htm.

[191] https://web.archive.org/web/20110716171312/http://www.lizardfire.com/html_nano/themovies.html.

the nanofactory output platform. Of course, these images represent idealized conceptualizations of just one possible nanofactory architecture. Many other architectural approaches for nanofactories are readily conceived.[192]

As shown in the conceptual image of the desktop nanofactory below,[193] the finished product in this example is a billion-CPU laptop supercomputer,[194] built to molecular precision all the way down to its constituent atoms. The laptop supercomputer product is emerging from the output port at the top of the nanofactory at the end of a production cycle.

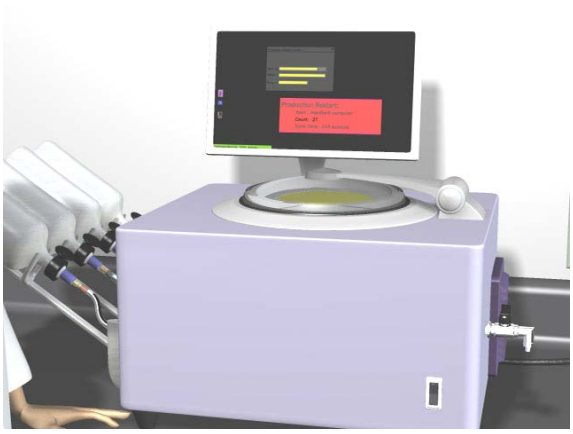

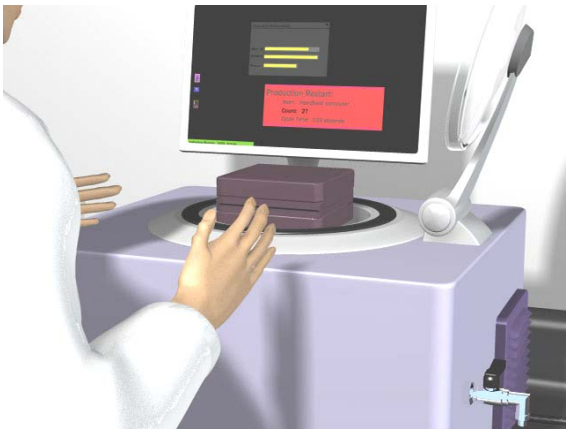

Rather than a laptop supercomputer, the nanofactory can be used to build medical nanorobots of modular design. The nanofactory for nanorobots would likely be a specialized type of limited-use nanofactory optimized for the fabrication and assembly of a small number of nanorobot modules that could be snapped together to make entire nanorobots at a ~1 kg/hour initial production rate.[195] The medical nanorobot factory might look something like the machine pictured above, except that a sterile container of medical nanorobots might be emerging from the output at the top of the device instead of a folded laptop supercomputer.

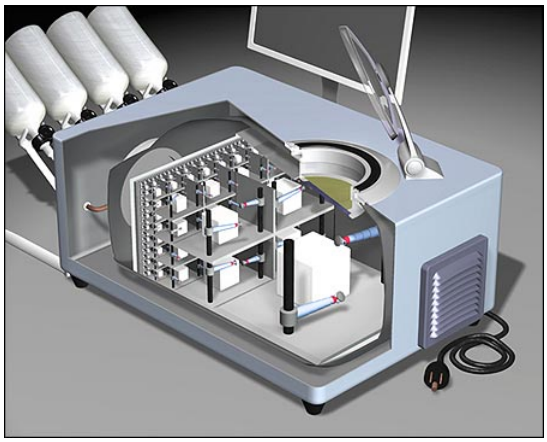

The end result of a dedicated nanofactory development program will be the creation of extremely clean, efficient, and inexpensive atomically precise manufacturing systems capable of producing macroscale quantities of atomically precise products. Nanofactories will make possible the manufacture of covalently-bonded products (e.g. nanomachines, including medical nanorobots; Section 1.2) having the intricate complexity and reliability of biological

---

[192] Freitas RA Jr., Merkle RC. Kinematic Self-Replicating Machines, Landes Bioscience, Georgetown, TX, 2004; Section 4; http://www.molecularassembler.com/KSRM/4.htm.

[193] https://web.archive.org/web/20110716171312/http://www.lizardfire.com/html_nano/themovies.html.

[194] Merkle RC, Freitas RA Jr., Hogg T, Moore TE, Moses MS, Ryley J. Molecular mechanical computing systems. IMM Report No. 46, 29 March 2016; http://www.imm.org/Reports/rep046.pdf.

[195] Drexler KE. Nanosystems: Molecular Machinery, Manufacturing, and Computation. John Wiley & Sons, New York, 1992, Section 14.4.3; https://www.amazon.com/dp/0471575186/.

systems combined with the greater speed, strength, power, and predictability of engineered mechanical systems.

After a call to action by Merkle and Freitas for cryonicists to support the development of molecular nanotechnology as a means to enable revivals,[196] the Alcor Scientific Advisory Board (SAB) met in Melbourne FL in Dec 2008[197] and issued the following formal recommendation, which was later officially endorsed by the Alcor Board of Directors:

Endorsement of Molecular Nanotechnology Research and Development

The development of molecular nanotechnology will speed solutions to the most difficult problems of medicine, including aging and reversible suspended animation. Molecular nanotechnology is the most compelling approach ever put forward for comprehensive repair of cryopreservation injury with maximum retention of original biological information. Support for immediate development of molecular nanotechnology by cryonicists and life extensionists could compress the historical timeline of this technology, bringing benefits decades sooner than otherwise.

1.4 Will Revivals Occur?

How do we know that efforts will be made to revive cryopatients in the future when this becomes technically feasible? There are at least three good reasons.

First of all, the charter of the Alcor Patient Care Trust[198] requires the organization to support the development of revival technologies, and to "build capital to eventually fund revival and reintegration" when the time is right. Also, an explicit part of Alcor's mission[199] is the "[f]uture restoration of good health and reintegration into society for all patients." Alcor Life Extension Foundation[200] is the leading cryonics service provider in the world. Other cryonics organizations have similar charters.[201]

Secondly, support from the broader society in this endeavor seems assured because cryopatients will almost certainly be regarded as priceless historical artifacts. Intact artifacts from the past are rare – especially

---

[196] Merkle RC, Freitas RA Jr. The Importance of MNT to the Cryonics Community. Cryonics 2008 Qtr 4;29(4);4-5; https://www.alcor.org/docs/cryonics-magazine-2008-04.pdf.

[197] Merkle RC. Alcor Scientific Advisory Board Meeting. Cryonics 2008 Qtr 4;29(4);4-5; https://www.alcor.org/docs/cryonics-magazine-2008-04.pdf.

[198] https://www.alcor.org/library/the-alcor-patient-care-trusts/.
[199] https://www.alcor.org/about/.
[200] https://www.alcor.org/.

[201] For example, **Cryonics Institute**, the other major U.S. cryonics service provider (https://www.cryonics.org/ci-landing/), "recognize[s] the responsibility we have to not only maintain, but to eventually revive our patients when and if that becomes scientifically possible." A new European cryonics provider, **Tomorrow Biostasis** (https://tomorrowbiostasis.com) collaborates with the European Biostasis Foundation, for whom (https://ebf.foundation/research/): "Eventually, restoration of human organ viability is the main goal….While potentially still many years away, we will start scientifically exploring possible routes to reanimation on the basis of small animal organs."

living, sentient artifacts – and, as such, cryopatients will likely be revived no matter what the cost, out of curiosity and in the spirit of scientific research, even if cryonics never becomes a widespread practice in mainstream society.

Finally, in a future world of material abundance[202] and self-actualization,[203] distant relatives will be eager and able to pay for the pleasure of meeting an ancestor in person. Wrote one cryonics advocate[204] in 2012: "Would my wife and I pay $50K, right here, right now, to repair and regenerate, say, my great-great grandfather who neither of us had ever known outside of family stories, had he been a soul on ice for many decades? Hell yes, and we'd consider it a bargain at the price."

It is worth quoting Alcor's official answer to this question:[205]

> Who will revive the patients?
>
> The short answer is "Alcor will revive them."
>
> The third item in Alcor's mission statement[206] is: "Eventually restore to health and reintegrate into society all patients in Alcor's care."
>
> Reviving the patients is also required by Alcor's contracts with members:[207] "When, in Alcor's best good faith judgement, it is determined that attempting revival is in the best interests of the Member in cryopreservation, Alcor shall attempt to revive and rehabilitate the Member."
>
> Reviving the patients is also a duty of the Alcor Patient Care Trust:[208] "At such time as Alcor deems that repair and revival of the Patients is feasible, the Trust shall expend whatever amounts of money are necessary to revive the Patients and reintroduce them to society, as long as on-going care of the Patients remaining in biostasis is not endangered. It is the intent of the Trust that such repair and revival proceed in such manner that ongoing Trust earnings reasonably can be predicted to provide for the eventual repair and revival of all Patients."
>
> Financially, the Patient Care Trust should grow in real value over time – compound interest should eventually produce sufficient assets to cover the costs of revival. At the same time, as technology progresses the cost of reviving patients should decrease over time. Eventually, the increasing funds available in the PCT should be sufficient to pay the costs of reviving and reintegrating patients into society.
>
> Socially, Alcor is a community. Some members of this community are alive and healthy, while others have been cryopreserved. This community forms an interconnected network of friendships and close ties. At any point in time the healthy members of this network have friends, relatives and loved ones in cryopreservation and will seek to revive them. Once revived, those members will in turn have other friends in cryopreservation, and they will in turn seek to revive them.
>
> The plan is not for "them" to revive us. The plan is that we, the Alcor community, will revive ourselves.

---

[202] https://en.wikipedia.org/wiki/Post-scarcity_economy.
[203] https://en.wikipedia.org/wiki/Self-actualization.
[204] https://www.overcomingbias.com/2012/01/brin-says-cryonics-selfish.html#comment-518228633.
[205] https://www.alcor.org/library/faq-general-questions/#whowillrevive.
[206] https://www.alcor.org/library/alcor-statements-of-mission-privacy-and-other-policies/.
[207] https://www.alcor.org/docs/alcor-form-cryopreservation-agreement.pdf.
[208] https://www.alcor.org/library/alcor-patient-care-trust-agreement/.

1.5 Organization of this Book

The discussion in this book is organized as follows:

Chapter 1 – what is the scientific rationale for human cryopreservation (Section 1.1), what are medical nanorobots (Section 1.2) and how will we manufacture them (Section 1.3), and how do we know that cryonics revivals will be attempted (Section 1.4)?

Chapter 2 – what are the key capabilities of revival technologies that are needed to preserve personal identity during a revival (Section 2.1), and what technical methods for revival have been proposed in the past (Section 2.2)?

Chapter 3 – the sources of biochemical and structural damage to which a cryopreserved patient will be exposed prior to revival include pre-mortem somatic (Section 3.1), post-mortem ischemic (Section 3.2), perfusion (Section 3.3), freezing or vitrification (Section 3.4), cryogenic storage (Section 3.5), and rewarming (Section 3.6) damage.

Chapter 4 – Plan A: the cryopreserved patient can be revived using conventional cell repair if the damage is not too great and if a nondestructive scan with ≥100 nm resolution is sufficient to preserve personal identity.

Chapter 5 – Plan B: the cryopreserved patient can be revived using molecular reconstruction if there is a lot of damage and if molecular-scale scan resolution is required to preserve personal identity, resulting in a new replacement body in the case of a destructive molecular scan (Section 5.2) or a repaired original body in the case of a nondestructive molecular scan (Section 5.3).

Chapter 6 – "neuro" (head-only) cryopreservation patients can obtain a replacement body by growing (Section 6.1.1) or nanofabricating (Section 6.1.2) an acephalic autologous biological body, or by attaching the cephalon to a head caddy or biocompatible artificial body (Section 6.1.3) .

Chapter 7 – revival prospects from pathways to preservation other than the ideal cryopreservation – including straight-freeze (Section 7.1.1), intermediate temperature storage (Section 7.1.2), xenon clathrate cryopreservation (Section 7.1.3), persufflation (Section 7.1.4), chemical fixation (Section 7.1.5), suspended animation (Section 7.1.6), genetic cloning (Section 7.1.7), and whole-body backups (Section 7.1.8) – are briefly described, followed by a discussion of medically sufficient animal-based (Section 7.2.1) or WBE (Whole Brain Emulation)-based (Section 7.2.2) methods of validating proposed revival protocols, ending with a summary of future research opportunities for advancing the field of human cryopreservation revival technology (Section 7.3).

2. Personal Identity and Cryostasis Revival

The central purpose of this book is to describe how to revive a cryopreserved patient who has been stored at liquid nitrogen (LN2) or similar cryogenic temperatures for some period of time, preserving all essential structures relevant to the patient's original personal identity that have (a) survived the cryopreservation process or (b) can be accurately inferred from surviving structures. While the exact definition of "personal identity" is much debated in philosophical circles,[209] in the present context we are primarily concerned with preserving the biological and structural elements that embody long-term memory[210] and the personality of the individual. Medical revival after such preservation does not invoke philosophical issues beyond those of resuscitation from states of absent brain function that already occur in medicine today.

A brain can stop working without losing long-term memories which are encoded in durable physical and chemical changes:

> "We know that secondary memory does not depend on continued activity of the nervous system, because the brain can be totally inactivated by cooling, by general anesthesia, by hypoxia, by ischemia, or by any method, and yet secondary memories that have been previously stored are still retained when the brain becomes active once again. Therefore, secondary memory must result from some actual alterations of the synapses, either physical or chemical." [211]

This Chapter starts by examining the requirements for the recovery of personal identity during revival from cryopreservation (Section 2.1), including the concept of "information-theoretic death" (with complete loss of personal identity) in cryonics (Section 2.1.1), the structural basis for personal identity (Section 2.1.2), the degree to which the patient's original identity can be recovered (Section 2.1.3), the role neurotransmitter levels play in long-term memory and personal identity (Section 2.1.4), other sources of personal identity beyond the brain (Section 2.1.5), and recommendations for choosing the revival method that best suits the patient's needs and expectations (Section 2.1.6). Perry[212] offers a simple but useful general recommendation for ***future research***: we should "[f]ind out more about the physical basis of memory in the brain."

After establishing that recovery of personal identity is the primary goal of revival, we review all known prior technical proposals for cryostasis revival (Section 2.2) to provide a proper contextual background for a deeper dive into the specific challenges and required technologies in subsequent Chapters. Brief synopses of the many fictional descriptions of cryopreservation and revival published during 1846-2020 are included in Appendix B, listed in chronological order of their appearance.

---

[209] Olson ET. Personal Identity. In: Zalta EN, ed. The Stanford Encyclopedia of Philosophy, Fall 2019 Edition; https://plato.stanford.edu/archives/fall2019/entries/identity-personal/. Bridge SW. I've Gotta Be Me! (But who will you be after cryonics revival?) Cryonics 2019 Qtr 3;40(3):52-56; https://www.alcor.org/docs/cryonics-magazine-2019-03.pdf. See also http://www.evidencebasedcryonics.org/.

[210] Note that "we can acquire new memories and change our interests and tastes without compromising our personal identity – i.e., we still feel ourselves to be the 'same person'." Best B. The Duplicates Paradox. 1998 Jan; https://www.benbest.com/philo/doubles.html.

[211] Guyton AC. Textbook of Medical Physiology, 7th edition, W.B. Saunders Company, Philadelphia PA, 1986, p. 658; https://www.amazon.com/Textbook-medical-physiology-Arthur-Guyton/dp/0721612601.

[212] Perry RM. Cryonics and Public Skepticism: Meeting the Challenges to Our Credibility. Cryonics 2019 Qtr 4;40(4):24-37; https://www.alcor.org/docs/cryonics-magazine-2019-04.pdf.

2.1 Recovery of Personal Identity

The biological foundation of personal identity starts with the genome: [213] "The molecular foundation upon which personal identity is built is the genomes – the nuclear genome, which is comprised of genetic material from both parents – and the mitochondrial genome, which is inherited from the mother in the form of the mitochondria in the cytoplasm of the maternal oocyte. In particular, the instructions for constructing the individual that are present in the form of the nuclear DNA most powerfully contribute to the fundamental structural composition of the individual. Additional determinants of brain and body structure occur during fetal development as a result of influence from the maternal biochemical environment; maternal circulating nutrient and hormone levels, harmful or beneficial maternal transmission of chemicals from the environment, and so on. Similarly, there are biophysical influences from the environment during the growth and development of the child – and continuing through life, which may shape personal identity. Once maturation is reached, such influences are likely to be less significant in shaping brain structure and biochemistry critical to memory and personality…. During and after the completion of [most] neurogenesis in the brain [avg ~2.9 years of age][214] the primary determinants of memory and personality will be experiential, and will take the form of long-term memories encoded in the molecular structure of the brain. It is the complex interaction of these 'recorded' experiences with the hardware encoding and processing them, that constitute personhood."

However, "only a limited number of biochemical and structural elements are candidates for encoding memory and personality, and it is now increasingly possible to image both this chemistry and structure. Similarly, without being able to succinctly define personal identity, we nevertheless find ourselves in the position of being able to determine when it is irretrievably lost by using the criterion of **information-theoretic death** [Section 2.1.1] as applied to the physical structures which encode and instantiate memory and personality."

2.1.1 Information-Theoretic Death

According to nanotechnology expert Ralph Merkle, originator of the concept of information-theoretic death:[215]

> "If we knew the coordinates of each and every atom in a person's brain then we would (at least in principle) be in a position to determine with absolute finality whether their memories and personality had been destroyed in the information theoretic sense, or whether they were preserved but could not, for some reason, be expressed. Considerations like this lead to the **information theoretic criterion of death**. A person is dead according to the information theoretic criterion if their memories, personality, hopes, dreams, etc. have been destroyed in the information theoretic sense. If the structures in the brain that encode memory and personality have been so disrupted that it is no longer possible in principle to recover them, then the person is dead. If they are

---

[213] Darwin M. Does Personal Identity Survive Cryopreservation? Chronosphere, 23 Feb 2011; http://chronopause.com/chronopause.com/index.php/2011/02/23/does-personal-identity-survive-cryopreservation/.

[214] Spalding KL, Bhardwaj RD, Buchholz BA, Druid H, Frisén J. Retrospective Birth Dating of Cells in Humans. Cell 2005 Jul 15;122(1):133-143; https://core.ac.uk/download/pdf/81197012.pdf.

[215] http://www.merkle.com/definitions/infodeath.html.

> sufficiently intact that inference of the state of memory and personality are feasible in principle, and therefore restoration to an appropriate functional state is likewise feasible in principle, then the person is not dead." [216]

Information-theoretic death can be understood as "the destruction of the human brain (or any cognitive structure capable of constituting a person) and the information within it to such an extent that recovery of the original person is theoretically impossible by any physical means. [The term] is intended to mean death that is absolutely irreversible by any technology, as distinct from clinical death and legal death, which denote limitations to contextually-available medical care rather than the true theoretical limits of survival….[A]s medical technology advances, conditions previously considered to be death, such as cardiac arrest, become reversible and are no longer considered to be death." [217]

A few years after inventing this concept in 1992, Merkle elaborated further[218] with a simple analogy:

> "It is essential [to] understand the gross difference between death by current clinical criteria and information-theoretic death. This is not a small difference of degree, nor just a small difference in viewpoint, nor a quibbling definitional issue that scholars can debate; but a major and fundamental difference. The difference between information-theoretic death and clinical death is as great as the difference between turning off a computer and dissolving that computer in acid. A computer that has been turned off, or even dropped out the window of a car at 90 miles per hour, is still recognizable. The parts, though broken or even shattered, are still there. While the short term memory in a computer is unlikely to survive such mistreatment, the information held on disk will survive. Even if the disk is bent or damaged, we could still read the information by examining the magnetization of the domains on the disk surface. It's not functional, but full recovery is possible."
>
> "If we dissolve the computer in acid, though, then all is lost."
>
> "So, too, with humans. Almost any small insult will cause clinical death. A bit of poison, a sharp object accidentally (or not so accidentally) thrust into a major artery, a failure of the central pump, a bit of tissue growing out of control: all can cause clinical death."
>
> "But information-theoretic death requires something much worse. Even after many minutes or hours of ischemia and even after freezing we can still recognize the cells, trace the paths of the axons, note where the synapses connect nerve cell to nerve cell – and this with our present rather primitive technology of light and electron microscopy (which is a far cry from what we will have in the future)."
>
> "For information-theoretic death to occur [during cryopreservation] we would have to damage the neuronal structures badly enough to cause loss of memory or personality. The structures that encode short term memory seem particularly sensitive: they are likely not preserved by cryonic suspension. The electrochemical activity of the brain is stopped when the temperature is lowered significantly (as in many types of surgery that are done after cooling the patient) so it is certainly

---

[216] Merkle RC. The Technical Feasibility of Cryonics. Med Hypotheses 1992 Sep;39(1):6-16; http://www.merkle.com/cryo/techFeas.html.

[217] Darwin M. Does Personal Identity Survive Cryopreservation? Chronosphere, 23 Feb 2011; http://chronopause.com/chronopause.com/index.php/2011/02/23/does-personal-identity-survive-cryopreservation/.

[218] Merkle RC. Cryonics, Cryptography, and Maximum-Likelihood Estimation. Cryonics 1995 Qtr 2;16(2):13-20; https://www.alcor.org/docs/cryonics-magazine-1995-02.pdf.

> stopped by freezing, with probable loss of short term memory. But human long term memory and the structural elements that encode our personality are likely to be more persistent, as they involve significant structural and morphological changes in the neurons and particularly in the synapses between neurons. Thus, we would like to know if the structures underlying human long term memory and personality are likely to be obliterated by freezing injury. The evidence available today suggests that the freezing injury and other injuries that are likely to occur in a cryonic suspension conducted under relatively favorable circumstances are unlikely to cause information-theoretic death."

De Wolf and Platt[219] note that "[t]he information-theoretic definition of death is not just a rationalization of the cryonics practice but reflects the mainstream view of physics and (bio) chemistry that the function and properties of a substance are defined by the specific organization of its molecules and extends this perspective to the concept of personhood. The criterion also arises in the context of diagnosing brain death or alternatives for cryonics such as chemical brain preservation."

2.1.2 Structural Basis for Long-Term Memory and Personality

Continuing with relevant observations[220] on the structural basis of personal identity: "Several mechanisms are currently understood to be in play in the formation of **long-term memory** (LTM). The earliest of these is **long-term potentiation** (LTP),[221] which is an enduring strengthening of signal transmission between two neurons that results from stimulating them synchronously. LTP is but one of many mechanisms that facilitate the ability of chemical synapses in the brain to change their strength, and thus exhibit what is known as synaptic plasticity. LTP appears to be the first step by which memories are encoded in the brain and it operates by modification of synaptic strength in response to

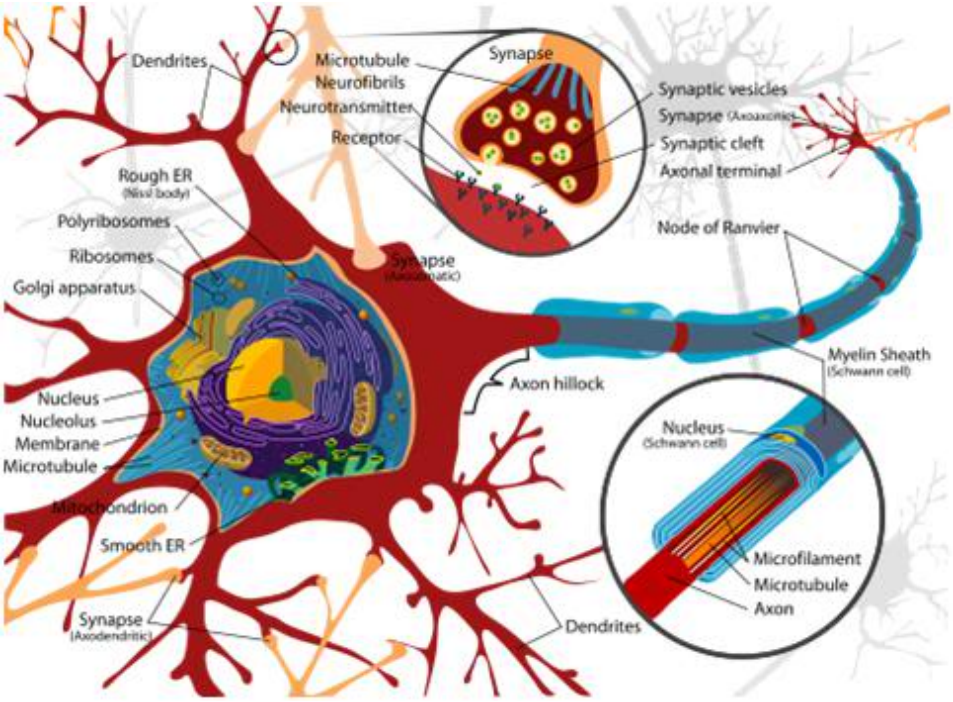

[219] De Wolf A, Platt C. Human Cryopreservation Procedures. Alcor Life Extension Foundation, 2020; https://www.alcor.org/library/human-cryopreservation-procedures/.

[220] Darwin M. Does Personal Identity Survive Cryopreservation? Chronosphere, 23 Feb 2011; http://chronopause.com/chronopause.com/index.php/2011/02/23/does-personal-identity-survive-cryopreservation/.

[221] https://en.wikipedia.org/wiki/Long-term_potentiation.

artificial stimulation (simulated inter-neuronal signaling) via the delivery of carefully modulated electrical pulses, or naturally, as a result of multi-pass filtered and integrated somatosensory signaling, generated as a result of life experience.…The creation of indefinitely durable LTM is presumably an even more complex process, and involves not just the addition, subtraction, or modification of one type of synapse, but of many." The image above is a "[s]imple schematic of a neuron and its axon, dendrites and synapses. The dendritic arbors that grow out of the neuronal soma and from the axon generate hundreds of thousands of synapses (up to 1 million per neuron) that serve as the signal switching mechanisms allowing inter-cellular communication and encoding LTM."

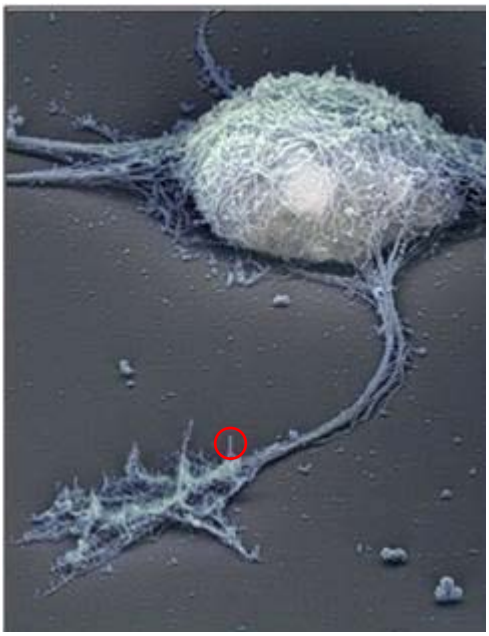

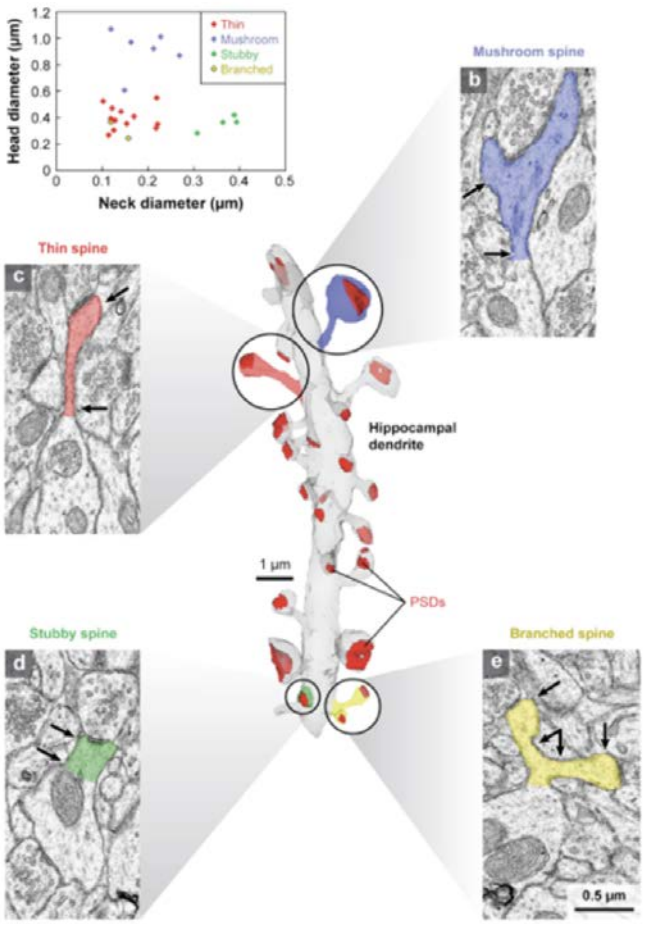

The image above[222] shows the cytoskeleton of a typical neuron from the hippocampus; a representative dendrite has been circled in red and is shown in greater detail in the image at right – a 10 µm long segment of a pyramidal cell dendrite with thin, stubby, and mushroom-shaped spines with spine synapses colored in red.[223]

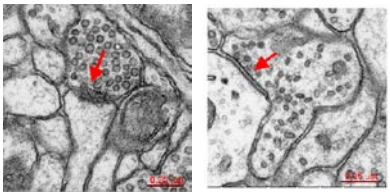

Gray's Type 1 synapses (far left) are found on dendritic spines and dendrite shafts, whereas Type 2 synapses (near left) occur primarily on dendrite shafts and neuronal cell bodies.[224]

---

[222] Stern S, Debre E, Stritt C, Berger J, Posern G, Knöll B. A nuclear actin function regulates neuronal motility by serum response factor-dependent gene transcription. J Neurosci. 2009 Apr 8;29(14):4512-8; https://www.jneurosci.org/content/29/14/4512.

[223] Bourne JN, Harris KM. Balancing structure and function at hippocampal dendritic spines. Annu Rev Neurosci. 2008;31:47-67; http://www.ncbi.nlm.nih.gov/pmc/articles/PMC2561948/.

[224] https://synapseweb.clm.utexas.edu/structure-chemical-synapses.

Darwin[225] provides an image (below, left) of "a three dimensional block of brain hippocampal tissue tomographically reconstructed from hundreds of slices of tissue 0.25 micron thick, using the same mathematical algorithms used in computerized tomography (CT) scanning employed in medical imaging (Section 4.1.2)….[A] single dendrite has been isolated from the tissue block to show the number and configuration of its synapses….At right is a hypothetical representation of the same neuron having undergone synaptic remodeling in response to the encoding of long-term memory, with new synaptic connections highlighted in yellow."

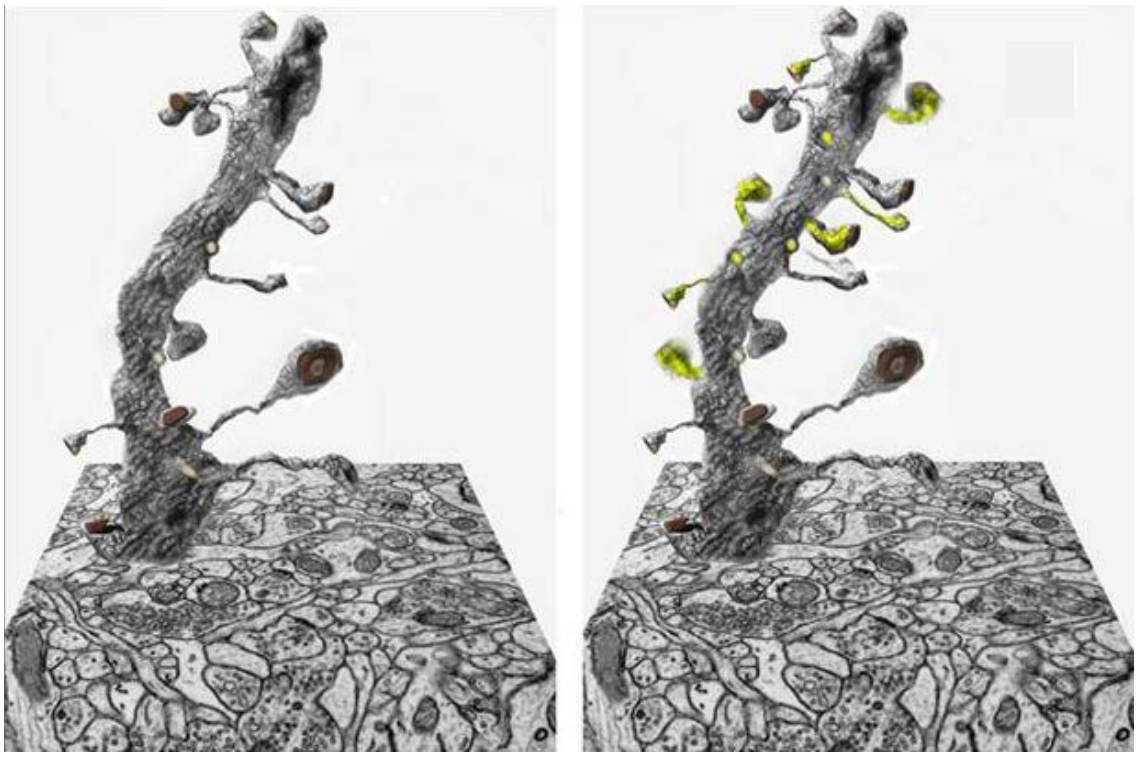

Dendritic spines[226] occur at a density of up to 5 spines per micron stretch of dendrite, with the smallest spine necks ≥100 nm in diameter; spines can rapidly change their volumes or shapes in response to stimuli and learning. The extension of spines has been directly photographed in rat brains – the micrograph at right shows 2 new spines that were observed to grow ~2 µm in ~2 days of training.[227] Extremely fast growth rates (e.g., ~4 µm

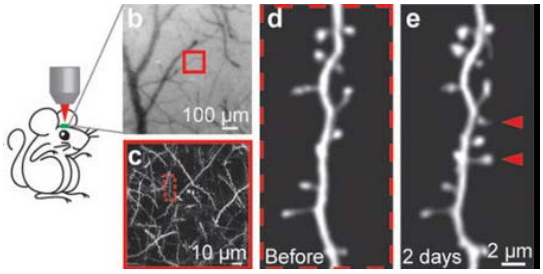

[225] Darwin M. Does Personal Identity Survive Cryopreservation? Chronosphere, 23 Feb 2011; http://chronopause.com/chronopause.com/index.php/2011/02/23/does-personal-identity-survive-cryopreservation/.

[226] https://en.wikipedia.org/wiki/Dendritic_spine.

[227] Yang G, Pan F, Gan WB. Stably maintained dendritic spines are associated with lifelong memories. Nature. 2009 Dec 17;462(7275):920-4; http://www.neuroscience.ubc.ca/CourseMat/Yang_et_al_2009.pdf.

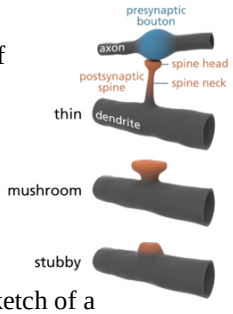

in ~10 minutes) have been observed in dendritic filopodia, and the maximum speed of one protrusion was reported as ~3 µm in just 30 sec.[228] Filopodia consist mostly of cytoskeletal elements, but they appear to be the first step in forming new dendritic spines (image, right) and new synaptic connections.

The tip of the spine has an electron-density region called the post-synaptic density (PSD)[229] that directly opposes the presynaptic active zone of the synapsing axon and comprises ~10% of the spine's membrane surface area; neurotransmitters released from the active zone bind receptors in the postsynaptic density of the spine.[230] The sketch of a "typical" excitatory synapse (below, left)[231] (see also Section 3.4.1(1)) shows "the presynaptic terminal where vesicles are released, and the postsynaptic element where glutamate receptors are located. The synapse is surrounded by astroglial processes containing glutamate transporters[232] (GLTs). Presynaptic vesicle fusion occurs at randomly selected locations, released glutamate (blue) diffuses in the cleft and binds to AMPARs (AMPA receptors)[233] (green) or GLTs (pink). AMPARs diffuse between the PSD, where they can attach to scaffolding molecules (orange) and the extrasynaptic regions, where they can undergo endocytosis (1) and exocytosis (2), maintaining the number of AMPARs at the post-synaptic terminal." The rightmost schematic at left shows the synapse as "two co-axial cylinders represent[ing] the pre- and postsynaptic terminal, forming a gap which represents the synaptic cleft. AMPARs (green) are distributed inside and outside the PSD. The trajectory of a glutamate molecule as illustrated by red, blue or green arrows corresponds to binding to AMPARs, GLTs, or diffusing away from the cleft (at 500 nm), respectively."[234] There have been rare observations of dendritic spines with segmented synapses having multiple active zones,[235] which

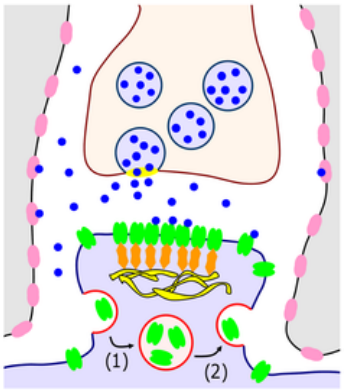

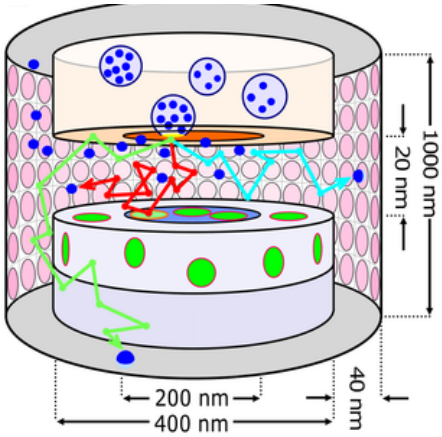

---

[228] Portera-Cailliau C, Pan DT, Yuste R. Activity-regulated dynamic behavior of early dendritic protrusions: evidence for different types of dendritic filopodia. J Neurosci. 2003 Aug 6;23(18):7129-42; https://www.jneurosci.org/content/jneuro/23/18/7129.full.pdf.

[229] https://en.wikipedia.org/wiki/Postsynaptic_density.
[230] https://en.wikipedia.org/wiki/Dendritic_spine.

[231] Freche D, Pannasch U, Rouach N, Holcman D. Synapse geometry and receptor dynamics modulate synaptic strength. PLoS One. 2011;6(10):e25122; https://www.ncbi.nlm.nih.gov/pmc/articles/PMC3184958/.

[232] https://en.wikipedia.org/wiki/Glutamate_transporter.
[233] https://en.wikipedia.org/wiki/AMPA_receptor.

[234] Freche D, Pannasch U, Rouach N, Holcman D. Synapse geometry and receptor dynamics modulate synaptic strength. PLoS One. 2011;6(10):e25122; https://www.ncbi.nlm.nih.gov/pmc/articles/PMC3184958/.

[235] Jones DG, Harris RJ. An analysis of contemporary morphological concepts of synaptic remodelling in the CNS: perforated synapses revisited. Rev Neurosci. 1995 Jul-Sep;6(3):177-219; https://pubmed.ncbi.nlm.nih.gov/8717635/.

appear to increase transiently after LTP induction in the hippocampus and then return to control levels within an hour.[236] These structures are uncommon, but "if segmented synapses are indeed lasting, and material to LTM, then the number of effective connections in the brain will have to be revised substantially upwards." [237]

Note that the physical dimensions of almost all significant dendritic features and synaptic structures reviewed above appear to be **≥100 nm** (≥0.1 μm) in size. Most of the smaller subcomponents composing these features and structures (and other brain structures[238]) are generic or can be inferred from the patient's DNA, or from neuronal connectivity patterns, from synapse type or size and shape[239] (indirectly evidencing relative synaptic strengths), from general knowledge of subcellular structures of specific types, and from other means. For example, the number of molecular AMPA receptors (AMPARs, ~14 nm in size),[240] whose concentration in the PSD increases as synaptic strength increases during learning, is somewhat correlated to synaptic type,[241] size,[242] and shape, allowing indirect inference of the receptor count from direct measurements of synapse size and shape (images, right[243] and below[244]). This is consistent with the recent finding that individual synapses may autonomously maintain synaptic strength at

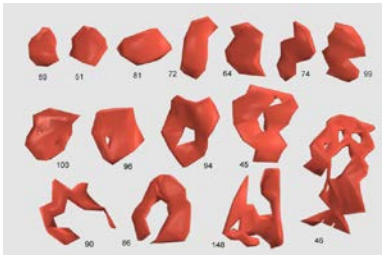

---

[236] Toni N, Buchs PA, Nikonenko I, Bron CR, Muller D. LTP promotes formation of multiple spine synapses between a single axon terminal and a dendrite. Nature. 1999 Nov 25;402(6760):421-5; http://synapseweb.clm.utexas.edu/sites/default/files/synapseweb/files/1999naturetonimullerltppromotesformationofmultspinesynapses.pdf.

[237] Darwin M. Does Personal Identity Survive Cryopreservation? Chronosphere, 23 Feb 2011; http://chronopause.com/chronopause.com/index.php/2011/02/23/does-personal-identity-survive-cryopreservation/.

[238] Mathiisen TM, Lehre KP, Danbolt NC, Ottersen OP. The perivascular astroglial sheath provides a complete covering of the brain microvessels: an electron microscopic 3D reconstruction. Glia. 2010 Jul;58(9):1094-1103; https://synapseweb.clm.utexas.edu/sites/default/files/synapseweb/files/2010gliamathiisenottersentheperivascastrosheath.pdf.

[239] Sorra KE, Harris KM. Occurrence and three-dimensional structure of multiple synapses between individual radiatum axons and their target pyramidal cells in hippocampal area CA1. J Neurosci. 1993 Sep;13(9):3736-48; https://www.jneurosci.org/content/jneuro/13/9/3736.full.pdf. Jones DG, Harris RJ. An analysis of contemporary morphological concepts of synaptic remodelling in the CNS: perforated synapses revisited. Rev Neurosci. 1995 Jul-Sep;6(3):177-219; https://pubmed.ncbi.nlm.nih.gov/8717635/.

[240] https://en.wikipedia.org/wiki/AMPA_receptor.

[241] Rubio ME, Fukazawa Y, Kamasawa N, Clarkson C, Molnár E, Shigemoto R. Target- and input-dependent organization of AMPA and NMDA receptors in synaptic connections of the cochlear nucleus. J Comp Neurol. 2014 Dec 15;522(18):4023-42; https://www.ncbi.nlm.nih.gov/pmc/articles/pmid/25041792/.

[242] Ganeshina O, Berry RW, Petralia RS, Nicholson DA, Geinisman Y. Synapses with a segmented, completely partitioned postsynaptic density express more AMPA receptors than other axospinous synaptic junctions. Neuroscience. 2004;125(3):615-23; https://pubmed.ncbi.nlm.nih.gov/15099675/. Fukazawa Y, Shigemoto R. Intra-synapse-type and inter-synapse-type relationships between synaptic size and AMPAR expression. Curr Opin Neurobiol. 2012 Jun;22(3):446-52; https://pubmed.ncbi.nlm.nih.gov/22325858/.

[243] Spacek J, Sorra Karin. Synapses of Stratum Radiatum. Figure 2: Variety of Synapse Morphologies. SynapseWeb, 2018 Mar 4; https://synapseweb.clm.utexas.edu/synapses-s-radiatum.

[244] Bailey CH, Kandel ER, Harris KM. Structural Components of Synaptic Plasticity and Memory Consolidation. Cold Spring Harb Perspect Biol. 2015 Jul 1;7(7):a021758; https://www.ncbi.nlm.nih.gov/pmc/articles/PMC4484970/.

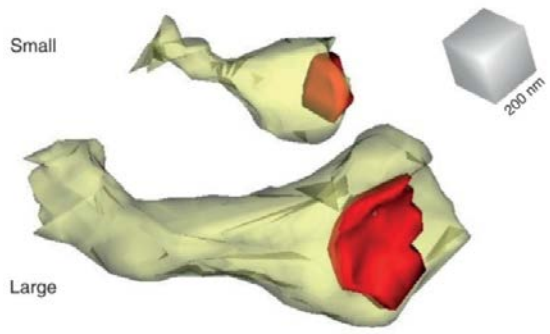

an intrinsic set point.[245] ***Future research*** should examine whether the exact number densities or spatial distributions of specific receptors (e.g., GLTs) or other molecular components within individual synapses are crucial to preserving long-term memory; and if so, whether this information can be adequately inferred solely from direct measurements of ≥100 nm features.

One seemingly relevant geometric factor could be the ~20 nm gap distance separating the presynaptic terminal from the postsynaptic density, called the **synaptic cleft**. But cleft height is not known to vary over time. Electron micrographs obtained with different tissue fixation methods suggest a relatively constant average distance between pre- and postsynaptic membranes.[246] The molecular basis of the relatively rigid cleft architecture derives from cadherin-type adhesion molecules[247] that provide transcellular structural scaffolding connecting pre- and postsynaptic membranes;[248] other factors also contribute to long-term synaptic stability.[249] While there is some computational evidence that cleft height might contribute to shaping the postsynaptic current over time,[250] there is as yet no evidence that the precise height of the cleft plays an important role in the storage of information in long-term memory,[251] nor that the height changes dramatically as memories accumulate. Indeed, one oft-cited computational study[252] found that there is an optimal cleft height driven by fundamental physiological factors to maximize synaptic strength. The same authors note that electron microscopy has been unable to definitively answer the question of whether cleft heights change "because the expected small range of change (few nanometers) is comparable with or less than the measurement error involved". If ***future research*** confirms that cleft height variations have no significant role in LTM, then in the absence of direct measurements of this sub-100-nm feature during revival-related scanning

---

[245] Levy JM, Chen X, Reese TS, Nicoll RA. Synaptic Consolidation Normalizes AMPAR Quantal Size following MAGUK Loss. Neuron. 2015 Aug 5;87(3):534-48; https://www.ncbi.nlm.nih.gov/pmc/articles/PMC4596923/.

[246] Peters A, Palay SL, Webster HDF. The Fine Structure of the Nervous System. Oxford University Press, New York, 1991. Zuber B, Nikonenko I, Klauser P, Muller D, Dubochet J. The mammalian central nervous synaptic cleft contains a high density of periodically organized complexes. Proc Natl Acad Sci U S A. 2005 Dec 27;102(52):19192-7; https://www.ncbi.nlm.nih.gov/pmc/articles/PMC1323199/.

[247] https://en.wikipedia.org/wiki/Cadherin.

[248] Tanaka H, Shan W, Phillips GR, Arndt K, Bozdagi O, Shapiro L, Huntley GW, Benson DL, Colman DR. Molecular modification of N-cadherin in response to synaptic activity. Neuron. 2000 Jan;25(1):93-107; https://core.ac.uk/download/pdf/82484472.pdf. Phillips GR, Huang JK, Wang Y, Tanaka H, Shapiro L, Zhang W, Shan WS, Arndt K, Frank M, Gordon RE, Gawinowicz MA, Zhao Y, Colman DR. The presynaptic particle web: ultrastructure, composition, dissolution, and reconstitution. Neuron. 2001 Oct 11;32(1):63-77; https://core.ac.uk/download/pdf/81973556.pdf.

[249] https://en.wikipedia.org/wiki/Synaptic_stabilization.

[250] Freche D, Pannasch U, Rouach N, Holcman D. Synapse geometry and receptor dynamics modulate synaptic strength. PLoS One. 2011;6(10):e25122; https://www.ncbi.nlm.nih.gov/pmc/articles/PMC3184958/.

[251] Ullah G. The role of transporters and synaptic cleft morphology in glutamate and GABA homeostasis and their effect on neuronal function. bioRxiv 2019 Jun 13; https://www.biorxiv.org/content/10.1101/670844v1.full.

[252] Savtchenko LP, Rusakov DA. The optimal height of the synaptic cleft. Proc Natl Acad Sci U S A. 2007 Feb 6;104(6):1823-8; https://www.ncbi.nlm.nih.gov/pmc/articles/PMC1783902/.

(Section 4.7) there will be no loss of LTM for the patient if the cleft is inferred to be the standard average height for that particular type of neuron and synapse.

Finally, ***future research*** must ask if there are any other <100 nm-scale or molecular-scale structures that might need to be precisely scanned and precisely repaired in order to recover personal identity, since the possible existence of such structures cannot yet be ruled out. Possibly relevant issues might include:

(1) Is it critical to know the exact positions of all the N-type calcium channels[253] that trigger release of neurotransmitters from vesicles in the presynaptic membrane, or is it only necessary to maintain the generic number density of ion channels with a standard spatial distribution,[254] allowing us to rely on the larger synaptic connectivity pattern and direct measurements of synapse size to carry the burden of preserving personality?

(2) Must we record and reproduce the original transcriptional state[255] of neurons and glial cells in order to ensure functionality of the revived neural tissues,[256] or will setting transcriptional state of neurons of a given type and location to generic default values suffice?

(3) Must we know the exact number and positions of all mechanotransductive cell adhesion molecules between neural cell membranes and the cytoskeleton intracellularly,[257] and between neural cell membranes and the ECM extracellularly,[258] through which outside mechanical forces can trigger cytochemical and cytomechanical responses in neurons?

---

[253] https://en.wikipedia.org/wiki/N-type_calcium_channel.

[254] Early studies* found that calcium channels located on the presynaptic face may have a preferred ~40 nm spacing (possibly from anchoring to a membrane-associated latticework of fixed mesh size). The absolute number of calcium channels in a synapse active zone in rats varies between 5-218 and may contribute to establishing synaptic strength in learning and memory,† but it remains undetermined if channel areal number density is constant (which would allow total channel number to be estimated from measurement of synaptic area alone).
* Haydon PG, Henderson E, Stanley EF. Localization of individual calcium channels at the release face of a presynaptic nerve terminal. Neuron. 1994 Dec;13(6):1275-80; https://lib.dr.iastate.edu/cgi/viewcontent.cgi?article=1022&context=zool_pubs.
† Sheng J, He L, Zheng H, Xue L, Luo F, Shin W, Sun T, Kuner T, Yue DT, Wu LG. Calcium-channel number critically influences synaptic strength and plasticity at the active zone. Nat Neurosci. 2012 Jun 10;15(7):998-1006; https://www.ncbi.nlm.nih.gov/pmc/articles/PMC4891200/.

[255] https://en.wikipedia.org/wiki/Transcription_(biology).

[256] One study of somatosensory neurons* found that neurogenesis produces cells in a transcriptionally unspecialized state, which then become restricted to specific subtypes as development proceeds. Learning and memory formation may be facilitated by transcriptional responses in the neuron,† but it is not yet clear whether particular transcriptional states are necessary to maintain existing memories that have already become embodied in synaptic physical structures. If necessary, mRNA transcripts can be removed from neurons under repair during molecular extraction (Section 4.10.1.5(V)), then decoded to determine neuronal transcriptional status.
* Sharma N, Flaherty K, Lezgiyeva K, Wagner DE, Klein AM, Ginty DD. The emergence of transcriptional identity in somatosensory neurons. Nature. 2020 Jan;577(7790):392-398; https://www.ncbi.nlm.nih.gov/pmc/articles/PMC7307422/.
† Abraham WC, Dragunow M, Tate WP. The role of immediate early genes in the stabilization of long-term potentiation. Mol Neurobiol. 1991;5(2-4):297-314; 45.79.91.117/Molecular%20Neurobiology/1991%20v.05/02-04%20%2861-433%29/297-314.pdf.

[257] Hemphill MA, Dauth S, Yu CJ, Dabiri BE, Parker KK. Traumatic brain injury and the neuronal microenvironment: a potential role for neuropathological mechanotransduction. Neuron. 2015 Mar 18;85(6):1177-92; https://core.ac.uk/download/pdf/82553770.pdf.

[258] Chighizola M, Dini T, Lenardi C, Milani P, Podestà A, Schulte C. Mechanotransduction in neuronal cell development and functioning. Biophys Rev. 2019 Oct;11(5):701-720; https://www.ncbi.nlm.nih.gov/pmc/articles/PMC6815321/.

(4) Is the exact arrangement of cytoskeletal components within a cell important enough to cell function such that if we don't scan and replicate it exactly, the revived person's personality or memory will not be precisely restored?

Neurobiologist Shawn Mikula[259] worries that we may need detailed neurochemical information in addition to complete knowledge of brain ultrastructure to fully infer neural function: "Certainly the existence of silent synapses,[260] gap junctions, more than 50 chemically-distinct neurotransmitters and myriad receptor subtypes with widely-varying post-synaptic responses would urge caution.[261] Gap junctions deserve special emphasis since they are prevalent in mammalian brains[262] and at least for *C. elegans*, form networks that are not correlated with synaptic networks.[263] [U]ltrastructural maps of whole-brain synaptic connectivity likely do not contain all requisite information for accurate whole-brain simulations but we will not know for certain what additional neurochemical information is needed until we are in possession of such connectional maps from mammalian whole-brains." These issues should be studied and resolved in ***future research***.

More generally, what is the extent of structural variation from the norm in neurons and larger neural tissues, and how do these variations affect personal identity (e.g., behavior, memories, etc.)? ***Future research*** should consider the effects of substituting structural norms for individual structures, especially in cases of damaged neurons or tissues where some original information has been lost.

2.1.3 How Much Personal Identity Can Be Recovered?

A more general concern is that even the tiniest error or omission in scanning or repairing a synaptic structure might result in some significant loss of memory, personality, or personal identity. However, this concern may be misinformed by our modern experience with digital computers. In computers, it is often possible that even a single flipped bit of data, if strategically located on a hard drive or in a software program, can produce disastrous consequences.

There is an argument that human long-term memory is vastly more robust than this. In 1986, Thomas Landauer estimated that the average rate at which humans accumulate information into long-term memory during the normal activities of life, such as reading text or exposure to visual images, approximates 1-2 bits/sec, asymptotically approaching a stable lifetime total (integrating memory gains with losses) of ~2 x

---

[259] Mikula S. Progress Towards Mammalian Whole-Brain Cellular Connectomics. Front Neuroanat. 2016 Jun 30;10:62; https://www.ncbi.nlm.nih.gov/pmc/articles/pmid/27445704/.

[260] Atwood HL, Wojtowicz JM. Silent synapses in neural plasticity: current evidence. Learn Mem. 1999 Nov-Dec;6(6):542-71; http://learnmem.cshlp.org/content/6/6/542.full.pdf.

[261] Bargmann CI, Marder E. From the connectome to brain function. Nat Methods. 2013 Jun;10(6):483-90; http://lab.rockefeller.edu/bargmann/assets/file/lab%20papers/2013_3_Cori_marder.pdf.

[262] Rozental R, Giaume C, Spray DC. Gap junctions in the nervous system. Brain Res Brain Res Rev. 2000 Apr;32(1):11-5; https://pubmed.ncbi.nlm.nih.gov/10928802/.

[263] Varshney LR, Chen BL, Paniagua E, Hall DH, Chklovskii DB. Structural properties of the *Caenorhabditis elegans* neuronal network. PLoS Comput Biol. 2011 Feb 3;7(2):e1001066; https://www.ncbi.nlm.nih.gov/pmc/articles/PMC3033362/.

10^9 bits for adults.[264] This figure should be compared to the best current estimates of ~86 x 10^9 neurons in the average human brain,[265] ~2 x 10^{14} synapses in the adult human neocortex,[266] and ~10^6 protein molecules per synapse.[267] While neurons and their synapses clearly perform many tasks unrelated to long-term memory storage, it would appear that up to ~43 neurons, ~100,000 synapses, and ~10^{11} protein molecules may be associated with each single bit of experienced, recallable, usable human memory. If long-term memory is truly this super-redundant, then it seems highly unlikely that the random loss of a single neuron, or the random corruption or misrepair of thousands of synapses or millions of proteins, could flip the associated single bit from "1" to "0" and destroy the tiniest piece of memory. This apparent robustness of the structures embodying long-term memory is consistent with the observation that human long-term memory persists over periods of many decades despite a turnover rate of ~0.7%/hour for synaptic proteins – a half-life of only 2-5 days.[268] Such turnover means that every few days, roughly 1 out of every 20 proteins in every synapse is replaced with a new protein incorporating at least one random peptide sequencing error[269] – yet memory and personal identity persist, in many cases over a lifetime. The extent of the robustness of long-term memory due to super-redundancy of neural data storage should be further explored in ***future research***.

A **lower bound** on the number of neurons that can be seriously damaged during cryopreservation or incorrectly repaired during revival without loss of personal identity is provided by the natural rate of neuron attrition. Early workers in the 1950s attempted the first assessment of the long-term rate of natural brain cell attrition.[270] Losses ranged from none at all to very many in various parts of the organ, but the brainwide average loss was ~100,000 neurons per day (~1 neuron/sec), a rate consistent with loss of all brain cells (in some parts of the organ) over a period of about 250-350 years. More recent work found a normal loss of ~**10%** of all neocortical neurons in normal human brains over a 70-year period from 20 to 90 years of age in both genders,[271] a 0.25%/yr long-term average loss rate of ~1 neuron/sec across the

---

[264] Landauer TK. How Much Do People Remember? Some Estimates of the Quantity of Learned Information in Long-term Memory. Cognitive Science 1986;10:477-493; https://onlinelibrary.wiley.com/doi/pdf/10.1207/s15516709cog1004_4. (The figure cited includes a generous allowance for motor memory, e.g., the information storage required when learning to play a piano, ride a bicycle, or perform gymnastics, which was not included in the original study; and incorporates an analysis of competing rates of both learning and forgetting.)

[265] Azevedo FA, Carvalho LR, Grinberg LT, Farfel JM, Ferretti RE, Leite RE, Jacob Filho W, Lent R, Herculano-Houzel S. Equal numbers of neuronal and nonneuronal cells make the human brain an isometrically scaled-up primate brain. J Comp Neurol. 2009 Apr 10;513(5):532-41; http://www.sakkyndig.com/psykologi/artvit/frederico2009.pdf.

[266] Pakkenberg B, Pelvig D, Marner L, Bundgaard MJ, Gundersen HJ, Nyengaard JR, Regeur L. Aging and the human neocortex. Exp Gerontol. 2003 Jan-Feb;38(1-2):95-9; http://citeseerx.ist.psu.edu/viewdoc/download?doi=10.1.1.332.5850&rep=rep1&type=pdf.

[267] assuming the average chemical synapse is ~1000 nm tall, ~400 nm in diameter, ~1 kg/L in density, and composed of ~75 kilodalton protein molecules.

[268] Cohen LD, Zuchman R, Sorokina O, Müller A, Dieterich DC, Armstrong JD, Ziv T, Ziv NE. Metabolic turnover of synaptic proteins: kinetics, interdependencies and implications for synaptic maintenance. PLoS One. 2013 May 2;8(5):e63191; https://www.ncbi.nlm.nih.gov/pmc/articles/PMC3642143/.

[269] The typical error rate in protein synthesis is ~10^{-4} (https://en.wikipedia.org/wiki/Kinetic_proofreading); assuming ~1000 residues/protein implies ~10% of all new protein molecules will contain at least one misincorporated amino acid.

[270] Brody H. Organization of the cerebral cortex, III. A study of aging in the human cerebral cortex. J Comp Neurol. 1955 Apr;102(2):511-556; https://onlinelibrary.wiley.com/doi/abs/10.1002/cne.901020206.

[271] Pakkenberg B, Gundersen HJ. Neocortical neuron number in humans: effect of sex and age. J Comp Neurol. 1997 Jul 28;384(2):312-20; http://www.ncbi.nlm.nih.gov/pubmed/9215725.

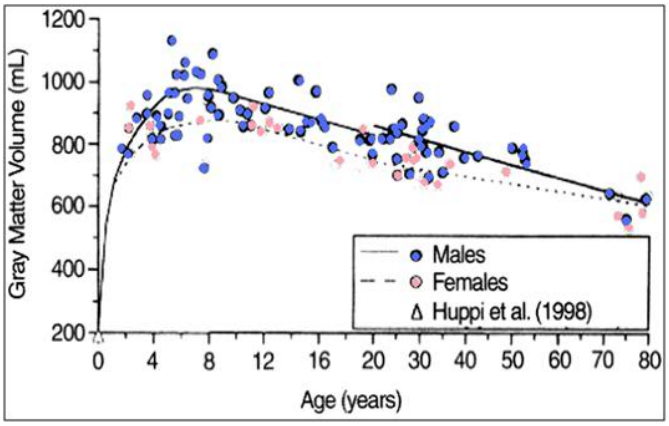

entire brain. Another study found a 0.5%/yr decline in whole-brain volume and weight.[272] MRI data shows gray matter[273] volume declines linearly with age (image, right).[274] A longitudinal MRI analysis of brain volume in patients aged 31-84 years found 0.32%/yr atrophy in the whole brain, 0.68%/yr in the temporal lobe, 0.82%/yr in the hippocampus, and ventricular[275] enlargement of 650 mm^3/yr.[276] Yet another study confirmed a 0.3%/yr neuronal loss in the human vestibular nuclear complex from 40 to 90 years of age.[277] It would appear that personal identity can survive at least a **10%-20% neuron loss** if the deletions are randomly distributed throughout the brain.

The **upper bound** of neuron attrition without loss of personal identity is not precisely known and should be assessed in ***future research***. The best-known neurodegenerative disease that results in loss of personal identity is Alzheimer's disease (AD). The whole-brain atrophy rate in AD brains can be ten times faster than the 0.2%-0.5%/yr seen with normal aging. One MRI study[278] reported a 1.9%/yr atrophy rate, and rates of whole brain atrophy for AD brains are typically reported as 2%/yr,[279] with a range of 1%-4%/yr

---

[272] Svennerholm L, Boström K, Jungbjer B. Changes in weight and compositions of major membrane components of human brain during the span of adult human life of Swedes. Acta Neuropathol. 1997 Oct;94(4):345-52; http://www.ncbi.nlm.nih.gov/pubmed/9341935/.

[273] Gray matter consists of neurons; white matter is mostly myelinated axons that carry nerve impulses between neurons; https://en.wikipedia.org/wiki/White_matter. Men have ~176,000 km of myelinated fibers at age 20 falling to ~97,200 km by age 80, a ~10%/decade length reduction, mostly due to the loss of thinner fibers.*
* Marner L, Nyengaard JR, Tang Y, Pakkenberg B. Marked loss of myelinated nerve fibers in the human brain with age. J Comp Neurol. 2003 Jul 21;462(2):144-52; https://pubmed.ncbi.nlm.nih.gov/12794739/.

[274] Courchesne E, Chisum HJ, Townsend J, Cowles A, Covington J, Egaas B, Harwood M, Hinds S, Press GA. Normal brain development and aging: quantitative analysis at *in vivo* MR imaging in healthy volunteers. Radiology. 2000 Sep;216(3):672-82; https://pubmed.ncbi.nlm.nih.gov/10966694/.

[275] The ventricles in the brain are cavities containing circulating cerebrospinal fluid, continuous with the central canal of the spinal cord; https://en.wikipedia.org/wiki/Ventricular_system.

[276] Scahill RI, Frost C, Jenkins R, Whitwell JL, Rossor MN, Fox NC. A longitudinal study of brain volume changes in normal aging using serial registered magnetic resonance imaging. Arch Neurol. 2003 Jul;60(7):989-94; http://archneur.jamanetwork.com/article.aspx?articleid=784396.

[277] Lopez I, Honrubia V, Baloh RW. Aging and the human vestibular nucleus. J Vestib Res. 1997 Jan-Feb;7(1):77-85; http://www.ncbi.nlm.nih.gov/pubmed/9057161.

[278] Sluimer JD, Vrenken H, Blankenstein MA, Fox NC, Scheltens P, Barkhof F, van der Flier WM. Whole-brain atrophy rate in Alzheimer disease: identifying fast progressors. Neurology. 2008 May 6;70(19 Pt 2):1836-41; http://dspace.ubvu.vu.nl/bitstream/handle/1871/19214/dissertation.pdf?sequence=12#page=105.

[279] Schott JM, Price SL, Frost C, Whitwell JL, Rossor MN, Fox NC. Measuring atrophy in Alzheimer disease: a serial MRI study over 6 and 12 months. Neurology. 2005 Jul 12;65(1):119-24; http://www.ncbi.nlm.nih.gov/pubmed/16009896.

brain volume loss among different populations.[280] Over a typical 5-10 year course of Alzheimer's disease, a 2%-4%/yr atrophy rate can amount to more than a **20%** loss of whole-brain volume.

If one assumes that no revival protocol can perfectly generate the ideal 100% recovery of original personal identity, what is the biggest percentage loss that we might find acceptable? As one crude calibration of our thinking on this question, we can consider the four clinical stages of Alzheimer's disease which display a progressive pattern of cognitive and functional impairment. We can peruse this list and decide how much impairment we might be willing to tolerate upon revival: [281]

Stage 1 (preclinical/prodromal AD): This stage is usually identified only in research settings. Patients will generally notice no symptoms of dementia, nor will those around them.

Stage 2 (AD, mild dementia): The patient may experience memory loss of recent events; have difficulty with problem-solving, complex tasks, and sound judgments; show a few noticeable changes in personality; have difficulty organizing and expressing thoughts; and may get lost or misplace belongings.

Stage 3 (AD, moderate dementia): The patient may experience increasingly poor judgment, deepening confusion, and even greater memory loss; may need help with some daily activities; and may undergo significant changes in personality and behavior. For example, patients may "confuse family members or close friends with one another or mistake strangers for family, forget details of their personal history such as their address or phone number or where they attended school, develop unfounded suspicions – e.g., to become convinced that friends, family or professional caregivers are stealing from them or that a spouse is having an affair – or may see or hear things that aren't really there."

Stage 4 (AD, severe dementia): The patient may lose the ability to communicate coherently; require daily assistance with personal care; and may experience a decline in physical abilities along with severe changes in personality.

A 2015 study counted the neuron losses at each stage of AD in three key areas of the brain – Layer II of the entorhinal cortex (EC),[282] the locus coeruleus (LC),[283] and the nucleus basalis of Meynert (NbM)[284] – in 101 Alzheimer's patients and 19 controls, with the results as shown in **Table 1**.

---

[280] Jack CR Jr, Shiung MM, Gunter JL, O'Brien PC, Weigand SD, Knopman DS, Boeve BF, Ivnik RJ, Smith GE, Cha RH, Tangalos EG, Petersen RC. Comparison of different MRI brain atrophy rate measures with clinical disease progression in AD. Neurology. 2004 Feb 24;62(4):591-600; http://www.ncbi.nlm.nih.gov/pmc/articles/PMC2730165/. Boyes RG, Rueckert D, Aljabar P, Whitwell J, Schott JM, Hill DL, Fox NC. Cerebral atrophy measurements using Jacobian integration: comparison with the boundary shift integral. Neuroimage. 2006 Aug 1;32(1):159-69; http://www.doc.ic.ac.uk/~pa100/pubs/boyesNeuroImage2006.pdf.

[281] "Alzheimer's stage: How the disease progresses." Mayo Clinic. 19 Apr 2019; https://www.mayoclinic.org/diseases-conditions/alzheimers-disease/in-depth/alzheimers-stages/art-20048448. See also: https://www.alz.org/alzheimers-dementia/stages.

[282] The EC is located in the medial temporal lobe and functions as a hub in a widespread network for memory, navigation and the perception of time, serving as the main interface between the hippocampus and neocortex and mediating declarative (autobiographical/episodic/semantic) and spatial memories; https://en.wikipedia.org/wiki/Entorhinal_cortex.

[283] The LC is a nucleus in the pons of the brainstem involved with physiological responses to stress and panic, and is the principal site for brain synthesis of norepinephrine (noradrenaline); https://en.wikipedia.org/wiki/Locus_coeruleus.

[284] The NbM is associated with arousing stimuli, both positive (appetitive) and negative (aversive), and may promote sustained attention, learning, and recall in long term memory; https://en.wikipedia.org/wiki/Nucleus_basalis.

Table 1. Average number of neurons present, and percentage neuron losses, in three specific brain regions during various stages of Alzheimer's dementia [285]

Location in Brain	Control	AD Stage 1 (preclinical)	AD Stage 2 (mild)	AD Stage 3 (moderate)	AD Stage 4 (severe)
EC	680,000	635,000 -7% loss	500,000 -26% loss	425,000 -38% loss	310,000 -54% loss
LC	17,550	16,130 -8% loss	11,750 -33% loss	9,650 -45% loss	5,250 -70% loss
NbM	170,000	155,000 -9% loss	114,500 -33% loss	69,500 -59% loss	25,000 -85% loss
Average of all 3		*-8% loss*	*-31% loss*	*-47% loss*	*-70% loss*

It is likely that there are some areas of the brain where relatively large neuron losses can occur without sacrificing personal identity. But in those regions of the brain that are most critical to personal identity, it appears that ~7%-9% neuron losses may result in only mild preclinical (i.e., barely observable) memory degradation (AD1), whereas losing ~26%-33% of critical neurons may produce some noticeable memory degradation (AD2), losing 38%-59% of these neurons can produce significant degradation of identity (AD3), and the absence of 54%-85% of critical neurons likely produces almost complete loss of original personal identity (AD4). Synapse losses as a function of Alzheimer's disease stage are similar.[286] Early stage AD shows a 15%-25% loss of synapses in the frontal cortex and limbic system while more advanced stages show 20%-40% synapse losses in frontal and cortical biopsies[287] and 44%-55% synapse depletion relatively early in the hippocampus[288] – although some areas of the brain may experience much less decline of synapses and dendritic spines during AD.[289] Similar losses occur with Parkinson's Disease.[290]

---

[285] Arendt T, Brückner MK, Morawski M, Jäger C, Gertz HJ. Early neurone loss in Alzheimer's disease: cortical or subcortical? Acta Neuropathol Commun. 2015 Feb 10;3:10; https://www.ncbi.nlm.nih.gov/pmc/articles/PMC4359478/.

[286] DeKosky ST, Scheff SW. Synapse loss in frontal cortex biopsies in Alzheimer's disease: correlation with cognitive severity. Ann Neurol. 1990 May;27(5):457-64; https://pubmed.ncbi.nlm.nih.gov/2360787/.

[287] Davies CA, Mann DM, Sumpter PQ, Yates PO. A quantitative morphometric analysis of the neuronal and synaptic content of the frontal and temporal cortex in patients with Alzheimer's disease. J Neurol Sci. 1987 Apr;78(2):151-64; https://pubmed.ncbi.nlm.nih.gov/3572454/. de Wilde MC, Overk CR, Sijben JW, Masliah E. Meta-analysis of synaptic pathology in Alzheimer's disease reveals selective molecular vesicular machinery vulnerability. Alzheimers Dement. 2016 Jun;12(6):633-44; https://www.ncbi.nlm.nih.gov/pmc/articles/PMC5058345/.

[288] Masliah E, Mallory M, Alford M, DeTeresa R, Hansen LA, McKeel DW Jr, Morris JC. Altered expression of synaptic proteins occurs early during progression of Alzheimer's disease. Neurology. 2001 Jan 9;56(1):127-9; https://pubmed.ncbi.nlm.nih.gov/11148253/.

[289] Poirel O, Mella S, Videau C, Ramet L, Davoli MA, Herzog E, Katsel P, Mechawar N, Haroutunian V, Epelbaum J, Daumas S, El Mestikawy S. Moderate decline in select synaptic markers in the prefrontal cortex (BA9) of patients with Alzheimer's disease at various cognitive stages. Sci Rep. 2018 Jan 17;8(1):938; https://www.ncbi.nlm.nih.gov/pmc/articles/PMC5772053/.

[290] At the onset of Parkinson's Disease (PD), only 385,000 neurons remain in the substantia nigra* region of the brain that normally has 810,000 neurons (a ~52% loss),† possibly falling to only ~240,000 neurons (a ~70% loss) just prior to PD death.

Another measure of personal identity retention as a function of percentage neural structure loss is provided by medical experience with supratentorial[291] (cerebral) ischemic stroke, wherein poor or interrupted blood flow to the brain causes neural cell death.[292] An analysis of the stroke damage rate literature (**Table 2**) found that a typical stroke patient loses ~**5%** of their brain, and up to **10%** in severe cases. A severe stroke can be associated with loss of significant blocks of personality and memory, depending on where in the brain it occurs, and the patient can often be seriously physically disabled afterwards – though medically and legally the patient is still considered to be the same person.

Table 2. Estimated neural circuitry loss during typical acute ischemic stroke[293]

Duration of Stroke	Neurons Lost	Synapses Lost	Myelinated Fibers Lost	Percentage Loss
Per Second	0.032×10^6	0.23×10^9	0.2 km	0.0001 %
Per Minute	1.9×10^6	14×10^9	12 km	0.009 %
Per Hour	120×10^6	830×10^9	714 km	0.5 %
Per Stroke	1200×10^6	8300×10^9	7140 km	**5 %**
Number in avg human forebrain:	*22×10^9*	*157×10^{12}*	*135,000 km*	*135,000 km*

A related perspective is provided by hemispherectomy,[294] a surgical procedure that originally involved removing an entire hemisphere of the brain (either right or left) to eliminate epileptic seizures, usually in children because their brains retain more neuroplasticity and can better compensate for the loss. Functional hemispherectomy has now become more common, in which less brain tissue (e.g., only the epileptic portions of one side of the brain) is removed – in one example,[295] leaving frontal and occipital lobes in place on both sides but removing the parietal and temporal lobes on one side (i.e., removal of ~199 cm^3 of lobe volume,[296] representing ~**24%** of total cortical gray matter or ~**14%** of total brain volume). Patients typically suffer no cognitive decline as a result of the surgery.[297]

---

[*] The substantia nigra is a basal ganglia structure located in the midbrain that plays an important role in reward and movement; https://en.wikipedia.org/wiki/Substantia_nigra.

[†] Pakkenberg B, Møller A, Gundersen HJ, Mouritzen Dam A, Pakkenberg H. The absolute number of nerve cells in substantia nigra in normal subjects and in patients with Parkinson's disease estimated with an unbiased stereological method. J Neurol Neurosurg Psychiatry. 1991 Jan;54(1):30-3; http://www.ncbi.nlm.nih.gov/pmc/articles/PMC1014294/pdf/jnnpsyc00499-0040.pdf.

[291] https://en.wikipedia.org/wiki/Supratentorial_region.

[292] https://en.wikipedia.org/wiki/Stroke#Ischemic.

[293] Saver JL. Time Is Brain – Quantified. Stroke 2006 Jan;37(1):263-266; https://www.ahajournals.org/doi/pdf/10.1161/01.str.0000196957.55928.ab.

[294] https://en.wikipedia.org/wiki/Hemispherectomy.

[295] Tinuper P, Andermann F, Villemure JG, Rasmussen TB, Quesney LF. Functional hemispherectomy for treatment of epilepsy associated with hemiplegia: rationale, indications, results, and comparison with callosotomy. Ann Neurol. 1988 Jul;24(1):27-34; https://pubmed.ncbi.nlm.nih.gov/3137858/.

[296] http://www.bic.mni.mcgill.ca/users/noor/brain_volume.html.

The loss of personal identity might also be correlated with the loss of neurons or neural capacity by associating standard measures of the depth of sedation (flowchart, below)[298] with specific dosage ranges of anesthetic agents. A ***future research*** project could ascertain the percentage of critical neuroreceptor occupancy or mean level of neuron functionality as a function of blood concentration or the degree of brain penetration of anesthetic agents, then use this information to generate an estimate of the fraction of neurons that must be quieted to eliminate episodic memory or consciousness, or to produce a given depth of sedation.

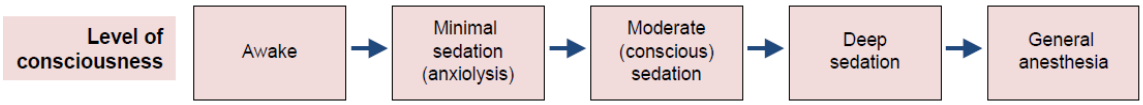

For example, propofol anesthesia depresses whole-brain metabolism by **55%**, with cortical metabolism reduced **58%** and subcortical reduced **48%** from normal values in an unconscious patient, as measured by PET scans.[299] Similarly, isoflurane depresses whole-brain metabolism by **46%**,[300] though xenon depresses by only **26%**.[301] Non-REM sleep exhibits a **23%** metabolic reduction across the entire brain.[302] More generally, the reduction in cerebral metabolism from a variety of causes (chart, below)[303] shows that consciousness may be retained at **10%** metabolic depression (i.e., locked-in syndrome or pseudocoma)[304] but is lost at **≥40%** metabolic depression.

---

[297] Cukiert A, Cukiert CM, Argentoni M, Baise-Zung C, Forster CR, Mello VA, Burattini JA, Mariani PP. Outcome after hemispherectomy in hemiplegic adult patients with refractory epilepsy associated with early middle cerebral artery infarcts. Epilepsia. 2009 Jun;50(6):1381-4; https://onlinelibrary.wiley.com/doi/pdf/10.1111/j.1528-1167.2008.01795.x.

[298] "Continuum of Depth of Sedation: Definition of General Anesthesia and Levels of Sedation/Analgesia," American Society of Anesthesiologists, Oct 1999; https://www.asahq.org/standards-and-guidelines/continuum-of-depth-of-sedation-definition-of-general-anesthesia-and-levels-of-sedationanalgesia.

[299] Alkire MT, Haier RJ, Barker SJ, Shah NK, Wu JC, Kao YJ. Cerebral metabolism during propofol anesthesia in humans studied with positron emission tomography. Anesthesiology. 1995 Feb;82(2):393-403; https://pubs.asahq.org/anesthesiology/article/82/2/393/34837.

[300] Alkire MT, Haier RJ, Shah NK, Anderson CT. Positron emission tomography study of regional cerebral metabolism in humans during isoflurane anesthesia. Anesthesiology. 1997 Mar;86(3):549-57; https://pubs.asahq.org/anesthesiology/article/86/3/549/35846.

[301] Rex S, Schaefer W, Meyer PH, Rossaint R, Boy C, Setani K, Büll U, Baumert JH. Positron emission tomography study of regional cerebral metabolism during general anesthesia with xenon in humans. Anesthesiology. 2006 Nov;105(5):936-43; https://pubs.asahq.org/anesthesiology/article-pdf/105/5/936/362483/0000542-200611000-00014.pdf.

[302] Buchsbaum MS, Gillin JC, Wu J, Hazlett E, Sicotte N, Dupont RM, Bunney WE Jr. Regional cerebral glucose metabolic rate in human sleep assessed by positron emission tomography. Life Sci. 1989;45(15):1349-56; https://pubmed.ncbi.nlm.nih.gov/2796606/.

[303] Laureys S, Owen AM, Schiff ND. Brain function in coma, vegetative state, and related disorders. Lancet Neurol. 2004 Sep;3(9):537-46; https://orbi.uliege.be/bitstream/2268/2213/1/LAUREYS_S_2004_LancetNeurol_3_9_537.pdf.

[304] "[P]atient is aware but cannot move or communicate verbally due to complete paralysis of nearly all voluntary muscles in the body except for vertical eye movements and blinking"; https://en.wikipedia.org/wiki/Locked-in_syndrome.

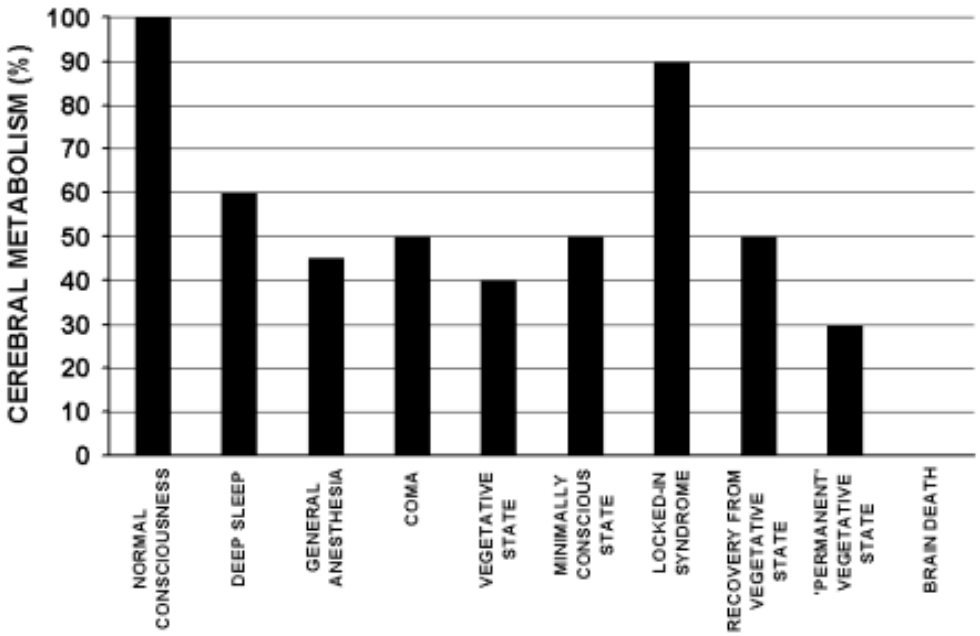

Our tentative conclusion: Holding neuron and synapse losses to a maximum of **10%-20%** (both globally and in localized regions of the brain) seems advisable to retain personal identity, although neuron losses in the **20%-35%** range might still yield an outcome that could be acceptable to some patients (e.g., in cases involving serious head trauma, advanced neurodegenerative disease, or extremely poor cryopreservation quality). It would be a useful exercise for ***future research*** to match the aforementioned correlates of personal identity with the time course of ischemic damage, to predict the approximate percentage of personal identity remaining after a given period of warm ischemia in past and current cryopreservation patients.

Regarding the likely incidence of at least partial amnesia in revived cryonics patients, Brian Wowk[305] observes: "Future technologies for molecular repair of the brain will be able to directly reverse structural and chemical changes caused by long periods without oxygen, making resuscitation after hours of clinical death theoretically possible….In the limiting case of a technology capable of completely general molecular repairs, restoration of a healthy state would always be possible. Whatever repairs were necessary to repair/reconstruct a functional, biologically healthy brain and body could always be performed. What would happen is that long periods of clinical death followed by repair would result in varying degrees of memory loss about prior events. If decomposition were severe enough, 'repair' would result in a new person. How much memory loss is required before the original patient is considered deceased? It is a tradition in medicine that if brain function can be restored, the original patient is considered recovered despite amnesia. This custom seems likely to continue in the future whenever clinically deceased patients can be restored to consciousness, even when the repaired injuries were severe."

In a subsequent 2014 paper,[306] Wowk further notes: "Instead of there being patients who can or cannot be resuscitated, repaired patients would wake on a continuum ranging from full memory retention to total

---

[305] Wowk B. Ethics of Non-ideal Cryonics Cases. Cryonics 2006 Fall;27(4):10-12; https://www.alcor.org/docs/cryonics-magazine-2006-04.pdf.

[306] Wowk B. The future of death. J Crit Care. 2014 Dec;29(6):1111-1113; https://pubmed.ncbi.nlm.nih.gov/25194588/.

retrograde amnesia. The latter states would not be as tragic as today's persistent vegetative state or minimally conscious states because intrinsic biological capacity for normal cognition could be restored. The result of extreme neurologic injury followed by repair would be the child-like beginning of a new life rather than a tragic-lingering end."

It seems unavoidable as a practical matter that many revived cryopatients will suffer at least some amnesia or memory distortion, since no revival process can be absolutely perfect. As Perry[307] adds: "The amnesia problem is the most serious one we are likely to face....Patients with amnesia but otherwise fully functional…could be helped through the use of records, including personal memorabilia. They should at minimum end up fully able to speak their native language, with basic knowledge and comprehension at former levels, and also know their name and other basic data which should be available from records. They should, in particular, know that they had been cryopreserved and resuscitated and when and where these events occurred. Personal memorabilia, photos, diaries and the like, could help to further fill out missing memories (and cryonicists are encouraged to maintain files of such memorabilia)."

2.1.4 Neurotransmitter Concentrations and Personal Identity

There will occur many random changes to the original precise spatial concentrations of **metabolites and neurotransmitters** during the post-mortem cryopreservation process, somewhat obscuring the exact original living concentrations, but the concentrations of many metabolites may remain stable or change in known ways after various exposure times post-mortem.[308] The large natural variation of these concentrations around known mean levels[309] (to which the intracellular concentrations can be reset during revival) is large enough[310] to suggest that the precise spatial concentration of these chemicals during life seems unlikely to be the key seat of personality and identity. Human brain tissue (even from autopsies carried out up to 24 hours or more post-mortem) generally "retains the metabolic machinery to reconstitute tissue metabolite and neurotransmitter pools,"[311] due in part to the high stability of enzymes, receptors, and nucleic acids in the post-mortem human brain.[312] It is therefore reasonable to assume that an accurately renovated connectome, once restored to functionality, will properly reconstitute all local metabolite and neurotransmitter concentrations to the original levels that are appropriate for that individual, in every neural compartment. This assumption should be experimentally verified in ***future research*** by demonstrating that

---

[307] Perry RM. Cryonics Under Fire: Meeting the Challenges of Hostile Scientists Then and Now. Cryonics 2016 Jan-Feb;37(1):8-15; https://www.alcor.org/docs/cryonics-magazine-2016-01.pdf.

[308] Perry TL, Hansen S, Gandham SS. Postmortem changes of amino compounds in human and rat brain. J Neurochem. 1981 Feb;36(2):406-10; https://www.ncbi.nlm.nih.gov/pubmed/7463068/.

[309] Banay-Schwartz M, Palkovits M, Lajtha A. Levels of amino acids in 52 discrete areas of postmortem brain of adult and aged humans. Amino Acids. 1993 Jun;5(2):273-87; https://www.ncbi.nlm.nih.gov/pubmed/24190671.

[310] Prabha M, Ravi V, Ramachandra Swamy N. Activity of hydrolytic enzymes in various regions of normal human brain tissue. Indian J Clin Biochem. 2013 Jul;28(3):283-91; https://www.ncbi.nlm.nih.gov/pmc/articles/PMC3689325/.

[311] "...incubated synaptosomes and brain slices from postmortem human brain respire, accumulate tissue potassium, maintain membrane potentials, release neurotransmitters in a calcium-dependent fashion, and possess active, sodium-dependent uptake systems." Dodd PR, Hambley JW, Cowburn RF, Hardy JA. A comparison of methodologies for the study of functional transmitter neurochemistry in human brain. J Neurochem. 1988 May;50(5):1333-45; https://onlinelibrary.wiley.com/doi/pdf/10.1111/j.1471-4159.1988.tb03013.x.

[312] Hardy JA, Dodd PR. Metabolic and functional studies on post-mortem human brain. Neurochem Int. 1983;5(3):253-66; https://www.ncbi.nlm.nih.gov/pubmed/20487948.

the particular concentrations of neurotransmitters and other chemical messenger molecules that are present some time after cooldown are largely unrelated to live function.

Darwin's comments[313] on the relevance of neurotransmitter levels to long-term memory and personal identity are worth repeating here:

> "What are neurotransmitters (NTs) and how is their concentration in brain synapses determined? Simply put, NTs are chemicals released at the synaptic junction which are responsible for not just the transmission of signals across the synapse, but for the 'strength' of the signal transmitted. Thus, they serve a 'weighting function' to signaling. How much NT gets made or released is *not* a function of the NT itself, anymore than how much smoke gets released from a fire being used to send smoke signals is a function of the smoke. NTs are smoke, they are the signal medium, not the signal itself, or the source of signal, or the signal's strength. Focusing on the conservation of NT levels in synapses as the key to the preservation of memory is analogous to focusing on the smoke in a smoke signal as the durable element of the underlying data set. Neurotransmitters are the smoke; the real question is, what causes the NTs to be made and released in predictable amounts and ways over long periods of time? In other words, who is controlling the amount and pattern of smoke release in a smoke signaling operation?"
>
> "The current consensus in the field of the neurobiology of learning and memory is that there is extensive biochemical change in the synapse itself, probably beginning with a process called Long Term Potentiation (LTP)….[I]n addition to biochemical changes in the synapse, there are also changes in the number and in the physical type and configuration of the synapses that occur during learning and memory encoding. There are well over 140 different physical *types of synapse* and the myriad new connections that form during learning may use many different synaptic morphologies. What's more, sometimes many of the synapses that initially form during encoding of learning, especially multiple synapses on the same dendrite, are pared down or disappear during what is believed to be the consolidation phase of memory encoding."
>
> "[S]ynapses are not transient fluctuations in the level of a biochemical, or signaling molecule – they are complex structures made of protein and protein gets made (and maintained) only as [a] result of signal transduction between the cell nucleus and the ribosomes: DNA > RNA > ribosomes > protein. Indeed, even the synaptic vesicles and the neurotransmitters inside them are manufactured in the cell bodies and subsequently transported to the synapses (the 'right' synapses) – all of which is presumably under nuclear control. Since memories persist at least a century in humans, it is clear that the biological structure(s) that encodes them is durable and well maintained. Put another way, the mechanism that controls and determines the pattern of smoke signaling is both robust and durable."
>
> "Our current understanding of the gating mechanisms of synapse firing suggests that the character, quantity and configuration of synapses is how memory 'works,' or is encoded. At this point, it should hopefully be clear that in theory, it should be possible to recover a brain with memories and personality intact, even if there was not a single molecule of NT present in any synapse, anywhere. The NTs are *made* by the neurons and released by the synapses in the 'right' amount at the 'right' time and in the 'right' way as a function of the *underlying* synapse and nerve cell structure. Not the other way around! The question that should be preoccupying cryonicists is

---

[313] Darwin MD. Ray Kurzweil on Memory and Cryonics. Cryonics 2012 Nov-Dec;33(6):9-10; https://www.alcor.org/library/kurzweil-memory-cryonics/; in response to: "Dialogue between Ray Kurzweil, Eric Drexler, and Robert Bradbury," following the Alcor 2002 Fifth Alcor Conference on Extreme Life Extension, 3 Dec 2002; https://web.archive.org/web/20120509071133/https://www.kurzweilai.net/dialogue-between-ray-kurzweil-eric-drexler-and-robert-bradbury.

whether there are sufficient intact neurons and synapses present to be preserved in the first place – not whether or not the NT levels are conserved in synapses following cryopreservation."

Future research should also examine the state of neurotransmitter concentrations in synapses after cessation of metabolism and brain activity during warm and cold ischemia, or during recovery from anesthesia, and so forth. Local neurotransmitter concentrations are significantly altered between the time of clinical death and the time the cryopreserved patient reaches cryogenic temperatures, since neurotransmitter half-time is only ~1 msec due to diffusion, re-uptake, receptor binding, and breakdown by enzymes.[314]

2.1.5 Other Elements of Personal Identity

Are important components of memory or personality encoded elsewhere than in purely neuronal or encephalic physical structures?

First, we should ask exactly which parts of the brain must be restored to capture personal identity? The neocortex (higher brain functions)[315] and the limbic system (emotion and long-term memory)[316] appear essential, but how much of personal identity resides in the basal ganglia[317] or "reptilian brain"[318] (instinct), the brain stem (autonomic regulation),[319] the spinal cord,[320] the peripheral nervous system[321] (limb and organ control), and other minor features of our nervous system? The ascending reticular activating system (ARAS)[322] also should not be overlooked, as without it there is no consciousness in the brain – likely making this ancient structure identity-critical. ***Future research*** should examine and resolve this issue so that the exact scope of essential revival tasks can be more clearly defined.[323]

Brain emulation scientist Randal Koene[324] does not rule out the possibility that full recovery of personal identity may require more than just the connectome and synaptome: "I think there is more to it than the connectome, where the connectome is just a list of which neuron is connected to which other neuron. Clearly, it will matter how they are connected, i.e., how the synaptic receptors involved respond, how the

---

[314] Scimemi A, Beato M. Determining the neurotransmitter concentration profile at active synapses. Mol Neurobiol. 2009 Dec;40(3):289-306; https://www.ncbi.nlm.nih.gov/pmc/articles/PMC2777263/.

[315] https://en.wikipedia.org/wiki/Neocortex.
[316] https://en.wikipedia.org/wiki/Limbic_system.
[317] https://en.wikipedia.org/wiki/Basal_ganglia.
[318] https://en.wikipedia.org/wiki/Triune_brain#Reptilian_complex.
[319] https://en.wikipedia.org/wiki/Brainstem.
[320] https://en.wikipedia.org/wiki/Spinal_cord.
[321] https://en.wikipedia.org/wiki/Peripheral_nervous_system.
[322] https://en.wikipedia.org/wiki/Reticular_formation#Ascending_reticular_activating_system.

[323] ***Future research*** should explore the degree to which it may be possible to correct corrupted memories by altering connectomic and synaptic brain structures to replace missing memories that have been destroyed, remove erroneous memories that are not real, or edit memories that have become corrupted. As early as 2015, neuroscientists had reportedly demonstrated a very limited ability to remove individual memories and to implant fake memories in the connectome of a living mouse using lasers and optogenetics.*
* Ramirez S, Liu X. A mouse, a laser beam, a manipulated memory. YouTube, 15 Aug 2015; https://www.youtube.com/watch?v=EXo3qA9V3eI.

[324] Weinstock N. Scholar Profile: Randal Koene. Cryonics 2019 Qtr 4;40(4):3-11; https://www.alcor.org/docs/cryonics-magazine-2019-04.pdf.

neurons involved respond to changes in their membrane potential caused by changes at synaptic sites somewhere along their somatic or dendritic structures. Such responses will be caused both by direct transmission of activity from neuron to neuron, but also by more diffuse pathways where cells in one location release chemicals that are subsequently received by neurons in various locations reached by those chemicals. There may even be subtle effects of electromagnetic fields, although we would have to determine if those rise beyond the brain's noise threshold. It might even be that we need some model of the modulatory effects of certain glial cell populations. In short, a good model of a specific brain that will faithfully produce desired functional responses will have to be more detailed than the mere connectome can probably provide....We may end up caring more about neural population dynamics and the activity of groups of neurons than about the delicate details of activity at individual cells. It's hard to predict this with any amount of certainty, because we haven't experimented and played with any advanced neural prosthesis or small-animal whole brain emulations yet." ***Future research*** must resolve the question of whether personal identity may reside in any of these places, and if so, to what level of significance.

Besides the estimated 86.1 x 10^9 signal-carrying neurons in the human brain,[325] the human connectome includes ~0.5 x 10^9 signal-carrying neurons in the **enteric nervous system** (ENS)[326] and ~0.1 x 10^9 signal-carrying neurons in the human **spinal cord**.[327] Thus ~0.7% of the human connectome lies outside of the brain and, in the conservative view, should be recovered along with the brain during a whole-body cryonics revival. It has recently been suggested that the enteric nervous system could be involved in specific aspects of memory and learning.[328] The ENS makes use of more than 30 neurotransmitters (including 90% of the body's serotonin and 50% of the body's dopamine)[329] that may well play a role in regulating mood and anxiety,[330] and this "second brain"[331] may be involved in aspects of emotion, appetite, and certain behavioral states[332] – important aspects (or at least modulators) of individual personality. The signal-

---

[325] Azevedo FA, Carvalho LR, Grinberg LT, Farfel JM, Ferretti RE, Leite RE, Jacob Filho W, Lent R, Herculano-Houzel S. Equal numbers of neuronal and nonneuronal cells make the human brain an isometrically scaled-up primate brain. J Comp Neurol. 2009 Apr 10;513(5):532-41; http://www.sakkyndig.com/psykologi/artvit/frederico2009.pdf.

[326] Furness JB. The enteric nervous system. Scholarpedia 2007;2(10)4064; http://www.scholarpedia.org/article/Enteric_nervous_system. Young E. Gut instincts: The secrets of your second brain. New Scientist, 2012 Dec 15;216(2895):38-42; https://web.archive.org/web/20130504175954/http://neurosciencestuff.tumblr.com/post/38271759345/gut-instincts-the-secrets-of-your-second-brain. Rao M, Gershon MD. The bowel and beyond: the enteric nervous system in neurological disorders. Nat Rev Gastroenterol Hepatol. 2016 Sep;13(9):517-28; https://www.ncbi.nlm.nih.gov/pmc/articles/PMC5005185/. See also: https://en.wikipedia.org/wiki/Enteric_nervous_system and https://en.wikipedia.org/wiki/Gut-brain_axis#Enteric_nervous_system.

[327] Hall JE. Neural Control of Gastrointestinal Function - Enteric Nervous System. Guyton and Hall Textbook of Medical Physiology, 12th edition, Saunders Elsevier, 2011, p. 755; https://www.amazon.com/Guyton-Hall-Textbook-Medical-Physiology/dp/1416045740/.

[328] Schemann M, Frieling T, Enck P. To learn, to remember, to forget-How smart is the gut? Acta Physiol (Oxf). 2020 Jan;228(1):e13296; https://pubmed.ncbi.nlm.nih.gov/31063665/.

[329] https://en.wikipedia.org/wiki/Gut-brain_axis#Enteric_nervous_system.

[330] Israelyan N, Del Colle A, Li Z, Park Y, Xing A, Jacobsen JPR, Luna RA, Jensen DD, Madra M, Saurman V, Rahim R, Latorre R, Law K, Carson W, Bunnett NW, Caron MG, Margolis KG. Effects of Serotonin and Slow-Release 5-Hydroxytryptophan on Gastrointestinal Motility in a Mouse Model of Depression. Gastroenterology. 2019 Aug;157(2):507-521; https://www.ncbi.nlm.nih.gov/pmc/articles/pmid/31071306/.

[331] Gershon MD. The Second Brain. Harper Collins, NY, 1998. Gershon MD. The enteric nervous system: a second brain. Hosp Pract (1995). 1999 Jul 15;34(7):31-2, 35-8, 41-2 passim; http://www.imhlk.com/wp-content/uploads/2018/02/The-Enteric-Nervous-System-A-Second-Brain-Michael-D.-Gershon.pdf.

[332] Li JH, Duan R, Li L, Wood JD, Wang XY, Shu Y, Wang GD. Unique characteristics of the second brain – The enteric nervous system. Sheng Li Xue Bao. 2020 Jun 25;72(3):382-390 [in Chinese]; https://pubmed.ncbi.nlm.nih.gov/32572435/.

carrying neurons in the spine might encode individual-specific signal routing patterns between brain and limbs, thus influencing the reaction speed of conscious motor functions and potentially impacting personality. ***Future research*** should assess the possible importance of the "gut brain" and the spinal cord[333] in human memory and personality. Any information these nonencephalic neurons might encode would be lost to neuro cryopatients (whose original body trunk has been discarded) but would likely remain fully recoverable for whole-body cryopatients.

It has also been suggested that gut bacteria,[334] aka. the **microbiome**, may influence mood, neural function, and even personality.[335] If true, it might be necessary to cryopreserve (and later revive and reimplant) a patient's original gut flora in order to fully recover their original personality, an issue that should be studied in ***future research***.

Some portion of personal identity is stored indirectly in the patient's body as "**physical memory**."[336] This includes physical characteristics such as individual-unique fingerprints,[337] dental patterns,[338] and brain fold patterns;[339] muscle distribution, muscle mass, and bone density; body shape and height; facial[340] and other[341] bodily asymmetries; and other physical features that are significantly determined by nongenetic and developmental factors such as environmental influences, parental behaviors, social behaviors, nutrition, exercise regimen, specialized physical performance activities, and personal choices during life (e.g., body piercings and tattoos), producing a set of physical traits that is utterly unique to each individual. These characteristics can help define how the individual relates to other people in the world,[342] provide

---

[333] We don't have reports of personality data before and after spinal injury, but one study* compared the personality assessment of veterans with **spinal cord injury** (SCI) to the personality assessment of their uninjured identical twins and found "no evidence that SCI is associated with long-term personality change," a finding that would at least be consistent with relatively low impact of non-encephalic neural structures on personality. This issue needs further study, as noted in the text.
* Hollick C, Radnitz CL, Silverman J, Tirch D, Birstein S, Bauman WA. Does spinal cord injury affect personality? A study of monozygotic twins. Rehab Psychol. 2001;46(1):58-67; https://psycnet.apa.org/record/2001-14028-004.

[334] Howes L. How your gut might modify your mind. Chem & Eng News 2019 Apr 8;97(14); https://cen.acs.org/biological-chemistry/microbiome/gut-might-modify-mind/97/i14.

[335] https://en.wikipedia.org/wiki/Gut-brain_axis#Anxiety_and_mood_disorders.

[336] O'Neal MB, de Wolf A. The Case for Whole-Body. Cryonics 2014 Feb;35(2):16-21; https://www.alcor.org/library/case-for-whole-body/.

[337] University of Applied Science. A Study in Finger Prints: Their Uses and Classification. Third Edition. Chicago: University of Applied Science, 1920; https://books.google.com/books?hl=en&lr=&id=lNUrAQAAMAAJ. Expert Working Group on Human Factors in Latent Print Analysis. Latent Print Examination and Human Factors: Improving the Practice through a Systems Approach. U.S. Department of Commerce, National Institute of Standards and Technology, 2012; https://doi.org/10.6028/NIST.IR.7842. See also: https://en.wikipedia.org/wiki/Fingerprint.

[338] Martin-de-Las-Heras S, Valenzuela A, Luna Jde D, Bravo M. The utility of dental patterns in forensic dentistry. Forensic Sci Int. 2010 Feb 25;195(1-3):166.e1-5; https://pubmed.ncbi.nlm.nih.gov/19963328/.

[339] Ebsworth-Gold E. 3-D mapping babies' brains. Washington University in St. Louis, 9 Mar 2018; https://source.wustl.edu/2018/03/3-d-mapping-babies-brains/. Garcia KE, Robinson EC, Alexopoulos D, Dierker DL, Glasser MF, Coalson TS, Ortinau CM, Rueckert D, Taber LA, Van Essen DC, Rogers CE, Smyser CD, Bayly PV. Dynamic patterns of cortical expansion during folding of the preterm human brain. Proc Natl Acad Sci U S A. 2018 Mar 20;115(12):3156-3161; https://www.ncbi.nlm.nih.gov/pmc/articles/PMC5866555/.

[340] https://en.wikipedia.org/wiki/Facial_symmetry.
[341] https://en.wikipedia.org/wiki/Fluctuating_asymmetry.
[342] https://en.wikipedia.org/wiki/Identity_(social_science).

compatible physicality to reinforce existing muscle memory,[343] and contribute to the coherence of the person's body image,[344] perceived body integrity,[345] and larger self-image.[346]

Future research should consider how much information contained in the **physical and informational artifacts** with which we surround ourselves during life (e.g., our books, houses, cars, collectibles, pets, and computer files) contributes to our personal identity by forming a kind of external long-term memory. People who have lost their homes (along with irreplaceable photographs, letters, and other personal or ancestral artifacts) during natural disasters often experience at least a partial loss of personal identity.[347]

This external memory includes our network of **personal and social relationships** with other people – our spouses, relatives, friends, and professional colleagues. O'Neal and de Wolf[348] note that "we store vast amounts of personal information that is important, or even essential, to our functioning as a person outside ourselves….the 'extended mind'. [This]…recognizes the role of external objects in the functioning of our mind and identity. Looking at the issue of identity preservation from this perspective makes even the whole-body option look limited because it does not take into account all the external objects and information outside of us that have become part of our person and self-image. For example, a Facebook account can be considered part of one's identity and it is not realistic to remember everything that one posted, liked, and shared. So it is not part of one's brain or body but it can be considered a part of one's identity and life history. We should not be surprised, then, that an increasing number of Alcor members are paying more attention to saving information and objects in addition to their own brain or body." In a later article,[349] de Wolf refers to this as the "extended self".

Similarly, the external societal, political, and **cultural milieu** in which a patient was immersed prior to cryopreservation can form an important part of personal identity. James Bedford, the longest-preserved

---

[343] https://en.wikipedia.org/wiki/Muscle_memory.
[344] https://en.wikipedia.org/wiki/Body_image.

[345] Edwards MJ, Alonso-Canovas A, Schrag A, Bloem BR, Thompson PD, Bhatia K. Limb amputations in fixed dystonia: a form of body integrity identity disorder? Mov Disord. 2011 Jul;26(8):1410-4; https://www.ncbi.nlm.nih.gov/pmc/articles/PMC3664409/. Brugger P, Lenggenhager B. The bodily self and its disorders: neurological, psychological and social aspects. Curr Opin Neurol. 2014 Dec;27(6):644-52; https://www.zora.uzh.ch/100466/1/Brugger%20%20Lenggenhager%202014%20(ZORA).pdf. Tatu L, Bogousslavsky J. Phantom Sensations, Supernumerary Phantom Limbs and Apotemnophilia: Three Body Representation Disorders. Front Neurol Neurosci. 2018;41:14-22; https://pubmed.ncbi.nlm.nih.gov/29145179/. Gibson RB. Elective Impairment Minus Elective Disability: The Social Model of Disability and Body Integrity Identity Disorder. J Bioeth Inq. 2020 Mar;17(1):145-155; https://www.ncbi.nlm.nih.gov/pmc/articles/PMC7260267/. Garbarini F, Fossataro C, Pia L, Berti A. What pathological embodiment/disembodiment tell us about body representations. Neuropsychologia. 2020 Dec;149:107666; https://pubmed.ncbi.nlm.nih.gov/33130159/.

[346] https://en.wikipedia.org/wiki/Self-image.

[347] Dugan B. Loss of identity in disaster: how do you say goodbye to home? Perspect Psychiatr Care. 2007 Feb;43(1):41-6; http://citeseerx.ist.psu.edu/viewdoc/download?doi=10.1.1.539.545&rep=rep1&type=pdf. Fox L. The Meaning of Home: A Chimerical Concept or a Legal Challenge? J Law and Society 2002 Dec;29(4):580-610; http://dro.dur.ac.uk/3268/1/3268.pdf.

[348] O'Neal MB, de Wolf A. The Case for Whole-Body. Cryonics 2014 Feb;35(2):16-21; https://www.alcor.org/library/case-for-whole-body/.

[349] de Wolf A. Beyond Skull and Skin: Concepts of Identity and the Growth of Cryonics. Cryonics 2015 Jun;36(6):10-13; https://www.alcor.org/library/beyond-skull-and-skin-concepts-of-identity-and-the-growth-of-cryonics/.

cryonics patient,[350] was cryopreserved more than 50 years ago,[351] and more decades will pass before he is revived. Over such long time frames, major changes can occur in the nature (and even existence) of specific occupations,[352] daily activities of life,[353] languages,[354] religions,[355] nations,[356] political parties,[357] definitions of crimes,[358] status of various groups (e.g., gender, racial, sexual orientation, etc.), and social norms and standards of acceptable behavior.[359] A patient whose sense of self was closely tied to a particular group, cause, or activity that no longer exists (or has changed beyond all recognition) may feel that a part of their personal identity has been lost forever.

---

[350] https://www.alcor.org/library/bedford-suspension/. From a 27 Nov 2015 press release:[*] "James Bedford, a psychology professor from Glendale CA who was cryopreserved on 12 Jan 1967 and is still maintained by Alcor, was born on April 20, 1893. That means that he is now the longest-surviving human being ever. Previously, Jeanne Calment was listed as the longest-lived human being ever verified. She was born on 21 February 1875 and died on 4 August 1997, making her 122 years, 164 days old (or 44,724 days). Bedford was cryopreserved on January 12, 1967, with the hope of eventual repair and revival with more advanced technology sometime in the future. It is true that Bedford is not currently, legally alive. But neither is he dead. He is in a third state akin to a deep coma but where all metabolic activity has halted. So long as he is maintained in that unchanging state, if he was sufficiently well-preserved to begin with, he should be considered as surviving."
[*] Cryonics 2016 Mar-Apr;37(2):8; https://www.alcor.org/docs/cryonics-magazine-2016-02.pdf.

[351] Nelson RF. We Froze the First Man, Dell Publishing Company, 1968; https://www.amazon.com/froze-first-man-Robert-Nelson/dp/B0006BTMOS/.

[352] "30 jobs that no longer exist," 13 Jul 2018; https://www.lovemoney.com/gallerylist/75436/30-jobs-that-no-longer-exist. "Obsolete occupations," https://en.wikipedia.org/wiki/Category:Obsolete_occupations.

[353] https://web.archive.org/web/20170226134342/http://mozy.com/blog/infographics/50-things-we-dont-do-anymore-due-to-technology/.

[354] "Atlas of the World's Languages in Danger," UNESCO, 5 Jul 2017; http://www.unesco.org/languages-atlas/en/statistics.html.

[355] Jason Palmer, "Religion may become extinct in nine nations, study says," BBC News, 22 Mar 2011; https://www.bbc.com/news/science-environment-12811197.

[356] Matt Rosenberg, "Countries That No Longer Exist," ThoughtCo., 10 Jul 2019; https://www.thoughtco.com/missing-countries-1435425. "List of former sovereign states," https://en.wikipedia.org/wiki/List_of_former_sovereign_states.

[357] "Defunct political parties in the United States," https://en.wikipedia.org/wiki/Category:Defunct_political_parties_in_the_United_States.

[358] "Things that were once illegal in America," https://stacker.com/stories/1355/things-were-once-illegal-america.

[359] https://en.wikipedia.org/wiki/Political_correctness.

Finally, among the religious, some might wonder about the preservation of the **soul**,[360] assuming such exists, after revival from cryopreservation. Retention of a soul could logically be regarded as a major component of personal identity. However, this seems more likely to be a concern prospectively rather than retrospectively. Theological conceptions of death tend to evolve with medical conceptions, so successfully resuscitated people may not be regarded as soul-less.

Future research might also systematically review, from a cryonics perspective, the many subtleties involved in the precise philosophical definition of death[361] and identity,[362] including issues such as the future of identity[363] and the copy problem,[364] all fascinating intellectual topics that normally spawn endless hours of vigorous debate,[365] usually repeating the conventional arguments on various sides without resolution, and which (fortunately!) lie beyond the scope of this book. However, cryostasis revival by *in situ* cell repair and rewarming is not qualitatively different from contemporary medical and surgical

---

[360] "Before considering resuscitation, some may ask what becomes of the soul of a person in biostasis. Some people would answer that the soul and the mind are aspects of the same thing, of a pattern embodied in the substance of the brain, active during active life and quiescent in biostasis. Assume, though, that the pattern of mind, memory, and personality leaves the body at death, carried by some subtle substance. The possibilities then seem fairly clear. Death in this case has a meaning other than irreversible damage to the brain, being defined instead by the irreversible departure of the soul. This would make biostasis a pointless but harmless gesture – after all, religious leaders have expressed no concern that the mere preservation of the body [e.g., being embalmed in a mausoleum] can somehow imprison a soul. Resuscitation would, in this view, presumably require the cooperation of the soul to succeed. The act of placing patients in biostasis has in fact been accompanied by both Catholic and Jewish ceremonies. With or without biostasis, cell repair cannot bring absolute immortality. Physical death, however greatly postponed, will remain inevitable for reasons rooted in the nature of the universe. Biostasis followed by cell repair thus seems to raise no fundamental theological issues. It resembles deep anesthesia followed by life-saving surgery: both procedures interrupt consciousness to prolong life." Drexler KE. Engines of Creation. Anchor Press/Doubleday, New York, 1986, pp. 138-9; https://web.archive.org/web/20180722191948/http://e-drexler.com/d/06/00/EOC/EOC_Chapter_9.html. See also: https://www.alcor.org/library/frozen-souls-why-a-religious-person-can-choose-cryonics/ and https://www.alcor.org/library/faq-spiritual-questions/. See also: Mercer C. Resurrection of the Body and Cryonics. Religions 2017;8(5):96; https://www.mdpi.com/2077-1444/8/5/96/pdf.

[361] More M. The Terminus of the Self. Cryonics 1994 Qtr 4 and 1995 Qtr 1; https://www.alcor.org/library/the-terminus-of-the-self/.

[362] Perry RM. Forever For All, Universal Publishers, 2000; https://www.amazon.com/Forever-All-Philosophy-Scientific-Immortality/dp/B00FFBJP28/. More M. The Diachronic Self, PhD Thesis, USC, 1995; http://digitallibrary.usc.edu/cdm/ref/collection/p15799coll17/id/482203. The "Ship of Theseus"; https://en.wikipedia.org/wiki/Ship_of_Theseus.

[363] When human neurological functions come fully under our technological control, we will have to reconcile the concept of a unique "personal identity" with the following scenarios:[*]
Identity Malleability: Parental, social and personal control of memory, identity and personality.
Posthuman Persons: Radically enhanced minds.
Identity Sharing: Memories, thoughts and skills, sold or shared.
Identity Cloning: Persons multiply copied into new media.
Distributed Identity: Distinct persons distributed over, or sharing, a set of bodies and machines.
Group Identity: Multiple bodies and machines integrated into a collective identity, without clear personal identity, e.g., Borg or "hive minds".
[*] Hughes JJ. The Future of Death: Cryonics and the Telos of Liberal Individualism. J Evol Technol. 2001 Jul;6(1); https://jetpress.org/volume6/death.pdf.

[364] Urban T. What Makes You You? Wait But Why, 12 Dec 2014; https://waitbutwhy.com/2014/12/what-makes-you-you.html. See also: https://www.cyberev.org/.

[365] e.g., https://www.reddit.com/r/cryonics/comments/lep7wx/who_is_being_revived/, https://www.econlib.org/archives/2009/11/whats_really_wr.html, https://alcorfoundation.org/forums/viewtopic.php?f=3&t=242&sid=9769b3dd14aa19f8b27543cfd4bc49b1.

treatments followed by resuscitation, and invokes no arcane or novel philosophical issues. Observes Aschwin de Wolf:[366]

> "These topics are of great philosophical and practical interest to some but have little relevance to the technical feasibility of cryonics. When a person goes in for surgery it is not common to engage medical personnel in abstract arguments about the nature of identity prior to induction of anesthesia. Similarly, when hypothermia is used to allow complete circulatory arrest in complex surgical brain procedures it is not common to object that this procedure puts the soul at risk. Even people who do not subscribe to the empiricist premise that underpins modern medicine have come to accept the procedures that are associated with it. Cryonics, as conceived and practiced by organizations like Alcor, is just an extension of the idea that metabolism can be reduced or stopped without inevitable irreversible death."

2.1.6 Choosing the Correct Method for Revival

The analysis that will be presented in Chapter 4 suggests that scans of the body and brain of a cryopreserved patient can be performed to a resolution of at least ~1 μm (Section 4.3), and probably down to a resolution of ~0.1 μm or ~100 nm (Section 4.7). If ***future research*** confirms that most or all surviving personal identity structures can be recovered using scans with ≥100 nm resolution for planning and executing the repairs, and if the patient received a "good" (i.e., thoroughly vitrified) cryopreservation, then revival may be successfully accomplished using the relatively less expensive and less complex method of **conventional cell repair** ("Plan A") as described in Chapter 4, which is entirely nondestructive[367] and only moderately invasive. This scenario should recover all of the connectome[368] and most of the synaptome[369] as well. Some researchers have tentatively assumed that the connectome may be sufficient to reconstruct individual identity and memory, although they acknowledge that the question of whether the connectome alone will provide sufficient information to enable revival remains open.[370]

On the other hand, if the identity, number, and location of structures smaller than 100 nanometers in size is determined to be essential for personal identity, and these structures are so damaged by cryopreservation that the repair process requires detailed knowledge of them to infer and restore the correct original state, then the conventional cell repair processes envisioned here ("Plan A") will likely not suffice and a fully invasive molecular scan and **molecular reconstruction** process ("Plan B") will be required for the revival

---

[366] de Wolf A. Cryonics as something else. Biostasis, 3 Dec 2009; https://www.biostasis.com/cryonics-as-something-else/.

[367] The simplest definition of "nondestructive" is "no part of the original was destroyed"; a dictionary definition is "no irreparable harm or damage was done". For further discussion, see Section 5.3.

[368] https://en.wikipedia.org/wiki/Connectome.

[369] The Mouse Brain Synaptome Atlas. University of Edinburgh, 2020; http://synaptome.genes2cognition.org/. Zhu F, Cizeron M, Qiu Z, Benavides-Piccione R, Kopanitsa MV, Skene NG, Koniaris B, DeFelipe J, Fransén E, Komiyama NH, Grant SGN. Architecture of the Mouse Brain Synaptome. Neuron. 2018 Aug 22;99(4):781-799; https://www.ncbi.nlm.nih.gov/pmc/articles/PMC6117470/. Curran OE, Qiu Z, Smith C, Grant SGN. A single-synapse resolution survey of PSD95-positive synapses in twenty human brain regions. Eur J Neurosci. 2020 Jun 3; https://www.researchgate.net/profile/Olimpia_Curran/publication/341885538_A_single-synapse_resolution_survey_of_PSD95-positive_synapses_in_twenty_human_brain_regions/links/5ef77c57299bf18816eaf868/A-single-synapse-resolution-survey-of-PSD95-positive-synapses-in-twenty-human-brain-regions.pdf.

[370] Phaedra C. Reconstructive Connectomics. Cryonics 2013 Jul;34(7):26-28; https://www.alcor.org/library/reconstructive-connectomics/.

of cryopreserved patients, as described in Chapter 5. This process may also be required in cases of extensive damage, very poor cryopreservation, or straight-freeze (Section 7.1.1). In these cases, as noted in Section 5.1, it may be useful to initially perform the scanning procedures described in Sections 4.1, 4.2, 4.3, 4.4, and 4.5, as this destroys no information and should permit a better assessment of the current physical state of the cryopreserved patient.

Either way, will it work? In a 1998 interview,[371] nanotechnology expert Eric Drexler responded as follows:

> "Somewhere in the back of our minds…we might ask, 'What about personal identity?' Here's where I think the standard medical model is excellent. Medical doctors never talk about personal identity that I've noticed. And likewise I don't hear educators talking about it, or bartenders, who give you mind-altering substances, talking about it. Brain surgeons certainly don't want to talk about it. Maybe they do a little bit on occasion, but it isn't a central conceptual issue in medicine. Rather the question is: the patient has come in the door, we do a procedure; can the patient get up and walk out, can the patient hold a job afterward, talk to friends and family? Have we damaged the patient's memory? Has the patient forgotten the last few days before the procedure? (With some procedures, or some accidents, certainly.) Does the patient remember his or her name? How much amnesia are we talking about in neurological cases? Ah, virtually none, or none detectable? Great!"
>
> "But that's the framework in which these things are discussed. So, will reanimation be successful? By medical criteria, yes. By more general functional criteria and so on, since physical health is not an issue with this kind of medical technology in place, the only remaining question is, are we talking about no amnesia or a little amnesia? And I think the answer there, in cases of suspensions performed using present techniques under good conditions as best I can judge from what I see in Greg Fahy's electron micrographs and discussions, and from what I understand from paying attention to the neurobiology literature for the last twenty years with this question in mind, is that: yes, we should be fine!"
>
> "The patient will not regard this as being a whole lot different from having been wheeled into a time machine, without any intervening freeze and repair process. I say that simply because of what the structure of memory seems to be, and what the nature of the perturbations caused by freezing seem to be. It's like asking, if you take a written page, and you rip it into four quarters and crumple it, and hand it to an art conservator, 'How many words will it forget?' Answer, 'None.' If it's a photograph, a half-tone photograph reproduction, you're probably going to lose a few half-tone dots, but I don't think anybody cares about a few half-tone dots in a page of print. Particularly since you can tell what the color was from either side in almost all cases. So, if one isn't concerned about learning something new, or forgetting the telephone number that you had when you were in dormitory in college, or the effect of a glass of wine, or the effects of living for the next five years – if those aren't terrifying things that you feel threaten your personal identity – then I basically would say, again premised on suspension under good conditions, forget the problem. Unless someone has something new to say that's negative, it's not a problem. I don't know any reason to think it's a problem, except the habit that people have of talking about it as though it is. The brain does not seem to be some delicate ethereal thing that evaporates when you chill it, or even freeze it."

---

[371] Cheney R. Cryonics Interview: Eric Drexler. Cryonics 1998 Qtr 3;19(3):32-39; https://www.alcor.org/docs/cryonics-magazine-1998-03.pdf.

2.2 Previously Proposed Technical Cryopreservation Revival Scenarios

This Section provides a list of all known prior technical proposals for cryopreservation revival,[372] along with an extensive extract from each.

Perhaps the earliest suggestion of human cryopreservation by a mainstream scientist was offered by John Hunter (1728-1793),[373] the prominent English surgeon and anatomist, who wrote[374] in 1778, years after he conducted his own fish-freezing experiments: "I had imagined that it might be possible to prolong life to any period by freezing a person in the frigid zone, as I thought all action and waste would cease until the body was thawed. I thought that if a man would give up the last ten years of his life to this kind of alternate oblivion and action, it might be prolonged to a thousand years: and by getting himself thawed every hundred years, he might learn what had happened during his frozen condition." Hunter's musings are not included in the list because his description does not quite rise to the level of a "technical proposal" – but it is interesting for its vintage, nevertheless.

Once the concept of using atomically precise nanomachinery and medical nanorobots to revive cryonics patients had been proposed in 1986 (Section 2.2.6), virtually all subsequent credible technical revival proposals have incorporated some form of nanomachinery or nanorobotics as a major part of their recommended procedures.

Culminating this tradition, in 2022, this book presents the first comprehensive conceptual protocol for revival from human cryopreservation, using medical nanorobotics (Chapter 1).

---

[372] Greg Fahy (personal communication, 30 Dec 2021) reports that he "put together a poster for a meeting of the Cryonics Societies of America, as hosted by the Cryonics Society of California, in Los Angeles, circa 1970, on revival using artificial enzymes such as 'membrane repairase' and 'DNA repairase' and 'membrane strengthenase' and I received an award for the contribution, as documented in Cryonics Reports. It was inspired by Barry Eldon's work on the aging of rat tail collagen and his comments about synthetic enzymes maybe being able to reverse it someday." Unfortunately, the poster was discarded and is now lost to history.

[373] https://en.wikipedia.org/wiki/John_Hunter_(surgeon).

[374] Palmer JF, ed. The Works of John Hunter, with Notes. Andesite Press, 2015, Vol. 1, p.284; https://books.google.com/books?id=OLgTAAAAQAAJ&pg=PA284. See also: https://www.amazon.com/Works-Hunter-Palmer-Illustr-Plates/dp/1297821742/.

2.2.1 Immortality Now (Cooper, 1962)

Evan Cooper[375] published the first cryonics book in 1962 under the pseudonym Nathan Duhring.[376] The work contained only the most general prescriptions for cryopreservation and revival, and Cooper's rambling writing style is not easy reading, but among his copious words[377] we can sense at least the earliest whiffs of a plan. Below are some extracts, slightly rearranged from the presentation order in the book to improve clarity.

> "The general theory of resurrection indicated that to recreate the individual identity the original pattern must be in existence in a form that has not deteriorated to any significant degree. Science can fill some of the lacunae, but the more there are to fill the more difficult the job and the less confidence that the copy is exactly representative of the original. So in short, it is desirable that the body be in the best possible condition by the time resuscitation methods are practical and reliable. The target date, let us say, rather hopefully, but arbitrarily chosen, is 2010."
>
> "[S]uppose you wish to be immortal but tomorrow you die from any one of a number of causes….This hypothetical person is dead, then. His relatives, or anyone concerned, finds that his wish is to hold his body in frozen storage. Thus, he is taken to the freezing plant as quickly as possible and entered for freezing….[I]n the case of an ordinary death the procedure is to get the body frozen as quickly as possible, relatively speaking, and then maintain that temperature with as little variation as possible….Then to make preservation still more perfect it would be best to have a coffin in which the air could be evacuated or removed as an inert gas is flooded in. An inert gas such as neon, krypton, argon, or helium inhibits any exchange of moisture or elements between the body and the environment provided the low temperature is maintained."
>
> "Now let us suppose that it is the year two thousand and something. It is the time when the processes of resuscitation and transmission have been practically achieved. For those in frozen storage, several avenues may open."

Cooper posits four possible methods for revival, which he calls "reanimation, transmission, replacement, or re-creation," and then describes each of them in somewhat sketchy terms:

(1) **Reanimation.** "The first avenue may be simple resuscitation. If you died of a heart attack, the heart may be repaired or replaced. For those who died of other causes, the problem of resuscitation or reanimation may be even less formidable….It is perhaps immensely difficult; much extension of the research done now will have to be accomplished, but what research has been done is quite hopeful and suggestive….It seems reasonable that within the next century research will show that first the smaller animals, just as is now true of certain small cellular structures, can be frozen for long periods of time and successfully resuscitated. Gradually it will be shown that more complex animals can be reanimated after being frozen for long periods of time….It seems reasonable that by sometime within the next century the

---

[375] It should be noted that Ev Cooper's efforts led to the formation of the Life Extension Society,[*] the first cryonics organization in the world, which unfortunately had ceased all activities by 1970.
[*] https://en.wikipedia.org/wiki/Life_Extension_Society.

[376] Duhring N. Immortality: Physically, Scientifically, Now. 20th Century Books, Washington DC, 1962; https://www.biostasis.com/pdfs/cooper_immortality.pdf.

[377] Reviewers cited in the Postscript said they found the book verbose. Cooper responds: "Some felt that the long disquisition on the machines and the more imaginative literature could have been trimmed. Perhaps they are right. But would we have the feeling we had written a book?"

researchers will have moved from golden hamsters, cats and dogs to successful resuscitation of men, even though they may have been frozen for considerable periods of time….Thus, we are assuming that resuscitation may be possible if they have a properly frozen body…. When it comes to human immortality it has been mentioned that if a person may die before the postulated breakthroughs of 2010, and he wishes to have his body stored, it is also wise to have as complete a record as is possible to aid the reanimation force. An encephalogram, encephalograph or brain print might just possibly be of some help."

(2) **Transmission.** "One alternative may be to be scanned...and transmitted into a more viable human body yet, maintaining his basic individual personal identity….A second alternative is to be transmitted from his body to a metallic and plastic body which might have many advantages. The basic advantage being that its structure is less susceptible to the aging processes that occur in the protoplasmic body as we know it…."

(3) **Replacement.** "In transplantation the spare parts must be gotten from somewhere: either growing them as might be envisioned in some brave new world laboratory or as now taking advantage of the death of other organisms…."

(4) **Re-Creation.** "Now let us consider in slightly greater detail the possibilities of the cybernetic method and some of its variations. The method implied by the ideas in Wiener's book might be called the transmitting re-creation method. A scanner goes over or through the individual picking up the pattern and transmitting it to any other point where the re-creation out of the same type of atoms is to take place. The degree of activity will be nil at anything above the molecular level and destroying the capacity for life in the tissue may not be of necessity depending on the capability of the scanning machine. This particular method would be a human to human, one to one relation between all of the atoms of the body, via the transmission device. In theory, it is excellent for storage and for transmission to distant points in time and space….Another possibility along this cybernetic line is the human to automaton….[I]f the scanner can pick up the pattern and re-create a duplicate individual it might even be easier and more advantageous to reconstruct the equivalent pattern in the frame of a unitary semi isolated mobile communication machine….In short, the pattern of the human may more easily be taped into the communication machine with its numerous structural advantages….The several apparent advantages are that putting the pattern into the machine is easier than re-creating another flesh and bone individual and the new metallic and plastic individual is then immortal, given minimal upkeep."

Amusingly, Cooper also proposed an idea which is gaining some currency among active cryonicists today:[378] "[I]n certain circumstances some individuals may wish to wear a minute radio transmitter which would continuously send body condition data to a central exchange or a mentamachine. In case of extreme danger or death rescue operations could begin without delay."

Cooper coined the classic cryonics slogan "Freeze-Wait-Reanimate" and published a newsletter[379] of mainly that title from Jan 1964 through Sep 1969.[380]

---

[378] "Alcor members requested a service to help monitor and improve response times for cases. Several monitoring services are available in the general market and some of them cost up to $50/month. Alcor extensively tested some of these services and formed a partnership to support an optional service that is now available exclusively for Alcor members." [*]
[*] Sarah Kelly, "Alcor Check-In Service Now Available," Alcor News, 19 Feb 2021; https://www.reddit.com/r/cryonics/comments/jycpwv/new_alcor_app_set_for_beta_testing_first_to/.

[379] https://www.biostasis.com/pdfs/freezewaitreanimate.pdf.

[380] During the first year of publication, through Dec 1964, the title was "Life Extension Society Newsletter", after which it became "Freeze-Wait-Reanimate". Perry M. The First Cryonics Newsletter. Biostasis, 19 Jan 2011; https://www.biostasis.com/the-first-cryonics-newsletter/.

2.2.2 Robot Surgeons of the Future (Ettinger, 1964)

In 1964, Robert Ettinger[381] published his landmark book, *The Prospect of Immortality*,[382] which claimed that future technological advances could be used to bring freeze-preserved people back to life, launching the field of cryonics.

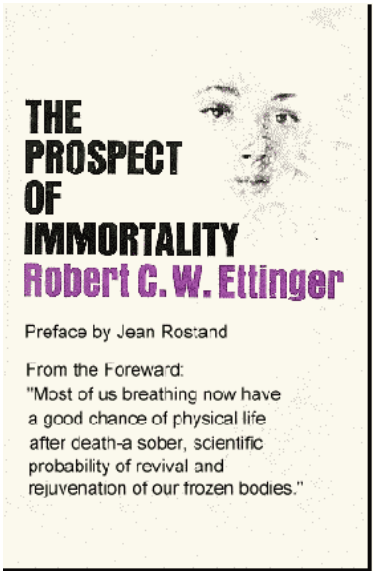

In the introduction to his book, Ettinger explains in general terms how this could occur:

"The robot surgeons of the future will have powers now only faintly foreshadowed, but beginnings have already been made in cell surgery. Individual cells have been successfully operated upon, e.g., transplanting nuclei into enucleated amoebae, even cross-species! Thus, if brute-force methods are necessary, it is not inconceivable that huge surgeon-machines, working twenty-four hours a day for decades or even centuries, will tenderly restore the frozen brains, cell by cell, or even molecule by molecule in critical areas. We hasten to add that in all likelihood the methods used will be much more elegant and yet unforeseen."

In the third chapter of his book, Ettinger provides a few more details, writing in an era that predates most of the science of genetic engineering and biotechnology, and long-predates all of the emerging modern discipline of nanotechnology:

> "[M]edical science should eventually be able to repair almost any damage to the human body, including freezing damage and senile debility or other cause of death….[W]e need only arrange to have our bodies, after we die, stored in suitable freezers against the time when science may be able to help us. No matter what kills us, whether old age or disease, and even if freezing techniques are still crude when we die, sooner or later our friends of the future should be equal to the task of reviving and curing us….We have investigated the proposition that a freshly dead body can be frozen, stored for a long time at low temperature, and thawed again without excessive damage….We need assurance that we can be revived, and not only that; if we die sick, we want to be made well; if we die broken, we want to be made whole…"
>
> "That future technicians will be able to repair and rejuvenate us cannot be proven, but it can be made convincing all the same….It is well known that hundreds of people have been revived after being clinically dead for many minutes, i.e., after heartbeat and breathing stopped. The people in the freezers – you and I – will have died mostly of disease or old age. The immediate cause of death will usually be the failure of some vital organ. The future medicos, then, will perhaps proceed somewhat as follows: first, either restore or provide respiration and circulation; next, repair or replace the defective organ that was the proximate cause of death; then cure any acute disease and make any other urgent repairs; lastly, and at leisure, make a general overhaul and rejuvenation."

---

[381] https://en.wikipedia.org/wiki/Robert_Ettinger.

[382] Ettinger RCW. The Prospect of Immortality. Doubleday, 1964; https://www.cryonics.org/images/uploads/misc/Prospect_Book.pdf.

> "The first stage, the restoration and support of life while biological repairs are being made, will demand the use of mechanical devices, some of which are already well known….Artificial organs and limbs will be used if natural repairs or replacements cannot be had; and they will probably be used again in the more distant future when they become so efficient that they are to be preferred over the biological….[T]he more urgent repairs will be made while the resuscitee is still unconscious, with new organs or tissues either grown in the lab and implanted or else gradually regenerated in the body. After this has been done he will be alive, and in much better health than just before he died….There seems a good chance that the supra-molecular circuitry can be read well enough after freezing. Hence it may well be that only a small percentage of the brain cells need escape with little damage; this may be enough for reasonably faithful reconstruction of the brain with freshly generated tissue."
>
> "When our resuscitee emerges from the hospital he may be a crazy quilt of patchwork. His internal organs – heart, lungs, liver, kidneys, stomach, and all the rest – may be grafts, implanted after being grown in the laboratory from someone else's donor cells. His arms and legs may be bloodless artifacts of fabric, metal and plastic, directed by his own will and complete with sense of touch but extended and flexed by tiny motors. His brain cells may be mostly new, regenerated from the few which could be saved, and some of his memories and personality traits may have had to be imprinted on or into the new cells by microtechniques of chemistry and physics, after being ascertained from the written records."

More than a decade later,[383] in 1976, Ettinger founded the Cryonics Institute,[384] one of the two major cryonics membership organizations in existence today that performs human cryopreservation and safeguards human patients in cryogenic storage. (Alcor Life Extension Foundation,[385] the other major cryonics organization, was founded four years earlier, in 1972.) In 1979 Ettinger published a call-to-arms for science fiction readers to join the cryonics effort,[386] describing the revival process only vaguely, as follows: "Medical progress will continue. Eventually, we may learn how to repair even serious freezing damage and major injuries, and how to cure all diseases, including senile debility….At best, the patient will awaken one day, as after a moment of sleep without dreams, and then…the science fiction writers should take it from there…" At that time, the earliest writings describing nanotechnology still lay 7 years in his future (Section 2.2.6), a new technical approach of which he ultimately took notice.[387]

---

[383] On page 59 of his follow-up book *Man Into Superman* (1972),[*] Ettinger proposed an idea in which a person's natural brain is maintained at a very secure location and communicates with the rest of the person in the (more dangerous) outside world: "One can go even beyond this to the concept of "extended bodies." The brain need not necessarily be mobile; in fact, it might be better protected and served if fixed at home base. The sensors and effectors-eyes, hands, etc-could be far away, and even widely scattered, with communication by appropriate signals (not necessarily radio)....He can have a variety of remote-control bodies-either organic, or mechanical, or a combination-and he can control and experience these bodies in exactly the same subjective way we control and experience our bodies....We cannot easily imagine what it would be like to enjoy such numerous and scattered limbs and organs..."

[*] http://www.cryonics.org/images/uploads/misc/ManIntoSuperman.pdf.

[384] https://en.wikipedia.org/wiki/Cryonics_Institute.

[385] https://en.wikipedia.org/wiki/Alcor_Life_Extension_Foundation.

[386] RCW Ettinger. A matter of life and death. Analog Sci Fiction Sci Fact. 1979 Jun;99(6):67-75; https://pubmed.ncbi.nlm.nih.gov/11661782/.

[387] Robert Ettinger, "Nanotechnology and Cryonics: An Introduction," apparently written sometime in the mid-1990s; https://www.cryonics.org/resources/nanotechnology-and-cryonics-an-introduction.

In a 1995 interview,[388] when asked if he would change his 1964 description of the proposed revival process, Robert Ettinger said: "I did make a goof in saying that although we expected giant machines that would be able to make repairs on a cell-by-cell or even a molecule-by-molecule basis. For some reason I assumed that the various aspects of the machinery other than the actual working parts would have to be rather large in order to accommodate all the computation. Of course I was wrong about all of that. In view of the work of Drexler and many others – especially in view of the many advances in electronics and computing – it turns out that the supporting machinery as well as the working parts will probably be very small."

2.2.3 Viral-Induced Repair (White, 1969)

In 1969, Jerome White advanced the first specific proposal[389] for the molecular repair of brain damage, "whatever its origin." White proposed the use of artificial viruses to direct specific repairs of damaged neurons under normothermic (~37 °C) conditions: "An organic cell is a self-repairing automaton, but if environmental interference exceeds a certain limit, damage will become total. Freezing can be used to halt progressive damage along with all metabolism, but means are required to restore or augment the cellular genetic control program, or enrich the environment to enhance repair ability. It has been proposed that appropriate genetic information be introduced by means of artificially constructed virus particles into a congenitally defective cell for remedy; similar means may be used for the more general case of repair."

According to the abstract of the paper, describing these microscopic repair machines: "An organic cell, as an automaton, derives energy from the metabolism of its own constituents for self-maintenance under the guidance of its genetic control program, which will not function properly if damaged or if a certain level of environmental deprivation or interference is exceeded; if allowed to proceed, such conditions lead to complete degradation. Although they increment it, methods exist for virtually halting such deterioration by stopping all biochemical processes; other means will be required to restore or augment a control program, or enrich the environment to enhance repair ability. It has been proposed that appropriate genetic information be introduced by means of artificially constructed virus particles into a congenitally defective cell for remedy; similar means may be used for the repair of more general cell damage exceeding the functional limit. Progress is being made in relevant areas such as virus/cell specificity, temperature-sensitive viral mutants, identification of RNA and DNA codon sequences, *in vitro* DNA synthesis, viral disassembly and assembly, and metabolic pathway determination. Further work is needed also in isolation of viral capsid programs, specific cell function subprograms, metabolic repair pathways, identification of enriching nutrients, replication of repair virions, infection methods, and quality control. *In situ*, the repair program must use means such as protein synthesis and metabolic pathways to diagnose and repair any damage. Applied to brain neurons, this may destroy long-term information content, which appears to be stored ultimately in molecular form, often proposed to be in a feedback cycle involving mRNA and protein synthesis. This information can be preserved by specifying that the repair program incorporate appropriate RNA tapes into itself upon entry and release them on termination of repair. This method of cell repair is applicable to many forms of brain damage and may be used as a research tool in investigating metabolic processes as well as information content and storage."

---

[388] Ryan D. The Prophet of Immortality: Derek Ryan interviews Robert Ettinger. Cryonics 1995 Qtr 3;16(3):12-17; https://www.alcor.org/docs/cryonics-magazine-1995-03.pdf.

[389] White JB. Viral-Induced Repair of Damaged Neurons with Preservation of Long-Term information Content. Paper presented to the Second Annual Conference of the Cryonic Societies of America, University of Michigan at Ann Arbor, 11-12 Apr 1969; http://alcor.org/Library/pdfs/White1969.pdf. See also: Jerome B. White. Viral-Induced Repair of Damaged Neurons with Preservation of Long-Term information Content. Cryonics 2014 Oct;35(10):8-17; https://www.alcor.org/docs/cryonics-magazine-2014-10.pdf.

White clearly realizes that his method – an early form of modern-day synthetic biology,[390] programmable bacteria[391] and engineered viruses[392] – can only be applied to reliquidified neural tissue, not to frozen or vitrified tissue, and that the repair processes his artificial viruses would stimulate must contend with a wide variety of structural and functional pathologies, including "freezing" (Section 3.4) and "thawing" (Section 3.6) damage, which can be quite severe: "The general method outlined here has its obvious use in the repair of nervous tissues especially human. Repair of all types of damage – caused by factors mechanical, chemical, pathological, aging, freezing, thawing, and so on – is intended." White also does not explain how his method would work if the cells, once having been warmed to the liquid state in heavily damaged condition, had become nonfunctional, which would likely forestall reparative molecular synthesis by now-moribund biocellular machinery, saying only that "similar means may be used for the repair of more general cell damage exceeding the functional limit."

In his review[393] of White's early proposal, Aschwin de Wolf similarly notes the difficulties: "Modifying a virus to change genes is one thing, but rebuilding damaged cell membranes and intracellular organelles is another and it is not fully clear how a virus can be modified to accomplish this. An even bigger challenge for biological repair is temperature limitations. This would seem to require that we first thaw the patient before conducting repairs. In the case of frozen patients, the ice will turn to water again and (damaged) biomolecules that were locked into place could dissolve into solution (which may constitute irreversible loss of identity-critical information). In the case of vitrified patients, ice nuclei that formed during the descent to cold temperatures (or continued forming during intermediate temperature storage) can organize themselves into ice during thawing. Another problem with conducting repairs after thawing is that ischemia will be permitted to continue, causing more damage."

These difficulties might not entirely close the door on biological approaches to cryostasis revival of patients perfused with future improved cryoprotectants, says de Wolf: "We can imagine breakthroughs in cryoprotectant design that reconcile negligible toxicity with extreme resistance to ice formation. Patients cryopreserved with such agents could be thawed without risk of ice damage. When temperatures are raised to a point where meaningful enzymatic activity is possible, various biological strategies (metabolic inhibition, reversible fixation) could be used to allow time for repairs. Another idea is to pursue a hybrid strategy in which (crude) nano-size mechanical machines are used to access and open the circulatory system while disrupting nucleation and/or delivering anti-nucleating molecules. After completing this task at cryogenic temperatures, the patient can be thawed and biological cell repair technologies introduced." (But see additional comments on the prospects for biological approaches in Section 4.17.)

---

[390] https://en.wikipedia.org/wiki/Synthetic_biology#Synthetic_life.

[391] Kotula JW, Kerns SJ, Shaket LA, Siraj L, Collins JJ, Way JC, Silver PA. Programmable bacteria detect and record an environmental signal in the mammalian gut. Proc Natl Acad Sci U S A. 2014 Apr 1;111(13):4838-43; https://www.ncbi.nlm.nih.gov/pmc/articles/PMC3977281/. Lammens EM, Nikel PI, Lavigne R. Exploring the synthetic biology potential of bacteriophages for engineering non-model bacteria. Nat Commun. 2020 Oct 20;11(1):5294; https://www.ncbi.nlm.nih.gov/pmc/articles/PMC7576135/.

[392] Lemire S, Yehl KM, Lu TK. Phage-Based Applications in Synthetic Biology. Annu Rev Virol. 2018 Sep 29;5(1):453-476; https://www.ncbi.nlm.nih.gov/pmc/articles/pmid/30001182/.

[393] de Wolf A. Biological Repair Technologies. Cryonics 2014 Oct;35(10):5-6; https://www.alcor.org/docs/cryonics-magazine-2014-10.pdf.

2.2.4 Anabolocytes: Artificial White Cells for Cryoinjury Repair (Darwin, 1977)

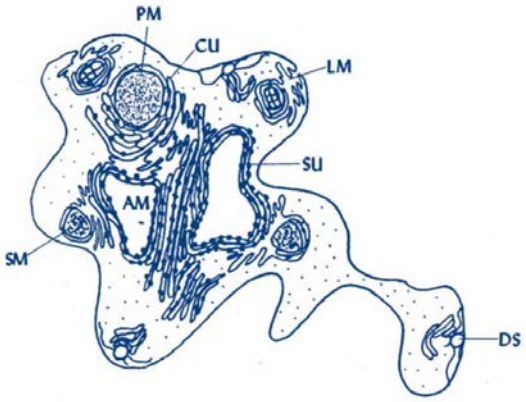

In 1977, Michael Darwin proposed using bioengineered white cells to take apart and reconstruct damaged tissue cells.[394] These artificial leukocytes, called "anabolocytes" (image, right), consist of various artificial intracellular organelles. The Program Module (PM) is the equivalent of the nucleus, responsible for directing anabolocyte activities from targeting through completion of the repair sequence. The Synthesis Unit (SU) fabricates new replacement organelles for the damaged originals. The Storage Module (SM) contains high-energy-compound reserves and necessary raw materials that are not available on-site. The Conduit Unit (CU) brings newly-assembled macromolecules or building blocks to the Synthesis Unit. The sensing (DS) and proteolysis (LM) units are used to vector the anabolocyte and to decompose damaged cell components for raw materials.

"If we start with something like a normal white blood cell and assume it could be modified in most any way, we could build an ultra-miniature, self-reduplicating repair unit. White cells are particularly good candidates for this type of transformation because they already embody several of the properties we are seeking. They have the capacity to move through the capillary walls to reach sites of injury and/or infection, they are compatible with human physiology, and perhaps more importantly, they have some (although very limited) capacity for attaching themselves to damaged or malignant cells to either repair them or donate a lysosome and destroy them. If we could modify white blood cells in any fashion, they could be used to crawl through the capillaries, seek out damaged cells (perhaps by following a 'track' of lysosomal enzymes which are related to cryoinjury) and initiate a repair sequence."

In the drawings below, the anabolocyte squeezes between two endothelial cells on a capillary wall and enters the extravascular space via diapedesis (image below, left), then attaches itself to a cell that has undergone catastrophic damage due to ischemia, freezing, and thawing (image below, right).

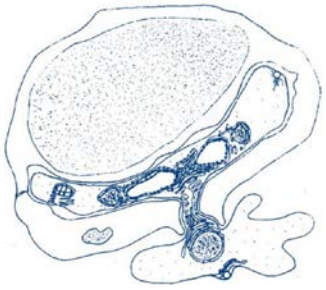

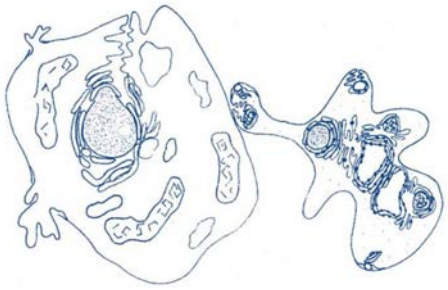

[394] Darwin M. The Anabolocyte: A Biological Approach to Repairing Cryoinjury. Life Extension Magazine, Jul/Aug 1977, pp. 80-83; http://www.alcor.org/Library/pdfs/anabolocyte.pdf or https://issuu.com/alcorlife/docs/cryonics-magazine-2008-4/16. Reprinted in: https://www.alcor.org/docs/cryonics-magazine-2008-04.pdf.

The anabolocyte opens the cell membrane and appropriates nuclear information (image A, below), pours out proteolytic enzymes to digest the old damaged structures (image B, below), begins fabricating a new cell by elaborating new structure into the Synthesis Module (image C, below), then completes a new operational cell identical to the original (image D, below). However, the anabolocyte is only designed to work "at high subzero temperatures (say, -15 °C or -20 °C) in the presence of some inert antifreeze agent such as one of the silicon based glycols," so it cannot be used for tissue repair work until the cryopreserved patient has been reliquidified from the solid (cryogenic) state.

Thirty years later, Darwin offered his perspective on how the anabolocyte concept came to be.[395]

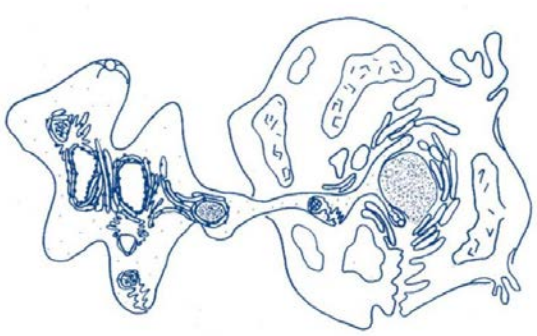

(A)

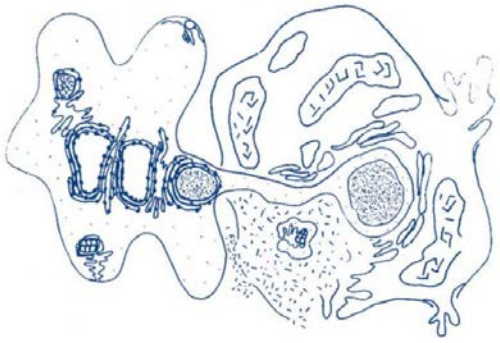

(B)

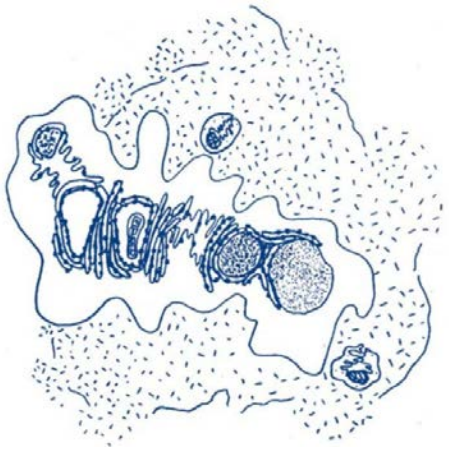

(C)

(D)

[395] Darwin M. Reflections on the Birth of the Anabolocyte. Cryonics 2008 Qtr 4;29(4):18; https://www.alcor.org/docs/cryonics-magazine-2008-04.pdf.

2.2.5 Artificial Macrophages, Repair Nets, and the Chrysalis (Donaldson, 1981, 1988)

In 1977, Thomas Donaldson privately circulated the idea of artificial macrophages and repair nets to conduct molecular repair of biological structures, which was finally published in 1981.[396] In 1988, Donaldson published a further elaboration of the repair net concept,[397] which he called the chrysalis.

According to Donaldson: "**Artificial macrophages** could pass through and between cells, reaching any body tissues. They could deliver genes or chemicals, take control of their target cells' metabolism, or even replace target cells entirely by budding off a new copy. Normal macrophages use the bloodstream for transport. Artificial macrophages could use the bloodstream too. Artificial macrophages will be able to communicate with one another. They could release diffusible chemicals to guide one another's behavior. Based on what one set found in the retina, for instance, others could carry out special modifications in the visual cortex. These devices could form an integrated repair system much larger than a single macrophage."

"Some repairs will need delivery of materials to a repair site much faster than the circulatory system provides. We'll need devices to grow their own support tissues into a patient. For instance, severe crushing or mangling injuries will require us to provide a new vascular system. The repair device might resemble a fungus, growing mycelia into the injured tissue. The mycelia would grow between existing cells rather than destroying any. We can call such devices **repair nets**. A repair net will work together with a whole family of macrophages. For instance, the macrophages could reach their target through the mycelia of the net."

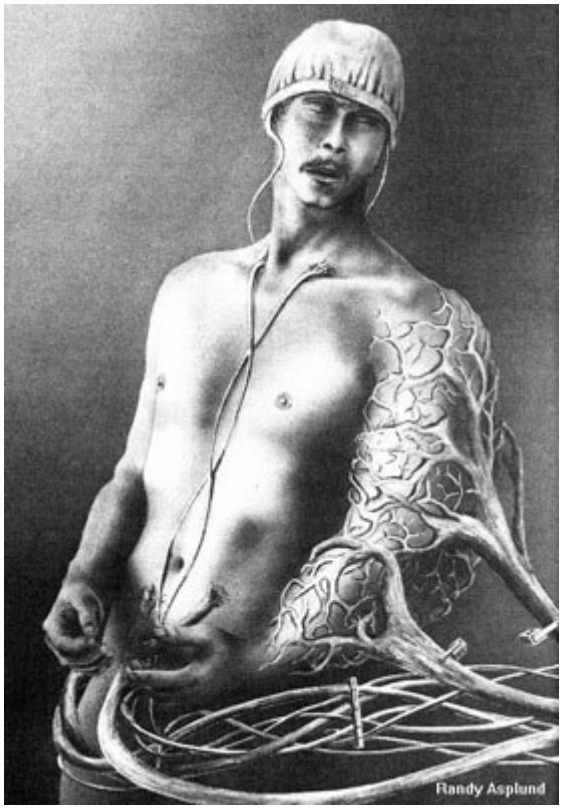

"We can therefore expect devices which would enfold a patient completely and carry out repair. We have a model for such devices already; the womb. It supports the infant by externally supplying blood and oxygen and removing wastes. But such a device would have even greater power to control growth and development of the patient inside it. It would take over from the patient's own genes, controlling growth according to the patient's own genetic program. Such a repair device would have a brain, to manage its control and maintain homeostasis. It could take apart a patient's entire body cell by cell, rework it into something new, and return the cells to their original location. I will call such a device a **chrysalis**."

"Chrysalises, repair nets, and macrophages are types

---

[396] Donaldson T. How Will They Bring Us Back, 200 Years From Now? The Immortalist 1981 Mar;12:5-10.

[397] Donaldson T. 24th Century Medicine. Analog Sci Fiction Sci Fact. 1988 Sep;108:64-80; http://www.alcor.org/Library/html/24thcenturymedicine.html.

of machines. They would have many specialized forms for different jobs. They would have programmability. Some would be adapted to replacing only particular organs. Some repair nets could force rapid wound repair. A broken bone, for instance, would be set inside a repair net bandage. This would grow into the tissue, controlling and promoting repair. Others would be adapted to reworking and repairing nervous tissue. Some chrysalises would specialize in reviving 'dead' tissue, such as severed limbs. These would be reattached after revival by another chrysalis."

"A chrysalis would first envelop the patient, then send tendrils of itself in between all of his cells. It disassembles the patient, surrounding each cell with its own repair machinery and vascular system. The disassembly process carefully preserves information about locations of the patient's cells and their relationships to each other. If necessary, though, morphogen chemical gradients could also retain this information. A patient would swell up to ten times his original volume. After repair, the chrysalis slowly withdraws the same way it entered re-establishing normal cell-to-cell relationships."

"Many current conditions of injury, including cryonic suspension, are very simple compared to problems for which chrysalises are needed. They probably won't need more than macrophages and nets for repair."

2.2.6 Cryonics Revival using Nanomachinery (Drexler, 1986)

While careful to avoid any explicit mention of cryonics so as not to offend mainstream scientific sensibilities, K. Eric Drexler first wrote of the possibility of using molecular nanotechnology for the repair of freezing damage to biological tissues and cells in his seminal 1981 paper[398] on molecular engineering:

> [M]olecular devices can characterize a frozen cell in essentially arbitrary detail by removal and characterization of successive layers of material (atomically thin layers, if desired). Although the amount of data involved is large (a typical cell contains billions of protein molecules), the physical bulk of a device able to store and manipulate this amount of data will be quite small.
>
> Such procedures would have special utility in analyzing the structure of tissue in the brain. Unlike, say, muscle or liver tissue, the function of brain tissue depends on the detailed three-dimensional structure of intertwined cells and their interfaces. The freezing process is far too slow to stop such dynamic processes as action potentials and synaptic transmission; short-term memory, however, is suspected to involve chemical modification of the neurons, and long-term memory is believed to involve the growth and modification of neuronal structures, particularly synapses. At the modest freezing rates possible in substantial pieces of tissue, ice crystals may be expected to nucleate and grow in the intercellular fluid, displacing the cell membranes as they do so. Electron micrographs, however, show that synapses (like many intercellular junctions) involve complementary structures on both sides of the intercellular gap, which should provide information enough to reconstruct the pre-freezing configurations of the cells almost regardless of ice crystal locations.
>
> The ability to reconstruct the prefreezing structure of tissue, when combined with the general synthetic capabilities outlined above, will make feasible the physical restoration of tissue damaged by ordinary freezing through characterization, reconstruction, and restoration of successive segments of frozen material. Although restored to a frozen condition, such tissue would lack the

---

[398] Drexler KE. Molecular engineering: An approach to the development of general capabilities for molecular manipulation. Proc Natl Acad Sci USA 1981 Sep;78(9):5275-5278; https://www.pnas.org/content/pnas/78/9/5275.full.pdf.

> characteristic damage caused by the freezing process. As many tissues can survive the gross insult of ordinary freezing, it seems likely that most could survive freezing followed by repair.
>
> [T]he eventual development of the ability to repair freezing damage (and to circumvent cold damage during thawing) has consequences for the preservation of biological materials today, provided a sufficiently long-range perspective is taken.

In 1986, Drexler published the first conceptual proposal for applying future molecular nanotechnology specifically to cryonics revival.[399] Virtually all credible revival proposals that have been advanced since 1986 have included some type of nanomachinery, nanorobotics, or other form of nanotechnology.

To reverse cryogenic biostasis, Drexler described the following procedure:

> "In the first stage of preparation, the patient lies in a tank of liquid nitrogen surrounded by equipment. Glassy protectant still locks each cell's molecular machinery in a firm embrace. This protectant must be removed, but simple warming might allow some cell structures to move about prematurely."
>
> "Surgical devices designed for use at low temperatures reach through the liquid nitrogen to the patient's chest. There they remove solid plugs of tissue to open access to major arteries and veins. An army of nanomachines equipped for removing protectant moves through these openings, clearing first the major blood vessels and then the capillaries. This opens paths throughout the normally active tissues of the patient's body. The larger surgical machines then attach tubes to the chest and pump fluid through the circulatory system. The fluid washes out the initial protectant-removal machines (later, it supplies materials to repair machines and carries away waste heat)."
>
> "Now the machines pump in a milky fluid containing trillions of devices that enter cells and remove the glassy protectant, molecule by molecule. They replace it with a temporary molecular scaffolding that leaves ample room for repair machines to work. As these protectant-removal machines uncover biomolecules, including the structural and mechanical components of the cells, they bind them to the scaffolding with temporary cross-links. (If the patient had also been treated with a cross-linking fixative, these cross-links would now be removed and replaced with the temporary links.) When molecules must be moved aside, the machines label them for proper replacement. Like other advanced cell repair machines, these devices work under the direction of on-site nanocomputers."
>
> "When they finish, the low-temperature machines withdraw. Through a series of gradual changes in composition and temperature, a water-based solution replaces the earlier cryogenic fluid and the patient warms to above the freezing point. Cell repair machines are pumped through the blood vessels and enter the cells. Repairs commence."
>
> "Small devices examine molecules and report their structures and positions to a larger computer within the cell. The computer identifies the molecules, directs any needed molecular repairs, and identifies cell structures from molecular patterns. Where damage has displaced structures in a cell, the computer directs the repair devices to restore the molecules to their proper arrangement, using temporary cross-links as needed. Meanwhile, the patient's arteries are cleared and the heart muscle, damaged years earlier, is repaired."

---

[399] Drexler KE. Engines of Creation: The Coming Era of Nanotechnology, Anchor Press/Doubleday, New York, 1986, pp. 133-138; https://web.archive.org/web/20060615004725/http://e-drexler.com/d/06/00/EOC/EOC_Chapter_9.html. This work was preceded by a privately-circulated analysis performed by Drexler titled "Cell Repair Machines and Tissue Reconstruction: Some notes on computational complexity and physical constraints" in 1984.

"Finally, the molecular machinery of the cells has been restored to working order, and coarser repairs have corrected damaged patterns of cells to restore tissues and organs to a healthy condition. The scaffolding is then removed from the cells, together with most of the temporary cross-links and much of the repair machinery. Most of each cell's active molecules remain blocked, though, to prevent premature, unbalanced activity."

"Outside the body, the repair system has grown fresh blood from the patient's own cells. It now transfuses this blood to refill the circulatory system, and acts as a temporary artificial heart. The remaining devices in each cell now adjust the concentration of salts, sugars, ATP, and other small molecules, largely by selectively unblocking each cell's own nanomachinery. With further unblocking, metabolism resumes step by step; the heart muscle is finally unblocked on the verge of contraction. Heartbeat resumes, and the patient emerges into a state of anesthesia. While the attending physicians check that all is going well, the repair system closes the opening in the chest, joining tissue to tissue without a stitch or a scar. The remaining devices in the cells disassemble one another into harmless waste or nutrient molecules."

2.2.7 Cell Repair Nanorobots (Wowk, 1988)

After writing a more general article on nanotechnology earlier in the year,[400] in 1988 Brian Wowk published a conceptual description of a generic cell repair nanorobot (image, below) that could be used for cryonics revival.[401]

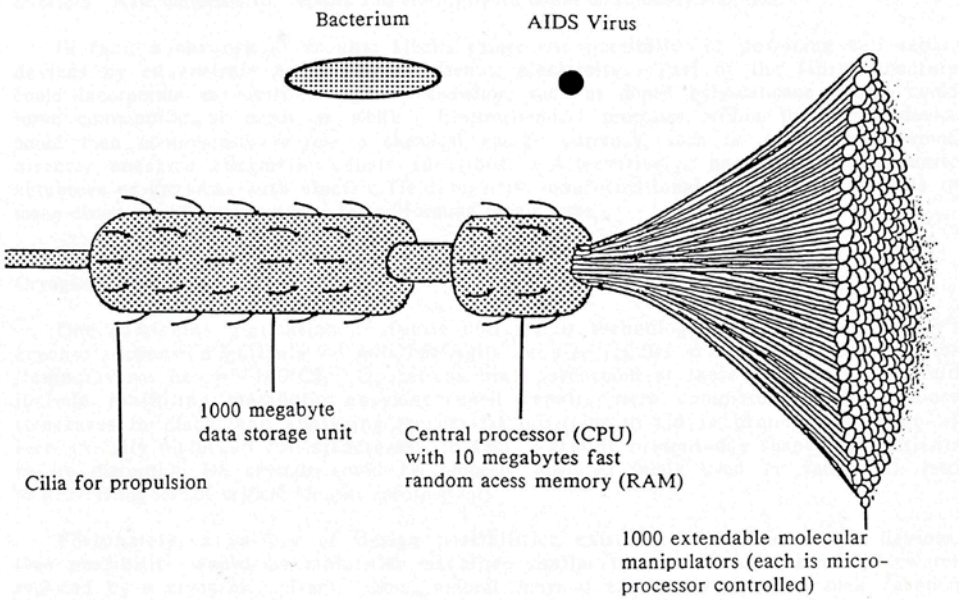

[400] Wowk B. Nanotechnology. Cryonics 1988 May;9(5):24-38; https://www.alcor.org/docs/cryonics-magazine-1988-05.txt. "Reversal of cryonic suspension will require a highly sophisticated future technology."

[401] Wowk. B. Cell repair technology. Cryonics 1988 Jul;9(7):21-29; https://www.alcor.org/library/cell-repair-technology/.

Writes Wowk: "Cells maintain themselves using a variety of molecular machines (machines constructed to molecular specifications), including enzymes for fine operations and cytoskeletal structures for grosser manipulations. Nanotechnology will allow us to build any of these molecular machines (and more), and to assemble them in ways not seen in nature – ways that achieve complex medical objectives. Among these objectives will be sophisticated cell repair."

"The development of nanotechnological cell repair systems can, in part, be viewed as the creation of artificial microorganisms for medical purposes. (Indeed, experimental usage of modified retroviruses for gene therapy today is a kind of cell repair technology.) It therefore follows that appropriately designed medical microbes, or cell repair devices, could at a minimum do anything that natural cells and their components are known to do today."

"[E]very basic capability required for a sophisticated cell repair technology is already demonstrated in nature. Molecular tools already exist (and undoubtedly others are possible) that could be implemented in future medical devices to allow controlled disassembly, analysis, and repair of cell structures at the molecular level. It remains for advancing molecular technology (which at a highly advanced point will become true nanotechnology) to integrate these tools into microscopic devices capable of advanced medical functions."

"Many repair tasks (especially ones as extensive as cryoinjury repair) will require communications between widely distributed devices both within and outside of cells. Rather than lugging a cubic micron nanocomputer all over a cell to perform repairs, for example, it would seem simpler to have the computer supervise the operation of many smaller devices from a central location in the cell. As well as providing a means for coordinating repairs within the body, it should also be noted that these communications channels could be used to transfer data processing tasks to computers outside the body. This might be useful in instances of extremely severe brain injury (such as a day of ischemia), when inferring the correct pre-injury state becomes a problem too complicated for *in-situ* computers. A communications system consisting of just one gigabaud channel per cell could, for example, transmit a complete atom-by-atom description of a biostatic brain (assuming one byte per atom) to external computers in less than a month."

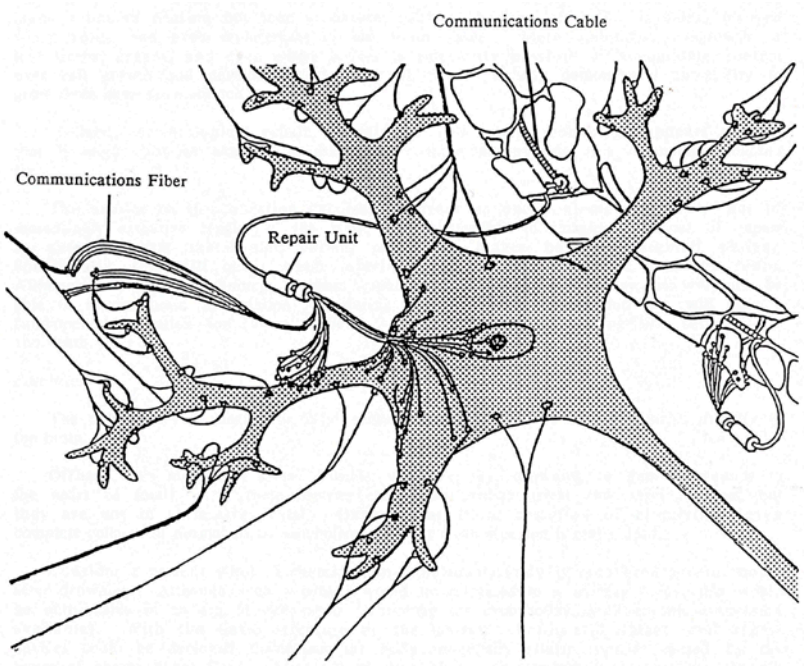

"One particular application of future cell repair technology – recovery of today's cryonic suspension patients – will optimally require repairs at cryogenic temperatures (temperatures below -100 °C). Operations best performed at these temperatures would include inhibiting metabolic enzymes (until repairs were completed), locking loose structures in place, and analyzing ice crystal positions to aid in proper restoration of mechanically disturbed cell structures. In fact, warming present-day suspension patients before disruptive ice crystals could be properly analyzed might even be fatal (i.e., lead to irreversible loss of critical identity information)."

"Fortunately, a variety of design possibilities exist for cryogenic repair devices. One possibility would be molecular machines similar to natural cells, but with water replaced by a cryogenic solvent. Of course, regardless of how they operate internally, repair devices will have to make chemical changes to tissues they

are repairing. Yet even this does not require high temperatures in the ordinary sense. Molecular tools driven by electrical (or low-temperature chemical) actuators could provide localized kinetic energy for forming or breaking chemical bonds. Indeed, by suitably "banging" or "grabbing" target molecules it is possible to create effectively any "temperature" at a single reaction site. Thus a fairly wide range of biological repair processes could in principle be carried out at cryogenic temperatures."

2.2.8 Nanorobotic Brain Repair with Biological Body Growth (Darwin, 1988)

Later in 1988, Michael Darwin wrote a "speculative exploration" of how revival might be carried out on patients who were cryopreserved using 1980s-era cryonics procedures.[402] Expecting much improved procedures to be developed, Darwin noted that "[p]atients cryopreserved today with modern vitrification methods under good conditions will require less extensive repairs than described here." The nanorobotic revival process would unfold as follows:

"The patient from the 1980s is removed from the icy vault that has held him for over a century. Slowly his temperature is raised to -130 °C [143 K], and his head is separated from the rest of his aged, diseased body with a high speed surgical saw and transferred to the fluid-filled receiving chamber of the revival unit. The fluid in the receiving chamber is tetrafluoromethane; a compound which is liquid even at -130 °C.[403] The revival unit [is] a combination of living creature and inorganic machine. An Artificial Intelligence, its 'brain' contains the sum of all human medical knowledge, which it keeps updated with its link to the worldwide medical information net."

"Connections are established between the patient's neck and the revival unit. Repairs begin. Countless millions of microscopic devices designed to operate at low temperatures begin to clear out ice from the patient's blood vessels. As they proceed, they assemble behind them fine fibers of electrically conductive polyacetylene which supply power to the ice removal devices. Later these fibers will serve as communications links as well."

"Once the circulatory system of the patient is free of ice, billions of nanocomputers (cell-sized computers) are moved into strategic positions along the network of conducting fibers. These interconnected computers will coordinate both short-range and long-range repair activities (such as repair of gross fractures). All these processes are carried out sufficiently slowly so that the patient's temperature does not rise significantly above -130 °C [143 K]: the tissues beyond his blood vessels remain virtually unchanged from the time of his suspension."

"New, more sophisticated devices, are introduced. Capillary walls are partially disassembled, and the devices begin to enter the inter-cellular spaces of the brain. These devices also remove ice, but much more carefully than the earlier ones. As ice crystals are disassembled at the molecular level, information concerning their position and orientation is transmitted back to supervising nanocomputers waiting in nearby blood vessels. When biological structures such as cell membranes or dendrite debris are encountered, they are carefully examined and tagged with special identifying molecules, and anchored to

---

[402] Darwin M. Resuscitation: A Speculative Scenario for Recovery. Cryonics 1988 Jul;9(7):33-37; https://www.alcor.org/library/resuscitation-a-speculative-scenario-for-recovery/.

[403] The boiling point of tetrafluoromethane is 145.3 K; https://en.wikipedia.org/wiki/Carbon_tetrafluoride.

nearby cells if necessary. Their original position is also relayed back to the supervising computers and to the revival unit."

"A week has now passed. Virtually all the ice has been removed from the patient's brain, and cryogenic fluid now freely circulates throughout the extracellular environment. The patient's temperature is now raised[404] until the contents of his cells become a thick liquid (at about -100 °C [173 K]). Devices for the first time begin to enter cell interiors. Their purpose is to lock up metabolic machinery to prevent premature, uncoupled activity. Enzymes are physically bonded to cell structures, and their active sites are blocked by specially fabricated molecules until repairs are completed."

"Once cell interiors have been adequately stabilized, the tetrafluoromethane is replaced with another solvent, and the patient's temperature is raised above the freezing point of water. Trillions of repair devices are now deployed. In sizes ranging from that of large molecules to small cells, the devices take up strategic positions both inside and outside cells. Among these devices are nanocomputers which will now supervise repairs from inside cells."

"With the repair system now in essentially complete control of the patient's brain, the most sophisticated operations begin. Small devices examine molecules and report their structures to larger controlling devices. Molecular damage due to oxygen and nutrient starvation (ischemia), freezing, and even aging is repaired by nanocomputer-directed repair enzymes. Independent DNA copies are obtained from many different cells, and DNA in these cells is restored to the damage-free sequence of youth inferred by nanocomputer comparison. As repairs proceed, virtually no cellular defects escape the detection and correction of the repair system."

"While repairs proceed inside cells, disrupted external structures are restored on the basis [of] information obtained during the ice removal process. Torn membranes are mended, disrupted cell connections restored, and gross fractures are repaired by microscopic surgeons which operate at a level a million times finer and more sophisticated than surgeons today. Where cells have been lost due to aging or other injury, new ones are fabricated and proper connections made. Gradually, over the course of several months, the patient's brain is restored to a healthy state."

"As repairs near completion, larger devices are removed, capillary membranes are repaired, and the network of nanocomputers and communications fibers is disassembled. A blood supply grown from the patient's own cells by the revival unit now begins to circulate, and the temperature is stabilized at 37 °C [98.5 °F]. Cell metabolism is restarted by selective unblocking of enzymes inhibited during the repair process, although consciousness is still suppressed by circulating chemicals which inhibit critical steps in nerve cell metabolism. The patient – an exposed pearly white brain floating within the womb of the revival unit – is now ready for the final phase of the revival process."

"On the surface of his brain a single cell begins to divide. Unlike the cancer which threatened the patient's life, the division of this cell is orderly and planned to restore life. A layer of dividing cells covers the restored but unconscious brain. The cells begin to differentiate, and slowly, like a newly conceived child, a

---

[404] Since the liquid range of tetrafluoromethane is 89.5 K – 145.3 K (-183.6 °C to -127.8 °C),[*] raising the temperature in the manner described will promptly vaporize the fluid unless ambient pressure is significantly raised. However, as temperature rises the CF_4 could be progressively replaced with perfluorocarbons having higher molecular weight, all of which will have the desirable characteristic of being immiscible in both fats and water. More complex fluorocarbons such as FC-87[†] manufactured by 3M remain liquid from -115 °C up to +30 °C; one issued U.S. patent[‡] describes a mixture of FC-77 and FC-87 that remains liquid from -140 °C up to room temperature.

[*] https://en.wikipedia.org/wiki/Carbon_tetrafluoride.

[†] https://multimedia.3m.com/mws/media/64896O/fluorinert-electronic-liquid-fc-87.pdf?&fn=prodinfo_FC87.pdf.

[‡] https://patents.google.com/patent/US6274303B1.

body begins to take shape within the revival unit….Just a little over a year from the start of the revival procedure, the patient awakens in his hospital bed."

2.2.9 Molecular Brain Repair (Merkle, 1989-1995)

In 1989, Ralph Merkle published the first[405] in a series of papers attempting to quantify several processes for brain repair using nanomachinery and nanorobotics. Merkle begins his analysis by estimating the amount of data needed to specify the location of every molecule in the brain and the structural requirements of memory preservation. He estimates the number of molecules in the brain, the amount of time needed to analyze and repair each one of them, and the number of repair machines (nanorobots) that may be required. Merkle then turns to "the physical deployment of these repair devices. That is, although the raw number of repair devices is sufficient, we must devise an orderly method of bringing each molecule, in turn, to the attention of a repair device. We shall presume that analysis takes place while the tissue is still frozen. While the exact temperature is left open, it seems better to perform analysis prior to warming. The thawing process itself causes damage and, once thawed, continued deterioration will proceed unchecked by the mechanisms present in healthy tissue. This cannot be tolerated during a repair time of several years. Either faster analysis or some means of blocking deterioration would have to be developed if analysis were to take place after warming."

Merkle divides repair scenarios into two classes that he calls "on-board repair" (only briefly mentioned) and "off-board repair" (which he favors and discusses at length):

"In the **on-board scenarios**, the repair devices are deployed within the volume of the brain. Existing structures are disassembled in place, their component molecules examined and repaired, and then reassembled on the spot. (We here class as 'on-board' those scenarios in which the repair devices operate within the physical volume of the brain, even though there might be substantial off-board support. That is, there might be a very large computational resource outside the tissue directing the repair process, but we would still refer to the overall repair approach as 'on-board'). The on-board repair scenario has been considered in some detail by Drexler [Section 2.2.6]….but [we] will not consider it [here] in any depth." In on-board repair, we might first logically partition the volume of the brain into a matrix of cubes, and then deploy each repair device in its own cube. Repair devices would first get as close as possible to their assigned cube by moving through the circulatory system (we presume it would be cleared out as a first step) and would then disassemble the tissue between them and their destination. Once in position, each repair device would repair every molecule in its assigned volume. [One] advantage of on-board repair is an easier evolutionary path from partial repair systems deployed in living human beings to the total repair systems required for repair of the more extensive damage found in the person who has been cryonically suspended. [Another] advantage of on-board repair is emotional….the original structure (you) is left intact at the macroscopic and even light microscopic level…. A third advantage is the ability to leave functional structures intact."

"**[O]ff-board scenarios** allow the total volume of repair devices to greatly exceed the volume of the human brain – any lingering concerns about volume and heat dissipation can be eliminated. If a ton of repair devices should prove necessary, then a ton can be provided. In addition, off-board repair scenarios do not require that the repair devices be mobile – simplifying communications and power distribution, and eliminating the need for locomotor capabilities (legs) and navigational abilities." Off-board repair scenarios would occur in four phases: (1) analyze the structure to determine its state; (2) determine the

---

[405] Merkle RC. Molecular Repair of the Brain. Cryonics 1989 Oct;10(10):21-44; http://www.alcor.org/cryonics/cryonics8910.txt.

healthy state; (3) repair planning; and (4) actual repair. Merkle considers just one variant, called "divide-and-conquer," in which the brain is removed and subdivided into progressively smaller pieces until the pieces are small enough to permit comprehensive analysis and repair, possibly inside a relatively large apparatus. "The division into halves continues until the pieces are small enough to allow direct analysis by repair devices. If we presume that division continues until each repair device is assigned its own piece to repair, then there will be both 1.8×10^{16} repair devices and pieces. If the 1350 cubic centimeter volume of the brain is divided into this many cubes, each cube would be about 0.4 microns (422 nanometers) on a side.[406] Each such cube could then be directly analyzed (disassembled into its component molecules) by a repair device during our three-year repair period….In the third phase of repair, repair planning, we must generate a plan for reassembly of the tissue components (the molecules) back into the healthy state described by the revised structural data base. That is, we must determine how to actually rebuild the healthy tissue. This problem is similar to generating an assembly sequence for a complex human-made structure, such as an airplane."

"The full power of molecular repair should now be evident: almost any damage that can be understood can be repaired. Almost any damage that can be identified – 'The mitochondria are swollen and non-functional,' 'The cell wall is ruptured,' 'The cell has been split,' 'The level of ATP in the cell is too low to support metabolism,' 'The cell is dehydrated,' etc., can now be repaired. For example, it would be theoretically possible to repair a cell even if it had been almost obliterated, provided that there were sufficient clues in the surrounding tissue to support the inference that the cell had been there, and what its function had been. For a nerve cell, it would be sufficient to know little more than the locations and types of the synapses and the courses of its axons and dendrites."

---

[406] The author of this book undertook a fresh analysis (which needs additional detail in ***future research***) of a similar version of this approach, where a frozen brain is divided into $N_{cubes} = 1350\ cm^3 / L_{cube}^3 = 1.8 \times 10^{16}$ tissue cubes of edge length $L_{cube} =$ 422 nm, and concluded that a whole-body destructive molecular scan using this extreme segmentation process might take $t_{bodyscan} \sim \alpha_{body/brain}\ t_{brainscan} = \alpha_{body/brain}\ (t_{initslice} + t_{cutslow} + t_{scan} + t_{transport}) = 1.63 \times 10^7$ sec (~**6 months**) to complete, using $M_{bodyscan} = M_{brainscan} = M_{CuttingLines} + M_{manipulators} + M_{boxes} \sim$ **26 kg** of nanomachinery of volume $V_{bodyscan} = V_{brainscan} = V_{manipulators} + V_{CuttingLines} + V_{boxes} + V_{channels} \sim$ **0.5 m^3** and power draw $P_{bodyscan} = P_{brainscan} = P_{cuttingslow} + P_{cubes} \sim$ **2000 watts**, and $\alpha_{body/brain} = V_{MSV} / V_{brain} = 29.3$ with whole-body molecular scan volume $V_{MSV} = 41{,}053\ cm^3$ and brain volume $V_{brain} = 1400\ cm^3$; whole-body estimate assumes all body tissue is cut into L_{cube}-sized cubes (Section 5.2.1.3).

The scan time once the brain tissue cubes are isolated is $t_{scan} = M_{cube} / (\mathfrak{m}_{BiomolAtomRemoval}\ n_{manip/cube}) = 4100$ sec if all cubes can be processed in parallel, where $M_{cube} \sim \rho_{water}\ L_{cube}^3 = 7.52 \times 10^{-17}$ kg per cube, $\rho_{water} = 1000\ kg/m^3$, $\mathfrak{m}_{BiomolAtomRemoval} \sim 1.83 \times 10^{-20}$ kg/manipulator-sec for tissue scanning, and $n_{manip/cube} = 1$ scanning manipulator per cube. To isolate the cubes, for simplicity we assume the brain is initially sliced into $N_{initslices} = V_{brain}^{1/3} / L_{cube} = 265{,}092$ slabs each L_{cube} thick, requiring $t_{initslice} = x_{diam}\ V_{brain}^{1/3} / c_{cutribbon} = 5.50 \times 10^5$ sec assuming a cutting line manipulator width allowance of $x_{diam} = 30$ nm and a cutting line capacity of $c_{cutribbon} = A_{cross} / (N_{ManipLine}\ \tau_{slice}) = 6.10 \times 10^{-15}\ m^2$/manipulator-sec. Once the slabs are separated, all cubes can be cut at once in each slab, with all slabs being cut simultaneously, in $t_{cutslow} = 100\ t_{cut} = 100\ a_{cube}\ x_{diam} / (c_{cutribbon}\ L_{cube}) = 1250$ sec, where cube surface area $a_{cube} = 6\ L_{cube}^2 = 1.07\ \mu m^2$/cube and the cutting speed is slowed 100-fold to avoid excessive waste heat generation. After cutting, each isolated cube must be transported through channels to its individual examination chamber ("box"), requiring a time $t_{transport} = L_{total} / v_{channel} = 100$ sec, where total transport distance $L_{total} \leq 1$ meter and transport speed is $v_{channel} \sim 1$ cm/sec.

The mass of all cutting lines is $M_{CuttingLines} = n_{manip/cutline}\ N_{cuttinglines}\ (m_{manipulator} + m_{cutlineoverhead}) = 0.277$ kg, where there are $n_{manip/cutline} = L_{cube}/x_{diam} = 14$ manipulators/cutting line, $N_{cuttinglines} = n_{cutline/cube}\ N_{cubes} = 1.8 \times 10^{16}$ cutting lines, $n_{cutline/cube} = 1$ cutline/cube, $m_{manipulator} = 10^{-19}$ kg, and the overhead mass that supports each cutting line manipulator is assumed to be $m_{cutlineoverhead} = 10\ m_{manipulator} = 10^{-18}$ kg. The mass of all scanning manipulators is $M_{manipulators} = m_{manipulator}\ N_{manipulators} = 1.8 \times 10^{-3}$ kg, where $N_{manipulators} = N_{cubes} = 1.8 \times 10^{16}$ manipulators. The mass of all examination chamber boxes is $M_{boxes} \sim 6\ y_{boxwall}\ L_{box}^2\ \rho_{diamond}\ N_{boxes} = 25.6$ kg, where the box walls are $y_{boxwall} = 100$ nm thick, the inside surface of the box is located $x_{boxclearance} = 100$ nm from the surface of the tissue cube that it encloses (i.e., manipulator length is 100 nm ~ $x_{boxclearance}$), box external edge length $L_{box} = L_{cube} + 2x_{boxclearance} + 2y_{boxwall} = 822$ nm, $\rho_{diamond} = 3510\ kg/m^3$, and $N_{boxes} = N_{cubes} = 1.8 \times 10^{16}$ boxes.

Scanning manipulator volume $V_{manipulators} = V_{manip}\ N_{manipulators} = 1.8 \times 10^{-5}\ m^3$ where $V_{manip} \leq (100\ nm)^3 = 1 \times 10^{-21}\ m^3$, cutting line volume $V_{CuttingLines} \sim M_{CuttingLines} / \rho_{diamond} = 7.90 \times 10^{-5}\ m^3$, and total box volume $V_{boxes} = L_{box}^3\ N_{boxes} = 0.010\ m^3$. The volume of all transport channels is $V_{channels} = w_{channel}^2\ L_{channel}\ N_{cubes} = 0.433\ m^3$, taking channel width $w_{channel} = L_{cube} + 2\ x_{boxclearance} = 622$ nm and average channel length $L_{channel} \sim 100\ w_{channel} = 62.2\ \mu m$. Cutting line power $P_{cuttingslow} = (1/100)\ n_{manip/cutline}\ N_{cuttinglines}\ P_{manipulator} = 252$ watts and $P_{cubes} = n_{manip/cube}\ N_{cubes}\ P_{manipulator} = 1800$ watts, taking $P_{manipulator} = 0.1$ pW.

After a public discussion of the ideas in the 1989 paper with Gregory Fahy in 1991,[407] Merkle published a summary of the arguments favoring the technical feasibility of cryonics in a mainstream medical journal in 1992,[408] followed by a revised version of his brain repair analysis in 1994[409] and two additional papers regarding the algorithmic feasibility of brain repair in 1994[410] and 1995.[411]

After his discussion with Merkle in 1991, Fahy published his own independent nanorobotic cryonics revival proposal later the same year (Section 2.2.10).

2.2.10 Nanotechnological Repair of Frozen Brain (Fahy, 1991)

In 1991, Gregory Fahy anonymously published a description of a nanotechnology-based "realistic" repair scenario for the restoration and revival of a cryopreserved human brain.[412] This was the first treatment of the subject[413] by an internationally-recognized professional cryobiologist, and included evaluations of the many forms of cryoinjury likely to be experienced by cryonics patients and likely to need repair during the procedure. "A scenario is developed which is based on (a) replacing brain ice with repair networks below T_g [the glass transition temperature], (b) carrying out gross structural repairs at temperatures in the range of about -100 to -30 degrees C, and (c) carrying out most intracellular repairs at more elevated temperatures, relying in part on ordinary biological self-assembly and self-repair for carrying out much of the work required." Starting at a temperature below the glass transition temperature, repair proceeds in 10 steps:

(1) **Stabilizing Fractures.** "[T]he very first step is to infiltrate surface fractures with specialized molecular devices which will form coatings or surface replicas of the fracture faces to molecular or near-molecular resolution. [T]he formation of sufficiently stable fracture face replicas at temperatures below T_g appears feasible and would maintain the overall geometry of the fracture faces after dissolution of the portion of the face that is ice and glass. Pores in the replicas of areas of pure ice or pure glass should be included to permit outgassing during the subsequent sublimation process (see below), which otherwise

---

[407] Fahy GM. Molecular Repair Of The Brain: A Scientific Critique, with a Response from Dr. Merkle. Cryonics 1991 Feb;12(2):8-11 and Cryonics 1991 May;12(5):15-19; http://www.alcor.org/Library/html/MolecularRepair-Critique.html.

[408] Merkle RC. The Technical Feasibility of Cryonics. Med Hypotheses 1992 Sep;39(1):6-16; http://www.merkle.com/cryo/TheTechnicalFeasibilityOfCryonics.pdf.

[409] Merkle RC. The Molecular Repair of the Brain. Cryonics 1994 Jan;15(1):16-31 (Part I) and Cryonics 1994 Apr;15(2):18-32 (Part II); http://www.alcor.org/Library/html/MolecularRepairOfTheBrain.htm.

[410] Merkle RC. Cryonics, Cryptography, and Maximum Likelihood Estimation. First Extropy Institute Conference, Sunnyvale CA, 1994; later published in Cryonics 1995;16(2):13-20; https://www.alcor.org/docs/cryonics-magazine-1995-02.pdf.

[411] Merkle RC. Algorithmic Feasibility of Molecular Repair of the Brain. Cryonics 1995;16(1):15-16; http://www.alcor.org/cryonics/cryonics1995-1.pdf.

[412] Fahy G. Appendix B. A "Realistic" Scenario for Nanotechnological Repair of the Frozen Human Brain. In: Wowk B, Darwin M, eds., Cryonics: Reaching for Tomorrow. Alcor Life Extension Foundation, 1991, pp. A-10 – A-26; https://alcor.org/Library/html/nanotechrepair.html.

[413] After Fahy's Feb 1991 critique of Merkle's approach* and Merkle's May 1991 response to Fahy,† during Aug-Sep 1991 Fahy sketched out several features of a nanorobotic-based fracture-stabilization and fracture-healing process that preceded his published scenario. Fahy's 12 pages of previously unpublished notes and drawings, which only became known to the author as this book was about to go to press, are reproduced in Appendix C for posterity, with the kind permission of Gregory Fahy.

* Fahy GM. "Molecular Repair of the Brain": A Scientific Critique. Cryonics 1991 Feb;12(2):8-11; https://www.alcor.org/docs/cryonics-magazine-1991-02.txt

† Merkle RC. Response to the critique of "Molecular Repair of the Brain." Cryonics 1991 May;12(5):15-19; https://www.alcor.org/docs/cryonics-magazine-1991-05.txt.

could tear holes in the replicas. After coating of opposite fracture faces, these faces could be computationally compared to verify complementarity. After complementarity analysis, the repair system could build filaments between the faces. The filaments on each side of the fracture would be complementary to each other and would connect so as to maintain fracture face registry later when the temperature is raised. The function of the wires later would be to direct each fracture face as a whole toward the other fracture face as the gap is later closed by normal thermal expansion in such a way as to continue to ensure perfect registry of the two fracture faces as the gap narrows. Molecular 'ratchets' along the guide wires could apply small forces to encourage closing where this is necessary."

(2) **Get the Big Picture.** "The frozen brain contains highly shrunken cells and neuronal processes compressed between sheets of ice and pools of vitreous cryoprotectant water-solute inclusions. There may be lipid extrusions, floating debris, ripped axons, hemorrhaged capillaries, stabilized fractures, unraveled myelin, crystallized regions of certain surface membranes, extruded cell contents in the extra-cellular space, and other relatively gross alterations. We desire to identify and stabilize all of these lesions before significant 'stirring' is permitted. This is difficult to do without large-scale cooperation of repair devices, for which a coordinate system needs to be set up, preferably one that does not in itself cause any damage."

(3) **Excavating the Extracellular Space.** "[A]bout 80% of the brain is nothing but water and cryoprotectant and … most of this exists in the form of pure ice located in the extracellular space. We first desire to remove the ice and most of the vitrified extracellular solution. This... creates room for the deployment of an extracellular communications complex which will be used to direct subsequent repairs....and it makes transmembrane diffusion in either direction ('stirring') effectively impossible when the temperature is subsequently raised. Our task might best be accomplished by a combination of direct excavation (done by relatively stupid molecular 'jackhammers'), which creates a certain amount of local warming, and by spontaneous ice sublimation, which offsets some of the local heating due to evaporative cooling. Excavation might proceed by digging out hollow tubular 'mines' through the ice perhaps 1 micron or more in diameter. The insides of the 'ice mines' are maintained at a strong vacuum. In a vacuum simulating that of deep space, ice evaporation rates have been shown to be sufficient near T_g to move sublimation boundaries at rates on the order of microns per day! If we maximize the surface area available for evaporation while also maximizing the rate of direct excavation, it might be possible to remove extracellular ice fairly rapidly – for example, in a few months."

(4) **Establishment of Extracellular Repair Network.** "As excavation/evacuation proceeds, an extracellular communication, transportation, and coordinate system could be laid down in the space made available. This system, penetrating throughout the extracellular portion of the brain and in intimate physical contact with the brain everywhere, could be thought of as a kind of 'meta-brain,' capable of relaying information about the brain over long distances while potentially having a volume amounting to more than 60% of the original volume of the entire brain (which is roughly the volume previously occupied by ice). This volume represents about 150% of the volume of the cellular components of the brain. The metabrain would permit all exposed lesions to be mapped and analyzed. Undamaged structures could be passed over without further action, except as they are needed to infer the proper locations of aberrant structures, such as debris resulting from ripped axons. Furthermore, the metabrain could be in contact with external computers, where most computation might occur."

(5) **Repair Computations for the Extracellular Space.** "[A]ll labile extracellular structures have been physically immobilized and a coordinate system is in place. No 'stirring' has taken place because all procedures have been carried out just below T_g. All significant extracellular anatomical elements of the brain have been registered. The 'wiring diagram' of the brain can now be deduced, and all damaged areas can be catalogued as to type and place. Where necessary, the loci of missing structures could be deduced at this point. To this point, no actual repairs have been made and the process has been completely noninvasive to brain cells. Based on the results obtained to this point, specialized repair devices are assigned to specific tasks and specific regions."

(6) **Warming above T_g.** "In order to proceed with repairs, warming of the brain is slowly induced. [This] induces changes in volume which permit fracture healing, it induces desirable changes in tissue pliability/deformability needed for moving structures such as cell membranes, and it permits both

diffusional transport of needed molecules and the chemical reactions needed for repair. At temperatures between about -110 and -50 degrees C, two major types of diffusional process can be identified: the diffusional motions that blur the fracture interfaces we have previously marked and prepared for healing, and diffusional motions within cells. By removing the great majority of the extracellular space and immobilizing extracellular debris, we have precluded transmembrane and extracellular diffusion, and by forming durable fracture replicas and establishing the relationships between them, we have precluded diffusional information loss at these sites. We therefore are able to proceed with the extracellular repair process first, and then to turn our attention to cellular interiors."

(7) **Fracture Healing.** "The key issues involved at this point are (a) the removal of the protective replica surfaces and (b) the union of tissue on either side of the fractures. Fractured surfaces will generally be cross-sections through various membrane-limited compartments (cells, myelinated axons, organelles), and planar separations between membrane bilayers. Within membrane-enclosed compartments, filamentous structures and molecular clusters such as enzyme complexes will be cleaved. In the case of membrane-bounded compartments that have been cleaved by fractures, one strategy would be to heal the limiting membrane first….As the naked membrane faces are brought together, they will tend to fuse spontaneously….If membrane fluidity is too low to permit good fusion at the prevailing temperatures, a small amount of specialty lipid can be added to the local area to enhance fluidity sufficiently to permit fusion to occur….[S]everal months ... should be more than enough time to carry out the required extracellular repairs."

(8) **Cell Repair.** [A] Debris consolidation. ("Having healed the fractures at about -80 degrees C, the next major extracellular task is to redistribute cellular debris to their proper locations.") [B] Stabilization against diffusional/biochemical deterioration. ("While limited, some diffusion is possible in cytoplasm at -60 degrees C. We exploit this by introducing metabolic inhibitors at this temperature into the cytoplasm. Since we have ready access to the external surfaces of cells, we can easily deposit inhibitors at regular intervals along cell processes. The inhibitors are designed to block the action of any enzymes that permit catabolism to proceed to beyond an acceptable point.") [C] Cell volume restoration. ("We…have to return cell volumes and cell water contents to normal.") [D] Rehydration. ("The perfusate contains necessary substrates, repair machines, and psychrophilic anabolocytes, as required. These new devices as well as the previously-deployed intracellular cell repair machines therefore now proceed to correct the most critical types of continuing damage. Their activities may include, for example: myelin synthesis and replacement; bacterial and viral killing; protein reaggregation; cytoskeletal reassembly; reversal of glycerol-induced biochemical reactions; *de novo* synthesis of key missing proteins and other key metabolites; reversal of exotic, unnatural chemical bonds formed in order to heal otherwise intractable lesions at lower temperatures; removal of specialty lipid; restoration of normal intracellular buffering and pH; repair or removal of peroxidized, racemized, oxidized, or otherwise modified structures, resulting in their replacement with undamaged structures.")

(9) **Metabolic Restoration.** "As temperature is elevated further, oxygen is reintroduced and many metabolic inhibitors are degraded or inactivated. Necessary protein repairs are completed. Successful repair is checked by examining certain key metabolite behaviors in each significant metabolic pathway that are indicative of proper metabolic startup. Departures from expectation are diagnostic of any lingering underlying problems, which are then specifically corrected to the degree necessary."

(10) **Disease Reversal and Reanimation.** "Brain temperature is raised to 25-37 degrees C. Cell metabolism may still be grossly abnormal in a variety of ways: it will not have been necessary to have previously reversed all details of the previously existing pathological state, but only those details required for subsequent cellular self-maintenance and self-repair. Cells 'know' what their proper state is and will spontaneously establish that state provided they are viable enough to continue to exist and to repair themselves. While this is happening, conventional medical nanotechnology will be at work on specific disease processes, reversing them, establishing proper connections to extracephalic structures, and, if need be, assisting with the provision of a new body. Given stable physiology, these curative processes, including the partial or even complete reversal of aging, can be allowed to proceed as long as needed. Very few constraints on repair exist at this point. Once the patient has been restored to a state approaching perfect physical health, consciousness is restored."

2.2.11 SCRAM Reanimation (Soloviov, 1994-1998)

In 1994, 1996 and 1998,[414] Michael Soloviov published proposals for reanimating cryonics patients via atom-by-atom reconstruction of the brain using "a big number of ATM-like needles united in matrix." This lightly-sketched scenario would unfold in three parts:

(1) **Scanning.** "A section of the frozen body is scanned to define the location and type of all atoms in the body. Generally this will be a destructive process – as one layer of atoms is scanned it is removed, exposing the next layer for scanning, until the whole interior structure is mapped."

(2) **Computer Reconstruction.** "The data file obtained in step (1) is processed. In effect, an electronic image of the body section is modified rather than the original material. In this way all necessary repairs, cure of diseases, etc. are carried out in cyberspace, again creating an electronic image – in this case, of the fully repaired body section. A procedure to rewarm the tissue is mapped out or updated."

(3) **Atomic Manufacture.** "The data file from step (2) is used by some STM-derived (or other type) device to assemble the body section atom-by-atom at low temperature. After all sections have been reconstructed in place, the frozen body is warmed to make it functional."

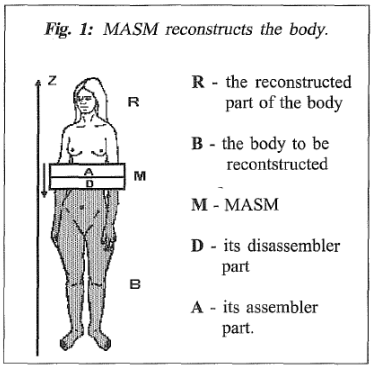

"The MASM [Macroscopic Atomic Scanner/Manufacturer] is the basic device for scanning and manufacture of the body. First it disassembles the body section and analyses its atomic structure (the scanning process). Then it assembles the body section from atoms anew (the manufacture process)....The MASM head is an array of 10^6 x 10^6 nanosyringes. Its size is 1 x 1 cm....The nanosyringe is a device to capture and recognize, or release and connect, atoms. Its maximal diameter is 10 nm. It is an STM-like needle with a nanotube inside....Transport of atoms could be effected through some sort of nanotube pipeline…." Unfortunately, the proposal evidences unawareness of many previously published crucial technical details[415] of atomic manipulation, positionally-controlled chemical reactions (mechanosynthesis), and molecular machine design.

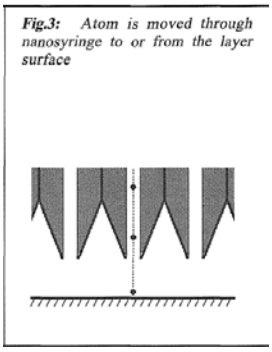

[414] Soloviov M. Atomic Printers or Time Estimation of Atom-by-atom Brain Assembling. Longevity Report 1994 Dec;6(48):12-15; http://www.quantium.plus.com/lr/lr48.htm#Atomic%20Printers. Soloviov MV. SCRAM Reanimation. Cryonics 1996 Qtr 1;17(1):16-18; https://alcor.org/cryonics/cryonics1996-1.pdf. Soloviov MV. A Cell Repair Algorithm. Cryonics 1998 Qtr 1;19(1):22-27; https://alcor.org/cryonics/cryonics1998-1.pdf.

[415] Drexler KE. Nanosystems: Molecular Machinery, Manufacturing, and Computation, John Wiley & Sons, New York, 1992; https://www.amazon.com/dp/0471575186/.

2.2.12 Reanimation Process (Drexler, 1998)

During a 1998 interview with Cryonics magazine,[416] interviewer Russell Cheney asked Eric Drexler to share his current thoughts on the specifics of the reanimation process. Having had 12 additional years to contemplate this issue since his first discourse on the subject in 1986 (Section 2.2.6), Drexler provided an updated scenario for cryonics revival:

> "I will just say in outline that if I had to sit down and sketch out a reasonably detailed technology scenario for how, given a lot of technology base, given a lot of knowledge in place, how would one go in and effect repair in a particular clinical case: I would say that, roughly speaking, first you start by not causing any thawing injury, sort of like reperfusion injury only much worse. So you would stay at liquid nitrogen temperature, or even below; it might be that there is an advantage to additional stabilization during some of these processes."
>
> "There's a lot of ice in the tissue; I think a good first move is to remove that ice, by a sort of mining operation. Have structures that would go in and say, 'Ah. yes, there's an icy surface and we'll remove a little bit of this material and yes, that's ice, a little bit of this.' And say, 'Ah, this here is stuck in place, this isn't ice; this is a protein, OK.' Once you had removed the ice and the ice crystals, keeping track of course of how much sodium and chlorine and potassium, and so on, were lodged in the crystal in different places, you'd find that you had a whole lot of working room and not a whole lot that's terribly blocking access to surfaces worth working on."
>
> "Where I think the scenario would proceed from there is essentially to moving things around so that they're in the right locations. OK, there's been dehydration and some tissue's been compressed. As a next step you do some stabilization. At some point here you probably want to raise the temperature so that various materials are a bit more pliable and flexible and not brittle. So now you have what in effect is a structure that is sort of cross-linked, but it's not by chemical reactions that just occurred haphazardly, maybe not chemical reactions *per se* at all, but rather there're a whole lot of little links holding things in place."
>
> "Now you can, at a gross morphological level, put things back where they belong. And at a finer scale move in and put things back where they belong. Once you've put everything back where it belongs and gone back to a lower temperature, you would put water back in. But now you put the water in without all the disturbances that are caused by an actual freezing process."
>
> "The naive idea of what freezing would do in an ideal world is that it makes everything just sort of stop, and maybe you get little microscopic bits of crystallization, but they don't really do much and everything is reasonably in place. Part of what Greg Fahy has been doing with vitrification shows that we are able to come increasingly close to that ideal with actual technologies of perfusion and cooling. But here you're not doing it by perfusion and cooling, but by construction, if your aim is to construct an ideal frozen state. What would a perfectly cryo-preserved tissue look like if you didn't have the nasty, concentrated cryoprotectants in there, but you had all the effects you wanted on the ice?"
>
> "Then, given that we already know that so many biological materials can tolerate thawing injury from accessible frozen states, it would seem that thawing from an idealized frozen state, that you can't get to by a real freezing process, would be pretty much a piece of cake, especially if you still have devices in there to do on-going adjustment of this and that. Presumably you'd like to have

---

[416] Cheney R. Cryonics Interview: Eric Drexler. Cryonics 1998 Qtr 3;19(3):32-39; https://www.alcor.org/docs/cryonics-magazine-1998-03.pdf.

the right ion concentrations and the right ATP concentrations, and there's some little corner where there are some stray molecules or something that wasn't convenient to mess with until there was a water phase for them to diffuse in, so you'd wait for the water phase to happen, then you'd catch them as they diffused."

"Probably what you'd like to do is to be sure you had enough mechanisms in place to prevent any metabolic activity. Although it's hard to say how the details will work out in practice, I think the sensible thing to do might well be to inhibit a large portion or some crucial subset of the enzymes and active transport mechanisms in the cells, and keep them in that state until you're up in some reasonable temperature regime, like 98 or so degrees."

"[T]he inhibition is initially done by temperature. You substitute a nonthermal mechanism for inhibition, stabilize, warm, and then after making sure that things are where they ought to be, and the concentrations of the various substances are what they ought to be, to be ready to roll. You then remove the blocks from the wheels and let her go. Given the robustness of biological systems, that scenario probably actually is a little bit more careful and cautious than is necessary. But on the other hand, why not?"

"The conservative thing to do would be to be restored to a healthy condition that's not terribly unlike the condition that they were in before suspension, but enough different that they obviously don't need suspension – to what is by present standards considered healthy. Then if people would like to arrange for a little bit more work so that they don't look quite so wretchedly unhealthy by the standards at the time of repair, then that would be a matter for voluntary choice, one would hope."

2.2.13 Low-Temperature Operation of Nanorobots (Freitas, 1999-2007)

In 1999 Robert Freitas published the first technical book on medical nanorobotics,[417] which included a subsection examining whether nanorobots would retain their functionality at unusually low operating temperatures…."an important question for nanodevices.... in situations requiring the repair and resuscitation of cold-vitrified or cryogenically-preserved tissues, organs, or whole organisms." After briefly considering questions of dimensional stability and material strength, the text next discusses the challenge of nanorobot locomotion in ice.[418]

"Just below freezing, crystalline ice viscosity is ~10^{10} kg/m-sec, requiring a 1-micron nanorobot to expend on the order of ~200,000 pW to creep forward at 1 micron/sec by viscoplastic flow in which ice crystals are deformed without breaking. Just halfway from freezing to liquid nitrogen temperature, at 164 K (-109 °C), viscosity has already risen to ~10^{21} kg/m-sec, roughly equivalent to solid mantle rock, and the power requirement has increased 100-billionfold, clearly prohibitive."

"One solution that avoids this problem at temperatures near the melting point is baronatation, which depends upon the fact that water, almost uniquely, is less dense as a solid than a liquid (i.e., ice floats),

---

[417] Freitas RA Jr. Nanomedicine, Volume I: Basic Capabilities. Landes Bioscience, Georgetown, TX, 1999; Section 10.5, "Temperature Effects on Medical Nanorobots"; http://www.nanomedicine.com/NMI/10.5.htm. Reprinted as: Freitas RA Jr. Chapter 3. Temperature Effects On Medical Nanorobots. In: Charles Tandy, ed. The Prospect of Immortality – Fifty Years Later. RIA University Press, Ann Arbor MI, 2014.

[418] Freitas RA Jr. Nanomedicine, Volume I: Basic Capabilities. Landes Bioscience, Georgetown, TX, 1999; Section 10.5.2, "Viscosity and Locomotion in Ice"; http://www.nanomedicine.com/NMI/10.5.2.htm.

suggesting a freezing point depression effect with increasing pressure that is visible as the short downleg from 0°C to -16 °C in the phase diagram for Ice I_h.[419] This is confirmed experimentally by suspending two heavy weights from a wire stretched across a block of ice. The wire passes slowly through the block, the wire exerting a pressure that melts a thin layer of water ahead of it, allowing the wire to progress; as the water passes behind the wire to the lower pressure region, it refreezes, a process known as regelation. The melting ice ahead of the wire absorbs the heat of fusion while the refreezing water gives up the heat of fusion, with heat steadily transferred by the wire, hence a good conductor cuts better than a poor one. The barostatic freezing point depression constant for ice is 134 atm/°C up to ~2100 atm. By exerting a higher pressure (force per unit area) ahead of it than behind it, a baronatating nanorobot of roughly conical geometry can progress slowly through ice that is no colder than -16 °C. Taking the heat of fusion for water-ice as ΔH_{fus} = 306 pJ/micron^3 (334 J/gm at 0 °C) and assuming at least ~3 micron^3 of ice must be melted to allow 1 micron of forward progress, then baronatation power requirement is very conservatively estimated as $P_{baro} \sim 3\ \Delta H_{fus}\ v_{nano} \sim 900$ pW for v_{nano} = 1 micron/sec."

"The freezing point depression effect[420] in which solute molecules are released ahead and recovered behind might serve as the basis for a similar drive system concept at temperatures just below the melting point." For example, ethanol (which has a much lower freezing point than water) melts ice[421] and is fully miscible with water; a 50% ethanol-water solution freezes at -32 °C.[422]

"Burrowing by progressive voids is yet another alternative that will work over a wider range of cold temperatures. The binding energy per hydrogen bond in the ice ahead is E_{HBond} = 33 zJ/bond (4.6 Kcal/mole), there are two hydrogen bonds [net] per water molecule, and $n_{water} = 3 \times 10^{10}$ water molecules/micron^3 in ice at 273 K (0 °C), so H-bond-breaking power is at most $P_{HBond} \sim 2\ E_{HBond}\ n_{water}\ L_{nano}^2\ v_{nano}$ = 2000 pW for a nanorobot of dimension L = 1 micron and velocity v_{nano} = 1 micron/sec. Moving ice in small chunks may be another energy-saving alternative."

In 1998, Freitas published the first medical nanorobot design paper[423] in a mainstream medical journal, describing the respirocyte – a simple medical nanorobot that performs the function of natural red blood cells but with 236 times greater capacity per unit volume.

In 2002, Freitas published the first scaling study and mission design for a whole-body artificial vascular transport system to replace blood, called a vasculoid,[424] a device that became a major component of a 2008 proposal for cryonics revival (Section 2.2.14) and provides the foundation for most of the revival scenarios described in this book (e.g., Chapter 4, Chapter 5).

---

[419] https://en.wikipedia.org/wiki/Ice_Ih.

[420] Freitas RA Jr. Nanomedicine, Volume I: Basic Capabilities. Landes Bioscience, Georgetown, TX, 1999; Section 10.5.3, "Solubility and Solvents"; http://www.nanomedicine.com/NMI/10.5.3.htm. See also: https://en.wikipedia.org/wiki/Freezing-point_depression.

[421] Technically, a solute melts ice by lowering the vapor pressure of the water-solute solution to less than the vapor pressure of pure ice at the same temperature, causing transfer of water molecules down their vapor pressure gradient from ice to liquid.

[422] "Ethanol Freeze Protected Water Solutions," The Engineering ToolBox, 2005; https://www.engineeringtoolbox.com/ethanol-water-d_989.html.

[423] Freitas RA Jr. Exploratory design in medical nanotechnology: a mechanical artificial red cell. Artif Cells Blood Substit Immobil Biotechnol. 1998 Jul;26(4):411-30; https://www.tandfonline.com/doi/pdf/10.3109/10731199809117682. A longer version of this paper appears at: https://web.archive.org/web/20100420085137/http://www.foresight.org/Nanomedicine/Respirocytes.html.

[424] Freitas RA Jr., Phoenix CJ. Vasculoid: A personal nanomedical appliance to replace human blood. J Evol Technol. 2002 Apr;11:1-139; http://www.jetpress.org/volume11/vasculoid.pdf.

Still later in 2007, Freitas published the first scaling study of a cell repair nanorobot, called a chromallocyte,[425] along with details of a specific cell repair mission (chromosome replacement in the cell nucleus). Sophisticated cell repair nanorobots of this general class figure prominently in most nanotechnology-based revival scenarios, including most of the ones presented in the present work.

2.2.14 Revival Scenario Using Molecular Nanotechnology (Merkle and Freitas, 2008)

As the most direct precursor of the present work, this 2008 proposal[426] for reviving cryopreserved patients is reproduced here in full.

We briefly outline one possible cryopreservation revival scenario using MNT (molecular nanotechnology). A full analysis will require much further work and detailed research. Our principal assumptions are that a reasonably mature MNT will exist, and that the patient has received a "good" cryopreservation by current standards, including the introduction of appropriate levels of cryoprotectants.

Pre-Repair Operations

The first question we face in designing a cryopreservation revival scenario is whether to warm the patient to provide a liquid environment before beginning, or to initiate repairs at low temperature (77 K / -196 °C for patients in LN2, or perhaps ~140 K / -133 °C for patients in the future who elect Intermediate Temperature Storage or ITS) [Section 7.1.2].

The obvious disadvantage of warming before initiating repairs is that further deterioration will take place, which might result in the loss of personality-relevant information (e.g., warming might cause deterioration of synaptic or neurological structures). We know that current methods of cryopreservation cause fractures. While these fractures, like fractures in glass, are expected to produce minimal information loss, they would nevertheless create problems with structural integrity that, upon warming, could lead to further deterioration. Without some form of stabilization, warming fractures would be like slicing the tissue with incredibly sharp knives – on its face, not something that we wish to do. Other forms of damage that had occurred either prior to cooling or during the cooling process might, upon warming, also cause continued deterioration of the tissue. As a consequence, initiating the repair process at low temperature is the more conservative approach.

The first step in low temperature repair is to clear out the circulatory system. This process would more closely resemble drilling a tunnel than anything else, and would require the use of molecular machines able to function at (for example) LN2 temperature (though the particular temperature could be adjusted as might be found useful).

This basic process will employ molecular machines that can operate at low temperature, and can sense and remove the kinds of materials found in the circulatory system. Fortunately, proposals for diamondoid molecular machines that operate at low temperature are common. Gears, bearings, ratchets, sliding interfaces and the rest work quite well regardless of temperature, and detailed analyses of molecular

---

[425] Freitas RA Jr. The Ideal Gene Delivery Vector: Chromallocytes, Cell Repair Nanorobots for Chromosome Replacement Therapy. J. Evol. Technol. 2007 Jun;16:1-97; http://jetpress.org/v16/freitas.pdf.

[426] Merkle RC, Freitas RA Jr. A Cryopreservation Revival Scenario using MNT. Cryonics 2008;29(4):6-8; http://www.alcor.org/cryonics/cryonics0804.pdf.

structures bear out this claim. Unlike biological systems that typically require liquid water in which to operate, diamondoid molecular machines can operate in vacuum with no need for lubricants and at temperatures as low as we might desire.

Logistics System Installation

Coordination, communication and power for these molecular machines can again be provided at low temperature. Designs for very compact molecular computers able to operate at arbitrarily low temperatures (specifically including rod logic, a type of molecular mechanical computation) are well known in the literature and could provide the computational power needed to coordinate repair activities. Several modes of communication are available, including molecular cables that should be able to transmit data at gigabit rates or higher.[427] By coupling activity of on-board repair devices to off-board computational resources, the overall repair process could be guided by massive computational resources located outside of the patient, thus avoiding concerns about patient heating caused by waste heat from the computational resources required to plan and coordinate repair activities. Finally, power distribution can take place by whatever means is convenient,[428] including distribution of electrical power via carbon nanotubes (which can have remarkably high conductivity).

During the repair process, various molecular inputs will be required and molecular outputs must be removed. A cryonics-specialized variant of an artificial vasculature or "vasculoid"[429] redesigned to operate at low temperatures could be installed to carry out this function. In this variant, the initial transport load would be orders of magnitude smaller than the load that a fully functional vasculoid would be required to handle in a normally metabolizing person even at basal rates. (The original vasculoid was scaled to handle peak metabolic rates.) Roughly speaking, a vasculoid is an artificial circulatory system that enables coordinated ciliary transport of containerized cargoes using a leak-tight coating of machinery on the inner vascular walls. The vasculoid appliance is readily modified to operate at low temperature, and can easily span relatively large cross-capillary breaks.

This initial stage brings medical nanodevices to within ~20 microns of any point in the brain via the circulatory system, and provides distributed power and control as well as massive computational resources located outside the tissue undergoing repair. Initial surveys of the tissue would provide damage estimates at specific sites, including a detailed mapping of fractures. A variety of imaging modalities[430] could be used to provide extensive information about the cellular structure throughout the immobilized tissue. At this stage, the external computer guiding repairs would come to possess detailed structural information of the entire system down to the cellular and subcellular level. If the cryopreservation had generally gone well, this fact would be apparent and relatively minimal analysis and repairs would be required. If the cryopreservation had produced more significant damage in some areas, this damage could be tabulated and assessed, and appropriate repair strategies could be planned. There is reason to believe that even very serious damage could be analyzed, the original healthy state determined, and appropriate repair strategies adopted.[431]

---

[427] Freitas RA Jr. Nanomedicine, Volume I: Basic Capabilities. Landes Bioscience, Georgetown, TX, 1999, Section 7.2.5, "Cable Communication"; http://www.nanomedicine.com/NMI/7.2.5.htm.

[428] Freitas RA Jr. Nanomedicine, Volume I: Basic Capabilities. Landes Bioscience, Georgetown, TX, 1999, Section 6.4, "Power Transmission"; http://www.nanomedicine.com/NMI/6.4.htm.

[429] Freitas RA Jr., Phoenix CJ. Vasculoid: A personal nanomedical appliance to replace human blood. J Evol Technol. 2002 Apr;11:1-139; http://www.jetpress.org/volume11/vasculoid.pdf.

[430] Freitas RA Jr. Nanomedicine, Volume I: Basic Capabilities, Landes Bioscience, Georgetown TX, 1999, Section 4.8, "Cellular Bioscanning"; http://www.nanomedicine.com/NMI/4.8.htm.

[431] Merkle RC. Cryonics, Cryptography, and Maximum-Likelihood Estimation. Cryonics 1995 Qtr 2;16(2):13-20; https://www.alcor.org/docs/cryonics-magazine-1995-02.pdf.

Fracture Stabilization

Current cryopreservation methods create fractures, some of which can have gaps that are tens or even hundreds of microns across. Unstabilized, these fractures would cause further tissue deterioration upon warming. Stabilization of fractures can be done by the synthesis of artificial surfaces specifically designed to conform to the exposed faces of the fractures. For example, we could make a stable support sheet of ~1 nanometer thickness to which arrays of hydrophilic and hydrophobic molecular surface "decorations" are attached. By making the decorations match the exposed face of the fracture, this support sheet would stabilize the fracture face on warming and prevent further deterioration. The success of this approach depends upon the ability of MNT to synthesize an appropriate support sheet – which we expect to be well within the capabilities of the technology.

Following stabilization of fracture surfaces the system temperature can be slowly increased without risk that the fractures will contribute to further deterioration. The support sheet would remain in contact with the fracture face even as the fracture face expands or contracts during warming – the thin support sheet would readily conform to such changes in shape.

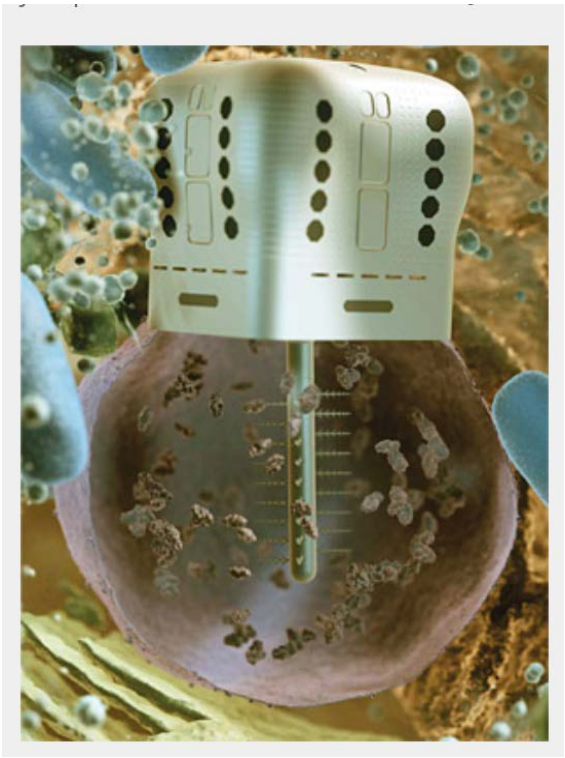

Advanced nanorobots will keep all human body cells in perfect repair, preventing disease and aging. Illustrated here is a cell repair robot called a chromallocyte. After the chromallocyte (in upper half of picture) locates and docks with the cell nucleus (in lower half of picture), it extends a tool-tipped robotic arm into the nucleoplasm. The job of this nanorobot is to replace old damaged chromosomes with new ones in every cell. ©2008 E-spaces 3danimation.e-spaces.com (artwork) and Robert A. Freitas Jr. www.rfreitas.com (concept/design).

Tissue Chemistry Restoration

As the temperature increases and some degree of fluidity is reintroduced into the tissue, the repair process can turn to other issues. In particular, some proteins have likely been denatured during the cryopreservation process. As most proteins should spontaneously recover, the technical challenge will be to identify those that are slow to recover and then either hasten their recovery (possibly by the use of artificially designed chaperones) or support their missing function by other means during recovery. (The recovery of many tissue types after cooling to low temperature supports this approach – if any significant fraction of proteins failed to recover, one would not expect any tissues to spontaneously survive such treatment.) In those cases where critical functionality does not spontaneously recover with sufficient rapidity, it would be possible to introduce new properly folded proteins at an appropriate temperature to take over the critical functions that have been compromised, and then let the tissue recover by itself later on, once it has resumed normal functioning. Re-denaturation of proteins can largely be avoided by delaying repairs to higher temperatures in a series of stages depending on which repairs are needed at various temperatures.

The cryopreservation process and the changes prior to cryopreservation have likely caused imbalances in the concentrations of specific chemicals. Concentrations of sodium, potassium, other ions, ATP, glucose, oxygen, and many other metabolites and chemicals are likely not at desirable values. Concentrations of cryoprotectants might or might not be at desired levels for the particular temperature, so it might be useful to remove cryoprotectants employed during the cryopreservation and replace them with newer

cryoprotectants that have more desirable properties. As the tissue becomes more fluid, concentrations of any specific chemical can be measured and adjusted. Direct access to cells surrounding the capillary lumen is available, and the use of tubular probes (which could be introduced from the lumenal vasculoid face once the liquid environment becomes sufficiently viscous to allow such probes to penetrate) would provide direct access to the intracellular contents of cells 10 or 20 microns from any capillary. Concentrations of reactive molecules such as oxygen and other reactive metabolites would be kept low until later in the recovery process, with metabolism also kept on hold during this time.

The support system and external computer would have essentially total control over the concentration of all chemical compounds in all cellular and even subcellular compartments in the recovering patient. The control system would adjust these concentrations as needed to minimize damage, both during the re-warming process and also later while metabolic activities were being re-established.

Fracture Sealing and Comprehensive Cell Repair

At some higher temperature, with sufficient fluidity for tissues to flow and reduce strain, the fracture faces can be brought together and the support sheets removed and exported from the body. One simple conceptual mechanism for bringing the fracture faces together involves using biologically inert "strings" attached to specific matching sites on two support sheets that are stabilizing the two opposing faces of a particular fracture. Pulling the strings tight draws the opposing fracture faces together. Even fracture gaps as large as 0.5 millimeters can be accommodated, since all the individual support sheets in a large block of tissue can be simultaneously manipulated as an incremental three-dimensional global strain release network to slowly heal the breaks.

Once the system is liquid it becomes possible to introduce other medical nanodevices to deal with specific forms of damage, including pre-existing damage – like the presence of lipofuscin or other undesired intracellular or extracellular junk, nuclear mutations or epimutations,[432] damaged mitochondria (which could simply be removed and replaced with new, functionally correct mitochondria), and a wide range of other conditions.

Patient Wake-up

After the patient has been repaired, stabilized and warmed to conditions of moderate hypothermia, metabolic activities and concentration gradients appropriate to a healthy functional state can be re-established. The vasculoid increases its transport activities to levels appropriate for a healthy human under normal conditions. The vasculoid can then be removed (in accordance with the sequence described in the vasculoid paper) and the patient is now fully restored but unconscious. Finally, the person is gently ramped through mild hypothermia up to normal body temperature with initiation of consciousness and full awareness of surroundings. The patient is now awake and healthy.

---

[432] Freitas RA Jr. The Ideal Gene Delivery Vector: Chromallocytes, Cell Repair Nanorobots for Chromosome Replacement Therapy. J. Evol. Technol. 2007 Jun;16:1-97; http://jetpress.org/v16/freitas.pdf.

2.2.15 Three Methods for Cryonics Revival (Merkle, 2018)

The most recent discussion of cryonics revival was published in 2018 by Ralph Merkle,[433] who suggests that "three primary methods by which revival from a state of cryopreservation might take place include [A] ***in situ* repair**, [B] **molecular scan-and-restore**, and [C] **scan-to-WBE** [Whole Brain Emulation]," as summarized in excerpts from the paper, below. This work is most notable for its emphasis on the need for WBE to validate cryonics revival technologies:

***In situ* Repair.** This uses the minimum repair methodology necessary for any given region of tissue. In this approach, any functional tissue, or tissue that can be restored to a state from which it can restore itself to a functional state, will be retained and repaired. *In situ* repair scenarios typically involve medical nanorobots called "cryobots" that might be 2 microns in diameter. "Cryobots operate in cryopreserved patients at cryogenic temperatures. Their first mission is to tunnel out the patients' circulatory system. Their second mission is to assess the state of each region of tissue. The primary purpose of this assessment is to determine if the local tissue can be warmed to enable further repairs to take place in the liquid state. The expectation is that well cryoprotected regions that are minimally damaged ('good regions') could be rewarmed until they are liquid, and repairs would continue in the liquid state. Regions where cryoprotectant did not penetrate, or which were otherwise subjected to significant damage ('bad regions'), would be processed at low temperature using *in situ* molecular scan-and-restore. Repair of fractures proceeds by taking a local molecular scan of the region near the fracture, and enough of the surrounding region to enable entry of cryobots into the extended fracture region, followed by rebuilding of the extended fracture region. On-site cryobots will report out to off-site computers, which will analyze the results of any regional molecular scans and develop a regional rebuilding plan for the bad regions compatible with the boundary conditions defined by the adjacent good regions."

"The primary requirement for correct functioning of cryobots is the ability to identify and tunnel through the circulatory system. For this to be possible, the circulatory system in the cryopreserved patient must be relatively intact and identifiable, especially the capillaries. If the circulatory system cannot be identified, or if it is not possible to create an appropriate network of tunnels without damaging the tissue, then it might be necessary to take a molecular scan of the cryopreserved patient as a whole. If, upon assessment, most of the tissue cannot be warmed to a liquid state but must be scanned in place, then a molecular scan of the cryopreserved patient as a whole would seem more appropriate. The level of damage that would prevent correct identification of the circulatory system, followed by tunneling into it by cryobots, would likely be severe."

---

[433] Merkle RC. Revival of Alcor Patients. Cryonics 2018 May-Jun;39(3):10-19 and Cryonics 2018 Jul-Aug;39(4):10-15; https://www.alcor.org/library/revival-of-alcor-patients/.

Molecular Scan-and-Restore. "The lower the quality of the cryopreservation, the more difficult it will be to accurately restore the tissue and the more important it will be to use a scan technology that provides as much information about the tissue as possible. The greatest amount of information would be provided by a molecular scan, which, by definition, produces exact information about the position and type of every atom and molecule in the scanned tissue. Molecular scan-and-restore should be effective even in cases of severe damage. It consists of three steps: (1) a molecular scan, (2) processing of the scan, and (3) physically restoring the patient from the processed scan. In this approach, the molecular scan gathers complete information about the molecular structure of the patient's tissues, particularly including the brain. A molecular scan gives the position and type of every atom. It provides the raw information that could, after processing, serve as the basis for restoring the scanned patient."

"Reliable methods for conducting destructive molecular scans that entirely disassemble the tissue are relatively easy to envision….Such methods might be based on high resolution Scanning Probe Microscopy (SPM) methods [that] rely on the physical interactions between a molecular-sized tip and the surface being scanned. A parallel array of SPM tips spaced approximately 100 nm (10^{-7} m) apart seems feasible, and would allow the surface of the brain (or other tissue) to be rapidly scanned. Assuming a moderately fast scan rate of 10 MHz (10 million pixels per second per tip) and an atomic resolution of 0.1 nm (10^{-10} m, one angstrom), means each tip would be able to scan its 100 nm x 100 nm square region in 0.1 second. Assuming a rate of penetration into the tissue of 1 nm per 0.1 second yields a molecular scan rate of approximately 10^6 nm/day, or 1 mm/day. A 100 mm thick brain could be completed in approximately 100 days….A molecular scan provides us with all the information about the cryopreserved tissue that it is possible to obtain. No further information can be obtained. If we can't restore a person with their memories and personality intact after a molecular scan, then there's too little information in their cryopreserved brain to do this."

Scan-to-WBE. "A third alternative that some patients might explicitly request is to process the information from a molecular scan and use it to directly construct a whole brain emulation (WBE). This 'scan-to-WBE' option might be simpler than the molecular scan-and-restore process, as it would eliminate the need for physically restoring a biological body. Scan-to-WBE would rely entirely on the information recovered from the cryopreserved tissue. It is possible that the technology for molecular scans and Whole Brain Emulations might become available before the technology for *in situ* repair. Alcor members wishing to return to an active life as quickly as possible might want to take advantage of whatever technology arrives first."

Scan-to-WBE assumes both the physical possibility of, and philosophical comfort with, identifying and abstracting out particular operations of biological brains, and computationally modeling them in a manner considered adequate for the functional survival of a human mind. The utility or desirability of Scan-to-WBE are questions that are neither specific to cryonics, nor necessary to address for cryonics revival. Scan-to-WBE is simply an option that future technologies might make available for people who are comfortable with the idea.

3. Accumulated Damage to the Cryopreserved Human Body

It is essential to lay out in some detail the nature and extent of the damage that must be repaired in order to restore tissues and organs to full viability before a cryonics revival protocol can be defined. Physical degradation will occur at every stage of the cryopreservation process, including damage from pre-mortem pathologies (Section 3.1), post-mortem ischemia (Section 3.2), cryoprotectant perfusion (Section 3.3), freezing or cold vitrification (Section 3.4), long-term cryogenic storage (Section 3.5), and rewarming/reperfusion (Section 3.6). Such damage, while extensive, does not appear to be beyond the likely repair capabilities of medical nanorobots (Section 4). Note that only lethal damage will be corrected during the revival process. Other nonlethal conditions ranging from medical flaws to purely cosmetic issues will not be corrected during revival, for reasons elaborated elsewhere (Section 5.2.2.2).

In the following discussion there is a modest emphasis on damage to the brain – both because the brain is the unique site of memory and personality, and because Alcor's 2021 cryopatient population included 122 neuro/brain patients and 62 whole-body patients.[434] However, nanorobotic scaling analyses performed in the present study generally assume that the subject of the revival is a whole-body patient.

3.1 Pre-Mortem Somatic Damage

The first type of injury that almost all[435] cryonics patients will exhibit is the physical damage caused by whatever pathology led to the formal pronouncement of death. Most cryopatients tend to be older, and these patients will most likely have fallen victim to one of the leading causes of aging-related death. For patients 65 years of age and older, heart disease (25%), cancer (21%), pulmonary disease (6%), stroke (6%), and Alzheimer's disease (6%) account for 65% of all U.S. deaths, and 57% of all deaths in the 45-64 age bracket; between ages 25-44, the leading causes of death are accidents (33%), suicide and homicide (17%), and heart disease or cancer (21%), representing 71% of the total.[436]

Patients with **heart disease** may have dead muscle cells in the heart, narrowing or hardening of the coronary arteries with indwelling plaques partially blocking the flow of blood, or other microvascular dysfunction.[437] **Cancer** patients will have exhibited carcinogenesis,[438] including one or more tumors in the brain, heart, or other tissues, caused by abnormal cell growth that can produce blockage of bronchial, esophageal, or colorectal passages, muscle or weight loss, skin changes, and chemical imbalances such as

---

[434] Complete List of Alcor Cryopreservations (all Alcor patients),1967-2021; https://www.alcor.org/library/complete-list-of-alcor-cryopreservations/. This data, marked as current through Nov 2021, was last verified in Dec 2021. The signed-up membership as of Feb 2021 was more evenly distributed: 687 whole body, 643 neuro, and 12 neuro with trunk.

[435] In many jurisdictions, terminally ill patients can voluntarily end their lives before a serious medical pathology forces death upon them (https://en.wikipedia.org/wiki/1994_Oregon_Ballot_Measure_16, https://en.wikipedia.org/wiki/Washington_Death_with_Dignity_Act, https://en.wikipedia.org/wiki/Euthanasia_in_Canada), but most legal systems do not encourage people to voluntarily seek death in the complete absence of medical pathology, e.g., euthanasia (https://en.wikipedia.org/wiki/Euthanasia), assisted death (https://en.wikipedia.org/wiki/Assisted_death), or right to die (https://en.wikipedia.org/wiki/Right_to_die), even for the purpose of life extension via cryonics.

[436] "How Americans die, in 5 charts," Advisory Board, 16 Jan 2019; https://www.advisory.com/daily-briefing/2019/01/16/deaths.

[437] https://en.wikipedia.org/wiki/Coronary_artery_disease#Pathophysiology.
[438] https://en.wikipedia.org/wiki/Carcinogenesis.

hypercalcemia or hyponatremia.[439] The cryopreserved cancer patient may also exhibit a variety of secondary injuries caused by contemporary treatments, possibly including systemic cell death due to chemotherapy[440] or localized radiation damage due to radiation therapy.[441] Patients suffering from chronic obstructive **pulmonary disease** may exhibit narrowed airways in the lung due to inflammation and scarring, focal lung pneumatoses (a persistent pocket of air larger than the alveoli), and a general breakdown of lung tissue as in emphysema and obstructive bronchiolitis.[442] **Stroke** victims will normally exhibit either a blood vessel blockage causing loss of blood to a part of the brain leading to death of local neural tissue (ischemic stroke), or a blood vessel rupture creating an expanding hematoma causing tissue compression and injury, again leading to local tissue death (hemorrhagic stroke).[443] **Alzheimer's** patients will suffer the most worrisome endogenous brain injuries, including loss of neurons and synapses in the cerebral cortex, gross atrophy of large regions of the brain, and widespread deposition of amyloid plaques and neurofibrillary tangles inside and around neurons throughout the brain.[444] Patients with any of the above injuries can be treated with medical nanorobots,[445] including cell repair nanorobots,[446] once other forms of damage have been repaired[447] after the patient has been warmed to a normal 310 K (37 °C) body temperature.

Patients who have experienced **homicide**, **suicide**, or **accidents** can exhibit more grievous physical injuries that may make it very difficult to achieve a high-quality cryopreservation. For example, a gunshot wound[448] to the head or chest may destroy parts of the brain and vascular network and can avulse significant bone and tissue masses from the body. Stabbing[449] injuries are a penetrating trauma that can produce broken bone, perforated tissues, embedded foreign objects, and infection.[450] A fall from a great height or an automobile accident may result in blunt trauma injuries[451] including torn arteries, systemic hemorrhage, and rupture of internal organs. Patients with such wounds might receive very poor cryopreservations if the vasculature is heavily compromised, with major regions of the body receiving an insufficient infusion of cryoprotectant to prevent massive mechanical damage and maceration of the tissues during subsequent cooling to cryogenic temperatures.

Besides the above causes of death, patients who are middle-aged or elderly will present a variety of aging-related depredations, including some that would be fairly easy to repair (e.g., gray hair from degenerate follicles or wrinkled skin from cross-linked dermal collagen) and some that would be more difficult to repair but apparently are less prevalent than commonly believed (e.g., general loss of neurons due to aging

---

[439] https://en.wikipedia.org/wiki/Cancer.
[440] https://en.wikipedia.org/wiki/Chemotherapy#Adverse_effects.
[441] https://en.wikipedia.org/wiki/Radiation_therapy#Side_effects.
[442] https://en.wikipedia.org/wiki/Chronic_obstructive_pulmonary_disease#Pathophysiology.
[443] https://en.wikipedia.org/wiki/Stroke#Pathophysiology.
[444] https://en.wikipedia.org/wiki/Alzheimer%27s_disease#Pathophysiology.

[445] Freitas RA Jr. Chapter 23. Comprehensive Nanorobotic Control of Human Morbidity and Aging. In: Fahy GM, West MD, Coles LS, Harris SB, eds, The Future of Aging: Pathways to Human Life Extension, Springer, New York, 2010, pp. 685-805; http://www.nanomedicine.com/Papers/Aging.pdf.

[446] e.g., Freitas RA Jr. The Ideal Gene Delivery Vector: Chromallocytes, Cell Repair Nanorobots for Chromosome Replacement Therapy. J. Evol. Technol. 2007 Jun;16:1-97; http://jetpress.org/v16/freitas.pdf.

[447] The repairs required for the partial or full recovery of normal brain function in Alzheimer's patients will be particularly extensive and challenging, but appear to lie within the anticipated capabilities of medical nanorobots. Freitas RA Jr. The Alzheimer Protocols: A Nanorobotic Cure for Alzheimer's Disease and Related Neurodegenerative Conditions. IMM Report No. 48, June 2016, 433 pp; http://www.imm.org/Reports/rep048.pdf.

[448] https://en.wikipedia.org/wiki/Gunshot_wound#Pathophysiology.
[449] https://en.wikipedia.org/wiki/Stab_wound.
[450] https://en.wikipedia.org/wiki/Penetrating_trauma.
[451] https://en.wikipedia.org/wiki/Blunt_trauma.

and alcohol consumption).[452] However, the repair of nonlethal medical deficiencies will normally be deferred until cryostasis revival has been successfully completed (Section 5.2.2.2).

Finally, we should recognize that the patient's actual cause of death may be due to somatic defects other than those officially reported on the death certificate. These additional defects must be identified and corrected as well. For example, one reference[453] from the early days of cryonics reported that: "...both patients apparently suffered from pathologies which contributed to or caused their deaths which were not listed on the death certificates. In addition to having suffered a cerebrovascular accident P1 was also found to have suffered a large, "recent" infarct of the posterior wall of the left ventricle. The heart was also hypertrophied secondary to chronic heart failure. P2 apparently died as a result of a massive intra-abdominal hemorrhage, not of an acute myocardial infarction as listed on the death certificate."

3.2 Post-Mortem Ischemic Damage

Global ischemia is the cessation of active blood flow throughout the body at death after the heart stops beating, which, if maintained systemically over a period of time, produces a cascade of biochemical reactions and structural changes resulting in tissue that is no longer viable by conventional medical standards, i.e., "cell death".[454] The ischemic cascade begins within minutes of cardiac arrest and usually proceeds for several hours or longer, via mechanisms illustrated in the simplified overview at right.[455] Damage results from the build-up of metabolic waste products, the inability to maintain cell membranes, mitochondrial injury, and eventual leakage of autolyzing proteolytic

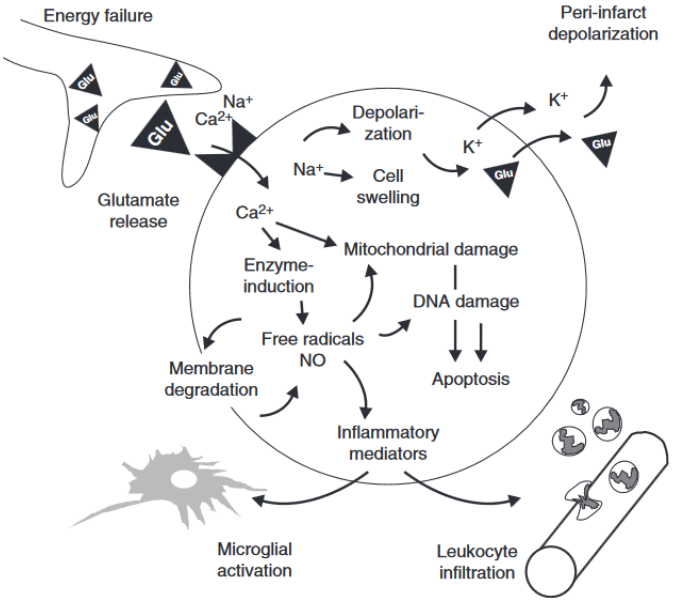

[452] von Bartheld CS. Myths and truths about the cellular composition of the human brain: A review of influential concepts. J Chem Neuroanat. 2018 Nov;93:2-15; https://www.ncbi.nlm.nih.gov/pmc/articles/PMC5834348/.

[453] Federowicz M, Hixon H, Leaf J. Postmortem examination of three cryonic suspension patients. Cryonics 1984 Sep;16(50):16-28; https://www.alcor.org/library/postmortem-examination-of-three-cryonic-suspension-patients/.

[454] Much of the discussion in this Section draws heavily from: Endres M, Dirnagl U, Moskowitz MA. The ischemic cascade and mediators of ischemic injury. Handb Clin Neurol. 2009;92:31-41; http://neuroutbildarna.se/files/7814/8647/7933/artikel-celldod-2-1.pdf; Darwin M. The pathophysiology of ischemic injury; https://www.alcor.org/library/the-pathophysiology-of-ischemic-injury/ (1995) and http://chronopause.com/chronopause.com/index.php/2011/02/15/the-pathophysiology-of-ischemic-injury-impact-on-the-human-cryopreservation-patient-part-4/index.html (2011); and Best B. Ischemia and Reperfusion Injury in Cryonics. December 2003; https://www.benbest.com/cryonics/ischemia.html.

[455] Dirnagl U, Iadecola C, Moskowitz MA. Pathobiology of ischaemic stroke: an integrated view. Trends Neurosci. 1999 Oct;22(9):391–397; http://citeseerx.ist.psu.edu/viewdoc/download?doi=10.1.1.946.3210&rep=rep1&type=pdf.

enzymes into the cell and surrounding tissues.[456]

The following subsections outline a few details of the global ischemic process.

3.2.1 Energy Failure, Ionic Imbalance, and Excitotoxicity

Ischemia immediately deprives the brain (and other tissues) of oxygen and glucose, causing anoxia and loss of function in both white and gray matter.[457] Lack of oxygen causes the neuron's normal process for making adenosine triphosphate (ATP) for energy to fail,[458] with high-energy phosphate levels almost fully depleted within 5 minutes of the onset of ischemia.[459] This forces the cell to switch to anaerobic metabolism, producing lactic acid. Lactic acidosis contributes to the pathophysiology of ischemia,[460] with lactate levels above a threshold of 18-25 μmol/gm resulting in currently irreversible neuronal injury.[461] The decrease in pH due to lactic acidosis also injures and inactivates mitochondria,[462] i.e., acidotoxicity.[463]

As ATP-reliant ion transport pumps fail, the cell becomes depolarized and allows the inflow of ions, especially calcium (Ca^{2+}), into the cell. Neuronal and non-neuronal cells become depolarized (e.g., anoxic depolarization)[464] and voltage-dependent calcium channels are activated[465] within minutes. The ion pumps

---

[456] https://en.wikipedia.org/wiki/Ischemia#Pathophysiology.

[457] Stys PK, Waxman SG, Ransom BR. Effects of temperature on evoked electrical activity and anoxic injury in CNS white matter. J Cereb Blood Flow Metab. 1992 Nov;12(6):977-986; https://journals.sagepub.com/doi/pdf/10.1038/jcbfm.1992.135.

[458] "In the first minute after stoppage of blood flow to the brain, ATP in neurons is primarily regenerated from ADP [adenosine diphosphate] by phosphate from phosphocreatine. Within two minutes without blood flow (due to heart stoppage or blood vessel occlusion) neurons lack the energy to power the sodium/potassium pump. Potassium ions rush out of the cell while sodium and chloride ions rush inward as the cell membranes depolarize. The net breakdown of ATP from glycolysis results in ADP, AMP (adenosine monophosphate), phosphate, lactate and acid accumulation (acidosis). Accumulation of carbon dioxide results in carbonic acid (H_2CO_3), which further increases acidity. Within two minutes of ischemia, extracellular pH can drop from about 7.3 to about 6.7." Best B. Ischemia and Reperfusion Injury in Cryonics. 2003 Dec; https://www.benbest.com/cryonics/ischemia.html.

[459] Siesjö BK. Cell damage in the brain: a speculative synthesis. J Cereb Blood Flow Metab. 1981 Jun 1;1(2):155-185; https://journals.sagepub.com/doi/pdf/10.1038/jcbfm.1981.18.

[460] Biros MH, Dimlich RV, Barsan WG. Postinsult treatment of ischemia-induced cerebral lactic acidosis in the rat. Ann Emerg Med. 1986 Apr;15(4):397-404; https://pubmed.ncbi.nlm.nih.gov/3954171.

[461] Rehncrona S, Rosén I, Siesjö BK. Brain lactic acidosis and ischemic cell damage: 1. Biochemistry and neurophysiology. J Cereb Blood Flow Metab. 1981;1(3):297-311; https://journals.sagepub.com/doi/pdf/10.1038/jcbfm.1981.34. Kalimo H, Rehncrona S, Söderfeldt B, Olsson Y, Siesjö BK. Brain lactic acidosis and ischemic cell damage: 2. Histopathology. J Cereb Blood Flow Metab. 1981;1(3):313-327; https://journals.sagepub.com/doi/pdf/10.1038/jcbfm.1981.35. Rehncrona S, Rosén I, Smith ML. Effect of different degrees of brain ischemia and tissue lactic acidosis on the short-term recovery of neurophysiologic and metabolic variables. Exp Neurol. 1985 Mar;87(3):458-473; https://pubmed.ncbi.nlm.nih.gov/3972049.

[462] Darwin M. The pathophysiology of ischemic injury. BioPreservation, Inc., 1995; https://www.alcor.org/Library/html/ischemicinjury.html.

[463] Simon RP. Acidotoxicity trumps excitotoxicity in ischemic brain. Arch Neurol. 2006 Oct;63(10):1368-71; https://jamanetwork.com/journals/jamaneurology/articlepdf/792466/NNR60010.pdf.

[464] Martin RL, Lloyd HG, Cowan AI. The early events of oxygen and glucose deprivation: setting the scene for neuronal death?. Trends Neurosci. 1994 Jun;17(6):251-257; https://pubmed.ncbi.nlm.nih.gov/7521086.

can no longer transport calcium out of the cell, and the presence of excessive intracellular calcium triggers the release of predominantly excitatory neurotransmitters from presynaptic terminals into the synaptic cleft,[466] especially glutamate that binds to AMPA receptors and Ca^{2+}-permeable NMDA receptors, inducing them to open and allow still more calcium into cells. An excess of excitatory neurotransmitters can cause neuronal injury and death even in the absence of hypoxic or ischemic injury.[467]

The excessive intracellular calcium levels trigger an array of calcium-dependent enzymes such as poly-ADPribose polymerase (PARP) and the calpains,[468] endonucleases,[469] phospholipases[470] and proteases[471] that degrade DNA, membranes, and proteins essential for cellular integrity (e.g., actin, spectrin, laminin).[472] Excess calcium can also induce microtubule depolymerization.[473] As the cell's membrane is broken down by phospholipases,[474] it becomes more permeable and allows more ions and harmful chemicals to flow into the cell, while intracellular potassium leaks rapidly out of the cell.[475]

---

[465] Paschen W. Role of calcium in neuronal cell injury: which subcellular compartment is involved?. Brain Res Bull. 2000 Nov 1;53(4):409-413; https://pubmed.ncbi.nlm.nih.gov/11136996.

[466] Zipfel GJ, Lee JM, Choi DW. Reducing calcium overload in ischemic brain. N Engl J Med 1999 Nov 11;341:1543-1544; https://www.nejm.org/doi/full/10.1056/NEJM199911113412011.

[467] Rothman S. Synaptic release of excitatory amino acid neurotransmitter mediates anoxic neuronal death. J Neurosci. 1984 Jul;4(7):1884-1891; https://www.jneurosci.org/content/jneuro/4/7/1884.full.pdf. Hagberg H, Lehmann A, Sandberg M, Nyström B, Jacobson I, Hamberger A. Ischemia-induced shift of inhibitory and excitatory amino acids from intra- to extracellular compartments. J Cereb Blood Flow Metab. 1985 Sep;5(3):413-419; https://journals.sagepub.com/doi/pdf/10.1038/jcbfm.1985.56.

[468] Mehta SL, Manhas N, Raghubir R. Molecular targets in cerebral ischemia for developing novel therapeutics. Brain Res Rev. 2007 Apr;54(1):34-66; https://www.ncbi.nlm.nih.gov/pubmed/17222914. Doyle KP, Simon RP, Stenzel-Poore MP. Mechanisms of ischemic brain damage. Neuropharmacology 2008 Sep;55(3):310-318; https://www.ncbi.nlm.nih.gov/pmc/articles/PMC2603601/.

[469] Tominaga T, Kure S, Narisawa K, Yoshimoto T. Endonuclease activation following focal ischemic injury in the rat brain. Brain Res. 1993 Apr 9;608(1):21-26; https://pubmed.ncbi.nlm.nih.gov/8388311.

[470] Muralikrishna Adibhatla R, Hatcher JF. Phospholipase A2, reactive oxygen species, and lipid peroxidation in cerebral ischemia. Free Radic Biol Med. 2006 Feb 1;40(3):376-387; http://citeseerx.ist.psu.edu/viewdoc/download?doi=10.1.1.204.3288&rep=rep1&type=pdf.

[471] del Zoppo GJ, Milner R, Mabuchi T, *et al*. Microglial activation and matrix protease generation during focal cerebral ischemia. Stroke. 2007 Feb;38(2 Suppl):646-651; http://stroke.ahajournals.org/content/38/2/646.

[472] Chen J, Nagayama T, Jin K, Stetler RA, Zhu RL, Graham SH, Simon RP. Induction of caspase-3-like protease may mediate delayed neuronal death in the hippocampus after transient cerebral ischemia. J Neurosci. 1998 Jul 1;18(13):4914-4928; https://www.jneurosci.org/content/jneuro/18/13/4914.full.pdf. Furukawa K, Fu W, Li Y, Witke W, Kwiatkowski DJ, Mattson MP. The actin-severing protein gelsolin modulates calcium channel and NMDA receptor activities and vulnerability to excitotoxicity in hippocampal neurons. J Neurosci. 1997 Nov 1;17(21):8178-8186; https://www.jneurosci.org/content/jneuro/17/21/8178.full.pdf. Endres M, Fink KB, Zhu J, Stagliano NE, Bondada V, Geddes JW, Azuma T, Mattson MP, Kwiatkowski DJ, Moskowitz MA. Neuroprotective effects of gelsolin during murine stroke. J Clin Invest 1999 Feb;103:347-354; https://www.ncbi.nlm.nih.gov/pmc/articles/PMC407902/.

[473] O'Brien ET, Salmon ED, Erickson HP. How calcium causes microtubule depolymerization. Cell Motil Cytoskeleton. 1997;36(2):125-135; https://pubmed.ncbi.nlm.nih.gov/9015201/.

[474] "Most ischemic brain damage is to the lipid portion of cell membranes through lipid peroxidation and phospholipase activity." Best B. Ischemia and Reperfusion Injury in Cryonics. December 2003; https://www.benbest.com/cryonics/ischemia.html.

[475] Heuser D, Guggenberger H. Ionic changes in brain ischaemia and alterations produced by drugs. Br J Anaesth. 1985 Jan;57(1):23-33; https://www.sciencedirect.com/science/article/pii/S0007091217432971/pdf.

Calcium and other ions enter mitochondria through the mitochondrial permeability transition pore, overloading the organelle with calcium, causing dysfunction and mitochondrial swelling, releasing toxins into the cell. Sodium and chloride ions enter neurons via channels for monovalent ions (e.g., the AMPA receptor) passively followed by water, creating a cytotoxic intracellular edema. Imbalances of other ions cause additional damage, as when large amounts of zinc stored in vesicles of excitatory neurons are released upon depolarization and contribute to excitotoxic cell death.[476]

Another consequence[477] of phospholipase activation is the production of free fatty acids (FFA)[478] including arachidonic acid, a potent prostaglandin inducer that causes a biochemical cascade ending with the production of thromboxane and leukotrienes – tissue irritants that can cause platelet aggregation, clotting, vasospasm, and edema.[479] FFA may have other degradative effects on cell membranes.[480]

3.2.2 Nitrosative Stress

Within minutes of the onset of ischemia, calcium-dependent neuronal type I nitric oxide synthase (nNOS) may be activated via calcium influx, causing cortical NO levels to rise from 10 nmol/L to 2000 nmol/L.[481] Inducible type II NO synthase (iNOS),[482] which is calcium/calmodulin-independent and normal absent from healthy brain tissue, is also induced during brain ischemia in non-neuronal cells such as microglia, leukocytes, astrocytes and endothelial cells, adding further to the NO output once expressed (usually ≥24

---

[476] Frederickson CJ. Neurobiology of zinc and zinc-containing neurons. Int Rev Neurobiol. 1989;31:145-238; https://www.sciencedirect.com/science/article/pii/S0074774208602792. Weiss JH, Hartley DM, Koh JY, Choi DW. AMPA receptor activation potentiates zinc neurotoxicity. Neuron. 1993 Jan;10(1):43-49; https://pubmed.ncbi.nlm.nih.gov/7678965. Sørensen JC, Mattsson B, Andreasen A, Johansson BB. Rapid disappearance of zinc positive terminals in focal brain ischemia. Brain Res. 1998 Nov 23;812(1-2):265-269; https://pubmed.ncbi.nlm.nih.gov/9813362. Granzotto A, Sensi SL. Intracellular zinc is a critical intermediate in the excitotoxic cascade. Neurobiol Dis. 2015 Sep;81:25-37; https://www.researchgate.net/profile/Stefano_Sensi/publication/275719559_Intracellular_zinc_is_a_critical_intermediate_in_the_excitotoxic_cascade/links/5c27e50b92851c22a34e7d1e/Intracellular-zinc-is-a-critical-intermediate-in-the-excitotoxic-cascade.pdf.

[477] Darwin M. The pathophysiology of ischemic injury. BioPreservation, Inc., 1995; https://www.alcor.org/Library/html/ischemicinjury.html.

[478] Duan XX, Zhang GP, Wang XB, Yu H, Wu JL, Liu KZ, Wang L, Long X. Elevated Serum and Cerebrospinal Fluid Free Fatty Acid Levels Are Associated with Unfavorable Functional Outcome in Subjects with Acute Ischemic Stroke. Mol Neurobiol. 2017 Apr;54(3):1677-1683; https://pubmed.ncbi.nlm.nih.gov/26873852.

[479] Wolfe LS. Eicosanoids: prostaglandins, thromboxanes, leukotrienes, and other derivatives of carbon-20 unsaturated fatty acids. J Neurochem. 1982 Jan;38(1):1-14; https://pubmed.ncbi.nlm.nih.gov/6286875. Raichle ME. The pathophysiology of brain ischemia. Ann Neurol. 1983 Jan;13(1):2-10; https://pubmed.ncbi.nlm.nih.gov/6299175. Mullane KM, Salmon JA, Kraemer R. Leukocyte-derived metabolites of arachidonic acid in ischemia-induced myocardial injury. Fed Proc. 1987 May 15;46(7):2422-2433; https://pubmed.ncbi.nlm.nih.gov/3106093.

[480] Wolfe LS. Eicosanoids: prostaglandins, thromboxanes, leukotrienes, and other derivatives of carbon-20 unsaturated fatty acids. J Neurochem. 1982 Jan;38(1):1-14; https://pubmed.ncbi.nlm.nih.gov/6286875.

[481] Dalkara T, Moskowitz MA. The complex role of nitric oxide in the pathophysiology of focal cerebral ischemia. Brain Pathol. 1994 Jan;4(1):49-57; https://pubmed.ncbi.nlm.nih.gov/7517769.

[482] Zheng L, Ding J, Wang J, Zhou C, Zhang W. Effects and Mechanism of Action of Inducible Nitric Oxide Synthase on Apoptosis in a Rat Model of Cerebral Ischemia-Reperfusion Injury. Anat Rec (Hoboken). 2016 Feb;299(2):246-255; https://anatomypubs.onlinelibrary.wiley.com/doi/epdf/10.1002/ar.23295.

hours after ischemia onset) and contributing to secondary late-phase tissue damage[483] as unattended ischemic injury evolves over several days. NO generation affects BBB permeability in the brain[484] and is linked to DNA damage and activation of the nuclear enzyme poly-ADP-ribose polymerase (PARP-1) by single-stranded DNA nicks (which may be generated by nitrosative damage), consuming large amounts of NAD^+ that depletes cellular energy and contributes to subsequent cell death.[485]

Autophagy,[486] a process in which damaged intracellular components are encased in phagosomes which then merge with lysosomes to be destroyed, can be induced by nitrosative stress.[487] Ischemia-derived nitrosative stress can also induce mitophagy (the autophagy of mitochondria).[488]

3.2.3 Inflammation

The expression of pro-inflammatory genes is triggered early after the onset of ischemia,[489] initiating a cascade of events[490] including the expression of adhesion molecules (e.g., intercellular and vascular

---

[483] Iadecola C, Zhang F, Casey R, Nagayama M, Ross ME. Delayed reduction of ischemic brain injury and neurological deficits in mice lacking the inducible nitric oxide synthase gene. J Neurosci. 1997 Dec 1;17(23):9157-9164; https://www.ncbi.nlm.nih.gov/pmc/articles/pmid/9364062/.

[484] Gu Y, Zheng G, Xu M, Li Y, Chen X, Zhu W, Tong Y, Chung SK, Liu KJ, Shen J. Caveolin-1 regulates nitric oxide-mediated matrix metalloproteinases activity and blood-brain barrier permeability in focal cerebral ischemia and reperfusion injury. J Neurochem. 2012 Jan;120(1):147-156; https://onlinelibrary.wiley.com/doi/full/10.1111/j.1471-4159.2011.07542.x.

[485] Zhang J, Dawson VL, Dawson TM, Snyder SH. Nitric oxide activation of poly(ADP-ribose) synthetase in neurotoxicity. Science. 1994 Feb 4;263(5147):687-689; https://pubmed.ncbi.nlm.nih.gov/8080500. Eliasson MJ, Sampei K, Mandir AS, Hurn PD, Traystman RJ, Bao J, Pieper A, Wang ZQ, Dawson TM, Snyder SH, Dawson VL. Poly(ADP-ribose) polymerase gene disruption renders mice resistant to cerebral ischemia. Nat Med. 1997 Oct;3(10):1089-1095; http://tonto.stanford.edu/~john/205/1999-2000/eliasson.pdf. Kim YH, Koh JY. The role of NADPH oxidase and neuronal nitric oxide synthase in zinc-induced poly(ADP-ribose) polymerase activation and cell death in cortical culture. Exp Neurol. 2002 Oct;177(2):407-418; https://pubmed.ncbi.nlm.nih.gov/12429187.

[486] https://en.wikipedia.org/wiki/Autophagy.

[487] Han F, Chen YX, Lu YM, *et al*. Regulation of the ischemia-induced autophagy-lysosome processes by nitrosative stress in endothelial cells. J Pineal Res. 2011 Aug;51(1):124-135; https://www.researchgate.net/profile/Gensheng_Zhang2/publication/50362494_Regulation_of_the_ischemia-induced_autophagy-lysosome_processes_by_nitrosative_stress_in_endothelial_cells/links/5a8bfce10f7e9b1a9556108c/Regulation-of-the-ischemia-induced-autophagy-lysosome-processes-by-nitrosative-stress-in-endothelial-cells.pdf.

[488] Feng J, Chen X, Guan B, Li C, Qiu J, Shen J. Inhibition of Peroxynitrite-Induced Mitophagy Activation Attenuates Cerebral Ischemia-Reperfusion Injury. Mol Neurobiol. 2018 Aug;55(8):6369-6386; https://pubmed.ncbi.nlm.nih.gov/29307080/.

[489] Pirttilä TR, Kauppinen RA. Recovery of intracellular pH in cortical brain slices following anoxia studied by nuclear magnetic resonance spectroscopy: role of lactate removal, extracellular sodium and sodium/hydrogen exchange. Neuroscience. 1992;47(1):155-164; https://pubmed.ncbi.nlm.nih.gov/1315933. Lindsberg PJ, Carpén O, Paetau A, Karjalainen-Lindsberg ML, Kaste M. Endothelial ICAM-1 expression associated with inflammatory cell response in human ischemic stroke. Circulation. 1996 Sep 1;94(5):939-945; https://www.ahajournals.org/doi/full/10.1161/01.CIR.94.5.939. Iadecola C. Bright and dark sides of nitric oxide in ischemic brain injury. Trends Neurosci. 1997 Mar;20(3):132-139; https://pubmed.ncbi.nlm.nih.gov/9061868.

adhesion molecules, ICAM, VCAM, and selectins), endothelial activation, pro-inflammatory and pro-thrombotic interactions between vessel wall and blood constituents promoting thrombogenesis, and microvascular plugging (e.g., granulocyte activation plugs ~27% of myocardial capillaries during acute myocardial ischemia[491]). Adhesion molecules expressed by the endothelium interact with receptors on neutrophils to promote their entry into the brain, followed days later by macrophages and monocytes in unattended ischemia.[492] Similar to leukocytes, activated microglia produce numerous pro-inflammatory cytokines along with toxic metabolites,[493] and macroglia such as astrocytes become activated and proliferate. Phagocytic cells may engulf damaged but still viable tissue. For example, increased production of IL-1 by microglia, astrocytes, and neurons may propagate tissue damage via arachidonic acid release, enhancement of NMDA mediated excitotoxicity, and stimulation of nitric oxide synthesis.[494] Increased expression of CINC and MCP-1 mRNA within 6 hours of cerebral arterial occlusion attracts neutrophils to ischemic tissue.[495]

Under conditions of complete circulatory arrest, neutrophil activation is a key factor in initiating the systemic cascade of inflammation/immune response that terminates in delayed multisystem organ failure.[496] Neutrophils accumulate in the brain within 30 minutes after complete occlusion of the middle cerebral artery during stroke, causing tissue damage by releasing oxygen free radicals and proteolytic enzymes.[497] Activated neutrophils can release (1) large amounts of hydrogen peroxide which quickly reacts with chloride to form bleach (HOCl)[498] capable of damaging a wide range of organic molecules,[499]

---

[490] Connolly ES Jr, Winfree CJ, Springer TA, Naka Y, Liao H, Yan SD, Stern DM, Solomon RA, Gutierrez-Ramos JC, Pinsky DJ. Cerebral protection in homozygous null ICAM-1 mice after middle cerebral artery occlusion. Role of neutrophil adhesion in the pathogenesis of stroke. J Clin Invest. 1996 Jan 1;97(1):209-216; https://www.ncbi.nlm.nih.gov/pmc/articles/PMC507081/. Stanimirovic D, Satoh K. Inflammatory mediators of cerebral endothelium: a role in ischemic brain inflammation. Brain Pathol. 2000 Jan;10(1):113-126; https://www.researchgate.net/profile/Danica_Stanimirovic/publication/12646245_Inflammatory_Mediators_of_Cerebral_Endothelium_A_Role_in_Ischemic_Brain_Inflammation/links/59deaca00f7e9bcfab240db3/Inflammatory-Mediators-of-Cerebral-Endothelium-A-Role-in-Ischemic-Brain-Inflammation.pdf. Frijns CJ, Kappelle LJ. Inflammatory cell adhesion molecules in ischemic cerebrovascular disease. Stroke. 2002 Aug;33(8):2115-2122; https://www.ahajournals.org/doi/full/10.1161/01.STR.0000021902.33129.69.

[491] Engler R. Consequences of activation and adenosine-mediated inhibition of granulocytes during myocardial ischemia. Fed Proc. 1987 May 15;46(7):2407-12; https://www.ncbi.nlm.nih.gov/pubmed/3569543.

[492] Iadecola C. Bright and dark sides of nitric oxide in ischemic brain injury. Trends Neurosci. 1997 Mar;20(3):132-139; https://pubmed.ncbi.nlm.nih.gov/9061868.

[493] Yrjanheikki J, Tikka T, Keinanan R, Goldsteins G, Chan PH, Koistinaho J. A tetracycline derivative, minocycline, reduces inflammation and protects against focal cerebral ischemia with a wide therapeutic window. Proc Natl Acad Sci USA 1999 Nov 9;96(23):13496-13500; https://www.ncbi.nlm.nih.gov/pmc/articles/PMC23976/.

[494] Huang J, Upadhyay UM, Tamargo RJ. Inflammation in stroke and focal cerebral ischemia. Surg Neurol. 2006 Sep; 66(3):232-45; https://www.ncbi.nlm.nih.gov/pubmed/16935624.

[495] Minami M, Satoh M. Chemokines and their receptors in the brain: pathophysiological roles in ischemic brain injury. Life Sci. 2003 Dec 5;74(2-3):321-7; http://labs.icb.ufmg.br/lbcd/prodabi5/homepages/hugo/Hugo/macrofago1.pdf

[496] Bersten A, Sibbald WJ. Acute lung injury in septic shock. Crit Care Clin. 1989 Jan;5(1):49-79; https://pubmed.ncbi.nlm.nih.gov/2647226.

[497] Doyle KP, Simon RP, Stenzel-Poore MP. Mechanisms of ischemic brain damage. Neuropharmacology 2008 Sep;55(3):310-318; https://www.ncbi.nlm.nih.gov/pmc/articles/PMC2603601/.

[498] 10^6 neutrophils can generate 2 x 10^7 mol of HOCl – enough to destroy 150 million *E. coli* in a matter of milliseconds. Klebanoff SJ. Phagocytic cells: Products of oxygen metabolism. In: Gallin JI, Goldstein IM, Snyderman R, eds. Inflammation: basic principles and clinical correlates. Raven Press, NY, 1988:391-444.

and (2) elastase and other proteolytic enzymes[500] that can decompose the proteinaceous extracellular matrix and degrade capillary integrity.[501]

Any ATP that has leaked into the extracellular spaces can activate inflammatory responses in macrophages and other innate immune cells.[502]

3.2.4 Protein, RNA, and DNA Stability

Cellular proteins are apparently quite stable under conditions of warm ischemia. Studies of protein stability in post-mortem rat cerebella show that the spectrum of abundant proteins is unchanged after up to 16 hours post-mortem at room temperature.[503] The expressed proteome in ovarian and breast cancer tissues is unchanged after 1 hour of cold ischemia, although phosphorylation modifications were observed in 24% of the >10,000 proteins detected,[504] and other studies have found some room temperature instability over 6-24 hours.[505] This is consistent with observations of reduced protein synthesis and degradation during conditions of warm ischemia[506] and anoxia.[507]

Messenger RNA molecules appear stable as well. According to one study:[508] "Both rat and human cerebellar mRNAs are surprisingly stable under a variety of post-mortem conditions, and biologically

---

[499] Test ST, Weiss SJ. The generation and utilization of chlorinated oxidants by human neutrophils. Adv Free Radical Biol Med 1986;2(1):91-116; https://www.sciencedirect.com/science/article/abs/pii/S8755966886800254.

[500] Henson PM, Henson JE, Fitlschen C, *et al*. Phagocytic cells: Degranulation and secretion. In: Gallin JI, Goldstein IM, Snyderman R, eds. Inflammation: Basic Principles and Clinical Correlates. Raven Press, NY, 1988:363-80.

[501] Darwin M. The pathophysiology of ischemic injury. BioPreservation, Inc., 1995; https://www.alcor.org/Library/html/ischemicinjury.html.

[502] Välimäki E, Cypryk W, Virkanen J, Nurmi K, Turunen PM, Eklund KK, Åkerman KE, Nyman TA, Matikainen S. Calpain Activity Is Essential for ATP-Driven Unconventional Vesicle-Mediated Protein Secretion and Inflammasome Activation in Human Macrophages. J Immunol. 2016;197(8):3315–3325; https://www.jimmunol.org/content/jimmunol/197/8/3315.full.pdf.

[503] Morrison MR, Griffin WST. The isolation and *in vitro* translation of undegraded messenger RNAs from human postmortem brain. Anal Biochem. 1981 May 15;113(2):318-24; https://www.sciencedirect.com/science/article/pii/000326978190083X.

[504] Mertins P, Yang F, Liu T, *et al*. Ischemia in tumors induces early and sustained phosphorylation changes in stress kinase pathways but does not affect global protein levels. Mol Cell Proteomics. 2014 Jul;13(7):1690-1704; https://www.mcponline.org/content/13/7/1690.long.

[505] Hennessy BT, Lu Y, Gonzalez-Angulo AM, *et al*. A Technical Assessment of the Utility of Reverse Phase Protein Arrays for the Study of the Functional Proteome in Non-microdissected Human Breast Cancers. Clin Proteomics. 2010 Dec;6(4):129-151; https://core.ac.uk/download/pdf/81552809.pdf.

[506] Williams EH, Kao RL, Morgan HE. Protein degradation and synthesis during recovery from myocardial ischemia. Am J Physiol. 1981 Mar;240(3):E268-E273; https://pubmed.ncbi.nlm.nih.gov/7212059.

[507] Chua B, Kao RL, Rannels DE, Morgan HE. Inhibition of protein degradation by anoxia and ischemia in perfused rat hearts. J Biol Chem. 1979 Jul 25;254(14):6617-6623; https://www.researchgate.net/profile/Race_Kao/publication/22694015_Inhibition_of_protein_degradation_by_anoxia_and_ischemia_in_perfused_rat_hearts/links/0912f506d9713aa5ac000000.pdf.

[508] Morrison MR, Griffin WST. The isolation and *in vitro* translation of undegraded messenger RNAs from human postmortem brain. Anal Biochem. 1981 May 15;113(2):318-24; https://www.sciencedirect.com/science/article/pii/000326978190083X.

active high-molecular-weight mRNAs can be isolated from post-mortem tissue. A comparison of RNA recoveries from fresh rat cerebella and from cerebella exposed to different post-mortem treatments showed that 83% of the total cytoplasmic RNAs present immediately post-mortem was recovered when rat cerebella were left at room temperature for 16 hours post-mortem and 90% was recovered when the cerebella were left at 4 °C for this length of time." Another study[509] found "no effect of post-mortem delay on RNA quality in both rat and human" and confirmed that post-mortem delays of as long as 48 hours "failed to reveal degradation of the specific rat brain mRNAs during the post-mortem period." A more recent study in 2001 found no significant degradation after 14 hours of mRNA recovered from post-mortem tissue samples in both Alzheimer's and nondemented brains.[510]

After cell death, DNA begins being cleaved into fragments by nucleases[511] and can be digested by microorganisms during decomposition.[512] Long-term DNA decay undergoes strand cleavage via hydrolysis of amino groups that accelerates the loss of purine residues (depurination).[513] A recent experimental study[514] estimated that the average molecular half-life for mitochondrial DNA depurination damage was $t_{DNA1/2} \sim \ln(2) / k_{242} = 521$ years for a 242 base-pair segment of mtDNA in buried bones of the extinct New Zealand moa, representing a fragmentation rate of $k_{DNAfrag} \sim 5.5 \times 10^{-6}$/nucleotide-year at a mean storage temperature of 286.25 K (13.1 °C), where $k_{242} = 1 - \exp(242\ k_{DNAfrag})$. The researchers helpfully estimated the temperature dependence of the mtDNA fragmentation rate as $\ln(k_{DNAfrag}) \sim 41.2 - (15267.6 / T)$, which implies:

* $k_{DNAfrag} \sim 3.2 \times 10^{-4}$/nucleotide-year at T = 310 K (37 °C), $t_{DNA1/2} \sim 9$ years
* $k_{DNAfrag} \sim 4.0 \times 10^{-7}$/nucleotide-year at T = 273 K (0 °C), $t_{DNA1/2} \sim 7200$ years; and
* $k_{DNAfrag} \sim 6.0 \times 10^{-69}$/nucleotide-year at T = 77 K (-196 °C), $t_{DNA1/2} \sim 5 \times 10^{65}$ years.

In other words, the long-term nonenzymatic chemical decay rate of DNA appears very low.

---

[509] Johnson SA, Morgan DG, Finch CE. Extensive postmortem stability of RNA from rat and human brain. J Neurosci Res. 1986;16(1):267-80; https://www.ncbi.nlm.nih.gov/pubmed/2427740.

[510] Cummings TJ, Strum JC, Yoon LW, Szymanski MH, Hulette CM. Recovery and expression of messenger RNA from postmortem human brain tissue. Mod Pathol. 2001 Nov;14(11):1157-1161; https://www.nature.com/articles/3880451.

[511] Darzynkiewicz Z, Juan G, Li X, Gorczyca W, Murakami T, Traganos F. Cytometry in cell necrobiology: analysis of apoptosis and accidental cell death (necrosis). Cytometry. 1997 Jan 1;27(1):1-20; http://www.cyto.purdue.edu/cdroms/cyto10a/cytometryhistory/individualhistories/media/darz/necrobiology.pdf.

[512] Eglinton G, Logan GA. Molecular preservation. Philos Trans R Soc Lond B Biol Sci. 1991 Sep 30;333(1268):315-328; https://royalsocietypublishing.org/doi/pdf/10.1098/rstb.1991.0081. Lindahl T. Instability and decay of the primary structure of DNA. Nature. 1993 Apr 22;362(6422):709-715; http://n.ethz.ch/~nbennett/download/Reading_NEW/DNA%20Damage%20and%20Repair/Lindahl.pdf.

[513] Lindahl T, Nyberg B. Rate of depurination of native deoxyribonucleic acid. Biochemistry. 1972 Sep 12;11(19):3610-3618; https://pubs.acs.org/doi/pdf/10.1021/bi00769a018. Lindahl T, Andersson A. Rate of chain breakage at apurinic sites in double-stranded deoxyribonucleic acid. Biochemistry. 1972 Sep 12;11(19):3618-3623, https://pubs.acs.org/doi/pdf/10.1021/bi00769a019.

[514] Allentoft ME, Collins M, Harker D, Haile J, Oskam CL, Hale ML, Campos PF, Samaniego JA, Gilbert MTP, Willerslev E, Zhang G, Scofield RP, Holdaway RN, Bunce M. The half-life of DNA in bone: measuring decay kinetics in 158 dated fossils. Proc Biol Sci. 2012 Dec 7;279(1748):4724-4733; https://royalsocietypublishing.org/doi/10.1098/rspb.2012.1745.

3.2.5 Apoptosis, Necrosis, and Structural Degradation

Mild ischemic injury can induce cell death via an apoptotic mechanism rather than necrosis. Triggers of apoptosis[515] include oxygen free radicals, death receptor ligation, DNA damage, and protease activation, and also ionic imbalance which triggers the release of cytochrome c from the outer mitochondrial membrane,[516] activating caspases that engage a complex apoptotic process to dismantle the cell by cleaving homeostatic, cytoskeletal, repair, metabolic, and cell signaling proteins, and by causing DNA fragmentation.[517] As a result, apoptosis-related molecules (image, right)[518] are likely to be present in many cryopreserved cells.

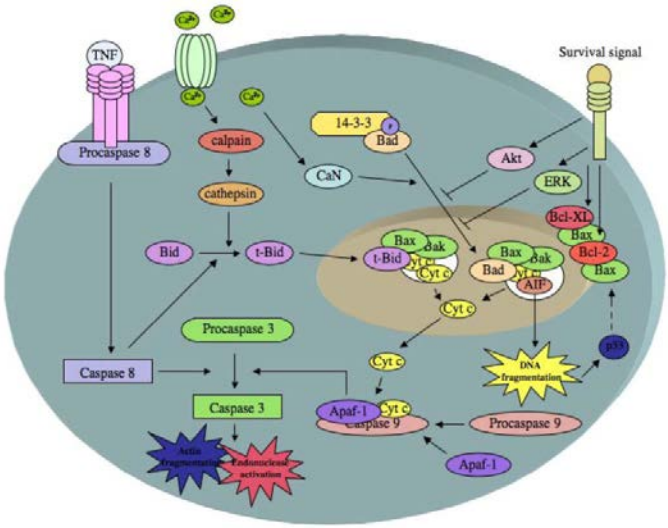

Autophagy,[519] a process in which damaged intracellular components are encased in phagosomes which then merge with lysosomes to be destroyed, is induced in neurons and other cells exposed to hypoxia,[520] excitotoxic stimuli,[521] hypoxia-ischemia,[522] closed head injury,[523] photoirradiation,[524] global ischemia,[525] focal cerebral ischemia,[526] or cold ischemia at 4 °C.[527]

---

[515] https://en.wikipedia.org/wiki/Apoptosis.

[516] Sims NR, Muyderman H. Mitochondria, oxidative metabolism and cell death in stroke. Biochim Biophys Acta. 2010 Jan;1802(1):80-91; https://core.ac.uk/download/pdf/82001859.pdf.

[517] Doyle KP, Simon RP, Stenzel-Poore MP. Mechanisms of ischemic brain damage. Neuropharmacology 2008 Sep;55(3):310-318; https://www.ncbi.nlm.nih.gov/pmc/articles/PMC2603601/.

[518] Doyle KP, Simon RP, Stenzel-Poore MP. Mechanisms of ischemic brain damage. Neuropharmacology 2008 Sep;55(3):310-318; https://www.ncbi.nlm.nih.gov/pmc/articles/PMC2603601/.

[519] https://en.wikipedia.org/wiki/Autophagy.

[520] Zhu C, Wang X, Xu F, Bahr BA, Shibata M, Uchiyama Y, Hagberg H, Blomgren K. The influence of age on apoptotic and other mechanisms of cell death after cerebral hypoxia-ischemia. Cell Death Differ 2005; 12:162-76; https://www.nature.com/articles/4401545/.

[521] Wang Y, Han R, Liang ZQ, Wu JC, Zhang XD, Gu ZL, Qin ZH. An autophagic mechanism is involved in apoptotic death of rat striatal neurons induced by the non-n-methyl-d-aspartate receptor agonist kainic acid. Autophagy 2008 Feb; 4:214-26; https://www.tandfonline.com/doi/pdf/10.4161/auto.5369.

[522] Balduini W, Carloni S, Buonocore G. Autophagy in hypoxia-ischemia induced brain injury: evidence and speculations. Autophagy. 2009 Feb;5(2):221-223; https://www.tandfonline.com/doi/pdf/10.4161/auto.5.2.7363. Balduini W, Carloni S, Buonocore G. Autophagy in hypoxia-ischemia induced brain injury. J Matern Fetal Neonatal Med. 2012 Apr;25 Suppl 1:30-34; https://pubmed.ncbi.nlm.nih.gov/22385271/.

[523] Diskin T, Tal-Or P, Erlich S, Mizrachy L, Alexandrovich A, Shohami E, Pinkas-Kramarski R. Closed head injury induces upregulation of beclin 1 at the cortical site of injury. J Neurotrauma 2005 Jul; 22:750-62; https://pubmed.ncbi.nlm.nih.gov/16004578/.

While components of the cell cycle machinery may become activated in neurons subjected to cell death stimuli,[528] necrosis[529] appears to follow acute permanent vascular occlusion.[530] The most prominent features of necrosis following brain ischemia are a loss of membrane integrity, cell swelling, and organelle failure.[531] For example, rat cortical neurons subjected to 3 hours of total hypoxia (0% oxygen) with an abundance of glucose retain 80% cell viability after 6 hours but only 30% viability after 24 hours, mostly due to necrosis rather than apoptosis.[532] Several experiments have found cell death occurring by necrosis in the central part of a cryogenic lesion but with apoptosis evident in the peripheral part of the lesion.[533] Elements of the cytoskeleton can also become disrupted during ischemia.

A marked increase in structural plasticity occurs near the trauma site after stroke. As with stroke, during ischemia dendrites disintegrate and reassemble rapidly with survivors showing a 5- to 8-fold increase in

---

[524] Kim I, Lemasters JJ. Mitophagy selectively degrades individual damaged mitochondria after photoirradiation. Antioxid Redox Signal. 2011 May 15;14(10):1919-28; https://www.ncbi.nlm.nih.gov/pmc/articles/PMC3078512/pdf/ars.2010.3768.pdf.

[525] Au AK, Chen Y, Du L, *et al*. Ischemia-induced autophagy contributes to neurodegeneration in cerebellar Purkinje cells in the developing rat brain and in primary cortical neurons *in vitro*. Biochim Biophys Acta. 2015 Sep;1852(9):1902-1911; https://core.ac.uk/download/pdf/82640642.pdf.

[526] Rami A, Langhagen A, Steiger S. Focal cerebral ischemia induces upregulation of beclin 1 and autophagy-like cell death. Neurobiol Dis 2008 Jan; 29:132-41; https://pubmed.ncbi.nlm.nih.gov/17936001/.

[527] Chen X, Wu JX, You XJ, Zhu HW, Wei JL, Xu MY. Cold ischemia-induced autophagy in rat lung tissue. Mol Med Rep. 2015 Apr;11(4):2513-2519; https://pdfs.semanticscholar.org/a616/6d11d3a3b9a2b1ef841c569ed91112508e2c.pdf.

[528] Katchanov J, Harms C, Gertz C, *et al*. Mild cerebral ischemia induces loss of cyclin-dependent kinase inhibitors and activation of cell cycle machinery before delayed neuronal cell death. J Neurosci. 2001 Jul 15;21(14):5045-5053; https://www.jneurosci.org/content/jneuro/21/14/5045.full-text.pdf. Herrup K, Arendt T. Re-expression of cell cycle proteins induces neuronal cell death during Alzheimer's disease. J Alzheimers Dis. 2002 Jan;4(3):243-247; https://www.ncbi.nlm.nih.gov/pubmed/12226544. Greene LA, Biswas SC, Liu DX. Cell cycle molecules and vertebrate neuron death: E2F at the hub. Cell Death Differ 2004 Jan;11:49-60; https://www.nature.com/articles/4401341.

[529] https://en.wikipedia.org/wiki/Necrosis.

[530] Du C, Hu R, Csernansky CA, Hsu CY, Choi DW. Very delayed infarction after mild focal cerebral ischemia: a role for apoptosis?. J Cereb Blood Flow Metab. 1996 Mar;16(2):195-201; https://journals.sagepub.com/doi/pdf/10.1097/00004647-199603000-00003. Endres M, Namura S, Shimizu-Sasamata M, Waeber C, Zhang L, Gómez-Isla T, Hyman BT, Moskowitz MA. Attenuation of delayed neuronal death after mild focal ischemia in mice by inhibition of the caspase family. J Cereb Blood Flow Metab. 1998 Mar;18(3):238–247; https://journals.sagepub.com/doi/pdf/10.1097/00004647-199803000-00002.

[531] Majno G, Joris I. Apoptosis, oncosis, and necrosis. An overview of cell death. Am J Pathol 1995 Jan;146(1):3-15; https://www.ncbi.nlm.nih.gov/pmc/articles/PMC1870771/pdf/amjpathol00049-0010.pdf. Lo EH, Moskowitz MA, Jacobs TP. Exciting, radical, suicidal. How brain cells die after stroke? Stroke 2005 Feb;36(2):189-192; https://www.ahajournals.org/doi/full/10.1161/01.STR.0000153069.96296.fd.

[532] Jones PA, May GR, McLuckie JA, Iwashita A, Sharkey J. Apoptosis is not an invariable component of *in vitro* models of cortical cerebral ischaemia. Cell Res. 2004 Jun;14(3):241-250; https://www.nature.com/articles/7290225.

[533] Steinbach JP, Weissenberger J, Aguzzi A. Distinct phases of cryogenic tissue damage in the cerebral cortex of wild-type and c-fos deficient mice. Neuropathol Appl Neurobiol. 1999 Dec;25(6):468-480; https://pdfs.semanticscholar.org/e6b6/73718f4387b6ed8c1c2de5da39c7d12010c1.pdf. Forest V, Peoc'h M, Campos L, Guyotat D, Vergnon JM. Effects of cryotherapy or chemotherapy on apoptosis in a non-small-cell lung cancer xenografted into SCID mice. Cryobiology. 2005 Feb;50(1):29-37; https://www.sciencedirect.com/science/article/pii/S0011224004001300. Wen J, Duan Y, Zou Y, Nie Z, Feng H, Lugnani F, Baust JG. Cryoablation induces necrosis and apoptosis in lung adenocarcinoma in mice. Technol Cancer Res Treat. 2007 Dec;6(6):635-640; https://journals.sagepub.com/doi/pdf/10.1177/153303460700600607.

dendritic spine turnover.[534] It is possible this may decrease the recoverability of neural structures encoding personal identity (Section 2.1.2).

Looking beyond the single cell to the larger neurovascular unit (i.e., cerebral endothelial cells, astrocytes, neurons, and extracellular matrix or ECM), the integrity of the blood-brain barrier depends primarily on the interaction of the extracellular matrix with endothelial cells and astrocytes. The ECM under ischemia suffers degradation of type IV collagen, laminin, and fibronectin due to the action of proteases such as cathepsins and heparanases, with contributions by plasminogen activator and matrix metalloproteinases MMP-2 and MMP-9 that are induced very early after ischemia onset and correlate with the risk for hemorrhagic transformation, edema formation, and the extent of tissue demise.[535] Cerebral edema (swelling of the brain) occurs due to leakage of large molecules like albumins from blood vessels through the damaged blood brain barrier.[536] The large-molecule leakage pulls water into the brain tissue via osmosis or vasogenic edema[537] that causes compression of, and damage to, brain tissue. The swelling of astrocytes compresses brain capillaries, eliminating reflow.[538]

There is also the danger of bacterial degradation. Best[539] points out that "people who deanimate in hospitals are typically placed in refrigeration units if they are not removed immediately by a funeral director. Hospitals tightly manage their space…, so the time [between] legal death and movement to a refrigeration unit is usually not very long. Refrigerator temperatures are usually in the range of 2 ºC – 7 ºC (35 ºF – 45 ºF).…The tolerable ischemic time in a hospital refrigerator could be at least 20 times that seen for warm ischemia, meaning 10 days or more. Unfortunately, this estimate is complicated by the fact that the growth of pathogens is inevitable in such a situation. Unpublished studies by cryonicists indicate that 5 days may be the maximum tolerable without bacterial autolysis."

---

[534] Brown CE, Li P, Boyd JD, Delaney KR, Murphy TH. Extensive turnover of dendritic spines and vascular remodeling in cortical tissues recovering from stroke. J Neurosci. 2007 Apr 11;27(15):4101-9; https://www.ncbi.nlm.nih.gov/pmc/articles/PMC6672555/. Brown CE, Murphy TH. Livin' on the edge: imaging dendritic spine turnover in the peri-infarct zone during ischemic stroke and recovery. Neuroscientist. 2008 Apr;14(2):139-46; https://pdfs.semanticscholar.org/f117/5bb53205567634ea8590ba9f96670e504341.pdf.

[535] Gasche Y, Fujimura M, Morita-Fujimura Y, Copin JC, Kawase M, Massengale J, Chan PH. Early appearance of activated matrix metalloproteinase-9 after focal cerebral ischemia in mice: a possible role in blood-brain barrier dysfunction. J Cereb Blood Flow Metab. 1999 Sep;19(9):1020-1028; https://journals.sagepub.com/doi/pdf/10.1097/00004647-199909000-00010. Heo JH, Lucero J, Abumiya T, Koziol JA, Copeland BR, del Zoppo GJ. Matrix metalloproteinases increase very early during experimental focal cerebral ischemia. J Cereb Blood Flow Metab. 1999 Jun;19(6):624-633; https://journals.sagepub.com/doi/pdf/10.1097/00004647-199906000-00005. Lapchak PA, Chapman DF, Zivin JA. Metalloproteinase inhibition reduces thrombolytic (tissue plasminogen activator)-induced hemorrhage after thromboembolic stroke. Stroke. 2000 Dec;31(12):3034-3040; http://citeseerx.ist.psu.edu/viewdoc/download?doi=10.1.1.328.4282&rep=rep1&type=pdf.

[536] Stokum JA, Gerzanich V, Simard JM. Molecular pathophysiology of cerebral edema. J Cereb Blood Flow Metab 2016 Nov 16;36(3):513-538; https://journals.sagepub.com/doi/10.1177/0271678X15617172.

[537] https://en.wikipedia.org/wiki/Cerebral_edema#Vasogenic.

[538] Ames A III, Wright RL, Kowada M, Thurston JM, Majno G. Cerebral ischemia II. The no-reflow phenomenon. Amer J Pathol 1968 Feb;52:437-53; https://www.ncbi.nlm.nih.gov/pmc/articles/PMC2013326/.

[539] Best B. Quantifying Ischemic Damage for Cryonics Rescue. 2009; https://www.benbest.com/cryonics/IR_Damage.html.

Outside of the brain and core organs, tourniquets that cut off all blood supply to the extremities for 1-2 hours are considered safe; e.g., local ischemic times of ~30 minutes allow sensory recovery in ~1 minute and full restoration of motor function in 10-17 minutes.[540]

3.2.6 White Matter Damage

By volume, the human brain contains >50% non-neuron white matter[541] composed of axons, oligodendrocytes, astrocytes, and blood vessels, enveloped by matrix proteins such as laminin, fibronectin, and chondroitin proteoglycans. Excitotoxic injury of white matter differs from that for gray matter (neuronal cell bodies)[542] as there are no synapses and vesicular release is minimal, but, similar to gray matter, energy deprivation leads to dysfunction of axons via activation of voltage-dependent sodium and calcium channels, and via consecutive activation of calcium-dependent disruptive pathways.[543] Oligodendrocytes, the myelin-forming cells of the central nervous system, are particularly vulnerable to ischemic injury because these cells express non-NMDA glutamate receptors and thus can be damaged or killed by glutamate excitotoxicity via intracellular calcium overload and subsequent calcium-dependent cascades.[544]

3.2.7 Histological Ultrastructural Change

Ischemic changes in brain cell architecture begin almost as rapidly as ischemic changes in biochemistry, over various time scales:[545] "Within seconds of the onset of cerebral ischemia, brain interstitial space almost completely disappears. Loss of interstitial space is a consequence of cell swelling secondary to sodium influx and failure of membrane ionic regulation." Only 20-40 seconds of stopped blood circulation after cardiac arrest depletes mammalian cerebral oxygen stores enough to cause brain electrical activity temporarily to cease.[546] Ultrastructural alterations observed in cat,[547] rat,[548] mouse,[549] and other models during prolonged global cerebral ischemia[550] (GCI) include:

---

[540] Haljamäe H, Enger E. Human skeletal muscle energy metabolism during and after complete tourniquet ischemia. Ann Surg. 1975 Jul;182(1):9-14; https://www.ncbi.nlm.nih.gov/pmc/articles/PMC1343870/pdf/annsurg00281-0019.pdf. Jacobson MD, Pedowitz RA, Oyama BK, Tryon B, Gershuni DH. Muscle functional deficits after tourniquet ischemia. Am J Sports Med. 1994 May-Jun;22(3):372-7; https://pubmed.ncbi.nlm.nih.gov/8037279/. See also: https://en.wikipedia.org/wiki/Emergency_tourniquet.

[541] https://en.wikipedia.org/wiki/White_matter.
[542] https://en.wikipedia.org/wiki/Grey_matter.

[543] Goldberg MP, Ransom BR. New light on white matter. Stroke. 2003 Feb;34(2):330-332; http://citeseerx.ist.psu.edu/viewdoc/download?doi=10.1.1.584.1695&rep=rep1&type=pdf.

[544] McDonald JW, Althomsons SP, Hyrc KL, Choi DW, Goldberg MP. Oligodendrocytes from forebrain are highly vulnerable to AMPA/kainate receptor-mediated excitotoxicity. Nat Med. 1998 Mar;4(3):291-297; https://www.researchgate.net/profile/Krzysztof_Hyrc/publication/51298339_McDonald_JW_Althomsons_SP_Hyrc_KL_Choi_DW_Goldberg_MPOligodendrocytes_from_forebrain_are_highly_vulnerable_to_AMPAkainate_receptor-mediated_excitotoxicity_Nat_Med_4291-297/links/0deec5355339d21a9b000000.pdf.

[545] Darwin M. The pathophysiology of ischemic injury. BioPreservation, Inc., 1995; https://www.alcor.org/Library/html/ischemicinjury.html.

[546] Lind B, Snyder J, Kampschulte S, Safar P. A review of total brain ischaemia models in dogs and original experiments on clamping the aorta. Resuscitation. 1975;4(1):19-31; https://pubmed.ncbi.nlm.nih.gov/1188189/.

* **Changes at 10 Minutes.** After 10 minutes of GCI, a significant number of cells (but not all) show clumping of nuclear chromatin (a reversible early change) and a modest increase in electron lucency (probably due to dilution of the cytosol by extracellular fluid). After 30 minutes, further changes include increased cytoplasmic swelling (particularly in the astrocytes), swelling and shape change of the mitochondria, and some loss of mitochondrial matrix density. Microtubules disappear and there is detachment of the ribosomes from the cisternae of the endoplasmic reticulum (ER). There is also dissociation of the polyribosomes, and single ribosomes lose their compact structure with associated failure of protein synthesis. Of note is the stability of the lysosomes over this time course.[551]

* **Changes at 1 Hour.** After 60 minutes of GCI, the above changes have become more pronounced with more conspicuous swelling of the ER cisternae. The mitochondria begin to show slight inner matrix swelling and occasional flocculent densities[552] (probably due to accumulated calcium). Endothelial edema and the beginning of blood-brain barrier breakdown is observed within 30 minutes of middle cerebral artery occlusion in mice.[553] The brains of monkeys subjected to 60 minutes of warm ischemia (but protected from reperfusion injury) show at least short-term recovery.[554]

* **Changes at 2 Hours.** After 120 minutes of GCI, the changes discussed above are more pronounced and a larger number of mitochondria exhibit the presence of flocculent densities evidencing calcium overload which is currently considered irreversible in the absence of technological means. Published electron micrographs reveal intact lysosomes and seem to confirm other studies which indicate that lysosomal rupture and subsequent catastrophic autolysis is not a feature of early (1-4 hours) ischemic injury:[555] "Lysosomes did not rupture for approximately 4 hours and in fact did not release the fluorescent

---

[547] Kalimo H, Garcia JH, Kamijyo Y, Tanaka J, Trump BF. The ultrastructure of "brain death". II. Electron microscopy of feline cortex after complete ischemia. Virchows Arch B Cell Pathol. 1977 Nov 3;25(3):207-220; https://www.ncbi.nlm.nih.gov/pubmed/413253.

[548] Karlsson U, Schultz RL. Fixation of the central nervous system for electron microscopy by aldehyde perfusion. III. Structural changes after exsanguination and delayed perfusion. J Ultrastruc Res 1966 Jan;14(1-2):57-63; https://www.sciencedirect.com/science/article/abs/pii/S0022532066800345. Van Nimwegen D, Sheldon, H. Early postmortem changes in cerebellar neurons of the rat. J Ultrastruc Res 1966 Jan;14(1-2):36-46; https://www.sciencedirect.com/science/article/abs/pii/S0022532066800333.

[549] Gonzalez-Riano C, Tapia-González S, García A, Muñoz A, DeFelipe J, Barbas C. Metabolomics and neuroanatomical evaluation of post-mortem changes in the hippocampus. Brain Struct Funct. 2017 Aug;222(6):2831-2853; https://www.ncbi.nlm.nih.gov/pmc/articles/PMC5541081/.

[550] https://en.wikipedia.org/wiki/Brain_ischemia#Global_brain_ischemia.

[551] Van Nimwegen D, Sheldon, H. Early postmortem changes in cerebellar neurons of the rat. J Ultrastruc Res 1966 Jan;14(1-2):36-46; https://www.sciencedirect.com/science/article/abs/pii/S0022532066800333.

[552] Itkonen P, Collan Y. Mitochondrial flocculent densities in ischemia. Digestion experiments. Acta Pathol Microbiol Immunol Scand A. 1983 Nov;91(6):463-8; https://pubmed.ncbi.nlm.nih.gov/6666582/.

[553] Krueger M, Mages B, Hobusch C, Michalski D. Endothelial edema precedes blood-brain barrier breakdown in early time points after experimental focal cerebral ischemia. Acta Neuropathol Commun. 2019 Feb 11;7(1):17; https://www.ncbi.nlm.nih.gov/pmc/articles/PMC6369548/.

[554] Bodsch W, Barbier A, Oehmichen M, Grosse Ophoff B, Hossmann KA. Recovery of monkey brain after prolonged ischemia. II. Protein synthesis and morphological alterations. J Cereb Blood Flow Metab. 1986 Feb;6(1):22-33; https://journals.sagepub.com/doi/pdf/10.1038/jcbfm.1986.4.

[555] Hawkins HK, Ericsson JL, Biberfeld P, Trump BF. Lysosome and phagosome stability in lethal cell injury. Morphologic tracer studies in cell injury due to inhibition of energy metabolism, immune cytolysis and photosensitization. Am J Pathol. 1972 Aug;68(2):255-8; https://www.ncbi.nlm.nih.gov/pmc/articles/PMC2032684/.

dye until after reaching the post-mortem necrotic phase of injury. Lysosomes appear to be relatively stable organelles." Kalimo[556] also reports: "After 120 min of complete blood deprivation we saw no evidence of membrane lysosomal breakdown, an observation which has also been reported in studies of *in vitro* lethal cell injury and in regional cerebral ischemia." Throughout even a 120-minute-period of normothermic cerebral ischemia, the appearance of the plasma membrane layers, including synapses and myelin sheaths, is only altered modestly. The first ultrastructural changes associated with what is currently considered lethal cell injury are to the mitochondria and ribosomes, and these do not usually appear until after 30 minutes of GCI.[557]

* **Changes at 3 Hours.** Hippocampal slice tissue (the most vulnerable to ischemic injury) retained significant spiking ability up to 3 hours after post-mortem extraction from rats.[558]

* **Changes at 5 Hours.** Significant metabolomic changes occurred at the 2 hour mark, but the integrity of neurons and glia, at the anatomical/neurochemical level, was not significantly altered for the majority of histological markers in mice maintained at room temperature for up to 5 hours post-mortem.[559] An earlier study of brain tissue of rats subjected to 5-6 hours of cardiac arrest showed normal synaptic activity after reperfusion.[560]

* **Changes at Longer Intervals.** Neurons of rats euthanized at room temperature showed the first signs of autolysis (ribosome disappearance and up to 2.5% of neurons strongly staining for caspase-3, an apoptosis indicator) after 9 hours.[561] Rats with an experimentally occluded middle cerebral artery showed few signs of neuron necrosis after 4 hours, with 15% of neurons necrotic after 6 hours and 65% necrotic after 12 hours.[562] Rat neuron ultrastructure 3 hours after onset of ischemia show severe cytoplasmic and moderate/severe mitochondrial swelling; after 24 hours the neuron mitochondria were still distinguishable,

---

[556] Kalimo H, Garcia JH, Kamijyo Y, Tanaka J, Trump BF. The ultrastructure of "brain death". II. Electron microscopy of feline cortex after complete ischemia. Virchows Arch B Cell Pathol. 1977 Nov 3;25(3):207-20; https://www.ncbi.nlm.nih.gov/pubmed/413253.

[557] Darwin M. The pathophysiology of ischemic injury. BioPreservation, Inc., 1995; https://www.alcor.org/Library/html/ischemicinjury.html.

[558] Leonard BW, Barnes CA, Rao G, Heissenbuttel T, McNaughton BL. The influence of postmortem delay on evoked hippocampal field potentials in the *in vitro* slice preparation. Exp Neurol. 1991 Sep;113(3):373-377; https://pubmed.ncbi.nlm.nih.gov/1915727/.

[559] Gonzalez-Riano C, Tapia-González S, García A, Muñoz A, DeFelipe J, Barbas C. Metabolomics and neuroanatomical evaluation of post-mortem changes in the hippocampus. Brain Struct Funct. 2017 Aug;222(6):2831-2853; https://www.ncbi.nlm.nih.gov/pmc/articles/PMC5541081/

[560] Charpak S, Audinat E. Cardiac arrest in rodents: maximal duration compatible with a recovery of neuronal activity. Proc Natl Acad Sci U S A. 1998 Apr 14;95(8):4748-4753; https://www.pnas.org/content/95/8/4748.full.

[561] Sheleg SV, Lobello JR, Hixon H, Coons SW, Lowry D, Nedzved MK. Stability and autolysis of cortical neurons in post-mortem adult rat brains. Int J Clin Exp Pathol. 2008 Jan 1;1(3):291-299; https://www.ncbi.nlm.nih.gov/pmc/articles/pmid/18784829/.

[562] Garcia JH, Liu KF, Ho KL. Neuronal necrosis after middle cerebral artery occlusion in Wistar rats progresses at different time intervals in the caudoputamen and the cortex. Stroke. 1995 Apr;26(4):636-643; https://www.ahajournals.org/doi/full/10.1161/01.str.26.4.636. Pulsinelli WA, Brierley JB, Plum F. Temporal profile of neuronal damage in a model of transient forebrain ischemia. Ann Neurol. 1982 May;11(5):491-498; https://pubmed.ncbi.nlm.nih.gov/7103425/.

though severely disrupted.[563] Rat cortical neurons subjected to 3 hours of total hypoxia (0% oxygen) with an abundance of glucose show 80% cell viability after 6 hours but only 30% viability after 24 hours.[564] Post-mortem mouse brains subjected to 6 hours at room temperature, then another 18 hours at 4 ºC, show half the neurons to be morphologically intact.[565] Recent tissue ultrastructure studies of warm and cold ischemia in rats found signs of vessel leakage and chromatin clumping after 1 hour at 37 °C (24 hours at 0 °C), synapse degradation after 6 hours at 37 °C (1 week at 0 °C), and advanced necrosis after 36 hours at 37 °C (2 months at 0 °C).[566] Structure and organelles can still be clearly identified in cortical electron micrographs of a rat brain after 21 hours of warm ischemia (image, right).[567] It takes many hours of normothermic global ischemia, and several weeks of cold global ischemia, to so damage the fine structure of the brain that the original structure can no longer be recognized or inferred.[568] Perry[569] recommends ***future research*** "to show persistence of mammalian brain structure and functions post-mortem. This research carries the caveat that success might provoke a negative mainstream reaction relating to brains formerly thought 'dead' now being seen as 'still alive' [which] would have to be managed."

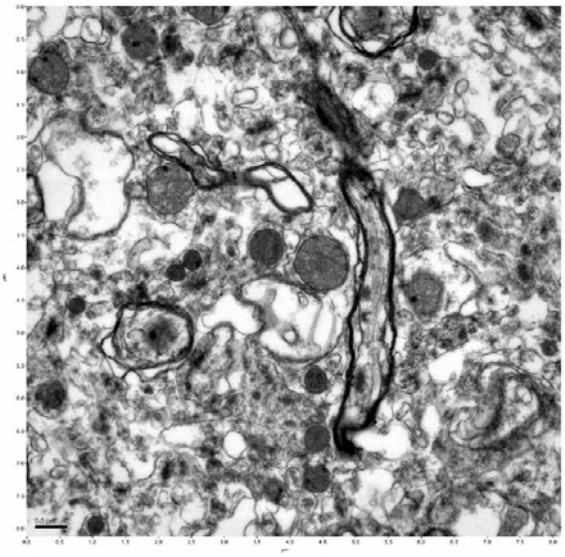

* **Changes in Humans.** At least one study of post-mortem ultrastructural degradation has been conducted on a small number of human subjects.[570] The histological and ultrastructural changes experienced in the brains of patients with 25-85 minutes of GCI,[571] and without extensive pre-mortem brain

---

[563] Solenski NJ, diPierro CG, Trimmer PA, Kwan AL, Helm GA. Ultrastructural changes of neuronal mitochondria after transient and permanent cerebral ischemia. Stroke. 2002 Mar;33(3):816-824; https://www.ahajournals.org/doi/full/10.1161/hs0302.104541.

[564] Jones PA, May GR, McLuckie JA, Iwashita A, Sharkey J. Apoptosis is not an invariable component of *in vitro* models of cortical cerebral ischaemia. Cell Res. 2004 Jun;14(3):241-250; https://www.nature.com/articles/7290225.

[565] Scheuerle A, Pavenstaedt I, Schlenk R, Melzner I, Rödel G, Haferkamp O. *In situ* autolysis of mouse brain: ultrastructure of mitochondria and the function of oxidative phosphorylation and mitochondrial DNA. Virchows Arch B Cell Pathol Incl Mol Pathol. 1993;63(6):331-4; https://pubmed.ncbi.nlm.nih.gov/8100657/.

[566] de Wolf A, Phaedra C, Perry RM, Maire M. Ultrastructural Characterization of Prolonged Normothermic and Cold Cerebral Ischemia in the Adult Rat. Rejuvenation Res. 2020 Jun;23(3):193-206; https://pubmed.ncbi.nlm.nih.gov/31631775/.

[567] Phaedra C. Reconstructive Connectomics. Cryonics 2013 Jul;34(7):26-28; https://www.alcor.org/library/reconstructive-connectomics/.

[568] de Wolf A, Phaedra C, Perry RM, Maire M. Ultrastructural Characterization of Prolonged Normothermic and Cold Cerebral Ischemia in the Adult Rat. Rejuvenation Res. 2020 Jun;23(3):193-206; https://pubmed.ncbi.nlm.nih.gov/31631775/.

[569] Perry RM. Cryonics and Public Skepticism: Meeting the Challenges to Our Credibility. Cryonics 2019 Qtr 4;40(4):24-37; https://www.alcor.org/docs/cryonics-magazine-2019-04.pdf.

[570] Kalimo H, Garcia, JH, Kamijyo Y, *et al*. Cellular and subcellular alterations of human CNS. Arc Pathol 1974 Jun;97(6):352-359; https://pubmed.ncbi.nlm.nih.gov/4596479.

[571] https://en.wikipedia.org/wiki/Brain_ischemia#Global_brain_ischemia.

trauma or pre-mortem cerebral no-reflow of prolonged duration, closely parallel those observed in animal models of GCI: astrocytic edema, clumping of nuclear chromatin, disassociation of the polyribosomes, detachment of the ribosomes from the ER cisternae, and swelling of the mitochondria with the presence of flocculent densities. Stability of the lysosomes and conservation of the structure of the neuropil over this time course are well documented. Sufficient structural integrity is retained for up to 24 hours post-mortem "to allow the various tissue compartments to remain relatively intact and distinct".[572]

In one early study, nearly two-thirds of all human neural tissue acquired within 6 hours of death was successfully grown in tissue culture (i.e., remained viable), whereas only one-third would grow when acquired more than 6 hours post-mortem.[573] Neurons in brain tissue extracted from humans post-mortem and subjected to normothermic conditions for 3-6 hours recovered oxidative metabolism and axon transport after suitable *in vitro* treatment.[574] Another study found that 70%-90% of neurons extracted from elderly humans an average of 2.6 hours post-mortem were still viable after 2 weeks *in vitro*.[575] Temporary functional recovery from up to 60 minutes of total ischemia has been demonstrated in cats,[576] with one study[577] of 143 animals subjected to one hour of warm global brain ischemia finding that spontaneous EEG activity returned after ischemia in 50% of the cats with one animal surviving 1 year having "no electrophysiologic deficit and with only minor neurologic and morphologic disturbances." But, as Merkle[578] notes: "Functional recovery is a more stringent criterion than the more relaxed information-theoretic criterion (Section 2.1.1),[579] which merely requires adequate structural preservation to allow inference about the pre-existing structure." Cooling substantially slows the rate of structural deterioration following warm ischemia.[580]

---

[572] Dodd PR, Hambley JW, Cowburn RF, Hardy JA. A comparison of methodologies for the study of functional transmitter neurochemistry in human brain. J Neurochem. 1988 May;50(5):1333-45; https://www.ncbi.nlm.nih.gov/pubmed/2896227.

[573] Gilden DH, Devlin M, Wroblewska Z, Friedman H, Rorke LB, Santoli D, Koprowski H. Human brain in tissue culture. I. Acquisition, initial processing, and establishment of brain cell cultures. J Comp Neurol. 1975 Jun 1;161(3):295-306; https://www.ncbi.nlm.nih.gov/pubmed/239028.

[574] Dai J, Swaab DF, Buijs RM. Recovery of axonal transport in "dead neurons". Lancet. 1998 Feb 14;351(9101):499-500; https://pubmed.ncbi.nlm.nih.gov/9482451/.

[575] Konishi Y, Lindholm K, Yang LB, Li R, Shen Y. Isolation of living neurons from human elderly brains using the immunomagnetic sorting DNA-linker system. Am J Pathol. 2002 Nov;161(5):1567-1576; https://www.ncbi.nlm.nih.gov/pmc/articles/PMC1850778/.

[576] Hossmann KA. Post-ischemic resuscitation of the brain: selective vulnerability versus global resistance. Prog Brain Res. 1985;63:3-17; https://www.ncbi.nlm.nih.gov/pubmed/3915126. Nordstrom CH, Siesjo BK. Neurochemical Determinants of Ischemic Cell Damage. In: Weinstein PR, Faden AA, eds., Protection of the Brain from Ischemia, Williams and Wilkens, 1990, pp. 49-66. Hossmann KA. Hemodynamics of Postischemic Reperfusion of the Brain. In: Weinstein PR, Faden AA, eds., Protection of the Brain from Ischemia, Williams and Wilkens, 1990, pp. 21-36.

[577] Hossmann KA. Resuscitation potentials after prolonged global cerebral ischemia in cats. Crit Care Med. 1988 Oct;16(10):964-71; https://www.ncbi.nlm.nih.gov/pubmed/3139367.

[578] Merkle RC. The molecular repair of the brain. Cryonics 1994 Jan;15(1) and Cryonics 1994 Apr;15(2); http://www.merkle.com/cryo/techFeas.html and https://www.alcor.org/library/molecular-repair-of-the-brain/.

[579] Merkle RC. The technical feasibility of cryonics. Med Hypotheses. 1992 Sep;39(1):6-16; https://www.ncbi.nlm.nih.gov/pubmed/1435395. See also: http://www.merkle.com/definitions/infodeath.html.

[580] Bowen ID, Lockshin RA, eds., Cell Death in Biology and Pathology, Chapman and Hall, 1981, p. 209 *et seq*.

Best[581] opines that "for those who believe that freezing damage can someday be repaired by nanotechnology, a cryonics patient could tolerate at least 5 hours of ischemia at room temperature before being straight-frozen while preserving most memory and identity."

Perry and de Wolf have created a mathematical metric that quantifies the ischemic exposure of a cryonics patient during the cooldown process to 0 °C and allows this exposure to be expressed as a normothermic-equivalent ischemic exposure time.[582] The chart below shows the median S-MIX (Standardized Measure of Ischemic Exposure)-based effective normothermic ischemic time, in hours, suffered by Alcor cryonics patients during 2000-2020; 4-6 hours appears typical.[583]

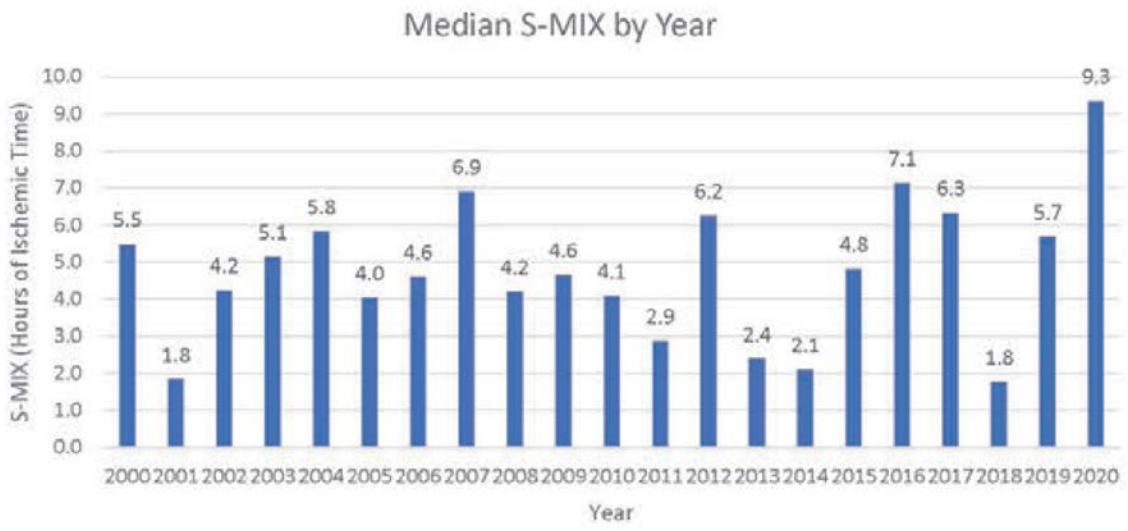

* **Systematic Studies.** The first systematic study comparing the ultrastructural effects of normothermic permanent ischemia with cold permanent ischemia in the mammalian brain was reported by de Wolf and colleagues in 2020.[584] From the abstract: "Complete cerebral ischemia was produced by cardiac arrest and the animals' temperature was maintained at 37 °C for periods ranging from 0 to 81 hours before electron microscopy preparation. Electron micrographs of cold cerebral ischemia were generated after stabilizing the rat's temperature at 0 °C after cardiac arrest for periods ranging from 0 hours to 6 months. A qualitative examination of the electron micrographs shows structural signatures of energy depletion such as vessel leaking and chromatin clumping after 1 hour at 37 °C and after 24 hours at 0 °C, followed by synapse degradation after 6 hours at 37 °C and 1 week at 0 °C. Evidence of advanced necrosis

---

[581] Best B. Quantifying Ischemic Damage for Cryonics Rescue. 2006 Feb; https://www.benbest.com/cryonics/IR_Damage.html.

[582] Perry RM, de Wolf A. The S-MIX: A Measure of Ischemic Exposure. Cryonics 2020 Qtr IV; 41(4):12-15; https://www.alcor.org/docs/measuring-ischemic-exposure.pdf. See also: de Wolf A. Implementing the S-MIX. Cryonics 2021 Qtr II; 42(2):33-34; https://www.alcor.org/docs/cryonics-magazine-2021-02.pdf.

[583] Benjamin M, de Wolf A. Alcor Case Metrics 2000-2020. Cryonics 2021 Qtr II; 42(2):10-30, chart "Median S-MIX by Year", p. 29; https://www.alcor.org/docs/cryonics-magazine-2021-02.pdf.

[584] de Wolf A, Phaedra C, Perry RM, Maire M. Ultrastructural Characterization of Prolonged Normothermic and Cold Cerebral Ischemia in the Adult Rat. Rejuvenation Res. 2020 Jun 16; 23(3):193-206; https://www.liebertpub.com/doi/10.1089/rej.2019.2225.

was observed after 36 hours at 37 °C and 2 months at 0 °C." Interestingly, the rate of degradation at the colder temperature was 2-3 times slower than the "Q10 rule" for biochemical activity rates as a function of temperature[585] would otherwise predict.

From these data, the authors concluded that "there appears to be a period of relative stability between the initial rapid, energy depletion-induced changes (most notably expressed as edema) and the global disintegration of the fine structure of the brain. During this period of relative stability, viable recovery is no longer possible, but the appearance of the original structure may still be inferred from the damaged state….[O]ur finding that the ultrastructure of the brain does not rapidly decompose after cardiac arrest supports the stronger, more rigorous, information-theoretic criterion of death, in which the criterion of viability is replaced by the stronger criterion of irreversible loss of identity-critical structure….[F]or the rat model used in this study, information-theoretic death occurs no sooner than at ~36 hours of normothermic ischemia or 2 months of cold ischemia."

3.2.8 Ischemic Damage in the Cryonics Context

An especially important consideration relevant to cryonics is that some cerebral ischemia damage mechanisms require metabolism, which requires restored blood circulation to supply oxygen and substrate. Such damage mechanisms are therefore forms of reperfusion injury (Section 3.6) that aren't significant in the context of the usual cryopreservation process used in cryonics.

When blood reperfusion is performed during cryonics stabilization, it's only for a very limited period of time. Apoptosis, for example, would require many hours of warm blood perfusion to run to completion. Inflammation is also limited in the context of cryonics because if blood circulation is restored, it's only for minutes instead of hours, and brain temperature is rapidly decreasing the whole time that circulation is restored. Brain swelling is limited for this same reason, is counteracted by osmotic effects of cryoprotectants, and is not allowed to progress when it occurs because Alcor performs burrhole monitoring of brain volume during cryoprotective perfusion.

Metaphorically speaking, notes Brian Wowk,[586] "cerebral ischemia lights the fuse of the bomb that goes off hours or days later in the brain of a patient on life support in ICUs after a cerebral ischemic insult." For example, Solenski *et al.*[587] show in Fig. 9 of their paper that even 24 hours of normothermic ischemia looks better than 3 hours of normothermic ischemia (called "transient ischemia" in the paper) followed by 24 hours of blood reperfusion.

As noted elsewhere,[588] most tissues and organs of the body can survive clinical death for considerable periods of time: "Although loss of function (after cardiac arrest) is almost immediate, there is no specific duration of clinical death at which the non-functioning brain clearly dies. The most vulnerable cells in the brain, CA1 neurons of the hippocampus, are fatally injured by as little as 10 minutes without oxygen.

---

[585] https://en.wikipedia.org/wiki/Q10_(temperature_coefficient).

[586] Personal communication from Brian Wowk to Robert Freitas, 30 Sep 2021.

[587] Solenski NJ, diPierro CG, Trimmer PA, Kwan AL, Helm GA. Ultrastructural changes of neuronal mitochondria after transient and permanent cerebral ischemia. Stroke. 2002 Mar;33(3):816-824; https://www.ahajournals.org/doi/full/10.1161/hs0302.104541.

[588] https://en.wikipedia.org/wiki/Clinical_death#Limits_of_reversal.

However, the injured cells do not actually die until hours after resuscitation.[589] This delayed death can be prevented *in vitro* by a simple drug treatment even after 20 minutes without oxygen.[590] In other areas of the brain, viable human neurons have been recovered and grown in culture hours after clinical death.[591] Brain failure after clinical death is now known to be due to a complex series of processes called reperfusion injury that occur after blood circulation has been restored, especially processes that interfere with blood circulation during the recovery period."

3.3 Perfusion Damage

Additional damage can occur to the patient during the perfusion process, when cryoprotective fluids are being introduced and cooldown has begun. Excessive ischemic damage to the blood vessels can increase the difficulty of obtaining a thorough perfusion of cryoprotectants.[592]

Some of this additional damage will be a consequence of the process itself, and occurs even when all procedures are performed perfectly from the standpoint of the medical practitioner (Section 3.3.1). Further damage may occur when the perfusion practitioner makes mistakes, whether due to inexperience or happenstance, causing iatrogenic damage (Section 3.3.2).

Can all ice formation can be inhibited in a cryonics patient? "Under ideal conditions it is reasonable to believe that this objective can be achieved in the brain because its high energy demands make it one of the most vascularized organs in the body. Since cryoprotectants are introduced into the cryonics patient's body using the circulatory system, the numerous blood vessels in the brain, generally speaking, allow cryoprotectants to be delivered with great efficiency. The degree to which the whole body of a human can be 100% vitrified is unknown at present but preliminary evidence from cryonics-associated cryobiology research labs indicates that a very good job can be done there, too (although, perhaps, still not 100%)." [593]

3.3.1 Endogenous Perfusion Damage

It is possible that perfusing the vascular system of a cryonics patient with cryoprotective fluids at normal temperatures, before the patient is cooled to cryogenic temperatures, might cause some incremental damage. At least one study shows that perfusion produces no additional observable chemical changes, alteration of vessel flow capacity, or histological damage, as compared to hypothermic complete circulatory

---

[589] Kirino T. Delayed neuronal death. Neuropathology. 2000 Sep;20 Suppl:S95-7; https://pubmed.ncbi.nlm.nih.gov/11037198/.

[590] Popovic R, Liniger R, Bickler PE. Anesthetics and mild hypothermia similarly prevent hippocampal neuron death in an in vitro model of cerebral ischemia. Anesthesiology. 2000 May;92(5):1343-9; https://pubs.asahq.org/anesthesiology/article/92/5/1343/441.

[591] Kim SU, Warren KG, Kalia M. Tissue culture of adult human neurons. Neurosci Lett. 1979 Feb;11(2):137-41; https://pubmed.ncbi.nlm.nih.gov/313541/.

[592] Best BP. Vascular and neuronal ischemic damage in cryonics patients. Rejuvenation Res. 2012 Apr;15(2):165-9; http://citeseerx.ist.psu.edu/viewdoc/download?doi=10.1.1.467.375&rep=rep1&type=pdf.

[593] Phaedra C, de Wolf A. Cryonics Protocols at the Cryonics Institute: Research and Practice. Part 3: Cryoprotection. Long Life 2018 Qtr 2;50(2):13-17; https://immortalistsociety.org/LongLifeV50-02.pdf.

arrest, in dogs.[594] However, this damage is generally regarded as relatively minor and easily reversed using the revival technologies likely to be available.[595]

Several types of perfusion damage may include:

(1) **Protein, ground substance, and cell debris removal.** Fahy[596] notes that perfusion, unlike freezing, has the potential to remove proteins and cellular debris from the brain. However, extensive protein loss from previously undamaged brains appears unlikely unless enormous concentrations (≥ 6 M) of glycerol are used. For example, rabbit brains fixed after perfusion with glycerol at temperatures above 10-15 °C and examined histologically[597] showed no loss of ground substance[598] or substantial morphological alterations. ***Future research*** can determine if the fluid flow rates needed for tissue washout cycling (Section 4.10.2) might be sufficient to risk removing larger molecular and biologically-derived structures.

(2) **Cerebral dehydration and brain shrinkage.** Under low temperature conditions, cryoprotectant perfusion to very high concentrations (≥ 6 M) can cause extensive shrinkage of the brain as a whole and of the component cells and processes. For instance, color-coded computed tomography (CT) scans of the head of one cryopreserved patient showed significant shrinkage of the brain within the skull, following cryopreservation (see below).[599]

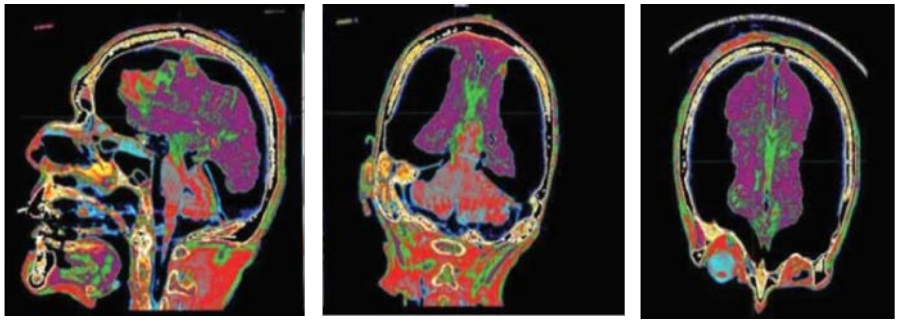

Side View Front View Back View

---

[594] Molina JE, Einzig S, Mastri AR, Bianco RW, Marks JA, Rasmussen TM, Clack RM. Brain damage in profound hypothermia. Perfusion versus circulatory arrest. J Thorac Cardiovasc Surg. 1984 Apr;87(4):596-604; https://www.sciencedirect.com/science/article/pii/S0022522319373635/pdf?md5=20721a74e1ecc1098c1c1d61c1dae2d6&pid=1-s2.0-S0022522319373635-main.pdf.

[595] Fahy G. Appendix B. A "Realistic" Scenario for Nanotechnological Repair of the Frozen Human Brain. In: Wowk B, Darwin M, eds., Cryonics: Reaching for Tomorrow. Alcor Life Extension Foundation, 1991, pp. A-10 – A-26; https://alcor.org/Library/html/nanotechrepair.html.

[596] Fahy G. Appendix B. A "Realistic" Scenario for Nanotechnological Repair of the Frozen Human Brain. In: Wowk B, Darwin M, eds., Cryonics: Reaching for Tomorrow. Alcor Life Extension Foundation, 1991, pp. A-10 – A-26; https://alcor.org/Library/html/nanotechrepair.html.

[597] Fahy GM, Takahashi T, Crane AM. Histological cryoprotection of rat and rabbit brains. Cryo-Letters 1984;5:33-46.

[598] Ground substance is an amorphous gel-like substance in the extracellular space that contains all components of the extracellular matrix except for fibrous materials such as collagen and elastin. https://en.wikipedia.org/wiki/Ground_substance.

[599] Linda Chamberlain. Alcor A-1990 Case Report. Cryonics, 2nd Quarter 2019, pp. 12-27; 27; https://www.alcor.org/cryonics/Cryonics2019-2.pdf.

While brain shrinkage did not prevent the apparent survival of a frozen cat brain in early studies,[600] cerebral dehydration was explicitly identified as a potential form of injury in a 2006 cryonics case report.[601] Aschwin de Wolf observes[602] that modern vitrification agents "do not cause cerebral dehydration because of their [chemical] properties as such, but because most cryoprotectants have poor blood brain barrier penetration." The problem of brain shrinking has in principle been solved in laboratory experiments through the use of blood brain barrier modifiers,[603] although this technology is not yet employed clinically in cryonics. The Suozzi cryopreservation case achieved a high level of cryoprotection without accompanying cerebral dehydration, now presumed due to opening of the blood brain barrier caused by the one hour of warm ischemia that preceded cryoprotectant perfusion.[604]

Although electron micrographs of brains cryopreserved with M22 and other cryoprotectants show ultrastructural alterations that are presumed to be due to cryoprotectant-induced dehydration,[605] these alterations represent minimal information loss because the alterations (A) appear to be inferentially reversible using cell repair nanorobots and (B) appear not to have damaged significant memory-critical cell or brain structures.

(3) **Whole-body edema.** Edema is the swelling of body tissues due to excessive fluid that prevents or limits perfusion of cryonics patients.[606] Based on research at Advanced Neural Biosciences,[607] "[a]s the duration of cold and/or normothermic ischemia increases, so does the degree of whole body (and cerebral) edema during cryoprotective perfusion….After 15 minutes of normothermic ischemia, weight loss is still routinely observed after completion of cryoprotective perfusion but this….[i]schemia-induced whole body edema cannot be mitigated by blood substitution, pharmaceutical treatment, or cryoprotectant carrier solution formulation."

(4) **Chemical alterations.** Tissues subjected to cryoprotectant perfusion can exhibit distorted histological staining (normally done when all protectant is removed from the tissue), possibly implying altered chemistry.[608] Fahy[609] notes that such altered staining may be the result of unusual fixation in the

---

[600] Suda I, Kito K, Adachi C. Bioelectric discharges of isolated cat brain after revival from years of frozen storage. Brain Res. 1974 Apr 26;70(3):527-531; https://www.sciencedirect.com/science/article/abs/pii/0006899374902637?via%3Dihub.

[601] de Wolf A, de Wolf C. Cryopreservation of Patient A-1097; https://www.alcor.org/Library/pdfs/casereportA1097.pdf.

[602] Dvorsky G. Generation Cryo: Fighting Death In The Frozen Unknown. Gizmodo, 23 Sep 2016; https://www.gizmodo.com.au/2016/09/generation-cryo-fighting-death-in-the-frozen-unknown/.

[603] The true honor of BBB modification goes to the cryobiologist Yuri Pichugin who discovered a class of molecules that could modify the BBB to allow for cryoprotection without shrinking of the brain. A provisional patent application* that was prepared but not filed discloses the work he did for Cryonics Institute on these molecules.
* Pichugin Y. Method of Cryopreservation of Whole Brains. U.S. Provisional Patent Application, 2007; https://www.cryonics.org/resources/blood-brain-barrier-preliminary-patent-application-disclousre.

[604] Corrigendum (correction) for Case A-2643. Alcor Life Extension Foundation, Mar 2016; https://www.alcor.org/Library/html/CorrigendumA2643.html.

[605] de Wolf A. Cryonics without cerebral dehydration? Biostasis, 21 Aug 2017; https://www.biostasis.com/cryonics-without-cerebral-dehydration/

[606] Ben Best, "Perfusion & Diffusion in Cryonics Protocol," https://www.benbest.com/cryonics/protocol.html#edema.

[607] De Wolf A, Phaedra C. Effect of Stabilization Medications on Cryopreservation of the Ischemic Brain. Cryonics 2017 Jan-Feb;38(1):10-12; https://www.alcor.org/docs/cryonics-magazine-2017-01.pdf.

[608] Fahy GM, Takahashi T, Crane AM, Sokoloff L. Cryoprotection of the mammalian brain. Cryobiology 1981;18:618. Fahy GM, Crane AM. Histological cryoprotection of rabbit brain with 3M glycerol. Cryobiology 1984;21:704.

presence of glycerol or similar artifacts: "If chemical changes have taken place as a result of glycerol exposure, these changes should be reversible due to their stereotypical nature and the identifiability of the chemically modified sites; actual information loss is not likely. Moreover, these chemical changes do not appear likely in the usual case, in which brains are perfused with lower concentrations of glycerol than 6 M."

Fahy also notes that some chemical alterations by glycerol are likely, but should mostly consist of altered levels of ordinary metabolic intermediates due to the actions of enzymes on glycerol[610] or due to the differential effects of glycerol on the kinetics of different enzymes.[611] "As such, they are fundamentally trivial and close to being spontaneously reversible. Glycerol has apparently never been documented to denature any protein under any conditions, with the possible exception of glycerol in concentrations in excess of 95% w/w,[612] a condition not remotely approached in cryonic suspension, even during the freezing phase of the process."[613]

(5) **Clotting and red cell sludging.** Patients who are subjected to a "straight freeze" with no cryoprotectants, or patients whose tissues receive incomplete cryoprotectant perfusion, may exhibit residual blood in the vasculature of the tissues subjected to poor perfusion, or may exhibit red cell aggregation[614] or "sludging" during low-flow or no-flow conditions.

(6) **Loss of synaptic contacts.** Both hibernation and external cooling induce expression of a number of cold-shock proteins in the brain, including the RNA binding protein RBM3.[615] In hibernating mammals, cooling induces loss of synaptic contacts which are reformed on rewarming, but in synaptically-compromised Alzheimer's mice the capacity to regenerate synapses after cooling declines in parallel with the loss of induction of RBM3. Alzheimer's mice lacking genes for RBM3 experience exacerbated synapse loss and accelerated disease, but enhanced expression of RBM3 in the hippocampus of Alzheimer's mice prevents this deficit and restores the capacity for synapse reassembly after cooling.

---

[609] Fahy G. Appendix B. A "Realistic" Scenario for Nanotechnological Repair of the Frozen Human Brain. In: Wowk B, Darwin M, eds., Cryonics: Reaching for Tomorrow. Alcor Life Extension Foundation, 1991, pp. A-10 – A-26; https://alcor.org/Library/html/nanotechrepair.html.

[610] Burch HB, Lowry OH, Meinhardt L, Max P Jr, Chyu K. Effect of fructose, dihydroxyacetone, glycerol, and glucose on metabolites and related compounds in liver and kidney. J Biol Chem. 1970 Apr 25;245(8):2092-2102; http://www.jbc.org/content/245/8/2092.full.pdf.

[611] Tanizaki MM, Bittencourt HM, Chaimovich H. Activation of low molecular weight acid phosphatase from bovine brain by purines and glycerol. Biochim Biophys Acta. 1977 Nov 23;485(1):116-123; https://pubmed.ncbi.nlm.nih.gov/199263.

[612] Bello J. The state of the tyrosines of bovine pancreatic ribonuclease in ethylene glycol and glycerol. Biochemistry. 1969 Nov;8(11):4535-4541; https://pubs.acs.org/doi/pdf/10.1021/bi00839a046.

[613] Jochem M, Körber Ch. Extended phase diagram for the ternary solutions H_2O-NaCl-glycerol and H_2O-NaCl-hydroxyethyI starch (HES) determined by DSC. Cryobiology 1987 Dec;24(6):513-536; https://www.sciencedirect.com/science/article/pii/0011224087900551.

[614] https://en.wikipedia.org/wiki/Erythrocyte_aggregation.

[615] Peretti D, Bastide A, Radford H, Verity N, Molloy C, Martin MG, Moreno JA, Steinert JR, Smith T, Dinsdale D, Willis AE, Mallucci GR. RBM3 mediates structural plasticity and protective effects of cooling in neurodegeneration. Nature. 2015 Feb 12;518(7538):236-9; http://www.ncbi.nlm.nih.gov/pmc/articles/PMC4338605/.

3.3.2 Iatrogenic Perfusion Damage

Human practitioners and organizations, even experienced and professional ones, occasionally err in one manner or another, in most cases amplifying an existing source of damage or in rare cases adding a new source of damage that must later be repaired.[616] This damage is iatrogenic, meaning "an inadvertent adverse effect or complication resulting from medical treatment…"[617]

For example, in the case of Patient A-1068 (a 68-year-old woman who was cryopreserved in 1985),[618] the surgeons who were attempting to create a fluidic circuit to enable continuous blood washout during the procedure quickly found and cannulated the right femoral artery but spent an hour searching for the right femoral vein without success, eventually switching to the left femoral vein to complete the circuit. It later turned out that the patient had a history of thrombophlebitis with extreme deep vein thrombosis of the right leg – in other words, the right femoral vein no longer existed. The failure to obtain medical records containing this information caused the patient to suffer ~1 hour of unnecessary additional cold ischemic damage.

Some documented examples of iatrogenic damage to cryopatients that occurred in past years due to improper perfusion procedures being followed by inexperienced practitioners include:[619]

* Allowing hydrobromide bleach (swimming pool disinfectant) to enter the portable ice bath (PIB), resulting in wall-water from the PIB containing bleach to be perfused into the patient.

* Allowing patients to be embolized by tiny air bubbles (thus blocking blood vessels, preventing proper cryopreservative perfusion) by failing to aspirate the arterial cannula and de-bubble the arterial line after connection to the cannula before going on bypass, by allowing air to enter the arterial filter while relying on the air separation membrane to remove gas emboli, failing to note the recirculating reservoir was empty, or allowing the aortic root cannula to "pop" out while leaving the venous return line unclamped.

* Reversing the connection of the arterial and venous bypass lines on a patient during blood washout resulting in massive vascular injury as evidenced by profuse bleeding from the sinuses, marked edema of the face, and distension of the eyeballs.

* Placing the venous reservoir above the level of the patient's right heart, thus preventing effective venous return and raising the central venous pressure to at least 30 mmHg with resultant massive pulmonary and systemic edema.

---

[616] Darwin M, *et al.*, Report of the Committee to Evaluate Alcor Procedures, Presented to the Alcor Board of Directors on April 4th, 2002, 114 pp.

[617] de Wolf A. Iatrogenesis and Cryonics. Cryonics 2013 Feb;34(2):5; https://www.alcor.org/docs/cryonics-magazine-2013-02.pdf.

[618] http://chronopause.com/chronopause.com/index.php/2011/04/11/you-be-the-judge-understanding-and-evaluating-the-quality-of-human-cryopreservations-from-cryonics-organization-literature-and-case-report-data-part-4/index.html.

[619] http://chronopause.com/chronopause.com/index.php/2012/04/29/cryonics-an-historical-failure-analysis-lecture-2-inherent-failure-mechanisms-and-risks-part-3/index.html.

These and similar practitioner-related errors can cause additional physical damage to the patient that must be detected, analyzed, and corrected during the nanorobotic repair procedures described elsewhere in this book.

3.4 Freezing or Vitrification Damage

Some damage inevitably occurs as tissue freezes or vitrifies, with different types of cells and tissues having different sensitivities to freezing temperatures.[620] One cryonicist[621] describes the effects on cells of a freezing process (images, below) that progresses at slow to moderate rates in the absence of cryoprotectant agents: "Ice begins forming outside cells, forming crystals of pure water. The salts and other solids that were formerly dissolved in the crystallized water are forced into a progressively smaller volume of unfrozen solution. This increase in the concentration of solids dissolved in the extracellular fluid osmotically extracts water from the cells, causing them to shrink. At about -20 °C no further water can be converted into ice and the interior of the cells remains in an unfrozen state – a highly concentrated solution of cell proteins and salts, from both inside and outside the cells. With further cooling this electrolyte gel will be converted to a crystal free glass at about -100 °C."

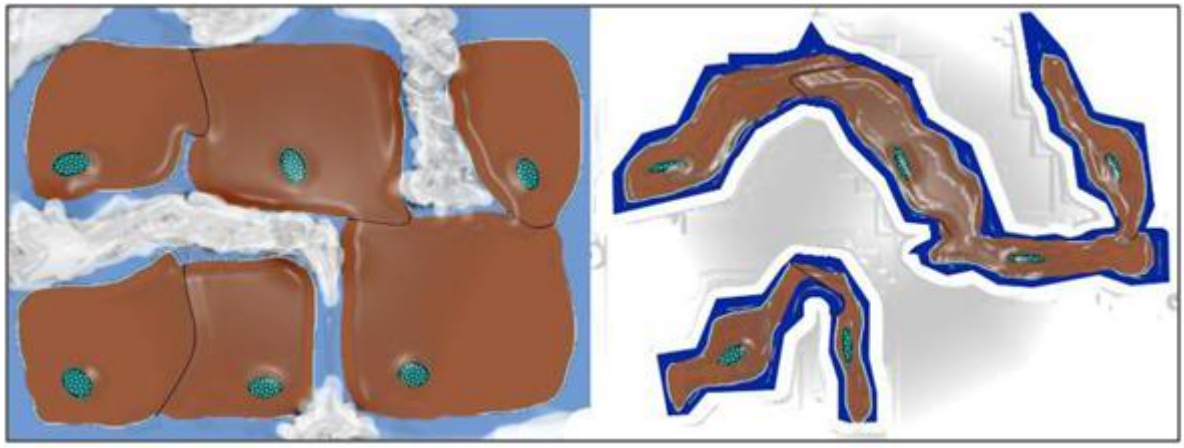

"Chemicals that provide cryoprotection are typically antifreeze compounds that are virtually identical in their action to that of ethylene glycol and propylene glycol, the chemicals used in automobile radiators and to winterize plumbing in recreational vehicles to protect them against freezing damage.[622] These antifreeze compounds work not only by decreasing the point at which a mixture of the agents and water will freeze,

---

[620] Gage AA, Baust JM, Baust JG. Experimental cryosurgery investigations *in vivo*. Cryobiology. 2009 Dec;59(3):229-43; https://www.ncbi.nlm.nih.gov/pmc/articles/PMC2821701/.

[621] Darwin M. Does Personal Identity Survive Cryopreservation? Chronosphere, 23 Feb 2011; http://chronopause.com/chronopause.com/index.php/2011/02/23/does-personal-identity-survive-cryopreservation/.

[622] Bank HL, Brockbank KG. Basic principles of cryobiology. J Card Surg. 1987 Mar;2(1 Suppl):137-43; https://pubmed.ncbi.nlm.nih.gov/2979966/. Karlsson JO, Toner M. Long-term storage of tissues by cryopreservation: critical issues. Biomaterials. 1996 Feb;17(3):243-56; https://pubmed.ncbi.nlm.nih.gov/8745321/. Pegg DE. The relevance of ice crystal formation for the cryopreservation of tissues and organs. Cryobiology. 2010 Jul;60(3 Suppl):S36-44; https://pubmed.ncbi.nlm.nih.gov/20159009/.

but also by reducing the amount of ice that forms when freezing does occur.[623] They do this by two mechanisms: (a) by the 'bulk effect' of taking up so much space in the solution that they physically interfere with the interaction of water molecules with each other, by providing a kinetic obstacle, and (b) by so strongly hydrogen bonding to water that they prevent the water from continuing to be converted into ice, once a certain amount of ice has been formed.[624] These mechanisms of action are termed 'colligative cryoprotection.'[625] Instead of the entire volume of solution freezing, only part of it does, whilst the rest becomes a thick, un-freezable liquid that, upon further cooling, solidifies[626] into a crystal-free and molecularly immobile glass."

In the discussion below, the lists in Section 3.4.1 and Section 3.4.2 are derived and updated mostly from items originally described by Fahy[627] of possible sources of freezing damage that may occur as the temperature of cryonics patients is lowered from room temperatures to cryogenic temperatures. Fahy evaluated these possible sources of damage for their relative ease of repair and for their potential to cause irreversible information loss according to the information-theoretic definition of death (Section 2.1.1),[628] and the present study updates the analysis in the context of repairability via medical nanorobots.

Future research should determine if there are any additional sources of potential freezing damage that have been overlooked in the present analysis.

3.4.1 Biochemical and Biophysical Cold Injury

Extracellular nucleating agents that are much less present intracellularly preferentially initiate water-ice formation in the extracellular spaces. Water excludes dissolved solutes as it freezes, increasing their concentration in the remaining liquid which draws water out of the cells by osmosis, dehydrating and shrinking the cells.[629] Typically ~60% of the volume of the brain of a (nonvitrified) cryopreserved patient

---

[623] Murthy SS. Some insight into the physical basis of the cryoprotective action of dimethyl sulfoxide and ethylene glycol. Cryobiology. 1998 Mar;36(2):84-96; https://pubmed.ncbi.nlm.nih.gov/9527870/.

[624] Greg Fahy clarifies (personal communication, 30 Dec 2021) that the specific technical mechanism is lowering of the vapor pressure of the liquid so as to bring the liquid vapor pressure of water down to the vapor pressure of ice at the same temperature.[*]

[*] Fahy GM. Analysis of "solution effects" injury. Equations for calculating phase diagram information for the ternary systems NaCl-dimethylsulfoxide-water and NaCl-glycerol-water. Biophys J. 1980 Nov;32(2):837-50; https://www.ncbi.nlm.nih.gov/pmc/articles/PMC1327241/pdf/biophysj00251-0161.pdf. Fahy GM. Simplified calculation of cell water content during freezing and thawing in nonideal solutions of cryoprotective agents and its possible application to the study of "solution effects" injury. Cryobiology. 1981 Oct;18(5):473-82; https://www.sciencedirect.com/science/article/abs/pii/0011224081902066.

[625] Wowk B, Darwin M, Harris SB, Russell SR, Rasch CM. Effects of solute methoxylation on glass-forming ability and stability of vitrification solutions. Cryobiology. 1999 Nov;39(3):215-27; https://pubmed.ncbi.nlm.nih.gov/10600255/.

[626] Wowk B. Thermodynamic aspects of vitrification. Cryobiology 2010;60:11-22; http://www.21cm.com/pdfs/2010-Thermodynamics.pdf.

[627] Fahy G. Appendix B. A "Realistic" Scenario for Nanotechnological Repair of the Frozen Human Brain. In: Wowk B, Darwin M, eds., Cryonics: Reaching for Tomorrow. Alcor Life Extension Foundation, 1991, pp. A-10 – A-26; https://alcor.org/Library/html/nanotechrepair.html.

[628] Merkle RC. The technical feasibility of cryonics. Med Hypotheses. 1992 Sep;39(1):6-16; https://www.ncbi.nlm.nih.gov/pubmed/1435395. See also: http://www.merkle.com/definitions/infodeath.html.

[629] Mazur P. Freezing of living cells: mechanisms and implications. Am J Physiol. 1984 Sep;247(3 Pt 1):C125-42; https://www.physiology.org/doi/pdf/10.1152/ajpcell.1984.247.3.C125.

has been converted into extracellular ice,[630] reducing cell volume because the freezing process extracts large fractions of the intracellular water.[631] (Early observations of briefly frozen hamsters found that at least 60% of the water in the brain could be converted into ice without damaging the ability of the hamsters to regain normal behavior after thawing,[632] and the lethal limit for freeze-tolerant animals appears to be ~65% ice.[633] The percentage of ice that forms varies from an ideal of 0% with vitrification to a very high percent with straight freezing.) The combination of cellular shrinkage, lowered temperature, and elevated cryoprotectant concentrations may cause the following kinds of damage:

(1) **Loss of membrane proteins into the extracellular space.** Loss of glutamate receptors and significant neurotransmitter receptor loss has been documented in brain tissue[634] and in other cells[635] frozen entirely without cryoprotectant, though such losses may be modest over short freeze periods up to 48 hours at -80 °C.[636] However, normal functionality is observed if even low concentrations of extracellular cryoprotectant (e.g., sucrose) are present during freezing.[637] Rat brain striatal synaptosomes[638] show up to 30% as much glutamate uptake as unfrozen controls after 5 days of cryopreservation at -80 °C,[639] and

---

[630] Leaf JD, Federowicz MG, Hixon H. Appendix A: The "Smith Criterion" for adequate cryoprotection. Cryonics 1985 Nov;6(11):38-39; https://alcor.org/cryonics/cryonics8511.txt.

[631] Mazur P. Freezing of living cells: mechanisms and implications. Am J Physiol. 1984 Sep;247(3 Pt 1):C125-42; https://www.physiology.org/doi/pdf/10.1152/ajpcell.1984.247.3.C125.

[632] Smith AU. Revival of mammals from body temperatures below zero. In: Smith AU, ed. Biological Effects of Freezing and Supercooling, Edward Arnold, London, 1961, pp.304-368. Lovelock JE, Smith AU. Studies on golden hamsters during cooling to and rewarming from body temperatures below 0 degrees C. III. Biophysical aspects and general discussion. Proc R Soc Lond B Biol Sci. 1956 Jul 24;145(920):427-442; https://royalsocietypublishing.org/doi/abs/10.1098/rspb.1956.0054.

[633] Storey KB, Storey JM. Freeze tolerance in animals. Physiol Rev. 1988 Jan;68(1):27-84; https://pdfs.semanticscholar.org/1933/ad336e2d05b8e4ce8c3554293bf767452558.pdf. Storey KB, Storey JM. Frozen and alive. Sci Am. 1990 Dec;263(6):92-97; https://www.researchgate.net/profile/Kenneth_Storey/publication/20884536_Frozen_and_Alive/links/0c96051f7dfd3ae26a000000/Frozen-and-Alive.pdf.

[634] Fagg GE, Mena EE, Monaghan DT, Cotman CW. Freezing eliminates a specific population of L-glutamate receptors in synaptic membranes. Neurosci Lett. 1983 Jul 29;38(2):157-162; https://pubmed.ncbi.nlm.nih.gov/6312382. Wu K, Carlin R, Siekevitz P. Binding of L-[3H]glutamate to fresh or frozen synaptic membrane and postsynaptic density fractions isolated from cerebral cortex and cerebellum of fresh or frozen canine brain. J Neurochem. 1986 Mar;46(3):831-841; https://pubmed.ncbi.nlm.nih.gov/2869103.

[635] Takahashi T, Inada S, Pommier CG, O'Shea JJ, Brown EJ. Osmotic stress and the freeze-thaw cycle cause shedding of Fc and C3b receptors by human polymorphonuclear leukocytes. J Immunol. 1985 Jun;134(6):4062-4068; https://pubmed.ncbi.nlm.nih.gov/3157755.

[636] Volz TJ, Farnsworth SJ, Hanson GR, Fleckenstein AE. Measurement of plasmalemmal dopamine transport, vesicular dopamine transport, and K(+)-stimulated dopamine release in frozen rat brain tissue. J Neurosci Methods. 2009 Jun 15;180(2):317-320; https://www.ncbi.nlm.nih.gov/pmc/articles/PMC2941190/.

[637] Haan EA, Bowen DM. Protection of neocortical tissue prisms from freeze-thaw injury by dimethyl sulphoxide. J Neurochem. 1981 Jul;37(1):243-246; https://pubmed.ncbi.nlm.nih.gov/6788904. Hardy JA, Dodd PR, Oakley AE, Perry RH, Edwardson JA, Kidd AM. Metabolically active synaptosomes can be prepared from frozen rat and human brain. J Neurochem. 1983 Mar;40(3):608-614; https://pubmed.ncbi.nlm.nih.gov/6827264. Dodd PR, Hardy JA, Baig EB, *et al*. Optimization of freezing, storage, and thawing conditions for the preparation of metabolically active synaptosomes from frozen rat and human brain. Neurochem Pathol. 1986 Jun;4(3):177-198; https://pubmed.ncbi.nlm.nih.gov/3561893.

[638] https://en.wikipedia.org/wiki/Synaptosome.

[639] Schwarcz R. Effects of tissue storage and freezing on brain glutamate uptake. Life Sci. 1981 Mar 9;28(10):1147-1154; https://www.sciencedirect.com/science/article/abs/pii/0024320581906925.

freezing rat and human tissues does not affect uptake sites of serotonin and dopamine neurotransmitters,[640] consistent with good retention of membrane proteins after freeze/thaw cycling. Intracellular organelles do not redistribute or mix proteins to a worrisome degree after brain tissue is frozen and thawed.[641] Thus, even excessive cellular shrinkage prior to freezing (caused by inadequate penetration of cryoprotectant) superimposed on subsequent freeze-induced cell shrinkage should not subject cells to greater osmotic stress than has been shown experimentally (by freezing with only extracellular sucrose present as cryoprotectant)[642] not to cause major loss of membrane proteins.

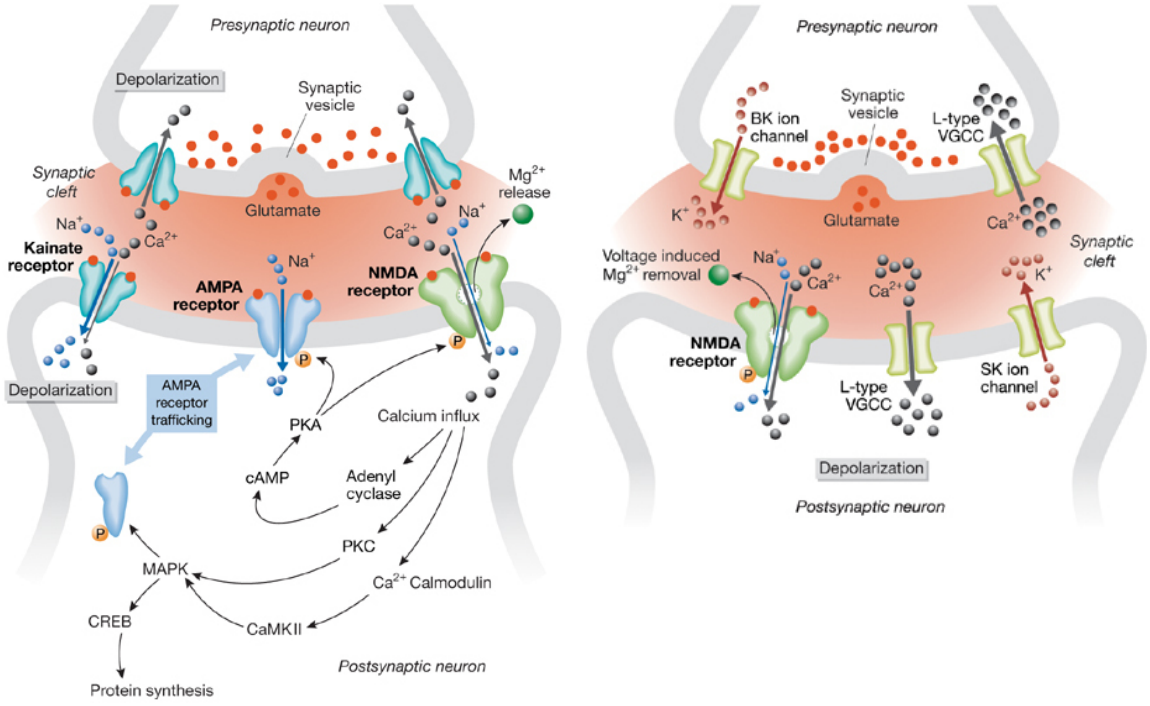

In 1991, Fahy[643] opined that "the number, state, and precise anatomical distribution of potassium channels in hippocampal dendrite membranes probably encodes memory to a large degree,[644] so the potential loss of these membrane proteins is of concern." Synaptic plasticity may be subject to regulation by synaptically

---

[640] Stenström A, Oreland L, Hardy J, Wester P, Winblad B. The uptake of serotonin and dopamine by homogenates of frozen rat and human brain tissue. Neurochem Res. 1985 May;10(5):591-599; https://pubmed.ncbi.nlm.nih.gov/4010874.

[641] Stahl WL, Swanson PD. Effects of freezing and storage on subcellular fractionation of guinea pig and human brain. Neurobiology. 1975 Dec;5(6):393-400; https://pubmed.ncbi.nlm.nih.gov/1207870.

[642] Hardy JA, Dodd PR, Oakley AE, Perry RH, Edwardson JA, Kidd AM. Metabolically active synaptosomes can be prepared from frozen rat and human brain. J Neurochem. 1983 Mar;40(3):608-614; https://pubmed.ncbi.nlm.nih.gov/6827264.

[643] Fahy G. Appendix B. A "Realistic" Scenario for Nanotechnological Repair of the Frozen Human Brain. In: Wowk B, Darwin M, eds., Cryonics: Reaching for Tomorrow. Alcor Life Extension Foundation, 1991, pp. A-10 – A-26; https://alcor.org/Library/html/nanotechrepair.html.

[644] Alkon DL. Memory storage and neural systems. Sci Am. 1989 Jul;261(1):42-50; https://www.jstor.org/stable/24987318. Alkon DL. Calcium-mediated reduction of ionic currents: a biophysical memory trace. Science. 1984 Nov 30;226(4678):1037-1045; https://science.sciencemag.org/content/226/4678/1037.full.pdf. Alkon DL, Rasmussen H. A spatial-temporal model of cell activation. Science. 1988 Feb 26;239(4843):998-1005; https://science.sciencemag.org/content/239/4843/998.full.pdf. Alkon DL. Memory Traces in the Brain, Cambridge University Press, 1988.

located K^+ channels that are dynamically trafficked in and out of synaptic compartments, contributing to the regulation of synaptic strength in the hippocampus.[645] The number of ion channels on the post-synaptic membrane affects the strength of the synapse (synapse schematic above, right).[646]

AMPA glutamate receptors (AMPAR) (synapse schematic above, left) play a role in long-term potentiation (LTP) of new memories (Section 2.1.2).[647] AMPAR are continuously trafficked (i.e., endocytosed, recycled, reinserted) into and out of the plasma membrane while preserving the total number of AMPAR in an activated synapse, a process responsible for the maintenance of new memories.[648] Because the AMPAR population is constantly in motion during life,[649] it seems likely that the synaptic activation level depends more on the total number of AMPAR present rather than on their precise positions within the local volume. The loss of a few of these proteins during cryopreservation should leave enough of the original population intact to permit inference of the original numbers and compensatory reinsertion of new AMPAR by medical nanorobots (Section 4.12). Similarly, synaptic NMDA receptors (NMDAR)[650] assist in LTP[651] while extrasynaptic NMDAR produce long term depression (LTD) of memory[652] (reducing the synaptic activation, the opposite of LTP) while inhibiting LTP.[653] Kainate receptors (which also have a role in synaptic plasticity)[654] and NMDAR lost during cryopreservation can be nanorobotically restored in similar manner to the AMPAR.

Associative learning involves both potassium channels and changes in several other characteristic proteins

---

[645] Kim J, Hoffman DA. Potassium channels: newly found players in synaptic plasticity. Neuroscientist. 2008 Jun;14(3):276-286; https://www.ncbi.nlm.nih.gov/pmc/articles/PMC2665047/.

[646] Voglis G, Tavernarakis N. The role of synaptic ion channels in synaptic plasticity. EMBO Rep. 2006 Nov;7(11):1104-1110; https://www.embopress.org/doi/full/10.1038/sj.embor.7400830.

[647] https://en.wikipedia.org/wiki/AMPA_receptor#Synaptic_plasticity.

[648] Malinow R, Mainen ZF, Hayashi Y. LTP mechanisms: from silence to four-lane traffic. Curr Opin Neurobiol. 2000 Jun;10(3):352-357; http://glutamate.med.kyoto-u.ac.jp/Shared/images/0/06/Malinow_Curr_Opin_Neurobiol.pdf. Shepherd JD, Huganir RL. The cell biology of synaptic plasticity: AMPA receptor trafficking. Annu Rev Cell Dev Biol. 2007;23:613-643; http://www.pai.utexas.edu/faculty/isaxena/BIO320/The%20cell%20biology%20of%20synaptic%20plasticity%20-%20AMPA%20receptor%20trafficking%20-%202007.pdf.

[649] Makino H, Malinow R. AMPA receptor incorporation into synapses during LTP: the role of lateral movement and exocytosis. Neuron. 2009 Nov 12;64(3):381-390; https://www.cell.com/neuron/pdf/S0896-6273(09)00675-8.pdf.

[650] https://en.wikipedia.org/wiki/NMDA_receptor#Neural_plasticity.

[651] Berg LK, Larsson M, Morland C, Gundersen V. Pre- and postsynaptic localization of NMDA receptor subunits at hippocampal mossy fibre synapses. Neuroscience. 2013 Jan 29;230:139-150; https://pubmed.ncbi.nlm.nih.gov/23159309.

[652] Li S, Jin M, Koeglsperger T, Shepardson NE, Shankar GM, Selkoe DJ. Soluble Aβ oligomers inhibit long-term potentiation through a mechanism involving excessive activation of extrasynaptic NR2B-containing NMDA receptors. J Neurosci. 2011 May 4;31(18):6627-6638; https://www.jneurosci.org/content/jneuro/31/18/6627.full.pdf. Papouin T, Ladépêche L, Ruel J, Sacchi S, Labasque M, Hanini M, Groc L, Pollegioni L, Mothet JP, Oliet SHR. Synaptic and extrasynaptic NMDA receptors are gated by different endogenous coagonists. Cell. 2012 Aug 3;150(3):633-646; https://www.cell.com/fulltext/S0092-8674(12)00786-6.

[653] Liu DD, Yang Q, Li ST. Activation of extrasynaptic NMDA receptors induces LTD in rat hippocampal CA1 neurons. Brain Res Bull. 2013 Apr;93:10-16; https://pubmed.ncbi.nlm.nih.gov/23270879.

[654] https://en.wikipedia.org/wiki/Kainate_receptor#Plasticity.

that induce and maintain the alterations of potassium conductance underlying memory.[655] Even loss of potassium channels should leave these remaining proteins behind, providing a clear indication of the "trained" vs. "untrained" state of given dendritic synapses and/or perisynaptic regions (Section 2.1.2). Durability and inferrability is further implied by the associative nature of memory, in which a given memory is stored redundantly (Section 2.1.3) in several brain regions in a number of independent forms,[656] all of which are unlikely to be extinguished simultaneously in their entirety.

(2) **Extrusion of pure lipid species from the plasma membrane**, either on tethers[657] or as free lipid droplets in the cytoplasm[658] or in the extracellular space (proportional to the reduction in membrane surface area produced by freezing). As long as any lipid extrusions are intracellular or remain attached to the cell of origin, it should be clear where to redistribute the lipid as long as the tissue remains solid. But upon warming, lipid extruded in this way is unable to spontaneously return to the plane of the membrane during reliquidification and volume expansion on thawing. The resulting inadequate membrane surface area upon restoration of approximately isotonic volume near the melting point causes cellular lysis in plant cells. Fortunately, this phenomenon has only been observed in plants and shedding of lipid to free-floating extracellular droplets has not been seen even in plants, so this problem is not expected to occur during the revival of human cryopatients.

(3) **Freezing of cell membrane lipids.** Darwin[659] notes that "[m]any cell membrane lipids freeze at or near room temperature, and almost all cellular lipid species are frozen at high subzero temperatures (i.e., above -20 °C).[660] Lipid phase change can result in a variety of alterations to membrane structure, and thus could alter function.[661] Reorganized lipids in the membrane may open up holes or pores which allow

---

[655] Alkon DL. Memory storage and neural systems. Sci Am. 1989 Jul;261(1):42-50; https://www.jstor.org/stable/24987318. Alkon DL. Calcium-mediated reduction of ionic currents: a biophysical memory trace. Science. 1984 Nov 30;226(4678):1037-1045; https://science.sciencemag.org/content/226/4678/1037.full.pdf. Alkon DL, Rasmussen H. A spatial-temporal model of cell activation. Science. 1988 Feb 26;239(4843):998-1005; https://science.sciencemag.org/content/239/4843/998.full.pdf. Alkon DL. Memory Traces in the Brain, Cambridge University Press, 1988.

[656] Kandel ER, Schwartz JH. Principles of Neural Science, Second Edition. Elsevier, New York, 1985. Alkon DL. Memory storage and neural systems. Sci Am. 1989 Jul;261(1):42-50; https://www.jstor.org/stable/24987318.

[657] Steponkus PL, Dowgert MF, Gordon-Kamm WJ. Destabilization of the plasma membrane of isolated plant protoplasts during a freeze-thaw cycle: the influence of cold acclimation. Cryobiology. 1983 Aug;20(4):448-465; https://pubmed.ncbi.nlm.nih.gov/6617234. Steponkus PL, Lynch DV, *et al*. Plant cryobiology: cellular and molecular aspects of freezing injury and cold acclimation. In: McGrath JJ, Diller KR, eds. Low Temperature Biotechnology: Emerging Applications and Engineering Contributions. ASME, New York, 1988, pp.47-56.

[658] Williams RJ, Hope HJ, Willemot C. Membrane collapse as a cause of osmotic injury and its reversibility in a hardy wheat. Cryobiology 1975;12:554-5.

[659] Darwin M. Does Personal Identity Survive Cryopreservation? Chronosphere, 23 Feb 2011; http://chronopause.com/chronopause.com/index.php/2011/02/23/does-personal-identity-survive-cryopreservation/.

[660] Fahy GM, da Mouta C, Tsonev L, Khirabagi BS, Mehl P, Meryman HT. Chapter 20. Cellular Injury Associated with Organ Cryopreservation: Chemical Toxicity and Cooling Injury. In: Lemasters JJ, Oliver C, eds., Cell Biology of Trauma, CRC Press, 1995, pp. 333-356. Balasubramanian SK, Wolkers WF, Bischof JC. Membrane hydration correlates to cellular biophysics during freezing in mammalian cells. Biochim Biophys Acta. 2009 May;1788(5):945-53; https://core.ac.uk/download/pdf/82611660.pdf.

[661] Schwarz W. Temperature experiments on nerve and muscle membranes of frogs. Indications for a phase transition. Pflugers Arch. 1979 Oct;382(1):27-34; https://pubmed.ncbi.nlm.nih.gov/316517/. Crowe JH, Tablin F, Tsvetkova N, Oliver AE, Walker N, Crowe LM. Are lipid phase transitions responsible for chilling damage in human platelets? Cryobiology. 1999 May;38(3):180-91; https://pubmed.ncbi.nlm.nih.gov/10328908/.

the leakage of water and ions into or out of the cells.[662] Cooling, independent of freezing, can also irreversibly alter the structure of glycolipids and lipid-protein complexes, rendering them inactive. Phase change in the membrane can also result in the precipitation, relocation, or extrusion of membrane proteins critical to cellular function....[with] extensive relocation of the sodium-potassium-ATPase from the interior domain of the membrane to the surface, as well as aggregation of the protein into visible particles." Fahy[663] warns of the possible reorganization of membrane bilayer structure into HexII forms (i.e., long narrow cylindrical lipid tubes on a hexagonal array)[664] or phase separation of lipid subclasses within the membrane, producing leaks secondary to the resulting molecular packing faults in the membrane.[665] These problems are functionally comparable to the possibility of osmotic or mechanically-induced leaks as noted above, though there is no direct evidence for HexII transitions in any mammalian system. HexII forms appear unlikely in the presence of 3-4 M glycerol before freezing, since HexII is a dehydration form[666] and glycerol can prevent the required level of dehydration for HexII formation from taking place.[667] (Tissue insufficiently infused with cryoprotectant solution or that receives no cryoprotectant might possibly have greater risk of this damage.) In both HexII formation and more conventional phase separations, all membrane material would remain in the membrane, so the challenge would be to minimize additional leakage from taking place during thawing and of redistributing solutes across membranes as needed after membrane resealing is completed, a task which nanorobots could perform (Section 4.12). In the case of HexII, spontaneous reversal of the phase transition upon warming and rehydration could lead to incorporation of lipid and protein into incorrect leaflets of the membrane, but nanorobots could detect and edit these incorrect leaflets, given sufficient time (which is likely available due to the planned induction of biochemical stasis; Section 4.10).

(4) **Local leakage of brain cell solute into the extracellular space.** The leakage of small ions (primarily potassium) and small metabolites should be negligible, assuming that most cell membranes remain intact – freeze-permeabilized cell membranes should normally reseal during warming and thawing.[668] Pumping potassium and small metabolites back into neurons is straightforward during

---

[662] Chow EI, Chuang SY, Tseng PK. Detection of a phase transition in red cell membranes using positronium as a probe. Biochim Biophys Acta. 1981 Aug 20;646(2):356-9; https://pubmed.ncbi.nlm.nih.gov/7295722/.

[663] Fahy G. Appendix B. A "Realistic" Scenario for Nanotechnological Repair of the Frozen Human Brain. In: Wowk B, Darwin M, eds., Cryonics: Reaching for Tomorrow. Alcor Life Extension Foundation, 1991, pp. A-10 – A-26; https://alcor.org/Library/html/nanotechrepair.html.

[664] Steponkus PL, Lynch DV. Freeze/thaw-induced destabilization of the plasma membrane and the effects of cold acclimation. J Bioenerg Biomembr. 1989 Feb;21(1):21-41; https://pubmed.ncbi.nlm.nih.gov/2651425. Koynova RD, Tenchov BG, Quinn PJ. Sugars favour formation of hexagonal (H_{II}) phase at the expense of lamellar liquid-crystalline phase in hydrated phosphatidylethanolamines. Biochem Biophys Acta 1989 Apr 28;980(3):377-380; https://www.sciencedirect.com/science/article/pii/0005273689903283.

[665] Lyons JM. Phase transitions and control of cellular metabolism at low temperatures. Cryobiology. 1972 Oct;9(5):341-350; https://www.sciencedirect.com/science/article/pii/0011224072901526. Quinn PJ. A lipid-phase separation model of low-temperature damage to biological membranes. Cryobiology. 1985 Apr;22(2):128-146; https://www.sciencedirect.com/science/article/pii/0011224085901671.

[666] Koynova RD, Tenchov BG, Quinn PJ. Sugars favour formation of hexagonal (H_{II}) phase at the expense of lamellar liquid-crystalline phase in hydrated phosphatidylethanolamines. Biochem Biophys Acta 1989 Apr 28;980(3):377-380; https://www.sciencedirect.com/science/article/pii/0005273689903283.

[667] Jochem M, Körber Ch. Extended phase diagram for the ternary solutions H_2O-NaCl-glycerol and H_2O-NaCl-hydroxyethyI starch (HES) determined by DSC. Cryobiology 1987 Dec;24(6):513-536; https://www.sciencedirect.com/science/article/pii/0011224087900551.

[668] Pegg DE, Diaper MP. On the mechanism of injury to slowly frozen erythrocytes. Biophys J. 1988 Sep;54(3):471-88; https://www.ncbi.nlm.nih.gov/pmc/articles/PMC1330346/.

nanorobot repair (Section 4.12). Leakage of proteins and other large molecules is more serious from a biological standpoint, but significant (e.g., 50%) uncorrected loss of intracellular soluble protein from cell bodies could probably be sustained without creating viability issues since it should be possible to institute compensatory controls over metabolic rate and membrane permeability consistent with the spontaneous ability of the cell to resynthesize missing proteins on warming.[669] Even massive protein loss from cell bodies would not be able to erase cell identification which will be preserved because cell identification is encoded (A) in the types of synapses the cell makes,[670] (B) by the pattern of genetic expression readable in the nucleus,[671] and (C) by membrane and perhaps non-soluble cytoplasmic protein markers.[672] The present "conventional cell repair" revival protocol (Chapter 4) is designed to handle even the worst case scenario where massive leakage has occurred from either cytosol or bloodstream into the extracellular spaces (e.g., Section 4.10.1.3).

Severe losses of axoplasmic proteins at sites of torn axon bundles[673] could make the identification of individual nerve fibers on both sides of tears more difficult, potentially limiting the ability to deduce the original connectivity of the brain. However, it is likely that a short distance away from the tear the axonal protein content should be largely unaffected by the lesion, especially given the gel-like nature of axoplasm[674] and the relatively rigid structures mediating axoplasmic traffic. Such tear sites should be visible from the micron (Section 4.3) and submicron (Section 4.7) resolution scans in the solid phase before significant tissue movement has occurred, enabling plans for nanorobotic repair to be devised for use during cell membrane repair (Section 4.11) following reliquidification. Some protein leakage will continue until the torn membranes are fully sealed, but the correct molecular populations can be restored nanorobotically during the detailed cell repair phase (Section 4.12).

(5) **Leakage of concentrated extracellular solute into brain cells.** Like membrane lipid loss (Section 3.4.1(2)), the main problem caused by this leakage would be expansion-induced lysis upon thawing.[675] Although the volume of extracellular space in the brain might be considered insufficient to

---

[669] Fahy G. Appendix B. A "Realistic" Scenario for Nanotechnological Repair of the Frozen Human Brain. In: Wowk B, Darwin M, eds., Cryonics: Reaching for Tomorrow. Alcor Life Extension Foundation, 1991, pp. A-10 – A-26; https://alcor.org/Library/html/nanotechrepair.html.

[670] Kuljis DA, Zemoura K, Telmer CA, Lee J, Park E, Ackerman DS, Xu W, Watkins SC, Arnold DB, Bruchez MP, Barth AL. Quantitative synapse analysis for cell-type specific connectomics. bioRxiv, 06 Aug 2018; https://www.biorxiv.org/content/10.1101/386912v1.full.pdf.

[671] Houlé JD, Das GD. Freezing and transplantation of brain tissue in rats. Experientia. 1980 Sep 15;36(9):1114-1115; https://pubmed.ncbi.nlm.nih.gov/7418856. Das GD, Houle JD, Brasko J, Das KG. Freezing of neural tissues and their transplantation in the brain of rats: technical details and histological observations. J Neurosci Methods. 1983 May;8(1):1-15; https://pubmed.ncbi.nlm.nih.gov/6876871. Sørensen T, Jensen S, Møller A, Zimmer J. Intracephalic transplants of freeze-stored rat hippocampal tissue. J Comp Neurol. 1986 Oct 22;252(4):468-482; https://onlinelibrary.wiley.com/doi/abs/10.1002/cne.902520404. Jensen S, Sørensen T, Zimmer J. Cryopreservation of fetal rat brain tissue later used for intracerebral transplantation. Cryobiology. 1987 Apr;24(2):120-134; https://pubmed.ncbi.nlm.nih.gov/3568740.

[672] Stahl WL, Swanson PD. Effects of freezing and storage on subcellular fractionation of guinea pig and human brain. Neurobiology. 1975 Dec;5(6):393-400; https://pubmed.ncbi.nlm.nih.gov/1207870.

[673] Suda I, Kito K, Adachi C. Bioelectric discharges of isolated cat brain after revival from years of frozen storage. Brain Res. 1974 Apr 26;70(3):527-531; https://www.sciencedirect.com/science/article/abs/pii/0006899374902637. Fahy GM, Takahashi T, Crane AM. Histological cryoprotection of rat and rabbit brains. Cryo-Letters 1984;5:33-46.

[674] Baker PF, Hodgkin AL, Shaw TI. Replacement of the axoplasm of giant nerve fibres with artificial solutions. J Physiol. 1962 Nov;164(2):330-54; https://www.ncbi.nlm.nih.gov/pmc/articles/PMC1359308/pdf/jphysiol01232-0142.pdf.

[675] Lovelock JE. The mechanism of the protective action of glycerol against haemolysis by freezing and thawing. Biochim Biophys Acta. 1953 May;11(1):28–36; https://www.sciencedirect.com/science/article/pii/0006300253900055.

permit lysis on warming, ultrastructural evidence of disruption of neuronal fine processes in frozen-thawed brain[676] as well as ultrastructural evidence of swelling of frozen-thawed synaptosomes[677] lends credibility to this possibility. However, since lysis can be avoided either by extruding extra intracellular osmolyte or actively managing the local osmotic environment during thawing, this is not considered a significant problem.

(6) **Cytoplasm structure breaks down into blobs of proteinaceous material.**[678] This may occur if there is a breach of the cell membrane or for other reasons that are currently only poorly understood. So far, this phenomenon has been seen only in kidney, not in brain, and does not pertain to all cells, even in the kidney.[679] While repair could be more complicated if this form of breakdown occurs in the brain, it is doubtful that any actual information loss would occur, and the change might be spontaneously reversible on warming, e.g., during prethaw phase (Section 4.9).

(7) **Precipitation of proteins and cellular buffers.** Little direct evidence exists for this mode of injury.[680] If it were to occur, the result would be reduced metabolic competence secondary to denatured or missing proteins or unfavorable pHs for normal metabolism. The remedies – supplying replacement buffer and/or proteins and restoring precipitated proteins and/or buffers to a soluble condition – are easy to deal with nanorobotically (Section 4.12).

(8) **Denaturation of proteins[681] and intracellular solute concentration effects.** Dehydration leading to solute concentration beyond some critical level could disrupt metabolism, denature cell proteins[682] and macromolecular complexes,[683] and weaken cell membranes.[684] According to one 2011

---

[676] Fahy G. Appendix B. A "Realistic" Scenario for Nanotechnological Repair of the Frozen Human Brain. In: Wowk B, Darwin M, eds., Cryonics: Reaching for Tomorrow. Alcor Life Extension Foundation, 1991, pp. A-10 – A-26; https://alcor.org/Library/html/nanotechrepair.html.

[677] Hardy JA, Dodd PR, Oakley AE, Perry RH, Edwardson JA, Kidd AM. Metabolically active synaptosomes can be prepared from frozen rat and human brain. J Neurochem. 1983 Mar;40(3):608-614; https://pubmed.ncbi.nlm.nih.gov/6827264.

[678] Fahy GM. Analysis of "solution effects" injury: cooling rate dependence of the functional and morphological sequellae of freezing in rabbit renal cortex protected with dimethyl sulfoxide. Cryobiology. 1981 Dec;18(6):550-570; https://www.sciencedirect.com/science/article/pii/0011224081901231. Jacobsen IA, Pegg DE, Starklint H, Hunt CJ, Barfort P, Diaper MP. Introduction and removal of cryoprotective agents with rabbit kidneys: assessment by transplantation. Cryobiology. 1988 Aug;25(4):285-299; https://pubmed.ncbi.nlm.nih.gov/3136972.

[679] Fahy G. Appendix B. A "Realistic" Scenario for Nanotechnological Repair of the Frozen Human Brain. In: Wowk B, Darwin M, eds., Cryonics: Reaching for Tomorrow. Alcor Life Extension Foundation, 1991, pp. A-10 – A-26; https://alcor.org/Library/html/nanotechrepair.html.

[680] Kylin H. Uber die Kalteresistenze der Meeresalgen. Eer. dtsch. bor. Ges. 1917;35:370-84. Van Den Berg L, Soliman FS. Effect of glycerol and dimethyl sulfoxide on changes in composition and pH of buffer salt solutions during freezing. Cryobiology. 1969 Sep-Oct;6(2):93-97; https://www.sciencedirect.com/science/article/pii/S0011224069804694.

[681] https://en.wikipedia.org/wiki/Denaturation_(biochemistry)#Protein_denaturation.

[682] Gu JH, Beekman A, Wu T, *et al*. Beyond glass transitions: studying the highly viscous and elastic behavior of frozen protein formulations using low temperature rheology and its potential implications on protein stability. Pharm Res. 2013 Feb;30(2):387–401; https://www.researchgate.net/profile/Michael_Hale5/publication/232256304_Beyond_Glass_Transitions_Studying_the_Highly_Viscous_and_Elastic_Behavior_of_Frozen_Protein_Formulations_Using_Low_Temperature_Rheology_and_Its_Potential_Implications_on_Protein_Stability/links/545d1fb40cf2c1a63bfa5f9b/Beyond-Glass-Transitions-Studying-the-Highly-Viscous-and-Elastic-Behavior-of-Frozen-Protein-Formulations-Using-Low-Temperature-Rheology-and-Its-Potential-Implications-on-Protein-Stability.pdf.

[683] Hochachka PW, Guppy M. Metabolic Arrest and the Control of Biological Time. Harvard University Press, 1987, p. 125.

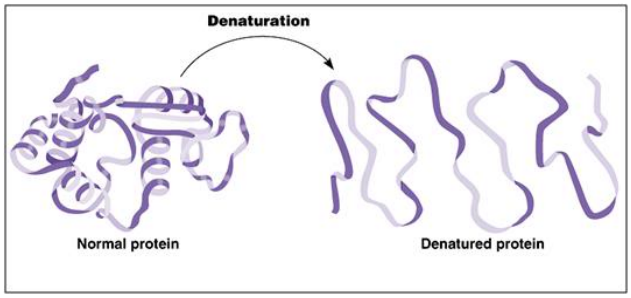

assessment:[685] "Many of the proteins that comprise the workhorses of cellular activity, including enzymes, DNA, RNA, and the structural proteins critical to the cell maintaining its shape and membrane integrity, require the presence of water to maintain their functional structure.[686] The water normally suspending and surrounding these proteins provides 'conformational support' and is essential to many proteins maintaining their functional shape. When too much water is removed from the medium suspending proteins, the proteins may become denatured (image, above). What this means is that the string of amino acids that make up the backbone of the protein can become unstable and lose its necessary folding configuration. Since a protein is made up of a 'bead work' of amino acids forming a long chain, it is often possible for that chain to be folded, or configured, in different ways. Unfortunately, usually only one folding configuration allows the protein to function in the lock and key fashion it requires in order to function properly – or at all. When very high concentrations of salts or cryoprotective chemicals replace the native cellular water, protein can become completely…or partially denatured. Sometimes this is reversible, but most often it is not, and the only solution to protein denaturation is for the cell to synthesize a replacement protein. However, if all of a species of protein that is essential to cellular metabolism is rendered inactive by denaturation, then the cell does not have the opportunity to restart metabolism, and thus replace the damaged protein(s)." Replacement proteins and nucleic acid structures can be synthesized in cell mills (Appendix D) and replaced during general cell repair (Section 4.12.2). Loss of identity-relevant information from this source of damage appears unlikely (Section 2.1.3).

(9) **Improper disulfide bridge formation between some proteins.**[687] An almost negligible problem, for similar reasons as with protein denaturation.

(10) **Intracellular freezing.** Intracellular freezing can occur in the absence of cryoprotectant if cooling is too fast to allow water within the cell to escape before it freezes, causing the intracellular contents to become supercooled, followed by abrupt freezing.[688] If cooling is slow enough to allow the osmotic removal of most water from the cell's interior, as typically occurs during cryopreservation, the high solute concentration prevents the small amount of remaining water from freezing and there is little damage unless membrane rupture allows extracellular ice to penetrate the intracellular region. This should not occur in vitrified cells and only rarely in cells lacking adequate cryoprotectant; membrane ruptures will be repaired by nanorobots (Section 4.11).

---

[684] Pegg D. Chapter 4. Principles of tissue preservation. In: Morris PJ, Tilney NL, eds. Progress in Transplantation, Volume 2, Churchill Livingstone, Edinburgh, 1985, pp. 69-105, 92.

[685] Darwin M. Does Personal Identity Survive Cryopreservation? Chronosphere, 23 Feb 2011; http://chronopause.com/chronopause.com/index.php/2011/02/23/does-personal-identity-survive-cryopreservation/.

[686] Tamiya T, Okahashi N, Sakuma R, Aoyama T, Akahane T, Matsumoto JJ. Freeze denaturation of enzymes and its prevention with additives. Cryobiology. 1985 Oct;22(5):446-56; https://pubmed.ncbi.nlm.nih.gov/2932302/.

[687] Goodin R, Levitt J. The cryoaggregation of bovine serum albumin. Cryobiology. 1970 Jan-Feb;6(4):333-338; https://www.sciencedirect.com/science/article/pii/S0011224070800876.

[688] Mazur P. Freezing of living cells: mechanisms and implications. Am J Physiol. 1984 Sep;247(3 Pt 1):C125-42; https://www.physiology.org/doi/pdf/10.1152/ajpcell.1984.247.3.C125.

(11) **Cold-induced microtubule depolymerization**. Microtubules (essential components of the cell cytoskeleton)[689] are sensitive to environmental conditions such as calcium concentration[690] or cold temperature,[691] the latter of which can cause depolymerization.[692] Repolymerization of the microtubular network can be observed after rewarming.[693] Vertebrates possess microtubule-associated proteins (MAP6) that protect microtubules against cold-induced depolymerization at least down to 4 °C.[694] While this mode of damage seems unlikely during cryonics revival, ***future research*** should verify that microtubule depolymerization does not occur (A) during tissue cooling to below 4 °C or (B) when cryopreserved tissue is warmed from cryogenic temperatures up to just above the melting point (e.g., 4 °C) during reliquidification; or its significance when it does occur.

(12) **Leakage of lysosomal enzymes into the cytoplasm, predisposing the cell to intracellular autolysis on warming.**[695] Despite early evidence that freezing and thawing might damage lysosomes,[696] the presence of cryoprotectant appears to reduce the freeze/thaw damage[697] and this failure has not yet been observed to occur in the cryonics context.[698] Cryoprotectants and low temperatures should limit autolysis

---

[689] https://en.wikipedia.org/wiki/Microtubule.

[690] Weisenberg RC. Microtubule formation *in vitro* in solutions containing low calcium concentrations. Science. 1972 Sep 22;177(4054):1104-1105; https://pubmed.ncbi.nlm.nih.gov/4626639/.

[691] Cassimeris LU, Wadsworth P, Salmon ED. Dynamics of microtubule depolymerization in monocytes. J Cell Biol. 1986 Jun;102(6):2023-32; https://www.ncbi.nlm.nih.gov/pmc/articles/PMC2114271/pdf/jc10262023.pdf.

[692] Li G, Moore JK. Microtubule dynamics at low temperature: evidence that tubulin recycling limits assembly. Mol Biol Cell. 2020 May 15;31(11):1154-1166; https://www.ncbi.nlm.nih.gov/pmc/articles/PMC7353160/.

[693] Breton S, Brown D. Cold-induced microtubule disruption and relocalization of membrane proteins in kidney epithelial cells. J Am Soc Nephrol. 1998 Feb;9(2):155-66; https://jasn.asnjournals.org/content/9/2/155/full-text.pdf.

[694] Delphin C, Bouvier D, Seggio M, *et al*. MAP6-F is a temperature sensor that directly binds to and protects microtubules from cold-induced depolymerization. J Biol Chem. 2012 Oct 12;287(42):35127-35138; https://www.jbc.org/content/287/42/35127.full.pdf. (Note that the earlier Breton and Brown paper cited in the previous footnote seemingly contradictorily reports microtubule network disruption at 4 °C.)

[695] Persidsky MD, Ellett MH. Lysosomes and cell cryoinjury. Cryobiology. 1971 Aug;8(4):345-349; https://www.sciencedirect.com/science/article/pii/0011224071901295.

[696] Erthet J, De Duve C. Tissue fractionation studies. I. The existence of a mitochondria-linked, enzymically inactive form of acid phosphatase in rat-liver tissue. Biochem J. 1951 Dec;50(2):174-181; https://www.ncbi.nlm.nih.gov/pmc/articles/PMC1197627/pdf/biochemj00911-0040.pdf. Bendall DS, De Duve C. Tissue-fractionation studies. 14. The activation of latent dehydrogenases in mitochondria from rat liver. Biochem J. 1960 Mar;74(3):444-50; https://www.ncbi.nlm.nih.gov/pmc/articles/PMC1204240/pdf/biochemj01015-0031.pdf.

[697] Osborne JA, Morris GJ, Lee D. Freezing of rat-liver lysosomes to -196 degrees C in the presence and absence of dimethylsulphoxide. Eur J Biochem. 1973 Jun 15;35(3):445-449; https://febs.onlinelibrary.wiley.com/doi/pdf/10.1111/j.1432-1033.1973.tb02857.x. Kravchenko LP, Lugovoĭ VI. Vliianie krioprotektorov na stabil 'nost' izosom pri okhlazhdenii [Effect of cryoprotectors on stability of lysosomes under cooling]. Ukr Biokhim Zh (1978). 1980 Sep-Oct;52(5):573-576; https://pubmed.ncbi.nlm.nih.gov/7256923. Rowe AW, Lenny LL. Cryopreservation of granulocytes for transfusion: studies on human granulocyte isolation, the effect of glycerol on lysosomes, kinetics of glycerol uptake and cryopreservation with dimethyl sulfoxide and glycerol. Cryobiology. 1980 Jun;17(3):198-212; https://www.sciencedirect.com/science/article/pii/0011224080900279.

[698] Fahy G. Appendix B. A "Realistic" Scenario for Nanotechnological Repair of the Frozen Human Brain. In: Wowk B, Darwin M, eds., Cryonics: Reaching for Tomorrow. Alcor Life Extension Foundation, 1991, pp. A-10 – A-26; https://alcor.org/Library/html/nanotechrepair.html.

during cooling,[699] and exogenous inhibitors[700] along with expeditious molecular extraction (Section 4.10) should be able to extinguish autolysis during warming if necessary.

(13) **Other chemical changes.** Freezing and thawing liver microsomes (vesicle-like bodies derived from the endoplasmic reticulum)[701] produce minimal or no change in resident enzyme activity.[702]

In sum, all of the sources of damage described herein (Section 3.4.1) appear reparable using medical nanorobots operating in reliquidified cryopreserved tissue that has been placed in biochemical stasis (Section 4.10) at icewater temperature (~273 K), consistent with the "conventional cell repair" revival protocol (Chapter 4) proposed here.

3.4.2 Non-Fracture-Related Mechanical Injury

The most pressing kinds of damage are mechanical forms of damage, not only because it is this type of injury that has actually been observed in frozen-thawed brains, but also because the potential for actual information loss is much more serious than is the case for the biochemical challenges reviewed in Section 3.4.1. It is not yet certain that high concentrations of cryoprotectant will prevent such injury consistently. Several kinds of mechanical injury other than fracture damage (Section 3.4.3) could occur, including the following.

(1) **Memory encoded in part in the shapes of dendritic trees might be altered by freezing.**[703] Dendritic remodeling associated with learning seems to involve massive changes such as deletion of unused synapses and unused dendritic branches. This remodeling is associated with the actions of many different proteins and, most likely, with considerable changes in the remaining synapses. The precise shape of the dendritic branchings are probably not as important as the specific pattern of connections, and this pattern in turn is presumably responsible for the changes of shape of the dendritic trees. Thus, any shape changes induced by freezing and thawing should be irrelevant as long as the synapses and dendrites remain physically intact.[704] Freezing is believed to spare synapses,[705] but a ***future research*** project could

---

[699] Fahy G. Appendix B. A "Realistic" Scenario for Nanotechnological Repair of the Frozen Human Brain. In: Wowk B, Darwin M, eds., Cryonics: Reaching for Tomorrow. Alcor Life Extension Foundation, 1991, pp. A-10 – A-26; https://alcor.org/Library/html/nanotechrepair.html.

[700] Persidsky MD. Lysosomes as primary targets of cryoinjury. Cryobiology. 1971 Oct;8(5):482-488; https://www.sciencedirect.com/science/article/pii/0011224071900393.

[701] https://en.wikipedia.org/wiki/Microsome.

[702] Pearce RE, McIntyre CJ, Madan A, Sanzgiri U, Draper AJ, Bullock PL, Cook DC, Burton LA, Latham J, Nevins C, Perkinson A. Effects of freezing, thawing, and storing human liver microsomes on cytochrome P450 activity. Arch Biochem Biophys. 1996 Jul 15;331(2):145-169; https://pubmed.ncbi.nlm.nih.gov/8660694.

[703] Alkon DL. Memory storage and neural systems. Sci Am. 1989 Jul;261(1):42-50; https://www.jstor.org/stable/24987318. Alkon DL. Calcium-mediated reduction of ionic currents: a biophysical memory trace. Science. 1984 Nov 30;226(4678):1037-1045; https://science.sciencemag.org/content/226/4678/1037.full.pdf. Alkon DL, Rasmussen H. A spatial-temporal model of cell activation. Science. 1988 Feb 26;239(4843):998-1005; https://science.sciencemag.org/content/239/4843/998.full.pdf. Alkon DL. Memory Traces in the Brain, Cambridge University Press, 1988.

[704] Fahy G. Appendix B. A "Realistic" Scenario for Nanotechnological Repair of the Frozen Human Brain. In: Wowk B, Darwin M, eds., Cryonics: Reaching for Tomorrow. Alcor Life Extension Foundation, 1991, pp. A-10 – A-26; https://alcor.org/Library/html/nanotechrepair.html.

specifically examine to what degree synaptic structures are damaged by freezing, or if there is little or no freezing damage at all.

Although there is evidence for axonal[706] and possibly cellular[707] tearing, light microscope evidence suggests that well-glycerolized hippocampal dendrites are not broken by freezing and thawing.[708] Tissues insufficiently infused with cryoprotectant solution or that receive no cryoprotectant are at risk of greater damage. But even considerable freeze-induced damage to dendrite branches should still leave the pattern of connections obvious from the remaining synapses. Dendrite branching patterns and their underlying biochemical correlates are biologically robust and should retain a high degree of inferrability, particularly given the availability of 3D micron (Section 4.3) and submicron (Section 4.7) resolution scans in the solid phase before any significant tissue movement might occur in the reliquidified phase.

(2) **Disruption of non-synaptic junctions between cells and capillary separation from the surrounding brain tissue.** Such problems have been observed[709] but appear not to involve direct information loss. Such separations could tear fine processes, so the imperative to reduce the effects of extracellular diffusion upon warming – whether by slow warming, deploying indwelling diffusion brakes, or by other means prior to molecular extraction (Section 4.10) – is reinforced by such observations.

(3) **Local (not global) ripping, twisting, and fraying of the torn ends of nerve tracts** by contraction of the brain cells and by the push of extracellular ice, creating debris-strewn gaps measured in microns in both length and thickness.[710] This is a potentially severe form of damage, with reconstruction requiring inferring the existence of positional relationships between nerve fibers in a given tract that do not vary significantly from one side of the gap to the other. If consistent positional relationships exist, inferring the proper connections at the site of a gap should be straightforward. But if the positional relationships happen to be changing near such a gap, additional information may be required for accurate inference of the pre-existing connectivity, perhaps in the form of molecular markers to identify individual fibers. Medical nanorobots operating in a cold reliquidified cell environment should be able to directly collect this data and report it back to external computers that can perform the necessary inferences (Section 4.11). Electrical tests across the gap may also be required to check for physiological consistency, e.g., axonal conductivity and circuit continuity.

---

[705] Haan EA, Bowen DM. Protection of neocortical tissue prisms from freeze-thaw injury by dimethyl sulphoxide. J Neurochem. 1981 Jul;37(1):243-246; https://pubmed.ncbi.nlm.nih.gov/6788904. Hardy JA, Dodd PR, Oakley AE, Perry RH, Edwardson JA, Kidd AM. Metabolically active synaptosomes can be prepared from frozen rat and human brain. J Neurochem. 1983 Mar;40(3):608-614; https://pubmed.ncbi.nlm.nih.gov/6827264. Welder HAD. The effect of freezing and rewarming on feline brain tissue: an electron microscope study. In: Wolstenholme GEW, O'Connor M, eds. The Frozen Cell. J. & A. Churchill, London, 1970, pp. 251-66; https://www.amazon.com/dp/0700014454/. [Welder could readily identify cell bodies, organelles, and neuronal processes despite considerable damage to the organization of the neuropil and to astrocyte cell membranes.]

[706] Fahy GM, Takahashi T, Crane AM. Histological cryoprotection of rat and rabbit brains. Cryo-Letters 1984;5:33-46.

[707] Suda I, Kito K, Adachi C. Bioelectric discharges of isolated cat brain after revival from years of frozen storage. Brain Res. 1974 Apr 26;70(3):527-531; https://www.sciencedirect.com/science/article/abs/pii/0006899374902637.

[708] Fahy GM, Takahashi T, Crane AM. Histological cryoprotection of rat and rabbit brains. Cryo-Letters 1984;5:33-46.

[709] Unpublished experimental results of Alcor Life Extension Foundation and Cryovita Laboratories, reported by G. Fahy.

[710] Suda I, Kito K, Adachi C. Bioelectric discharges of isolated cat brain after revival from years of frozen storage. Brain Res. 1974 Apr 26;70(3):527-531; https://www.sciencedirect.com/science/article/abs/pii/0006899374902637. Fahy GM, Takahashi T, Crane AM. Histological cryoprotection of rat and rabbit brains. Cryo-Letters 1984;5:33-46. Also: Unpublished experimental results of Alcor Life Extension Foundation and Cryovita Laboratories, reported by G. Fahy.

Even if molecular markers are indistinguishable from one fiber to another, and if positional relationships prove unreliable, and if electrical tests give ambiguous results, enough information for correct reconstruction may still be present in the debris pattern that exists in the frozen state, given (A) the limited opportunities for diffusion during freezing and (B) the availability of 3D micron (Section 4.3) and submicron (Section 4.7) resolution scans of biological structures ≥ 100 nm in size in the solid phase before any significant movement might occur in the cold reliquidified phase. For example, reconstruction might be possible based on tiny but consistent size differences between fibers, as measured haptically by medical nanorobots operating in reliquidified tissue. Finally, the relative infrequency of these gaps and the generic effects of many connections as well as the vast redundancy of the brain may make incorrect inference of a few proper connections still consistent with an adequate ultimate clinical outcome – as clinical observations suggest that even severe local damage can be consistent with maintenance of identity and personality.[711]

(4) **Stripping of myelin from axons**,[712] including formation of gaps between the axon membrane and the myelin, unraveling of the myelin, and possible tearing of the axolemma resulting in loss of intra-axonal material at moderately low temperatures. Myelin[713] is inert, generic, non-information-containing material. Despite the types of myelin damage described, there should be no problem in inferring which regions of axolemma were previously covered by myelin and which were exposed. Myelin's function is only important under physiological conditions. Myelin repair might therefore not be necessary until the patient was reliquidified and able to allow medical nanorobots to conduct the necessary cell repairs (Section 4.12.4.1), or even restored to normal body temperature (Section 4.13.1) at which point restoration might possibly be carried out by ordinary or modified oligodendroglial cells[714] which lay down myelin under normal conditions,[715] without need for further nanorobotic intervention. Leakage of axonal material may be reduced by the presence of even a tattered myelin sheath which could act as a diffusion barrier.

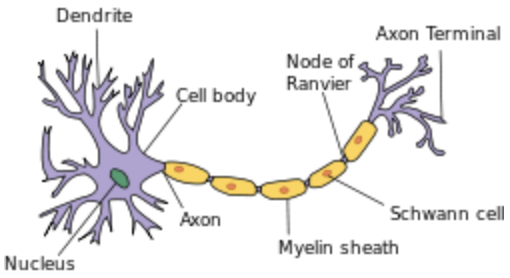

(5) **Physical disruption of capillaries due to intracapillary ice formation**, including rupture of capillary wall, tearing of endothelial cells, or stripping of endothelial cells from their underlying capillary wall material resulting in incompetent vessels littered with emboli.[716] Brain tissue may have 3-30 μm pericapillary tears, e.g., where the basement membrane has torn away from the surrounding neuropil, believed to result from cryoprotectant-induced dehydration rather than from cooling to vitrification temperature.[717] While this is potentially a very serious form of injury, no unique memory- or personality-relevant information is contained in capillaries *per se*. The entire capillary network could likely be cleared out and replaced with generic capillary transplants without any effect on the identity of the patient. Repair or replacement of existing capillaries can be conducted by medical nanorobots operating in a reliquidified

---

[711] Fahy G. Appendix B. A "Realistic" Scenario for Nanotechnological Repair of the Frozen Human Brain. In: Wowk B, Darwin M, eds., Cryonics: Reaching for Tomorrow. Alcor Life Extension Foundation, 1991, pp. A-10 – A-26; https://alcor.org/Library/html/nanotechrepair.html.

[712] Unpublished experimental results of Alcor Life Extension Foundation and Cryovita Laboratories, reported by G. Fahy.

[713] https://en.wikipedia.org/wiki/Myelin.
[714] https://en.wikipedia.org/wiki/Oligodendrocyte#Myelination.
[715] https://en.wikipedia.org/wiki/Myelinogenesis.

[716] Unpublished experimental results of Alcor Life Extension Foundation and Cryovita Laboratories, reported by G. Fahy.

[717] http://chronopause.com/chronopause.com/index.php/2012/06/13/semantics-and-cryonics-propaganda/index.html.

tissue environment and is conceptually less demanding than the abilities needed to repair fractures (Section 4.9). Tears in the neuropil may be repaired similarly to damaged tissue ECM (Section 4.12.3.3).

(6) **Localized tissue maceration**. Localized freezing damage involving random microscale tissue fragmentation might occur in some areas of the brain that received insufficient perfusion of cryoprotectants during the cryopreservation process. Alcor has documented a few cases where perfusion insufficiency was clearly visible in CT scans,[718] whereupon above-normal incidence of local tissue maceration might be expected. In these circumstances, the methods described above in Section 3.4.2(3) will be available for tissue typing, allowing either the missing tissue structure to be restored (Section 4.11) or the cell debris to be extracted (Section 4.10.1.8(4)) followed by cellular repair of the inferred original structure pursuant to a maximum likelihood estimation procedure (Section 4.8.2).[719]

In sum, all of the sources of damage described herein (Section 3.4.2) appear reparable using medical nanorobots operating in reliquidified cryopreserved tissue that has been placed in biochemical stasis (Section 4.10) at icewater temperature (~273 K), consistent with the "conventional cell repair" revival protocol (Chapter 4) proposed here.

3.4.3 Fracture-Related Mechanical Injury

As the cryoprotected patient's temperature drops below the glass transition temperature of ~150 K (-123 °C), the solid phase material can fracture due to tensile stress in the glassy material, with separation of fractured halves of cells, axons, dendrites, capillaries, and other brain elements by distances up to the millimeter size range.[720]

How big are the typical ice fractures in a cryopreserved patient? Cracking is caused by differential contraction as the ice is cooled. Patients are generally cooled very slowly to minimize cracking, but it still occurs, typically around 110-140 K (-163 °C to -133 °C),[721] and patients cryopreserved in the early years of cryonics are expected to have more fracturing than modern-day patients. If we know the linear thermal expansion coefficient of ice $\alpha_{ice}(T)$ at temperature T, then we can estimate the worst case displacement by assuming that one side of the ice is locked into its zero-stress condition at freezing (T_{melt} = 273 K / 0 °C) and the other side is cooled to the final liquid nitrogen storage temperature of T_{LN2} = 77 K (-196 °C), in which case the total linear displacement necessary to relieve all the pressure caused by differential contraction could be as large as $L_{displace} \sim L_0 \, \alpha_{ice,avg} \, (T_{melt} - T_{LN2})$ = 739 μm (~0.7 mm) for an L_0 ~ 11 cm

---

[718] Baldwin C. Alcor A-1088 Case Report. Alcor Life Extension Foundation, Aug 2013; https://www.alcor.org/Library/pdfs/casereportA1088DennisRoss.pdf. See also: https://www.alcor.org/Library/html/CTscan1088.html.

[719] Merkle RC. Cryonics, Cryptography, and Maximum Likelihood Estimation. Proc 1st Extropy Inst Conf 1994; http://www.merkle.com/cryo/cryptoCryo.html. See also: https://en.wikipedia.org/wiki/Maximum_likelihood and http://mathworld.wolfram.com/MaximumLikelihood.html.

[720] Fahy GM, Saur J, Williams RJ. Physical problems with the vitrification of large biological systems. Cryobiology. 1990 Oct;27(5):492-510; https://pubmed.ncbi.nlm.nih.gov/2249453. Also: Unpublished experimental results of Alcor Life Extension Foundation and Cryovita Laboratories, reported by G. Fahy. Observations of the gaps referred to in Section 3.4.2(3) might also reflect microfractures that became "mushy" upon warming and thereby resulted in molecular blurring of the fracture faces.

[721] Rabin Y, Steif PS, Hess KC, Jimenez-Rios JL, Palastro MC. Fracture formation in vitrified thin films of cryoprotectants. Cryobiology. 2006 Aug;53(1):75-95; https://www.ncbi.nlm.nih.gov/pmc/articles/PMC2190754/.

block of ice,[722] where the average expansion coefficient $\alpha_{ice,avg} \sim (\alpha_{ice}(T_{melt}) + \alpha_{ice}(T_{LN2})) / 2 = 32 \times 10^{-6}\ K^{-1}$ because the experimental variation is roughly linear over the entire indicated temperature range[723] (chart, right),[724] with $\alpha_{ice}(273\ K) = 55.8 \times 10^{-6}\ K^{-1}$ and $\alpha_{ice}(77\ K) \sim 7.7 \times 10^{-6}\ K^{-1}$. If the block of ice suffers ~10 separate cracks to relieve the strain during cooling then the average crack size may be ~70 µm; if there were ~100 cracks, the average crack size might be ~7 µm. Related experiments show that thermally stressed ice undergoes cracking when the ice layer exceeds 1-3 µm in thickness.[725] Note that the expansion coefficient is somewhat higher for cryoprotectant chemicals such as DMSO,[726] which at -100 °C has $\alpha_{DMSO}(173\ K) \sim 152 \times 10^{-6}\ K^{-1}$, about five times higher than for pure water-ice and boosting the maximum strain-relieving displacement into the millimeter range.

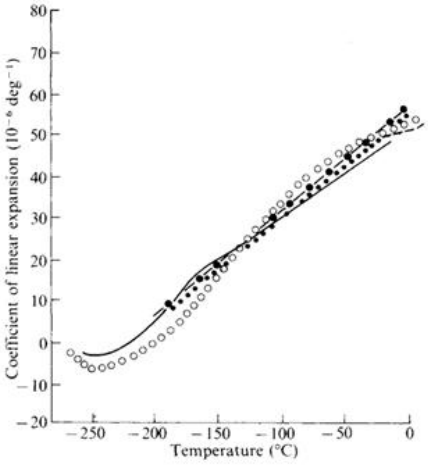

Cracking in frozen animal tissues has been studied for years,[727] including at least one study that published histological images appearing to show (1) large cracks ~200 µm wide and 2 mm long, (2) microcracks 3-15 µm wide and up to 0.9 mm long, evidence of cell rupture alongside the cracks, and (3) perhaps ~1% of total tissue volume occupied by cracks for cryogenically frozen rabbit liver tissue (image, below).[728]

---

[722] 11 cm is roughly the mean linear dimension of a ~1400 cm^3 human brain.

[723] Powell RW. Preliminary measurements of the thermal conductivity and expansion of ice. Proc Roy Soc. 1958;247:464-466; cited in https://nvlpubs.nist.gov/nistpubs/Legacy/MONO/nbsmonograph29.pdf.

[724] https://physics.stackexchange.com/questions/342707/coefficient-of-linear-expansion-of-ice.

[725] Westley MS, Baratta GA, Baragiola RA. Density and index of refraction of water ice films vapor deposited at low temperatures. J Chem Phys. 1998 Feb 22;108(8):3321-3326; https://pdfs.semanticscholar.org/a0c8/c132f4618eaed6dfb24c814398cefa8ad1b9.pdf. Bu C, Dukes C, Baragiola RA. Charging and Discharging of Amorphous Solid Water Ice: The effects of Cracking and Implications for x 10-ring Grain Surface Potential. 47th Lunar and Planetary Science Conference (2016); https://www.hou.usra.edu/meetings/lpsc2016/pdf/2917.pdf. Bu C, Bahr DA, Dukes CA, Baragiola RA. The effects of cracking on the surface potential of icy grains in Saturn's x 10-ring: Laboratory studies. Astrophys J. 2016 Jul 10;825(2):106-112; http://jupiter.chem.uoa.gr/thanost/papers/papers1/ApJ_825(2016)106.pdf.

[726] Rabin Y, Steif PS, Hess KC, Jimenez-Rios JL, Palastro MC. Fracture formation in vitrified thin films of cryoprotectants. Cryobiology. 2006 Aug;53(1):75-95; https://www.ncbi.nlm.nih.gov/pmc/articles/PMC2190754/.

[727] Hunt CJ, Song YC, Bateson EA, Pegg DE. Fractures in cryopreserved arteries. Cryobiology. 1994 Oct;31(5):506-15; https://www.ncbi.nlm.nih.gov/pubmed/7988160. Rabin Y, Steif PS, Taylor MJ, Julian TB, Wolmark N. An experimental study of the mechanical response of frozen biological tissues at cryogenic temperatures. Cryobiology. 1996 Aug;33(4):472-82; http://www.prostatecancercentre.ca/wp-content/uploads/2014/10/Rabin_Pub210.pdf. Pegg DE, Wusteman MC, Boylan S. Fractures in cryopreserved elastic arteries. Cryobiology. 1997 Mar;34(2):183-92; https://www.ncbi.nlm.nih.gov/pubmed/9130389. H Zezhao, X Hongyan, Z Guoyan, L Jinfen, H Huimin, D Wenxiang. Analyses of thermal stress and fracture during cryopreservation of blood vessel. Sci in China Ser E: Technol Sci. 2001 Apr;44(2):158-163; https://link.springer.com/article/10.1007/BF03014626.

[728] Rabin Y, Olson P, Taylor MJ, Steif PS, Julian TB, Wolmark N. Gross damage accumulation on frozen rabbit liver due to mechanical stress at cryogenic temperatures. Cryobiology. 1997 Jun;34(4):394-405; http://www.andrew.cmu.edu/user/yr25/RabinPublications/Rabin_Pub214.pdf. A crude estimate from the histological image above is that 0.042 of the tissue area is cracks, which suggests that $(0.042)^{3/2} = 0.9\%$ of the tissue volume may be in cracks, assuming the image is representative of the whole.

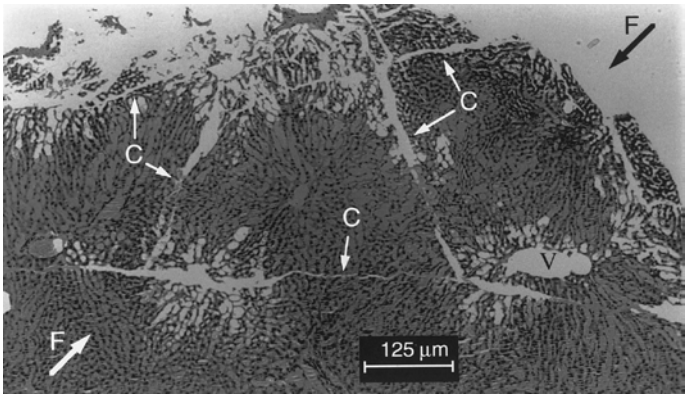

A 1983 study[729] of fracture damage in cats cooled to LN2 temperatures and then thawed found that fracturing was "most pronounced in delicate, high flow organs which are poorly fiber-reinforced," with the most serious damage in the brain, spleen, pancreas and kidney. "In these organs fractures would often completely divide or sever the organ into one or more discrete pieces. Tougher, more fiber-reinforced tissues such as myocardium, skeletal muscle, and skin were less affected by fracturing; there were fewer fractures, and they were smaller, and less frequently penetrated the full thickness of the organ." Large arteries such as the aorta were heavily fractured. The spinal cord was severed by multiple transverse fractures at intervals of 5 mm to 15 mm over its entire length and exhibited the appearance of a broken candle stick.

Cryopreserved human tissues are less studied. The first published direct physical examination of discarded cryopreserved human tissue from three Alcor patients in 1983[730] found "serious fracturing in all of the suspension patients....Examination of the internal organs of P3 revealed fractures present in almost every organ. The spinal cord, aorta, thoracic inferior vena cava, pulmonary artery, myocardium, right lung, liver, pericardium, stomach, ileum, colon, mesentery, spleen, skeletal muscle, and pancreas, were all seriously fractured. In some organs, such as the spleen, lung, liver and great vessels, fractures penetrated the organ to the point of completely or almost completely severing them. In other instances the fractures were confined to the capsule, serous coat, or first two or three millimeters of the organ....A length of spinal cord approximately 20 cm in length...had fractured into three pieces, each approximately 6 cm long. These fractures completely transected the cord giving the impression of a broken glass rod." However, "it was not possible to examine the brain and head for post-thaw fracturing."

The first published examination of a cryopreserved brain by Hixon in 1995[731] found that the subject brain had neatly cracked into 5 major pieces: "cerebellum (cracks at spinal cord and pons), the two hemispheres of the cerebrum (crack along the corpus callosum), and the frontal lobes (approximately the first third of each hemisphere of the cerebrum; transverse, symmetrical, and along no recognizable anatomical feature). The tip of one of the temporal lobes was fractured transversely. No other cracks were noted." Hixon further reported: "The abdominal and thoracic organs in the 1983 autopsies were fractured in no particular pattern. Animal organs (including the brain) frozen at Alcor by Michael Darwin ten years ago cracked extensively on a scale of about a centimeter."

Hixon[732] also reported in 1995 the first use of the crackphone, a means for recording the acoustic pulse generated every time a fracture occurs during the cooldown process. In one experiment, crackphone

---

[729] Darwin M, Leaf J, Hizon HL. The effects of cryopreservation on the cat, Part 1. Chronosphere 13 Feb 2012; http://chronopause.com/chronopause.com/index.php/2012/02/13/the-effects-of-cryopreservation-on-the-cat-part-1/index.html.

[730] Federowicz M, Hixon H, Leaf J. Postmortem examination of three cryonic suspension patients. Cryonics 1984 Sep;16(50):16-28; https://www.alcor.org/library/postmortem-examination-of-three-cryonic-suspension-patients/.

[731] Hixon H. Exploring cracking phenomena. Box 1. Observations at an Autopsy. Cryonics 1995 Qtr 1;16(1):28-29; https://alcor.org/cryonics/cryonics1995-1.pdf.

[732] Hixon H. Exploring cracking phenomena. Cracking Pilot Study. Cryonics 1995 Qtr 1;16(1):32; https://alcor.org/cryonics/cryonics1995-1.pdf.

sensors recorded 53 distinct sonic events (each likely representing a separate fracture event) while a dog's head perfused with 9.4 M glycerol cryoprotectant was cooled from 195 K (-78 °C) to 77 K (-196 °C). Several years later, Wowk[733] reported that 19 acoustic events believed to be fractures in the brain were recorded by crackphone between 155 K (-118 °C) and 84 K (-189 °C) during the cryopreservation of Alcor patient A-2063, who had received B2C vitrification (cryoprotectant) solution.[734]

The use of vitrification solutions can reduce the severity of fracturing but does not eliminate it altogether in storage systems employing LN2 temperatures.[735] Notes Wowk:[736] "Vitrified brain...under liquid nitrogen...is almost certainly fractured, yet it remains an integrated whole. Fracturing does not cause tissue to break into widely separated pieces at the time of fracture....[F]ractures are not macroscopically obvious at cryogenic temperature. Movements between fracture planes appear to remain microscopic provided that tissue stays cold and solid. The actual physical displacements associated with fracturing are small, and are believed to remain small as long as tissue remains solid. Fractures in bare cryoprotectant solutions are observed to be optically smooth. In other words, the fracture surfaces are smooth on a scale smaller than a wavelength of light, which is less than one millionth of a meter [≤ 1 μm]. Although the fracture faces of vitrified tissue have not been specifically studied, it is assumed that they are also relatively smooth. When frozen tissue is fractured for microscopy in a procedure called 'freeze fracture,' the resulting faces are smooth enough for electron micrographic study of cell membranes. From an information-theoretic [Section 2.1.1] standpoint, it seems likely that fracturing does not cause loss of neural connectivity information provided that tissue remains vitrified, and provided that some future means exists to match and restore structure across fracture faces." Some theoretical analysis of fracture mechanics during cryopreservation via vitrification has been done,[737] but more research is needed,[738] along with experimental validation[739] of the models employed.

---

[733] Wowk B. Systems for intermediate temperature storage for fracture reduction and avoidance. Cryonics 2011 Qtr 3; https://www.alcor.org/library/systems-for-intermediate-temperature-storage-for-fracture-reduction-and-avoidance/.

[734] De Wolf A. The first vitrification agent in cryonics: B2C. Biostasis, 11 Jun 2008; https://www.biostasis.com/the-first-vitrification-agent-in-cryonics-b2c/.

[735] Fahy GM, Saur J, Williams RJ. Physical problems with the vitrification of large biological systems. Cryobiology. 1990 Oct;27(5):492-510; https://www.ncbi.nlm.nih.gov/pubmed/2249453.

[736] Wowk B. Systems for intermediate temperature storage for fracture reduction and avoidance. Cryonics 2011 Qtr 3; https://www.alcor.org/library/systems-for-intermediate-temperature-storage-for-fracture-reduction-and-avoidance/.

[737] Steif PS, Palastro MC, Rabin Y. The Effect of Temperature Gradients on Stress Development During Cryopreservation via Vitrification. Cell Preserv Technol. 2007;5(2):104-115; http://www.andrew.cmu.edu/user/yr25/RabinPublications/Rabin_Pub260.pdf. Steif PS, Palastro MC, Rabin Y. Continuum mechanics analysis of fracture progression in the vitrified cryoprotective agent DP6. J Biomech Eng. 2008 Apr;130(2):021006; https://www.ncbi.nlm.nih.gov/pmc/articles/PMC2566949/. Eisenberg DP, Steif PS, Rabin Y. On the Effects of Thermal History on the Development and Relaxation of Thermo-Mechanical Stress in Cryopreservation. Cryogenics (Guildf). 2014 Nov-Dec;64:86-94; https://www.ncbi.nlm.nih.gov/pmc/articles/PMC4360916/.

[738] Unpublished experimental studies of fracturing in 60-80 kg (whole-body) pigs by Greg Fahy in 2014 observed 4 fractures in 2 sites at -130 °C, 9-12 fractures in 3-5 sites at -140 °C, and 50-60 fractures near -180 °C; personal communication, 30 Dec 2021.

[739] Steif PS, Palastro M, Wan CR, Baicu S, Taylor MJ, Rabin Y. Cryomacroscopy of vitrification, Part II: Experimental observations and analysis of fracture formation in vitrified VS55 and DP6. Cell Preserv Technol. 2005 Sep;3(3):184-200; https://www.ncbi.nlm.nih.gov/pmc/articles/PMC1533993/. Feig JS, Eisenberg DP, Rabin Y. Polarized light scanning cryomacroscopy, part I: Experimental apparatus and observations of vitrification, crystallization, and photoelasticity effects. Cryobiology. 2016 Oct;73(2):261-71; https://www.ncbi.nlm.nih.gov/pmc/articles/PMC5420075/. Feig JS, Solanki PK, Eisenberg DP, Rabin Y. Polarized light scanning cryomacroscopy, part II: Thermal modeling and analysis of experimental observations. Cryobiology. 2016 Oct;73(2):272-81; https://europepmc.org/articles/pmc5420076. Solanki PK, Rabin Y. Analysis of polarized-light effects in glass-promoting solutions with applications to cryopreservation and organ banking. PLoS One. 2018 Jun 18;13(6):e0199155; https://www.ncbi.nlm.nih.gov/pmc/articles/PMC6005522/.

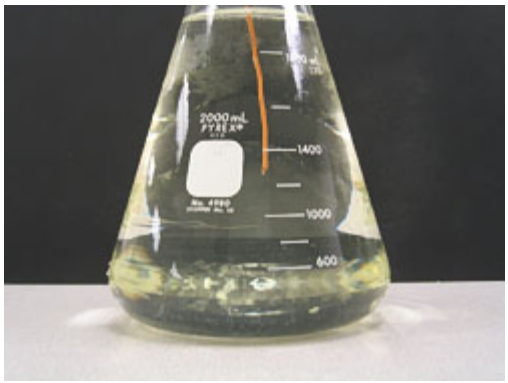

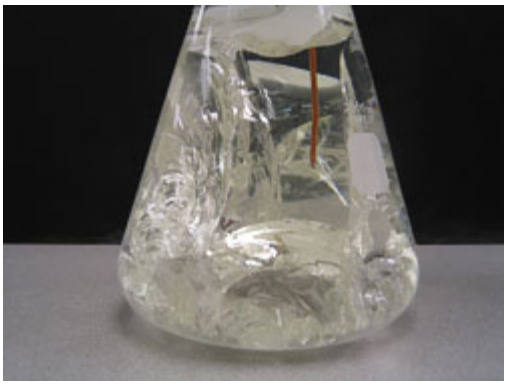

Specifically, more systematic experimental ***future research*** is required to measure and quantify the number density, organ or tissue specificity (if any), the preferred propagation directions and patterns (if any), and the exact lateral and length dimensions of fractures in blocks of frozen water-ice and frozen cryoprotectant, in cryogenic vitrification solutions (see above, before (left) and after (right) fracturing during cooling),[740] and in cryopreserved human tissue, including specific organs and whole bodies. This may include scanning probe microscope or other direct *in situ* experimental observation of micron- and submicron-scale features of ice fractures. ***Future research*** should also seek simple methods for reducing or eliminating cracking at cryogenic temperatures – such as thermal annealing[741] or intermediate temperature storage (Section 7.1.2) – to reduce the severity (or entirely eliminate) this problem for future cryopatients.

In the meantime, it seems plausible to assume that individual cracks may occupy up to ~1% of tissue volume and produce tissue displacements up to ~100 μm (0.1 mm) in width, running for considerable lengths (typically up to ~1 mm) throughout a tissue mass inside a cryopreserved patient maintained at LN2 temperatures. Vitrified cryopatients, pre-vitrification classically-cryopreserved patients, and straight-freeze cryopatients may have different numbers, sizes, and shapes of cracks, but any set of cracks that might be found in different patients should be accommodated by the "conventional cell repair" revival protocols (esp. Section 4.4 through Section 4.8) proposed in the present work.

Aschwin de Wolf notes that ischemia-induced perfusion impairment causes no or incomplete distribution of the vitrification agent. These tissue volumes of poor distribution freeze at high subzero temperatures and are thus subject to significantly more thermal stress than the vitrified areas that are only at risk below the glass transition temperature. Thus in a sense, high subzero fracturing is an indirect measure of ischemia.

---

[740] "Cryopreservation and Fracturing,"; https://www.alcor.org/library/cryopreservation-and-fracturing/.

[741] Wowk B. Systems for intermediate temperature storage for fracture reduction and avoidance. Cryonics 2011 Qtr 3; https://www.alcor.org/library/systems-for-intermediate-temperature-storage-for-fracture-reduction-and-avoidance/. See also: https://www.alcor.org/library/cryopreservation-and-fracturing/.

3.5 Cryogenic Storage Damage

Once the cryopreserved patient has reached liquid nitrogen temperatures, biological decay processes essentially halt. A biochemical process that would require $\tau_{ischemic}$ ~ **6 minutes**[742] at normal human body temperature[743] (310 K / 37 °C) would require[744] **1.8 hours** at the pure water-ice freezing point (273 K / 0 °C), **4.5 years** at dry-ice temperature (193 K / -80 °C), **81,000 years** at the aqueous glass transition temperature (T_g ~ 150 K / -123 °C) proposed for intermediate-temperature storage in cryonics,[745] and ~**10^{23} years** at the boiling point of liquid nitrogen (77 K / -196 °C).

Even these are conservative estimates because the Arrhenius equation used in the above calculation assumes the presence of a gaseous or fluid medium in which normal diffusion-driven chemistry can take place. The absolute viscosity of water-ice and aqueous solutions at the calorimetric glass transition temperature has been observed to be ~10^{12} Pa-sec,[746] compared to 6.915 x 10^{-4} Pa-sec for liquid water at 310 K. Relative diffusion time is classically inversely proportional to absolute viscosity and independent of particle size,[747] so a glucose molecule that could diffuse 1 nanometer in 0.7 nanoseconds at 310 K (37

---

[742] This is the classical time limit for the onset of warm ischemic damage after cardiac arrest. For example: "Resuscitation after cardiac arrest longer than 4 to 6 minutes at normal body temperature typically results in irreversible brain injury, coma, or death." https://alcor.org/FAQs/faq02.html#resuscitation

[743] "The longest normothermic no-flow time yet reversed to good functional survival of heart, brain and the entire organism appears to be not 5 min, but between 10 and 20 min." Safar P. Resuscitation from clinical death: pathophysiologic limits and therapeutic potentials. Crit Care Med. 1988 Oct;16(10):923-941; https://pubmed.ncbi.nlm.nih.gov/3048894/.

[744] These times are calculated from the Arrhenius equation, or $k_1/k_2 = \exp[(E_a/R)(T_2^{-1} - T_1^{-1})]$, where k_1 is the reaction rate at temperature T_1, k_2 is the reaction rate at temperature T_2, E_a is the activation energy for the reaction (e.g., using E_a = 54,810 J/mol for lactate dehydrogenase (LDH) enzyme in water;[*] muscle enzymes may span a range of 14,300-70,800 J/mol[†]) and the universal gas constant R = 8.314 J/mol-K.
[*] Best BP. Scientific justification of cryonics practice. Rejuvenation Res. 2008 Apr;11(2):493-503; https://www.ncbi.nlm.nih.gov/pmc/articles/PMC4733321/.
[†] Fudge DS, Ballantyne JS, Stevens ED. A test of biochemical symmorphosis in a heterothermic tissue: bluefin tuna white muscle. Am J Physiol Regul Integr Comp Physiol. 2001 Jan;280(1):R108-14; https://journals.physiology.org/doi/pdf/10.1152/ajpregu.2001.280.1.r108.

[745] Wowk B. Systems for intermediate temperature storage for fracture reduction and avoidance. Cryonics 2011 Qtr 3; https://www.alcor.org/library/systems-for-intermediate-temperature-storage-for-fracture-reduction-and-avoidance/.

[746] Angell CA. Liquid fragility and the glass transition in water and aqueous solutions. Chem Rev. 2002 Aug;102(8):2627-50; https://citeseerx.ist.psu.edu/viewdoc/download?doi=10.1.1.620.1853&rep=rep1&type=pdf. Debenedetti PG, Stillinger FH. Supercooled liquids and the glass transition. Nature. 2001 Mar 8;410(6825):259-67; http://www.physics.emory.edu/faculty/weeks/lab/papers/debenedetti-nat01.pdf. One estimate is that the absolute viscosity of solidified aqueous vitrification solutions at 77 K may be as low as ~3 x 10^{21} Pa-sec (Ben Best, "Molecular Mobility at Low Temperature," 2007; https://www.benbest.com/cryonics/mobility.html).

[747] The Einstein-Stokes approximation[*] gives $D \sim k_B T / (6 \pi \eta R)$, where D is the diffusion constant for rigid spherical particles of radius R ($R >> R_{H20molecule}$) in a liquid of absolute viscosity η at temperature T, where k_B = 1.381 x 10^{-23} J/K (Boltzmann's constant), hence relative diffusion $D_1/D_2 = (T_1 \eta_2) / (T_2 \eta_1)$ = 2.93 x 10^{15}, where D_1 is the aqueous diffusion constant at temperature T_1 in water of absolute viscosity η_1, and similarly for D_2, and taking T_1 = 310 K, η_1 = 6.915 x 10^{-4} Pa-sec, $T_2 = T_g$ = 153 K, and η_2 ~10^{12} Pa-sec.
[*] Einstein A. Über die von der molekularkinetischen Theorie der Wärme geforderte Bewegung von in ruhenden Flüssigkeiten suspendierten Teilchen. Annalen der Physik. 1905;322(8):549-560 (in German); https://en.wikipedia.org/wiki/Einstein_relation_(kinetic_theory)#Stokes%E2%80%93Einstein_equation.

°C) would in principle require ~24 days to diffuse the same distance at T_g.[748] By this measure, a diffusion-driven chemical process that required ~**6 minutes** at 310 K would require ~**34 billion years** at T_g ~ 150 K / -123 °C (typical T_g for water-based vitrification solutions),[749] not 81,000 years as estimated above using the Arrhenius equation. As a practical matter, biological stasis can be regarded as complete below the glass transition temperature.[750]

Additionally, as noted by Mazur,[751] there is insufficient thermal energy for thermally-driven chemical reactions to take place at 77 K (-196 °C): "The only reactions that can occur in aqueous systems at -196 °C are photophysical events such as the formation of free radicals and the production of breaks in macromolecules as a direct result of 'hits' by background ionizing radiation or high-energy particles.[752] Over a sufficiently long period of time, these direct ionizations could produce enough breaks in DNA to become deleterious, especially since no enzymatic repair can occur at these very low temperatures. The dose of ionizing radiation that kills 63% of representative cultured mammalian cells [i.e., $(1 - e^{-1})$ survival] is 200 to 400 rads.[753] Since terrestrial background radiation is ~0.1 rad/yr, it ought to require some 2,000 to 4,000 years at -196 °C to kill 63% of a population of typical mammalian cells." Further experimental work in the field of cryochemistry[754] has concluded that natural background radiation might require ~32,000 years to kill 90% of Chinese hamster ovary (CHO) cells.[755] Later work has found no radiation damage to

---

[748] Applying the Einstein approximation[*] for the root-mean-square displacement of a particle of radius R as $\Delta X \sim (k_B T \Delta t / 3\pi \eta R)^{1/2}$, the time required for a molecule of diffusion constant D to diffuse a distance ΔX is $\Delta t \sim \Delta X^2/2D = 7 \times 10^{-10}$ sec for a glucose molecule having $D = 7.1 \times 10^{-10}$ m^2/sec in 310 K water.[†] Relative diffusion time is therefore $\tau_{diffusion} \sim \Delta t (D_1/D_2) \sim 2.1 \times 10^6$ sec ~ 23.8 days.
[*] Einstein A. Über die von der molekularkinetischen Theorie der Wärme geforderte Bewegung von in ruhenden Flüssigkeiten suspendierten Teilchen. Annalen der Physik. 1905;322(8):549-560 (in German).
[†] Freitas RA Jr. Nanomedicine, Volume I: Basic Capabilities, Landes Bioscience, Georgetown, TX, 1999; Table 3.3; http://www.nanomedicine.com/NMI/Tables/3.3.jpg.

[749] Wowk B. Thermodynamic aspects of vitrification. Cryobiology 2010;60:11-22; http://www.21cm.com/pdfs/2010-Thermodynamics.pdf.

[750] The polymerization rate of formaldehyde at 4 K is 110 orders of magnitude higher than that predicted by the Arrhenius equation, due to quantum mechanical tunneling,[*] indicating that at least some reactions can continue to occur at cryogenic temperatures. This is deemed[†] not to be a problem for the long-term stability of cryopreserved patients because (1) these are reactions mediated by free radicals that should not be present unless the tissue has been bombarded with electron beams or gamma rays, (2) most biological molecules susceptible to radical formation are present in only relatively low concentrations, and (3) the reaction rates from tunneling are expected to be negligible; but this should be verified in ***future research***.
[*] Goldanskii VI. Quantum chemical reactions in the deep cold. Sci Am 1986 Feb; 254(2):38-53; https://www.jstor.org/stable/24975889.
[†] Alcor Staff. Does quantum mechanics threaten cryonics? Cryonics 1986 Mar;7(3):29-32; https://www.alcor.org/docs/cryonics-magazine-1986-03.txt.

[751] Mazur P. Limits to life and low temperatures and at reduced water contents and water activities. To be published in "The Limits to Life," Proceedings of the 4th College Park Colloquium on Chemical Evolution, 18-20 Oct 1978, University of Maryland (CONF-7810136-2); https://www.osti.gov/servlets/purl/5483758/.

[752] Rice FO, History of radical trapping. In: Bass AM, Broida HP, eds., Formation and Trapping of Free Radicals, Academic Press, NY, 1960, p. 7; https://www.amazon.com/dp/B0000CKLQ4/.

[753] Elkind MM, Whitmore GF. The Radiobiology of Cultured Mammalian Cells. Gordon and Breach, NY, 1967; https://www.amazon.com/dp/0677109202/.

[754] McGee HA Jr, Martin WJ. Cryochemistry. Cryogenics 1962 Sep;2(5):1-11; https://www.sciencedirect.com/science/article/abs/pii/0011227562900012.

[755] Ashwood-Smith MJ, Grant E. Genetic stability in cellular systems stored in the frozen state. Ciba Found Symp. 1977 Jan 18-20;(52):251-72; https://pubmed.ncbi.nlm.nih.gov/244398/. Reprinted in: Elliott K, Whelan J (eds) The freezing of mammalian embryos. Elsevier/Excepta Medica, North-Holland Amsterdam, pp 251-267; https://books.google.com/books?hl=en&lr=&id=AmV4KJglbPsC&oi=fnd&pg=PA251.

mouse embryos at -196 °C after exposure to the equivalent of 2000 years of background radiation,[756] with no reported cases of cell death ascribable to storage at -196°C for some 2-15 years and none even when cells are exposed to levels of ionizing radiation some 100 times background for up to 5 years.[757] There is no evidence that storage at -196°C results in the accumulation of chromosomal or genetic changes.[758]

Table 3. Estimated natural endoradioactivity in the human body (70-kg human adult)[759]

Radionuclide	**Total Mass Found in a Human Body** (gm)	**Total Activity in a Human Body***	**Half-Life of the Radionuclide** (yr)
^{40}K	1.7×10^{-2}	120 nCi (4400 Bq)	1.2×10^{9}
^{14}C	2.2×10^{-8}	100 nCi (3700 Bq)	5730
^{210}Po	2×10^{-13}	1 nCi (37 Bq)	0.38
^{3}H	6×10^{-14}	0.6 nCi (23 Bq)	12.32
$^{235/238}U$	9×10^{-5}	30 pCi (1.1 Bq)	$0.7/4.5 \times 10^{9}$
^{226}Ra	3.1×10^{-11}	30 pCi (1.1 Bq)	1600
^{232}Th	3×10^{-5}	3 pCi (0.11 Bq)	1.4×10^{10}

* 1 becquerel (Bq) = 1 nuclear disintegration/sec; 1 curie (Ci) = 37×10^{9} nuclear disintegrations/sec.

Besides background radiation and cosmic rays, cryopatients are continuously subject to damage from endoradiation – the radioactivity naturally present in the human body (**Table 3**). Emissions from these natural radionuclides combine to produce a net whole-body endoradiation dose of ~0.03-0.04 rad/yr[760] (δ_{endo} ~ 0.3 milliSieverts/yr (mSv/yr) from ~8162 Bq of endoradioactivity) which is a modest addition to the ~0.1 rad/yr (δ_{exo} ~ 1 mSv/yr) total from cosmic rays and terrestrial gamma ray sources for a cryopreserved patient.[761] (An additional ~2 mSv/yr dose due to inhaled radon and its decay products to

---

[756] Lyon MF, Glenister PH, Whittingham DG. Long-term viability of embryos stored under irradiation. In: Zeilmaker GH (ed) Frozen storage of laboratory animals. Gustav Fischer Verlag, Stuttgart, 1981:139-147; https://www.amazon.com/Storage-Laboratory-Animals-Zeilmaker-Workshop/dp/3437303422/. Glenister PH, Whittingham DG, Lyon MF. Further studies on the effect of radiation during the storage of frozen 8-cell mouse embryos at -196 degrees C. J Reprod Fertil. 1984 Jan;70(1):229-34; http://citeseerx.ist.psu.edu/viewdoc/download?doi=10.1.1.533.6055&rep=rep1&type=pdf.

[757] Glenister PH, Whittingham DG, Wood MJ. Genome cryopreservation: a valuable contribution to mammalian genetic research. Genet Res Camb. 1990;56:253-258; https://www.cambridge.org/core/services/aop-cambridge-core/content/view/1858198F060E24A6B385D46FA91D0ACB/S0016672300035357a.pdf/genome_cryopreservation_a_valuable_contribution_to_mammalian_genetic_research.pdf.

[758] Ashwood-Smith MJ, Friedmann GB. Lethal and chromosomal effects of freezing, thawing, storage time, and x-irradiation on mammalian cells preserved at -196 degrees in dimethyl sulfoxide. Cryobiology. 1979 Apr;16(2):132-40; https://www.ncbi.nlm.nih.gov/pubmed/573193.

[759] "Radioactivity in Nature", The Radiation Information Network (ISU Health Physics Radinf); https://sites.google.com/isu.edu/health-physics-radinf/radioactivity-in-nature.

[760] "Radioactivity in Nature", The Radiation Information Network (ISU Health Physics Radinf); https://sites.google.com/isu.edu/health-physics-radinf/radioactivity-in-nature. Note also that 1 rad = 0.01 J/kg of absorbed radiation dose; https://en.wikipedia.org/wiki/Rad_(unit).

[761] "Table 1. Average radiation dose from natural sources", in: Report of the United Nations Scientific Committee on the Effects of Atomic Radiation to the General Assembly; http://www.unscear.org/docs/reports/gareport.pdf.

which living humans are normally exposed[762] doesn't apply to cryopreserved patients, who are not breathing.) This endoradiation dose remains essentially constant over a 100-1000 year cryopreservation period due to the long half-lives of the two largest components (^{40}K and ^{14}C), and is the minimum possible long-term dosage even in a hypothetical perfectly-shielded cryonics storage facility that eliminated all background radiation and cosmic ray exposure.

Note that the natural background radiation from the dewar itself is a negligible $\leq 0.5 \times 10^{-3}$ of the whole-body endoradiation dose,[763] and the other packing materials[764] surrounding the cryopreserved patient should be similarly or even less radioactive. Radon gas originally trapped in the patient's tissues initially produces radiation ≤0.001 of the whole-body endoradiation dose,[765] and this declines quickly after death due to the short half-life of ^{222}Rn (3.82 days) and radon's decay products,[766] and due to the lack of replacement gas entering the tissues. Radon diffusing into the dewar's liquid nitrogen from the

---

[762] "Radioactivity in Nature", The Radiation Information Network (ISU Health Physics Radinf); https://sites.google.com/isu.edu/health-physics-radinf/radioactivity-in-nature.

[763] A Bigfoot dewar made of #304 stainless steel (https://alcor.org/FAQs/faq02.html#bigfoot) of density $\rho_{steel} \sim 8000$ kg/m^3 and mean molecular weight $MW_{steel} \sim 0.056$ kg/mole has a maximum carbon mass fraction of $f_{steelC} = 8 \times 10^{-4}$ (https://www.lenntech.com/stainless-steel-304.htm), of which $\alpha_{14C} = 10^{-12}$ of the carbon is the isotope ^{14}C (https://en.wikipedia.org/wiki/Carbon-14) which disintegrates via β^- emission with a decay energy of $E_{decay} = 0.158$ MeV = 2.53×10^{-14} J with a half-life of $\tau_{1/2} = 5730$ yr = 1.80×10^{11} sec (https://en.wikipedia.org/wiki/Carbon#Isotopes), irradiating matter of normal density $\rho_{normal} = 1000$ kg/m^3 inside the dewar within a typical ~200 μm stopping distance of β^- particles in water. Taking $N_A = 6.022 \times 10^{23}$ molecules/mole (Avogadro's number) and $k_{rad} = 0.01$ J/kg-rad energy of absorbed radiation dose, then the maximum possible radiation dose received from the dewar is $\delta_{dewar} \sim \alpha_{14C} f_{steelC} \rho_{steel} E_{decay} N_A / (2 k_{rad} MW_{steel} \rho_{normal} \tau_{1/2}) = 1.52 \times 10^{-5}$ rad/yr, which is $\leq 0.5 \times 10^{-3}$ of the natural endoradiation dose. Other than ^{14}C, there are no other naturally occurring radioisotopes of the other elements comprising #304 stainless steel (Fe 66-74%, Cr 18-20%, Ni 8-11%, Mn <2%, Si <1%, S <0.03%, and P <0.045% by weight; http://asm.matweb.com/search/SpecificMaterial.asp?bassnum=mq304a).

[764] Besides the stainless steel walls, each Bigfoot dewar includes a vacuum superinsulation consisting of a wrapping of multiple layers of glass fiber paper and aluminum foil. There are 10-12 lbs of synthetic zeolite getters (Union Carbide Type 5A aluminosilicate molecular sieve) with a hydrogen scavenger consisting of 5 gm of palladium oxide. A floating trunnion (sleeved with 1/8" Mycardia G-10 plastic composite) is a metal bar in a metal cage with a 1/4" ring separated by vacuum that serves to keep the hanging inner shell from rattling around during moving or shipping. There is ~80 feet of vacuum-grade TIG welding (using TIG rods with 2% thorium dioxide) with no more than one or two helium-permeable pinholes in the first pass. The dewar is topped with a circular styrafoam cork ~1 m in diameter and 14" thick. Inside the dewar, whole bodies are encased in medium-weight mummy bags (~2.2 kg, mostly polyester, perhaps some nylon) within custom aluminum pods (~20.6 kg, mostly aluminum with a little steel and nylon); neuros reside in 1.8 kg metal cans. Personal communications from Hugh Hixon to Robert Freitas, 15-17 Nov 1999.

[765] The typical indoor concentration of radioactive radon (^{222}Rn) is ~48 Bq/m^3.[*] Studies of radon solubility in rat tissue[†] found tissue/air ratios of 4.83 (i.e., 232 Bq/m^3 for indoor air) for omental fat, 0.405 for venous blood, 0.309 for brain, 0.306 for liver, 0.285 for kidney, 0.221 for heart, 0.184 for testis, and 0.154 (7 Bq/m^3 for indoor air) for skeletal muscle. Direct measurements[‡] of radon in human blood and urine have reported levels as high as 570 Bq/m^3 and 209 Bq/m^3, respectively. Generously assuming 200 Bq/m^3 are evenly distributed throughout a ~0.06 m^3 adult human body, the resulting 12 Bq whole-body exposure equates to ~0.0004 mSv/yr or ~0.001 of other endoradiation sources.

[*] https://en.wikipedia.org/wiki/Radon#Concentration_units.

[†] Nussbaum E, Hursh JB. Radon solubility in rat tissues. Science. 1957 Mar 22;125(3247):552-3; https://science.sciencemag.org/content/125/3247/552.

[‡] Salih NF, Jafri ZM, Aswood MS. Measurement of radon concentration in blood and urine samples collected from female cancer patients using RAD7. J Rad Res Appl Sci. 2016 Jul;9(3):332-336; https://www.sciencedirect.com/science/article/pii/S168785071600011X.

[766] https://en.wikipedia.org/wiki/Isotopes_of_radon.

surrounding air could produce radiation ≤0.0003 of the whole-body endoradiation dose;[767] LN2 boiloff might provide a counterflow to the ^{222}Rn diffusion path, though it has been observed that some oxygen from the external environment does accumulate into the dewar from normal day-to-day operations.[768] (The boiling point of oxygen (90 K) is higher than the boiling point of nitrogen (77 K) so liquid oxygen can co-exist with LN2, both as a remnant of the original liquefaction[769] from air and acquired by diffusion after liquefaction. However, at cryogenic temperatures any oxidation damage of cryopreserved tissue from this source should be minimal.)

A cryopreserved patient thus accumulates a "lethal dose" of D_{lethal} ~ 10,000 mSv[770] in $\tau_{lethal} \sim D_{lethal} / (\delta_{exo} + \delta_{endo})$ = 7700 years for a conventionally-shielded cryopreserved patient, or $\tau_{lethal} \sim D_{lethal} / \delta_{endo}$ = 33,000 years for a perfectly externally-shielded patient. We might therefore expect at most ~0.1% of cryopreserved DNA to be seriously (but randomly) damaged for every decade of cryostorage[771] (though it should be noted that radiation damage to biological molecules decreases several-fold with temperature for a given absorbed dose[772]). However, such damage is readily repaired by medical nanorobots[773] as soon as the patient is restored to the reliquidified (i.e., diffusional) state.

---

[767] The solubility of radon in liquid nitrogen has not been reported. However, if the typical ~48 Bq/m^3 indoor air concentration of ^{222}Rn is representative for liquid nitrogen continuously exposed to radon-laden air, then the concentration if liquefied will be roughly proportional to the ratio of densities of LN2 and air, or (48 Bq/m^3) (807 kg/m^3) / (1.29 kg/m^3) ~ 30,000 Bq/m^3. Since the range in liquid media (e.g., water) of the 5.59-MeV α-particle emitted during ^{222}Rn decay is ~38 μm,[*] the maximum radiation source volume surrounding a ~2 m^2 surface area human body in the dewar is (2 m^2) (38 μm) ~ 7.6 x 10^{-5} m^3, creating a (30,000 Bq/m^3) (7.6 x 10^{-5} m^3) ~ 2.3 Bq whole-body exposure that equates to ~0.00008 mSv/yr or ~0.0003 of all other endoradiation sources.

[*] de Carvalho HG, Yagoda H. The range of alpha-particles in water. Phys Rev. 1952 Oct 15;88(2):273-8; https://journals.aps.org/pr/abstract/10.1103/PhysRev.88.273.

[768] Personal communication from Hugh Hixon to Robert Freitas, 19 Nov 1999.

[769] https://en.wikipedia.org/wiki/Liquefaction_of_gases.

[770] "Acute Radiation Syndrome: A Fact Sheet for Clinicians," Centers for Disease Control and Prevention, 4 Apr 2018; https://www.cdc.gov/nceh/radiation/emergencies/arsphysicianfactsheet.htm?CDC_AA_refVal=https%3A%2F%2Femergency.cdc.gov%2Fradiation%2Farsphysicianfactsheet.asp.

[771] If the relative abundance of radioactive ^{14}C in the human body is ~10^{-12} relative to ^{12}C (https://en.wikipedia.org/wiki/Carbon-14), then a 70 kg reference male human body contains ~7.9 x 10^{14} atoms of ^{14}C and ~7.9 x 10^{26} atoms of ^{12}C; the full DNA complement of a single cell has ~10^{11} carbon atoms, hence each cellular DNA set incorporates an average of ~0.1 ^{14}C atoms. Thus only about one DNA set in ten incorporates a single potentially destructive ^{14}C atom, and after 5730 years of cryopreservation only half of these ^{14}C atoms will have disintegrated, in the worst case inducing one randomly-placed error in the DNA set of one in ten cells, which seems negligible. Brian Wowk (personal communication with Robert Freitas, 1 May 2000) believes the error rate will be even lower: "Carbon 14 decays via 0.15 MeV negative beta emission. The ejected electron will lose energy over a 200 micron track in water, with a peak energy loss at the end of its track, several cells away from the original decay event. The probability of the electron interacting with nearby atoms is negligible. The sole local result of a ^{14}C decay in DNA will be the conversion of the carbon atom into a tetravalent N^+ ion. This will ruin (mutate) the nucleotide, but it won't break the DNA molecule. Even if the decay occurs in one of the three carbons per nucleotide that hold the backbone together, all these carbons have attached hydrogens. This means that the carbon will merely become a protonated amine – the natural state of amines at physiological pH. Even if that conversion to nitrogen [could] break the molecule, single-stranded DNA breaks are easily repaired by cells. It is a truism of radiation biology that a double-stranded break is necessary to kill a cell. With the extremely low abundance of ^{14}C, this is of course very unlikely. In short, if every ^{14}C atom in your body were to convert to ^{14}N right now, I doubt you'd even notice it. The total radiation dose would only be about 5 rads – equivalent to two medical CT scans."

[772] Ashwood-Smith MJ, Friedmann GB. Lethal and chromosomal effects of freezing, thawing, storage time, and x-irradiation on mammalian cells preserved at -196 degrees in dimethyl sulfoxide. Cryobiology. 1979 Apr;16(2):132-40; https://www.ncbi.nlm.nih.gov/pubmed/573193. See also: Beauregard G, Potier M. Temperature dependence of the radiation inactivation of proteins. Anal Biochem. 1985 Oct;150(1):117-20; https://www.ncbi.nlm.nih.gov/pubmed/4083473.

[773] Freitas RA Jr. The Ideal Gene Delivery Vector: Chromallocytes, Cell Repair Nanorobots for Chromosome Replacement Therapy. J. Evol. Technol. 2007 Jun;16:1-97; http://jetpress.org/v16/freitas.pdf.

Far higher radiation doses would be required before biological molecules stored at cryogenic temperatures would be so severely damaged as to be unrecoverable by advanced nanotechnology. For example, one study[774] found that X-ray accumulations on the order of 10^{16} photons/mm^2, corresponding to a dose of tens of millions of rads, are necessary to severely alter biomolecules in a frozen matrix.

Finally, no formal estimate of the spontaneous rate of sublimation of water-based frozen or vitrified cryoprotectant solution or extracellular water-ice in a patient stored at 77 K (-196 °C) and at ambient atmospheric pressure has yet been published, but the rate is expected to be negligibly small, possibly on the order of ~2 x 10^{-19} nm/day.[775]

3.6 Rewarming Damage

Additional damage may occur when the cryopreserved patient is rewarmed from LN2 temperatures to temperatures high enough to reliquidify tissues. Classical **reperfusion** injury, aka. ischemia-reperfusion injury (IRI) or reoxygenation injury, is the tissue damage caused when blood supply returns to tissue after a period of anoxia or hypoxia such that the restoration of circulation results in inflammation and oxidative damage through the induction of oxidative stress.[776] Reperfusion injury can be more damaging than the initial ischemia, when restoration of blood flow brings oxygen back to the tissues that: (1) increases the production of free radicals and reactive oxygen species that damage cells, (2) brings more calcium ions to the tissues causing further calcium overloading and potentially fatal cardiac arrhythmias, and (3) exaggerates the inflammation response of damaged tissues causing white blood cells to destroy damaged cells that may otherwise still be viable.[777] For example, 17% of cardiomyocytes died when kept ischemic for 4 hours straight, but 73% of those cells died when reperfused for 3 hours after 1 hour of ischemia.[778]

Much of the classical reperfusion damage mechanisms cannot occur if the patient's vasculature is filled with cryoprotectant fluid (or with vasculoid; Section 4.6) instead of blood. Damage should also be avoided if the patient's blood flow and oxygen supply are not resumed immediately upon rewarming, or,

---

[774] Burmeister WP. Structural changes in a cryo-cooled protein crystal owing to radiation damage. Acta Crystallogr D Biol Crystallogr. 2000 Mar;56(Pt 3):328-41; https://www.researchgate.net/profile/Wim_Burmeister/publication/12601379_Structural_changes_in_a_cryo-cooled_protein_crystal_owing_to_radiation_damage/links/0fcfd50f7fa5b868a4000000.pdf.

[775] The measured sublimation rate of Antarctic ice[*] is ~1 mm/day at ~0 °C / 273 K (water-ice saturation vapor pressure ~600 Pa)[†] and ~0.1 mm/day at -30 °C / 243 K (water-ice saturation vapor pressure ~60 Pa),[†] which implies a sublimation rate at -196 °C / 77 K (water-ice saturation vapor pressure ~10^{-22} Pa)[‡] approximating ~2 x 10^{-19} nm/day assuming sublimation rate is linearly proportional to saturation vapor pressure.
[*] Clow GD, McKay CP, Simmons GM Jr, Wharton RA Jr. Climatological observations and predicted sublimation rates at Lake Hoare, Antarctica. J Clim. 1988 Jul;1(7):715-728; https://journals.ametsoc.org/jcli/article-pdf/1/7/715/3748674/1520-0442(1988)001_0715_coapsr_2_0_co_2.pdf.
[†] Andreas EL. New estimates for the sublimation rate for ice on the Moon. Icarus 2007 Jan;186(1):24-30; https://people.nwra.com/resumes/andreas/publications/Icarus_Moon.pdf.
[‡] Feistel R, Wagner W. Sublimation pressure and sublimation enthalpy of H_2O ice Ih between 0 and 273.16 K. Geochim et Cosmochim Acta. 2007 Jan 1;71(1):36-45; http://www.personal.psu.edu/mrh318/Feistel-Wagner-GCA-2007.pdf.

[776] https://en.wikipedia.org/wiki/Reperfusion_injury.
[777] https://en.wikipedia.org/wiki/Ischemia#Pathophysiology.

[778] Vanden Hoek TL, Shao Z, Li C, Zak R, Schumacker PT, Becker LB. Reperfusion injury on cardiac myocytes after simulated ischemia. Am J Physiol. 1996 Apr;270(4 Pt 2):H1334-41; https://pubmed.ncbi.nlm.nih.gov/8967373/.

even better, if systemic biochemical stasis has been established during tissue reliquidification (Section 4.10). Some cell debris creation and migration will also occur as tissue is thawed, so incremental rewarming damage is probably inevitable because full biochemical stasis will take some time to initially establish (~1 hour; Section 4.10.1), during reliquidification.

Major types of rewarming damage include:

(1) **Oxidative stress.** Reactive free oxygen species are generated as a consequence of ischemia, especially after reperfusion, and can be key mediators of tissue damage in organs such as heart or kidney that are subjected to reperfusion injury.[779] Free radicals trigger a vicious cycle in mitochondria with inhibition of electron transport mechanisms leading to excess superoxide production and activation of a mitochondrial permeability transition.[780] Additional sources of reactive free oxygen species are enzymatic processes such as the cyclooxygenase-dependent conversion of arachidonic acid to prostanoids, or the degradation of hypoxanthine – in fact, oxidative stress is closely linked to excitotoxicity, energy loss, and ionic imbalances (Section 3.2.1), all of which may contribute to tissue damage.[781] Reactive oxygen species (ROS) rise slowly during ischemia but spike sharply at the onset of perfusion.[782] For example, rabbit hearts spike ROS after only 10-20 seconds of reperfusion following 10-30 minutes of ischemia, with no trace of ROS after 5 minutes of reflow.[783]

These forms of damage are less likely to occur when reactive molecules are quickly extracted from the tissues (Section 4.10) and no oxygen is reintroduced.

(2) **Neutrophil activation.** Inflammatory cytokines such as TNF-α and IL-1β appear within hours of ischemia, followed by neutrophils after 4-6 hours.[784] Polymorphonuclear leukocytes (PMNLs) and monocytes/macrophages have been implicated as significant causes of pathology in reperfusion injury.[785] Early research[786] focused on PMNL-mediated reperfusion injury to the myocardium,[787] establishing that

---

[779] Endres M, Dirnagl U, Moskowitz MA. The ischemic cascade and mediators of ischemic injury. Handb Clin Neurol. 2009;92:31-41; http://neuroutbildarna.se/files/7814/8647/7933/artikel-celldod-2-1.pdf.

[780] Fiskum G, Murphy AN, Beal MF. Mitochondria in neurodegeneration: acute ischemia and chronic neurodegenerative diseases. J Cereb Blood Flow Metab. 1999 Apr;19(4):351-369; https://journals.sagepub.com/doi/pdf/10.1097/00004647-199904000-00001. Kroemer G, Reed JC. Mitochondrial control of cell death. Nat Med. 2000 May;6(5):513-519; https://www.nature.com/articles/nm0500_513. Chan PH. Reactive oxygen radicals in signaling and damage in the ischemic brain. J Cereb Blood Flow Metab. 2001 Jan;21(1):2-14; https://journals.sagepub.com/doi/pdf/10.1097/00004647-200101000-00002.

[781] Endres M, Dirnagl U, Moskowitz MA. The ischemic cascade and mediators of ischemic injury. Handb Clin Neurol. 2009;92:31-41; http://neuroutbildarna.se/files/7814/8647/7933/artikel-celldod-2-1.pdf.

[782] Vanden Hoek TL, Li C, Shao Z, Schumacker PT, Becker LB. Significant levels of oxidants are generated by isolated cardiomyocytes during ischemia prior to reperfusion. J Mol Cell Cardiol. 1997 Aug 31;29(9):2571-2583; https://europepmc.org/article/med/9299379.

[783] Zweier JL, Kuppusamy P, Williams R, Rayburn BK, Smith D, Weisfeldt ML, Flaherty JT. Measurement and characterization of postischemic free radical generation in the isolated perfused heart. J Biol Chem. 1989 Nov 15;264(32):18890-5; https://www.jbc.org/content/264/32/18890.full.pdf.

[784] Rosenberg GA. Ischemic brain edema. Prog Cardiovasc Dis. 1999 Nov-Dec;42(3):209-16; https://pubmed.ncbi.nlm.nih.gov/10598921/.

[785] Vinten-Johansen J. Involvement of neutrophils in the pathogenesis of lethal myocardial reperfusion injury. Cardiovasc Res. 2004 Feb 15;61(3):481-497; https://academic.oup.com/cardiovascres/article/61/3/481/404101.

[786] https://www.alcor.org/Library/html/ischemicinjury.html.

PMNL activation and subsequent plugging and degranulation (resulting in release of oxidizing compounds) is responsible for the no-reflow phenomenon following myocardial ischemia, with PMNL activation responsible for plugging at least 27% of myocardial capillaries.[788] Activated PMNLs and endothelial cells in the brain secrete adhesion molecules, causing leukocytes to stick to blood vessel walls and infiltrate ischemic tissue 6-12 hours after reperfusion.[789] PMNL activation is also responsible for the development of edema and arrhythmias upon reperfusion.[790] Neutrophils are thought to be a major mediator of ischemic injury in a variety of organ systems,[791] and their acute activation may be responsible for many of the effects of ischemia observed in the brain and other body tissues including the loss of capillary integrity and the degradation of ultrastructure upon reperfusion.[792]

During revival from cryopreservation, from the moment that cryopreserved tissue first reliquidifies near 273 K (0 °C) the entire vasculature is filled with vasculoid machinery (Section 4.6) and remains so, blocking entrance or passage by motile cells until the later stages of revival. Energy molecules will be quickly extracted (Section 4.10), quickly causing motile cells to become anergic. Damaged endothelial cells and other vascular faults are detected and repaired (Section 4.11 and Section 4.12), unwanted cells are identified and removed by nanorobots (Section 4.12.1), and ECM ultrastructure faults and other cell damage is repaired (Section 4.12) before the vasculoid is removed, forestalling capillary plugging or rewarming damage by activated PMNLs which are already relatively inactive due to the near-freezing temperature.

(3) **Hypoperfusion or "no reflow" following reperfusion**. Cerebral hypoperfusion (decreased blood flow through an organ) after restoration of spontaneous circulation can cause a range of brain injuries[793] and may be a significant contributor to the potential for reperfusion injury in cryonics patients.[794]

---

[787] Go LO, Murry CE, Richard VJ, Weischedel GR, Jennings RB, Reimer KA. Myocardial neutrophil accumulation during reperfusion after reversible or irreversible ischemic injury. Am J Physiol. 1988 Nov;255(5 Pt 2):H1188-H1198; https://pubmed.ncbi.nlm.nih.gov/2461099.

[788] Engler RL, Dahlgren MD, Morris DD, Peterson MA, Schmid-Schönbein GW. Role of leukocytes in response to acute myocardial ischemia and reflow in dogs. Am J Physiol. 1986 Aug;251(2 Pt 2):H314-H323; https://www.physiology.org/doi/pdf/10.1152/ajpheart.1986.251.2.H314. Schmid-Schönbein GW. Capillary plugging by granulocytes and the no-reflow phenomenon in the microcirculation. Fed Proc. 1987 May 15;46(7):2397-2401; https://pubmed.ncbi.nlm.nih.gov/3552737. Engler R. Consequences of activation and adenosine-mediated inhibition of granulocytes during myocardial ischemia. Fed Proc. 1987 May 15;46(7):2407-2412; https://pubmed.ncbi.nlm.nih.gov/3569543.

[789] Kuroda S, Siesjö BK. Reperfusion damage following focal ischemia: pathophysiology and therapeutic windows. Clin Neurosci. 1997;4(4):199-212; https://pubmed.ncbi.nlm.nih.gov/9186042/.

[790] Mullane KM, Salmon JA, Kraemer R. Leukocyte-derived metabolites of arachidonic acid in ischemia-induced myocardial injury. Fed Proc. 1987 May 15;46(7):2422-2433; https://pubmed.ncbi.nlm.nih.gov/3106093.

[791] Nakazawa D, Kumar SV, Marschner J, Desai J, Holderied A, Rath L, Kraft F, Lei Y, Fukasawa Y, Moeckel GW, Angelotti ML, Liapis H, Anders HJ. Histones and Neutrophil Extracellular Traps Enhance Tubular Necrosis and Remote Organ Injury in Ischemic AKI. J Am Soc Nephrol. 2017 Jun;28(6):1753-1768; https://www.ncbi.nlm.nih.gov/pmc/articles/PMC5461800/. Oliveira THC, Marques PE, Proost P, Teixeira MMM. Neutrophils: a cornerstone of liver ischemia and reperfusion injury. Lab Invest. 2018 Jan;98(1):51-62; https://www.nature.com/articles/labinvest201790.

[792] Halliwell B, ed. Oxygen Radicals and Tissue Injury: Proceedings of a Brook Lodge Symposium. Augusta MI, USA, 27-29 April 1987, Federation of American Societies for Experimental Biology, Bethesda MD, 1988, pp.1-143; https://www.amazon.com/dp/0913822159/.

[793] De Georgia M, Miller B. Chapter 87 – Brain Injury From Cerebral Hypoperfusion. Primer on Cerebrovascular Diseases, 2nd edition, 2017, pp. 423-426; https://www.sciencedirect.com/science/article/pii/B9780128030585000874.

[794] Darwin M. The pathophysiology of ischemic injury. BioPreservation, Inc., 1995; https://www.alcor.org/Library/html/ischemicinjury.html.

The onset of "no reflow" conditions (image, below)[795] may occur due to a multitude of causative mechanisms including endothelial blebbing in capillary lumens,[796] regional endothelial swelling,[797] blood clots and neutrophil plugs,[798] vessel compression from swollen myocytes or astrocytes,[799] edema,[800] hyperviscosity of blood due to red cell aggregation,[801] and so forth. However, all of these mechanisms that result in structural damage or vascular blockages will be repaired (Section 4.12) prior to the re-establishment of normal circulation (Section 4.14.2). Also, many of the rapid-onset effects of reperfusion might be reduced or eliminated by the injection of inhibitory agents at the outset of molecular extraction (Section 4.10).

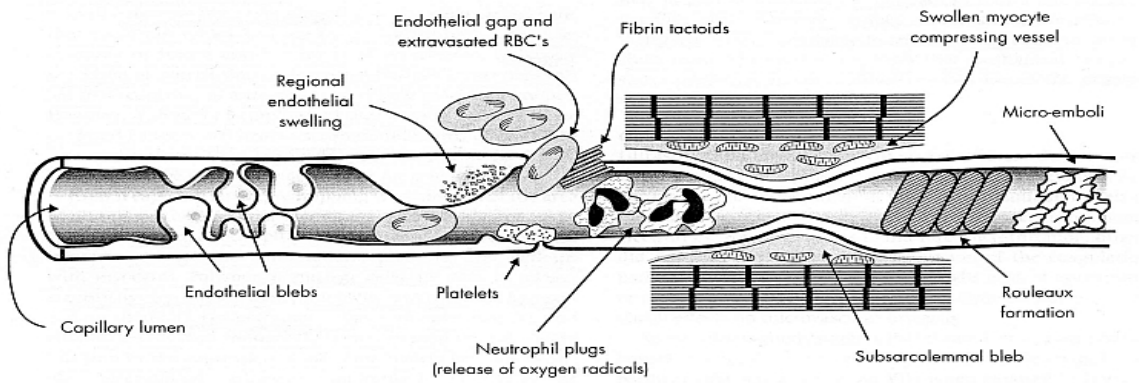

---

[795] Best B. Ischemia and Reperfusion Injury in Cryonics. December 2003; https://www.benbest.com/cryonics/ischemia.html.

[796] Chiang J, Kowada M, Ames A 3rd, Wright RL, Majno G. Cerebral ischemia. III. Vascular changes. Am J Pathol. 1968 Feb;52(2):455-476; https://www.ncbi.nlm.nih.gov/pmc/articles/PMC2013336/pdf/amjpathol00559-0199.pdf.

[797] Garcia JH, Liu KF, Yoshida Y, Chen S, Lian J. Brain microvessels: factors altering their patency after the occlusion of a middle cerebral artery (Wistar rat). Am J Pathol. 1994 Sep;145(3):728-740; https://www.ncbi.nlm.nih.gov/pmc/articles/PMC1890335/pdf/amjpathol00057-0234.pdf. Dawson DA, Ruetzler CA, Hallenbeck JM. Temporal impairment of microcirculatory perfusion following focal cerebral ischemia in the spontaneously hypertensive rat. Brain Res. 1997 Feb 28;749(2):200-8; https://pubmed.ncbi.nlm.nih.gov/9138719/.

[798] del Zoppo GJ, Schmid-Schönbein GW, Mori E, Copeland BR, Chang CM. Polymorphonuclear leukocytes occlude capillaries following middle cerebral artery occlusion and reperfusion in baboons. Stroke. 1991 Oct;22(10):1276-1283; https://www.ahajournals.org/doi/pdf/10.1161/01.str.22.10.1276.

[799] Ames A III, Wright RL, Kowada M, Thurston JM, Majno G. Cerebral ischemia II. The no-reflow phenomenon. Amer J Pathol 1968 Feb;52:437-53; https://www.ncbi.nlm.nih.gov/pmc/articles/PMC2013326/.

[800] Sage JI, Van Uitert RL, Duffy TE. Early changes in blood brain barrier permeability to small molecules after transient cerebral ischemia. Stroke. 1984 Jan-Feb;15(1):46-50; https://www.ahajournals.org/doi/pdf/10.1161/01.STR.15.1.46. Gotoh O, Asano T, Koide T, Takakura K. Ischemic brain edema following occlusion of the middle cerebral artery in the rat. I: The time courses of the brain water, sodium and potassium contents and blood-brain barrier permeability to 125I-albumin. Stroke. 1985 Jan-Feb;16(1):101-9; https://www.ahajournals.org/doi/pdf/10.1161/01.str.16.1.101. Slivka A, Murphy E, Horrocks L. Cerebral edema after temporary and permanent middle cerebral artery occlusion in the rat. Stroke. 1995 Jun;26(6):1061-5; https://www.ahajournals.org/doi/full/10.1161/01.STR.26.6.1061. Rosenberg GA, Estrada EY, Dencoff JE. Matrix metalloproteinases and TIMPs are associated with blood-brain barrier opening after reperfusion in rat brain. Stroke. 1998 Oct;29(10):2189-95; http://citeseerx.ist.psu.edu/viewdoc/download?doi=10.1.1.320.5384&rep=rep1&type=pdf.

[801] Dintenfass L. Red cell aggregation in cardiovascular diseases and crucial role of inversion phenomenon. Angiology. 1985 May;36(5):315-26; http://citeseerx.ist.psu.edu/viewdoc/download?doi=10.1.1.861.4612&rep=rep1&type=pdf.

(4) **Recrystallization of intracellular ice.** Lacking cryoprotectants, very rapid cooling produces intracellular ice with very small crystals[802] that are invisible at the ultramicroscopic level. Small ice crystals are thermodynamically unstable relative to larger ice crystals,[803] so during warming there will be a tendency for small crystals to aggregate to form larger crystals, a process referred to as recrystallization.[804] Slow warming is thought to be harmful to frozen cells because it allows time for such recrystallization to occur, hence fast warming likely should be employed (Section 4.9.1). A correlation between the recrystallization of intracellular ice observed under the microscope and cell death has been demonstrated in yeast,[805] higher plant cells,[806] ascites tumor cells,[807] and hamster tissue culture cells.[808]

The presence of cryoprotectants should forestall major ice formation in tissues and cells. Modern cryoprotectants such as M22 incorporate ice blockers,[809] and the search for better ice recrystallization inhibitors is an active field of research today.[810] Tissues with recrystallization damage that occurs in regions of insufficient cryoprotectant penetration will first have all plasma membrane compartments resealed (Section 4.11) followed by comprehensive cellular repair (Section 4.12), after any ice that has recrystallized has melted following tissue reliquidification (Section 4.9). The cryogenic phases of the repair process could also replace some water molecules with extra cryoprotectant molecules that can slow or prevent both devitrification (see below) and ice recrystallization.

---

[802] Nei T. Structure and function of frozen cells: freezing patterns and post-thaw survival. J Microsc. 1978 Mar;112(2):197-204; https://pubmed.ncbi.nlm.nih.gov/349159. Shimada K. Effects of cryoprotective additives on intracellular ice formation and survival in very rapidly cooled HeLa cells. Contrib Inst Low Temp Sci Ser B. 1978 May 22;19:49-69; http://citeseerx.ist.psu.edu/viewdoc/download?doi=10.1.1.1029.8424&rep=rep1&type=pdf.

[803] Mazur P. The role of cell membranes in the freezing of yeast and other single cells. Ann N Y Acad Sci. 1965 Oct 13;125(2):658-676; https://nyaspubs.onlinelibrary.wiley.com/doi/abs/10.1111/j.1749-6632.1965.tb45420.x. Mazur P. Chapter 6. Physical and chemical basis of injury in single-celled microorganisms subjected to freezing and thawing. In: Meryman HT, ed., Cryobiology, Academic Press, London, 1966, pp. 213-315.

[804] Mazur P. Freezing of living cells: mechanisms and implications. Am J Physiol. 1984 Sep;247(3 Pt 1):C125-42; https://www.physiology.org/doi/pdf/10.1152/ajpcell.1984.247.3.C125.

[805] Mazur P. The role of cell membranes in the freezing of yeast and other single cells. Ann N Y Acad Sci. 1965 Oct 13;125(2):658-676; https://nyaspubs.onlinelibrary.wiley.com/doi/abs/10.1111/j.1749-6632.1965.tb45420.x.

[806] Sakai A, Otsuka K. Survival of plant tissue at super-low temperatures v. An electron microscope study of ice in cortical cells cooled rapidly. Plant Physiol. 1967 Dec;42(12):1680-94; https://www.ncbi.nlm.nih.gov/pmc/articles/PMC1086783/pdf/plntphys00504-0028.pdf.

[807] Shimada K, Asahina E. Visualization of intracellular ice crystals formed in very rapidly frozen cells at -27 degree C. Cryobiology. 1975 Jun;12(3):209-218; https://www.sciencedirect.com/science/article/pii/001122407590019X.

[808] Farrant J, Walter CA, Lee H, McGann LE. Use of two-step cooling procedures to examine factors influencing cell survival following freezing and thawing. Cryobiology. 1977 Jun;14(3):273-286; https://www.sciencedirect.com/science/article/pii/0011224077901766.

[809] Fahy GM, Wowk B, Wu J, Phan J, Rasch C, Chang A, Zendejas E. Cryopreservation of organs by vitrification: perspectives and recent advances. Cryobiology. 2004 Apr;48(2):157-78; http://www.21cm.com/pdfs/cryopreservation_advances.pdf.

[810] Briard JG, Poisson JS, Turner TR, Capicciotti CJ, Acker JP, Ben RN. Small molecule ice recrystallization inhibitors mitigate red blood cell lysis during freezing, transient warming and thawing. Sci Rep. 2016 Mar 29;6:23619; https://www.ncbi.nlm.nih.gov/pmc/articles/PMC4810524/. Poisson JS, Acker JP, Briard JG, Meyer JE, Ben RN. Modulating Intracellular Ice Growth with Cell-Permeating Small-Molecule Ice Recrystallization Inhibitors. Langmuir. 2019 Jun 11;35(23):7452-7458; https://pubmed.ncbi.nlm.nih.gov/30119611/.

(5) **Devitrification.** As Wowk explains it,[811] the initial process of ice formation begins with ice nucleation, the local rotational reorientation of water molecules at the nanoscale to form the initial nucleus of an ice crystal. This ice nucleation process is favored at low temperatures, and reaches a maximum rate at deep sub-zero temperatures near the glass transition temperature, T_g.[812] The growth of the ice nucleus into a larger ice crystal requires diffusion of water molecules to join the surface of a growing ice crystal. This growth process is inhibited by high viscosity at low temperatures, so ice growth, unlike ice nucleation, is favored at higher sub-zero temperatures closer to the melting temperature, T_m, of the cryoprotectant solution (i.e., -55 °C for M22). Ice growth during cooling occurs because there is some overlap between the higher ice growth temperature zone and the lower ice nucleation temperature zone such that ice can nucleate and still grow before the viscosity increase with continued cooling stops growth. Simultaneous ice nucleation and ice growth isn't necessary for ice growth during warming. Even after water molecules become translationally immobilized by increasing viscosity during cooling, local rotation of water molecules will continue to produce nanoscale ice nuclei until at least 10 °C below the glass transition temperature. When tissue is rewarmed above the glass transition temperature and water becomes translationally mobile again, the previously-formed nanoscopic ice nuclei will begin to grow into microscopic and even macroscopic ice crystals. As a consequence, any ice formation tendency during cooling of tissues cryopreserved by vitrification will be far exceeded by ice formation tendency during warming.

Ice growth that occurs during warming above the glass transition temperature until the melting temperature is reached is called **devitrification**. It can be mitigated by rapid warming to outrun the growth process of ice nuclei and/or using a cryoprotectant concentration high enough to slow or eliminate both ice nucleation and ice growth. In principle, devitrification could be mitigated during revival of cryonics patients by replacing enough water molecules with cryoprotectant molecules while still at cryogenic temperature to make tissue immune to devitrification during the warming process.

The cryobiology literature sometimes confuses devitrification with ice recrystallization. These are distinct processes. Devitrification is growth of ice during rewarming. Recrystallization is preferential growth of larger ice crystals at the expense of smaller ones (aka. Ostwald ripening).[813] This preferential growth is a consequence of the thermodynamic instability of a mixture of many ice crystals of difference sizes, wherein the melting point of small crystals with a smaller radius of curvature is lower than the melting point of larger crystals with a larger radius of curvature. Thus during slow warming, a dispersion of many ice crystals will tend to become one large damaging ice crystal. Ultrafast warming can allow cells with even extensive intracellular freezing to survive because fast warming prevents intracellular ice from growing to a damaging size (e.g., >200 nm).

Ice recrystallization is distinct from devitrification but the mitigations can be the same: for example, fast warming and/or raising the cryoprotectant concentration to slow ice growth by raising viscosity and making fewer water molecules available. Whatever slows ice growth will also slow recrystallization. 21CM's "X-1000" ice blocker is an especially potent inhibitor of ice recrystallization because it adsorbs onto ice surfaces, but with its high molecular weight (~1000 gm/mole) it doesn't naturally get inside cells. Research

---

[811] Personal communication from Brian Wowk to Robert Freitas, 30 Sep 2021.

[812] Wowk B. Thermodynamic aspects of vitrification. Cryobiology 2010;60:11-22; http://www.21cm.com/pdfs/2010-Thermodynamics.pdf.

[813] https://en.wikipedia.org/wiki/Ostwald_ripening.

groups are working on smaller-molecule ice recrystallization inhibitors (IRIs)[814] that would be better suited to intracellular use, even if temporarily placed there by nanorobots during a repair process.

(6) **Osmotic shock.** When excess solute is loaded into cells during slow freezing, and insufficient time is allowed for the excess solute to diffuse back out when thawing is rapid, cells can swell and lyse as the medium becomes abruptly diluted by the melting of extracellular ice.[815] Osmotic shock[816] can also kill cells when they are returned to isotonic medium.

During the revival protocol, if thawing (Section 4.9) cannot be performed slowly enough to allow cytosolic solutes to exit the cell, then molecular extraction (Section 4.10) from the reliquidified tissue must be performed both inside and outside the cellular compartments, albeit at a rate governed by diffusion speed, thus relieving any osmotic imbalances.

Alternatively, Wowk[817] suggests that tissue burdened by large quantities of extracellular ice could have that ice excavated and replaced at cryogenic temperature with a combination of water and cryoprotectant molecules isotonic with the intracellular space so that upon warming there would be no osmotic stress. For originally vitrified tissue, or frozen tissue transformed into vitrified tissue by cryogenic molecular replacement, removal of the cryoprotectant molecules both inside and outside cells at warmer temperatures to transition to a cryoprotectant-free composition at a temperature above 0 °C is not osmotically difficult because this is already done successfully in contemporary organ cryopreservation research.[818]

(7) **Leakage from damaged fluid compartments**. Leaks from unrepaired fluid compartments can destroy viability when the patient is rewarmed. For instance, in one experiment where primates (*Galago crassicaudatus*) were frozen without cryoprotectant and then rewarmed,[819] all animals died within one day from pulmonary edema (due to fluid leaking into the lungs through freeze-damaged pulmonary alveoli) or from intraperitoneal bleeding (due to gastric juice that leaked from the freeze-damaged stomach or biliary glands into abdominal tissue). Fahy[820] refers to this form of damage as "stirring" that is normally held in check by extracellular diffusion barriers presented by ice and high viscosity extracellular media, but which, during thawing, may occur due to declining viscosity, thermal expansion, convection, and cellular expansion, allowing transmembrane diffusion in either direction.

---

[814] Briard JG, Poisson JS, Turner TR, Capicciotti CJ, Acker JP, Ben RN. Small molecule ice recrystallization inhibitors mitigate red blood cell lysis during freezing, transient warming and thawing. Sci Rep. 2016 Mar 29;6:23619; https://www.ncbi.nlm.nih.gov/pmc/articles/PMC4810524/. Poisson JS, Acker JP, Briard JG, Meyer JE, Ben RN. Modulating Intracellular Ice Growth with Cell-Permeating Small-Molecule Ice Recrystallization Inhibitors. Langmuir. 2019 Jun 11;35(23):7452-7458; https://pubmed.ncbi.nlm.nih.gov/30119611/.

[815] Mazur P. Slow-freezing injury in mammalian cells. Ciba Found Symp. 1977 Jan 18;(52):19-48; https://books.google.com/books?hl=en&lr=&id=AmV4KJglbPsC&oi=fnd&pg=PA19.

[816] Mazur P. Freezing of living cells: mechanisms and implications. Am J Physiol. 1984 Sep;247(3 Pt 1):C125-42; https://www.physiology.org/doi/pdf/10.1152/ajpcell.1984.247.3.C125

[817] Personal communication from Brian Wowk to Robert Freitas, 30 Sep 2021.

[818] Fahy GM, Wowk B, Wu J, Phan J, Rasch C, Chang A, Zendejas E. Cryopreservation of organs by vitrification: perspectives and recent advances. Cryobiology. 2004 Apr;48(2):157-78; http://www.21cm.com/pdfs/cryopreservation_advances.pdf.

[819] Smith AU. Viability of supercooled and frozen mammals. Ann N Y Acad Sci. 1959 Sep 14;80:291–300; https://nyaspubs.onlinelibrary.wiley.com/doi/abs/10.1111/j.1749-6632.1959.tb49209.x.

[820] Fahy G. Appendix B. A "Realistic" Scenario for Nanotechnological Repair of the Frozen Human Brain. In: Wowk B, Darwin M, eds., Cryonics: Reaching for Tomorrow. Alcor Life Extension Foundation, 1991, pp. A-10 – A-26; https://alcor.org/Library/html/nanotechrepair.html.

The “conventional cell repair” revival protocol described in Chapter 4 includes the installation of a watertight vascular membrane called a vasculoid (Section 4.6), the prompt extraction of leaked or degradative biochemicals in a ~3600 sec timeframe (Section 4.10) after fast whole-body warming in a ≤200 sec timeframe (Section 4.9.1 and Section 5.2.3.1(B)), followed by rapid nanorobotic repair of damaged cellular membrane compartments (Section 4.11) to minimize or forestall “stirring” damage.

(8) **Creation and migration of cell debris during thawing**. Minimal cellular tearing should occur during the descent to cryogenic temperatures if the patient’s tissues have been adequately cryoprotected and vitrified. In this case, any torn cell structures will remain locked in place at cryogenic temperatures producing little loss of structural information. However, modest information loss may occur when cryopreserved tissue is thawed (Section 4.9), both because some ice may form if the rate of warming is too slow (Section 4.9.1), causing tissue maceration and cell debris formation (especially in regions of poor cryoprotectant perfusion), and because pieces of cell debris can randomly migrate as the viscosity of the local environment declines with rising temperature (Section 4.11.1). A cell debris-handling protocol is proposed in Section 4.11.1.

4. Plan A: Nanorobotic Revival via Conventional Cell Repair

Since at least the mid-1980s, it has been clear that some form of nanorobotic repair procedure would be required to revive human cryopreservation patients. Conceptual designs for simple nanorobots that mimic the activity of biological red cells,[821] white cells,[822] and platelets[823] were published during 1998-2005, along with the first technical books on medical nanorobot design[824] and biocompatibility,[825] and the first conceptual design for a cell repair nanorobot was published in 2007.[826] Detailed proposals for using nanorobots to cure seemingly intractable maladies such as Alzheimer's disease[827] and aging[828] in living human patients were published during 2010-2016.

But how can nanomedical devices be used to revive human patients who have been cryopreserved – a condition requiring extensive repairs that represents perhaps the most technically challenging application in the field of medical nanorobotics?

One fundamental difficulty has long been apparent.

The cryopreserved patient is resting at cryogenic temperatures, typically 77 K (-196 °C), the temperature of liquid nitrogen (LN2). Nanorobots and nanorobotic machinery should perform quite well in cryogenic environments – for example, molecular vibrations are of lower amplitude compared to room-temperature operation, allowing more accurate sensing, reduced frictional losses, vacuum operations on biological tissues without desiccating them (Section 5.2.1), and more reliable atomic printing (Section 5.2.3.1(2)) via mechanosynthesis (Section 1.3.1). However, at these temperatures the patient is in the solid state, either frozen or vitrified. Nanorobots can have great mobility and facility with cell repair when operating in the liquid state at normal human body temperature, but these devices will find it extremely difficult to enter frozen cells and manipulate the immobilized biological materials trapped therein.

---

[821] Freitas RA Jr. Exploratory design in medical nanotechnology: a mechanical artificial red cell. Artif Cells Blood Substit Immobil Biotechnol. 1998 Jul;26(4):411-30; https://www.tandfonline.com/doi/pdf/10.3109/10731199809117682. A longer version of this paper appears at: https://web.archive.org/web/20100420085137/http://www.foresight.org/Nanomedicine/Respirocytes.html.

[822] Freitas RA Jr. Microbivores: Artificial Mechanical Phagocytes using Digest and Discharge Protocol. J. Evol. Technol. 2005 Apr;14:55-106; http://www.jetpress.org/volume14/freitas.pdf.

[823] Freitas RA Jr. Clottocytes: Artificial Mechanical Platelets. Foresight Update 2000 Jun 30;41:9-11; https://web.archive.org/web/20060212200540/http://www.imm.org/Reports/Rep018.html.

[824] Freitas RA Jr. Nanomedicine, Volume I: Basic Capabilities, Landes Bioscience, Georgetown, TX, 1999; http://www.nanomedicine.com/NMI.htm.

[825] Freitas RA Jr. Nanomedicine, Volume IIA: Biocompatibility, Landes Bioscience, Georgetown, TX, 2003; http://www.nanomedicine.com/NMIIA.htm.

[826] Freitas RA Jr. The Ideal Gene Delivery Vector: Chromallocytes, Cell Repair Nanorobots for Chromosome Replacement Therapy. J. Evol. Technol. 2007 Jun;16:1-97; http://jetpress.org/v16/freitas.pdf.

[827] Freitas RA Jr. The Alzheimer Protocols: A Nanorobotic Cure for Alzheimer's Disease and Related Neurodegenerative Conditions. IMM Report No. 48, June 2016, 433 pp; http://www.imm.org/Reports/rep048.pdf.

[828] Freitas RA Jr. Chapter 23. Comprehensive Nanorobotic Control of Human Morbidity and Aging. In: Fahy GM, West MD, Coles LS, Harris SB, eds, The Future of Aging: Pathways to Human Life Extension, Springer, New York, 2010, pp. 685-805; http://www.nanomedicine.com/Papers/Aging.pdf.

To appreciate the degree of difficulty, consider that solid pure water-ice just a few degrees below the freezing point already has an absolute viscosity of $\eta_{water\text{-}ice} \sim 10^{10}$ Pa-sec, nearly 13 orders of magnitude higher than the viscosity of liquid water near the freezing point of 273 K / 0 °C (i.e., $\eta_{water} = 1.787 \times 10^{-3}$ Pa-sec).[829] One published analysis of the possibility of nanorobotic locomotion in ice[830] found that even in this relatively soft ice, a 1 μm diameter nanorobot would have to expend ~200,000 pW of power to creep forward at ~1 μm/sec by viscoplastic flow in which ice crystals are deformed without breaking. (Bloodborne nanorobot power consumption is typically ~1-1000 pW per robot.) At LN2 temperatures, the absolute viscosity of water-ice may rise as high as $\sim 10^{21}$ Pa-sec, almost equivalent to solid mantle rock,[831] causing the conventional locomotion power requirement to increase by *another* 100-billionfold, clearly prohibitive. Baronatation (melting ice using a freezing point depression effect caused by the application of mechanical pressure) is one proposed workaround for this problem,[832] but it can only be used in the softest and warmest ice. The only other option is to mechanosynthetically disassemble the frozen or vitrified tissue virtually atom by atom (Section 5.2.1), taking great care to avoid damaging biological structures as the nanorobot moves forward (Section 5.3.1).

What about vitrified tissue? Pure vitrified solution is much less viscous than water-ice at most temperatures of relevance (Section 4.9). But well-cryopreserved patients will always have some water-ice present, and even in vitrified 100% pure M22 the viscosity of this cryoprotectant is already ~20 times higher than normothermic water at 0 °C (273 K), 100-fold higher at -30 °C (243 K), and 1000-fold higher than normothermic water at the M22 melting point of -55 °C (218 K),[833] making nanorobot locomotion energy-problematic even in a purely glassy operating environment because normothermic fluid locomotion is typically scaled around 1%-10% of mobile nanorobot onboard power.[834] The absolute viscosity of M22 is $\sim 10^{15}$ times higher than for normothermic water at -123 °C (150 K), closer to LN2 temperatures (Section 4.9).

However, if the cryopreserved patient is warmed enough to reliquidify the tissues sufficiently to permit nanorobots to locomote effectively, then the patient risks losing valuable unique structural information as the solid matrix softens and melts, allowing internal matter to mobilize and mix randomly. Additionally, biochemical activity rates double with each 10 °C rise in temperature,[835] so degradative chemical reactions that might theoretically require $\sim 10^{23}$ years at 77 K / -196 °C might take only ~1.8 hours at the water-ice

---

[829] Freitas RA Jr., Nanomedicine, Volume I: Basic Capabilities, Landes Bioscience, Georgetown, TX, 1999, Table 9.4 "Absolute Viscosity of Some Common Materials"; http://www.nanomedicine.com/NMI/Tables/9.4.jpg.

[830] Freitas RA Jr. Nanomedicine, Volume I: Basic Capabilities, Landes Bioscience, Georgetown TX, 1999, Section 10.5.2, "Viscosity and Locomotion in Ice"; http://www.nanomedicine.com/NMI/10.5.2.htm.

[831] The compressive strength of granite is ~200 MPa (https://en.wikipedia.org/wiki/Granite), reasonably near the ~120 MPa compressive strength of ice at 100 K (~LN2 temp), acc. to: Wu X, Prakash V. Dynamic compressive behavior of ice at cryogenic temperatures. Cold Regions Sci Technol. 2015;118:1-13; https://www.researchgate.net/profile/Xianqian_Wu/publication/278744289_Dynamic_Compressive_Behavior_of_Ice_at_Cryogenic_Temperatures/links/5be3f2f04585150b2ba6eb12/Dynamic-Compressive-Behavior-of-Ice-at-Cryogenic-Temperatures.pdf.

[832] "By exerting a higher pressure (force per unit area) ahead of it than behind it, a baronatating nanorobot of roughly conical geometry can progress slowly through ice that is no colder than -16 °C [257 K]." [*]

[*] Freitas RA Jr. Nanomedicine, Volume I: Basic Capabilities, Landes Bioscience, Georgetown TX, 1999, Section 10.5.2, "Viscosity and Locomotion in Ice"; http://www.nanomedicine.com/NMI/10.5.2.htm#p3.

[833] Data provided in a personal communication from Brian Wowk to Robert Freitas, 12 Oct 2020.

[834] Freitas RA Jr. Nanomedicine, Volume I: Basic Capabilities, Landes Bioscience, Georgetown TX, 1999, Section 9.4.2.4, "Force and Power Requirements"; http://www.nanomedicine.com/NMI/9.4.2.4.htm.

[835] https://en.wikipedia.org/wiki/Q10_(temperature_coefficient).

freezing point of ~273 K / 0 °C (Section 3.5), allowing biological decay and information loss to progress over time, slowly destroying the patient's molecular structure.

The key difficulty may be summarized as follows: Nanorobots cannot readily locomote in cryogenic tissue where the physical structure information could be preserved for indefinite periods of time, but physical structure information is gradually destroyed if the cryogenic tissue is warmed enough to create a reliquidified environment in which nanorobots can locomote freely. So how can conventional nanorobots be employed for cryonics revival?

The solution described here in Chapter 4 is to scan and record all relevant physical structure to subcellular (~0.1 μm or 100 nm) resolution while the patient is still in the solid state. After this information has been obtained and processed into a plan for repair, the patient is warmed sufficiently to allow rapid extraction of all metabolic and degradative molecules as cells reliquidify, quickly establishing complete biostasis at the higher temperature. Conventional medical nanorobots can then be introduced to comprehensively restore at the subcellular level the cryopatient's previously recorded (and now therapeutically edited) physical structure, over an extended period with reduced time urgency. Chapter 5 explores an alternative solution in which all significant data collection necessary to revive a cryopreservation patient is performed via planar scans in the solid state at cryogenic temperatures.

Accordingly, we propose that a conventional cell repair approach can be employed for cryonics revival, aka. "Plan A", that involves executing the following 15 operational steps:

Step 1. **Millimeter Vascular Scan** (Section 4.1). In a cryopreserved patient stored at ~77 K (-196 °C), noninvasively scan and map all major blood and lymphatic vessels down to 0.1-1 mm (100-1000 μm) in diameter.

Step 2. **Large Vessel Excavation** (Section 4.2). Employ nanorobots or suitable macroscale technical means to mechanically excavate interior ice from all major blood and lymphatic vessels down to 0.1-1 mm (100-1000 μm) in diameter.

Step 3. **Microvascular Scans** (Section 4.3). Scan and map the blood and lymphatic microvasculatures, including all arterioles, venules, capillary beds, and lymphatic precollecting ducts.

Step 4. **Microvascular Excavations** (Section 4.4). Employ nanorobots to mechanically excavate interior ice from all blood and lymphatic microvasculatures, all void spaces between ice crackfaces, all exposed perimeter surfaces of organs and other tissues, and some extracellular spaces.

Step 5. **Recondition and Map Exposed Ice Surfaces** (Section 4.5). Clear excavation debris from all exposed ice surfaces, then recondition those surfaces. Geometrically and biochemically map the reconditioned exposed ice surfaces to ~1 nm resolution, locating and identifying all vascular faults and fracture planes in crackfaces throughout the ice.

Step 6. **Install Vasculoid** (Section 4.6). Install the vasculoid appliance – a mechanical ciliary transport system previously proposed as a means for replacing the vascular transport function in a living person – to provide rapid and reliable transport of nanorobots and materiel throughout the excavated vasculature of the cryopreserved human body. Vasculoid basic plates cover the walls of the entire vasculature, bridge any empty gaps across crack voids, and are installed across all major crackfaces using periodically-spaced anchors onto the ice to temporarily stabilize the faces.

Step 7. **Submicron Tissue Scans** (Section 4.7). Using sensor components mounted on the ubiquitous vasculoid, all tissues in which the vasculoid is embedded are scanned and mapped to ~100 nm feature resolution in three dimensions, clearly identifying most major organelles in all tissue cells and all other cytoplasmic and extracellular structures down to ~100 nm in size including neuronal synapses and boutons.

Step 8. **Compute Whole-Body Repair Plan** (Section 4.8). Compile existing scan data into detailed whole-body maps covering all exposed ice surfaces, vascular faults, fracture planes, tissue components to 100 nm resolution in 3D, the neural connectome, and cell plasma membrane faults. These maps are used to create data-driven computational models to plan, simulate, and direct repairs.

Step 9. **Prethaw and Crackface Fusion** (Section 4.9). The cryopreserved patient is warmed to 223-273 K (-50 °C to 0 °C), producing whole-body tissue reliquidification. During the warming process, thermal stresses in the cryogenic tissue are relaxed, allowing separated crackfaces on either side of ice fractures to be drawn together, closing all crackface voids.

Step 10. **Molecular Extraction** (Section 4.10). Microprobes using pumps with molecularly specific binding sites at their distal termini are inserted from the vasculoid into all tissue cells at a 2-5 μm spacing. Tens of thousands of key fuel, metabolic, intermediate, and other molecules are rapidly extracted from the cells, establishing biochemical stasis throughout the tissues within ~1 hour of reliquidification.[836] The extraction microprobes are then withdrawn from the tissues.

Step 11. **Reseal Plasma Membrane Compartments and Rehydrate** (Section 4.11). Nanorobots are released from the vasculoid to repair all cellular plasma membranes, reseal all compartments against fluid leakage, and rehydrate the cells in part via extracellular water transfers.

Step 12. **Conventional Cellular and Tissue Repair** (Section 4.12). Nanorobots are employed to remove unwanted cells and microbodies, inspect and repair (or replace) existing cells, and then perform various supplemental repair tasks on tissues and neurons.

Step 13. **Patient Warmup and Molecular Instillation** (Section 4.13). The patient is warmed to normal human body temperature (310 K). Microprobes inserted into cells from the vasculoid instill thousands of essential molecules into intracellular cytoplasm and organelles, omitting only those molecules that could restart active metabolism. The microprobes are then withdrawn from the tissues. Molecules capable of restarting metabolism are loaded into storage nanorobots that are parked intracellularly, awaiting a future signal to release their cargoes.

Step 14. **Uninstall Vasculoid and Finish Repairs** (Section 4.14). The vasculoid is rapidly withdrawn from the body and replaced with a temporary blood substitute that includes nanorobots capable of supporting normal metabolic and material transport functions. The patient's metabolism, heartbeat, circulation, and respiration are restarted as key metabolic chemicals are released from the parked storage nanorobots (which are then removed), and final neural repairs are completed. The temporary blood substitute is replaced with manufactured natural blood.

Step 15. **Patient Wakeup** (Section 4.15). Anesthetic agents are removed and the patient awakens to full consciousness.

The remainder of Chapter 4 provides additional details on each of these 15 steps for achieving cryopreservation revival using conventional nanorobots, called "**Plan A**".

Alternative approaches involving a full molecular scan and molecular reconstruction of the cryopatient's body, called "**Plan B**", are presented in Chapter 5.

---

[836] Biochemical degradative processes that would proceed in ~6 minutes (the traditional nondamaging ischemic limit) at the normal human body temperature of 310 K require ~1.8 hours to occur at the pure water-ice melt temperature of 273 K, and even longer at slightly lower temperatures (Section 3.5).

4.1 Macrovascular Scan

The first step of the "Plan A" cryonics revival protocol aims to noninvasively create a coarse 3D map of the entire macroscale vasculature (especially of the brain), including the lymphatics,[837] down to some minimum vessel diameter, which is then used to guide the initial excavation process (Section 4.2). The specific objective is to locate and map the major vasculature down to a size resolution of ~0.1 mm (100 μm), something akin to a noninvasive "digital autopsy".[838]

The available noninvasive vascular scanning methods include:

(1) **Magnetic Resonance Angiography** (Section 4.1.1) uses the techniques of magnetic resonance imaging – which typically include large magnets, radio waves, and flowing blood with or without contrast agents (that cannot easily be injected into cryopatients after they've been cryopreserved) – to create vascular images. This can produce 0.1-mm-resolution 3D images of vasculature in live patients, but with conventional methods there is no signal from frozen tissue (as would obtain in the case of cryopreserved patients). New methods might be able to furnish a detectable signal.

(2) **Computed Tomography Angiography** (Section 4.1.2) uses X-rays to scan a number of virtual planar slices through the patient which are then computationally combined to create 3D vascular images. Conventional CT can provide resolutions of 0.1-0.2 mm (both with and without contrast agent), and synchrotron radiation CT can resolve features down to 0.02-0.1 mm at the cost of higher radiation exposure and other complications. Conventional CT works fine in ice.

(3) **Ultrasound Angiography** (Section 4.1.3) uses ultrasonic acoustic pulses to map internal body structures including blood vessels, by measuring either echoes from interfaces in reflection mode or attenuation through tissues of differing density in transmission mode, with typical feature resolution of 0.5-4 mm in live tissues. Probes placed outside of direct contact with ice cannot see inside the ice, but direct ice-contacting probes should be able to map the interior of iceballs given a sufficient duration of scanning. Intravascular ultrasound typically achieves a feature resolution of 0.15 mm resolution and has the potential to reach 0.1 mm resolution.

(4) **A few other noninvasive scanning techniques** (Section 4.1.4) should also be investigated for possible applicability to cryopatient vascular scanning.

Future research should verify our tentative conclusion that bloodstream and lymphatic vascular scans with feature resolution down to ~0.1 mm in cryopreserved tissues are already available, or are likely to become available in the not-too-distant future; or, if not, should determine the best performance that might become available using the aforementioned or analogous means in the future technological era of nanorobotically-enabled revivals.

---

[837] Freitas RA Jr. Nanomedicine, Volume I: Basic Capabilities, Landes Bioscience, Georgetown TX, 1999, Section 8.2.1.3, "Lymphatic System"; http://www.nanomedicine.com/NMI/8.2.1.3.htm.

[838] https://en.wikipedia.org/wiki/Digital_autopsy.

4.1.1 Magnetic Resonance Angiography

Magnetic resonance imaging (MRI) is a medical imaging technique that uses strong magnetic fields, magnetic field gradients, and radio frequency magnetic fields to generate images of the organs inside the body without the use of ionizing radiation (X-rays) or radioactive tracers. In MRI (image, right), energy from an oscillating magnetic field is applied to a patient at the appropriate resonance frequency, causing excited hydrogen atoms in water molecules to emit a radio frequency signal (measured by a receiving coil) that can be made to encode position information by varying the main magnetic field using gradient coils.[839] Conventional MRI at a 3 tesla field strength[840] provides a volumetric resolution of about ~1 mm^3. Ultra High Field (UHF) MRI using 7 tesla fields in a whole-body scanner has demonstrated feature resolution down to 0.15 mm in post-mortem formalin-fixed[841] entire human brains at room temperature, and the first 10.5 tesla MRI machine became available in 2018.[842] A typical UHF brain image[843] might be acquired in ~6 hours and generate >200 GB of raw data that takes >25 days to process offline using adaptive reconstruction in MATLAB on an advanced server (e.g., 24 CPUs and 128 GB of physical memory). Assuming a 1:20 brain/body length ratio, a whole-body scan of this type might take ~**120 hours**.

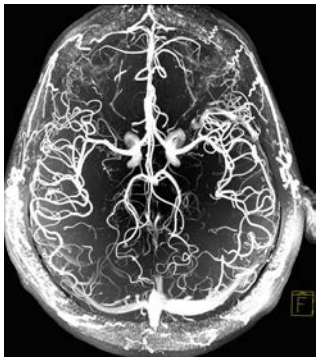

Magnetic resonance angiography (MRA)[844] can obtain images of blood vessels down to ~0.2 mm resolution (image, left)[845] and magnetic resonance microscopy (MRM)[846] routinely produces resolutions better than 0.1 mm,

---

[839] https://en.wikipedia.org/wiki/Magnetic_resonance_imaging.

[840] Edelman RR, Dunkle E, Koktzoglou I, Griffin A, Russell EJ, Ankenbrandt W, Ragin A, Carrillo A. Rapid whole-brain magnetic resonance imaging with isotropic resolution at 3 Tesla. Invest Radiol. 2009 Jan;44(1):54-9; https://www.ncbi.nlm.nih.gov/pubmed/19060723.

[841] Formalin fixation produces a higher gradient echo signal than *in vivo* scans, enabling somewhat higher resolution than unfixed tissue.

[842] "U Scientists Scan World's First 10.5-Tesla Human MRI Image," Center for Magnetic Resonance Research (https://www.cmrr.umn.edu/), Univ. of Minnesota, 28 Feb 2018; https://research.umn.edu/inquiry/post/u-scientists-scan-worlds-first-105-tesla-human-mri-image.

[843] e.g., Yang S, Yang Z, Fischer K, Zhong K, Stadler J, Godenschweger F, *et al*. Integration of Ultra-High Field MRI and Histology for Connectome Based Research of Brain Disorders. Front Neuroanat. 2013;7(31) https://www.ncbi.nlm.nih.gov/pmc/articles/PMC3784919/.

[844] https://en.wikipedia.org/wiki/Magnetic_resonance_angiography.

[845] Stucht D, Danishad KA, Schulze P, Godenschweger F, Zaitsev M, Speck O. Highest Resolution *In Vivo* Human Brain MRI Using Prospective Motion Correction. PLoS One. 2015 Jul; 10(7):e0133921; https://www.ncbi.nlm.nih.gov/pmc/articles/PMC4520483/. 7-tesla MRA image by Jon Polimeni, MGH/HST Martinos Center for Biomedical Imaging; https://i.pinimg.com/originals/bc/34/75/bc3475d32161ad7f322051ac9cc03d52.png.

[846] Alexandra B, Allan JG. Magnetic resonance microscopy. Anal Cell Pathol (Amst). 2012; 35(4):205-227; https://www.ncbi.nlm.nih.gov/pmc/articles/mid/NIHMS420859/.

but both methods usually exploit the flow of blood (e.g., Time-of-Flight MRA) or the injection of contrast agents into the bloodstreams of living patients, neither of which can be employed in cryogenically preserved tissue. Non-contrast-enhanced MRA (NCE -MRA)[847] and even flow-independent non-contrast-enhanced methods are available,[848] most notably using balanced steady state-free precession (bSSFP) imaging,[849] but many of these techniques rely on the difference between the systole and diastole blood signal which will not be present in cryopreserved static brains. Related techniques such as functional MRI (fMRI)[850] and arterial spin labeling (ASL)[851] that rely on the paramagnetic properties of oxygenated and deoxygenated hemoglobin or contrast agents to visualize changing blood flow in a living brain associated with neural activity also are not applicable to cryopreserved brains.

It is generally known that frozen tissues have no perceptible MR signal[852] because the T_2* response[853] of most crystalline solids is too short.[854] Daniel *et al.*[855] found weakening MR signal in frozen liver tissue as

---

[847] Koktzoglou I, Lim RP, Flanagan O, Edelman RR. Non-contrast Enhanced MRA. In Syed MA, Raman SV, Simonetti OP, eds. Basic Principles of Cardiovascular MRI, Springer, 2015, pp. 297-314; https://link.springer.com/chapter/10.1007/978-3-319-22141-0_21.

[848] Tan EJ, Tirukonda P, Tang TY, Chong LR. REACT – Clinical Utility of a Free-Breathing, Non-Gated, Non-Contrast 3D Magnetic Resonance Angiography Technique. ECR 2018 Congress, Poster C-0536; http://dx.doi.org/10.1594/ecr2018/C-0536. Dillman JR, Trout AT, Merrow AC, Moore RA, Rattan MS, Crotty EJ, Fleck RJ, Yoneyama M, Wang H, Tkach JA. Non-contrast three-dimensional gradient recalled echo Dixon-based magnetic resonance angiography/venography in children. Pediatr Radiol. 2019 Mar;49(3):407-414; https://www.ncbi.nlm.nih.gov/pubmed/30406414.

[849] Cukur T, Lee JH, Bangerter NK, Hargreaves BA, Nishimura DG. Non-contrast-enhanced flow-independent peripheral MR angiography with balanced SSFP. Magn Reson Med. 2009 Jun;61(6):1533-9; https://www.ncbi.nlm.nih.gov/pmc/articles/PMC2760085/. Glockner JF, Lee CU. Balanced steady state-free precession (b-SSFP) imaging for MRCP: techniques and applications. Abdom Imaging. 2014 Dec;39(6):1309-22; https://www.ncbi.nlm.nih.gov/pubmed/24811765. Knobloch G, Lauff MT, Hirsch S, Schwenke C, Hamm B, Wagner M. Nonenhanced magnetic resonance angiography (MRA) of the calf arteries at 3 Tesla: intraindividual comparison of 3D flow-dependent subtractive MRA and 2D flow-independent non-subtractive MRA. Eur Radiol. 2016 Dec;26(12):4585-4594; https://www.ncbi.nlm.nih.gov/pubmed/26863895.

[850] https://en.wikipedia.org/wiki/Functional_magnetic_resonance_imaging.
[851] https://en.wikipedia.org/wiki/Arterial_spin_labelling.

[852] Isoda H. Sequential MRI and CT monitoring in cryosurgery--an experimental study in rats. Nihon Igaku Hoshasen Gakkai Zasshi. 1989 Dec 25;49(12):1499-508 (in Japanese); https://www.ncbi.nlm.nih.gov/pubmed/2633129. Rubinsky B, Gilbert JC, Onik GM, Roos MS, Wong ST, Brennan KM. Monitoring cryosurgery in the brain and in the prostate with proton NMR. Cryobiology. 1993 Apr;30(2):191-9; https://www.ncbi.nlm.nih.gov/pubmed/8319488. Gilbert JC, Rubinsky B, Roos MS, Wong ST, Brennan KM. MRI-monitored cryosurgery in the rabbit brain. Magn Reson Imaging. 1993;11(8):1155-64; https://www.ncbi.nlm.nih.gov/pubmed/8271902.

[853] Spin-spin relaxation is the mechanism by which the transverse component of the magnetization vector exponentially decays towards its equilibrium value; T_2 is a time constant characterizing the signal decay, called the spin-spin relaxation time; https://en.wikipedia.org/wiki/Spin–spin_relaxation. In any real NMR experiment, the transverse magnetization decays much faster than would be predicted by natural atomic and molecular mechanisms. This faster rate is denoted as T_2*, which can be considered an "observed" or "effective" T_2, whereas the first T_2 can be considered the "natural" or "true" T_2 of the tissue being imaged; T_2* is always less than or equal to T_2; http://mriquestions.com/t2-vs-t2.html.

[854] Slichter CP. Principles of Magnetic Resonance. 3rd ed., Springer-Verlag, NY, 1992; https://www.amazon.com/dp/0387501576/.

the material was cooled below 0 °C (273 K), reaching zero signal at -34 °C (239 K) and on down to -130 °C (143 K) (image, right). This is consistent with the authors' conclusion that the weak MR signal from incompletely frozen tissue arises from excluded liquid-phase protons and that the volume of liquid-phase protons decreases with decreasing temperature.

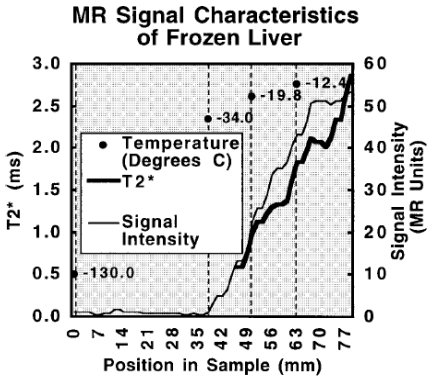

As the primary authors explain:[856] "There are three water compartments in biological tissues: free water, hydration water, and crystalline water. Free water has the same behavior as bulk water. Crystalline water is tightly bound to macromolecular structure, while hydration water is associated with macromolecules but is more loosely bound. The transverse relaxation times of these water compartments are very different (crystalline ~10 μs, hydration ~10 ms, and free water ~100 ms). The effective relaxation time of the hydration water is shortened by spin-spin exchange with crystalline water. Free water freezes at the temperature expected from its solute concentration. Water molecules close to the hydrophilic surface of tissue require more energy to remove them and so have a lower freezing point. The observable MR signal in frozen tissue comes primarily from unfrozen hydration water. Crystalline water and frozen free water do not contribute to the observed MR signal even with a UTE [Ultrashort Echo Time] sequence with a TE [echo time] of 100 μs because their T_2 values are too short. The decrease in the fraction of hydration water that is not frozen during tissue freezing results in a temperature-dependent reduction in equilibrium nuclear magnetization as the tissue temperature is decreased. The T_2 of the MR signal in the frozen tissue is further shortened by the field inhomogeneity created by the difference in the susceptibilities of liquid- and solid-phase water in a heterogeneous system as well as nonzero dipolar interactions. These effects decrease T_2 and T_2* as the temperature of frozen tissue is lowered....T_1 has also been demonstrated to change with temperature in *ex vivo* frozen tissue sample experiments at different frequencies."

The coldest temperature from which MR signal has been reliably measured from frozen tissue is apparently about -40 °C (233 K).[857] Cryopreserved tissue is normally stored at liquid nitrogen (LN2) temperature (-196 °C, 77 K), and intermediate temperature storage between -120 °C (153 K) and -130 °C (143 K) has been proposed,[858] both of which are far colder than the temperatures at which an MR signal can currently be measured. It might be possible to slowly warm cryopreserved tissue until some MR signal appears, but the creation of numerous randomly-located microscale liquid phase regions, however temporary, might

---

[855] Daniel BL, Butts K, Block WF. Magnetic resonance imaging of frozen tissues: temperature-dependent MR signal characteristics and relevance for MR monitoring of cryosurgery. Magn Reson Med. 1999 Mar;41(3):627-30; https://onlinelibrary.wiley.com/doi/pdf/10.1002/(SICI)1522-2594(199903)41:3%3C627::AID-MRM28%3E3.0.CO;2-Q. See also: Wansapura JP, Daniel BL, Vigen KK, Butts K. *In vivo* MR thermometry of frozen tissue using R2* and signal intensity. Acad Radiol. 2005 Sep;12(9):1080-4; https://www.ncbi.nlm.nih.gov/pubmed/16112510. Kaye EA, Josan S, Lu A, Rosenberg J, Daniel BL, Pauly KB. Consistency of signal intensity and T2* in frozen *ex vivo* heart muscle, kidney, and liver tissue. J Magn Reson Imaging. 2010 Mar;31(3):719-24; https://www.ncbi.nlm.nih.gov/pmc/articles/PMC2832094/. Lu A, Daniel BL, Kaye E, Butts Pauly K. MRI of frozen tissue demonstrates a phase shift. Magn Reson Med. 2011 Dec;66(6):1582-9; https://www.ncbi.nlm.nih.gov/pmc/articles/PMC3166360/.

[856] Lu A, Daniel BL, Pauly KB. Chapter 33. Ultrashort TE Imaging of Cryotherapy. In: Bydder GM, Fullerton GD, Young IR, eds. MRI of Tissues with Short T2s or T2*s. Wiley, 2013; https://books.google.com/books?id=1bPM7YF-DLoC&pg=PT862.

[857] Overduin CG, Fütterer JJ, Scheenen TW. 3D MR thermometry of frozen tissue: Feasibility and accuracy during cryoablation at 3T. J Magn Reson Imaging. 2016 Dec;44(6):1572-1579; https://www.ncbi.nlm.nih.gov/pubmed/27160336.

[858] Wowk B. Systems for intermediate temperature storage for fracture reduction and avoidance. Cryonics 2011 Qtr 3; https://www.alcor.org/library/systems-for-intermediate-temperature-storage-for-fracture-reduction-and-avoidance/.

allow biologically damaging chemical reactions or structural rearrangements to occur and thus seems inadvisable from a strict information-theoretic[859] (Section 2.1.1) perspective.

There has been recent interest in employing hyperpolarized ^{13}C in biomolecules[860] or in nanodiamonds[861] that could produce an MRI signal at cryogenic temperatures. However, these special molecules would need to be prepositioned in the patient's vasculature prior to cryopreservation, perhaps by adding them in nanoparticulate form to the cryosuspension fluids during the perfusion process prior to cooldown, hence this method would not apply to existing cryopreserved patients or to future patients preserved using existing cryoprotectants that lack these additives.

UTE signal measurement is currently limited to about 100 μs.[862] If nanotechnology-based fast-response rf emitters and receivers, or some other means, could be employed to obtain pulse and detection times below 10 μs, then a ***future research*** project could explore whether it might be possible to detect MR signal from hard-frozen tissue. If some signal could be detected, MRI scans of cryopreserved brains could be extended to **2 weeks** or even longer (vs. current MRI scan times limited to 1-2 hours due to considerations of live patient comfort), improving the signal-to-noise ratio and potentially increasing the conventional achievable MRI resolution by approximately tenfold.[863]

If frozen tissues of various types are found to differ sufficiently in mechanical stiffness, it might be possible to obtain 3D vascular data using magnetic resonance elastography.[864]

The possibility of detecting an MR signal from cryogenic-temperature vitrification solutions[865] that might mostly fill the vasculature of a cryopreserved brain should also be investigated in ***future research***.

MRI scans typically cost $300-$700/hour in research institutions.[866]

---

[859] Merkle RC. The technical feasibility of cryonics. Med Hypotheses. 1992 Sep;39(1):6-16; https://www.ncbi.nlm.nih.gov/pubmed/1435395.

[860] Siddiqui S, Kadlecek S, Pourfathi M, Xin Y, Mannherz W, Hamedani H, Drachman N, Ruppert K, Clapp J, Rizi R. The use of hyperpolarized carbon-13 magnetic resonance for molecular imaging. Adv Drug Deliv Rev. 2017 Apr;113:3-23; https://www.ncbi.nlm.nih.gov/pmc/articles/PMC5783573/.

[861] Hyperdiamond Project, European Union Horizon 2020 programme, No. 667192, 2019; https://www.hyperdiamond-project.eu/page/en/about-the-project/state-of-the-art-ndash-background.php.

[862] Zhu A, Hernando D, Johnson KM, Reeder SB. Characterizing a short T2* signal component in the liver using ultrashort TE chemical shift-encoded MRI at 1.5T and 3.0T. Magn Reson Med. 2019 Dec;82(6):2032-2045; https://www.ncbi.nlm.nih.gov/pubmed/31270858.

[863] The standard deviation of a series of independent measurements of a noisy variable is proportional to the inverse square root of the number of observations (https://en.wikipedia.org/wiki/Standard_deviation). Maximum scan resolution as a function of total scan time t_{scan} should therefore approximate $\sim t_{scan}^{-1/2}$ if the number of observations per second is constant, whereupon the improvement in scan resolution to be achieved by increasing t_{scan} from 2 hours ($\sim 10^4$ sec) to 2 weeks ($\sim 10^6$ sec) should be a factor of $\sim (10^6)^{1/2} / (10^4)^{1/2} \sim 10$.

[864] "Magnetic resonance elastography (MRE) is a non-invasive medical imaging technique that measures the stiffness of soft tissues by generating shear waves in tissue, imaging their propagation using MRI, and processing the images to generate a stiffness map (elastogram)." https://en.wikipedia.org/wiki/Magnetic_resonance_elastography.

[865] e.g., M22: Fahy GM, Wowk B, Wu J, Phan J, Rasch C, Chang A, Zendejas E. Cryopreservation of organs by vitrification: perspectives and recent advances. Cryobiology. 2004 Apr;48(2):157-78; http://www.21cm.com/pdfs/cryopreservation_advances.pdf.

[866] Yale University Magnetic Resonance Research Center, usage Charges, 1 Jul 2020; https://medicine.yale.edu/mrrc/users/charges/. Brigham and Women's Hospital, BWH Research Imaging Core Pricing, Nov 2020; https://www.brighamandwomens.org/radiology/research-imaging-core/pricing.

4.1.2 Computed Tomography Angiography

Computed tomography (CT) (aka. Computerized Axial Tomography or CAT) scanning[867] is a medical imaging technique in which X-ray measurements[868] taken from many different angles are computationally combined to produce cross-sectional "tomographic" images (virtual "slices") of specific areas of a scanned object. A motorized table moves the patient through the CT imaging system (image, below).[869] Digital processing allows visualizing a complete 3D volume of the inside of the object from a large series of two-dimensional radiographic images taken around a single axis of rotation. Features can be distinguished based on the differing abilities of various tissues to absorb X-rays. CT has become the diagnostic modality of choice for head trauma due to its accuracy, reliability, safety, and wide availability.[870]

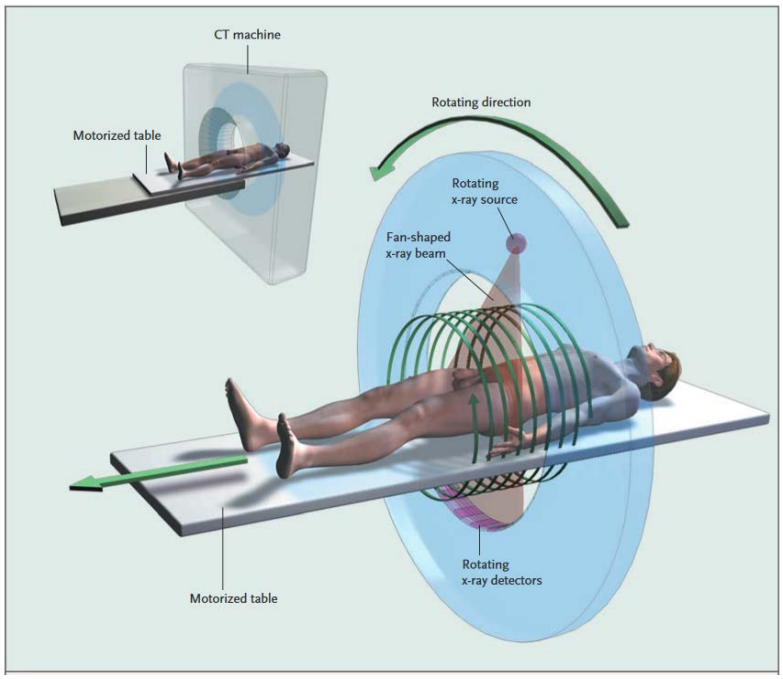

Computed tomography angiography (aka. CT angiography or CTA)[871] often employs radiocontrast agents (usually iodine-based) injected into the blood vessels of a living patient to visualize blockages, aneurysms (dilations of walls), dissections (tearing of walls), and stenoses (narrowing of vessels) in the vasculature of the heart,[872] the aorta and other large blood vessels, and in the major arteries of the lungs, the

---

[867] https://en.wikipedia.org/wiki/CT_scan.

[868] Other types of non-X-ray CT exist, such as Positron Emission Tomography or PET (https://en.wikipedia.org/wiki/Positron_emission_tomography) and Single-Photon Emission Computed Tomography or SPECT (https://en.wikipedia.org/wiki/Single-photon_emission_computed_tomography), both of which provide only 4-10 mm spatial resolution and require injection of radionuclide-containing material into the bloodstream of living patients in order to perform the scan, hence are inapplicable to the vascular scanning of cryopreserved patients.

[869] Brenner DJ, Hall EJ. Computed tomography--an increasing source of radiation exposure. N Engl J Med. 2007 Nov 29;357(22):2277-84; http://www.members.tripod.com/enotes/CT_radiation2007.pdf.

[870] https://en.wikipedia.org/wiki/Computed_tomography_of_the_head.
[871] https://en.wikipedia.org/wiki/Computed_tomography_angiography.
[872] https://en.wikipedia.org/wiki/Coronary_CT_angiography.

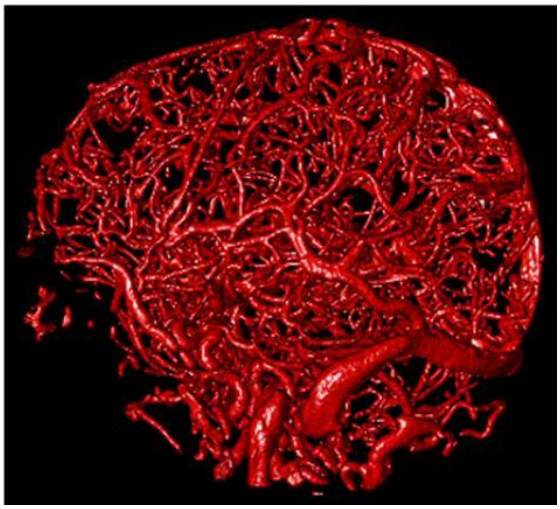

kidneys, the head and neck, and the arms and legs, as small as 1 mm in diameter.[873] By 2003, multidetector scanners used in Multislice Computed Tomography (MSCT) were available with up to 16 axial slices per rotation which allowed, for example, the entire heart to be covered in a single breath-hold with a slice thickness (spatial resolution) of ~1 mm.[874] Current CT scanners have a spatial resolution of 0.35-0.625 mm,[875] and can distinguish tissues whose densities differ by less than 1%.[876] Flat-panel volume CT scanners can achieve an isotropic spatial resolution of 0.2-0.3 mm and can allow visualizing a contrast difference of as few as 5 Hounsfield Units (HU) without difficulty.[877] (For comparison, soft tissue in vascular walls typically has 100-300 HU, compared to water at 0 HU, unclotted blood at 13-50 HU, clotted blood at 50-75 HU, and bone at 300-1900 HU.[878]) The image above is a 3D rendering of CT angiography data for the brain of a living human patient, acquired using a 320-row Toshiba CT scanner after injection of contrast agent, then computer-processed using custom vessel segmentation detection software in a pattern recognition framework with a voxel spacing of 0.43 mm and a method that "emphasizes completeness over accuracy in defining the vessel boundaries".[879]

Unlike MRI, CT scans employ ionizing radiation that can potentially damage biological materials. Will heavy doses of X-rays from lengthy scans impose unacceptable damage to DNA or other frozen cellular substructures within a cryopreserved patient? CT scans often have 100-1000 times higher doses than the lowest-dose conventional X-ray techniques,[880] but the estimated lifetime cancer mortality risk from an

---

[873] Kumamaru KK, Hoppel BE, Mather RT, Rybicki FJ. CT angiography: current technology and clinical use. Radiol Clin North Am. 2010 Mar;48(2):213-35; https://www.ncbi.nlm.nih.gov/pmc/articles/PMC2901244/.

[874] Peebles CR. Non-invasive coronary imaging: computed tomography or magnetic resonance imaging? Heart. 2003 Jun;89(6):591-4; https://www.ncbi.nlm.nih.gov/pmc/articles/PMC1767702/.

[875] Lin E, Alessio A. What are the basic concepts of temporal, contrast, and spatial resolution in cardiac CT? J Cardiovasc Comput Tomogr. 2009 Nov-Dec;3(6):403-8; https://www.ncbi.nlm.nih.gov/pmc/articles/PMC4752333/. Otero HJ, Steigner ML, Rybicki FJ. The "post-64" era of coronary CT angiography: understanding new technology from physical principles. Radiol Clin North Am. 2009 Jan;47(1):79-90; https://www.ncbi.nlm.nih.gov/pmc/articles/PMC2893874/.

[876] https://en.wikipedia.org/wiki/CT_scan#Advantages.

[877] Gupta R, Cheung AC, Bartling SH, Lisauskas J, Grasruck M, Leidecker C, Schmidt B, Flohr T, Brady TJ. Flat-panel volume CT: fundamental principles, technology, and applications. Radiographics. 2008 Nov-Dec;28(7):2009-22; https://pubs.rsna.org/doi/full/10.1148/rg.287085004.

[878] https://en.wikipedia.org/wiki/Hounsfield_scale.

[879] Meijs M, Patel A, van de Leemput SC, Prokop M, van Dijk EJ, de Leeuw FE, Meijer FJA, van Ginneken B, Manniesing R. Robust Segmentation of the Full Cerebral Vasculature in 4D CT of Suspected Stroke Patients. Sci Rep. 2017 Nov 15;7(1):15622; https://www.ncbi.nlm.nih.gov/pmc/articles/PMC5688074/.

[880] Brenner DJ, Hall EJ. Computed tomography--an increasing source of radiation exposure. N Engl J Med. 2007 Nov 29;357(22):2277-84; http://www.members.tripod.com/enotes/CT_radiation2007.pdf.

abdominal CT on a 1-year-old patient is only 0.1% or 1:1000 scans.[881] This suggests that CT scans on cryopreserved patients could probably be safely extended in total dose by at least several orders of magnitude beyond the doses employed in conventional scans before any kind of "irreparable" harm could occur to a cryopatient for whom the conventional cell repair (Chapter 4) revival protocol is available. Typical CT scans take 15-60 minutes to complete. Assuming applied X-ray dosage is linear with exposure time, then using the previous methodology a 1000-fold longer scan time (**250-1000 hr**) might allow a 32-fold improvement in achievable spatial resolution.[882] Alternatively, the higher dosage might partially or wholly compensate for the lack of contrast enhancement (~linearly proportional to contrast agent concentration)[883] that would normally be provided by an iodinated contrast agent injected into the bloodstreams of living patients but will be absent in the case of cryopreserved patients. The degree of such resolution and contrast compensation and the maximum tolerable scan times for cryopreserved tissue are appropriate subjects for ***future research***.

A standard rule of thumb is that the necessary X-ray dose needed to preserve a fixed signal-to-noise ratio in a CT scan voxel when scanning an object of fixed size varies inversely with the fourth power of voxel linear dimension.[884] This requirement is not machine-specific or X-ray source-specific but is a direct result of the necessary mathematics for CT image reconstruction and assumed perfect detection of all X-ray photons successfully passing through the object.

A related but non-tomographic technique called **synchrotron radiation microangiography**[885] uses monochromatic X-rays, a high-definition video system, and nonionic contrast media to provide 2D images of small collateral arteries with diameters of 0.03-0.1 mm. Synchrotron radiation (SR) based micro-computed tomography with contrast agent regularly images microvessels to a resolution of 0.020-0.030 mm in microsectioned tissue samples,[886] but SR has also produced 3D images of the microvasculature of

---

[881] Furlow B. Radiation dose in computed tomography. Radiol Technol. 2010 May-Jun;81(5):437-50; https://www.ncbi.nlm.nih.gov/pubmed/20445138.

[882] Using the ~$t_{scan}^{-1/2}$ estimation method (Section 4.1.1), the improvement in scan resolution to be achieved by increasing available scan time from 1 time unit to 1000 time units should be a factor of ~ $(1000)^{1/2}$ / $(1)^{1/2}$ ~ 32.

[883] Murphy DJ, Aghayev A, Steigner ML. Vascular CT and MRI: a practical guide to imaging protocols. Insights Imaging. 2018 Apr;9(2):215-236; https://www.ncbi.nlm.nih.gov/pmc/articles/PMC5893493/.

[884] Ford NL, Thornton MM, Holdsworth DW. Fundamental image quality limits for microcomputed tomography in small animals. Med Phys. 2003 Nov;30(11):2869-77; https://pubmed.ncbi.nlm.nih.gov/14655933/.

[885] Takeshita S, Isshiki T, Mori H, Tanaka E, Eto K, Miyazawa Y, Tanaka A, Shinozaki Y, Hyodo K, Ando M, Kubota M, Tanioka K, Umetani K, Ochiai M, Sato T, Miyashita H. Use of synchrotron radiation microangiography to assess development of small collateral arteries in a rat model of hindlimb ischemia. Circulation. 1997 Feb 18;95(4):805-8; https://www.ahajournals.org/doi/full/10.1161/01.cir.95.4.805.

[886] Gu S, Xue J, Xi Y, Tang R, Jin W, Chen JJ, Zhang X, Shao ZM, Wu J. Evaluating the effect of Avastin on breast cancer angiogenesis using synchrotron radiation. Quant Imaging Med Surg. 2019 Mar;9(3):418-426; https://www.ncbi.nlm.nih.gov/pmc/articles/PMC6462576/.

various animal organs *in vivo* at similar resolution within intact animals.[887] SR microangiography[888] in live mice to 0.020 mm resolution typically requires X-ray dosages of ~3 mGy per image[889] with 50 msec exposure times. ***Future research*** should assess whether such high image resolutions can be achieved without the use of contrast agent, which would not be available in the case of cryopreserved patients. Also, sources of synchrotron radiation (image, right)[890] are typically very large and specialized, such as nuclear particle accelerators or storage rings.[891]

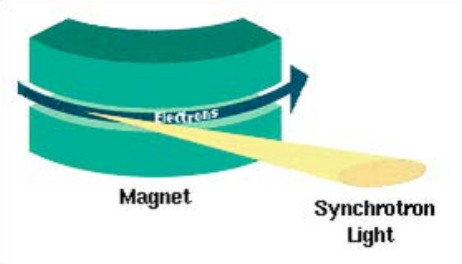

Modern MSCT or **Multi Detector Computed Tomography** (MDCT) machines may generate 64-640 slices per scan and by 2018 could obtain slice thicknesses of ~0.1 mm in high-resolution bone images even without intravenously administered iodinated contrast agent.[892] Contrast-free **high-resolution X-ray microtomography** (micro-CT) scans have not yet been performed on cryopreserved human tissue at cryogenic temperatures, but the image below of a similarly solid and hard material (a fossilized embryo) shows a 3D tomographic reconstruction created using synchrotron-radiation X-ray tomographic microscopy (SRXTM).[893] No contrast agent was used and the 10 μm scale bar indicates that nonvascular

---

[887] Shirai M, Schwenke DO, Eppel GA, Evans RG, Edgley AJ, Tsuchimochi H, Umetani K, Pearson JT. Synchrotron-based angiography for investigation of the regulation of vasomotor function in the microcirculation *in vivo*. Clin Exp Pharmacol Physiol 2009 Jan;36(1):107-16; https://www.ncbi.nlm.nih.gov/pubmed/18986322. Liu P, Sun J, Zhao J, Liu X, Gu X, Li J, Xiao T, Xu LX. Microvascular imaging using synchrotron radiation. J Synchrotron Radiat 2010 Jul;17(4):517-21; https://www.ncbi.nlm.nih.gov/pubmed/20567084. Liu X, Zhao J, Sun J, Gu X, Xiao T, Liu P, Xu LX. Lung cancer and angiogenesis imaging using synchrotron radiation. Phys Med Biol 2010 Apr 21;55:2399-409; https://www.ncbi.nlm.nih.gov/pubmed/20360634. Shirai M, Schwenke DO, Tsuchimochi H, Umetani K, Yagi N, Pearson JT. Synchrotron radiation imaging for advancing our understanding of cardiovascular function. Circ Res 2013 Jan 4;112(1):209-21; http://citeseerx.ist.psu.edu/viewdoc/download?doi=10.1.1.975.256&rep=rep1&type=pdf. Zhang M, Peng G, Sun D, Xie Y, Xia J, Long H, Hu K, Xiao B. Synchrotron radiation imaging is a powerful tool to image brain microvasculature. Med Phys 2014;41(3):031907; https://aapm.onlinelibrary.wiley.com/doi/pdf/10.1118/1.4865784.

[888] Torii M, Fukui T, Inoue M, Kanao S, Umetani K, Shirai M, Inagaki T, Tsuchimochi H, Pearson JT, Toi M. Analysis of the microvascular morphology and hemodynamics of breast cancer in mice using SPring-8 synchrotron radiation microangiography. J Synchrotron Radiat. 2017 Sep 1;24(Pt 5):1039-1047; https://www.ncbi.nlm.nih.gov/pmc/articles/PMC5580789/.

[889] Radiation doses (1 Gy = 1 joule of absorbed ionizing radiation per kg of tissue; https://en.wikipedia.org/wiki/Gray_(unit)) in humans have ~10% mortality at 2 Gy, ~50% at 3 Gy, and ~80% at 4 Gy; https://en.wikipedia.org/wiki/Acute_radiation_syndrome#Cause. If a cryopreserved patient can tolerate radiation damage from SR scans equivalent to ~50% mortality for a living person, then ~1000 SR images at 3 mGy/image could be collected during the scanning process.

[890] https://en.wikipedia.org/wiki/Synchrotron_radiation.
[891] https://en.wikipedia.org/wiki/Synchrotron_light_source.

[892] De Foer B, Wuyts L, Bernaerts A, van Dinther J, Offeciers E, Casselman JW. Chapter 6. Temporal Bone Tumors. In: Chong V, ed. Skull Base Imaging, Elsevier, 2018, pp. 99-143; https://www.sciencedirect.com/science/article/pii/B9780323485630000064. Summary in https://www.sciencedirect.com/topics/medicine-and-dentistry/multidetector-computed-tomography.

[893] Donoghue PC, Bengtson S, Dong XP, Gostling NJ, Huldtgren T, Cunningham JA, Yin C, Yue Z, Peng F, Stampanoni M. Synchrotron X-ray tomographic microscopy of fossil embryos. Nature. 2006 Aug 10;442(7103):680-683; https://seis.bristol.ac.uk/~jc1224/Publications/assets/Donoghue_et_al_2006b.pdf.

cellular features crudely resembling capillary tubes are clearly resolved at the 2-5 μm size scale; synchrotron μCT can reach ~1 μm^3 voxels.[894]

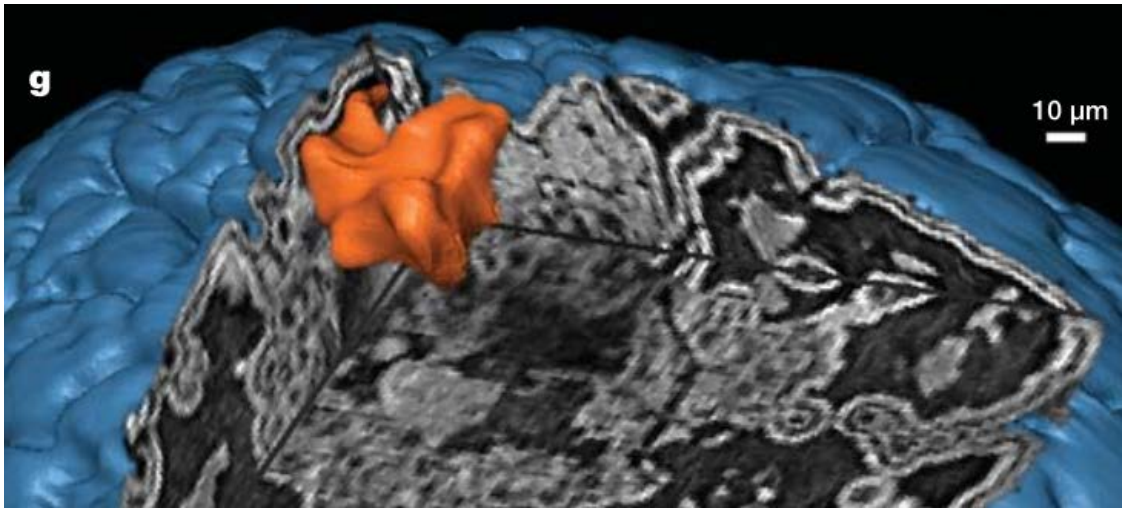

Micro CT machines employ amazingly small voxel sizes because they are imaging very small objects, like rodents. There appear to be no theoretical obstacles to building a micro CT machine that can image a cryopreserved human body at 0.1 mm resolution. However, Brian Wowk[895] notes that the laws of physics will unavoidably require a dose on the order of 10,000 times the ~1 centigray typical whole body medical CT dose with a ~1 mm voxel size, or ~100 Gray. This is about 200 times the lethal dose by contemporary medical criteria (cf. Section 3.5), though perhaps not that much of a concern relative to the nanomedical repair task of a badly cryoinjured patient. Says Wowk: "An order-of-magnitude reduction in dose might be possible with improved detector quantum efficiencies, but the fourth-power law remains, as does the general conclusion that the doses required for high resolution CT imaging inside large objects are quite large."

Other forms of CT scans also require no contrast agents (aka. **Non-contrast-Enhanced CT**, or **NECT**), such as coronary calcium scans,[896] non-contrast-enhanced urography,[897] scans for abdominal cancers (though venous thrombosis can be missed),[898] screens for abdominal aortic aneurysms,[899] and first-pass

---

[894] Dyer EL, Gray Roncal W, Prasad JA, Fernandes HL, Gürsoy D, De Andrade V, Fezzaa K, Xiao X, Vogelstein JT, Jacobsen C, Körding KP, Kasthuri N. Quantifying Mesoscale Neuroanatomy Using X-Ray Microtomography. eNeuro. 2017 Sep-Oct 16;4(5); https://www.ncbi.nlm.nih.gov/pmc/articles/PMC5659258/.

[895] Personal communication from Brian Wowk to Robert Freitas, 30 Sep 2021.

[896] https://en.wikipedia.org/wiki/Coronary_CT_calcium_scan.

[897] Smith RC, Rosenfield AT, Choe KA, Essenmacher KR, Verga M, Glickman MG, Lange RC. Acute flank pain: comparison of non-contrast-enhanced CT and intravenous urography. Radiology. 1995 Mar;194(3):789-94; https://www.ncbi.nlm.nih.gov/pubmed/7862980.

[898] Semaan H, Bazerbashi MF, Siesel G, Aldinger P, Obri T. Diagnostic accuracy of non-contrast abdominal CT scans performed as follow-up for patients with an established cancer diagnosis: a retrospective study. Acta Oncol. 2018 Mar;57(3):426-430; https://www.tandfonline.com/doi/pdf/10.1080/0284186X.2017.1360512.

[899] Liisberg M, Diederichsen AC, Lindholt JS. Abdominal ultrasound-scanning versus non-contrast computed tomography as screening method for abdominal aortic aneurysm - a validation study from the randomized DANCAVAS study. BMC Med Imaging. 2017 Feb 14;17(1):14; https://core.ac.uk/download/pdf/50624310.pdf.

imaging scans for brain tumors.[900] This is convenient because contrast agents will generally not be available in the vasculature of the cryopreserved patient unless they were placed there during perfusion prior to cooldown.

NECT has been demonstrated to provide images of structures inside frozen human tissue at least since the 1990s,[901] and was the method of choice for nondestructive scanning of the prehistoric frozen "Iceman".[902] CT scanners can distinguish between CT tissues with and without cryoprotectant,[903] and can distinguish tissues having CT densities differing by less than 1%.[904] (In comparison to pure water, the CT density of the white matter of the brain is 2% greater, gray matter is 4% greater, and cryopreserved tissue with target concentrations of M22 cryoprotectant solution is 26% greater.[905])

Over the last several years Alcor has acquired numerous low-resolution NECT scans of cryopreserved patients' brains (e.g., image, right, of one scan slice),[906] showing almost no ice (blue) and decent saturation levels of cryoprotectant (green, purple, and orange). As of 2021, none of these datasets had been computer-processed to extract vascular segmentation data or to compile a proper 3D vascular map. Doing so could be a useful ***future research*** project.

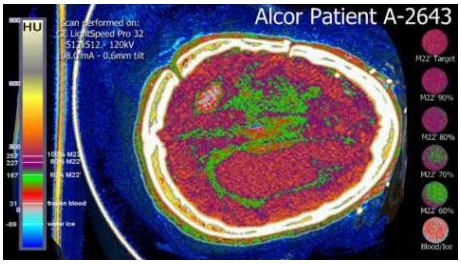

In the past several years, Alcor has introduced CT scanning for neuro patients using a CT scanner, purchased with donated funds, at an external imaging center. This capability will enable Alcor "to do CT scans not only after cooling but prior to surgical procedures for perfusion."[907] Alcor is pursuing its own in-house scanning capabilities to scan all patients but as of 2021 this was still a work in progress.

---

[900] "Brain Tumor," American Society of Neuroradiology, 2012-17; https://www.asnr.org/patientinfo/conditions/brain_tumor.shtml. Minné C, Kisansa ME, Ebrahim N, Suleman FE, Makhanya NZ. The prevalence of undiagnosed abnormalities on non-contrast-enhanced computed tomography compared to contrast-enhanced computed tomography of the brain. S Afr J Rad. 2014;18(1); http://www.scielo.org.za/scielo.php?script=sci_arttext&pid=S2078-67782014000100008.

[901] Saliken JC, McKinnon JG, Gray R. CT for Monitoring Cryotherapy. AJR Am J Roentgenol. 1996 Apr;166(4):853-5; https://www.ajronline.org/doi/pdfplus/10.2214/ajr.166.4.8610562.

[902] Murphy WA Jr, Nedden Dz Dz, Gostner P, Knapp R, Recheis W, Seidler H. The iceman: discovery and imaging. Radiology. 2003 Mar;226(3):614-29; https://www.researchgate.net/profile/Seidler_Horst/publication/10887853_The_Iceman_Discovery_and_Imaging1/links/55fa510d08aec948c4a472b2.pdf.

[903] Bischof JC, Mahr B, Choi JH, Behling M, Mewes D. Use of X-ray tomography to map crystalline and amorphous phases in frozen biomaterials. Ann Biomed Eng. 2007 Feb;35(2):292-304; https://www.ncbi.nlm.nih.gov/pubmed/17136446.

[904] https://en.wikipedia.org/wiki/CT_scan#Advantages.

[905] https://www.alcor.org/Library/html/CTcalibration.html.

[906] "Post Cryopreservation CT Scan for Alcor Case A-2643," Cryonics, Mar 2014; 35(3):15-21; https://www.alcor.org/library/complete-list-of-alcor-cryopreservations/ct-scan-a-2643/.

[907] "Q&A with Max More, Ph.D.," Cryonics 2020 Qtr 3; 41(3):11-14; https://www.alcor.org/docs/cryonics-magazine-2020-03.pdf.

4.1.3 Ultrasound Angiography

Ultrasound imaging (aka. medical ultrasound, diagnostic sonography, ultrasonography, or US scanning)[908] is a medical imaging technique in which sound waves with frequencies higher than those audible to humans (>20 KHz) are used to create an image of internal body structures such as tendons, muscles, joints, blood vessels, and internal organs, usually with the aim to identify a source of a disease, to exclude pathology, or to monitor a developing fetus (i.e., obstetric ultrasound[909]). Ultrasonic images are made by sending pulses of ultrasound into tissue using a probe, whereupon the pulses echo off tissues with different reflection properties and are recorded and displayed as an image. Sonograms can display many different kinds of useful information, including brightness (the acoustic impedance of a 2D cross-section of tissue), blood flow, motion of tissue over time, the location of blood, the presence of specific molecules, the stiffness of tissue, or the anatomy of a three-dimensional region.[910]

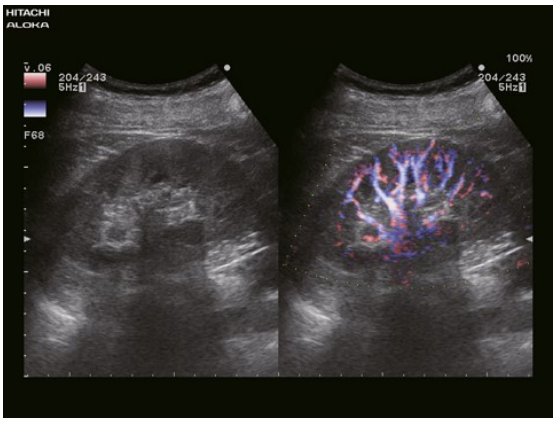

Conventional vascular ultrasound most often relies upon the Doppler effect[911] in fluids moving inside a live patient's body, which is useless for cryopreserved patients whose tissues and fluids are entirely solid. For example, Transcranial Doppler (TCD)[912] and cranial ultrasound[913] measure the velocity of blood flow through the brain's vasculature, Doppler echocardiography[914] measures the direction of blood flow and the velocity of both blood and cardiac tissue in the heart at a spatial resolution of ~0.5-2.0 mm,[915] and renal ultrasonography[916] uses Doppler data to measure blood flow in the kidneys. The image at left shows large blood vessel ultrasound imaging using the Hitachi directional eFLOW high-definition blood flow imaging mode.[917] Contrast agent (microbubbles) can also enhance the resolution of vascular sonography[918] (e.g., image below, right),[919] but it is not possible to inject contrast agent into cryopreserved tissue without first thawing the tissue.

---

[908] https://en.wikipedia.org/wiki/Medical_ultrasound.
[909] https://en.wikipedia.org/wiki/Obstetric_ultrasonography.

[910] Zhou Z, Wu W, Wu S, Jia K, Tsui PH. A Review of Ultrasound Tissue Characterization with Mean Scatterer Spacing. Ultrason Imaging. 2017 Sep;39(5):263-282; https://www.ncbi.nlm.nih.gov/pubmed/28797220.

[911] The Doppler effect is the change in frequency of a wave as detected by an observer who is in motion relative to the source; https://en.wikipedia.org/wiki/Doppler_effect.

[912] https://en.wikipedia.org/wiki/Transcranial_Doppler.
[913] https://en.wikipedia.org/wiki/Cranial_ultrasound.
[914] https://en.wikipedia.org/wiki/Doppler_echocardiography.

[915] Nissen SE, Yock P. Intravascular ultrasound: novel pathophysiological insights and current clinical applications. Circulation. 2001 Jan 30;103(4):604-16; https://www.ncbi.nlm.nih.gov/pubmed/11157729/.

[916] https://en.wikipedia.org/wiki/Renal_ultrasonography.

[917] "eFLOW - New High-definition Blood Flow Imaging Mode," © 2019 Hitachi Medical Systems Holding; http://www.hitachi-medical-systems.eu/products-and-services/ultrasound/technologies/eflow.html.

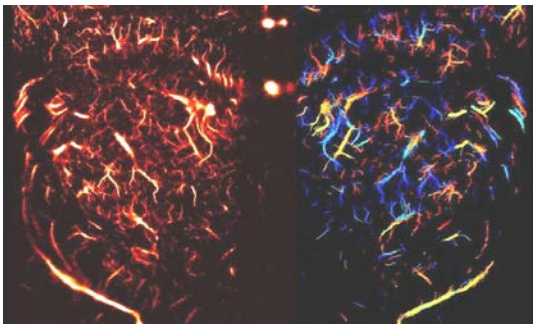

The 1-18 MHz frequencies typically used in medical ultrasound[920] equate to acoustic wavelengths (e.g., ~maximum spatial resolution) of 4-0.2 mm, given the 3940 m/sec speed of sound in bubble-free ice at ~210 K.[921] (Higher frequencies have exponentially worse attenuation and lower range in frozen tissue.) In sonography, the sound wave is partially reflected from the layers between different tissues or is scattered from smaller structures, wherever there are acoustic impedance changes at interfaces between two different kinds of material. However, the acoustic energy reflected from a wide variety of soft tissue and aqueous interfaces is ~1% or less,[922] so these interfaces (such as those defining vascular walls) will likely be very hard to distinguish in a sonograph of frozen tissue.

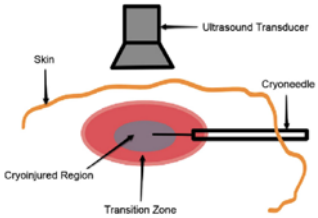

Virtually all attempts at sonographic visualization of frozen tissue have assumed that the acoustic transceiver is not in direct contact with the ice. Most notably, sonographic cryosurgery[923] employs ultrasound to monitor the exterior extent of an iceball created inside a block of unfrozen tissue near the tip of a cold probe inserted into the tissue, but the ultrasound transducer is not in direct contact with the ice (image, left).[924]

A common observation in this situation is that "cryotherapy performed under sonographic guidance is often unsatisfactory because sonography is unable to image beyond the near edge of ice, which reflects 99% of

---

[918] Pfister K, Schierling W, Jung EM, Apfelbeck H, Hennersperger C, Kasprzak PM. Standardized 2D ultrasound versus 3D/4D ultrasound and image fusion for measurement of aortic aneurysm diameter in follow-up after EVAR. Clin Hemorheol Microcirc. 2016;62(3):249-60; https://www.ncbi.nlm.nih.gov/pubmed/26484714.

[919] Bob Yirka, "New way to use ultrasound allows for imaging live blood vessels with more clarity," Medical Xpress, 26 Nov 2015; https://medicalxpress.com/news/2015-11-ultrasound-imaging-blood-vessels-clarity.html.

[920] https://en.wikipedia.org/wiki/Medical_ultrasound#Sound_in_the_body.

[921] Vogt C, Laihem K, Wiebusch C. Speed of sound in bubble-free ice. J Acoust Soc Am. 2008 Dec;124(6):3613-8; https://www.researchgate.net/publication/23997391_Speed_of_sound_in_bubble-free_ice. The speed of sound in vitrified tissue will be slightly different from this number.

[922] Freitas RA Jr. Nanomedicine, Volume I: Basic Capabilities, Landes Bioscience, Georgetown TX, 1999, Table 6.6, "Acoustic Energy Reflected and Transmitted at Various Tissue Interfaces"; http://www.nanomedicine.com/NMI/Tables/6.6.jpg.

[923] Onik G, Kane R, Steele G, McDermott W, Khettry U, Cady B, Jenkins R, Katz J, Clouse M, Rubinsky B, *et al*. Monitoring hepatic cryosurgery with sonography. AJR Am J Roentgenol. 1986 Oct;147(4):665-9; https://www.ncbi.nlm.nih.gov/pubmed/3529893. Onik G, Cobb C, Cohen J, Zabkar J, Porterfield B. US characteristics of frozen prostate. Radiology. 1988 Sep;168(3):629-31; https://www.ncbi.nlm.nih.gov/pubmed/3043544. Onik GM, Reyes G, Cohen JK, Porterfield B. Ultrasound characteristics of renal cryosurgery. Urology. 1993 Aug;42(2):212-5; https://www.ncbi.nlm.nih.gov/pubmed/8367932. Saliken JC, McKinnon JG, Gray R. CT for monitoring cryotherapy. AJR Am J Roentgenol. 1996 Apr;166(4):853-5; https://www.ajronline.org/doi/pdfplus/10.2214/ajr.166.4.8610562. Sheng L, Wang G, Li F, Luo J, Liu J. Ultrasound signal wavelet analysis to quantify the microstructures of normal and frozen tissues *in vitro*. Cryobiology. 2014 Feb;68(1):29-34; https://www.ncbi.nlm.nih.gov/pubmed/24269529.

[924] Sheng L, Wang G, Li F, Luo J, Liu J. Ultrasound signal wavelet analysis to quantify the microstructures of normal and frozen tissues *in vitro*. Cryobiology. 2014 Feb;68(1):29-34; https://www.semanticscholar.org/paper/Ultrasound-signal-wavelet-analysis-to-quantify-the-Sheng-Wang/6e95a857572c53f3d9fe80bee6c1a6a82b2833ee.

incident acoustic energy."[925] While sonography can distinguish frozen and unfrozen tissue, it cannot readily visualize distinct features within the iceball under these circumstances (image, right).[926]

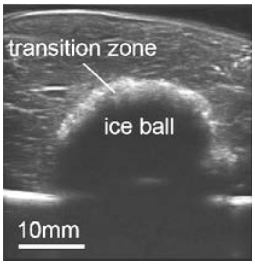

Similarly, the images below show vibroacoustic scans of an excised human prostate gland, before (leftmost) and after (rightmost) freezing to dry ice temperature.[927] As noted by one research group: "The primary challenge in ultrasound monitoring of cryosurgery[928] is the high absorption of the ultrasound energy by the frozen region, which leads to (i) opacity of the frozen region on the ultrasound monitor, (ii) shadow effect behind the frozen region, and (iii) clear demarcation of the freezing front in areas close to the ultrasound transducer."[929]

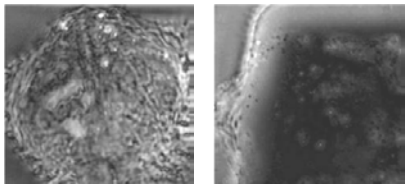

However, the potential imaging capabilities of ice-contacting ultrasound transducers should be explored in ***future research***, after verifying that ultrasound will not induce cracking in cryogenic, possibly highly mechanically stressed, frozen tissue. In particular, **intravascular ultrasound** (IVUS)[930] is a technique that could in principle be applied in direct contact with cryopreserved tissue. In IVUS, a specially designed catheter with a miniaturized ultrasound probe attached to its distal end is threaded into a blood vessel; the proximal end of the catheter is attached to computerized ultrasound equipment that allows sound waves generated by a piezoelectric transducer to visualize the endothelium (inner wall) of blood vessels in living individuals, with an aqueous resolution of 0.15 mm because it can employ somewhat higher frequencies (20-50 MHz)[931] – equivalent to 0.20-0.08 mm acoustic wavelengths in ice. (A 57.5 MHz ultrasound needle transducer <1 mm in size was demonstrated almost a decade ago,[932] and <0.5 mm transducers are now available.[933]) Because of its limited range, this technique could only be applied locally, perhaps in conjunction with simultaneous arterial ice excavation (Section 4.2.2).

---

[925] Saliken JC, McKinnon JG, Gray R. CT for monitoring cryotherapy. AJR Am J Roentgenol. 1996 Apr;166(4):853-5; https://www.ajronline.org/doi/pdfplus/10.2214/ajr.166.4.8610562.

[926] Sheng L, Wang G, Li F, Luo J, Liu J. Ultrasound signal wavelet analysis to quantify the microstructures of normal and frozen tissues *in vitro*. Cryobiology. 2014 Feb;68(1):29-34; https://www.semanticscholar.org/paper/Ultrasound-signal-wavelet-analysis-to-quantify-the-Sheng-Wang/6e95a857572c53f3d9fe80bee6c1a6a82b2833ee.

[927] Mitri FG, Davis BJ, Alizad A, Greenleaf JF, Wilson TM, Mynderse LA, Fatemi M. Prostate cryotherapy monitoring using vibroacoustography: preliminary results of an *ex vivo* study and technical feasibility. IEEE Trans Biomed Eng. 2008 Nov;55(11):2584-92; https://www.ncbi.nlm.nih.gov/pmc/articles/PMC2758914/.

[928] Cryosurgery is the local application of cryogenic temperatures to biological tissues in order to therapeutically selectively destroy them; https://en.wikipedia.org/wiki/Cryosurgery.

[929] Thaokar C, Rossi MR, Rabin Y. A new method for temperature-field reconstruction during ultrasound-monitored cryosurgery using potential-field analogy. Cryobiology. 2016 Feb;72(1):69-77; https://www.ncbi.nlm.nih.gov/pmc/articles/PMC5172398/.

[930] https://en.wikipedia.org/wiki/Intravascular_ultrasound.

[931] Nissen SE, Yock P. Intravascular ultrasound: novel pathophysiological insights and current clinical applications. Circulation. 2001 Jan 30;103(4):604-16; https://www.ncbi.nlm.nih.gov/pubmed/11157729/.

[932] Hsu HS, Zheng F, Li Y, Lee C, Zhou Q, Kirk Shung K. Focused high frequency needle transducer for ultrasonic imaging and trapping. Appl Phys Lett. 2012 Jul 9;101(2):24105; https://www.ncbi.nlm.nih.gov/pmc/articles/PMC3407142/.

[933] Chen R, Jiang L, Zhang T, *et al*. Eco-Friendly Highly Sensitive Transducers Based on a New KNN-NTK-FM Lead-Free Piezoelectric Ceramic for High-Frequency Biomedical Ultrasonic Imaging Applications. IEEE Trans Biomed Eng. 2019 Jun;66(6):1580-1587; https://pubmed.ncbi.nlm.nih.gov/30452346/.

Future research should also investigate other ultrasound-based scanning modalities for possible relevance in scanning cryopreserved tissue, including various forms of **ultrasound computed tomography**[934] such as **ultrasonic refractive index tomography** and **ultrasonic attenuation tomography**.[935] The latter, aka. **ultrasound transmission tomography**,[936] measures the delay in the passage of ultrasound pulses through tissue, allowing directional mapping of the attenuation coefficient. Tumors typically have a higher speed of sound than the surrounding tissue,[937] so experimentalists could investigate the degree to which variation in the speed of sound can differentiate between frozen vascular wall tissue, frozen cryopreservative fluid that presumably fills the vascular lumen, and frozen extravascular soft tissues generally – at this early stage in the revival protocol, we only need to noninvasively map the larger vessels. Ultrasound waves don't travel solely in straight lines like X-rays but are deflected at each boundary, potentially complicating the analysis. **High frequency ultrasound biomicroscopy**[938] at 35-50 MHz can achieve 0.02 mm axial resolution and 0.1 mm lateral resolution with a depth of penetration of 8-9 mm at 50 MHz in conventional applications.[939]

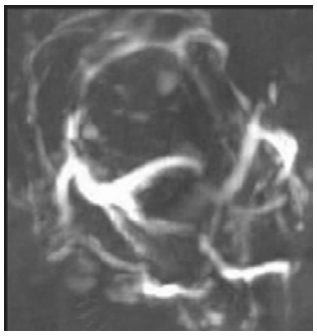

Thermoacoustic imaging[940] and thermoacoustic computed tomography (TCT)[941] might also work in cryopreserved tissue. In this scheme, the tissue is irradiated by an energy source (e.g., radio waves or microwaves)[942] that is absorbed by the body. The absorbed energy is converted to heat, which raises the temperature of the tissue (typically <0.001 °C), causing the tissue to mechanically expand in volume very slightly, producing an acoustic wave that propagates outward in all directions from the site of energy absorption at the velocity of sound. The image at left is a 3D TCT image of the vasculature inside the head of a (non-frozen) mouse to a resolution of 0.35 mm,[943] though the researchers used near infrared radiation and exploited the higher optical absorption of blood compared to the surrounding tissue.

---

[934] https://en.wikipedia.org/wiki/Ultrasound_computer_tomography.

[935] Kak AC, Slaney M. Principles of Computerized Tomographic Imaging. Society of Industrial and Applied Mathematics, 2001; "Section 4.3 Ultrasonic Computed Tomography"; https://engineering.purdue.edu/~malcolm/pct/CTI_Ch04.3.pdf.

[936] https://en.wikipedia.org/wiki/Ultrasound_transmission_tomography.

[937] Opielinski KJ, Gudra T. Multi-parameter ultrasound transmission tomography of biological media. Ultrasonics. 2006 Dec 22;44 Suppl 1:e295-302; https://www.ncbi.nlm.nih.gov/pubmed/17005227.

[938] Pavlin CJ, McWhae JA, McGowan HD, Foster FS. Ultrasound biomicroscopy of anterior segment tumors. Ophthalmology. 1992 Aug;99(8):1220-1228; https://pubmed.ncbi.nlm.nih.gov/1513574/. Kanellopoulos AJ, Asimellis G. Comparison of high-resolution Scheimpflug and high-frequency ultrasound biomicroscopy to anterior-segment OCT corneal thickness measurements. Clin Ophthalmol. 2013;7:2239-47; https://www.ncbi.nlm.nih.gov/pmc/articles/PMC3838761/.

[939] Shung KK. High Frequency Ultrasonic Imaging. J Med Ultrasound 2009;17(1):25-30; https://core.ac.uk/download/pdf/82448478.pdf.

[940] https://en.wikipedia.org/wiki/Thermoacoustic_imaging.

[941] Kruger RA, Kopecky KK, Aisen AM, Reinecke DR, Kruger GA, Kiser WL Jr. Thermoacoustic CT with radio waves: a medical imaging paradigm. Radiology. 1999 Apr;211(1):275-8; https://www.ncbi.nlm.nih.gov/pubmed/10189483.

[942] When laser pulses of visible light or near infrared radiation are used, the technology is often called photoacoustic imaging or optoacoustic imaging; https://en.wikipedia.org/wiki/Photoacoustic_imaging.

[943] Kruger RA, Kiser WL, Reinecke DR, Kruger GA, Miller KD. Thermoacoustic molecular imaging of small animals. Mol Imaging. 2003 Apr;2(2):113-23; https://journals.sagepub.com/doi/pdf/10.1162/15353500200303109.

Radio waves can achieve good penetration in ice, so ***future research*** should consider whether this technique might work in cryopreserved tissue.

If frozen tissues of various types are found to differ sufficiently in mechanical stiffness, it might be possible to obtain 3D vascular data using **ultrasound elastography**,[944] including **shear-wave elasticity imaging**[945] or **supersonic shear imaging**.[946]

The methods of three-dimensional **ultrasound tissue characterization**,[947] **quantitative ultrasound imaging**,[948] and **beamforming ultrasound tomography**[949] should also be reviewed for their potential applicability to 3D ultrasound angiography in frozen or cryopreserved tissue.

4.1.4 Other Conventional Millimeter-Resolution Techniques

Aside from MRI (Section 4.1.1), CT (Section 4.1.2), and US (Section 4.1.3) scanning, a few other conventional techniques might be feasible for noninvasively obtaining millimeter- or submillimeter-resolution vascular map data from a cryopreserved human body:

(1) **Terahertz tomography**[950] employs sectional imaging using terahertz (THz, or 10^{12} Hz; aka. far-infrared) electromagnetic radiation.[951] Terahertz time-domain spectroscopy allows for measurements

---

[944] https://en.wikipedia.org/wiki/Elastography#Ultrasound_elastography.

[945] Sarvazyan AP, Rudenko OV, Swanson SD, Fowlkes JB, Emelianov SY. Shear wave elasticity imaging: a new ultrasonic technology of medical diagnostics. Ultrasound Med Biol. 1998; 24(9): 1419-35; https://pdfs.semanticscholar.org/71da/899e63a3e92ed61f54d9015025943f5ccfc1.pdf.

[946] Bercoff J, Tanter M, Fink M. Supersonic shear imaging: a new technique for soft tissue elasticity mapping. IEEE Trans Ultrason Ferroelectr Freq Control. 2004 Apr;51(4):396-409; https://www.researchgate.net/profile/Jeremy_Bercoff/publication/8565554_Supersonic_Shear_Imaging_a_new_technique_for_soft_tissue_elasticity_mapping/links/02bfe50efec541f210000000/Supersonic-Shear-Imaging-a-new-technique-for-soft-tissue-elasticity-mapping.pdf. Gennisson JL, Rénier M, Catheline S, Barrière C, Bercoff J, Tanter M, Fink M. Acoustoelasticity in soft solids: assessment of the nonlinear shear modulus with the acoustic radiation force. J Acoust Soc Am. 2007 Dec;122(6):3211-9; https://www.researchgate.net/profile/Jeremy_Bercoff/publication/5604041_Acoustoelasticity_in_soft_solids_Assessment_of_the_nonlinear_shear_modulus_with_the_acoustic_radiation_force/links/02bfe50efec5475260000000.pdf.

[947] Zhou Z, Wu W, Wu S, Jia K, Tsui PH. A Review of Ultrasound Tissue Characterization with Mean Scatterer Spacing. Ultrason Imaging. 2017 Sep;39(5):263-282; https://www.ncbi.nlm.nih.gov/pubmed/28797220.

[948] Mercado KP, Helguera M, Hocking DC, Dalecki D. Noninvasive Quantitative Imaging of Collagen Microstructure in Three-Dimensional Hydrogels Using High-Frequency Ultrasound. Tissue Eng Part C Methods. 2015 Jul;21(7):671-82; https://www.ncbi.nlm.nih.gov/pmc/articles/PMC4499776/. Ruland A, Gilmore KJ, Daikuara LY, Fay CD, Yue Z, Wallace GG. Quantitative ultrasound imaging of cell-laden hydrogels and printed constructs. Acta Biomater. 2019 Jun;91:173-185; https://www.ncbi.nlm.nih.gov/pubmed/31055120.

[949] Jovanovic I, Hormati A, Littrup P, Duric N, Rama O, Vetterli M. Temperature monitoring during tissue freezing using ultrasound speed measurements. Proc of SPIE 2009;7265:72650Q-1-72650Q-8; https://infoscience.epfl.ch/record/112677/files/72650Q_1.pdf.

[950] Guillet JP, Recur B, Frederique L, Bousquet B, Canioni L, Manek-Hönninger I, Desbarats P, Mounaix P. Review of Terahertz Tomography Techniques. J Infrared Millimeter and Terahertz Waves. 2014;35(4):382-411; https://hal.archives-ouvertes.fr/hal-00968839/PDF/GuilletJIMTW2014_PostPrint.pdf.

[951] https://en.wikipedia.org/wiki/Terahertz_radiation.

(e.g., thickness, density, defect location) on difficult-to-probe materials, as the depth of buried structures can be inferred through timing of their reflections of these ultrashort-width terahertz pulses.[952]

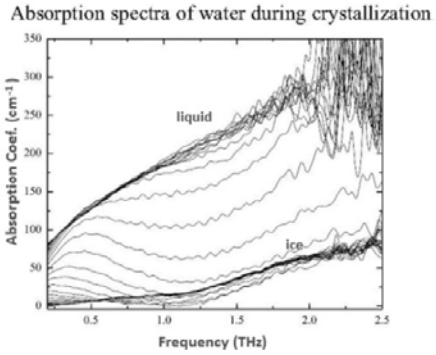

THz radiation, which has many medical uses,[953] is nonionizing and induces molecular rotations and vibrations that are far less damaging to biological tissues and DNA than X-rays. The effective penetration of THz is normally limited to a tissue depth of 0.2-0.3 mm at body temperature because of the enormous absorption of this radiation in liquid water, which comprises the bulk of most biological tissues. However, in the 0.1-2.0 THz frequency range there is a huge disparity between liquid water absorption and ice absorption, with ice being ~100 times more permeable to the radiation than liquid water (chart, right).[954] The intensity of transmitted THz energy is inversely exponentially proportional to absorption and tissue thickness. For 0.3 THz (1 mm wavelength) radiation, the absorption coefficient of ~100 cm^{-1} in water[955] allows only <0.0001% of the radiation to penetrate 1 mm in depth, whereas the absorption coefficient of ~1 cm^{-1} in ice[956] allows ~90% of the radiation to penetrate 1 mm in depth.[957] The images below show clear differences between healthy and cancerous tissue in terahertz scans.[958]

---

[952] https://en.wikipedia.org/wiki/Terahertz_time-domain_spectroscopy#Uses_of_THz_radiation.

[953] Son JH, Oh SJ, Cheon H. Potential clinical applications of terahertz radiation. J Appl Phys. 2019;125:190901; https://aip.scitation.org/doi/full/10.1063/1.5080205. "Some frequencies of terahertz radiation can penetrate several millimeters of tissue with low water content (e.g., fatty tissue) and reflect back. Terahertz radiation can also detect differences in water content and density of a tissue. Such methods could allow effective detection of epithelial cancer with an imaging system that is safe, non-invasive, and painless." https://en.wikipedia.org/wiki/Terahertz_radiation

[954] Ashworth PC, Zeitler JA, Pepper M, Wallace VP. Terahertz spectroscopy of biologically relevant liquids at low temperatures. 2006 Joint 31st International Conference on Infrared Millimeter Waves and 14th International Conference on Teraherz Electronics, 18-22 Sep 2006, Paper No. TueB6-2, p. 184; https://ieeexplore.ieee.org/document/4222126.

[955] Hasted JB, Husain SK, Frescura FA, Birch JR. The temperature variation of the near millimetre wavelength optical constants of water. Infrared Physics 1987 Jan;27(1):11-15; https://www.sciencedirect.com/science/article/pii/0020089187900443. Liebe HJ, Hufford GA, Manabe T. A model for the complex permittivity of water at frequencies below 1 THz. Intl J Infrared and Millimeter Waves 1991;12(7):659-675; https://www.researchgate.net/profile/Takeshi_Manabe/publication/225967810_A_model_for_the_complex_permittivity_of_water_at_frequencies_below_1_THz/links/546d99550cf2193b94c589ad.pdf.

[956] Zhang C, Lee KS, Zhang XC, Wei X, Shen YR. Optical constants of ice Ih crystal at terahertz frequencies. Appl Phys Lett. 2001 Jul 16;79(4):491-493; https://aip.scitation.org/doi/abs/10.1063/1.1386401. Nakajima S, Hoshina H, Yamashita M, Otani C, Miyoshi N. Terahertz imaging diagnostics of cancer tissues with a chemometrics technique. Appl Phys Lett. 2007 Jan 22;90(4):041102; http://www2.riken.jp/lab-www/THz-img/hoshina/PDF/Hosina_APL_02.pdf. Takeya K, Fukui T, Takahashi R, Kawase K. Dielectric constants of H_2O and D_2O ice in the terahertz frequency regime over a wide temperature range. J Optics. 2014;16(9):094005; https://iopscience.iop.org/article/10.1088/2040-8978/16/9/094005/. Cheon H, Yang HJ, Son JH. Toward Clinical Cancer Imaging Using Terahertz Spectroscopy. IEEE J. Sel. Top. Quantum Electron. 2017;23(4):8600109; https://ieeexplore.ieee.org/abstract/document/7929316.

[957] Vilagosh Z, Lajevardipour A, Wood AW. Computational phantom study of frozen melanoma imaging at 0.45 terahertz. Bioelectromagnetics. 2019 Feb;40(2):118-127; https://www.ncbi.nlm.nih.gov/pubmed/30699238.

[958] Chen H, Lee WJ, Huang HY, Chiu CM, Tsai YF, Tseng TF, Lu JT, Lai WL, Sun CK. Performance of THz fiber-scanning near-field microscopy to diagnose breast tumors. Opt Express. 2011 Sep 26;19(20):19523-19531; https://www.osapublishing.org/viewmedia.cfm?uri=oe-19-20-19523&seq=0.

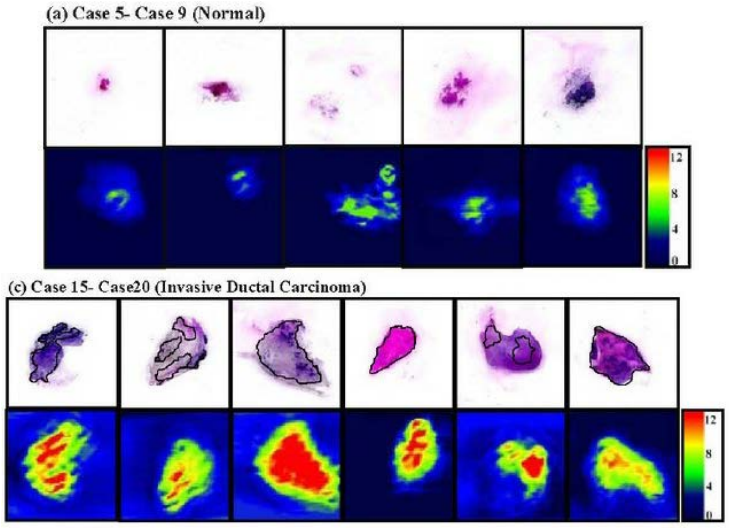

Experimental work on human tissue at cryogenic temperatures has demonstrated the ability of THz radiation to distinguish cancerous from noncancerous tissue in both frozen oral[959] and lymphatic[960] tissues, and to distinguish porcine striated muscle from adipose tissues frozen to below -33 °C.[961] The possibility of identifying melanoma in frozen skin tissue has also been studied,[962] and THz radiation has been used to characterize frozen brain tissue samples altered by Alzheimer's disease.[963] The THz resonance of methylated DNA from solid cancer cell lines, otherwise difficult to observe in aqueous solution, has been measured using the freezing technique.[964]

The response of frozen or vitrified cryoprotectants to THz radiation has not yet been tested. However, it has been pointed out that it is the dielectric properties, not the conductive ones, that cause water to absorb terahertz frequencies.[965] The main ingredients in the commonly used cryoprotectant solution M22 are

---

[959] Sim YC, Park JY, Ahn KM, Park C, Son JH. Terahertz imaging of excised oral cancer at frozen temperature. Biomed Opt Express. 2013 Jul 23;4(8):1413-21; https://www.osapublishing.org/viewmedia.cfm?uri=boe-4-8-1413&seq=0. Sim YC, Ahn KM, Park JY, Park C, Son JH. Temperature-Dependent Terahertz Imaging of Excised Oral Malignant Melanoma. IEEE J. Biomed. Health Inform. 2013 Apr 29;17(4):779-784; https://ieeexplore.ieee.org/document/6509416.

[960] Park JY, Choi HJ, Cheon H, Cho SW, Lee S, Son JH. Terahertz imaging of metastatic lymph nodes using spectroscopic integration technique. Biomed Opt Express. 2017 Jan 25;8(2):1122-1129; https://www.osapublishing.org/viewmedia.cfm?uri=boe-8-2-1122&seq=0.

[961] Hoshina H, Hayashi A, Miyoshi N, Fukunaga Y, Otani C. Terahertz pulsed imaging of frozen biological tissues. Appl Phys Lett. 2009 Mar 23;94(12):123901; http://www2.riken.jp/lab-www/THz-img/hoshina/PDF/Hoshina_APL_02.pdf.

[962] Vilagosh Z, Lajevardipour A, Wood AW. Computational phantom study of frozen melanoma imaging at 0.45 terahertz. Bioelectromagnetics. 2019 Feb;40(2):118-127; https://www.ncbi.nlm.nih.gov/pubmed/30699238.

[963] Png GM, Falconer RJ, Fischer BM, Zakaria HA, Mickan SP, Middelberg AP, Abbott D. Terahertz spectroscopic differentiation of microstructures in protein gels. Opt Express. 2009 Jul 20;17(15):13102-15; https://www.osapublishing.org/viewmedia.cfm?uri=oe-17-15-13102&seq=0.

[964] Cheon H, Yang HJ, Lee SH, Kim YA, Son JH. Terahertz molecular resonance of cancer DNA. Sci Rep. 2016 Nov 15;6:37103; https://www.nature.com/articles/srep37103.

[965] Armstrong CM. The truth about terahertz. IEEE Spectrum, 17 Aug 2012; https://spectrum.ieee.org/aerospace/military/the-truth-about-terahertz.

water, dimethyl sulfoxide, ethylene glycol, and formamide.[966] Comparing the dielectric constants of the liquid and solid (frozen) forms, we find $\varepsilon_{liq} = 78$ and $\varepsilon_{solid} = 3.2$ for water,[967] $\varepsilon_{liq} = 46.7$ and $\varepsilon_{solid} = 2.5$ for DMSO at 1.5 GHz,[968] and $\varepsilon_{liq} = 37$ and $\varepsilon_{solid} = 1.6$ for ethylene glycol at 1.5 GHz,[969] which suggests that frozen M22 might be as transparent to THz radiation as is water-ice. This looks like an excellent topic for a ***future research*** project.

(2) **Diffuse optical imaging** (DOI)[970] is a medical imaging modality which uses near infrared light to generate images of the body via near-infrared spectroscopy (NIRS)[971] or fluorescence-based methods.[972] When used to create 3D volumetric models of the imaged material, DOI is called diffuse optical tomography or DOT. The technique normally measures the optical absorption spectrum of hemoglobin that varies with its oxygenation status as blood circulates, so if applied in the usual manner would likely be inapplicable to cryopreserved patients who lack both blood circulation and red cells containing hemoglobin (due to blood washout). However, different tissues exhibit different thermal conductivity,[973] so it seems possible in theory to discern vascular structures as distinct from nonvascular tissue.

(3) **Fourier transform infrared spectro-microtomography**[974] is a nondestructive 3D imaging approach that reveals the distribution of distinctive chemical compositions throughout an intact biological or materials sample, using a synchrotron-based mid-infrared beamline at the University of Wisconsin–Madison Synchrotron Radiation Center. However, it is unclear if this method can be scaled up to accommodate 10 cm sized blocks of cryopreserved tissue.

(4) **Electrical Impedance Tomography** (EID)[975] is a medical imaging technique in which the electrical conductivity, permittivity, and impedance of a part of the body is inferred from surface electrode measurements and used to form a tomographic image of that part. Electrical conductivity varies

---

[966] Fahy GM, Wowk B, Wu J, Phan J, Rasch C, Chang A, Zendejas E. Cryopreservation of organs by vitrification: perspectives and recent advances. Cryobiology. 2004 Apr;48(2):157-78; http://www.21cm.com/pdfs/cryopreservation_advances.pdf.

[967] https://www.quora.com/What-is-the-dielectric-constant-of-water-ice.

[968] "Dielectric Chart," Univ. Washington; https://depts.washington.edu/eooptic/linkfiles/dielectric_chart%5B1%5D.pdf; Macklis JD, Ketterer FD. Microwave properties of cryoprotectants. Cryobiology. 1978 Dec;15(6):627-35; https://pdfs.semanticscholar.org/b64a/ed2704a698072a3d121edb863232c7956e88.pdf.

[969] "Dielectric Constants of Common Liquids," The Engineering Toolbox; https://www.engineeringtoolbox.com/liquid-dielectric-constants-d_1263.html; Macklis JD, Ketterer FD. Microwave properties of cryoprotectants. Cryobiology. 1978 Dec;15(6):627-35; https://pdfs.semanticscholar.org/b64a/ed2704a698072a3d121edb863232c7956e88.pdf.

[970] https://en.wikipedia.org/wiki/Diffuse_optical_imaging.

[971] Durduran T, Choe R, Baker WB, Yodh AG. Diffuse Optics for Tissue Monitoring and Tomography. Rep Prog Phys. 2010 Jul;73(7):076701; https://www.ncbi.nlm.nih.gov/pmc/articles/PMC4482362.

[972] Boas G. Imaging Technologies: Diffuse Optical Imaging. Athinoula A. Martinos Center for Biomedical Imaging, Jan 2005; https://web.archive.org/web/20120616155545/http://www.nmr.mgh.harvard.edu/martinos/research/technologiesDOI.php.

[973] Giering K, Minet O, Lamprecht I, Muller G. Review of thermal properties of biological tissues. SPIE PM 1995;25:45-65; https://www.researchgate.net/profile/Olaf_Minet/publication/294698829_Review_of_Thermal_Properties_of_Biological_Tissues/links/5b69f556299bf14c6d951e8e/Review-of-Thermal-Properties-of-Biological-Tissues.pdf.

[974] Martin MC, Dabat-Blondeau C, Unger M, Sedlmair J, Parkinson DY, Bechtel HA, Illman B, Castro JM, Keiluweit M, Buschke D, Ogle B, Nasse MJ, Hirschmugl CJ. 3D spectral imaging with synchrotron Fourier transform infrared spectro-microtomography. Nat Methods. 2013 Sep;10(9):861-4; https://www.fpl.fs.fed.us/documnts/pdf2013/fpl_2013_martin001.pdf.

[975] https://en.wikipedia.org/wiki/Electrical_impedance_tomography.

considerably among various biological tissues, and sufficient conductivity of frozen tissue, perhaps loaded with cryoprotectant, would have to be established for this technique to be successful. Also, in contrast to the X-rays used in Computed Tomography that travel in straight lines, electric currents travel three dimensionally along the paths of least resistivity, so inevitably parts of the electric current leave the transverse plane, greatly complicating 3D image reconstruction. Nevertheless, radiofrequency imaging of tissues for cancer detection and identification is now commonplace.[976]

4.2 Macrovascular Excavation

Once a 3D map of the large vessels of the vasculature of a cryopreserved human patient has been noninvasively compiled (Section 4.1), the next step is to cleanly excavate the frozen water-ice or vitrified cryoprotectant from the interior of these vessels. This excavation should clear ice from the lumena of all major blood vessels, lymph vessels, and cerebrospinal fluid channels and other intracerebral fluid chambers, probably replacing the removed contents with oxygen-free cold nitrogen gas or liquid nitrogen. Excavation will extend from the heart chambers to the most distal termini of all vessels identified in the map, including vessel diameters at least as small as 1 mm but ideally as small as 0.1 mm (Section 4.1).

The large-bore vasculature can be conveniently excavated at LN2 temperatures – either relatively quickly by map following (i.e., cartographic excavation; Section 4.2.1) or more slowly by exploratory methods if necessary (i.e., exploratory excavation; Section 4.2.2). For many cryopatients, some combination of both methods may be required if the maps of the large-bore vasculature are not entirely complete.

4.2.1 Cartographic Excavation

Excavation nanorobots are employed to remove mainly frozen water-ice or vitrification cryoprotectant materials[977] from all major blood vessels identified on the large-vessel 3D vascular map, a process that may be called cartographic excavation. Due to the presence of the map, there can be some reasonable assurance that most major vessels, including the lymphatics,[978] will have been identified and can be excavated, and it will be possible to calculate the safest pathways between termini of broken vessels that have been bisected and separated by up to 0.1 mm due to cracking (Section 3.4.3). For the few large vessels that might be missed during the scan, they can be found later either by excavation upward in size from the capillary beds reaching the other (missing) side of the vessel, or, in the case of vessel segments completely isolated by separate breaks on either side and not detected by the original scan, by capillary bed analysis that should detect blocks of tissue that appear to lack sufficient vascularization, followed by exploratory excavation (Section 4.2.2) of those few blocks of tissue.

If only a 1 mm vascular map was available, this excavation would involve clearing out ~11,541 arterial vessels (including aorta, large arteries, main artery branches, and terminal artery branches) of lumenal

---

[976] Kaufman Z, Paran H, Haas I, Malinger P, Zehavi T, Karni T, Pappo I, Sandbank J, Diment J, Allweis T. Mapping breast tissue types by miniature radio-frequency near-field spectroscopy sensor in *ex-vivo* freshly excised specimens. BMC Med Imaging. 2016 Oct 10;16(1):57; https://www.ncbi.nlm.nih.gov/pmc/articles/PMC5057390/.

[977] Some large blood clots may also need to be removed.

[978] Freitas RA Jr. Nanomedicine, Volume I: Basic Capabilities, Landes Bioscience, Georgetown TX, 1999, Section 8.2.1.3, "Lymphatic System"; http://www.nanomedicine.com/NMI/8.2.1.3.htm.

volume ~500 cm^3, plus another ~11,541 venous vessels (including vena cava, large veins, main venous branches, and terminal veins)[979] of lumenal volume ~3350 cm^3,[980] for a blood vessel excavation volume of ~3850 cm^3, out of the total ~5400 cm^3 blood volume. The excavation must also clear out ~12 large lymphatic vessels (including the thoracic duct, right lymphatic duct, main trunks, and cisterna chylii) and ~100 minor lymphatic trunks of lumenal volume ~11 cm^3,[981] the entire cardiac chamber volume of ~450 cm^3, and the entire ~150 cm^3 volume of cerebrospinal fluid,[982] giving a total clearance volume of $V_{ice,1mm}$ ~ 4461 cm^3.

If a 0.1 mm-resolution vascular map is available, the excavation will include an additional ~4,500,000 arterioles of lumenal volume ~70 cm^3 and ~4,500,000 venules of lumenal volume ~355 cm^3, increasing the blood vessel excavation volume by ~425 cm^3 to a grand total of ~4275 cm^3 for the blood vessels, out of the total ~5400 cm^3 blood volume. To this must be added ~618,700 lymphonodal collecting ducts of lumenal volume ~363 cm^3 and ~68,000,000 lymphatic precollecting ducts of lumenal volume ~1200 cm^3, representing another ~1563 cm^3 of lymphatic volume, making a grand total of ~1574 cm^3, out of the total ~3300 cm^3 lymphatic system volume. These extra vessels add ~1988 cm^3, increasing the total clearance volume to $V_{ice,0.1mm}$ ~ 6449 cm^3. All these volumes would be ~43 times smaller[983] if only the brain is considered.

Note that these excavation volumes refer to fully-patent liquid-filled vessels in living patients and might change in as yet unmeasured amounts due to: (A) a volume increase due to the osmotic outflow of water from tissues into blood vessels during the cryopreservation process (e.g., brain blood vessels are maximally dilated during cryoprotectant perfusion); (B) a volume change ranging from +9% expansion for pure water as it freezes at 0 °C (273 K) to -5% contraction of pure M22 cryoprotective solution as it solidifies during cooling from 0 °C to -150 °C (123 K) (see chart, Section 5.2.3.1(B)); or (C) an increase or decrease in vessel mechanical patency compared to living vasculature, after perfusion with cryoprotectant and subsequent solidification of lumenal contents during cryopreservation. Measuring and modeling the exact changes would be a useful experimental project for ***future research***.

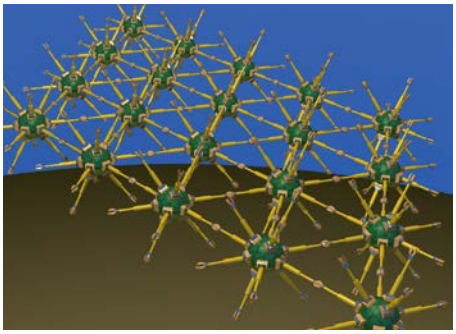

The excavation nanorobots may be conceptualized as a loosely-space-filling utility fog[984] (image, left) that advances

---

[979] The venous tree including the hepatic portal system (https://en.wikipedia.org/wiki/Hepatic_portal_system) and the hypophyseal portal system (https://en.wikipedia.org/wiki/Hypophyseal_portal_system), which transport venous blood between two capillary beds.

[980] Freitas RA Jr. Nanomedicine, Volume I: Basic Capabilities, Landes Bioscience, Georgetown TX, 1999, Table 8.1, "Approximate Quantification of the Human Arteriovenous System"; http://www.nanomedicine.com/NMI/Tables/8.1.jpg.

[981] Freitas RA Jr. Nanomedicine, Volume I: Basic Capabilities, Landes Bioscience, Georgetown TX, 1999, Table 8.5, "Approximate Quantification of the Human Lymphatic System"; http://www.nanomedicine.com/NMI/Tables/8.5.jpg.

[982] Freitas RA Jr. Nanomedicine, Volume I: Basic Capabilities, Landes Bioscience, Georgetown TX, 1999, Table 8.9, "Mass, Volume, and Scale Size of the Organs of the Human Body"; http://www.nanomedicine.com/NMI/Tables/8.9.jpg.

[983] [average human brain volume ~1.4 L (https://en.wikipedia.org/wiki/Brain_size)] / [average human body volume ~ 60 L (http://www.nanomedicine.com/NMI/8.2.5.htm)] = 1/43.

[984] Hall JS. Utility fog: A universal physical substance. Vision 21: Interdisciplinary Science and Engineering in the Era of Cyberspace, NASA-Lewis Research Center (N94-27367), Dec 1993, pp. 115-126; https://ntrs.nasa.gov/archive/nasa/casi.ntrs.nasa.gov/19940022864.pdf. See also: https://www.autogeny.org/Ufog.html and https://en.wikipedia.org/wiki/Utility_fog.

slowly from the entry point(s) throughout the vascular space to be cleared, filling that space as it moves forward like an extensible "mining worm". Active robots at the forward end follow the map and remove bits of ice, clearing the vessel lumen all the way to the cold-immobilized endothelial cell surfaces lining the vessel walls. The bits of ice are transported rearward through relatively inactive robots comprising the body of the "worm" and thence out of the body. Excavation proceeds until all vessels identified in the map have been cleared of ice and replaced with liquid nitrogen. Entry points can include any convenient large vessel located near the skin surface, or accessible via open respiratory volumes, or even the heart. During cryopreservation the entry point for washout is the femoral artery (for whole-body) or the carotid artery (for neuro) and the cannula is normally left in place,[985] providing a convenient entry point for tunneling nanorobots.

The **hepatic portal vein**[986] is a special case because it does not carry blood directly from the arterial to the venous circuit, but rather connects two capillary beds, carrying blood to the liver[987] from the gastrointestinal tract, the gallbladder, the pancreas, and the spleen. Because the large 6-12 mm diameter[988] portal vein is not directly accessible from large vessels on either the arterial or venous side of the circulation, special arrangements might be made for its early excavation, possibly employing a targeted nanosyringe (Section 4.12.2.8) or nanocatheter (Section 4.12.3.1) apparatus. The only other portal system[989] found in humans, the **hypophyseal portal system**[990] that transports hormones between the hypothalamus and the anterior pituitary in the brain, has venules that are 300 μm long and 32 μm in diameter (in rats)[991] that will be excavated along with the rest of the microvasculature (Section 4.4), hence require no special handling here. The efferent arterioles[992] in the human kidney that carry blood from the glomerular capillaries to a second peritubular capillary network, sometimes mistaken for the renal portal system[993] that is found only in non-mammalian kidneys, are also microscale in size and will be excavated later in due course (Section 4.4).

Another interesting minor challenge is how the nanorobots will nondestructively pass through numerous venous,[994] lymphatic,[995] and heart[996] valves, most of which consist of simple bicuspid flaps of tissue that

---

[985] https://www.alcor.org/library/alcor-human-cryopreservation-protocol/.
[986] https://en.wikipedia.org/wiki/Portal_vein.

[987] The liver receives 75% of its blood supply from the hepatic portal vein and 25% from the regular arterial circulation; https://en.wikipedia.org/wiki/Liver#Blood_supply.

[988] Wanless IR, Huang WY. "Vascular Disorders," in: Burt AD, Portmann BC, Ferrell LD, eds., MacSween's Pathology of the Liver, 6th Edition, 2012, pp. 601-643; https://www.sciencedirect.com/science/article/pii/B978070203398800012X.

[989] https://en.wikipedia.org/wiki/Portal_venous_system.
[990] https://en.wikipedia.org/wiki/Hypophyseal_portal_system.

[991] Gross PM, Joneja MG, Pang JJ, Polischuk TM, Shaver SW, Wainman DS. Topography of short portal vessels in the rat pituitary gland: a scanning electron-microscopic and morphometric study of corrosion cast replicas. Cell Tissue Res. 1993 Apr;272(1):79-88; https://pubmed.ncbi.nlm.nih.gov/8481959/.

[992] https://en.wikipedia.org/wiki/Efferent_arteriole.
[993] https://en.wikipedia.org/wiki/Renal_portal_system.

[994] Caggiati A. The venous valves of the lower limbs. Phlebolymphology 2013;20(2):87-95; https://www.phlebolymphology.org/wp-content/uploads/2014/09/Phlebolymphology78.pdf. See also: https://www.jobst.com/mainnavigation/leg-health/veins-valves.html and https://en.wikipedia.org/wiki/Vein.

[995] Scallan JP, Zawieja SD, Castorena-Gonzalez JA, Davis MJ. Lymphatic pumping: mechanics, mechanisms and malfunction. J Physiol. 2016 Oct 15;594(20):5749-5768; https://www.ncbi.nlm.nih.gov/pmc/articles/PMC5063934/. See also: https://en.wikipedia.org/wiki/Lymphatic_vessel.

will be frozen solid in the cryopreserved patient. ***Future research*** should determine the typical states of these valves following cryopreservation.[997] If valves are typically blocked open with bits of interposed ice, then robot passage should be easy once the bits of ice are cleared away. If valves are completely sealed, then a small amount of valve tissue holing or trimming by the robots might be required, mindful that only a few microns of clearance may be needed for successful excavation operations to proceed. Precapillary sphincters[998] (smooth muscle fibers encircling the entrance to capillaries, found uniquely in the mesenteric[999] circulation) might have squeezed shut some vessels, so the typical states of these sphincters following cryopreservation should also be the subject of ***future research***.

The precise workings of nanorobots that perform ice excavation have not yet been detailed but don't seem conceptually complex. One published estimate[1000] of the power requirements for a $d_{robot} = 1$ μm diameter nanorobot mechanically locomoting at $v_{robot} \sim 1$ μm/sec through solid ice via viscoplastic flow in which ice crystal at a temperature just below freezing is deformed without breaking is $P_{robot} \sim 200{,}000$ pW. However, this seems excessive compared to an excavation scheme in which most of the spoil is exported from the ice face through the utility fog "mining worms" and thence out of the body as still-unmelted microchunks of ice, with the mining robots and local environment maintained at cryogenic temperatures by the suffusion of liquid nitrogen throughout the theater of operation.

For simplicity of analysis, consider an excavation robot that removes a cubic block of ice of linear dimension L_{ice} by passing a cutting instrument[1001] around the perimeter of the ice cube in order to free it from the larger ice face. The cutting instrument cleaves a narrow layer of thickness t_{cut} across all five unexposed sides,[1002] removing spoil of volume $V_{spoil} \sim 5\ t_{cut}\ L_{ice}^2$ to release an ice cube of volume $V_{cube} = (L_{ice} - 2t_{cut})^3$ from the ice face which is then transported intact and still frozen out of the body.

---

[996] Ayoub S, Ferrari G, Gorman RC, Gorman JH, Schoen FJ, Sacks MS. Heart Valve Biomechanics and Underlying Mechanobiology. Compr Physiol. 2016 Sep 15;6(4):1743-1780; https://www.ncbi.nlm.nih.gov/pmc/articles/PMC5537387/. See also: https://en.wikipedia.org/wiki/Heart_valve.

[997] This may vary considerably from one patient to another, both on an individual basis and as a function of cryopreservation quality, and will be useful information to determine how much variation the algorithms and nanorobots must be able to handle.

[998] Sakai T, Hosoyamada Y. Are the precapillary sphincters and metarterioles universal components of the microcirculation? An historical review. J Physiol Sci. 2013 Sep;63(5):319-31; https://www.ncbi.nlm.nih.gov/pmc/articles/PMC3751330/.

[999] https://en.wikipedia.org/wiki/Mesentery.

[1000] Freitas RA Jr. Nanomedicine, Volume I: Basic Capabilities, Landes Bioscience, Georgetown TX, 1999, Section 10.5.2, "Viscosity and Locomotion in Ice"; http://www.nanomedicine.com/NMI/10.5.2.htm.

[1001] Concepts in the existing nanomachinery literature include a rotating cylindrical "core sampler" tool and "coarse shearing" tools,[*] and morcellation and mincing cutting tools.[†]
[*] Freitas RA Jr. Nanomedicine, Volume I: Basic Capabilities, Landes Bioscience, Georgetown TX, 1999, Section 9.3.2, "Nanoscale End-Effectors and Tool Tips"; http://www.nanomedicine.com/NMI/9.3.2.htm.
[†] Freitas RA Jr. Nanomedicine, Volume I: Basic Capabilities, Landes Bioscience, Georgetown TX, 1999, Section 9.3.5.1, "Morcellation and Mincing"; http://www.nanomedicine.com/NMI/9.3.5.1.htm.

[1002] While simple ice core augers are well-known,[*] there are many ways to gain cutting access to the fifth side at the bottom of the cube being extracted. For example, a starter hole can be drilled to the depth of the bottom face that is sufficiently wide to admit a sideways cutting instrument, from which the rest of that cutting plane becomes readily accessible across the entire face. Alternatively, the initial cut could be made at a downward angle, establishing a cutting plane ramp that zigzags deeper with each traverse, thus avoiding the need to drill a starter hole for each new plane of ice (though producing slanted cubes). Circumferential side-cutting devices have also been patented for medical use.[†]
[*] https://en.wikipedia.org/wiki/Ice_core and https://en.wikipedia.org/wiki/Ice_drilling#Coring_augers.
[†] McGuckin JF Jr. Breast surgery method and apparatus. U.S. Patent 7,753,920, 13 Jun 2010; https://patents.google.com/patent/US7753920.

The energy required to free the ice cube can be conservatively estimated as the energy required to melt the spoil. The energy cost to (locally) melt the spoil ice is $E_{D,melt} = \rho_{ice}\ H_{fusion,water} = 3.1 \times 10^8$ J/m^3, where ρ_{ice} = 916.7 kg/m^3 (the density of ice at 0 °C) and $H_{fusion,water}$ = 333,550 J/kg (the heat of fusion of water at 0 °C),[1003] plus the energy cost to (locally) warm the ice from T_{LN2} = 77 K to $T_{ice,melt}$ ~ 273 K (~0 °C) which is $E_{D,warm} \sim \rho_{ice}\ c_{ice}\ (T_{ice,melt} - T_{LN2}) = 2.5 \times 10^8$ J/m^3, where c_{ice} ~ 1400 J/kg-K (the average specific heat capacity of ice over the indicated temperature range).[1004] (Nonaqueous cryopreservative chemicals such as DMSO[1005] and ethylene glycol[1006] have lower heats of fusion and heat capacities, hence their inclusion in the above calculations would only lower the total energy estimate.) Taking the total reliquidification energy as $E_{D,liq} = E_{D,warm} + E_{D,melt} = 5.6 \times 10^8$ J/m^3 for our crude estimate of the energy cost of excavation yields $E_{Excavation} \sim E_{D,liq}\ V_{spoil}$ = 28 pJ per ice cube of volume V_{cube} = 0.941 μm^3 with L_{ice} = 1 μm, t_{cut} = 10 nm, and V_{spoil} = 0.05 μm^3. The energy cost for hand-over-hand transport of one intact microscale ice cube using a telescoping manipulator arm is ~10 zJ/nm,[1007] or $E_{transport}$ ~ 10 pJ to move the ice cube ~1 meter to exit the body.

Expending only ~28 pJ/ice cube, a P_{robot} = 100 pW excavation nanorobot should be able to target a removal rate of n_{cubes} ~ 1 ice cube per second, allowing a rate of advance through the vasculature of $v_{clearance}$ ~ 1 μm/sec. If the average path length of a complete vascular circuit (mainly noncapillaries) is L_{vasc} ~ 1.5 m,[1008] then the time required to clear ice from noncapillary vessels is on the order of $t_{clearance} \sim L_{vasc} / v_{clearance} = 1.5 \times 10^6$ sec ~ **17 days**. Taking the ice removal rate by front-line active excavation nanorobots as $r_{removal}$ = 1 μm^3/nanorobot-sec, then the excavation fleet required to clear a 1-mm resolution vascular map must include $N_{nanorobots,1mm} = V_{ice,1mm} / (r_{removal}\ t_{clearance}) = 2.97 \times 10^9$ front-line nanorobots with a continuous average fleet power generation of $P_{fleet,1mm} = P_{robot}\ N_{nanorobots,1mm}$ = 0.30 W, or $N_{nanorobots,0.1mm} = V_{ice,0.1mm} / (r_{removal}\ t_{clearance}) = 4.30 \times 10^9$ nanorobots to clear a 0.1-mm resolution vascular map with $P_{fleet,0.1mm} = P_{robot}\ N_{nanorobots,0.1mm}$ = 0.43 W. These figures do not include the much larger number of nanorobots trailing behind the front-line devices that will be relatively inactive, engaging only in relatively low-power hand-over-hand transport tasks. The total number of ice cubes that are removed and must be transported is $N_{icecubes,0.1mm} \sim V_{ice,0.1mm} / L_{ice}^3 = 6.449 \times 10^{15}$, adding only a modest $P_{transport,0.1mm} = N_{icecubes,0.1mm}\ E_{transport} / t_{clearance}$ = 0.043 W to the continuous average fleet power requirement.

Frozen tissue at 77 K (-196 °C) with a density of ~ 932 kg/m^3 (if mostly water-ice)[1009] should have a specific heat capacity of ~0.63 pJ/μm^3-K,[1010] so even if there are many cubic microns of frozen tissue

---

[1003] https://en.wikipedia.org/wiki/Properties_of_water.

[1004] Robert C. Weast, Handbook of Chemistry and Physics, 49th Edition, CRC, Cleveland OH, 1968; "Specific Heat of Ice," -200 °C to -2.2 °C, p. D-95. See also: https://www.engineeringtoolbox.com/ice-thermal-properties-d_576.html.

[1005] The heat of fusion for solid DMSO is ~ 2 x 10^8 J/m^3 (https://en.wikipedia.org/wiki/Dimethyl_sulfoxide_(data_page)), well below the 3.1 x 10^8 J/m^3 value for solid water-ice. The heat capacity of liquid DMSO is ~2 x 10^6 J/m^3-K (https://en.wikipedia.org/wiki/Dimethyl_sulfoxide_(data_page)), well below the 4.22 x 10^6 J/m^3-K value for liquid water at 0 °C (https://www.engineeringtoolbox.com/specific-heat-capacity-water-d_660.html).

[1006] The heat of fusion for solid ethylene glycol is ~ 1.8 x 10^8 J/m^3 (https://en.wikipedia.org/wiki/Ethylene_glycol_(data_page)), well below the 3.1 x 10^8 J/m^3 value for solid water-ice. The heat capacity of liquid ethylene glycol at 0 °C is ~2.7 x 10^6 J/m^3-K (https://www.engineeringtoolbox.com/ethylene-glycol-d_146.html), well below the 4.22 x 10^6 J/m^3-K value for liquid water at 0 °C (https://www.engineeringtoolbox.com/specific-heat-capacity-water-d_660.html).

[1007] Freitas RA Jr. Nanomedicine, Volume I: Basic Capabilities, Landes Bioscience, Georgetown TX, 1999, Section 3.4.3, "Internal Transport Streams"; http://www.nanomedicine.com/NMI/3.4.3.htm#p5.

[1008] Freitas RA Jr. Nanomedicine, Volume I: Basic Capabilities, Landes Bioscience, Georgetown TX, 1999, Table 8.1, "Approximate Quantification of the Human Arteriovenous System"; http://www.nanomedicine.com/NMI/Tables/8.1.jpg.

[1009] Handle PH, Loerting T. Temperature-induced amorphisation of hexagonal ice. Phys Chem Chem Phys. 2015 Feb 21;17(7):5403-5417; https://pubs.rsc.org/en/content/articlehtml/2015/cp/c4cp05587j.

surrounding each active excavation site the temperature rise could be unacceptable without active cooling. Heating of frozen tissue due to thermalization of waste heat from excavation operations can be minimized by circulating a small amount of liquid nitrogen coolant throughout the theater of operation. The specific heat capacity of LN2 at 77 K and 1 atm ambient pressure is $c_{LN2} = 8.73 \times 10^5$ J/m^3-K,[1011] hence the coolant temperature change resulting from the active clearance of a 0.1-mm resolution vascular map can be held to $\Delta T_{coolant} = 1$ K with a modest average coolant flow of LN2 through all opened spaces in the whole-body vasculature of $V_{coolant} \sim (P_{fleet,0.1mm} + P_{transport,0.1mm}) / (c_{LN2}\ \Delta T_{coolant}) = 0.54$ cm^3/sec, with flow and counterflow enabled in cul-de-sac tunnels using patterned groupings of the transport nanorobots to create incoming and outgoing channels.[1012] A ***future research*** project should attempt a preliminary design for the excavation nanorobots and their mission requirements that would permit more refined size, number, time, power, and thermal balance estimates.

Excavation nanorobots should include an appropriate sensor suite to detect the cellular walls of the vascular cavity so that those walls are not damaged by the burrow tools. A means must be devised to reliably detect seriously damaged endothelium,[1013] although significant spatial distortion or displacement of the lumena of these larger vessels seems unlikely except in the case of ice fractures. Such fractures are major features that should be visible, hence torn ends and their likely displacements can be anticipated and appropriate detours planned and executed. Endothelial cells lining the interior surface of blood vessels and lymphatic vessels may be <1μm thick with a flat surface area of 300-1200 μm^2 and a 10-20 nm gap junction of several different types between neighboring cell membranes. During close approach to vascular walls, the incremental depth of all progressive cuts should probably be restricted to ~25 nm to allow early sensor detection of the ~110 nm thick endothelial glycocalyx,[1014] permitting excavation in a particular direction to be halted before mechanical damage is done to the vascular endothelium.

The lumenal plasma membrane surface of the endothelial cell has a rich proteome consisting of at least 1800 different lipid-embedded proteins,[1015] affording a wide variety of potential sensor targets for a

---

[1010] Robert C. Weast, Handbook of Chemistry and Physics, 49th Edition, CRC, Cleveland OH, 1968; "Specific Heat of Ice," -200 °C to -2.2 °C, p. D-95.

[1011] https://www.aiche.org/resources/publications/cep/2015/september/cool-down-liquid-nitrogen and https://www.engineeringtoolbox.com/nitrogen-d_1421.html.

[1012] Note that the entire fleet waste heat of $P_{fleet} = P_{fleet,0.1mm} + P_{transport,0.1mm} = 0.473$ W could be absorbed by allowing only $P_{fleet} / P_{melt} = 38\%$ of the transported ice cubes to melt during transport, where the power required to melt all of the transported ice is $P_{melt} = n_{cubes}\ N_{nanorobots,0.1mm}\ V_{cube}\ \rho_{ice}\ H_{fusion,water} = 1.24$ W.

[1013] Hadi HA, Carr CS, Al Suwaidi J. Endothelial dysfunction: cardiovascular risk factors, therapy, and outcome. Vasc Health Risk Manag. 2005 Sep;1(3):183-98; https://www.ncbi.nlm.nih.gov/pmc/articles/PMC1993955/. Fisher M. Injuries to the vascular endothelium: vascular wall and endothelial dysfunction. Rev Neurol Dis. 2008;5 Suppl 1:S4-S11; http://medreviews.com/sites/default/files/2016-11/RIND_5Suppl1_S4_0.pdf. Rajendran P, Rengarajan T, Thangavel J, Nishigaki Y, Sakthisekaran D, Sethi G, Nishigaki I. The vascular endothelium and human diseases. Int J Biol Sci. 2013 Nov 9;9(10):1057-69; https://www.ncbi.nlm.nih.gov/pmc/articles/PMC3831119/.

[1014] Uchimido R, Schmidt EP, Shapiro NI. The glycocalyx: a novel diagnostic and therapeutic target in sepsis. Crit Care. 2019 Jan 17;23(1):16; https://d-nb.info/1178412806/34. Delgadillo LF, Marsh GA, Waugh RE. Endothelial Glycocalyx Layer Properties and Its Ability to Limit Leukocyte Adhesion. Biophys J. 2020 Feb 15;S0006-3495(20):30131-4; https://pubmed.ncbi.nlm.nih.gov/32135082/.

[1015] Jacobson BS, Stolz DB, Schnitzer JE. Identification of endothelial cell-surface proteins as targets for diagnosis and treatment of disease. Nat Med. 1996 Apr;2(4):482-484; https://www.nature.com/articles/nm0496-482. Li Y, Massey K, Witkiewicz H, Schnitzer JE. Systems analysis of endothelial cell plasma membrane proteome of rat lung microvasculature. Proteome Sci. 2011 Mar 29;9(1):15; https://proteomesci.biomedcentral.com/articles/10.1186/1477-5956-9-15.

chemotactic sensor pad.[1016] Lymphocytes were observed to adhere to the high endothelial venules in rat lymph node tissue that was frozen to -15 °C, then fixed in glutaraldehyde at 4 °C,[1017] and lymphocytes adhere similarly in frozen mouse mesenteric lymph nodes,[1018] so molecular recognition on frozen tissue surfaces by microscale devices appears plausible. Lateral excavation can be controlled so as not to penetrate too deeply.

In the special case of crackface void excavation, the strengths of the non-covalent bonds holding together cell membrane bilayers are very much lower than the strengths of the non-covalent bonds holding together the vitreous matrix of the solid cryopreservative, so any excavation energy delivered to dislodge segments of the vitreous residue should avoid unnecessarily dislodging lipids from cell membranes. Fahy[1019] suggests designing the geometry of the force application process so as to ensure that only a few molecules are dislodged at any one time, the excavation force being applied not to the medium at large but to a very local area when nanorobots are operating very close to a vascular wall.

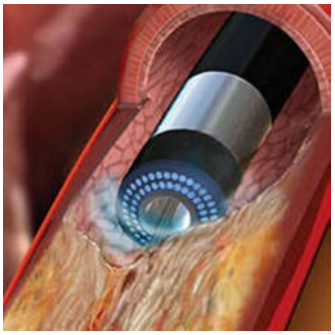

A ***future research*** project might explore the possibility of alternative excavation scenarios, perhaps employing an upgraded variant of one of many catheter-based scanning modalities such as: (1) conventional angiography[1020] or invasive coronary catheterization[1021] in which a snake-like manipulator traverses and carefully follows the branchings of the vascular tree, providing scan information typically with a spatial resolution of ~0.16 mm;[1022] or (2) the ultrasound-based IVUS approach (Section 4.1.3) that may employ 20-50 MHz acoustic frequencies,[1023] potentially providing scan image resolution commensurate to 0.20-0.08 mm wavelengths in ice. These scanning modalities could be combined with a modified version of one or more catheter-based vascular ablation systems such as directional, orbital, rotational, or laser atherectomy systems[1024] as commonly used for plaque removal in endovascular surgery (image, above). These approaches are generally deprecated for cryonics revival work because of their higher energy cost and their

---

[1016] Freitas RA Jr. Nanomedicine, Volume I: Basic Capabilities, Landes Bioscience, Georgetown TX, 1999, Section 8.5.2.1, "Identification of Self"; http://www.nanomedicine.com/NMI/8.5.2.1.htm#p8.

[1017] Stamper HB Jr, Woodruff JJ. Lymphocyte homing into lymph nodes: *in vitro* demonstration of the selective affinity of recirculating lymphocytes for high-endothelial venules. J Exp Med. 1976 Sep 1;144(3):828-33; http://citeseerx.ist.psu.edu/viewdoc/download?doi=10.1.1.285.2270&rep=rep1&type=pdf.

[1018] Butcher EC, Scollay RG, Weissman IL. Lymphocyte adherence to high endothelial venules: characterization of a modified *in vitro* assay, and examination of the binding of syngeneic and allogeneic lymphocyte populations. J Immunol. 1979 Nov;123(5):1996-2003; https://www.jimmunol.org/content/123/5/1996.short.

[1019] Fahy G. Appendix B. A "Realistic" Scenario for Nanotechnological Repair of the Frozen Human Brain. In: Wowk B, Darwin M, eds., Cryonics: Reaching for Tomorrow. Alcor Life Extension Foundation, 1991, pp. A-10 – A-26; https://alcor.org/Library/html/nanotechrepair.html.

[1020] https://en.wikipedia.org/wiki/Invasive_angiography.
[1021] https://en.wikipedia.org/wiki/Coronary_catheterization.

[1022] Lin E, Alessio A. What are the basic concepts of temporal, contrast, and spatial resolution in cardiac CT? J Cardiovasc Comput Tomogr. 2009 Nov-Dec;3(6):403-8; https://www.ncbi.nlm.nih.gov/pmc/articles/PMC4752333/.

[1023] Nissen SE, Yock P. Intravascular ultrasound: novel pathophysiological insights and current clinical applications. Circulation. 2001 Jan 30;103(4):604-16; https://www.ncbi.nlm.nih.gov/pubmed/11157729/.

[1024] Bhat TM, Afari ME, Garcia LA. Atherectomy in Peripheral Artery Disease: A Review. J Invasive Cardiol. 2017 Apr;29(4):135-144; https://www.invasivecardiology.com/articles/atherectomy-peripheral-artery-disease-review.

lack of precision and flexibility – both in turning tight corners and in safely penetrating and operating beyond narrow barriers (e.g., through valves and precapillary sphincters) – though a scheme involving front-steered microcatheters might prove workable. The potential of vacuum sublimation systems (Section 2.2.10(3)) as an alternative excavation methodology should also be investigated in more detail as already recommended elsewhere (Section 5.2.1).

4.2.2 Exploratory Excavation

While cartographic excavation (Section 4.2.1) employs a 3D map to allow quick and efficient removal of ice from a cryopreserved patient, exploratory excavation (aka. **sensor-guided excavation**) involves a slower process in which local sensor data alone is employed to detect vascular pathways and boundaries, and ice is progressively removed from within those regions only as the boundaries are affirmatively detected, e.g., by nanorobots extending probes tipped with chemotactic sensor pads.[1025] If the proper forward path in a vessel under exploration in the 0.1-1 mm size range cannot be reliably located, excavation can be halted in that direction, awaiting guidance from the next round of higher-resolution mapping (Section 4.3). Exploratory excavation is necessarily a longer and more painstaking process than cartographic excavation, probably exhibiting at least a tenfold slower speed of progression.

Exploratory excavation will be needed wherever vascular maps are incomplete. Sensor-guided removal of interstitial ice may be required to search beyond the surviving terminus of a vessel that has been fractured in order to locate the continuation of the same vessel, which may lie 100 μm or farther away. In addition, cryorobotic systems must remove the ice that separates regions of more or less intact tissue that is contained within cracks caused by thermal fracturing during cooldown to cryogenic temperatures. If such fracture ice amounts to $f_{crackvol}$ ~ 1% of total tissue volume (Section 3.4.3), then the total volume of fracture ice to be cleared might be as large as $V_{fractureice,0.1mm} \sim f_{crackvol}\ V_{body} = 600\ cm^3$, or ~9% of the volume of vascular ice to be cleared from a 0.1-mm resolution vascular map (i.e., $V_{ice,0.1mm} \sim 6449\ cm^3$; Section 4.2.1), taking $V_{body} = 0.06\ m^3$ (mean human whole-body volume).[1026] Sensor-guided excavation of fracture ice may be required if the geometry of crack surfaces proves difficult to map in advance or exhibits significant random aspects. ***Future research*** should investigate the best algorithms[1027] for estimating the number, size, and positions of missing or incomplete vasculature based on the available scanning data.

[1025] Freitas RA Jr. Nanomedicine, Volume I: Basic Capabilities, Landes Bioscience, Georgetown TX, 1999, Section 8.5.2.1, "Identification of Self"; http://www.nanomedicine.com/NMI/8.5.2.1.htm#p8.

[1026] Freitas RA Jr. Nanomedicine, Volume I: Basic Capabilities, Landes Bioscience, Georgetown TX, 1999, Table 8.9, "Mass, Volume, and Scale Size of the Organs of the Human Body"; http://www.nanomedicine.com/NMI/Tables/8.9.jpg.

[1027] e.g., Merkle RC. Cryonics, Cryptography, and Maximum Likelihood Estimation. Proc 1st Extropy Inst Conf 1994; http://www.merkle.com/cryo/cryptoCryo.html. See also: https://en.wikipedia.org/wiki/Maximum_likelihood and http://mathworld.wolfram.com/MaximumLikelihood.html.

4.3 Microvascular and Related Scans

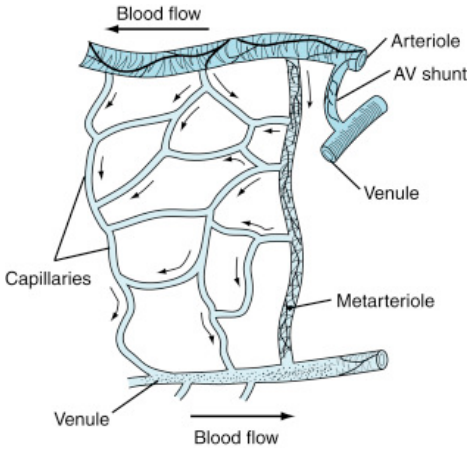

After externally scanning (Section 4.1) and excavating (Section 4.2) the entire vascular tree down to ~0.1 mm (100 μm) diameter vessels, we now have access to a whole-body tunnel system with a total of $N_{termini}$ ~ 77 million excavation endpoints, including:

* 4.5 million arteriole[1028] termini (image above, right) averaging 100 μm in diameter and 9,000 m in total length;[1029]

* 4.5 million venule[1030] termini (image above, right) averaging 150 μm in diameter, 20,000 m in total length;[1031] and

* 68 million lymphatic precollecting duct termini (image below) averaging 100-300 μm in diameter[1032] and ~70,000 m in total length.[1033]

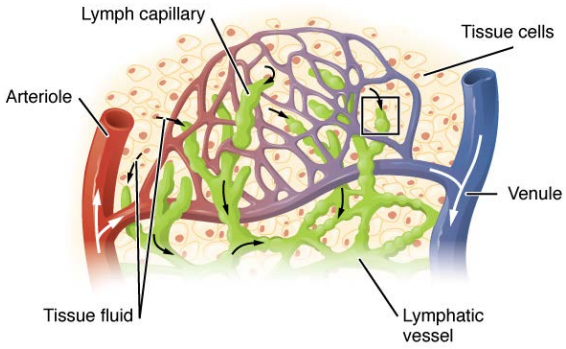

[1028] Non-retinal arterioles receive autonomic nervous system innervation and respond to various circulating hormones in order to regulate their diameter,[*] which ranges from 0.04-0.25 mm.[†]
[*] https://en.wikipedia.org/wiki/Arteriole.
[†] Auer RN. Histopathology of Brain Tissue Response to Stroke and Injury. In: Stroke: Pathophysiology, Diagnosis, and Management, 6th Edition, 2016, pp. 47-59; https://www.sciencedirect.com/science/article/pii/B9780323295444000049.

[1029] Freitas RA Jr. Nanomedicine, Volume I: Basic Capabilities, Landes Bioscience, Georgetown TX, 1999, Table 8.1, "Approximate Quantification of the Human Arteriovenous System"; http://www.nanomedicine.com/NMI/Tables/8.1.jpg.

[1030] https://en.wikipedia.org/wiki/Venule.

[1031] Freitas RA Jr. Nanomedicine, Volume I: Basic Capabilities, Landes Bioscience, Georgetown TX, 1999, Table 8.1, "Approximate Quantification of the Human Arteriovenous System"; http://www.nanomedicine.com/NMI/Tables/8.1.jpg.

[1032] Lymph capillaries drain lymph fluid to larger contractile collecting lymphatics (which have valves and smooth muscle walls) via the precollecting ducts. Pan WR, Suami H, Taylor GI. Lymphatic drainage of the superficial tissues of the head and neck: anatomical study and clinical implications. Plast Reconstr Surg. 2008 May;121(5):1614-1626; http://klosetraining.com/wp-content/uploads/2015/09/Hiro-Suami-Kopf-Hals.pdf.

[1033] Freitas RA Jr. Nanomedicine, Volume I: Basic Capabilities, Landes Bioscience, Georgetown TX, 1999, Table 8.5, "Approximate Quantification of the Human Lymphatic System"; http://www.nanomedicine.com/NMI/Tables/8.5.jpg.

If arteriovenous (image below, left) and lymphatic (image below, right) termini were more-or-less evenly distributed throughout a human body volume of V_{body} = 0.06 m^3, then each terminus would be surrounded by an average tissue volume of $V_{termini} = V_{body} / N_{termini}$ = 0.779 mm^3, with a mean separation of $V_{termini}^{1/3}$ = 0.92 mm between termini.

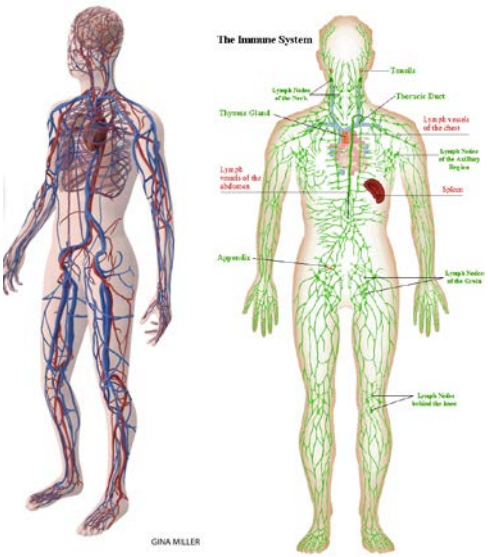

The next step in the revival protocol is to scan the entire frozen tissue to a resolution sufficient to resolve all capillary vessels 4-8 μm in diameter, then use this information to excavate all frozen material from all arteriovenous and lymphatic microvasculature and crackface voids (Section 4.4.1) and similarly from organ and other tissue perimeters (Section 4.4.2).

To initiate the scan process, nanorobotic energy transceivers could be placed at all previously-excavated termini, creating a 3D microarray of $N_{termini}$ sensors that could, over a sufficient data collection time, produce high-resolution tomographic images of the entire frozen tissue mass. However, the number of sensor points can be dramatically increased by placing the microscale transceivers every $x_{sensors}$ ~ 100 μm/sensor along the $L_{macroexcavate}$ = 9,000 m + 20,000 m + 70,000 m ~ 10^5 m total length of all previously excavated vessels, yielding a total sensor count of $N_{sensors} = L_{macroexcavate} / x_{sensors}$ ~ 10^9 sensors and thus an average per-sensor service volume of $V_{sensors} \sim V_{body} / N_{sensors}$ = 60 million μm^3, with a mean separation of $x_{sep} = V_{sensors}^{1/3}$ = 390 μm between closest-neighbor transceivers, again assuming more-or-less even distribution throughout the body.

Several methods have been tentatively identified that may provide the required microvascular, crackface void and organ perimeter scans at sufficient resolution to guide cartographic excavation (as previously described in Section 4.2.1) of the microvasculature. These scanning methods include: gigahertz acoustic microscopy (Section 4.3.1), terahertz infrared imaging (Section 4.3.2), optical coherence tomography (Section 4.3.3), confocal microscopy (Section 4.3.4), and high-resolution X-ray microtomography (Section 4.3.5). Some details of the excavation are described in Section 4.4.

Care must be taken not to unduly raise the cryogenic body temperature of the cryopreserved patient during the scanning process. For example, whole-body gigahertz acoustic scanning is estimated to generate 0.03-0.3 watts of waste heat using a GHz acoustic pulse rate of ~1 KHz for $N_{sensors}$ = 10^9 transmitters (requiring a 30-300 pW/nanorobot power supply assuming 1 transmitter per nanorobot, the large range being due to the current uncertainty in GHz signal attenuation during passage through a cryogenic tissue mass; Section 4.3.1). If necessary to keep the cryopreserved tissue from softening or melting: (1) liquid nitrogen can be flushed through the tunnel network to carry away excess heat as previously described in Section 4.2.1; or (2) the GHz pulse rate can be reduced to whatever is deemed thermally acceptable, allowing the patient to remain physically safe and unchanging at cryogenic temperatures. In this manner, the scanning process can take as long as necessary – be it days, weeks, or even months.

4.3.1 Gigahertz Acoustic Microscopy

Given the $v_{sound/ice}$ ~ 3940 m/sec speed of sound in bubble-free ice at ~210 K,[1034] achieving a feature resolution of $d_{capillary}$ ~ 4-8 μm requires an acoustic frequency on the order of $v_{ice} \geq v_{sound/ice} / d_{capillary}$ ~ 0.5-1 GHz. 1 GHz ultrasound scanning is now fairly routine.[1035] Although there are no reports of GHz ultrasound microscope scans in ice, acoustic microscopy has had notable successes that seem relevant to the present application, including:

* acoustic waves with a wavelength of **0.01 μm** have been generated and studied in cryogenic quartz crystals;[1036]
* a cryogenic acoustic microscope operated at 8 GHz has demonstrated **0.02 μm** lateral resolution in 0.1 K superfluid helium;[1037]
* an acoustic resolution of **0.2 μm** has been achieved with water as the coupling fluid at a frequency of up to 4.4 GHz;[1038] and
* acoustic images of MOS transistor circuits clearly resolve **1 μm** features using frequencies of 1.1-1.8 GHz.[1039]

In normal biological tissues, ultrasound attenuation is approximately linearly proportional to frequency,[1040] with 50 MHz ultrasound having a penetration depth of 8-9 mm in most tissues,[1041] implying a penetration

---

[1034] Vogt C, Laihem K, Wiebusch C. Speed of sound in bubble-free ice. J Acoust Soc Am. 2008 Dec;124(6):3613-8; https://www.researchgate.net/publication/23997391_Speed_of_sound_in_bubble-free_ice. The speed of sound in vitrified tissue will be slightly different from this number.

[1035] Brand S, Lapadatu A, Djuric T, Czurratis P, Schischka J, Petzold M. Scanning acoustic gigahertz microscopy for metrology applications in three-dimensional integration technologies. J Micro/Nanolithography, MEMS, and MOEMS 2014 Feb 20;13(1):011207; https://www.spiedigitallibrary.org/journals/journal-of-micro-nanolithography-mems-and-moems/volume-13/issue-01/011207/Scanning-acoustic-gigahertz-microscopy-for-metrology-applications-in-three-dimensional/10.1117/1.JMM.13.1.011207.full?SSO=1. Balasubramanian PS, Singh A, Xu C, Lal A. GHz Ultrasonic Chip-Scale Device Induces Ion Channel Stimulation in Human Neural Cells. Sci Rep. 2020 Feb 20;10(1):3075; https://www.ncbi.nlm.nih.gov/pmc/articles/PMC7033194/. Mohamed ETA, Declercq NF. Giga-Hertz ultrasonic microscopy: Getting over the obscurity - A short review on the biomedical applications. Physics in Medicine 2020 Jun;9:100025; https://www.sciencedirect.com/science/article/pii/S2352451020300019.

[1036] Ilukor J, Jacobsen EH. Coherent elastic wave propagation in quartz at ultramicrowave frequencies, in: Mason WP, ed., Physical Acoustics, Academic Press, NY, 1968, vol. V, Ch. 5, pp. 221-231; https://www.amazon.com/dp/0124332846/. Anderson CH, Sabisky ES. Spin-phonon spectrometer, in: Mason WP, ed., Physical Acoustics, Academic Press, NY, 1971, Vol. VIII, Ch. 1, pp. 2-57; https://www.amazon.com/dp/0124313949/.

[1037] Hadimioglu B, Foster JS. Advances in superfluid helium acoustic microscopy. J Appl Phys. 1984 Oct 1;56(7):1976-1980; https://aip.scitation.org/doi/abs/10.1063/1.334230.

[1038] Hadimioglu B, Quate CF. Water acoustic microscopy at suboptical wavelengths. Appl Phys Lett. 1983 Dec 1;43(11):1006-1007; https://aip.scitation.org/doi/abs/10.1063/1.94223. See also: Luers H, Bereiter-Hahn J, Litniewski J, in: Ermert H, Harjes HP, eds., Acoustical Imaging, Volume 19, Plenum Press, NY, 1992, pp. 511-516.

[1039] Quate CF, Atalar A, Wickramasinghe HK. Acoustic microscopy with mechanical scanning – a review. Proc IEEE 1979 Aug;67(8):1092-1114; http://repository.bilkent.edu.tr/bitstream/handle/11693/50766/Acoustic_microscopy_with_mechanical_scanning%20A_review.pdf?sequence=1.

[1040] Zagzebski JM. Essentials of Ultrasound Physics. Mosby, St. Louis MO, 1996. Szabo T. Diagnostic Ultrasound Imaging: Inside Out, Elsevier, NY, 2004. Shung KK. Diagnostic Ultrasound: Imaging and Bloodflow Measurements, CRC Press, Boca Raton FL, 2006. Cobbold RSC. Foundations of Biomedical Ultrasound. Oxford University Press, NY, 2007; https://www.amazon.com/dp/B001PIHTKA/.

depth of 400-450 μm at 1 GHz – very close to the required x_{sep} = 390 μm separation of closest-neighbor transceivers.

If operated in transmission mode, the acoustic pulse must travel the full x_{sep} from transmitter to receiver, but if operated in reflection mode, less attenuated data can be received from reflections off structures considerably closer to the transmitter than x_{sep}. A previously-published theoretical estimate suggests that acoustic reflection microscopy (echolocation) using 1.5 GHz acoustic chirps at the maximum safe *in vivo* power density of 1000 W/m^2 in warm aqueous tissue might resolve ~1 μm features at a depth of x_{range} ~ 46 μm into the tissue mass.[1042] If this approximately holds for water-ice-rich cryopreserved tissue at ~77 K (-196 °C), then two apposed nanorobots located x_{sep} = 390 μm apart could scan the nearest x_{range} / 2 = 23 μm of tissue in reflection mode, including in the direction towards each other, map the vascular features that are observed, excavate the vascular tunnels within the 23 μm mapped volume, then reposition themselves x_{range} = 46 μm closer and repeat the procedure, closing the 390 μm gap between them in a total of x_{sep} / x_{range} ~ 9 iterations. This procedure should yield a comprehensive tissue map down to micron-scale feature resolution with all capillaries and crackface voids fully mapped and excavated.

High-resolution lithium niobate ~0.3 GHz ultrasound transducers measuring 9 μm in size have provided 6.4 μm lateral resolution and 6.2 μm axial resolution in scans of a zebrafish eye;[1043] a ~0.5 GHz acoustic microscope with a 125 μm lens radius has achieved a 4 μm lateral resolution;[1044] and ~1 GHz acoustic microscopes are available.[1045]

Power demand can be estimated for the worst-case scenario (transmission mode). Reports of GHz acoustic attenuation coefficients for ice are scarce in the literature, but if we assume an attenuation coefficient in the range of α_{GHzIce} = 1-7 Np/mm at GHz frequencies based on related data in **Table 4**, then the power attenuation of a 1 GHz acoustic pulse traversing cryopreserved human tissue at LN2 temperatures (~77 K) is $k_{atten} = P_{receiver}/P_{transmitter} \sim \exp(-\alpha_{GHzIce}\ x_{sep})$ = 0.7-0.065 in transmission mode for x_{sep} = 390 μm. Taking the minimum detectable energy for a 1 μm^3 acoustic sensor with a signal-to-noise ratio (SNR) of ~3 as $E_{receiver} \sim k_B T\ e^{SNR}$ = 21 zJ at T = 77 K,[1046] the receiver power $P_{receiver} = E_{receiver} / t_{pulse}$ = 0.021 pW for a single minimally-detectable pulse of duration $t_{pulse} = 10^{-6}$ sec, in which case the power required to transmit the pulses is $P_{transmitter} = P_{receiver} / k_{atten}$ = 0.03-0.3 pW per pulse and the power requirement for all $N_{sensors}$ transmitters to emit one pulse is $P_{pulse,total} = P_{transmitter}\ N_{sensors}$ = 30-300 μW/pulse. Thus a pulse rate of ~1

[1041] Shung KK. High Frequency Ultrasonic Imaging. J Med Ultrasound 2009;17(1):25-30; https://core.ac.uk/download/pdf/82448478.pdf.

[1042] Freitas RA Jr. Nanomedicine, Volume I: Basic Capabilities, Landes Bioscience, Georgetown TX, 1999, Section 4.9.2, "Transcellular Acoustic Microscopy"; http://www.nanomedicine.com/NMI/4.8.2.htm.

[1043] Fei C, Chiu CT, Chen X, Chen Z, Ma J, Zhu B, Shung KK, Zhou Q. Ultrahigh Frequency (100 MHz-300 MHz) Ultrasonic Transducers for Optical Resolution Medical Imagining. Sci Rep. 2016 Jun 22;6:28360; https://www.nature.com/articles/srep28360.

[1044] Rohrbach D, Jakob A, Lloyd HO, Tretbar SH, Silverman RH, Mamou J. A Novel Quantitative 500-MHz Acoustic Microscopy System for Ophthalmologic Tissues. IEEE Trans Biomed Eng. 2017 Mar;64(3):715-724; https://www.ncbi.nlm.nih.gov/pmc/articles/PMC5490248/.

[1045] Rantamaa A, Hyvönen J, Meriläinen A, Salmi A, Hæggström E. Optimized Signal Generation Circuit for Coded GHz Acoustic Microscope. 2019 IEEE International Ultrasonics Symposium (IUS), 6-9 Oct 2019; https://ieeexplore.ieee.org/abstract/document/8926073.

[1046] Freitas RA Jr. Nanomedicine, Volume I: Basic Capabilities, Landes Bioscience, Georgetown TX, 1999, Section 4.5.1, "Minimum Detectable Pressure"; http://www.nanomedicine.com/NMI/4.5.1.htm.

KHz could be sustained for all $N_{sensors} = 10^9$ transmitters within a whole-body scanning power budget of 0.03-0.3 watts.

Table 4. High-frequency acoustic attenuation coefficients

Type of Ice or Other Solid Material	Acoustic Frequency	Attenuation Coefficient (Np/mm)[1047]	Reference*
Sea ice	1 MHz	0.0069	[1]
Hard (glaze) ice	1.1 MHz	0.0102	[2]
Sea & freshwater ice	1.1 MHz	0.0173	[3]
Soft (rime) ice	1.1 MHz	0.0374	[2]
Water	15 MHz	0.0055	[2]
Hard (glaze) ice	15 MHz	0.04	[2]
Soft (rime) ice	15 MHz	0.17	[2]
α_{glaze} (Np/mm) = 0.002 x f (MHz) + 0.008 (glaze ice) (empirical model)	1 MHz	0.01	[2]
	10 MHz	0.03	[2]
	100 MHz	0.21	[2]
	1 GHz	2.01	[2]
α_{rime} (Np/mm) = 0.0067 x f (MHz) + 0.03 (rime ice) (empirical model)	1 MHz	0.04	[2]
	10 MHz	0.10	[2]
	100 MHz	0.70	[2]
	1 GHz	6.73	[2]
Biofilm	100 MHz	4.0	[4]
Metals, insulators, ceramics, & semiconductors	1 GHz	0.0023-0.18	[5]
Titanium @ 300 K	1 GHz	0.12	[5]
Gold @ 300 K	0.7-0.8 GHz	1.15	[5]

* [1],[1048] [2],[1049] [3],[1050] [4],[1051] and [5][1052]

[1047] The neper (Np) is a logarithmic unit for ratios of measurements of physical field and power quantities; https://en.wikipedia.org/wiki/Neper.

[1048] Pounder ER, Langleben MP. Acoustic attenuation in sea ice. In: Ward W, ed., Commission of Snow and Ice, Intl Union of Geodesy and Geophysics and Intl Assn of Scientific Hydrology, Publ. No. 79, 1968, pp. 161-169 ; http://hydrologie.org/redbooks/a079/079015.pdf.

[1049] Liu Y, Bond LJ, Hu H. Ultrasonic-Attenuation-Based Technique for Ice Characterization Pertinent to Aircraft Icing Phenomena. AIAA J. 2017 May;55(5):1-8; http://www.aere.iastate.edu/~huhui/paper/journal/2017-AIAA-J-Ultrasonic-Yang-Liu.pdf.

[1050] Bogorodskii VV, Gavrilo VP, Nikitin VA. Sound Propagation in Ice Crystallized from Salt-Water. Soviet Physics Acoustics 1976;22(2):158-159.

[1051] Anastasiadis P, Mojica KD, Allen JS, Matter ML. Detection and quantification of bacterial biofilms combining high-frequency acoustic microscopy and targeted lipid microparticles. J Nanobiotechnology. 2014 Jul 6;12:24; https://core.ac.uk/download/pdf/81776877.pdf.

The design of a GHz acoustic scanning system for whole-body cryogenic vascular mapping at microscale resolution is an appropriate topic for ***future research***.

4.3.2 Terahertz Infrared Imaging

Because of its 100-fold greater penetrating power in solid ice as compared to liquid water, terahertz (THz = 10^{12} Hz) or far-infrared electromagnetic radiation can traverse ~1000 μm of frozen tissue with ~90% of the original transmitted energy reaching the receiver (Section 4.1.4(1)). Terahertz imaging for biological scanning most commonly occupies the ν_{THz} = 0.1-10 THz frequency range (wavelength $\lambda_{THz} = c / \nu_{THz}$ ~ 3000-30 μm, taking speed of light c = 3 x 10^8 m/sec), though the upper bound is considered by some sources to be as high as ~30 THz,[1053] representing a wavelength as low as λ_{THz} ~ 10 μm which might be small enough to localize most capillaries sufficiently well to enable exploratory excavation (Section 4.2.2).

Terahertz radiation is not ionizing radiation and thus does not damage DNA and living tissues, and may detect differences in density between different biological structures in part because proteins have intramolecular vibrations in the THz range. While the initial attraction of THz imaging was its strong absorption by water (with tissue water content assumed to be the dominant contrast mechanism),[1054] it has subsequently been shown that THz imaging can distinguish between (1) rat tissues from different healthy organs,[1055] (2) healthy adipose and healthy fibrous breast tissue,[1056] and (3) normal and diseased liver due to differences in absorption of the tissue structure.[1057] The greatest contrast between cancerous and normal tissue apparently occurs in the lower frequency ranges between 0.15-2 THz,[1058] so ***future research*** should

---

[1052] Quate CF, Atalar A, Wickramasinghe HK. Acoustic microscopy with mechanical scanning – a review. Proc IEEE 1979 Aug;67(8):1092-1114; http://repository.bilkent.edu.tr/bitstream/handle/11693/50766/Acoustic_microscopy_with_mechanical_scanning%20A_review.pdf?sequence=1.

[1053] Dhillon SS, *et al*. The 2017 terahertz science and technology roadmap. J Phys D: Appl Phys. 2017;50(4):1-49; https://www-thz.physics.ox.ac.uk/papers/Dhillon2017_4463.pdf.

[1054] Hu BB, Nuss MC. Imaging with terahertz waves. Opt Lett. 1995 Aug 15;20(16):1716-1718; https://pdfs.semanticscholar.org/82ab/a984ba2c031f65d668eb78aef26c9d84891f.pdf.

[1055] Huang SY, Wang YJ, Yeung DKW, Ahuja AT, Zhang YT, Pickwell-MacPherson E. Tissue characterization using terahertz pulsed imaging in reflection geometry. Phys Med Biol. 2009;54:149-160; https://www.researchgate.net/profile/Yi_Xiang_Wang2/publication/23656242_Tissue_characterization_using_terahertz_pulsed_imaging_in_reflection_geometry/links/548795e90cf2ef34478ecbfc.pdf.

[1056] Ashworth PC, Pickwell-MacPherson E, Provenzano E, Pinder SE, Purushotham AD, Pepper M, Wallace VP. Terahertz pulsed spectroscopy of freshly excised human breast cancer. Opt Express. 2009 Jul 20;17(15):12444-12454; https://www.osapublishing.org/viewmedia.cfm?uri=oe-17-15-12444&seq=0.

[1057] Sy S, Huang S, Wang YX, Yu J, Ahuja AT, Zhang YT, Pickwell-MacPherson E. Terahertz spectroscopy of liver cirrhosis: investigating the origin of contrast. Phys Med Biol. 2010 Dec 21;55(24):7587-7596; https://www.researchgate.net/profile/Yi_Xiang_Wang2/publication/251963201_Investigating_the_role_of_water_content_on_the_terahertz_properties_of_rat_liver_cirrhosis/links/548797620cf268d28f072602/Investigating-the-role-of-water-content-on-the-terahertz-properties-of-rat-liver-cirrhosis.pdf.

[1058] Ashworth PC, Pickwell-MacPherson E, Provenzano E, Pinder SE, Purushotham AD, Pepper M, Wallace VP. Terahertz pulsed spectroscopy of freshly excised human breast cancer. Opt Express. 2009 Jul 20;17(15):12444-12454; https://www.osapublishing.org/viewmedia.cfm?uri=oe-17-15-12444&seq=0.

investigate the available contrast at higher frequencies near 10-30 THz and determine if this contrast is sufficient to resolve cryoprotectant-filled capillary vessels. Compact sources of THz radiation such as cryogenic quantum cascade lasers are known,[1059] and laser terahertz microscopy has imaged the surface of an integrated circuit chip to a spatial resolution below 3 μm,[1060] but ***future research*** must identify or develop microscale emitters and receivers of THz radiation[1061] suitable for conveyance and use by nanorobots in order to make this approach feasible.

4.3.3 Optical Coherence Tomography

Optical coherence tomography (OCT) is an imaging technique that uses low-coherence light to capture micron-resolution 2D and 3D subsurface images from within translucent or opaque optical scattering media such as biological tissue.[1062] OCT can probe as deep as 500 μm with a lateral resolution of ~10 μm and an axial resolution (depth) of ~3 μm in ophthalmology.[1063] Intracoronary OCT,[1064] and especially intravascular OCT,[1065] are catheter-based systems that typically deliver and collect near-infrared light (λ_{OCT} ~ 1300 nm) to create cross-sectional images of the artery lumen and wall. Time-domain OCT provides 12-18 μm axial resolution of 12-18 μm and 20-90 μm lateral resolution with tissue penetration of 1-3 mm, while frequency-domain OCT can achieve 10-15 μm axial resolution, 20-40 μm lateral resolution, and 2-3.5 mm tissue penetration.[1066]

"OCT delivers high resolution because it is based on light, rather than sound or radio frequency. An optical beam is directed at the tissue, and a small portion of this light that reflects from sub-surface features is collected. Most light is not reflected but, rather, scatters off at large angles. In conventional imaging, this diffusely scattered light contributes background that obscures an image. However, in OCT, interferometry is used to record the optical path length of received photons allowing rejection of most photons that scatter

---

[1059] For example: Walther C, Fischer M, Scalari G, Terazzi R, Hoyler N, Faist J, Quantum cascade lasers operating from 1.2 to 1.6 THz. Appl Phys Lett. 2007 Sep;91(13):131122; https://aip.scitation.org/doi/abs/10.1063/1.2793177. Dean P, Lim YL, Valavanis A, *et al*. Terahertz imaging through self-mixing in a quantum cascade laser. Opt Lett. 2011 Jul 1;36(13):2587-2589; http://eprints.whiterose.ac.uk/43114/4/OptLett_Dean_2011.pdf.

[1060] Yamashita M, Kawase K, Otani C, Kiwa T, Tonouchi M. Imaging of large-scale integrated circuits using laser-terahertz emission microscopy. Opt Express. 2005 Jan 10;13(1):115-120; http://www.agri.tohoku.ac.jp/thz/jp/71_k03.pdf.

[1061] Jornet JM, Akyildiz IF. Graphene-based Plasmonic Nano-Antenna for Terahertz Band Communication in Nanonetworks. IEEE J Select Areas in Commun/Suppl. 2013 Dec;31(12, Pt. 2):685-694; http://bwn.ece.gatech.edu/papers/2013/j17.pdf. Cocker TL, Huber R. THz microscopy. J Phys D: Appl Phys. 2017;50:26-27; https://www-thz.physics.ox.ac.uk/papers/Dhillon2017_4463.pdf. See also: https://en.wikipedia.org/wiki/Terahertz_radiation#Artificial.

[1062] https://en.wikipedia.org/wiki/Optical_coherence_tomography.

[1063] Drexler W, Morgner U, Ghanta RK, Kärtner FX, Schuman JS, Fujimoto JG. Ultrahigh-resolution ophthalmic optical coherence tomography. Nat Med. 2001 Apr;7(4):502-7; https://www.ncbi.nlm.nih.gov/pmc/articles/PMC1950821/.

[1064] https://en.wikipedia.org/wiki/Intracoronary_optical_coherence_tomography.

[1065] Tearney GJ, Regar E, Akasaka T, *et al*. Consensus standards for acquisition, measurement, and reporting of intravascular optical coherence tomography studies: a report from the International Working Group for Intravascular Optical Coherence Tomography Standardization and Validation. J Am Coll Cardiol. 2012 Mar 20;59(12):1058-1072; http://www.incathlab.com/files/STJUDE/2012_Tearney_Consensus_OCT.pdf.

[1066] Bezerra HG, Costa MA, Guagliumi G, Rollins AM, Simon DI. Intracoronary optical coherence tomography: a comprehensive review clinical and research applications. JACC Cardiovasc Interv. 2009 Nov;2(11):1035-1046; https://core.ac.uk/download/pdf/81942083.pdf.

multiple times before detection. Thus OCT can build up clear 3D images of thick samples by rejecting background signal while collecting light directly reflected from surfaces of interest. The technique is limited to imaging 1-2 mm below the surface in biological tissue, because at greater depths the proportion of light that escapes without scattering is too small to be detected." [1067]

Future research should establish the performance and limitations of this method on cryopreserved human tissue at cryogenic temperatures.

4.3.4 Confocal Microscopy

Confocal microscopy[1068] is an optical imaging technique for increasing optical resolution and contrast of a micrograph by using a spatial pinhole to block out-of-focus light during image formation – capturing multiple 2D images at different depths in a sample enables the reconstruction of 3D structures within an object, a process known as optical sectioning.[1069] Most applications of confocal microscopy achieve submicron resolution by using special mounting media or by staining the specimen,[1070] neither of which will be available in the case of cryopreserved tissue at cryogenic temperatures. *Ex vivo* confocal microscopy avoids the need for tissue embedding, processing, or sectioning, without altering the tissue. When used in reflectance mode (with an 830 nm wavelength laser) rather than fluorescence mode on excised dermal tissue, the microscope produces horizontal images of 750 x 750 μm of the different layers of the skin up to a thickness of 200 μm with lateral and axial spatial resolutions of 1 μm and 3 μm, respectively.[1071]

A recently developed optical scanning technology called laser scanning reflection-matrix microscopy uses computational adaptive optics to see through mouse skull and acquire a microscopic map of neural networks within the brain tissues. The reflection matrix microscope is said to work without any fluorescent labeling,[1072] and was able to realize reflectance imaging of myelinated axons *in vivo* underneath an intact mouse skull at 450 nm resolution over a field of view >100 μm^2, and to visualize neuronal dendrites and their spines at 500 nm resolution albeit using two-photon fluorescence (which would not be possible on cryopreserved brains).[1073]

[1067] https://en.wikipedia.org/wiki/Optical_coherence_tomography#Layperson's_explanation.

[1068] https://en.wikipedia.org/wiki/Confocal_microscopy.

[1069] Pawley JB, ed. Handbook of Biological Confocal Microscopy, Third Edition, Springer, Berlin, 2006; https://www.amazon.com/dp/B0086HWP4I/.

[1070] For example: Schermelleh L, Heintzmann R, Leonhardt H. A guide to super-resolution fluorescence microscopy. J Cell Biol. 2010 Jul 26;190(2):165-175; http://www.aomf.ca/pdfs/OMUG2011/JCB_GuideToSuperResolution.pdf. Fouquet C, Gilles JF, Heck N, Dos Santos M, Schwartzmann R, Cannaya V, Morel MP, Davidson RS, Trembleau A, Bolte S. Improving axial resolution in confocal microscopy with new high refractive index mounting media. PLoS One. 2015 Mar 30;10(3):e0121096; https://www.ncbi.nlm.nih.gov/pmc/articles/PMC4379090/pdf/pone.0121096.pdf.

[1071] Cinotti E, Perrot JL, Labeille B, Cambazard F, Rubegni P. *Ex vivo* confocal microscopy: an emerging technique in dermatology. Dermatol Pract Concept. 2018 Apr 30;8(2):109-119; https://www.ncbi.nlm.nih.gov/pmc/articles/PMC5955077/pdf/dp0802a08.pdf.

[1072] https://www.ibs.re.kr/cop/bbs/BBSMSTR_000000000738/selectBoardArticle.do?nttId=19379.

[1073] Yoon S, Lee H, Hong JH, Lim YS, Choi W. Laser scanning reflection-matrix microscopy for aberration-free imaging through intact mouse skull. Nat Commun. 2020 Nov 12;11(1):5721; https://www.ncbi.nlm.nih.gov/pmc/articles/PMC7665219/.

Future research should investigate (1) the workability of these scanning methods on cryopreserved human tissue at cryogenic temperatures, and (2) whether operational optical emitting, masking, and receiving equipment can be reduced in size to microscopic dimensions to enable convenient deployment and use by medical nanorobots deployed in vascular spaces.

4.3.5 High-Resolution X-Ray Microtomography

As previously noted in Section 4.1.2, contrast-free high-resolution X-ray microtomography (micro-CT) scans on fossilized biological specimens that are as solid and hard as cryopreserved human tissue at cryogenic temperatures permit 3D tomographic reconstructions in which nonvascular cellular features crudely resembling capillary tubes are clearly resolved at the 2-5 μm size scale.[1074] ***Future research*** should explore the limits of this technology for the proposed application.

4.4 Microvascular and Related Excavations

With all microvascular capillaries and crackface voids having been scanned and geometrically defined, and with the physical extent of organs, bones and other tissues known to a geometrical resolution of microns, excavation can now be finished for three particular tissue volumes:

* the capillaries and crackface void spaces (Section 4.4.1),

* the accessible perimeter spaces surrounding organs and related structures (Section 4.4.2), and

* the extracellular spaces where pure water-ice has accumulated, occupying space vacated by the shrinking brain and other organs as water exits the cells and then freezes during the cryopreservation process (Section 4.4.3).

4.4.1 Capillary, Lymphatic, and Crackface Void Excavation

In regions of cryopreserved tissue where the micron-scale scanning has been successful, excavation may proceed cartographically as previously outlined in Section 4.2.1 wherein the vasculature with vessel diameters ≥100 μm has already been excavated. For the remaining vasculature with vessel diameters <100 μm that has been scanned as described in Section 4.3, there is now an additional V_{avcap} = 5400 cm^3 – 4275 cm^3 = 1125 cm^3 of small-vessel arteriovenous volume and an additional $V_{lymphcap}$ = 3300 cm^3 – 1574 cm^3 = 1726 cm^3 of lymphatic system volume to be cleared of ice using the same excavation nanorobots as before. To this must be added the crackface void volume, with individual cracks occupying $f_{crackvol}$ ~ 1% of total cryopreserved tissue volume (Section 3.4.3). Taking tissue volume as V_{body} = 0.06 m^3 (mean human whole-body volume),[1075] then $V_{crackvoid} = f_{crackvol}\ V_{body}$ ~ 600 cm^3.

[1074] Donoghue PC, Bengtson S, Dong XP, Gostling NJ, Huldtgren T, Cunningham JA, Yin C, Yue Z, Peng F, Stampanoni M. Synchrotron X-ray tomographic microscopy of fossil embryos. Nature. 2006 Aug 10;442(7103):680-683; https://seis.bristol.ac.uk/~jc1224/Publications/assets/Donoghue_et_al_2006b.pdf.

[1075] Freitas RA Jr. Nanomedicine, Volume I: Basic Capabilities, Landes Bioscience, Georgetown TX, 1999, Table 8.9, "Mass, Volume, and Scale Size of the Organs of the Human Body"; http://www.nanomedicine.com/NMI/Tables/8.9.jpg.

Thus the total capillary and crackface void volume to be excavated is $V_{ice,\mu m} = V_{avcap} + V_{lymphcap} + V_{crackvoid}$ ~ 3451 cm^3. Applying the same methodology for microvascular excavation as was used for macrovascular excavation in Section 4.2.1, $N_{nanorobots,\mu m} = V_{ice,\mu m} / (r_{removal}\ t_{clearance})$ = **2.3 x 10^9** active tunneling nanorobots are needed to clear the ice from the microtunnels identified in a ~4 μm resolution vascular map (Section 4.3), with a fleet power demand of $P_{fleet,\mu m} = P_{robot}\ N_{nanorobots,\mu m}$ = 0.23 W, again taking $r_{removal}$ = 1 μm^3/nanorobot-sec, $t_{clearance}$ ~ 1.5 x 10^6 sec (~**17 days**), and P_{robot} = 100 pW. As before, additional support nanorobots will also be required.

In regions of tissue where mapping has been unsuccessful or is incomplete, exploratory excavation may proceed as described earlier in Section 4.2.2.

An additional complication of small-vessel excavation is the likely presence of various blockages attributable to extended periods of warm ischemia (Section 3.2). In the most common cases involving erythrocyte-rich blood clots, sludged red cells, broken platelets, neutrophil plugs, and other micro-emboli, the blockage material is readily removed by conventional excavation as long as the frozen biological debris is clearly distinguishable from the endothelium forming the capillary walls, allowing excavation to proceed without damaging vessel integrity. In less-common cases involving endothelial swelling or blebbing that seriously occludes the capillary lumen (Section 3.6(3)), clean installation of vasculoid (Section 4.6) may require excision of the (still frozen or solidified) blocking material, with the location and other details of the excision recorded for inclusion in the future vasculoid installation (Section 4.6.2) and vascular cell repair (Section 4.11.1) procedures.

4.4.2 Organ and Tissue Surface Perimeter Excavation

It is reasonable to expect that many accessible organ and body surfaces should be coated with vasculoid applications plates to maintain the gross physical integrity of the patient's body after warmup and reliquidification. These plates will create a watertight barrier providing protection against tissue desiccation, fluid leakage, and material contamination during and after reliquidification, and will also provide physical support and resistance to gravitational sagging and other geometric deformations as the body is warmed and softens. The surfaces to be plated would include the exterior surfaces of organs, the exterior surface of the human body (i.e., the skin), the inside and outside surfaces of macroscale fluid-filled compartments (e.g., Bowman's capsule in a renal glomerulus; image, right), pleural surfaces, and the surfaces of the lung and alimentary tract that are exposed to air and chyme, respectively. As estimated in Appendix E, these additional surfaces may have a total surface area of $A_{surfaceplates}$ ~ 90.841 m^2.

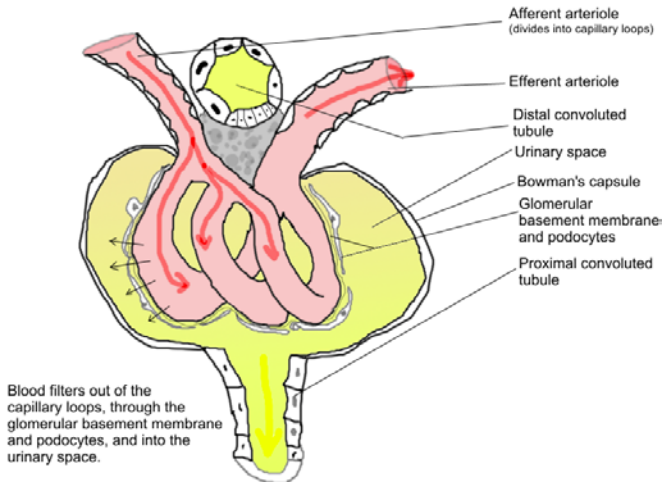

These potentially plateable surfaces must be excavated to a depth of at least $d_{excavsurf}$ ~ 1 μm, the thickness of an applications plate (Section 4.6.1), giving a minimum excavation volume of $V_{excavsurf} \sim d_{excavsurf}\ A_{surfaceplates}$ = 91 cm^3 which is a 2.6% addition to the previously estimated $V_{ice,\mu m}$ ~ 3451 cm^3 microvascular excavation volume (Section 4.4.1), requiring only an additional **0.06 x 10^9** active tunneling nanorobots operating for ~2.6% $t_{clearance}$ ~ 39,000 sec (~**11 hr**). While slightly greater depths of up to a few microns may be needed to provide excavation and plate-emplacing nanorobots with sufficient room to operate conveniently, it is also likely that not all identified surfaces can or must be excavated, e.g.,

due to the physical impediment of pleural attachments to certain organs. The extent and specifics of perimeter excavation requirements is a matter to be examined in greater detail in ***future research***.

4.4.3 Extracellular Ice Excavation

The brain of a cryopreserved patient is perhaps 80% water and cryoprotectant, and some of this will exist in the form of pure water-ice located in the extracellular space due to osmotic outflows of cytosolic water during the original cryopreservation process,[1076] sometimes causing significant organ shrinkage (Section 3.3(2)). These organs will expand to their original volumes during rehydration (Section 4.11.3). By removing the extracellular ice, empty space is created into which (A) rehydrating organs can expand, and (B) cell repair nanorobots can operate. ***Future research*** should ascertain where and how much extracellular ice is likely to be present in cryonics patients of early vs. modern vintage, using various cryoprotectants and different cryopreservation protocols. Excavation of unwanted water-ice can proceed as outlined earlier (Section 4.2).

Extracellular ice excavation may result in additional (but presently unquantified) exposed surface ice requiring reconditioning (Section 4.5.2), surface mapping (Section 4.5.4 and Section 4.5.5), and vasculoid plating (Section 4.6.5(4)).

4.5 Recondition and Map Exposed Ice Surfaces

Following the excavation of all arteriovenous, capillary and lymphatic vasculature, along with all crackface voids and organ perimeters as previously described (Section 4.4), the next step in the revival process is to thoroughly clean, recondition, scan and map all exposed ice surfaces to nanometer resolution.

Reconditioning and nanometric mapping of exposed ice surfaces (Section 4.5.1) is necessary: (A) to provide useful structural and biochemical data enabling the creation of a comprehensive whole-body computational model sufficient to allow planning of the repairs needing to be completed (Section 4.8) and to guide crackface fusion (Section 4.9.2); (B) to ensure smooth installation of the vasculoid transport system (Section 4.6) during the next step of the revival protocol, including the plates that will coat the vascular, crackface, and tissue walls; and (C) for planning the proper placement and deployment procedures for probes that will perform molecular extraction (Section 4.10). Once this scan data has been collected and processed, all breaks, faults and other damage in the vascular system will be known to high resolution (~1 nm; Section 4.5.6), which should be good enough to allow computation of a comprehensive vascular repair plan. This data will also reveal the exact number, type, and location of all likely cancerous tumors that had grown large enough to display pathological vascularization pre-mortem, enabling a repair plan (possibly to include DNA sampling to confirm the cancerous identity), a tumor excision plan, and a plan for rebuilding vascular thoroughfares in future excised regions of tissue.

[1076] Fahy G. Appendix B. A "Realistic" Scenario for Nanotechnological Repair of the Frozen Human Brain. In: Wowk B, Darwin M, eds., Cryonics: Reaching for Tomorrow. Alcor Life Extension Foundation, 1991, pp. A-10 – A-26; https://alcor.org/Library/html/nanotechrepair.html.

In the special case of crackface surfaces, Fahy[1077] notes that the strengths of the non-covalent bonds holding together cell membrane bilayers are very much lower than the strengths of the non-covalent bonds holding together the vitreous matrix of the solid cryopreservative, hence whole planes of cells might have one half of their bilayer structure ripped apart from the other half along a crackface. Fracture planes often proceed along the plane of the middle of the membrane bilayer in ordinary freeze-fracture microscopy.[1078] For this reason it is important to scan the surfaces of crackfaces to detect and to measure the extent of this pathology, so that subsequent computational reconstruction can match the two sides and determine where significant membrane replacement will be required for the fissioned cells.

All exposed ice surfaces must be cleaned, reconditioned, and mapped. The ice surface to be treated in this manner has a total surface area of $A_{recondition} = A_{arteriovenous} + A_{lymphovascular} + A_{crackface} + A_{surfaceplates}$ = **664.3 m^2**, where arteriovenous vascular area $A_{arteriovenous}$ = 312.9 m^2,[1079] lymphatic surface area $A_{lymphovascular}$ = 248.6 m^2 (Section 4.6.4), crackface surface area $A_{crackface}$ = 12 m^2 (Section 4.6.3), and organ/tissue perimeter surface area $A_{surfaceplates}$ = 90.841 m^2 (Section 4.4.2; Appendix E).

Specific tasks to be completed are briefly outlined in the following subsections.

4.5.1 Clear Excavation Debris from all Exposed Ice Surfaces

The total volume of material removed from the V_{body} = 60,000 cm^3 human body during the various excavation processes outlined in previous Sections is approximately $V_{excavation} = V_{ice,0.1mm} + V_{avcap} + V_{lymphcap} + V_{crackvoid} + V_{excavsurf}$ = **12,842 cm^3**, where excavation volumes are $V_{ice,0.1mm}$ ~ 6449 cm^3 for arteriovenous and large lymphatic vasculature (Section 4.2.1), V_{avcap} = 1125 cm^3 for arteriovenous capillaries (Section 4.4.1), $V_{lymphcap}$ = 1726 cm^3 for lymphatic capillaries (Section 4.4.1), $V_{crackvoid}$ ~ 3451 cm^3 for crackface voids (Section 4.4.1), and $V_{excavsurf}$ ~ 91 cm^3 for organ and tissue perimeters (Section 4.4.2).

The excavation cutting process proposed in Section 4.2.1 produces an estimated spoil fraction $f_{spoil} \sim V_{spoil} / V_{cube}$ = 5.3% of the excavated volume, crudely comparable to the production of sawdust when a carpenter saws wood. The calculations in Section 4.2.1 assumed that all ice "sawdust" is removed, but perhaps f_{debris} = 1% is left behind as debris. In that case, the "sawdust" volume generated by all excavations in a whole-body patient is $V_{debris} \sim f_{debris}\ f_{spoil}\ V_{excavation}$ = 6.81 cm^3 requiring $n_{janitorial} = V_{debris} / V_{janstorage}$ = 6.81 x 10^{12} janitorial nanorobot excursions from the pickup site to the external dump, taking $V_{janstorage}$ = 1 μm^3/nanorobot of onboard debris storage capacity.

[1077] Fahy G. Appendix B. A "Realistic" Scenario for Nanotechnological Repair of the Frozen Human Brain. In: Wowk B, Darwin M, eds., Cryonics: Reaching for Tomorrow. Alcor Life Extension Foundation, 1991, pp. A-10 – A-26; https://alcor.org/Library/html/nanotechrepair.html.

[1078] Orci L. Freeze-Etch Histology. A Comparison Between Thin Sections and Freeze-Etch Replicas, Springer-Verlag, NY, 1975; https://www.amazon.com/dp/0387070435/.

[1079] Freitas RA Jr. Nanomedicine, Volume I: Basic Capabilities, Landes Bioscience, Georgetown, TX, 1999; Table 8.1 "Approximate Quantification of the Human Arteriovenous System"; http://www.nanomedicine.com/NMI/Tables/8.1.jpg.

If the average nanorobot excursion speed is $v_{janitor}$ ~ 1 mm/sec over the average pickup-to-dump circuit path length of L_{vasc} ~ 1.5 m (comparable to the average vascular circuit path length),[1080] and if we want excavation debris removal to be completed in τ_{debris} ~ 10^6 sec (~**12 days**), then the total number of janitorial nanorobots required for continuous operation during that time period is $N_{janitorial} = n_{janitorial} L_{vasc} / (\tau_{debris} v_{janitor})$ ~ 1 x 10^{10} janitorial nanorobots.

A per-robot power budget of $P_{janitor}$ ~ 100 pW for janitorial nanorobots creates $P_{janitorfleet} = N_{janitorial} P_{janitor}$ ~ 1 W of continuous waste heat throughout the patient's entire cryopreserved body over the τ_{debris} ~ 10^6 sec duration of the janitorial mission.

4.5.2 Recondition Exposed Ice Surfaces

Nanorobots must next remove any irregularities and protruding shards of ice, leaving a smooth continuous cryogenic tissue surface to which vasculoid plates (Section 4.6.2) can be gaplessly attached. This activity should also remove the top few molecular layers of frozen ice or cryoprotectant that might have melted along a crackface at the time a fracture occurred.[1081]

If f_{irreg} = 10% of the exposed ice surface exhibits an x_{irreg} = 0.1 μm tall irregularity, then the removal volume $V_{irreg} = f_{irreg} x_{irreg} A_{recondition}$ = 6.64 cm^3, requiring the continuous operation of ~10^{10} nanorobots over a $\tau_{recondition}$ ~ 10^6 sec mission duration generating $P_{reconditionfleet} = N_{recondition} P_{janitor}$ ~ 1 W of waste heat with a power density $P_{icesurf} = P_{reconditionfleet} / A_{recondition}$ = 1.51 x 10^{-3} W/m^2 (= 0.00151 pW/μm^2) throughout a whole-body patient, which dumps $E_{icesurf} = P_{icesurf} \tau_{recondition}$ ~ 1500 J/m^2 (= 1500 pJ/μm^2) onto the exposed ice surfaces or ~1 MJ of energy into the whole body over the course of the 10^6 sec (~**12 day**) mission, assuming the use of $N_{recondition}$ ~ 10^{10} reconditioning nanorobots similar to the janitorial nanorobots described in Section 4.5.1.

The time constant for thermal diffusion from an $A_{thermal}$ = 1 μm^2 patch of ice is $\tau_{thermal} \sim A_{thermal} c_{ice} / K_{ice}$ = 0.6 μsec, taking specific heat capacity c_{ice} = 1.28 x 10^6 J/m^3-K and thermal conductivity K_{ice} = 2.21 W/m-K for ice,[1082] giving a temperature change in the topmost x_{layer} = 1 nm ice layer from this heat flux of $\Delta T \sim \tau_{thermal} P_{icesurf} / (x_{layer} c_{ice})$ = 0.7 μK, which seems negligible.

[1080] Freitas RA Jr. Nanomedicine, Volume I: Basic Capabilities, Landes Bioscience, Georgetown TX, 1999, Table 8.1, "Approximate Quantification of the Human Arteriovenous System"; http://www.nanomedicine.com/NMI/Tables/8.1.jpg.

[1081] Fahy G. Appendix B. A "Realistic" Scenario for Nanotechnological Repair of the Frozen Human Brain. In: Wowk B, Darwin M, eds., Cryonics: Reaching for Tomorrow. Alcor Life Extension Foundation, 1991, pp. A-10 – A-26; "The Repair Scenario. I. Stabilizing Fractures"; https://alcor.org/Library/html/nanotechrepair.html.

[1082] Freitas RA Jr. Nanomedicine, Volume I: Basic Capabilities, Landes Bioscience, Georgetown TX, 1999, Section 10.5.4, "Heat Conductivity and Capacity, and Refrigeration"; http://www.nanomedicine.com/NMI/10.5.4.htm.

4.5.3 Sensor-Driven Ice Peel

Taking care to avoid creating hills, valleys, or divots at the micron and submicron size scales, exploratory nanorobots will gently peel away molecular layers of frozen water-ice and vitrified cryoprotectant molecules from the reconditioned exposed ice surfaces until small molecular groups that are covalently bonded to still-submerged key biological features such as glycocalyx are exposed. The peeling operation may then be halted, or alternatively it may be deemed advisable to sacrifice certain nonessential molecular groups (e.g., of a conventional glycocalyx) to allow deeper digging to expose key cellular damage (e.g., a fractured lipid bilayer needing repair in a vascular endothelial cell). ***Future research*** should enumerate these situations and evaluate the technical tradeoffs involved.

A nanorobot budget of $N_{peel} \sim 10^{10}$ nanorobots generating $P_{peelfleet} \sim 1$ W of waste heat over a $\tau_{peel} \sim 10^6$ sec (~**12 days**) mission duration seems reasonable for this operation.

4.5.4 Geometrical Mapping

Perambulating metrological nanorobots are sent throughout the excavated spaces to comprehensively map all reconditioned exposed ice surfaces totaling $A_{recondition} = 664.3$ m^2 in surface area.

While *in vivo* cartotaxic- and transponder-based navigational systems can readily achieve positional accuracies of a few microns,[1083] a "conga line"[1084] metrological motif can achieve nanometer positional accuracies because, unlike living systems which are flexible and floppy, a cryopreserved patient is very rigid and highly dimensionally stable. Single-file lines of metrological nanorobots maintaining intimate physical contact can create a nanometric yardstick to measure the length of a vascular route to very high accuracy. An $L_{path} = 1.5$ m vascular circuit path length traversed by metrological nanorobots of size $L_{maprobot} = 1$ µm/robot requires a conga line of only $N_{maprobot} = L_{path} / L_{maprobot} = 1.5 \times 10^6$ nanorobots. If the nanorobots comprising the line can collectively adjust their positions by 0.1% of their length (equivalent to a ~2 m tall human moving one finger by ~2 mm) in the same direction in one step, then linear position along the vascular tunnels or crackface walls can be determined to ~1 nm positional accuracy.

Once the conga line is in place, each robot takes a local circumferential measurement of the geometry of the tunnel walls at its position by extending a 5-10 µm long probe terminating in a metrological scanning tip with 10 sensors at 1 nm intervals, then shifts forward by 10 nm, repeats the measurement, and so on for 100 cycles, after which the entire surface along that pathway has been geometered to $q_{resol} = 1$ nm accuracy along two surface dimensions (axial and circumferential). More than 95% of the vascular surface area to

---

[1083] Freitas RA Jr. Nanomedicine, Volume I: Basic Capabilities, Landes Bioscience, Georgetown TX, 1999, Section 8.3, "Positional Navigation"; http://www.nanomedicine.com/NMI/8.3.htm.

[1084] https://en.wikipedia.org/wiki/Conga_line.

be mapped is in the capillaries,[1085] but metrological nanorobots located in ice tunnels or other spaces that are larger than capillary diameter can employ circumferential ringsets[1086] to complete their measurements.

A 3D map of all exposed ice surfaces thus requires $n_{pixelGeom} = A_{recondition} / q_{resol}^2 = 6.64 \times 10^{20}$ pixels; allowing $I_{pixelGeom} \sim 30 + 3 \log_2(\sim 1 \text{ meter} / 1 \text{ nm}) = 120$ bits/pixel for three Cartesian dimensions of 10^9:1 precision plus 30 bits to specify up to 10^9 unique data point identifiers per nanorobot, the entire 3D map requires $I_{mapGeom} = n_{pixelGeom} I_{pixelGeom} \sim 8 \times 10^{22}$ bits of storage. If each nanorobot employs one metrological scanning tip with a 10x10 array of 100 q_{resol}^2 sensors that can be moved at a scan velocity of $v_{scan} \sim 1$ μm/sec, giving an areal scan rate of 10 $q_{resol} v_{scan} = 0.01$ μm^2/sec for each robot, then all exposed ice surfaces can be scanned to 1 nm resolution in $N_{scan} = A_{recondition} / 10 q_{resol} v_{scan} = 6.64 \times 10^{16}$ robot-sec. A fleet of $N_{mapfleet} \sim 10^{10}$ nanorobots could complete the whole-body geometrical map in $\tau_{map} = N_{scan} / N_{mapfleet} \sim 6.64 \times 10^6$ sec (~**77 days**) generating ~1 W of continuous waste heat assuming ~100 pW power draw for each metrological nanorobot.

4.5.5 Biochemical Mapping

Perambulating biomolecular-sensing nanorobots are sent throughout the excavated spaces to comprehensively examine all reconditioned exposed ice surfaces and record the character and position of any exposed molecular groups, allowing preliminary inference of the underlying biological structures to which they are mostly likely covalently bonded. Rather than metrological tips, these nanorobots use probes tipped with chemotactic sensor pads[1087] to detect, measure, and if possible identify any exposed chemical groups or biomolecules.

The number density of mappable biomolecular features is unknown because the extent of their exposure has been left to ***future research*** (Section 4.5.3), hence the number of robots, their scan speed and power draw, and the size of the resulting data cache are difficult to estimate. For convenience, the following device estimates are adopted from Section 4.5.4: $\sim 10^{10}$ biomolecular-sensing nanorobots, generating ~1 W of continuous waste heat assuming ~100 pW power draw for each robot, completing the whole-body biochemical map in $\tau_{map} \sim 6.64 \times 10^6$ sec (~**77 days**). Assigning each geometered pixel (Section 4.5.4) a unique numerical address requires $I_{pixelBio} \geq \log_2(n_{pixelGeom}) \sim 70$ bits/pixel; conservatively allowing for $\sim 10^6$ alternative biomolecular entities that might possibly be observed in each $q_{resol}^2 = 1$ nm^2 pixel requires another $I_{pixelBioM} \geq \log_2(10^6) \sim 20$ bits/pixel, giving a total data storage requirement of $I_{mapBio} = n_{pixelGeom} (I_{pixelBio} + I_{pixelBioM}) \sim 6 \times 10^{22}$ bits of storage, taking $n_{pixelGeom} = 6.64 \times 10^{20}$ pixels (Section 4.5.4).

[1085] Freitas RA Jr. Nanomedicine, Volume I: Basic Capabilities, Landes Bioscience, Georgetown TX, 1999, Table 8.1, "Approximate Quantification of the Human Arteriovenous System"; http://www.nanomedicine.com/NMI/Tables/8.1.jpg.

[1086] Hogg T, Freitas RA Jr. Acoustic Communication for Medical Nanorobots. Nano Commun Networks 2012 Jun;3(2):83-102; https://arxiv.org/pdf/1202.0568.pdf.

[1087] Freitas RA Jr. Nanomedicine, Volume I: Basic Capabilities, Landes Bioscience, Georgetown TX, 1999; Section 4.2.8, "Chemotactic Sensor Pads", http://www.nanomedicine.com/NMI/4.2.8.htm; Section 8.5.2.1, "Identification of Self", http://www.nanomedicine.com/NMI/8.5.2.1.htm#p8; and Section 8.5.2.2, "Identification of Cell Type", http://www.nanomedicine.com/NMI/8.5.2.2.htm#p23.

4.5.6 Locate and Identify Vascular Faults

Using data already collected above, computational analysis will locate and identify all breaks, faults, and other structural pathologies (e.g., Section 3.6(3)) in the arteriovenous or lymphatic vascular systems, at a sufficient resolution to permit computation of a comprehensive vascular repair plan (Section 4.8.4).

This data will also reveal the exact number, type, and location of all likely cancerous tumors that had grown large enough to display pathological vascularization pre-mortem, enabling construction of a repair plan (possibly to include DNA sampling to confirm the cancerous identity), a tumor excision plan, and a plan for rebuilding vascular thoroughfares in the resulting excised regions of tissue (Section 4.12).

4.5.7 Locate and Identify Crackface Fracture Planes

Fahy[1088] notes that the process of freeze-fracturing releases energy that creates a very high but brief local elevation of temperature, possibly causing the first several molecular layers on each side of a fracture to become somewhat melted or disordered. After peeling and scanning these surfaces, apposing faces can be computationally compared to verify complementarity. Using data already collected above, computational analysis will locate and identity instances of fracture faces that proceed along the plane of the middle of the membrane bilayer of cells.

It is important to scan the surfaces of crackfaces to detect and to measure the extent of this pathology so that subsequent computational reconstruction can match the two sides for future alignment and determine where significant membrane replacement will be required for all bisected cells. This will be primarily a computational effort, since the physical data supporting the inference will already have been collected in Section 4.5.4 and Section 4.5.5, above.

[1088] Fahy G. Appendix B. A "Realistic" Scenario for Nanotechnological Repair of the Frozen Human Brain. In: Wowk B, Darwin M, eds., Cryonics: Reaching for Tomorrow. Alcor Life Extension Foundation, 1991, pp. A-10 – A-26; https://alcor.org/Library/html/nanotechrepair.html.

4.6 Install Vasculoid

By this point in the revival process, crackface networks and all capillaries and other vessels and fluid-filled cavities (including the arterial and venous channels, lymphatic vessels, the ventricular system of the brain including the subarachnoid spaces where most of the cerebrospinal fluid volume resides, the synovial fluid in joints, the pleural fluid in the pleural cavities, the pericardial fluid in the cardiac sac, the peritoneal fluid in the peritoneal cavity, and the aqueous humor of the eye)[1089] have been cleared of debris and their hard frozen surfaces have been smoothed, cleaned, scanned and spatially- and surface-mapped to high resolution (Section 4.5). It is now time to erect a comprehensive nanorobotic logistics system that will enable the final submicron scanning effort (Section 4.7) and allow subsequent tissue repair work to proceed by providing transport of materials and information through the cryopreserved body.

Besides having the ability to transport materials, the installed logistics system must offer at least two additional features. First, the logistics system must provide a leak-proof barrier to fluid migration once the temperature of the cryopreserved patient is raised to ~273 K / 0 °C (Section 4.9) and body tissues have been reliquidified. Second, the logistics system must provide a mechanically stable framework that is sufficiently rigid to allow the insertion of tissue-penetrating sensor probes (Section 4.6.5), crackface tensioning and tissue retraction mechanisms (Section 4.9), and temporary installation of branched plumbing architectures during molecular extraction (Section 4.10), as well as overall mechanical support against gravity. Third, the logistics system must provide a mechanical support system adequate to prevent any possibility of "structural collapse due to declining cellular rigidity with rising temperature, causing cellular structures to sag in the absence of extracellular supports."[1090]

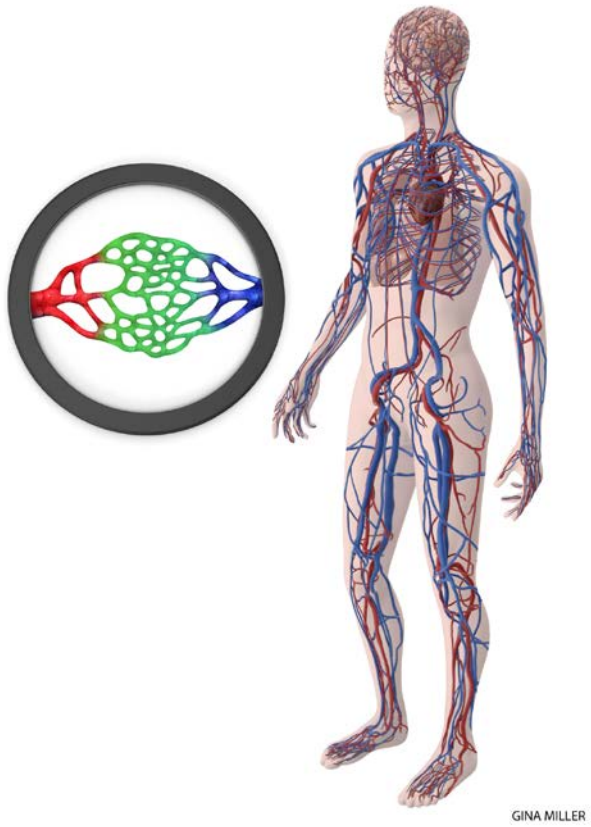

[1089] https://opentextbc.ca/anatomyandphysiology/chapter/26-1-body-fluids-and-fluid-compartments/.

[1090] Fahy G. Appendix B. A "Realistic" Scenario for Nanotechnological Repair of the Frozen Human Brain. In: Wowk B, Darwin M, eds., Cryonics: Reaching for Tomorrow. Alcor Life Extension Foundation, 1991, pp. A-10 – A-26; https://alcor.org/Library/html/nanotechrepair.html.

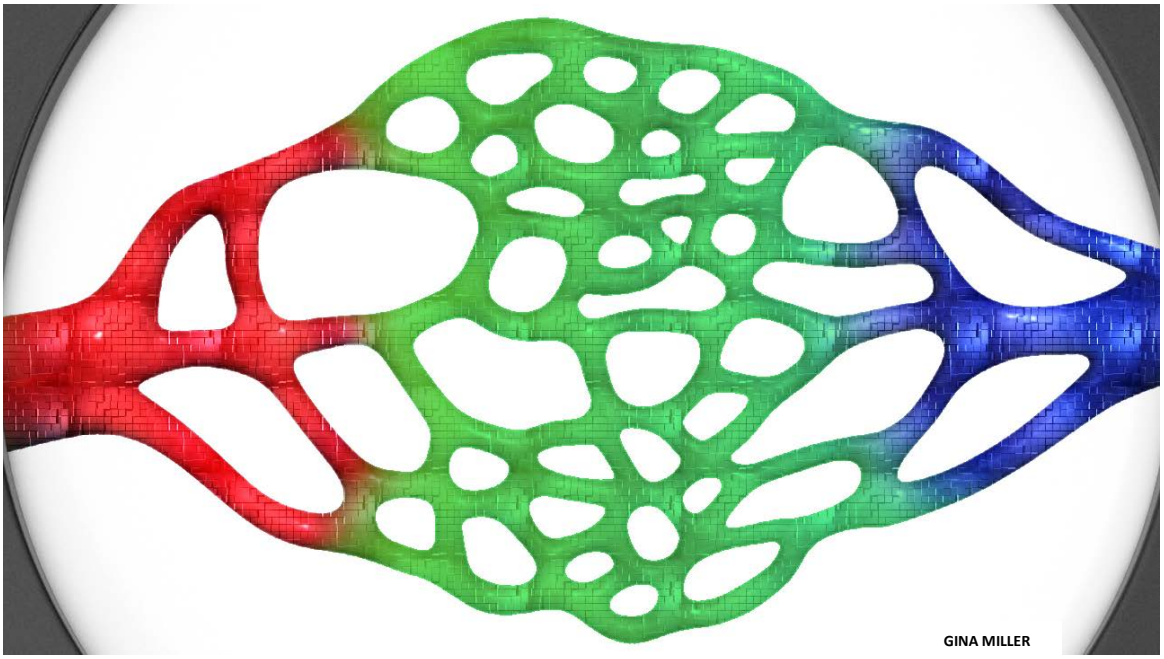

These objectives can be accomplished by coating all frozen surfaces with an artificial vasculature or vasculoid[1091] redesigned to operate at cryogenic (LN2), icewater, and normal human body temperatures. In this variant, the initial transport load would be orders of magnitude smaller than the load that a fully functional vasculoid would be required to handle in a normally metabolizing person even at basal rates. (The original vasculoid was designed to replace all blood transport functions and was scaled to handle peak metabolic rates.) Roughly speaking, a vasculoid is an artificial circulatory system that enables coordinated ciliary transport of containerized cargoes using a leak-tight coating of nanomachinery on the inner vascular walls -- the square vasculoid plates are visible with close inspection of the image above. The vasculoid appliance is readily modified to operate at low temperature, and can easily span relatively large cross-capillary breaks. This initial stage brings medical nanodevices to within 20-40 μm of any point in the brain via the circulatory system, and provides distributed power and control as well as massive computational resources located outside of the tissue undergoing repair.

4.6.1 General Description of Vasculoid

The original vasculoid[1092] was designed as a complete replacement for human blood. It is a single, complex, multisegmented nanotechnological medical robotic system capable of duplicating all essential thermal and biochemical transport functions of the blood, including circulation of respiratory gases, glucose, hormones, cytokines, waste products, and cellular components. This nanorobotic system, a very

---

[1091] Freitas RA Jr., Phoenix CJ. Vasculoid: A personal nanomedical appliance to replace human blood. J Evol Technol. 2002 Apr;11:1-139; http://www.jetpress.org/volume11/vasculoid.pdf.

[1092] Freitas RA Jr., Phoenix CJ. Vasculoid: A personal nanomedical appliance to replace human blood. J Evol Technol. 2002 Apr;11:1-139; http://www.jetpress.org/volume11/vasculoid.pdf.

aggressive and physiologically invasive macroscale nanomedical device comprised of ~500 trillion stored or active individual nanorobots, would weigh ~2 kg and consume from 30-200 watts of power in the basic human model, depending on activity level. The vasculoid system conforms to the shape of existing blood vessels and forms a watertight coating of nanomachinery distributed across the lumenal surface of the entire human vascular tree of approximate surface area $A_{arteriovenous}$ ~ 312.9 m^2.[1093] This nanomachinery uses a ciliary array to transport important nutrients and biological cells to the tissues, containerized either in "tankers" (for molecules) or "boxcars" (for cells).

The most important basic structural component of the electrically-powered vasculoid appliance (**Table 5**) is a ~312.9 m^2 two-dimensional vascular-surface-conforming array of ~150 trillion diamondoid **basic plates**. These square plates are nanorobots that cover the entire lumenal surface of all blood vessels in the body to one-plate thickness. Each basic plate is an individual self-contained nanorobot ~1 μm thick and A_{plate} ~ 2 μm^2 in surface area, a size small enough to allow adequate clearance even in the narrowest human capillaries.

Molecule-conveying **docking bays** comprise ~24 trillion, or 16%, of all vasculoid basic plates. **Tankers** containing molecules for distribution can dock at these bays and load or unload their cargo. Tankers are 1 μm^3 hollow diamondoid (possibly chamfered) cubes with useful interior storage volume of V_{tanker} = 0.75 μm^3 and ~8 x 10^{-16} kg dry mass. Gases are stored in tankers at 1000 atm pressure;[1094] this is highly conservative, as the tensile strength of diamond exceeds ~100,000 atm.[1095] Liquids and solids are packed at normal macroscopic densities.

Cell-conveying **cellulocks** are built on cellulock plates that span the area of 30 basic plates, or 60 μm^2 (e.g., 7.75 μm x 7.75 μm) each, and were originally designed to be spaced ~96 μm apart (mean center-to-center separation) along vessel walls. **Boxcars** containing biological cells for distribution can dock at these cellulocks and load or unload their cargo, with cellulocks acting as "airlock" interfaces between boxcar and tissue environments. Boxcars are 1000 μm long and 6 μm in diameter, of which 75% (V_{boxcar} = 2120 μm^3) is usable internal storage volume. Tankers and boxcars normally circulate once every $\tau_{VasculoidCirc}$ = 140 sec. Boxcars can be loaded or unloaded through a cellulock in $\tau_{BoxcarLoad}$ = 163 sec,[1096] so the maximum volume transport capacity of the entire boxcar/cellulock system is $\upsilon_{capacityB/C} = N_{boxcars}\ V_{boxcar} / (\tau_{VasculoidCirc} + \tau_{BoxcarLoad})$ = 0.22 cm^3/sec for a total vasculoid population of $N_{boxcars}$ = 32 x 10^9 boxcars. With only 32.6 billion cellulock plates in the entire vasculoid design, cellulocks occupy the area of 0.978 trillion basic plates or only 0.65% of the entire vasculoid surface. In the context of cryonics revival, boxcars are also used to transport cell repair nanorobots and other nanodevices that are released into, or retrieved from, body tissues via the cellulocks.

[1093] Freitas RA Jr. Nanomedicine, Volume I: Basic Capabilities, Landes Bioscience, Georgetown, TX, 1999; Table 8.1 "Approximate Quantification of the Human Arteriovenous System"; http://www.nanomedicine.com/NMI/Tables/8.1.jpg.

[1094] Freitas RA Jr. Exploratory design in medical nanotechnology: a mechanical artificial red cell. Artif Cells Blood Substit Immobil Biotechnol. 1998 Jul;26(4):411-30; https://web.archive.org/web/20100613040242/https://foresight.org/Nanomedicine/Respirocytes1.html (Sec. 2.2.1). Freitas RA Jr. Nanomedicine, Volume I: Basic Capabilities, Landes Bioscience, Georgetown, TX, 1999; Section 10.3.1 "Fluid Storage Tank Scaling"; http://www.nanomedicine.com/NMI/10.3.1.htm.

[1095] Freitas RA Jr. Nanomedicine, Volume I: Basic Capabilities, Landes Bioscience, Georgetown, TX, 1999; Table 9.3, "Mechanical Strength of Nanomedical Materials"; http://www.nanomedicine.com/NMI/Tables/9.3.jpg.

[1096] Freitas RA Jr., Phoenix CJ. Vasculoid: A personal nanomedical appliance to replace human blood. J Evol Technol. 2002 Apr;11:1-139; Section 2.4.2 "Cellulocks for Boxcars"; http://www.jetpress.org/volume11/vasculoid.pdf.

Table 5. Number, mass and volume of baseline vasculoid system components[1097]			
System Component	**Number of Nanorobots**	**Subsystem Mass**	**Subsystem Volume**
Basic Plates		1.05 kg	
Applications plates	125×10^{12}	----	250.0 cm^3
Docking bays	24×10^{12}	----	48.0 cm^3
Cellulocks	0.0326×10^{12}	----	1.956 cm^3
Container Fleet			
Tankers			
Active	166.2×10^{12}	0.133 kg	166.2 cm^3
Backups in storage	166.2×10^{12}	(0.133 kg)*	(166.2 cm^3)*
Boxcars			
Active	0.032×10^{12}	0.0768 kg	91.7 cm^3
Backups in storage	0.032×10^{12}	(0.0768 kg)*	(91.7 cm^3)*
Vasculocytes			
Active	0.200×10^{12}	0.002 kg	0.6 cm^3
Backups in storage	2.000×10^{12}	(0.02 kg)*	(6.0 cm^3)*
Storage Vesicles	0.5×10^{6}	0.460 kg	500.0 cm^3
Other structure, unspecified	16.3×10^{12}	0.2782 kg	141.544 cm^3
TOTALS	**500.0×10^{12}**	**2.000 kg**	**1200.0 cm^3**
* *mass and volume already included in storage vesicles*			

The remaining ~125 trillion basic plates are reserved for special equipment and other as-yet undefined applications. All nanomachinery within each plate is of modular design, permitting easy replacement and repair by legged mobile repair nanorobots called **vasculocytes** that are under 3 μm in size.[1098] Each vasculocyte is replete with ambulatory appendages, manipulator arms, repair and assembly tools/materials, redundant onboard computers with mass memories, communications and sensory equipment, and an onboard energy store. With a vasculocyte mass of ~10 pg, volume ~3 μm^3, and power demand ranging from ~1 pW for continuous simple walking up to ~50 pW to allow bursts of more intensive computation (at up to nearly ~1 megaflop/sec)[1099] or other activity, a 10-watt vasculocyte fleet energy budget permits the deployment of 200 billion continuously active devices, a total 2-gm mass of nanorobots.

In the original design, **storage vesicles** were each ~1 mm^3 in volume, providing enough space to store ~1 billion tankers, ~300 million vasculocytes, or 350,000 boxcars, and were to be attached directly to the vasculoid surface using struts affixed to reinforced base plates, or attached to each other in convenient

---

[1097] Freitas RA Jr., Phoenix CJ. Vasculoid: A personal nanomedical appliance to replace human blood. J Evol Technol. 2002 Apr;11:1-139; Section 1.1 "The Vasculoid Concept"; http://www.jetpress.org/volume11/vasculoid.pdf.

[1098] Freitas RA Jr. Chapter 23. Comprehensive Nanorobotic Control of Human Morbidity and Aging, Section 6.2.3 "Heart and Vascular Disease". In: Fahy GM, West MD, Coles LS, Harris SB, eds, The Future of Aging: Pathways to Human Life Extension, Springer, New York, 2010, pp. 685-805; http://www.nanomedicine.com/Papers/Aging.pdf.

[1099] Freitas RA Jr. Microbivores: Artificial Mechanical Phagocytes using Digest and Discharge Protocol. J. Evol. Technol. 2005 Apr;14:55-106; Section 3.2.3 "Onboard Computers"; http://www.jetpress.org/volume14/freitas.pdf.

three-dimensional configurations (e.g., "bunch of grapes" formations). The vesicles were intended to serve as storage garages containing reserves of mobile and cargo-carrying nanodevices, other auxiliary nanodevices, spare parts, replacement modules and repair materials, critical biochemical consumables, nanoscale bioprocess plants, and compressed refuse. Given the ability to exchange robots and materials with the external environment throughout a revival procedure, storage vesicles might be reduced in size or number, or eliminated altogether, in the cryonics application.

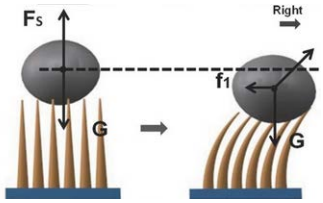

Mechanical cilia[1100] (image, right) protrude from the lumenal surface of each basic plate, forming a robotic array that can grapple, laterally transport, and then release individual tankers and boxcars. Each cilium is a cylindrical assembly 100 nm long and 30 nm in diameter, having a transverse travel of 100 nm and a lateral speed of 1 cm/sec, consuming 0.1 pW during continuous operation at >100 KHz while applying ~1 nN at the tip, sufficient force to accelerate a 1 μm^3 block of water (weight ~0.01 pN) at 10^5 G or a 100-µm long, 6-µm wide water-filled cylindrical boxcar at ~30 G. Mechanical cilia are spaced at most 0.32 µm apart on basic plates (see image below, with ciliary arms only partially extended), and a minimum of 3000 trillion cilia are needed to achieve 100% service over the entire ~300 m^2 vascular (mostly capillary) surface,[1101] physically occupying ~2.1 m^2 (~7%) of the vasculoid lumenal surface.

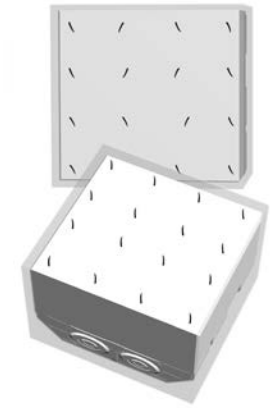

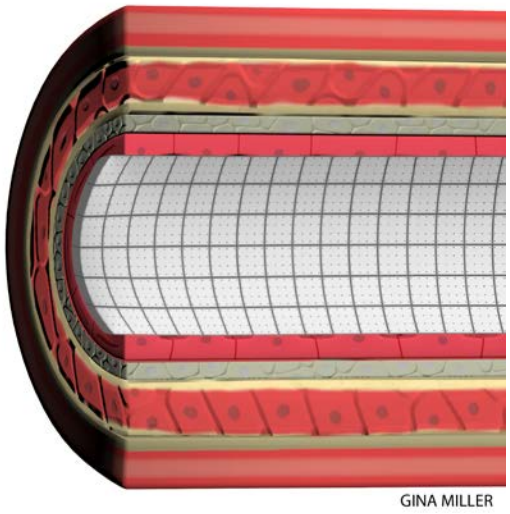
GINA MILLER

Adjacent plates abut through flexible but watertight mechanical interfaces on metamorphic bumpers[1102] along the entire perimeter of each plate (images, right). Vasculoid plate bumpers can alter plate width from 1.4 µm to 1.6 µm, providing a ~14% controllable variability in linear dimension and a ~30% controllable variability in surface area.[1103] With controllable variable volume, bumpers permit the vasculoid surface to: (A) slightly expand or contract in area, or (B) flex, either in response to macroscale body movements or in response to vascular surface corrugations or other irregularities to the same degree or better than the natural endothelium. Thus,

---

[1100] Freitas RA Jr. Nanomedicine, Volume I: Basic Capabilities, Landes Bioscience, Georgetown, TX, 1999; Section 9.3.1.2, "Nanocilium Manipulators"; http://www.nanomedicine.com/NMI/9.3.1.2.htm. Ben S, Tai J, Ma H, Peng Y, Zhang Y, Tian D, Liu K, Jiang L. Cilia-inspired flexible arrays for intelligent transport of viscoelastic microspheres. Adv Functional Mater. 2018 Apr 18;28(16):1706666; https://onlinelibrary.wiley.com/doi/pdf/10.1002/adfm.201706666.

[1101] Freitas RA Jr. Nanomedicine, Volume I: Basic Capabilities, Landes Bioscience, Georgetown, TX, 1999; Table 8.1, "Approximate Quantification of the Human Arteriovenous System"; http://www.nanomedicine.com/NMI/Tables/8.1.jpg.

[1102] Freitas RA Jr. Nanomedicine, Volume I: Basic Capabilities, Landes Bioscience, Georgetown, TX, 1999; Section 5.4, "Metamorphic Bumpers"; http://www.nanomedicine.com/NMI/5.4.htm.

[1103] Freitas RA Jr., Phoenix CJ. Vasculoid: A personal nanomedical appliance to replace human blood. J Evol Technol. 2002 Apr;11:1-139; Section 7.4 "Vascular Plating"; http://www.jetpress.org/volume11/vasculoid.pdf.

plated surfaces could accommodate the natural cyclical volume changes of various organs such as lung, bladder, or spleen during life. Also, due to cell shrinkage during cryopreservation the blood vessels may be slightly smaller than in living tissue, and during rehydration (Section 4.11.3) the vessel diameters might increase. The vasculoid must have metamorphic surfaces with enough adjustability to accommodate all such size changes that may occur during the revival process. Rigidity of the plate array is subject to engineering control and to localized real-time control as well, via the bumpers, since diamondoid plating may be made substantially stiffer than natural endothelium if desired. The rupture strength of individual plates is ~40,000 atm and bumper actuation power is of order ~0.1 pW,[1104] comparable to the power draw of a single basic plate cilium.

The original design envisioned deployment of sensor probes that could leave the vasculoid and enter the surrounding tissues to detect and monitor remote events (such as angiogenesis, tumors, or pathogens) that otherwise might not be conveniently detected from within the vasculoid.[1105] The vasculoid variant used for cryonics revival will also be required to extend a variety of sensors, pumps, and mechanical probes from the underside of each vasculoid basic plate that is in contact with the underlying frozen tissue.[1106]

The maximum $P_{vasc,max}$ = 200 watts of waste heat produced by the vasculoid appliance could be conveniently exported for external disposal either by:

(A) allowing $P_{vasc,max} / H_{vapLN2}$ = **1.24 cm^3/sec of liquid nitrogen (LN2)** to absorb heat and evaporate inside the $V_{vascint}$ ~ 4200 cm^3 interior volume[1107] of the arteriovenous vasculoid; or

(B) filling $(P_{vasc,max}\ \tau_{VasculoidCirc} / V_{tanker}) / (C_{V,avg}\ \Delta T_{77\text{-}273K} + H_{water\text{-}ice})$ = **6.38 x 10^{13} tankers** (~38% of the active fleet) with water-ice at 77 K (-196 °C) and allowing it to circulate, absorb heat, and melt to water at 271 K (-2 °C), taking LN2 heat of vaporization H_{vapLN2} = 1.61 x 10^8 J/m^3, $\tau_{VasculoidCirc}$ = 140 sec, V_{tanker} = 0.75 μm^3, average heat capacity of water over the $\Delta T_{77\text{-}273K}$ = 273 K – 77 K = 196 K range as $C_{V,avg}$ = 1.28 x 10^6 J/m^3-K, and the heat of fusion of water-ice as $H_{water\text{-}ice}$ = 3.34 x 10^8 J/m^3.

Design of the vasculoid in general, and more specifically a vasculoid optimized for cryonics revival work, will be a major undertaking for ***future research***. The exemplar system described here is just one point in a rich design space which should be more thoroughly explored with the cryonics revival application in mind.

[1104] Freitas RA Jr. Nanomedicine, Volume I: Basic Capabilities, Landes Bioscience, Georgetown, TX, 1999; Section 5.3.3, "Metamorphic Power and Control"; http://www.nanomedicine.com/NMI/5.3.3.htm.

[1105] Freitas RA Jr., Phoenix CJ. Vasculoid: A personal nanomedical appliance to replace human blood. J Evol Technol. 2002 Apr;11:1-139; Section 8.6 "Extravasculoid Devices"; http://www.jetpress.org/volume11/vasculoid.pdf.

[1106] Greg Fahy (personal communication, 15 Jan 2022) notes that inserting things into tissue implies that there is room available for such insertions. In particular, thermal contraction exists below the glass transition temperature T_g. If thermal contraction were relieved by inserting other elements into the glassy matrix, stresses would theoretically be reduced, and items could be inserted into the volume lost by thermal contraction. However, native structures would have to be separated (very hard below T_g) and expansion upon rewarming might run into problems because the restored volume would exceed the starting volume.

[1107] The blood volume which the vasculoid is designed to replace is 5400 cm^3; subtracting the 1200 cm^3 displacement volume of the vasculoid appliance machinery (**Table 5**) implies a 4200 cm^3 interior free volume.

4.6.2 Arteriovenous Emplacement

Two vasculoid installation scenarios intended to be used on a living human body have been proposed.[1108] Either could be adapted for use in the cryonics revival application, but for simplicity only the less aggressive approach is presented here.

Vasculoid installation takes place at a temperature just slightly above the boiling point of liquid nitrogen (LN2), perhaps 80 K. This allows the excavated vascular tunnels to be flushed with pure nitrogen gas in order to positively exclude potentially reactive oxygen from the worksite. **The patient is maintained under a nitrogen atmosphere** until the vasculoid is uninstalled near the end of the revival process (Section 4.14.2).

In the case of vasculoid emplacement in a living human recipient, each 3 μm^3 vasculocyte grasps a single 2 μm^3 plate, ready for installation. An infusant solution containing 10% v/v cargo-bearing vasculocytes (i.e., ~20 x 10^9 vasculocytes/cm^3) is injected into the vasculature of the live patient to begin the vascular plating process, through one or more large veins to permit rapid infusion and exfusion. Installing ~150 x 10^{12} basic plates demands a minimum of 7500 cm^3 of vasculo-infusant, requiring ~3800 sec or ~**1 hour** assuming a very gentle flow rate of only ~2 cm^3/sec. Each vasculocyte drifts quietly in the flow until it encounters a vessel wall, causing it to attempt to release its cargo in a clear space. If the immediate area is already fully plated, the legged vasculocyte walks across the surface until it reaches a clear area to deposit its cargo, using corner registration of adjacent plates prior to plate release to ensure a maximally dense tiling pattern. Once its cargo plate is in place, the vasculocyte releases back into the flowing fluid, powers down, and is eventually exfused from the body. Approximately 42 billion plates/sec are deposited during this 1-hour process.

In the case of vasculoid emplacement in a cryopreserved human patient, following microvascular excavation (Section 4.4) the vascular spaces are initially an empty network of continuous[1109] rigid hollow tunnels through ice at cryogenic (~LN2) temperatures, not supple living surfaces at human body temperature. Rather than flowing in on a carrier fluid, the vasculocytes simply walk into the frozen vascular tunnels along the walls, carrying their plate cargoes to a predetermined destination following an efficient plating algorithm (to be designed and simulated as a ***future research*** project) that minimizes plating time subject to fleet power limits designed to avoid significantly heating the ice. To satisfy this thermal constraint it is anticipated that the plating operation will require an installation time significantly longer than 1 hour. Since all activities take place at cryogenic temperatures, cryopreserved tissue suffers no continuing degradation so the installation can take as long as needed without harm.

The plates are not passive during the installation process. Besides the ~20 cilia positioned atop each plate to provide tanker and boxcar mobility as part of the ciliary subsystem, plates also possess a few motive cilia to assist in both installation and repair operations. Each motive cilium is fully retractable when not in use. Complete positional, rotational and translational control during installation (and functional redundancy) requires at least one motive cilium on each of the 4 sides and at least four on the underside to establish a stable tripod while walking. The motive cilia allow limited trans-endothelial cytoambulation by each plate

---

[1108] Freitas RA Jr., Phoenix CJ. Vasculoid: A personal nanomedical appliance to replace human blood. J Evol Technol. 2002 Apr;11:1-139; Section 7 "Hypothetical Vasculoid Installation Scenarios"; http://www.jetpress.org/volume11/vasculoid.pdf.

[1109] Any existing gaps in the vasculature will be temporarily bridged by adjacent plates. Such gaps might be due to avulsion wounds or other processes that have wholly or partially removed local endothelium, or might have resulted from the necessary excision of endothelial material during microvascular excavation (Section 4.4.1) due to endothelial swelling or blebbing that seriously occluded the capillary lumen.

(using reversibly adherent foot pads) and fine control of plate/plate jostling motions. A working cilium consumes 0.1 pW during continuous operation at 1 cm/sec, roughly the speed of jostling movements involving motions of ~1% plate width per microsecond. Plate power dissipation is under ~1 pW even if all motive cilia are operating at once. The motive ciliary power draw of the entire plate population normally should not exceed ~1 watt during installation because once properly positioned in a regular grid pattern (in <1 sec) all local plate jostling ceases and the motive cilia are stowed.

Cellulocks (which are 30 times larger than a basic plate) also must be installed. With respect to a body-temperature installation into a living human, the original paper[1110] notes: "Specific procedures for cellulock installation have not been examined in detail because these vasculoid components are relatively few in number and require a net installation rate of only ~9 million/sec (compared to 42 billion/sec for basic plates). To the extent cellulock placement can be governed by easily detected geometric factors such as vascular diameter (e.g., near capillary entrances), cellulock placement may occur similarly to plate deposition, but using vasculocytes programmed with specific geometric release criteria. Some modest number of cellulocks destined for specific vascular addresses may be installed after plate initialization using a combination of vasculocytes and now-active cargo cilia, by replacing temporary plates with cellulocks."

Following supravascular positioning and subsystem validation, each plate inflates fluidtight metamorphic bumpers[1111] along its contact perimeter with its neighbors. This provides at least ~14% linear effective elasticity (1.6 μm vs. 1.4 μm, center-to-center, comparable to the usual stretch requirements of the elastic arteries during normal cardiac pumping) and permits plates to track lateral movements of the underlying tissue while avoiding any relative movement of the opposing surfaces later on in the revival process. Neighboring plates lock their bumpers firmly together with reversible fasteners embedded in the bumpers. The entire plate fleet can then be initialized and activated. The vasculoid is now fully operational and self-contained.

Instances of endothelial swelling or blebbing that seriously occlude the capillary lumen (Section 3.6(3)) will require excision of the (still frozen or solidified) blocking material (Section 4.5.2). The location and other details of this excision must be recorded in the Vascular Fault Map (Section 4.8.1(2)) so that the vasculoid installation can proceed across these incisions, and so that conventional cell repair operations can later heal the damage (Section 4.12.2).

4.6.3 Crackface Voids

Crackface voids created by fracture damage during freezing (Section 3.4.3) must also receive vasculoid plating to establish and maintain high-fidelity registration between the opposing faces. Prior mapping (Section 4.4) will have revealed the exact size, location, and geometry of the surfaces of all such features. Physical access to fracture voids and crackfaces may be provided from the exposed open termini of blood vessels, or by small ad hoc ice tunnels in the rare case of fracture voids totally isolated from all vascular entry points.

[1110] Freitas RA Jr., Phoenix CJ. Vasculoid: A personal nanomedical appliance to replace human blood. J Evol Technol. 2002 Apr;11:1-139; Section 7.4 "Vascular Plating"; http://www.jetpress.org/volume11/vasculoid.pdf.

[1111] Freitas RA Jr. Nanomedicine, Volume I: Basic Capabilities, Landes Bioscience, Georgetown, TX, 1999; Section 5.4, "Metamorphic Bumpers"; http://www.nanomedicine.com/NMI/5.4.htm.

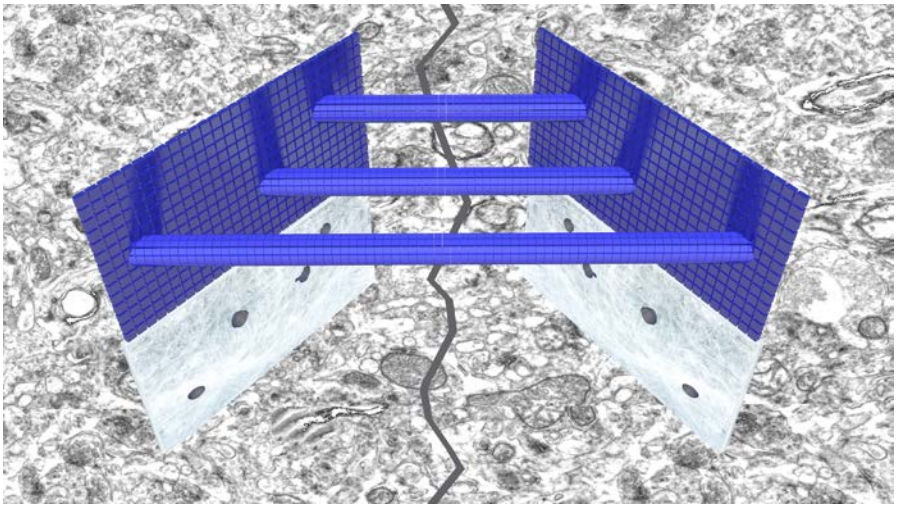

At the perimeter of a crackface, vasculoid plates are placed in intimate contact with the crackface surfaces to stabilize them. Plates are installed across all major crackfaces with small temporary anchors into the ice spaced periodically. Free-hanging vasculoid microtubes can span empty gaps across crack voids to create a mechanical bridge between the separated termini of bisected capillaries. Imagine two opposing faces with a similar hole on either side representing the two ends of a cleaved capillary vessel, and a void between them. The vasculoid plating tunnel emerges from the capillary hole in one face, spans the void unsupported, and joins to the vasculoid in the matching capillary hole on the other face, giving the appearance of a narrow flexible pipe spanning the open space between two walls (image, above; vasculoid plates in blue). The holes on each face are matched to the correct holes on the opposing face via the hollow plated microtubes, so the entire vascular network is topologically complete with no volumetric gaps. The freehanging vasculoid microtube segments are then placed under mild mechanical tension by reverse-telescoping the freehanging segments via bumper contraction. This tension is maintained later as the tissue is warmed and softens, allowing the separated capillaries to be slowly drawn together in exactly the right configuration during the prethaw and crackface fusion process (Section 4.9), crudely analogous to the use of drawstrings to assemble a ship-in-a-bottle (image, right),[1112] or surgical suturing,[1113] shoelacing, or stitching in textile work.

For an initial crude quantification estimate, we assume that individual cracks may occupy perhaps $f_{crackvol}$ ~ 1% of tissue volume, producing tissue displacements with two crackfaces separated on average by $L_{cracksep}$ ~ 100 μm (Section 3.4.3). Thus the total crackface area is $A_{crackface} \sim 2\ f_{crackvol}\ V_{body} / L_{cracksep}$ ~ 12 m^2 (taking V_{body} ~ 60 L as the mean human whole-body volume),[1114] requiring $N_{crackplates} = A_{crackface} / A_{plate} \sim 6 \times 10^{12}$ additional vasculoid basic plates for complete crackface coverage, representing only a small fraction (~4.8%) of the entire 125 x 10^{12} basic plate population for applications (**Table 5**). Additionally, assuming an average capillary number density[1115] of $n_{capillary}$ ~ 600 capillaries/mm^2 and taking each bridging vasculoid microtube as $L_{cracksep}$ ~ 100 μm in length and $d_{capillary}$ ~ 8 μm in diameter, then the total surface area of vasculoid microtubes bridging the separated termini of

---

[1112] https://www.instructables.com/Building-A-Ship-In-A-Bottle/.
[1113] https://en.wikipedia.org/wiki/Surgical_suture#Techniques.

[1114] Freitas RA Jr. Nanomedicine, Volume I: Basic Capabilities, Landes Bioscience, Georgetown TX, 1999, Table 8.9, "Mass, Volume, and Scale Size of the Organs of the Human Body"; http://www.nanomedicine.com/NMI/Tables/8.9.jpg.

[1115] Schmidt RF, Thews G, eds., Human Physiology, Second Edition, Springer-Verlag, New York, 1989; https://www.amazon.com/dp/3540116699/.

bisected capillaries, spanning the empty space from one crackface to the opposing crackface, is of order $A_{crackbridge} \sim (0.5\ n_{capillary}\ A_{crackface})\ (\pi\ d_{capillary}\ L_{cracksep}) \sim 9.05\ m^2$, requiring $N_{cracktubes} = A_{crackbridge} / A_{plate} \sim 4.5 \times 10^{12}$ additional vasculoid basic plates for complete coverage of all vasculoid microtube bridges, another modest 3.6% of the basic plate population. These plates cannot employ simple free-flow installation as in the arteriovenous case (Section 4.6.2), so we will allocate ~**1 day** to complete this process.

Fahy[1116] notes that fractures may occur preferentially along local planes of bilayer membranes. If this happens, it is possible that there could be a relative paucity of traversable capillaries between any two particular opposed crackfaces.[1117] In such cases, "blind capillaries" (vasculoid plates formed into hollow microtubes substituting for the missing capillaries) should be installed at regular intervals spanning the two crackfaces, after those crackfaces have been plated and the blind microtubes can be joined to either side. The blind capillaries can then serve the same function as the crackface-spanning microtubes connecting the separated ends of actual capillaries – e.g., maintaining proper tension between the two crackfaces and slowly pulling them together as the tissue warms, softens, and eventually reliquidifies during the prethaw phase of the revival protocol (Section 4.9). These blind capillaries provide a similar function as the "guide wires" proposed by Fahy in 1991 "to maintain fracture face registry later when the temperature is raised."[1118]

With crackfaces separated by an average of ~100 μm,[1119] there should be plenty of room (and time) for mobile nanorobots perhaps ~1 μm in size to perform the installation of all crackface plates and bridging vasculoid microtubes. Additional strategies may need to be developed in ***future research*** for cracks that are narrower than 1 μm if experimental work determines that such cracks exist in significant numbers; Fahy also believes that different plate designs might be necessary for blood vessels and for crackfaces, given the differences between these structures.

[1116] Fahy G. Appendix B. A "Realistic" Scenario for Nanotechnological Repair of the Frozen Human Brain. In: Wowk B, Darwin M, eds., Cryonics: Reaching for Tomorrow. Alcor Life Extension Foundation, 1991, pp. A-10 – A-26; https://alcor.org/Library/html/nanotechrepair.html.

[1117] Greg Fahy notes (personal communication, 15 Jan 2022) that "fractures through cell membranes will not extend farther than the diameter of an individual cell, at the most. The gap between capillaries is more like 40 microns, which is much larger than the diameter of a single tissue cell. So I don't think you need to worry about crack healing vis a vis capillaries due to bilayer-separating fractures. In fact, if registry can be maintained, bilayer-separating fractures should heal spontaneously. There is even an experiment in which nerves were deliberately frozen and fractured and then thawed while maintaining registry between the fracture faces, and the nerves healed."

[1118] "After complementarity analysis, the repair system could build filaments between the faces. The filaments on each side of the fracture would be complementary to each other and would connect so as to maintain fracture face registry later when the temperature is raised. Given sufficiently strong replicas, these 'guide wires' could be attached only to the replicas (the replicas in turn being tightly adherent to the fracture faces themselves at all points). The function of the wires later would be to direct each fracture face as a whole toward the other fracture face as the gap is later closed by normal thermal expansion in such a way as to continue to ensure perfect registry of the two fracture faces as the gap narrows. Molecular 'ratchets' along the guide wires could apply small forces to encourage closing where this is necessary. If the 'guide wires' are built onto the replica faces at the sites of special pores, then as the gap is closed and the faces approach each other, the 'guide wires' can be allowed to protrude into safe regions of tissue on each side of the gap, and/or they could be disassembled at a pace set by the narrowing of the gap." Fahy G. Appendix B. A "Realistic" Scenario for Nanotechnological Repair of the Frozen Human Brain. In: Wowk B, Darwin M, eds., Cryonics: Reaching for Tomorrow. Alcor Life Extension Foundation, 1991, pp. A-10 – A-26; https://alcor.org/Library/html/nanotechrepair.html.

[1119] Cracks will exist in a variety of sizes, ranging from microcracks 3-15 μm wide to large cracks up to ~200 μm wide; Section 3.4.3. Mobile nanorobots ~1 μm in size can fit inside all of these.

4.6.4 Lymphatic Vasculature and Tissue Perimeter Surfaces

The lymphatic vasculature must receive a lumenal coating of application plates during the cryonics revival process. This differs from the original vasculoid proposal that envisioned replacing only the arteriovenous circulatory system with the vasculoid transport system. **Table 6** provides an estimate of the lumenal surface area of the lymphatic vasculature that must be coated with applications plates. The total plateable area of $A_{lymphovascular}$ = 248.6 m^2 is slightly less than the 312.9 m^2 plateable area of the arteriovenous vasculature, and will require the fielding of $N_{lymphplates} = A_{lymphovascular} / A_{plate} \sim 124.3 \times 10^{12}$ vasculoid plates for this purpose.

Table 6. Plateable surfaces of the lymphovascular system[1120]

Lymphatic Vessels	Estimated Surface Area
Thoracic duct	5655 mm^2
Right lymphatic duct	132 mm^2
Main lymphatic trunks	4899 mm^2
Cisterna chyli	3063 mm^2
Minor lymphatic trunks	3142 mm^2
Lymphonodal collecting ducts	2,915,555 mm^2
Precollecting ducts	32,044,245 mm^2
Lymphatic capillaries	213,628,300 mm^2
TOTAL	248.6 m^2

An additional $N_{surfaceplates} = A_{surfaceplates} / A_{plate} \sim 45.4 \times 10^{12}$ vasculoid basic plates and ~**5 days** may be required to plate several organs and tissue surfaces as detailed in Appendix E, which reports an estimate of $A_{surfaceplates} \sim 90.841$ m^2 for this purpose. Space will have been cleared in the ice for the installation of these plates during previous excavation (Section 4.4.2). These two requirements essentially double the total applications plate requirement as compared to a conventional arteriovenous vasculoid installation in a living human. Note that all vasculoid components will be removed after the completion of tissue repair (Section 4.12.3.4).

The cellular contents that are removed from the lymphovasculature and lymph nodes during vasculoid installation could be recovered and retained for possible later use (Section 4.14.1.2).

[1120] Surface area estimated as (π) x (vessel diameter) x (vessel length) x (number of vessels), using data in: Freitas RA Jr. Nanomedicine, Volume I: Basic Capabilities, Landes Bioscience, Georgetown TX, 1999, Table 8.5, "Approximate Quantification of the Human Lymphatic System"; http://www.nanomedicine.com/NMI/Tables/8.5.jpg.

4.6.5 Cryorevival-Specific Equipment

Prior to prethaw and reliquidification (Section 4.9), vasculoid plates and cellulocks can easily be changed out and replaced by contracting the bumpers of neighboring plates, temporarily opening enough space around a plate or cellulock to allow it to be removed and replaced with other components. In addition to the original-design equipment and capabilities described above, several additional capabilities must be added to the original vasculoid system which was designed for operation in warm living human bodies, not in cryopreserved bodies at cryogenic temperatures. These additions include:

(1) **Circumferential Cellulocks.** Circumferential cellulocks may be installed during the submicron scanning phase of revival (Section 4.7) and used to deploy and operate specialized high-resolution scanning instrumentalities, after which these special cellulocks can be removed and replaced with conventional cellulocks that can accommodate the transport of cell repair nanorobots or biological cells as originally designed. In any case, circumferential cellulocks are removed and replaced with standard basic plates prior to vasculoid removal (Section 4.14.2).

(2) **Scanning Patches.** A scanning patch is a 3D group of scanning instruments that can be repositioned as a group to intensively scan a block of tissue to ~100 nm resolution. Power and communication can be supplied to each patch using one or more single lines of connected vasculoid plates (rather than a full cylindrical wrap of plates). This feedline can be moved around the circumference of a capillary, possibly using roundhouse joints at capillary branch points off the nearest feeder arteriole. Essentially this is a small bit of vasculoid acting as a giant scanning head to do the high resolution 3D scan of the frozen tissue prior to full vasculoid installation, supporting the submicron scanning phase of revival (Section 4.7). Scanning patches are removed and replaced with standard basic plates as soon as the high-resolution scans are complete.

(3) **Extraction Plates.** Extraction plates support the molecular extraction activity described in Section 4.10. Molecular extraction probes could perhaps be operated from existing plates but, more likely, will be operated from a new form of "extraction plate" that can extend telescoping extraction probes into post-thaw reliquidified tissue, extend the sorting rotors or appropriate pipeage (Section 4.10.1.9), and operate the molecule-selective pumps, carrying the extracted materials back to the vasculoid for removal in fleet tankers. Extraction plates are removed and replaced with standard basic plates immediately after their last use for molecular instillation (Section 4.13.2) but prior to vasculoid removal (Section 4.14.2). A few plumbing details for an exemplar probe design are presented in Section 4.10.1.9.

(4) **Tissue Surface Perimeter Plates.** To maintain gross physical integrity of the patient's body after warmup and reliquidification, certain accessible organ and tissue surface perimeters will be coated with vasculoid applications plates (Section 4.6.4). These plates will serve at least two important purposes: (A) to create a watertight barrier that provides protection against tissue desiccation, fluid leakage, and material contamination during and after reliquidification; and (B) to provide physical support and resistance to gravitational sagging and other geometric deformations as the body is warmed and softens, using mechanical inter-plate 2D force tensioning to selectively stiffen the entire plate array. Significant organ shrinkage may have occurred due to osmotic outflows of cytosolic water during the original cryopreservation process, and these organs will expand to their original volumes during rehydration (Section 4.11.3). Thus it will be necessary to devise a protocol allowing plated surfaces to expand as the organs they surround regain their original size. ***Future research*** must devise a specific protocol for inserting new plates into an existing plate array without breaking the watertight seal and without significantly disrupting any directional tensioning that is being employed by the array. Perimeter plates are removed after all tissue repairs (Section 4.12.3.4) are complete.

(5) **Acoustic Navigational Beacons.** The vasculoid may support the presence of ~10^{11} acoustic transponder devices located an average of ~100 μm apart throughout the human body volume, providing a microtransponder network supporting a 3-μm resolution internal navigational network as described

elsewhere[1121] using standalone nanorobots. These beacons can support the internal navigational requirements of cell repair and related accessory nanorobots (Section 4.12). If these devices are integral components of the vasculoid, then they should be removed and replaced with standard basic plates prior to vasculoid removal (Section 4.14.2); if they are standalone nanorobots, they may be left in the tissue after vasculoid removal and extracted later via conventional means (e.g., ECM migration followed by diapedesis into the vasculature, then bloodstream exfusion) after their work is finished.

(6) **Mobile Data Carriers.** While the vasculoid includes some network communications capability through interconnected plates, additional data handling demands may require the deployment of mobile data carriers inside the vasculoid. These data carriers are tankers or boxcars filled with solid-state nanomechanical memory that can pick up data at a plate or cellulock and transport this data out of the appliance to an external reader, allowing repair models to be updated in real time. Information can also flow in the opposite direction as required. For example, an excess dataflow requirement of $I_{carriers} \sim 10^{16}$ bits/sec allowing each application plate to send ~100 bits/sec can be transported by $N_{datatankers} = I_{carriers} \tau_{VasculoidCirc} / i_{nano} V_{tanker} \sim 2 \times 10^{11}$ data tankers (~0.1% of all tankers) incorporating nanocomputer read/write memory with a fairly modest storage density of $i_{nano} = 10^7$ bits/μm^3 (Section 4.8.5).

(7) **Intentional Heat Generation.** The vasculoid may be used to provide global or localized heating for prethaw warming (Section 4.9.1) or final patient warmup (Section 4.13.1). Heating can be achieved by operating motors within each basic plate at high speed to generate a surplus of waste heat, or by importing specialized "heating tankers" whose function is to dock in good thermal contact with each heat-conductive diamondoid basic plate and then consume energy in a manner optimized to generate waste heat (conceptually equivalent to electrical joule heating in a wire), or by similar other simple means.

4.7 Submicron Tissue Scan

Following the cleaning, reconditioning, scanning and mapping of all exposed ice surfaces to nanometer resolution (Section 4.5) and the partial or complete installation of the vasculoid (Section 4.6), the next step is to perform submicron scans up to ~20 μm below each exposed ice surface to detect and map all tissue structures down to ~0.1 μm (~100 nm) in size. (If each tissue cell lies within 1-3 cell widths of a capillary,[1122] and if the average cell size is 20 μm,[1123] then the typical tissue-crossing distance between nearest-neighboring points on capillaries is ~40 μm.)

Submicron scans to 100 nm resolution are necessary to: (A) provide useful structural data to support creation of the comprehensive whole-body computational model and repair plan (Section 4.8); (B) prepare a whole-body neural connectome map (Section 4.8.1(5)); and (C) provide actionable information on possible damage to subsurface tissues and the location and possible identity of macerated cell structures to enable resealing damaged membrane compartments (Section 4.11) and detailed cell repair operations (Section 4.12) after tissue reliquidification. Note that the minimum limit of 100 nm resolution for structural data, here deemed essential for preserving memory and personal identity, was tentatively proposed in Section 2.1.6 following an initial analysis of requirements but is the proper subject of ***future research*** to modify or confirm.

[1121] Freitas RA Jr. Nanomedicine, Volume I: Basic Capabilities, Landes Bioscience, Georgetown TX, 1999, Section 8.3.3, "Microtransponder Network"; http://www.nanomedicine.com/NMI/8.3.3.htm.

[1122] Freitas RA Jr. Nanomedicine, Volume I: Basic Capabilities, Landes Bioscience, Georgetown, TX, 1999; Section 8.2.1.2, "Arteriovenous Microcirculation"; http://www.nanomedicine.com/NMI/8.2.1.2.htm#p11.

[1123] Freitas RA Jr. Nanomedicine, Volume I: Basic Capabilities, Landes Bioscience, Georgetown, TX, 1999; Fig. 8.36 in Section 8.5.3.1, "Overall Cellular Structure"; http://www.nanomedicine.com/NMI/8.5.3.1.htm.

In this Section we briefly examine four technologies that are theoretically capable of providing the required submicron data: acoustic scanning (Section 4.7.1), optical microscopy (Section 4.7.2), electron microscopy (Section 4.7.3), and direct chemohaptic sensing (Section 4.7.4). Each of these techniques has advantages and disadvantages. All are very challenging in the intended application and all will require significant additional ***future research*** to better define and perfect them.

As previously noted, these scans may be facilitated by specialized vasculoid scanning patches (Section 4.6.5(2)) that should be removed from the patient and replaced with standard basic plates after the scanning processes described in Section 4.7 are complete.

4.7.1 Submicron Acoustic Scanning

Given the $v_{sound/ice}$ ~ 3940 m/sec speed of sound in bubble-free ice at ~210 K,[1124] achieving a feature resolution of $x_{capillary}$ ~ 0.1 μm (100 nm) requires an acoustic frequency on the order of $\nu_{ice} \geq v_{sound/ice} / x_{feature}$ ~ 40 GHz. As previously noted (Section 4.3.1), there are no reports of GHz ultrasound microscope scans in ice media. However, one 2014 paper[1125] reports acoustic experiments in solid media at 10 GHz using ~100 nm acousto-plasmonic resonators that have been hailed as "an advance…towards next generation ultrasonic imaging with potentially 1,000 times higher resolution than today's medical ultrasounds."[1126] Another 2011 paper[1127] reports measuring the attenuation of 50 GHz and 100 GHz longitudinal acoustic waves in amorphous silicon, and of 50 GHz acoustic waves in crystalline silicon. Properly designed atomically-precise nanorobotic devices should readily generate 40 GHz acoustic vibrations. For example, as early as 1995 CalTech researchers performed molecular dynamics simulations (and vibrations were observed) on a 3557-atom planetary gear mechanism rotating at ~83 GHz (the input unit completing one revolution every 12.0 picoseconds).[1128]

Assuming these signals can be generated by microscale emitters, what is the attenuation of 40 GHz acoustic waves in ice? It may be invalid to extend the empirical estimates for GHz sound attenuation in water-ice in **Table 4** to much higher frequencies than they were modeled for, but the empirical model for hard glaze ice in **Table 4** (Section 4.3.1) appears to predict an acoustic attenuation coefficient of $\alpha_{GHzIce} = \alpha_{glaze} = 80$ Np/mm for 40 GHz. If average cells are 20 μm in size and all cells lie within ~2 cell widths of a capillary, then the shortest path through cells between the nearest transmitter/receiver pairs in neighboring capillaries is ~40 μm. The power attenuation of a 40 GHz acoustic pulse traversing x_{sep} = 40 μm of cryopreserved

---

[1124] Vogt C, Laihem K, Wiebusch C. Speed of sound in bubble-free ice. J Acoust Soc Am. 2008 Dec;124(6):3613-8; https://www.researchgate.net/publication/23997391_Speed_of_sound_in_bubble-free_ice. The speed of sound in vitrified tissue will be slightly different from this number.

[1125] O'Brien K, Lanzillotti-Kimura ND, Rho J, Suchowski H, Yin X, Zhang X. Ultrafast acousto-plasmonic control and sensing in complex nanostructures. Nat Commun. 2014 Jun 4;5:4042; http://xlab.me.berkeley.edu/pdf/243.pdf.

[1126] Yarris L. Manipulating and Detecting Ultrahigh Frequency Sound Waves. LBL News Center, 11 Jun 2014; https://newscenter.lbl.gov/2014/06/11/ultrahigh-frequency-sound-waves/.

[1127] Hondongwa DB, Daly BC, Norris TB, Yan B, Yang J, Guha S. Ultrasonic attenuation in amorphous silicon at 50 and 100 GHz. Phys Rev B 2011 Mar 10;83:121303; https://journals.aps.org/prb/abstract/10.1103/PhysRevB.83.121303.

[1128] Cagin T, Jaramillo-Botero A, Gao G, Goddard WS III. Molecular mechanics and molecular dynamics analysis of Drexler-Merkle gears and neon pump. Nanotechnology 1998;9:143-152; https://authors.library.caltech.edu/526/1/CAGnanotech98.pdf. Paper originally presented at Fifth Foresight Conference on Molecular Nanotechnology, 1995; https://web.archive.org/web/20100613014250/https://foresight.org/Conferences/MNT05/Papers/index.html.

human tissue at LN2 temperatures (~77 K) can be estimated as $k_{atten} = P_{receiver}/P_{transmitter} \sim \exp(-\alpha_{GHzIce}\ x_{sep})$ = 0.04 in transmission mode. Following the methodology previously outlined in Section 4.3.1 with SNR ~ 3 for t_{pulse} = 1 μsec pulses at 40 GHz with $P_{receiver} = E_{receiver} / t_{pulse}$ = 0.021 pW, the power required to transmit the pulses is $P_{transmitter} = P_{receiver} / k_{atten}$ = 0.53 pW per pulse and the power requirement for all $N_{sensors} = 10^9$ transmitters to emit one pulse is $P_{pulse,total} = P_{transmitter}\ N_{sensors}$ ~ 0.5 mW/pulse. Thus a pulse rate of ~1 KHz could be sustained for all $N_{sensors} = 10^9$ transmitters within a whole-body scanning power budget of 0.5 watts. This whole-body power fluence is too low to defrost or significantly warm cryopreserved tissue, especially since small thermal gradients caused by localized acoustic waste heat generation can be actively opposed by vasculoid-provided cooling resources. Because the wavelength is ~100 nm, features as small as this wavelength may be made visible with a scanning program of sufficient duration.

The vasculoid (Section 4.6) provides a sturdy fixed reference frame from which to deploy scanning instruments, a reliable platform for supplying electrical power to scanning transmitters and receivers, and a ready-made network through which scan data can be collected and transported to external computers for further analysis. The vasculoid can also provide precise timing signals throughout the network – without these timing signals, precisely synchronized and highly accurate timers would likely be needed inside each individual nanorobot.

It should be possible to detect and visualize many cellular and subcellular features by taking sufficient time to scan and re-scan over enough cycles to accumulate excellent statistics. Resolving intracellular features ~0.1 μm and larger would capture all major organelles including the nucleus, the Golgi, the endoplasmic reticulum (ER), and other organelles around ~1 μm in size such as mitochondria, lysosomes, peroxisomes, and possibly the nucleolus. A ~100 nm scan resolution should also allow detailed identification of all key synaptic structures (Section 2.1.2), enabling compilation of a comprehensive neural connectivity map of the frozen brain by tracing all individual axons and dendrites. For example, unmyelinated parallel fibers are 200-300 nm in diameter, while myelinated parallel fibers (axons) are typically 400-1100 nm wide.[1129]

In one possible deployment scenario, scanning instruments are emplaced directly onto tissue ice through modified cellulocks in a completely installed vasculoid (Section 4.6.2). The original vasculoid design positioned cellulocks at a mean center-to-center separation of ~96 μm, but decreasing their separation to only ~40 μm should permit sufficient resolution on the underlying frozen tissue while increasing their numbers by about $(96\ \mu m / 40\ \mu m)^2$ ~ 6-fold, also increasing their occupancy of the entire vasculoid surface from 0.65% (Section 4.6.1) to 3.9%. These cellulocks should be restructured as circumferential rings (Section 4.6.5(1)) so they can service the entire 360 degree region surrounding the vascular tube. The cellulocks would then become sensor/ice access ports, with transmitters and receivers transported between sites inside vasculoid boxcars. These devices can be selectively removed after the scan, whereupon conventional cellulocks and boxcars could be installed prior to commencing cell repair operations (Section 4.12). Conventional boxcars are 6 μm (diameter) x 1000 μm in size with 2120 μm^3 of usable internal storage volume and thus can be used to import large numbers of tissue-crawling repair nanorobots later in the process (after tissue reliquidification), in addition to any mobile cells that might be needed for repairs or for return to normal metabolism (Section 4.14.3) and normal biological function at the end of the revival process.

A second possible deployment scenario would be to perform scans only in small local sectors at a time to avoid excessive heat generation – in essence, deploying a moving block of temporary vasculoid-like systems through all the capillary beds in the body, slowly scanning and recording every section over a very long time period, only installing the complete vasculoid after all scans have been completed. It might be useful to employ mobile scanning elements that can slide along the capillary walls, taking measurements as

---

[1129] Wyatt KD, Tanapat P, Wang SS. Speed limits in the cerebellum: constraints from myelinated and unmyelinated parallel fibers. Eur J Neurosci. 2005 Apr;21(8):2285-90; https://www.ncbi.nlm.nih.gov/pmc/articles/PMC1201546/.

they go. If these walls have previously been precisely mapped, then roving nanorobotics transmitters and receivers could establish their precise position within the tunnels for each measurement they take.

A third possible deployment scenario would excavate, using sensor guidance, small boreholes into tissue ice beneath the vasculoid, taking care to avoid any critical biological structures (e.g., the nucleus and DNA). Acoustic transmitter and receiver equipment could then be positioned inside the boreholes at depth, allowing (A) reduced attenuation between transmitters and receivers because of the reduced distance over which the acoustic pulses must travel, and (B) greater geometric flexibility in siting transmitters relative to receivers in 3D space making available a far greater number of potential scanning pathways through the ice and improved resolution of objects buried in the ice.

Future research should identify suitably efficient deployable microscale transmitters and receivers for ~40 GHz acoustic waves, establish efficient coupling mechanisms between these devices and vitrified or frozen water-ice at 77 K (-196 °C), determine actual attenuation coefficients in this ice for ~40 GHz acoustic waves, and assess which deployment scenario offers the most favorable technical tradeoffs.

4.7.2 Optical Microscopy

The optical microscope, also referred to as a light microscope, commonly uses visible light and a system of lenses to generate magnified images of small objects.[1130] Transparent objects can be lit from below and solid objects can be lit with light coming through (bright field) or around (dark field) the objective lens. There are many variants of optical microscopes,[1131] too numerous to review here.

In a lens system with negligible optical aberrations, the far-field optical resolution limit is $d_{resol} = \lambda / 2$ NA, where λ is the wavelength of the light and the maximum "numerical aperture" NA ~ 0.95 in air, 1.5 in oil. The optical wavelength is usually taken as $\lambda \sim 550$ nm (green light), giving a theoretical resolution of $d_{resol} = 289$ nm in air with a photon energy of $E_{photon} = hc/\lambda = 2.26$ eV, well below the 3.6 eV needed to break the weakest single carbon (C-C) covalent bonds in organic molecules,[1132] taking $c = 3 \times 10^8$ m/sec (speed of light) and $h = 6.63 \times 10^{-34}$ J-sec (Planck constant). Pushing photon energy to an organic molecule-destroying threshold energy of 3.6 eV requires a $\lambda = 346$ nm photon ("soft UV" in the middle of the "ultraviolet A" (UVA) range),[1133] a resolution limit of $d_{resol} = 182$ nm in air. Pushing the resolution limit all the way to $d_{resol} = 100$ nm in air would require even higher-energy and more destructive photons: $\lambda \sim$ 190 nm ("hard UV") with $E_{photon} = 6.53$ eV, energetic enough to break even C=C double bonds (at 6.24 eV bond energy).

In practice, the lowest value of d_{resol} obtainable with conventional lenses is about **200 nm**.[1134] A new type of lens called a HIRES lens has used multiple scattering of biostructure-safe $\lambda = 561$ nm light to improve the resolution to ~**100 nm**.[1135] ***Future research*** is required to ascertain whether this or some other optical

---

[1130] https://en.wikipedia.org/wiki/Optical_microscope.
[1131] https://en.wikipedia.org/wiki/Optical_microscope#Other_microscope_variants.

[1132] C-C bond energy is 346 KJ/mole; "Common Bond Energies"; http://www.wiredchemist.com/chemistry/data/bond_energies_lengths.html.

[1133] https://en.wikipedia.org/wiki/Ultraviolet#Subtypes.
[1134] https://en.wikipedia.org/wiki/Optical_microscope#Limitations.

[1135] van Putten EG, Akbulut D, Bertolotti J, Vos WL, Lagendijk A, Mosk AP. Scattering lens resolves sub-100 nm structures with visible light. Phys Rev Lett. 2011;106(19):193905; http://www.koenderink.info/reading/MoskLens.pdf.

scanning methodology is sufficiently general to be applicable to scanning *in situ* cryopreserved tissue blocks. For instance, photons passing through living soft tissue in a scanning beam are removed from their path mostly by scattering (σ_{scat} ~10^4-10^5 m^{-1}; average ~30,000 m^{-1}). As a result, the mean free path of an optical photon in living human soft tissue is $\Lambda_{optical} \sim \sigma_{scat}^{-1}$ ~ 10-100 μm (average ~30 μm).[1136] The scattering coefficient can be lower in exceptionally clear tissues (e.g., σ_{scat} ~1000 m^{-1}, $\Lambda_{optical}$ ~ 1000 μm)[1137] and even lower for pure water-ice (e.g., σ_{scat} ~ 2 m^{-1})[1138] so optical photons can probably penetrate the necessary 20-40 μm required for submicron tissue scans (Section 4.7).

Near-field scanning optical microscopy (NSOM)[1139] breaks the far-field optical resolution limit by exploiting the properties of evanescent waves.[1140] When a sample is scanned at a close distance below an aperture that is smaller than the wavelength of the laser light being focused through it, then the optical resolution of transmitted or reflected light is limited only by the diameter of the aperture, enabling a maximum lateral resolution of 20 nm[1141] and a vertical resolution of 2-5 nm[1142] to be demonstrated. Unfortunately, because NSOM makes use of evanescent fields that exist only near the surface of the object (which carry the high frequency spatial information about the object, with intensities that drop off exponentially with distance from the object), the detector must be placed within a few nanometers of the sample in the near field zone. As a result, near field microscopy remains primarily a surface inspection technique. Other techniques such as optical absorption microscopy[1143] can also provide nanometer-scale resolution during surface scans, while techniques like Structured Illumination Microscopy[1144] can reach ~100 nm resolution but apparently require fluorophores. The potential applicability of these methods to submicron cryopreserved tissue scanning should be explored in ***future research***.

[1136] Freitas RA Jr. Nanomedicine, Volume I: Basic Capabilities, Landes Bioscience, Georgetown TX, 1999, Section 4.10.4, "Optical Macrosensing"; http://www.nanomedicine.com/NMI/4.9.4.htm#p4.

[1137] Jacques SL. Time-resolved reflectance spectroscopy in turbid tissues. IEEE Trans Biomed Eng. 1989 Dec;36(12):1155-61; https://pubmed.ncbi.nlm.nih.gov/2606489/. Cheong WF, Prahl SA, Welch AJ. A Review of the Optical Properties of Biological Tissues. IEEE J Quantum Electronics 1990 Dec;26:2166-2185; http://citeseerx.ist.psu.edu/viewdoc/download?doi=10.1.1.420.8912&rep=rep1&type=pdf.

[1138] Katlein C, Nicolaus M, Petrich C. The anisotropic scattering coefficient of sea ice. J Geophys Res: Oceans. 2014 Feb;119(2):842-855; https://core.ac.uk/download/pdf/19773389.pdf.

[1139] https://en.wikipedia.org/wiki/Near-field_scanning_optical_microscope.
[1140] https://en.wikipedia.org/wiki/Evanescent_field.

[1141] Dürig U, Pohl DW, Rohner F. Near-field optical-scanning microscopy. J Appl Phys. 1986;59(10):3318; https://www.researchgate.net/profile/Dieter_Pohl/publication/224419975_Near-Field_Optical_Scanning_Microscopy_in_Reflection/links/00b7d5270d75651937000000.pdf.

[1142] Oshikane Y, Kataoka T, Okuda M, Hara S, Inoue H, Nakano M. Observation of nanostructure by scanning near-field optical microscope with small sphere probe. Sci Technol Adv Mater. 2007 Apr 30;8(3):181-185; https://iopscience.iop.org/article/10.1016/j.stam.2007.02.013/pdf.

[1143] Weaver J, Walpita L, Wickramasinghe H. Optical absorption microscopy and spectroscopy with nanometre resolution. Nature 1989 Dec 14;342(6251):783–785; https://www.nature.com/articles/342783a0. Chien MH, Brameshuber M, Rossboth BK, Schütz GJ, Schmid S. Single-molecule optical absorption imaging by nanomechanical photothermal sensing. Proc Natl Acad Sci U S A. 2018 Oct 30;115(44):11150-11155; https://www.ncbi.nlm.nih.gov/pmc/articles/pmid/30254155/. Dutta BK, Panchadhyayee P, Bayal I, Das N, Mahapatra PK. Optical absorption microscopy of localized atoms at microwave domain: two-dimensional localization based on the projection of three-dimensional localization. Sci Rep. 2020 Jan 17;10(1):536; https://www.ncbi.nlm.nih.gov/pmc/articles/PMC6969140/.

[1144] Ströhl F, Kaminski CF. Frontiers in structured illumination microscopy. Optica 2016;3(6):667-677; https://www.osapublishing.org/optica/fulltext.cfm?uri=optica-3-6-667&id=344732.

4.7.3 Electron Microscopy

Electron microscopes[1145] use a beam of electrons to illuminate a sample that is being scanned. Because the wavelength of electrons is ~100,000 times shorter than the wavelength of visible light photons, certain electron microscopes can reveal structures as small as **0.05 nm**,[1146] as compared with optical microscopes that are classically diffraction-limited to ~200 nm (Section 4.7.2). Electron microscopes are commonly used to investigate the ultrastructure of a wide range of biological and inorganic specimens including large molecules, cells, microorganisms, and biopsy samples. Electron microscopy offers extremely high spatial resolution but at high risk of physical destruction of some of the biological structures being scanned. ***Future research*** on submicron scanning using electron microscopy could examine the tradeoff between scan intensity and the tolerable limits of biological damage, given the posited super-redundancy of neural storage data (Section 2.1.3).

For example, FIB-SEM (Focused Ion Beam[1147] - Scanning Electron Microscope[1148]) brain tissue scans to below 10 nm resolution have been demonstrated,[1149] some with pixel size as small as 4 nm,[1150] and similar resolution has been demonstrated using SEM/TEM (Transmission Electron Microscope[1151]) techniques.[1152] The Zeiss MultiSEM Scanning Electron Microscope uses 91 separate electron beams operating in parallel to image a 1 cm^2 area to 4 nm pixel size in ~3 hours.[1153] Most of these techniques currently require using ultramicrotome brain tissue sections that are only 30-100 nm thick. At least one possible future path to achieve a whole human brain scan to nanoscale resolution using conventional electron scanning technologies has been proposed.[1154]

Much electron microscopy is done under high vacuum conditions (because air molecules scatter electrons) and require conductive samples (nonconductive samples are traditionally thinly coated with conductive

---

[1145] https://en.wikipedia.org/wiki/Electron_microscope.

[1146] Erni R, Rossell MD, Kisielowski C, Dahmen U. Atomic-resolution imaging with a sub-50-pm electron probe. Phys Rev Lett. 2009;102(9):096101; https://escholarship.org/content/qt3cs0m4vr/qt3cs0m4vr.pdf.

[1147] https://en.wikipedia.org/wiki/Focused_ion_beam.
[1148] https://en.wikipedia.org/wiki/Scanning_electron_microscope.

[1149] Hayworth KJ, Xu CS, Lu Z, Knott GW, Fetter RD, Tapia JC, Lichtman JW, Hess HF. Ultrastructurally smooth thick partitioning and volume stitching for large-scale connectomics. Nat Methods. 2015 Apr;12(4):319-22; http://www.ncbi.nlm.nih.gov/pmc/articles/PMC4382383/.

[1150] Knott G, Rosset S, Cantoni M. Focussed ion beam milling and scanning electron microscopy of brain tissue. J Vis Exp. 2011 Jul 6;(53):e2588; http://www.ncbi.nlm.nih.gov/pmc/articles/PMC3196160/.

[1151] https://en.wikipedia.org/wiki/Transmission_electron_microscopy.

[1152] Briggman KL, Bock DD. Volume electron microscopy for neuronal circuit reconstruction. Curr Opin Neurobiol. 2012 Feb;22(1):154-61; http://web.stanford.edu/class/cs379c/archive/2015/calendar_invited_talks/articles/BriggmanandBockCON-12.pdf.

[1153] https://www.zeiss.com/microscopy/us/products/scanning-electron-microscopes/multisem.html.

[1154] Merkle RC. Large Scale Analysis of Neural Structures. Xerox PARC CSL-89-10 Nov 1989 (P89-00173); http://www.merkle.com/merkleDir/brainAnalysis.html. Hayworth KJ. Electron imaging technology for whole brain neural circuit mapping, Int J Machine Consciousness, 2012; 4(1):87-108; http://web.archive.org/web/20150428052029/http://www.brainpreservation.org/sites/default/files/ElectronImagingTechnologyForWholeBrainNeuralCircuitMapping_Hayworth2012.pdf.

metal). However, the low-voltage mode[1155] of modern electron microscopes permits the observation of non-conductive specimens without metal coatings. Nonconductive materials can also be imaged by a variable pressure[1156] (or environmental)[1157] scanning electron microscope, or by various alternative cryogenic electron microscopy techniques (see below) that should be explored for cryonics applications in ***future research***.

4.7.3.1 Low Voltage Electron Microscopy

A low-voltage electron microscope (LVEM)[1158] is operated at a relatively low electron accelerating voltage between 5-25 KV, attaining scan resolutions of 1-3 nm. Low voltage increases the image contrast which reduces or eliminates the need for sample staining, an important consideration both for living biological specimens and for scanning cryopreserved tissue which cannot readily be stained or implanted with fluorescent molecules. However, low voltage limits the maximum thickness of samples that can be studied in the TEM (transmission electron microscopy)[1159] or STEM (scanning TEM)[1160] mode – only 20-65 nm thick samples can be used in conventional LVEM @ 5 KV compared to 50-90 nm thick samples for conventional high-energy TEM – though high quality LVEM results are claimed to have been obtained on L_{sample} = 100 nm thick samples using a 25 KV LVEM.[1161] Of course, electrons carrying an energy of 5000-25,000 eV may cleave any chemical bond that they encounter, exemplifying an inverse relationship between scan duration (i.e., radiation dose) and biochemical integrity of the sample.

Miniaturized SEMs with 100 nm resolution and ~14 cm^3 device volume have been developed for NASA,[1162] but an electrostatic accelerator tube capable of boosting electron voltages to $V_{electron}$ = 5-25 KV could have a length dimension as small as $L_{accelerator} \geq V_{electron} / V_{breakdown}$ ~ 5-25 μm, creating a steerable scanning beam of electrons of energy $E_{electron}$ = 5-25 KeV (8-40 x 10^{-16} J/electron), possibly to be used in a microscopic low-voltage electron microscope apparatus, given the maximum breakdown voltage for diamond of $V_{breakdown}$ ~ 1 volt/nm (~10^9 volt/m).[1163] To hold whole-body total waste heat generation to P_{escan} ~ 100 watts, each V_{evoxel} = (~20 μm)^3 = 8000 μm^3 scan voxel would have to be held to a maximum of $P_{evoxel} = P_{escan} (V_{evoxel} / V_{body})$ = 13.4 pW, which implies an electron scanning beam fluence of only $N_{electrons} = P_{evoxel} / E_{electron}$ = 3400-16,800 electrons/sec through each scan voxel, or $N_{electrons} (L_{sample}^2 / V_{evoxel}^{2/3})$ = 0.09-0.4 electrons/sec through each (100 nm)^2 cross-sectional pixel in a 20 μm voxel. Beam fluence can be increased in one voxel by reducing the simultaneous fluence in other voxels or by operating each beam at a higher frequency but shorter duty cycle. ***Future research*** should determine if a practical

---

[1155] https://en.wikipedia.org/wiki/Low-voltage_electron_microscope.

[1156] Stokes DL. Principles and practice of variable pressure/environmental scanning electron microscopy (VP-SEM). Wiley, Chichester, West-Sussex, 2008; https://www.amazon.com/dp/0470065400/.

[1157] https://en.wikipedia.org/wiki/Environmental_scanning_electron_microscope.
[1158] https://en.wikipedia.org/wiki/Low-voltage_electron_microscope.
[1159] https://en.wikipedia.org/wiki/Transmission_electron_microscopy.
[1160] https://en.wikipedia.org/wiki/Scanning_transmission_electron_microscopy.
[1161] https://en.wikipedia.org/wiki/Low-voltage_electron_microscope#Limitations.

[1162] Gaskin JA, *et al*. Miniature Scanning Electron Microscope for *in-situ* planetary studies: electron gun development. 40th Lunar and Planetary Science Conference, 2009; https://www.lpi.usra.edu/meetings/lpsc2009/pdf/2318.pdf. "Scientists shrink electron gun to matchbox size," DESY News, 2016 Nov 22; https://www.desy.de/news/news_search/index_eng.html?openDirectAnchor=1144.

[1163] CVD diamond dielectric strengths are typically listed around 1 x 10^9 V/m, but some researchers and manufacturers report they have achieved dielectric strengths of 3 x 10^9 V/m or more. Kardys G. What is the ultimate dielectric material? IEEE GlobalSpec, 30 Aug 2018; https://insights.globalspec.com/article/9768/what-is-the-ultimate-dielectric-material-diamond-materials-part-4.

low-voltage electron-based scanning system can be defined and assess whether the use of ice boreholes (Section 4.7.1) can assist in reducing the required scan distances in ice.

4.7.3.2 Cryogenic Electron Microscopy

Cryogenic Electron Microscopy (cryoEM)[1164] is an electron microscopy (EM) technique applied on samples cooled to cryogenic temperatures and embedded in an environment of vitreous water. An aqueous sample solution is applied to a grid-mesh and plunge-frozen in liquid ethane or a mixture of liquid ethane and propane.[1165] While development of the technique began in the 1970s, recent advances in detector technology and software algorithms have allowed for the determination of biomolecular structures at near-atomic resolution,[1166] and the 2017 Nobel Prize in Chemistry was awarded for the development of cryo-electron microscopy for the high-resolution structure determination of biomolecules in solution.[1167] In the first successful demonstration of cryoEM in 1981, pure water was vitrified in a thin film by spraying it onto a hydrophilic carbon film that was rapidly plunged into liquid propane or liquid ethane at 100 K (-173 °C), creating a <1 µm thick layer of amorphous/vitreous ice as confirmed by an electron diffraction pattern.[1168] In 1984 the same group used cryoEM to visualize feature sizes well below 100 nm (1000 Å) in the structural biology of vitrified adenovirus type 2, T4 bacteriophage, Semliki Forest virus (image, above), Bacteriophage CbK, and Vesicular-Stomatitis-Virus.[1169]

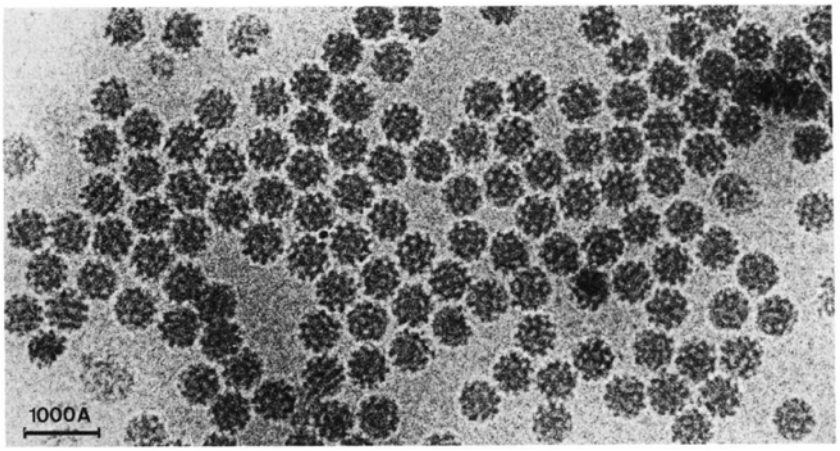

[1164] https://en.wikipedia.org/wiki/Cryogenic_electron_microscopy.

[1165] Tivol WF, Briegel A, Jensen GJ. An improved cryogen for plunge freezing. Microsc Microanal. 2008 Oct;14(5):375-379; https://www.ncbi.nlm.nih.gov/pmc/articles/PMC3058946/pdf/nihms278822.pdf.

[1166] Cheng Y, Grigorieff N, Penczek PA, Walz T. A primer to single-particle cryo-electron microscopy. Cell. 2015 Apr 23;161(3):438-449; https://www.cell.com/cell/pdf/S0092-8674(15)00370-0.pdf.

[1167] Cressey D, Callaway E. Cryo-electron microscopy wins chemistry Nobel. Nature. 2017;550(7675):167; https://www.nature.com/news/cryo-electron-microscopy-wins-chemistry-nobel-1.22738.

[1168] Dubochet J, McDowall AW. Vitrification of pure water for electron microscopy. J Microsc. 1981 Dec;124(3):RP3-RP4; https://onlinelibrary.wiley.com/doi/epdf/10.1111/j.1365-2818.1981.tb02483.x.

[1169] Adrian M, Dubochet J, Lepault J, McDowall AW. Cryo-electron microscopy of viruses. Nature. 1984 Mar 1;308(5954):32-36; https://serval.unil.ch/resource/serval:BIB_BEC796503260.P001/REF.pdf.

4.7.3.3 Transmission Electron Cryomicroscopy

CryoTEM or transmission electron cryotomography,[1170] the most common form of cryoEM, can provide up to 1.8 Å resolution for samples embedded in vitrified ice at LN2 temperatures. In 2020 a German research team reported using cryoEM to produce a 3D image of the apoferritin molecule to 0.125 nm (1.25 Å) resolution, representing the first truly atomic resolution image of a protein molecule.[1171]

The energy of the electrons used for imaging (80-300 KeV) is high enough to break covalent bonds, so it is necessary to limit the electron exposure used to acquire the image when imaging specimens vulnerable to radiation damage. Typically the biological material is spread on an electron microscopy grid and quick-frozen to LN2 temperature, allowing the specimen to be introduced into the high vacuum of the electron microscope column. Most biological specimens are extremely radiosensitive and must be imaged with low-dose techniques, although the low temperature of cryoTEM provides an additional protective factor against radiation damage. The method is limited to thin biological specimens typically < 500 nm because the electrons cannot cross thicker samples without multiple scattering events.[1172] Thicker specimens are vitrified by cryofixation up to tens of microns in thickness, then are cut into thin sections 40-200 nm thick using a diamond knife in a cryoultramicrotome at temperatures below -135 °C (devitrification temperature).

4.7.3.4 Electron Cryotomography

Cryo electron tomography (cryoET) or electron cryotomography (ECT)[1173] is a specialized application of cryoTEM in which samples are imaged as they are tilted, resulting in a series of 2D images that can be combined to produce high-resolution (1-4 nm) 3D views of samples, typically biological macromolecules and cells (analogous to a CT scan of the human body).

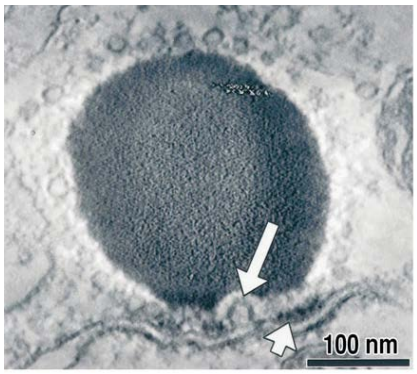

The image at right is a tomographic slice of a synapse showing a synaptic body (dense round body ~200 nm wide), an Ω-shaped presynaptic membrane invagination (long arrow) and presynaptic density (short arrow).

The image below is an electron cryotomographic slice of part of a Golgi body from a normal rat kidney cell, showing, e.g., the ER-Golgi intermediate compartment (colored yellow) and the *trans*-most cisterna (red).[1174] Again, sample thickness is typically limited to ~500

[1170] https://en.wikipedia.org/wiki/Transmission_electron_cryomicroscopy.

[1171] Nakane T, *et al*. Single-particle cryo-EM at atomic resolution. bioRxiv 2020 May 22; https://www.biorxiv.org/content/biorxiv/early/2020/05/22/2020.05.22.110189.full.pdf. Yip KM, Fischer N, Paknia E, Chari A, Stark H. Breaking the next Cryo-EM resolution barrier – Atomic resolution determination of proteins! bioRxiv 2020 Dec 21; https://www.biorxiv.org/content/10.1101/2020.05.21.106740v1.full.pdf. See also: Callaway E. 'It opens up a whole new universe': Revolutionary microscopy technique sees individual atoms for first time. Nature News, 3 Jun 2020; https://www.nature.com/articles/d41586-020-01658-1.

[1172] https://en.wikipedia.org/wiki/Transmission_electron_cryomicroscopy#Biological_specimens.
[1173] https://en.wikipedia.org/wiki/Electron_cryotomography.

[1174] Gan L, Jensen GJ. Electron tomography of cells. Q Rev Biophys. 2012;45(1):27-56; https://authors.library.caltech.edu/29858/1/Gan2012p17514Q_Rev_Biophys.pdf.

nm to achieve macromolecular (~4 nm) resolution, though thicker samples may be tolerable if only 50-100 nm resolution is required. It may also be possible to sacrifice resolution using low-number density scan patterns to avoid prohibitively long scan times.

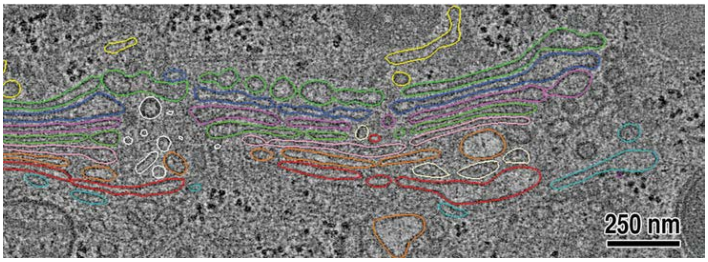

4.7.4 Direct Chemohaptic Sensing

Even if the 100-nm resolution acoustic-, optical-, and electron-based scanning methods described in the preceding subsections prove unworkable, an extremely laborious alternative called chemohaptic (Appendix F) sensing should still be available.

Using this method, tiny flexible sensor probes would be carefully drilled into the ice, following open-ice channel pathways that avoid any large biological structures that are detected buried in the ice. These "nanosnakes" could be slowly moved through the ice, sampling by haptic and chemical sensing the outlines of all structures encountered, without disturbing their positions and without cutting or damaging them. After circumnavigation of such structures, each probe would move on to the next structure, traversing the frozen cytosol between structures where only isolated small molecules reside. If the patient has been vitrified, then the ice will not be solid crystalline but will be amorphous, which might ease the transit of the nanosnake.

The nanosnake could be a hyperredundant manipulator (e.g., a tentacle manipulator), with its apex festooned with nanomotors, chemical sensors, and other appropriate mechanisms. Locally excavated water-ice can be backfilled after the probe is finished mapping all ≥100 nm structures in a given tissue volume. Scanning this way could take a very long time, perhaps months and possibly years. But for a cryopreservation patient maintained at 77 K (-196 °C), biochemical activity and particle diffusion should be minimized so all necessary time may be taken to avoid exceeding heat generation and other technical limitations on the process. ***Future research*** should assess the viability and limitations of this approach.

If some additional structural or biochemical information below the 100-nm resolution limit is required to preserve personal identity (Section 2.1), direct chemohaptic sensing may be able to provide it in the manner described above. But this will be a very time-consuming process because of the control complexity in operating the many manipulators required and because of the need to avoid exceeding strict waste heat generation limits. The possibility of obtaining sub-100-nm information by this means should be investigated in ***future research***.

4.8 Compute Whole-Body Repair Plan

Upon completion of whole-body mapping (Section 4.5) and submicron scans to 100 nm spatial resolution (Section 4.7), the detailed structural information thus obtained is analyzed to determine the probable location, identity, and integrity of all significant biological structures in the body of the cryopreserved patient. These data and analyses are employed to devise a corrective plan that can be used to effectuate all necessary repairs. The corrective plan will include a model of the cryopreserved body as it currently exists, a second model of the body as we wish it to exist after repairs are completed, and a sequence of tasks and operations ("the plan") to be executed by medical nanorobots that will convert the patient's body from the description in the first model to the description in the second model.

Future research might also investigate whether the whole-body maps described in this Section can provide sufficient information to initialize a human brain emulation (Section 5.2.3.4), and if so, what degree of personal identity might be expected to be recoverable in the absence of a full molecular scan (Chapter 5).

4.8.1 Analysis of Scan Data for Cryonics Repair

Extensive scan data collection by various means enables the compilation of six detailed whole-body maps representing the current physical state of the cryopreserved patient, comprising $I_{mapCryo} \sim 1.5 \times 10^{23}$ bits of structure information, as follows:

(1) Exposed Ice Surfaces Map. The data storage requirement for a whole-body map of all exposed ice surfaces involving 6.64×10^{20} pixels of size $q_{resol}^2 = 1$ nm^2/pixel is $I_{mapGeom} \sim 8 \times 10^{22}$ bits of storage (Section 4.5.4), plus an additional $I_{mapBio} \sim 6 \times 10^{22}$ bits of storage for a whole-body biochemical map of all exposed ice surfaces (Section 4.5.5), giving a total storage requirement for the Exposed Ice Surfaces Map of $I_{mapEISM} \sim$ **1.4×10^{23} bits**. This map has the largest datafile, in part because of its high spatial resolution.

(2) Vascular Fault Map. Assuming that vascular faults (Section 4.5.6) represent $f_{Vascfault} \sim 10\%$ of the total arteriovenous ($A_{arteriovenous} = 312.9$ m^2)[1175] and lymphatic ($A_{lymphovascular} = 248.6$ m^2; Section 4.6.4) vascular surface area, where each fault can be adequately flagged as being one of $\sim 10^6$ possible types or modes of fault thus requiring $I_{pixelVascfault} \geq \log_2(10^6) \sim 20$ bits/pixel to encode for pixels of size $q_{resol}^2 = 1$ nm^2/pixel, then the additional data storage requirement to add a map of all vascular faults atop the Exposed Ice Surfaces Map is $I_{mapVascfault} = f_{Vascfault}\ I_{pixelVascfault}\ (A_{arteriovenous} + A_{lymphovascular}) / q_{resol}^2 \sim$ **1×10^{21} bits**.

(3) Fracture Plane Map. Assuming that crackface fracture planes (Section 4.5.7) represent $f_{Fracplanes} \sim 10\%$ of the total crackface surface area ($A_{crackface} = 12$ m^2; Section 4.6.3), where each fracture plane occurrence can be adequately flagged as being one of $\sim 10^3$ possible types thus requiring $I_{pixelFracplanes} \geq \log_2(10^3) \sim 10$ bits/pixel to encode for pixels of size $q_{resol}^2 = 1$ nm^2/pixel, then the additional data storage requirement to add a map of all crackface fracture planes atop the Exposed Ice Surfaces Map is $I_{mapFracplanes} = f_{Fracplanes}\ I_{pixelFracplanes}\ A_{crackface} / q_{resol}^2 \sim$ **1×10^{19} bits**.

(4) 3D Submicron Tissue Map. A whole-body 3D tissue map that records minimum feature sizes of $q_{resol3D} = 100$ nm during submicron tissue scans (Section 4.7) for an entire cryopreserved human body of total volume $V_{body} = 0.06$ m^3 ($\approx$ mean human whole-body volume)[1176] requires $n_{voxelBody} = V_{body} / q_{resol3D}^3 = 6 \times 10^{19}$ voxels of size $q_{resol3D}^3 = 10^6$ nm^3/voxel in volume. If $I_{voxelBody} \sim 3 \log_2(\sim 1$ meter / 100 nm) = 70 bits/voxel for three Cartesian dimensions of $\sim 10^7$:1 precision are sufficient to uniquely identify the geometric location of each voxel in 3D space to ~100 nm precision, and if each voxel can be encoded as having one of $\sim 10^6$ possible types, modes, colors, or other relevant characteristics, thus requiring $I_{voxeltype} \geq \log_2(10^6) \sim 20$ bits/voxel to encode, then the total data storage requirement for a 3D Submicron Tissue Map is $I_{mapBody} = n_{voxelBody}\ (I_{voxelBody} + I_{voxeltype}) \sim$ **5.4×10^{21} bits**.

[1175] Freitas RA Jr. Nanomedicine, Volume I: Basic Capabilities, Landes Bioscience, Georgetown, TX, 1999; Table 8.1, "Approximate Quantification of the Human Arteriovenous System"; http://www.nanomedicine.com/NMI/Tables/8.1.jpg

[1176] Freitas RA Jr. Nanomedicine, Volume I: Basic Capabilities, Landes Bioscience, Georgetown TX, 1999, Table 8.9, "Mass, Volume, and Scale Size of the Organs of the Human Body"; http://www.nanomedicine.com/NMI/Tables/8.9.jpg.

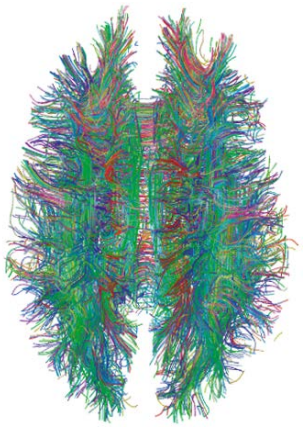

(5) Whole-Body Neural Connectome Map. The data provided by the 3D Submicron Tissue Map can be used to compile[1177] a whole-body neural connectome[1178] map – essentially, the "wiring diagram" of the brain (image, right).[1179] The human brain is currently estimated to contain 86.1 x 10^9 signal-carrying neurons,[1180] 2.4 x 10^{14} signal-routing synapses,[1181] and 84.6 x 10^9 non-signaling glial cells,[1182] to which must be added ~0.5 x 10^9 signal-carrying neurons in the enteric nervous system[1183] and ~0.1 x 10^9 signal-carrying neurons in the human spinal cord[1184] – hence f_{brain} = 99.3% of the signal-conducting human connectome resides in the human brain. Assuming the $q_{resol3D}$ = 100 nm feature size available from the 3D Submicron Tissue Map is sufficient to uniquely identify all neuron bodies (i.e., axons and dendrites) and all neuronal synapses that are present in a human brain of volume[1185] V_{brain} = 1400 cm^3, then a 100-nm precision physical map of the human connectome can be specified with $I_{mapConnectomeB} = n_{voxelBrain} (I_{voxelBrain} + I_{voxeltype}) \sim 1.1 \times 10^{20}$ bits, assuming $n_{voxelBrain} = V_{brain} / q_{resol3D}^3 = 1.4 \times 10^{18}$ voxels of size $q_{resol3D}^3 = 10^6$ nm^3/voxel in volume and taking $I_{voxelBrain} \sim 3 \log_2$(~0.1 meter / 100 nm) = 60 bits/voxel for three Cartesian dimensions of ~10^6:1 precision. If non-brain neurons average 10 times longer in length than brain neurons and thus contribute an additional $I_{mapConnectomeNB} = 10 (1 - f_{brain}) I_{mapConnectomeB}$ = 7.7 x 10^{18} bits, then a whole-body neural connectome map can be compiled in $I_{mapConnectome}$ =

[1177] Phaedra C. Reconstructive Connectomics. Cryonics 2013 Jul;34(7):26-28; https://www.alcor.org/library/reconstructive-connectomics/.

[1178] Seung S. Connectome: How the Brain's Wiring Makes Us Who We Are. Houghton Mifflin, 2012; https://www.amazon.com/dp/0547678592/. See also: https://en.wikipedia.org/wiki/Connectome.

[1179] Gigandet X, Hagmann P, Kurant M, Cammoun L, Meuli R, Thiran JP. Estimating the confidence level of white matter connections obtained with MRI tractography. PLoS One. 2008;3(12):e4006; https://www.ncbi.nlm.nih.gov/pmc/articles/PMC2603475/.

[1180] Azevedo FA, Carvalho LR, Grinberg LT, Farfel JM, Ferretti RE, Leite RE, Jacob Filho W, Lent R, Herculano-Houzel S. Equal numbers of neuronal and nonneuronal cells make the human brain an isometrically scaled-up primate brain. J Comp Neurol. 2009 Apr 10;513(5):532-41; http://www.sakkyndig.com/psykologi/artvit/frederico2009.pdf.

[1181] Martins NRB, Erlhagen W, Freitas RA Jr. Non-destructive whole-brain monitoring using nanorobots: neural electrical data rate requirements. Intl J Machine Consciousness 2012 Jun;4(1):109-140; http://citeseerx.ist.psu.edu/viewdoc/download?doi=10.1.1.962.7895&rep=rep1&type=pdf (Table 2).

[1182] Azevedo FA, Carvalho LR, Grinberg LT, Farfel JM, Ferretti RE, Leite RE, Jacob Filho W, Lent R, Herculano-Houzel S. Equal numbers of neuronal and nonneuronal cells make the human brain an isometrically scaled-up primate brain. J Comp Neurol. 2009 Apr 10;513(5):532-41; http://www.sakkyndig.com/psykologi/artvit/frederico2009.pdf. See also: von Bartheld CS, Bahney J, Herculano-Houzel S. The search for true numbers of neurons and glial cells in the human brain: A review of 150 years of cell counting. J Comp Neurol. 2016 Dec 15;524(18):3865-3895; https://www.ncbi.nlm.nih.gov/pmc/articles/PMC5063692/.

[1183] Young E. Gut instincts: The secrets of your second brain. New Scientist, 2012 Dec 15;216(2895):38-42; https://web.archive.org/web/20130504175954/http://neurosciencestuff.tumblr.com/post/38271759345/gut-instincts-the-secrets-of-your-second-brain.

[1184] Hall JE. Neural Control of Gastrointestinal Function - Enteric Nervous System. Guyton and Hall Textbook of Medical Physiology, 12th edition, Saunders Elsevier, 2011, p. 755; https://www.amazon.com/Guyton-Hall-Textbook-Medical-Physiology/dp/1416045740/.

[1185] https://en.wikipedia.org/wiki/Brain_size.

$I_{mapConnectomeB} + I_{mapConnectomeNB}$ ~ **1.2×10^{20} bits**.[1186] Alternatively, encoding just the 3D coordinates of all $n_{synap} = 2.4 \times 10^{14}$ signal-routing synapses might compress the map to as small as n_{synap} ($I_{voxelBrain} + I_{voxeltype}$) ~ 1.9×10^{16} bits, assuming one synapse per voxel.

Note that the human brain expresses ~86% of all genes encoded in the genome at some point during development[1187] and at least a third of all genes are expressed primarily in the brain (the highest of any organ) – genes that are thought to influence the development and function of the brain.[1188] If a cryopatient's genome specifies some core brain or network architecture[1189] that does not reflect environmental growth, then it might be possible to create initial crude brain maps of cryonics patients based on their genomes, or at least guided by this information.

(6) Cell Plasma Membrane Fault Map. The data provided by the 3D Submicron Tissue Map can also be used to compile a map of cell plasma membranes that can be inspected for damage. If there are $N_{braincells} \sim 200 \times 10^9$ cells in the human brain each with plasma membrane surface area of $A_{braincell} \sim 24{,}000$ μm^2,[1190] and if these have been mapped to $q_{braincell} = 100$ nm resolution yielding $n_{pixelbrain} = A_{braincell} / q_{braincell}^2 = 2{,}400{,}000$ pixels/neuron requiring $I_{pixelcell} \sim 80$ bits/pixel to describe, then the total data storage requirement for a brain cell plasma membrane map is $I_{mapbraincells} = n_{pixelbrain}\ N_{braincells}\ I_{pixelcell} \sim$ **3.8×10^{19} bits**, or $I_{mapbodycells} = I_{mapbraincells} + n_{pixelbody}\ N_{bodycells}\ I_{pixelcell} \sim$ **1.1×10^{20} bits** for a whole-body Cell Plasma Membrane Fault Map, taking $A_{bodycell} \sim 2400\ \mu m^2$/cell,[1191] $q_{bodycell} = q_{braincell} = 100$ nm, $n_{pixelbody} = A_{bodycell} / q_{bodycell}^2 = 240{,}000$ pixels/cell, and $N_{bodycells} \sim 3.5 \times 10^{12}$ tissue cells in the entire human body.[1192]

[1186] This seems like a conservative estimate, given that recording the 3D geometric positions and types of all $n_{synapse} = 2.4 \times 10^{14}$ synapses to 100 nm precision allowing $I_{synapse} = 80$ bits/synapse would require only $n_{synapse}\ I_{synapse} =$ **1.9×10^{16} bits**. However, the full model of the connectome of a *C. elegans* worm, which has only 302 neurons, required 12 terabytes (9.6×10^{13} bits) of data storage.[*] A simpleminded linear extrapolation from 302 neurons to the 86.1×10^9 neurons of the human brain might imply (9.6×10^{13} bits) (86.1×10^9 neurons) / (302 neurons) ~ **3×10^{22} bits** for the human connectome. ***Future research*** is needed to more precisely quantify the essential description of the human connectome.

[*] Achacoso TB, Fernandez V, Nguyen DC, Yamamoto WS. Computer Representation of the Synaptic Connectivity of *Caenorhabditis Elegans*. Proc Annu Symp Comput Appl Med Care. 1989 Nov 8:330-4; https://www.ncbi.nlm.nih.gov/pmc/articles/PMC2245716/pdf/procascamc00017-0327.pdf.

[1187] Kang HJ, Kawasawa YI, Cheng F, Zhu Y, Xu X, Li M, *et al*. Spatio-temporal transcriptome of the human brain. Nature 2011; 478:483-489; https://www.ncbi.nlm.nih.gov/pmc/articles/PMC3566780/.

[1188] https://www.ninds.nih.gov/Disorders/Patient-Caregiver-Education/Genes-Work-Brain#1.

[1189] Bertolero MA, Blevins AS, Baum GL, Gur RC, Gur RE, Roalf DR, Satterthwaite TD, Bassett DS. The human brain's network architecture is genetically encoded by modular pleiotropy. Eprint axXiv, 2019 May; https://arxiv.org/pdf/1905.07606.

[1190] A "typical" ~8000 μm^3 body cell with a roughly cubic shape would have an external surface area of $A_{bodycell} \sim 2400$ μm^2/cell, but ~24,000 μm^2/neuron seems more typical for the surface area of a neuronal dendritic tree. Donohue DE, Ascoli GA. A comparative computer simulation of dendritic morphology. PLoS Comput Biol. 2008 Jun 6;4(5):e1000089; http://www.ncbi.nlm.nih.gov/pmc/articles/PMC2376061/.

[1191] Freitas RA Jr., Nanomedicine, Volume I: Basic Capabilities, Landes Bioscience, Georgetown, TX, 1999, Table 8.17, "Approximate Quantification of the Components of a Typical 20-µm Human Tissue Cell"; http://www.nanomedicine.com/NMI/Tables/8.17.jpg.

[1192] Freitas RA Jr. Nanomedicine, Volume I: Basic Capabilities, Landes Bioscience, Georgetown TX, 1999, Section 8.5.1, "Cytometrics"; http://www.nanomedicine.com/NMI/8.5.1.htm#p5.

The compilation of these maps is a result of extensive analysis of the raw data. Some early neural connectome analysis[1193] software already exists (**Table 7**), but more sophisticated computational neuroscience[1194] and neuroinformatics[1195] algorithms and software packages[1196] will be needed for cryonics repair due to the possible presence of extensive damage – a suitable topic for ***future research***. For example, de Wolf and colleagues recently introduced a deep learning algorithm that distinguishes the early stages of permanent cerebral ischemia from the late stages of permanent cerebral ischemia, based on electron micrographs of the two damage states.[1197]

Fahy[1198] described the assembly of brain structure data where modest damage has occurred: "All significant extracellular anatomical elements of the brain have been registered. The 'wiring diagram' of the brain can now be deduced, and all damaged areas can be catalogued as to type and place. Where necessary, the loci of missing structures could be deduced at this point. For example, ripped bundles of axons are analyzed to deduce how to infer the pattern of connections between the two ripped ends based on the direct physical remains of the ripped axons and any other available information. The loci of missing cell membranes are deduced. Extracellular debris is assigned to appropriate destinations."

Merkle[1199] cautions that any revisions to the database that might damage the patient's memory should be avoided, but that other revisions might be safe. "One set of safe alterations would be those that correspond to real-world changes that are non-damaging. For instance, moving sub-cellular organelles within a cell would be safe – such motion occurs spontaneously in living tissue. Likewise, gently pushing aside tissue to open a small space should also be safe. Indeed, some operations that might at first appear dubious are almost certainly safe. For example, any alteration that produces damage that can be repaired by the tissue

---

[1193] Oberlaender M, Dercksen VJ, Egger R, Gensel M, Sakmann B, Hege HC. Automated three-dimensional detection and counting of neuron somata. J Neurosci Methods. 2009 May 30;180(1):147-60; http://homes.mpimf-heidelberg.mpg.de/~mhelmsta/pdf/2009%20Oberlaender%20..%20JNeurosciMeth.pdf. Kasthuri N, Hayworth KJ, Berger DR, Schalek RL, Conchello JA, Knowles-Barley S, Lee D, Vázquez-Reina A, Kaynig V, Jones TR, Roberts M, Morgan JL, Tapia JC, Seung HS, Roncal WG, Vogelstein JT, Burns R, Sussman DL, Priebe CE, Pfister H, Lichtman JW. Saturated Reconstruction of a Volume of Neocortex. Cell. 2015 Jul 30;162(3):648-61; http://seunglab.org/wp-content/uploads/2015/09/saturatedreconstruction.pdf. Berning M, Boergens KM, Helmstaedter M. SegEM: Efficient Image Analysis for High-Resolution Connectomics. Neuron. 2015 Sep 23;87(6):1193-1206; https://core.ac.uk/download/pdf/82642900.pdf. Staffler B, Berning M, Boergens KM, Gour A, Smagt PV, Helmstaedter M. SynEM, automated synapse detection for connectomics. Elife. 2017 Jul 14;6:e26414; https://www.ncbi.nlm.nih.gov/pmc/articles/PMC5658066/. Motta A, Berning M, Boergens KM, Staffler B, Beining M, Loomba S, Hennig P, Wissler H, Helmstaedter M. Dense connectomic reconstruction in layer 4 of the somatosensory cortex. Science. 2019 Nov 29;366(6469):eaay3134; https://neurophysics.ucsd.edu/courses/physics_171/eaay3134.full.pdf. "The Human Connectome Project", https://en.wikipedia.org/wiki/Human_Connectome_Project. "Connectome Coordination Facility"; http://www.humanconnectome.org/.

[1194] Bauer R. Computational Neuroscience and Cryonics: Strangers that are Just Friends Waiting to happen. Cryonics 2020 Qtr 2;41(2):9-13; https://www.alcor.org/docs/cryonics-magazine-2020-02.pdf. See also: https://www.nature.com/subjects/computational-neuroscience.

[1195] https://en.wikipedia.org/wiki/Neuroinformatics.

[1196] Breitwieser L, Hesam A, de Montigny J, Vavourakis V, Iosif A, Jennings J, Kaiser M, Manca M, Di Meglio A, Al-Ars Z, Rademakers F, Mutlu O, Bauer R. BioDynaMo: an agent-based simulation platform for scalable computational biology research. bioRxiv; 2020; https://www.biorxiv.org/content/10.1101/2020.06.08.139949v1.full.pdf.

[1197] de Wolf A, Phaedra C, Perry RM, Maire M. Ultrastructural Characterization of Prolonged Normothermic and Cold Cerebral Ischemia in the Adult Rat. Rejuvenation Res. 2020 Jun;23(3):193-206; https://pubmed.ncbi.nlm.nih.gov/31631775/.

[1198] Fahy G. Appendix B. A "Realistic" Scenario for Nanotechnological Repair of the Frozen Human Brain. In: Wowk B, Darwin M, eds., Cryonics: Reaching for Tomorrow. Alcor Life Extension Foundation, 1991, pp. A-10 – A-26; https://alcor.org/Library/html/nanotechrepair.html.

[1199] Merkle RC. Molecular Repair of the Brain. Cryonics 1989 Oct;10(10):21-44; http://www.alcor.org/cryonics/cryonics8910.txt.

itself once it is restored to a functional state is in fact safe – though we might well seek to avoid such alterations (and they do not appear necessary). While the exact range of alterations that can be safely applied to the structural data base is unclear, that a fairly wide range exists should be evident."

Maximum likelihood estimation (Section 4.8.2) may be required in critical tissue regions such as the brain where more extensive damage has occurred.

Table 7. A few representative databases and datasets containing information about neuroanatomical connections[1200]

Database	Available Connectivity Information	URL
Brain Architecture Management System (BAMS)	Projections in rodent brain, curated manually from existing literature	http://brancusi.usc.edu/bkms/
Collations of Connectivity Data on the Macaque Brain (CoCoMac)	Projections in macaque brain, curated manually from existing literature	http://www.cocomac.org
Functional Anatomy of the Cerebro–Cerebellar System (FACCS)	3D atlas of axonal tracing data in rat cerebro–cerebellar system	http://ocelot.uio.no/nesys/
BrainMaps.org	Tables of connections from literature and primary data for some tracer injections	http://brainmaps.org
BrainPathways.org	Multiscale visualization of connectivity data from collated literature reports	http://brainpathways.org
Human Brain Connectivity Database	Curated reports of connectivity studies in post-mortem human brain tissue	http://brainarchitecture.org
Internet Brain Connectivity Database	Estimated connectional data between human cortical gyral areas	http://www.cma.mgh.harvard.edu/ibcd/
Surface Management System DataBase (SumsDB)	Connection densities from macaque retrograde tracer injections mapped to surface-based atlas	http://sumsdb.wustl.edu/sums/
SynapseWeb	Reconstructed volumes and structures from serial section electron microscopy	http://synapses.clm.utexas.edu/
Neocortical Microcircuit Database	Connection data between single cells in mammalian cortex	http://microcircuit.epfl.ch/
ICBM DTI-81 Atlas	Probabilistic atlas of human white matter tracts based on diffusion tensor imaging	http://www.loni.ucla.edu/Atlases/Atlas_Detail.jsp?atlas_id=15
Anatomy Toolbox Fiber Tracts	Probabilistic atlas of human white matter tracts based on post-mortem studies	http://www.fz-juelich.de/ime/spm_anatomy_toolbox
WormAtlas	Full neuronal wiring data for *C. elegans*	http://www.wormatlas.org

[1200] Bohland JW, *et al*. A proposal for a coordinated effort for the determination of brainwide neuroanatomical connectivity in model organisms at a mesoscopic scale. PLoS Comput Biol. 2009 Mar;5(3):e1000334; http://www.ncbi.nlm.nih.gov/pmc/articles/PMC2655718/.

4.8.2 Maximum Likelihood Estimation

In regions of the cryopreserved body where damage is particularly extensive, and especially in the brain where loss of information should be maximally avoided, it may be necessary to resort to the technique of maximum likelihood estimation[1201] to obtain a tissue structure that is most likely to be the correct end target for repair – something like a form of neural archeology,[1202] deducing from surviving structures the missing structure of a vanished memory in order to restore it.

As first described by Merkle[1203] in connection with the cryonics revival process:

> "Analysis of the frozen tissue will, on a local basis, allow the recovery of what might be called Local Neuronal Structure or LNS. If the cryopreservation took place under favorable circumstances, the LNS will be substantially correct with little ambiguity, that is, we will be able to assign a single interpretation based on local information (e.g., this synapse connects this neuron to that neuron; this axon carries information from one well identified location to another well identified location, etc.). Under adverse circumstances, the LNS will become increasingly ambiguous. An axon might have one of two possible targets, which cannot be fully disambiguated based only on local information. Which axon a synapse is connected to might not be distinguishable based on the remaining local structure. This will result in a situation where the LNS will not be a single, specific neuronal structure, but will instead be a set of possible structures with initial probabilities assigned based on local information."
>
> "Consider as an example the neuronal structures that process visual information. The retina is exposed to photons which describe the visual scene. The output coming from the primary visual cortex is highly characteristic: the image has been processed and basic image elements have been isolated and identified. From our point of view, the interesting thing is that certain types of input to the retina (a spot of light, a line, a moving line, etc) produce characteristic outputs from the primary visual cortex. Given that we have knowledge derived from the frozen tissue about the LNS in the retina…and the primary visual cortex, we can then enter 'plaintext' (images on the retina) and observe the resulting 'ciphertext' (neuronal outputs from the primary visual cortex). If the 'ciphertext' is inappropriate for the 'plaintext,' we can incrementally modify the descriptions of the LNS and see if the resulting plaintext-ciphertext pairs become more or less reasonable. If the result is more reasonable, we are moving in the right direction and should continue. If the result is less reasonable we are moving in the wrong direction and should stop and try some other direction. More generally, the brain has many cortical areas connected by projections. The processing in each cortical area and the information that can pass along these projections is characteristic of the function being performed. When inappropriate responses are observed, we can incrementally change the relevant LNS in an appropriate direction (e.g., we can change the initial probability vector which describes the state of the LNS by taking a small step in the multi-dimensional hyperspace)."

[1201] https://en.wikipedia.org/wiki/Maximum_likelihood_estimation.

[1202] Donaldson T. Neural Archeology. Cryonics 1987 Feb;8(2):24-33; https://www.alcor.org/library/neural-archaeology/.

[1203] Merkle RC. Cryonics, Cryptography, and Maximum-Likelihood Estimation. Cryonics 1995 Qtr 2;16(2):13-20; https://www.alcor.org/docs/cryonics-magazine-1995-02.pdf. Merkle RC. Cryonics, Cryptography, and Maximum Likelihood Estimation. Proc 1st Extropy Inst Conf. 1994; http://www.merkle.com/cryo/cryptoCryo.html.

To successfully perform this kind of iterative analysis, our computational sophistication must be advanced enough to accurately simulate the neuroelectrical function of a particular block of neuronal tissue, knowing only the physical structure of that tissue. We must be able to correctly simulate the stimulation and transmission of neural impulses in and through the modeled tissue. Such simulations necessarily will be more computationally intense than other purely structural analyses, but nevertheless should remain tractable: (A) given the tremendous computer power and simulation expertise that will be available in a nanotechnological milieu advanced enough to permit cryostasis revivals, and (B) because this level of analysis is assumed to be needed for only a modest fraction of the tissue that is seriously damaged in any particular cryopreserved patient. (***Future research*** should seek to validate both of these assumptions.)

The maximum likelihood estimation procedure would work like this: Based on the available scan data, a trial model of a particular block of neural tissue is created. The desired ideal performance of this tissue is specified. The block's performance is simulated by providing it with any number of varied inputs and measuring the outputs. The divergence of the simulated outputs from the desired outputs is quantified. The trial model is then altered in some small degree, the simulation repeated, and the divergence measured again. If the divergence is smaller than before, the alteration to the model is deemed successful and is retained. If the divergence is larger than before, the alteration is discarded in favor of the original model. The process is repeated, slowly lowering the divergence by repeated testing of alterations to the trial model until the divergence becomes small enough to be deemed inconsequential or at least acceptable. The resulting altered model represents a maximum likelihood estimation of the desired ideal structure of the block of tissue, and this structure now becomes our target to achieve during physical repair. This estimation procedure is somewhat analogous to molecular structure energy minimizations or geometry optimizations in computational chemistry,[1204] which use a similar iterative process[1205] to arrive at the correct structure.[1206]

How can we be sure that the required computations will not prove intractable? According to Tad Hogg,[1207] "there is no reason to expect the enormous number of possible arrangements [of imperfectly cryopreserved neural structures] will in fact require infeasibly enormous computations. Instead, much of the difficulty is likely to be in properly formulating, rather than solving, the computational problem. This formulation requires learning the details of what arrangements constitute adequate repairs and the nature of the damage process….For repair, [combinatorial] heuristics are likely to be more relevant since the goal is to find any one of the 'solutions', i.e., arrangements that correspond to adequate restoration, rather than necessarily the single one that is in some sense 'best'. Particularly useful in this context are methods, such as heuristic repair,[1208] simulated annealing,[1209] and genetic algorithms,[1210] that rely on making a relatively small number of adjustments to an initial guess based on evaluating a few possible changes at a time. These

---

[1204] https://en.wikipedia.org/wiki/Energy_minimization.
[1205] https://en.wikipedia.org/wiki/Maximum_likelihood_estimation#Iterative_procedures.

[1206] Well-known techniques for finding "global minimums" while avoiding getting trapped in "local minimums" and other related methods in computational chemistry (e.g., gradients, simulated annealing) might also be useful in the cryonics revival context.

[1207] Hogg T. Letters to the Editor. Cryonics 1994 Qtr 4;15(4):3-4; https://www.alcor.org/docs/cryonics-magazine-1994-04.pdf.

[1208] Minton S, Johnston MD, Philips AB, Laird P. Minimizing Conflicts: A Heuristic Repair Method for Constraint Satisfaction and Scheduling Problems. Artificial Intelligence 1992 Dec;58(1-3):161-205; https://core.ac.uk/download/pdf/208171735.pdf.

[1209] Kirkpatrick S, Gelatt CD Jr, Vecchi MP. Optimization by simulated annealing. Science. 1983 May 13;220(4598):671-80; http://www.stat.duke.edu/~scs/Courses/Stat376/Papers/TemperAnneal/KirkpatrickAnnealScience1983.pdf.

[1210] Forrest S. Genetic algorithms: principles of natural selection applied to computation. Science. 1993 Aug 13;261(5123):872-8; https://pubmed.ncbi.nlm.nih.gov/8346439/.

often succeed within quite reasonable computational costs when one can start with an initial guess that is already fairly close to a solution and one has a reasonably accurate way to evaluate whether the individual changes are likely to be closer or further from a solution. If the initial guess (as provided by the tissue structure) is not sufficiently close, more global information can be used for this evaluation in locally ambiguous cases, [for example by using] the maximum likelihood estimation technique."

Elsewhere,[1211] Hogg notes: "Many studies of constraint satisfaction problems have demonstrated, both empirically and theoretically, that easily computed structural parameters of these problems can predict, on average, how hard the problems are to solve by a variety of search methods. A major result of this work is that hard instances of NP-complete problems are concentrated near an abrupt transition between under- and over-constrained problems. This transition is analogous to phase transitions seen in some physical systems." Responds Merkle:[1212] "An interpretation of this statement in the context of cryonics would be that the computational problems of determining the healthy state of a frozen structure are likely to remain tractable until the damage approaches the point where actual information-theoretic loss [Section 2.1.1] is sustained. As this transition is approached, computational tractability will rapidly deteriorate. Beyond this point, finding a solution consistent with the available data will again become easy because there are many possible solutions (and many differing people) whose brain structure would be consistent with the remaining frozen tissue. When all information is lost, any brain structure at all would be consistent with the frozen remains and the 'search problem' would become entirely trivial (and of debatable value)."

The creation of efficient maximum likelihood estimation algorithms, techniques, and software applicable to the problem of revival from cryopreservation is a suitable topic for ***future research***.

Using maximum likelihood to improve vasculoid-based mapping. In a recent personal communication,[1213] Tad Hogg pointed out that an under-appreciated aspect of maximum likelihood estimation (MLE) is that it doesn't just produce parameters giving the best value, but it also gives an indication of errors in those estimates. Locally, the "error bars" on the estimated parameters come from the curvature of the likelihood function at the maximum. This not only gives error bars for each parameter individually but also gives the correlations among parameter errors. (The likelihood may be thought of as a ridge at some angle in a high-dimensional space of the parameters). Globally, one could check for other maxima (e.g., 2nd and 3rd largest values), and if these are orders of magnitude smaller than the maximum, the maximum is likely the correct reconstruction. (If the other maxima are similar, then there's ambiguity among several different reconstructions.)

Hogg observes that the reconstruction algorithm could use this error information to decide among variations in the revival process. Sensors in the vasculoid could spend days or weeks collecting data to improve signal-to-noise, if necessary. Since this map won't be as detailed as the molecular scan, reconstruction that just uses this "vasculoid scan" will lean more on the inference capabilities of the reconstruction algorithm (Plan A) than Plan B will probably need. The error estimates that MLE provides could be used in a variation on Plan B by inserting a computational step after the vasculoid map wherein

---

[1211] Hogg T. Phase Transitions in Search. Xerox/PARC Dynamics of Computation Group, 5 Aug 1997; https://web.archive.org/web/19990221080420/http://www.parc.xerox.com/spl/groups/dynamics/www/constraints.html. See also: Williams CP, Hogg T. Using deep structure to locate hard problems. Proc 10th Natl Conf on Artif Intelligence (AAAI92), 1992 Jul, pp. 472-477; https://citeseerx.ist.psu.edu/viewdoc/download?doi=10.1.1.40.6465&rep=rep1&type=pdf. Hogg T. Statistical Mechanics of Combinatorial Search. Proc of the Workshop on Physics and Computation (PhysComp94); http://citeseerx.ist.psu.edu/images/pdf_icon.png;jsessionid=40E9B6AEA6D880C07151B96545C92C88.

[1212] Merkle RC. Algorithmic Feasibility of Molecular Repair of the Brain. Cryonics 1995 Qtr 1;16(1):15-16; https://www.alcor.org/docs/cryonics-magazine-1995-01.pdf.

[1213] Personal communication from Tad Hogg to Robert Freitas, 21 Aug 2021.

we compute how well that coarse map allows reconstruction. For structures where that's good enough, the molecular scan becomes unnecessary.

Otherwise, before going to the molecular scan, the revival process could trace the highly uncertain parameters back to the data that is most relevant for determining their values, indicating where to focus for additional information. Perhaps only a few cubic millimeters at specific locations in the brain contribute to most of the uncertainty in the estimates. The revival procedure could return to those areas to collect more information using the vasculoid by extending the sensing time or by sending specialized sensors to those locations. Given the extra cost and time for molecular scan, spending a bit more effort with the vasculoid could make sense.

The error estimates from the MLE might not only say where to get more information but also which type of information would be most useful to reduce the uncertainty. This could exploit the identified correlations among different parameters included in the MLE error estimates. It may be easier to improve information on parameters other than the high-error parameter, and then use correlations from the more-easily measured parameters to improve the high-error parameter indirectly. Molecular scan could be used when even extra information from the vasculoid is not enough.

Unlike the default "get information → compute → repair" sequential procedure of Plan A and B, we would have an iterative process in which the algorithm first evaluates the vasculoid scan, decides where and what additional information it needs (if any), then repeats the scan until it either (1) has enough information for a high confidence inference, or (2) decides that it needs more resolution than the vasculoid can provide. If there's a lot of variation in the amount of damage in different parts of the body, the molecular scan may only be needed in a small portion of the body. Having a "first pass" reconstruction based on the vasculoid map would also serve as a partial backup in case something goes wrong with the molecular scan, and limiting any destructive scans to just the locations that really need it for the reconstruction algorithm would reduce the amount of destruction.

Adequate inference from vasculoid scanning seems very likely for the body, but is this good enough for brain repair? Notes Hogg: "Given our limited understanding of how identity is stored, and how redundantly, it seems at least plausible that a vasculoid scan could give enough information for reconstruction, especially when combined with prior information about the person and what we will learn about memory storage from research-class nanorobots." If so, then this less-destructive but more computationally intensive form of vasculoid mapping could drastically reduce how much of body structure requires molecular scan – allowing repair mostly using Plan A and only applying Plan B to parts of the body with too much damage for reconstruction from the vasculoid map alone.

Hogg continues: "In practice, the inference for the repair algorithm will use prior information for a Bayesian inference.[1214] So instead of maximizing the likelihood (i.e., maximum likelihood), it would aim to maximize the posterior probability (i.e., the product of likelihood and prior). The prior reduces the amount of overfitting or 'fitting to noise' that may occur using just the likelihood. If there's little damage, I expect the likelihood will be narrowly peaked and so MAP [maximum *a posteriori*] and ML [maximum likelihood] estimates will be nearly the same. On the other hand, for places with extensive damage, ML may have wide or multiple peaks of similar size. In that case, the prior may be the main factor to identify the best reconstruction. Such priors could come from high-resolution biology research on what tissue should look like, and will likely rapidly improve in the process of revivals, e.g., starting from less damaged people. More generally, Bayesian inference can combine MAP with a penalty evaluation of the consequences of wrong decisions (e.g., missing a minor memory of what you recently had for breakfast vs. more identity-significant ones). This is how the algorithm could incorporate prior information (both from

[1214] https://en.wikipedia.org/wiki/Bayesian_inference.

research on generic tissue structure and in specific cases, e.g., via WBE or memory tests [such as] 'do you remember this photo from your childhood?')."

4.8.3 Creating Computational Models to Direct Repairs

By the time the first cryonics revivals are attempted, databases should exist that contain high-resolution scans of actual human brains and bodies representing a variety of genders, races, nationalities, ages, and states of health, including computerized "typical", "consensus", "standard", or "generic" human models based upon actual scan data. Early precursors of such databases already exist,[1215] although in 2020 one leading practitioner of computational neuroscience glumly observed that "the usage of computational tools in cryopreservation (what one might call 'computational cryopreservation') has not advanced much since the 1970s".[1216] If the necessary detailed databases do not exist, then ***future research*** projects should be undertaken to create them.

The computational reconstruction process begins with selecting an appropriate baseline whole-body model that best matches the cryopreserved patient's evident physical characteristics. If none exists, then the process should start with a "standard" body model. This might include a subcellular-resolution whole-body model requiring $I_{mapBody} \sim 5.4 \times 10^{21}$ bits of storage, combined with a 1-nm resolution geometrical map of all arteriovenous ($A_{arteriovenous} = 312.9\ m^2$)[1217] and lymphatic ($A_{lymphovascular} = 248.6\ m^2$; Section 4.6.4) vascular surfaces consisting of $n_{pixelGeomModel} = (A_{arteriovenous} + A_{lymphovascular}) / q_{resol}^2 = 5.62 \times 10^{20}$ pixels for $q_{resol}^2 = 1\ nm^2$ pixels requiring $I_{mapVascModel} = n_{pixelGeomModel}\ (I_{voxelBody} + I_{voxeltype}) \sim 5.1 \times 10^{22}$ bits of storage, for a total of $I_{StdBodyModel} = I_{mapBody} + I_{mapVascModel} \sim$ **5.6×10^{22} bits** of data storage for the baseline whole-body model.

Next, a composite cryopreserved whole-body model is assembled using the data from each of the six maps previously compiled (Section 4.8.1), comprising $I_{mapCryo} \sim 1.5 \times 10^{23}$ bits as previously described. The tissue reconstruction software then computationally performs the sequence of repair operations as described in Section 4.9 (crackface fusions with fracture void closings), Section 4.11 (resealing membrane compartments, including damaged vascular compartments and damaged cell membranes, and rehydration), and Section 4.12 (detailed cell repair), simulating the effects of each repair procedure on the cryopreserved whole-body model and updating the model after each incremental repair is completed. Note that the model must properly incorporate the mechanical and hydrodynamic properties of tissues at various temperatures between 77 K (-196 °C) and 273 K (0 °C), but biochemical and bioelectric tissue properties can be largely ignored in these simulations as the tissue will be quickly rendered biochemically inactive upon thawing (Section 4.10). It's probably also unnecessary to model and simulate in detail the workings of billions of individual nanorobots as they go about their tasks. Only the effects of nanorobot reparative activities need

---

[1215] Human Cell Atlas; https://www.humancellatlas.org/. Horwitz R, Johnson GT. Whole cell maps chart a course for 21st-century cell biology. Science. 2017 May 26;356(6340):806-807; https://files.gitter.im/embryo-digital-atlas/Lobby/wLSl/whole_cell_maps.pdf. Allen Brain Atlas; https://portal.brain-map.org/. Chandran KB, Udaykumar HS, Reinhardt JM, eds. Image-Based Computational Modeling of the Human Circulatory and Pulmonary Systems: Methods and Applications. Springer, 2011. Visible Human Project; https://en.wikipedia.org/wiki/Visible_Human_Project. Visualizing Anatomy; https://blog.wolfram.com/2017/03/10/visualizing-anatomy/. Hester RL, Brown AJ, Husband L, Iliescu R, Pruett D, Summers R, Coleman TG. HumMod: A Modeling Environment for the Simulation of Integrative Human Physiology. Front Physiol. 2011 Apr 13;2:12; https://www.ncbi.nlm.nih.gov/pmc/articles/PMC3082131/.

[1216] Bauer R. Computational neuroscience and cryonics: Strangers that are just friends waiting to happen. Cryonics 2020 Qtr 2;41(2):9-13; https://alcor.org/cryonics/Cryonics2020-2.pdf.

[1217] Freitas RA Jr. Nanomedicine, Volume I: Basic Capabilities, Landes Bioscience, Georgetown, TX, 1999; Table 8.1, "Approximate Quantification of the Human Arteriovenous System"; http://www.nanomedicine.com/NMI/Tables/8.1.jpg

be modeled and simulated as long as: (A) the reparative activities are clearly within the operational capability of the repair nanorobots envisioned for use; and (B) sufficient physical space is allocated in the computational model to allow for nanorobot access to all tissues to be repaired.

Correctly modeling the brain is the most critical task if memory and personality are to be preserved. As noted elsewhere,[1218] software to automate the construction of a cytoarchitectural brain map can be developed to process data supplied from previous nanorobot brain scans. The computational problem is crudely analogous to the problem domain of jigsaw puzzles, which has already been applied to fields as diverse as biology,[1219] chemistry,[1220] literature,[1221] archeology,[1222] reconstruction of historical statues (e.g., a billion-polygon model),[1223] speech descrambling,[1224] cryptography,[1225] image editing,[1226] and the recovery of shredded documents or photographs.[1227] Numerous automated jigsaw puzzle assembly

---

[1218] Freitas RA Jr. The Alzheimer Protocols: A Nanorobotic Cure for Alzheimer's Disease and Related Neurodegenerative Conditions. IMM Report No. 48, June 2016, 433 pp; Section 5.3.1 "Brain Mapping and Neural Repair Plan"; http://www.imm.org/Reports/rep048.pdf.

[1219] Marande W, Burger G. Mitochondrial DNA as a genomic jigsaw puzzle. Science. 2007 Oct 19;318(5849):415; http://3dinformatics.com/genome_in_pieces3.pdf.

[1220] Wang C-SE. Determining molecular conformation from distance or density data . PhD thesis, Massachusetts Institute of Technology, Dept. of Electrical Engineering and Computer Science, 2000; http://dspace.mit.edu/bitstream/handle/1721.1/16736/45147791.pdf?sequence=1&origin=publication_detail

[1221] Morton AQ, Levison M. The computer in literary studies. IFIP Congress (2), 1968:1072-81.

[1222] Leitao HCG, Stolfi J. Automatic reassembly of irregular fragments. Tech. Report IC-98-06, Univ. of Campinas, 1998; http://citeseerx.ist.psu.edu/viewdoc/download?doi=10.1.1.37.6671&rep=rep1&type=pdf. Leitao HCG. Information Contents of Fracture Lines. Tech. Report, Univ. of Campinas, 1999; https://dspace.zcu.cz/bitstream/handle/11025/15481/Leitao.pdf?sequence=1. Levoy M. Digital Forma Urbis Romae Project, 2015; http://www.graphics.stanford.edu/projects/forma-urbis. Koller D, Levoy M. Computer-aided reconstruction and new matches in the forma urbis romae. Bullettino Della Commissione Archeologica Comunale di Roma, 2006:103-125; http://graphics.stanford.edu/papers/forma-bullcom/forma-bullcom-text.pdf. Brown B, Toler-Franklin C, Nehab D, Burns M, Dobkin D, Vlachopoulos A, Doumas C, Rusinkiewicz S, Weyrich T. A system for high-volume acquisition and matching of fresco fragments: Reassembling Theran wall paintings. ACM Transactions on Graphics 2008;27(3):84; http://dl.acm.org/citation.cfm?id=1360683.

[1223] Levoy M. The Digital Michelangelo Project, 2015; http://www.graphics.stanford.edu/projects/mich/.

[1224] Zhao Y, Su M, Chou Z, Lee J. A puzzle solver and its application in speech descrambling. WSEAS Int.Conf. Comput Eng Appl, 2007:171-176; http://citeseerx.ist.psu.edu/viewdoc/download?doi=10.1.1.499.356&rep=rep1&type=pdf.

[1225] Farn EJ, Chen CC. Novel steganographic method based on jig swap puzzle images. J Electronic Imaging. 2009 Jan-Mar;18(1):013003; http://citeseerx.ist.psu.edu/viewdoc/download?doi=10.1.1.154.9766&rep=rep1&type=pdf.

[1226] Cho TS, Butman M, Avidan S, Freeman WT. The patch transform and its applications to image editing. IEEE Conference on Computer Vision and Pattern Recognition, 2008:1-8; http://people.csail.mit.edu/billf/papers/CVPRPatch.pdf.

[1227] Justino E, Oliveira LS, Freitas C. Reconstructing shredded documents through feature matching. Forensic Sci Int. 2006 Jul 13;160(2-3):140-7; http://citeseerx.ist.psu.edu/viewdoc/download?doi=10.1.1.90.2640&rep=rep1&type=pdf. Zhu L, Zhou Z, Hu D. Globally consistent reconstruction of ripped-up documents. IEEE Trans Pattern Anal Mach Intell. 2008 Jan;30(1):1-13; http://www.ncbi.nlm.nih.gov/pubmed/18000320. Marques MAO, Freitas COA. Reconstructing strip-shredded documents using color as feature matching. ACM Symp Appl Comput. 2009:893-894. Cao S, Liu H, Yan S. Automated assembly of shredded pieces from multiple photos. IEEE Int. Conf. Multimedia Expo 2010:358-363; http://ieeexplore.ieee.org/xpl/articleDetails.jsp?tp=&arnumber=5582544. Deever A, Gallagher A. Semi-automatic assembly of real cross-cut shredded documents. ICIP 2012:233-236; http://citeseerx.ist.psu.edu/viewdoc/download?doi=10.1.1.362.7366&rep=rep1&type=pdf. Gallagher A. Jigsaw puzzles with pieces of unknown orientation. IEEE Conf Comput Vision Pattern Recog 2012:382-389; http://citeseerx.ist.psu.edu/viewdoc/download?doi=10.1.1.405.927&rep=rep1&type=pdf. DARPA Shredder Challenge 2011; https://en.wikipedia.org/wiki/DARPA_Shredder_Challenge_2011.

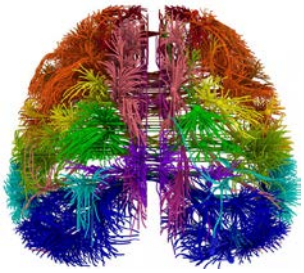

algorithms have been published,[1228] including one package that can assemble 10,000 pieces using software that is "fully automatic, requires no manually provided hints, operates on puzzles having thousands of pieces, and does so with near perfect performance."[1229] More recently, another package that uses a genetic algorithm has solved a 22,834-piece puzzle in only 13.2 hr of runtime on a single modern PC and allegedly could solve "more difficult variations of the jigsaw problem, including unknown piece orientation, missing and excessive puzzle pieces, unknown puzzle dimensions, and three-dimensional puzzles."[1230] The possible application of automated puzzle-solving to 3D images and models of cryopreserved neural tissue in particular, and to cryonics revival in general, should be explored in ***future research***.

Construction of a cytoarchitectural brain map also has conceptual similarities to the reverse engineering of machines[1231] and to the growing field of computer-aided reverse engineering.[1232] A whole-brain cellular-level wiring diagram for the mouse brain has been published (image above, left),[1233] and algorithms for automated neuronal arbor analysis[1234] and neuron classification[1235] are available, including a gamified

---

[1228] Kosiba DA, Devaux PM, Balasubramanian S, Kasturi R. An automatic jigsaw puzzle solver. Proc. 12th Int. Conf. Pattern Recognition, Vol. 1,1994:616-618; http://citeseerx.ist.psu.edu/viewdoc/download?doi=10.1.1.344.1536&rep=rep1&type=pdf. Goldberg D, Malon C, Bern M. A global approach to automatic solution of jigsaw puzzles. Proc 18th Ann Symp Comput Geom ACM, 2002 Jun 5;82-87; http://www.parc.com/content/attachments/global_approach_automatic_4365_parc.pdf. Cho TS, Avidan S, Freeman WT. A probabilistic image jigsaw puzzle solver. Proc. 2010 IEEE CVPR, 2010; http://people.csail.mit.edu/taegsang/Documents/JigsawSolver.pdf. Pomeranz D, Shemesh M, Ben-Shahar O. A fully automated greedy square jigsaw puzzle solver. IEEE Conference on Computer Vision and Pattern Recognition, 2011:9-16; http://citeseerx.ist.psu.edu/viewdoc/download?doi=10.1.1.298.3227&rep=rep1&type=pdf. Paikin G, Tal A. Solving multiple square jigsaw puzzles with missing pieces. Proc. IEEE Conf Comput Vision Pattern Recog. 2015:4832-4839; http://webee.technion.ac.il/~ayellet/Ps/15-PT.pdf.

[1229] Gallagher A. Jigsaw puzzles with pieces of unknown orientation. IEEE Conf Comput Vision Pattern Recog 2012:382-389; http://citeseerx.ist.psu.edu/viewdoc/download?doi=10.1.1.405.927&rep=rep1&type=pdf. "Computational Jigsaw Puzzle Solving," Interdisciplinary Computational Vision laboratory, 2012; http://www.cs.bgu.ac.il/~icvl/icvl_projects/automatic-jigsaw-puzzle-solving/.

[1230] Sholomon D, David O, Netanyahu NS. A Genetic Algorithm-Based Solver for Very Large Jigsaw Puzzles. 2013 IEEE Conf. Comp. Vision Pattern Recog. 2013 Jun:1767-1774; http://www.cv-foundation.org/openaccess/content_cvpr_2013/papers/Sholomon_A_Genetic_Algorithm-Based_2013_CVPR_paper.pdf, https://www.aaai.org/ocs/index.php/AAAI/AAAI14/paper/viewFile/8650/8638, and http://www.genetic-programming.org/hc2014/Sh-Paper.pdf.

[1231] Varady T, Martin R, Cox J. Reverse engineering of geometric models–an introduction. Computer-Aided Design 1997;29(4):255–268; http://ralph.cs.cf.ac.uk/papers/Geometry/RE.pdf. "The Rise of Reverse Engineering," ASME, Feb 2012; https://www.asme.org/engineering-topics/articles/modeling-computational-methods/the-rise-of-reverse-engineering. Kumar A, Jain PK, Pathak PM. Reverse engineering in product manufacturing: an overview. DAAAM International Scientific Book 2013, pp. 665-678; http://www.daaam.info/Downloads/Pdfs/science_books_pdfs/2013/Sc_Book_2013-039.pdf.

[1232] Sarfraz M. Computer-aided reverse engineering using evolutionary heuristics on NURBS. Chapter 14 in: Interactive Curve Modeling, Springer, 2008:297-330; http://link.springer.com/chapter/10.1007%2F978-1-84628-871-5_14#page-1. Oancea G, Ivan NV, Pescaru R. Computer aided reverse engineering system used for customized products. Acad J Manuf Eng 2013;11(4):p30-35; http://www.auif.utcluj.ro/images/v11_4/6-Oancea%20Gh.pdf.

[1233] Oh SW, *et al.* A mesoscale connectome of the mouse brain. Nature. 2014 Apr 10;508(7495):207-14; https://www.ncbi.nlm.nih.gov/pmc/articles/PMC5102064/. Image: Allen Institute for Brain Science.

[1234] Sümbül U, Zlateski A, Vishwanathan A, Masland RH, Seung HS. Automated computation of arbor densities: a step toward identifying neuronal cell types. Front Neuroanat. 2014 Nov 25;8:139; http://journal.frontiersin.org/article/10.3389/fnana.2014.00139/full.

version called EyeWire that elicits help from human volunteers in tracing neuron connectivity.[1236] Far more sophisticated techniques will exist in the era of cryostasis revivals, though it is plausible to presume that cryonics-targeted ***future research*** in this area could greatly hasten the arrival of such techniques and ensure their existence when needed.

Detailed whole-cell modeling[1237] will also be required to support cryostasis revivals. The first computational structural model of an entire cell at macromolecular detail was published in early 2022,[1238] intended to serve as "a worked example of how a whole cell structural model can be constructed with the current state of knowledge and current technologies". The image below shows one view of the modeled cell of the small bacterium *Mycoplasma genitalium*. All molecular "ingredients" are defined by existing experimental data and individually modeled, then assembled into the complete cell. "During construction, a coarse-grain representation is used, and each ingredient is comprised of a collection of beads of 17 Å radius. During optimization, each ingredient (molecule or molecular assembly) is treated as a rigid body. Atomic models are then generated by overlaying the original atomic models of the ingredients onto this coarse-grain model."

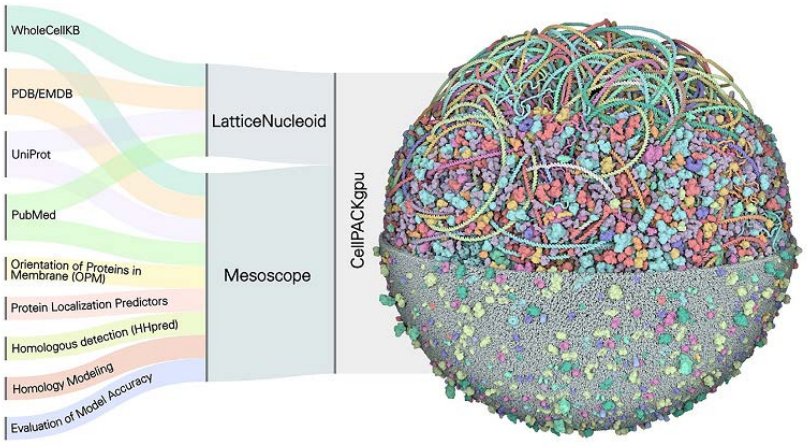

4.8.4 Computational Requirements for Repair Simulations

The minimum computational requirements for repair simulations might be as follows:

* If the **crackface fusion repairs** described in Section 4.9 are computationally performed upon all fractures simultaneously, then closing each crackface in $x_{closefrac}$ ~ 1 μm increments over a typical fracture length of $L_{fracture}$ ~ 1 mm (Section 3.4.3), and allowing $n_{compcycle}$ = 100 computational cycles for each

---

[1235] Sümbül U, Song S, McCulloch K, Becker M, Lin B, Sanes JR, Masland RH, Seung HS. A genetic and computational approach to structurally classify neuronal types. Nat Commun. 2014 Mar 24;5:3512; http://www.nature.com/ncomms/2014/140324/ncomms4512/pdf/ncomms4512.pdf.

[1236] https://en.wikipedia.org/wiki/EyeWire.

[1237] Tomita M. Whole-cell simulation: a grand challenge of the 21st century. Trends Biotechnol. 2001 Jun;19(6):205-10; http://fizz.cmp.uea.ac.uk/Research/ivis/papers/tomita01wholecell.pdf. Goldberg AP, Szigeti B, Chew YH, Sekar JA, Roth YD, Karr JR. Emerging whole-cell modeling principles and methods. Curr Opin Biotechnol. 2018 Jun;51:97-102; https://www.ncbi.nlm.nih.gov/pmc/articles/pmid/29275251/.

[1238] Maritan M, Autin L, Karr J, Covert MW, Olson AJ, Goodsell DS. Building Structural Models of a Whole Mycoplasma Cell. J Mol Biol. 2022 Jan 30;434(2):167351; https://www.sciencedirect.com/science/article/abs/pii/S002228362100588X.

positional increment, requires $n_{increment} = L_{fracture} / x_{closefrac} \sim 1000$ iterations[1239] or updates of the $I_{mapCryo} \sim 1.5 \times 10^{23}$ bit composite cryopreserved whole-body model, which in turn requires at least $Z_{crackfusion} \sim n_{compcycle}\ n_{increment}\ I_{mapCryo} = 1.5 \times 10^{28}$ bits of computation. Note that many smaller simulations of alternative reparative operations in numerous local areas may need to be tested via simulation prior to updating the entire model at the end of each iteration, but the data processing requirements for these smaller runs should be modest in comparison to the whole-model simulation iterations.

* The whole-body vascular fault map (Section 4.5.6) requires $I_{mapVascfault} \sim 1 \times 10^{21}$ bits to describe, so performing **vascular repairs** (Section 4.11) in $n_{increment} \sim 1000$ iterations requires at least $Z_{vascrepair} \sim n_{compcycle}\ n_{increment}\ I_{mapVascfault} = 1 \times 10^{26}$ bits of computation for the whole-body map. The record of these simulations is the first draft of a vascular repair plan.

* Performing $n_{increment} \sim 1000$ iterations involving **plasma membrane repairs** (Section 4.11) on all cells in the whole body with $N_{bodycells} \sim 3.5 \times 10^{12}$ tissue cells and a whole-body cell plasma membrane map of $I_{mapbodycells} \sim 6.7 \times 10^{19}$ bits requires at least $Z_{plasmamembranerepair} \sim n_{compcycle}\ n_{increment}\ I_{mapbodycells} = 6.7 \times 10^{24}$ bits of computation.

* The **rehydration and detailed cell repairs** (Section 4.12) will be conducted on all tissues (both cellular and acellular) in the body whose physical structure can be described in a map with $I_{mapcellrepair} \sim I_{mapBody} \sim 5.4 \times 10^{21}$ bits, requiring at least $Z_{cellrepair} \sim n_{compcycle}\ n_{increment}\ I_{mapcellrepair} = 5.4 \times 10^{26}$ bits of computation assuming $n_{increment} \sim 1000$ computational repair iterations.

Hence the computation required to simulate all whole-body repairs is on the order of $Z_{SimBodyrepair} = Z_{crackfusion} + Z_{vascrepair} + Z_{plasmamembranerepair} + Z_{cellrepair} \sim 1.6 \times 10^{28}$ bits of computation, driven principally by the crackface fusion repair computational budget.

The various reparative steps that are simulated (and proven successful) and incorporated into the iterated composite whole-body model during "computational repair" are recorded and compiled into a rational sequence of prioritized operations for which nanorobots can be programmed and tasked to perform in the cryopreserved patient, collectively constituting the repair plan.

Comparison of the resulting "computationally-repaired" patient to the baseline whole-body model of the patient should reveal no unacceptable gaps or anomalies between the two structures. The two structures will not be identical in their cellular and synaptic details, but they should be similar enough to confirm that the computationally-repaired model describes a healthy and fully functional human brain and body. Creation of these brain and body models, the metrics to be used for comparison of similarity, the standards of success to be applied, the design of the simulation algorithms to be employed, and the precise data storage and computational requirements for executing those algorithms are all proper subjects for ***future research***.

[1239] Physically moving tissue in 1 μm increments seems like a reasonably conservative assumption. The assumption of 100 computational cycles per iteration for each 1 μm movement also seems reasonable, based on the typical requirements for computational convergence when computing minimum energy optimizations of small molecular structures using quantum chemistry simulation packages such as Gaussian. Using 10 computational cycles to iterate each 100 nm of movement (the assumed scan resolution limit) might also be reasonable. However, these are at best poorly-supported assumptions, and ***future research*** is needed to more precisely define the computational processes to be employed in these simulations (e.g., molecular dynamics, continuum models, etc.) and to more accurately estimate the required computational effort.

4.8.5 Data Storage and Computational Processing Requirements

The above estimates suggest that whole-body repair computations will require at least $I_{StdBodyModel} \sim 5.6 \times 10^{22}$ bits of data storage (Section 4.8.3) for the baseline whole-body model and $I_{mapCryo} \sim 1.5 \times 10^{23}$ bits of data storage (Section 4.8.3) for the composite cryopreserved whole-body model that is iterated, a total of $I_{Body} \sim 2.1 \times 10^{23}$ bits of data storage for whole-body repair computations. We will also require at least $Z_{SimBodyrepair} \sim 1.6 \times 10^{28}$ bits of computation (Section 4.8.4) to perform the whole-body repair simulations, or $Z_{comp} \sim 1 \times 10^{30}$ bits of floating-point computation assuming one 64-bit word is required to support each bit of repair model computation.

By the time the first cryonics revivals are attempted, such storage and computational capabilities will be readily and commonly available. According to classical descriptions of high-density nanocomputing,[1240] a 3D array of diamondoid register rods can achieve a storage density of $i_{nano} = 10^7$ bits/μm^3 with a $t_{nano} = 10^{10}$ bit/sec data access speed, and a specific processing power of $U_{nano} \sim 10^{30}$ bit/sec-m^3.[1241] Hence the entire $I_{Body} \sim 2.1 \times 10^{23}$ bit data cache can be stored in a nanocomputer memory unit of volume $V_{nanomemory} \sim I_{Body} / i_{nano} =$ **21,000 cm^3** (21 L); if there are $c_{lines} = 10^{10}$ independent parallel input/output lines into the memory unit, the entire data cache can be read or written in $t_{read/write} \sim I_{Body} / c_{lines}\ t_{nano} =$ **2100 sec** (~0.6 hours), requiring $t_{revivalcalc} \sim (n_{increment}\ t_{read/write}) \sim 600$ hours (~**25 days**) for $n_{increment} \sim 1000$ iterations to complete the simulations. Processing $Z_{comp} \sim 1 \times 10^{30}$ bits in $t_{read/write} \sim 2100$ sec (~0.6 hours) would require $V_{nanocomp} \sim Z_{comp} / (t_{read/write}\ U_{nano}) \sim$ **500 cm^3** (0.5 L) of diamondoid mechanical nanocomputers.

A mechanical computing system[1242] that could make full use of reversible computing and is built using the kind of mature nanotechnology that will be required to execute other aspects of a cryonics revival should be able to achieve ~10^{12} GFLOPS/watt or ~10^{-21} J/bit assuming erasure of one bit for every logical operation.[1243] This is very close to the experimentally-confirmed[1244] classical Landauer limit[1245] for non-

---

[1240] Drexler KE. Nanosystems: Molecular Machinery, Manufacturing, and Computation, John Wiley & Sons, New York, 1992, Chapter 12 "Nanomechanical Computational Systems"; https://www.amazon.com/dp/0471575186/. Freitas RA Jr. Nanomedicine, Volume I: Basic Capabilities, Landes Bioscience, Georgetown TX, 1999, Section 10.2.1, "Nanomechanical Computers"; http://www.nanomedicine.com/NMI/10.2.1.htm.

[1241] Assuming 1 GHz operation of a (400 nm)^3 CPU,* and using 64-bit words: (64 bits/operation) (10^9 operations/sec) / (400 nm)^3 = 1 x 10^{30} bits/sec-m^3.
* Drexler KE. Nanosystems: Molecular Machinery, Manufacturing, and Computation, John Wiley & Sons, New York, 1992, Chapter 12 "Nanomechanical Computational Systems"; https://www.amazon.com/dp/0471575186/.

[1242] Merkle RC, Freitas RA Jr, Hogg T, Moore TE, Moses MS, Ryley J. Molecular mechanical computing systems. IMM Report No 46, Apr 2016; http://www.imm.org/Reports/rep046.pdf. Merkle RC, Freitas RA Jr, Hogg T, Moore TE, Moses MS, Ryley J. Mechanical computing systems using only links and rotary joints. J Mechanisms Robotics 2018 Dec;10(6):061006; https://arxiv.org/pdf/1801.03534.pdf.

[1243] Tad Hogg notes that the erasure of one bit per logical operation is a design choice that reversible computers allow but don't require – you can throw away energy unnecessarily, but don't have to, in contrast to irreversible logic. You could instead choose to use logically reversible gates, thereby avoiding the energy of one bit erased for every operation. This could substantially reduce the energy for the computation, provided the design doesn't throw away possibly recoverable energy from going over potential energy barriers. For example, in nanomechanical computers we can arrange for neighboring gates to have offsets so that while one gate is going down into a potential well, this energy pushes another gate up, analogous to using counterweights in elevators rather than dissipating all the potential energy of an elevator as it descends. This makes a more complex nanocomputer design but such designs should be available, if desired, by the time revivals are attempted. There appears to be considerable leeway in trading off computer energy use (and associated cost) with the time required for the computation, with the greatest benefit from reversible gates coming from running them slowly.

[1244] Bérut A, Arakelyan A, Petrosyan A, Ciliberto S, Dillenschneider R, Lutz E. Experimental verification of Landauer's principle linking information and thermodynamics. Nature. 2012 Mar 7;483(7388):187-189; https://www.nature.com/articles/nature10872.

reversible computational energy dissipation of $E_{Landauer77K} \sim k_B T \ln(2)$ J/bit = 7.4 x 10^{-22} J/bit using an LN2-cooled nanocomputer at T = 77 K (-196 °C), taking Boltzmann's constant k_B = 1.38 x 10^{-23} J/K. LN2-temperature computation would imply a continuous power draw of $P_{comp} \sim Z_{comp} E_{Landauer77K} / t_{read/write} \sim$ 0.352 MW, costing ~$36/hr for electricity at today's typical commercial rate of ~$0.10/KW-hr ($e_\$$ ~ 2.78 x 10^{-8} $/J; Appendix G) and a total electricity cost of ($e_\$ t_{revivalcalc} P_{comp}$) ~ $21,000 to complete these calculations for a single whole-body revival.[1246]

The possible utility of quantum computers[1247] for performing the many calculations required for cryostasis revival should be investigated in ***future research***.

[1245] Landauer R. Irreversibility and heat generation in the computing process. IBM J Res Devel. 1961;5:183-191; http://fab.cba.mit.edu/classes/MAS.862/notes/computation/Landauer-1961.pdf. Bennett C, Landauer R. The fundamental physical limits of computation. Sci Am. 1985 Jul;253(1):48-57; http://web.eecs.umich.edu/~taustin/EECS598-HIC/public/Physical-Limits.pdf.

[1246] Computation at liquid helium temperatures (T ~ 4 K / -269 °C) may also be feasible, implying a continuous power draw of $P_{comp} \sim Z_{comp} E_{Landauer4K} / t_{read/write} \sim$ 18.2 KW for $E_{Landauer4K}$ = 3.8 x 10^{-23} J/bit, costing ~$1.82/hr for electricity and a total electricity cost of ($e_\$ t_{revivalcalc} P_{comp}$) ~ $1100 to complete these calculations for a single revival. Of course, the cost of continuously cooling an 18.2 KW cryogenic computer to 4 K must be added to this figure – e.g., a liquid nitrogen plant that could provide 18.2 KW of cooling capacity might cost ~$350,000 according to Air Liquide, and a liquid helium plant of similar capacity would likely be 10-100 times more expensive.

[1247] https://en.wikipedia.org/wiki/Quantum_computing.

4.9 Prethaw and Crackface Fusion

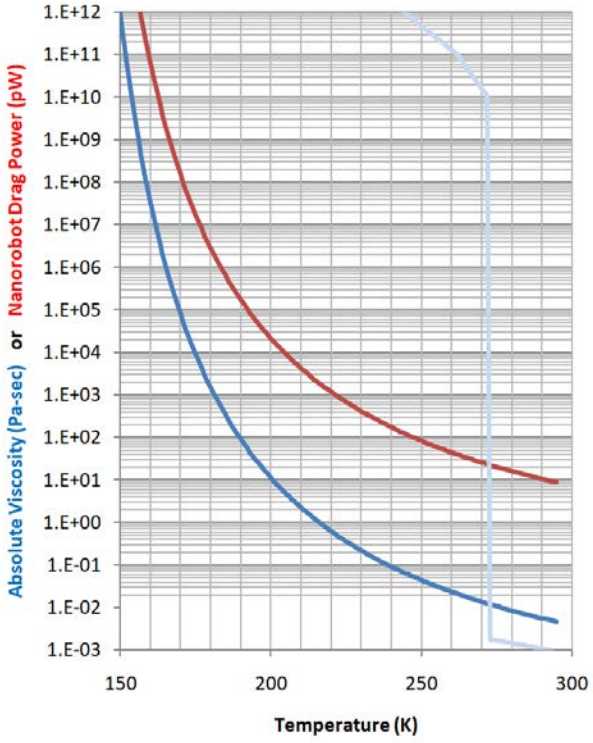

After acquiring knowledge of the position and identity of all biologically relevant structures down to 100 nm feature sizes and putting the vasculoid infrastructure in place, the principal reparative procedures can now be initiated. The first step is to warm the patient. As the patient warms, the cryogenic-temperature cryopreserved tissue softens, allowing the crackfaces to be rejoined, with the fusion process completing as all tissues reach normal fluidity during tissue reliquidification at some temperature between **218 K** (-55 °C) (the melting temperature of M22)[1248] and **273 K** (0 °C).[1249] Note that the temperature-dependent viscosity profile η(T) for pure M22 vitrification solutions commonly used in cryopreservation (chart, dark blue curve)[1250] differs from pure water-ice (chart, pale blue curve) in having no sharp viscosity step-up below a freezing point, so nanorobots might plausibly operate in M22-saturated tissue down to about 248 K (-25 °C) wherein the power drag $P_{drag} = 6\pi\ \eta(T)\ R_{nano}\ v_{nano}^2$ (chart, red curve) for a nanorobot of radius R_{nano} = 1 μm and velocity v_{nano} = 1 cm/sec remains in the acceptable 10-100 pW range. Nanorobots that can successfully perform their missions while migrating through cryogenic tissue at velocities as slow as v_{nano} = 10 μm/sec might plausibly operate down to 171 K (-102 °C) within the 100 pW maximum drag power limit, but at the risk of significantly increased ice growth below 218 K (-55 °C) (Section 4.9.1). ***Future research*** should review which nanorobot activities can be successfully performed while employing transit velocities as slow as 10 μm/sec, and consider the impact if any on cryostasis revival mission design.

[1248] Personal communication from Brian Wowk to Robert Freitas, 16 Oct 2020.

[1249] The addition of pressure can produce at least a small freezing point depression effect that could allow reliquidification to occur at a slightly lower temperature, thus reducing biochemical reaction rates (and the potential tissue degradation) during molecular extraction (Section 4.10) and subsequent repair operations. For example, the freezing point of water drops from **273 K** (0 °C) at normal 1 atm atmospheric pressure to **251 K** (-22 °C) at ~2100 atm pressure[*] – comparable to most household freezers that keep meat cold between -18 °C and -23 °C (i.e., https://en.wikipedia.org/wiki/Refrigerator#Freezer). Whether the resulting ~4-fold decrease in biochemical reaction rates at the lower reliquidification temperature is worth the trouble of workspace pressurization is an appropriate topic for ***future research***.

[*] Bridgman PW. The Pressure-Volume-Temperature Relations of the Liquid, and the Phase Diagram of Heavy Water. J Chem Phys. 1935 Oct;3:597-605; https://aip.scitation.org/doi/abs/10.1063/1.1749561. See also: https://en.wikipedia.org/wiki/Phase_diagram#Crystals.

[1250] Reparameterized M22 data for the Vogel-Tammann-Fulcher (VTF) equation was provided to Robert Freitas by Brian Wowk on 14 Oct 2020, based on original source: Mullen SF, Fahy GM. Chapter 12. Fundamental aspects of vitrification as a method of reproductive cell, tissue and organ cryopreservation. In: Donnez J, Kim SS, eds. Principles and Practice of Fertility Preservation, Cambridge University Press, 2011, pp. 145-163; https://www.amazon.com/dp/0521196957/.

Assuming that fracture features involve crackfaces of length $L_{cracklength}$ ~ 1 mm (Section 3.4.3) and width $W_{crackwidth}$ ~ 100 μm separated by $L_{cracksep}$ ~ 100 μm (Section 4.6.3) occupying $f_{crackvol}$ ~ 1% of tissue volume, then there are $N_{fractures} \sim V_{crackvoid} / L_{cracklength} W_{crackwidth} L_{cracksep}$ = 60 million fractures of total crackface surface area $A_{crackface}$ = 12 m^2 of crackfaces to be joined (Section 4.6.3), occupying $V_{crackvoid} = f_{crackvol} V_{body}$ ~ 600 cm^3 or ~1% of patient body volume (Section 4.4.1). Whether these number and volume estimates are accurate or conservatively high can be resolved by ***future research*** employing appropriate microhistological studies of a representative variety of animal tissues that have been cryogenically preserved using several relevant cryoprotectants, cooling rate profiles, terminal temperature targets, and storage conditions and durations.

In this Section we describe the process of prethaw warming that leads to tissue reliquidification (Section 4.9.1), then outline the procedure for rejoining the separated crackfaces and closing all crackface voids (Section 4.9.2).

4.9.1 Prethaw Warming

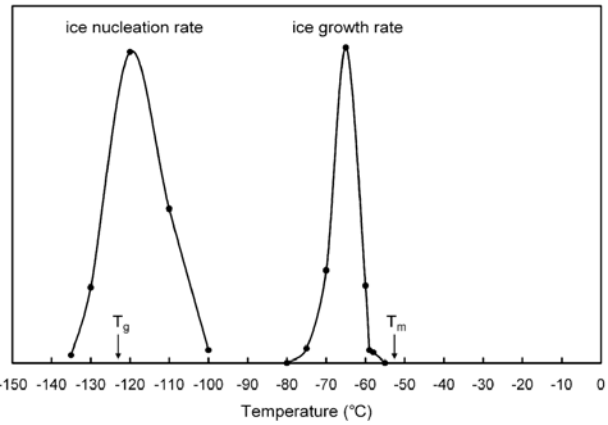

The cryopreserved patient is warmed, in most cases starting from LN2 temperatures around 77 K (-196 °C). The vasculoid infrastructure (Section 4.6.5(7)) can be employed to apply precisely distributed and timed increments of heat energy[1251] to the entire cold tissue mass simultaneously.[1252] If necessary, vasculoid-sourced warming can be supplemented with heat energy imported into the body using whole-body acoustic, inductive, or dielectric heating.[1253] Our best current understanding is that this heating process should be performed very rapidly.[1254] Wowk[1255] notes that because the maximum ice nucleation rate in M22-perfused patients peaks

---

[1251] The vasculoid could distribute the energy $E_{Tg-Tm} \sim \rho_{ice} c_{ice} (T_m - T_g) V_{MSV,water}$ = 2.6 MJ that is required to warm a volume $V_{MSV,water}$ = 0.0275 m^3 (Section 5.2.1.3) of human body-tissue water-ice from T_g (150 K or -123 °C) to T_m (218 K or (-55 °C) in just **10 sec** by deploying 260 KW of power delivered via prepositioned thermocytes (Section 5.2.3.1(B)) or other means, taking ρ_{ice} ~ 930 kg/m^3 and c_{ice} ~ 1500 J/kg-K for water-ice in that temperature range. Note that T_m ranges from -55 °C for full-strength M22-protected tissue to 0 °C for poorly-protected tissue (i.e., ~all ice).

[1252] If the mean separation between heat-emitting elements located in the capillary components of the vasculoid is $L_{vascsep}$ ~ 40 μm (~2 "typical cell" widths), then the thermal equilibration time of such emitted heat is $t_{EQ} = L_{botsep}^2 C_V / K_t \sim 0.5$ msec taking volumetric heat capacity $C_V \sim 10^6$ J/m^3-K and thermal conductivity K_t ~ 3 W/m-K as average values for water-ice over the 77-273 K range. Such a fast equilibration time ensures that heated tissues will remain essentially isothermal as they are warmed, even in cases where the temperature rise is relatively rapid.

[1253] A proposal to use nanodevices operating at cryogenic temperatures to carefully excavate and replace water with unfreezable cryoprotectant, reconstituting the composition of every extracellular and intracellular compartment containing water to eliminate any possible devitrification during warming, probably would also require the installation (and subsequent removal) of stabilizing scaffolding around damaged structures, which seems considerably more challenging than simply warming the tissue rapidly.

[1254] Fast warming (A) minimizes the risk of devitrification (of cryoprotectant-vitrified tissue), (B) lowers the risk of rewarming damage called "recrystallization of intracellular ice" (Section 3.6(4)) and devitrification (Section 3.6(5)) especially in regions of tissue that may be less-well perfused with cryoprotectant chemicals, as tissue temperature rises (approaching reliquidification), and (C) lowers the risk of damage caused by "stirring"* (Section 3.6(6)) and cell debris migration (Section 3.6(7)).

near the glass transition temperature (T_g ~ 150 K or -123 °C) but the maximum ice growth occurs around 205 K (-68 °C) just below the T_m ~ 218 K (-55 °C) melting temperature of M22 (chart, above),[1256] the more time spent near T_g in the presence of M22 the faster the warming rate must be when later passing through the high ice growth rate temperature zone: "Nucleation at very low temperatures primes the solution for extensive ice growth at warmer temperatures." ***Future research*** should examine whether a pulsed warming regimen that hurries through both regions (e.g., 137 K / -136 °C to 173 K / -100 °C, and 193 K / -80 °C to 217 K / -56 °C) during a transition from 77 K (-196 °C) to 273 K (0 °C) can maximally suppress the formation of ice during prethaw. (See also the discussion of ultrafast warming by embedded thermocytes and the warming rates required to prevent devitrification, in Section 5.2.3.1(B), and how nucleation as a function of temperature may affect Intermediate Temperature Storage in cryonics, in Section 7.1.2.)

By adjusting the size of its interplate bumpers, the vasculoid can alter its geometry to accommodate slight changes in cellular and extracellular volume that occur as the body warms. These adjustments in tissue geometry are recorded as changes in positional coordinates to update the whole-body maps that support the current repair plan, as the revival protocol proceeds.

The application of slightly different amounts of heat at different locations can be modeled and actively managed in such a way as to maintain the whole of the body in a solid state for as long as possible as average temperature rises, maximizing immobility of biomolecules and biological structures until the final moment when whole-body reliquidification is to be triggered. Virtually no enzymatic activity should be possible at temperatures starting from **77 K** (-196 °C) all the way up to about **223 K** (-50 °C).[1257] Fahy[1258] notes that "deterioration at this temperature is likely to be due to slow intracellular diffusional processes perhaps accompanied by slow spontaneous breakdown of certain relatively rare labile molecules. Any enzymatic activity that could occur is likely to be arrested in time due to lack of available substrate or accumulated product inhibition, and thus is unlikely to proceed for very long. A special class of proteins, catabolic enzymes, may pose the most serious problems. However, the fraction of enzymes represented by key catabolic enzymes is small and all such activity can be blocked by specific inhibitors. We can…also ignore problems arising from any protein denaturation that may exist. Denatured proteins are not likely to catalyze troublesome reactions and are not needed for any functional role, so there is no reason to worry about them until temperatures are brought to near-zero. At that point, many or most of them will have spontaneously renatured, or will renature spontaneously given additional warming."

The initial portion of actual repair thus involves coping with diffusional processes. At temperatures between **163 K** (-110 °C) and **223 K** (-50 °C), two major types of diffusional process can be identified: (1) the diffusional motions that would normally blur the fracture interfaces, and (2) intracellular diffusional motions. By anchoring vasculoid plates into the crackfaces (Section 4.6.3) we have mostly precluded

---

[*] Fahy G. Appendix B. A "Realistic" Scenario for Nanotechnological Repair of the Frozen Human Brain. In: Wowk B, Darwin M, eds., Cryonics: Reaching for Tomorrow. Alcor Life Extension Foundation, 1991, pp. A-10 – A-26; https://alcor.org/Library/html/nanotechrepair.html.

[1255] Personal communication from Brian Wowk to Robert Freitas, 16 Oct 2020.

[1256] Wowk B. Thermodynamic aspects of vitrification. Cryobiology 2010;60:11-22; http://www.21cm.com/pdfs/2010-Thermodynamics.pdf.

[1257] Douzou P. Cryobiochemistry: An Introduction. Academic Press, NY, 1977; https://www.amazon.com/dp/B012YSOWEK/. Franks F. Biophysics and Biochemistry at Low Temperature. Cambridge University Press, NY, 1985; https://www.amazon.com/dp/0521269326/.

[1258] Fahy G. Appendix B. A "Realistic" Scenario for Nanotechnological Repair of the Frozen Human Brain. In: Wowk B, Darwin M, eds., Cryonics: Reaching for Tomorrow. Alcor Life Extension Foundation, 1991, pp. A-10 – A-26; https://alcor.org/Library/html/nanotechrepair.html.

diffusional information loss at interface sites. Intracellular diffusion is relatively trivial over the short run, so we can first proceed with extracellular and membrane repair processes (Section 4.11), only later turning our attention to cellular interiors (Section 4.12).

Molecular extraction (Section 4.10) should be initiated wherever and whenever reliquidification occurs in any tissue, somewhere above 223 K (-50 °C) (a starting point that should be quantified in ***future research***). Fast extraction establishes the conditions of biochemical stasis as quickly as possible throughout the cryopreserved body. Because premature extraction of cryoprotectant would increase the relative concentration of water and potentially raise the tissue melting point closer to the **273 K** (0 °C) freezing point of pure water-ice, risking resolidification of initially-reliquidified tissue, it may be best to remove cryoprotectants (Section 4.10.1.7) only after more biochemically active molecules such as oxygen (Section 4.10.1.1), glucose (Section 4.10.1.2), and the rest (Section 4.10.1) have been safely deconcentrated via molecular extraction.[1259] This procedure should allow the extraction of newly-liquid-mobilized molecules from the reliquidified state at the lowest possible temperature, thus ensuring minimum biochemical activity rates from these molecules between the time when they enter the liquid state and the time when they are sufficiently extracted,[1260] a period tentatively specified as ~1 hour or less (Section 4.10.1).

It has been noted (Section 3.4.2(2)) that non-synaptic junctions between cells could be disrupted and capillaries could become separated from the surrounding brain tissue during the cryopreservation process, possibly resulting in the tearing of fine processes. Insufficiently perfused tissues could also suffer tissue maceration (Section 3.4.2(6)) in which key pieces of cell debris become detached and able to drift upon tissue reliquidification. ***Future research*** should assess the severity of this problem and the need for additional corrective measures. For instance, besides the physical barriers to diffusion that will already be provided by the temporary installation of branched plumbing architectures during molecular extraction (Section 4.10.1.9), indwelling mechanical diffusion brakes could be deployed (if necessary) by inserting retractable grids or screens in a 3D pattern inside the cell, creating an additional physical barrier to free diffusion. Alternatively (but with more complications), viscosity-enhancing materials could be temporarily injected from the vasculoid into the solid tissue as it softens and eventually melts, decreasing the distance diffusion can carry untethered isolated tissue fragments.

4.9.2 Crackface Fusion

As the cryopreserved tissue warms, thermal stresses relax and the crackfaces start to move together. The separated tissues are gently dragged together across the crackfaces as they warm. Some plastic movement will begin to occur just below the meltpoint temperature, allowing the drawing together to be a gradual continuous process, with the tensile force being adjusted continuously in response to locally measured temperatures, forces, and tissue viscosities. The rejoinment process is guided by two mechanisms.

[1259] Brian Wowk notes that during revival, cryoprotectants should not be replaced with water in a manner that causes T_m to rise significantly above the temperature of the patient at any stage of the repair process warmer than T_g because this would make the system thermodynamically unstable, allowing ice to nucleate unpredictably and grow uncontrollably.

[1260] Following this procedure may also ensure that the extraction of bioactive molecules will take place in a somewhat more viscous fluid environment, since fluid at 223 K (-50 °C) is generally more viscous than a similar fluid at 273 K (0 °C). Diffusion is slower in more viscous fluid, so a course of molecular extraction will take longer at 223 K than at 273 K. Is it better to have slower unwanted biochemical reaction rates with longer active biomolecule extraction times, or the reverse? ***Future research*** should analyze and quantify this technical tradeoff and determine the optimum protocol for cryostasis revival. For computational convenience, the discussion of molecular extraction in Section 4.10 assumes extraction occurs at 273 K. Performing these extractions from reliquidified tissue in the same timeframe but at a lower temperature requires small increases in the total mass of the specified extraction nanodevices.

First, the fracture void-spanning elements of the vasculoid (Section 4.6.3) can apply gentle retractive tension through the linked array of plates to assist in the process of pulling together the separated crackfaces, and to ensure that the two crackfaces remain continuously aligned until the two walls are rejoined, ultimately eliminating the fracture and restoring a seamless microvasculature. While the tensile strength of a 60% w/v concentration of cryoprotectant M22 in water has not yet been measured, one 1954 measurement[1261] of commercial water-ice under modest loading conditions reported a tensile failure strength of 2.41 MPa (~24 atm) at 223 K (-50 °C) falling to 1.34 MPa (~13 atm) at 273 K (0 °C), largely confirmed by a later 1978 study[1262] (though a still later paper[1263] reported somewhat lower values). The tensile strength of *in situ* solid-state M22 at various subfreezing temperatures should be determined by experimental measurements in ***future research***. Restricting vasculoid tensioning to ~0.1 MPa (~1 atm) or less as temperature rises should ensure both that plate anchors will not be ripped out of the ice or glassy solid and that plates will not become dislodged from crackface tissue surfaces during retraction. ***Future research*** can model the rate of rejoining (e.g., due to creep in the ice) as a function of applied force, shear rate, and temperature. It may also be possible for the vasculoid that is resident in the evacuated circulatory system to apply selected bulk pressure to local sections of solid tissue to help steer specific fracture planes to proper closure.

Second, the crackface vasculoid plating can be retracted off of the crackfaces as the faces move together, keeping them well-aligned until they rejoin. The applied tension is maintained as the tissue warms and softens, allowing the separated capillaries to be slowly drawn together in the best possible configuration. The likely path of the crackface rejoining can be simulated during repair process planning, so planar force vectors that should be applied and the exit routes for the retreating crackface vasculoid can be specified in advance. Alignment during the rejoining should be close enough that many fissioned cell membranes will spontaneously reseal as they regain some fluidity. To the extent there are large gaps that diverge from the repair plan in Section 4.8, small amounts of membrane could be locally exuded from the vasculoid as a temporary patch to slow the leakage of liquidifying cell contents into the extracellular spaces.

Procedures must be designed or specified for the extraction of excess plates as the crackfaces are pulled together, as follows:

Microtube bridging capillaries. Extraction of the 9.05 m^2 surface of microtube bridging capillaries comprising ~4.5 x 10^{12} plates (Section 4.6.3) involves gradually shortening the total length of the tensioning bridging capillaries. If the interior diameter of capillary bridges is d_{cap} ~ 8 μm and the plates are only A_{plate} ~ 2 μm^2 area and 1 μm thick, a procedure can be designed in which plates are removed from the inside of each microtube and then transported through that interior volume out of the local area as the bridge length shortens. (The microtubes are hollow with ciliary transport mechanisms coating interior surfaces, readily permitting these removal operations.) The bridges are under tension, so force pathways should have multiple redundancy permitting tension to be maintained while one plate is removed. There are $n_{circum} = \pi d_{cap} / A_{plate}^{1/2}$ ~ 18 plates around the circumference of a bridging microtube. These plates could be tiled in a staggered configuration so that some of them can maintain the tensile load while others

---

[1261] Butkovich TR. Ultimate Strength of Ice. Research Paper 11, Snow, Ice and Permafrost Research Establishment, U.S. Army Corps of Engineers, Wilmette IL, Dec 1954, Table 3, p.11; https://books.google.com/books?hl=en&lr=&id=5Aa-TJbh3lMC&oi=fnd&pg=PA11.

[1262] Haynes FD. Effect of temperature on the strength of snow-ice. CRREL Report 78-27, Cold Regions Research and Engineering Laboratory, U.S. Army Corp of Engineers, Dec 1978, Table II, pp. 6-8; https://books.google.com/books?hl=en&lr=&id=fX5CHYos1rMC&oi=fnd&pg=PA6.

[1263] Richter-Menge JA, Jones KF. The tensile strength of first-year sea ice. J Glaciology 1993;39(133):609-618; https://www.cambridge.org/core/services/aop-cambridge-core/content/view/3D163667916EFABC21415F7AF81496FB/S0022143000016506a.pdf/tensile_strength_of_firstyear_sea_ice.pdf.

are removed. For example, if every other plate were offset by half a plate length ($A_{plate}^{1/2}$ / 2 ~ 0.7 μm), then any 9 of them could maintain tension while another 9 were removed. But a 50% stagger would require that each plate must be able to telescope half its length or 0.7 μm – well beyond the posited ~0.2 μm expandability range of both vasculoid plates (i.e., 1.4 μm to 1.6 μm diameter range)[1264] and vasculoid bumpers (100-300 nm throw).[1265] ***Future research*** can develop a staggering scheme that allows removing one plate one at a time, so that each of the remaining plates only has to shrink (using contractile bumpers) by 1/18th of their length, or $A_{plate}^{1/2}$ / n_{circum} ~ 0.078 μm, well within the ~0.2 μm expandability range of the vasculoid plates.

Crackface plates. The 12 m^2 or ~6 x 10^{12} plates (Section 4.6.3) covering the crackfaces must also be removed as the two faces are brought together. The fracture voids bounded by crackface surfaces (to which vasculoid plates are attached) should mostly consist of two general types: V-cracks and slip planes. For V-cracks, the crack can be "zipped up" from the apical end of the V to the wide end as the patient warms, while slowly peeling back the vasculoid coating as the crackface surfaces are drawn into close alignment. Plates are removed from the apical end of the V first, allowing the narrowest end of the V to close first, slowly proceeding to the other end like a zipper closing up a seam. For slip planes, the two crackfaces will normally be coated with anchored vasculoid plates – although in a few cases it may be necessary to ratchet the two planes slightly farther apart if they're closer together than a few microns, in order to allow enough room to install the plates. As the tissue thaws, the contractile-force-applying vasculoid can apply sufficiently more force on one end of the crack than on the other so as to slowly tilt the faces together slightly closer at one end, allowing a "zipping" process to proceed roughly similarly as with the V-cracks. Other fracture void geometries should be specified and explored in ***future research***.

An average tissue capillary number density[1266] of $n_{capillary}$ ~ 600 capillaries/mm^2 implies that vascular capillaries are spaced an average of $x_{capillary}$ ~ $(n_{capillary})^{-1/2}$ ~ 40 μm apart. As temperature rises from T_{LN2} = 77 K (-196 °C) to T_{melt} = 273 K (0 °C), the ice field between two bracketing capillaries expands by $\Delta x_{expansion} = x_{capillary}\ \alpha_{ice,avg}\ (T_{melt} - T_{LN2})$ ~ 250 nm, taking the average coefficient of expansion of ice over this temperature range as $\alpha_{ice,avg} \sim (\alpha_{ice}(T_{melt}) + \alpha_{ice}(T_{LN2})) / 2 = 32 \times 10^{-6}\ K^{-1}$ (Section 3.4.3). But feature misalignment or loss of registration between two opposed crackfaces occurs only when the ice fields of the two crackfaces expand at different rates or when some additional positional shift occurs between them. If the entire differential motion between two crackfaces during thawing can be held to x_{diff} ~ 1 μm, then the expansion-related misalignment between two bracketing capillaries is only $\Delta x_{diff} = x_{diff}\ \alpha_{ice,avg}\ (T_{melt} - T_{LN2})$ ~ 6 nm, close to the typical 6-10 nm lipid bilayer plasma membrane thickness in cells,[1267] potentially allowing correct spontaneous membrane self-sealing in most instances during tissue warm-up. Membrane repair is further discussed in Section 4.11.

Excess vasculoid plates that are removed from bridging capillaries and crackfaces may be exported out of the body, via the vasculoid.

[1264] Freitas RA Jr., Phoenix CJ. Vasculoid: A personal nanomedical appliance to replace human blood. J Evol Technol. 2002 Apr;11:1-139; Section 7.4 "Vasculoid Plating"; http://www.jetpress.org/volume11/vasculoid.pdf.

[1265] Freitas RA Jr. Chapter 23. Comprehensive Nanorobotic Control of Human Morbidity and Aging, Section 6.2.3 "Heart and Vascular Disease". In: Fahy GM, West MD, Coles LS, Harris SB, eds, The Future of Aging: Pathways to Human Life Extension, Springer, New York, 2010, pp. 685-805; http://www.nanomedicine.com/Papers/Aging.pdf.

[1266] Schmidt RF, Thews G, eds., Human Physiology, Second Edition, Springer-Verlag, New York, 1989; https://www.amazon.com/dp/3540194320/.

[1267] Freitas RA Jr. Nanomedicine, Volume I: Basic Capabilities, Landes Bioscience, Georgetown TX, 1999, Section 8.5.3.2, "Cell Membranes"; http://www.nanomedicine.com/NMI/8.5.3.2.htm.

4.10 Molecular Extraction

Warming cryopreserved tissues before repair carries two principal risks – first, that formerly solid-locked isolated fragments of tissues or other biological material may drift in a reliquidified medium, possibly destroying identity-relevant information, and second, that harmful biochemical reactions can more easily occur in the now less-viscous fluid medium and at the higher temperatures, risking further ischemic-like damage.

The molecular extraction process as described in this Section avoids both of these risks. First, prior to rewarming, the positions of all ≥100 nm major fragments of tissues have been mapped and their likely originating source and composition has been identified, so their role in the forthcoming nanorobotic repair process has already been incorporated into the repair plan. A viable cell debris-handling protocol is proposed in Section 4.11.1. Second, molecular extractions are tentatively designed to be completed within ~1 hour at ~273 K (0 °C), an exposure to newly-reactive chemistry that should create equivalent (negligible) incremental ischemic risk during the extraction hour as would an exposure of the same materials to normothermic temperatures (310 K / 37 °C) for ~3 minutes. Faster extractions can be employed if deemed necessary in ***future research***. Afterwards, molecular extraction maintains the patient in a state of **comprehensive metabolic arrest** for the duration of the repair and revival process.

As a practical matter, any given cryopatient will have some regions of their body well perfused with cryoprotectant, other regions that have received almost no cryoprotectant and are little better than a "straight freeze," with much of the body enjoying some intermediate state of perfusion completeness. Because cryoprotectants and other solutes lower the freezing point of water, well-perfused areas will reliquidify first at the lowest temperatures during rewarming, while poorly perfused areas will reliquidify last at higher temperatures nearer to 273 K. As temperature rises and tissue reliquidifies, the risk of rewarming damage (Section 3.6) and reperfusion injury grows. The purpose of molecular extraction is to ameliorate or eliminate most of this risk.

Sensors on the previously-installed vasculoid (Section 4.6) can detect the telltale drop in viscosity of the underlying extracellular and cytosolic environments during localized melting. As small sections of mostly vitrified tissue begin to reliquidify, the vasculoid inserts probes festooned with sorting rotors into the softened tissue to begin the selective extraction of key molecules in a prioritized order. The objective of the sorting rotors is to extract potentially biologically active free molecules from the extracellular fluid and from the cytosol of all individual cells – fluids which may be commingled in cases of cells with damaged plasma membranes. The removal of free molecules that could potentially serve as biologically active agents (i.e., enabling unwanted chemical reactions during or after the warming process to ~273 K) metabolically deactivates each cell, leaving it effectively chemically inert and no longer subject to internal chemical degradation. It should be noted that many possible chemical reaction pathways will already have been carried to completion after a period of warm ischemia and subsequent cooldown through temperatures above the freezing point where solidification occurs, leaving fewer reaction possibilities after reliquidification.

As the temperature slowly rises, more and more tissue water enters the liquid state. The molecular extraction process continues until all tissue accessible to the vasculoid has been reliquidified and subjected to molecular extraction. The vasculoid transports all of these materials out of the body, potentially recording the molecule type, number count, and approximate cellular addresses (because many cell membranes will lack structural integrity while awaiting resealing; Section 4.11) of some or all extracted molecules, allowing extensive computations on this data using massive external computers to prepare revisions to the original repair plan (Section 4.8). The warmup (above M22 melting point T_m ~ 218 K, or -55 °C) and extraction process may be conducted slowly enough to enable molecular recognition and transport to occur within well-defined time, energy, and heat budgets consistent with the ability of the vasculoid to maintain continuous thermal stability.

As any given subvolume of tissue reliquidifies, specific free molecules will be extracted in the priority order detailed in Section 4.10.1. This defines "targeted extraction" – an approach in which nanorobotic mechanisms are employed to recognize and extract only the specific targeted free-floating molecules that are deemed sufficient to ensure biochemical stasis, while leaving other molecules behind (or reserved for later extraction). Targeted extraction can identify and record which molecules came from where, in case that information proves useful or necessary for revival – the exact extent to which this has utility should be determined by ***future research***. Targeted extraction may require the design and implementation of up to ~25,000 unique binding sites mounted on sorting rotors to perform the targeted extractions. The order of these extractions can be designed to maintain continuous liquidity at the lowest possible temperatures while the patient thaws – another possible topic for ***future research***.

Section 4.10.2 summarizes a possibly simpler "tissue washout" approach that appears to avoid much of the complexity of targeted extraction but also sacrifices most of the ability to determine and record the number and location of extracted molecules. It is a ***future research*** project to examine the merits of both approaches and make a recommendation favoring one or the other. Which kind of extraction (and its priorities) may be sufficient to establish metabolic stasis is an experimentally accessible question that could be researched now. Note that conventional extracorporeal perfusion techniques could not be started until large reliquidified channels existed through the tissue to permit flow circuits to exist, losing valuable time.

Under either approach, the molecular extractions can be completed to sub-physiological solute concentrations in ~1 hour, presumptively establishing a condition of biochemical stasis. A 1-hour exposure to potentially damaging biochemical reactions at 273 K (0 °C) should produce roughly the same incremental damage as normothermic exposure to the same materials for ~3 minutes at 310 K (37 °C), according to the Arrhenius equation (Section 3.5), so added ischemic risk during the extraction hour should be minimal.[1268] Once initial biostasis has been achieved, the extraction process could be continued indefinitely to arbitrarily low concentration levels for all solutes, taking as much time as deemed necessary by even the most conservative criteria.

Possible Nonextraction Targets. Just as an excess of calcium ion can cause microtubule depolymerization[1269] (hence calcium extraction reduces the likelihood of depolymerization), a ***future research*** project should determine which (if any) ions or solutes must be left in place at some minimum active concentration and not maximally extracted, in order to prevent cellular structural deterioration or destabilization. A few possible examples might include:

* Microtubules are dynamic cytoskeletal structures – constantly being assembled and disassembled – and require GTP[1270] (the guanosine form of ATP) for assembly. Reducing the concentration of GTP in the cytosol to sub-biologic levels might allow excess microtubule depolymerizations and destabilize the cell, as microtubule destabilization has been linked to various neurodegenerative diseases such as Parkinson's[1271] and Alzheimer's.[1272]

[1268] If even ~3 minutes of additional normothermic ischemia must be avoided, ***future research*** can specify a number of key molecules that can be extracted at least an order of magnitude faster by varying the selection of sorting rotor binding sites and by other means.

[1269] Weisenberg RC. Microtubule formation *in vitro* in solutions containing low calcium concentrations. Science. 1972 Sep 22;177(4054):1104-1105; https://pubmed.ncbi.nlm.nih.gov/4626639/. O'Brien ET, Salmon ED, Erickson HP. How calcium causes microtubule depolymerization. Cell Motil Cytoskeleton. 1997;36(2):125-135; https://pubmed.ncbi.nlm.nih.gov/9015201/.

[1270] https://en.wikipedia.org/wiki/Guanosine_triphosphate.

[1271] Pellegrini L, Wetzel A, Grannó S, Heaton G, Harvey K. Back to the tubule: microtubule dynamics in Parkinson's disease. Cell Mol Life Sci. 2017 Feb;74(3):409-434; https://link.springer.com/article/10.1007/s00018-016-2351-6.

* There is at least a small risk that excessive extraction of cyclase-association proteins (e.g., CAP2) from brain tissue could modify neuronal architecture and spine morphology.[1273]

* Excessive extraction of drebrin (an actin-binding protein) might risk altering hippocampal dendritic spines leading to synaptic pathology.[1274]

* Establishing hypotonic (low salt concentration) conditions in the cytosol can alter the usual spectrin dimer-tetramer reversible equilibrium from favoring tetramers to favoring dimers instead, diminishing the structural stability of these membrane skeletons.[1275]

The selection of the molecules to be extracted and the degree of extraction required must be done carefully with the objective of preventing destabilization of preexisting cellular structures while establishing conditions of sustainable biochemical stasis in the cytosolic and extracellular compartments.

Possible Injection Targets. After expressing concern that significant diffusion could occur even at low temperatures up to and during reliquidification, Fahy[1276] proposed the injection of metabolic inhibitors[1277] into the cytoplasm to immediately "block the action of any enzymes that permit catabolism to proceed to beyond an acceptable point. Once deposited, they can be ignored, since these relatively low molecular weight inhibitors will reach their targets by diffusion as rapidly as the normal substrates would otherwise reach these catabolic enzymes." Injection of metabolic inhibitors (that could perhaps later be selectively removed via sorting rotors prior to patient warmup; Section 4.13) are at least a partial third conceptual approach if ***future research*** determines that molecular extraction in a 1-hour time frame is insufficiently fast. However, any additional degradation that may occur during the 1-hour extraction period is likely to be small compared to the degradation that has already occurred due to the many other sources of damage (Chapter 3), especially including the many hours of warm ischemia (Section 3.2) normally already suffered

---

[1272] Bamburg JR, Bloom GS. Cytoskeletal pathologies of Alzheimer disease. Cell Motil Cytoskeleton. 2009 Aug;66(8):635-649; https://www.ncbi.nlm.nih.gov/pmc/articles/PMC2754410/.

[1273] Kumar A, Paeger L, Kosmas K, Kloppenburg P, Noegel AA, Peche VS. Neuronal Actin Dynamics, Spine Density and Neuronal Dendritic Complexity Are Regulated by CAP2. Front Cell Neurosci. 2016 Jul 26;10:180; https://www.ncbi.nlm.nih.gov/pmc/articles/pmid/27507934/.

[1274] Harigaya Y, Shoji M, Shirao T, Hirai S. Disappearance of actin-binding protein, drebrin, from hippocampal synapses in Alzheimer's disease. J Neurosci Res. 1996 Jan 1;43(1):87-92; https://pubmed.ncbi.nlm.nih.gov/8838578/. Counts SE, Nadeem M, Lad SP, Wuu J, Mufson EJ. Differential expression of synaptic proteins in the frontal and temporal cortex of elderly subjects with mild cognitive impairment. J Neuropathol Exp Neurol. 2006 Jun;65(6):592-601; https://academic.oup.com/jnen/article/65/6/592/2645294.

[1275] Liu SC, Palek J. Spectrin tetramer-dimer equilibrium and the stability of erythrocyte membrane skeletons. Nature. 1980 Jun 19;285(5766):586-588; https://www.nature.com/articles/285586a0.

[1276] Fahy G. Appendix B. A "Realistic" Scenario for Nanotechnological Repair of the Frozen Human Brain. In: Wowk B, Darwin M, eds., Cryonics: Reaching for Tomorrow. Alcor Life Extension Foundation, 1991, pp. A-10 – A-26; https://alcor.org/Library/html/nanotechrepair.html.

[1277] e.g., Gullans SR, Brazy PC, Soltoff SP, Dennis VW, Mandel LJ. Metabolic inhibitors: effects on metabolism and transport in the proximal tubule. Am J Physiol. 1982 Aug;243(2):F133-40; https://pubmed.ncbi.nlm.nih.gov/7114212/. Zhao Y, Butler EB, Tan M. Targeting cellular metabolism to improve cancer therapeutics. Cell Death Dis. 2013 Mar 7;4(3):e532; https://www.ncbi.nlm.nih.gov/pmc/articles/pmid/23470539/. Ramesh V, Brabletz T, Ceppi P. Targeting EMT in Cancer with Repurposed Metabolic Inhibitors. Trends Cancer. 2020 Nov;6(11):942-950; https://portal.findresearcher.sdu.dk/files/174150289/1_s2.0_S2405803320301898_main.pdf.

by most cryopatients prior to cryopreservation. Neutralization of membrane-bound enzymes is discussed below (Section 4.10.1.8(2)).

Future research should also determine the advisability of injecting a few specialized inhibitor molecules to reduce the risk of fast-spiking reperfusion injuries (Section 3.6) as cells are warmed enough to reliquidify. For example, ROS injury (Section 3.6(1)) can be nearly eliminated by injecting antioxidants,[1278] and reperfusion-related cerebral edema (Section 3.6(3)) might be reduced using antioxidant enzymes,[1279] VEGF antagonists,[1280] and other agents.[1281] Methylene blue can protect against reperfusion injury by suppressing formation of nitric oxide metabolites (Section 3.2.2).[1282] No-reflow effects (Section 3.6(3)) might be reduced by injecting the monoclonal antibody IB4.[1283] Neurons might be protected from ischemic and reperfusion injury by blocking harmful calcium influx with nimodipine,[1284] by blocking TNF receptors[1285] and other receptors using anti-apoptotic proteins.[1286]

Is the Vasculoid Essential for Molecular Extraction? In principle, the molecular extractions described in this Section could be performed by infusing ~6 liters of mobile storage nanorobots as described for

---

[1278] Vanden Hoek TL, Shao Z, Li C, Schumacker PT, Becker LB. Mitochondrial electron transport can become a significant source of oxidative injury in cardiomyocytes. J Mol Cell Cardiol. 1997 Sep;29(9):2441-50; https://www.sciencedirect.com/science/article/abs/pii/S0022282897904818.

[1279] Armstead WM, Mirro R, Thelin OP, Shibata M, Zuckerman SL, Shanklin DR, Busija DW, Leffler CW. Polyethylene glycol superoxide dismutase and catalase attenuate increased blood-brain barrier permeability after ischemia in piglets. Stroke. 1992 May;23(5):755-62; https://www.ahajournals.org/doi/pdf/10.1161/01.STR.23.5.755.

[1280] van Bruggen N, Thibodeaux H, Palmer JT, Lee WP, Fu L, Cairns B, Tumas D, Gerlai R, Williams SP, van Lookeren Campagne M, Ferrara N. VEGF antagonism reduces edema formation and tissue damage after ischemia/reperfusion injury in the mouse brain. J Clin Invest. 1999 Dec;104(11):1613-20; https://www.ncbi.nlm.nih.gov/pmc/articles/PMC409867/.

[1281] Takahashi M, Macdonald RL. Vascular aspects of neuroprotection. Neurol Res. 2004 Dec;26(8):862-9; https://pubmed.ncbi.nlm.nih.gov/15727270/. Trinkl A, Vosko MR, Wunderlich N, Dichgans M, Hamann GF. Pravastatin reduces microvascular basal lamina damage following focal cerebral ischemia and reperfusion. Eur J Neurosci. 2006 Jul;24(2):520-6; https://pubmed.ncbi.nlm.nih.gov/16836638/. He ZJ, Huang ZT, Chen XT, Zou ZJ. Effects of matrix metalloproteinase 9 inhibition on the blood brain barrier and inflammation in rats following cardiopulmonary resuscitation. Chin Med J (Engl). 2009 Oct 5;122(19):2346-51; https://journals.lww.com/cmj/Fulltext/2009/10010/Effects_of_matrix_metalloproteinase_9_inhibition.28.aspx.

[1282] Miclescu A, Sharma HS, Martijn C, Wiklund L. Methylene blue protects the cortical blood-brain barrier against ischemia/reperfusion-induced disruptions. Crit Care Med. 2010 Nov;38(11):2199-206; https://pubmed.ncbi.nlm.nih.gov/20711066/.

[1283] Mori E, del Zoppo GJ, Chambers JD, Copeland BR, Arfors KE. Inhibition of polymorphonuclear leukocyte adherence suppresses no-reflow after focal cerebral ischemia in baboons. Stroke. 1992 May;23(5):712-8; https://www.ahajournals.org/doi/pdf/10.1161/01.STR.23.5.712.

[1284] Babu CS, Ramanathan M. Post-ischemic administration of nimodipine following focal cerebral ischemic-reperfusion injury in rats alleviated excitotoxicity, neurobehavioural alterations and partially the bioenergetics. Int J Dev Neurosci. 2011 Feb;29(1):93-105; https://pubmed.ncbi.nlm.nih.gov/20713150/.

[1285] Martin-Villalba A, Hahne M, Kleber S, Vogel J, Falk W, Schenkel J, Krammer PH. Therapeutic neutralization of CD95-ligand and TNF attenuates brain damage in stroke. Cell Death Differ. 2001 Jul;8(7):679-86; https://www.nature.com/articles/4400882.

[1286] Sawitzki B, Amersi F, Ritter T, Fisser M, Shen XD, Ke B, Busuttil R, Volk HD, Kupiec-Weglinski JW. Upregulation of Bag-1 by *ex vivo* gene transfer protects rat livers from ischemia/reperfusion injury. Hum Gene Ther. 2002 Aug 10;13(12):1495-1504; https://pubmed.ncbi.nlm.nih.gov/12215270/. Tuttolomondo A, Di Sciacca R, Di Raimondo D, Arnao V, Renda C, Pinto A, Licata G. Neuron protection as a therapeutic target in acute ischemic stroke. Curr Top Med Chem. 2009;9(14):1317-34; https://pubmed.ncbi.nlm.nih.gov/19849659/.

performing nanostasis (Section 7.1.6.5) on a warm living human body. However, in the situation where the extraction must be performed on a cold solid body as it warms and unevenly reliquidifies, the process will take longer because the nanorobots must be transported throughout the patient by some other means than a vasculoid distribution system, and because the nanorobots must wait for local reliquidification to occur before they can attempt tissue penetration to reach their targets. Export of extracted molecules is expedited by the vasculoid which can rapidly transport containerized material out of the body as quickly as it is acquired, whereas the storage robots must retain these materials in onboard storage thus requiring a just-tolerable maximally-intrusive total volume of nanorobots to be employed.

4.10.1 Targeted Extraction

One method for removing specific molecules from intracellular and extracellular spaces is to perform targeted extraction of specific molecular types. Typically, this might involve a nanoscale mechanical device called a sorting rotor[1287] (images, below: classical (left) and revolver (right) designs) equipped with binding sites for each targeted molecular type, and a means for transferring the captured molecule from its native environment inside the body to an internal reservoir from whence the molecule can be transported out of the body, inside vasculoid tankers (Section 4.6.1).

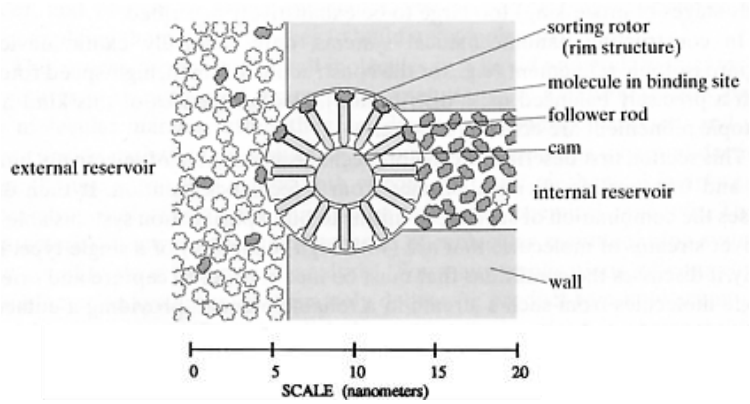

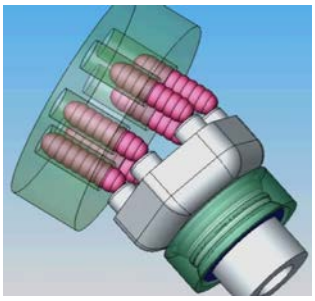

A classical sorting rotor mechanism measuring 7 nm x 14 nm x 14 nm (V_{rotor} = 1372 nm^3/rotor, M_{rotor} ~ 2 x 10^{-21} kg/rotor) equipped with molecular binding sites[1288] targeting 99% occupancy could bind, extract and transport ~10^6 molecules/sec starting from a high ambient concentration of c_{max} ~ 10^{-3} molecules/nm^3, slowing to ~10^{-2} molecules/sec in a low ambient concentration of ~10^{-11} molecules/nm^3,[1289] a rotor

---

[1287] Drexler KE. Nanosystems: Molecular Machinery, Manufacturing, and Computation, John Wiley & Sons, New York, 1992, Section 13.2.1(a) "Modulated receptors for selective transport: Basic concepts"; https://www.amazon.com/dp/0471575186/. Freitas RA Jr. Nanomedicine, Volume I: Basic Capabilities, Landes Bioscience, Georgetown, TX, 1999; Section 3.4.2, "Sorting Rotors"; http://www.nanomedicine.com/NMI/3.4.2.htm.

[1288] Freitas RA Jr. Exploratory design in medical nanotechnology: a mechanical artificial red cell. Artif Cells Blood Substit Immobil Biotechnol. 1998 Jul;26(4):411-30; https://web.archive.org/web/20100613040242/https://foresight.org/Nanomedicine/Respirocytes1.html (Sec. 2.2.3). Freitas RA Jr. Nanomedicine, Volume I: Basic Capabilities, Landes Bioscience, Georgetown, TX, 1999; Section 3.5.7, "Receptor Configurations"; 7http://www.nanomedicine.com/NMI/3.5.7.htm

[1289] Freitas RA Jr. Nanomedicine, Volume I: Basic Capabilities, Landes Bioscience, Georgetown, TX, 1999; Section 3.4.2, "Sorting Rotors"; http://www.nanomedicine.com/NMI/3.4.2.htm; and Section 4.2.3, "Counting Rotors"; http://www.nanomedicine.com/NMI/4.2.3.htm.

pumping rate that can be crudely modeled for scaling purposes as $r_{pump} = 10^{[9+\log10(cm(t))]}$ molecules/rotor-sec at a concentration of c_m (molecules/nm^3). We assume there is a maximum pump rate of ~10^6 molecules/sec at any concentration due to rotor design limits. It is a major task for ***future research*** to create designs (and automated design processes) for reversible binding sites with the necessary specificity and affinity for the numerous target molecules required to complete the molecular extraction task (Appendix H).

The pumping rate is also constrained by the ability of the target molecules to diffuse from their random locations within the rotor service volume to the binding site of the sorting rotor where they may become bound. The maximum pumping rate is $r_{pump,max} \sim 2\ D_{mol} / \Delta X^2$,[1290] where the diffusion coefficient for a molecule of molecular weight MW (gm/mole) in water at temperature $T_{icewater} \sim 273$ K (0 °C) may be crudely modeled for scaling purposes as $D_{mol} \sim 10^{(-0.35 \log10(MW) - 9.3)}$, which represents the trendline (chart, below) of the data on diffusion coefficient vs. molecular weight for a variety of molecules in $T_{bodytemp} = 310$ K (37 °C) water published elsewhere,[1291] this data having been adjusted to account for the lower diffusion coefficient at higher viscosity at lower temperature ($T_{icewater}$) by dividing by $\eta_{icewater} / \eta_{bodytemp} = 2.584$, where $\eta_{icewater} = 1.787 \times 10^{-3}$ Pa-sec and $\eta_{bodytemp} = 0.6915 \times 10^{-3}$ Pa-sec.[1292] ΔX, the radius of an assumed-spherical rotor service volume, is the maximum distance a target molecule might need to diffuse to reach the binding site of a sorting rotor that is attempting to extract it. Rotor service volume radius ΔX is typically 2-5 μm for the molecules and concentrations considered here.[1293]

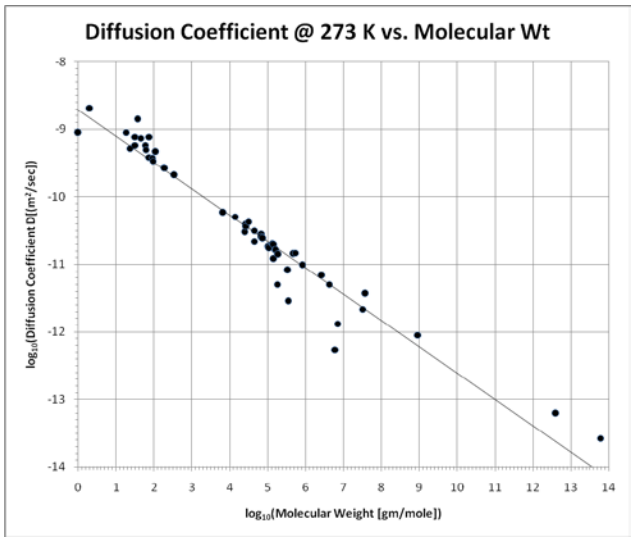

How long will it take a single sorting rotor with appropriate binding sites to reduce the concentration of a target molecule from its initial concentration $c_{m,high}$ to a desired lower concentration $c_{m,low}$ in the fluid service volume $V_{service}$ of the sorting rotor? The initial number of molecules in the service volume is $n_{molecule}(t) = c_m(t)\ V_{service}$ at t = 0. During an increment of time Δt, the rotor operates to extract $\Delta n_{molecule}(t) = \Delta t\ r_{pump}(t)$ molecules, reducing the concentration of the target molecule to $c_m(t+\Delta t) = [n_{molecule}(t) - \Delta n_{molecule}(t)] / V_{service}$ molecules/nm^3. Iteration over multiple Δt cycles reduces concentration from $c_{m,high}$ to $c_{m,low}$ in the rotor service volume, after a total pumping time of τ_{total}. On average, no net molecules of a particular type will enter or leave the service volume during the pumping activity other than through the sorting rotor, if a complete 3D array of rotors is simultaneously pumping the selected molecule at equal

---

[1290] Freitas RA Jr. Nanomedicine, Volume I: Basic Capabilities, Landes Bioscience, Georgetown TX, 1999, Section 3.2.4, "Diffusion Cascade Sortation"; http://www.nanomedicine.com/NMI/3.2.4.htm.

[1291] Freitas RA Jr. Nanomedicine, Volume I: Basic Capabilities, Landes Bioscience, Georgetown, TX, 1999; Table 3.3; http://www.nanomedicine.com/NMI/Tables/3.3.jpg.

[1292] The cytosol, interstitial fluid, and leaked blood plasma are mostly water but have variable viscosities somewhat higher than the pure water model assumed here. It is a ***future research*** task to model and quantify the effects of such higher viscosity on the extraction operations at ~273 K described in this Section.

[1293] In actual tissue the diffusion of a solute molecule will not take place in pure water but will be slowed by the presence of semipermeable membranes, organelles, intracellular cytoskeleton scaffolding, and other solute molecules, a factor whose inclusion is beyond the scope of the present scaling study.

rates from the centers of all adjacent service volumes. The rotor service volume is $V_{service} \sim V_{fluid} / N_{fleet}$, where $V_{fluid} \sim 38.5$ L is the whole-body intracellular (~28 L) plus the interstitial (~10.5 L) fluid volume[1294] of a 70 kg human body, and N_{fleet} is the total number of sorting rotors deployed in the patient's body for molecular extraction purposes, having total volume $V_{fleet} = N_{fleet} V_{rotor}$ and total mass $M_{fleet} = N_{fleet} M_{rotor}$.[1295]

The minimum energy required to pump uncharged molecules is the change in free energy[1296] in transporting the species from one environment having concentration c_m to a second environment having concentration $c_{transport}$, which may be estimated as $\Delta G(t) = k_B T_{icewater} \ln(c_{transport}/c_m(t))$, where $k_B = 1.38 \times 10^{-23}$ J/K (Boltzmann constant). For example, transport of one uncharged molecule from a low concentration inside the body to a high concentration environment such as an interior reservoir or a vasculoid tanker across a $c_{transport}/c_m = 1000$ concentration gradient (typical in biology) costs $\Delta G \sim 26$ zJ/molecule at 273 K (0 °C). In cases where the ambient concentration exceeds c_{max} and the target molecule is being pumped into a lower concentration reservoir at ~10^{-3} molecules/nm^3,[1297] energy can in principle be recovered but we assume the energy cost is zero. The pumping energy during each increment of time is $\Delta E(t) = \Delta G(t) \Delta n_{molecule}(t)$ and the total average power draw by all rotors in the fleet by the conclusion of the extraction is $P_{fleet} = \Sigma \Delta E(t) / \tau_{total}$ watts.

As noted earlier (Section 3.5), $\tau_{ischemic} \sim 6$ minutes is the classical time limit for the onset of warm ischemic damage after cardiac arrest in humans,[1298] although a 14-16 minute window of survivability has been demonstrated in dogs[1299] and a 60-minute (1 hour) window has been reported in cats[1300] at normothermic body temperature. Following the Arrhenius equation,[1301] a metabolic process that would require 6 minutes at normal human body temperature (310 K / 37 °C) would require ~1.8 hours (6500 sec) at the water-ice

---

[1294] https://en.wikipedia.org/wiki/Fluid_compartments.

[1295] Tad Hogg suggests that the model might be clearer if stated as an exponential decrease from a differential equation, rather than the approximate incremental change in Δt. The aforestated model for pumping rate corresponds to $r_{pump} = a\, c_m(t)$, taking $a = 10^9$ nm^3/sec, whereupon the number of molecules in the service volume changes as $d/dt[n(t)] = - r_{pump} = -(a/V_{service})\, n(t)$, so $n(t)$ decreases exponentially from its initial value with time constant $V_{service}/a$. Similarly, the sum over increments approximates the integral in the discussion of energy use. The incremental numerical method employed here makes the unstated approximation that the time increment Δt is small enough that the quantities don't change during that interval (which, strictly, is only correct in the limit of $\Delta t \rightarrow 0$) and yet large enough not to be swamped by numerical roundoff error. This numerical method for solving differential equations is conceptually simple but can have roundoff and stability problems, and other methods give better accuracy with fewer steps, e.g., by adjusting step size. Interested readers are encouraged to use whatever method they prefer to solve this model, including via simulation software packages such as Comsol (https://en.wikipedia.org/wiki/COMSOL_Multiphysics) or Modelica (https://en.wikipedia.org/wiki/Modelica).

[1296] Freitas RA Jr. Nanomedicine, Volume I: Basic Capabilities, Landes Bioscience, Georgetown TX, 1999, Section 3.4.1, "Transporter Pumps"; http://www.nanomedicine.com/NMI/3.4.1.htm.

[1297] In the case of high-concentration cryoprotectants (Section 4.10.1.7), we conservatively assume the reservoir concentration is ~1 molecule/nm^3 for the energy calculations.

[1298] e.g., Zimmermann KA. Respiratory system: Facts, function and diseases, LiveScience, July 2021; https://www.livescience.com/22616-respiratory-system.html; https://web.archive.org/web/20160705121054/http://www.nlm.nih.gov/medlineplus/ency/article/000013.htm.

[1299] Lemler J, Harris SB, Platt C, Huffman TM. The arrest of biological time as a bridge to engineered negligible senescence. Ann N Y Acad Sci. 2004 Jun;1019:559-63; http://www.alcor.org/Library/pdfs/Lemler-Annals.pdf.

[1300] Hossmann KA, Schmidt-Kastner R, Grosse Ophoff B. Recovery of integrative central nervous function after one hour global cerebro-circulatory arrest in normothermic cat. J Neurol Sci. 1987 Feb;77(2-3):305-320; https://pubmed.ncbi.nlm.nih.gov/3819770.

[1301] https://en.wikipedia.org/wiki/Arrhenius_equation.

melting point (273 K) – the maximum temperature at which molecular extraction should occur. The goal of molecular extraction is to reduce the concentrations of O_2, glucose, and all other biologically reactive free molecules to subreactive levels in a sub-ischemic time of τ_{total} ~ 1 hour (3600 sec). The required concentration reduction appears to be to 0.1%-0.3% of ambient for O_2 (Section 4.10.1.1) and to ~1% of ambient for glucose (Section 4.10.1.2). The latter seems more representative for most free molecules, so the 1%-of-ambient target is adopted in this preliminary scaling study, with the exception of oxygen (Section 4.10.1.1) and cryoprotectants (Section 4.10.1.7) for which a 0.1% target seems advisable.[1302] With no significant degradative biochemical reactions occurring after the first hour of intensive extraction operations, molecular pumping could continue indefinitely if desired, driving the concentrations of all relevant free molecules arbitrarily low with little further temporal urgency.

The standard 70 kg human body has a total volume ~60 L (0.060 m^3),[1303] which includes V_{blood} = 5.4 L of whole blood and V_{fluid} ~ 38.5 L of non-vascular fluid, including $V_{intracell}$ ~ 28 L of intracellular fluid and $V_{extracell}$ ~ 10.5 L of interstitial fluid.[1304] A cryopreserved patient who has had their blood removed and replaced with vasculoid (Section 4.6) thus contains V_{fluid} ~ 38.5 L of fluid volume at the water-ice melting temperature of 273 K (0 °C). This is the total fluid volume from which free molecules must be extracted.

The following subsections describe the technical means for molecular extraction, properly scaled to reduce free molecule concentrations in biological tissue to subreactive levels within a ~3600 sec window of time, achieving complete metabolic deactivation and stasis. The principal targets of molecular extraction include, in priority order: oxygen (Section 4.10.1.1), glucose (Section 4.10.1.2), metabolites and leaked blood components (Section 4.10.1.3), free ions (Section 4.10.1.4), neurotransmitters and other signaling molecules (Section 4.10.1.5), pre-mortem drugs (Section 4.10.1.6), cryoprotectants (Section 4.10.1.7), and unwanted cells, organelles, virions, and toxins (Section 4.10.1.8). A general summary of the process follows in Section 4.10.1.9.

[1302] It is a ***future research*** task to determine the actual threshold concentrations of all biologically relevant free molecules below which no significant degradative biochemical reactions will occur.

[1303] Freitas RA Jr. Nanomedicine, Volume I: Basic Capabilities, Landes Bioscience, Georgetown TX, 1999, Section 8.2, "Human Somatography"; http://www.nanomedicine.com/NMI/8.2.htm.

[1304] https://en.wikipedia.org/wiki/Fluid_compartments.

4.10.1.1 Oxygen

The most chemically reactive substance likely to be present in the cryopreserved human body is **molecular oxygen**. Oxygen is the primary oxidant facilitating chemical power in the body, so its presence risks prematurely restarting metabolic processes once molecular mobility is restored during tissue reliquidification. Oxygen could also chemically degrade biological structures, and this damage would go unrepaired and possibly grow during the time the body remains metabolically deactivated. Therefore molecular oxygen is the highest priority chemical substance that should be extracted from the cryopreserved body during reliquidification.

Oxygen is normally transported throughout the living body reversibly bound to hemoglobin trapped inside red blood cells called erythrocytes that constitute nearly half the volume of whole blood. During the cryopreservation process, the patient's blood is removed[1305] and replaced with cryoprotectant fluid that contains no red cells, so this principal source of O_2 will be largely absent during reliquidification. Similarly, residual gaseous oxygen present in the lungs, nasal passages, gastrointestinal tract and elsewhere will likely be entirely replaced by nitrogen by the time a patient who is being cryopreserved finally resides in a bath of liquid nitrogen as long-term storage begins. Molecular extraction should be performed in an oxygen-free environment (e.g., under pure nitrogen atmosphere) to prevent additional oxidation damage to exposed tissue surfaces.

The remaining source of molecular oxygen in a cryopreserved human body is the amount dissolved in the extracellular fluids and the cytosol of cells prior to freezing or vitrification. One estimate considers that the dissolved O_2 concentration in both arterial and venous blood plasma ranges between 1.6-3.9 mg/L (1.6-3.9 x 10^{-3} kg/m^3),[1306] and it might be reasonable to consider this the maximum plausible concentration in both extracellular fluid and cytosol.

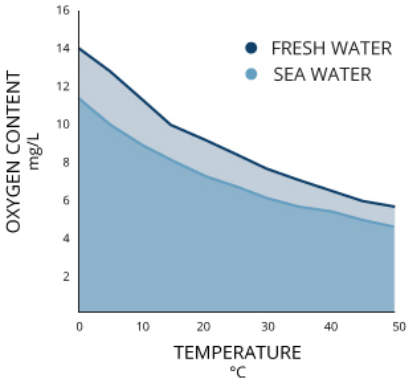

However, consideration of the solubility of oxygen in fresh and salt water as a function of temperature (chart, left),[1307] pressure, and salinity gives a slightly higher estimate. Solubility increases as temperature falls, and the chart shows that ~11 mg/L of O_2 (11 x 10^{-3} kg/m^3) will dissolve at 273 K (0 ºC) at sea level pressure in seawater, which has salinity very close to that of human blood plasma and extracellular fluid. We conservatively adopt this larger figure as representing the worst-case scenario ($c_{O2,high}$ = 11 x 10^{-3} kg/m^3), despite plausible arguments favoring the lower figure based on concentration gradient and diffusive flow.[1308]

How much oxygen must we extract? The partial pressure of oxygen in air at STP is 21.3 KPa (160 mmHg), falling to 13.3 KPa (100 mmHg) in the alveolar gas.[1309] Tissue cells are considered to be hypoxic at 0.5-2.5 KPa (4-19 mmHg) O_2 partial pressure,[1310] or 6.8-34 x

---

[1305] Unless there were few agonal morbidities and little ischemia, some residual blood should be assumed.

[1306] Freitas RA Jr. "Appendix B. Concentrations of Human Blood Components", Nanomedicine, Volume I: Basic Capabilities, Landes Bioscience, Georgetown, TX, 1999, pp. 387-392; http://www.nanomedicine.com/NMI/AppendixB.htm.

[1307] Fondriest Environmental, Inc. "Dissolved Oxygen." Fundamentals of Environmental Measurements. 19 Nov 2013; https://www.fondriest.com/environmental-measurements/parameters/water-quality/dissolved-oxygen/.

[1308] https://en.wikipedia.org/wiki/Diffusion#Diffusion_vs._bulk_flow.

10^{-3} kg/m^3, which is very close to the aqueous solubility limit. But metabolic activity continues during hypoxia.[1311] Even at O_2 levels as low as 0.005% (50 ppm, 0.005 KPa, 0.0375 mmHg), cell division will continue until reaching the late G_1 stage.[1312] It is only below 0.001% O_2 (10 ppm, 0.001 KPa, 0.0075 mmHg) or $c_{O2,low}$ = 1.3 x 10^{-5} kg/m^3 that no respiratory metabolism takes place.[1313]

Therefore, the extraction process must reduce the concentration of oxygen in the fluid water of the reliquidified cryopreserved human body by ~1000-fold, from an initial high concentration of $c_{O2,high}$ = 11 x 10^{-3} kg/m^3 (2.07 x 10^{-4} molecules/nm^3) down to a final low concentration of $c_{O2,low}$ = 1.3 x 10^{-5} kg/m^3 (2.45 x 10^{-7} molecules/nm^3), reducing the total mass of dissolved oxygen in the body from $c_{O2,high}$ V_{fluid} = 4.24 x 10^{-4} kg O_2 down to $c_{O2,low}$ V_{fluid} = 5.01 x 10^{-7} kg O_2. Using molecular sorting rotors with an appropriate O_2 binding site (Section H.2)[1314] and the iterative numerical model described in Section 4.10.1, this target may be accomplished in a τ_{total} = 3600 sec extraction time using an O_2 sorting rotor fleet of N_{fleet} = 3.01 x 10^{15} sorting rotors having total volume V_{fleet} = 4.13 x 10^{-3} cm^3, total mass M_{fleet} = 6.02 x 10^{-3} gm, and an average total power draw over the entire τ_{total} extraction time of $P_{fleet,avg}$ = 0.0214 watts. These figures may be compared to the entire vasculoid appliance which has a much larger device volume of ~**1200 cm^3**, mass ~**2000 gm**, and power draw of **30-200 watts**.[1315]

Even if reducing tissue oxygen to $c_{O2,low}$ = 1.3 x 10^{-5} kg/m^3 forecloses all respiratory metabolism in newly reliquidified cryopreserved tissues, nonenzymatic purely chemical oxidation can still take place. For example, lipid oxidation[1316] occurs in refrigerated foods when a random free radical abstracts a hydrogen from a fatty acid, leaving an alkyl radical that rapidly combines with oxygen to form a fatty acid peroxyl radical, which then abstracts a hydrogen from an adjacent fatty acid to form a hydroperoxide molecule and a new fatty acid alkyl radical, thus propagating the process.[1317] While spontaneous decomposition is

---

[1309] Sharma S, Hashmi MF, Rawat D. Partial Pressure of Oxygen (PO2). StatPearls, 2019 Sep 13; https://www.ncbi.nlm.nih.gov/books/NBK493219/.

[1310] Sitkovsky M, Lukashev D. Regulation of immune cells by local-tissue oxygen tension: HIF1 alpha and adenosine receptors. Nat Rev Immunol. 2005 Sep;5(9):712-21; https://www.ncbi.nlm.nih.gov/pubmed/16110315.

[1311] Ebbesen P, Eckardt KU, Ciampor F, Pettersen EO. Linking measured intercellular oxygen concentration to human cell functions. Acta Oncol. 2004;43(6):598-600; https://www.tandfonline.com/doi/pdf/10.1080/02841860410020220.

[1312] Graff P, Amellem O, Andersson KK, Pettersen EO. Role of ribonucleotide reductase in regulation of cell cycle progression during and after exposure to moderate hypoxia. Anticancer Res. 2002 Jan-Feb;22(1A):59-68; https://www.researchgate.net/profile/Erik_Pettersen/publication/11355055_Role_of_ribonucleotide_reductase_in_regulation_of_cell_cycle_progression_during_and_after_exposure_to_moderate_hypoxia/links/5857989f08ae81995eb7f67b/Role-of-ribonucleotide-reductase-in-regulation-of-cell-cycle-progression-during-and-after-exposure-to-moderate-hypoxia.pdf.

[1313] Froese G. The respiration of ascites tumour cells at low oxygen concentrations. Biochim Biophys Acta. 1962 Mar 12;57:509-19; https://www.sciencedirect.com/science/article/pii/0006300262911587. Amellem O, Pettersen EO. Cell inactivation and cell cycle inhibition as induced by extreme hypoxia: the possible role of cell cycle arrest as a protection against hypoxia-induced lethal damage. Cell Prolif. 1991 Mar;24(2):127-41; https://www.ncbi.nlm.nih.gov/pubmed/2009318.

[1314] Freitas RA Jr. Exploratory design in medical nanotechnology: a mechanical artificial red cell. Artif Cells Blood Substit Immobil Biotechnol. 1998 Jul;26(4):411-30; Section 2.2.3 "Sorting Rotor Binding Sites" (extended version); https://web.archive.org/web/20100613040242/https://foresight.org/Nanomedicine/Respirocytes1.html (Sec. 2.2.3).

[1315] Freitas RA Jr., Phoenix CJ. Vasculoid: A personal nanomedical appliance to replace human blood. J Evol Technol. 2002 Apr;11:1-139; http://www.jetpress.org/volume11/vasculoid.pdf.

[1316] Domínguez R, Pateiro M, Gagaoua M, Barba FJ, Zhang W, Lorenzo JM. A Comprehensive Review on Lipid Oxidation in Meat and Meat Products. Antioxidants (Basel). 2019 Sep 25;8(10): E429; https://www.mdpi.com/2076-3921/8/10/429/pdf.

[1317] Erickson MC. Lipid Oxidation: Flavor and Nutrition Quality Deterioration in Frozen Foods. In: Erickson MC, Hung YC, eds., Quality in Frozen Food. Springer, Boston MA, 1997, pp. 141-173; https://link.springer.com/chapter/10.1007/978-1-4615-5975-7_9.

unlikely at freezing temperatures,[1318] hydroperoxide breakdown during frozen storage is dominated by one-electron transfer from metal ions found principally in any heme and nonheme iron that may be present. In one food-related experiment, storage of mince at -20 ºC strongly retarded lipid oxidation compared to storage of similar material at -7 ºC.[1319] Other experiments have shown that uncooked ground beef had higher thiobarbituric acid content when stored at -12 ºC than when stored at -23 ºC or -34 ºC,[1320] and fish stored at -20 ºC for 13 months exhibited significant lipid and protein oxidation compared to similar samples stored at -30 ºC and -80 ºC.[1321] The phenomenon of "freezer burn", due in part to tissue oxidation, is well-known.[1322] This line of research is also relevant to understanding the condition of cryopreserved patients that spent a prolonged period at freezer temperatures prior to deep cooling. Further research is needed to determine to what extent these results may be due to exposure to high-concentration atmospheric oxygen, whether protein oxidation can be prevented by the infusion of antioxidants,[1323] and if concentrations of residual molecular oxygen lower than $c_{O2,low}$ will be required to prevent significant oxidation in newly reliquidified cryopreserved tissue.

Residual oxygen can also be converted to free radicals by ionizing radiation. If molecules suffer ~10^{15} "inactivating hits" per kg per rad of radiation exposure,[1324] and if we naively apply this rate to the breakage of O_2 molecules to form radicals, then the background terrestrial radiation level of ~0.1 rad/yr might create $n_{rad} = 1.69 \times 10^{-19}$ radicals/sec per residual O_2 molecule.[1325] If there are $n_{O2resid} = c_{O2,low} V_{fluid} / m_{O2} \sim 10^{19}$ residual O_2 molecules in the body, taking $m_{O2} = 5.31 \times 10^{-26}$ kg/molecule of O_2, then the rate of whole-body radiation-induced O_2 radical creation is $R_{O2radical} = n_{rad}\ n_{O2resid} = 1.7$ radicals/sec. A 30-week ($t_{P-E} \sim 1.8 \times 10^7$ sec) post-extraction revival procedure (**Table 13** in Section 4.16) would produce only $N_{radicals} = t_{P-E}\ R_{O2radical} = 3 \times 10^7$ radicals. Even if each radical alters the bonding of $n_{damage} = 10$ atoms before it is quenched, the total damage rate for a human body with $n_{body} \sim 7 \times 10^{27}$ atoms is $n_{damage}\ N_{radicals} / n_{body} \sim 10^{-19}$ which seems entirely negligible.

Carbon dioxide, the other major respiratory gas, has a similar distribution to molecular oxygen in cryopreserved bodies. At normal atmospheric concentrations and 25 ºC, CO_2 dissolves in water to a concentration of ~1.2×10^{-5} mole/L and red blood cells containing carbonic anhydrase produce bicarbonate

---

[1318] Terao J. Reactions of lipid hydroperoxides. In: Vigo-Pelfrey C, ed. Membrane Lipid Oxidation. CRC Press, Boca Raton FL, 1990, pp. 219-238.

[1319] Hwang KT, Regenstein JM. Protection of menhaden mince lipids from rancidity during frozen storage. J Food Sci. 1988;54:1120-1124; https://pubag.nal.usda.gov/catalog/1387397.

[1320] Bhattacharya M, Hanna MA, Mandigo RW. Lipid oxidation in ground beef patties as affected by time-temperature and product packaging parameters. J Food Sci. 1988;53:714-717; https://pubag.nal.usda.gov/catalog/1387354.

[1321] Baron CP, Kjaersgård IV, Jessen F, Jacobsen C. Protein and lipid oxidation during frozen storage of rainbow trout (*Oncorhynchus mykiss*). J Agric Food Chem. 2007 Oct 3;55(20):8118-25; https://www.ncbi.nlm.nih.gov/pubmed/17713921. See also: Tanaka R, *et al*. Effects of Chilled Storage, Freezing Rates, and Frozen Storage Temperature on Lipid Oxidation in Meat Blocks from Cultured Bluefin Tuna *Thunnus thynnus*. J Aquatic Food Prod Technol 2016;25(7):1073-1085; https://www.tandfonline.com/doi/abs/10.1080/10498850.2015.1010679.

[1322] https://en.wikipedia.org/wiki/Freezer_burn.

[1323] Saeed S, Howell NK. Effect of lipid oxidation and frozen storage on muscle proteins of Atlantic mackerel (*Scomber scombrus*). J Sci Food Agricul. 2002 Apr;82(5):579-586; https://onlinelibrary.wiley.com/doi/abs/10.1002/jsfa.1080.

[1324] Drexler KE. Nanosystems: Molecular Machinery, Manufacturing, and Computation, John Wiley & Sons, New York, 1992, Section 6.6.2 "Classical radiation target theory", p. 155; https://www.amazon.com/dp/0471575186/.

[1325] $n_{rad} = [(10^{15}$ hits/kg-rad)(0.032 kg/mole O_2)(1 radical/hit)(0.1 rad/yr)] / [(6.022 x 10^{23} molecules/mole)(3.14 x 10^7 sec/yr)] = 1.69 x 10^{-19} radicals/sec per residual O_2 molecule.

ion (HCO_3^-) at a concentration of ~2.2 x 10^{-6} mole/L,[1326] the extraction of which is discussed below in Section 4.10.1.5. Dissolved CO_2 can also form weak (pH 5.7) carbonic acid (H_2CO_3) in amounts (~2 x 10^{-8} mole/L or 8.8 x 10^{-7} kg/m^3) that seem too small to pose any serious risk of tissue damage. Interestingly, an artificially lowered systemic concentration of CO_2, or hypocapnia,[1327] could pose another set of risks during the post-warmup normal metabolic phase of revival (Section 4.14.3).[1328]

4.10.1.2 Glucose and ATP

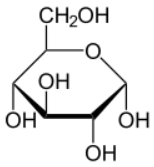

Glucose (image, right) is the most ubiquitous fuel molecule in biology. It is used as an energy source by almost all living organisms from bacteria to humans,[1329] and is the human body's principal source of energy via aerobic respiration.[1330] As the primary energy fuel in the body, the presence of glucose risks prematurely restarting metabolic processes once molecular mobility is restored during tissue reliquidification. (Fatty acids[1331] and amino acids[1332] can also be combined with oxygen to produce energy in the cell; their extraction from reliquidified tissue is described in Section 4.10.1.3.)

There are typically ~18 gm of native glucose in the human body,[1333] of which 4 gm are present in the blood[1334] (which has a normal glucose concentration of 0.7-1.05 kg/m^3).[1335] Since all blood has been replaced in cryopreserved patients, this might leave up to ~14 gm of native free glucose in the body tissues,[1336] needing to be extracted. There is normally a somewhat higher concentration of glucose outside of the cell. In contrast to the normal blood glucose concentration of 4-6 mM (0.7-1.05 kg/m^3), a typical

---

[1326] https://en.wikipedia.org/wiki/Carbonic_acid#pH_and_composition_of_carbonic_acid_solutions.
[1327] https://en.wikipedia.org/wiki/Hypocapnia.

[1328] Laffey JG, Engelberts D, Kavanagh BP. Injurious effects of hypocapnic alkalosis in the isolated lung. Am J Respir Crit Care Med. 2000 Aug;162(2 Pt 1):399-405; http://citeseerx.ist.psu.edu/viewdoc/download?doi=10.1.1.333.7618&rep=rep1&type=pdf.

[1329] https://en.wikipedia.org/wiki/Glucose#Energy_source.
[1330] https://en.wikipedia.org/wiki/Cellular_respiration#Aerobic_respiration.

[1331] Stryer L. Fatty acid metabolism. In: Biochemistry, 4th Ed, W.H. Freeman and Company, New York, 1995, pp. 603-628. See also: https://en.wikipedia.org/wiki/Fatty_acid_metabolism.

[1332] Sakami W, Harrington H. Amino acid metabolism. Annu Rev Biochem. 1963;32:355-98; https://www.annualreviews.org/doi/abs/10.1146/annurev.bi.32.070163.002035?journalCode=biochem. Felig P, Owen OE, Wahren J, Cahill GF Jr. Amino acid metabolism during prolonged starvation. J Clin Invest. 1969 Mar;48(3):584-94; https://dm5migu4zj3pb.cloudfront.net/manuscripts/106000/106017/JCI69106017.pdf. Felig P. Amino acid metabolism in man. Annu Rev Biochem. 1975;44:933-55; https://www.annualreviews.org/doi/abs/10.1146/annurev.bi.44.070175.004441?journalCode=biochem.

[1333] Satyanarayana U. Biochemistry. Elsevier Health Sciences, 2014, p. 674; https://www.amazon.com/Biochemistry-Dr-U-Satyanarayana/dp/8187134801/.

[1334] Wasserman DH. Four grams of glucose. Am J Physiol Endocrinol Metab. 2009 Jan;296(1):E11-21; https://www.ncbi.nlm.nih.gov/pmc/articles/PMC2636990/.

[1335] Freitas RA Jr. "Appendix B. Concentrations of Human Blood Components", Nanomedicine, Volume I: Basic Capabilities, Landes Bioscience, Georgetown, TX, 1999, pp. 387-392; http://www.nanomedicine.com/NMI/AppendixB.htm.

[1336] Some of this may be concentrated in the liver, an organ that produces 180-220 gm/day of glucose while the patient is alive. Satyanarayana U. Biochemistry. Elsevier Health Sciences, 2014, p. 674.

intracellular glucose concentration might be, for example, 2 mM (0.36 kg/m^3) in rat adipose cells[1337] or 0.7-2.5 mM (0.13-0.45 kg/m^3) for the *in vivo* cytosolic neuronal glucose concentration in cortical neurons from awake mice.[1338] The brain gets most of its energy from the oxygen-dependent metabolism of glucose,[1339] although the brain can also derive energy from other sources including ketones,[1340] medium chain fatty acids (caprylic and heptanoic acids),[1341] lactate,[1342] acetate,[1343] and possibly amino acids,[1344] the extractions of which are covered in Section 4.10.1.3.

Glucose concentrations in the brain are typically 4-6 mM (0.72-1.08 kg/m^3) in normal times, 2-3 mM (0.36-0.54 kg/m^3) when fasting,[1345] and <1 mM (<0.18 kg/m^3) during confusion and coma. When blood glucose levels fall below 0.55 mM (0.1 kg/m^3),[1346] most neurons become electrically silent and nonfunctional, resulting in neuroglycopenia[1347] and coma. While rat cortical neurons subjected to 3 hours of total oxygen and glucose deprivation show 60% cell viability after 1 hour (25% after 3 hours, 10% after 6 hours, and 0% after 24 hours),[1348] it has been determined experimentally[1349] that the glycolytic rate[1350]

[1337] Foley JE, Cushman SW, Salans LB. Intracellular glucose concentration in small and large rat adipose cells. Am J Physiol. 1980 Feb;238(2):E180-5; https://www.ncbi.nlm.nih.gov/pubmed/6987896.

[1338] Díaz-García CM, Lahmann C, Martínez-François JR, Li B, Koveal D, Nathwani N, Rahman M, Keller JP, Marvin JS, Looger LL, Yellen G. Quantitative *in vivo* imaging of neuronal glucose concentrations with a genetically encoded fluorescence lifetime sensor. J Neurosci Res. 2019 Aug;97(8):946-960; https://onlinelibrary.wiley.com/doi/pdf/10.1002/jnr.24433.

[1339] https://en.wikipedia.org/wiki/Brain#Metabolism.
[1340] https://en.wikipedia.org/wiki/Ketone_bodies#Fuel_utilization_across_different_organs.

[1341] Ebert D, Haller RG, Walton ME. Energy contribution of octanoate to intact rat brain metabolism measured by ^{13}C nuclear magnetic resonance spectroscopy. J Neurosci. 2003 Jul 2;23(13):5928-35; https://www.ncbi.nlm.nih.gov/pmc/articles/PMC6741266/. Marin-Valencia I, Good LB, Ma Q, Malloy CR, Pascual JM. Heptanoate as a neural fuel: energetic and neurotransmitter precursors in normal and glucose transporter I-deficient (G1D) brain. J Cereb Blood Flow Metab. 2013 Feb;33(2):175-82; https://www.ncbi.nlm.nih.gov/pmc/articles/PMC3564188/.

[1342] Boumezbeur F, Petersen KF, Cline GW, Mason GF, Behar KL, Shulman GI, Rothman DL. The contribution of blood lactate to brain energy metabolism in humans measured by dynamic ^{13}C nuclear magnetic resonance spectroscopy. J Neurosci. 2010 Oct 20;30(42):13983-91; https://www.ncbi.nlm.nih.gov/pmc/articles/PMC2996729/.

[1343] Deelchand DK, Shestov AA, Koski DM, Uğurbil K, Henry PG. Acetate transport and utilization in the rat brain. J Neurochem. 2009 May;109 Suppl 1:46-54; https://www.ncbi.nlm.nih.gov/pmc/articles/PMC2722917/.

[1344] Soengas JL, Aldegunde M. Energy metabolism of fish brain. Comp Biochem Physiol B Biochem Mol Biol. 2002 Mar;131(3):271-96; https://www.ncbi.nlm.nih.gov/pubmed/11959012

[1345] Dwyer D. Glucose Metabolism in the Brain. Academic Press, NY, 2002, p. xiii; https://www.amazon.com/Glucose-Metabolism-International-Review-Neurobiology-dp-0123668522/dp/0123668522/.

[1346] https://en.wikipedia.org/wiki/Hypoglycemia#Pathophysiology.
[1347] https://en.wikipedia.org/wiki/Neuroglycopenia.

[1348] Jones PA, May GR, McLuckie JA, Iwashita A, Sharkey J. Apoptosis is not an invariable component of *in vitro* models of cortical cerebral ischaemia. Cell Res. 2004 Jun;14(3):241-250; https://www.nature.com/articles/7290225.

[1349] Vander Heiden MG, Plas DR, Rathmell JC, Fox CJ, Harris MH, Thompson CB. Growth factors can influence cell growth and survival through effects on glucose metabolism. Mol Cell Biol. 2001 Sep;21(17):5899-912; https://www.ncbi.nlm.nih.gov/pmc/articles/PMC87309/.

[1350] The glycolytic rate is the rate at which glycolysis, the first step in glucose metabolism, occurs in living cells. Glycolysis (https://en.wikipedia.org/wiki/Glycolysis) is the metabolic pathway that converts glucose ($C_6H_{12}O_6$) into pyruvate (CH_3COCOO^-) and a hydrogen ion (H^+), the initial step in glucose metabolism.

falls essentially to zero at a glucose concentration of ≤0.01 mM (≤0.0018 kg/m^3). This suggests that the presence of glucose at ≤0.01 mM is insufficient for glucose-based metabolism to proceed.

Assuming that the extraction requirement is to reduce a post-mortem native glucose concentration of $c_{Glucose,high}$ ~ 1 mM (0.18 kg/m^3 or 6 x 10^{-4} molecules/nm^3) to a post-extraction glucose concentration of $c_{Glucose,low}$ ~ 0.01 mM (0.0018 kg/m^3 or 0.06 x 10^{-4} molecules/nm^3) throughout the V_{fluid} ~ 38.5 L whole-body intracellular and interstitial fluid volume of a 70 kg human body, sorting rotors (Section 4.10.1) with appropriate glucose binding sites[1351] (Section H.2) can accomplish this in a τ_{total} = 3600 sec extraction time using a glucose sorting rotor fleet of N_{fleet} = 1.00 x 10^{16} sorting rotors having total volume V_{fleet} = 1.45 x 10^{-2} cm^3, total mass M_{fleet} = 2.12 x 10^{-2} gm, and an average total power draw over the entire τ_{total} extraction time of $P_{fleet,avg}$ = 0.0353 watts.

It should be noted that glucose is also present at a 90 mM concentration in the carrier solution for the commonly used M22 cryoprotectant. At this concentration, assuming 60% of the aqueous intracellular and interstitial volume (V_{fluid} = 38.5 L) has been replaced by M22 components, the tissues of a whole-body patient could contain up to 375 gm of non-native glucose that must also be removed. The extraction of this non-native glucose is described in Section 4.10.1.7.

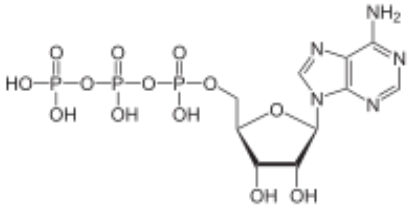

Adenosine triphosphate (ATP)[1352] (image, right) is a complex organic chemical that provides energy to drive many processes in living cells such as muscle contraction, nerve impulse propagation, and chemical synthesis. ATP is found in all forms of life and is often referred to as the "molecular unit of currency" of intracellular energy transfer.[1353] The live human body recycles its own body weight equivalent in ATP each day.[1354] The typical intracellular concentration of ATP (0.5072 kg/mole) is 1-10 μmole per gm of tissue (0.53-5.3 kg/m^3, taking ρ_{tissue} ~ 1064 kg/m^3) in many eukaryotes,[1355] implying the presence of 0.03-0.3 kg ATP in an entire 0.06 m^3 live human body. However, ATP is very actively recycled to an equivalent of 500-750 times per day[1356] in normal human metabolism (wherein ~30 ATP molecules are produced from each molecule of glucose),[1357] so a living patient's existing intracellular ATP energy stores should be metabolically exhausted after only 2-3 minutes of warm ischemia,[1358] leaving virtually none to be extracted

---

[1351] Bennett WS Jr, Steitz TA. Glucose-induced conformational change in yeast hexokinase. Proc Natl Acad Sci U S A. 1978 Oct;75(10):4848-52; https://www.ncbi.nlm.nih.gov/pmc/articles/PMC336218/. Hresko RC, Hruz PW. HIV protease inhibitors act as competitive inhibitors of the cytoplasmic glucose binding site of GLUTs with differing affinities for GLUT1 and GLUT4. PLoS One. 2011;6(9):e25237; https://www.ncbi.nlm.nih.gov/pmc/articles/PMC3179492/. Palani K, Kumaran D, Burley SK, Swaminathan S. Structure of a periplasmic glucose-binding protein from *Thermotoga maritima*. Acta Crystallogr Sect F Struct Biol Cryst Commun. 2012 Dec 1;68(Pt 12):1460-4; https://www.ncbi.nlm.nih.gov/pmc/articles/PMC3509965/.

[1352] https://en.wikipedia.org/wiki/Adenosine_triphosphate.

[1353] Knowles JR. Enzyme-catalyzed phosphoryl transfer reactions. Annu Rev Biochem. 1980;49:877-919; https://pdfs.semanticscholar.org/3afc/f5cd92c824e192da25465b30fe78883301c2.pdf.

[1354] Törnroth-Horsefield S, Neutze R. Opening and closing the metabolite gate. Proc Natl Acad Sci U S A. 2008 Dec 16;105(50):19565-6; https://www.ncbi.nlm.nih.gov/pmc/articles/PMC2604989/.

[1355] Beis I, Newsholme EA. The contents of adenine nucleotides, phosphagens and some glycolytic intermediates in resting muscles from vertebrates and invertebrates. Biochem J. 1975 Oct;152(1):23-32; https://www.ncbi.nlm.nih.gov/pmc/articles/PMC1172435/pdf/biochemj00546-0037.pdf.

[1356] https://en.wikipedia.org/wiki/Adenosine_triphosphate#ATP_recycling.
[1357] https://en.wikipedia.org/wiki/Adenosine_triphosphate#Production,_aerobic_conditions.

[1358] Longevity of metabolically interrupted ATP recycling: (86,400 sec/day) / (500-750 cycles/day) = 115-173 sec/cycle.

from a cryopreserved patient. Nevertheless, the full physiological cellular concentration of ATP is conservatively assumed to be present and necessary to extract in the inventory of cell metabolites analyzed in Section 4.10.1.3, below; if less is present, as could be directly measured experimentally in ***future research***, the required number of sorting rotors and the power draw can be correspondingly reduced.

Note that when ATP has been exhausted during ischemia, a cell derives its energy from the pyrophosphate bonds of ADP as they are degraded, first to adenosine monophosphate (AMP), and then to adenosine which diffuses freely out of the cell, dramatically reducing the intracellular pool of adenine nucleotides which are the precursors for ATP.[1359]

How much ATP might still be present after a long cessation of metabolic function? The normal cell-free human plasma concentration of ATP is commonly reported as ~1000 nmol/L (5×10^{-4} kg/m^3), but when the measured effects of hemolysis (i.e., damaged circulating erythrocytes spilling their contents into the plasma) are statistically removed, the background plasma concentration of ATP is estimated as only 28 nmol/L (1.42×10^{-5} kg/m^3).[1360] This is ~100,000 times lower than the normal intracellular levels in metabolically active cells and may approximate the baseline ATP concentration in metabolically inactive tissue, and thus also approximate the residual ATP concentration in the extracellular fluids of cryopreserved tissue. A ***future research*** task is to validate the assumption that an ATP concentration as low as 28 nmol/L is sufficient to ensure no biological activity, and thus that no further ATP needs to be extracted from the cryopreserved tissue during the revival process. ATP extraction, if necessary, would add only a small number of new sorting rotors to the estimated total.

During prolonged ischemia in the post-mortem period prior to cryopreservation, the cell also exhausts its intracellular stores of glycogen.[1361]

4.10.1.3 Cell Metabolites and Leaked Blood Plasma Components

Each cell in the body of a cryopreserved patient will contain a large number of metabolites – small reactive molecules that participate in metabolic processes during life – including biochemical reactants, products, and reaction intermediates. As the worst-case scenario, we must conservatively assume that cell membrane damage during the post-mortem ischemic and cooldown period has allowed the chemical contents of all cells to escape into the interstitial fluid compartment to occupy the entire fluid volume (V_{fluid}), and at the same concentrations as are found in the cell. While lists of cryotissue-degradation-active mammalian cytoplasmic metabolites are not readily available, databases of *all* known human metabolites do exist. For example, in March 2021 the Human Metabolome Database (HMDB)[1362] provided information on 114,304 metabolite species, though most will probably not contribute to cell degradation in warmed cryotissue if unextracted. An inventory of the 103 most abundant metabolite molecules present in a glucose-fed *E. coli* cell,[1363] yielding a total cytosolic concentration of 231 mM for all metabolites, may be more representative

---

[1359] Goudin M, Dubois P. Impact of ischemia on cellular metabolism. In: Aronow WS, ed., Artery Bypass, 2013 Mar 13; https://www.intechopen.com/books/artery-bypass/impact-of-ischemia-on-cellular-metabolism.

[1360] Gorman MW, Feigl EO, Buffington CW. Human plasma ATP concentration. Clin Chem. 2007 Feb;53(2):318-25; http://clinchem.aaccjnls.org/content/clinchem/53/2/318.full.pdf.

[1361] https://en.wikipedia.org/wiki/Glycogen.

[1362] The Human Metabolome Database, HMDB Version 4.0; https://hmdb.ca/.

[1363] Table 1. Intracellular concentrations of the most abundant metabolites in glucose-fed, exponentially growing *E. coli* measured via mass spectroscopy. Adapted from: Bennett *et al.*, Nature Chemical Biology, 2009. http://book.bionumbers.org/what-are-the-concentrations-of-free-metabolites-in-cells/.

of the most important metabolites requiring extraction (Appendix I). The amounts listed as being physiologically present (conservatively including full physiological ATP; Section 4.10.1.2) are assumed to be biologically active at that concentration.

We will also conservatively assume, as a worst-case scenario, that the vascular compartment has become completely porous during the post-mortem ischemic and cooldown period, and to a lesser degree during the prethaw warmup period, allowing blood plasma components to diffuse into, and become thoroughly mixed with, the nonvascular fluid volume. An inventory of 232 blood plasma components and their maximum normal concentrations in human blood[1364] should be representative of the numbers and types of molecules involved (Appendix J). Since the vascular volume is subsequently emptied during vasculoid installation, the contribution of blood plasma molecule concentration to the total small-molecule concentration in the remaining fluid volume of the cryopreserved patient is $k_{leak} = V_{blood} / (V_{blood} + V_{fluid}) \sim 12.3\%$. The contribution of metabolite concentration to the total is taken as $(1 - k_{leak}) = V_{fluid} / (V_{blood} + V_{fluid}) \sim 87.7\%$. These two sets of components are weighted accordingly in the calculations here.

Assuming that the extraction requirement is to reduce post-mortem metabolite and leaked blood plasma molecules to 1% of their maximum living concentrations throughout the $V_{fluid} \sim 38.5$ L whole-body intracellular and interstitial fluid volume of a 70 kg human body, and using the iterative numerical model described in Section 4.10.1, sorting rotors with appropriate binding sites (Appendix H) are estimated to perform the deconcentration in a $\tau_{total} = 3600$ sec extraction time using a fleet of $N_{fleet,metabolite} = 2.19 \times 10^{18}$ sorting rotors to collect the 103 metabolite molecules and a fleet of $N_{fleet,plasma} = 4.76 \times 10^{17}$ sorting rotors to collect the 232 leaked plasma molecules, with a combined fleet volume of $V_{fleet} = 3.65$ cm^3, fleet mass of $M_{fleet} = 5.32$ gm, and an average total fleet power draw over the entire τ_{total} extraction time of $P_{fleet,avg} = 2.21$ watts.

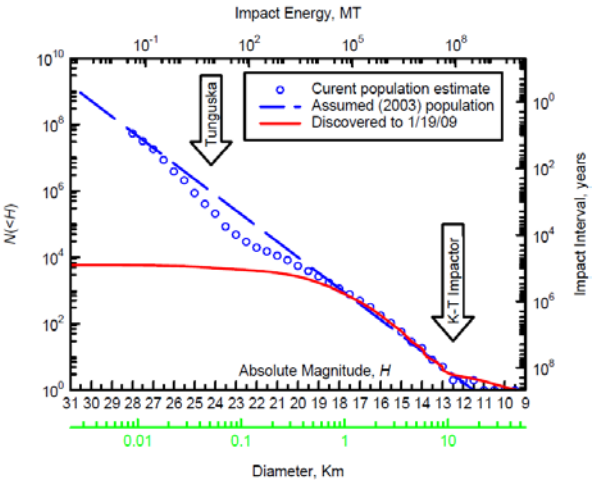

This may be an acceptable first estimate for the mass and power draw of sorting rotors needed to deconcentrate the 335 molecules on both lists. However, there are likely to be many moderate- to low-concentration components that are missing from both lists because of our incomplete knowledge of the precise contents of blood plasma and cytoplasm. If the lists are assumed to be nearly complete for the most common molecules at the highest concentrations, there is a simple method to estimate how much may be missing. One well-known example is the method used by astronomers to estimate the size distribution of asteroids. The log-log chart above shows the number of asteroids on the leftmost vertical axis and the size of those asteroids on the bottommost horizontal axis, in green.[1365] The red curve shows the distribution of telescopically observed asteroids as of 2009. The linear trend observed in the rightmost part of the red curve (the actual data) can be extended to predict the log-linear size distribution (blue curve) of the missing

---

[1364] Freitas RA Jr. "Appendix B. Concentrations of Human Blood Components", Nanomedicine, Volume I: Basic Capabilities, Landes Bioscience, Georgetown, TX, 1999, pp. 387-392; http://www.nanomedicine.com/NMI/AppendixB.htm.

[1365] National Research Council. Defending Planet Earth: Near-Earth Object Surveys and Hazard Mitigation Strategies. National Academies Press, Washington DC, 2010, Table 2.4, p. 17; https://www.boulder.swri.edu/~bottke/Reprints/National_Academies_NEO_Report_Defending_Planet_Earth.pdf.

asteroids (the gap between red and blue curves) that had not yet been observed because they are too distant or too small.

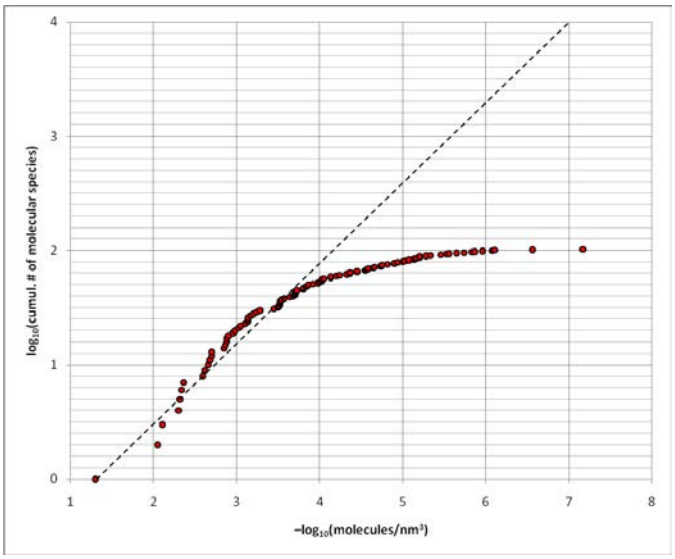

In similar manner, the chart at left shows a log-log graph of the cumulative number of cell metabolite molecular species as a function of cytosolic concentration using the core data from Appendix I. Analogously to the asteroid size chart, the observed metabolite list becomes incomplete at concentrations of ~10^{-4} molecules/nm^3 and below. To crudely assess the number of missing metabolites, we estimate the gap between the assumed "actual" line (dashed line) and the "observed data" curve (red data points) at four concentration levels (10^{-4}, 10^{-5}, 10^{-6}, and 10^{-7} molecules/nm^3). This estimation process implies the existence of ~12,127 extra molecular species requiring 3.26 x 10^{18} additional rotors to complete all new extractions in τ_{total} = 3600 sec.

The chart at right, based on Appendix J data for leaked blood plasma chemicals, shows the same pattern, with incomplete observations of distinct molecular species appearing at concentrations below ~10^{-5} molecules/nm^3. Estimates of the number of missing species at four concentration levels (10^{-6}, 10^{-7}, 10^{-8}, and 10^{-9} molecules/nm^3) suggests the possible existence of ~12,591 extra molecular species requiring 1.09 x 10^{18} additional rotors to complete the new extractions in τ_{total} = 3600 sec.

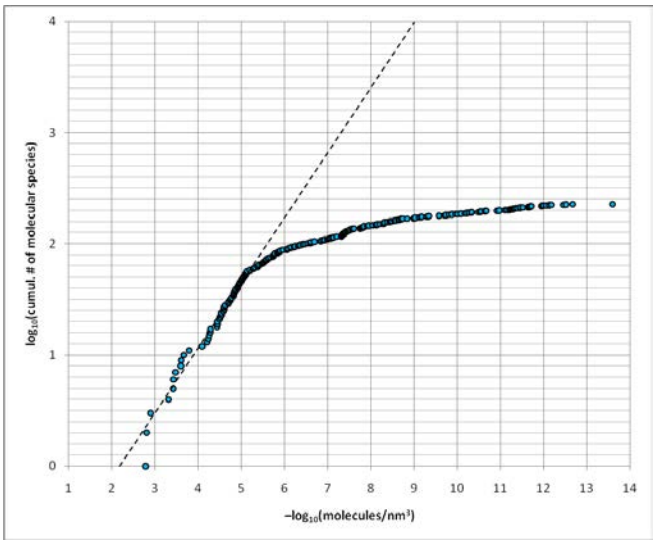

If this latter analysis was extended to even lower concentrations (e.g., to somewhere between 10^{-10} and 10^{-13} molecules/nm^3), and included all **114,184** metabolite species listed in the Human Metabolome Database[1366] instead of just the 12,127 + 12,591 = 24,718 species estimated above, this would add only (114,184 species – 24,718 species) (9.84 x 10^{-5} gm/species; Appendix J) = 8.8 grams of extra rotor mass to the existing ~15.7 gram total (**Table 9** in Section 4.10.1.9), a minor factor that would not alter the general conclusions of the present study.[1367]

[1366] The Human Metabolome Database, HMDB Version 4.0; https://hmdb.ca/.

[1367] Ellert van Koperen estimated that in 2014 there were ~9.8 million synthetic and natural compounds available to purchase, of which the naturally-occurring compounds might represent up to ~5% of the total, or ~**500,000** natural compounds; https://chemistry.stackexchange.com/a/16952.

These results also appear relatively insensitive to the targeted concentration decrement. For example, if the extraction of glutamate (the highest-concentration free metabolite in Appendix I) is extended beyond 1% to only 0.1% of its maximum normal concentration in the same τ_{total} = 3600 sec extraction time, the estimated number of rotors required increases only very slightly from 3.00 x 10^{17} rotors to 3.02 x 10^{17} rotors although the average power drawn by the glutamate extraction fleet increases tenfold from 2.71 x 10^{-3} W to 2.71 x 10^{-2} W. In the case of adenosine (the lowest-concentration free metabolite in Appendix I), extending the concentration decrement target from 1% to 0.1% increases the estimated number of rotors slightly from 1.12 x 10^{14} rotors to 1.29 x 10^{14} rotors while the average power drawn by the adenosine extraction fleet is almost unchanged, rising from 2.88 x 10^{-5} W to only 2.92 x 10^{-5} W.

This approach potentially requires designing perhaps ~25,000 binding sites (Appendix H) targeting each of the molecules we seek to extract. Some of the leaked blood plasma components listed in Appendix J need multiple binding site designs because of the many distinct molecular types within that category, e.g., there are many different kinds of lipids, fatty acids, triglycerides, amino acids, ketone bodies, mucopolysaccharides, and bile acids, but this adds only modestly to the total workload. Fortunately, computational binding site design (Appendix H) should be heavily automated[1368] by the time cryostasis revival technologies are implemented.

Future research tasks include:

(1) compiling a comprehensive inventory of reactive intracellular metabolites, including molecular types and concentrations, in post-mortem human tissue;

(2) compiling a comprehensive inventory of reactive plasma components, including molecular types and concentrations, in post-mortem human blood plasma;

(3) validation or correction of the assumption made here that a 100-fold decrement in the concentration of each of the cell metabolite or blood plasma reactive molecular species is sufficient dilution to effectively ensure complete biochemical stasis (i.e., negligible reaction rates) at ~273 K (0 ºC) temperatures over the timespans that may be required to complete all post-extraction revival processes, perhaps on the order of ~10^{6}-10^{7} sec (12-120 days; **Table 13** in Section 4.16);

(4) determining the priority sequence in which molecular species should be extracted in order to minimize the risk of biochemical reaction, chemical degradation, enzymatic synthesis, enzymatic decomposition, and biological activation; and

(5) developing the technology of automated binding site design, so that highly selective binding sites for large numbers of target molecules can be generated quickly with a minimum of scarce human labor.

[1368] Salis HM, Mirsky EA, Voigt CA. Automated design of synthetic ribosome binding sites to control protein expression. Nat Biotechnol. 2009;27(10):946–950; https://www.ncbi.nlm.nih.gov/pmc/articles/PMC2782888/pdf/nihms145791.pdf. Jiménez J, Doerr S, Martínez-Rosell G, Rose AS, De Fabritiis G. DeepSite: protein-binding site predictor using 3D-convolutional neural networks. Bioinformatics. 2017;33(19):3036–3042; https://eclass.uoa.gr/modules/document/file.php/D464/Course%20Projects/deepsite.pdf. Khersonsky O, Lipsh R, Avizemer Z, *et al*. Automated Design of Efficient and Functionally Diverse Enzyme Repertoires. Mol Cell. 2018;72(1):178–186.e5; https://www.ncbi.nlm.nih.gov/pmc/articles/PMC6193528/pdf/emss-79915.pdf. Krivák R, Hoksza D. P2Rank: machine learning based tool for rapid and accurate prediction of ligand binding sites from protein structure. J Cheminform. 2018 Aug 14;10(1):39; https://www.ncbi.nlm.nih.gov/pmc/articles/PMC6091426/. Hossain A, Lopez E, Halper SM, Cetnar DP, Reis AC, Strickland D, Klavins E, Salis HM. Automated design of thousands of nonrepetitive parts for engineering stable genetic systems. Nat Biotechnol. 2020 Dec;38(12):1466-1475; https://pubmed.ncbi.nlm.nih.gov/32661437/.

4.10.1.4 Free Ions

Free ions mediate action potentials in neurons, participate in molecular signaling and enzymatic activity, and can poison cell metabolism if present in excessive concentrations, hence are the next highest priority species for molecular extraction from the body of the cryopreserved patient. The most common free ions found in human blood plasma, interstitial fluid, and the cytosol are K^+, Na^+, Cl^-, free Ca^{2+}, free Mg^{2+},[1369] HCO_3^-, HPO_4^{2-}, and H^+ (H_3O^+) or hydronium ion at the typical cytosolic pH ~ 7.[1370]

The minimum energy required to pump charged ions is the change in free energy[1371] in transporting the charged species from one environment having concentration c_m to a second environment having concentration $c_{transport}$, which may be estimated as $\Delta G_{ion}(t) = k_B T_{icewater} \ln(c_{transport}/c_m(t)) + (Z_e F \Delta V / N_A)$, where Z_e = 1 or 2 (the number of charges transported per ion), ΔV = the electrical potential across which the ion is transported (typically 40-80 mV for biological cell membranes and 70-80 mV resting potential for excitable cells),[1372] F = 9.65 x 10^4 coul/mole (Faraday constant), and N_A = 6.022 x 10^{23} molecules/mole (Avogadro's number).

Appendix K lists the typical concentrations of these ions in the mammalian cytosol (intracellular) and the blood plasma or interstitial (extracellular) compartments.[1373] Conservatively assuming that complete mixing has occurred during the post-mortem ischemic/cooldown and the prethaw/warmup periods, the contribution of the intracellular components to the total ion concentration in the fluid volume is $k_{intracell} = V_{intracell} / (V_{intracell} + V_{extracell}) \sim 72.7\%$. The contribution of extracellular concentration to the total is taken as $k_{extracell} = (1 - k_{intracell}) = V_{extracell} / (V_{intracell} + V_{extracell}) \sim 27.3\%$. These two sets of components are weighted accordingly in the calculations here.

Assuming that the extraction requirement is to reduce post-mortem ions to 1% of their typical living concentrations (a ~100-fold decrement)[1374] throughout the $V_{fluid} = V_{intracell} + V_{extracell} \sim 38.5$ L whole-body intracellular and extracellular fluid volume of a 70 kg human body, and using the iterative numerical process described in Section 4.10.1, sorting rotors with appropriate binding sites are estimated to accomplish this task in a τ_{total} = 3600 sec extraction time using a fleet of N_{fleet} = 8.32 x 10^{17} ion extraction sorting rotors with a combined fleet volume of V_{fleet} = 1.14 cm^3, total mass M_{fleet} = 1.66 gm, and an average total fleet power draw over the entire τ_{total} extraction time of $P_{fleet,avg}$ = 16.0 watts. Rapid

---

[1369] Magnesium inside mammalian cells is mostly bound to ATP, ribosomes, and other macromolecules and metabolites.

[1370] https://en.wikipedia.org/wiki/Intracellular_pH.

[1371] Freitas RA Jr. Nanomedicine, Volume I: Basic Capabilities, Landes Bioscience, Georgetown TX, 1999, Section 3.4.1, "Transporter Pumps"; http://www.nanomedicine.com/NMI/3.4.1.htm.

[1372] https://en.wikipedia.org/wiki/Membrane_potential.

[1373] Lodish HF. Molecular Cell Biology. Scientific American Books, New York, 1999; http://book.bionumbers.org/what-are-the-concentrations-of-different-ions-in-cells/; and https://opentextbc.ca/anatomyandphysiology/chapter/26-1-body-fluids-and-fluid-compartments/.

[1374] Extracellular/intracellular sodium ion concentration in neurons is 145 mM / 5-15 mM, giving a 10-29X decrement; intracellular/extracellular potassium ion concentration in neurons is 140 mM / 5 mM, giving a 29X decrement.* Normal sodium ion blood concentration is ~135-145 mM, whereas severe hyponatremia ensues at only 115 mM causing confusion, seizures, and coma (https://en.wikipedia.org/wiki/Hyponatremia). Potassium ion blood concentration is normally 3.5-5 mM, falling to 2-2.5 mM (a ~2X decrement) during severe hypokalemia which causes flaccid paralysis, hyporeflexia, rhabdomyolysis and respiratory depression (https://en.wikipedia.org/wiki/Hypokalemia).

* Izhikevich EM. Dynamical systems in neuroscience: the geometry of excitability and bursting. Cambridge: MIT Press; 2007; http://math.tut.fi/courses/MAT-35006/pIIexam/Izhikevich_Ch1-2.pdf

extraction of ions demands the highest power draw of any molecular component due to charge repulsion. Note that if extraction of intracellular K^+ and extracellular Na^+ and Cl^- is allowed to take 12 hours instead of 1 hour, the ion extraction fleet is nearly halved to 4.41 x 10^{17} rotors and the total power demand is cut by two-thirds to 5.18 W.

While direct measurement of free intracellular phosphate concentration supports the 0.5-5 mM range used here,[1375] other sources mention intracellular phosphate concentrations as high as 95 mM.[1376] These higher figures might include bound inorganic polyphosphate – a linear polymer comprising 15-750 phosphate residues that is present in intracellular vacuoles in all cell types where it functions as a phosphate store.[1377] (Poly P has been found in mammalian cells at 0.15-1.5 μM.)[1378] ***Future research*** should include a comprehensive literature search and direct experimental measurements if necessary to resolve this apparent ambiguity, since higher intracellular free phosphate concentrations could increase the ion-extraction rotor power requirements by up to ~50%.

Binding site designs will be fewer in number but more challenging, since ions generally don't exist in isolation but are complexed with water or other molecules. For example, Na^+ ion in aqueous solution is usually present as $[Na(H_20)_6]^+$,[1379] and similarly for chloride ions, so rotor binding sites must accommodate these bulky complexes. Specific binding sites for the sodium ion/water cluster,[1380] chloride ion/water cluster,[1381] and magnesium ion/water cluster[1382] are known, but ***future research*** should expand this knowledge and extend it to additional relevant ion/water clusters.

Most free radicals[1383] that might have been created during the ischemic, cryopreservative, or warmup phases will have quickly reacted and quenched, doing some small damage but no longer needing extraction. If free radicals are being generated at too high a rate during the time period allotted for post-extraction revival processes (~10^6-10^7 sec), antioxidants or damage-reducing enzymes could be injected to neutralize

---

[1375] Bevington A, Mundy KI, Yates AJ, Kanis JA, Russell RG, Taylor DJ, Rajagopalan B, Radda GK. A study of intracellular orthophosphate concentration in human muscle and erythrocytes by ^{31}P nuclear magnetic resonance spectroscopy and selective chemical assay. Clin Sci (Lond) 1986;71(6):729-735; https://pdfs.semanticscholar.org/1c2c/6e47a484636cac38e323818602667de33f69.pdf.

[1376] e.g., Figure 4. The Concentrations of Different Elements in Key Bodily Fluids. In: "181 26.1 Body Fluids and Fluid Compartments," Human Anatomy and Physiology, Rice University; OpenStax, Anatomy & Physiology. OpenStax CNX. Feb 26, 2016; https://opentextbc.ca/anatomyandphysiology/chapter/26-1-body-fluids-and-fluid-compartments/#fig-ch27_01_04.

[1377] Docampo R, de Souza W, Miranda K, Rohloff P, Moreno SN. Acidocalcisomes – conserved from bacteria to man. Nat Rev Microbiol. 2005 Feb 28;3(3):251-261; http://www.bio.umass.edu/micro/klingbeil/590s/Reading/Docampo2005.pdf.

[1378] Kumble KD, Kornberg A. Inorganic polyphosphate in mammalian cells and tissues. J Biol Chem. 1995 Mar 17;270(11):5818-5822; https://www.jbc.org/content/270/11/5818.long.

[1379] Lincoln SF, Richens DT, Sykes AG. Metal Aqua Ions. Comprehensive Coordination Chemistry II 2003;1:515-555; https://www.sciencedirect.com/science/article/pii/B0080437486010550.

[1380] Gutiérrez-de-Terán H, Massink A, Rodríguez D, Liu W, Han GW, Joseph JS, Katritch I, Heitman LH, Xia L, IJzerman AP, Cherezov V, Katritch V, Stevens RC. The Role of a Sodium Ion Binding Site in the Allosteric Modulation of the A2A Adenosine G Protein-Coupled Receptor. Structure 2013 Dec;21(12):2175-2185; https://core.ac.uk/download/pdf/82711619.pdf.

[1381] Custelcean R, Gorbunova MG. A metal-organic framework functionalized with free carboxylic acid sites and its selective binding of a $Cl(H_2O)^{4(-)}$ cluster. J Am Chem Soc. 2005 Nov 30;127(47):16362-3; https://www.ncbi.nlm.nih.gov/pubmed/16305200.

[1382] Miller MD, Cai J, Krause KL. The active site of *Serratia* endonuclease contains a conserved magnesium-water cluster. J Mol Biol. 1999 May 21;288(5):975-87; https://www.ncbi.nlm.nih.gov/pubmed/10329193.

[1383] https://en.wikipedia.org/wiki/Radical_(chemistry)#In_biology.

the radicals. For example, the formation of new reactive oxygen species (ROS)[1384] such as superoxide (O_2^-)[1385] can be detoxified by superoxide dismutase.[1386] Other ROS's, such as hydroxyl radical (OH^-)[1387] which cannot be sanitized by enzymatic reaction,[1388] may be greatly curtailed by the rapid extraction of oxygen from all tissues (Section 4.10.2).

Osmotic imbalances could be a problem during many higher temperature operations and might require some continued nanobot-monitored osmolality operations to maintain or restore osmolality, especially during the extraction phase. It might be necessary to introduce certain solutes or ions into the cytosol in order to prevent existing vesicular organelles from shrinking, swelling, or bursting due to unwanted osmotic imbalances (Section 4.12.2.3(II)). Care must be taken to ensure that selected ions and solutes essential to maintain cellular structural stability are not excessively removed – any essential molecules in deficit concentration could be imported via the vasculoid transport system and reintroduced into the cytoplasm wherever and whenever needed (Section 4.10.2).

4.10.1.5 Signaling Molecules

Secretory signaling molecules (e.g., hormones) generally don't participate in chemical reactions *per se*, but rather bind to specific receptors which trigger some chemical event or a subsequent signaling event. These molecules are typically chemically unchanged during the course of this signaling process, though they are often rapidly broken down by local enzymes into relatively chemically-unreactive signal-inert components. With energy molecules deconcentrated from the body (Section 4.10.1.2), signal-induced enzyme-driven chemical events will be unlikely to occur even if a signaling event is triggered during patient warmup and reliquidification. Hence removing signaling molecules provides secondary protection but is, in most cases, not a primary line of defense against unwanted chemical reactions.

A list of signaling molecules published elsewhere[1389] identifies several general classes of such chemicals, most of which are transmitted through the body via the bloodstream and many of which are already counted in the analysis of metabolites and leaked serum chemicals described in Section 4.10.1.3 and listed in Appendix J. Much like the other serum molecules, signal molecules in the blood would seep into the tissue spaces during prolonged ischemia and early cooldown, thus must suffer a similar $V_{blood} / (V_{blood} + V_{fluid}) \sim$ 12.3% dilution effect (Section 4.10.1.3).

Six major classes of signaling molecules include:

I. Endocrine Hormones. Included in Appendix J: Aldosterone, Calcitonin, Cholecalciferol (Vitamin D_3), Cortisol (hydrocortisone), Dehydroepiandrosterone (DHEA), Estradiol (E_2), Estrone (E_1), Insulin, Pancreatic Polypeptide, Parathyroid Hormone (PTH), Progesterone, Relaxin, Secretin, Somatotropin Growth Hormone (GH), Testosterone, and Thyroxine (FT_4); missing are:

[1384] https://en.wikipedia.org/wiki/Reactive_oxygen_species.
[1385] https://en.wikipedia.org/wiki/Superoxide.
[1386] https://en.wikipedia.org/wiki/Superoxide_dismutase.
[1387] https://en.wikipedia.org/wiki/Hydroxyl_radical.

[1388] Reiter RJ, Melchiorri D, Sewerynek E, Poeggeler B, Barlow-Walden L, Chuang J, Ortiz GG, Acuña-Castroviejo D. A review of the evidence supporting melatonin's role as an antioxidant. J Pineal Res. 1995 Jan;18(1):1-11; https://www.ncbi.nlm.nih.gov/pubmed/7776173.

[1389] Freitas RA Jr. Nanomedicine, Volume I: Basic Capabilities, Landes Bioscience, Georgetown, TX, 1999; Table 7.2; http://www.nanomedicine.com/NMI/Tables/7.2.jpg.

Adrenocorticotropic Hormone (ACTH), Atrial Natriuretic Factor (ANF), Follicle Stimulating Hormone (FSH), Inhibin, Leptin, Lipotropin (LPH), Luteinizing Hormone (LH), Melanocyte Stimulating Hormone (MSH), Motilin, and Ovarian Growth Factor.

II. Local Chemical Mediators. Included in Appendix J: Epidermal Growth Factor (EGF), Erythropoietin, Nerve Growth Factor (NGF), Platelet Derived Growth Factor (PDGF), and Prostaglandin (PGE); missing are: Fibroblast Growth Factor (FGF), Histamine, Interferon, Interleukins, Leukotrienes, Macrophage Growth Factor (MGF), Macrophage Inflammatory Factor, Neutrophil Chemotactic Factor, Platelet Activating Factor (PAF), Prostacyclin, Thromboxanes, Thrombopoietin (TPO), Transforming Growth Factor (TGF), Tumor Necrosis Factor (TNF), and Vascular Endothelial Growth Factor (VEGF).

III. Neurotransmitters and Neuropeptides. Included in Appendix J: Acetylcholine, Angiotensin II (Renin), Bradykinin, Dopamine, Epinephrine (adrenalin), Glutamate (the anion of glutamic acid), Glycine, Melatonin, Norepinephrine (noradrenalin) (NEP), Oxytocin, Serotonin, and Vasopressin; missing are: Acetylserotonin, Endorphin, Enkephalin, GABA, Galanin, Kyotorphin, Neurokinin, Neuropeptide Y, Neuropeptide P, Neurotensin, Nitric Oxide (NO), Octopamine, Somatostatin, and Tachykinin.

IV. Intracellular Messengers. Included in Appendix J: Cyclic AMP, Cyclic GMP, and Inositol; missing are: Arachidonic Acid, Diacylglycerol, GTPase-Activating Proteins, Guanine Nucleotide Exchange Factors, and Inositol Triphosphate.

Most of these chemicals are present in blood in only very minute quantities. Most of them are rapidly degraded by enzymes specific to them, in order to ensure that the stimulatory chemical signal will be rapidly extinguished shortly after receipt. As a result, the representative concentrations employed in Appendix J are probably serious overestimates of the quantities that would actually be present in a cryopreserved patient who has suffered hours of warm ischemia. All relevant species included in the above four categories should be extracted, but it is unlikely that adding the molecular species currently omitted from Appendix J would materially increase the extraction device requirements estimated in the present study.

Two other classes of potential "signaling molecules" deserve attention:

V. Messenger RNA. "Messenger RNA (mRNA) is a large family of intracellular RNA molecules that convey genetic information from DNA to the ribosome, where they specify the amino acid sequence of the protein products of gene expression. The RNA polymerase enzyme transcribes genes into primary transcript mRNA (known as pre-mRNA) leading to processed, mature mRNA. This mature mRNA is then translated into a polymer of amino acids: a protein, as summarized in the central dogma of molecular biology."[1390] In net effect, mRNA molecules convey an information-laden signal to ribosomes inside the cell, activating them to produce proteins. One objective of the molecular extraction procedure proposed here is to ensure that all ribosome-mediated protein translation in the reliquidified cell is halted.

It has been estimated that the typical mammalian cell contains ~4 x 10^5 mRNA molecules made up of ~12,000 different transcripts each measuring ~2000 base pairs in length (MW ~ 10^6 gm/mole), representing perhaps ~0.1% of cell mass.[1391] In a living cell, mRNA is synthesized by polymerases and destroyed by

---

[1390] https://en.wikipedia.org/wiki/Messenger_RNA.

[1391] "How much RNA does a typical mammalian cell contain?" QIAGEN, FAQ ID-2946, 2020; https://www.qiagen.com/us/resources/faq?id=06a192c2-e72d-42e8-9b40-3171e1eb4cb8&lang=en.

nucleases. The estimated median mRNA half-life in live human cells is ~10 hours,[1392] so one might naively assume that most of a patient's pre-mortem mRNA at the time of death will be degraded by the time the patient enters the solid state if many mRNA half-lives have passed prior to cryopreservation. However, several studies have found that mRNA remains stable in the post-mortem human brain for up to 48 hours (Section 3.2.4), so apparently at least some degradative processes are shut off shortly after cell death occurs.

Can more mRNA be created? mRNA is manufactured by RNA polymerase[1393] acting on DNA strands in the nucleus, but RNA polymerase requires ATP to activate transcription complexes.[1394] Since ATP has been rapidly depleted (Section 4.10.1.2), no new mRNA transcripts should be created after a few minutes post-mortem.

Should existing mRNA be extracted? Protein translation from mRNA is an energy-intensive process[1395] that depends on the presence of ATP to create high-energy tRNA (transfer RNA) amino acid carriers with which ribosomes can catalyze the formation of peptide chains and proteins. With ATP exhausted early in the ischemic timeline prior to cryopreservation, ribosomal production of proteins will have halted and will not be able to resume upon patient reliquidification during revival because the ATP will not yet have been replenished. This analysis suggests that no special effort need be made to extract free mRNA molecules (or ribosomes) following reliquidification of the patient's body. Leaving mRNA transcripts in place also allows for the possibility of confirming normal cell identity or cancer status during cell repair, e.g., during the removal of cancer cells (Section 4.12.1.6) , or of reproducing the original transcriptional states of neurons under repair to ensure preservation of personal identity (Section 2.1.2(2)).

Cell-free DNA is found in blood plasma in short segments with a size distribution peaking at ~162 base pairs (~106,920 gm/mole) in length[1396] in concentrations ranging from 0-3.4 ng/ml[1397] (Appendix J). Small amounts of extracellular RNA and DNA are also found in normal human blood plasma[1398] and some of this might have been retained in cryopreserved tissue, but it is probably not worth the trouble to extract it.

[1392] Greenberg JR. High stability of messenger RNA in growing cultured cells. Nature. 1972 Nov 10;240(5376):102-4; https://www.nature.com/articles/240102a0. Yang E, van Nimwegen E, Zavolan M, Rajewsky N, Schroeder M, Magnasco M, Darnell JE Jr. Decay Rates of Human mRNAs: Correlation With Functional Characteristics and Sequence Attributes. Genome Res. 2003 Aug; 13(8): 1863-1872; https://www.ncbi.nlm.nih.gov/pmc/articles/PMC403777/.

[1393] https://en.wikipedia.org/wiki/RNA_polymerase.

[1394] Kopytek SJ, Peterson DO. ATP-mediated activation of RNA polymerase II transcription complexes. Gene Expr. 1998;7(2):75-86; https://www.ncbi.nlm.nih.gov/pmc/articles/PMC6190198/.

[1395] Stouthamer AH. A theoretical study on the amount of ATP required for synthesis of microbial cell material. Antonie Van Leeuwenhoek. 1973;39(3):545-65; https://link.springer.com/article/10.1007/BF02578899.

[1396] Fan HC, Blumenfeld YJ, Chitkara U, Hudgins L, Quake SR. Analysis of the size distributions of fetal and maternal cell-free DNA by paired-end sequencing. Clin Chem. 2010 Aug;56(8):1279-86; https://pdfs.semanticscholar.org/363d/fe1c99870190a781d20f7d31a5b0a9fbd2f4.pdf.

[1397] Fernando MR, Jiang C, Krzyzanowski GD, Ryan WL. New evidence that a large proportion of human blood plasma cell-free DNA is localized in exosomes. PLoS One. 2017 Aug 29;12(8):e0183915; https://www.ncbi.nlm.nih.gov/pmc/articles/PMC5574584/.

[1398] Max KEA, Bertram K, Akat KM, Bogardus KA, Li J, Morozov P, Ben-Dov IZ, Li X, Weiss ZR, Azizian A, Sopeyin A, Diacovo TG, Adamidi C, Williams Z, Tuschl T. Human plasma and serum extracellular small RNA reference profiles and their clinical utility. Proc Natl Acad Sci U S A. 2018 Jun 5;115(23):E5334-E5343; https://pdfs.semanticscholar.org/8d6c/9e8e0389050ce6afe4605f891cdda87b75db.pdf.

VI. Apoptotic Signaling Molecules. Apoptosis is a form of programmed cell death that occurs in multicellular organisms. In apoptosis, biochemical events lead to characteristic cell changes including a cascade of protein cleavage by proteolytic caspase enzymes, cell blebbing and shrinkage, nuclear fragmentation, chromatin condensation and chromosomal DNA fragmentation, mRNA decay, and cell death – a highly regulated process that cannot stop (in nature) once it has begun.[1399] Several kinds of events are known to elicit apoptosis in a eukaryotic cell – such as when a cell loses its normal contact with its surroundings or sustains irreparable internal damage[1400] – that seem possible to occur during ischemia or the cryopreservation and revival processes.

Apoptosis can be initiated by a number of cell suicide trigger molecules. It would probably be wise to extract all of them if they are present in the reliquidified cryopatient. For example, pore formation[1401] in damaged mitochondria may release **cytochrome c**[1402] into the cytoplasm, which then binds with Apaf-1 (apoptotic protease activating factor) and ATP to initiate the proteolytic caspase cascade.[1403] Kluck *et al.*[1404] report a threshold concentration of cytochrome *c* needed to trigger caspase activation – no activation at 20 nM (~2.4 x 10^{-7} gm/cm^3), a lag of 3 hr to activation at 40 nM, and a lag of only 15 min to caspase activation at 80 nM (~9.6 x 10^{-7} gm/cm^3). Another experiment[1405] that subjected rats to cardiac arrest injury measured the subsequent blood plasma cytochrome c concentration as <2 μg/ml in survivors and up to 4.6 μg/ml in non-survivors (e.g., 1.6-4.6 x 10^{-6} gm/cm^3; see Appendix J). A 100-fold reduction to 4.6 x 10^{-8} gm/cm^3 would be well below the 2.4 x 10^{-7} gm/cm^3 threshold for activation. Damaged mitochondria also release a protein into the cytosol called **Smac** (second mitochondria-derived activator of caspase) that binds to IAPs (inhibitors of apoptosis) and prevents them from blocking the apoptotic process, thus enabling apoptosis to proceed.[1406] Two further examples:

* **TNFα** (tumor necrosis factor), a 25,644 dalton[1407] cytokine produced by activated macrophages, initiates caspase activity upon binding to the TNFR1 receptor present on most cells in the human body.[1408]

[1399] https://en.wikipedia.org/wiki/Apoptosis.

[1400] Ashkenazi A, Dixit VM. Death receptors: signaling and modulation. Science. 1998 Aug 28;281(5381):1305-8; https://pdfs.semanticscholar.org/95bd/4c74539a6521f2f4760c8961b2242ead3033.pdf.

[1401] Uren RT, Iyer S, Kluck RM. Pore formation by dimeric Bak and Bax: an unusual pore? Philos Trans R Soc Lond B Biol Sci. 2017 Aug 5;372(1726); https://www.ncbi.nlm.nih.gov/pmc/articles/PMC5483520/.

[1402] https://en.wikipedia.org/wiki/Cytochrome_c_family.

[1403] Riedl SJ, Salvesen GS. The apoptosome: signalling platform of cell death. Nat Rev Mol Cell Biol. 2007 May;8(5):405-13; https://www.ncbi.nlm.nih.gov/pubmed/17377525/. Ripple MO, Abajian M, Springett R. Cytochrome c is rapidly reduced in the cytosol after mitochondrial outer membrane permeabilization. Apoptosis. 2010 May;15(5):563-73; https://www.ncbi.nlm.nih.gov/pmc/articles/PMC2863113/.

[1404] Kluck RM, Martin SJ, Hoffman BM, Zhou JS, Green DR, Newmeyer DD. Cytochrome c activation of CPP32-like proteolysis plays a critical role in a *Xenopus* cell-free apoptosis system. EMBO J. 1997 Aug 1;16(15):4639-49; https://www.ncbi.nlm.nih.gov/pmc/articles/PMC1170090/.

[1405] Radhakrishnan J, Wang S, Ayoub IM, Kolarova JD, Levine RF, Gazmuri RJ. Circulating levels of cytochrome c after resuscitation from cardiac arrest: a marker of mitochondrial injury and predictor of survival. Am J Physiol Heart Circ Physiol. 2007 Feb;292(2):H767-75; https://www.ncbi.nlm.nih.gov/pmc/articles/PMC1796625/.

[1406] Du C, Fang M, Li Y, Li L, Wang X. Smac, a mitochondrial protein that promotes cytochrome c-dependent caspase activation by eliminating IAP inhibition. Cell. 2000 Jul 7;102(1):33-42; https://core.ac.uk/download/pdf/82197854.pdf.

[1407] https://www.phosphosite.org/proteinAction?id=8542247.

[1408] https://en.wikipedia.org/wiki/Tumor_necrosis_factor_alpha.

(Serum concentration of TNFα ranges up to 1.2 x 10^{-11} gm/cm^3 for carcinoma patients;[1409] see Appendix J.)

* **Nitric oxide** may promote apoptosis in some circumstances.[1410] Physiological concentrations of NO range from 0.01-1 μM with an estimated half-life of 0.15-15 hours due to the reaction with oxygen,[1411] but human blood serum NO concentrations have been reported as high as 30 μM (3 x 10^{-8} gm/cm^3; see Appendix J) for patients with stage IV carcinoma.[1412] Because of its modest half-life, most NO should already be mostly degraded in the cryopreserved patient so the amount present should normally fall far short of the aforementioned maximum concentration.

A ***future research*** project should explore and identify the types and concentrations of all apoptotic signaling molecules, then include them in the molecular extraction protocol to be executed immediately following reliquidification of the cryopreserved patient's body.

Signaling molecules that have become bound to plasma membrane receptors and are no longer free in cytosolic or extracellular fluids may be removed in a later stage of the repair process (Section 4.12.2.2).

4.10.1.6 Drugs

Depending on the particular circumstances, a cryopreservation patient may have been administrated a variety of drugs as a part of the normal medical procedures for treatment or for palliative care at or near the original time of death, or even during the process of cryopreservation (Appendix L) including cryonics stabilization medications.[1413] Some amount of these substances may remain in the tissues and should be extracted because of their possible chemical reactivity, biological activity, or their potential to interfere with subsequent nanorobotic repair operations (e.g., Section 4.11 and Section 4.12). Since most of these substances would not pose an immediate risk of tissue degradation, they may be extracted at leisure with low time pressure after all higher-priority extractions have been completed.

Ideally, records will exist for each patient that describe which substances were taken or administered, and when, and in what quantities, to help guide the molecular extraction process. As there are a finite number of possible substances, it might be prudent to include a prophylactic selection of sorting rotor-based pumps with binding sites for a wide variety of chemical agents that were known to be commonly employed in the late 20th and early 21st centuries in the patient's last country(ies) of residence. Relevant drugs[1414] and other chemical agents might include:

[1409] Wang YY, Lo GH, Lai KH, Cheng JS, Lin CK, Hsu PI. Increased serum concentrations of tumor necrosis factor-alpha are associated with disease progression and malnutrition in hepatocellular carcinoma. J Chin Med Assoc. 2003 Oct;66(10):593-8; http://homepage.vghtpe.gov.tw/~jcma/6610/661005.pdf.

[1410] Brüne B, von Knethen A, Sandau KB. Nitric oxide (NO): an effector of apoptosis. Cell Death Differ. 1999 Oct;6(10):969-75; https://www.nature.com/articles/4400582.pdf. Wang Y, Chen C, Loake GJ, Chu C. Nitric oxide: promoter or suppressor of programmed cell death? Protein Cell. 2010 Feb;1(2):133-42; https://www.ncbi.nlm.nih.gov/pmc/articles/PMC4875162/.

[1411] Kelm M. Nitric oxide metabolism and breakdown. Biochim Biophys Acta. 1999 May 5;1411(2-3):273-89; https://core.ac.uk/download/pdf/82014905.pdf.

[1412] Ratajczak-Wrona W, Jablonska E, Antonowicz B, Dziemianczyk D, Grabowska SZ. Levels of biological markers of nitric oxide in serum of patients with squamous cell carcinoma of the oral cavity. Int J Oral Sci. 2013 Sep;5(3):141-5; https://www.ncbi.nlm.nih.gov/pmc/articles/PMC3967335/.

[1413] https://www.alcor.org/library/alcor-human-cryopreservation-protocol/#administration.

[1414] https://en.wikipedia.org/wiki/List_of_drugs.

* **Surgical antiseptics**[1415] such as chlorhexidine gluconate,[1416] iodopovidone,[1417] and polyhexanide[1418];

* **Local anesthetics**[1419] such as lidocaine,[1420] novocaine,[1421] and prilocaine;[1422]

* **General anesthetics**[1423] including inhalables (e.g., ether,[1424] nitrous oxide,[1425] halothane,[1426] enflurane,[1427] methoxyflurane,[1428] desflurane,[1429] isoflurane,[1430] sevoflurane[1431]) and injectibles (e.g., propofol,[1432] etomidate,[1433] barbiturates[1434] (e.g., methohexital,[1435] thiopentone[1436]), benzodiazepines[1437] (e.g., diazepam,[1438] midazolam[1439]), and ketamine[1440]);

* **Hypnotics and soporifics**[1441] including barbiturates,[1442] benzodiazepines,[1443] melatonin,[1444] nonbenzodiazepines[1445] and quinazolinones;[1446]

* **Tranquilizers**[1447] including antidepressants,[1448] antipsychotics,[1449] mood stabilizers,[1450] and sedatives;[1451]

* **Neuromuscular relaxants**[1452] including alcuronium,[1453] aminosteroids,[1454] gallamine,[1455] suxmethonium,[1456] and tetrahydroisoquinoline derivatives;[1457]

[1415] https://en.wikipedia.org/wiki/Antiseptic.
[1416] https://en.wikipedia.org/wiki/Chlorhexidine_gluconate.
[1417] https://en.wikipedia.org/wiki/Povidone-iodine.
[1418] https://en.wikipedia.org/wiki/Polyhexanide.
[1419] https://en.wikipedia.org/wiki/Local_anesthetic.
[1420] https://en.wikipedia.org/wiki/Lidocaine.
[1421] https://en.wikipedia.org/wiki/Procaine.
[1422] https://en.wikipedia.org/wiki/Prilocaine.
[1423] https://en.wikipedia.org/wiki/General_anaesthetic.
[1424] https://en.wikipedia.org/wiki/Diethyl_ether#Anesthetic_use.
[1425] https://en.wikipedia.org/wiki/Nitrous_oxide_(medication).
[1426] https://en.wikipedia.org/wiki/Halothane.
[1427] https://en.wikipedia.org/wiki/Enflurane.
[1428] https://en.wikipedia.org/wiki/Methoxyflurane.
[1429] https://en.wikipedia.org/wiki/Desflurane.
[1430] https://en.wikipedia.org/wiki/Isoflurane.
[1431] https://en.wikipedia.org/wiki/Sevoflurane.
[1432] https://en.wikipedia.org/wiki/Propofol.
[1433] https://en.wikipedia.org/wiki/Etomidate.
[1434] https://en.wikipedia.org/wiki/Barbiturate.
[1435] https://en.wikipedia.org/wiki/Methohexital.
[1436] https://en.wikipedia.org/wiki/Thiopentone.
[1437] https://en.wikipedia.org/wiki/Benzodiazepine.
[1438] https://en.wikipedia.org/wiki/Diazepam.
[1439] https://en.wikipedia.org/wiki/Midazolam.
[1440] https://en.wikipedia.org/wiki/Ketamine.
[1441] https://en.wikipedia.org/wiki/Hypnotic.
[1442] https://en.wikipedia.org/wiki/Barbiturate.
[1443] https://en.wikipedia.org/wiki/Benzodiazepine.
[1444] https://en.wikipedia.org/wiki/Melatonin.
[1445] https://en.wikipedia.org/wiki/Nonbenzodiazepine.
[1446] https://en.wikipedia.org/wiki/Quinazolinone.
[1447] https://en.wikipedia.org/wiki/Tranquilizer.
[1448] https://en.wikipedia.org/wiki/Antidepressant.
[1449] https://en.wikipedia.org/wiki/Antipsychotic.
[1450] https://en.wikipedia.org/wiki/Mood_stabilizer.
[1451] https://en.wikipedia.org/wiki/Sedation.
[1452] https://en.wikipedia.org/wiki/Neuromuscular-blocking_drug.
[1453] https://en.wikipedia.org/wiki/Alcuronium_chloride.
[1454] https://en.wikipedia.org/wiki/Aminosteroid.
[1455] https://en.wikipedia.org/wiki/Gallamine.

* **Analgesics (painkillers)**[1458] including acetaminophen,[1459] COX-2 inhibitors,[1460] flupirtine,[1461] narcotics,[1462] nefopam,[1463] NSAIDs[1464] (e.g., aspirin,[1465] ibuprofen,[1466] and naproxen[1467]), opioids[1468] (e.g., fentanyl,[1469] morphine[1470]), and ziconotide;[1471]

* **Emergency medications** including adenosine,[1472] atropine,[1473] bronchodilators,[1474] dextrose,[1475] heparin,[1476] naloxone,[1477] nitroglycerin,[1478] P2Y12 inhibitors,[1479] and TPA;[1480]

* **Chemotherapy**[1481] **and chemotherapeutic agents**[1482] including cisplatin,[1483] doxorubicin,[1484] methotrexate,[1485] quinazolines,[1486] and vincristine;[1487]

* **Drugs for common medical conditions**[1488] including AIDS drugs,[1489] amphetamines,[1490] anti-aging drugs,[1491] antibiotics,[1492] anticoagulants,[1493] antidiarrheals,[1494] antihistamines,[1495] anti-malarial drugs,[1496] anti-obesity medications,[1497] antiprotozoal drugs,[1498] antipyretics,[1499] antiviral drugs,[1500] appetite

---

[1456] https://en.wikipedia.org/wiki/Suxamethonium.
[1457] https://en.wikipedia.org/wiki/Tetrahydroisoquinoline.
[1458] https://en.wikipedia.org/wiki/Analgesic.
[1459] https://en.wikipedia.org/wiki/Paracetamol.
[1460] https://en.wikipedia.org/wiki/COX-2_inhibitor.
[1461] https://en.wikipedia.org/wiki/Flupirtine.
[1462] https://en.wikipedia.org/wiki/Narcotic.
[1463] https://en.wikipedia.org/wiki/Nefopam.
[1464] https://en.wikipedia.org/wiki/Nonsteroidal_anti-inflammatory_drug.
[1465] https://en.wikipedia.org/wiki/Aspirin.
[1466] https://en.wikipedia.org/wiki/Ibuprofen.
[1467] https://en.wikipedia.org/wiki/Naproxen.
[1468] https://en.wikipedia.org/wiki/Opioids.
[1469] https://en.wikipedia.org/wiki/Fentanyl.
[1470] https://en.wikipedia.org/wiki/Morphine.
[1471] https://en.wikipedia.org/wiki/Ziconotide.
[1472] https://en.wikipedia.org/wiki/Adenosine.
[1473] https://en.wikipedia.org/wiki/Atropine.
[1474] https://en.wikipedia.org/wiki/Bronchodilator.
[1475] https://en.wikipedia.org/wiki/Dextrose.
[1476] https://en.wikipedia.org/wiki/Heparin.
[1477] https://en.wikipedia.org/wiki/Naloxone.
[1478] https://en.wikipedia.org/wiki/Nitroglycerin_(medication).
[1479] https://en.wikipedia.org/wiki/P2Y12.
[1480] https://en.wikipedia.org/wiki/Tissue_plasminogen_activator.
[1481] https://en.wikipedia.org/wiki/Chemotherapy.
[1482] https://en.wikipedia.org/wiki/List_of_chemotherapeutic_agents.
[1483] https://en.wikipedia.org/wiki/Cisplatin.
[1484] https://en.wikipedia.org/wiki/Doxorubicin.
[1485] https://en.wikipedia.org/wiki/Methotrexate.
[1486] https://en.wikipedia.org/wiki/Quinazoline.
[1487] https://en.wikipedia.org/wiki/Vincristine.
[1488] https://en.wikipedia.org/wiki/Medication.
[1489] https://en.wikipedia.org/wiki/Management_of_HIV/AIDS.
[1490] https://en.wikipedia.org/wiki/Amphetamine.
[1491] https://en.wikipedia.org/wiki/Life_extension#Anti-aging_drugs.
[1492] https://en.wikipedia.org/wiki/Antibiotic.
[1493] https://en.wikipedia.org/wiki/Anticoagulant.
[1494] https://en.wikipedia.org/wiki/Antidiarrhoeal.
[1495] https://en.wikipedia.org/wiki/Antihistamine.
[1496] https://en.wikipedia.org/wiki/Antimalarial_drug.
[1497] https://en.wikipedia.org/wiki/Anti-obesity_medication.
[1498] https://en.wikipedia.org/wiki/Antiprotozoal.
[1499] https://en.wikipedia.org/wiki/Antipyretic.

suppressants,[1501] blood pressure medications,[1502] contraceptives,[1503] diuretics[1504] and antidiuretics,[1505] headache medications,[1506] hormone replacements,[1507] laxatives,[1508] and statins;[1509] and

* **Recreational drugs**[1510] including alcohol,[1511] caffeine,[1512] cannabis,[1513] cocaine,[1514] euphorants,[1515] LSD,[1516] nicotine,[1517] other stimulants,[1518] psychoactive drugs,[1519] and viagra.[1520]

Since these substances are potentially numerous in number, differ widely in concentration for individual patients, and may be extracted at leisure because they will be biologically inactive in metabolically biostatic tissue, we've selected for the present analysis one high-concentration item to represent what might more commonly be an extraction task involving multiple substances but having similar total concentration. Ethanol (MW = 46.1 gm/mole), if present in a likely-lethal[1521] maximum blood alcohol concentration or BAC = 0.400% (4×10^{-3} gm/cm^3), can be reduced 400-fold to a negligible concentration (e.g., BAC = 0.001% (1×10^{-5} gm/cm^3) using 1.54×10^{16} rotors of volume 0.021 cm^3 and mass 0.031 gm, with an average fleet power draw of 0.003 W over a leisurely 12-hour extraction period. Other pre-mortem drugs should be present, if at all, in far lower concentrations than this. Some patients might have few or no pre-mortem drugs requiring extraction, aside from those introduced during cryopreservation.

A ***future research*** effort could be directed at specifying the pharmaceutical agents that might typically be found in a cryopreserved patient and their anticipated concentration ranges, evaluating the risk they might pose if they are not extracted, and creating a ranked priority list for molecular extraction.

[1500] https://en.wikipedia.org/wiki/Antiviral_drug.
[1501] https://en.wikipedia.org/wiki/Anorectic.
[1502] https://en.wikipedia.org/wiki/Antihypertensive_drug.
[1503] https://en.wikipedia.org/wiki/Oral_contraceptive_pill and https://en.wikipedia.org/wiki/Combined_oral_contraceptive_pill.
[1504] https://en.wikipedia.org/wiki/Diuretic.
[1505] https://en.wikipedia.org/wiki/Antidiuretic.
[1506] https://en.wikipedia.org/wiki/Management_of_chronic_headaches.
[1507] https://en.wikipedia.org/wiki/Hormone_replacement.
[1508] https://en.wikipedia.org/wiki/Laxative.
[1509] https://en.wikipedia.org/wiki/Statin.
[1510] https://en.wikipedia.org/wiki/Recreational_drug_use.
[1511] https://en.wikipedia.org/wiki/Alcohol_(drug).
[1512] https://en.wikipedia.org/wiki/Caffeine.
[1513] https://en.wikipedia.org/wiki/Cannabis_(drug).
[1514] https://en.wikipedia.org/wiki/Cocaine.
[1515] https://en.wikipedia.org/wiki/Euphoriant.
[1516] https://en.wikipedia.org/wiki/Lysergic_acid_diethylamide.
[1517] https://en.wikipedia.org/wiki/Nicotine.
[1518] https://en.wikipedia.org/wiki/Stimulant.
[1519] https://en.wikipedia.org/wiki/Category:Psychoactive_drugs.
[1520] https://en.wikipedia.org/wiki/Sildenafil.
[1521] https://en.wikipedia.org/wiki/Short-term_effects_of_alcohol_consumption.

4.10.1.7 Cryoprotectants

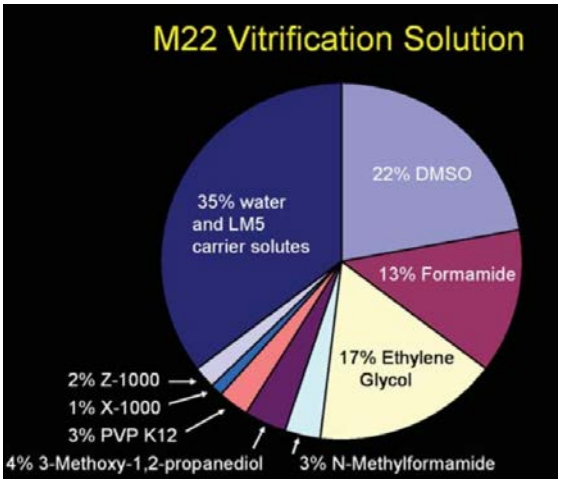

Cryoprotectants are chemicals used to protect biological tissues from freezing damage. During human cryopreservation, over a period of hours the patient's vasculature is flushed with ~32 liters of a special cryoprotective solution known as M22 (image, right;[1522] and **Table 8**). According to laboratory tests on rabbit kidneys,[1523] M22 achieves 55%-60% tissue saturation in a perfusion time of 25 minutes. For the present analysis, this is interpreted to mean that up to 60% of the aqueous intracellular and interstitial volume (V_{fluid} = 38.5 L) has been replaced by M22 components.

Toxicity is a major concern when developing cryoprotectant solutions,[1524] and there is an ongoing search for nontoxic cryoprotectants,[1525] but M22 is one of the two most widely used vitrification cryoprotectant solution in cryonics.[1526] Given the high tissue concentrations of M22 achieved during perfusion (with all major components of M22 well above LD_{50} in mammals), it is necessary to ask how much of its constituent chemicals must be extracted to avoid residual cell toxicity.

DMSO. A 0.1% (v/v) or ~14.1 mM solution of DMSO is commonly considered nontoxic in cell assays, although small changes in gene expression in cardiac and hepatic microtissues[1527] and in intestinal inflammatory response[1528] have been reported at 0.1% (v/v), and a slight increase in human multiple

---

[1522] Wowk B. How cryoprotectants work. Cryonics, 3rd Qtr 2007, pp. 3-7; https://alcor.org/Library/pdfs/How-Cryoprotectants-Work.pdf.

[1523] Table 4 in Fahy GM, Wowk B, Wu J, Phan J, Rasch C, Chang A, Zendejas E. Cryopreservation of organs by vitrification: perspectives and recent advances. Cryobiology. 2004 Apr;48(2):157-78; http://www.21cm.com/pdfs/cryopreservation_advances.pdf.

[1524] Clark P, Fahy GM, Karow AM Jr. Factors influencing renal cryopreservation. II. Toxic effects of three cryoprotectants in combination with three vehicle solutions in nonfrozen rabbit cortical slices. Cryobiology. 1984 Jun;21(3):274-284; https://pubmed.ncbi.nlm.nih.gov/6734240/. Fahy GM. Cryoprotectant toxicity neutralization. Cryobiology. 2010 Jul;60(3 Suppl):S45-S53; http://www.21cmpublications.com/PubFiles/12/2010Fahytoxneutral.pdf. Best BP. Cryoprotectant Toxicity: Facts, Issues, and Questions. Rejuv Res. 2015 Oct;18(5):422-436; https://www.liebertpub.com/doi/10.1089/rej.2014.1656.

[1525] Matsumura K, Hayashi F, Nagashima T, Rajan R, Hyon SH. Molecular mechanisms of cell cryopreservation with polyampholytes studied by solid-state NMR. Commun Mater. 2021;2(15); https://www.nature.com/articles/s43246-021-00118-1.pdf. See also: https://phys.org/news/2021-02-insights-mechanisms-safely-cryopreserving-biological.html.

[1526] Alcor uses M22, whereas Cryonics Institute uses an alternative vitrification solution called VM-1; https://www.biostasis.com/vitrification-agents-in-cryonics-vm-1/.

[1527] Verheijen M, Lienhard M, Schrooders Y, Clayton O, Nudischer R, Boerno S, Timmermann B, Selevsek N, Schlapbach R, Gmuender H, Gotta S, Geraedts J, Herwig R, Kleinjans J, Caiment F. DMSO induces drastic changes in human cellular processes and epigenetic landscape *in vitro*. Sci Rep. 2019 Mar 15;9(1):4641; https://www.ncbi.nlm.nih.gov/pmc/articles/PMC6420634/.

[1528] Hollebeeck S, Raas T, Piront N, Schneider YJ, Toussaint O, Larondelle Y, During A. Dimethyl sulfoxide (DMSO) attenuates the inflammatory response in the *in vitro* intestinal Caco-2 cell model. Toxicol Lett. 2011 Oct 30;206(3):268-75; https://www.ncbi.nlm.nih.gov/pubmed/21878375.

myeloma cell growth has been reported at 0.05% (v/v).[1529] Another study on immortalized odontoblast-like MDPC-23 cells found no significant effects on cell viability or protein production at DMSO concentrations from 0.0004% to 0.008%.[1530] Reducing DMSO concentration from the maximum of (60%)(2855 mM) = 1713 mM found in an M22-cryopreserved patient to the highest concentration reported to have no effect (0.008% or 1.1 mM) requires a concentration decrement of **1500X**.

Table 8. Components of M22 cryoprotectant solution commonly employed in human cryopreservation[1531]

Component	Molar Concentration (M = moles/L)	Molec. Weight (gm/mole)	Mass Concentration (g/L) or (kg/m^3)	Molecular Concentration ($molec/nm^3$)
Cryoprotectants				
Dimethyl sulfoxide (DMSO)	2.855	78.1	223.05	1.719
Formamide	2.855	45.0	128.58	1.719
Ethylene glycol	2.713	62.1	168.37	1.634
N-methylformamide	0.508	59.1	30.0	0.306
3-Methoxy,1,2-propanediol	0.377	106.2	40.0	0.227
Polyvinyl pyrrolidone K12	~0.0056	~5000	28.0	0.003
X-1000 ice blocker	~0.005	~2000	10.0	0.003
Z-1000 ice blocker	~0.0267	~749	20.0	0.016
Subtotals	*9.345*	---	*648.00*	*5.627*
LM5 Carrier Solution				
Glucose	0.090	180.2	16.22	0.054
Mannitol	0.045	182.2	8.20	0.027
Lactose	0.045	342.3	15.40	0.027
KCl	0.0282	74.6	2.10	0.017
K_2HPO_4	0.0072	174.2	1.25	0.004
Reduced glutathione	0.005	307.3	1.54	0.003
Adenine HCl	0.001	171.6	0.17	0.0006
$NaHCO_3$	0.010	84.0	0.84	0.006
Subtotals	*0.231*	---	*45.72*	*0.139*
Totals	**9.576**	---	**693.72**	**5.766**

Formamide. Based on an extensive review[1532] of the 20th century literature on formamide toxicity in rats, mice, rabbits, and other mammals, a NOAEL (no observed adverse effects limit) of 100 mg/kg of animal

[1529] Wen J, Tong Y, Zu Y. Low Concentration DMSO Stimulates Cell Growth and *In vitro* Transformation of Human Multiple Myeloma Cells. J Adv Med Medical Res. 2015;5(1):65-74; http://journaljammr.com/index.php/JAMMR/article/view/12313/22497.

[1530] Hebling J, Bianchi L, Basso FG, Scheffel DL, Soares DG, Carrilho MR, Pashley DH, Tjäderhane L, de Souza Costa CA. Cytotoxicity of dimethyl sulfoxide (DMSO) in direct contact with odontoblast-like cells. Dent Mater. 2015 Apr;31(4):399-405; https://www.ncbi.nlm.nih.gov/pmc/articles/PMC4757809/.

[1531] Fahy GM, Wowk B, Wu J, Phan J, Rasch C, Chang A, Zendejas E. Cryopreservation of organs by vitrification: perspectives and recent advances. Cryobiology. 2004 Apr;48(2):157-78; http://www.21cm.com/pdfs/cryopreservation_advances.pdf.

body weight has been tentatively established for oral, intravenous, and intraperitoneal administration of formamide. For a 70 kg human with a 60 L body volume, this equates to a 2.6 mM concentration. Reducing formamide concentration from the maximum of (60%)(2855 mM) = 1713 mM found in an M22-cryopreserved patient to the suggested NOAEL concentration of 2.6 mM requires a concentration decrement of **659X**.

Ethylene glycol. A human serum concentration of 20 mg/dL (~3 mM) has been recommended as the threshold of ethylene glycol toxicity,[1533] and a subsequent examination of hospital cases confirmed that serum levels between 6-13 mg/dL (1.0-2.1 mM) produced mild acidosis but no significant metabolic abnormalities after ingestion and absorption of the chemical by humans.[1534] Reducing ethylene glycol concentration from the maximum of (60%)(2713 mM) = 1628 mM found in an M22-cryopreserved patient to the recommended NOAEL threshold concentration of ~3 mM requires a concentration decrement of **543X**. It should also be noted that the toxic mechanism of ethylene glycol poisoning is mainly due to its breakdown metabolites (e.g., oxalic acid) in the liver, so trouble from this source could be forestalled by establishing biochemical stasis in the liver as a priority during molecular extraction. If such metabolic processes do occur, they will take hours at 273 K (0 °C) versus minutes at 310 K (37 °C), which gives the 1-hour extraction process sufficient time to establish biochemical stasis.

N-methylformamide. The hepatotoxic threshold of N-methylformamide (NMF) in mice is 100 mg/kg (~2.6 mM equivalent in humans)[1535] but the NOAEL threshold for developmental toxicity in rats and rabbits is 10-50 mg/kg (0.3-1.3 mM).[1536] NMF can be used as a radiosensitizer for human cancer radiotherapy in well-tolerated doses of 600 mg/m^2/wk (~0.3 mM for a ~2 m^2 human).[1537] Reducing NMF concentration from the maximum of (60%)(508 mM) = 305 mM found in an M22-cryopreserved patient to the apparent NOAEL threshold concentration in rats, rabbits and humans of ~0.3 mM requires a concentration decrement of **1017X**.

3-methoxy-1,2-propanediol. Threshold toxicity has not yet been established. At the high end of 3-MPD concentration, the subcutaneous LD_{50} in mice is reported as 2.547 gm/kg (~28 mM for a 70 kg/60 L

[1532] "Formamide", study completed 3 Jan 2001, The MAK Collection, 2013; https://onlinelibrary.wiley.com/doi/pdf/10.1002/3527600418.mb7512e3213.

[1533] Barceloux DG, Krenzelok EP, Olson K, Watson W. American Academy of Clinical Toxicology Practice Guidelines on the Treatment of Ethylene Glycol Poisoning. Ad Hoc Committee. J Toxicol Clin Toxicol. 1999;37(5):537-60; https://www.ncbi.nlm.nih.gov/pubmed/10497633. Boyer EW, Mejia M, Woolf A, Shannon M. Severe ethylene glycol ingestion treated without hemodialysis. Pediatrics. 2001 Jan;107(1):172-3; https://www.ncbi.nlm.nih.gov/pubmed/11134452.

[1534] Caravati EM, Erdman AR, Christianson G, Manoguerra AS, Booze LL, Woolf AD, Olson KR, Chyka PA, Scharman EJ, Wax PM, Keyes DC, Troutman WG. Ethylene Glycol Exposure: an Evidence-Based Consensus Guideline for Out-of-Hospital Management. J Clin Toxicol. 2005;43(5):327-345; https://www.tandfonline.com/doi/full/10.1080/07313820500184971.

[1535] Whitby H, Gescher A, Levy L. An investigation of the mechanism of hepatotoxicity of the antitumour agent N-methylformamide in mice. Biochem Pharmacol. 1984 Jan 15;33(2):295-302; https://www.ncbi.nlm.nih.gov/pubmed/6704151. Tulip K, Timbrell JA. Comparative hepatotoxicity and metabolism of N-methylformamide in rats and mice. Arch Toxicol. 1988;62(2-3):167-76; https://www.ncbi.nlm.nih.gov/pubmed/3196150.

[1536] Kelich SL, Mercieca MD, Pohland RC. Developmental toxicity of N-methylformamide administered by gavage to CD rats and New Zealand white rabbits. Fundam Appl Toxicol. 1995 Sep;27(2):239-46; https://www.ncbi.nlm.nih.gov/pubmed/8529819.

[1537] Rowinsky EK, Grochow LB, Hantel A, Ettinger DS, Vito BL, Donehower RC. Assessment of N-methylformamide (NMF) administered orally on a three times weekly schedule: a phase I study. Invest New Drugs. 1989 Nov;7(4):317-25; https://www.ncbi.nlm.nih.gov/pubmed/2599802.

human).[1538] At the low end, wine was spiked with 3-MPD at possible concentrations of 0.12-3.1 mg/L (0.001-0.03 mM) in a taste experiment, with no ill effects to the human tasters.[1539] A decrement of **1000X** from the maximum 3-MPD tissue concentration of (60%)(377 mM) = 226 mM in an M22-cryopreserved patient would yield a post-extraction concentration of 0.23 mM remaining in the tissues. (3-MPD is said to be somewhat more toxic than its non-methoxylated variant 1,2-propanediol or propylene glycol,[1540] for which the FDA claims 23 mg/kg (~0.35 mM) is a safe daily intake for humans.[1541]) ***Future research*** should more accurately determine the NOAEL threshold for 3-methoxy,1,2-propanediol.

Long before cryoprotective perfusion with M22 can occur (immediately prior to and during cryogenic cooldown), the cryonics patient must first be packed in ice and immediately administered a set of "stabilization" medications,[1542,1543] including small volume drugs such as 50,000 IU (100 mg)[1544] of heparin, 40 IU (0.075 mg)[1545] of vasopressin, and 250,000 IU (522.5 mg)[1546] of streptokinase, and large-volume medications such as 400 ml of decaglycerol/THAM[1547] and 420 ml of Vital-Oxy.[1548] The

---

[1538] Journal of Pharmacology and Experimental Therapeutics. Vol. 93, Pg. 470, 1948; cited in https://pubchem.ncbi.nlm.nih.gov/compound/3-Methoxy-1_2-propanediol#section=General-Manufacturing-Information.

[1539] Fauhl C, Wittkowski R, Lofthouse J, Hird S, Brereton P, Versini G, Lees M, Guillou C. Gas chromatographic/mass spectrometric determination of 3-methoxy-1,2-propanediol and cyclic diglycerols, by-products of technical glycerol, in wine: interlaboratory study. J AOAC Int. 2004 Sep-Oct;87(5):1179-88; https://www.researchgate.net/profile/Claude_Guillou/publication/8222751_Gas_chromatographicmass_spectrometric_determination_of_3-methoxy-12-propanediol_and_cyclic_diglycerols_by-products_of_technical_glycerol_in_wine_Interlaboratory_study/links/00463515c3c702e48d000000/Gas-chromatographic-mass-spectrometric-determination-of-3-methoxy-1-2-propanediol-and-cyclic-diglycerols-by-products-of-technical-glycerol-in-wine-Interlaboratory-study.pdf.

[1540] https://www.biostasis.com/vitrification-agents-in-cryonics-m22/.

[1541] "Ethylene Glycol and Propylene Glycol Toxicity - What is Propylene Glycol?" Agency for Toxic Substances & Disease Registry, 3 Oct 2007; https://www.atsdr.cdc.gov/csem/csem.asp?csem=12&po=14.

[1542] "Human Cryopreservation Stabilization Medications," 30 Jan 2007; https://www.alcor.org/library/human-cryopreservation-stabilization-medications/.

[1543] "Alcor Human Cryopreservation Protocol," updated Feb 2019; https://www.alcor.org/library/alcor-human-cryopreservation-protocol/#administration.

[1544] 500 IU/mg for heparin; https://www.researchgate.net/post/If_you_want_a_final_concentration_of_Heparin_of_10_ug_mL_in_500_ml_of_media_with_a_stock_conc_of_heparin_5000U_mL_how_many_mL_do_you_add.

[1545] 530 IU/mg for vasopressin; https://www.uspnf.com/official-text/revision-bulletins/vasopressin-0.

[1546] Bangham DR, Walton PL. The international standard for streptokinase-streptodornase. Bull World Health Organ. 1965;33(2):235-42; https://www.ncbi.nlm.nih.gov/pmc/articles/PMC2475839/.

[1547] "Decaglycerol/THAM is administered as a custom formulation of 20% w/v decaglycerol and 4.5% w/v THAM (tromethamine) in water, packaged in 2 x 200 ml sterile vials." (https://www.alcor.org/library/alcor-human-cryopreservation-protocol/#administration) Stated dose is interpreted as 64.3 gm of decaglycerol + 14.5 gm of tromethamine + 321.2 gm of water.

[1548] 6 ml/kg body weight of Vital-Oxy: "…proprietary emulsion of the antioxidants melatonin [1.55 mg], vitamin E (as D-alpha tocopherol) [198 IU], PBN (alpha Phenyl t-Butyl Nitrone) [19.4 mg], and the anti-inflammatory agent carprofen [3.24 mg]" provided "in an emulsion of Cremaphor EL and 155 mg ethanol in water." 6 ml/kg x 70 kg human = 420 ml; unfortunately, this item had to be omitted from the current analysis because of the incomplete quantification of the ingredients and the lack of a precisely-specified dilution per patient (https://www.alcor.org/library/alcor-human-cryopreservation-protocol/#administration, https://www.alcor.org/docs/cryopreservation-procedures-section-13-medications.pdf).

calculations here conservatively assume that the full infused weight of all medications is retained in the body and thus requires subsequent molecular extraction, most likely a significant overestimate.

Based on the foregoing analysis, a concentration decrement of ~1000X during molecular extraction is tentatively set for all cryoprotective chemicals. Additionally, because biochemical stasis will have been established within the first hour of molecular extraction, we can afford to take a much longer time – e.g., $\tau_{total} = 10^6$ sec (~12 days) – to pump out the very large quantities of cryoprotectant chemicals that are present in the M22-cryopreserved patient. (Estimated fleet numbers have been doubled for the three ionic compounds that will form separate anions and cations in aqueous solution.)

Using the iterative numerical process described in Section 4.10.1 to estimate the results shown in Appendix L, sorting rotors with appropriate binding sites should perform the molecular extraction of both cryoprotective chemicals and carrier solution chemicals (e.g., non-native glucose) in $\tau_{total} = 10^6$ sec using a fleet of $N_{fleet} = 2.41 \times 10^{17}$ rotors with a combined fleet volume of $V_{fleet} = 0.33$ cm^3, total mass $M_{fleet} = 0.48$ gm, and an average total fleet power draw over the entire τ_{total} extraction time of $P_{fleet,avg} = 0.7$ watts. Molecular extractions on patients infused with cryoprotectant solutions other than M22 may differ in the details but will have similar requirements.

Performing the same cryoprotectant extraction operation in $\tau_{total} = 3600$ sec (1 hour) would require a ~30 times larger sorting rotor fleet with ~300-fold higher average power draw than for a $\tau_{total} = 10^6$ sec mission, possibly exceeding available vasculoid appliance capacities.[1549]

A ***future research*** project should ascertain whether the extraction of cryoprotectant chemicals can safely be postponed until later in the revival protocol, either after resealing major membrane compartments (Section 4.11) or after primary cell repair operations (Section 4.12) using nanorobots. Full postponement would allow starting nanorobotic repair operations only 3600 sec (1 hour) after reliquidification begins, rather than having to wait until after ~10^6 sec (~278 hours, ~12 days) have elapsed to initiate those repairs. Postponement might also allow repairs to proceed at slightly lower temperatures, permitting molecular extractions to begin at temperatures well below the 273 K (0 °C) icewater temperature, further delaying any possible rewarming damage that might occur.

Another ***future research*** project is to determine if there are any chemicals or materials that could be added to the carrier solution of cryoprotectants used today that might assist in future scanning, re-warming, or repair efforts during one of the revival processes described in this book.

4.10.1.8 Other Potential Extraction Targets

Other potential extraction targets might include:

(1) **Poisons and Toxins.** If a cryopreserved patient died as a result of exposure to an acute poisoning[1550] agent or a toxin[1551] generated from a biological source, that chemical should be extracted from the patient's reliquidified tissue if the chemical can be mobilized and is not tightly bound to a membrane or a macromolecular anchor. Bound poison molecules will remain inactive, and toxin-damaged organelles can be detected and replaced during subsequent nanorobot-repair phases of the revival protocol,

---

[1549] Cryoprotective extraction in $\tau_{total} = 3600$ sec requires $N_{fleet} = 7.02 \times 10^{18}$ sorting rotors, fleet volume $V_{fleet} = 9.64$ cm^3, total mass $M_{fleet} = 14.0$ gm, and average total fleet power draw $P_{fleet,avg} = 181.6$ watts.

[1550] https://en.wikipedia.org/wiki/Poison.
[1551] https://en.wikipedia.org/wiki/Toxin.

because those bound molecules or damaged organelles should remain biochemically inactive given the lack of available energy and substrate molecules.

Some poisonous chemicals[1552] must be present in relatively large concentrations to cause death. For example, a human who has suffered asphyxiation from accidental acetylene inhalation[1553] could have as much as 10^{-3} gm/cm^3 of the gas dissolved in their bloodstream.[1554] If the tissue water concentration were the same, it could require 1.30 x 10^{17} sorting rotors of volume 0.2 cm^3 and mass 0.3 gm, drawing 4.3 W over τ_{total} = 1 hour to reduce the concentration 100-fold. At the other extreme is botulinum toxin,[1555] a toxic protein whose active component is a free-floating 50-kDa zinc metalloprotease in the neuron cytosol that cleaves the SNAP-25 protein, preventing the release of the neurotransmitter acetylcholine from axon endings. The intravenous or intramuscular human LD_{50} of ~2.1 ng/kg of body weight for this toxin,[1556] equivalent to ~4 x 10^{-12} gm/cm^3 in the 38.5 L water volume of a 70 kg human, could be 99% extracted in τ_{total} = 1 hour using only 4.92 x 10^{13} additional sorting rotors. Botulinum poisoning might occur from an overdose following the use of the toxin for medical purposes.[1557]

The presence of lipopolysaccharide (LPS) endotoxin in the human blood can cause septic shock in living humans,[1558] and the killing of bacteria using even traditional antibiotic regimens can liberate up to ~10^5 ng/ml of endotoxin.[1559] Extraction of any free LPS endotoxin is essential, but most will not be free, since the toxin operates by binding to the CD14/TLR4/MD2 receptor complex in monocytes, dendritic cells, macrophages and B cells, thus promoting secretion of pro-inflammatory cytokines, nitric oxide, and eicosanoids.[1560] Since none of these cells will be biochemically active, extraction of LPS can be postponed until later in the revival protocol when whole bacteria will be removed (Section 4.12.1.4).

Neutrophils activated during ischemia-triggered inflammation (Section 3.2.3) can produce large quantities of hydrogen peroxide (H_2O_2) and bleach (HOCl). If small quantities of these or related toxic chemicals persist during cryopreservation, they should be extracted. Other leaked corrosive chemicals (Section 3.6(7)) should also be extracted.

[1552] https://en.wikipedia.org/wiki/List_of_chemical_warfare_agents.

[1553] Acetylene has a very low acute toxicity (https://scialert.net/fulltext/?doi=jms.2005.21.25). The gas is an inhalation anesthetic when administered at 10%-40% in air; at such high air concentrations, the blood concentration is probably near saturation at the maximum solubility in water (https://stacks.cdc.gov/view/cdc/19368/cdc_19368_DS1.pdf). There are rare cases of death due to abuse via inhalation (https://www.ncbi.nlm.nih.gov/pubmed/11327229) or ill effects due to inhaling 100% pure gas (https://www.ncbi.nlm.nih.gov/pubmed/11244734), but "acetylene rebreathing" is a commonly used and medically safe technique for measuring cardiac output in sports medicine (https://www.ncbi.nlm.nih.gov/pubmed/9156963) and in pulmonary medicine (https://www.ncbi.nlm.nih.gov/pubmed/10894104).

[1554] Freitas RA Jr., Nanomedicine, Volume I: Basic Capabilities, Landes Bioscience, Georgetown, TX, 1999, Table 9.2; http://www.nanomedicine.com/NMI/Tables/9.2.jpg.

[1555] https://en.wikipedia.org/wiki/Botulinum_toxin.

[1556] Arnon S, *et al.* Botulinum Toxin as a Biological Weapon: Medical and Public Health Management. JAMA 2001 Feb 28;285(8):1059-1070; https://pubmed.ncbi.nlm.nih.gov/11209178.

[1557] https://en.wikipedia.org/wiki/Botulinum_toxin#Medical_uses.
[1558] https://en.wikipedia.org/wiki/Lipopolysaccharide#Health_effects.

[1559] Frieling JT, Mulder JA, Hendriks T, Curfs JH, van der Linden CJ, Sauerwein RW. Differential induction of pro- and anti-inflammatory cytokines in whole blood by bacteria: effects of antibiotic treatment. Antimicrob Agents Chemother. 1997 Jul;41(7):1439-43; https://aac.asm.org/content/aac/41/7/1439.full.pdf.

[1560] Abbas A. Basic Immunology. Elsevier, 2006.

(2) Enzymes. Molecular extraction of enzymes[1561] – the engines of metabolism, signal transduction, regulation, and movement in the cell – would ensure complete biochemical deactivation of the cryopreserved patient, providing extra assurance of biological stasis after all sources of enzymatic energy (Section 4.10.1.1 and Section 4.10.1.2) and substrates (Section 4.10.1.3) have been removed. The comprehensive BRENDA database[1562] currently lists ~7000 known enzymes,[1563] of which ~1000 are found in *E. coli* cells[1564] and ~1300 are known or suspected to be present in human cells,[1565] ranging in size from 62 residues for the monomer of 4-oxalocrotonate tautomerase[1566] up to 2500 residues for the animal fatty acid synthase.[1567] A ***future research*** project should compile a comprehensive list of all ~1300 enzymes and their concentrations in various human cells, both free and membrane-bound, unless such a list already exists.

A few enzymes may be particularly troublesome if not extracted. For example, caspases[1568] will probably have been released during the initial post-mortem ischemic phase and may persist in cryopreserved tissue. Members of the caspase family proteolytically degrade a host of intracellular proteins to carry out the cell death program of apoptosis,[1569] so these molecules should be extracted to absolutely ensure that they cannot perform their degradative function, producing uncontrolled and unwanted cell damage after tissue reliquidification. Small quantities of matrix metalloproteinases[1570] secreted early during ischemia (Section 3.2.5) and surviving post-cryopreservation that could potentially cause damage after reliquidification should also be extracted.

Enzymes are very resistant to freezing damage,[1571] hence should survive largely intact. However, much like secretory signaling molecules (Section 4.10.1.5), enzymes generally don't participate in chemical reactions *per se* but serve as catalysts either to enable two otherwise nonreactive molecules to react or to cleave one molecule into two or more pieces. Enzymes requiring ATP[1572] will be unable to operate with energy molecules deconcentrated from the body, and other enzyme-driven chemical events will be unlikely to occur even over fairly long periods of time with enzyme substrates having been extracted to relatively low nonreactive concentrations. Hence removing free enzymes from the cytosol or interstitial fluid might provide secondary protection but is, in most cases, not a primary line of defense against unwanted chemical reactions. However, any enzymes irreversibly damaged (e.g., permanently denatured) by the cryopreservation process should be removed.

[1561] https://en.wikipedia.org/wiki/Enzyme.
[1562] https://en.wikipedia.org/wiki/BRENDA.
[1563] https://en.wikipedia.org/wiki/List_of_enzymes.
[1564] https://science.howstuffworks.com/life/cellular-microscopic/cell2.htm.
[1565] https://enzyscience.com/pages/enzyme-faq.

[1566] Chen LH, Kenyon GL, Curtin F, Harayama S, Bembenek ME, Hajipour G, Whitman CP. 4-Oxalocrotonate tautomerase, an enzyme composed of 62 amino acid residues per monomer. J Biol Chem. 1992 Sep 5;267(25):17716-21; https://pdfs.semanticscholar.org/2f8a/e4783544644f8996fa526d01736759106796.pdf.

[1567] Smith S. The animal fatty acid synthase: one gene, one polypeptide, seven enzymes. FASEB J. 1994 Dec;8(15):1248-59; https://www.ncbi.nlm.nih.gov/pubmed/8001737.

[1568] https://en.wikipedia.org/wiki/Caspase.
[1569] https://en.wikipedia.org/wiki/Apoptosis#TNF_path.
[1570] https://en.wikipedia.org/wiki/Matrix_metallopeptidase.

[1571] Mazur P. Freezing of living cells: mechanisms and implications. Am J Physiol. 1984 Sep;247(3 Pt 1):C125-42; https://www.physiology.org/doi/pdf/10.1152/ajpcell.1984.247.3.C125.

[1572] e.g., https://en.wikipedia.org/wiki/Endonuclease#Categories.

Many of the enzymes in human cells are not floating freely in the cytosol but are attached to internal membrane structures (e.g., the Golgi,[1573] endoplasmic reticulum,[1574] proteasomes,[1575] or the outer mitochondrial membrane[1576]) or are confined to protein compartments (e.g., lysosomes,[1577] peroxisomes,[1578] or the mitochondrial matrix[1579]) inside the cell.

Regarding the attached enzymes, ***future research*** should investigate any possible residual activity from membrane-bound enzymes that are not extracted. Such activity is expected to be low if all relevant enzyme substrates and metabolites that are ordinarily freely floating in the cytosol have previously been extracted (Section 4.10.1.3). If any troublesome activity is suspected, reversible inhibitors could be released into the cytosol to "block the action of any enzymes that permit catabolism to proceed to beyond an acceptable point. Once deposited, they can be ignored, since these relatively low molecular weight inhibitors will reach their targets by diffusion as rapidly as the normal substrates would otherwise reach these catabolic enzymes."[1580] Enzymes thusly blocked can be selectively removed and replaced by cell repair nanorobots during the final whole-body check (Section 4.13.3), or simply ignored if their number is few or their function is noncritical.

Regarding the confined enzymes, the spilled contents from protein compartments inside organelles that have burst open during cryopreservation should also be extracted from both cytosol and interstitial fluid. ***Future research*** should investigate the nature and frequency of damage to organelles with compartmented enzymes in response to cryoinjury, and to what extent enzymes are freed from membranes suffering cryoinjury.

(3) **Organelles.** A typical 8000 μm^3 cell may include ~20 μm^3 of proteosomes[1581] and ~90 μm^3 of lysosomes[1582] (both requiring ATP to maintain activity, so the absence of ATP should deactivate them), 90 μm^3 of peroxisomes,[1583] ~80 μm^3 of ribosomes[1584] (some free in the cytosol, others attached to membranes of the rough endoplasmic reticulum, though many may have detached during ischemia; Section 3.2.7), and ~1000 μm^3 of mitochondria (which generate ATP by metabolizing glucose derivatives produced elsewhere in the cytosol,[1585] so the absence of cytosolic glucose should deactivate them).[1586] Microsomes[1587] are heterogeneous vesicle-like artifacts (~20-200 nm in diameter) that re-formed from pieces of the

---

[1573] https://en.wikipedia.org/wiki/Golgi_apparatus#Structure.

[1574] Yeagle PL. The Membranes of Cells, 3rd Edition, Elsevier, 2016, "1.4.2 Endoplasmic Reticulum Membranes"; https://www.sciencedirect.com/topics/neuroscience/endoplasmic-reticulum.

[1575] https://en.wikipedia.org/wiki/Cytosol#Protein_compartments.
[1576] https://en.wikipedia.org/wiki/Mitochondrion#Outer_membrane.
[1577] https://en.wikipedia.org/wiki/Lysosome.
[1578] https://en.wikipedia.org/wiki/Peroxisome.
[1579] https://en.wikipedia.org/wiki/Mitochondrial_matrix.

[1580] Fahy G. Appendix B. A "Realistic" Scenario for Nanotechnological Repair of the Frozen Human Brain. In: Wowk B, Darwin M, eds., Cryonics: Reaching for Tomorrow. Alcor Life Extension Foundation, 1991, pp. A-10 – A-26; https://alcor.org/Library/html/nanotechrepair.html.

[1581] https://en.wikipedia.org/wiki/Proteasome.
[1582] https://en.wikipedia.org/wiki/Lysosome.
[1583] https://en.wikipedia.org/wiki/Peroxisome.
[1584] https://en.wikipedia.org/wiki/Ribosome.
[1585] https://en.wikipedia.org/wiki/Mitochondrion#Energy_conversion

[1586] Freitas RA Jr., Nanomedicine, Volume I: Basic Capabilities, Landes Bioscience, Georgetown, TX, 1999, Table 8.17, "Approximate Quantification of the Components of a Typical 20-μm Human Tissue Cell"; http://www.nanomedicine.com/NMI/Tables/8.17.jpg.

[1587] https://en.wikipedia.org/wiki/Microsome.

endoplasmic reticulum when eukaryotic cells are broken up in the laboratory. Microsomes are not present in healthy living cells, but might be present in cryoinjured cells.

Extraction of intact but inactive organelles has at best a secondary benefit in ensuring biochemical stasis. If organelle compartments are damaged and have leaked their contents (e.g., enzymes), the leaked contents should be extracted and the residual membrane debris should be disposed as described below.

(4) **Cell debris.** Mechanical grinding may produce debris from damaged cell membranes or organelles. Membrane debris is unlikely to be strongly chemically reactive, so its removal can be postponed until subsequent phases of the repair process (Section 4.11). When the debris is from membranes of broken organelles, the spilled contents of these compartments, if chemically reactive, will already have been extracted as previously described.

(5) **Unwanted cells.** A number of foreign or nontissue whole cells or virions, including bacteria, may have become embedded in the cryopreserved tissues. Since all energy sources and signaling molecules will have been removed during the first hour of tissue reliquidification, all of these cells should remain inert, so their removal can be postponed until subsequent phases of the repair process (Section 4.12.1).

(6) **Extracellular vesicles.** Extracellular vesicles of three types may be found in the blood, and a small number of them may find their way into cryopreserved tissue. First, there are microvesicles[1588] 100-1000 nm in diameter, generated by outward budding of cell plasma membranes and subsequent shedding into the extracellular space, averaging ~200 nm in diameter with a mean concentration of 5.9×10^9 particles/ml of peripheral blood plasma.[1589] Second are exosomes,[1590] 30-260 nm in diameter and numbering ~2×10^{10}/ml of plasma (~10^{-5} ml/ml),[1591] containing proteins that help cell penetration, invasion, and fusion (e.g., CD81, CD63, CD9), proteins involved in exosome biogenesis (e.g., alix, TSG101, clathrin),[1592] and DNA, mRNAs, and microRNAs – an online database[1593] lists 9769 exosome proteins, 3408 mRNAs, 2838 miRNAs, and 1116 lipids – letting them modulate the immune system[1594] and transfer genetic material.[1595]

[1588] https://en.wikipedia.org/wiki/Microvesicles.

[1589] Menck K, Bleckmann A, Schulz M, Ries L, Binder C. Isolation and Characterization of Microvesicles from Peripheral Blood. J Vis Exp. 2017 Jan 6;(119):55057; https://www.ncbi.nlm.nih.gov/pmc/articles/PMC5408706/.

[1590] https://en.wikipedia.org/wiki/Exosome_(vesicle).

[1591] Fernando MR, Jiang C, Krzyzanowski GD, Ryan WL. New evidence that a large proportion of human blood plasma cell-free DNA is localized in exosomes. PLoS One. 2017 Aug 29;12(8):e0183915; https://www.ncbi.nlm.nih.gov/pmc/articles/PMC5574584/.

[1592] Ostrowski M, Carmo NB, Krumeich S, Fanget I, Raposo G, Savina A, Moita CF, Schauer K, Hume AN, Freitas RP, Goud B, Benaroch P, Hacohen N, Fukuda M, Desnos C, Seabra MC, Darchen F, Amigorena S, Moita LF, Thery C. Rab27a and Rab27b control different steps of the exosome secretion pathway. Nat Cell Biol. 2010 Jan;12(1):19-30; http://arca.igc.gulbenkian.pt/bitstream/10400.7/200/1/Ostrowski%20M.pdf.

[1593] Exo-Carta; http://www.exocarta.org/.

[1594] Raposo G, Nijman HW, Stoorvogel W, Liejendekker R, Harding CV, Melief CJ, Geuze HJ. B lymphocytes secrete antigen-presenting vesicles. J Exp Med. 1996 Mar 1;183(3):1161-72; https://www.ncbi.nlm.nih.gov/pmc/articles/PMC2192324/.

[1595] Valadi H, Ekström K, Bossios A, Sjöstrand M, Lee JJ, Lötvall JO. Exosome-mediated transfer of mRNAs and microRNAs is a novel mechanism of genetic exchange between cells. Nat Cell Biol. 2007 Jun;9(6):654-9; http://gene-quantification.net/valadi-et-al-mrna-microrna-transfer-2007.pdf.

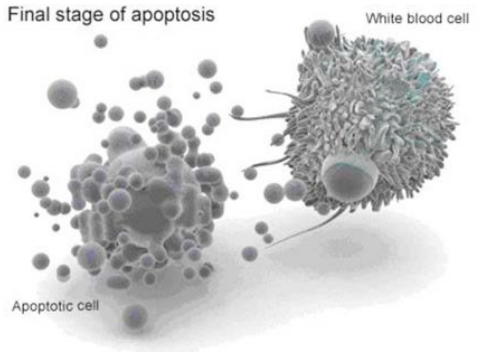

The third type of extracellular vesicles are the apoptotic bodies[1596] (image, right) which are released from cells that have undergone apoptosis. These vesicles, typically 1-5 μm in diameter, contain intracellular fragments, cellular organelles, and fragmented DNA,[1597] and are released by all cell types during the late stages of apoptosis. It is claimed that during life the typical adult human can lose up to 50-70 billion cells each day due to apoptosis,[1598] which phagocytic cells are usually able to engulf and remove before the contents of affected cells can spill out into the interstitial spaces or bloodstream to cause further damage.[1599] Some apoptotic bodies escape into the bloodstream where their typical concentration in neurological patients has been measured at ~1 x 10^8 bodies/ml plasma (~5 x 10^{-5} ml/ml assuming ~1 μm diameter bodies) in the plasma of patients with ischemic stroke, ~5 x 10^8 bodies/ml (~3 x 10^{-4} ml/ml) from patients with multiple sclerosis, and ~4 x 10^8 bodies/ml (~2 x 10^{-4} ml/ml) from patients with Parkinson's disease.[1600]

Future research should determine the number density of microvesicles, exosomes, and apoptotic bodies that may be found in the interstitial spaces of the tissues of normal cryopreserved patients, but the present analysis assumes that these concentrations are small enough to preclude chemical reactivity. If this is true, then removal of these vesicles, if deemed necessary, can await nanorobot-based tissue repair operations in a subsequent phase of the revival protocol (Section 4.12.1.1).

4.10.1.9 Summary of Extraction Mechanisms and Prioritized Molecular Targets

The estimated number, volume, mass, and power draw of sorting rotors needed to extract the numbers and masses indicated of prioritized molecular extraction targets from the interstitial and intracellular fluid compartments of a reliquidified cryopreserved patient are summarized below in **Table 9**. All of the molecules except cryoprotectants are extracted down to presumed sub-reactive concentrations in an extraction time of τ_{total} = 3600 sec (1 hour). If lower concentrations are deemed advisable or required,

---

[1596] https://en.wikipedia.org/wiki/Apoptosis#Apoptotic_cell_disassembly.

[1597] Orlando KA, Stone NL, Pittman RN. Rho kinase regulates fragmentation and phagocytosis of apoptotic cells. Exp Cell Res. 2006 Jan 1;312(1):5-15; https://www.ncbi.nlm.nih.gov/pubmed/16259978. György B, Szabó TG, Pásztói M, Pál Z, Misják P, Aradi B, László V, Pállinger E, Pap E, Kittel A, Nagy G, Falus A, Buzás EI. Membrane vesicles, current state-of-the-art: emerging role of extracellular vesicles. Cell Mol Life Sci. 2011 Aug;68(16):2667-88; https://www.ncbi.nlm.nih.gov/pmc/articles/PMC3142546/.

[1598] Stillwell W. An Introduction to Biological Membranes: Composition, Structure and Function, 2nd Edition, 2016, p. 540; https://www.google.com/books/edition/An_Introduction_to_Biological_Membranes/Q_WpCwAAQBAJ.

[1599] "Chapter 18 Apoptosis: Programmed Cell Death Eliminates Unwanted Cells," in: Alberts B, Johnson A, Lewis J, Raff M, Roberts K, Walter P. Molecular Biology of the Cell, 5th ed., Garland Science, 2008, p. 1115; https://www.amazon.com/dp/B00HMVGL3A/.

[1600] Serrano-Heras G, Díaz-Maroto I, Carrión B, Perona-Moratalla AB, Gracia J, Arteaga S, Hernández-Fernández F, García-García J, Castro-Robles B, Ayo-Martín O, Segura T. Isolation and quantification of blood apoptotic bodies in neurological patients. bioRxiv, 12 Sep 2019; https://www.biorxiv.org/content/10.1101/757872v1.full.pdf.

these extractions can always be continued to whatever arbitrarily low concentration levels are considered desirable.

Table 9. Number, volume, mass, and power draw of sorting rotors needed to extract prioritized extraction targets from interstitial and intracellular fluid compartments, in one hour

Prioritized Molecular Species	# of Different Molecules	# of Sorting Rotors	Mass of Molecules Extracted (gm)	Volume of Rotors (cm^3)	Mass of Rotors (gm)	Average Fleet Power (W)
Oxygen	1	3.01×10^{15}	0.4	0.0041	0.0060	0.0214
Glucose	1	1.06×10^{16}	6.9	0.0145	0.0212	0.0353
Leaked blood plasma components	12,822	1.57×10^{18}	957.5	2.1492	3.1330	0.5931
Cell metabolites	12,230	5.44×10^{18}	2465.4	7.4662	10.8837	3.6653
Free ions	8	8.32×10^{17}	304.0	1.1415	1.6640	15.9727
Signaling molecules	---	---	---	---	---	---
Pre-mortem drugs (e.g., 0.4% ethanol)	>1	1.54×10^{16}	153.6	0.0210	0.0310	0.0030
Cryoprotectants	25	2.41×10^{17}	16,047.5	0.3302	0.4813	0.6666
Totals	**25,088**	**7.87×10^{18}**	**19,969.1**	**10.8**	**15.7**	**20.3**

We assume that sorting rotors will be deployed throughout a V_{body} = 60 L human whole-body volume (of which V_{fluid} = 38.5 L is fluid) to perform the molecular extractions. Depending on the target molecule's concentration and molecular weight, these rotors must be positioned in a 3D array at spacings of $x_{rotor} = 2\ \Delta X \sim$ 4-10 μm, given a rotor service volume radius $\Delta X \sim$ 2-5 μm (Section 4.10.1). We shall assume x_{rotor} = 5 μm as a reasonable number. This choice implies that we need a total of $N_{cluster} = V_{body} / x_{rotor}^3 = 4.8 \times 10^{14}$ service points throughout the body.

The number of distinct molecules we will be simultaneously extracting is $N_{moleculetypes} \sim$ 25,088 (**Table 9**). We assume the use of one rotor device (possibly including up to a dozen individual binding sites around the rim) per molecule to be extracted, hence $N_{rotortypes} = N_{moleculetypes} \sim$ 25,088. Each service point throughout the body will include a cluster of $N_{rotortypes}$ = 25,088 rotors, each of volume V_{rotor} = 1372 nm^3/rotor, hence the single-cluster volume $V_{onecluster} = N_{rotortypes}\ V_{rotor}$ = 0.0344 μm^3/service point and the total volume of all rotor clusters in the array is $V_{clusters} = N_{cluster}\ V_{onecluster}$ = **16.5 cm^3**.

It must be noted that our estimate of ~25,088 molecules needing extraction should probably be regarded as a worst-case estimate. ***Future research*** should determine the minimum possible number and identity of molecules that must be extracted to ensure acceptable levels of metabolic stasis during the revival process described here. Reducing the number and mass of essential extractable molecules reduces the analysis, design, and operational complexity of the nanorobotic systems needed for a successful revival from cryostasis. It is also possible that a more detailed understanding of (and specific intervention in) deleterious processes in sub-zero cryoprotected cells on a timescale of hours might make possible sub-zero metabolic stabilization methods less complex than those contemplated here.

While more efficient branched plumbing architectures are surely available – and ***future research*** should be directed at designing them – for simplicity in the present scaling analysis we assume that one cylindrical probe, each tipped with a sorting rotor cluster, will be extended straight from the lower surface of the vasculoid to each service point in the human body. Since the vasculoid only has 1.5×10^{14} basic plates in contact with the vascular surface,[1601] in this highly inefficient architecture at least 3 probes would be extended from the underside of each vasculoid plate.

A rotor service volume radius of $\Delta X \sim$ 2-5 μm (Section 4.10.1) implies that extraction probes will be extended not just into sessile tissue cells but also into normally nonsessile cells such as microglia[1602] and other phagocytic cells. These cells should be nearly immobile at the beginning of extraction, both because of the biologically low temperature (~0 °C) at the time of reliquidification and because the nutrients and oxygen necessary to enable cell motility will have been largely exhausted during the period of warm ischemia prior to cryopreservation. As extraction proceeds, any surviving motility in these cells will be further suppressed as oxygen and nutrient concentrations are quickly reduced to submetabolic levels, forcing these cells into complete biochemical dormancy and immobility.

If the average cell is 20 μm in width and the average cell lies within 1-2 cell diameters of a capillary serviced by the vasculoid, then the mean length of each probe is $L_{probe} \sim 30$ μm. The model predicts that the rotors extract a maximum of $n_{extract,max} = 1780$ molecules/sec for the highest concentration metabolite (e.g., glutamate; Appendix I), hence the maximum rate of molecule transport would be $N_{transport} = n_{extract,max} N_{moleculetypes} = 4.47 \times 10^7$ molecules/sec for each extraction probe.

Crudely approximating molecular density as $\rho_{molec} \sim 600$ daltons/nm^3 for organic molecules of normal density (~1 gm/cm^3), the volume of the average metabolite molecule of molecular weight $MW_{metabolite} \sim 320.1$ daltons (Appendix I) is $V_{metabolite} \sim MW_{metabolite} / \rho_{molec} = 0.534$ nm^3 with diameter $d_{metabolite} \sim 2(3V_{metabolite}/4\pi)^{1/3} \sim 1.01$ nm if the shape is taken as approximately spherical. If the metabolite molecules are packed into cubic voxels of cross-sectional area $d_{metabolite}^2 = 1.02$ nm^2 and the voxels are moved through a hollow channel at $n_{transport} \sim 10^6$ molecules/sec,[1603] then the cross-sectional area of the hollow channel is $A_{channel} = (N_{transport} / n_{transport}) d_{metabolite}^2 = \underline{45.6\ nm^2}$, equivalent to a square cross-section channel of width $A_{channel}^{1/2} = 6.75$ nm. A square probe of width $w_{probe} = 30$ nm ($\underline{900\ nm^2}$ in cross-sectional area, ~20X larger than the hollow channel within) should be sufficient to accommodate the structural support, conveyor systems and other machinery needed to move this many molecules at speed. Hence the volume of each probe is $V_{probe} = w_{probe}^2 L_{probe} = 0.027$ μm^3 and the total volume of the entire 3D probe array that must be extended from the vasculoid's outer surface is $V_{array} = N_{cluster} V_{probe} =$ **13 cm^3**. (The ~0.08 μm^3 solid volume of 3 probes is only ~4% of the 2 μm^3 volume of the vasculoid basic plate from which they are deployed.) The transport power demand in a single channel for a belt-on-rollers molecular transport system with reagent-binding devices mounted on the belt is $P_{channel} = L_{probe} n_{transport} E_{molecule} = 3 \times 10^{-17}$ W, where the transport energy per molecule is $E_{molecule} \sim 10^{-6}$ zJ/nm-molecule (= 10^{-18} J/m-molecule),[1604] giving the total system power draw for all transport channels in the 3D array as $P_{allchannels} = P_{channel} N_{cluster} = 0.01$ W.

Probe cylinders this skinny (similar in axial ratio to a human hair) lack sufficient stiffness to be pushed through the reliquidified cytoplasmic and interstitial spaces, so a locomotive head of characteristic size

---

[1601] Freitas RA Jr, Phoenix CJ. Vasculoid: A Personal Nanomedical Appliance to Replace Human Blood. J Evol Technol. 2002 Apr;11(1):1-139, Section 1.1 and Table 1; http://www.jetpress.org/volume11/vasculoid.pdf.

[1602] https://en.wikipedia.org/wiki/Microglia.

[1603] Freitas RA Jr. Nanomedicine, Volume I: Basic Capabilities, Landes Bioscience, Georgetown, TX, 1999; Section 3.4.3, "Internal Transport Streams"; http://www.nanomedicine.com/NMI/3.4.3.htm.

[1604] Freitas RA Jr. Nanomedicine, Volume I: Basic Capabilities, Landes Bioscience, Georgetown, TX, 1999; Section 3.4.3, "Internal Transport Streams"; http://www.nanomedicine.com/NMI/3.4.3.htm.

L_{head} will be attached to the terminus of each probe. This head can slowly drag the probe through the aqueous medium during the extension and lateral movement phases, can help to immobilize and penetrate (sluggish) motile cells, and can later assist in reverse movement during the retraction phase of probe deployment. Allowing $L_{head} \sim 0.1\ x_{rotor} = 0.5$ μm for all locomotive mechanisms in the head and assuming for convenience a cubical form factor, the total volume of all locomotive head mechanisms is $V_{heads} = N_{cluster}\ L_{head}^3 =$ **60 cm^3**.

Hence the estimated total volume of all extraction mechanisms to be deployed outside of the vasculoid is $V_{exmech} = V_{clusters} + V_{array} + V_{heads} = 89.5$ cm^3. If an additional ~10.5 cm^3 of system volume are allocated to provide mechanisms for dealing with bigger but more infrequent molecules such as large proteins, then the entire molecular extraction system has a design volume of ~**100 cm^3**, representing just ~8% of the 1200 cm^3 total system volume of the vasculoid appliance (Section 4.6.1).

The entire extraction system delivers a maximum of $R_{extraction} = N_{cluster}\ n_{extract,max} = 8.544 \times 10^{17}$ metabolite molecules/sec to the vasculoid for export from the body. Upon delivery to the vasculoid, extracted molecules are packed into vasculoid "tankers" circulating once every $\tau_{VasculoidCirc} = 140$ sec with each tanker having $V_{tanker} = 0.75$ μm^3 of useful internal storage volume, giving a per-tanker metabolite molecule transport rate of $n_{metabolite} = V_{tanker} / \tau_{VasculoidCirc}\ V_{metabolite} = 1 \times 10^7$ molecules/tanker-sec. The tankers are moved by ciliary transport to a distant exit port embedded in the vasculoid through which the molecules can be conveniently transferred out of the body. If deemed useful, rotor clusters can employ counting rotors[1605] allowing some or all of these devices to maintain an exact count of the number of molecules of each targeted molecule type that is removed. This information, along with the time and location of the source cluster for each load of molecules, can be transferred to the tanker's onboard ~39 kilobit cargo manifest[1606] and later aggregated with all other tanker data at the exit port when the tanker is unloaded, providing a fairly detailed whole-body 3D molecular extraction map.[1607]

The maximum extraction system output can be transported using just $R_{extraction} / n_{metabolite} = 8.544 \times 10^{10}$ tankers, which is a mere 0.05% of the available 1.662×10^{14} vasculoid tanker fleet. Thus it appears that the

---

[1605] Freitas RA Jr. Nanomedicine, Volume I: Basic Capabilities, Landes Bioscience, Georgetown, TX, 1999; Section 4.2.3, "Counting Rotors"; http://www.nanomedicine.com/NMI/4.2.3.htm.

[1606] Freitas RA Jr, Phoenix CJ. Vasculoid: A Personal Nanomedical Appliance to Replace Human Blood. J Evol Technol. 2002 Apr;11(1):1-139; Section 5 "Control Systems and Computational Requirements"; http://www.jetpress.org/volume11/vasculoid.pdf.

[1607] An alternative architecture that also permits partial tracking of source would involve emplacing $N_{cluster} = 4.8 \times 10^{14}$ nanorobots (equal to the number of deployed service points) in the body, most conveniently at the tips of each extraction probe, replacing the rotor clusters. The intention would be to store all extracted material inside the nanorobots throughout the extraction process rather than immediately exporting material using vasculoid tankers, then subsequently extracting the fully-loaded nanorobots at leisure. The size of each storage nanorobot would be $V_{storagebot} = M_{material} / (f_{storage}\ \rho_{material}\ N_{cluster}) = 10.89$ μm^3, with a 1.38 μm radius assuming a spherical geometry, taking the mass of material to be removed $M_{material} = 3.9216$ kg (excluding cryoprotectant) from **Table 9**, average density of the material to be removed as $\rho_{material} \sim 1000$ kg/m^3, and the fraction of nanorobot volume available for storage $f_{storage} = 75\%$ (similar to vasculoid tankers; Section 4.5.1). Adding a storage robot fleet volume of $V_{storagefleet} = V_{storagebot}\ N_{cluster} = 5.23$ L to the $V_{body} = 60$ L human body volume represents an increase of $V_{storagefleet} / V_{body} = 8.7\%$, very near the maximum whole-body intrusiveness limit of 1-10% recommended in the literature.[*] Excluding cryoprotectant, from **Table 9** the storage robots would require a total of 7.87×10^{18} sorting rotors with a volume of $V_{rotorfleet} = 10.8$ cm^3, drawing $P_{rotorfleet} = 20.3$ W of average power, to complete the extraction in $\tau_{total} = 3600$ sec. In this case, the sorting rotors would occupy only $f_{rotor/bot} = V_{rotorfleet} / [(1 - f_{storage})\ V_{storagefleet}] = 0.83\%$ of available storage nanorobot structural volume. This fraction could plausibly be increased to ~10% in an attempt to decrease the extraction time to as low as (0.83%/10%) $\tau_{total} = 299$ sec, but only at the cost of increasing average power dissipation to $P_{rotorfleet} / (0.83\%/10\%) = 245$ W which would require increased cooling capacity in the vasculoid by 12-fold to avoid undue tissue warming prior to undertaking tissue repair operations (e.g., Section 4.11).

[*] Freitas RA Jr. Nanomedicine, Volume IIA: Biocompatibility, Landes Bioscience, Georgetown, TX, 2003; Section 15.6.1, "Somatic Intrusiveness"; http://www.nanomedicine.com/NMIIA/15.6.1.htm#p15.

vasculoid tanker fleet could be operated at <0.1% of rated capacity and still meet the minimum requirements for molecular extraction during cryopreservation revival.

4.10.2 Alternative to Targeted Extraction: Tissue Washout

In order to avoid the complexity of designing, deploying, and operating sorting rotors equipped with up to ~25,000 different binding sites, ***future research*** should evaluate an alternative approach: to simply wash out tissue solutes by locally infusing a bolus of aqueous solution, allowing dissolved solutes to leach into the infused bolus, and then pumping the bolus out again, removing some fraction of the solutes with each rinse cycle. Unwanted solutes can be perfused/diffused out on a decreasing osmotic or concentration gradient over sufficient time to avoid osmotic damage, allowing solutes to be unloaded against a concentration gradient while staying equimolar. (Animal cells exposed to pure water can osmotically explode.)[1608] Multiple rinse cycles can drive the concentration of unwanted solutes as low as is deemed desirable, with the leach fluid containing appropriate concentrations of solvated ions and other molecules consistent with maintenance of proper cell membrane integrity. The leaching fluid is pumped in and out using an array of micropipes similar in concept to the probe array described in Section 4.10.1.9.

The spacing of the micropipe termini $L_{terminus}$ apart defines an approximate micropipe service volume $V_{service} \sim L_{terminus}^3$. If the volume of leach water infused during each rinse cycle is $V_{infused} = (1/2)\ V_{service} = V_{exfused}$ (the volume of equilibrated water exfused), then the number of rinse cycles is $N_{rinse} = \log_2(c_{start}/c_{end}) \sim 10$, where c_{start} is the starting solute concentration, c_{end} is the final concentration after all rinse cycles are complete, and the maximum required concentration decrement is $c_{start}/c_{end} \sim 1000$ as described in Section 4.10.1.

Completing N_{rinse} rinse cycles in a $\tau_{total} = 3600$ sec total extraction time defines a rinse cycle time of $\tau_{rinse} = \tau_{total} / N_{rinse} = 360$ sec. Assuming for convenience equal time allotments for the three rinse cycle phases of fluid infusion, osmotic equilibration, and fluid exfusion, then $\tau_{infusion} = \tau_{equilibration} = \tau_{exfusion} = \tau_{rinse} / 3 = 120$ sec. The largest tissue fluid solute molecule with a molecular weight of $MW_{rinse} \sim 2 \times 10^6$ daltons (Appendix J) and an estimated diffusion constant (Section 4.10.1) of $D_{rinse} \sim 10^{(-0.35 \log_{10}(MWrinse) - 9.3)} \sim 3.1 \times 10^{-12}$ m^2/sec can diffuse a distance $\Delta x_{rinse} \sim (2\ D_{rinse}\ \tau_{equilibration})^{1/2} \sim 27$ μm ~ $L_{terminus}$ in $\tau_{equilibration} = 120$ sec, hence $V_{service} \sim \Delta x_{rinse}^3 \sim 19{,}700$ μm^3 and $V_{infused} = 9850$ μm^3.

In the most naïve plumbing architecture, a pipe is extended a distance L_{pipe} ~30 μm into the tissue from the underside of the vasculoid, again following the reasonable assumption that the average tissue cell is 20 μm in width and the average cell lies within 1-2 cell diameters of a capillary serviced by the vasculoid (Section 4.10.1.9). If the nozzles at the apexes of each micropipe have a separation of $L_{terminus}$, then the number of pipes necessary to create a 3D rinse array is $N_{pipes} = V_{body} / L_{terminus}^3 = 3 \times 10^{12}$ pipes throughout a $V_{body} = 60$ L human whole-body volume (of which $V_{fluid} = 38.5$ L is fluid). The volume flow rate passing through each pipe during the fluid infusion phase is $\tilde{V} = V_{infused} / \tau_{infusion} = 82$ μm^3/sec, so the Hagen-Poiseuille law requires an end-to-end pressure differential of $\Delta P = 8\ \eta_{icewater}\ L_{pipe}\ \tilde{V} / \pi\ r_{pipe}^4 = 0.0018$ atm (1.3 mmHg) for micropipes of diameter $2r_{pipe} \sim 1$ μm, representing a per-pipe power draw of $P_{pump} \sim \tilde{V}\ \Delta P = 1.5 \times 10^{-14}$ W

[1608] For example, when red blood cells are placed in pure water, water rapidly enters the cells by osmosis and causes the cells to burst, a phenomenon known as hemolysis.* More generally, rupture of the plasma membrane due to immersion of animal cells in hypotonic solution is called osmotic lysis.†

* https://science.jrank.org/pages/4930/Osmosis-Cellular-Osmosis-in-red-blood-cells.html.

† "Section 15.8 Osmosis, Water Channels, and the Regulation of Cell Volume," in Lodish H, Berk A, Zipursky SL, *et al.*, Molecular Cell Biology, 4th Edition, W.H. Freeman, NY, 2000; https://www.ncbi.nlm.nih.gov/books/NBK21739/.

and a total plumbing system power draw of $P_{rinse} \sim P_{pump}\ N_{pipes} = 0.045$ W.[1609] The infusion or exfusion fluid velocity is $v_{rinse} \sim r_{pipe}^2\ \Delta P / 8\ \eta_{icewater}\ L_{pipe} \sim 1$ mm/sec through the micropipes. However, resident tissue microstructures should be only gently displaced by the moving outermost wall of the expanding fluid bolus. The diameter of a hypothetical spherical fluid bolus would increase at only 5.4 μm/sec during the first second of infusion when the bolus is smallest but would slow to 0.046 μm/sec in the last second of infusion as the swelling bolus reaches its maximum size.[1610] This seems slow enough to avoid significant disturbance of existing tissue structures because the bolus speed is comparable to the ~0.1 μm/sec chromosome transport speed during mitosis,[1611] the ~0.3 μm/sec velocity of biomolecular diffusion estimated above,[1612] the 0.05-0.7 μm/sec speed of leukocyte and fibroblast amoeboid movement through extracellular tissue,[1613] the 2-4 μm/sec speed of axonal transport of membrane-bound vesicles in neurons,[1614] and the ~10 μm/sec speed at which micron-sized mitochondria are shuttled around the cellular interior.[1615]

The repeated forward and reverse cycling through each nozzle provides a backflushing effect to help resist clogging and biofouling at the intake aperture. Additional mechanical filters and wipers may be needed to keep the opening clear during the entire 10 cycles of operation. The direction of pumping from adjacent pipe termini can be alternated so that the total bolus volumes remain approximately constant at any given time thus preventing ballooning of tissue mass, with half of the pipe termini injecting fluid and the other half extracting the same volume of leachate fluid at any point in each cycle.

The lateral apically-applied buckling force of a hollow pipe of inside radius $r_{pipe} = 500$ nm, wall thickness $w_{pipe} = 33$ nm, outside radius $R_{pipe} = r_{pipe} + w_{pipe}$, length $L_{pipe} = 30$ μm, and Young's modulus $E_{pipe} = 1.05 \times 10^{12}$ N/m^2 for diamond is $F_{buckle} = \pi^3\ E_{pipe}\ (R_{pipe}^4 - r_{pipe}^4) / 4\ L_{pipe}^2 = 165{,}000$ nN, ~1000-fold higher than the ~165 nN lateral force exerted by a fibroblast locomoting through tissue.[1616] Such a pipe has a material volume of $V_{pipe} = 2\pi\ r_{pipe}\ L_{pipe}\ w_{pipe} = 3.1\ \mu m^3$, so the entire pipe array has a material volume of $V_{pipearray} = V_{pipe}\ N_{pipes} =$ **9.3 cm^3**, a small fraction of the ~1200 cm^3 vasculoid material volume (Section 4.6.1).

[1609] Freitas RA Jr. Nanomedicine, Volume I: Basic Capabilities, Landes Bioscience, Georgetown, TX, 1999; Section 9.2.5, "Pipe flow"; http://www.nanomedicine.com/NMI/9.2.5.htm.

[1610] $2([(3/4\pi)(1\text{ sec})(82\ \mu m^3/\text{sec})]^{1/3}) / (1\text{ sec}) = 5.4$ μm/sec; $2([(3/4\pi)(19{,}700\ \mu m^3)]^{1/3} - [(3/4\pi)(19{,}618\ \mu m^3)]^{1/3}) / (1\text{ sec}) = 0.046$ μm/sec.

[1611] Forer A. Chapter 23. Chromosome movements during cell-division. In: Lima-de-Faria A, ed., Handbook of Molecular Cytology, Volume 15, North Holland Publ. Co., Amsterdam, 1969, pp. 553-601; https://www.amazon.com/dp/072047115X/.

[1612] 27 μm / 120 sec = 0.3 μm/sec.

[1613] Peacock EE Jr. Wound Repair, W.B. Saunders Company, Philadelphia, 1984; https://www.amazon.com/dp/0721671454/. Keller HU, Zimmermann A, Cottier H. Cell shape, movement, and chemokinesis. Adv Biosciences 1987;66:21-27. Stefano GB, Shipp MA, Scharrer B. A possible immunoregulatory function for Met-enkephalin-Arg^6-Phe^7 involving human and invertebrate granulocytes. J Neuroimmunol. 1991 Feb;31(2):97-103; https://www.sciencedirect.com/science/article/abs/pii/016557289190015Y.

[1614] Loewy AG, Siekevitz P, Menninger JR, Gallant JAN. Cell Structure and Function: An Integrated Approach, Third Edition, Saunders College Publishing, Philadelphia PA, 1991; https://www.amazon.com/dp/0030474396/. Becker WM, Deamer DW. The World of the Cell, Second Edition, Benjamin/Cummings Publishing Company, Redwood City CA, 1991; https://www.amazon.com/dp/0805308709/.

[1615] Ashkin A, Schutze K, Dziedzic JM, Euteneuer U, Schliwa M. Force generation of organelle transport measured *in vivo* by infrared laser trap. Nature 1990 Nov 22;348(6299):346-348; https://www.nature.com/articles/348346a0.

[1616] James DW, Taylor JF. The stress developed by sheets of chick fibroblasts *in vitro*. Exp Cell Res. 1969 Jan;54(1):107-110; https://www.sciencedirect.com/science/article/abs/pii/0014482769902997?via%3Dihub.

During each rinse cycle, a volume $V_{in} = V_{infused}\ N_{pipes}$ = 29.6 L of leach water must be infused into the patient from the vasculoid in an infusion time of $\tau_{infusion}$ = 120 sec, giving a total volumetric transport rate of $\tilde{V}_{in} = V_{in} / \tau_{infusion}$ = 246 cm^3/sec on the infusion side. (A similar volume of solute-equilibrated leach water must be transported out of the body on the exfusion side.) Unfortunately, the entire N_{tanker} = 332.4 x 10^{12} tanker vasculoid fleet has a maximum volumetric transport rate of $\tilde{V}_{tankerfleet} = V_{tanker}\ N_{tanker} / \tau_{trankfer}$ = 1.8 cm^3/sec, too small by ~100X to accommodate the rinse water volumes involved. However, the interior volume of vasculoid ($V_{vascint}$ ~ 4200 cm^3)[1617] can be employed to accommodate a 246 cm^3/sec flow rate if the fluid filling this interior volume can be recycled once every $\tau_{recycle} \sim V_{vascint} / \tilde{V}_{in}$ = 17 sec, representing a very reasonable average fluid flow velocity of $L_{vasc} / \tau_{recycle}$ ~ 8 cm/sec through the average L_{vasc} ~ 1.4 m body circuit distance in the human vasculature. This is only ~4 times faster than the ~2 cm/sec mean blood flow velocity[1618] in the live human vasculature.

Care must be taken to ensure that selected ions and solutes deemed essential to maintain cellular structural stability are not excessively removed by the washout procedure. If necessary, such essential molecules could be imported via the vasculoid transport system and reintroduced into the cytoplasm after the primary tissue washout process is complete.

The design and analysis of a less naïve plumbing architecture is another appropriate task for ***future research***.

4.11 Reseal Plasma Membrane Compartments and Rehydrate

Restoring the integrity of whole-cell plasma membrane compartments is the highest priority objective of early repair because cells are the basic units of biology. If cells lose integrity, or if their broken integrity is not restored, they cannot function and the tissue will lose structure and die. Repairing non-plasma membrane compartments of intracellular organelles such as lysosomes and mitochondria is deferred until a later time when detailed cell repair is being performed (Section 4.12).

As the cryopreserved tissue warms toward 273 K (0 °C), softens and thaws, all fracture crackfaces will have been drawn together (Section 4.9), closing pathological voids and enabling the spontaneous refusion of many cellular plasma membranes that had become separated during fracture events. However, not all membranes will have properly resealed even if intact, and some membranes that had been torn during fracture will retain tears or gaps. Both of these membrane faults must be repaired wherever they occur.

Simultaneously and over a relatively short period of time (~1 hr; Section 4.10), molecular extraction will have rapidly reduced the local concentrations of all biochemically active or potentially degradative chemical substances by at least 100-fold, effectively placing the newly reliquidified tissue in a state of biochemical stasis (or at least minimal biochemical activity) at the lowest feasible reliquidification temperature over the time period of relevance to subsequent repair operations. Potentially lethal[1619]

[1617] The blood volume which the vasculoid (Section 4.5) is designed to replace is 5400 cm^3; subtracting the 1200 cm^3 displacement volume of the vasculoid appliance machinery (**Table 5**) implies a 4200 cm^3 interior free volume.

[1618] (mean 1.4 m circuit distance) / (60 sec mean circulation time) ~ 2 cm/sec mean flow velocity.

[1619] For example, primates frozen without cryoprotectant and then thawed died from pulmonary edema (due to fluid leaking into the lungs through freeze-damaged pulmonary alveoli) or from intraperitoneal bleeding (due to gastric juice that leaked from the freeze-damaged stomach or biliary glands into abdominal tissue). Smith AU. Viability of supercooled and frozen mammals. Ann N Y Acad Sci. 1959 Sep 14;80:291–300; https://nyaspubs.onlinelibrary.wiley.com/doi/abs/10.1111/j.1749-6632.1959.tb49209.x.

digestive enzymes, corrosive acids, or toxins accumulated during cryopreservation or thawing that leaked from cells whose plasma membranes have lost integrity or that spilled from broken organelles will have been extracted previously, leaving only low concentrations of these chemicals that will not cause immediate further degradation.

Restoration of damaged cell plasma membranes comes first (Section 4.11.1), followed by the repair of plasma membranes that were improperly fused at fracture face interfaces (Section 4.11.2). As plasma membrane integrity is restored, cells are rehydrated to biologically healthy levels (Section 4.11.3).

4.11.1 Restore Damaged Cell Plasma Membranes

Cell plasma membrane repairs may be performed by medical nanorobots imported into the body via the vasculoid transport system and locally deployed via periodically positioned cellulocks. Nanorobots can patrol the newly reliquidified tissues using locomotive methods described elsewhere,[1620] employ contact sensing[1621] to determine the integrity (or lack thereof) of all cell plasma bilayer membranes encountered, report out these results for comparison with the repair plan, and then perform local repairs as necessary either by mechanically inducing membrane resealing of *in situ* materials[1622] or by adding new lipid bilayer membrane material (image, below) imported from external cell mills (Appendix D) and installed at the site of a membrane break or breach. (The reinsertion of proteins into the damaged plasma membrane is deferred until later; Section 4.12.2.5.) The restoration of cell plasma membranes should verifiably establish the presence of complete cell enclosures at the positions and in the orientations and shapes described in the repair plan devised in Section 4.8. Membrane repair includes all endothelial cells, including swollen or blebbed endothelial cells that were trimmed during microvascular excavation (Section 4.4.1) prior to vasculoid installation (Section 4.6.2), thus ensuring restoration of the cellular integrity of the vasculature. Cells that have been sealed after suffering deeper avulsion wounds should be subjected to comprehensive cell repair (Section 4.12.2).

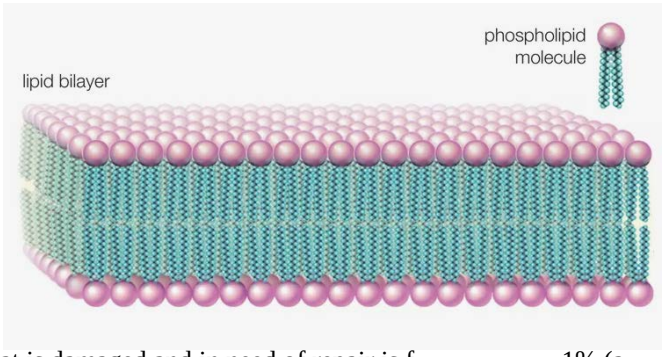

If the estimated fraction of cryopreserved tissue cell plasma membrane surface area that is damaged and in need of repair is $f_{CellPMdamaged} \sim 1\%$ (a figure to be determined by ***future research***, including direct experimental measurements), then the total plasma surface area to be repaired is $A_{CellPMrepair} = f_{CellPMdamaged}\ A_{CellPM} \sim 1.32 \times 10^{14}\ \mu m^2$, where total cell plasma membrane area in the whole body is $A_{CellPM} = N_{braincells}\ A_{braincell} + N_{bodycells}\ A_{bodycell} \sim 1.32 \times 10^{16}\ \mu m^2$, $N_{braincells} \sim 200 \times 10^9$ cells in the human brain each with plasma membrane surface area of $A_{braincell} \sim$

[1620] Freitas RA Jr. Nanomedicine, Volume I: Basic Capabilities, Landes Bioscience, Georgetown TX, 1999, Section 9.4.3, "Cytoambulation", http://www.nanomedicine.com/NMI/9.4.3.htm; and Section 9.4.4, "Histonatation"; http://www.nanomedicine.com/NMI/9.4.4.htm.

[1621] Freitas RA Jr. Nanomedicine, Volume I: Basic Capabilities, Landes Bioscience, Georgetown TX, 1999, Section 4.2.8, "Chemotactic Sensor Pads", http://www.nanomedicine.com/NMI/4.2.8.htm; and Section 8.5.2.1, "Identification of Self"; http://www.nanomedicine.com/NMI/8.5.2.1.htm#p8.

[1622] Freitas RA Jr. Nanomedicine, Volume I: Basic Capabilities, Landes Bioscience, Georgetown TX, 1999, Section 9.4.5.6, "Breach Sealing and Intrusiveness", http://www.nanomedicine.com/NMI/9.4.5.6.htm

24,000 μm^2/cell (Section 4.8.1(6)), and $N_{bodycells} \sim 3.5 \times 10^{12}$ tissue cells in the entire human body[1623] with average plasma membrane surface area $A_{bodycell} \sim 2400\ \mu m^2$/cell.[1624] Allowing one scanning nanorobot and one repair nanorobot per cell, and conservatively assuming for this calculation that brain cells are not a subset of the body cell count, the estimated scan + repair time is $\tau_{CellPMrepair} = [(A_{CellPM} / \kappa_{PMscan}) + (A_{CellPMrepair} / \kappa_{PMrepair})] / (N_{braincells} + N_{bodycells}) \sim 714{,}000$ sec (**8.3 days**) using a total of $N_{PMscanbots} = N_{braincells} + N_{bodycells} = 3.7 \times 10^{12}$ scanning nanorobots and $N_{PMrepairbots} = N_{PMscanbots} = 3.7 \times 10^{12}$ repair nanorobots, assuming a plasma membrane scan rate of $\kappa_{PMscan} = 10^{-2}\ \mu m^2$/ nanorobot-sec (Section 4.5.4) and a plasma membrane repair rate of $\kappa_{PMrepair} = 0.01\ \kappa_{PMscan} = 10^{-4}\ \mu m^2$/nanorobot-sec (i.e., arbitrarily assumed to be 100 times slower than scanning). These are at best crude estimates of achievable nanorobot scan and repair rates, so a more comprehensive analysis of the logistics of complete scan and repair operational cycles should be undertaken during ***future research***. Taking nanorobot power $P_{nanorobot} \sim 100$ pW in continuous opera-tion,[1625] whole-body nanorobotic waste heat generation is $P_{CellPM} \sim N_{PMrepairbots}\ P_{nanorobot} = 370$ watts, likely requiring vasculoid-assisted systemic cooling to hold body temperature near the desired 273 K (0 °C).

Mechanical ice grinding during thawing may produce large debris from damaged cell plasma membranes or from the damaged membranes of intracellular organelles. All pre-thaw debris will have been mapped down to debris sizes as small as ~0.1 μm (Section 4.7). A small piece of cell debris having a characteristic size $L_{debris} \sim$ **0.1 μm** and volume $V_{debris} \sim L_{debris}^3 \sim 0.001\ \mu m^3$ with an effective molecular weight $MW_{debris} \sim \rho_{molec}\ V_{debris} = 6 \times 10^8$ daltons, assuming molecular density $\rho_{molec} \sim 600$ daltons/nm^3 for organic molecules of normal density (~1 gm/cm^3), should have an effective diffusion constant in melted cytosolic water at 273 K (0 °C) of $D_{debris} \sim 10^{(-0.35\ \log_{10}(MWdebris)\ -\ 9.3)} \sim 4.2 \times 10^{-13}\ m^2$/sec (Section 4.10.1), hence may diffuse a distance $\Delta x_{debris} \sim (2\ D_{debris}\ \Delta t)^{1/2} \sim$ **55 μm** during a post-reliquidification time interval of $\Delta t \sim$ 3600 sec (1 hour).[1626] For larger debris particles with $L_{debris} \sim$ **1 μm**, $MW_{debris} \sim 6 \times 10^{11}$ daltons, and $D_{debris} \sim 3.8 \times 10^{-14}\ m^2$/sec, $\Delta x_{debris} \sim$ **16 μm** during $\Delta t \sim 3600$ sec.

This implies that visible debris items may be able to random-walk a distance of up to 1-2 cell diameters by the end of the 1-hour molecular extraction period (Section 4.10) except where impeded by obstacles such as cytoskeletal microtubules, intact membranes, or ECM fiber networks. However, the previous solid-phase mapping should still provide a record of the size, shape, and probable source, hence likely composition, of all ≥0.1 μm pre-thaw debris items, enabling nanorobots encountering these items in the fluid to make a positive identification. Note that debris flow through the fluid during thawing will have a Reynolds number[1627] of $N_R \sim \rho_{water}\ v_{flow}\ L_{debris} / \eta_{water} \sim 10^{-10}$, taking $\rho_{water} \sim 1000$ kg/m^3, $v_{flow} \sim \Delta x_{debris} / \Delta t \sim 1.5 \times 10^{-8}$ m/sec, $L_{debris} \sim 0.1$ μm, and $\eta_{water} = 1.787 \times 10^{-3}$ Pa-sec at 273 K (0 °C). A Reynolds number of $N_R \leq 1$

[1623] Freitas RA Jr. Nanomedicine, Volume I: Basic Capabilities, Landes Bioscience, Georgetown TX, 1999, Section 8.5.1, "Cytometrics"; http://www.nanomedicine.com/NMI/8.5.1.htm#p5.

[1624] Freitas RA Jr., Nanomedicine, Volume I: Basic Capabilities, Landes Bioscience, Georgetown, TX, 1999, Table 8.17, "Approximate Quantification of the Components of a Typical 20-μm Human Tissue Cell"; http://www.nanomedicine.com/NMI/Tables/8.17.jpg.

[1625] Freitas RA Jr. Microbivores: Artificial Mechanical Phagocytes using Digest and Discharge Protocol. J. Evol. Technol. 2005 Apr;14:55-106; http://www.jetpress.org/volume14/freitas.pdf. Freitas RA Jr. The Ideal Gene Delivery Vector: Chromallocytes, Cell Repair Nanorobots for Chromosome Replacement Therapy. J. Evol. Technol. 2007 Jun;16:1-97; http://jetpress.org/v16/freitas.pdf.

[1626] Another estimate of the diffusion distance uses the Einstein approximation* for the root-mean-square displacement $\Delta x \sim (k_B T\ \Delta t / 3\pi\ \eta\ R)^{1/2} \sim$ **127 μm** for a particle of radius R = 0.05 μm in liquid water of viscosity $\eta = 1.787 \times 10^{-3}$ Pa-sec at temperature T = 273 K, with $\Delta t = 3600$ sec.
* Einstein A. Über die von der molekularkinetischen Theorie der Wärme geforderte Bewegung von in ruhenden Flüssigkeiten suspendierten Teilchen. Annalen der Physik. 1905;322(8):549-560 (in German).

[1627] https://en.wikipedia.org/wiki/Reynolds_number.

indicates laminar,[1628] not turbulent, flow. Swimming microscale bacteria typically have $N_R \sim 10^{-5}$, so a highly laminar $N_R \sim 10^{-10}$ minimizes the prospect of long-range chaotic "stirring" that may occur, making it computationally tractable to backtrack the laminar flow path of a particular debris item to somewhere near its originating locale. The Reynolds number is even lower for smaller debris items or more viscous fluid at lower temperatures. ***Future research*** should experimentally measure the paths and rates of passive migration of nanoscale and microscale objects of irregular shape through cytosol and extracellular matrix as a function of temperature and viscosity.

As for post-thaw debris items that arise during warming, and also for debris items <0.1 μm in size, upon detection these items could have their positions recorded, then be removed intact from the tissue by nanorobots and exported from the body through the vasculoid, then externally examined and characterized for molecular content to provide identification and consistency with the repair plan (Section 4.8). The repair plan can now be updated to reflect the new information. Replacement cell structures may be manufactured using external cell mills (Appendix D) and imported back into the body for installation at local repair sites as needed. ***Future research*** should investigate the size, quantity, and character of cell debris items likely to be created during cryopreservation and subsequent thawing, as a function of tissue type and the extent of cryoprotectant perfusion in that tissue, in order to more accurately estimate nanorobotic debris-processing requirements.

As a crude initial estimate of such requirements, debris scavenging nanorobots patrolling a typical V_{cell} = 8000 μm^3 tissue cell[1629] at an intracellular natation velocity of $v_{celldebris}$ = 1-10 μm/sec[1630] while sampling a circumferential cross-sectional area around the nanorobot of $A_{debrisscanarea}$ = 10 μm^2 can complete one pass through the entire cell volume in $\tau_{celldebrispass} = V_{cell} / v_{celldebris} A_{debrisscanarea}$ = 80-800 sec. Allowing tenfold more time for debris acquisition and multiple round trips to and from the nearest vasculoid cellulock to deliver the debris item for export, debris clearance can probably be completed in $\tau_{celldebris} \sim 8000$ sec (~2.2 hr) per cell. This implies that a fleet of $N_{debrisbots} \sim 10^{12}$ debris removal nanorobots generating $P_{celldebris} \sim N_{debrisbots} P_{nanorobot}$ = 100 watts of continuous whole-body waste heat could complete all debris removal operations in all body tissue cells in $t_{debrisremoval} \sim \tau_{celldebris} N_{bodycells} / N_{debrisbots}$ = 28,000 sec (~**7.8 hr**).

Applying Stokes drag,[1631] a spherical scavenging nanorobot of radius R_{nano} = 1 μm can be driven through pure liquid water-ice of absolute viscosity $\eta_{cell} = \eta_{icewater} = 1.787 \times 10^{-3}$ Pa-sec at 273 K (0 °C) at a velocity of v_{nano} = 10 μm/sec by applying a locomotive power of $P_{nanovisc} = 6 \pi \eta_{cell} R_{nano} v_{nano}^2 = 3.3 \times 10^{-6}$ pW,[1632] or $P_{nanovisc}$ = 0.06 pW taking a cytosolic viscosity of $\eta_{cell} \sim 30$ Pa-sec for representative human white cells

---

[1628] "Laminar flow occurs at low Reynolds numbers, where viscous forces are dominant, and is characterized by smooth, constant fluid motion"; https://en.wikipedia.org/wiki/Reynolds_number#Definition.

[1629] Freitas RA Jr., Nanomedicine, Volume I: Basic Capabilities, Landes Bioscience, Georgetown, TX, 1999, Table 8.17, "Approximate Quantification of the Components of a Typical 20-μm Human Tissue Cell"; http://www.nanomedicine.com/NMI/Tables/8.17.jpg.

[1630] Freitas RA Jr. Nanomedicine, Volume I: Basic Capabilities, Landes Bioscience, Georgetown TX, 1999, Section 9.4.6, "In Cyto Locomotion", http://www.nanomedicine.com/NMI/9.4.6.htm.

[1631] https://en.wikipedia.org/wiki/Stokes%27_law#Statement_of_the_law. Stokes drag for a sphere provides a good order of magnitude estimate for nanorobot locomotive power. This idealized formula is for an isolated sphere, far from any boundaries such as vessel walls. Boundaries impose a no-slip condition on the flow which increases the drag on nearby objects. Studies of drag power on small objects near walls in viscous fluids suggest at most a factor of 10 increase, still small compared to a 100 pW nanorobot power budget.

[1632] Freitas RA Jr. Nanomedicine, Volume I: Basic Capabilities, Landes Bioscience, Georgetown TX, 1999, Section 9.4.2.4, "Force and Power Requirements", http://www.nanomedicine.com/NMI/9.4.2.4.htm.

at 273 K,[1633] either of which is a tiny fraction of the previously stated available nanorobot power budget of $P_{nanorobot}$ ~ 100 pW.

4.11.2 Repair Improperly Rejoined Fracture Face Plasma Membranes

The location of all potentially improper fractured-membrane rejoins will be known from previous mapping, so nanorobots can be targeted to those locations to inspect the quality and completeness of the results. The same repair procedures (Section 4.11.1) can then be used to correct plasma membrane reseal errors that have occurred during crackface fusion (Section 4.9).

Fahy[1634] notes that "fractured surfaces will generally be cross-sections through various membrane-limited compartments (cells, myelinated axons, organelles), and planar separations between membrane bilayers. Within membrane-enclosed compartments, filamentous structures and molecular clusters such as enzyme complexes will be cleaved. In most cases, relatively free molecules such as cytoplasmic globular proteins should not be fractured, and the few that might be lost in this way can be neglected. Fractured microtubules, actin, etc. can be healed enzymatically. Steric hindrance is not a likely problem for individual molecules. Disrupted enzyme clusters can be reclustered (and will often recluster spontaneously when warmed sufficiently).[1635] As the naked membrane faces are brought together, they will tend to fuse spontaneously.[1636] This is also true for bringing together membranes fractured between leaflets. No specific chemical bonding will have to be induced to heal the major portion of the fracture. If membrane fluidity is too low to permit good fusion at the prevailing temperatures, a small amount of specialty lipid

---

[1633] Freitas RA Jr., Nanomedicine, Volume I: Basic Capabilities, Landes Bioscience, Georgetown, TX, 1999, Table 9.4, "Absolute Viscosity of Some Common Materials"; http://www.nanomedicine.com/NMI/Tables/9.4.jpg.

[1634] Fahy G. Appendix B. A "Realistic" Scenario for Nanotechnological Repair of the Frozen Human Brain. In: Wowk B, Darwin M, eds., Cryonics: Reaching for Tomorrow. Alcor Life Extension Foundation, 1991, pp. A-10 – A-26; https://alcor.org/Library/html/nanotechrepair.html.

[1635] "Both proteins and membranes exist in the form they do because of the immiscibility of water and hydrocarbons. This immiscibility causes these structures to self-assemble spontaneously if permitted to do so; this is the basis of spontaneous protein renaturation and membrane assembly. Protein clusters often involve hydrophobic associations as well, but even when other contributions are more important, mis-clustering is, in principle, equally spontaneously reversible. Self-assembly can happen incorrectly, but, given a little guidance, can surely be directed to happen correctly." Fahy G. Appendix B. A "Realistic" Scenario for Nanotechnological Repair of the Frozen Human Brain. In: Wowk B, Darwin M, eds., Cryonics: Reaching for Tomorrow. Alcor Life Extension Foundation, 1991, pp. A-10 – A-26; https://alcor.org/Library/html/nanotechrepair.html.

[1636] "Fat exposed to water preferentially associates with other fat if any is available. A fractured membrane presents two 'greasy' surfaces to water, which is entropically unfavorable; it is thermodynamically favorable for these two cut surfaces to fuse together so as to eliminate the unfavorable water-fat interface. This tendency is, however, reduced by low temperatures (which reduce the energy cost of hydrating fat) and by solidification of the membrane. A good general discussion of these issues is given in The Hydrophobic Effect, Formation of Micelles and Biological Membranes, by Charles Tanford (2nd Edition, 1980, John Wiley & Sons, New York). As Tanford notes (p. vii): 'The hydrophobic effect is perhaps the most important single factor in the organization of the constituent molecules of living matter into complex structural entities such as cell membranes and organelles.'" Fahy G. Appendix B. A "Realistic" Scenario for Nanotechnological Repair of the Frozen Human Brain. In: Wowk B, Darwin M, eds., Cryonics: Reaching for Tomorrow. Alcor Life Extension Foundation, 1991, pp. A-10 – A-26; https://alcor.org/Library/html/nanotechrepair.html.

can be added to the local area to enhance fluidity sufficiently to permit fusion to occur.[1637] After membrane fusion has occurred, some individual molecular species (particularly cross-linked proteins) associated with the formerly fractured area of the membrane might exist in a damaged (cleaved) form. These damaged components can be examined later, at higher temperatures, where they can be enzymatically[1638] healed."

Restoration can proceed as previously described in Section 4.11.1. If total crackface void volume is ~1% of all tissue volume (Section 4.6.3), and if the plasma membrane damage rate for fractured tissue cells (Section 4.9.2) is similar to the damage rate for nonfractured tissue cells, then the operating times and the number of nanorobots needed to correct improperly rejoined fracture face plasma membranes should be ~1% of the numbers needed to repair the damaged plasma membranes of nonfractured tissue cells (Section 4.11.1).

4.11.3 Cell Rehydration and Extracellular Water Transfers

With cell plasma membranes repaired and sealed against gross leakage, we can now initiate rehydration to return cell volumes and cell water contents to normal. This will be done in coordination with cryoprotectant extraction (Section 4.10.1.7) to maintain liquidity at our preferred temperature for cell repair (to be determined by ***future research***). Because metabolic activity has been largely eliminated via molecular extraction (Section 4.10), we can favor higher temperatures near the water-ice freezing point to "maximize membrane fluidity and minimize problems that may arise from unreversed membrane lipid phase transitions during cellular and membrane re-expansion."[1639]

[1637] "'Specialty lipids' could be made by reducing the number of carbon atoms in the fatty acid tails of ordinary membrane phospholipids, increasing the number of double bonds (especially *cis* double bonds) in these tails, fluorinating the fatty acid tails, modifying polar head groups to prevent close association of the lipid tails (by preventing clumping of these head groups), or by any combination of these maneuvers. These modifications are all known to reduce the freezing points of lipids and/or hydrocarbons and hence increase their fluidity. (See also: Small, D. M., *et al*, The Physical Chemistry of lipids: From Alkanes to Phospholipids. Plenum Press, New York, 1986 [Handbook of Lipid Research, Vol. 4].) Specialty lipids based on such modifications should, therefore, enhance the ability of lipid phases doped with them to fuse. It does not seem likely that the specialty lipids must reverse membrane phase separations to effect membrane fusion. Even small, free molecules such as pentane or its relatives could suffice: as long as the molecule is insoluble in water and preferentially associates with hydrophobic species, it should produce the desired effect. (The fact that membranes continue to exist at low temperatures suggests that hydrophobic forces will remain strong enough at these temperatures to promote self-assembly of hydrophobic entities in an aqueous environment.) Even if a molecule such as pentane becomes volatile on warming, the membrane will not be affected, provided it becomes sufficiently fluid before the small species evaporates." Fahy G. Appendix B. A "Realistic" Scenario for Nanotechnological Repair of the Frozen Human Brain. In: Wowk B, Darwin M, eds., Cryonics: Reaching for Tomorrow. Alcor Life Extension Foundation, 1991, pp. A-10 – A-26; https://alcor.org/Library/html/nanotechrepair.html.

[1638] "Evidence that it is permissible to heal some fracture damage at higher temperatures is provided by the results of Dr. Luiz de Medinaceli, who found he could regenerate rat sciatic nerves that he had first frozen and then cut cleanly at temperatures just below 0 degrees C. The nerve ends were held together by special tethers and extracellular potassium was elevated to keep the cut axons alive. Only very cleanly cut nerves regenerated well. His work was discussed in a series of papers that appeared in Experimental Neurology, Volume 81 (pages 459-468; 469-487; and 488-496) and Volume 84 (396-408), in 1983 and 1984. See particularly Vol. 81, pp. 469-496. His work is now being extended to human patients (personal communication)." Fahy G. Appendix B. A "Realistic" Scenario for Nanotechnological Repair of the Frozen Human Brain. In: Wowk B, Darwin M, eds., Cryonics: Reaching for Tomorrow. Alcor Life Extension Foundation, 1991, pp. A-10 – A-26; https://alcor.org/Library/html/nanotechrepair.html.

[1639] Fahy G. Appendix B. A "Realistic" Scenario for Nanotechnological Repair of the Frozen Human Brain. In: Wowk B, Darwin M, eds., Cryonics: Reaching for Tomorrow. Alcor Life Extension Foundation, 1991, pp. A-10 – A-26; https://alcor.org/Library/html/nanotechrepair.html.

Frozen cells will have been greatly dehydrated by the freezing process because during equilibrium freezing, the intracellular space equalizes osmolality with the freeze-concentrated increasing osmolality of the extracellular space principally by losing water to the extracellular space. The extraction of cryoprotectant from the cytosol of cells with intact plasma membranes should permit the spontaneous diffusion of water from the extracellular spaces (where liquid water is again present) to intracellular compartments. However, the previous extraction of many soluble solutes (Section 4.10) will greatly reduce the osmotic pressures that would normally lead to spontaneous rehydration. To the extent that all necessary water diffusion does not occur, or does not occur fast enough, pumping nanodevices similar to those that were deployed from the vasculoid for intracellular molecular extraction (Section 4.10.1.9) may be used to transfer water directly into dehydrated cells, including sufficient solutes to maintain osmolal stability, as determined by ***future research***. In the worst case, a transfer of the entire V_{fluid} = 38.5 L of aqueous intracellular and interstitial volume using a vasculoid with $N_{tankers} = 166.2 \times 10^{12}$ tankers, each circulating once every $\tau_{VasculoidCirc}$ = 140 sec and each having $V_{TankerInt}$ = 0.75 μm^3 of usable internal storage, would take $t_{watertransfer} = V_{fluid} / (V_{TankerInt}\ N_{tankers} / \tau_{VasculoidCirc})$ ~ **12 hours** to complete. The same system can be used to export excess water out of the body from any regions where it is not needed, or to import water from outside of the body to any internal regions where it is in short supply.

As cells rehydrate and expand, any tensile stresses that appear in the plasma membrane can be relieved by the insertion of additional exogenous plasma membrane material (Section 4.11.1) or specialty lipid (Section 4.11.2) as described earlier.

4.12 Conventional Cellular and Tissue Repair

With all plasma membranes repaired and cells (illustration, right)[1640] fully hydrated and no longer prone to gross leakage, we can now undertake extensive repair operations designed to correct all the forms of damage identified in Chapter 3, using conventional cell repair and tissue repair nanorobots resourced with power,[1641] communication[1642] and navigation[1643] in the usual manner.

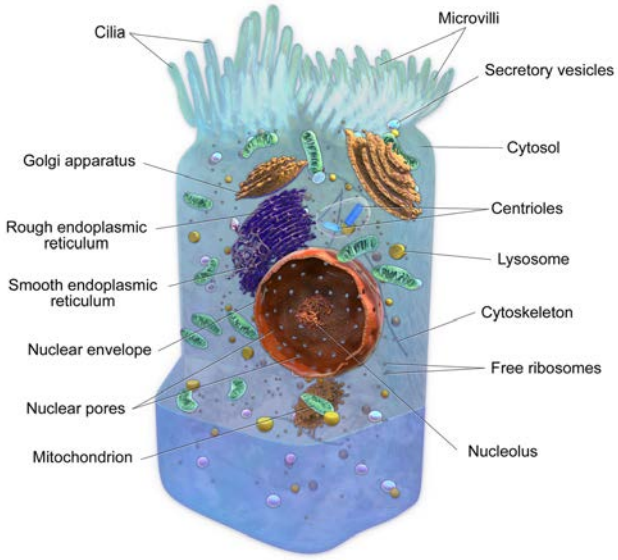

Repairs begin with the removal of unwanted cells and microbodies in the tissues (Section 4.12.1), then proceed with the inspection and repair or replacement of the interior organelles of all existing cells (Section 4.12.2), followed

---

[1640] Blausen.com staff (2014). "Medical gallery of Blausen Medical 2014". WikiJournal of Medicine **1** (2). DOI:10.15347/wjm/2014.010.

[1641] Freitas RA Jr. Nanomedicine, Volume I: Basic Capabilities, Landes Bioscience, Georgetown TX, 1999, Chapter 6, "Power", http://www.nanomedicine.com/NMI/6.1.htm.

[1642] Freitas RA Jr. Nanomedicine, Volume I: Basic Capabilities, Landes Bioscience, Georgetown TX, 1999, Chapter 7, "Communication", http://www.nanomedicine.com/NMI/7.1.htm.

[1643] Freitas RA Jr. Nanomedicine, Volume I: Basic Capabilities, Landes Bioscience, Georgetown TX, 1999, Chapter 8, "Navigation", http://www.nanomedicine.com/NMI/8.1.htm.

by supplemental tissue and vascular repairs with reconditioning of the extracellular matrix (Section 4.12.3) along with supplemental repair of axons and neuron membranes and the restoration of missing brain tissue (Section 4.12.4), as described at length below.

4.12.1 Remove Unwanted Cells and Microbodies

Nontissue or foreign whole cells or other membrane-bound bodies may have become embedded in cryopreserved tissues. Their removal has been postponed to this point in time because the extraction of all energy sources and signaling molecules during the first hour of tissue reliquidification (Section 4.10) virtually guarantees that these objects will remain biologically inert even if rewarmed to 273 K (0 °C).

It is now time to remove six specific classes of unwanted items: extracellular vesicles (Section 4.12.1.1), red cells and platelets (Section 4.12.1.2), white cells (Section 4.12.1.3), bacteria (Section 4.12.1.4), other pathological microbes (Section 4.12.1.5), and cancer cells (Section 4.12.1.6).

4.12.1.1 Extracellular Vesicles

As noted in Section 4.10.1.8(6), there are three main types of extracellular vesicles (image, right)[1644] that may be present in cryopreserved tissue, though likely in concentrations small enough to preclude significant biochemical activity. While ***future research*** should determine the size distribution and number density of these microbodies, for present purposes we shall assume that we must find and remove:

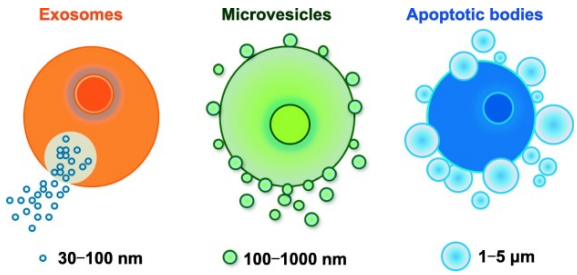

(a) $n_{mv} \sim 5.9 \times 10^{9}$/ml of ~200 nm diameter ($V_{mv} \sim 0.004\ \mu m^3$) **microvesicles**[1645] present in blood plasma of total volume $V_{plasma} = 0.59\ V_{blood} = 3.2$ L,[1646] of which $f_{leak} = V_{plasma}/V_{interstitial} = 30\%$ is assumed to leak into the total interstitial volume[1647] $V_{interstitial} \sim 10.5$ L of a 70 kg human body prior to cryopreservation, leaving a total of $N_{mv} = f_{leak}\ n_{mv}\ V_{interstitial} = 1.9 \times 10^{13}$ microvesicles;

(b) $n_{exo} \sim 2 \times 10^{10}$/ml plasma of ~90 nm diameter ($V_{exo} \sim 0.00004\ \mu m^3$) **exosomes**[1648] of which up to $N_{exo} = f_{leak}\ n_{exo}\ V_{interstitial} = 6.3 \times 10^{13}$ exosomes are assumed to leak into the tissues prior to cryopreservation; and

---

[1644] Chen Y, Li G, Liu ML. Microvesicles as Emerging Biomarkers and Therapeutic Targets in Cardiometabolic Diseases. Genomics Proteomics Bioinformatics. 2018 Feb;16(1):50-62; https://www.ncbi.nlm.nih.gov/pmc/articles/PMC6000161/.

[1645] Menck K, Bleckmann A, Schulz M, Ries L, Binder C. Isolation and Characterization of Microvesicles from Peripheral Blood. J Vis Exp. 2017 Jan 6;(119):55057; https://www.ncbi.nlm.nih.gov/pmc/articles/PMC5408706/.

[1646] https://www.sciencedirect.com/topics/engineering/plasma-volume.
[1647] https://en.wikipedia.org/wiki/Fluid_compartments.

[1648] Fernando MR, Jiang C, Krzyzanowski GD, Ryan WL. New evidence that a large proportion of human blood plasma cell-free DNA is localized in exosomes. PLoS One. 2017 Aug 29;12(8):e0183915; https://www.ncbi.nlm.nih.gov/pmc/articles/PMC5574584/. See also: https://en.wikipedia.org/wiki/Exosome_(vesicle).

(c) n_{apop} ~ 2 x 10^8/ml plasma of ~1 μm (V_{apop} ~ 0.5 μm^3) **apoptotic bodies**[1649] of which up to $N_{apop} = f_{leak}\ n_{apop}\ V_{interstitial}$ = 6.3 x 10^{11} are assumed to have leaked into the tissues prior to cryopreservation;

giving a total vesicle removal volume of $V_{ev} = N_{mv}\ V_{mv} + N_{exo}\ V_{exo} + N_{apop}\ V_{apop}$ ~ 0.39 cm^3 of microbodies comprising a total of $N_{ev} = N_{mv} + N_{exo} + N_{apop}$ ~ 8.3 x 10^{13} microparticles. This may include removing an unknown number of phagosomes[1650] caused by the triggering of autophagy during ischemia (Section 3.2.2 and Section 3.2.5), and an unknown but probably modest number of cells that were far enough along in the process of apoptosis,[1651] autolysis,[1652] or autophagic programmed cell death[1653] at the time of cryopreservation that they have already been reduced to debris or are otherwise not worth trying to restore.

Future research should determine if these microbodies are likely to be distributed roughly uniformly throughout the human extracellular tissue volume (as assumed here), or instead will have some nonuniform distribution that could allow a more focused and speedier extraction process.

A fleet of $N_{robots} = 10^{12}$ extracellular vesicle scavenging nanorobots, distributed using vasculoid boxcars and released or retrieved via cellulocks (Section 4.6.1), searching a human body of extracellular tissue volume[1654] $V_{intercellular}$ ~ 17 L at a nanorobot transit velocity of $v_{intercellular}$ = 1-10 μm/sec[1655] while sampling a circumferential cross-sectional area of $A_{scanarea}$ = 10 μm^2 around the nanorobot, can complete one pass through the entire cell volume in $\tau_{celldebrispass} = V_{intercellular} / N_{robots}\ v_{intercellular}\ A_{scanarea}$ = 170-1700 sec.

Allowing tenfold more time for vesicle recognition, acquisition, and multiple round trips to and from the nearest vasculoid cellulock to deliver the captured vesicles for export, comprehensive microbody clearance can probably be completed in $t_{microbody}$ ~ 17,000 sec (~**4.7 hours**), generating $P_{microbody} \sim N_{robots}\ P_{nanorobot}$ = 100 watts of continuous whole-body waste heat during the removal process. (Detailed specification of these additional tasks is a subject for ***future research***.)

4.12.1.2 Red Cells and Platelets

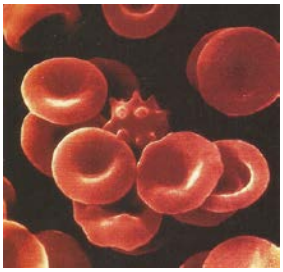

Blood cells that have escaped the vasculature and become embedded in body tissue prior to cryopreservation are in the wrong place and should be removed. Blood is drained from the human body during cryonics washout,[1656] an early part of the cryopreservation process, carrying off most of the ~28.5 x 10^{12}

[1649] Serrano-Heras G, Díaz-Maroto I, Carrión B, Perona-Moratalla AB, Gracia J, Arteaga S, Hernández-Fernández F, García-García J, Castro-Robles B, Ayo-Martín O, Segura T. Isolation and quantification of blood apoptotic bodies in neurological patients. bioRxiv, 12 Sep 2019; https://www.biorxiv.org/content/10.1101/757872v1.full.pdf.

[1650] https://en.wikipedia.org/wiki/Phagosome.
[1651] https://en.wikipedia.org/wiki/Apoptosis#Proteolytic_caspase_cascade:_Killing_the_cell.
[1652] https://en.wikipedia.org/wiki/Autolysis_(biology).
[1653] https://en.wikipedia.org/wiki/Programmed_cell_death.

[1654] Freitas RA Jr. Nanomedicine, Volume I: Basic Capabilities, Landes Bioscience, Georgetown TX, 1999, Section 9.4.4.2, "ECM Brachiation", http://www.nanomedicine.com/NMI/9.4.4.2.htm.

[1655] Freitas RA Jr. Nanomedicine, Volume I: Basic Capabilities, Landes Bioscience, Georgetown TX, 1999, Section 9.4.4.2, "ECM Brachiation", http://www.nanomedicine.com/NMI/9.4.4.2.htm.

[1656] https://www.alcor.org/library/alcor-human-cryopreservation-protocol/.

erythrocytes (red cells; image, right) and ~2.1 x 10^{12} platelets that are normally present in the blood.[1657]

Defective or senescent red cells are filtered out of the blood and may be found in the monocyte phagocyte system including the spleen, liver, and lymph nodes,[1658] especially if the cells are undergoing eryptosis[1659] or red cell programmed death.[1660] The normal 120-day erythrocyte lifespan implies that up to 1/120th or ~0.83 % of the red cell population ($N_{cryoRBC}$ ~ 2.4 x 10^{11} RBCs each of volume V_{RBC} = 94 μm^3) may be present even in a perfectly washed-out cryopreserved patient, if we assume that roughly one day's worth of cells remain intact due to a combination of ischemic time and the time required for the completion of phagocytosis. A few red cells will also have been cryopreserved in the red marrow of large bones where these cells are newly generated,[1661] trapped behind the bone marrow barrier,[1662] but these developing cells need not be removed because they are not refugees from the bloodstream, and thus might simply be repaired in the normal manner (Section 4.12.3).

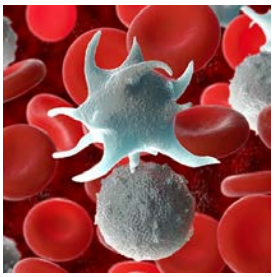

Platelets (image, left) typically circulate for 8-9 days before being removed via phagocytosis in the liver and spleen.[1663] Making similar assumptions as for red cells, these two organs might contain up to ~10% of the circulating platelet population ($N_{cryoPlatelet}$ ~ 2.1 x 10^{11} cells each of volume $V_{platelet}$ = 10 μm^3) in various stages of disassembly in the body of a cryopreserved patient.

It should be possible to remove all $V_{cryoBloodCell} = (N_{cryoRBC}\ V_{RBC}) + (N_{cryoPlatelet}\ V_{platelet})$ = 25 cm^3 of unwanted blood cells in $t_{cryoBloodCell}$ ~ **6.9 hours** using a ~100 watt fleet of N_{robots} ~ 10^{12} nanorobots each having $V_{NanorobotIntStore}$ ~ 10 μm^3/nanorobot of internal storage space, allowing each nanorobot $\tau_{cryoBloodCell} = t_{cryoBloodCell}\ N_{robots}\ V_{NanorobotIntStore} / V_{cryoBloodCell}$ ~ 10,000 sec (2.8 hours) per round trip delivery time between the cell and the vasculoid export dropoff locations. This seems sufficient if nanorobots can travel at 1-10 μm/sec, enabling transit of even millimeter-long round trip circuits in 100-1000 sec, and if the maximum transport capacity of the entire boxcar/cellulock system is $\upsilon_{capacityB/C}$ = 0.22 cm^3/sec (Section 4.6.1) which would allow $V_{cryoBloodCell}$ = 25 cm^3 of RBC or platelet material to be exported from the body in $V_{cryoBloodCell} / \upsilon_{capacityB/C}$ ~ 112 sec.

Since tissue-trapped RBCs and platelets are likely to be concentrated in specific organs or in specific subregions of particular bones, it may be possible to design a more focused removal process that allows expedited removal as compared to the generic scenario assumed above. The precise number and location of blood cells to be removed from a cryopreserved human body, and the ideal procedure for their removal, is a suitable subject for ***future research***.

[1657] Freitas RA Jr. Nanomedicine, Volume I: Basic Capabilities, Landes Bioscience, Georgetown TX, 1999, Section 8.5.1, "Cytometrics", http://www.nanomedicine.com/NMI/8.5.1.htm.

[1658] https://en.wikipedia.org/wiki/Red_blood_cell#Senescence.

[1659] Repsold L, Joubert AM. Eryptosis: An Erythrocyte's Suicidal Type of Cell Death. Biomed Res Int. 2018 Jan 3;2018:9405617; https://www.ncbi.nlm.nih.gov/pmc/articles/pmid/29516014/.

[1660] Lang F, Lang E, Föller M. Physiology and pathophysiology of eryptosis. Transfus Med Hemother. 2012 Oct;39(5):308-314; https://www.ncbi.nlm.nih.gov/pmc/articles/pmid/23801921/.

[1661] https://en.wikipedia.org/wiki/Erythropoiesis.
[1662] https://en.wikipedia.org/wiki/Bone_marrow#Bone_marrow_barrier.
[1663] https://en.wikipedia.org/wiki/Platelet#Development.

4.12.1.3 Errant White Cells

Blood drained from the human body during cryonics washout[1664] also carries off ~0.4 x 10^{12} white cells that are normally present in the blood,[1665] so neutrophils and other bloodborne white cells will be seriously depleted[1666] with the removal of all blood. Nonspecific white cells that remain embedded in body tissues should be relatively few in number and can be removed using minimal resources.

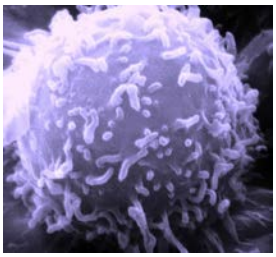

The lymphatic system is not usually subjected to cryoprotectant washout during cryopreservation. At least ~0.7 x 10^{12} lymphocyte cells (image, right) reside in lymphoid organs and tissues,[1667] providing long-term immunologic memory,[1668] that should also be repaired *in situ* in the normal manner (Section 4.12.3), as should any of the >0.2 trillion macrophages[1669] (image, left) or other mononuclear phagocytes.[1670] All such phagocytic cells should remain functionally immobilized and thus can be repaired in place, because they will be anergic due to the previous extraction (Section 4.10) of all biochemically active fuels, oxidants, and metabolites from the body.

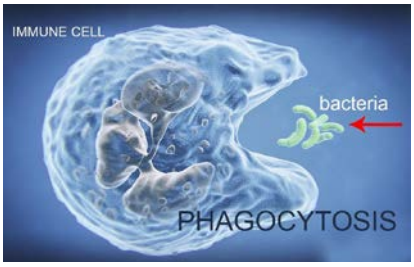

In the interest of preserving all possible structural information in the brain prior to repair, brain-specific phagocytic cells[1671] (e.g., microglia[1672]) may be identified but otherwise should not be disturbed until the start of the inspection and repair processes described in Section 4.12.2 as applied to neurons and other tissue cells. ***Future research*** should examine whether replacement of phagocytic cells in the brain, rather than repair, is a feasible repair alternative.

[1664] https://www.alcor.org/library/alcor-human-cryopreservation-protocol/.

[1665] Freitas RA Jr. Nanomedicine, Volume I: Basic Capabilities, Landes Bioscience, Georgetown TX, 1999, Section 8.5.1, "Cytometrics", http://www.nanomedicine.com/NMI/8.5.1.htm.

[1666] Romson JL, Hook BG, Kunkel SL, Abrams GD, Schork MA, Lucchesi BR. Reduction of the extent of ischemic myocardial injury by neutrophil depletion in the dog. Circulation. 1983 May;67(5):1016-1023; https://www.ahajournals.org/doi/pdf/10.1161/01.CIR.67.5.1016.

[1667] Freitas RA Jr. Nanomedicine, Volume I: Basic Capabilities, Landes Bioscience, Georgetown TX, 1999, Table 8.5, "Approximate Quantification of the Human Lymphatic System"; http://www.nanomedicine.com/NMI/Tables/8.5.jpg.

[1668] https://en.wikipedia.org/wiki/Lymphocyte.
[1669] https://en.wikipedia.org/wiki/Macrophage.

[1670] Lee GR, Bithell TC, Foerster J, Athens JW, Lukens JN, eds., Wintrobe's Clinical Hematology, Ninth Edition, Lea & Febiger, Philadelphia PA, 1993.

[1671] Galloway DA, Phillips AEM, Owen DRJ, Moore CS. Phagocytosis in the Brain: Homeostasis and Disease. Front Immunol. 2019 Apr 16;10:790; https://www.ncbi.nlm.nih.gov/pmc/articles/PMC6477030/.

[1672] https://en.wikipedia.org/wiki/Microglia.

4.12.1.4 Bacteria

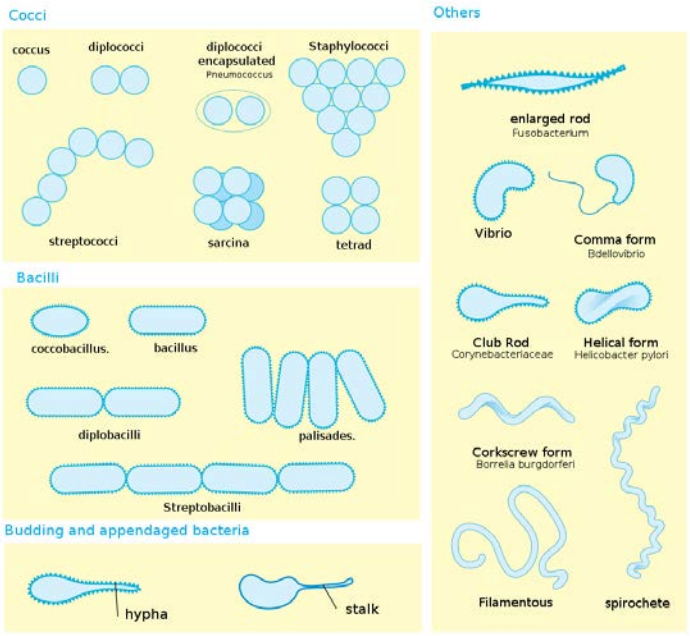

It is possible that an intact bacterium[1673] located anywhere in a reliquidified human body might be able to function for a short time running on internal energy or nutrient stores, though any such activity should not last long because of the previous extraction of all biochemically active fuels, oxidants, and metabolites from the body, down to hypometabolic concentrations (Section 4.10). Nevertheless, excepting gut flora, most bacterial presence inside the human body is at least nonessential for health and is usually undesirable. Because bacteria represent potential point sources of unmonitored and uncontrolled biochemical activity, it is recommended that all bacteria should be removed from the reliquidified cryopreserved human body prior to commencing general cell repair operations. As for gut flora, alimentary digestion can be temporarily bypassed during intensive care with missing micronutrients supplied intravenously.[1674] Because colonic bacteria often escape intestinal confinement and enter the surrounding tissues or bloodstream,[1675] it is recommended that any bacteria found in the alimentary canal of the cryopreserved patient should be entirely removed as soon as possible following reliquidification.

A fleet of $N_{robots} = 10^{12}$ bacterium-scavenging nanorobots searching human tissue with a fluid volume $V_{fluid} = 38.5$ L at a nanorobot transit velocity of $v_{intercellular} = 1\text{-}10$ μm/sec[1676] while sampling a circumferential cross-sectional area of $A_{scanarea} = 10\ \mu m^2$ around the nanorobot can complete one pass through the entire fluid volume in $\tau_{bacterial} = V_{fluid} / N_{robots}\ v_{intercellular}\ A_{scanarea} = 385\text{-}3850$ sec.

[1673] https://en.wikipedia.org/wiki/Bacteria.

[1674] Singer P, Berger MM, Van den Berghe G, *et al*. ESPEN Guidelines on Parenteral Nutrition: intensive care. Clin Nutr. 2009 Aug;28(4):387-400; https://www.clinicalnutritionjournal.com/article/S0261-5614(09)00098-3/fulltext.

[1675] See I, Soe MM, Epstein L, Edwards JR, Magill SS, Thompson ND. Impact of removing mucosal barrier injury laboratory-confirmed bloodstream infections from central line-associated bloodstream infection rates in the National Healthcare Safety Network, 2014. Am J Infect Control. 2017 Mar 1;45(3):321-323; https://www.ncbi.nlm.nih.gov/pmc/articles/PMC5523439/. Tamburini FB, Andermann TM, Tkachenko E, Senchyna F, Banaei N, Bhatt AS. Precision identification of diverse bloodstream pathogens in the gut microbiome. Nat Med. 2018 Dec;24(12):1809-1814; https://www.ncbi.nlm.nih.gov/pmc/articles/PMC6289251/.

[1676] Freitas RA Jr. Nanomedicine, Volume I: Basic Capabilities, Landes Bioscience, Georgetown TX, 1999, Section 9.4.4.2, "ECM Brachiation", http://www.nanomedicine.com/NMI/9.4.4.2.htm.

Allowing tenfold more time for bacterial recognition and acquisition,[1677] and multiple round trips to and from the nearest vasculoid cellulock to deliver the captured microbes for export, comprehensive bacterial clearance can probably be completed in $t_{bacterial}$ ~ 38,500 sec (~**10.7 hours**), generating $P_{bacterial} \sim N_{robots} P_{nanorobot}$ = 100 watts of continuous whole-body waste heat during the removal process.

4.12.1.5 Other Pathological Microbes

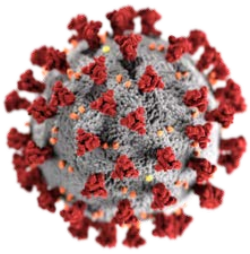

All virus[1678] particles (image, right) and their components should be removed from the reliquidified cryopreserved human body. Retroviruses[1679] that have inserted their genomes into the DNA of the patient's cells must await subsequent cell repair operations (Section 4.12.2.2) to delete. The antivirus activity is not time-critical because all virions will be biologically inert – following molecular extraction (Section 4.10), all cellular metabolic machinery is inoperative, thus cannot be hijacked.

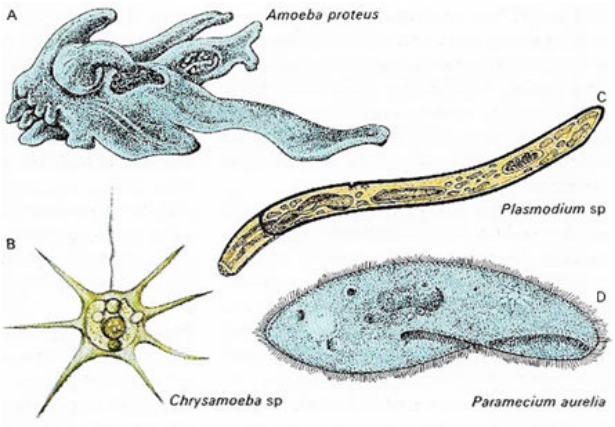

The same requirement for removal applies to a great many microbes of lesser, variable, or uncertain risk, including viroids,[1680] virusoids,[1681] virophages,[1682] bacteriophages,[1683] protozoa (image, left),[1684] fungi,[1685] and other parasites[1686] that are known to be present or which might be present in a particular patient. Each of these classes of objects has unique external biochemical signatures that can be recognized by patrolling nanorobots, permitting ready removal. ***Future research*** should determine which microbes must be removed and which can be ignored during the cryopreservation revival process.

Future engineered bioweapons,[1687] if any are found, should also be removed at this stage. This includes any bioengineered microbes or viruses specifically designed to inflict harm on biological systems, such as bacteriological warfare agents.[1688]

The mission requirements and nanorobotics equipment needed to eliminate a wide range of pathological microbes should be similar to those used to remove bacteria (Section 4.12.1.4).

[1677] Freitas RA Jr. Microbivores: Artificial Mechanical Phagocytes using Digest and Discharge Protocol. J. Evol. Technol. 2005 Apr;14:55-106; http://www.jetpress.org/volume14/freitas.pdf.

[1678] https://en.wikipedia.org/wiki/Virus.
[1679] https://en.wikipedia.org/wiki/Retrovirus.
[1680] https://en.wikipedia.org/wiki/Viroid.
[1681] https://en.wikipedia.org/wiki/Virusoid.
[1682] https://en.wikipedia.org/wiki/Virophage.
[1683] https://en.wikipedia.org/wiki/Bacteriophage.
[1684] https://en.wikipedia.org/wiki/Protozoan_infection.
[1685] https://en.wikipedia.org/wiki/Fungus#Pathogenic_mechanisms.
[1686] https://en.wikipedia.org/wiki/Parasitology#Medical.
[1687] https://en.wikipedia.org/wiki/Biological_warfare.
[1688] https://en.wikipedia.org/wiki/Biological_agent.

4.12.1.6 Cancer Cells

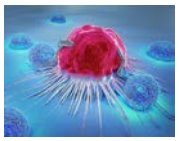

A cell that has lost its normal control mechanisms and thus exhibits unregulated growth is called a cancer. Cancer cells (image, right)[1689] can arise from normal cells in any tissue or organ, and during this process their genetic material undergoes change. As these cells grow and multiply, they form a mass of cancerous tissue that invades adjacent tissues and can metastasize around the body, usually with excess vascularization[1690] that may be visible in geometrical maps (Section 4.5.4) created during microvascular scans (Section 4.3), and possibly confirmed by data from previously compiled biochemical maps of the intravascular surfaces (Section 4.5.5).

Smaller clumps of cancer cells (image, left) that have not yet excessively vascularized must be located by direct inspection. The bodies of most older people and many middle-aged people are riddled with pre-cancerous microtumors,[1691] and these microtumors will have been cryopreserved along with the normal cells. While no single universal tumor cell biomarker has been found, a biomarker likely exists for every type of cancer.[1692] A trillion-nanorobot survey fleet that spends ~100 seconds examining the biochemical surface signatures for evidence of specific cancer biomarkers[1693] on the plasma membranes of ~10 trillion native non-blood cells in the body,[1694] using probes tipped with chemotactic

---

[1689] Myrna Buiser Schnur, "How Are Cancer Cells Different from Normal Cells?", Lippincott Nursing Center, 15 Jul 2019; https://www.nursingcenter.com/ncblog/july-2019/cancer-cells-vs-normal-cells.

[1690] Nico B, Benagiano V, Mangieri D, Maruotti N, Vacca A, Ribatti D. Evaluation of microvascular density in tumors: pro and contra. Histol Histopathol. 2008 May;23(5):601-607; https://digitum.um.es/digitum/bitstream/10201/29811/1/Evaluation%20of%20microvascular%20density%20in%20tumors%2C%20pro%20and%20contra.pdf.

[1691] Autopsies have shown that every person over 50 years old has microscopic tumors in their thyroid glands, and more than one-third of autopsied women aged 40-50 have *in situ* microtumors in their breasts.[*] Microscopic tumors are clumps of cells without dedicated supporting blood vessels, representing the avascular phase of tumor growth.[†]
[*] Folkman J, Kalluri R. Cancer without disease. Nature. 2004 Feb 26;427(6977):787; http://health120years.com/Hamlet/Hamlet_Cancer-without-disease.pdf.
[†] Tang L, van de Ven AL, Guo D, Andasari V, Cristini V, Li KC, Zhou X. Computational Modeling of 3D Tumor Growth and Angiogenesis for Chemotherapy Evaluation. PLoS One 2014 Jan 3; https://journals.plos.org/plosone/article?id=10.1371/journal.pone.0083962.

[1692] https://en.wikipedia.org/wiki/Biomarker_(cell)#Examples_of_Biomarkers.

[1693] Biomarker databases: Early Detection Research Network (EDRN), National Cancer Institute; https://edrn.nci.nih.gov/. Cancer Biomarkers database, Cancer Genome Interpreter (CGI); https://www.cancergenomeinterpreter.org/biomarkers. Tumor Markers, BioRad; https://www.bio-rad-antibodies.com/tumor-markers.html. See also: Zhang S, *et al*. Selection of tumor antigens as targets for immune attack using immunohistochemistry. Intl J Cancer 1997 Sep 26;73(1):42-49; https://onlinelibrary.wiley.com/doi/pdf/10.1002/(SICI)1097-0215(19970926)73:1%3C42::AID-IJC8%3E3.0.CO;2-1; Intl J Cancer 1997 Sep 26;73(1):50-56; https://onlinelibrary.wiley.com/doi/pdf/10.1002/%28SICI%291097-0215%2819970926%2973%3A1%3C50%3A%3AAID-IJC9%3E3.0.CO%3B2-0; and Clin Cancer Res. 1998 Nov;4:2669-2676; https://clincancerres.aacrjournals.org/content/4/11/2669.full-text.pdf. Malyankar UM. Tumor-associated antigens and biomarkers in cancer and immune therapy. Int Rev Immunol. 2007 May-Aug;26(3-4):223-247; https://pubmed.ncbi.nlm.nih.gov/17558745/. Even-Desrumeaux K, Baty D, Chames P. State of the art in tumor antigen and biomarker discovery. Cancers (Basel). 2011 Jun 9;3(2):2554-2596; https://www.ncbi.nlm.nih.gov/pmc/articles/PMC3757432/. Kim WT, Ryu CJ. Cancer stem cell surface markers on normal stem cells. BMB Rep. 2017 Jun;50(6):285-298; https://www.ncbi.nlm.nih.gov/pmc/articles/pmid/28270302/. Hong Y, Park C, Kim N, *et al*. QSurface: fast identification of surface expression markers in cancers. BMC Syst Biol. 2018 Mar 19;12(Suppl 2):17; https://www.ncbi.nlm.nih.gov/pmc/articles/PMC5861488/. Townsend MH, Shrestha G, Robison RA, O'Neill KL. The expansion of targetable biomarkers for CAR T cell therapy. J Exp Clin Cancer Res. 2018 Jul;37(1):163-186; https://www.ncbi.nlm.nih.gov/pmc/articles/pmid/30031396/.

sensor pads,[1695] nominally might require ~1000 sec to complete the survey while recording the navigational position of each cell that is found to be cancerous. To this scan time must be added the travel time to reach the vicinity of most organs and tissues in the body (about one vasculoid circulation time or ~140 sec); plus the travel time between ten neighboring cells which lie within ~40 microns (~2 cell widths) of a capillary exit point, requiring ~40 sec even traveling at a very slow ~1 micron/sec crawl through the tissues (comparable to leukocyte and fibroblast speeds),[1696] which adds another ~400 sec for all 10 neighboring cells. This gives an apparent requirement of 1000 sec + 140 sec + 400 sec = 1540 sec for the fleet to complete its survey of all native nonblood cells, so perhaps we should allow ~**1 hour** (3600 sec) for the entire detection and mapping process.

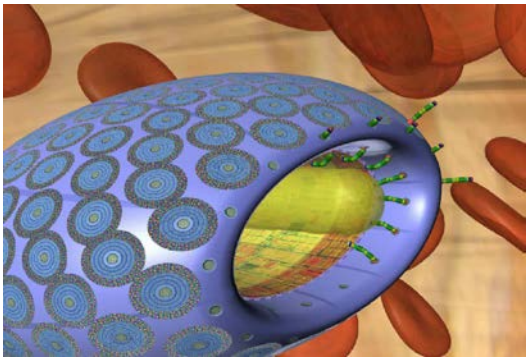

Once we have a comprehensive whole-body cancer cell map in hand, another round of nanorobotic inspection devices can revisit all presumptively cancerous cells and reconfirm their cancerous identity, possibly via direct sampling of cytosolic mRNA transcripts (which were not extracted from the cell; Section 4.10.1.5(V)). Once their cancerous identity has been verified, the cancer cells may be mechanically excised by microbivore-class[1697] devices (image, left; Section 1.2.2) or related nanorobots. One published estimate[1698] is that each active microbivore crowding on the exterior surface of a tumor mass could excavate and digest a tumor mass beneath it at ~1 μm/min, requiring ~1 hour for ~4000 devices to digest a 100 μm diameter tumor mass or ~400,000 devices and ~10 hours for a 1 mm diameter tumor. The number of cancer cells and tumors will vary from patient to patient, but a plausible resource allocation for this task would be ~10^{12} nanorobots working for ~**12 hours** generating ~100 watts of fleet waste heat. ***Future research*** can determine under what circumstances it may be more efficient to excise tumor masses using a nanocatheter or nanosyringe extraction apparatus (Section 4.12.2.8)

A special exception must be made for cancer cells located in the brain. Detection and mapping of these pathological cells may proceed as described above, but their removal and replacement with undamaged brain tissue should await the repair process described in Section 4.12.4.3 because it is important to preserve all possible structural information in the existing brain tissue prior to repair.

[1694] Freitas RA Jr. Nanomedicine, Volume I: Basic Capabilities, Landes Bioscience, Georgetown, TX, 1999; Section 8.5.1, "Cytometrics"; http://www.nanomedicine.com/NMI/8.5.1.htm.

[1695] Freitas RA Jr. Nanomedicine, Volume I: Basic Capabilities, Landes Bioscience, Georgetown TX, 1999; Section 4.2.8, "Chemotactic Sensor Pads", http://www.nanomedicine.com/NMI/4.2.8.htm; Section 8.5.2.1, "Identification of Self", http://www.nanomedicine.com/NMI/8.5.2.1.htm#p8; and Section 8.5.2.2, "Identification of Cell Type", http://www.nanomedicine.com/NMI/8.5.2.2.htm#p23.

[1696] Freitas RA Jr. Nanomedicine, Volume I: Basic Capabilities, Landes Bioscience, Georgetown, TX, 1999; Section 9.4.4.2, "ECM Brachiation"; http://www.nanomedicine.com/NMI/9.4.4.2.htm.

[1697] Freitas RA Jr. Microbivores: Artificial Mechanical Phagocytes using Digest and Discharge Protocol. J. Evol. Technol. 2005 Apr;14:55-106; http://www.jetpress.org/volume14/freitas.pdf.

[1698] Freitas RA Jr. Chapter 23. Comprehensive Nanorobotic Control of Human Morbidity and Aging. In: Fahy GM, West MD, Coles LS, Harris SB, eds, The Future of Aging: Pathways to Human Life Extension, Springer, New York, 2010, pp. 685-805; Section 6.2.2 "Cancer"; http://www.nanomedicine.com/Papers/Aging.pdf.

4.12.2 Inspect and Repair Existing Cells

With unwanted cells removed, it is now time to inspect and repair or replace all the remaining cells in the body of the cryopreserved patient. The conventional cell repair process begins with a preliminary cell inspection and removal of small debris from within the cell using nanorobots (Section 4.12.2.1). Then, starting with the innermost components and progressing to the outermost components, we repair or replace the nucleus (Section 4.12.2.2), the non-nucleus organelles (Section 4.12.2.3), the cytosolic cytoskeleton (Section 4.12.2.4), any poisoned receptors (Section 4.12.2.5), other membrane and transmembrane proteins (Section 4.12.2.6), and finally the glycocalyx (Section 4.12.2.7). One author[1699] once referred to these sorts of detailed cellular repair operations as "Humpty Dumpty" work (a metaphor for seemingly impossibly difficult repair tasks analogous to fixing a broken egg).[1700] It appears that cell repair work, while truly an impossible task "for all the king's men" (i.e., modern surgeons), is well within the grasp of a coordinated swarm of a trillion medical nanorobots equipped with a wide assortment of nanoscale scanning and manipulation capabilities.

For computational convenience, the completion time estimates given here generally presume that all instances of a particular cell component must be replaced, allowing none of the original instances of that component to remain in place and allowing none of the originals to be repaired (i.e., we replace all of the mitochondria, rather than leaving most intact and just repairing the few that are damaged, which will likely be the case most often). The time estimates given here also assume that each task must be done in series by separate nanorobot fleets, with each task fleet waiting until the previous one has completely finished before starting the next task in the sequence. In practice, these constraints can probably be relaxed to provide more efficient operation and significantly shorter overall task execution times.

Finally, this Section assumes that most intact cells will be repaired *in situ* by repairing or replacing intracellular components such as individual organelles, chromosomes, or receptor molecules in each cell. ***Future research*** should investigate: (1) the feasibility and desirability of replacing entire cells with externally remanufactured whole cells sourced from a cell mill (Appendix D), (2) the limitations and potential difficulties of such wholesale replacement, and (3) the circumstances under which such replacement would be preferable or more efficient than component-level *in situ* repair, as briefly described in Section 4.12.2.8.

4.12.2.1 Preliminary Cell Inspection and Small Debris Cleanup

The first task in cell repair is to assess the current status of each existing intact cell so that repair activities can be adequately planned, scheduled, resourced, and executed. During this assessment, inspection nanorobots will verify the type of cell being encountered, then enter into each cell and record the number, distribution, and apparent external condition of organelles, while also cataloguing any other evidence of gross intracellular damage. These nanorobots should also find, identify, and extract intracellular debris smaller than 100 nm in size that was not previously scavenged in Section 4.11.1. Preliminary identification of this small debris can provide useful information on which intracellular structures might be damaged or are missing components.

[1699] Fahy G. Appendix B. A "Realistic" Scenario for Nanotechnological Repair of the Frozen Human Brain. In: Wowk B, Darwin M, eds., Cryonics: Reaching for Tomorrow. Alcor Life Extension Foundation, 1991, pp. A-10 – A-26; https://alcor.org/Library/html/nanotechrepair.html.

[1700] https://en.wikipedia.org/wiki/Humpty_Dumpty.

Inspection nanorobots should determine the current apoptotic or necrotic status of each cell, even though the degradative process (Section 3.2.5) might have exhausted itself during the period of warm ischemia or may be in complete stasis following molecular extraction (Section 4.10). During a prior stage of repair (Section 4.11.1), plasma membrane repair may have been performed on cells that were already in an advanced apoptotic or necrotic state, with large amounts of internal disassembly in evidence. Such membrane repair may be appropriate for neurons whose network connectivity pattern must be preserved long enough to verify the future integrity of the repaired connectome (Section 4.12.4). For non-neuronal cells with severe internal damage, the appropriate action may be whole-cell replacement in which case the prior membrane repair will have served mainly to expedite cell removal. ***Future research*** should determine the correct protocol for cells that are determined to be in various stages of apoptosis or necrosis, and should specify how this protocol will vary based on cell type and cell location.

An inspection nanorobot patrolling a typical V_{cell} = 8000 μm^3 tissue cell[1701] at a conservative intracellular natation velocity of $v_{cellinspect}$ = 1 μm/sec[1702] while sampling a circumferential cross-sectional area around the nanorobot of $A_{inspectscanarea}$ = 10 μm^2 can complete one pass through the entire cell volume in $\tau_{cellinspectpass} = V_{cell} / v_{cellinspect} A_{inspectscanarea}$ = 800 sec. Allowing 100-fold more time to type, count, and cursorily inspect organelles for damage, to make multiple round trips to and from the nearest vasculoid cellulock to deliver scavenged debris items for export, and to report out the cell data that has been gathered, preliminary cell inspection and small debris cleanup can probably be completed in $\tau_{cellinspect}$ ~ 80,000 sec (~22 hr) per cell, assuming one nanorobot per cell. (Detailed specification of these additional tasks is a subject for ***future research***.) This implies that a fleet of $N_{inspectbots} \sim 10^{12}$ inspection nanorobots generating $P_{cellinspect} \sim N_{inspectbots} P_{nanorobot}$ = 100 watts of continuous whole-body waste heat could complete all inspection and small debris removal operations in all $N_{bodycells} \sim 3.5 \times 10^{12}$ body tissue cells in $t_{cellinspect} \sim \tau_{cellinspect} N_{bodycells} / N_{inspectbots}$ = 280,000 sec (~**78 hr**).

Once inspection is complete, the nanorobots exit the body and offload their last tranche of data to an external computer. The external computer system analyzes all the data, compiles lists of likely repairs needed for each cell, prioritizes all the punchlists, then sends repair nanorobots to named cells in priority order to perform organelle repair. Lightly damaged organelles needing only minor membrane repair may be reparable using membrane materials fabricated in cell mills (Appendix D). Moderately or seriously damaged organelles will normally be removed and replaced with damage-free organelles (Section 4.12.2.3) manufactured in a cell mill.

4.12.2.2 Cell Nucleus Repair or Replacement

The first step in cell nucleus restoration is to repair any damage to the outer nuclear membrane of the nuclear envelope, which nanorobots will have already detected during the preliminary cell inspection (Section 4.12.2.1). The previously described methodology for estimating the requirements for plasma membrane repair (Section 4.11.1) can be applied here because the nuclear membrane is qualitatively similar (though different in detail) to the plasma membrane. The surface area of the typical cell nucleus is $A_{nucleus} \sim 200\ \mu m^2$, much smaller than the typical plasma membrane surface area of $A_{bodycell} \sim 2400$

[1701] Freitas RA Jr., Nanomedicine, Volume I: Basic Capabilities, Landes Bioscience, Georgetown, TX, 1999, Table 8.17, "Approximate Quantification of the Components of a Typical 20-μm Human Tissue Cell"; http://www.nanomedicine.com/NMI/Tables/8.17.jpg.

[1702] Freitas RA Jr. Nanomedicine, Volume I: Basic Capabilities, Landes Bioscience, Georgetown TX, 1999, Section 9.4.6, "In Cyto Locomotion", http://www.nanomedicine.com/NMI/9.4.6.htm

μm^2/cell,[1703] so the resource requirements estimated for plasma membrane repair can be reduced by a factor of $A_{bodycell} / A_{nucleus} \sim 12$ for nuclear membrane repair – or $\tau_{NucleusMrepair} = \tau_{CellPMrepair} / 12 = 59{,}500$ sec (~**16.5 hr**) using 3.7×10^{12} repair nanorobots with a 370 watt fleet power budget.

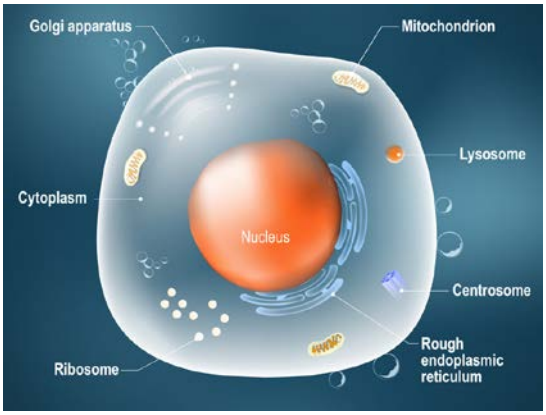

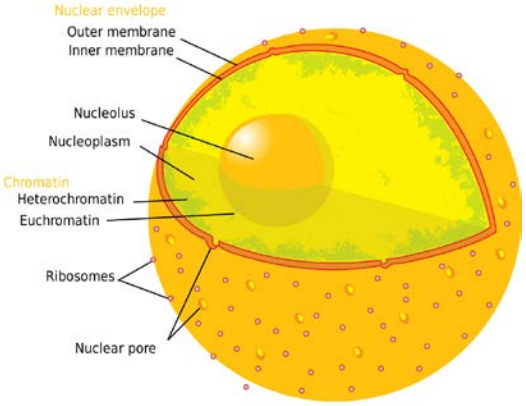

Given the rotor service volume radius of $\Delta X \sim 2$-5 μm during molecular extraction (Section 4.10.1) and the typical nucleus diameter of ~8 μm, it is presumed that molecular extraction probes will have extended into the interior of each cell nucleus, resulting in full biochemical stasis within the nucleoplasm. ***Future research*** should determine the likely state(s) of a cell nucleus inside a cell that has first been cooled to LN2 temperatures (with or without cryoprotectants) after a period of warm ischemia and then rewarmed to icewater temperatures. If there is normally only light damage, then spot repairs could be undertaken, but if heavy damage is anticipated then it may be more efficient to simply replace the entire contents of the nucleus with newly remanufactured material that is identical to the patient's original biological structures. Taking this as the "worst-case" scenario, the present analysis assumes that full nucleus replacement is necessary. Note that the initial spot repair of nuclear envelope damage should make it easier to extract and replace the entire nucleus intact in this scenario.

Nanorobotic devices called chromallocytes[1704] (image, below) are capable of such replacement activity in a cell nucleus. Chromallocytes (Section 1.2.3) were primarily designed to perform chromosome replacement therapy, wherein the entire chromatin content of the nucleus in a living cell is extracted and promptly replaced with a new set of prefabricated chromosomes which have been artificially manufactured as defect-free copies of the originals (Section D.1.2.2). This process has been described in a 26-step protocol,[1705] though a few steps will be unnecessary in the cryonics revival situation due to the previously established biostatic state of the reliquidified cell.

Chromallocytes can also function as more general-purpose cell repair devices or "delivery trucks" because they possess multiple manipulators and a large $V_{chromstorage} = 40\ \mu m^3$ internal storage volume. This storage volume permits large amounts of replacement materials to be imported and installed in cells during each

---

[1703] Freitas RA Jr., Nanomedicine, Volume I: Basic Capabilities, Landes Bioscience, Georgetown, TX, 1999, Table 8.17, "Approximate Quantification of the Components of a Typical 20-μm Human Tissue Cell"; http://www.nanomedicine.com/NMI/Tables/8.17.jpg.

[1704] Freitas RA Jr. The Ideal Gene Delivery Vector: Chromallocytes, Cell Repair Nanorobots for Chromosome Replacement Therapy. J. Evol. Technol. 2007 Jun;16:1-97; http://jetpress.org/v16/freitas.pdf.

[1705] Freitas RA Jr. The Ideal Gene Delivery Vector: Chromallocytes, Cell Repair Nanorobots for Chromosome Replacement Therapy. J. Evol. Technol. 2007 Jun;16:1-97; Section 5.2, "Detailed Sequence of Chromallocyte Activities"; http://jetpress.org/v16/freitas.pdf.

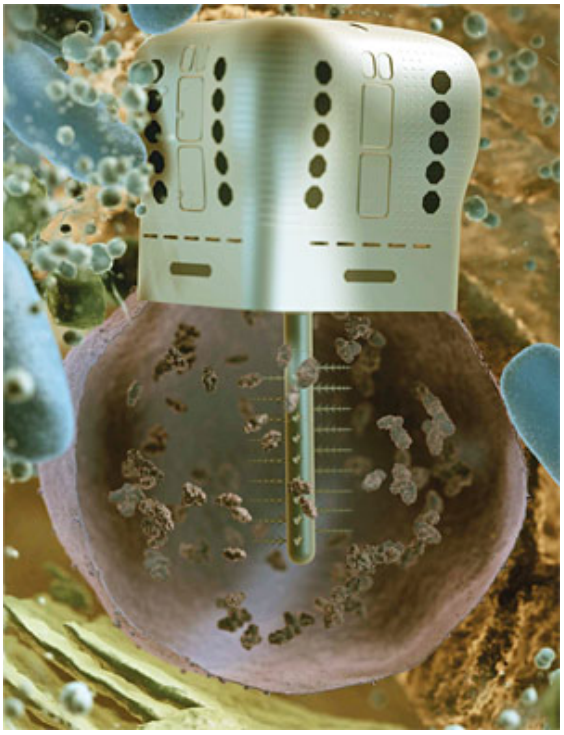

visit. Without knowing the exact state of the nuclear interior (e.g., chromatin condensed or extended? nuclear pores detached? nuclear lamina torn?) a specific replacement protocol is difficult to define *a priori*. However, as a very coarse estimate of the required effort, the typical cell nucleus has a volume of $V_{nucleus} \sim 268\ \mu m^3$ so in principle $V_{nucleus} / V_{chromstorage} \sim 7$ round-trip deliveries of a single chromallocyte to a single cell can transport a sufficient volume of material to completely replace the entire nucleus. According to the published technical paper, each chromallocyte requires ~3 hours to complete all 26 steps in the sequence – to travel to the target organ, complete its tasks in its assigned target cell in that organ, and then return to the entry point. Because several steps can be eliminated and because the nanorobots only need to travel to the nearest vasculoid cellulock and not all the way out of the body via the bloodstream, this time estimate is likely very conservative. Hence it seems safe to estimate that no more than $\tau_{chromcell} \sim$ 21 hours would be required for a single chromallocyte to visit a single cell 7 times to effectuate a complete replacement of the nucleus. A fleet of $N_{chromallocytes} = 10^{12}$ chromallocytes of total displacement volume ~69 cm^3 releases ~100 watts of nanorobotic waste heat and completes nuclear replacement in all $N_{bodycells} \sim 3.5 \times 10^{12}$ body tissue cells in $t_{replacenucl} \sim \tau_{chromcell}\ N_{bodycells} / N_{chromallocytes} \sim$ **74 hr**.

The replacement material will include duplicates of the patient's chromosomes manufactured in an external Chromosome Sequencing and Manufacturing Facility[1706] (Section D.1.2.1 and Section D.1.2.2), along with many other nucleus components that can be manufactured in cell mills (Appendix D), and will possess protein, carbohydrate, and antigenic signatures that precisely match the patient's native tissue types, eliminating any histocompatibility[1707] or biocompatibility concerns. The patient's genome must be fully sequenced in order to enable the cell mill to manufacture genetically identical replacement biological materials. Therefore, it should also be a simple matter – though not absolutely essential for revival – to clean the patient's genome of all accumulated defects[1708] (whether due to aging or cryopreservation) and then use the corrected genome as the basis for restoring the chromosomes in every cell of the patient's body.

Uniquely in the case of the neuron nucleus, ***future research*** should examine the extent to which the chromatin state of individual neurons may differ from their neighbors in ways that might affect long-term memory, and should determine the extent to which neural genomes may require special handling by chromallocytes if generic autologous genomic structures will not suffice. For example, in experiments with

---

[1706] Freitas RA Jr. The Ideal Gene Delivery Vector: Chromallocytes, Cell Repair Nanorobots for Chromosome Replacement Therapy. J. Evol. Technol. 2007 Jun;16:1-97; Section 4, "*Ex vivo* Chromosome Sequencing and Manufacturing Facility"; http://jetpress.org/v16/freitas.pdf.

[1707] https://en.wikipedia.org/wiki/Histocompatibility.

[1708] Freitas RA Jr. The Ideal Gene Delivery Vector: Chromallocytes, Cell Repair Nanorobots for Chromosome Replacement Therapy. J. Evol. Technol. 2007 Jun;16:1-97; Section 4.1, "Genome Sampling and Modification"; http://jetpress.org/v16/freitas.pdf.

rats exposed to an intense learning experience,[1709] long-term memory of the event produced >5000 differently methylated DNA regions in the hippocampus neuronal genome, at 1 and 24 hours after training. These methylation pattern alterations occurred in many down-regulated genes (often due to the formation of new 5-methylcytosine sites in CpG-rich regions of the genome) and up-regulated genes (likely due to hypomethylation), creating a unique pattern of induced and repressed genes in brain neurons. During learning and memory formation, dynamic regulation of chromatin structure occurs in postmitotic neurons[1710] and DNA methylation is highly involved.[1711]

4.12.2.3 Non-Nucleus Organelles

The next step in the repair of existing cells is to locate and replace all non-nucleus intracellular organelles. It is technically possible to individually examine each organelle, assess any structural and functional damage, then repair whatever damage has been detected. However, this would require much scanning, handling, probing, and internal manipulation of each organelle. The detected damage could be a random collection of some or all of the forms of damage described in Chapter 3, combined with the various forms of damage that might have occurred during the patient's life including a wide variety of DNA-defect-driven deficiencies, chronic environmental insults, and acute injuries. The result of all this detailed repair activity would be a healthy organelle that is functionally indistinguishable from any other healthy generic organelle from the same patient.

Since healthy new organelles can be manufactured quickly and easily in cell mills (Appendix D), the most efficient protocol is to replace all existing organelles in the cell with perfect new ones without bothering to assess the current damage state of the originals. This restores cell components to a pristine standard of biological health without having to repair any of the many possible defects the original organelles might have accumulated over time or during cryopreservation.

Table 10 below provides a list of the 14 most important intracellular organelles. The "average" ~8000 μm^3 cell includes ~3500 μm^3 of organelles (~44% of total cell volume). There are ~26 million organelles in each individual cell, mostly accounted for by 20 million ribosomes and 5.7 million proteasomes. Three general classes of non-nucleus organelles can be distinguished:

I. Five **macromolecular organelles**, including (A) 11 nm proteasomes,[1712] (B) 25 nm ribosomes,[1713] (C) 10-40 nm glycogen granules,[1714] (D) 30-60 nm vaults,[1715] and (E) 400 nm centrioles[1716] (images, below). These are all self-assembling proteins or nucleoproteins that are easily synthesized and transported in large numbers onboard a chromallocyte.

[1709] Duke CG, Kennedy AJ, Gavin CF, Day JJ, Sweatt JD. Experience-dependent epigenomic reorganization in the hippocampus. Learn Mem. 2017 Jun 15;24(7):278-288; https://www.ncbi.nlm.nih.gov/pmc/articles/pmid/28620075/.

[1710] Morris MJ, Monteggia LM. Role of DNA methylation and the DNA methyltransferases in learning and memory. Dialogues Clin Neurosci. 2014 Sep;16(3):359-71; https://www.ncbi.nlm.nih.gov/pmc/articles/pmid/25364286/.

[1711] Poon CH, Chan YS, Fung ML, Lim LW. Memory and neuromodulation: A perspective of DNA methylation. Neurosci Biobehav Rev. 2020 Apr;111:57-68; https://pubmed.ncbi.nlm.nih.gov/31846654/.

[1712] https://en.wikipedia.org/wiki/Proteasome.
[1713] https://en.wikipedia.org/wiki/Ribosome.
[1714] https://en.wikipedia.org/wiki/Glycogen.
[1715] https://en.wikipedia.org/wiki/Vault_(organelle).
[1716] https://en.wikipedia.org/wiki/Centriole.

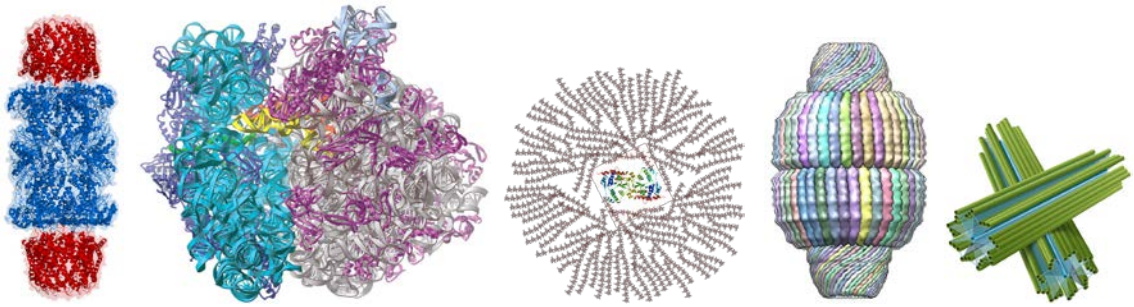

(A) (B) (C) (D) (E)

Table 10. Approximate number of non-nucleus replacement intracellular organelles needed for a 70 kg human whole-body cryopreservation patient[1717]

Organelle	Volume of Organelle (μm^3)	Avg Volume per Cell (μm^3)	Total Number in 70 kg Patient	Total Volume in 70 kg Patient (cm^3)
Rough ER	1120	1120	3.5×10^{12}	3900
Mitochondria	1	1000	3.5×10^{15}	3500
Golgi apparatus	410-520	450	3.5×10^{12}	1600
Smooth ER	420	420	3.5×10^{12}	1500
Secretory vesicles	4×10^{-3}	210	1.8×10^{17}	740
Lysosomes	0.31	90	1×10^{15}	320
Peroxisomes	0.31	90	1×10^{15}	320
Ribosomes	4×10^{-6}	80	7×10^{19}	280
Proteasomes	3.4×10^{-6}	20	2×10^{19}	70
Golgi vesicles	6.5×10^{-5}	13	7×10^{17}	50
Lipid droplets	0.1	10	3.5×10^{14}	35
Glycogen granules	1×10^{-5}	1	3.5×10^{17}	4
Vaults	5×10^{-5}	0.16	1.1×10^{16}	0.6
Centrioles	0.007	0.014	7×10^{12}	0.05
TOTALS		***3500***	***9.1×10^{19}***	***12,300***

II. Six **vesicular organelles**, including 30-80 nm Golgi vesicles and 0.1-1 μm secretory vesicles,[1718] 0.2-5 μm lipid droplets,[1719] 0.5-1 μm lysosomes,[1720] 0.5-1 μm peroxisomes,[1721] and 0.5-1 μm mitochondria.[1722] Each of these organelles consists of a phospholipid monolayer or a lipid bilayer

---

[1717] Assumes 3.5×10^{12} cells in a 70-kg human body; organelle data from: Freitas RA Jr., Nanomedicine, Volume I: Basic Capabilities, Landes Bioscience, Georgetown, TX, 1999, Table 8.17, "Approximate Quantification of the Components of a Typical 20-μm Human Tissue Cell"; http://www.nanomedicine.com/NMI/Tables/8.17.jpg.

[1718] https://en.wikipedia.org/wiki/Golgi_apparatus#Vesicular_transport.
[1719] https://en.wikipedia.org/wiki/Lipid_droplet.
[1720] https://en.wikipedia.org/wiki/Lysosome.
[1721] https://en.wikipedia.org/wiki/Peroxisome.
[1722] https://en.wikipedia.org/wiki/Mitochondrion.

membrane enclosing a roughly spherical or cylindrical space filled with lipids, digestive enzymes, material being transported, or, in the case of the mitochondrion (image, right), a system of internal membranes, ribosomes, granules, and DNA almost as complex as a complete living cell but much smaller, reflecting its ancient bacterial evolutionary origin. All six organelles are readily manufactured in cell mills (Appendix D) and are small enough for transport in numbers inside a chromallocyte.

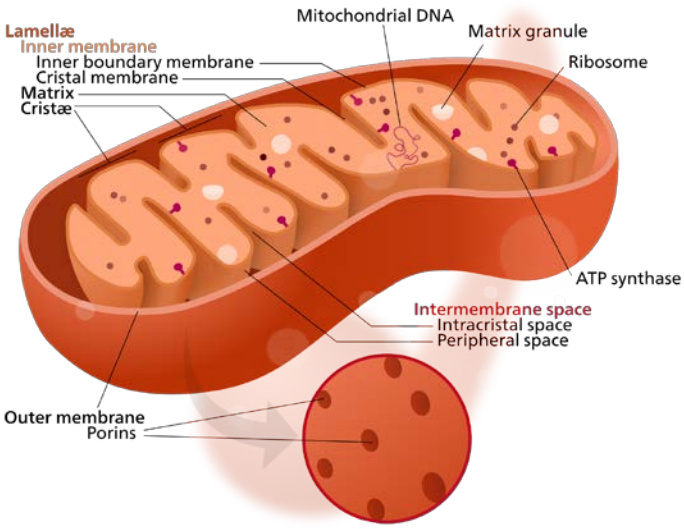

It might be necessary to introduce certain solutes or ions into the cytosol (Section 4.10.2) in order to prevent newly introduced vesicular organelles from shrinking, swelling, or bursting due to unwanted osmotic imbalances. Preventing this activity is especially important since new organelles may be introduced with inventories of enzymes and at least some reactive chemicals. This issue and its specific resolution are the proper subject of ***future research***.

III. Three **membraneous organelles**, including the Golgi apparatus (below, left),[1723] the rough endoplasmic reticulum[1724] and the smooth endoplasmic reticulum[1725] (below, right).[1726]

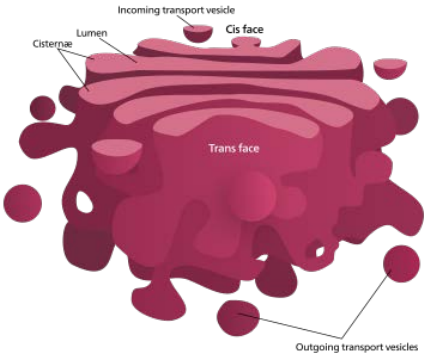

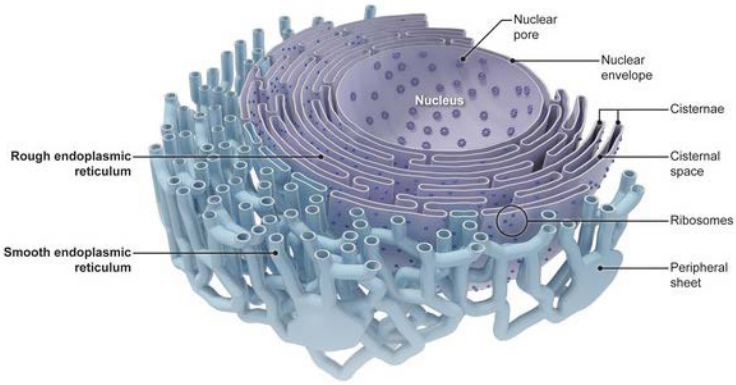

The membraneous organelles are too large to be transported intact inside a single chromallocyte nanorobot. However, the material comprising these organelles is readily manufactured inside a cell mill (Appendix D). The Golgi apparatus is known to disintegrate prior to cell mitosis and then reassemble with remarkable

---

[1723] https://en.wikipedia.org/wiki/Golgi_apparatus.
[1724] https://en.wikipedia.org/wiki/Endoplasmic_reticulum#Rough_endoplasmic_reticulum.
[1725] https://en.wikipedia.org/wiki/Endoplasmic_reticulum#Smooth_endoplasmic_reticulum.

[1726] Goyal U, Blackstone C. Untangling the web: mechanisms underlying ER network formation. Biochim Biophys Acta. 2013 Nov;1833(11):2492-8; https://www.ncbi.nlm.nih.gov/pmc/articles/pmid/23602970/.

precision after cytokinesis,[1727] so deployment of manufactured Golgi material in the correct intracellular position after extraction of the original material should result in self-assembly of a fully functional Golgi stack.[1728] Self-assembly of endoplasmic reticulum (ER) from manufactured material also appears likely,[1729] though the viability of both Golgi and ER self-assembly processes must be tested and experimentally confirmed by ***future research***.

One chromallocyte can transport up to $V_{chromstorage}$ = 40 μm^3 of organelle material during each round trip between the vasculoid cellulock and the cell under repair, so transporting $V_{organelle}$ = 3500 μm^3 of material per cell (**Table 10**) requires $n_{orgcycles} = V_{organelle} / V_{chromstorage}$ = 88 round trips per cell. Allowing $\tau_{organelle}$ ~1 hour per round trip to each of $N_{bodycells}$ = 3.5 x 10^{12} human body cells using a fleet of $N_{chromallocytes}$ = 10^{12} chromallocytes to make all the deliveries enables complete whole-body non-nucleus organelle replacement in $t_{replaceorganelle} \sim \tau_{organelle}\ n_{orgcycles}\ N_{bodycells} / N_{chromallocytes}$ ~ 308 hours (**12.8 days**) with a continuous nanorobotic fleet power draw of ~100 watts. During this time period, the cell mill must manufacture ~9 x 10^{19} organelles or roughly 12.3 liters (**Table 10**) of whole organelles or organelle material needed to complete the revival of a 70 kg cryopreservation patient. ***Future research*** should investigate and ascertain the additional resource overhead required for the detachment and reattachment of organelles to the cytoskeleton during the replacement operation.

The infusion of lipid droplet (~10 μm^3 or ~0.1% of cell volume) and glycogen granule (~1 μm^3 or ~0.01% of cell volume) organelles may be postponed if ***future research*** determines that this delay is necessary to maintain biochemical stasis throughout the remainder of repair activities until it is time to re-energize the cell via full instillation of activating molecules (Section 4.14.3).

4.12.2.4 Cytoskeleton and Related Intracellular Components

With the nucleus and other intracellular organelles successfully replaced, the next step is to inspect and repair (or replace) the many cytoskeletal components in the cell. **Table 11** suggests that there are ~17 meters of cytoskeletal fibers and filaments crammed into each cell (about 8 times the ~2-meter length[1730] of all DNA strands in the nucleus if fully stretched out), occupying ~11% of total cell volume.

[1727] Lowe M, Nakamura N, Warren G. Golgi division and membrane traffic. Trends Cell Biol. 1998 Jan;8(1):40-44; https://pubmed.ncbi.nlm.nih.gov/9695807/. Zaal KJM, Smith CL, Polishchuk RS, Altan N, Cole NB, Ellenberg J, Hirschberg K, Presley JF, Roberts TH, Siggia E, Phair RD, Lippincott-Schwartz J. Golgi membranes are absorbed into and reemerge from the ER during mitosis. Cell. 1999 Dec 10;99(6):589-601; https://core.ac.uk/download/pdf/82536976.pdf.

[1728] Rabouille C, Misteli T, Watson R, Warren G. Reassembly of Golgi stacks from mitotic Golgi fragments in a cell-free system. J Cell Biol. 1995 May;129(3):605-18; http://citeseerx.ist.psu.edu/viewdoc/download?doi=10.1.1.273.3233&rep=rep1&type=pdf. Puri S, Linstedt AD. Capacity of the golgi apparatus for biogenesis from the endoplasmic reticulum. Mol Biol Cell. 2003 Dec;14(12):5011-5018; https://www.ncbi.nlm.nih.gov/pmc/articles/PMC284802/. Kühnle J, Shillcock J, Mouritsen OG, Weiss M. A modeling approach to the self-assembly of the Golgi apparatus. Biophys J. 2010 Jun 16;98(12):2839-2847; https://www.ncbi.nlm.nih.gov/pmc/articles/PMC2884245/. Tachikawa M, Mochizuki A. Golgi apparatus self-organizes into the characteristic shape via postmitotic reassembly dynamics. Proc Natl Acad Sci U S A. 2017 May 16;114(20):5177-5182; https://www.ncbi.nlm.nih.gov/pmc/articles/PMC5441826/.

[1729] Ferencz CM, Guigas G, Veres A, Neumann B, Stemmann O, Weiss M. Shaping the endoplasmic reticulum *in vitro*. Biochim Biophys Acta. 2016 Sep;1858(9):2035-2040; https://www.sciencedirect.com/science/article/pii/S0005273616302127. Ferencz CM, Guigas G, Veres A, Neumann B, Stemmann O, Weiss M. *In Vitro* Reconstitution of the Endoplasmic Reticulum. Curr Protoc Cell Biol. 2017 Sep 1;76:11.22.1-11.22.16; https://pubmed.ncbi.nlm.nih.gov/28862340/. Li Q, Han X. Self-Assembled Rough Endoplasmic Reticulum-Like Proto-Organelles. iScience. 2018 Oct 26;8:138-147; https://www.ncbi.nlm.nih.gov/pmc/articles/PMC6180236/.

[1730] McGraw-Hill Encyclopedia of Science and Technology, McGraw-Hill, NY, 2012. Ashworth H. How long is your DNA? Science Focus, 2020; https://www.sciencefocus.com/the-human-body/how-long-is-your-dna/.

Table 11. Approximate quantification of cytoskeletal components possibly needing repair[1731]

Cytoskeletal Fiber Component	Fiber Thickness (nm)	Total Volume per Cell (μm^3)	Total Surface Area per Cell (μm^2)	Total Length per Cell (m)
Microfilaments	5-7	360	200,000	10
Superfine filaments	2-4	45	40,000	5
Intermediate filaments	8-12	100	30,000	1
Microtubules	25	370	10,000	0.6
Thick filaments	15	< 9	2,000	0.04
TOTALS		***884***	***282,000***	***17***

The exact extent of cytoskeletal damage caused by cryopreservation is presently unknown but should be the subject of ***future research***. As with organelles, a decision must be made if it is more efficient to scan, measure, and repair cytoskeletal fibers in place, or if time and effort can be saved by simply extracting the existing fiber network and replacing it with new fibers manufactured in cell mills (Appendix D) and installed intracellularly by nanorobots.

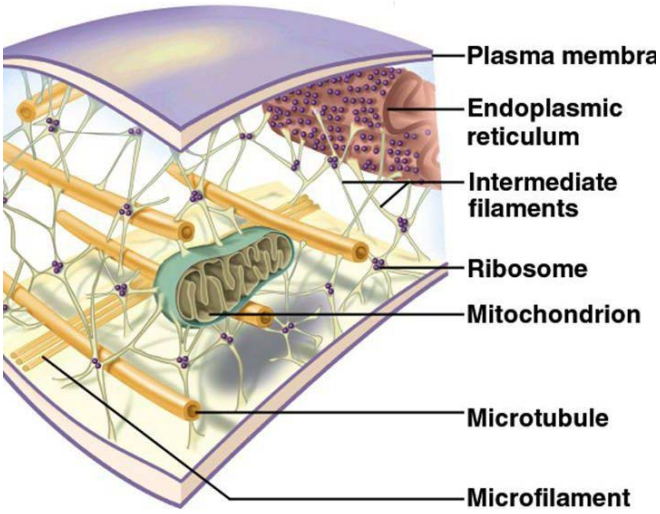

One can readily imagine a nanorobot optimized for cytoskeletal inspection and repair work. It would possess the ability to reversibly transit the plasma membrane and locomote intracellularly. It would possess inspection appendages tipped with chemotactic sensor pads[1732] enabling it to physically sample the entire 282,000 μm^2 of fiber surface and inspect it for faults or breaks. It would maintain an onboard inventory of fiber construction material to be applied wherever repairs are needed. Certain bacteria can locomote through cytoskeleton-rich animal cells at 0.1-1 µm/sec;[1733] if intracellular nanorobots can achieve $v_{scanbots}$ = 10 µm/sec, then inspection of the entire $L_{cytoskel}$ ~ 17 meter

[1731] Freitas RA Jr., Nanomedicine, Volume I: Basic Capabilities, Landes Bioscience, Georgetown, TX, 1999, Table 8.17, "Approximate Quantification of the Components of a Typical 20-µm Human Tissue Cell"; http://www.nanomedicine.com/NMI/Tables/8.17.jpg; and Section 8.5.3.11, "Cytoskeleton", http://www.nanomedicine.com/NMI/8.5.3.11.htm

[1732] Freitas RA Jr. Nanomedicine, Volume I: Basic Capabilities, Landes Bioscience, Georgetown TX, 1999; Section 4.2.8, "Chemotactic Sensor Pads", http://www.nanomedicine.com/NMI/4.2.8.htm; Section 8.5.2.1, "Identification of Self", http://www.nanomedicine.com/NMI/8.5.2.1.htm#p8; and Section 8.5.2.2, "Identification of Cell Type", http://www.nanomedicine.com/NMI/8.5.2.2.htm#p23.

[1733] Freitas RA Jr. Nanomedicine, Volume I: Basic Capabilities, Landes Bioscience, Georgetown TX, 1999; Section 9.4.6, "In Cyto Locomotion", http://www.nanomedicine.com/NMI/9.4.6.htm.

length of all cytoskeleton fibers in the cell using a fleet of 10^{12} robots could require at least [$L_{cytoskel}$ / $v_{scanbots}$] ($N_{bodycells}$ / $N_{PMscanbots}$) ~ 6 million sec (~69 days), plus at least several multiples of this time that must be allocated for the actual repair work. A nanorobot with multiple appendages operated in parallel could locomote more slowly or could process all the fibers in less time.

On the other hand, a nanorobot that made just one pass through the cell, simultaneously extracting existing fibers (regardless of their condition) and emplacing new fibers (recently manufactured in known good condition) at a net extraction/deposition speed of 10 μm/sec could complete the cytoskeleton replacement operation in the aforementioned **69 days**, using a fleet of 10^{12} nanorobots with the usual 100 watt power budget.

In addition to the fibers, the nanorobots must replace a few 400 nm centrioles,[1734] two of which are arranged at right angles and surrounded by an organized mass of protein,[1735] together constituting a centrosome organelle (of which there are normally two per cell).[1736] We may also need to inspect and replace any damaged or missing kinesin[1737] or dynein[1738] transport motor molecules that normally convey vesicles and granules at up to ~2 μm/sec through the cell on microtubule tracks. (These motor molecules will be biologically inert because the ATP that powers them will have previously been extracted from the cytoplasm; Section 4.10.1.2.)

4.12.2.5 Extract and Replace Maloccupied Membrane Receptors

A number of undesirable molecules will no longer be free in the extracellular or cytosolic fluids because they will have become chemically bound to receptors in cell membranes (images, below). These mal-occupied receptor molecules must be extracted, in many cases using the methods of transmembrane protein editing (Section 4.12.2.6).

One class of potentially undesirable receptor-bound molecules are signaling molecules (Section 4.10.1.5). For example, TNFα (tumor necrosis factor), a 25,644 dalton[1739] cytokine produced by activated macrophages, normally initiates caspase activity upon binding to the TNFR1 receptor present on most cells in the human body.[1740] Because the molecule becomes bound to a membrane receptor, it will not be removed during

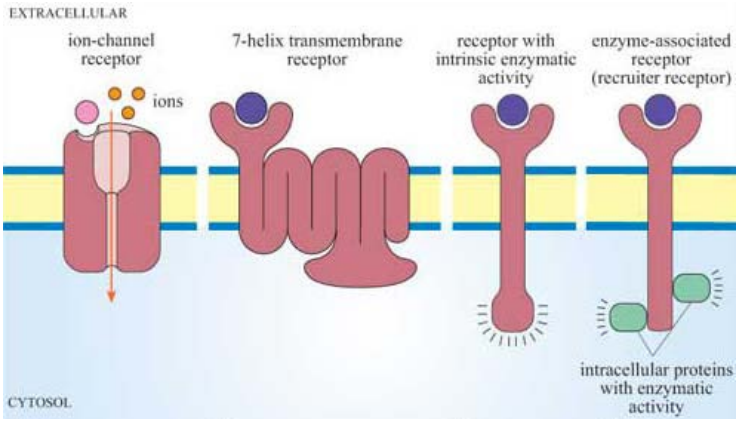

[1734] https://en.wikipedia.org/wiki/Centriole.
[1735] https://en.wikipedia.org/wiki/Pericentriolar_material.
[1736] https://en.wikipedia.org/wiki/Centrosome.
[1737] https://en.wikipedia.org/wiki/Kinesin.
[1738] https://en.wikipedia.org/wiki/Dynein.
[1739] https://www.phosphosite.org/proteinAction?id=8542247.
[1740] https://en.wikipedia.org/wiki/Tumor_necrosis_factor_alpha.

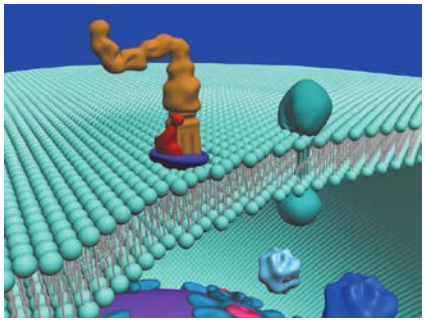

molecular extraction (Section 4.10). To remove these molecules, nanorobots must examine the relevant receptors on cell surfaces using probes tipped with chemotactic sensor pads,[1741] often inserted into cell-cell interfaces. These probes can identify which receptors may have signaling molecules bound to them, then extract those occupied receptors from the membrane, replacing them with identical new ones that are unoccupied. In such extractions, even inside the brain, it should be sufficient to restore the original number density and general distribution of receptors in the cell membrane because the exact position of individual receptors is unlikely to represent specific data comprising the patient's memory or personality (Section 2.1.2).

Bacterial toxins may produce another class of undesired occupied receptors. For example, the presence of lipopolysaccharide (LPS) endotoxin in the human blood can cause septic shock in living humans,[1742] but most of this endotoxin will not be free because the toxin operates by binding to the CD14/TLR4/MD2 receptor complex in monocytes, dendritic cells, macrophages and B cells.[1743] If left unattended, these occupied receptors could eventually induce production of cytokines such as IL-1β and IL-6 that can elicit inflammatory reactions. Again, nanorobots must examine the relevant receptors on cell surfaces, identify which ones may have been poisoned by toxin binding, and then extract those occupied receptors from the membrane, replacing them with identical new ones that are unoccupied. ***Future research*** should compile a comprehensive list of undesirable molecules likely to bind to membrane receptors, requiring replacement of the whole receptor complex.

Signaling molecules, toxins and the like will normally be present in fairly minute quantities. For example, humans can develop symptoms of toxemia when exposed to as little as 500 pg of *E. coli* lipopolysaccharide (the amount present in ~5 x 10^5 bacteria) per kilogram of body weight.[1744] This represents ~3.5 x 10^{-8} gm in a 70 kg human body, or ~3.5 x 10^{-14} molecules/nm^3 assuming 10^4-dalton endotoxin molecules in a 60 L human body (the same concentration reported for TNFα; Appendix J), or ~0.6 endotoxin molecules per cell if distributed evenly over $N_{bodycells}$ = 3.5 x 10^{12} tissue cells. Given the relatively small number of likely afflicted receptors per cell, the inspection time rather than the extraction/replacement time should dominate in this task. Following the method of estimation in Section 4.11.1, inspecting a total plasma membrane surface area of A_{CellPM} ~ 1.32 x 10^{16} μm^2 requires a scan time of $\tau_{CellPMscan}$ = [(A_{CellPM} / κ_{PMscan}) / $N_{PMscanbots}$] ($N_{bodycells}$ / $N_{PMscanbots}$) ~ 1.2 x 10^6 sec (**14 days**) using a total of $N_{PMscanbots}$ = 1 x 10^{12} scanning nanorobots assuming a plasma membrane scan rate of κ_{PMscan} = 10^{-2} μm^2/ nanorobot-sec (Section 4.5.4), while generating P_{CellPM} ~ 100 watts of continuous waste heat throughout the task duration.

[1741] Freitas RA Jr. Nanomedicine, Volume I: Basic Capabilities, Landes Bioscience, Georgetown TX, 1999; Section 4.2.8, "Chemotactic Sensor Pads", http://www.nanomedicine.com/NMI/4.2.8.htm; Section 8.5.2.1, "Identification of Self", http://www.nanomedicine.com/NMI/8.5.2.1.htm#p8; and Section 8.5.2.2, "Identification of Cell Type", http://www.nanomedicine.com/NMI/8.5.2.2.htm#p23.

[1742] https://en.wikipedia.org/wiki/Lipopolysaccharide#Health_effects.

[1743] Abbas A, Lichtman AH. Basic Immunology. Elsevier, 2006; https://www.amazon.com/dp/1416029745/.

[1744] https://en.wikipedia.org/wiki/Depyrogenation#Maximum_acceptable_endotoxin_level

4.12.2.6 Plasma Membrane and Transmembrane Protein Editing

With the intracellular cytoskeleton network repaired and the plasma membrane intact, the next task is to reinsert extruded lipids along with membrane and transmembrane proteins, including both integral and peripheral proteins (image, right), as required.

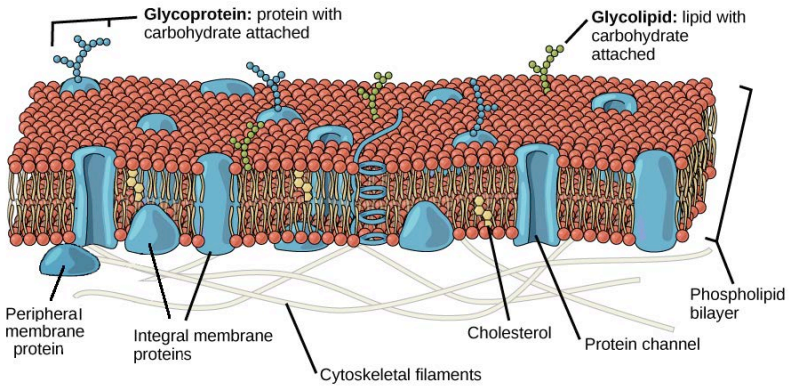

For cells other than neurons, it should suffice to restore the generic number density of appropriate lipids,[1745] lipid rafts,[1746] and proteins[1747] into or upon the plasma membrane. Careful scanning of the entire 2400 μm^2 external surface of each individual cell using probes tipped with chemotactic sensor pads[1748] can reveal the existing protein population, including any pathological proteins needing removal and replacement. Missing lipids and proteins can be added from manufactured stock provided by cell mills (Appendix D), restoring the established generic number density for the particular cell type (to be established by ***future research***). Many proteins will have attachments to various elements of the cytoskeleton, so the typical replacement operation will involve four steps: (1) detach old protein from cytoskeleton, (2) extract protein from membrane, (3) insert new protein into membrane, and (4) reconnect new protein to cytoskeleton. ***Future research*** should investigate possible strategies for expediting the fourth step by employing self-assembly or complementary surfaces to facilitate protein reattachment to the cytoskeleton or to peripheral proteins.[1749]

The time for a nanorobot to scan the plasma membrane can be estimated as $t_{PMproteinscan} \sim A_{bodycell} / \kappa_{PMscan} \sim$ 240,000 sec (2.8 days) taking $A_{bodycell} \sim 2400$ μm^2 for a typical cell[1750] and assuming a scan rate of $\kappa_{PMscan} = 10^{-2}$ μm^2/ nanorobot-sec (Section 4.5.4).

The total protein volume in the plasma membrane of a typical cell is $V_{PMprotein} \sim f_{PMprotein} V_{PM} \sim 10$ μm^3 if the plasma membrane is $f_{PMprotein} \sim 50\%$ protein by volume,[1751] the plasma membrane volume is $V_{PM} =$

[1745] https://en.wikipedia.org/wiki/Cell_membrane#Lipids.
[1746] https://en.wikipedia.org/wiki/Lipid_raft.
[1747] https://en.wikipedia.org/wiki/Cell_membrane#Proteins.

[1748] Freitas RA Jr. Nanomedicine, Volume I: Basic Capabilities, Landes Bioscience, Georgetown TX, 1999; Section 4.2.8, "Chemotactic Sensor Pads", http://www.nanomedicine.com/NMI/4.2.8.htm; Section 8.5.2.1, "Identification of Self", http://www.nanomedicine.com/NMI/8.5.2.1.htm#p8; and Section 8.5.2.2, "Identification of Cell Type", http://www.nanomedicine.com/NMI/8.5.2.2.htm#p23.

[1749] e.g., https://en.wikipedia.org/wiki/Peripheral_membrane_protein#Membrane_binding_mechanisms, https://en.wikipedia.org/wiki/Transmembrane_protein#Proteins_with_alpha-helical_transmembrane_anchors.

[1750] Freitas RA Jr., Nanomedicine, Volume I: Basic Capabilities, Landes Bioscience, Georgetown, TX, 1999, Table 8.17, "Approximate Quantification of the Components of a Typical 20-μm Human Tissue Cell"; http://www.nanomedicine.com/NMI/Tables/8.17.jpg.

[1751] Cooper GM. The Cell: A Molecular Approach. 2nd edition. Sunderland (MA): Sinauer Associates; 2000; "Cell Membranes"; https://www.ncbi.nlm.nih.gov/books/NBK9928/.

w_{PM} $A_{bodycell}$ ~ 20 μm^3, and the lipid bilayer[1752] averages w_{PM} ~ 8 nm thick.[1753] If the typical membrane protein molecule volume is $V_{protein}$ ~ 100 nm^3, then there are $N_{PMproteins}$ ~ $V_{PMprotein}$ / $V_{protein}$ ~ 10^8 protein molecules in the plasma membrane.[1754] A chromallocyte nanorobot has ~1000 "grapple arms" deployable from its hull for mobility purposes.[1755] If a chromallocyte-class protein replacement nanorobot can simultaneously employ just N_{arm} = 100 manipulator arms that can extract and insert protein molecules at a rate of $\chi_{insertion}$ ~ 1 molecule/manipulator-sec, then all plasma membrane proteins could be replaced in an individual cell in $t_{PMproteinreplace}$ ~ $N_{PMproteins}$ / ($\chi_{insertion}$ N_{arm}) ~ 10^6 sec (11.6 days), the worst-case scenario. Note that a single chromallocyte-class nanorobot with $V_{chromstorage}$ = 40 μm^3 of internal storage has the space to transport the entire membrane protein content of up to $V_{chromstorage}$ / $V_{PMprotein}$ ~ 4 cells.

A fleet of $N_{chromallocytes}$ = 10^{12} nanorobots consuming 100 watts of power could complete the membrane protein scan and replace mission in a maximum of $t_{PMprotein}$ = ($t_{PMproteinscan}$ + $t_{PMproteinreplace}$) ($N_{bodycells}$ / $N_{chromallocytes}$) = 4.3 x 10^6 sec (~**50 days**).

For neurons, using the aforementioned process with greater care in the vicinity of synapses and similar neural features to avoid disturbing memory- or personality-encoding structures seems prudent, although the living neuron plasma membrane replaces its protein content fairly quickly (turnover rates for neuron plasma membrane proteins[1756] and synaptic proteins[1757] are in the range of several days). The greater surface area of neurons compared to average tissue cells shouldn't increase the whole-body processing time estimated in the previous paragraph by more than ~25%.

4.12.2.7 Glycocalyx Repair

Finally, the plasma membrane also contains small amounts of carbohydrate[1758] that might have suffered damage during cryopreservation (the extent of which should be investigated in ***future research***). This carbohydrate is covalently linked to some of the membrane lipids and proteins. Carbohydrate portions of the membrane glycoproteins are always located at the extracellular surface, forming the **glycocalyx** (together with collagen proteins and glycosaminoglycans). The red cell membrane, for instance, contains 52% protein, 40% lipid, and 8% carbohydrate by weight.[1759] A small proportion of membrane

---

[1752] https://en.wikipedia.org/wiki/Lipid_bilayer.

[1753] Freitas RA Jr., Nanomedicine, Volume I: Basic Capabilities, Landes Bioscience, Georgetown, TX, 1999, Table 8.17, "Approximate Quantification of the Components of a Typical 20-μm Human Tissue Cell"; http://www.nanomedicine.com/NMI/Tables/8.17.jpg.

[1754] Freitas RA Jr. Nanomedicine, Volume I: Basic Capabilities, Landes Bioscience, Georgetown TX, 1999; Section 8.5.3.2, "Cell Membrane", http://www.nanomedicine.com/NMI/8.5.3.2.htm.

[1755] Freitas RA Jr. The Ideal Gene Delivery Vector: Chromallocytes, Cell Repair Nanorobots for Chromosome Replacement Therapy. J. Evol. Technol. 2007 Jun;16:1-97; Section 3.5, "Mobility System"; http://jetpress.org/v16/freitas.pdf.

[1756] Dörrbaum AR, Kochen L, Langer JD, Schuman EM. Local and global influences on protein turnover in neurons and glia. Elife. 2018 Jun 19;7:e34202; https://www.ncbi.nlm.nih.gov/pmc/articles/PMC6008053/.

[1757] Cohen LD, Zuchman R, Sorokina O, Müller A, Dieterich DC, Armstrong JD, Ziv T, Ziv NE. Metabolic turnover of synaptic proteins: kinetics, interdependencies and implications for synaptic maintenance. PLoS One. 2013 May 2;8(5):e63191; https://www.ncbi.nlm.nih.gov/pmc/articles/PMC3642143/.

[1758] https://en.wikipedia.org/wiki/Cell_membrane#Carbohydrates.

[1759] Becker WM, Deamer DW. The World of the Cell, Second Edition, Benjamin/Cummings Publishing Company, Redwood City CA, 1991; https://www.amazon.com/dp/0805308709/.

carbohydrate is glycolipids, but most is in the form of glycoproteins, and the sugar units are usually short oligosaccharide chains attached to serine, threonine, or asparagine side chains.

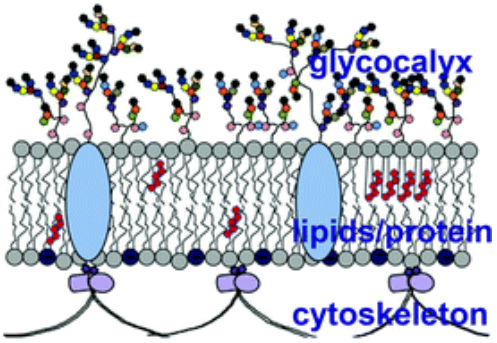

The glycocalyx (image, right),[1760] or fuzzy coat, lies exterior to the plasma membrane. In most cell types, the glycocalyx is 10-100 nm thick consisting of tangled strands of up to ~10,000-atom glycoproteins each measuring 5-8 nm thick and up to 100-200 nm in length.[1761] The experimentally-measured thickness of the glycocalyx of various human cells ranges from ~6 nm for blood-group A erythrocytes[1762] to 30-60 nm for bladder cells,[1763] 40-70 nm for lymphocytes,[1764] ~50 nm for myocardial cells,[1765] 90 nm for cochlear hair cells,[1766] and up to 150 nm in intestinal epithelial cells where the fuzzy coat consists primarily of oligosaccharide chains 1.2-2.5 nm in diameter.[1767] The glycoproteins of the glycocalyx provide a set of highly specific biological markers that should be readily recognizable by suitably equipped medical nanorobots. These markers assist normal cellular interactions by allowing blood group recognition and providing bacterial and toxin binding sites, egg recognition by sperm, immune responses, guidance of embryonic development, and cellular lifespan determination (e.g., the red cell coat thins with age which may serve as an RBC removal signal for phagocytes and in the liver).[1768] ***Future research*** should determine the level of effort required for glycocalyx editing, but for now a crude time estimate of **3 days** for ~10^{12} nanorobots should suffice.

A few other cytosolic components might need attention and should be considered in ***future research***:[1769] (1) repair or removal of peroxidized, racemized, oxidized, or otherwise modified structures, resulting in

---

[1760] Atukorale PU, Yang YS, Bekdemir A, Carney RP, Silva PJ, Watson N, Stellacci F, Irvine DJ. Influence of the glycocalyx and plasma membrane composition on amphiphilic gold nanoparticle association with erythrocytes. Nanoscale. 2015 Jul 14;7(26):11420-32; https://core.ac.uk/download/pdf/189512268.pdf.

[1761] de Robertis EDP, de Robertis EMF. Cell and Molecular Biology, Eighth Edition, Lea & Febiger, Philadelphia PA, 1987; https://www.amazon.com/dp/0812110129/. Alberts B, Bray D, Lewis J, Raff M, Roberts K, Watson JD. The Molecular Biology of the Cell, Second Edition, Garland Publishing, Inc., NY, 1989; https://www.amazon.com/dp/0824036956/.

[1762] Linss W, Pilgrim C, Feuerstein H. How thick is the glycocalyx of human erythrocytes? [in German]. Acta Histochem. 1991;91(1):101-104; https://pubmed.ncbi.nlm.nih.gov/1801510/.

[1763] Romanenko AM. Ultrastructural diagnostic markers of the urinary bladder precancer. Bull Assoc Anat (Nancy). 1989 Mar;73(220):31-35; https://pubmed.ncbi.nlm.nih.gov/2765681/.

[1764] Schneider GB, Pockwinse SM, Billings-Gagliardi S. Binding of concanavalin-A to critical-point-dried and freeze-dried human lymphocytes. Am J Anat. 1979 Sep;156(1):121-129; https://pubmed.ncbi.nlm.nih.gov/517445/.

[1765] Langer GA. The structure and function of the myocardial cell surface. Am J Physiol. 1978 Nov;235(5):H461-H468; https://journals.physiology.org/doi/pdf/10.1152/ajpheart.1978.235.5.H461.

[1766] Santi PA, Anderson CB. A newly identified surface coat on cochlear hair cells. Hear Res. 1987;27(1):47-65; https://pubmed.ncbi.nlm.nih.gov/3583936/.

[1767] Becker WM, Deamer DW. The World of the Cell, Second Edition, Benjamin/Cummings Publishing Company, Redwood City CA, 1991; https://www.amazon.com/dp/0805308709/.

[1768] Marieb EN. Human Anatomy and Physiology, Benjamin/Cummings Publishing Company, Redwood City CA, 1989; https://www.amazon.com/dp/0805301224/.

[1769] Fahy G. Appendix B. A "Realistic" Scenario for Nanotechnological Repair of the Frozen Human Brain. In: Wowk B, Darwin M, eds., Cryonics: Reaching for Tomorrow. Alcor Life Extension Foundation, 1991, pp. A-10 – A-26; https://alcor.org/Library/html/nanotechrepair.html.

their replacement with undamaged structures; (2) protein reaggregation; and (3) reversal of glycerol-induced biochemical reactions.

4.12.2.8 Whole-Cell Replacement Option

Future research should undertake a trade study to investigate whether much of the complexity of the repair operations described in the previous seven subsections might be avoided by simply importing whole cells that are manufactured in the cell mill (Appendix D) and installing them directly into the tissue, while simultaneously extracting and discarding the old cells.

Vasculoid boxcars have a limit of V_{boxcar} = 2120 μm^3 of usable internal storage volume. This is too small for carrying even a single whole V_{cell} = 8000 μm^3 replacement tissue cell. However, a nanosyringe[1770] can be used to import macroscale quantities of cells to any location inside the body. A nanosyringe (to be designed as a ***future research*** exercise) is a 1-10 micron diameter flexible tube that could be inserted directly through the skin and steered[1771] into specific locations inside organs or tissues, much like the molecular extraction probe (Section 4.10.1.9). Nanorobotic mechanisms embedded on the external surfaces of a nanosyringe can assist in actively propelling the telescoping apparatus gently through the tissues[1772] while (1) avoiding embedded vasculoid components, (2) sampling the local chemical environment,[1773] and (3) providing a torrent of mechanical and optical sensory feedback along with precision positional metrology to allow the surgical operator to maintain complete locational awareness throughout the procedure.

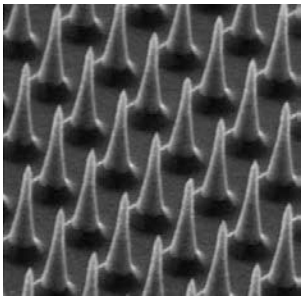

For example, a 1 cm^3 volume of 125 million 20-micron tissue cells, arranged in planar 10-cell slabs moving perpendicular to the slab plane through a tube, could be imported at ~1 m/sec through a 10-cm long nanosyringe with a 100 micron inside diameter (possibly coated with mechanical cilia to facilitate efficient transport) to virtually anywhere inside the human body in ~250 sec (~4 min). A modest-sized array of 1000 nanosyringes arranged in the manner of common microneedles (image, right)[1774] having a ~10 mm^2 total penetration cross-section for the entire array could transport ~1500 cm^3 of cells – the volume of the human liver, one of the largest human organs – into the body during a ~6 minute transfer. Nanorobots positioned at or near the in-tissue terminus of the nanosyringe can assist in receiving and installing the arriving cells. A second nanosyringe could export a matching volume of body fluid or comminuted pathological tissue and discarded cells to precisely maintain conservation of volume/mass, if necessary.

[1770] Freitas RA Jr. Chapter 23. Comprehensive Nanorobotic Control of Human Morbidity and Aging, Section 6.3.5.4 "Nanosyringoscopy". In: Fahy GM, West MD, Coles LS, Harris SB, eds, The Future of Aging: Pathways to Human Life Extension, Springer, New York, 2010, pp. 685-805; http://www.nanomedicine.com/Papers/Aging.pdf.

[1771] Glozman D, Shoham M. Flexible needle steering for percutaneous therapies. Comput Aided Surg. 2006 Jul;11(4):194-201; https://www.tandfonline.com/doi/pdf/10.3109/10929080600893019.

[1772] Freitas RA Jr. Nanomedicine, Volume I: Basic Capabilities, Landes Bioscience, Georgetown TX, 1999, Section 9.4.4, "Histonatation"; http://www.nanomedicine.com/NMI/9.4.4.htm.

[1773] Freitas RA Jr. Nanomedicine, Volume I: Basic Capabilities, Landes Bioscience, Georgetown TX, 1999, Chapter 4, "Sensors and Nanoscale Scanning"; http://www.nanomedicine.com/NMI/4.1.htm.

[1774] Gittard SD, Ovsianikov A, Chichkov BN, Doraiswamy A, Narayan RJ. Two-photon polymerization of microneedles for transdermal drug delivery. Expert Opin Drug Deliv. 2010 Apr;7(4):513-533; https://www.ncbi.nlm.nih.gov/pmc/articles/PMC2844933/. Ingrole RSJ, Gill HS. Microneedle Coating Methods: A Review with a Perspective. J Pharmacol Exp Ther. 2019 Sep;370(3):555-569; https://pubmed.ncbi.nlm.nih.gov/31175217/.

Whole-cell replacement could provide dramatically shorter repair times for non-neuron cells. Replacing whole neurons that are uniquely the seat of memory and personality will require special care because: (1) neurons are packed more tightly in the brain than are cells in other tissues, leaving less space for nanodevices to operate; (2) neural axons and dendrites are intricately threaded around other cells, making it harder to correctly extract and insert lengthy cytoplasmic processes into the embedding neuropil while avoiding additional damage; and (3) precise positional matching of synapses to axonal locations on contacting neurons will require excellent metrology and careful handling.[1775] The details of how this can be accomplished is a suitable conceptual design exercise for ***future research***.

4.12.3 Supplemental Tissue Repair

With all existing cells now in good repair, our attention turns to three remaining items of general tissue repair that must be addressed before the patient can be awakened:

(1) the extraction of unwanted **macroscale objects**, whether biological or nonbiological in origin, from the body, and insertion of appropriate whole cells and other viable tissue into the voids created by this extraction (Section 4.12.3.1).

(2) Repair of **blood vessel damage** caused by (A) vascular trimming operations during vasculoid installation, (B) freeze damage during cryopreservation, and (C) the need to re-create vascular thoroughfares where essential blood vessels are missing (Section 4.12.3.2).

(3) Reconditioning of selected subvolumes of the **extracellular matrix** that may have suffered significant damage in tissues receiving insufficient cryoprotectant perfusion (Section 4.12.3.3).

4.12.3.1 Foreign Object Extraction and Avulsion Wound Repair

The nanocatheter or nanosyringe (Section 4.12.2.8) can be used to remove large foreign objects from the body of the cryopreserved patient, including objects resulting from biological pathology (e.g., cancer tumors, granulomas, scar tissue), trauma (e.g., bullets, shrapnel), surgery (e.g., surgical pins that are no longer required), or cosmetic modifications (e.g., metal body piercings, tattoos, breast implants). Carefully poking a needle-like 100-micron diameter nanosensor-tipped self-steering nanosyringe quickly through all intervening soft tissues to the immediate vicinity of a foreign object should cause minimal tissue damage that can be rapidly repaired or in some cases even ignored.

After tissue penetration to the vicinity of the target foreign object, ~10^{10} μm^3/sec of nanorobots flowing at ~1 m/sec through the tube (a typical rate for contemporary medical syringes) could surround a cubic 1 cm^3 target object to a coating thickness of 100 μm in ~10 seconds. The coating nanorobots would then dig out 1 μm wide grooves at a volumetric excavation rate of 1% of nanorobot volume per second to partition the 1 cm^3 object into 10^6 100-μm microcubes in ~300 seconds, after which the foreign object microcubes are transported out of the patient in single file at 1 m/sec through the nanosyringe in ~100 seconds, followed by the exiting nanorobots taking ~10 seconds, completing a ~7 minute object-removal procedure through a ~100-μm diameter hole.

[1775] Freitas RA Jr. The Alzheimer Protocols: A Nanorobotic Cure for Alzheimer's Disease and Related Neurodegenerative Conditions. IMM Report No. 48, June 2016, 433 pp; Section 5.3.2.3, "Cell Insertion and Emplacement," pp. 327-332; http://www.imm.org/Reports/rep048.pdf.

Removal of the foreign object will leave a vacancy that must be filled. Depending on the type of tissue in which the foreign object was embedded, specific whole cells manufactured in cell mills (Appendix D) could be delivered directly to the site via the nanosyringe (Section 4.12.2.8) and installed by tissue-assembly nanorobots (also delivered on site by the nanosyringe), after which all nanorobots exit the body through the nanosyringe, and then the nanosyringe is removed.

Additional tissue vacancies may be present in the likely rare cases of avulsion[1776] wounds suffered by the patient prior to cryopreservation. Wound healing will be a specialty in the field of medical nanorobots,[1777] and may require debridement,[1778] manufacture of replacement cells using a cell mill (Appendix D), and cell insertion and replacement[1779] and neural incorporation[1780] operations, possibly using scaffolded tissue printing (Section 5.2.3.3.1) or other methods of fluidic 3D cell printing (Section 5.2.3.3).

4.12.3.2 Residual Vascular Repair

The structural and functional integrity of the entire vascular system must be restored before the patient can be resanguinated. All existing cells have been physically restored by this stage, so there are five remaining sources of possible vascular fault (Section 4.8.1(2)) requiring repair:

(1) **Trim Damage.** Endothelial cells lining the vascular walls with only plasma membrane damage or serious cytoplasmic avulsion wounds will already have been repaired, but in some cases endothelial cells that were more heavily trimmed during vasculoid installation (Section 4.6.2) due to endothelial swelling or blebbing (Section 3.6(3)) may fail to have remained recognizable as viable cells after trimming and may have been removed as cell debris (Section 4.12.2.1), leaving a void where one or more cells should reside. The missing cells of the appropriate types can be restored or rebuilt *in situ* from manufactured components (Appendix D) that are installed via conventional nanomedical means (Section 4.12.2).

(2) **Freeze Damage.** Blood vessels with serious structural damage due to cryopreservation stresses must be repaired to allow proper conduction of biological fluids, and pieces of shredded or torn endothelium (or the interior components of endothelial cells) could migrate throughout the ECM or even into cytological spaces to the detriment of tissue health. These cells should be rebuilt *in situ* from manufactured components (Appendix D) that are installed via conventional means (Section 4.12.2). The migrating pieces should already have been detected (Section 4.8.1 or Section 4.11.1) and removed (Section 4.12.1.1 or Section 4.12.2.1).

[1776] https://en.wikipedia.org/wiki/Avulsion_injury.

[1777] Freitas RA Jr. Chapter 23. Comprehensive Nanorobotic Control of Human Morbidity and Aging. In: Fahy GM, West MD, Coles LS, Harris SB, eds, The Future of Aging: Pathways to Human Life Extension, Springer, New York, 2010, pp. 685-805; Section 6.3.4 "Wound Healing"; http://www.nanomedicine.com/Papers/Aging.pdf.

[1778] Freitas RA Jr. The Alzheimer Protocols: A Nanorobotic Cure for Alzheimer's Disease and Related Neurodegenerative Conditions. IMM Report No. 48, June 2016, 433 pp; Section 5.3.2.2 "Intracranial Debridement"; http://www.imm.org/Reports/rep048.pdf.

[1779] Freitas RA Jr. The Alzheimer Protocols: A Nanorobotic Cure for Alzheimer's Disease and Related Neurodegenerative Conditions. IMM Report No. 48, June 2016, 433 pp; Section 5.3.2.3 "Cell Insertion and Replacement"; http://www.imm.org/Reports/rep048.pdf.

[1780] Freitas RA Jr. The Alzheimer Protocols: A Nanorobotic Cure for Alzheimer's Disease and Related Neurodegenerative Conditions. IMM Report No. 48, June 2016, 433 pp; Section 5.3.2.4 "Neural Incorporation"; http://www.imm.org/Reports/rep048.pdf.

(3) **Missing Vascularization.** Localized macerated tissue due to freezing with insufficient cryoprotectant perfusion (Section 3.4.2(6)) will undergo debris clearance followed by cell repopulation of *de novo* tissue, and then the building of vascular thoroughfares throughout the replaced material. New endothelial cells can be reconstructed from manufactured components (Appendix D), as can the other cells comprising the fresh tissue. In the case of well-vascularized cancer tumors that are eradicated by individual cell deletion, vasculoid will still fill the capillaries of the now vacant tissue, so new vasculature can be constructed around the external surface of the vasculoid plating in a manner analogous to scaffolded tissue printing (Section 5.2.3.3.2), with other missing cells also added via conventional means (Section 4.12.2). Tumors that are eradicated by whole tumor deletion (Section 4.12.3.1) may leave a vasculoid-free void that can be packed with appropriate cells using a nanosyringe apparatus (Section 4.12.2.8).

(4) **Lymphatic Damage.** The three vascular restoration tasks described above must also be applied to the lymphatic vasculature, which should repaired in similar manner as required, after which all vasculoid components residing in lymphatic tissue that were previously installed (Section 4.6.4) should be uninstalled and removed from the patient.

(5) **BBB Damage.** Disruptions to the blood-brain barrier (BBB) may need to be repaired if the BBB has been deliberately damaged during future cryonics protocols designed to improve the penetration of cryoprotective agents into the brain.

4.12.3.3 ECM Reconditioning

Tissues are dynamic structures that exhibit continual turnover of molecular and cellular components. The extracellular matrix[1781] (ECM) helps to maintain tissue pattern integrity, allowing cells that are lost due to injury or aging to be replaced in an organized fashion. For instance, when tissue cells are killed by freezing or poisoning, all of the cellular components may die and be removed, but the basement tissue membrane often remains intact. (The image at right shows (gray) cells surrounded by (white) spaces filled with extracellular matrix.)[1782] These residual scaffoldings ensure correct repositioning of cells (e.g., cell polarity) and proper restoration of different cell types to their correct locations (e.g., muscle cells in muscle basement tissue membrane, nerve cells in nerve sheaths, endothelium within blood vessels). Conversely, loss of ECM integrity during wound healing may cause permanent disorganization of tissue patterns, producing dermal scars.[1783]

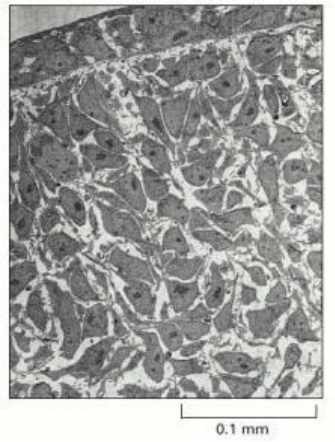

The mesh size of the fibrous components of the ECM varies widely according to tissue type. Collagens are the major proteins of the ECM and comprise ~25% of total mammalian protein mass.[1784] The typical

---

[1781] Frantz C, Stewart KM, Weaver VM. The extracellular matrix at a glance. J Cell Sci. 2010 Dec 15;123(Pt 24):4195-200; https://www.ncbi.nlm.nih.gov/pmc/articles/PMC2995612/. See also: https://en.wikipedia.org/wiki/Extracellular_matrix.

[1782] "The Extracellular Matrix of Animals," Fig. 19-33, in: Alberts B, Johnson A, Lewis J, Raff M, Roberts K, Walter P, eds. Molecular Biology of the Cell, 4th edition, Garland Science, New York, 2002; https://www.ncbi.nlm.nih.gov/books/NBK26810/.

[1783] Ingber DE. Chapter 7. Mechanochemical Switching Between Growth and Differentiation by Extracellular Matrix. In: Lanza RP, Langer R, Chick WL, eds., Principles of Tissue Engineering, R.G. Landes Company, Georgetown TX, 1997, pp. 89-100; https://www.amazon.com/dp/0124366252/.

collagen molecule is a long (~300 nm), thin (~1.5 nm) fiber, the center of which is a characteristic triple helix running ~95% of the length. Photomicrographs of excised tissue samples show a gap of 4-12 μm between adjacent collagen fibrils in skin tissue and in tendons.[1785] Cartilage (which contains much collagen) has large aggregates of proteoglycans, with as many as 100 molecules attached to a single hyaluronic acid, giving a length of ~10 μm and a diameter of 500-600 nm. A tissue micrograph of fibrous cartilage in the disks between the vertebral bodies[1786] shows gaps of 10-30 microns between adjacent fibrils.[1787] Fibronectins or laminins may be present in ECM at low density (<1 ng/mm^3) or high density (>5 ng/mm^3),[1788] giving an estimated typical intermolecular spacing of 4-10 μm. Although the matrix grid can be as narrow as 0.3-3 microns in special cases such as the ECM between the epidermis and the somites of the axolotl embryo, or between the highly flexible elastin fibers in the walls of the aorta,[1789] in most cases the gaps between ECM elements should be wide enough (schematic, above)[1790] for micron-size nanorobots to slip through without much difficulty.

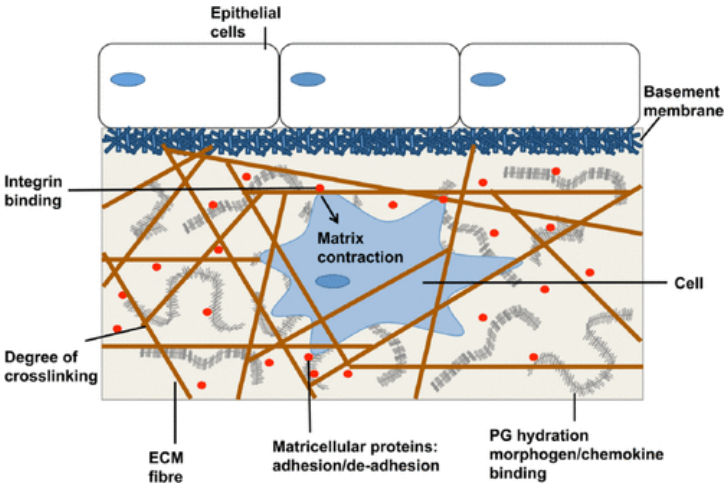

Nanorobots with at least two appendages can alternately grasp and release a succession of adjacent ECM elements, brachiating[1791] "hand over hand" through tissue in a manner crudely analogous to scuba divers pulling themselves along an underwater rope mesh ladder. The maximum safe nanorobot brachiation speed

---

[1784] Stryer L. Biochemistry, 4th Edition, W.H. Freeman and Company, New York, 1995; https://www.amazon.com/dp/0716720094/.

[1785] Loewy AG, Siekevitz P, Menninger JR, Gallant JAN. Cell Structure and Function: An Integrated Approach, Third Edition, Saunders College Publishing, Philadelphia PA, 1991; https://www.amazon.com/dp/0030474396/.

[1786] https://en.wikipedia.org/wiki/Vertebral_column.

[1787] Loewy AG, Siekevitz P, Menninger JR, Gallant JAN. Cell Structure and Function: An Integrated Approach, Third Edition, Saunders College Publishing, Philadelphia PA, 1991; https://www.amazon.com/dp/0030474396/.

[1788] Ingber DE. Chapter 7. Mechanochemical Switching Between Growth and Differentiation by Extracellular Matrix. In: Lanza RP, Langer R, Chick WL, eds., Principles of Tissue Engineering, R.G. Landes Company, Georgetown TX, 1997, pp. 89-100; https://www.amazon.com/dp/0124366252/.

[1789] Loewy AG, Siekevitz P, Menninger JR, Gallant JAN. Cell Structure and Function: An Integrated Approach, Third Edition, Saunders College Publishing, Philadelphia PA, 1991; https://www.amazon.com/dp/0030474396/.

[1790] Kular JK, Basu S, Sharma RI. The extracellular matrix: Structure, composition, age-related differences, tools for analysis and applications for tissue engineering. J Tiss Eng. 2014 Dec 21; 5; https://journals.sagepub.com/doi/full/10.1177/2041731414557112.

[1791] Nakanishi J, Fukuda T, Koditschek DE. Preliminary Studies of a Second Generation Brachiation Robot Controller. Proc. 1997 IEEE International Conference on Robotics and Automation, 20-25 Apr 1997, IEEE Robotics and Automation Society, pp. 2050-2056.

through the ECM has been estimated[1792] as ~100 μm/sec although the natural movement of biological entities through ECM is much slower – e.g., leukocyte and fibroblast amoeboid motion through extracellular tissue is typically ~0.05-0.70 μm /sec.[1793] Nanorobot locomotion through ECM to perform previous stages of repair or replacement should not cause significant additional ECM damage or elicit any cellular changes. ECM in living cells transmits mechanical forces to mechanosensors in nearby cells which would normally respond to the stimulus by altering cell behavior, gene expression, and differentiation. However, these responses will be inactive during nanorobot passage or ECM repair operations because of the previous molecular extractions producing metabolic stasis (Section 4.10).

Future research should quantify the exact nature and amount of damage to tissue ECM that should be expected during warm ischemia, perfusion, and cryopreservation by performing experiments to directly test and measure these effects. During cryopreservation, water leaves the cells and expands the extracellular spaces, then vitrifies or freezes. ECM damage could be substantial in those areas lacking sufficient cryoprotectant. This knowledge, together with previously compiled tissue damage maps (Section 4.8.1), cryoprotectant concentration maps accumulated during the molecular extraction process (Section 4.10.1.7), and the record of cryorevival interventions to this point should provide a clear guide as to which sections of ECM may be most in need of repair.

It seems unlikely that matrix-bound nanovesicles[1794] (similar to exosomes; Section 4.12.1.1) will be seriously damaged by cryopreservation, although a few may have detached and require reattachment.

In the worst case scenario, most or all of the ECM would need some kind of repair or reconditioning. The ECM occupies the interstitial fluid volume,[1795] which we may estimate as $V_{ECM} \sim 10$ L for the reference 70 kg human body. If $f_{ECMfiber} = 1\%$ of the volume of the ECM is occupied by fibers averaging $w_{fiber} \sim 2$ nm in width, then the total length of all ECM fibers in the human body may be approximated as $L_{ECM} \sim f_{ECMfiber} V_{ECM} / w_{fiber}^2 \sim 2.5 \times 10^{13}$ m. A fleet of $N_{fibrobot} = 10^{12}$ ECM repair nanorobots called fibrobots[1796] (to be designed as a ***future research*** exercise) with a ~100 W fleet power budget could perform all necessary ECM repairs in $t_{ECMrepair} \sim (L_{ECM} / v_{fibrobot} N_{fibrobot}) = 2.5 \times 10^6$ sec (~**29 days**), assuming fibrobots can scan ECM fibers at a linear velocity of ~100 μm/sec but achieve a net repair velocity of only $v_{fibrobot} \sim 10$ μm/sec taking into account the occasional need to stop and make repairs. These velocities are only ~2 orders of magnitude faster on both measures than is typically achieved by biological fibroblasts, well within the envisioned typical performance improvement of nanorobots over biological systems. Repair materials may be locally sourced from damaged ECM, extruded from onboard stores, or reprovisioned via the nearby vasculoid.

[1792] Freitas RA Jr. Nanomedicine, Volume I: Basic Capabilities, Landes Bioscience, Georgetown TX, 1999, Section 9.4.4.2, "ECM Brachiation"; http://www.nanomedicine.com/NMI/9.4.4.2.htm.

[1793] Freitas RA Jr. Nanomedicine, Volume I: Basic Capabilities, Landes Bioscience, Georgetown TX, 1999, Section 9.4.3.7, "Amoeboid Locomotion"; http://www.nanomedicine.com/NMI/9.4.3.7.htm.

[1794] Huleihel L, Hussey GS, Naranjo JD, Zhang L, Dziki JL, Turner NJ, Stolz DB, Badylak SF. Matrix-bound nanovesicles within ECM bioscaffolds. Sci Adv. 2016;2(6):e1600502; https://www.ncbi.nlm.nih.gov/pmc/articles/PMC4928894/.

[1795] https://en.wikipedia.org/wiki/Extracellular_fluid.

[1796] Fibrobots would perform a similar function as **fibroblasts** (https://en.wikipedia.org/wiki/Fibroblast), the most common mobile cell in connective tissue that synthesizes and maintains the structural framework of the ECM, mobile **chondrocytes** (https://en.wikipedia.org/wiki/Chondrocyte), the only cells found in healthy cartilage, that produce the cartilaginous matrix, and **osteoblasts** (https://en.wikipedia.org/wiki/Osteoblast) that perform a similar function in bone.

4.12.3.4 Withdraw Vasculoid from Tissue Perimeter Surfaces

With the plasma membranes resealed and cells rehydrated (Section 4.11), existing cells repaired (Section 4.12.2), and tissue repair complete (Section 4.12.3) including ECM reconditioning (Section 4.12.3.3), tissue structure now has sufficient integrity and support strength to allow the withdrawal of all vasculoid components that were previously installed on the tissue perimeter surfaces (Section 4.6.5(4)) as enumerated in Appendix E.

All removed vasculoid components should be exported out of the body, via the vasculoid.

4.12.4 Supplemental Neural Repair

A whole-body neural connectome map – essentially, a "wiring diagram" of the brain that uniquely identifies all neuron bodies (i.e., axons and dendrites) and all neuronal synapses – was previously compiled (Section 4.8.1(5)). This map should have been updated to reflect physical changes that occurred during the foregoing cell reconstruction processes (Section 4.12.2).

At this point in the neural reconstruction process, all plasma membranes will have been sealed. The final tasks to complete neural repair will include sealing all axon breaks (Section 4.12.4.1), neuron membrane editing to correct receptor molecules in plasma membranes (Section 4.12.4.2), and the restoration of missing brain tissue (Section 4.12.4.3).

4.12.4.1 Axonal Repair

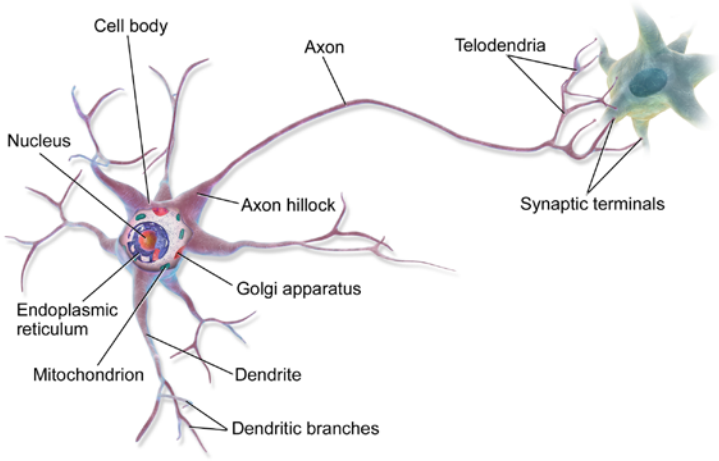

The axon[1797] is a long, slender projection of a neuron that conducts electrical impulses away from the nerve cell body in order to transmit information to remote neurons, muscles, and glands.

While the main neuron cell body will have previously been repaired (Section 4.12.2), and synapses are believed to be spared from freezing damage (Section 3.4.2(1)), there is some evidence for axonal tearing during cryopreservation.[1798] Even major loss of axoplasmic proteins at sites of torn axon bundles should not complicate the identification of individual nerve fibers on either side of a tear because the axonal protein content should be largely unaffected by the lesion a short distance from the tear (Section 3.4.1(4)). Local ripping, twisting, and fraying of the torn ends of nerve tracts by contraction of the brain cells and by the push of extracellular ice, creating debris-strewn

---

[1797] https://en.wikipedia.org/wiki/Axon.

[1798] Fahy GM, Takahashi T, Crane AM. Histological cryoprotection of rat and rabbit brains. Cryo-Letters 1984;5:33-46; https://iifiir.org/en/fridoc/histological-cryoprotection-of-rat-and-rabbit-brains-77106.

gaps measured in microns in both length and thickness, may require inference of positional relationships between nerve fibers in a given tract that do not vary significantly from one side of the gap to the other. This inference may be done using nanorobots as previously described (Section 3.4.2(3)). Such tears may have been temporarily sealed during plasma membrane repair operations to permit rehydration but may not have been properly reconnected.

Tear sites should be visible in the 3D Submicron Tissue Map (Section 4.8.1(4)) created from the submicron tissue scan (Section 4.7) in the solid phase before significant tissue movement has occurred, enabling the computational inference of the original connectivity of the brain (Section 4.8.3). Using this map and the inferential repair plan, cell repair nanorobots can be directed to the sites of axonal breakage and can reconnect or bridge the torn axons with remanufactured material with a minimum of time and effort – probably under ~**1 day** using a fleet of only ~10^{11} nanorobots (~1 per neuron) requiring ~10 watts of power for whole-brain treatment.

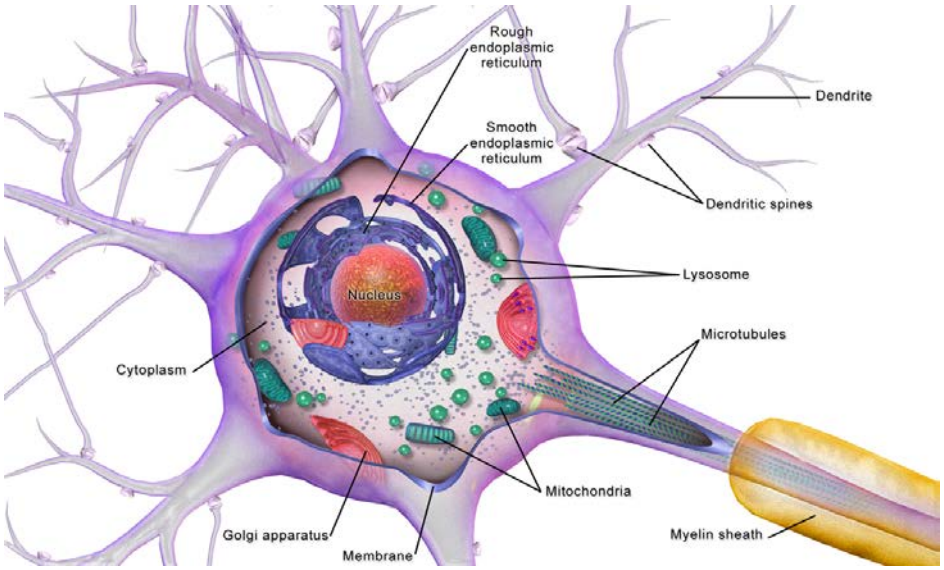

In the nervous system, axons may be unmyelinated or myelinated (possessing an insulating layer called a myelin sheath; images, above and below).[1799] Axons in the peripheral nervous system are myelinated by glial cells called Schwann cells that myelinate a single axon, whereas axons in the central nervous system are myelinated by another type of glial cell called the oligodendrocyte that can myelinate up to 50 axons.[1800] In myelination, one cell literally wraps around another cell.

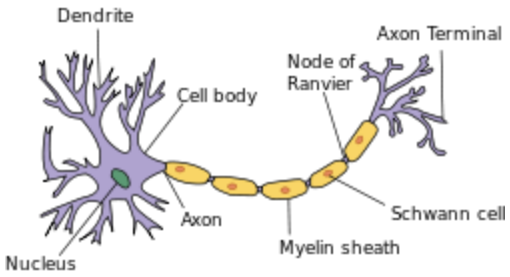

The stripping of myelin from axons – including formation of gaps between the axon membrane and the myelin, unraveling of the myelin, and possible tearing of the axolemma resulting in loss of intra-axonal material at moderately low temperatures – has been proposed as a possible damage mechanism resulting from

[1799] https://en.wikipedia.org/wiki/Axon#/media/File:Neuron_Cell_Body.png.

[1800] Sadler T. Langman's Medical Embryology, 11th Edition, Lippincott William & Wilkins, Philadelphia PA, 2010, p. 300; https://www.amazon.com/dp/B004HOZ5KK/.

cryopreservation,[1801] one that should be confirmed and quantified by direct experiments in ***future research***. If damage does occur, there should be no difficulty inferring which regions of axolemma were previously covered by myelin and which were exposed.[1802] Schwann cells and oligodendrocytes forming the sheaths might already have been repaired or replaced during conventional cell repair procedures (Section 4.12.2). If those myelinating cells are too badly damaged or macerated to be repaired, they can be restored using whole-cell replacement (Section 4.12.2.8) or by nanorobots performing a similar function as ordinary or modified oligodendroglial cells[1803] which lay down myelin under normal conditions.[1804]

4.12.4.2 Neuron Membrane Editing

The number, state, and possibly the distribution of potassium channels in hippocampal dendrite membranes might encode memory,[1805] and AMPA glutamate receptors (AMPAR),[1806] which are an example of such a channel and the most common plasma membrane receptor molecule in the nervous system, do play a role in long-term potentiation (LTP) of new memories.[1807] As previously noted (Section 3.4.1(1)), AMPAR (image, right[1808]) are continuously trafficked (i.e., endocytosed,

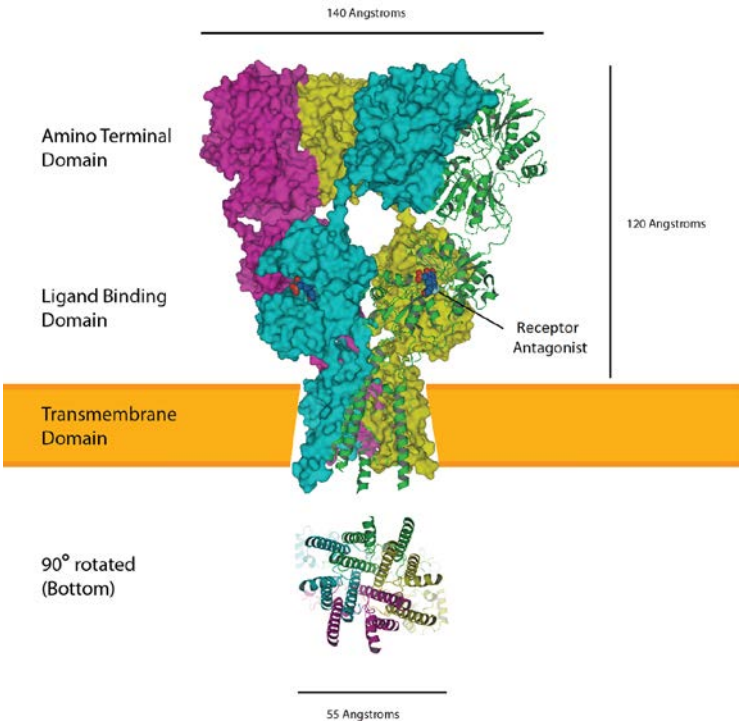

[1801] Unpublished experimental results of Alcor Life Extension Foundation and Cryovita Laboratories, reported by G. Fahy.

[1802] Fahy G. Appendix B. A "Realistic" Scenario for Nanotechnological Repair of the Frozen Human Brain. In: Wowk B, Darwin M, eds., Cryonics: Reaching for Tomorrow. Alcor Life Extension Foundation, 1991, pp. A-10 – A-26; https://alcor.org/Library/html/nanotechrepair.html.

[1803] https://en.wikipedia.org/wiki/Oligodendrocyte#Myelination.
[1804] https://en.wikipedia.org/wiki/Myelinogenesis.

[1805] Alkon DL. Memory storage and neural systems. Sci Am. 1989 Jul;261(1):42-50; https://www.jstor.org/stable/24987318. Alkon DL. Calcium-mediated reduction of ionic currents: a biophysical memory trace. Science. 1984 Nov 30;226(4678):1037-1045; https://science.sciencemag.org/content/226/4678/1037.full.pdf. Alkon DL, Rasmussen H. A spatial-temporal model of cell activation. Science. 1988 Feb 26;239(4843):998-1005; https://science.sciencemag.org/content/239/4843/998.full.pdf. Alkon DL. Memory Traces in the Brain, Cambridge University Press, 1988.

[1806] https://en.wikipedia.org/wiki/AMPA_receptor.
[1807] https://en.wikipedia.org/wiki/AMPA_receptor#Synaptic_plasticity.
[1808] https://en.wikipedia.org/wiki/AMPA_receptor#/media/File:AMPA_receptor.png.

recycled, reinserted) into and out of the plasma membrane while generally preserving the total number of AMPAR in an activated synapse, a process responsible for the maintenance of new memories.[1809] Because the AMPAR population is constantly turning over during life,[1810] the synaptic activation level probably depends more on the total number of AMPAR present rather than on their precise locations within the local volume. The loss of a few AMPAR proteins during cryopreservation should still leave enough of the original population intact to permit inference of the original numbers by medical nanorobots.

Similarly, synaptic NMDA receptors (NMDAR)[1811] assist in LTP[1812] while extrasynaptic NMDAR produce long term depression (LTD) of memory[1813] (reducing the synaptic activation, the opposite of LTP) while inhibiting LTP.[1814] Kainate receptors (which also have a role in synaptic plasticity)[1815] and NMDAR lost during cryopreservation can be nanorobotically restored in similar manner to the AMPAR.

Future research should comprehensively survey all key plasma membrane receptors employed in neural function and establish nominal membrane number density concentrations for each, for every cell type. These benchmarks, when combined with measured residual concentrations of each receptor on every type of cell, should suffice to infer the desired original concentrations consistent with preservation of memory and personality, potentially allowing nanorobots to "top up" each cell membrane to the correct concentration of each receptor – possibly including, for example, the compensatory reinsertion of new AMPAR. At the same time, any damaged, malformed, or corrupted receptor proteins can be replaced with new remanufactured ones; or, alternatively if deemed necessary, all receptors could be exchanged for new ones without regard to their current damage status.

Assuming $N_{braincells} \sim 200 \times 10^9$ cells in the human brain each with plasma membrane surface area $A_{braincell} \sim 24{,}000\ \mu m^2$/cell (Section 4.8.1(6)) for a total plasma membrane area of $A_{BrainPM} = A_{braincell}\ N_{braincells} = 4800\ m^2$ in the brain, the estimated scan + protein insertion time is $\tau_{BrainPMrepair} \sim A_{BrainPM} / (\kappa_{PMscan}\ N_{BrainPMbots}) \sim 480{,}000$ sec (**5.6 days**) using a total of $N_{BrainPMbots} = 1 \times 10^{12}$ scanning/insertion nanorobots, assuming a plasma membrane scan rate of $\kappa_{PMscan} = 10^{-2}\ \mu m^2$/ nanorobot-sec (Section 4.5.4) and a negligible time to insert premanufactured proteins in the plasma membrane which can mostly be done while scans of other areas of the same cell membrane are still in progess. Assuming nanorobot power

---

[1809] Malinow R, Mainen ZF, Hayashi Y. LTP mechanisms: from silence to four-lane traffic. Curr Opin Neurobiol. 2000 Jun;10(3):352-357; http://glutamate.med.kyoto-u.ac.jp/Shared/images/0/06/Malinow_Curr_Opin_Neurobiol.pdf. Shepherd JD, Huganir RL. The cell biology of synaptic plasticity: AMPA receptor trafficking. Annu Rev Cell Dev Biol. 2007;23:613-643; http://www.pai.utexas.edu/faculty/isaxena/BIO320/The%20cell%20biology%20of%20synaptic%20plasticity%20-%20AMPA%20receptor%20trafficking%20-%202007.pdf.

[1810] Makino H, Malinow R. AMPA receptor incorporation into synapses during LTP: the role of lateral movement and exocytosis. Neuron. 2009 Nov 12;64(3):381-390; https://www.cell.com/neuron/pdf/S0896-6273(09)00675-8.pdf.

[1811] https://en.wikipedia.org/wiki/NMDA_receptor#Neural_plasticity.

[1812] Berg LK, Larsson M, Morland C, Gundersen V. Pre- and postsynaptic localization of NMDA receptor subunits at hippocampal mossy fibre synapses. Neuroscience. 2013 Jan 29;230:139-150; https://pubmed.ncbi.nlm.nih.gov/23159309.

[1813] Li S, Jin M, Koeglsperger T, Shepardson NE, Shankar GM, Selkoe DJ. Soluble Aβ oligomers inhibit long-term potentiation through a mechanism involving excessive activation of extrasynaptic NR2B-containing NMDA receptors. J Neurosci. 2011 May 4;31(18):6627-6638; https://www.jneurosci.org/content/jneuro/31/18/6627.full.pdf. Papouin T, Ladépêche L, Ruel J, Sacchi S, Labasque M, Hanini M, Groc L, Pollegioni L, Mothet JP, Oliet SHR. Synaptic and extrasynaptic NMDA receptors are gated by different endogenous coagonists. Cell. 2012 Aug 3;150(3):633-646; https://www.cell.com/fulltext/S0092-8674(12)00786-6.

[1814] Liu DD, Yang Q, Li ST. Activation of extrasynaptic NMDA receptors induces LTD in rat hippocampal CA1 neurons. Brain Res Bull. 2013 Apr;93:10-16; https://pubmed.ncbi.nlm.nih.gov/23270879.

[1815] https://en.wikipedia.org/wiki/Kainate_receptor#Plasticity.

$P_{nanorobot}$ ~ 100 pW in continuous operation,[1816] whole-body nanorobotic waste heat generation is $P_{BrainPMbots}$ ~ $N_{BrainPMbots}$ $P_{nanorobot}$ = 100 watts.

4.12.4.3 Missing Brain Tissue

With the exception of the brain, macroscale blocks of tissue that have been removed by decay, avulsion wound, or other misadventure can be replaced with a generic tissue architecture customized to match the patient's existing tissue at the interface to the undamaged tissue, and reconstructed from the patient's own genome using cells and tissues manufactured in cell mills (Appendix D).

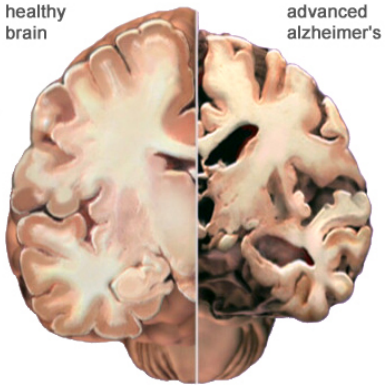

This approach is not advisable in the case of missing brain tissue, because the brain is the seat of memory and personality and encodes information unique to the particular patient. For cryonics cases, the most likely scenarios in which brain tissue is missing involve cases of advanced Alzheimer's disease[1817] (images, above and below[1818]) or related neurodegenerative diseases.

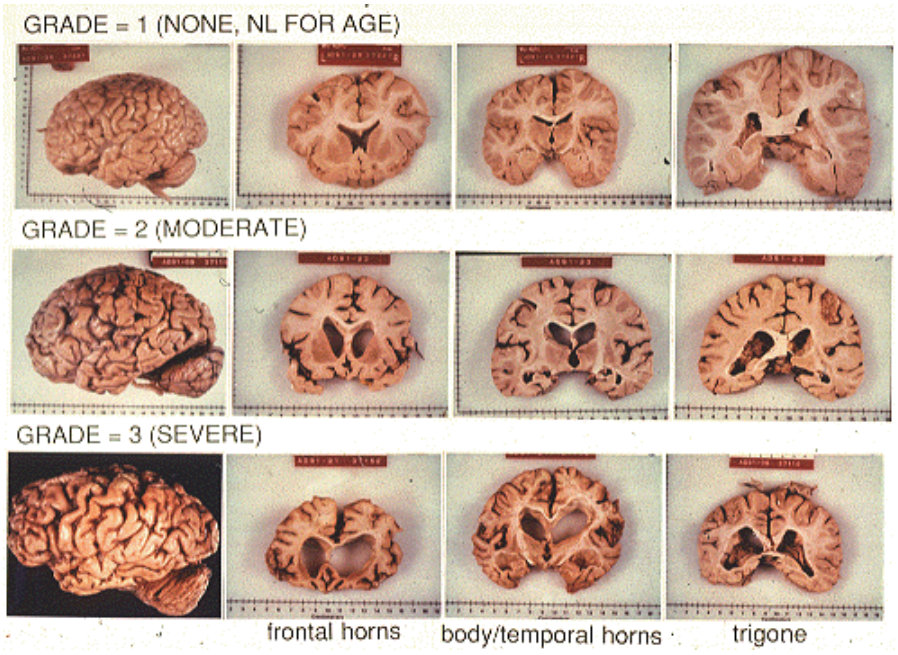

[1816] Freitas RA Jr. Microbivores: Artificial Mechanical Phagocytes using Digest and Discharge Protocol. J. Evol. Technol. 2005 Apr;14:55-106; http://www.jetpress.org/volume14/freitas.pdf. Freitas RA Jr. The Ideal Gene Delivery Vector: Chromallocytes, Cell Repair Nanorobots for Chromosome Replacement Therapy. J. Evol. Technol. 2007 Jun;16:1-97; http://jetpress.org/v16/freitas.pdf.

[1817] https://en.wikipedia.org/wiki/Alzheimer%27s_disease.

[1818] http://unionlosangeles.com/2012/09/21/pink-is-for-breast-cancer-purple-is-for-alzheimers-disease/.

As noted elsewhere,[1819] the rate of whole-brain atrophy due to normal aging is 0.2%-0.5%/yr, roughly equivalent to ~1 neuron/sec. The whole-brain atrophy rate in Alzheimer brains can be ten times faster. One MRI study[1820] reported a 1.9%/yr atrophy rate and rates of whole brain atrophy for AD brains are typically reported at 2%/yr,[1821] with a range of 1%-4%/yr brain volume loss among different populations.[1822] Over a typical 5-10 year course of Alzheimer's disease, a 2%-4%/yr atrophy rate can amount to a 20%+ loss of whole-brain volume, over and above the expected 2% brain volume loss due to normal aging. Losses in specialized areas of the AD brain can be much higher.

Table 12. Nanorobot count and treatment time to execute nanorobotic tasks for the Third Alzheimer Protocol (neural reconstruction)[1823]

Nanorobotic Protocol Task	# of Nanorobots	Treatment Time
3A. Brain mapping	86 billion	13 hr
3B. Compile neural repair plan	external computers	24 hr
Damaged area close inspection	20 billion	
3C. Manufacture replacement cells	external cell mill	1 hr
3D. Intracranial debridement		2 hr
Debridement	10-100 billion	
Support	1000 billion	
Injury suppression	86 billion	
3E. Cell emplacement/incorporation		46 hr
Shepherd	68 billion	
Support	86 billion	
TOTALS	***1356-1446 billion***	***86 hr***

A process for neural reconstruction of brains exhibiting lost tissue mass, using medical nanorobots, has been proposed[1824] in the context of a living Alzheimer's patient: "Our proposed Third Alzheimer Protocol

---

[1819] Freitas RA Jr. The Alzheimer Protocols: A Nanorobotic Cure for Alzheimer's Disease and Related Neurodegenerative Conditions. IMM Report No. 48, June 2016, 433 pp; http://www.imm.org/Reports/rep048.pdf.

[1820] Sluimer JD, Vrenken H, Blankenstein MA, Fox NC, Scheltens P, Barkhof F, van der Flier WM. Whole-brain atrophy rate in Alzheimer disease: identifying fast progressors. Neurology. 2008 May 6;70(19 Pt 2):1836-41; http://dspace.ubvu.vu.nl/bitstream/handle/1871/19214/dissertation.pdf?sequence=12#page=105.

[1821] Schott JM, Price SL, Frost C, Whitwell JL, Rossor MN, Fox NC. Measuring atrophy in Alzheimer disease: a serial MRI study over 6 and 12 months. Neurology. 2005 Jul 12;65(1):119-24; http://www.ncbi.nlm.nih.gov/pubmed/16009896.

[1822] Jack CR Jr, Shiung MM, Gunter JL, O'Brien PC, Weigand SD, Knopman DS, Boeve BF, Ivnik RJ, Smith GE, Cha RH, Tangalos EG, Petersen RC. Comparison of different MRI brain atrophy rate measures with clinical disease progression in AD. Neurology. 2004 Feb 24;62(4):591-600; http://www.ncbi.nlm.nih.gov/pmc/articles/PMC2730165/. Boyes RG, Rueckert D, Aljabar P, Whitwell J, Schott JM, Hill DL, Fox NC. Cerebral atrophy measurements using Jacobian integration: comparison with the boundary shift integral. Neuroimage. 2006 Aug 1;32(1):159-69; http://www.doc.ic.ac.uk/~pa100/pubs/boyesNeuroImage2006.pdf.

[1823] Freitas RA Jr. The Alzheimer Protocols: A Nanorobotic Cure for Alzheimer's Disease and Related Neurodegenerative Conditions. IMM Report No. 48, June 2016, 433 pp; Table 4; http://www.imm.org/Reports/rep048.pdf.

begins with extensive brain mapping and the compilation of a neural repair plan. The next step is reconstruction of the missing neural tissue. Reconstruction requires manufacturing replacement neural cells, debridement of neural detritus in heavily damaged or envoided areas, insertion and emplacement of replacement cells via a nanocatheter array, and incorporation of the replacement cells into the existing neural tissues." Some of these Alzheimer procedures (e.g., debridement) must be carefully coordinated with previous steps proposed in the present document (e.g., neural connectome mapping (Section 4.8.1(5)), plasma membrane repair (Section 4.11.1), debris cleanup (Section 4.12.2.1), etc.). No more than ~1.4 x 10^{12} nanorobots of several types should be needed to perform the necessary neural reconstruction in a previously estimated repair time of ~**86 hours** (**Table 12**).

The nanorobots are released into the tissues through specialized circumferential cellulocks in the vasculoid structure (Section 4.6.5(1)), after which the specialty cellulocks are no longer required and should be detached from the vasculoid, replaced with standard basic plates, and removed from the patient. When the nanorobots' tasks are ultimately finished, the devices can be extracted via ECM migration, then diapedesis into the vasculature, followed by bloodstream exfusion by nanapheresis or nanorobot washout (Appendix M), or by relocation to the conventional excretory organs.

4.13 Patient Warmup and Molecular Instillation

With cellular and tissue repairs mostly complete, it is now time to prepare the patient for full vasculoid removal.

To accomplish this, the still-unconscious patient is first warmed to normal human body temperature (Section 4.13.1). The vasculoid is then employed to instill, into cells and extracellular spaces, thousands of different molecules that are essential for normal metabolism but will not yet initiate any biochemical activity (Section 4.13.2). The vasculoid instillation mechanisms are then withdrawn from the tissues and a small fleet of mobile nanorobots are dispatched to examine the current biochemical state and correctively edit a variety of essential bulk body fluids (Section 4.13.3). Finally, a second fleet of storage nanorobots are loaded with a select group of molecules that are capable of initiating biochemical activity if released, and are distributed appropriately into the tissues (Section 4.13.4).

Storage nanorobots will remain stationed inside tissue cells, awaiting the broadcast command to release their contents as soon as the vasculoid has been removed from the body (Section 4.14).

4.13.1 Warm the Patient

The first step of the preparative process is to raise the patient's temperature from icewater temperature near 273 K (~0 °C) to near normal human body temperature at 310 K (~37 °C). The ubiquitous presence of the vasculoid makes it easy to warm the entire body very uniformly (Section 4.6.5(7)).

Biochemical stasis is still in effect, so we can take our time warming the patient. A conservative scaling analysis might simplistically estimate that the energy required to raise a human body-volume of V_{body} = 60 L filled with water at 310 K with a heat capacity of C_{Vwater} = 4.19 x 10^6 J/m^3-K by ΔT = 37 K is E_{37K} =

[1824] Freitas RA Jr. The Alzheimer Protocols: A Nanorobotic Cure for Alzheimer's Disease and Related Neurodegenerative Conditions. IMM Report No. 48, June 2016, 433 pp; Section 5.3, "Third Alzheimer Protocol: Neural Reconstruction," pp. 290-360; http://www.imm.org/Reports/rep048.pdf.

$V_{body}\ C_{Vwater}\ \Delta T \sim 9.3 \times 10^6$ J, or $E_{37Kplate} = E_{37K} / N_{plates} \sim 74{,}000$ pJ/plate if emitted from each of $N_{plates} = 125 \times 10^{12}$ individual vasculoid application plates, requiring a very modest nanorobotic waste heat power output of $P_{37Kplate} = E_{37Kplate} / t_{heating} \sim 21$ pW/plate over a heating time of $t_{heating} \sim 3600$ sec (**1 hour**). The thermal equilibration time during heating is very fast, roughly $t_{EQ} \sim L_{serv}^2\ C_{Vwater} / K_t = 0.006$ sec,[1825] taking thermal conductivity $K_t = 0.623$ W/m-K for liquid water with a tissue service volume surrounding each warming plate of characteristic size $L_{serv} \sim 30$ μm.

4.13.2 Instill Nonactivating Molecules via Vasculoid

Nonactivating molecules are molecules that cannot initiate, activate, or sustain any biochemical activity on their own in the absence of other molecules, called "activating molecules," that provide the necessary energy or catalytic assistance to drive biochemical reactions (e.g., oxygen, glucose, ATP) or provide specific substrates that can be acted upon by various enzymes. The best strategy is probably to restore cytoplasmic and extracellular molecular concentrations of nonactivating molecules to their normal default settings, as additionally informed by quantitative measurements of the number and locations of small molecules removed during molecular extraction that could allow us to adjust the defaults toward some measure of customization to the particular individual, taking careful account of the patient's health, medical history, and specific circumstances of clinical death and cryopreservation.

In this phase of the revival process, the vasculoid re-extends its extraction plumbing (Section 4.10.1.9) into the body tissues at $N_{cluster} = 4.8 \times 10^{14}$ service points and instills nonactivating molecules of thousands of different types into desired cytosolic locations at the desired concentrations. Sorting rotors in the extraction mechanisms could be replaced with simpler bulk distribution devices for instillation that can provide higher throughput than sorting rotors, such as pressurized molecules driven through mechanically gated nozzles. These instillation devices should be positionally controllable with a spatial resolution of at least ~1 μm or better.

Ignoring pre-mortem drugs and cryoprotectants that need not be returned to the body, **Table 9** in Section 4.10.1.9 lists five classes of molecules (oxygen, glucose, leaked plasma components, cell metabolites, and free ions) of which a total of 3734.2 gm were previously extracted from the entire body of the cryopreserved patient during the molecular extraction phase (Section 4.10). However, a some of these molecules may be "activating molecules" that would risk initiating significant biochemical activity if they were returned to the body at this stage of the revival process, and thus must be excluded from instillation at this time. Many other molecules need not be returned to the body at all, as they would contribute nothing to healthy functioning of the cell or could be deleterious or even toxic.

In the worst case scenario where all 3734.2 gm of relevant extracted molecules had to be returned to the body, a typical molecular volume of 0.534 nm^3 with normal density of ~1 gm/cm^3 (Section 4.10.1.9) gives a whole-body instillation requirement of $n_{extracted} \sim 7 \times 10^{24}$ previously extracted molecules. While molecular extraction is limited by diffusion time because the sorting rotors must wait for the target molecules to migrate to the vicinity of the binding sites, gated nozzle instillation is not limited by diffusion because molecules can be released in bulk at higher rates constrained only by effervescence and crystallescence limits,[1826] typically $R_{solute} \sim 10^{10}$ molecules/sec for solutes (to avoid localized

---

[1825] Freitas RA Jr. Nanomedicine, Volume I: Basic Capabilities, Landes Bioscience, Georgetown TX, 1999, Section 10.5.4, "Heat Conductivity and Capacity, and Refrigeration"; http://www.nanomedicine.com/NMI/10.5.4.htm.

[1826] It is possible that such high release rates might cause damage by briefly producing localized concentrations of mixed molecules high enough to produce protein misfolding, molecular dehydration, enzyme poisoning, or other pathologies. ***Future research*** should identify and quantify relevant situations of this type, if any, that could provide more restrictive constraints on maximum release rates.

crystallization) and $R_{gas} \sim 10^9$ molecules/sec for gases (to avoid local bubble formation).[1827] Although most nonactivating molecules are not gases, a conservative estimate for the whole-body nozzled instillation time would be $t_{instillNA} \sim n_{extracted} / (N_{cluster} R_{gas}) \sim 15$ sec.

If they have previously been removed or diluted (Section 4.10.1.6), appropriate general anesthetic agents should be re-introduced so that the patient remains definitively unconscious throughout warmup and instillation (Section 4.13) and vasculoid removal (Section 4.14.2) procedures, all of which might be uncomfortable for the patient to experience if awake. To the extent that pharmaceutical-based general anesthetics[1828] might involve the mechanical distortion of neuronal lipid bilayer membranes,[1829] direct nanorobotic suppression of consciousness (perhaps by intervening in specific brainstem cells)[1830] might be employed if ***future research*** determines that anesthetic-based distortion might affect the process or reliability of plasma membrane repair as described in Section 4.11.1.

As soon as instillation operations are completed, the extraction plumbing is retracted and the vasculoid extraction plates (Section 4.6.5(3)) used in the molecular instillation process are removed and replaced with standard basic plates.

4.13.3 Whole-Body Fluid Check and Perimeter Surface Cleanup

After vasculoid instillation devices complete their work and are retracted (Section 4.13.2), mobile nanorobots are dispatched from the vasculoid through the cellulocks to examine the current biochemical state of a variety of bulk body fluids including lymphatic fluid, the cerebrospinal fluid occupying the ventricular system of the brain including the subarachnoid spaces, the synovial fluid in joints, the pleural fluid in the pleural cavities, the pericardial fluid in the cardiac sac, the peritoneal fluid in the peritoneal cavity, and the aqueous humor of the eye.[1831] This examination should be designed to detect both unwanted components that are present (and then remove them) and desired components that are missing (and then restore them). The identity and quantity of these components, and their likely appearance or disappearance as a result of the cryopreservation process, is a suitable subject for ***future research***.

If any metabolic inhibitors were installed in an earlier phase to assist in molecular extraction (Section 4.10), they should now be removed. Any enzymes that have been permanently poisoned by these inhibitors should be replaced. This is also the appropriate time to restore normal intracellular buffering and pH levels.[1832]

[1827] Freitas RA Jr. Nanomedicine, Volume I: Basic Capabilities, Landes Bioscience, Georgetown TX, 1999, Section 9.2.6, "Effervescence and Crystallescence"; http://www.nanomedicine.com/NMI/9.2.6.htm.

[1828] https://en.wikipedia.org/wiki/General_anaesthetic.
[1829] https://en.wikipedia.org/wiki/Theories_of_general_anaesthetic_action.

[1830] Injury to the cerebral cortex or the reticular activating system in the brainstem is sufficient to induce coma (https://en.wikipedia.org/wiki/Coma#Pathophysiology). Nanorobots resident in appropriate cortical neurons could reversibly inhibit normal neural function, temporarily simulating coma-inducing injury. Nanorobots might also directly activate sleep-promoting neurons in the ventrolateral preoptic nucleus (https://en.wikipedia.org/wiki/Ventrolateral_preoptic_nucleus) to induce and maintain an unconscious state.

[1831] https://opentextbc.ca/anatomyandphysiology/chapter/26-1-body-fluids-and-fluid-compartments/.

[1832] Fahy G. Appendix B. A "Realistic" Scenario for Nanotechnological Repair of the Frozen Human Brain. In: Wowk B, Darwin M, eds., Cryonics: Reaching for Tomorrow. Alcor Life Extension Foundation, 1991, pp. A-10 – A-26; https://alcor.org/Library/html/nanotechrepair.html.

A fleet of ~10^{12} mobile nanorobots operating for ~1 day should be sufficient to perform these functions.

In addition, all tissue perimeter surfaces (e.g., gut lumenal walls, sinus cavity surfaces, etc.; Appendix E) are examined for possible small amounts of broken cells, microbial remains, small protein tangles, and other organic loose debris, and when these are found they are removed, leaving behind clean microbe- and detritus-free surfaces. (The original vasculoid plating of these surfaces was removed earlier; Section 4.12.3.4.) The incremental time and nanorobot resource requirements to perform this additional function should be minimal.

4.13.4 Instill Storage Nanorobots that Carry Activating Molecules

Chemical substances that can initiate, activate, assist or sustain biochemical activity (e.g., oxygen, glucose, ATP, etc.) are called "activating molecules". Other "activating molecules" may include "inhibitory metabolites that are normally present and needed to control the overactivity of other proteins" or "necessary protein cofactors",[1833] as ***future research*** may enumerate. These are expected to be a relatively small fraction of all previously extracted molecules. Once these "activating molecules" are released into the cell, biochemical activity will immediately begin; but until these key molecules are released, biochemical activity remains suspended. It is still too early to initiate active biochemistry in this phase of the revival process, so the strategy is to load all activating molecules into nanorobots, park the nanorobots in tissue cells, and then order the nanorobots to release their cargo at a convenient later time of our choosing.

Thus in this phase, we instill the activating molecules into medical nanorobot carriers similar in size to chromallocytes.[1834] These carriers should have significant internal tankage and pumps to allow quick offloading of contents, and mobility systems good enough to permit the devices to exfuse themselves from the body when their mission is completed. Purely for computational convenience in the present scaling exercise, we tentatively allocate one such storage nanorobot to each of the $N_{bodycells}$ = 3.5 trillion tissue cells, hence $N_{storagebots}$ ~ 3.5 x 10^{12} robots are deployed throughout the whole body. Each nanorobot is loaded with the full complement of "activating molecules" destined for its particular target cell. These nanorobots are distributed to the vicinity of their target cells via the vasculoid internal transport system (Section 4.6.1). This marks the last major operational task of the vasculoid system, prior to its uninstallation (Section 4.14.2).

After being released into the tissue, each storage nanorobot migrates to its target cell, enters that cell and parks there, awaiting the command to release its multimolecular cargo either into the cytosol or into specific cytoplasmic subcompartments inside the cell. Pre-positioning all storage nanorobots in the patient's tissues may take ~**1 hour**.

Again assuming a typical molecular volume of $V_{molecule}$ ~ 0.534 nm^3 with normal density of ~1 gm/cm^3 (Section 4.10.1.9), if each storage nanorobot has an internal storage volume of $V_{storagebots}$ ~ $V_{chromstorage}$ = 40 μm^3 then a fleet of $N_{storagebots}$ ~ 3.5 x 10^{12} robots has a total storage volume of V_{active} = $N_{storagebots}$ $V_{storagebots}$ ~ 140 cm^3 (mass ~**140 gm**) containing n_{active} ~ V_{active} / $V_{molecule}$ ~ 2.6 x 10^{23} "activating molecules" or ~4%

[1833] Fahy G. Appendix B. A "Realistic" Scenario for Nanotechnological Repair of the Frozen Human Brain. In: Wowk B, Darwin M, eds., Cryonics: Reaching for Tomorrow. Alcor Life Extension Foundation, 1991, pp. A-10 – A-26; https://alcor.org/Library/html/nanotechrepair.html.

[1834] Freitas RA Jr. The Ideal Gene Delivery Vector: Chromallocytes, Cell Repair Nanorobots for Chromosome Replacement Therapy. J. Evol. Technol. 2007 Jun;16:1-97; http://jetpress.org/v16/freitas.pdf.

of all $n_{extracted}$ ~ 7 x 10^{24} previously extracted molecules (Section 4.13.2). This seems sufficient, since only 0.4 gm of oxygen and 6.9 gm of glucose were previously extracted (**Table 9**) and an entire 70 kg live human body contains only ~14 gm of available glucose outside of the bloodstream and may need as little as ~30 gm of ATP to restart the entire body (Section 4.10.1.2).

If a higher percentage of "activating molecules" must be instilled, then either: (A) additional storage nanorobots may be stationed inside tissue cells, or nanorobots with somewhat larger internal storage space may be employed; or (B) lower concentrations of particular "activating molecules" could be instilled by the vasculoid in the same manner as nonactivating molecules are instilled, producing some low-level biochemical activity but at an intensity well below normal metabolic levels.

4.14 Uninstall Vasculoid and Finish Repairs

All that remains is to remove the vasculoid appliance, restart the patient's metabolism, and transfuse manufactured natural blood into the arteriovenous vasculature. The patient will then be ready for awakening (Section 4.15).

The following discussion describes the manufacture of replacement blood (Section 4.14.1), the uninstallation of the vasculoid and replacement of persufflated nitrogen gas with an artificial nanorobot-rich blood substitute (Section 4.14.2), the reactivation of the patient's metabolism and the restoration of heartbeat and respiration (Section 4.14.3), and the replacement of the nanorobot-rich blood substitute with manufactured natural blood (Section 4.14.4).

4.14.1 Manufacture Replacement Blood

The process of uninstalling the vasculoid will create an empty space inside the vasculature that must be filled with replacement blood. The filling of the vasculature with replacement blood occurs in two phases.

In the first phase, a temporary **blood substitute** (Section 4.14.1.1), consisting mostly of active storage nanorobots suspended in an aqueous carrier fluid, immediately replaces the patency-preserving humid nitrogen gas that will be insufflated into the total enclosed volume vacated by the vasculoid as the appliance is withdrawn.

In the second phase, the temporary blood substitute is replaced by **manufactured natural blood** (Section 4.14.1.2) – containing autologous red cells, platelets, white cells, and a variety of organic materials and biochemicals – all produced by a cell mill (Appendix D).

The initial use of a temporary blood substitute serves to decouple the timing of vasculoid removal (Section 4.14.2) from the timing of the subsequent activation and removal of storage nanorobots from tissues that initiates normal metabolism in tissue cells (Section 4.14.3). With the artificial blood substitute (Section

4.14.1.1) in place first, the patient's body is parked in a medically stable state[1835] that can be maintained as long as necessary to complete the next stages of the revival process – including the synthesis (Section 4.14.1.2) and infusion (Section 4.14.4) of the manufactured natural blood. While parked, there is no requirement to maintain proper nutrient levels for circulating blood cells, since no such cells have been introduced yet. Employing artificial blood first, then natural blood later, temporally decouples two processes that need not be coupled, enhancing operational flexibility. ***Future research*** should critically examine the validity of this procedure, and investigate the circumstances under which manufactured natural blood could be transfused without a temporary blood substitute precursor.

4.14.1.1 Blood Substitute

Upon initial withdrawal of the vasculoid, the arteriovenous vasculature will be filled with a blood substitute consisting of respirocyte-class remote-controlled-release storage nanorobots suspended in an aqueous saline carrier fluid. The majority of these nanorobots will probably be standard spherical respirocytes[1836] (image, right)[1837] to provide temporary respiratory support, preloaded with full tanks of 1000-atm pressurized oxygen, onboard glucose for power, and empty CO_2 tanks waiting to be filled during circulation. A 56 cm^3 injection of a 50% (by volume) aqueous colloidal respirocyte suspension containing ~54 x 10^{12} fully charged respirocytes, if injected into the 5400 cm^3

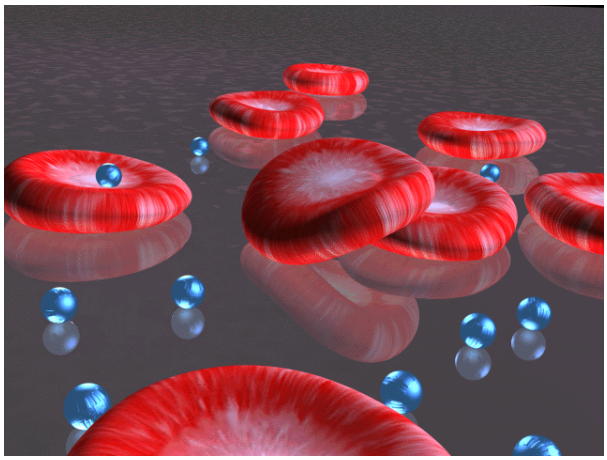

[1835] It is assumed that a blood substitute comprising various types of medical nanorobots suspended in an aqueous medium can perform all of the special biological functions of natural blood for a period of time sufficient to complete the tasks described in Section 4.14. ***Future research*** to enumerate the totality of these special functions will be required in order to ensure that nanorobots can be designed to supply all necessary functionality. For example, blood vessels can leak in the absence of natural platelets, which apparently have a role in maintaining proper function of capillary gap junctions.[*] However, the reference cited notes that this function "may rely on secretion of the various platelet granules and their many active components" (which nanorobots could be programmed to secrete as well), and that while platelets might physically block potential gaps in the endothelial lining without eliciting clotting, and "defects in endothelial junctions would definitely lead to leakage of fluid and proteins into tissues," nevertheless the absence of platelets is "unlikely sufficient to cause bleeding". Under certain circumstances, platelets can also amplify or maintain vascular permeability.[†]

[*] Ho-Tin-Noé B, Demers M, Wagner DD. How platelets safeguard vascular integrity. J Thromb Haemost. 2011 Jul;9 Suppl 1(Suppl 1):56-65; https://www.ncbi.nlm.nih.gov/pmc/articles/PMC3229170/.

[†] Cloutier N, Paré A, Farndale RW, Schumacher HR, Nigrovic PA, Lacroix S, Boilard E. Platelets can enhance vascular permeability. Blood. 2012 Aug 9;120(6):1334-43; https://www.sciencedirect.com/science/article/pii/S000649712046536X.

[1836] Freitas RA Jr. Exploratory design in medical nanotechnology: a mechanical artificial red cell. Artif Cells Blood Substit Immobil Biotechnol. 1998 Jul;26(4):411-30; https://www.tandfonline.com/doi/pdf/10.3109/10731199809117682. A longer version of this paper appears at: https://web.archive.org/web/20100420085137/http://www.foresight.org/Nanomedicine/Respirocytes.html.

[1837] Image of respirocytes (blue) in repose, with red blood cells, courtesy of artist Forrest Bishop; https://web.archive.org/web/20210508220644/https://foresight.org/Nanomedicine/Gallery/Captions/Image140.html.

human blood volume, would be sufficient to provide oxygen and carbon dioxide transport equivalent to the normal human red cell mass for ~20 minutes prior to the onset of normal respiration.[1838] This respirocyte fleet would generate ~16 watts of nanorobotic waste heat while supplying oxygen at the human basal rate, producing at most a negligible ~0.1 ^{o}F rise in core body temperature.

Some additional number of storage nanorobots suspended in the blood substitute may contain onboard supplies of glucose with the objective of establishing bloodstream concentrations in acceptable ranges when the time comes to terminate metabolic stasis, and after normal circulation begins (Section 4.14.3). Other storage nanorobots may contain a selection of chemicals necessary to maintain life including specific ions, nutrients, or signaling molecules, while still other nanorobots may provide available onboard storage space to absorb metabolic waste products that would normally be conveyed by the bloodstream. While the reduction of cerebral blood flow by 50% can produce marked disturbances in brain metabolism,[1839] and at 20% of normal flow the neurons can depolarize with rapid loss of intracellular potassium into extracellular spaces,[1840] the storage nanorobots in the blood substitute can be adjusted to maintain physiological electrolyte (esp. Na^{+}, K^{+}, and Ca^{++}) concentrations and osmotic balances and to extract any excitotoxins that might be released.[1841] The ideal mix of nanorobots, transport capabilities, and solutes to be dissolved in the blood substitute carrier fluid are a suitable topic for ***future research***.

All nanorobots can be activated or reprogrammed by acoustic broadcast signaling, and all material transactions in and out of robot tankage are guided by sensor data and locally controlled by onboard computers with software designed to support an awakening metabolism and to provide the necessary biochemical homeostasis.

4.14.1.2 Manufactured Natural Blood

After the vasculoid has been uninstalled (Section 4.14.2) and the patient's metabolism has been restarted (Section 4.14.3), the circulating blood substitute (Section 4.14.1.1) that was initially deployed (Section 4.14.2) will be replaced (Section 4.14.4) by manufactured natural blood that is indistinguishable from the patient's (healthy) original.

The medical team has access to the patient's cellular and mitochondrial genomes, plus samples of erythrocytes or red blood cells (RBCs), platelets, and white cells that were scavenged from various places in the body (Section 4.12.1), along with access to a cell mill (Appendix D). Lymphocytes, especially B cells[1842] and memory T cells[1843] that encode the body's adaptive immune system, will have been harvested (Section 4.6.4) from the lymph nodes[1844] and decoded, after which their antigenic signatures can be re-

---

[1838] Freitas RA Jr. Exploratory design in medical nanotechnology: a mechanical artificial red cell. Artif Cells Blood Substit Immobil Biotechnol. 1998 Jul;26(4):411-30; https://web.archive.org/web/20100613011849/https://foresight.org/Nanomedicine/Respirocytes3.html (Sec. 4.1).

[1839] Dearden NM. Ischaemic brain. Lancet. 1985 Aug 3;2(8449):255-259; https://www.sciencedirect.com/science/article/abs/pii/S0140673685903010.

[1840] Hertz L. Features of astrocytic function apparently involved in the response of central nervous tissue to ischemia-hypoxia. J Cereb Blood Flow Metab. 1981;1(2):143-153; https://journals.sagepub.com/doi/pdf/10.1038/jcbfm.1981.17.

[1841] Diemer NH, Johansen FF, Benveniste H, Bruhn T, Berg M, Valente E, Jørgensen MB. Ischemia as an excitotoxic lesion: protection against hippocampal nerve cell loss by denervation. Acta Neurochir Suppl (Wien). 1993;57:94-101; https://link.springer.com/chapter/10.1007/978-3-7091-9266-5_14.

[1842] https://en.wikipedia.org/wiki/B_cell and https://en.wikipedia.org/wiki/Memory_B_cell.
[1843] https://en.wikipedia.org/wiki/Memory_T_cell.
[1844] https://en.wikipedia.org/wiki/Lymph_node.

instantiated in the correct proportions in the new manufactured lymphocyte cell population,[1845] if such is deemed necessary.[1846] The aforementioned resources should allow the manufacture of a sufficient quantity of natural blood for final transfusion into the patient (Section 4.14.4).

It is estimated that ~20 liters of natural blood may be required to adequately flush the blood vessels of all components of the blood substitute, using conventional transfusion techniques.[1847] Natural blood contains ~5.2 x 10^9 erythrocytes/cm^3, 2.5 x 10^8 platelets/cm^3, 1.1 x 10^7 leukocytes/cm^3 (e.g., neutrophils, eosinophils, basophils, lymphocytes, monocytes, and phagocytes), and up to 0.2 gm/cm^3 of blood serum biochemicals (e.g., fatty acids, proteins, etc.).[1848] Creating 20 liters of natural blood thus requires the manufacture of 1.04 x 10^{14} RBCs (~10,800 gm),[1849] 5.0 x 10^{12} platelets (~53 gm),[1850] 2.2 x 10^{11} white cells (~92 gm),[1851] plus ~4000 gm of blood serum chemicals, for a total cell mill product mass of ~14.9 kg comprising 10.9 kg of cells and 4 kg of biochemicals. Given a cell mill production rate of ~1 kg/hr (Appendix D), the manufacture of ~20 L of natural blood will require ~**14.9 hours**.

[1845] Perfusion with cryoprotectants should only flush out the contents of the arteriovenous vasculature and not the contents of the lymphatic vasculature or the lymph nodes, hence the lymphocyte cell population of lymph nodes can be captured and stored during vasculoid plating of the lymphovasculature (Section 4.6.4) and therefore should remain intact and available for replication after cryopreservation – but this is an assumption that should be verified in ***future research***.

[1846] In the future era in which cryonics revivals are being performed, it may be commonplace to infuse the blood of all living humans with a designed selection of prophylactic manufactured artificial lymphocytes expressing a wide selection of antigens to which the individual has never been personally exposed, but which provides a wide spectrum defense to all known extant viruses, bacteria, and other microbial attackers. Alternatively, future medicine may employ nanorobotic immune system recognition and deployment implants that provide immune responses 1-2 orders of magnitude faster than the natural system, or may instead rely upon the use of readily injectable doses of reconfigurable microbivores entirely freeing patients from reliance on their natural biological immune system.

[1847] A conventional four-volume blood exchange transfusion (i.e., where four times the patient's total blood volume is exchanged, or ~20 liters) replaces ~98% of the original blood substitute; e.g., "Exchange Transfusion (ExTx)," Univ. of California, Intensive Care Nursery House Staff Manual, 2004, p. 42; https://www.ucsfbenioffchildrens.org/pdf/manuals/11_ExchangeTransfusion.pdf.

[1848] Freitas RA Jr. "Appendix B. Concentrations of Human Blood Components", Nanomedicine, Volume I: Basic Capabilities, Landes Bioscience, Georgetown, TX, 1999, pp. 387-392; http://www.nanomedicine.com/NMI/AppendixB.htm.

[1849] Average erythrocyte volume ~ 94 μm^3 [Freitas RA Jr. Nanomedicine, Volume I: Basic Capabilities, Landes Bioscience, Georgetown TX, 1999, Section 8.2.1.2, "Arteriovenous Microcirculation"; http://www.nanomedicine.com/NMI/8.2.1.2.htm#p7], density ~ 1.110 gm/cm^3 [Norouzi N, Bhakta HC, Grover WH. Sorting cells by their density. PLoS One. 2017 Jul 19;12(7):e0180520; https://www.ncbi.nlm.nih.gov/pmc/articles/PMC5516969/]; mass = 1.04 x 10^{-10} gm/cell.

[1850] Average platelet volume ~10 μm^3 and density ~ 1.0645 gm/cm^3 [Martin JF, Shaw T, Heggie J, Penington DG. Measurement of the density of human platelets and its relationship to volume. Br J Haematol. 1983 Jul;54(3):337-352; https://pubmed.ncbi.nlm.nih.gov/6860588/]; mass = 1.06 x 10^{-11} gm/cell.

[1851] Average neutrophil volume ~ 468 μm^3 and density ~ 1.080 gm/cm^3, average lymphocyte volume = 247 μm^3 and density ~ 1.075 gm/cm^3, and average monocyte volume ~ 534 μm^3 and density ~ 1.072 gm/cm^3 [Zipursky A, Bow E, Seshadri RS, Brown EJ. Leukocyte density and volume in normal subjects and in patients with acute lymphoblastic leukemia. Blood. 1976 Sep;48(3):361-371; https://pdfs.semanticscholar.org/863b/20f7f63902383754bd3dd357b031b8c1e907.pdf]; average blood concentrations are 3.65 x 10^6/cm^3 for neutrophils, 2.50 x 10^6/cm^3 for lymphocytes, and 0.43 x 10^6/cm^3 for monocytes [Freitas RA Jr. "Appendix B. Concentrations of Human Blood Components", Nanomedicine, Volume I: Basic Capabilities, Landes Bioscience, Georgetown, TX, 1999, pp. 387-392; http://www.nanomedicine.com/NMI/AppendixB.htm]; concentration-weighted average white cell volume ~ 389 μm^3 and density ~ 1.077 gm/cm^3; concentration-weighted avg mass ~ 4.2 x 10^{-10} gm/cell.

4.14.2 Uninstall Vasculoid and Transfuse Blood Substitute

Numerous additional components of the original vasculoid appliance were emplaced during installation (Section 4.6). At this stage of the revival process, all of these additional components have already been (or must now be) removed, as follows:

* **Crackface void plates** (Section 4.6.3) are removed during crackface fusion (Section 4.9.2).
* **Lymphatic plates** (Section 4.6.4) are removed after the completion of tissue repair operations (Section 4.12.3.2).
* **Tissue perimeter surface plates** (Section 4.6.4, Section 4.6.5(4), and Appendix E) are removed after the completion of tissue repair operations (Section 4.12.3.4).
* **Circumferential cellulocks** (Section 4.6.5(1)) should now be removed and replaced with standard basic plates.
* **Scanning patches** (Section 4.6.5(2)) are removed and replaced with standard basic plates as soon as the high-resolution scans (Section 4.7) are complete.
* **Extraction plates** (Section 4.6.5(3)) are removed and replaced with standard basic plates as soon as the instillation of nonactivating molecules (Section 4.13.2) is complete.
* **Acoustic navigation beacons** (Section 4.6.5(5)), if they are integral components of the vasculoid, should now be removed and replaced with standard basic plates.

Once these tasks are completed, only the vasculoid arteriovenous subsystem (Section 4.6.2) remains to be uninstalled.

A published paper[1852] describes two installation procedures for the vasculoid appliance.

The first installation procedure is a conservative 6.5-hour-long process "that would be feasible using the technology available in 2002" (the year the original study was published) had the vasculoid otherwise been available at that time. The lengthy process was designed for comfortable installation in a live human patient and is fully reversible at each step, so these steps could be described in reverse order for uninstallation with minor modifications.

The second installation procedure[1853] is "considerably more convenient and up to 100 times faster" and is expected to be feasible "by the time a vasculoid-class device can be built [when] medical technology will have advanced significantly." This procedure can be completed in minutes and has steps that are easier to describe in reverse order and are more readily adapted to the specifics of a cryonics revival, and thus will be the basis for the uninstall process detailed here.

Prior to the uninstall procedure, the vasculoid has previously been introduced into the arteriovenous vasculature directly through the heart via cardiopuncture[1854] or cardiocentesis.[1855] Cardiocentric

---

[1852] Freitas RA Jr., Phoenix CJ. Vasculoid: A personal nanomedical appliance to replace human blood. J Evol Technol. 2002 Apr;11:1-139; Section 7 "Hypothetical Vasculoid Installation Scenarios"; http://www.jetpress.org/volume11/vasculoid.pdf.

[1853] Freitas RA Jr., Phoenix CJ. Vasculoid: A personal nanomedical appliance to replace human blood. J Evol Technol. 2002 Apr;11:1-139; Section 7.8 "Aggressive Installation Scenario"; http://www.jetpress.org/volume11/vasculoid.pdf.

[1854] "Cardiac Puncture"; National Center for the Replacement Refinement & Reduction of Animals in Research, Jan 2015; https://www.nc3rs.org.uk/mouse-cardiac-puncture-terminal. Weis HJ, Baas EU. Die Herzpunktion bei der Ratte zur wiederholten Blutentnahme und Injektion [Cardiopuncture in the rat for repeated sampling of blood and injection]. Z Gesamte Exp Med. 1971;156(4):314-316; https://pubmed.ncbi.nlm.nih.gov/5144492/.

installation is required because the human circulation consists of two independent arterial circuits (pulmonary and systemic) each containing their own capillary beds. The appliance is installed as a continuously-everting concentric tube, a process called progressive fractal eversion analogous to turning a thin latex glove inside out to remove it from the hand. Basic plates, docking bays and cellulocks are prefastened in the proper configuration to fit the various diameters and branchings of the blood vessels that they will coat. The necessary flexibility of this sheet of plates is provided by "hinging" watertight interplate bumpers, with eversion powered by compressed gas, ciliary action between opposed plates, or other appropriate means.

To begin the vasculoid uninstall process, all tankers, boxcars, and other mobile components are withdrawn and exported from the appliance, requiring at most one ciliary circulation time of $\tau_{VasculoidCirc}$ ~ 140 sec (Section 4.6.1). The ciliary transport system is then shut down. Retraction of the vasculoid "sheet" begins in the capillaries, with each capillary tube breaking at mid-vessel. One half then retracts to the arterial side while the other half retracts to the venous side. The vasculoid exits the capillaries via reverse eversion that may be assumed to progress at only ~10 micron/sec of travel, the same as the specified conservative installation speed, requiring ~100 sec to uninstall all capillary plating assuming a typical capillary bed length of ~1 mm. (Human capillaries contain ~14% of blood volume but comprise ~95% of the surface area of the vascular system,[1856] so most of the appliance's plates are withdrawn during this initial ~100 seconds.) Retraction speed may increase to ~1 cm/sec in the larger vessels, requiring another ~70 sec to unplate the maximum ~70-cm main arterial or venous course.[1857] The entire reverse eversion process thus may require as little as ~310 sec (~**5.2 min**) to complete, although more time can be taken if necessary to ensure safety and completeness of the retraction. If all 150 trillion plates are active throughout this process, the power draw is a physiologically-tolerable 150 watts.[1858]

Reversing the course of the installation, vasculoid retraction proceeds cardiocentrically in two primary segments exported via two cardiopuncture entry points (that are designed for easy reseal, e.g., by using nanodevices similar to vascular gates[1859]) through the relatively thin walls of the right atrium and the left atrium,[1860] respectively.

Uninstallation works inward from the distal capillary beds toward each chamber opening. Toward the right atrial entry point, the retracting right atrial appliance segment has four "fingers" and simultaneously unplates: (1) the superior vena cava; (2) the inferior vena cava; (3) the coronary sinus (which receives cardiac veins from heart tissue); and returns through (and unplates) the right atrial and ventricular chambers after unplating (4) the pulmonary artery. The right atrial segment also must unplate all of the numerous Thebesian veins;[1861] these venules return blood from the myocardium without entering the venous current, and open directly into the right atrium. From the left atrial entry point, the retracting left

---

[1855] Sarno AP Jr, Wilson RD. Fetal cardiocentesis: a review of indications, risks, applications and technique. Fetal Diagn Ther. 2008;23(3):237-244; https://pubmed.ncbi.nlm.nih.gov/18417985/.

[1856] Freitas RA Jr. Nanomedicine, Volume I: Basic Capabilities, Landes Bioscience, Georgetown TX, 1999, Table 8.1, "Approximate Quantification of the Human Arteriovenous System"; http://www.nanomedicine.com/NMI/Tables/8.1.jpg.

[1857] Freitas RA Jr. Nanomedicine, Volume I: Basic Capabilities, Landes Bioscience, Georgetown TX, 1999, Table 8.1, "Approximate Quantification of the Human Arteriovenous System"; http://www.nanomedicine.com/NMI/Tables/8.1.jpg.

[1858] Freitas RA Jr., Phoenix CJ. Vasculoid: A personal nanomedical appliance to replace human blood. J Evol Technol. 2002 Apr;11:1-139; Section 7.4 "Vascular Plating"; http://www.jetpress.org/volume11/vasculoid.pdf.

[1859] Freitas RA Jr. Chapter 23. Comprehensive Nanorobotic Control of Human Morbidity and Aging, Section 6.3.5.1 "Vascular Gates". In: Fahy GM, West MD, Coles LS, Harris SB, eds, The Future of Aging: Pathways to Human Life Extension, Springer, New York, 2010, pp. 685-805; http://www.nanomedicine.com/Papers/Aging.pdf.

[1860] https://en.wikipedia.org/wiki/Atrium_(heart).
[1861] https://en.wikipedia.org/wiki/Smallest_cardiac_veins.

atrial appliance segment has five "fingers" and simultaneously unplates: (1&2) the two left pulmonary veins (which frequently terminate by a common opening); (3&4) the two right pulmonary veins; and returns through (and unplates) the left atrial and ventricular chambers after unplating (5) the aorta. Additionally, a third vasculoid segment called the portal segment must be retracted through a third abdominal entry point in order most efficiently to unplate the portal vein,[1862] which lies midway between the hepatic and intestinal capillary beds.

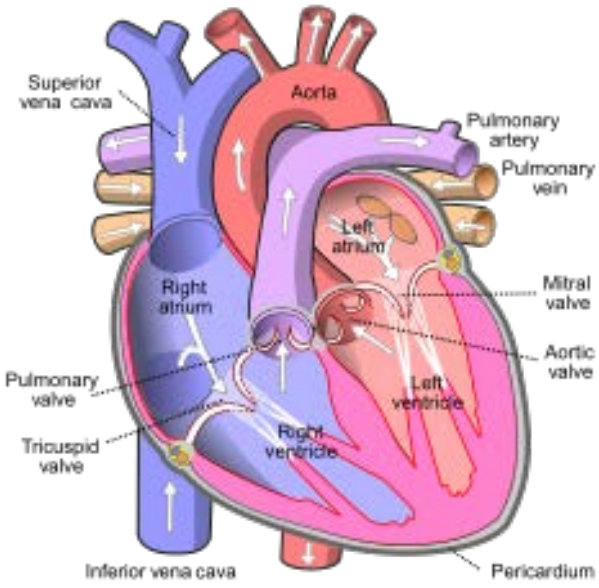

As the vasculoid is withdrawn, humid inert nitrogen gas is be introduced into the vacated blood vessels at sufficient pressure (well below burst pressure)[1863] to maintain vascular patency,[1864] without disturbing the viability of endothelial cells lining the vessel walls for extended times.[1865] (Persufflation of vasculature with cold gas instead of cold liquid has been proposed as an alternative to conventional cryoprotectant-based organ cryopreservation.[1866])

Once the vasculoid has been entirely retracted and exported from the body, the vasculature is quickly filled with 5.4 liters of the temporary liquid blood substitute (Section 4.14.1.1), replacing the prior persufflated nitrogen gas. The abdominal entry point and the two cardiopuncture entry points are resealed, restoring full vascular integrity.

[1862] https://en.wikipedia.org/wiki/Portal_vein.

[1863] Roeder R, Wolfe J, Lianakis N, Hinson T, Geddes LA, Obermiller J. Compliance, elastic modulus, and burst pressure of small-intestine submucosa (SIS), small-diameter vascular grafts. J Biomed Mater Res. 1999 Oct;47(1):65-70; https://pubmed.ncbi.nlm.nih.gov/10400882/.

[1864] Fung YC, Sobin SS, Tremer H, Yen MR, Ho HH. Patency and compliance of pulmonary veins when airway pressure exceeds blood pressure. J Appl Physiol Respir Environ Exerc Physiol. 1983 Jun;54(6):1538-1549; https://journals.physiology.org/doi/pdf/10.1152/jappl.1983.54.6.1538. Papas K. Humidified oxygen gas perfusion (persufflation) in organ preservation and cryobanking. Cryobiology 2015 Aug;71(1):177-178; https://www.sciencedirect.com/science/article/pii/S0011224015001637.

[1865] Fischer JH, Funcke C, Yotsumoto G, Jeschkeit-Schubbert S, Kuhn-Régnier F. Maintenance of physiological coronary endothelial function after 3.3 h of hypothermic oxygen persufflation preservation and orthotopic transplantation of non-heart-beating donor hearts. Eur J Cardiothorac Surg. 2004 Jan;25(1):98-104; https://academic.oup.com/ejcts/article/25/1/98/356315.

[1866] Suszynski TM, Rizzari MD, Scott WE, Eckman PM, Fonger JD, John R, Chronos N, Tempelman LA, Sutherland DE, Papas KK. Persufflation (gaseous oxygen perfusion) as a method of heart preservation. J Cardiothorac Surg. 2013 Apr 22;8:105; https://core.ac.uk/download/pdf/207071160.pdf. Van Sickle S, Jones T. Improved technology for organ cryopreservation by vitrification. SENS6 Conference, Sep 2013; https://web.archive.org/web/20130918185729/http://www.sens.org/outreach/conferences/sens6/accepted-abstracts/improved-technology-organ-cryopreservation. Robitzski D. Freezing and storing donated organs could eliminate some transplant waitlists. Futurism.com, 15 Aug 2018; https://futurism.com/neoscope/freezing-donated-organs-arigos.

The pure nitrogen atmosphere externally surrounding the reviving cryopatient is now replaced with regular air.

4.14.3 Initiate Normal Metabolism and Remove Storage Nanorobots

With the vasculoid removed (Section 4.14.2) and the vasculature filled with functional blood substitute (Section 4.14.1.1), it is time to restart biochemical activity throughout the patient's body. An acoustic command is broadcast to all storage nanorobots that were previously emplaced (Section 4.13.4) inside each of the ~3.5 x 10^{12} tissue cells throughout the body, commanding the robots to release their cargoes of activating molecules, possibly employing specific cytosolic release times, sequences, patterns, or organelle locations for each of the different molecules (with details to be determined by ***future research***). Once finished, the storage nanorobots should exit the cell and migrate at leisure through the ECM, enter the vasculature via diapedesis, and finally exfuse or be removed from the bloodstream (Appendix M). All tissue cells are now metabolically active.[1867]

Simultaneously, an acoustic command is broadcast to all nanorobots present in the blood substitute, causing them to begin providing temporary supportive active chemical exchange and transport services at need.[1868]

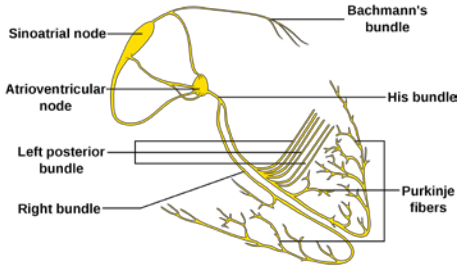

The administration of ACLS,[1869] particular medications,[1870] or electrical signals[1871] can stimulate the patient's heart to begin pumping and the lungs to begin normal respiration; an appropriate protocol can be determined by ***future research***. Other appropriate means for heart stimulation could also be used. For example, the sinoatrial node[1872] (image, right)[1873] is a small group of cells in the heart that spontaneously generates rhythmic electrical signals that serve as a natural pacemaker for the heartbeat. A few "jumper cable" nanorobots positioned in or near these natural pacemaker cells[1874] could chemically or electrically stimulate them into action, after which the node's generation of regular periodic action potentials driving heart muscle contractions would likely become self-sustaining, allowing the stimulatory nanorobots to be removed. Similar conventional[1875] or nanorobotic[1876] means can be used to trigger the onset of respiration. ***Future research*** must also specify

---

[1867] ***Future research*** should determine if caution dictates first re-starting metabolism at temperatures just warm enough for spontaneous heartbeat, then monitoring the effects at the slower metabolic rate.

[1868] Metabolic activation could be done in stages. Because storage nanorobots can be individually addressed at their target destination cells, it would be possible to restart metabolism only in selected tissues or organs before it was restarted in others, if this is deemed useful in ***future research***. For example, the metabolism of cells in the heart, lung, and vasculature could be restarted first to ensure that the respirocyte fleet's limited oxygen carrying capacity was not overtaxed trying to support the entire body before circulation and respiration that would permit respirocyte recharge in the lungs could be fully restored.

[1869] https://en.wikipedia.org/wiki/Advanced_cardiac_life_support.
[1870] https://en.wikipedia.org/wiki/Epinephrine_(medication).
[1871] https://en.wikipedia.org/wiki/Defibrillation.
[1872] https://en.wikipedia.org/wiki/Sinoatrial_node.
[1873] https://en.wikipedia.org/wiki/File:ConductionsystemoftheheartwithouttheHeart-en.svg.
[1874] https://en.wikipedia.org/wiki/Cardiac_pacemaker.

[1875] Holmes GW, Buckingham WB, Cugell DW, Kirchner K. Electric stimulation of breathing in chronic lung diseases. J Am Med Assoc. 1958 Mar 29;166(13):1546-1551; https://jamanetwork.com/journals/jama/article-abstract/323590. Yu J, Zhang JF, Fletcher EC. Stimulation of breathing by activation of pulmonary peripheral afferents in rabbits. J Appl Physiol (1985). 1998 Oct;85(4):1485-1492; https://journals.physiology.org/doi/full/10.1152/jappl.1998.85.4.1485.

[1876] e.g., by direct nanorobotic stimulation of cells in the respiratory center* of the brainstem.†
* https://en.wikipedia.org/wiki/Respiratory_center.
† https://en.wikipedia.org/wiki/Brainstem.

whether some similar stimulus or circulating biochemicals[1877] may be required to restart normal neural signal processing and other electrical activity in the brain.

The patient is now alive, though still unconscious because of the presence of appropriate general anesthetic agents that were previously emplaced in the tissues and bloodstream (Section 4.13.2).

The general state of repair at this point does not need to be perfect. It only needs to be survivable. As Fahy[1878] notes: "Cell metabolism may still be grossly abnormal in a variety of ways. It will not have been necessary to have previously reversed all details of the previously existing pathological state, but only those details required for subsequent cellular self-maintenance and self-repair. Cells 'know' what their proper state is and will spontaneously establish that state provided they are viable enough to continue to exist and to repair themselves." For example, after the restart of active metabolism we may discover that some biochemical or signal transduction processes are out of synchronization or are otherwise not performing exactly right. This pathological circumstance becomes a separate "illness" – perhaps called "cellular cryorevival dysfunction syndrome" – that must be assigned for diagnosis and correction to a second wave of medical nanorobots. The possible nature and range of such complications are a suitable subject for ***future research***.

4.14.4 Replace Blood Substitute with Manufactured Natural Blood

After removing the vasculoid, transfusing the nanorobot-laden blood substitute into the vasculature, activating the patient's metabolism and vital functions, and extracting all cell-dwelling storage nanorobots from the body, the last step before awakening the patient is to perform a conventional blood exchange transfusion.[1879] Vascular access for the transfusion is obtained by conventional venipuncture.[1880] The exchange transfusion replaces substantially all of the temporary blood substitute with the previously manufactured natural blood (Section 4.14.1.2), readying the patient for reawakening (Section 4.15). We can allocate ~**12 hours** to finish this process using conventional perfusion transfusion, although the process might be completed much faster using nanorobot washout (Appendix M).

Adequate levels of general anesthetic should be maintained in the bloodstream throughout the exchange transfusion to ensure that the patient remains unconscious until the proper time for awakening arrives.

[1877] Vrselja Z, Daniele SG, Silbereis J, Talpo F, Morozov YM, Sousa AMM, Tanaka BS, Skarica M, Pletikos M, Kaur N, Zhuang ZW, Liu Z, Alkawadri R, Sinusas AJ, Latham SR, Waxman SG, Sestan N. Restoration of brain circulation and cellular functions hours post-mortem. Nature. 2019 Apr;568(7752):336-343; https://www.ncbi.nlm.nih.gov/pmc/articles/PMC6844189/.

[1878] Fahy G. Appendix B. A "Realistic" Scenario for Nanotechnological Repair of the Frozen Human Brain. In: Wowk B, Darwin M, eds., Cryonics: Reaching for Tomorrow. Alcor Life Extension Foundation, 1991, pp. A-10 – A-26; https://alcor.org/Library/html/nanotechrepair.html.

[1879] https://en.wikipedia.org/wiki/Exchange_transfusion.
[1880] https://en.wikipedia.org/wiki/Venipuncture.

4.15 Patient Wakeup and Post-Awakening Protocols

At this point in the revival process, the formerly cryopreserved patient has undergone comprehensive whole-body cell repair. The integrity of the vasculature is fully restored. All cryoprotectants and the nanorobotic instruments of cellular repair have been removed from the body. The patient has a heartbeat, respiration, normal blood circulation and brainstem electrical activity, and is at normal human body temperature while remaining sedated under general anesthesia.

Depending on the method of anesthesia employed, nanorobots can be introduced into the patient's bloodstream to quickly remove all circulating anesthetic agents, or the anesthetic agents can be allowed to disperse more gradually by conventional natural means.

The patient awakens!

A protocol must be devised to monitor patient vital signs during awakening, and the appropriate personnel must be in attendance, both for monitoring purposes and for psychological purposes. The patient will undoubtedly have many questions, and the attending staff should be prepared to provide good answers to all questions, subject to the proviso that some information might be embargoed for a time if it is believed that accurate answer(s) would be extremely upsetting to the patient.[1881] ***Future research*** must define an appropriate set of awakening protocols.

Certain natural body processes such as eating, drinking, and eliminating probably must be re-introduced gradually and gracefully. For instance, the patient's gut will have been deflorated and can be nutritionally reflorated with appropriate gastrointestinal microbiota[1882] if desired, unless nanomedicine at the time of cryostasis revivals can provide nanorobotic substitutes making gut flora replacement redundant or unnecessary. Other medically desirable treatments not directly related to cryopreservation revival – ranging from cosmetic issues like hair restoration to more serious issues like anti-aging treatments[1883] and long-term eradication of genetic causes of neurodegenerative diseases[1884] can be considered as elective procedures at the patient's discretion and choice, resources permitting.

Perhaps the most difficult medical issue to confront upon awakening may be whether or not cryopatients have been revived with sufficient memory and personality to retain their sense of identity (Section 2.1.5)

[1881] In a 2009 short story* describing one such Q&A session, the revived patient is informed by staff that "in 2021, a virus wiped out most of the Earth's population…probably released from a research lab…" – an interesting passage, given the 2020-21 lab-sourced "COVID-19" coronavirus pandemic which by the end of Dec 2021 had killed 5.5 million people with 280 million cases reported worldwide.†

* Tennant DJ. And 1 Makes 76. Cryonics 2009 Qtr 4;30(4):16-17; https://www.alcor.org/docs/cryonics-magazine-2009-04.pdf.

† https://coronavirus.jhu.edu/map.html.

[1882] https://en.wikipedia.org/wiki/Human_gastrointestinal_microbiota.

[1883] Freitas RA Jr. Chapter 23. Comprehensive Nanorobotic Control of Human Morbidity and Aging. In: Fahy GM, West MD, Coles LS, Harris SB, eds, The Future of Aging: Pathways to Human Life Extension, Springer, New York, 2010, pp. 685-805; http://www.nanomedicine.com/Papers/Aging.pdf.

[1884] Freitas RA Jr. The Alzheimer Protocols: A Nanorobotic Cure for Alzheimer's Disease and Related Neurodegenerative Conditions. IMM Report No. 48, June 2016, 433 pp; Section 5.1, "First Alzheimer Protocol: Genetic Derisking," pp. 240-251; http://www.imm.org/Reports/rep048.pdf.

and subjectively still "feel like themselves"[1885] – or, in other words, how bad is the amnesia? If the connectome has not been perfectly restored, or if neurotransmitter levels or receptor number densities in neuron membranes are not quite right, it could feel like something is missing.[1886] In that case, it may be necessary to assist the patient with additional treatment procedures in order to regain a fuller sense of selfness.

Restoring missing increments of memory and personality from a well-repaired but still somewhat physically damaged brain is exactly the task that the final stages of the Third Alzheimer Protocol were designed to perform – including neural incorporation[1887] and neural network retraining.[1888] These final stages involve steps that can only be taken after the patient has been restored to full consciousness and a modicum of good health, and can actively participate in intellectual exercises designed to recapture as much of the missing data as possible: "Full incorporation is elicited and guided by an intensive program of neural network retraining, enabling significant restoration of function to the … patient. Network retraining relies on the experimentally-proven beneficial effects of environmental enrichment, which includes activities designed to elicit recovery of brain memory data and mental algorithms." For instance, if the patient has forgotten how to play the piano, they could receive piano lessons to retrain that skill.

The awakened patient can be exposed to recordings[1889] or other records that depict or describe the unique person they used to be. Hogg[1890] provided an early list of such materials, which could include items targeting memories (e.g., diaries, events, knowledge, skills), personality (preferences, interests, hobbies, personality test results, jokes, personal philosophy), individual psychophysical behavior (voice, handwriting), materials the patient created (writings, artistic compositions), and live or recorded recollections of the patient by friends and colleagues. Of course, the patient, after being awakened, can be provided with this information as useful input but should remain free to accept or reject it depending on

---

[1885] Bridge SW. I've Gotta Be Me! (But who will you be after cryonics revival?) Cryonics 2019 QIII; 40(3);52-56; https://alcor.org/CryonicsMagazine/cryonics2020.html#n3.

[1886] A useful project for ***future research*** would be to design a test – perhaps a customized list of questions or tasks – that the patient could take to quantify exactly how much of their original memory and personality remain. This could be a useful diagnostic tool to assist the patient in deciding if more work was necessary to restore missing elements of memory or personality. Care must be taken in designing such a test as the result could have legal implications – e.g., whether a revived person was lawfully entitled to receive assets previously placed in a cryonics asset preservation trust.

[1887] Freitas RA Jr. The Alzheimer Protocols: A Nanorobotic Cure for Alzheimer's Disease and Related Neurodegenerative Conditions. IMM Report No. 48, June 2016, 433 pp; Section 5.3.2.4, "Neural Incorporation," pp. 333-346; http://www.imm.org/Reports/rep048.pdf.

[1888] Freitas RA Jr. The Alzheimer Protocols: A Nanorobotic Cure for Alzheimer's Disease and Related Neurodegenerative Conditions. IMM Report No. 48, June 2016, 433 pp; Section 5.3.3, "Neural Network Retraining," pp. 347-360; http://www.imm.org/Reports/rep048.pdf.

[1889] Linda Chamberlain recommended that prospective cryonics patients should make a video self-interview during their lifetime, and provides a list of questions whose answers would be maximally informative to your future post-revival self. Chamberlain L. Preserving Your Memory and Identity. Cryonics 2000 Qtr 2;21(2):18-23; https://www.alcor.org/docs/cryonics-magazine-2000-02.pdf.

[1890] Hogg T. Information Storage and Computational Aspects of Repair. Cryonics 1996 Qtr 3;17(3):18-25; https://www.alcor.org/docs/cryonics-magazine-1996-03.pdf.

their judgment of the relevance of the information to their current views and circumstances.[1891] Alternatively, they may choose to voluntarily submit to neurophysical memory implantation[1892] by memory engineers to establish closer psychological continuity between "the person who is revived from cryopreservation…[and] the one who went into cryopreservation."[1893] Ultimately it may be possible to implant complete memories of new knowledge and new skillsets directly into the post-revival living brain, sparing the revived person the need for extensive schooling or retraining in order to operate productively in the new world into which they've awakened.[1894] People would presumably be pleased to discover that there will be no need to spend years post-revival "repeating high school" to become a fully functioning citizen of the future.

[1891] In principle, a Whole-Brain Emulation (WBE) (Section 5.2.3.4) of the patient's brain could be created, the WBE could be run in simulation to determine its response to various inputs, and to the extent the responses to these inputs were inconsistent with the pre-cryopreservation records, the WBE parameters could be adjusted so that the simulation produced results more consistent with the historical information. The "corrected" WBE could then be used as the basis for physical or virtual brain reconstruction and revival. One major difficulty with this approach would be that changes imposed to correct one set of "erroneous" responses could create unforeseen changes in other responses, especially including ones that were not tested. An ethical difficulty would also arise if a conscious WBE "emulated person" was "awakened" and then forcibly subjected *in silico* to repeated incremental mental alterations not of their choosing, a process that could be likened to mind rape. A different ethical issue arises if a possibly incompletely- or imperfectly-emulated WBE-person is allowed to choose the memory status of his future physically-instantiated self.

[1892] Neuroscientists have already demonstrated a very limited ability to remove individual memories and to implant fake memories in the connectome of a living mouse using lasers and optogenetics.[*] By the time cryorevivals are taking place, memory implantation techniques should be far more advanced than today, as will the analysis of the ethics of memory enhancement vs. memory editing.[†]

[*] Liu X, Ramirez S, Pang PT, Puryear CB, Govindarajan A, Deisseroth K, Tonegawa S. Optogenetic stimulation of a hippocampal engram activates fear memory recall. Nature. 2012 Mar 22;484(7394):381-5; https://www.ncbi.nlm.nih.gov/pmc/articles/PMC3331914/. Tonegawa S, Liu X, Ramirez S, Redondo R. Memory Engram Cells Have Come of Age. Neuron. 2015 Sep 2;87(5):918-31; https://www.sciencedirect.com/science/article/pii/S0896627315006777. Vetere G, Tran LM, Moberg S, Steadman PE, Restivo L, Morrison FG, Ressler KJ, Josselyn SA, Frankland PW. Memory formation in the absence of experience. Nat Neurosci. 2019 Jun;22(6):933-940; https://www.ncbi.nlm.nih.gov/pmc/articles/PMC7592289/. Lau JMH, Rashid AJ, Jacob AD, Frankland PW, Schacter DL, Josselyn SA. The role of neuronal excitability, allocation to an engram and memory linking in the behavioral generation of a false memory in mice. Neurobiol Learn Mem. 2020 Oct;174:107284; https://www.ncbi.nlm.nih.gov/pmc/articles/pmid/32745601/.

[†] Erler A. Does Memory Modification Threaten Our Authenticity? Neuroethics. 2011 Nov;4(3):235-249; https://www.ncbi.nlm.nih.gov/pmc/articles/PMC3189328/.

[1893] More M. Survival Through Inference. Cryonics 2007 Qtr 2;28(2):10-11; https://www.alcor.org/docs/cryonics-magazine-2007-02.pdf.

[1894] In the original Matrix movie, the ability to connect your neural network to the information network all around you means that learning a new skill takes a matter of seconds, as illustrated in a scene where Trinity, leading a rescue mission, gets "taught" how to pilot a helicopter in the blink of an eye (https://www.youtube.com/watch?v=6AOpomu9V6Q). We can't directly upload knowledge yet, although transcranial direct current stimulation has been shown to modulate the brain processes of novice pilots who are fed signals from experienced pilots,[*] and techniques such as decoded neurofeedback[†] are slowly leading in the direction of Matrix-style "instant learning". Natural learning requires establishing new synaptic connections between neurons in the brain, which takes time because biological growth processes are relatively slow. Nanorobots in the brain could create artificial electrical pathways between neurons in seconds if we can determine which connections, if established, would encode the desired knowledge or skills.

[*] Choe J, Coffman BA, Bergstedt DT, Ziegler MD, Phillips ME. Transcranial Direct Current Stimulation Modulates Neuronal Activity and Learning in Pilot Training. Front Hum Neurosci. 2016 Feb 9;10:34; https://www.ncbi.nlm.nih.gov/pmc/articles/pmid/26903841/.

[†] Shibata K, Lisi G, Cortese A, Watanabe T, Sasaki Y, Kawato M. Toward a comprehensive understanding of the neural mechanisms of decoded neurofeedback. NeuroImage 2019 Mar; 188:539-556; https://www.sciencedirect.com/science/article/pii/S1053811918321669.

Future research must also define a process by which the revived patient can be re-integrated into society,[1895] especially if they awaken lost in a world of, say, extreme superabundance[1896] or incomprehensible sexual practices.[1897] This may require language training, skills training, or other behavioral adaptations necessary to succeed in the new world in which the patient has awakened, possibly including some time in an interactive virtual reality history simulator.[1898]

In Oct 2020, Alcor Life Extension Foundation initiated a Reintegration Working Group[1899] to explore relevant issues. According to their announcement: "Alcor will not be able to revive any patients for many decades to come. Although that time is a long way off, we should be thinking about it and planning for it now. For one thing, that's part of Alcor's mission: Future restoration of good health and reintegration into society for all patients….Cryonics will be less scary to some if we have a clearer picture of the challenges revived patients will face and the ways we can prepare for them. The Reintegration Working Group (RWG) aims to develop ideas and plans relating to:

- Asset trusts and future-income trusts;
- 'Memory books' and ways to fill in any missing memories;
- Legal structures to allow patients to claim their identities and their status as persons;
- An organizational culture that fosters interest in and desire to help those who return from biostasis;
- Supporting and protecting newly revived patients as they gradually reintegrate into the new world; and
- Facilitating contact with other revived cryonauts,[1900] if this is desired."

Part of the accumulated wealth available to revive cryopatients might someday fund a "Cryonics Halfway House".[1901] Revivees could live there in an environment comfortingly similar to the cultural milieu that

---

[1895] Krieger D. Revival. Cryonics 1993 Jun;14(6):22-24; https://www.alcor.org/docs/cryonics-magazine-1993-06.pdf. Macintosh K. Reintegration, Personalized. Cryonics 2013 May;34(5):13-14; https://www.alcor.org/docs/cryonics-magazine-2013-05.pdf. Grove RS. Speculations: Post-Cryopreservation Mentation. Cryonics 2004 Mar/Apr;25(2):10-14; https://www.alcor.org/docs/cryonics-magazine-2004-02.pdf.

[1896] "The Germans have a word for this condition: Zerrissenheit – loosely, 'falling-to-pieces-ness'. This is the loss of internal coherence that can come from living a multitasking, pulled-in-a-hundred-directions existence. This is what Kierkegaard called 'the dizziness of freedom'. When the external constraints are loosened, when a person can do what he wants, when there are a thousand choices and distractions, then life can lose coherence and direction if there isn't a strong internal structure." David Brooks. The Road to Character. Random House, 2015, p. 218; https://www.amazon.com/Road-Character-David-Brooks/dp/0812983416/.

[1897] Freitas RA Jr. Nanomedicine, Volume III: Applications. Landes Bioscience, Georgetown, TX, in preparation; Chapter 27, "Sex, Gender, and Reproduction"; http://www.nanomedicine.com/NMIII.htm.

[1898] Michael Darwin has suggested[*] "having patients virtually live through the interval between the time they were cryopreserved and the time they were revived in order to catch up, or adjust. This would be an accelerated process where a week, a day or even an hour of real time would equate to a year of subjective time "lost" in storage. Clearly, this would take place as a simulation, and beyond the purpose of defusing shock, it could also serve to educate and rehabilitate. The patient would wake up one day in his life at a point before his cardiac arrest deemed appropriate, get out of bed, and continue, as usual, with the normal routine of his life. The trajectory of his experience would alter gradually, probably in ways not now imaginable; in order to ultimately equip him with the insights, knowledge and skills needed to survive in a world transformed by time and technology."
[*] http://chronopause.com/chronopause.com/index.php/2011/03/17/1968-ad-cryonics-reboot/index.html.

[1899] https://www.alcor.org/2020/10/introducing-the-reintegration-working-group/.

[1900] "U.S. man wakes from 19-year coma"; http://news.bbc.co.uk/2/hi/americas/3052433.stm.

[1901] https://en.wikipedia.org/wiki/Halfway_house.

existed at the time of their cryopreservation. Other volunteer cryonicists will be there to provide support and coping skills against future shock.[1902] As a revivee, you could stay as long as you like – forever, if you so choose. While staying at the House, you might volunteer to perform whatever tasks are helpful to keep the place going, from menial tasks to just chatting with other residents, teaching, or entertaining. You would also get progressive access to whatever new technologies are available, including anti-aging therapies and meetings with surviving relatives[1903] and friends, should you wish to begin a comfortably slow period of integration with the outside society at whatever pace is comfortable for you. If and when you're ready to leave, you can choose to do so. If you're an adventurous thrillseeker who craves variety and change, you might choose to go "cold turkey" and jump right into the outside world, secure in the knowledge that you'll always be welcome back at the Cryonics House if things don't work out well.

[1902] Beighley P. Culture Shock: Thinking About Reintegration after Preservation. Cryonics 2021 Qtr 1;42(1):3-4; https://www.alcor.org/docs/cryonics-magazine-2021-01.pdf.

[1903] Apparently James Bedford, the first person to be cryopreserved, in 1967, will have at least one family member who will be present and eager to help when he is revived: "Dan Shilstone replied on June 26, 2015: Was pleasantly surprised to open my alumni magazine and find this article about my great grandfather, James Bedford. Can't wait to meet him!" Comment posted in: Smith CA. Into the Deep Freeze: What Kind of Person Chooses to Get Cryonically Preserved? California Magazine, Summer 2015; https://alumni.berkeley.edu/comment/19626#comment-19626.

4.16 Summary of Conventional Cell Repair

Table 13 lists the number of nanorobots and the estimated time required to complete each stage of the revival protocol using the conventional nanorobotic cell repair approach, for both whole-body (estimated from Sections 4.1-4.15) and neuro (informal estimate) cryopreservation patients.

Table 13. Nominal list of conventional repair tasks for human cryopreservation revival, with estimated task durations for whole-body and neuro patients

Cryopreservation Revival Task	Section Reference	Number of Nanorobots	Task Duration (Whole-Body)	Task Duration (Neuro)
Macrovascular scan	4.1	---	>5 days	~1 day
Macrovascular excavation	4.2	2.97×10^9	17 days	~1 day
Microvascular scans	4.3	$\sim 3 \times 10^9$	~7 days	~1 day
Microvascular excavations				
Capillaries & crackface voids	4.4.1	2.3×10^9	17 days	~2 days
Organ & tissue surface perimeters	4.4.2	6×10^7	~0.5 day	~0.5 day
Extracellular ice	4.4.3	(variable)	(variable)	(variable)
Recondition & map ice surfaces				
Clear excavation debris	4.5.1	1×10^{10}	12 days	~0.5 day
Recondition exposed ice surfaces	4.5.2	1×10^{10}	12 days	~1 day
Ice peel	4.5.3	1×10^{10}	12 days	~1 day
Geometrical mapping	4.5.4	1×10^{10}	77 days	~2 days
Biochemical mapping	4.5.5	1×10^{10}	77 days	~2 days
Install vasculoid				
Arteriovenous emplacement	4.6.2	1.5×10^{14}	0.04 day	~0.04 day
Crackface void emplacement	4.6.3	1.05×10^{13}	~1 day	~0.5 day
Lymphatic & perimeter surfaces	4.6.4	4.54×10^{13}	~5 days	~0.5 day
Submicron tissue scan	4.7	$\sim 3 \times 10^9$	~21 days	~1 day
Compute whole-body repair plan	4.8.5	---	25 days	~2 days
Prethaw and crackface fusion	4.9.1	---	1 day	~0.5 day
Molecular extraction				
Extraction probe deployment	4.10.1.9	---	~1 day	~0.5 day
Extraction pumping	4.10.1.9	---	0.04 day	~0.04 day
Cryoprotectant extraction	4.10.1.7	---	12 days	~12 days
Reseal membrane compartments				
Restore cell plasma membranes	4.11.1	7.4×10^{12}	8.3 days	~1 day
Debris removal	4.11.1	1×10^{12}	0.3 day	~0.1 day
Repair fracture face membranes	4.11.2	1×10^{12}	~1 day	~1 day
Cell rehydration & water transfers	4.11.3	---	0.5 day	~0.5 day
Remove cells & microbodies				
Extracellular vesicles	4.12.1.1	1×10^{12}	0.2 day	~0.2 day
Red cells & platelets	4.12.1.2	1×10^{12}	0.3 day	~0.3 day
Bacteria	4.12.1.4	1×10^{12}	0.4 day	~0.4 day
Cancer cells – detection & mapping	4.12.1.6	1×10^{12}	0.04 day	~0.04 day
Cancer cells – excision	4.12.1.6	1×10^{12}	0.5 day	~0.5 day
Inspect & repair existing cells				

Prelim inspection & debris cleanup	4.12.2.1	1 x 10^{12}	3.3 days	~0.5 day
Cell nucleus repair/replacement	4.12.2.2	1 x 10^{12}	3.1 days	~2 days
Non-nucleus organelles	4.12.2.3	1 x 10^{12}	12.8 days	~4 days
Cytoskeleton & rel. components	4.12.2.4	1 x 10^{12}	69 days	~4 days
Replace membrane receptors	4.12.2.5	1 x 10^{12}	14 days	~2 days
Membrane protein editing	4.12.2.6	1 x 10^{12}	50 days	~4 days
Glycocalyx repair	4.12.2.7	1 x 10^{12}	3 days	~1 day
ECM reconditioning	4.12.3.3	1 x 10^{12}	29 days	~2 days
Supplemental neural repair				
Axonal repair	4.12.4.1	1 x 10^{11}	~1 day	~1 day
Neuron membrane editing	4.12.4.2	1 x 10^{12}	5.6 days	~5.6 days
Restore missing brain tissue	4.12.4.3	1.4 x 10^{12}	3.6 days	~3.6 days
Patient warmup & molec. instillation				
Warm the patient to 310 K	4.13.1	---	0.04 day	~0.04 day
Instillation probe deployment	4.10.1.9	---	~1 day	~1 day
Instillation pumping	4.13.2	---	0.4 day	~0.4 day
Fluid check & perimeter cleanup	4.13.3	1 x 10^{12}	~1 day	~1 day
Instill storage nanorobots	4.13.4	3.5 x 10^{12}	0.4 day	~0.4 day
Uninstall vasculoid & finish repairs				
Manufacture replacement blood	4.14.1.2	---	0.6 day	~0.6 day
Retract vasculoid	4.14.2	---	0.004 day	~0.004 day
Transfuse replacement blood	4.14.4	---	0.5 days	~0.5 day
TOTALS			***512 days*** *(1.4 years)*	***~66 days*** *(~2.2 months)*
Minimum time assuming whole-cell replace + high energy density repair:			**244 days** *(8.1 months)*	**46 days** *(1.5 months)*

The nominal serial revival protocol for **whole-body patients** as described in Sections 4.1-4.15 appears to require ~512 days (~**1.4 years**) of calendar repair time to complete. If it becomes feasible to shift cell repair (Section 4.12) from organelle repair/replacement to exclusively whole-cell replacement operations (Section 4.12.2.8), then it may be possible to cut the cellular and tissue repair time (Section 4.12) from 155 days to only ~15 days, reducing total calendar time for revival from 512 days to 372 days (~**1.0 year**). If it becomes feasible to tolerate 300 watts (~5 watts/liter) of waste heat generation from nanorobot operations instead of just 100 watts (~1.7 watts/liter), then it might be possible to cut the calendar time for reconditioning and mapping exposed ice surfaces (Section 4.5) from 190 days to only ~63 days, and the calendar time for removing unwanted cells and microbodies (Section 4.12.1) from 1.44 days to ~0.48 days, further reducing the total calendar time for revival from 372 days to 244 days (~**8.1 months**). It seems possible that the total repair time for whole-body patients might be further modestly reduced by parallelizing some or all of these serial operations. The extent to which the nominal serial revival protocol using conventional cell repair can be further temporally shortened or made more efficient is a suitable topic for ***future research***.

The nominal serial revival protocol for **neuro patients** is crudely estimated as requiring ~66 days (~**2.2 months**) of calendar repair time to complete. If it becomes feasible to shift cell repair (Section 4.12) from organelle repair/replacement to exclusively whole-cell replacement operations (Section 4.12.2.8), then it may be possible to cut the cellular and tissue repair time (Section 4.12) for neuro patients from 17.5 days to only ~3 days, reducing total calendar time for revival from 66 days to 52 days (~**1.7 months**). If it becomes feasible to tolerate ~5 watts/liter of waste heat generation from nanorobot operations instead of just ~1.7 watts/liter in the cranial theater of operations, then it might be possible to cut the calendar time for reconditioning and mapping exposed ice surfaces (Section 4.5) from 6.5 days to only ~2 days, and the calendar time for removing unwanted cells and microbodies (Section 4.12.1) from 1.44 days to ~0.48 days, further reducing the total calendar time for revival from 52 days to 46 days (~**1.5 months**). Parallelizing

some or all of these serial operations might further modestly reduce the total repair time for neuro patients. The neuro repair time estimates listed in **Table 13** exclude whatever time may be required to print or regrow an acephalonic replacement body and then reattach it to the fully repaired formerly cryopreserved cephalon (Section 6.1), which might occur in parallel.

While neuro revival takes (512 days / 66 days =) **7.8-fold** less repair time than whole-body revival in the nominal serial case, or (244 days / 46 days =) **5.3-fold** less time in the whole-cell-replacement high-waste-heat-energy-density scenario, this is not quite as big an advantage as the V_{body}/V_{brain} = 60 L / 1.4 L ~ **43 body/brain volume ratio** might suggest. This is because many tasks may have certain irreducible fixed setup costs, and extracting cryoprotectant takes the same time in either scenario. ***Future research*** can analyze whether neuro or whole-body repair procedures may be easier to parallelize.

Note that nanomedical practitioners must design and build all of the same nanorobot types and the same repair missions for whole-body or neuro patients. Once all necessary nanorobots and mission designs for either revival scenario are in hand, they can be equally well employed for either type of patient. This means that the initial investment in revival technology will be about the same, regardless of which type of patient might be targeted first. In the case of whole-body patients, some additional mission design work will be required to deal with the repair specifics for multiple organs other than the brain – although the brain is expected to be the most technically challenging organ to repair and the least tolerant of error. In the case of neuro patients, additional development work will be required to design, build, and operate the acephalonic body manufacturing and reattachment technology (Chapter 6) – technologies that might invoke additional legal complications beyond those involved in repairing a patient's original natural body. These factors together seem not to significantly favor either type of patient for early revival attempts.

Key Technical Uncertainty. The key technology underlying much of the conventional cell repair is the vasculoid appliance (Section 4.6). The vasculoid is an extremely complex device that will be the product of a mature molecular manufacturing technology and an intimate knowledge of human physiology and cytoarchitecture. The ability to perform a cryonics revival using conventional cell repair depends on the prior development of the vasculoid or some similar technology. The revival of cryonics patients will probably not provide sufficient economic motivation to develop the vasculoid quickly, because there are so few such patients. Vasculoid development outside of the cryonics context likely must await either (1) some motivation derived from more conventional and more widespread medical purposes, such as the treatment of extensive global ischemia and trauma, or (2) the intervention by a benefactor willing to invest the necessary resources regardless of conventional economic motivations.

However, once the vasculoid has been developed as described, its operation should easily meet the specifications needed for the cryonics revival application. That's because the vasculoid was originally designed to be operated inside a living human body whose metabolism must be continuously maintained after the replacement of natural blood. In the cryonics application, the operational requirements are less severe because the patient's body is maintained in metabolic stasis throughout the procedure. In the cryonics revival application, the vasculoid is being operated well below its maximum design specifications and thus should have no difficulty meeting the operational requirements of this scenario.

4.17 Why Biological Methods of Cryostasis Revival are Likely Infeasible

Backing off to a "bigger picture" perspective, the foregoing discussions should make it clear why purely biological approaches to cryostasis revival (e.g., Sections 2.2.3, 2.2.4, and 2.2.5) are most likely to be infeasible. There are two main reasons for this: high viscosity and slow reaction rates at cold temperatures.

Viscosity. As noted earlier (Section 4.0), frozen water-ice has extremely high viscosity, making locomotion energetically infeasible even for diamondoid nanorobots at cryogenic temperatures. Motile

biological cells such as engineered bacteria would have negligible mobility in slightly-subfreezing "warm" (i.e., 0 °C > T ≥ -20 °C) water-ice,[1904] and no mobility whatsoever in undisturbed colder (or cryogenic) ice. Cold-solidified vitrified solutions are less viscous than water-ice at most temperatures of relevance but are likely sufficiently viscous to immobilize bacteria, even assuming toxicity could be avoided. Well-cryopreserved patients will always have some impenetrable water-ice present, and even in vitrified 100% pure M22 the viscosity (Section 4.9) of this cryoprotectant is already ~20 times higher than normothermic water at 0 °C (273 K), 100-fold higher at -30 °C (243 K), and 1000-fold higher than water at the M22 melting point of -55 °C (218 K), making microbial locomotion mechanically- and energy-prohibitive even in a purely glassy operating environment.

Reaction Rates. Enzymes, which drive biological and biochemical processes in the cell, lose their activity when frozen,[1905] especially due to cold denaturation near ~0 °C,[1906] although a few psychrophile (cold-loving)[1907] enzymes retain useful activity as low as -20 °C[1908] which is thought to be close to the lowest operating temperature limit for free-living microbes[1909] and for terrestrial biological organisms generally.[1910] Regarding psychrophilic bioengineering, at least one psychrophilic enzyme (subtilisin S41)[1911] has been submitted to directed evolution in an attempt to create improved artificial variants, and one mutant variant showed increased thermostability "without sacrificing its low-temperature activity,"[1912] but its minimum operating temperature was not reduced. At present, there is no evidence that any kind of psychrophile organism can be bioengineered to operate much below -20 °C, let alone a complex reparative biological organism for cryonics revival purposes operating down to LN2 temperatures.

[1904] Price PB. Microbial life in glacial ice and implications for a cold origin of life. FEMS Microbiol Ecol. 2007 Feb;59(2):217-31; https://academic.oup.com/femsec/article/59/2/217/2908360. Rohde RA, Price PB. Diffusion-controlled metabolism for long-term survival of single isolated microorganisms trapped within ice crystals. Proc Natl Acad Sci U S A. 2007 Oct 16;104(42):16592-7; https://www.pnas.org/content/104/42/16592. Pandey R, Usui K, Livingstone RA, Fischer SA, Pfaendtner J, Backus EH, Nagata Y, Fröhlich-Nowoisky J, Schmüser L, Mauri S, Scheel JF, Knopf DA, Pöschl U, Bonn M, Weidner T. Ice-nucleating bacteria control the order and dynamics of interfacial water. Sci Adv. 2016 Apr 22;2(4):e1501630; https://www.ncbi.nlm.nih.gov/pmc/articles/PMC4846457/. Bar Dolev M, Bernheim R, Guo S, Davies PL, Braslavsky I. Putting life on ice: bacteria that bind to frozen water. J R Soc Interface. 2016 Aug;13(121):20160210; https://www.ncbi.nlm.nih.gov/pmc/articles/pmid/27534698/.

[1905] http://www.worthington-biochem.com/introBiochem/tempEffects.html and https://sciencing.com/effects-boiling-freezing-enzyme-activity-23207.html.

[1906] Privalov PL. Cold denaturation of proteins. Crit Rev Biochem Mol Biol. 1990;25(4):281-305; http://citeseerx.ist.psu.edu/viewdoc/download?doi=10.1.1.1023.8655&rep=rep1&type=pdf.

[1907] https://en.wikipedia.org/wiki/Psychrophile.

[1908] Deming JW. Psychrophiles and polar regions. Curr Opin Microbiol. 2002 Jun;5(3):301-9; https://lasp.colorado.edu/home/wp-content/uploads/2011/07/deming2002.pdf.

[1909] Price PB, Sowers T. Temperature dependence of metabolic rates for microbial growth, maintenance, and survival. Proc Natl Acad Sci U S A. 2004 Mar 30;101(13):4631-6; https://www.ncbi.nlm.nih.gov/pmc/articles/pmid/15070769/.

[1910] Clarke A, Morris GJ, Fonseca F, Murray BJ, Acton E, Price HC. A Low Temperature Limit for Life on Earth. PLoS One. 2013 Jun 19;8(6):e66207; https://www.ncbi.nlm.nih.gov/pmc/articles/pmid/23840425/.

[1911] Davail S, Feller G, Narinx E, Gerday C. Cold adaptation of proteins. Purification, characterization, and sequence of the heat-labile subtilisin from the Antarctic psychrophile *Bacillus TA41*. J Biol Chem. 1994 Jul 1;269(26):17448-53; https://www.sciencedirect.com/science/article/pii/S0021925817324602.

[1912] Miyazaki K, Wintrode PL, Grayling RA, Rubingh DN, Arnold FH. Directed evolution study of temperature adaptation in a psychrophilic enzyme. J Mol Biol. 2000 Apr 7;297(4):1015-26; https://pdfs.semanticscholar.org/3bbf/7558df5f9883e3abbe1466ede09bda70c40d.pdf. Wintrode PL, Miyazaki K, Arnold FH. Patterns of adaptation in a laboratory evolved thermophilic enzyme. Biochim Biophys Acta. 2001 Sep 10;1549(1):1-8; https://pubmed.ncbi.nlm.nih.gov/11566363/.

Cell membrane ion transport is also highly temperature dependent, with voltage-gated H^+ transport activity falling almost ten-fold for every 10 °C drop near ice-water temperatures,[1913] and molecular endocytosis is negligible below 5-15 °C.[1914] With key cell machinery effectively "frozen out" at cryogenic temperatures, viruses (Section 2.2.3) and similar parasitic biological entities will be prevented from successful reproduction by their usual method of commandeering the metabolism of cells. Thus only metabolically competent organisms like bacteria could be employed for cryostasis revival, and these organisms, to remain functional, must be used at temperatures above -20 °C or thereabouts.

Nanorobot internal operating speed is largely unaffected by temperature. In contrast, bacterial internal operating speed is highly temperature dependent. At temperatures nearer the water-ice freezing point, mobility is possible but biochemical activity is painfully slow. For instance, enzyme activity decreases by a factor of ~2 for every ~10 °C drop in temperature,[1915] so chemical processes will run $k_{chem} \sim 2^{(310\ K - 253\ K)/(10\ K)} \sim 52$ times slower at -20 °C (253 K) than at 37 °C (310 K), the normal human body temperature. This means that a reparative microbial organism working at -20 °C would only have $k_{chem}\ \tau_{ischemic} \sim 5$ hours of operating time before tissue would suffer the same degradative damage (Section 3.2) as a normothermic body would experience in $\tau_{ischemic} \sim 6$ minutes. At operating temperatures warmer than -20 °C, the microbes would have still less time to finish their work.

Even nanorobots, which can work much faster than microbes at any temperature, require weeks or months to complete all necessary cryostasis repairs on a human brain or body (Section 4.16). But nanorobots can avoid creating new ischemic damage at warmer temperatures by performing molecular extraction (Section 4.10) to place the cryopatient in a state of complete metabolic stasis that halts further accumulation of damage, thus "buying time" for extensive repair work. It seems unlikely that any microbial organism could be engineered to be capable of rapid molecular extraction (or inhibition) of possibly many thousands of relevant metabolic chemicals from every cell in the brain or body tissues of a reliquidified cryopatient, especially given the relatively large volumes of metabolic chemicals that may be involved (Section 7.1.6.5). Tens of thousands of different binding sites could be required, and onboard storage would have to be at ordinary low pressures (hence not compact) and would have to use a biological containment vessel that can resist degradation from a mixed soup of potentially reactive chemicals. Operating power would need to be provided to the engineered microbes in some artificial form that does not participate in normal cellular metabolism – perhaps via synthetic chemicals, electromagnetic waves, or acoustics – or else the microbe might place itself in stasis as a result of its own extraction activities. Consequently, it seems unlikely that engineered microbes would be able to establish whole-body or whole-brain cellular metabolic stasis sufficient to forestall ongoing ischemic damage to the cryopatient during very long repair times.

Ischemic damage accrues slowly at lower temperatures, but the lower temperatures also slow the activities of the reparative biological organisms. At higher temperatures, the speed of both damage accumulation and repair activities can increase. Optimistically assuming that engineered reparative organisms could be promptly suffused throughout the cryopatient's entire body to ~1% (1/100) of total tissue volume (i.e.,

---

[1913] DeCoursey TE, Cherny VV. Temperature dependence of voltage-gated H^+ currents in human neutrophils, rat alveolar epithelial cells, and mammalian phagocytes. J Gen Physiol. 1998 Oct;112(4):503-22; https://www.ncbi.nlm.nih.gov/pmc/articles/PMC2229433/.

[1914] Weigel PH, Oka JA. Temperature dependence of endocytosis mediated by the asialoglycoprotein receptor in isolated rat hepatocytes. Evidence for two potentially rate-limiting steps. J Biol Chem. 1981 Mar 25;256(6):2615-7; https://www.sciencedirect.com/science/article/pii/S0021925819696560. Faghihi Shirazi M, Aronson NN Jr, Dean RT. Temperature dependence of certain integrated membrane functions in macrophages. J Cell Sci. 1982 Oct;57:115-27; https://jcs.biologists.org/content/joces/57/1/115.full.pdf. Chanaday NL, Kavalali ET. Time course and temperature dependence of synaptic vesicle endocytosis. FEBS Lett. 2018 Nov;592(21):3606-3614; https://febs.onlinelibrary.wiley.com/doi/pdfdirect/10.1002/1873-3468.13268.

[1915] https://en.wikipedia.org/wiki/Q10_(temperature_coefficient).

~600 cm^3 in a 60 L adult human body), these reparative engineered organisms would have to be $(1/100)^{-1}$ ~ 100 times more efficient (volume for volume) than the patient's own natural cells in repairing ischemic damage just to keep pace with the new damage as it accrues. Reversing pre-existing cryopreservation-related damage would require a still larger infusion of engineered biological devices or even greater relative efficiency of the engineered microbes over natural biological cells. But there are no reports of engineered white cells,[1916] macrophages,[1917] fibroblasts,[1918] or other artificial reparative cells providing significant multiples of superior performance over their natural counterparts, let alone multiple *orders of magnitude* of superior performance.

Effective repair likely requires a great deal of rapid computation. The maximum clock speed of biochemical computation inside engineered organisms may be on the order of KHz,[1919] far below the GHz clock speeds that should be available with nanomechanical computers.[1920] Computational systems using organic or bioelectronic components[1921] might exhibit above-KHz clock speeds, but these would not be purely biological structures and thus may be difficult to incorporate into biological organisms that must be manufactured using conventional cell reproduction and growth processes, or using laboratory cell reactors.

Many additional advantages of nanorobotic systems over biological systems have already been enumerated in Section 1.2.5.

[1916] Robbins Y, Greene S, Friedman J, Clavijo PE, Van Waes C, Fabian KP, Padget MR, Abdul Sater H, Lee JH, Soon-Shiong P, Gulley J, Schlom J, Hodge JW, Allen CT. Tumor control via targeting PD-L1 with chimeric antigen receptor modified NK cells. Elife. 2020 Jul 7;9:e54854; https://www.ncbi.nlm.nih.gov/pmc/articles/PMC7340502/.

[1917] Moyes KW, Lieberman NA, Kreuser SA, Chinn H, Winter C, Deutsch G, Hoglund V, Watson R, Crane CA. Genetically Engineered Macrophages: A Potential Platform for Cancer Immunotherapy. Hum Gene Ther. 2017 Feb;28(2):200-215; https://pubmed.ncbi.nlm.nih.gov/27758144/. Villanueva MT. Macrophages get a CAR. Nat Rev Immunol. 2020 May;20(5):273; https://www.nature.com/articles/s41577-020-0302-9.pdf. Brempelis KJ, Cowan CM, Kreuser SA, Labadie KP, Prieskorn BM, Lieberman NAP, Ene CI, Moyes KW, Chinn H, DeGolier KR, Matsumoto LR, Daniel SK, Yokoyama JK, Davis AD, Hoglund VJ, Smythe KS, Balcaitis SD, Jensen MC, Ellenbogen RG, Campbell JS, Pierce RH, Holland EC, Pillarisetty VG, Crane CA. Genetically engineered macrophages persist in solid tumors and locally deliver therapeutic proteins to activate immune responses. J Immunother Cancer. 2020 Oct;8(2):e001356; https://www.ncbi.nlm.nih.gov/pmc/articles/PMC7594542/.

[1918] Ortiz-Urda S, Lin Q, Green CL, Keene DR, Marinkovich MP, Khavari PA. Injection of genetically engineered fibroblasts corrects regenerated human epidermolysis bullosa skin tissue. J Clin Invest. 2003 Jan;111(2):251-5; https://www.ncbi.nlm.nih.gov/pmc/articles/PMC151880/. Roy B, Yuan L, Lee Y, Bharti A, Mitra A, Shivashankar GV. Fibroblast rejuvenation by mechanical reprogramming and redifferentiation. Proc Natl Acad Sci U S A. 2020 May 12;117(19):10131-10141; https://www.ncbi.nlm.nih.gov/pmc/articles/PMC7229653/.

[1919] Freitas RA Jr. Nanomedicine, Volume I: Basic Capabilities. Landes Bioscience, Georgetown, TX, 1999; Section 10.2.3.1, "Biochemical Computers"; http://www.nanomedicine.com/NMI/10.2.3.1.htm#p9.

[1920] Freitas RA Jr. Nanomedicine, Volume I: Basic Capabilities. Landes Bioscience, Georgetown, TX, 1999; Section 10.2.1, "Nanomechanical Computers"; http://www.nanomedicine.com/NMI/10.2.1.htm.

[1921] Freitas RA Jr. Nanomedicine, Volume I: Basic Capabilities. Landes Bioscience, Georgetown, TX, 1999; Section 10.2.3.3, "Organic and Bioelectronic Computers"; http://www.nanomedicine.com/NMI/10.2.3.3.htm

5. Plan B: Nanorobotic Revival via Molecular Reconstruction

Mobile nanorobots cannot readily operate in frozen tissue where the physical structure could be preserved for indefinite periods of time. But if the frozen tissue is warmed enough to create a reliquidified environment in which nanorobots can operate effectively, physical structure is gradually destroyed. One general approach, called "**Plan A**" or "conventional cell repair" (Chapter 4), is to scan and record all relevant physical structure while the cryopreserved patient is still in the solid state, then to warm the patient sufficiently to allow rapid extraction of all metabolic and degradative molecules and quickly establish complete biostasis at the higher temperature, after which conventional medical nanorobots can be introduced to comprehensively restore at the subcellular level the previously recorded original physical structure, with necessary corrections.

This Chapter describes a second general approach, called "**Plan B**" or "molecular reconstruction". Cryopreserved tissue at cryogenic temperature is literally as hard as solid rock, making nanorobotic locomotion prohibitively energy-intensive. But cryogenic solid materials can be disassembled or assembled atom by atom using the techniques of mechanosynthesis[1922] – the emerging technology of positionally-controlled site-specific mechanically-driven single-atom chemical reactions (Section 1.3.1). In Plan B, subtractive mechanosynthesis can be used to abstract one atom (or one small chemical moiety such as a methyl ($–CH_3$) or amino ($–NH_2$) group) at a time from a specific site on the patient's physical structure (Section 5.2.1.2); additive mechanosynthesis can also be used to donate one atom (or one small chemical moiety) at a time to a specific site. Recording the identity and precise location of every atom as it is removed or added creates an atomically-precise map of the entire cryopreserved body. The cryopatient's physical structure is then known to a resolution of ~0.1 nm, which is roughly 1000-fold more detailed than the ~100 nm resolution potentially available using Plan A. This is the best resolution that is physically obtainable and virtually guarantees that all available structural information is captured and retained. After the initial scan data has been processed and corrected to eliminate medical flaws, the patient's body can be reconstructed using the corrected scan data.

After nonstructural bulk materials (e.g., frozen fluid in frozen veins) is extracted from the cryopreserved patient's body (Section 5.1), there are two broad pathways to revival that can be followed, depending on the philosophical preferences (and financial means) of the patient:

(1) **Destructive Scan and Molecular Reconstruction of a Replacement Body** (Section 5.2). In a destructive molecular scan (Section 5.2.1), the patient's cryopreserved body is disassembled atom by atom, the precise location and type of atom is recorded in a data file, and the atoms are discarded as the process unfolds. After the initial scan file is digitally corrected to incorporate all necessary medical repairs (Section 5.2.2), a new replacement body is manufactured via 3D printing that is a near-exact copy of the original cryopreserved body, but incorporating the specified repairs (Section 5.2.3). This pathway appears to be somewhat faster and less expensive.

(2) **Nondestructive Scan and Molecular Reconstruction of the Original Body** (Section 5.3). In a nondestructive molecular scan (Section 5.3.1), the patient's cryopreserved body is temporarily progressively separated into its constituent atoms or molecules, a small piece at a time, during which the precise location and type of each atom is recorded in a data file, after which the same atoms are carefully reassembled back into the original molecules, and the original molecules are reassembled back into their original positions, maintaining the original physical cryopreserved body, completely intact. At any time

---

[1922] Freitas RA Jr., Merkle RC. A minimal toolset for positional diamond mechanosynthesis. J Comput Theor Nanosci. 2008;5:760-861; http://www.molecularassembler.com/Papers/MinToolset.pdf.

during the proposed nondestructive scan, fully 99.99999% of the patient's solid body is undisturbed while only one thin tissue slice ~200 nm thick is being processed at a time, over a period of ~10 sec. Successive slices are then scanned in turn, resulting in a 39-month total scan time. Faster processing times are available by adding additional scan slices, simultaneously processed. The initial scan file that results from this process is then digitally corrected to incorporate all necessary medical repairs (Section 5.3.2). Finally, the original cryopreserved body is repaired by repeating the nondestructive molecular scan, this time inserting the digital corrections incorporating all necessary medical repairs (Section 5.3.3). This pathway appears to be somewhat slower and more expensive than the destructive pathway.

5.1 Extract Nonstructural Bulk Materials

The first phase of a molecular reconstruction is to extract from the body all non-tissue and other loose matter that can later be replaced with fresh bulk materials. These items are not components of the patient's physical structure and make no essential contribution to structural integrity at the molecular scale, or to memory and personal identity, hence there is no need to retain or to map them to atomic precision. Their extraction reduces the total number of molecules that must be precisely mapped and later precisely repaired or replaced. Additionally, the removal process produces a coarse mapping of all interior void spaces that can provide a guide for the more precise atomically-precise mapping that is yet to come.

The bulk extraction process may proceed as follows:

(1) **Millimeter Vascular Scan** (Section 4.1). In a cryopreserved patient stored at ~77 K (-196 °C), noninvasively scan and map all major blood and lymphatic vessels down to 0.1 mm (100 μm) in diameter.

(2) **Large Vessel Excavation** (Section 4.2). Employ nanorobots or other suitable macroscale technical means to mechanically excavate interior ice from all major blood and lymphatic vessels down to 0.1 mm (100 μm) in diameter, an estimated excavation volume of V_{LVE} ~ 6449 cm^3 when a ~0.1 mm resolution map has been compiled.

(3) **Microvascular Scans** (Section 4.3). Scan and map the blood and lymphatic microvasculatures, including all arterioles, venules, capillary beds, and lymphatic precollecting ducts, to micron resolution.

(4) **Microvascular Excavations** (Section 4.4). Employ nanorobots to mechanically excavate interior ice from all blood and lymphatic microvasculatures and void spaces between ice crackfaces, an estimated V_{ME} ~ 3451 cm^3 of additional capillary and crackface void volume to be excavated (Section 4.4.1).

(5) **Organ System Excavations**. Employ nanorobots to mechanically excavate interior ice from the interior gas or fluid volumes of the lungs (~4800 cm^3), gastrointestinal tract (~2600 cm^3), urinary bladder (~500 cm^3), heart (~450 cm^3), kidney (~270 cm^3), spleen (~150 cm^3), the ventricular system of brain and spine (~150 cm^3), gall bladder (~50 cm^3), synovial fluid capsules in joints (~50 cm^3), and the aqueous humor of the eyes (~27 cm^3),[1923] an additional excavation volume of V_{OSE} ~ 9047 cm^3 requiring nanorobotic resources and excavation times comparable to the two prior excavations combined. These excavations are done primarily to avoid the need to process informationally redundant bulk fluids during

[1923] Freitas RA Jr. Nanomedicine, Volume I: Basic Capabilities, Landes Bioscience, Georgetown TX, 1999, Table 8.9, "Mass, Volume, and Scale Size of the Organs of the Human Body"; http://www.nanomedicine.com/NMI/Tables/8.9.jpg.

molecular reconstruction, which would be wasteful of time, energy, and manufacturing resources. All bulk substance removed in this manner can be restored during the whole-body fluid check, either as original or freshly manufactured material according to preference (Section 4.13.3).

(6) **Clear Excavation Debris** (Section 4.5.1). Clear excavation debris from all exposed ice surfaces.

The aforementioned processes will have removed a total of $V_{NBM} = V_{LVE} + V_{ME} + V_{OSE} \sim 18{,}947\ cm^3$ of nonstructural bulk materials from the standard 70 kg human body of volume $V_{body} \sim 60{,}000\ cm^3$, leaving a molecular scan volume of approximately $V_{MSV} = V_{body} - V_{NBM} = 41{,}053\ cm^3$.

With (mostly) only structural features remaining, the cryopreserved patient is now ready for a full molecular scan, which may be either destructive (Section 5.2.1) or nondestructive (Section 5.3.1).

5.2 Molecular Reconstruction of a New Replacement Body

The most accurate molecular reconstruction of a fully repaired and healthy human body requires comprehensive high quality information on the atomic structure of the cryopreserved patient's body. This information can be acquired the most quickly, and at lowest cost, using a destructive molecular scan.

In a destructive molecular scan (Section 5.2.1), the patient's cryopreserved body is disassembled atom by atom. The precise location and type of every atom is recorded in a data file. Once removed, atoms can be discarded because all atoms of a given element (of the same isotope) are absolutely identical, hence retaining the original atoms is not strictly necessary for manufacturing the replacement body. Atoms of the required elements from any source will produce an identical physical structure from a given molecular plan. Eliminating the necessity to individually retain, index, track, and re-use the original atoms after a molecular scan, and during the fabrication process, reduces the complexity of the manufacturing process. Once scanned and recorded, the original atoms can be discarded in the most expeditious manner available, probably involving convenient bulk waste material handling. A reconstruction process that requires retention of the original atoms for fabrication, after scanning, is considerably more complex (Section 5.3), but may nonetheless be preferred by patients who believe that discarding the original body is technically risky or philosophically objectionable, despite its additional complexity and cost.

Note that a destructive scan must work flawlessly on the first pass because the original tissue is destroyed in the scanning process. There is no possibility of a do-over if mistakes are made. As a result, the means of data collection, data transmission, data storage, and follow-up computational analysis must all be extremely reliable or some data could be irretrievably lost, an event that varies in severity of consequences depending on what is lost.

A molecular scan allows acquisition of the greatest possible amount of information on the atomic structure of a cryopreserved patient's body. But the patient's body includes a multitude of structural faults that must be corrected, along with data that can be harmlessly compacted (Section 5.2.2). Once the initial scan file has been compiled, it may be useful to eliminate redundant information to reduce data storage and computational requirements, perhaps by eliminating the precise positions of all water molecules (which can be inferred from other data) or by compacting the atomic descriptions of all nonwater molecules. The file must also be corrected by computationally repairing specific medical flaws, including many of the sources of damage caused by the patient's original fatal illness and by the cryoprotective process itself (Chapter 3).

With the corrected scan file in hand, a print file may be created to drive the chosen fabrication process for manufacturing the replacement patient body (Section 5.2.3), of which there are at least four major variants: **Cryogenic 3D Atomic Print** (Section 5.2.3.1), **Cryogenic 3D Molecular Print** (Section 5.2.3.2), **Fluidic 3D Cell Print** (Section 5.2.3.3), and **Virtual 3D Bit Print**, aka. "uploading" (Section 5.2.3.4).

5.2.1 Destructive Molecular Scan

The revival team can perform a **destructive scan** of the molecular scan volume $V_{MSV} = V_{body} - V_{NBM} =$ 41,053 cm^3 of the cryopreserved patient's solid-state body at cryogenic temperatures ($T_{LN2} = 77$ K). During this scan, the body is taken apart atom by atom, breaking many covalent bonds in the process. The identity and 3D position of each atom is recorded as it is removed, after which the removed atom is discarded. The compiled result of this process is a whole-body map of the cryopreserved patient's molecular structure at atomic or near-atomic resolution, called the "initial scan file".

The removal of each atom requires the scission of a covalent bond that previously bound the removed atom to the rest of the patient's body. This creates a highly reactive radical site at the molecular location where the atom was removed. If this process is not conducted under vacuum conditions, ambient contaminant atoms or molecules may chemically react at the radical site, bonding to the molecular site previously vacated by the removed atom and making it difficult to distinguish native atoms from contaminant atoms – and requiring the subsequent removal of the contaminant atoms. Temporarily capping the radical by adding a known passivating atom after atom removals will require detachment and reattachment of the capping atom before and after each atom removal operation, tripling the number of mechanosynthetic operations and increasing the probability of error. These difficulties are further complicated if two radicals are created during an atom removal from a workpiece.

Ambient poisoning of the molecular radical site can occur very rapidly. For example, the minimum lifetime of a radical site in an atmospheric environment may be estimated as the time required for a binding event to occur as a function of the molecular impingement rate,[1924] which for ambient pressure $P_{atm} = 1$ atm is given by: $t_{radical} \sim (N_{encounters} / A_{radical}\ n_{gas}\ P_{atm}) (\pi\ MW_{kg} / 2\ k_B T\ N_A)^{1/2} =$ **7.2×10^{-8} sec**, where a carbon radical site created by the breaking of a C-C bond of length $L_{C\text{-}C} = 0.154$ nm has cross-sectional area $A_{radical} \sim L_{C\text{-}C}^2 \sim 0.0237\ nm^2$, the number density of ideal gas molecules in a gaseous ambient atmospheric environment is $n_{gas} = N_A / R_{gas}\ T_{gas} = 2.45 \times 10^{25}$ molecules/m^3-atm at temperature $T_{gas} = 300$ K (27 °C), taking $N_{encounters} \sim 10$ random molecule-radical encounters required for a binding event, $MW_{kg} = 0.028$ kg/mole for N_2 which is the most abundant molecule in air, $k_B = 1.381 \times 10^{-23}$ J/K (Boltzmann constant), universal gas constant $R_{gas} = 8.206 \times 10^{-5}$ m^3-atm/mole-K, and $N_A = 6.023 \times 10^{23}$ molecules/mole (Avogadro's number).

Radical lifetime can be greatly extended by performing the destructive molecular scan in a vacuum environment. Driving the probability of radical site poisoning down to one radical in a billion ($p_{poison} \sim 10^{-9}$/atom) at a molecular scan rate of $r_{removal} \sim 10^6$ atoms/sec requires a radical site lifetime of $t_{radical} \sim (p_{poison}\ r_{removal})^{-1} \sim 1000$ sec, which for cryogenic operation at T = 77 K (-196 °C) requires a vacuum pressure of $P_{atm} \sim 10^{-12}$ atm (~10^{-9} torr, ~10^{-9} mbar, ~10^{-7} Pa). This is about 1000-fold better than the 10^{-9} atm used in commercial vacuum tubes[1925] but well within the pressure range of high vacuum (10^{-6}-10^{-12} atm)[1926] and ultrahigh vacuum (UHV)[1927] laboratory systems (10^{-12}-10^{-15} atm)[1928] as found in high-quality research equipment and on the lunar surface (~3×10^{-15} atm).[1929]

[1924] Freitas RA Jr. Nanomedicine, Volume I: Basic Capabilities, Landes Bioscience, Georgetown TX, 1999; Section 4.2.1, "Broadband Receptor Arrays", http://www.nanomedicine.com/NMI/4.2.1.htm#p8.

[1925] https://en.wikipedia.org/wiki/Vacuum_tube#Vacuum.
[1926] https://en.wikipedia.org/wiki/Vacuum#Measurement.
[1927] https://en.wikipedia.org/wiki/Ultra-high_vacuum.
[1928] https://en.wikipedia.org/wiki/Vacuum#Measurement.
[1929] https://en.wikipedia.org/wiki/Atmosphere_of_the_Moon.

Future research should determine whether continuous vacuum pumping will be required throughout the entire molecular scan procedure, since the excavated cryopreserved body cannot be subjected to the customary high-temperature bakeout process[1930] to prevent outgassing[1931] but must be maintained at cryogenic temperatures for the duration. The main sources of UHV outgassing are plastics, elastomers, glues, porous ceramics and porous metals, most lubricants and heat transfer greases, and human fingerprints, hair, skin cells, dust, and food. The most predominant gases or vapors outgassing from surfaces are water vapor, oil and grease vapor, solvents, and organic materials. In the most rarified range of UHV, the stainless steel used to manufacture much of the chamber itself outgasses hydrogen and carbon monoxide to some degree.[1932] All of the outgassed molecules except H_2 will be either solids or liquids at 77 K (-196 °C), hence susceptible to cold-trapping,[1933] which should minimize radical site poisoning inside the cryogenic molecular scanning chamber.

Water-ice represents nearly 99% of all molecules in the cryopreserved patient and can sublimate directly to vapor at low enough pressures, a process akin to freeze-drying[1934] that was once proposed as a possible means of rapid dehydration of cryopatients during revival.[1935] At the glass transition temperature of T_g ~ 150 K (-123 °C), pure ice has a saturation vapor pressure of $P_{svpH20} \sim 10^{-5}$ Pa and will sublimate at a rate of $\chi_{icesublime} \sim 10^{-5}$ kg/m^2-hr at lunar UHV pressures,[1936] or $x_{icesublime} = \chi_{icesublime} / \rho_{ice150K} \sim$ **0.26 µm/day**, taking ice density[1937] $\rho_{ice150K} \sim 930$ kg/m^3.[1938] However, at the normal cryopreservation temperature of $T_{LN2} = 77$ K ($< T_g$) the pure ice saturation vapor pressure falls to $P_{svpH20} \sim 10^{-17}$ Pa with a sublimation rate of $\chi_{icesublime} \sim 10^{-12}$ kg/m^2-hr,[1939] or $x_{icesublime} = \chi_{icesublime} / \rho_{ice77K} \sim$ **2.6 x 10^{-8} µm/day** (~0.01 nm/year, taking ice density

---

[1930] https://en.wikipedia.org/wiki/Bake-out.
[1931] https://en.wikipedia.org/wiki/Ultra-high_vacuum#Outgassing.
[1932] https://www.accuglassproducts.com/outgassing.
[1933] https://en.wikipedia.org/wiki/Cold_trap.
[1934] https://en.wikipedia.org/wiki/Freeze-drying).

[1935] Fahy G. Appendix B. A "Realistic" Scenario for Nanotechnological Repair of the Frozen Human Brain. In: Wowk B, Darwin M, eds., Cryonics: Reaching for Tomorrow. Alcor Life Extension Foundation, 1991, pp. A-10 – A-26; "The Repair Scenario. III. Excavating the Extracellular Space"; https://alcor.org/Library/html/nanotechrepair.html.

[1936] Andreas EL. New estimates for the sublimation rate for ice on the Moon. Icarus 2007 Jan;186(1):24-30; https://people.nwra.com/resumes/andreas/publications/Icarus_Moon.pdf.

[1937] https://en.wikipedia.org/wiki/Water_(data_page)#Liquid_physical_properties.

[1938] The papers by Kramers and Stemerding[*] and Andreas[†] describing the sublimation of ice in vacuum appear to report rates about three orders of magnitude higher than the paper by Clow *et al.*[‡] describing the sublimation of Antarctic ice in air. Assuming no methodological errors in the three papers, Wowk[**] speculates that the difference in sublimation rates might be related to a boundary layer of vapor pressure gradient at the surface of the ice that can't exist in a big unconfined vacuum. This suggests that schemes for sublimating ice *in-situ* inside excavated cryogenic tissue microcaverns could be very sensitive to gas composition and pressure within those caverns, including the pressure of the evolved water vapor itself which would be dependent upon the strategies for removing it. ***Future research*** should resolve this issue, perhaps including some study of the vacuum freeze-drying literature, other relevant literature sources, additional theoretical analyses, and direct experimental measurements if necessary.
[*] Kramers H, Stemerding S. The sublimation of ice in vacuum. Appl Sci Res. 1951 Apr;A3:73-82; http://www.personal.psu.edu/mrh318/Kramers-Stemerding-ASRS-1951.pdf.
[†] Andreas EL. New estimates for the sublimation rate for ice on the Moon. Icarus 2007 Jan;186(1):24-30; https://people.nwra.com/resumes/andreas/publications/Icarus_Moon.pdf.
[‡] Clow GD, McKay CP, Simmons GM Jr, Wharton RA Jr. Climatological observations and predicted sublimation rates at Lake Hoare, Antarctica. J Clim. 1988 Jul;1(7):715-728; https://journals.ametsoc.org/jcli/article-pdf/1/7/715/3748674/1520-0442(1988)001_0715_coapsr_2_0_co_2.pdf.
[**] Personal communication from Brian Wowk to Robert Freitas, 30 Sep 2021.

[1939] Andreas EL. New estimates for the sublimation rate for ice on the Moon. Icarus 2007 Jan;186(1):24-30; https://people.nwra.com/resumes/andreas/publications/Icarus_Moon.pdf.

ρ_{ice77K} ~ 935 kg/m^3), representing a negligible sublimation rate of about one 0.2-nm atomic monolayer of ice every 21 years at lunar UHV pressures.

5.2.1.1 Abstraction of Water Molecules

Water molecules should comprise nearly ~99% of all molecules present in the bulk-excavated (Section 5.1) body of the cryopreserved human patient (image below, left), so the removal of water may be the most common molecular removal operation in this revival protocol. Water is a charge-polarized molecule, so water molecules in ice form a regular 3D lattice (image below, right) in which the slightly negative oxygen atoms (in red) are attracted to neighboring slightly positive hydrogen atoms (in white), forming networks of relatively weak hydrogen bonds.

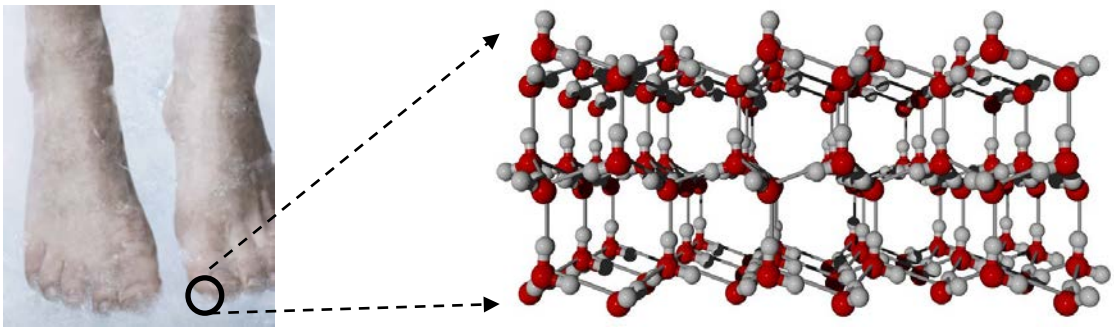

One simple method for removing a molecule of ice from its lattice is to move a mechanosynthetic tool into the vicinity of a specific single molecule of water, lower the tool toward the lattice until the active tip of the tool covalently bonds with the targeted water molecule, then retract the mechanosynthetic tool from the lattice, ripping the whole water molecule out of the lattice. The extracted water molecule can then be carried off elsewhere for disposal.

Future research must fully investigate the best tool for this purpose – an exercise that lies beyond the scope of this book – but a simple quantum chemistry simulation can demonstrate the basic feasibility of this approach. An exemplar molecular tool (below, left) consists of a 6-carbon ring on the right side with two C=C double bonds above and below and a carbene radical (C:) on the carbon atom (in black) at farthest right. A carbene radical can form two covalent bonds to other atoms. The ring is attached to an adamantane cage, the smallest possible chunk of diamond, on the left side. This cage is readily attached to a larger diamondoid handle structure that is capable of convenient 3D positional motion control. The target water molecule (H_2O) is at right.

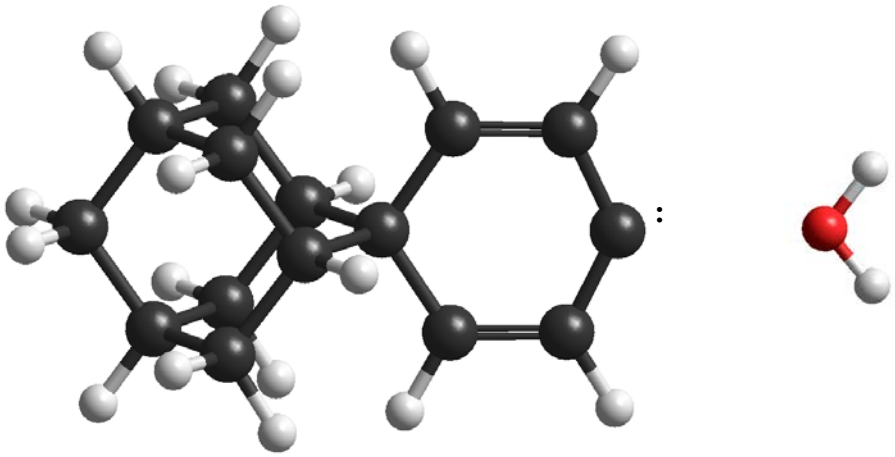

When the carbene[1940] radical tool approaches the water-ice molecule, one reaction that can occur is that a hydrogen atom (H) in the water bonds to the first radical site on the carbene, and the remaining two atoms (OH) bond to the second radical site on the carbene (see below). A simple quantum chemistry simulation of this reaction using Density Functional Theory (DFT)[1941] and the standard 6-31G* basis set[1942] with the popular B3LYP exchange correlation functional[1943] (but no zero-point correction[1944]) using the Gaussian software package[1945] indicates that this reaction is strongly energetically favorable (exoergic) by -2.99 eV (479 zJ).[1946] No further examinations of possible pathological alternative reactions, tool stability, spin multiplicities, normal mode analysis or higher levels of theory have yet been made, but this operation is illustrative of the likely UHV mechanosynthetic capabilities of properly designed molecular abstraction tools.

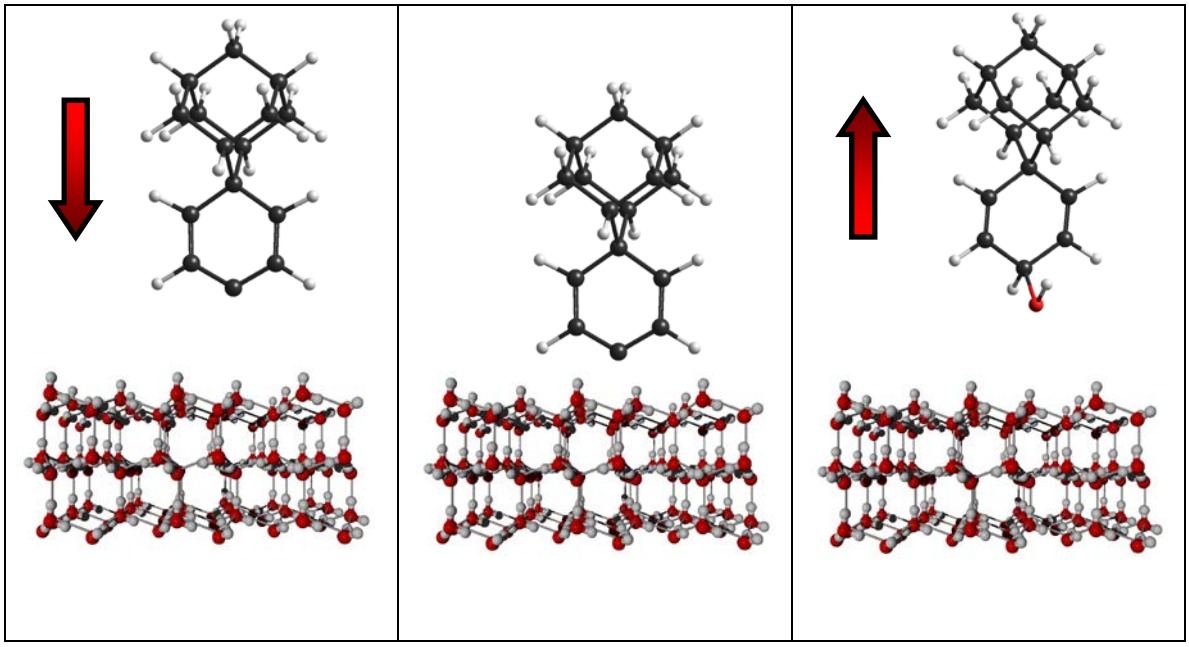

After completing the aforementioned water molecule abstraction reaction and recording the exact 3D position of the removal site, the carbene tool is transferred to an analysis bay where chemical sensors[1947] confirm the identity of the attached water molecule. The tool is then transferred to a recharge station

---

[1940] https://en.wikipedia.org/wiki/Carbene.
[1941] https://en.wikipedia.org/wiki/Density_functional_theory.
[1942] https://en.wikipedia.org/wiki/Basis_set_(chemistry)#Pople_basis_sets.
[1943] https://en.wikipedia.org/wiki/Hybrid_functional#B3LYP.

[1944] Foresman JB, Frisch A. Exploring Chemistry with Electronic Structure Methods, Second Edition, Gaussian Inc., Pittsburgh PA; 1996, pp. 68-69; https://www.amazon.com/dp/0963676938/.

[1945] https://en.wikipedia.org/wiki/Gaussian_(software).

[1946] Note that about +0.51 eV (49.4 kJ/mole), the sublimation enthalpy of ice at 77 K,* is the energy that must be added to a water molecule that is hydrogen-bonded to the ice lattice surface in order to remove it to the vapor phase.
* Feistel R, Wagner W. Sublimation pressure and sublimation enthalpy of H_2O ice Ih between 0 and 273.16 K. Geochim et Cosmochim Acta. 2007 Jan 1;71(1):36-45; http://www.personal.psu.edu/mrh318/Feistel-Wagner-GCA-2007.pdf.

[1947] Freitas RA Jr. Nanomedicine, Volume I: Basic Capabilities, Landes Bioscience, Georgetown TX, 1999; Section 4.2, "Chemical and Molecular Sensors", http://www.nanomedicine.com/NMI/4.2.htm.

where, with the application of additional mechanosynthetic reactions and the likely addition of ~479 zJ of reaction energy, the water molecule is removed from the carbene, restoring the molecular tool to its previous active state. The carbene tool is then returned to service, allowing it to participate in another cycle of operation, while the abstracted water molecule is discarded to an external dump.

Some ions and additional small molecules such as isolated amino acids, glucose, and the like may also be visible and identifiable, hence extractable *in situ* by similar means. Such targets should be enumerated and quantified, and molecular abstraction tools for all such targets should be designed and simulated in ***future research***. Most biomolecules will be much larger, though fewer in number, and will require special handling as described later (Section 5.2.1.2).

Carbene radical tools may be applied to the icy surfaces of the cryopreserved patient using an array of molecular manipulators (image, below) with a 100 nm x 100 nm lateral range of motion and a central tool handling volume through which carbene and other tools may be transported.[1948]

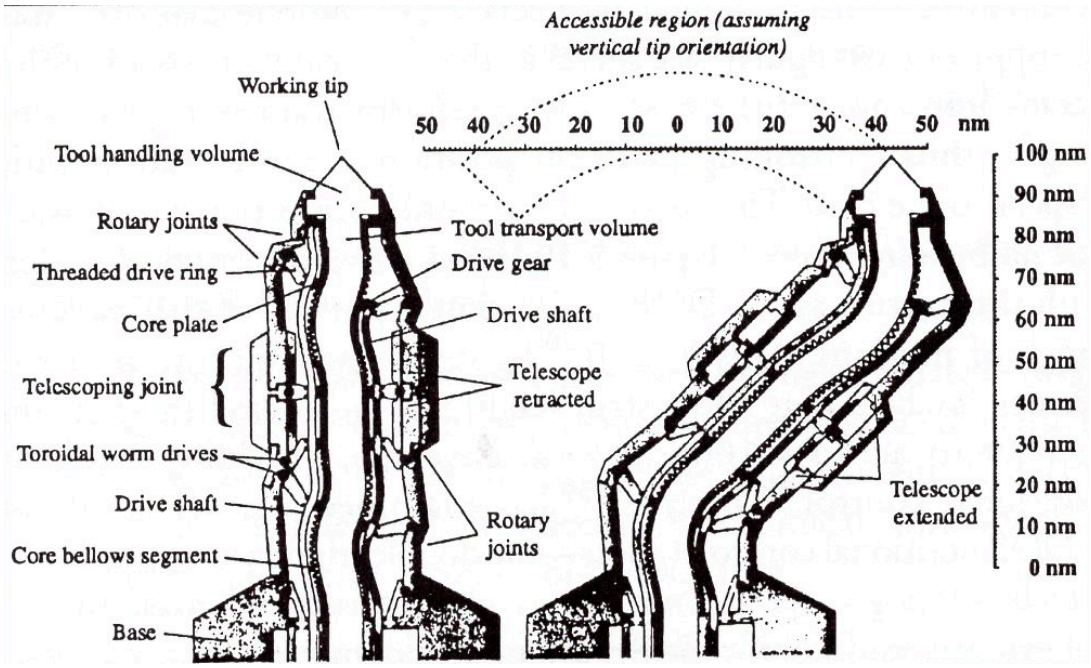

The one-way tool path down through the body of the manipulator is ~100 nm long, so the minimum time required to exchange a water-laden carbene tool with a fresh active carbene tool is **~0.2 µsec**, assuming an internal transport speed of ~1 m/sec, because a new tool must wait for the old one to exit the nanomanipulator before it can enter the 7 nm diameter tool transport volume and be reinstalled within the tool handling volume at the apex of the device. The manipulator can move between adjacent 77 K water-ice molecules separated by an average of x_{IceSep} = 0.32 nm in the lattice,[1949] assuming a conservative lateral

---

[1948] Freitas RA Jr. Nanomedicine, Volume I: Basic Capabilities, Landes Bioscience, Georgetown TX, 1999, Fig. 9.8; http://www.nanomedicine.com/NMI/Figures/9.8.jpg. Adapted from: Drexler KE. Nanosystems: Molecular Machinery, Manufacturing, and Computation, John Wiley & Sons, New York, 1992, Section 13.4.1, "A bounded-continuum design for a stiff manipulator"; https://www.amazon.com/dp/0471575186/.

[1949] $x_{IceSep} = (MW_{ice} / \rho_{ice77K} N_A)^{1/3}$ = 0.32 nm, taking water-ice molecular weight MW_{ice} = 0.018 kg/mole, density of 77 K ice ρ_{ice77K} ~ 935 kg/m^3, and N_A = 6.022 x 10^{23} molecules/mole (Avogadro's number).

speed of ~1 cm/sec, in ~**0.032 µsec**, dissipating $P_{manipulator}$ ~ 0.1 pW of power while in continuous motion at a ~1 MHz operating frequency.[1950]

A typical mechanosynthetic reaction requires nanoseconds or less to run to completion, so allowing ~**1 µsec** per abstraction operation seems plausible as an initial performance target, yielding a water-ice abstraction rate of $\mathfrak{A}_{water}$ ~ 10^6 molecules/sec and a water molecule volumetric clearance rate of $\mathfrak{V}_{IceClear}$ = $x_{IceSep}^3 \mathfrak{A}_{water}$ ~ 32,768 nm^3/sec for each nanomanipulator system. There would be $N_{IcePlane} = A_{manip} / x_{IceSep}^2$ ~ 100,000 ice molecules comprising each 0.32 nm thick layer of ice underneath the $A_{manip} = H_{manip}^2$ = 10,000 nm^2 work area of a nano-manipulator with H_{manip} = 100 nm of accessible horizontal space, assuming a field of solid ice.

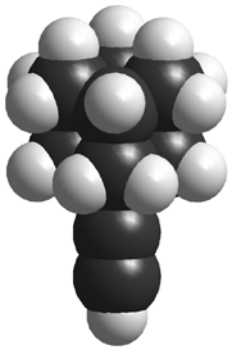

It is also necessary to inspect the abstraction site to determine which molecules are located where, in part to determine the location of water molecules to be abstracted because the carbene radical tool could abstract atoms from nonwater molecules if mispositioned. In a typical inspection cycle, the nanomanipulator described above may be provisioned with an appropriate molecular inspection tool (possibly an atomically sharp tip such as the HAbst-H molecule;[1951] image, left), requiring ~0.4 µsec for the toolhead round trip through the body of the nanomanipulator. If the entire 10^4 nm^2 surface accessible to the tool is raster-scanned to determine the positions and probable atomic composition of all visible molecules (using methods described in Appendix F), and if successive scan lines are 0.01 nm (10 pm) apart with ~10,000 scan lines each 100 nm in length, this gives a total continuous scanline length of 10^6 nm (1 mm). (A singly-bonded carbon atom is 0.154 nm, or 154 pm, in diameter.) A tip scan speed of ~1 cm/sec[1952] implies a total inspection time of ~**0.1 sec**, about the same as the $N_{IcePlane} / \mathfrak{A}_{water}$ ~ **0.1 sec** abstraction time for an entire 0.32 nm thick ice layer underneath the nanomanipulator's 10^4 nm^2 scan area, assuming a field of solid ice.

Alternatively, a square inspection area of 0.32 nm x 0.32 nm covering one water molecule requires a continuous scanline length of (0.32 nm) (0.32 nm / 0.01 nm) ~ 10 nm producing an inspection time of (10 nm) / (1 cm/sec) ~ **1 µsec**, similar to the ~1 µsec water molecule abstraction time. If every abstraction operation requires a site inspection operation, this effectively halves the operating frequency, reducing the net water abstraction rate to only ~0.5 $\mathfrak{A}_{water}$ ~ 0.5 x 10^6 molecules/sec and the net water molecule volumetric clearance rate to only $\mathfrak{V}_{IceRemoval}$ = 0.5 $\mathfrak{V}_{IceClear}$ ~ **16,384 nm^3/manipulator-sec**.

5.2.1.2 Positional Disassembly of Biomolecules

Most biomolecules comprising the human body are lengthy chains, or polymers, of simpler monomeric molecules such as amino acids (in proteins), sugars (in carbohydrates), nucleic acids (in DNA and RNA),

---

[1950] Freitas RA Jr. Nanomedicine, Volume I: Basic Capabilities, Landes Bioscience, Georgetown TX, 1999, Section 9.3.1.4, "Telescoping Manipulators"; http://www.nanomedicine.com/NMI/9.3.1.4.htm.

[1951] Freitas RA Jr., Merkle RC. A minimal toolset for positional diamond mechanosynthesis. J Comput Theor Nanosci. 2008;5:760-861; http://www.molecularassembler.com/Papers/MinToolset.pdf.

[1952] "Lateral tip speeds of 5 mm/s can be achieved with full feedback on surfaces with significant roughness…higher speed MEMS scanners...are currently under development." Disseldorp EC, Tabak FC, Katan AJ, Hesselberth MBS, Oosterkamp TH, Frenken JWM, van Spengen WM. MEMS-based high speed scanning probe microscopy. Rev Sci Instrum. 2010 Apr;81(4):043702; https://pdfs.semanticscholar.org/3863/c8311d544c1e635f79985c2941e27c649861.pdf.

or mixtures of these several types (e.g., glycoproteins that combine sugars and amino acids).[1953] Amino acid monomers range in size from glycine at 10 atoms to arginine and tryptophan at 27 atoms. Proteins vary widely in size, but the average human protein is 38.2 KDa[1954] with ~300 covalently bonded amino acid monomers[1955] or "residues" comprising ~3,000 atoms. The glucose dehydrogenase enzyme protein consists of 4 identical subunits totaling 1048 amino acid residues with a molecular weight of 113,408 gm/mole.[1956] Due to hydrogen bonding, chains of amino acids naturally curl up into 3D helices, sheets, and other higher-order "secondary structure".[1957] In the tissues of the cryopreserved patient, these molecules will be embedded in a solid water-ice matrix from which they must be extracted and measured, atom by atom.

An exemplar peptide chain of 10 amino acids, all of them glycine (Gly; image, right), is shown below (C = black, H = white, O = red, N = blue) in its natural alpha helix conformation. This simple peptide may be regarded as a proxy for protein molecules that can illustrate the positional disassembly of biomolecules.

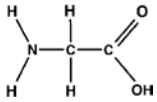

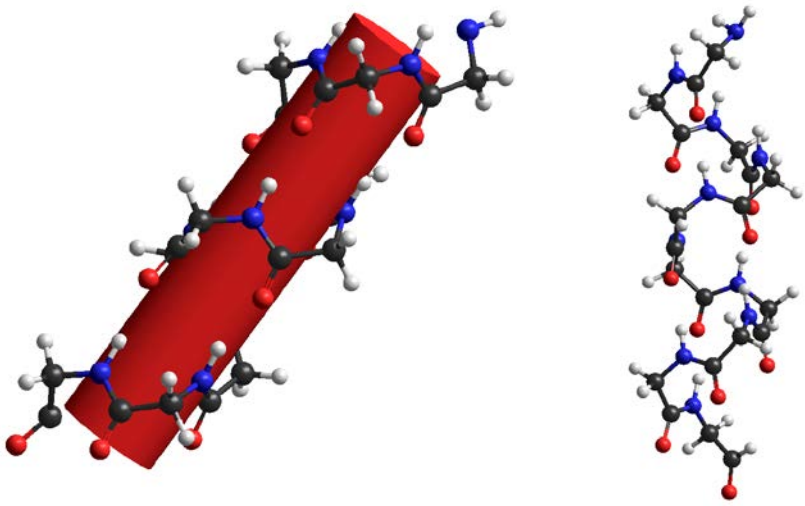

Positional disassembly refers to the atom-by-atom deconstruction of a covalently bonded molecule, while keeping track of the atom type, 3D position, and bonding pattern of each atom that is removed. For a simple illustration of the process, we assume that a single protein molecule is embedded in a lattice of water-ice molecules. As water molecules are successively removed (Section 5.2.1.1) and the workspace surface is reinspected, eventually the first atoms attached to an embedded protein become visible on the surface (top of image below, left). Water molecules continue to be removed near the same site with reinspection, allowing inference of the exact position of the emerging protein molecule in both its current and original fully-embedded state. Eventually a sufficient number of atoms of the embedded protein have been freed from the ice and become available for convenient mechanosynthetic removal (image below,

---

[1953] Lipids are usually not considered polymers but rather oligomers of fatty acids consisting of hydrocarbon $(CH_2)_n$ chains of 5-26 carbon atoms; https://en.wikipedia.org/wiki/Fatty_acid#Length_of_fatty_acids.

[1954] https://incenp.org/notes/2013/average-protein-size.html.
[1955] https://www.sciencedaily.com/terms/protein_structure.htm.

[1956] Jany KD, Ulmer W, Fröschle M, Pfleiderer G. Complete amino acid sequence of glucose dehydrogenase from *Bacillus megaterium*. FEBS Lett. 1984 Jan 2;165(1):6-10; https://core.ac.uk/download/pdf/82592893.pdf.

[1957] https://en.wikipedia.org/wiki/Protein_secondary_structure.

right). Based on inspection results, the probable identity of the exposed protein atoms and their covalent bonding pattern is inferred. A plan for the positional disassembly of the exposed portion of the biomolecule is formulated, employing an ordered sequence of subtractive mechanosynthetic reaction steps.

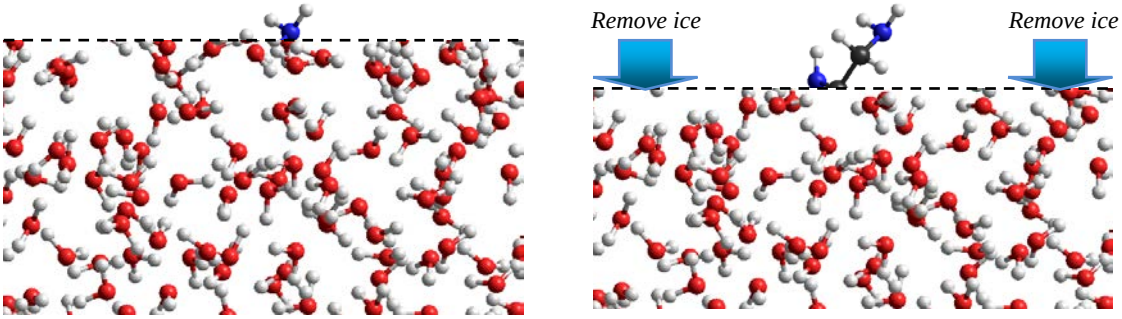

Assuming for illustrative purposes that the first amino acid residue to be exposed is a simple glycine, the positionally controlled disassembly of this molecule may be simulated using Density Functional Theory (DFT)[1958] and the standard 6-31G* basis set[1959] with the popular B3LYP exchange correlation functional[1960] (without zero-point correction[1961]) using the Gaussian software package[1962] in three successive steps, in each case applying the well-studied ethynyl radical-based Hydrogen Abstraction or "HAbst" tool[1963] (●C≡C-$C_{10}H_{15}$) starting at the –NH_2 terminus of a Gly_2 dipeptide for computational convenience. As noted in the previous Section, no further examinations of possible pathological alternative reactions, tool stability, spin multiplicities, normal mode analysis or higher levels of theory have yet been made, but the reactions described below are illustrative of the likely capabilities of properly designed subtractive mechanosynthetic tools and pathways.

Step 1. Remove the NH_2 group

According to the simulation runs, attacking the NH_2 group with the HAbst molecular tool can remove this group in any one of three different ways, all of which are energetically favorable. In Reaction 1-1, the entire NH_2 group is removed. In Reaction 1-2, an H is removed, followed by the remaining NH group. In Reaction 1-3, the atoms are removed one at a time – first an H, then the second H, and finally the N. Examination of the atom(s) captured on the tip of the HAbst tool (images below, far right) will be required to ascertain which of these paths was taken in any particular circumstance. In each case, the position of the tool at the time of abstraction is also known, so the 3D coordinates of the abstracted atom(s) can be recorded with precision.

[1958] https://en.wikipedia.org/wiki/Density_functional_theory.
[1959] https://en.wikipedia.org/wiki/Basis_set_(chemistry)#Pople_basis_sets.
[1960] https://en.wikipedia.org/wiki/Hybrid_functional#B3LYP.

[1961] Foresman JB, Frisch A. Exploring Chemistry with Electronic Structure Methods, Second Edition, Gaussian Inc., Pittsburgh PA; 1996, pp. 68-69.

[1962] https://en.wikipedia.org/wiki/Gaussian_(software).

[1963] Freitas RA Jr., Merkle RC. A minimal toolset for positional diamond mechanosynthesis. J Comput Theor Nanosci. 2008;5:760-861; http://www.molecularassembler.com/Papers/MinToolset.pdf.

Reaction 1-1. Abstract NH_2 group using HAbst tool			–1.70 eV
Reactants		Products	
OH-CO-CH_2-NH-CO-CH_2-NH_2	●C≡C-$C_{10}H_{15}$	OH-CO-CH_2-NH-CO-CH_2●	NH_2-C≡C-$C_{10}H_{15}$
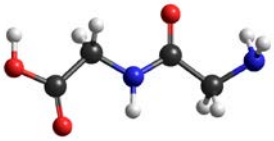	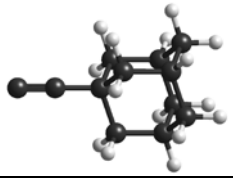	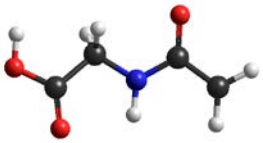	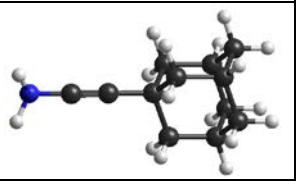

Reaction 1-2A. Abstract H from NH_2 group using HAbst tool			–1.56 eV
Reactants		Products	
OH-CO-CH_2-NH-CO-CH_2-NH_2	●C≡C-$C_{10}H_{15}$	OH-CO-CH_2-NH-CO-CH_2-NH●	H-C≡C-$C_{10}H_{15}$
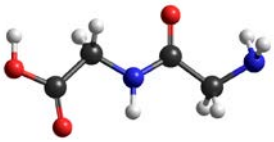	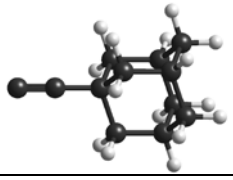	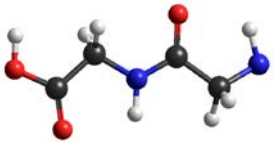	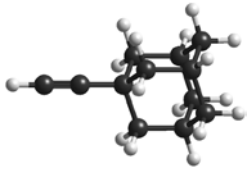

Reaction 1-2B. Abstract NH using HAbst tool			–2.49 eV
Reactants		Products	
OH-CO-CH_2-NH-CO-CH_2-NH●	●C≡C-$C_{10}H_{15}$	OH-CO-CH_2-NH-CO-CH_2●	●NH-C≡C-$C_{10}H_{15}$
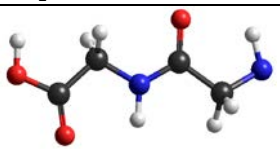	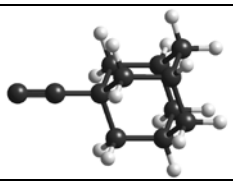	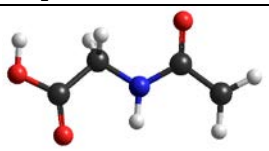	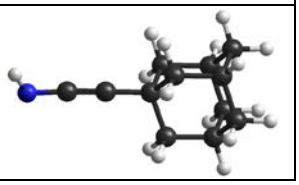

Reaction 1-3A. Abstract H from NH_2 group using HAbst tool			–1.56 eV
Reactants		Products	
OH-CO-CH_2-NH-CO-CH_2-NH_2	●C≡C-$C_{10}H_{15}$	OH-CO-CH_2-NH-CO-CH_2-NH●	H-C≡C-$C_{10}H_{15}$
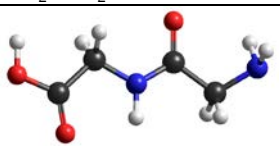	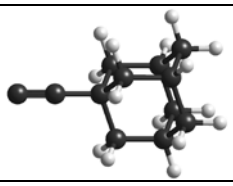	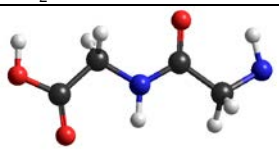	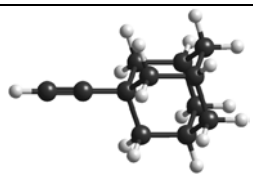

Reaction 1-3B. Abstract H from NH group using HAbst tool			–2.11 eV
Reactants		Products	
OH-CO-CH_2-NH-CO-CH_2-NH●	●C≡C-$C_{10}H_{15}$	OH-CO-CH_2-NH-CO-CH_2-N:	H-C≡C-$C_{10}H_{15}$
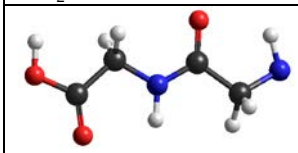	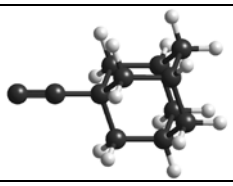	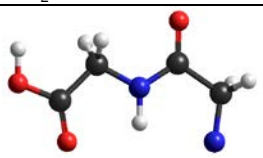	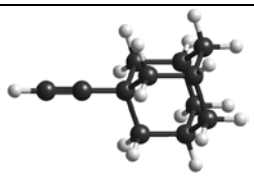

Reaction 1-3C. Abstract N from CH_2 group using HAbst tool			–3.21 eV
Reactants		Products	
OH-CO-CH_2-NH-CO-CH_2-N:	●C≡C-$C_{10}H_{15}$	OH-CO-CH_2-NH-CO-CH_2●	:N-C≡C-$C_{10}H_{15}$
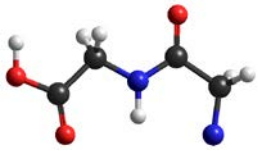	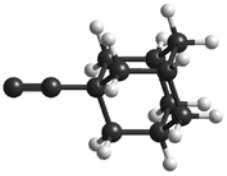	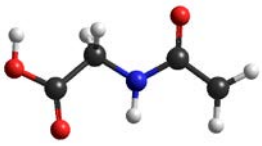	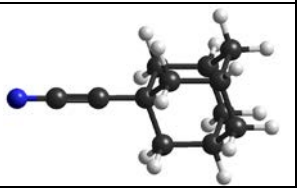

Step 2. Remove the CH_2 group

The HAbst molecular tool can next be used to remove the CH_2 group in these simulation runs in any of three different ways, all of which are again energetically favorable. In Reaction 2-1, the entire CH_2 group is removed. In Reaction 2-2, an H is removed, followed by the remaining CH group. In Reaction 2-3, the atoms are removed one at a time – first an H, then the second H, and finally the C. As before, examination of the atom(s) captured on the tip of the HAbst tool is required to ascertain which of these paths was taken in any particular circumstance, and the 3D coordinates of the abstracted atom(s) at the time of abstraction can be precisely recorded.

Reaction 2-1. Abstract CH_2 group using HAbst tool			–2.13 eV
Reactants		Products	
OH-CO-CH_2-NH-CO-CH_2●	●C≡C-$C_{10}H_{15}$	OH-CO-CH_2-NH-CO●	●CH_2-C≡C-$C_{10}H_{15}$
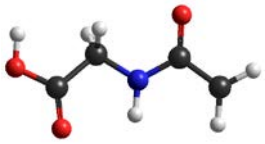	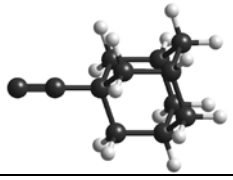	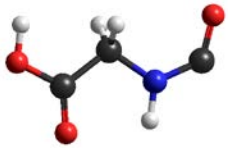	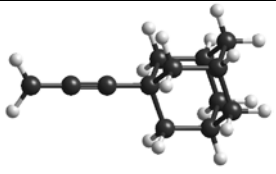

Reaction 2-2A. Abstract H from CH_2 group using HAbst tool			–1.05 eV
Reactants		Products	
OH-CO-CH_2-NH-CO-CH_2●	●C≡C-$C_{10}H_{15}$	OH-CO-CH_2-NH-CO-CH:	H-C≡C-$C_{10}H_{15}$
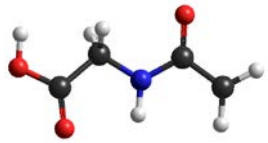	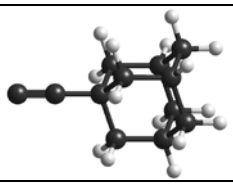	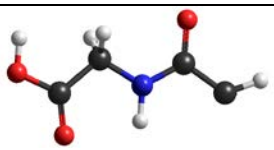	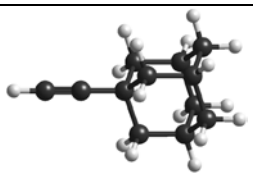

Reaction 2-2B. Abstract CH using HAbst tool			–2.61 eV
Reactants		Products	
OH-CO-CH_2-NH-CO-CH:	●C≡C-$C_{10}H_{15}$	OH-CO-CH_2-NH-CO●	:CH-C≡C-$C_{10}H_{15}$
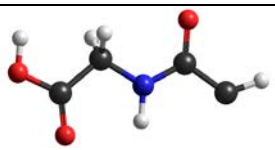	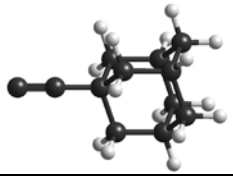	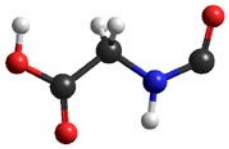	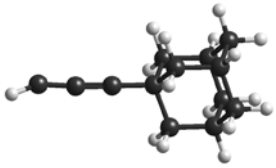

Reaction 2-3A. Abstract H from CH_2 group using HAbst tool			–1.05 eV
Reactants		Products	
OH-CO-CH_2-NH-CO-CH_2●	●C≡C-$C_{10}H_{15}$	OH-CO-CH_2-NH-CO-CH:	H-C≡C-$C_{10}H_{15}$
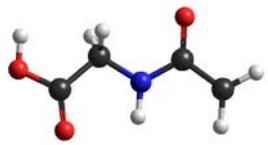	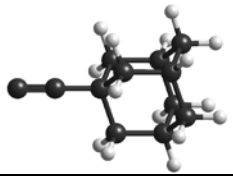	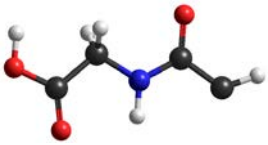	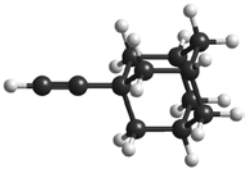

Reaction 2-3B. Abstract H from CH group using HAbst tool			–0.64 eV
Reactants		Products	
OH-CO-CH_2-NH-CO-CH:	●C≡C-$C_{10}H_{15}$	OH-CO-CH_2-NH-CO-C:●	H-C≡C-$C_{10}H_{15}$
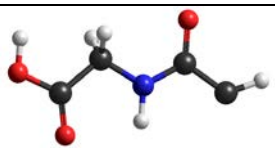	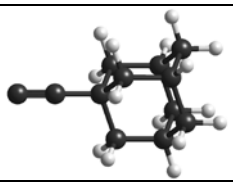	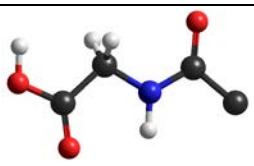	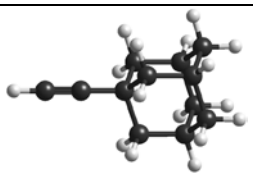

Reaction 2-3C. Abstract C from CO group using HAbst tool			–2.27 eV
Reactants		Products	
OH-CO-CH_2-NH-CO-C:●	●C≡C-$C_{10}H_{15}$	OH-CO-CH_2-NH-CO●	●:C-C≡C-$C_{10}H_{15}$
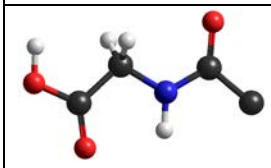	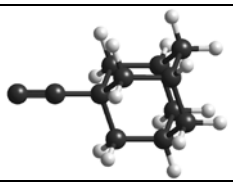	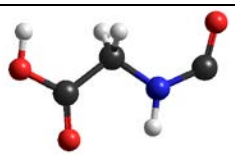	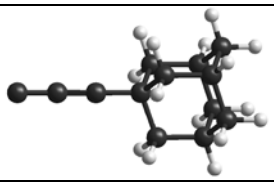

Step 3. Remove the CO group

According to DFT simulations, the CO group can be removed by the HAbst molecular tool with favorable energetics (Reaction 3-1), but the HAbst tool cannot remove the O from the CO group because the reaction energetics are unfavorably uphill (Reaction 3-2). As a final consistency check, the removal of the remaining NH group using an HAbst tool (Reaction 4) is energetically favorable by –2.51 eV, almost exactly the same as the –2.49 eV calculated for the same reaction earlier in the polymer chain (Reaction 1-2B). Again, the precise 3D coordinates of the abstracted atoms can be recorded because the position of the tool at the time of abstraction is known.

Reaction 3-1. Abstract CO group using HAbst tool			–1.32 eV
Reactants		Products	
OH-CO-CH_2-NH-CO●	●C≡C-$C_{10}H_{15}$	OH-CO-CH_2-NH●	●CO-C≡C-$C_{10}H_{15}$
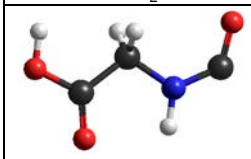	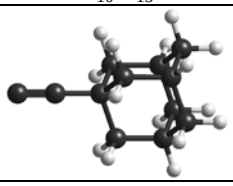	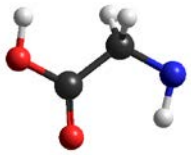	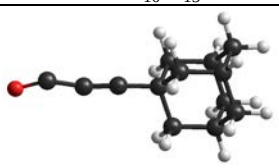

Reaction 3-2. Abstract O from CO group using HAbst tool			+3.44 eV
Reactants		Products	
OH-CO-CH_2-NH-CO●	●C≡C-$C_{10}H_{15}$	OH-CO-CH_2-NH-C:●	●O-C≡C-$C_{10}H_{15}$
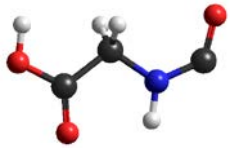	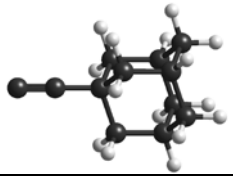	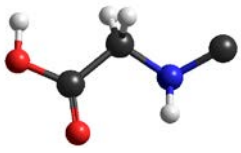	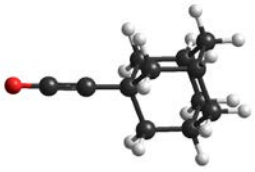

Reaction 4. Abstract second NH group using HAbst tool			–2.51 eV
Reactants		Products	
$OH\text{-}CO\text{-}CH_2\text{-}NH\bullet$	$\bullet C{\equiv}C\text{-}C_{10}H_{15}$	$OH\text{-}CO\text{-}CH_2\bullet$	$\bullet NH\text{-}C{\equiv}C\text{-}C_{10}H_{15}$
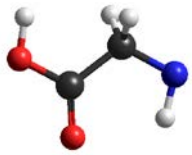	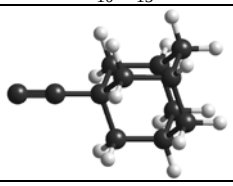	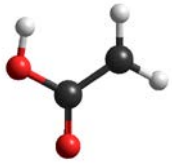	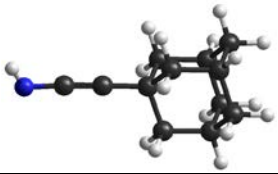

A whole set of useful reactions for the positionally controlled mechanosynthetic disassembly of organic molecules including proteins, carbohydrates, lipids, and others should be designed, simulated, and tested in ***future research***. There are numerous complications and special cases beyond the simple peptide disassembly sequence illustrated above (e.g., how a protein should be disassembled starting from somewhere in the middle of the molecule, rather than at the $–NH_2$ terminus as illustrated here), but it appears likely that similar tools and procedures can be designed to handle these additional situations.

For example, it may frequently occur that a protein emerges from the ice as an inverted U-shaped loop rather than a terminal end, forcing abstraction to be undertaken from mid-strand. When inspection reveals such a situation, one solution may be to deploy a compound molecular tool, possibly combining a GeRad-H tool[1964] and a GeRad tool on a hinged mount that permits 1-DOF (degrees of freedom) actuation and can force the GeRad-H and GeRad either into or out of proximity with each other. After identifying a target break point on the protein chain, a radical site may be created on atoms residing on either side of the break point, e.g., via hydrogen abstraction using an HAbst tool. Two of the compound tools are then brought up to the break point, bonding the GeRad component of each compound tool to one of the two radical sites. The two compound tools are then pulled in opposite directions, breaking the protein chain at the target break point,[1965] but with each of the two separate strands held firmly by the GeRad tool on one or the other of the two compound tools. The actuator on each compound tool then moves its GeRad-H tool into apical contact with its GeRad tool, causing the GeRads on each compound tool bond together, forming a Ge-Ge bond between them and allowing the H from the GeRad-H tool to bond to the radical on the protein strand created by the debonding of the GeRad, passivating that end of the strand on both sides of the break point. There are now two passivated protein half-strands emerging from the embedding ice, and these can be processed as individual strands in the manner previously described.[1966] Given the close packing of large biomolecules in cells, it is likely that many such loops will emerge during scanning and may be fairly close together on the active scan surface. The repair process must keep track of which isolated strands correspond to which loops in different nearby biomolecules.

[1964] A GeRad-H is a germanium radical to which a hydrogen atom is weakly covalently bound, making it a hydrogen donation tool that will readily transfer the H atom to a carbon radical or other radical sites, leaving an active germanium radical or GeRad tool behind. Freitas RA Jr., Merkle RC. A minimal toolset for positional diamond mechanosynthesis. J Comput Theor Nanosci. 2008;5:760-861; http://www.molecularassembler.com/Papers/MinToolset.pdf.

[1965] Two Ge-C bonds have a combined scission force of 2 x 3.64 nN = **7.28 nN** which exceeds the **5.53 nN** C-C bond scission force or even weaker bonds such as C-N in protein chains.* If this proves insufficient to break a C-C bond due to geometric constraints, two SiRad tools could be used in place of the GeRads to create Si-C bonds that would provide an even stronger combined scission force of 2 x 4.4 nN = **8.8 nN**.

* Freitas RA Jr., Merkle RC. A minimal toolset for positional diamond mechanosynthesis. J Comput Theor Nanosci. 2008;5:760-861; http://www.molecularassembler.com/Papers/MinToolset.pdf.

[1966] This proposal has not been rigorously examined using quantum chemistry simulations or other related means, but provides an illustration of one possible procedure that could allow the reliable passivation of both sides of a positionally controlled protein strand break.

It may sometimes be expedient to donate a hydrogen atom to an exposed radical on an intermediate structure during molecular disassembly, passivating the site to temporarily stabilize it. When the focus of activity later returns to that site, the passivating hydrogen can easily be removed, restoring the radical and allowing subsequent disassembly operations to proceed.

After completing each abstraction reaction and recording the exact 3D position of the removal site, the HAbst tool (or alternate molecular tool) is transferred to an analysis bay where chemical sensors[1967] confirm the identity of the attached atom(s). The tool is then transferred to a recharge station where the attached atom(s) are removed with the application of additional mechanosynthetic reactions, restoring the molecular tool to its previously active state.

One example of a three-step **reaction sequence to recharge the HAbst tool** is illustrated below[1968] (Ge = yellow). In the first step, a germanium-substituted adamantane radical (GeRad) tool is brought up to the apical carbon atom of the exhausted HAbst-H tool, forming a covalent Ge–C bond in a reaction that is energetically favorable by -0.43 eV. In the second step, an adamantane radical (AdamRad) tool approaches the H atom to be removed, and the H atom bonds to the carbon radical, breaking the C–H bond on the HAbst-H tool and forming a new H-C bond on the AdamRad with an energy favorability of -0.84 eV. In the third step, the GeRad tool is mechanically pulled away from the HAbst tool, breaking the relatively weak Ge-C covalent bond, requiring a mechanical energy input of +4.81 eV. This operation frees the original GeRad tool and produces a recharged HAbst tool that is ready to perform another abstraction reaction. Alternative recharge reaction sequences that may be required for exhausted HAbst-X tools bearing payloads of "X" other than hydrogen should be pursued in ***future research***.

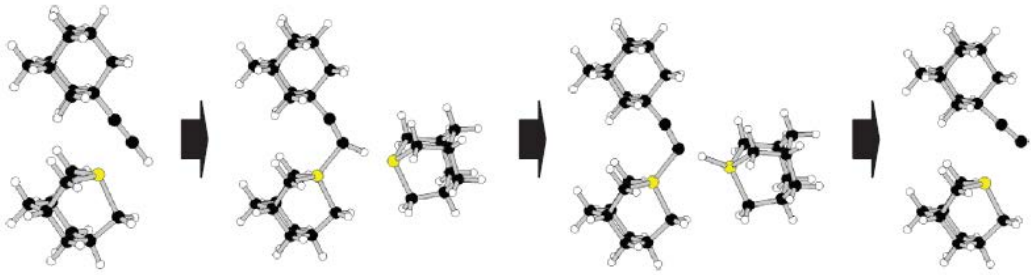

Following recharge, the abstraction tool can be returned to service to participate in another cycle of operation, while the abstracted atom(s) are discarded to an external dump.

After the removal of some number of atoms from the biomolecule has stripped it down very near to the embedding ice plane, the last accessible radical site(s) can be protectively hydrogenated, passivating the remaining portion of the biomolecule until more of it can be exposed by the abstraction of additional embedding water-ice molecules, allowing further disassembly work to be done on the biomolecule at a later time. This process continues until the entire biomolecule has been excavated, positionally disassembled, and recorded.

The foregoing analysis suggests that some combination of 1-, 2-, and 3-atom removals will occur during subtractive mechanosynthetic processing of cryopreserved tissue. Pending ***future research*** on the statistics

---

[1967] Freitas RA Jr. Nanomedicine, Volume I: Basic Capabilities, Landes Bioscience, Georgetown TX, 1999; Section 4.2, "Chemical and Molecular Sensors", http://www.nanomedicine.com/NMI/4.2.htm.

[1968] e.g., see Reaction Sequence RS5 (p. 767) in: Freitas RA Jr., Merkle RC. A minimal toolset for positional diamond mechanosynthesis. J Comput Theor Nanosci. 2008;5:760-861; http://www.molecularassembler.com/Papers/MinToolset.pdf.

of atom removal for proteins, carbohydrates and other polymeric biomolecules, we will assume for scaling purposes that, on average, 2 atoms are removed per subtractive operation.

Following the same estimation method as used in Section 5.2.1.1 suggests a biomolecule atom abstraction rate of $\mathfrak{A}_{BiomolAtom} \sim 2 \times 10^{6}$ atoms/sec and a biomolecule specific clearance rate of $\mathfrak{M}_{BiomolAtomClear} = m_{BiomolAtom}\ \mathfrak{A}_{BiomolAtom} \sim 3.65 \times 10^{-20}$ kg/sec for each nanomanipulator system, taking $m_{BiomolAtom} \sim MW_{BiomolAtom} / N_A = 1.83 \times 10^{-26}$ kg/atom in biomolecules where $MW_{BiomolAtom} \sim 0.011$ kg/mole for the average atom in a CHON-based biomolecule and $N_A = 6.022 \times 10^{23}$ atoms/mole (Avogadro's number). If every abstraction operation is assumed to require a prior inspection operation, then the net biomolecule abstraction rate is only ~0.5 $\mathfrak{A}_{BiomolAtom} \sim 1 \times 10^{6}$ atoms/sec and the net biomolecule specific clearance rate is $\mathfrak{M}_{BiomolAtomRemoval} = 0.5\ \mathfrak{M}_{BiomolAtomClear} \sim$ **1.83×10^{-20} kg/manipulator-sec**.

Future research must (A) determine the optimum subtractive mechanosynthesis protocols for performing this kind of scan on all types of biomolecules found in the human body, (B) design and simulate the specific mechanosynthetic tools needed to do it, and (C) more accurately assess the achievable biomolecule atom abstraction rate, in case the above estimate for $\mathfrak{A}_{BiomolAtom}$ is too optimistic. ***Future research*** should also examine possible mechanosynthetic tools, tool motions, and reaction sequences necessary for performing subtractive mechanosynthesis on more densely-bonded structures, such as 3D cage molecules and sp^3-dense structures, with solid diamond structures representing the most extreme circumstance.

Future research should also examine the feasibility and relative efficiency of molecular rather than atomic disassembly of cryopreserved human tissue. In this alternative procedure, whole molecules would be extracted from the ice to minimize handling cycles, at the cost of some molecular positional information and the possibility of molecule breakage in many cases, especially when particularly long molecules are extracted. The force required to extract the molecule from cryogenic ice must be estimated by simulations or directly measured, then compared to the mechanochemical scission force needed to break C-C (~5.53 nN)[1969] and C-N (est. ~4.8 nN) backbone bonds in organic molecules to determine where and how often these polymer molecules will fragment when pulled using large forces.

5.2.1.3 Destructive Molecular Scan System Scaling

The envisioned destructive molecular scanning process can be loosely described as follows:

1. Inspect the target patch of frozen tissue to be molecularly scanned.

2. Identify what seems to be there, making a preliminary estimate as to which molecules are where, including their element type, position, and orientation, including the positions of all water-ice molecules.

3. Remove the water-ice molecules one at a time, recording the position and orientation of all molecules removed and reinspecting the surface site periodically to account for any surface rearrangements that may have occurred, until one or more biomolecules are sufficiently exposed to allow their positional disassembly.

[1969] Freitas RA Jr., Merkle RC. A minimal toolset for positional diamond mechanosynthesis. J Comput Theor Nanosci. 2008;5:760-861; http://www.molecularassembler.com/Papers/MinToolset.pdf.

4. Disassemble the biomolecule(s) as far as possible, recording positions and identity of all atom(s) removed. Repeat Step 3, removing more water-ice molecules to expose more of the biomolecule(s) and continue positional disassembly operations until all biomolecules in the target patch are disassembled.

5. Repeat from Step 1 on successive target patches until all water-ice has been removed and all biomolecules have been positionally disassembled. The recorded data – after some digital processing (Section 5.2.2) – can be used to compile a detailed atomic scale 3D map of the entire original body of the cryopreserved patient. At the completion of this stage, the cryopreserved patient's original physical body no longer exists.

Table 14 shows that water molecules comprise 65% of the mass of a typical tissue cell but represent ~98.73% of all molecules present. At the molecular scale, the cell looks like large tracts of water molecules with a few solute molecules mixed in, plus a moderate number of very long or bulky macromolecules (e.g., carbohydrates, proteins) embedded among huge numbers of water molecules. In the cryopreserved patient, many water molecules will have migrated out of the cells into the extracellular spaces during the process of cryopreservation, but the total mass of water-ice in the body will remain the same, just differently distributed.

In one early study of whole bodies, the standard adult human male of mass ~70 kg and volume ~60 L was measured to contain ~67% water by mass (~46.9 kg, ~46.9 L) and ~33% non-water by mass (~23.1 kg, ~13.1 L).[1970] These numbers can vary significantly by age, gender, state of health, and so forth, but will suffice for the present scaling exercise.

Table 14. Estimated gross molecular contents of a typical 20 µm human cell[1971]

Molecule Type	Molecular Weight *(daltons)*	Number of Molecules	Fraction of all Molecules	Fraction of all Molecule Mass
Water	18	1.74×10^{14}	98.73 %	65 %
Other Inorganics	55	1.31×10^{12}	0.74 %	1.5 %
Lipids	700	8.4×10^{11}	0.475 %	12 %
Other Organics	250	7.7×10^{10}	0.044 %	0.4 %
Proteins	50,000	1.9×10^{10}	0.011 %	20 %
RNA	1×10^{6}	5×10^{7}	3×10^{-5} %	1.0 %
DNA	1×10^{11}	46	3×10^{-11} %	0.1 %
Totals	---	1.76×10^{14}	100 %	100 %

In preparation for the molecular scan, a large quantity of nonstructural bulk materials has already been removed from the body (Section 5.1), leaving a V_{MSV} ~ 41,053 cm^3 molecular scan volume in the

[1970] Mitchell HH, Hamilton TS, Steggerda FR, Bean HW. The chemical composition of the adult human body and its bearing on the biochemistry of growth. J Biol Chem. 1945;168:625-637; http://bionumbers.hms.harvard.edu/files/625.full.pdf.

[1971] Freitas RA Jr. Nanomedicine, Volume I: Basic Capabilities, Landes Bioscience, Georgetown, TX, 1999; Table 3.2; http://www.nanomedicine.com/NMI/Tables/3.2.jpg.

cryopreserved patient. Half of the removed volume is blood and lymph fluid which are probably close to the 67% water / 33% nonwater ratio in composition. If we apply the same ratio to the entire molecular scan volume, the result is a net molecular scan volume of $V_{MSV,water} \sim 0.67\ V_{MSV} \sim$ **27.5 L of water**, representing a mass of $M_{MSV,water} \sim \rho_{water}\ V_{MSV,water} \sim 27.5$ kg for water, taking $\rho_{water} \sim 1$ kg/L. The net molecular scan volume for nonwater is therefore of $V_{MSV,nonwater} \sim V_{MSV} - V_{MSV,water} \sim 13.6$ L, with a molecular scan mass of $M_{MSV,nonwater} \sim (23.1 \text{ kg} / 13.1 \text{ L})\ V_{MSV,nonwater} \sim$ **24.0 kg of nonwater**.

Based on the estimated net water molecule volumetric clearance rate of $\mathfrak{V}_{IceRemoval} \sim 16{,}384$ nm^3/manipulator-sec with per-operation site scanning (Section 5.2.1.1) and the biomolecule specific clearance rate of $\mathfrak{M}_{BiomolAtomRemoval} \sim 1.83 \times 10^{-20}$ kg/manipulator-sec with per-operation site scanning (Section 5.2.1.2), the whole-body clearance requirement can be approximated as $N_{Removal} = (V_{MSV,water} / \mathfrak{V}_{IceRemoval}) + (M_{MSV,nonwater} / \mathfrak{M}_{BiomolAtomRemoval}) = 3 \times 10^{21}$ manipulator-sec, if we assume that all nonwater molecules are biomolecules purely for computational convenience. ***Future research*** should undertake a more detailed estimate.

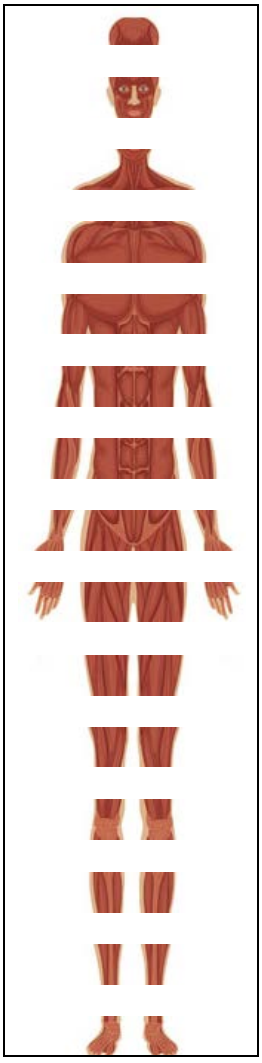

A simple whole-body destructive scan time estimate might assume that a cryopreserved patient of height $L_{body} \sim 1.85$ m (~6 feet) and volume $V_{body} = 60{,}000\ cm^3$ with a mean cross-sectional area of $A_{cross} = V_{body} / L_{body} \sim 324\ cm^2$ (e.g., ~18 cm x ~18 cm) is scanned using a planar array of nanomanipulators each having a 100 nm x 100 nm accessible work area of $A_{manipulator} \sim 10{,}000\ nm^2$ that scans the patient in a linear sweep that starts at the bottom of the patient's feet and finishes at the top of the patient's head. The planar scanning array includes $n_{manipulator} = A_{cross} / A_{manipulator} = 3.24 \times 10^{12}$ nanomanipulators, giving a total scan time of $\tau_{SinglePlane} = N_{Removal} / n_{manipulator} = 9.26 \times 10^8$ sec (29.5 yrs).

This time can be cut in half by scanning the patient simultaneously in two directions, both from the feet up and from the head down, meeting in the middle. This doubles the number of active scanning manipulators at work, giving a scan time of $\tau_{2\text{-}Plane} = N_{Removal} / 2\ n_{manipulator} = 4.63 \times 10^8$ sec (14.7 yrs), with a nanorobotic power consumption of $P_{scan} = N_{manipulators}\ P_{manipulator} \sim 0.6$ watts, taking $N_{manipulators} = 2\ n_{manipulator} = 6.48 \times 10^{12}$ nanomanipulators and $P_{manipulator} \sim 0.1$ pW (Section 5.2.1.1).

More generally, scan time can be reduced (at the cost of more scanning hardware) by segmenting the patient into a multiplicity of cross-sectional slices, then separately processing each slice simultaneously from its top and bottom faces. For example, scan time may be reduced to $\tau_{30\text{-}Plane}$ = **1 year** by separating the patient into roughly 15 separate scan slices, each averaging ~12 cm thick (image, right), requiring $N_{manipulators} \sim 30\ n_{manipulator} = 9.72 \times 10^{13}$ nanomanipulators generating $P_{scan} = N_{manipulators}\ P_{manipulator} \sim 10$ watts of continuous nanomechanical waste heat while processing all 15 slices, or $P_{15\text{-}slice} \sim P_{scan} / 15 \sim 0.65$ watts per slice. The processing of different slices can take place in well-separated and thermally isolated locations.

Alternatively, scan time may be reduced to $\tau_{360\text{-}Plane}$ = **1 month** by separating the patient into 180 separate scan slices, each ~1 cm thick, requiring $N_{manipulators} \sim 360\ n_{manipulator} = 1.17 \times 10^{15}$ nanomanipulators collectively generating $P_{scan,1mo} = N_{manipulators}\ P_{manipulator} \sim 117$ watts, or $P_{180\text{-}slice} \sim P_{scan} / 180 \sim 0.65$ watts/slice, of continuous nanomechanical waste heat for the duration of the procedure.

Some geometry other than simplistic planar slices will most likely be required for maximum efficiency, and investigation of ideal such geometries and the optimum degree of segmentation is a proper subject for ***future research***. Perhaps the most aggressive segmentation proposal is Merkle's description[1972] of dividing the frozen brain tissue into 1.8 x 10^{16} individual cubes of dimensions 422 nm x 422 nm x 422 nm, then applying one nanorobotic device per cube to atomically scan each cube during a scanning process originally believed to require ~3 years. Preliminary analysis (Section 2.2.9) by the author of this book suggests that a destructive whole-body molecular scan using this extreme segmentation process might take $t_{bodyscan}$ ~ **6 months** to complete using $M_{bodyscan}$ ~ 26 kg of atomically-precise nanomachinery of volume $V_{bodyscan}$ ~ 0.5 m^3 and power draw $P_{bodyscan}$ ~ 2000 watts, an estimate that includes only the nanomachinery and none of the required macroscale support infrastructure.

Segmentation of the body of the cryopreserved patient can be performed using a thin cutting ribbon ~1 mm in width and wedge-shaped in cross-section, with the thin leading cutting edge ~30 nm thick populated by a continuous line of adjacent nanoscale manipulators x_{diam} ~30 nm in diameter and ~100 nm in length (Section 5.2.1.1), the thick trailing edge ~1 μm deep, and the bulk of the segmentation ribbon mechanism filled with tool transport tubes, fluid transfer pipes, electrical power cables, control and data transfer wiring, mechanical segment positioners, and the like. The nanomanipulator line carefully separates cryogenic tissues at the molecular scale and records tip motions and tip sensor data for future compilation, with tip motions largely constrained to the plane of the ribbon. As the tissue separates and flows over the two 1 mm wide faces, chemical and mechanical sensors on the two ribbon faces collect data on the physical structure of the separated tissue, allowing identification and direct measurement of the positions, sizes, types, and physical state of cells, many of which will have been bisected by the cutting. Bisected collagen and other fibers under tension would normally retract when cut inside warm reliquidified tissue. But because the cutting takes place at cryogenic temperatures, the tissues are as hard as rock, preventing significant retraction of cut fibers and allowing the sensory surface to detect, identify and measure these strands as well.

The segmentation nanomanipulators cut and remove only a thin slice of tissue of thickness t_{slice} ~ 3 nm through a cross-sectional area A_{cross} = 324 cm^2 of the body, removing a volume $V_{slice} = t_{slice}\ A_{cross}$ = 9.72 x 10^{-11} m^3 and a mass M_{slice} ~ $\rho_{water}\ V_{slice}$ ~ 9.72 x 10^{-8} kg of tissue. A line of $N_{ManipLine} = A_{cross}^{1/2} / x_{diam}$ = 6 x 10^6 nanomanipulators along the leading edge of the segmentation ribbon requires $\tau_{slice} \sim M_{slice} / N_{ManipLine}\ \mathfrak{M}_{BiomolAtomRemoval}$ = 8.85 x 10^5 sec (~**10 days**) to complete the cut at a fairly negligible power cost of $P_{slice} = N_{ManipLine}\ P_{manipulator}$ = 6 x 10^{-7} watts, taking $\mathfrak{M}_{BiomolAtomRemoval}$ ~ 1.83 x 10^{-20} kg/manipulator-sec and $P_{manipulator}$ ~ 0.1 pW. ***Future research*** should further examine the ideal methods and geometries for segmentation of the body of the cryopreserved patient for quick molecular scanning, including nanorobotically-enabled atomically-fine cutting methods that preserve structural information across all matched cut planes.

In addition to the mechanical waste heat generated by the operation of the scanning and segmentation nanomechanisms, a certain amount of energy will be released during the exoergic processes of subtractive mechanosynthesis. A crude estimate of the waste heat from this source starts with the observation that the 70 kg human body contains an estimated $N_{HBatoms}$ ~ 6.71 x 10^{27} atoms,[1973] of which V_{MSV} / V_{body} ~ 68% or $N_{MSVatoms}$ ~ 4.6 x 10^{27} atoms may be present in the molecular scan volume. If whole-body scanning requires breaking an average of $n_{bondscission}$ ~ 2 bonds per atom, and if each bond scission liberates an average of $E_{bondscission}$ ~ 600 zJ/bond (~3.75 eV/bond) of waste heat, then a whole-body destructive molecular scan will release $E_{scission,total} \sim n_{bondscission}\ E_{bondscission}\ N_{MSVatoms}$ = 5.5 x 10^9 J of total

---

[1972] Merkle RC. The molecular repair of the brain. Cryonics 1994 Jan;15(1) and Cryonics 1994 Apr;15(2); http://www.merkle.com/cryo/techFeas.html and https://www.alcor.org/library/molecular-repair-of-the-brain/.

[1973] Freitas RA Jr. Nanomedicine, Volume I: Basic Capabilities, Landes Bioscience, Georgetown, TX, 1999; Table 3.1; http://www.nanomedicine.com/NMI/Tables/3.1.jpg.

mechanosynthetic waste heat over the course of the procedure. A 15-slice scan performed over the course of a year thus creates a continuous ~180 watts of additional waste heat, or ~12 watts/slice; a 180-slice scan performed over the course of one month creates $P_{1mo,\ bonds}$ ~ 2100 watts of additional continuous waste heat for the whole body (but the same ~12 watts/slice) – and the slices can be processed in thermal isolation from each other.

Aside from computing requirements (Section 5.2.2), there has been no attempt here to design or estimate the size of the chemically and mechanically active atomically-precise supporting infrastructure. However, an extremely crude estimate would start with the manipulators. Each nanomanipulator is commonly conceived as comprising ~4 million atoms excluding the base and external power and control structures, with a typical mass of $m_{manipulator} \sim 10^{-19}$ kg.[1974] A single 324 cm^2 plane of $n_{manipulator} \sim 3.24 \times 10^{12}$ nanomanipulators would thus have a mass of $m_{plane} = m_{manipulator}\ n_{manipulator} \sim 3.24 \times 10^{-7}$ kg. The plane of 100-nm long nanomanipulators lies atop a support sheet of atomically precise infrastructure that includes power supplies and mechanical actuators to drive the manipulator joints, tunnels and transport mechanisms to deliver tools and other materiel to and from the nanomanipulator tips, and so forth. The support sheet must also provide sufficient structural rigidity to maintain the necessary positional registration as the support sheets are moved around in space and as the manipulators perform their various operations on cryogenic tissues.

Lacking a detailed design of these support sheets (a suitable exercise for ***future research***), we observe that household aluminum foil[1975] has a thickness of 16-24 μm and that diamond with a 10-fold larger Young's modulus would have 10-fold greater flexural rigidity[1976] for the same thickness, which is probably sufficient. A diamond support sheet of thickness t_{ss} = 20 μm, area A_{ss} = 324 cm^2, and density $\rho_{diamond}$ = 3510 kg/m^3 has a mass of $m_{ss} = t_{ss}\ A_{ss}\ \rho_{diamond} = 2.27 \times 10^{-3}$ kg, giving a total mass of active nanorobotic components in a single-plane scanning plate system of $m_{ss} + m_{plane} = 2.270324 \times 10^{-3}$ kg ~ m_{ss}. The most aggressive $\tau_{360\text{-}Plane}$ = 1 month scanning process described above would require 360 copies of the same nanomanipulators and infrastructure, giving a total active nanorobotic system mass of $M_{DMS} \sim 360\ m_{ss} \sim$ 0.8 kg. If early molecular manufacturing of atomically precise nanomachinery has an energy cost of $C_{mmE\$} \sim \$100{,}000/kg$,[1977] then building $M_{DMS} \sim 0.8$ kg of scanning nanomachinery could have an initial capital cost of up to $C_{mm\$} = C_{mmE\$}\ M_{DMS} \sim \$80{,}000$.

Allocating ~1,000,000 nm^3 (i.e., ~100 million atoms, or 0.1% the size of a full Lab Module; Section F.2.1) for one analysis bay performing a 1-3 atom moiety identification that is paired with each of $N_{manipulators} \sim 360\ n_{manipulator} = 1.17 \times 10^{15}$ nanomanipulators adds a negligible $\sim 10^{-6}\ m^3$ or $\sim 10^{-3}$ kg to the total atomically-precise infrastructure mass.

The atomically-imprecise macroscale supporting infrastructure (e.g., circulating coolant pumps and pipes, electrical power supplies, cryogenic vacuum systems, patient support crib, slice-handling mechanisms, etc.) might be 1-3 orders of magnitude larger in total mass than the atomically-precise nanorobotic system components, but its specification and design is beyond the scope of this book and must be left for ***future research***.

[1974] Freitas RA Jr. Nanomedicine, Volume I: Basic Capabilities, Landes Bioscience, Georgetown TX, 1999, Section 9.3.1.4, "Telescoping Manipulators"; http://www.nanomedicine.com/NMI/9.3.1.4.htm.

[1975] https://en.wikipedia.org/wiki/Aluminium_foil.
[1976] https://en.wikipedia.org/wiki/Flexural_rigidity.

[1977] Freitas RA Jr., Merkle RC. Kinematic Self-Replicating Machines, Landes Bioscience, Georgetown, TX, 2004; Fig. 4.42, "Physical device specifications for the Merkle-Freitas hydrocarbon molecular assembler"; http://www.molecularassembler.com/KSRM/Figures/4.42.JPG.

5.2.2 Computational Cost of Fault Correction

Section 5.2.2.1 provides a high-level description of the data storage requirements for the initial scan file, both in its original complete form and after compactification, for both whole-body and neuro patients.

Section 5.2.2.2 distinguishes the medical flaws that will be computationally corrected from those that will not be corrected, briefly describes the function of the Digital Repair Algorithm that will perform the fault corrections, then estimates the computer time, memory, volume, and power that may be required to execute the desired corrections in both whole-body and neuro situations, producing a corrected scan file.

The possibility of converting the corrected scan file to a description of a synthetic (biological, nonbiological, or nanorobotic) physical system is briefly discussed in Section 5.2.2.3.

5.2.2.1 Initial Scan File

The molecular scan volume of the average cryopreserved 70 kg human body, after nonessential bulk materials needing no atomically precise specification have been removed, will include an estimated $N_{MSVatoms} \sim 4.6 \times 10^{27}$ atoms (Section 5.2.1.3).

The initial atomic scan file of the cryopreserved patient must specify the 3D position of every single atom in the molecular scan volume, ideally to a resolution at least as small as the maximum atomic placement positional variance that ensures a correct single-atom placement during positional mechanosynthesis. Diamond has the shortest crystalline bonds, hence the positional tolerance for reliable diamond mechanosynthesis represents a conservative requirement for scan file precision involving biological materials. The minimum tolerable variance for reliable diamond mechanosynthesis positioning operations has long been established as $\lambda_{mechanosynthesis} \sim 20$ pm for C_2 dimer placement on the C(110) surface, which avoids creating any unwanted metastable or defect structures.[1978] The maximum dimension of a human whole-body scan volume is $L_{HBmax} \sim 2$ meters, roughly the maximum height of the vast majority of humans. Hence the positional data in each dimension for each atom might include $\log_{10}(L_{HBmax} / \lambda_{mechanosynthesis}) \sim 11$ significant decimal figures, requiring $I_{MSVposition} = 3 \log_2(L_{HBmax} / \lambda_{mechanosynthesis}) \sim 110$ bits/atom to record the 3D position of each atom to 11 significant figures. To this must be added $I_{MSVtype} = \log_2(N_{elements}) \sim 7$ bits/atom, to identify which one of the possible $N_{elements} = 92$ natural chemical elements was present at the particular location. We could include an additional $I_{MSVbonds} = 4 \log_2(N_{MSVatoms}) \sim 368$ bits/atom to incorporate the digital names of up to four neighboring atoms to which each atom is covalently bonded, but this seems unnecessary because a 20 pm positional specification should allow ready inference of the bonding partners and bond types of each atom in the molecular scan volume. Hence the size of a patient's initial atomic scan file may approximate $I_{MSVatoms} \sim (I_{MSVposition} + I_{MSVtype}) N_{MSVatoms} =$ **5.4×10^{29} bits**. An aggressive scan time of $\tau_{360\text{-}Plane} = 2.57 \times 10^6$ sec (~1 month; Section 5.2.1.3) requires an average data acquisition rate of $t_{MSVatoms} \sim I_{MSVatoms} / \tau_{360\text{-}Plane} =$ **2.1×10^{23} bits/sec**.

[1978] Peng J, Freitas RA Jr., Merkle RC. Theoretical Analysis of Diamond Mechanosynthesis. Part I. Stability of C_2 Mediated Growth of Nanocrystalline Diamond C(110) Surface. J Comput Theor Nanosci. 2004 Mar;1(1):62-70; http://www.molecularassembler.com/Papers/JCTNPengMar04.pdf. Peng J, Freitas RA Jr., Merkle RC, Von Ehr JR, Randall JN, Skidmore GD. Theoretical Analysis of Diamond Mechanosynthesis. Part III. Positional C_2 Deposition on Diamond C(110) Surface using Si/Ge/Sn-based Dimer Placement Tools. J Comput Theor Nanosci. 2006 Feb;3(1):28-41; http://www.molecularassembler.com/Papers/JCTNPengFeb06.pdf.

To acquire this data, we must remove $N_{MSVwater}$ = 8.95 x 10^{26} water molecules[1979] (Section 5.2.1.1), each of which requires the processing of $I_{waterextract}$ = 702 bits/molecule of data,[1980] so the total data handling requirement for the metrological removal of all water molecules from the cryopreserved patient is $I_{MSVwaterAll} = I_{waterextract}\ N_{MSVwater}$ ~ 6.28 x 10^{29} bits. We must also remove $N_{MSVnonwaterA} \sim N_{MSVatoms} - 3\ N_{MSVwater}$ ~ 1.92 x 10^{27} nonwater atoms, ~96% of which are incorporated in biomolecules (**Table 14**). Assuming each atom requires the processing of up to $I_{nonwaterextract} \sim I_{waterextract} / 3$ = 234 bits/atom (since the step-by-step mechanochemical disassembly of biomolecules may result in the removal of 1-, 2-, or 3-atom moieties; Section 5.2.1.2), then the metrological removal of all nonwater molecules from the cryopreserved patient has a data handling requirement of $I_{MSVnonwaterAll} = I_{nonwaterextract}\ N_{MSVnonwaterA}$ ~ 4.49 x 10^{29} bits, giving a total data processing requirement for acquiring the initial scan file of $I_{MSVprocess} = I_{MSVwaterAll} + I_{MSVnonwaterAll}$ ~ 1.08 x 10^{30} bits. This adds $t_{MSVprocess} \sim I_{MSVAll} / \tau_{360\text{-}Plane}$ = 4.2 x 10^{23} bits/sec to the required $t_{MSVatoms}$ ~ 2.1 x 10^{23} bits/sec average data acquisition rate for the initial scan file itself.

Hence, the total data storage requirement is $I_{MSV} = I_{MSVatoms} + I_{MSVprocess}$ ~ **1.62 x 10^{30} bits** and a total data processing requirement of $t_{MSV} \sim t_{MSVatoms} + t_{MSVprocess}$ ~ **6.3 x 10^{23} bits/sec** for the duration of the initial scan. The CPU volume[1981] and power consumption[1982] needed to support the data processing requirement are modest, but data storage is a bottleneck. Specifically, storing I_{MSV} in nanomechanical RAM using a 3D array of diamondoid register rods with storage density i_{nanoRR} = 10^7 bits/μm^3 as previously assumed (Section 4.8.5) would require a nanomechanical memory unit of volume $V_{nanomemoryRR} \sim I_{MSV} / i_{nanoRR}$ = 162,000 m^3. However, storing the same data in a high-density read/write-capable spooled hydrofluorocarbon tape memory[1983] with storage density $i_{nanoHFC}$ = 10^{10} bits/μm^3 reduces memory unit volume to $V_{nanomemoryHFC} \sim I_{MSV} / i_{nanoHFC}$ = **162 m^3**, with some loss of access speed and convenience compared to the lower-storage-density RAM.

162 m^3 of high-density nanocomputer memory seems like a lot of resources to devote to the revival of a single person. Fortunately, memory volume can be reduced by compactification that degrades data quality in two specific ways that might be deemed acceptable pending the concurrence of ***future research***:

(1) **Delete water molecule data**. We can eliminate ~60% of the nanocomputer memory volume by throwing away all data on the positions of water molecules. This will require us to infer the presence of missing water molecules based on the extremely precise positional data for the atoms in the nonwater molecules. Performing such inference will slightly increase the computational load but can cut the data storage requirement from ~1.62 x 10^{30} bits to $I_{MSVNoWater} = I_{MSVatomsNoWater} + I_{MSVprocessNoWater}$ ~ **6.8 x 10^{29}**

[1979] There are ~1.74 x 10^{14} water molecules per (20 μm)^3 = 8000 μm^3 tissue cell (**Table 14**), or $\rho_{water\#}$ = 2.18 x 10^{10} water molecules/μm^3, so a crude estimate of the total number of water molecules that must be removed from the molecular scan volume is $N_{MSVwater} \sim \rho_{water\#}\ V_{MSV}$ = 8.95 x 10^{26} water molecules, taking V_{MSV} ~ 41,053 cm^3 (Section 5.2.1.3).

[1980] Extracting each water molecule requires the extraction to be transported between three locations (the removal site, the analysis bay, and the tool recharge station), which demands three sets of 3D coordinates accurate to ~20 pm; another three sets of 3D coordinates of similar prevision record the result of the raster-scan of the water molecule's pre-extraction position, assuming one set for each of the three atoms in the molecule (Section 5.2.1.1). Hence the minimum data requirement to extract each water molecule is $I_{waterextract} = 6\ (I_{MSVposition} + I_{MSVtype})$ = 702 bits/molecule.

[1981] Using a nanomechanical CPU able to achieve $U_{nano} \sim 10^{30}$ bit/sec-m^3 (Section 4.8.5), the data processing load would require only $V_{nanocomputer} \sim t_{MSV} / U_{nano}$ ~ **0.63 cm^3** of diamondoid mechanical nanocomputers.

[1982] Assuming energy dissipation at the classical Landauer limit (Section 4.8.5) of $E_{Landauer77K} \sim k_B T \ln(2)$ J/bit = 7.4 x 10^{-22} J/bit (for LN2 temperature T = 77 K and Boltzmann's constant k_B = 1.38 x 10^{-23} J/K), the power requirement for processing this data is a fairly modest $P_{comp} = t_{MSV}\ E_{Landauer77K}$ ~ 466 watts.

[1983] Freitas RA Jr. Nanomedicine, Volume I: Basic Capabilities, Landes Bioscience, Georgetown TX, 1999, Section 10.2.1, "Nanomechanical Computers"; http://www.nanomedicine.com/NMI/10.2.1.htm.

bits, taking $I_{MSVatomsNoWater} \sim (I_{MSVposition} + I_{MSVtype}) N_{MSVnonwaterA} = 2.3 \times 10^{29}$ bits and $I_{MSVprocessNoWater} = I_{MSVnonwaterAll} \sim 4.5 \times 10^{29}$ bits, consequently reducing hydrofluorocarbon tape storage volume from ~162 m^3 to $V_{nanomemoryHFCNoWater} = I_{MSVNoWater} / i_{nanoHFC} \sim$ **68 m^3**.

(2) **Compaction of molecular descriptors**. Rather than tracking the position of every atom in every molecule, we could:

(a) assign each molecular type a unique index number (e.g., $I_a = \log_2(10^9) \sim 30$ bits/molecule to allow a billion different molecule types);[1984]

(b) record the precise atomic coordinates of the terminal atom at either end of the molecule (i.e., $I_b = 2(I_{MSVposition} + I_{MSVtype}) \sim 234$ bits/molecule for the two atoms indicated);

(c) record the fold type for each protein molecule (e.g., $I_c = \log_2(10^9) \sim 30$ bits/molecule to allow a billion different protein fold configurations); and

(d) record the geometrical rotational position of the molecule around its three primary 3D axes (i.e., pitch, roll, and yaw) to within ~1 deg of arc (e.g., $I_d = 3 \log_2(360°/1°) \sim 25$ bits/molecule), for a grand total of 319 bits/molecule.

There are $N_{MSVnonwaterM} \sim 1.03 \times 10^{25}$ nonwater molecules in the molecular scan volume,[1985] so molecular descriptor compaction additionally reduces the data storage requirement from $I_{MSVnowater} \sim 6.8 \times 10^{29}$ bits to $I_{MSVnowaterM} = (I_a + I_b + I_c + I_d) N_{MSVnonwaterM} =$ **3.29×10^{27} bits** and reduces hydrofluorocarbon tape storage volume from ~68 m^3 to $V_{nanomemoryHFCnowaterM} = I_{MSVnowaterM} / i_{nanoHFC} \sim$ **0.33 m^3** (~330 L). Of course, the reduced atomic detail may make it more difficult to accurately infer the location of all water molecules (algorithms for performing this function should be developed in ***future research***), and the highly compact molecular descriptions may require significant additional computational processing to unpack the data during fault analysis and correction (Section 5.2.2.2).[1986]

Note that the above estimates, if applied solely to the cryopreserved brain, would suggest $N_{MSVnonwaterMbrain} \sim (V_{brain} / V_{body}) N_{MSVnonwaterM} \sim$ **2.40×10^{23}** nonwater molecules in the brain with a data storage requirement of $I_{MSVnowaterMbrain} \sim (V_{brain} / V_{body}) I_{MSVnowaterM} \sim$ **7.68×10^{25} bits** for the brain alone, needing only $V_{nanomemoryHFCnowaterB} = I_{MSVnowaterMbrain} / i_{nanoHFC} \sim$ **0.008 m^3** (~8 L) of high-density spooled hydrofluorocarbon tape memory to store all the data, taking $V_{brain} = 1.4$ L and $V_{body} = 60$ L. This is in fairly close agreement with a previously published estimate[1987] of ~2×10^{23} nonwater "significant molecules" in the brain with a total data storage requirement of ~**10^{25} bits**.

[1984] Note that the 40-atom InChI string for the 40-atom morphine molecule is the 148-character string "InChI=1S/C17H19NO3/c1-18-7-6-17-10-3-5-13(20)16(17)21-15-12(19)4-2-9(14(15)17)8-11(10)18/h2-5,10-11,13,16,19-20H,6-8H2,1H3/t10-,11+,13-,16-,17-/m0/s1" (https://en.wikipedia.org/wiki/International_Chemical_Identifier#Example), and 148/40 = 3.7 alphanumeric characters/molecule x 8 bits/character ~ 30 bits/molecule.

[1985] There are ~2×10^{12} nonwater molecules per $(20\ \mu m)^3 = 8000\ \mu m^3$ tissue cell (**Table 14**), or $\rho_{nonwater\#} = 2.5 \times 10^8$ nonwater molecules/μm^3, so a crude estimate of the total number of nonwater molecules in the molecular scan volume is $N_{MSVnonwaterM} \sim \rho_{nonwater\#} V_{MSV} = 1.03 \times 10^{25}$ nonwater molecules, taking $V_{MSV} \sim 41{,}053\ cm^3$ (Section 5.2.1.3).

[1986] We could also reduce data storage volume from 162 m^3 to 0.33 m^3 without sacrificing the water or biomolecule detail data by dividing the molecular scan volume into (162/0.33) ~ 491 separate segments, then retaining the data for only one segment at a time while we work on it. This would require the fault analysis, the preparation of the corrected scan file, and all repairs for a given segment to be correctly processed before the system could move on to processing the next segment (whereupon all data from the previous segment is forever erased). This would eliminate the possibility of coordinating repairs and repair planning involving structures spanning two or more segments (e.g., neural axons, long fibers in connective tissues, muscle cells, etc.), and would intimately couple the molecular scanning and repairing activities possibly reducing performance and reliability compared to systems in which scan and repair activities are decoupled and can occur asynchronously. These tradeoffs should be further examined in ***future research***.

[1987] Merkle RC. The molecular repair of the brain. Cryonics 1994 Jan;15(1) and Cryonics 1994 Apr;15(2); http://www.merkle.com/cryo/techFeas.html and https://www.alcor.org/library/molecular-repair-of-the-brain/.

5.2.2.2 Corrected Scan File

We have the compacted initial scan file describing the now-disassembled physical structure of the cryopreserved patient to atomic (or nearly-atomic) accuracy. The next step is to identify all relevant biological flaws in the initial data file, and then to correct them. These flaws will include contributions from all of the sources of accumulated damage described in Chapter 3 except for the last source (rewarming damage; Section 3.6), all of which would be lethal if left uncorrected and thus all of which must be corrected to enable a viable replacement body to be printed.[1988] A second set of highly desirable alterations might also be imagined, ranging from nonlethal medical flaws (e.g., excising microtumors,[1989] cleanout of mild arteriosclerosis, correction of genetic defects, whole-body rejuvenation) to nonlethal purely cosmetic issues (e.g., changing eye, hair, or skin color; muscle rebulking; skin tag removal and tooth straightening; increasing body height; breast enlargement; correction of body asymmetries[1990]). We will assume that only lethal or near-lethal flaws will be corrected, for two primary reasons:

(1) **Lack of informed consent.** A patient can rationally give consent to procedures deemed essential to reverse lethal damage prior to cryopreservation, because otherwise viable revival – life itself – would be impossible. However, physical alterations beyond the minimum necessary to eliminate prompt lethality should be undertaken only with the fully informed consent of the patient and in the context of their future life. Since the details of as yet unrealized nanorobotic techniques and their attendant risks are largely unknown at the time the patient is cryopreserved, informed consent[1991] must necessarily await the awakening, education, and assent of the patient. In other words, informed consent to correct nonlethal defects[1992] may not be possible prior to revival.[1993]

(2) **Limited resources.** Correcting nonlethal flaws in addition to lethal flaws will take more time, require more computation, and may be more costly than correcting only the lethal flaws. Unless the organization performing the revivals has unlimited resources or unless the costs of revival are unexpectedly low, the reviving organization will be able to awaken more cryopatients more quickly by attending to only the most essential repairs needed to guarantee viability for each patient. Since nonlethal flaws should be easily correctable post-revival at leisure using conventional medical nanorobotics,[1994] it seems difficult to

---

[1988] Additionally, any virions, bacteria, microbes or pathogens present in the cryopreserved body will be faithfully recorded in the initial scan file but must be recognized and deleted in the corrected scan file.

[1989] Autopsies have shown that every person over 50 years old has microscopic tumors in their thyroid glands, and more than one-third of autopsied women aged 40-50 have *in situ* microtumors in their breasts. Folkman J, Kalluri R. Cancer without disease. Nature. 2004 Feb 26;427(6977):787; http://health120years.com/Hamlet/Hamlet_Cancer-without-disease.pdf.

[1990] https://en.wikipedia.org/wiki/Facial_symmetry, https://en.wikipedia.org/wiki/Physical_attractiveness.

[1991] https://en.wikipedia.org/wiki/Informed_consent.

[1992] An interesting edge case for ***future research*** would be the existence of a nonlethal mental defect – e.g., a case of moderate dementia that might preclude the possibility of informed consent if left uncorrected but would otherwise not affect the immediate viability of the patient's printed replacement body.

[1993] ***Future research*** should examine the philosophical, legal, ethical, and technical aspects of a hypothetical procedure in which the scan file of a cryopreserved patient is repaired sufficiently to allow the generation of a computer-simulated conscious upload (Section 5.2.3.4), whereupon the uploaded person is fully informed, educated, and assents to additional procedures that will be applied to the replacement body (though not necessarily applied to the uploaded person). Further analysis of this possibility is beyond the scope of this book.

[1994] Freitas RA Jr. Chapter 23. Comprehensive Nanorobotic Control of Human Morbidity and Aging. In: Fahy GM, West MD, Coles LS, Harris SB, eds, The Future of Aging: Pathways to Human Life Extension, Springer, New York, 2010, pp. 685-805; http://www.nanomedicine.com/Papers/Aging.pdf.

argue that the value of nonessential "elective" procedures outweighs the value of *earlier* restoration of life for *more* cryopatients.

An earlier analysis of the computational requirements for repair simulations during conventional cell repair (Section 4.8.4) assumed that repairs would be made by nanorobotic systems that physically move tissue components in incremental steps along continuous motion paths leading from initial to final states, and that all intermediate states occurring after each increment of movement must be simulated to verify workability of the intended motions and the stability of the resulting physical state.

In the present case, the repair strategy is not to convert one block of biomatter into another block of biomatter via a series of incremental internal physical transformations, but rather to fabricate a wholly new replacement block of biomatter based on an atomically-precise description of a previous block of biomatter that has been disassembled during scanning and no longer physically exists. Since incremental physical modifications are unnecessary, this scenario eliminates the need for simulations of incremental stages and requires only the execution of a Digital Repair Algorithm that is smart enough to convert the lethal initial scan file into a nonlethal corrected scan file.

To perform its function, the Digital Repair Algorithm will require information pertaining to the faults needing repair, minimally including at least the six maps described in Section 4.8.1 and the computational models described in Section 4.8.3 in the context of conventional cell repair. Additional maps and models will likely be required to capture the impact of sub-100-nm- and molecular-scale faults that are invisible in the previous maps but are now available from the molecular scan data, e.g., variations in the fine structure of the myelin sheaths responsible for insulating axons, which exhibit a periodicity between 15-18 nm (image, right).[1995] The Digital Repair Algorithm would accept these maps as inputs, along with the initial scan file, and would compute the corrected scan file in a single cycle (or just a few cycles) of computation, crudely analogous to a matrix multiplication operation but vastly more complex. (Again, the computation could be performed in segments to reduce computer memory requirements.)

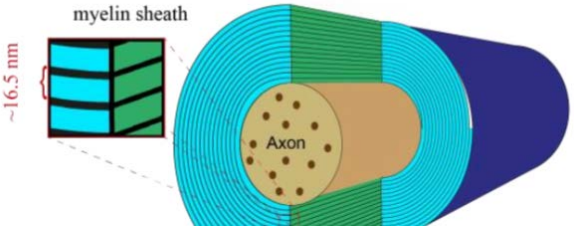

Design of the Digital Repair Algorithm awaits ***future research***, but it seems likely that at least part of its function will involve comparing observed structures detected in the initial scan file with the structures of biological components whose state is considered healthy, normal, or ideal, e.g., possibly using deep learning[1996] algorithms aided by cytoarchitectural whole-organism models that are only in their infancy today.[1997] It is the job of the Digital Repair Algorithm to computationally transform a description of the observed state into the description of a normal state. The normal state of each biological component may be specified by an ideal normative structure accompanied by a permissible range of variation around the normative structure that would still be regarded as healthy or acceptable. These ranges may be greater or lesser in various characteristics (e.g., sizes, shapes, atom counts, fold structures, etc.), and may also be tagged with a number of conditional acceptance levels (e.g., Rule X: if an observed muscle cell mitochondrion has a total volume larger than 1.0 μm^3, then it is permissible for its length to be up to 10% greater than the normative value of 3.1 μm, but no longer).

[1995] Schulz G, Deyhle H, Bikis C, Bunk O, Muller B. Imaging the orientation of myelin sheaths in a non-stained histological slice of human brain. Precis Nanomed. 2020 Oct;3(4):656-665; https://precisionnanomedicine.com/article/17211-imaging-the-orientation-of-myelin-sheaths-in-a-non-stained-histology-slide-of-human-brain.

[1996] https://en.wikipedia.org/wiki/Deep_learning.
[1997] https://en.wikipedia.org/wiki/OpenWorm.

A key function of the Digital Repair Algorithm will be to search the entire initial scan file for pattern matches to the premises or conditions specified by all the rules, and then to apply the limitations or actions prescribed by each rule in a predetermined priority order. This process may require multiple sweeps through the entire datafile because the exercise of rule actions may create new pattern patches to the premises or conditions of previously-triggered or new rules. Additional process rules may also be required to ensure that the aforementioned iterative process remains stable, producing changes within acceptable limits and not pathological results or infinite loops. Further description and development of the Digital Repair Algorithm is beyond the scope of this book but represents an essential challenge for the future.

The initial scan data in compacted form contains an estimated $I_{MSVnowaterM} \sim 3.29 \times 10^{27}$ bits and may be stored in a high-density read/write-capable spooled hydrofluorocarbon tape memory of volume $V_{nanomemoryHFCnowaterM} \sim 0.33$ m^3 (Section 5.2.2.1) with a $t_{nanoHFC} = 10^9$ bit/sec data access speed.[1998] If there are $c_{linesHFC} = 10^{15}$ independent parallel input/output lines into the memory unit, the entire data cache can be read or written in $t_{read/writeHFC} \sim I_{MSVnowaterM} / c_{linesHFC}\ t_{nanoHFC}$ = **3290 sec** (~0.9 hours). For scaling purposes, we make the unsupported but not unreasonable assumption that to perform its work the Digital Repair Algorithm must execute calculations that process an amount of data equivalent to $n_{DRAoperations} \sim 1000$ times the size of the initial scan file, or $(n_{DRAoperations}\ I_{MSVnowaterM}) = 3.29 \times 10^{30}$ bits. This will require $t_{revivalcalcHFC} \sim (n_{DRAoperations}\ t_{read/writeHFC}) = 3.29 \times 10^6$ sec (~914 hours, ~**38 days**) to complete all read/write operations from the $V_{nanomemoryHFCnowaterM} \sim 0.33$ m^3 hydrofluorocarbon tape storage unit (Section 5.2.2.1).

If we further assume that one 64-bit word is required to support the computational repair of each bit of the initial scan file by the Digital Repair Algorithm, then the entire whole-body repair calculation requires processing $Z_{compHFC} \sim 64\ n_{DRAoperations}\ I_{MSVnowaterM} = 2.1 \times 10^{32}$ bits of floating-point computation.

Processing $Z_{compHFC} \sim 2.1 \times 10^{32}$ bits in $t_{read/writeHFC} \sim 3290$ sec requires $V_{nanocompHFC} \sim Z_{compHFC} / (t_{read/writeHFC}\ U_{nano}) \sim$ **0.064 m^3** (64 L) of diamondoid mechanical nanocomputers with specific processing power of $U_{nano} \sim 10^{30}$ bit/sec-m^3, and a continuous power draw of $P_{compHFC} \sim Z_{compHFC}\ E_{Landauer77K} / t_{read/writeHFC} \sim 47.2$ MW[1999] for $E_{Landauer77K} \sim k_B T \ln(2)$ J/bit = 7.4×10^{-22} J/bit using an LN2-cooled nanocomputer at T = 77 K (-196 °C), costing ~$4720/hr for electricity at today's typical commercial rate of ~$0.10/KW-hr ($e_\$ \sim 2.78 \times 10^{-8}$ $/J; Appendix G) for a total electricity cost of $(e_\$\ t_{revivalcalcHFC}\ P_{compHFC}) \sim$ **$4.3M** to complete the calculations for a single whole-body revival.[2000]

[1998] Freitas RA Jr. Nanomedicine, Volume I: Basic Capabilities, Landes Bioscience, Georgetown TX, 1999, Section 10.2.1, "Nanomechanical Computers"; http://www.nanomedicine.com/NMI/10.2.1.htm.

[1999] Note that this represents a power density of only $P_{compHFC} / V_{nanocompHFC} \sim 8 \times 10^8$ W/m^3, well below the typical ~10^{12} W/m^3 power density commonly assumed for mechanical nanocomputers; e.g., Freitas RA Jr. Nanomedicine, Volume I: Basic Capabilities, Landes Bioscience, Georgetown TX, 1999, Section 6.5.6(E), "Power Analysis in Design: Computation"; http://www.nanomedicine.com/NMI/6.5.6.htm#p6.

[2000] Assuming computation at liquid helium temperatures (~4 K), $P_{compHFC} \sim Z_{compHFC}\ E_{Landauer4K} / t_{read/writeHFC} \sim 2.4$ MW for $E_{Landauer4K} = 3.8 \times 10^{-23}$ J/bit, costing ~$240/hr for electricity and giving a total electricity cost of $(e_\$\ t_{revivalcalcHFC}\ P_{compHFC}) \sim$ $220,000 to complete the calculations for a single whole-body revival. However, the cost of continuously maintaining a 4 K operating temperature for a cryogenic computer that is generating 2.4 MW could be substantial and must be added to the total cost figure. For example, a liquid nitrogen plant capable of supplying ~3000 liters/minute of LN_2 (77 K), sufficient to extract a continuous 1 MW of waste heat, would have a ground footprint of 20 meters x 40 meters and would cost ~$20M to buy, according to Air Liquide, a major supplier of turnkey cryogenic systems. A liquid helium plant producing LHe (4 K) of similar cooling capacity would likely be at least 10-100 times more expensive. It might be less costly and more efficient to employ a spaceborne computer system, e.g., located in the Hermite Crater on the Moon whose surface temperature has been measured at 24 K (https://lola.gsfc.nasa.gov/feature20110331.html), which is even colder than the 44 K average surface temperature of Pluto (https://www.universetoday.com/13893/temperature-of-pluto/).

Applied solely to a cryopreserved brain, the above estimates would require processing $Z_{compHFCbrain} \sim (V_{brain} / V_{body}) Z_{compHFC} = 4.9 \times 10^{30}$ bits using $V_{nanocompHFCbrain} \sim Z_{compHFCbrain} / (t_{read/writeHFCbrain} U_{nano}) \sim$ **0.064 m^3** (64 L) of diamondoid mechanical nanocomputers, taking $t_{read/writeHFCbrain} \sim (V_{brain} / V_{body}) t_{read/writeHFC} = 77$ sec, $t_{revivalcalcHFCbrain} \sim (n_{DRAoperations} t_{read/writeHFCbrain}) = 7.68 \times 10^4$ sec (~**21 hours**), $V_{brain} = 1.4$ L, and $V_{body} = 60$ L. The continuous power draw is still $P_{compHFCbrain} \sim Z_{compHFCbrain} E_{Landauer77K} / t_{read/writeHFCbrain} \sim 47.2$ MW assuming LN2-temperature computation at ~$4720/hr for electricity, but with a total electricity cost of only $(e_{\$} t_{revivalcalcHFCbrain} P_{compHFCbrain}) \sim$ **$101,000** to complete the calculations for a single neuro revival.[2001]

All of the above estimates depend critically upon the specific assumptions chosen. ***Future research*** should attempt to improve the accuracy and reliability of these assumptions.

5.2.2.3 Optional Synthetic Conversion File

Once we have the corrected scan file for the patient's brain, it would be theoretically possible to re-analyze the file and computationally replace all biological neurons with artificial neurons[2002] of similar or smaller size, producing a synthetic conversion file. In this scenario, the artificial neurons would be designed to possess exactly the same connectome and synaptic connectivity among themselves as was present in the original neurons and neural network of the brain. Accurate computational models of the biological neurons would allow adjusting the operating parameters of the artificial neurons to mimic the exact same behaviors and responses to stimuli in terms of voltages, frequencies, delays, firing patterns, and so forth, as the biological neurons. At the perimeter of the artificial neuron mass, a custom interface would be needed to bridge the gap to the remaining biological tissues.

In principle, all of the biological structures in the patient's body could be replaced with artificial modules that mimicked the original biological function of all the patient's tissues, eliminating the need for a synthetic/biological interface system. Some biological functions would probably become obsolete and could be deleted from the synthetic conversion design. The artificial neurons or modules could be constructed of more functional and durable materials than proteins, lipids, and carbohydrates, such as diamondoid nanomachinery, ceramic optical components, lightweight graphene composite structural members, and so forth. Scan file additions such as embedded cryoprotectant molecules could be deleted from the new design if the artificial structures were no longer subject to damage upon being rewarmed to normal temperatures.

Once the new synthetic conversion motif has been properly designed, simulated, and computationally validated, the replacement patient body could be printed in place of the original biological body,[2003]

[2001] Assuming liquid helium temperature computation, the continuous power draw could be $P_{compHFCbrain} \sim Z_{compHFCbrain} E_{Landauer4K} / t_{read/writeHFCbrain} \sim 2.4$ MW with a total electricity cost of $(e_{\$} t_{revivalcalcHFCbrain} P_{compHFCbrain}) \sim$ $5100 to complete the calculations for a single revival, taking $t_{revivalcalcHFCbrain} \sim 76{,}800$ sec. The cautions expressed in the previous footnote about the expense of providing liquid helium coolant for cryogenic computers would apply here as well.

[2002] Abu-Hassan K, Taylor JD, Morris PG, Donati E, Bortolotto ZA, Indiveri G, Paton JFR, Nogaret A. Optimal solid state neurons. Nat Commun. 2019 Dec 3;10(1):5309; https://www.ncbi.nlm.nih.gov/pmc/articles/PMC6890780/. See also: https://techxplore.com/news/2019-12-world-artificial-neurons-chronic-diseases.html.

[2003] as in the Star Trek TOS episode where humans are copied into android bodies; https://en.wikipedia.org/wiki/What_Are_Little_Girls_Made_Of%3F.

possibly using the 3D atomic print method described in Section 5.2.3.1. The many fascinating variations enabled by this approach[2004] can be explored in ***future research*** but are beyond the scope of this book.

5.2.3 Print Replacement Patient Body

It is now time to print a replacement body for the cryopreserved patient, since the patient's original physical body has been completely disassembled and no longer exists. The corrected scan file must be converted into a print file, but the size and nature of the print file depends upon which printing method has been selected. There are at least four general classes of printing methods that can be employed:

(1) **Cryogenic 3D Atomic Print**: 3D printing of a repaired copy of the original body in the solid state at cryogenic temperature, atom by atom, which involves making and breaking covalent bonds on the "workpiece", with atoms or small multi-atom moieties provided as feedstock from an external source (Section 5.2.3.1).

(2) **Cryogenic 3D Molecular Print**: 3D printing of a repaired copy of the original body in the solid state at cryogenic temperature, molecule by molecule, which involves making and breaking noncovalent bonds almost exclusively, with all covalently-bonded whole molecules provided as feedstock from an external source such as a cell mill (Section 5.2.3.2).[2005]

(3) **Fluidic 3D Cell Print**: 3D printing of a repaired copy of the original body in the liquid state using a combination of noncellular and cellular components provided as feedstock from an external source such as a cell mill; placement will not be atomically precise but will be guided by a repair plan that has been informed by atomically precise knowledge of the desired end structure (Section 5.2.3.3).[2006]

(4) **Virtual 3D Bit Print (Upload)**: 3D virtual reconstruction of a repaired copy of the original body as virtual reality software that emulates the form and function of a human body, operating in an emulated virtual reality environment, i.e., an "upload" (Section 5.2.3.4).

[2004] Moravec* proposed a process by which nanorobots would replace individual neurons with artificial neurons, one by one over some period of time, in a conscious living human patient for the purpose of ensuring continuity of consciousness as the biological brain is progressively replaced by an artificial brain composed of a different (and presumably more durable) substrate (Section 5.2.3.4.1). This is possible in principle, though it may take a relatively long time to complete, given the length of many axons and the large number of synaptic connections that must be precisely matched in a densely packed neuropil.

* Moravec H. Mind Children: The Future of Robot and Human Intelligence. Harvard University Press, 1988; https://www.amazon.com/Mind-Children-Future-Robot-Intelligence/dp/0674576187.

[2005] Methods for 3D printing of frozen biological materials were being developed in 2021, including a prototype system* that uses "multilayer cryolithography to make biological products…by simultaneously printing 2D layers in parallel and assembling the layers into a 3D at an assembly site,…[using] freezing to bind the 2D layers together into a 3D object." According to the team leader: "The problem with 3D bioprinting is that it is a very slow process, so you can't print anything big because the biological materials will deteriorate by the time you finish. We freeze the material as it is being printed so that the biological material is preserved, and we can control the freezing rate."

* Ukpai G, Sahyoun J, Stuart R, Wang S, Xiao Z, Rubinsky B. A Parallel Multiple Layer Cryolithography Device for the Manufacture of Biological Material for Tissue Engineering. J Med Devices 2019 Sep;13(3):035001; https://asmedigitalcollection.asme.org/medicaldevices/article-abstract/13/3/035001/632797/A-Parallel-Multiple-Layer-Cryolithography-Device. See also: Linda Vu, "Mass-producing biomaterials," Berkeley Engineering News, 8 Apr 2019; https://engineering.berkeley.edu/news/2019/04/mass-producing-biomaterials-2/.

[2006] Organovo (https://organovo.com/) and Cellink (https://www.cellink.com/) are early companies in the emerging 3D tissue bioprinting industry,* using live biological components and other conventional biomaterials in their "inks".

* https://en.wikipedia.org/wiki/3D_bioprinting and https://en.wikipedia.org/wiki/Applications_of_3D_printing#Bio-printing.

5.2.3.1 Cryogenic 3D Atomic Print

The most precise reconstruction of the patient's physical body using the corrected scan file will be achieved by printing the body as a solid block of biomatter, essentially atom by atom,[2007] with each tissue atom installed in almost exactly the correct place. Atomic print jobs are subject to two general constraints:

(1) **Ultra-High Vacuum (UHV)**. Chemically reactive atoms are bound together into chemically stable molecules via covalent bonds, hence printing a block of matter atom-by-atom necessarily involves the making and breaking of covalent bonds, e.g., via mechanosynthesis. In the most straightforward case, covalent bonds are formed by radical-radical coupling, such as the addition of a carbon atom to a chain in the reaction CH_3-CH_2-CH_2● + ●CH_3 → CH_3-CH_2-CH_2-CH_3, where "●" denotes an unpaired valence or reactive site on each of the reactant molecules. Special cases of mechanosynthetic addition reactions do not involve the creation of radical sites (e.g., insertion reactions employing carbon atoms with multiple bonds such as CH_3-CH=CH_2 + CH_4 → CH_3-CH_2-CH_2-CH_3) and it is possible to design mechanosynthetic tools that avoid the existence or creation of radical sites on the tool itself during operation.[2008] But it is not clear how to add atoms to single-bonded structures (the most common molecular situation) in the general case without the use of radicals. Radical sites are rapidly poisoned by the presence of solvent or stray gas molecules which quickly react with the radical. So it appears that the use of an ultra-high vacuum (UHV) workspace environment at $P_{atm} \leq 10^{-12}$ atm (Section 5.2.1) is essential for general-purpose radical-based mechanosynthetic constructions. Special cases of solution-based mechanosynthesis have been demonstrated experimentally,[2009] so ***future research*** should investigate the theoretical possibility of a general-purpose radical-free mechanochemistry that could remove this constraint from the atomic printing process.

(2) **Cryogenic Temperatures**. While room temperature mechanosynthesis has been demonstrated experimentally,[2010] operation at cryogenic temperatures helps ensure the extreme reliability that is essential for negligible-error large-scale production runs. There are several reasons for this. **First**, mechanosynthesis typically involves one reaction pathway leading from reactants to a favored product accompanied by one or more alternative pathways, blocked by an energy barrier, that lead to undesired products. The lower the operating temperature, the lower the probability that the system can surmount one of these blocking barriers and reach an undesired state, resulting in an erroneous structure. For example, the probability of an erroneous reaction for carbon transfer operations in which there exists a +0.40 eV barrier to a pathological state is estimated as 2×10^{-7} at 300 K but only 5×10^{-26} at 80 K.[2011] **Second**, mechanosynthetic tooltips vibrate with larger amplitude at higher temperature, increasing the probability that the reactive tip will miss its intended target atom and hit a neighboring atom instead, triggering an

---

[2007] Small moieties such as $–CH_3$, $–NH_2$, or –OH can be substituted for C, N, and O with little or no loss of atomic fidelity.

[2008] Allis DG, Drexler KE. Design and analysis of a molecular tool for carbon transfer in mechanosynthesis. J Comput Theor Nanosci. 2005;2:45-55; http://citeseerx.ist.psu.edu/viewdoc/download?doi=10.1.1.162.2411&rep=rep1&type=pdf.

[2009] Duwez AS, Cuenot S, Jérôme C, Gabriel S, Jérôme R, Rapino S, Zerbetto F. Mechanochemistry: targeted delivery of single molecules. Nat Nanotechnol. 2006 Nov;1(2):122-5; http://citeseerx.ist.psu.edu/viewdoc/download?doi=10.1.1.188.9873&rep=rep1&type=pdf.

[2010] Duwez AS, Cuenot S, Jérôme C, Gabriel S, Jérôme R, Rapino S, Zerbetto F. Mechanochemistry: targeted delivery of single molecules. Nat Nanotechnol. 2006 Nov;1(2):122-5; http://citeseerx.ist.psu.edu/viewdoc/download?doi=10.1.1.188.9873&rep=rep1&type=pdf.

[2011] Freitas RA Jr., Merkle RC. A minimal toolset for positional diamond mechanosynthesis. J Comput Theor Nanosci. 2008;5:760-861; http://www.molecularassembler.com/Papers/MinToolset.pdf.

erroneous reaction. For instance, the positional uncertainty of a DCB6Ge carbon dimer placement tool in the horizontal UV plane is far lower at 20 K (dark purple scatter) than at 300 K (yellow scatter), according to molecular dynamics simulations (image below, right).[2012] (High-reliability mechanosynthetic carbon placement typically requires ±20 pm (±0.2 Å) positional accuracy;[2013] the stiffer crossbar motif of DCB6Ge (image below, left; C = cyan, Ge = purple, H = white) achieves ±14 pm in $\hat{x}$, ±7 pm in $\hat{y}$, and ±9 pm in $\hat{z}$ at 80 K.[2014]) **Third**, surface migration of atoms is reduced at cold temperatures, and the sublimation of small molecules (e.g., water) in vacuum falls to negligible levels at cryogenic temperatures (Section 5.2.1), allowing construction or deposition of small molecules during an atomic print and ensuring their positional stability over periods of time that are long in comparison with the duration of the print run.

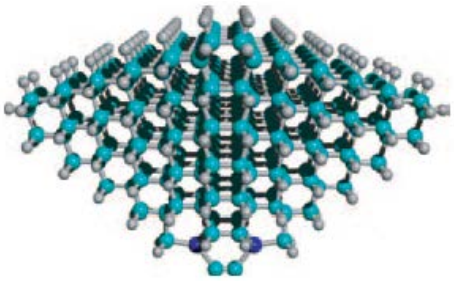

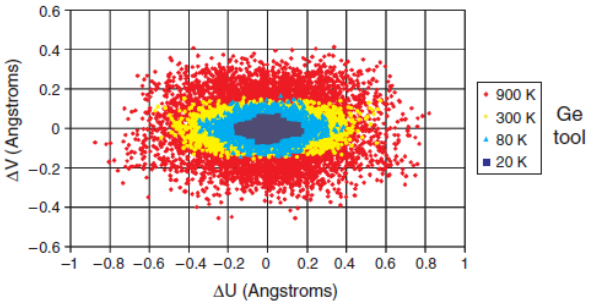

These considerations appear to require that an atomically-precise 3D-printed replacement body must be constructed in a cryogenic fabrication chamber under UHV, probably at ~10^{-12} atm pressure and at LN2 or LHe temperatures, but this is an assumption that should be critically evaluated in ***future research***. Once simple mechanosynthetic systems of molecular manufacturing are in more widespread experimental use, enumeration and quantification of other potential sources of mechanosynthetic process error (e.g., the mechanical instability of tooltip placement mechanisms, metrological measurement errors, etc.) will become a proper subject of ***future research***, in order to properly evaluate the reliability of such operations over trillions of successive cycles.

The compacted corrected scan file[2015] must now be translated into an atomic print file providing build instructions for the 3D atomic printer. To perform this translation, we must next ask: What is the correct target structure to print? A human body with normal tissues, ions and water content fabricated atom-by-atom *de novo* at 77 K (-196 °C) might resemble a normal human body that had been instantly and uniformly flash-frozen to liquid nitrogen temperatures. A close analog of this state is known to be produced by ultra-rapid cooling (e.g., 100-10,000 K/sec), which promotes intracellular fluid supercooling

---

[2012] Peng J, Freitas RA Jr., Merkle RC, Von Ehr JR, Randall JN, Skidmore GD. Theoretical Analysis of Diamond Mechanosynthesis. Part III. Positional C_2 Deposition on Diamond C(110) Surface using Si/Ge/Sn-based Dimer Placement Tools. J Comput Theor Nanosci. 2006 Feb;3(1):28-41; http://www.molecularassembler.com/Papers/JCTNPengFeb06.pdf.

[2013] Peng J, Freitas RA Jr., Merkle RC. Theoretical Analysis of Diamond Mechanosynthesis. Part I. Stability of C_2 Mediated Growth of Nanocrystalline Diamond C(110) Surface. J Comput Theor Nanosci. 2004 Mar;1(1):62-70; http://www.molecularassembler.com/Papers/JCTNPengMar04.pdf. Peng J, Freitas RA Jr., Merkle RC, Von Ehr JR, Randall JN, Skidmore GD. Theoretical Analysis of Diamond Mechanosynthesis. Part III. Positional C_2 Deposition on Diamond C(110) Surface using Si/Ge/Sn-based Dimer Placement Tools. J Comput Theor Nanosci. 2006 Feb;3(1):28-41; http://www.molecularassembler.com/Papers/JCTNPengFeb06.pdf.

[2014] Peng J, Freitas RA Jr., Merkle RC, Von Ehr JR, Randall JN, Skidmore GD. Theoretical Analysis of Diamond Mechanosynthesis. Part III. Positional C_2 Deposition on Diamond C(110) Surface using Si/Ge/Sn-based Dimer Placement Tools. J Comput Theor Nanosci. 2006 Feb;3(1):28-41; http://www.molecularassembler.com/Papers/JCTNPengFeb06.pdf.

[2015] An uncompacted corrected scan file would provide the maximum atomic fidelity but would require storing and processing ~500 times more data (Section 5.2.2.1), probably for negligible added benefit.

and vitrification[2016] without intracellular ice formation or cellular water out-migration (as occurs during slow programmable freezing[2017]). It is said[2018] that during vitrification, a metastable glass forms before water molecules can self-aggregate to form ice nuclei and grow crystals,[2019] and that in dilute solutions, water vitrifies at about 138 K[2020] and cooling to this temperature must occur at >20,000 K/sec to prevent ice formation.[2021] More precise experimental data compiled by Mullen and Fahy[2022] (chart, below) shows the **critical cooling rate** necessary to achieve vitrification as a function of concentrations for three common cryoprotective agents (CPA) in water solution – propylene glycol (PG), ethylene glycol (EG), and glycerol. The concentration typically sought for M22 in cryopreserved human patients is ~60% w/v (Section 4.10.1.7), which will have the lowest critical cooling rate.

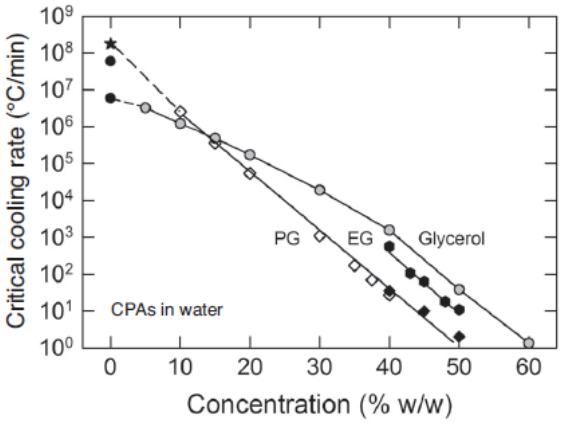

Since all water molecules have been deleted from the initial scan file (Section 5.2.2.1(1)) and thus are also missing from the corrected scan file (so that their presence must be inferred from the positions of the remaining non-water molecules), the 3D atomic printer can simply emplace the water molecules one by one into the tissue

---

[2016] Franks F. Biophysics and biochemistry at low temperatures. Cambridge University Press, Cambridge UK, 1985; https://www.amazon.com/Biophysics-Biochemistry-at-Low-Temperatures/dp/0521269326. Mazur P. Equilibrium, quasi-equilibrium and non-equilibrium freezing of mammalian embryos. Cell Biophysics. 1990 Aug;17(1):53-92; https://pubmed.ncbi.nlm.nih.gov/1704816/. Bald WB. Real cooling and warming rates during cryopreservation. CryoLetters. 1993;14:207-216. Vajta G, Nagy ZP. Are programmable freezers still needed in the embryo laboratory? Review on vitrification. Reproductive BioMedicine Online. 2006 Jun;12(6):779-796; https://www.rbmojournal.com/article/S1472-6483(10)61091-7/pdf. Fahy GM. Theoretical considerations for oocyte cryopreservation by freezing. Reproductive BioMedicine Online. 2007 May 31;14(6):709–714; http://www.21cm.com/pdfs/RBMO%202007%20Fahy.pdf. Walters C, Wesley-Smith J, Crane J, Hill LM, Chmielarz P, Pammenter NW, Berjak P. Cryopreservation of recalcitrant (desiccation-sensitive) seeds. In: Reed BM, ed. Plant cryopreservation: a practical guide. Springer, New York, 2008, pp. 465–484; https://link.springer.com/chapter/10.1007/978-0-387-72276-4_18.

[2017] https://en.wikipedia.org/wiki/Cryopreservation#Slow_programmable_freezing.

[2018] Wesley-Smith J, Berjak P, Pammenter NW, Walters C. Intracellular ice and cell survival in cryo-exposed embryonic axes of recalcitrant seeds of *Acer saccharinum*: an ultrastructural study of factors affecting cell and ice structures. Ann Bot. 2014 Mar;113(4):695-709; https://www.ncbi.nlm.nih.gov/pmc/articles/PMC3936581/.

[2019] Fahy GM, MacFarlane DR, Angell CA, Meryman HT. Vitrification as an approach to cryopreservation. Cryobiology. 1984;21:407-426; https://www.sciencedirect.com/science/article/pii/0011224084900798. Vajta G, Nagy ZP. Are programmable freezers still needed in the embryo laboratory? Review on vitrification. Reproductive BioMedicine Online. 2006 Jun;12(6):779-796; https://www.rbmojournal.com/article/S1472-6483(10)61091-7/pdf. Fahy GM. Theoretical considerations for oocyte cryopreservation by freezing. Reproductive BioMedicine Online. 2007 May 31;14(6):709–714; http://www.21cm.com/pdfs/RBMO%202007%20Fahy.pdf. Liu J, Phy J, Yeomans E. Theoretic considerations regarding slow cooling and vitrification during cryopreservation. Theriogenology. 2012 Nov;78(8):1641-1652; https://pubmed.ncbi.nlm.nih.gov/22818092/.

[2020] Franks F. Biophysics and biochemistry at low temperatures. Cambridge University Press, Cambridge UK, 1985; https://www.amazon.com/Biophysics-Biochemistry-at-Low-Temperatures/dp/0521269326.

[2021] Bald WB. Quantitative cryofixation. Adam Hilger, Bristol UK, 1987; https://www.amazon.com/Quantitative-Cryofixation-W-B-Bald/dp/085274448X.

[2022] Mullen SF, Fahy GM. Chapter 12. Fundamental aspects of vitrification as a method of reproductive cell, tissue and organ cryopreservation. In: Donnez J, Kim SS, eds. Principles and Practice of Fertility Preservation, Cambridge university Press, 2011, pp. 145-163.

positions they would have occupied had the original body been cooled at ultra-high speed – i.e., into a perfect glassy state.[2023]

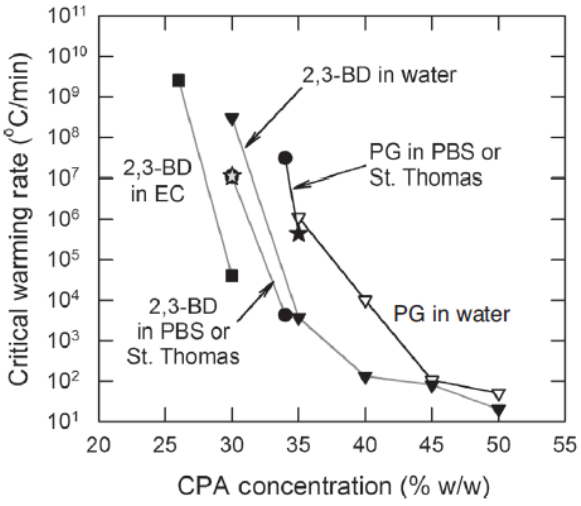

However, a problem arises when the temperature of a replacement human body initially fabricated in the glassy state at cryogenic temperatures is warmed to above the glass transition temperature as part of an effort to awaken the patient. Where cryoprotectants are absent, ice crystals may form, damaging many cells – a previously-discussed mode of rewarming damage called "recrystallization of intracellular ice" (Section 3.6(4)). If cryoprotectant is present and the tissues are vitrified rather than frozen (i.e., no crystalline ice is present), the tissue must be rewarmed fast enough to outrun devitrification (Section 3.6(5)). The **critical warming rate** for one cryoprotectant agent (VS41A) was estimated as 40-270 °C/min,[2024] or 0.7-4.5 K/sec. More recent data from Mullen and Fahy[2025] (chart, left) showing the critical warming rate necessary to avoid devitrification for two cryoprotective agents – propylene glycol (PG) and 2,3-butanediol (2,3-BD) – solvated in water or two other solution carriers confirms that cryopatients with typical CPA concentrations at 50% or higher (Section 4.10.1.7) require only fairly modest warming rates in the 10-100 °C/min range to avoid devitrification during warming, and the critical warming rate for high-concentration M22 may be < 1 °C /min.[2026]

There are several ways to prevent such rewarming damage:

(A) **Embedded Cryoprotectants.** Molecular descriptions of the various components of the M22 cryoprotectant mixture[2027] (**Table 8** in Section 4.10.1.7) could be inserted into the atomic print file, displacing enough water molecules to establish a high-quality >9.6 molar concentration uniformly distributed throughout the entire body. Ideal concentrations and mixtures of cryoprotectant chemicals for

---

[2023] Since vitrified water is amorphous, not crystalline, this suggests that while the presence of a water molecule in a specific location may be important to viability and structural preservation, the exact rotational orientation of the water molecules may not be important, so our suggestion to delete this information from the stored initial scan file is probably correct. This view is supported by the notion that the exact linear and rotational positions of the patient's water molecules at the time of death pronouncement will most likely be dramatically different from the positions occupied by those same molecules once the patient finally reaches the storage temperature of 77 K after cryopreservation – or even after only 6 minutes of warm ischemia.

[2024] Mehl PM. Nucleation and Crystal Growth in a Vitrification Solution Tested for Organ Cryopreservation by Vitrification. Cryobiology. 1993 Oct;30(5):509-518; https://pubmed.ncbi.nlm.nih.gov/11987991/.

[2025] Mullen SF, Fahy GM. Chapter 12. Fundamental aspects of vitrification as a method of reproductive cell, tissue and organ cryopreservation. In: Donnez J, Kim SS, eds. Principles and Practice of Fertility Preservation, Cambridge university Press, 2011, pp. 145-163.

[2026] Fahy GM, Wowk B, Wu J, Phan J, Rasch C, Chang A, Zendejas E. Cryopreservation of organs by vitrification: perspectives and recent advances. Cryobiology. 2004 Apr;48(2):157-78; http://www.21cm.com/pdfs/cryopreservation_advances.pdf.

[2027] Fahy GM, Wowk B, Wu J, Phan J, Rasch C, Chang A, Zendejas E. Cryopreservation of organs by vitrification: perspectives and recent advances. Cryobiology. 2004 Apr;48(2):157-78; http://www.21cm.com/pdfs/cryopreservation_advances.pdf.

each cell, tissue, and organ type could be inserted as deemed desirable. When the vitrified body is later quickly warmed, it will pass through the intermediate temperature ranges where ice might normally begin to form (e.g., ~173 K),[2028] and through the aqueous freezing point (~273 K), without any ice formation and without creating any additional cellular damage needing repair. After parking the process near 273 K (0 °C) in the reliquidified state, revival would then entail (1) installation of vasculoid (Section 4.6), (2) molecular extraction of the cryoprotectant (Section 4.10.1.7), (3) patient warmup to 310 K (37 °C) and molecular instillation (Section 4.13), (4) vasculoid uninstallation and blood substitution (Section 4.14), and (5) patient wakeup (Section 4.15). The validity of this protocol and the details of cryoprotectant embedding should be critically reviewed in ***future research***.

(B) **Embedded Thermocytes.** To enable sufficiently fast and uniform whole-body warming, fully-energized thermal generator nanorobots could be inserted into the atomic print file and distributed uniformly throughout the body in sufficient quantity to permit widespread positionally-controlled ultra-rapid warming. These devices would be manufactured alongside the biomaterial and could be triggered simultaneously or in a rolling wave, promptly raising whole-body temperature through the freezing point up to 310 K (37 °C) normal body temperature and forestalling freezing damage due to warming. After warmup, the nanorobots could be removed. The technical and mission design of thermocyte nanorobots should be undertaken in ***future research***.

The energy required to warm water-ice from 77 K (-196 °C) to 273 K (0 °C), melt it, then warm it from 273 K to 310 K (37 °C), is $E_{thaw,body} \sim \rho_{ice}\ c_{ice}\ (T_{273K} - T_{77K}) + \rho_{ice}\ H_{fusion,water} + C_{V,water}\ (T_{310K} - T_{273K}) = 6.68 \times 10^8$ J/m^3, taking $\rho_{ice} = 916.7$ kg/m^3 (the density of ice at 0 °C), $c_{ice} \sim 1400$ J/kg-K (the average specific heat capacity of ice over the indicated temperature range),[2029] $H_{fusion,water} = 333{,}550$ J/kg (the heat of fusion of water at 0 °C),[2030] and $C_{V,water} \sim 3 \times 10^6$ J/m^3-K (over the indicated temperature range). If the entire human body volume $V_{body} = 0.06$ m^3 was water (the most conservative assumption), the thermal generator nanorobots would have to release $E_{vitriwarm} = E_{thaw,body}\ V_{body} = 4 \times 10^7$ J of energy. A release time of $t_{warm} \sim$ **200 sec** would produce a highly-uniform body-wide power pulse at $E_{vitriwarm} / t_{warm} \sim$ **200 KW**[2031] producing a $(T_{310K} - T_{77K}) / t_{warm} \sim$ **60 °C/min** (~1 K/sec) heating rate, roughly comparable to tissue "nanowarming".[2032] This would require embedding a total volume of $V_{thermbots} = E_{vitriwarm} / f_{flywheel}\ E_D \sim 0.9$ L of thermal generator nanorobots (each with $f_{flywheel} = 50\%$ of their volume devoted to 1-μm diameter diamond flywheels mounted on single-atom acetylenic bearings spun up to the maximum energy density of $E_D \sim 90$ MJ/L with a half-life of ~50 days),[2033] occupying only $V_{thermbots} / V_{body} \sim 1.5\%$ of the human body

---

[2028] Personal communication from Brian Wowk to Robert Freitas, 16 Oct 2020.

[2029] Robert C. Weast, Handbook of Chemistry and Physics, 49th Edition, CRC, Cleveland OH, 1968; "Specific Heat of Ice," -200 °C to -2.2 °C, p. D-95. See also: https://www.engineeringtoolbox.com/ice-thermal-properties-d_576.html.

[2030] https://en.wikipedia.org/wiki/Properties_of_water.

[2031] A 200 KW power level externally applied to an entire human body through a mean skin surface area ~2 m^2 would imply a surface intensity of ~100 KW/m^2, which is only slightly above the conservative maximum recommended safe exposure limit for incident ultrasonic acoustic power for whole-body exposures of 10-100 sec. Freitas RA Jr. Nanomedicine, Volume I: Basic Capabilities, Landes Bioscience, Georgetown TX, 1999, Fig. 6.8; http://www.nanomedicine.com/NMI/Figures/6.8.jpg.

[2032] Magnetically-driven nanoparticle heating in cryoprotectant solutions has achieved up to **320 °C/min** in "nanowarming".[*] Another group has reached >130 °C/min warming rates with similar particles.[†]

[*] Chiu-Lam A, Staples E, Pepine CJ, Rinaldi C. Perfusion, cryopreservation, and nanowarming of whole hearts using colloidally stable magnetic cryopreservation agent solutions. Science Advances 2021 Jan 8;7(2):eabe3005; https://advances.sciencemag.org/content/7/2/eabe3005.full.

[†] Manuchehrabadi N, Gao Z, Zhang J, Ring HL, Shao Q, Liu F, McDermott M, Fok A, Rabin Y, Brockbank KG, Garwood M, Haynes CL, Bischof JC. Improved tissue cryopreservation using inductive heating of magnetic nanoparticles. Sci Transl Med. 2017 Mar 1;9(379):eaah4586; https://www.ncbi.nlm.nih.gov/pmc/articles/PMC5470364/.

[2033] Freitas RA Jr. Energy Density. IMM Report No. 50, 25 June 2019; Section 5.3.2, "Rotational Motion"; http://www.imm.org/Reports/rep050.pdf.

volume. If each nanorobot has volume V_{bot} = 10 μm^3/nanorobot, then we require $N_{bots} = V_{thermbots} / V_{bot}$ = **9 x 10^{13} nanorobots** distributed evenly throughout a human body volume of V_{body} = 0.06 m^3 with a mean separation of $L_{botsep} = (V_{body} / N_{bots})^{1/3}$ = 8.7 μm between nanorobots, having a thermal equilibration time of $t_{EQ} = L_{botsep}^2 C_V / K_t$ ~ 0.025 msec taking volumetric heat capacity C_V ~ 10^6 J/m^3-K and thermal conductivity K_t ~ 3 W/m-K as average values for water-ice over the 77-273 K range. Further analysis of this technical approach, including determining (1) the minimum rapid-warming rate needed to avoid ice formation (see discussion of ice nucleation in regard to Intermediate Temperature Storage in Section 7.1.2), (2) the warming power needed using thermophysical parameters for M22 solution rather than pure water, (3) the safe maximum heating rate and maximum tolerable uniform body-wide power density,[2034] and (4) the potential utility of a spatially patterned heating wave rather than simultaneous uniform nanorobot activation throughout the entire body, should be undertaken in ***future research***.

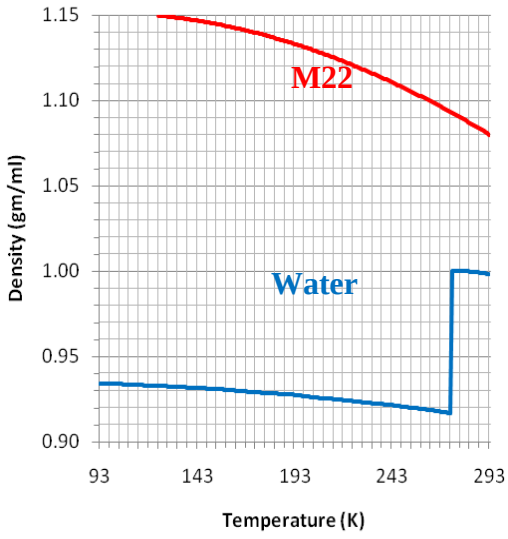

The compacted corrected scan file is modified as described with the addition of embedded cryoprotectant molecules or thermocyte nanorobots, and is further modified to create a description of a human body in full metabolic stasis, with all metabolic biochemicals removed from all tissues as described in Section 4.10.

One last potential difficulty is differential thermal expansion of ice upon warming. Conventional hexagonal water-ice has a density of 0.935 gm/ml at the LN2 storage temperature of 77 K (-196 °C), falling gradually to 0.917 gm/ml as it warms to 273 K (0 °C) with the ice slowly expanding +2% in volume and +0.7% in linear dimension, then suddenly contracting -9% in volume or -2.9% in linear dimension as the ice melts to liquid water at 273 K with density spiking to 1.000 gm/ml (blue curve in the chart at left).[2035] Thermal stresses caused by the initial modest expansion of tissue filled with pure water-ice as it warms from 77 K to 273 K could probably be

---

[2034] In 1990, Merkle proposed[*] emplacing ~10^{15} high-energy H_2/F_2-fueled chemical pellets X_{pellet} ~ 1 μm apart uniformly throughout a frozen brain, which, upon simultaneously releasing all their stored chemical energy (E_{pell} ~ 10^6 J for 75 gm ~ 75 cm^3 of HF, or ~5% of brain volume), would raise the temperature of the V_{brain} ~ 1.4 liter brain from its cryogenic storage temperature (T_1 = 140 K) to human body temperature (T_2 = 310 K) in "a few microseconds" (i.e., τ_{bang} ~ 3 μsec) giving a heating rate of **3.4 billion °C/min** and a power density of $P_D \sim E_{pell} / V_{brain} \tau_{bang}$ ~ 2.4 x 10^{14} W/m^3 (about 1/4 of the ~10^9 MW/m^3 power density of a Type II supernova[†]) during the period of operation, possibly imposing interesting thermomechanical stresses on the frozen material. For example, linear expansion of $L_{displace} = L_0 \alpha_{ice,avg} (T_2 - T_1)$ ~ 1.3 mm for an L_0 ~ 15 cm long block of ice with expansion coefficient α_{ice} ~ 50 x 10^{-6} K^{-1} (Section 3.4.3) in only τ_{bang} sec would generate an acoustic pulse velocity of $v_{bang} = L_{displace} / \tau_{bang}$ ~ 400 m/sec, which is the initial velocity of a nitroglycerine impact explosion,[‡] given that the thermal equilibration time $t_{EQ} \sim X_{pellet}^2 C_{V,ice} / K_{t,ice}$ = 0.8 μsec << τ_{bang}, taking $C_{V,ice}$ ~ 1.7 x 10^6 J/m^3-K and $K_{t,ice}$ ~ 2.2 W/m-K. For isolated individual cells, heating can be very rapid. The fastest single-cell nanowarming to date was accomplished by placing gold nanorods inside a zebrafish embryo filled with cryoprotectant that was submerged in LN2 and cooled at **90,000 °C/min**, then warmed with a 1 msec burst from a 1064 nm infrared laser, heating the cell to room temperature at **14 million °C/min** without devitrification (reversion from glass to ice) of the cytosol.[**]

[*] Merkle RC. Cold starting. Cryonics 1990 Nov;11(11):11; https://www.alcor.org/docs/cryonics-magazine-1990-11.txt.

[†] https://en.wikipedia.org/wiki/Type_II_supernova.

[‡] Bowden FP, Gurton OA. Birth and growth of the explosion in solids initiated by impact. Nature 1948 Mar 6;161:348; https://www.nature.com/articles/161348a0.

[**] Khosla K, Wang Y, Hagedorn M, Qin Z, Bischof J. Gold Nanorod Induced Warming of Embryos from the Cryogenic State Enhances Viability. ACS Nano. 2017 Aug 22;11(8):7869-7878; https://pubmed.ncbi.nlm.nih.gov/28702993/.

[2035] https://en.wikipedia.org/wiki/Properties_of_water#Density_of_water_and_ice.

avoided by printing water-ice molecules at 2% lower number density than would otherwise be indicated, giving the ice some space in which to expand as it warms. When the ice reliquidifies and quickly shrinks in volume at 273 K (0 °C), there will arise a net -9% deficit in water volume that must later be replaced during molecular instillation (e.g., Section 4.13). Apparently the densities of hexagonal ice and amorphous or vitrified ice are about the same in the solid state.[2036]

The thermal expansion profile of M22 cryoprotectant (Section 4.10.1.7) is different, as indicated by the density data[2037] (red curve) in the chart above. M22 smoothly declines in density and expands in volume by a total of +6.5% (or +2.1% in linear dimension) as it warms from 123 K (-150 °C) to 293 K (20 °C), with no sudden melt-related volume contraction as occurs for water. For a pure M22 solution, the body could be printed with M22 molecules at an overall 6.5% lower number density than would otherwise be indicated, leaving sufficient room for the warmup expansion. The ideal low-density distribution print pattern to minimize the buildup of mechanical stress and warmup fracturing, for the particular cryoprotectant compositions and concentrations chosen, should be explored in ***future research***.

The resulting datafile is then translated into a suitable atomic print file – e.g., by unpacking the compacted molecular descriptions in the corrected scan file into full atomistic descriptions – that can direct the operation of the 3D atomic printer. The printer then fabricates the cryopreserved patient's replacement body inside a cryogenic UHV chamber, atom by atom (or moiety by moiety). Since the atomic printing process is essentially the time-reversed version of the atomic scanning process previously described in Section 5.2.1, the same equipment and procedures can be employed with similar quantification as estimated in Section 5.2.1.3, using similar amounts of nanocomputer mass and power. In the most expeditious scenario considered in this work, the 3D atomic printer would require a print time of $\tau_{360\text{-Plane}}$ = **1 month** to fabricate the replacement body as 180 separate vitreous slices averaging ~1 cm thick.[2038]

The slices are subsequently combined into a seamless whole body by operating the segmentation ribbon mechanism in reverse, reattaching the segments across matching faces, molecule by molecule. The time required to reassemble n_{slice} = 180 separate vitreous slices may be roughly comparable to the time required to perform the original segmentation into separate slices, or τ_{slice} ~ 10 days, involving an additional n_{slice} $N_{ManipLine}$ ~ 1.07 x 10^9 nanomanipulators on 179 nanosegmentation ribbons (Section 5.2.1.3).

The total active nanorobotic system mass in the 3D atomic printer has been estimated as ~**0.1 kg** (Section 5.2.1.3), although the complete printing system might be several orders of magnitude larger in total mass, especially including the mass of the cryogenic UHV chamber and its support equipment. A continuous power draw of $P_{1mo,print}$ ~ $P_{scan,1mo}$ + $P_{1mo,\ bonds}$ ~ 1217 watts was estimated for the fastest operation of the nanomechanical equipment alone.

These resource requirements might be reduced by a factor of up to (V_{brain} / V_{body}) ~ 43 for a print job involving only the human brain, in the case of neuro patients.

Future research must also define the appropriate molecular tools and procedures for handling two special circumstances that will occur repeatedly during an atomic print run: (1) how to initiate the fabrication of a

---

[2036] Ghormley JA, Hochanadel CJ. Amorphous ice: density and reflectivity. Science 1971 Jan 8;171(3966):62-64; https://science.sciencemag.org/content/171/3966/62.full.pdf.

[2037] Estimated density data for M22 as a function of temperature in the chart (using the Rabin model for VS55 thermal expansion fitted to M22 density at room temperature) was kindly provided by Brian Wowk of 21st Century Medicine on 12 Oct 2020.

[2038] ***Future research*** should parameterize the key variables and explore the optimum volume, geometry, and dimensions of the "slices" based on technical tradeoffs -- e.g., weighing the benefits and demerits of replacing large slices with vastly more numerous manufactured cubes 1 mm^3 or even 1 μm^3 in size, or with mixed tissue blocks of various sizes and shapes.

new biomolecule[2039] when no atoms have yet been laid down to anchor the initial structure onto the "workpiece" as the next atoms are emplaced; and (2) how to pick and place water molecules[2040] onto the growing "workpiece".

After stabilization in the reliquidified state, revival then entails (A) installation of vasculoid (Section 4.6), (B) molecular extraction of any cryoprotectant (Section 4.10.1.7), (C) patient warmup to 310 K (37 °C) and molecular instillation (Section 4.13), (D) vasculoid uninstallation and blood substitution (Section 4.14), and (E) patient wakeup (Section 4.15). The details and validity of this protocol should be critically reviewed in ***future research***.

5.2.3.2 Cryogenic 3D Molecular Print

A very high-quality reconstruction of the patient's physical body using the corrected scan file can be achieved by printing the body as a solid block of biomatter, using molecules as the primitive building blocks rather than individual atoms or small chemical moieties. The compacted corrected scan file contains a highly accurate description of the identity, position, and orientation of every molecule in the patient's body. All molecules needed for construction can be manufactured in the Biosynthesis Module of the cell mill (Appendix D). Working solely with molecules eliminates the need for mechanosynthesis in the final printing process, hence eliminates the requirement that highly reactive radical sites on a partially printed human body must be continually protected from poisoning by stray molecules in the environment. However, stray environmental molecules, ions, and even free radicals[2041] could still attach or insert themselves into a growing construction, creating an erroneous structure, so it remains a necessity for fabrication to occur in an ultra-high vacuum (UHV) chamber. The use of cryogenic (LN2, but especially LHe) temperatures during assembly of the replacement body also ensures a high-quality vacuum, freezing out virtually all ambient contaminants.

Regarding the temperature of operation, thermal vibrations and Brownian motion at room temperature would thoroughly disrupt the physical structure as it's being built. By fabricating at LN2 (~77 K) or LHe (~4 K) temperatures, we ensure that molecules will stay where we put them with minimal disruption as the physical structure is assembled like a 3D jigsaw puzzle. For example, the root mean square displacement[2042] of a molecule of radius R = 1 nm over an observation period of $\tau \sim 10^6$ sec (~2 weeks) is

---

[2039] Several possibilities include: (1) restrain the nascent molecule with a weak covalent bond on a temporary holder while enough atoms are added to ensure a stable base for further work, then bring in an H donation tool that breaks the weak bond, passivates the resulting radical, and releases the molecule from the temporary holder; (2) build a fragment of the molecule on the temporary holder, then insert and release it into a reversible binding site after passivating the resulting radical site on the molecule fragment, then position the binding site over the desired transfer location and switch the binding site from attractive to repulsive, releasing the molecular fragment, after which molecular fabrication can resume to completion at the transfer location; (3) fabricate and insert the entire molecule into a nanotube whose terminus is positioned over the desired deposition site, then slowly force the linearized molecule out of the nanotube in a manner that allows control of positioning and folding (in the case of proteins).

[2040] Several possibilities include: (1) design a reversible water molecule binding site which is positioned over the deposition site as the binding site is switched from attractive to repulsive, releasing the weakly bound water molecule; (2) push water molecules one by one out of a nanotube using a piston, analogous to a medicine dropper, with the terminus of the nanotube positioned over the intended deposition site; (3) design a mechanosynthetic tool with two heads that can be pushed together or pulled apart, with H• bonded to one head and •OH to the other, such that a nonradical HOH molecule is formed and released when the two heads are forced together over the desired deposition site.

[2041] Sly PD, Cormier SA, Lomnicki S, Harding JN, Grimwood K. Environmentally Persistent Free Radicals: Linking Air Pollution and Poor Respiratory Health? Am J Respir Crit Care Med. 2019 Oct 15;200(8):1062-1063; https://www.atsjournals.org/doi/full/10.1164/rccm.201903-0675LE.

[2042] Freitas RA Jr. Nanomedicine, Volume I: Basic Capabilities, Landes Bioscience, Georgetown TX, 1999; Section 3.2.1, "Brownian Motion", http://www.nanomedicine.com/NMI/3.2.1.htm#p2.

$\Delta X = (k_B T \tau / 3\pi \eta R)^{1/2}$ = **600 pm** in frozen water-ice of viscosity $\eta \sim 10^{12}$ Pa-sec at the moderately high sub-melt temperature of T ~ 260 K,[2043] taking Boltzmann's constant $k_B = 1.38 \times 10^{-23}$ J/K, but only $\Delta X \sim$ **0.01 pm** in frozen water-ice of viscosity $\eta \sim 10^{21}$ Pa-sec at temperature T ~ 77 K,[2044] which is a negligible spontaneous random displacement compared to the **154 pm** length of a single C–C bond in a typical organic molecule. At cryogenic temperatures, nonbonded interactions (e.g., van der Waals attractive forces) should suffice to hold the growing assembly in place as later molecules are added to the structure in the correct order. Thus, much like the 3D atomic print scenario (Section 5.2.3.1), a 3D molecular print job should be conducted inside a cryogenic fabrication chamber under UHV.

To create the 3D molecular print datafile, the objective is again to fabricate a vitrified version of the cryopreserved patient's body, with cryoprotectant molecules inserted into the dataset at sufficient concentration and in the ideal pattern to forestall rewarming damage when the replacement body is warmed above the glass transition temperature in preparation for awakening the patient. Hence, the first task is to modify the corrected scan file to reflect the addition of cryoprotectant molecules, as previously described (Section 5.2.3.1(A)). As before, the scan file is also modified to create a description of a human body in full metabolic stasis, with all metabolic biochemicals removed from all tissues as described in Section 4.10.

Second, we must extract from the cryoprotectant-corrected scan file a complete list of the molecules to be fabricated, including all required variants, both generic and personalized, along with the exact number of each molecule that is needed. This creates a "parts list" that can be sent to the Biosynthesis Module of the cell mill (Appendix D) for manufacture.

Third, we must translate the cryoprotectant-corrected scan file into an ordered sequence of assembly steps that specifies which molecule to lay down first and in what orientation, then where to put the second molecule and in what orientation, and so forth. This computational translation process will employ a Molecular Assembly Sequencing Algorithm (MASA) that is yet to be developed. As previously noted (Section 4.8.3), early versions of MASA-related algorithms already exist in extremely primitive form. For

---

[2043] Fowler AC. Glaciers and ice sheets. In: Diaz JI, ed., The Mathematics of Models for Climatology and Environment, NATO ASI Series 1: Global Environmental Change, Vol. 48, Springer-Verlag Berlin Heidelberg, 1977, pp. 301-336; https://link.springer.com/chapter/10.1007%2F978-3-642-60603-8_9. Debenedetti PG, Stillinger FH. Supercooled liquids and the glass transition. Nature. 2001 Mar 8;410(6825):259-67; http://www.physics.emory.edu/faculty/weeks/lab/papers/debenedetti-nat01.pdf. Angell CA. Liquid fragility and the glass transition in water and aqueous solutions. Chem Rev. 2002 Aug;102(8):2627-50; https://citeseerx.ist.psu.edu/viewdoc/download?doi=10.1.1.620.1853&rep=rep1&type=pdf.

[2044] One estimate is that the absolute viscosity of solidified aqueous vitrification solutions at 77 K may be as low as ~3×10^{21} Pa-sec (Ben Best, "Molecular Mobility at Low Temperature," 2007; https://www.benbest.com/cryonics/mobility.html). The compressive strength of granite ($\eta \sim 10^{21}$ Pa-sec in Earth's mantle) is ~200 MPa (https://en.wikipedia.org/wiki/Granite), very near the ~120 MPa compressive strength of ice at 100 K (close to LN2 temperatures); Wu X, Prakash V. Dynamic compressive behavior of ice at cryogenic temperatures. Cold Regions Sci Technol. 2015;118:1-13; https://www.researchgate.net/profile/Xianqian_Wu/publication/278744289_Dynamic_Compressive_Behavior_of_Ice_at_Cryogenic_Temperatures/links/5be3f2f04585150b2ba6eb12/Dynamic-Compressive-Behavior-of-Ice-at-Cryogenic-Temperatures.pdf.

example, numerous automated jigsaw puzzle assembly algorithms have been published,[2045] including one package that can assemble 10,000 pieces using software that is "fully automatic, requires no manually provided hints, operates on puzzles having thousands of pieces, and does so with near perfect performance",[2046] and another package that used a genetic algorithm to solve a 22,834-piece puzzle in only 13.2 hr of runtime on a PC and could allegedly solve "more difficult variations of the jigsaw problem."[2047]

A defluidized 70 kg (~60 L) cryopreserved human body with a molecular scan volume of $V_{MSV} \sim 41{,}053$ cm^3 (Section 5.1) may include $N_{MSVwater} \sim 8.95 \times 10^{26}$ water molecules and $N_{MSVnonwaterM} \sim 1.03 \times 10^{25}$ nonwater molecules (Section 5.2.1.1), or $N_{MSVparts} \sim 10^{27}$ "puzzle pieces", so the Molecular Assembly Sequencing Algorithm must be able to successfully complete a vastly larger jigsaw puzzle problem than has ever been attempted before. The problem appears tractable because the complexity will usually be confined to fairly localized volumes of interlocking molecules, so the computational requirements should be workable using much smaller subpuzzle segments. One crude measure of feasibility is provided by the Sholomon algorithm cited above, which solved an $N_{Sholomon} = 22{,}834$ piece puzzle in $t_{Sholomon} = 47{,}520$ sec (13.2 hr) using a 2013-vintage ~1 GHz personal computer ($\nu_{Sholomon} \sim 10^9$ bits/sec), giving a puzzle computational intensity of $Z_{puzzlecomp} = \nu_{Sholomon}\ t_{Sholomon} / N_{Sholomon} = 2.08 \times 10^9$ bits/part. We will assume that a future more efficient algorithm can reduce this computational intensity by a factor of $r_x = 10$ to $Z_{puzzlecompx} = \nu_{Sholomon}\ t_{Sholomon} / r_x\ N_{Sholomon} = 2.08 \times 10^8$ bits/part. Applying a Molecular Assembly Sequencing Algorithm with this reduced computational intensity to a biomolecular puzzle with $N_{MSVparts} \sim 10^{27}$ parts (likely comprising numerous much smaller and more tractable subpuzzles) would solve the whole-body molecular assembly puzzle problem in $t_{compute} = Z_{puzzlecompx}\ N_{MSVparts} / V_{nanocomp}\ U_{nano} = 2.08 \times 10^6$ sec (~**24 days**) using $V_{nanocomp} \sim 0.1\ m^3$ of diamondoid mechanical nanocomputers having a specific processing power $U_{nano} \sim 10^{30}$ bit/sec-m^3 (Section 4.8.5), while drawing $P_{comp} \sim Z_{puzzlecompx}\ N_{MSVparts}\ E_{Landauer77K} / t_{compute} \sim 74$ MW of power, costing ~$7400/hr for electricity at today's typical commercial rate of ~$0.10/KW-hr ($e_\$ \sim 2.78 \times 10^{-8}$ $/J; Appendix G) with a total electricity cost of ($e_\$\ t_{compute}\ P_{comp}$) ~ **$4,300,000** to complete these calculations for a single whole-body revival, or perhaps a bit less,[2048] using an LN2-cooled nanocomputer with $E_{Landauer77K} \sim k_B T \ln(2)$ J/bit $= 7.4 \times 10^{-22}$ J/bit at T = 77 K (-196 °C). The specifications, software concepts and designs, and computer hardware required to create and run the

---

[2045] Kosiba DA, Devaux PM, Balasubramanian S, Kasturi R. An automatic jigsaw puzzle solver. Proc. 12th Int. Conf. Pattern Recognition, Vol. 1,1994:616-618; http://citeseerx.ist.psu.edu/viewdoc/download?doi=10.1.1.344.1536&rep=rep1&type=pdf. Goldberg D, Malon C, Bern M. A global approach to automatic solution of jigsaw puzzles. Proc 18th Ann Symp Comput Geom ACM, 2002 Jun 5;82-87; http://www.parc.com/content/attachments/global_approach_automatic_4365_parc.pdf. Cho TS, Avidan S, Freeman WT. A probabilistic image jigsaw puzzle solver. Proc. 2010 IEEE CVPR, 2010; http://people.csail.mit.edu/taegsang/Documents/JigsawSolver.pdf. Pomeranz D, Shemesh M, Ben-Shahar O. A fully automated greedy square jigsaw puzzle solver. IEEE Conference on Computer Vision and Pattern Recognition, 2011:9-16; http://citeseerx.ist.psu.edu/viewdoc/download?doi=10.1.1.298.3227&rep=rep1&type=pdf. Paikin G, Tal A. Solving multiple square jigsaw puzzles with missing pieces. Proc. IEEE Conf Comput Vision Pattern Recog. 2015:4832-4839; http://webee.technion.ac.il/~ayellet/Ps/15-PT.pdf.

[2046] Gallagher A. Jigsaw puzzles with pieces of unknown orientation. IEEE Conf Comput Vision Pattern Recog 2012:382-389; http://citeseerx.ist.psu.edu/viewdoc/download?doi=10.1.1.405.927&rep=rep1&type=pdf. "Computational Jigsaw Puzzle Solving," Interdisciplinary Computational Vision laboratory, 2012; http://www.cs.bgu.ac.il/~icvl/icvl_projects/automatic-jigsaw-puzzle-solving/.

[2047] Sholomon D, David O, Netanyahu NS. A Genetic Algorithm-Based Solver for Very Large Jigsaw Puzzles. 2013 IEEE Conf. Comp. Vision Pattern Recog. 2013 Jun:1767-1774; http://www.cv-foundation.org/openaccess/content_cvpr_2013/papers/Sholomon_A_Genetic_Algorithm-Based_2013_CVPR_paper.pdf, https://www.aaai.org/ocs/index.php/AAAI/AAAI14/paper/viewFile/8650/8638, and http://www.genetic-programming.org/hc2014/Sh-Paper.pdf.

[2048] It is estimated that the cost of commercial electricity might decline up to 100-fold in the era of widespread atomically-precise manufacturing using nanofactories (Appendix G), in which case the energy cost of the nondestructive scan might fall to only $43,000 whereupon other costs (e.g., labor) might predominate.

MASA code package, including at least a tenfold improvement in computational efficiency over the Sholomon algorithm, may be suitable development projects for ***future research***.

Unlike atomic print jobs, in which radical sites are created to join atoms or small chemical moieties with strong covalent bonds, molecular print jobs use no radical sites and employ only nonbonded interactions (e.g., van der Waals adhesive forces) to induce whole molecules to stick to each other. One example of this "weak bonding" approach is found in the plasma membranes of cells, wherein phospholipid molecules weakly bond into sheets or membranes using radical-free noncovalent bonds (Section D.2.1). In fact, most multi-molecular structures in the human body are held together in this manner, and we can use this same approach to assemble a replacement human body using whole molecules as the fundamental building blocks.

Both generic and personalized whole molecules can be synthesized in the Biomolecule Synthesis Module of the cell mill (Section D.1), then delivered to the construction site via a nanomechanical conveyor belt (image, right)[2049] that can deliver molecules trapped in binding sites, aka. "reagent devices," one at a time. According to one analysis of this theoretical design,[2050] a 20-roller conveyor line 1 micron long might have a ~2 micron long belt with 500 closely packed reagent devices measuring 4 nm x 4 nm x 2 nm (32 nm^3), while delivering $\alpha_{transport} = 10^6$ molecules/sec at a belt speed of 4 mm/sec, with a total conveyor line mass of $M_{conveyor} \sim 6 \times 10^{-20}$ kg (~3 million carbon atoms) or $m_{conveyor} \sim 6 \times 10^{-14}$ kg/meter of conveyor length. Operation is in cryogenic UHV vacuum conditions. Total power dissipation is $P_{conveyor} \sim 1.4 \times 10^{-18}$ watts, a rate of ~0.001 zJ per moiety (or per reagent device) delivered or $E_{transport} \sim 10^{-6}$ zJ/nm (~10^{-18} J/m) traveled per reagent device. Transporting $N_{MSVparts} \sim 10^{27}$ molecules across a distance $x_{transport} \sim 1$ meter between cell mill and assembly chamber during a $t_{assembly} \sim 2.1 \times 10^6$ sec (~25 day) assembly time requires a continuous molecular transport power of $P_{transport} = x_{transport}\ E_{transport}\ N_{MSVparts} / t_{assembly} \sim 480$ watts and a conveyor system of mass ($m_{conveyor}\ x_{transport}$) ~ 6×10^{-14} kg. This does not include the mass of the motors, gearing, housings, control systems, and other support mechanisms, but is consistent with the assumption that the import transport system as a whole should have modest power and mass requirements compared to the rest of the system. Note that a cell mill scaled to produce ~1 kg/hr of biomolecules (Appendix D) can produce all whole molecules necessary to manufacture a 70 kg replacement human body in ~ 70 hours.

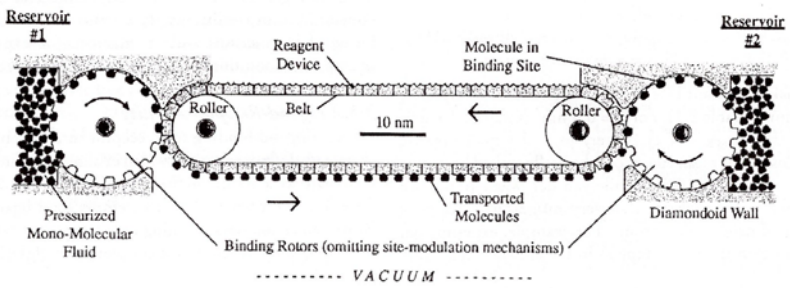

Manufactured whole molecules are transported into the central channels of robotic nanomanipulator devices 30 nm in diameter and 100 nm in length with a 100 nm x 100 nm range of motion at the tip (Section 5.2.1.1), which emplace these molecules onto the worksite in the desired position and orientation as specified by the molecular print file. Transported molecules travel up the central shaft of the nanomanipulator and could be temporarily noncovalently bound in programmable reconfigurable "pin

---

[2049] Freitas RA Jr. Nanomedicine, Volume I: Basic Capabilities, Landes Bioscience, Georgetown TX, 1999, Fig. 3.9; http://www.nanomedicine.com/NMI/Figures/3.9.jpg. Adapted from: Drexler KE. Nanosystems: Molecular Machinery, Manufacturing, and Computation, John Wiley & Sons, New York, 1992, Section 13.3.1, "Reactive encounters using belt and roller systems"; https://www.amazon.com/dp/0471575186/.

[2050] Freitas RA Jr. Nanomedicine, Volume I: Basic Capabilities, Landes Bioscience, Georgetown TX, 1999; Section 3.4.3, "Internal Transport Streams", http://www.nanomedicine.com/NMI/3.4.3.htm#p2.

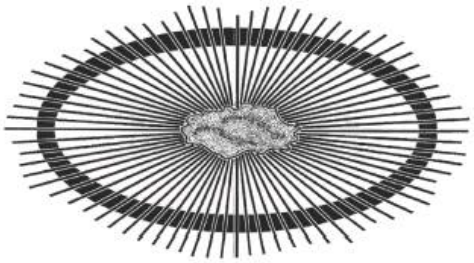

cushion" binding sites (image, left).[2051] These binding sites use a 3D array of narrow sliding rods to create a custom binding pocket "on the fly" that has maximum affinity for the particular target molecule. Once the molecule is in place on the workpiece, the pins are retracted, returning the affinity of the binding nearly to zero, and repulsive pins can be extended, forcing release of the molecule onto the workpiece.[2052] The binding site can then be automatically reconfigured for the next molecule that is set to arrive. Most molecules may be relatively stiff and unmoving at cryogenic temperatures, but for very long molecules with tortuous, coiled, or twisted emplacement geometries, it may become necessary to emplace temporary support jigs to allow smaller molecules to be packed around the constrained larger twisted molecule, locking the larger molecule into a specific position or orientation. These temporary jigs would then be removed once the large-molecule assembly is sufficiently stable and unlikely to rearrange itself. The further specification and design of these reversible binding sites, temporary jigs, and assembly procedures are a suitable topic for ***future research***.

If the molecule volumetric placement rate is similar to that for the removal of water molecules (which are also treated as whole molecules; Section 5.2.1.1), then the biomolecule placement rate is $\mathfrak{V}_{MolecularEmplacement} \sim \mathfrak{V}_{IceRemoval} \sim 16{,}384$ nm^3/manipulator-sec,[2053] in which case the whole-body build time may be crudely estimated as $t_{assembly} = V_{MSV} / N_{manipulators}\ \mathfrak{V}_{MolecularEmplacement} \sim 2.1 \times 10^6$ sec (~25 days), taking $V_{MSV} \sim 41{,}053$ cm^3 (Section 5.1) and $N_{manipulators} \sim 1.17 \times 10^{15}$ nanomanipulator devices for performing a whole-body molecular print job on 180 separate slices each ~1 cm thick dissipating $P_{scan,1mo} \sim 117$ watts of total continuous energy (Section 5.2.1.3). The 180 slices are subsequently restacked into a completed body by joining the matched faces of slice pairs using a segmentation ribbon mechanism (Section 5.2.1.3) operated in reverse to rejoin rather than separate the opposed tissue planes. As in the previous Section, the optimum volume, geometry, and dimensions of the "slices" are a subject for ***future research***.

The end state of the print process described in this Section is a fully repaired and viable replacement human body in biochemical stasis that has been rapidly rewarmed to near 273 K (0 °C) in the reliquidified state, exactly as we have at the end of Section 4.12 but with greater molecular fidelity to the original cryopreserved body. As in the cryogenic 3D atomic print scenario, revival then entails (A) installation of vasculoid (Section 4.6), (B) molecular extraction of the cryoprotectant (Section 4.10.1.7), (C) patient warmup to 310 K (37 °C) and molecular instillation (Section 4.13), (D) vasculoid uninstallation and blood substitution (Section 4.14), and (E) patient wakeup (Section 4.15). The details and validity of this protocol should be critically reviewed in ***future research***.

Future research must also define the special mechanosynthetic tools, reaction sequences, and related procedures needed to fabricate extended regions of noncovalently bonded ionic solids such as hydroxyapatite[2054] that are found in the teeth (e.g., enamel,[2055] dentin,[2056] and cementum[2057]) and bones[2058] of the human body.

[2051] Freitas RA Jr. Nanomedicine, Volume I: Basic Capabilities, Landes Bioscience, Georgetown TX, 1999, Fig. 3.14; http://www.nanomedicine.com/NMI/Figures/3.9.jpg.

[2052] Freitas RA Jr. Nanomedicine, Volume I: Basic Capabilities, Landes Bioscience, Georgetown TX, 1999; Section 3.5.7.4, "Pin Cushion Model", http://www.nanomedicine.com/NMI/3.5.7.4.htm.

[2053] The 16,384 nm^3/manipulator-sec figure corresponds to a single manipulator achieving a molecule placement rate of ~164 molecules/sec for ~100,000-dalton protein molecules each of volume ~100 nm^3, which seems aggressive but plausible. Reasonable estimates for molecule placement rates should be further examined in ***future research***.

[2054] https://en.wikipedia.org/wiki/Hydroxyapatite.

[2055] https://en.wikipedia.org/wiki/Human_tooth#Enamel.

5.2.3.3 Fluidic 3D Cell Print

A good-quality reconstruction of the patient's physical body using the corrected scan file can be achieved by printing the replacement human body from its constituent cells as the primary building blocks, in combination with a variety of biological fibers, meshes, mineralized structures, and other binding and connective materials. The compacted corrected scan file, which contains a highly accurate description of the identity, position, and orientation of every molecule in the patient's body, must be computationally segregated into cellular and noncellular components, after which all identified individual cells can be manufactured in the Cell Assembly Module of the cell mill (Section D.3) and the noncellular materials can be manufactured in the Biosynthesis Module of the cell mill (Section D.1). ***Future research*** must confirm that this approach can recreate a replacement body with sufficient fidelity to the (repaired) original patient as to preserve acceptable levels of patient memory and personal identity.[2059]

It might be possible to manufacture whole cells in the solid frozen state, with their protruding and possibly quite lengthy processes (e.g., the axons and dendrites of neurons) pre-manufactured with the exactly correct twists, folds, coils, and geometrically complementary surfaces exactly matching their final emplaced geometry that could in theory permit their subsequent assembly into solid tissue alongside other similar frozen cells, much like the solid rigid pieces of a jigsaw puzzle are fitted together but in 3D. Unfortunately, given cells with more than a minimum of geometric feature complexity, it seems likely that in many cases these physical constraints could be sufficiently restrictive to leave no available assembly pathway. Installing whole cells in a flexible reliquidified state, perhaps just slightly above the melting point of water-ice near 273 K (0 °C), eliminates this problem, just as 3D jigsaw pieces composed of jointed sections or even putty would be more assemblable than solid pieces composed of a rigid ceramic. Reliquidified cells manipulated under vacuum conditions would rapidly desiccate, so a fluidic cell print should be conducted in a liquid environment.

The most convenient liquid assembly environment is pure water. Because ions and many soluble small molecules could leach out of the cells into a watery bath via osmosis during a long assembly process, to use water-based assembly the corrected scan file must not only have all metabolites removed from the description, but all water-soluble molecules must also be deleted from the scan file description and thereupon omitted from cells that are manufactured in the cell mill, creating osmotically-inactive cells. (Such deleted molecules can later be restored to cells during the instillation phase of revival, e.g., Section 4.13.) It might be possible to identify some alternative inert fluid in which water-soluble molecules were insoluble, hence would not support small-molecule leaching from cells, but no such solvent has yet been identified. For example, the noble gas xenon under 41.54 bars pressure becomes a liquid at 273.35 K just above the melting point of water;[2060] unfortunately, liquid xenon's high polarizability allows it to readily dissolve small organic molecules such as formaldehyde and methanol up to 0.0002-0.02 M

[2056] https://en.wikipedia.org/wiki/Human_tooth#Dentin.
[2057] https://en.wikipedia.org/wiki/Human_tooth#Cementum.
[2058] https://en.wikipedia.org/wiki/Bone#Composition.

[2059] Numerous issues must be resolved by ***future research***. For instance, can a cell mill reproduce the original molecular structure of fabricated cells to sufficient accuracy and completeness to preserve memory and personal identity? Are biological printed structures stable enough over the course of a fluidic print job that may take many days or weeks to complete – e.g., might normal thermal agitation in 273 K water cause sufficient physical displacement of a precisely positioned synapse to reduce the fidelity or information content of a particular unit of memory?

[2060] Xenon, Physical Properties, Air Liquide, 2020; https://encyclopedia.airliquide.com/sites/gas_encyclopedia/files/014-xenon.xls.

concentrations,[2061] naphthalene,[2062] large organic hydrocarbons and biological molecules,[2063] polymers such as poly(dimethyl-siloxane),[2064] large organic neutral species though not free ions or ion pairs,[2065] and even water,[2066] hence could damage biological membranes, making liquid xenon unsuitable as an alternative cell print environmental fluid.[2067] ***Future research*** could investigate other non-water possibilities for the cell print assembly fluid.

For the present analysis, we will assume that cell printing occurs in an aqueous environment at ~273 K (0 °C) and ~1 atm ambient pressure, and that all cells are manufactured without any water-leachable soluble molecules, metabolites, or ions (all of which are restored to the cell later, by nanorobots, during molecular instillation, e.g., Section 4.13). The corrected scan file is condensed to create an appropriate corrected cell print file, which should detail each cell that needs to be built, where each cell should be positioned and oriented, and the interfaces between each cell and other cells or biomaterials. The corrected scan file can also provide the cell mill with molecular descriptions for each cell to be fabricated, which the cell mill can reproduce to the fullest limits of manufacturing fidelity of which it is capable. ***Future research*** may examine the computational details by which the corrected scan file can be converted into a cell print file appropriate to each of the specific print techniques described below.

At least three alternative techniques for performing a fluidic 3D cell print of a replacement human body have been identified: planar tissue printing (Section 5.2.3.3.1), scaffolded tissue printing (Section 5.2.3.3.2), and nanorobot-guided organic growth (Section 5.2.3.3.3). ***Future research*** should investigate the details of these and other possible fluidic 3D cell printing techniques, then perform a trade study to determine which method may produce the most desirable results with the greatest efficiency and lowest cost.

For the first two cell printing techniques, ***future research*** must also define the appropriate size and shape of fragments of noncovalently bonded ionic solids such as hydroxyapatite[2068] that may be fabricated in a cell mill (Appendix D), and the bonding methods appropriate for joining these fragments into extended proteinaceous matrices as found in human teeth (e.g., enamel,[2069] dentin,[2070] and cementum[2071]) and bones.[2072]

[2061] Beattie WH, Maier WB II, Holland RF, Freund SM, Stewart B. Spectroscopy And Photochemistry In Cryogenic Solutions. Proc SPIE 0158, Laser Spectroscopy: Applications and Techniques, 9 Nov 1978; https://ui.adsabs.harvard.edu/abs/1978SPIE..158..113B/abstract.

[2062] Krukonis VJ, McHugh MA, Seckner AJ. Xenon as a supercritical solvent. J Phys Chem 1984;88:2687-2689; https://pubs.acs.org/doi/pdf/10.1021/j150657a004.

[2063] Rentzepis PM, Douglass DC. Xenon as a solvent. Nature 1981 Sep 10;293:165-166; https://www.nature.com/articles/293165a0.

[2064] Everett DH, Stageman JF. Preparation and stability of novel polymer colloids in a range of simple liquids. Disc Faraday Soc. 1978;65:230-241; https://pubs.rsc.org/en/content/articlelanding/1978/dc/dc9786500230.

[2065] Marshall DB, Strohbusch F, Eyring EM. Solubility of organic substances in liquid xenon. J Chem Eng Data 1981 Jul 1;26(3):333-334; https://pubs.acs.org/doi/pdf/10.1021/je00025a034.

[2066] Rentzepis PM, Douglass DC. Xenon as a solvent. Nature 1981 Sep 10;293:165-166; https://www.nature.com/articles/293165a0.

[2067] The possible use of xenon as a cryoprotectant agent is discussed in Section 7.1.3.

[2068] https://en.wikipedia.org/wiki/Hydroxyapatite.
[2069] https://en.wikipedia.org/wiki/Human_tooth#Enamel.
[2070] https://en.wikipedia.org/wiki/Human_tooth#Dentin.
[2071] https://en.wikipedia.org/wiki/Human_tooth#Cementum.
[2072] https://en.wikipedia.org/wiki/Bone#Composition.

It is of interest that 3D printing of models of human brains to 30 μm (i.e., ~cellular) resolution using photopolymers of specific colors and transparencies was achieved in 2018,[2073] translating CT and MRI scans of the brains of living patients into UV-hardened rubberlike plastic models.

5.2.3.3.1 Planar Tissue Printing

In the seemingly simplest approach, cell-mill-manufactured cells (Appendix D) and accompanying noncellular biomaterials are laid down layer by layer, plane upon plane, building up large blocks of cell-infused living tissue in the manner of present-day 3D printing[2074] and organ printing[2075] systems, but using robotic manipulators capable of achieving more precise positioning – the details of which should be set forth in ***future research***.

For crude scaling purposes, we can imagine a Tissue Assembly Plate coated with large millimanipulators 100 times larger in every dimension than the micromanipulators described in Section D.3. Millimanipulators are D_{milli} = 2 R_{milli} = 300 μm in cylindrical diameter and L_{milli} = 1000 μm (1 mm) in length, with a central transport channel ~100 μm in diameter, large enough to convey even the largest human cell[2076] through the device. The millimanipulator has a 1 mm x 1 mm lateral motion range, an operating volume of $V_{millimanip}$ = 1 mm^3, an arm velocity of v_{manip} ~ 1 cm/sec, and a ~10^4 W/m^3 power density, giving a power dissipation estimate of $P_{millimanipVac}$ ~ 1,000,000 pW (1 μW) for the millimanipulator (compared to ~1000 pW for the micromanipulator and ~1 pW for the nanomanipulator) when operating in vacuum. The activities of the manipulator-covered frontal face of the Tissue Assembly Plate would be supported by a network of transfer tubes, fluid pipes, electrical power and control lines, and other essential infrastructure behind the frontal face and extending to the backside of the Tissue Assembly Plate, as needed to support 3D cell printing operations.

If the replacement human body to be manufactured by 3D cell printing can fit inside a rectangular print chamber that is ~2 meters in length and ~40 cm wide, then a Tissue Assembly Plate of these dimensions with area A_{TAP} = 2 m x 40 cm = 0.8 m^2 with adjacent millimanipulators spaced $x_{millispace}$ = L_{milli} = 1 mm apart has $n_{millimanip}$ = A_{TAP} / $x_{millispace}^2$ = 800,000 millimanipulators mounted on its surface. A millimanipulator traversing the maximum L_{milli} = 1 mm lateral motion range of the millimanipulator to install each V_{cell} ~ 8000 μm^3 cell could install $n_{millicellsV}$ = v_{manip} / L_{milli} ~ 10 cells/manipulator-sec, but we will allow ten-fold longer to ensure correct cell positioning giving $n_{millicells}$ = $n_{millicellsV}$ / 10 = 1 cell/manipulator-sec, thus requiring $N_{MilliCellPlace}$ = $N_{bodycells}$ / $n_{millicells}$ = 3.5 x 10^{12} manipulator-sec to install all $N_{bodycells}$ ~ 3.5 x 10^{12} tissue cells in the entire human body[2077] in $\tau_{cellinstall}$ ~ $N_{MilliCellPlace}$ / $n_{millimanip}$ = 4.4 x

---

[2073] Hosny A, Keating SJ, Dilley JD, Ripley B, Kelil T, Pieper S, Kolb D, Bader C, Pobloth AM, Griffin M, Nezafat R, Duda G, Chiocca EA, Stone JR, Michaelson JS, Dean MN, Oxman N, Weaver JC. From Improved Diagnostics to Presurgical Planning: High-Resolution Functionally Graded Multimaterial 3D Printing of Biomedical Tomographic Data Sets. 3D Printing and Additive Manuf. 2018 Jun;5(2):103-113; https://www.liebertpub.com/doi/10.1089/3dp.2017.0140.

[2074] https://en.wikipedia.org/wiki/3D_printing.
[2075] https://en.wikipedia.org/wiki/Organ_printing.

[2076] The ovum is the largest compact cell in the human body with a diameter of ~100 μm.* Longer cells could be transported as segments capped with temporary sealed interfaces that can be removed at the time of final *in situ* assembly or installation.
* Alberts B, Johnson A, Lewis J, Raff M, Roberts K, Walter P, eds. Molecular Biology of the Cell, 4th edition, Garland Science, New York, 2002; https://www.ncbi.nlm.nih.gov/books/NBK26842/.

[2077] Freitas RA Jr. Nanomedicine, Volume I: Basic Capabilities, Landes Bioscience, Georgetown TX, 1999, Section 8.5.1, "Cytometrics"; http://www.nanomedicine.com/NMI/8.5.1.htm#p5.

10^6 sec (~51 days). If the print job was taking place in vacuum, the power requirement to drive all manipulator motions would be $P_{cellinstallVac} = n_{millimanip}\ P_{millimanipVac} \sim 0.8$ watts. Since the millimanipulators are instead moving in liquid water at T = 273 K (0 °C) having an absolute viscosity of $\eta = 1.787 \times 10^{-3}$ Pa-sec, they will also experience viscous drag. The drag power for a cylindrical robot arm translating normal to its central axis[2078] is $P_{millimanipDrag} = 8\pi\ \eta\ L_{milli}\ v_{manip}^2 / [1 + \ln(L_{milli}^2 / R_{milli}^2)] = 940$ pW/manipulator, hence additional drag power needed to drive all 800,000 millimanipulators on the Tissue Assembly Plate is a modest $P_{cellinstallDrag} = n_{millimanip}\ P_{millimanipDrag} \sim 8 \times 10^{-4}$ watts.

If the total cell volume in a 70 kg human body is $V_{bodycells} = N_{bodycells}\ V_{cell} \sim 28{,}000$ cm^3, then the millimanipulators must also install $V_{noncell} = V_{MSV} - V_{bodycells} = 13{,}053$ cm^3 of noncellular biomaterials, taking the molecular scan volume as $V_{MSV} \sim 41{,}053$ cm^3 (Section 5.1). If we arbitrarily assume that noncellular material takes a similar amount of time to install as cells per unit volume because this material isn't as neatly packaged, then this adds $\tau_{noncellinstall} = \tau_{cellinstall}\ V_{noncell} / V_{bodycells} \sim 2.1 \times 10^6$ sec (~24 days) to the print job, which would therefore be expected to take $t_{ptp} \sim \tau_{cellinstall} + \tau_{noncellinstall} \sim 6.5 \times 10^6$ sec (~**75 days**).

Even if the aforementioned processes can serve as the foundation for fabricating much of the replacement human body, there are some specific cases involving overlong cells that will require special handling in addition to the Tissue Assembly Plate mechanism. The most important example is neurons, whose axons can range from 500 μm to 1 meter in length. The axon of the longest motor neuron[2079] in the human body is a few microns in diameter and runs from the base of the spine to the feet, a distance of up to 1 meter.[2080] Muscle cells are another example of a special case. A typical muscle cell is cylindrical, 10-50 μm in diameter but up to 1-40 mm in length.[2081]

Both of these cell types are too large to be transported inside the 100 μm central channel of the millimanipulator because they are much longer than the $L_{milli} = 1$ mm central channel length, and they cannot be deterministically emplaced in a tissue workpiece because their great length and 3D positioning requirements into varying tissue depths may greatly exceed the ~1 mm^3 operating volume of a single millimanipulator or the reach of a plane of millimanipulators with a ~1 mm maximum vertical reach. Transport and emplacement of such cells may require the intervention of a small fleet of coordinated mobile shepherd nanorobots,[2082] which can push and pull the overlong cell into arbitrary depths and patterns inside the growing printed tissue mass. For instance, a fleet of 100,000 shepherd nanorobots might grasp and guide the installation of a sinuous 1 meter motor axon, with the robots spaced every 10 μm along the length of the axon. ***Future research*** should enumerate the types and likely numbers of overlong cells, describe and parameterize the process of their emplacement using shepherd nanorobots, and estimate the size, number, time and power consumption of the nanorobots required to complete the 3D cell print of the replacement body in concert with other Tissue Assembly Plate mechanisms and operations.

[2078] Freitas RA Jr. Nanomedicine, Volume I: Basic Capabilities, Landes Bioscience, Georgetown TX, 1999, Eqn. 9.75 in Section 9.4.2.4, "Force and Power Requirements"; http://www.nanomedicine.com/NMI/9.4.2.4.htm#p6.

[2079] https://biologydictionary.net/motor-neuron/.

[2080] Fletcher DA, Theriot JA. An introduction to cell motility for the physical scientist. Phys Biol. 2004 Feb 12;1(1):T1-10; http://rpdata.caltech.edu/courses/aph161/Handouts/Fletcher2004.pdf.

[2081] Lodish H, Berk A, Zipursky SL, *et al*. Molecular Cell Biology, 4th edition, W.H. Freeman, NY, 2000; https://www.ncbi.nlm.nih.gov/books/NBK21670/.

[2082] Freitas RA Jr. The Alzheimer Protocols: A Nanorobotic Cure for Alzheimer's Disease and Related Neurodegenerative Conditions. IMM Report No. 48, June 2016, 433 pp; Section 5.3.2.3, "Cell Insertion and Emplacement," pp. 327-332; http://www.imm.org/Reports/rep048.pdf.

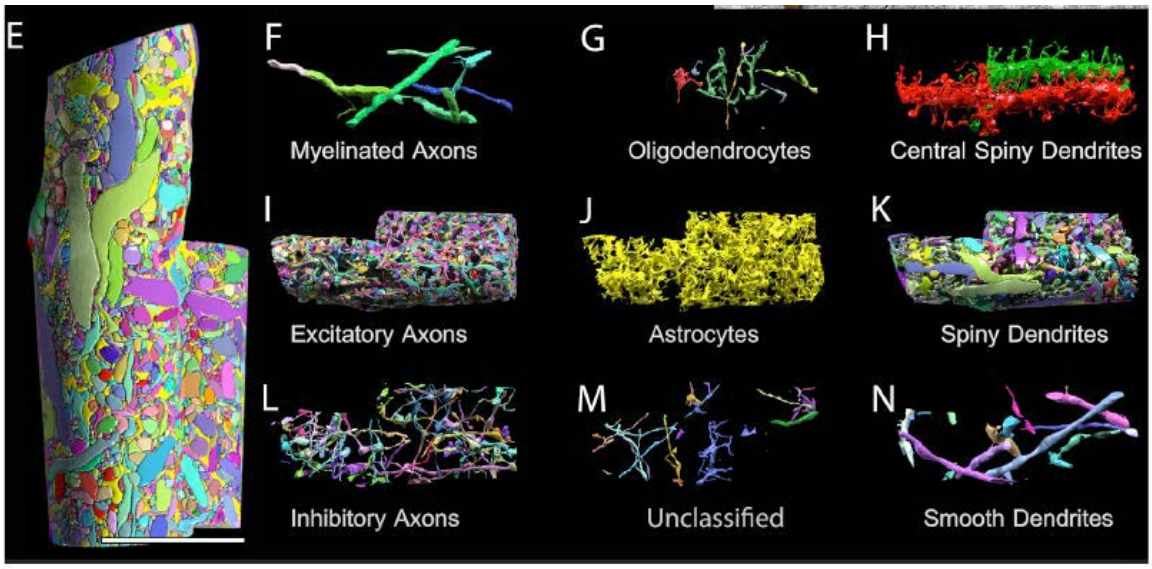

The neuropil of the brain is very densely packed with cells and axonal processes, as illustrated in a multiscale reconstruction of generic cortical neuronal somata of mouse brain (image, above; scale bar = 7 μm),[2083] and as such is ideally suited to positional assembly by shepherd nanorobots as described above. But elsewhere in the body where cells are packed less densely or intricately, large volumes of extracellular matrix (ECM) may occupy much of the spaces between cells. ECM is filled with lengthy intertwined fibers of various types that vary widely according to tissue type (Section 4.12.3.3). For example, collagens representing ~25% of total mammalian protein mass[2084] may exist as strands ~300 nm long and ~1.5 nm wide, spaced 4-12 μm apart in the ECM. Cartilage consisting of ~10 μm strands that are ~500-600 nm in diameter may be spaced 10-30 μm apart in the ECM.[2085] Rather than attempting to positionally assemble this multitude of fibers one by one during the planar tissue print, we may be able to rely upon the cell mill (Appendix D) to assemble specified chunks of ECM containing prefabricated fiber networks that can be deployed as building blocks by the aforementioned millimanipulators during the print job. ***Future research*** should further examine the challenge of nanoscale and microscale fiber network assembly during planar tissue printing, and devise multiple technical strategies that can be compared in an engineering trade study to select the best alternative.

By the end of the planar printing process, the replacement body has been printed in a pure water environment at 273 K (0 °C), using cells that were manufactured without incorporating any water-leachable soluble molecules, metabolites, or ions. The revival process is then completed by (A) installation of

---

[2083] Kasthuri N, Hayworth KJ, Berger DR, Schalek RL, Conchello JA, Knowles-Barley S, Lee D, Vázquez-Reina A, Kaynig V, Jones TR, Roberts M, Morgan JL, Tapia JC, Seung HS, Roncal WG, Vogelstein JT, Burns R, Sussman DL, Priebe CE, Pfister H, Lichtman JW. Saturated Reconstruction of a Volume of Neocortex. Cell. 2015 Jul 30;162(3):648-61; http://seunglab.org/wp-content/uploads/2015/09/saturatedreconstruction.pdf.

[2084] Stryer L. Biochemistry, 4th Edition, W.H. Freeman and Company, New York, 1995; https://www.amazon.com/dp/0716720094/.

[2085] Loewy AG, Siekevitz P, Menninger JR, Gallant JAN. Cell Structure and Function: An Integrated Approach, Third Edition, Saunders College Publishing, Philadelphia PA, 1991; https://www.amazon.com/dp/0030474396/.

vasculoid (Section 4.6), (B) patient warmup to 310 K (37 °C) and molecular instillation (Section 4.13), (C) vasculoid uninstallation and blood substitution (Section 4.14), and (D) patient wakeup (Section 4.15).

5.2.3.3.2 Scaffolded Tissue Printing

An alternative method for 3D cell printing of a replacement body may be termed the "print on scaffold" approach, wherein a whole-body scaffolding is first laid down, after which nanorobots install whole cells and other biological materials onto the scaffolding to build out the rest of the body tissues – the more complete details of which should be set forth in ***future research***.

To initiate the printing process, a 2 m x 0.4 m x 0.4 m water-filled print chamber is injected with vasculoid basic plates (Section 4.6.1) which are unfurled into a free-hanging complete vascular network as dictated by the patient's personalized ~4 μm resolution vascular map (Section 4.3). This vascular map was previously compiled at the completion of microvascular scans in which nanorobots scanned and mapped (Section 4.3), then excavated (Section 4.4), the blood and lymphatic microvasculatures, including all arterioles, venules, capillary beds, and lymphatic precollecting ducts, as directed in Section 5.1.

Rather than the arteriovenous installation procedure described in Section 4.6.2, the plates will be emplaced using a more aggressive procedure in which the vasculoid is manufactured as a folded, pre-assembled custom appliance tailored to the patient's unique vasculature. As previously described elsewhere,[2086] the appliance unfurls as a continuously-everting concentric tube, a process called progressive fractal eversion that may be visualized as turning a glove inside out. Basic plates, docking bays and cellulocks are prefastened in the proper configuration to fit the various diameters and branchings of the blood vessels that they would normally coat. The necessary flexibility of this sheet of plates is provided by sophisticated watertight jointed interplate bumpers that have yet to be designed. Eversion may be powered by compressed gas, ciliary action between opposed plates, or by other appropriate means; the presence of pressurized gas (e.g., pure dry N_2) would also help to minimize the occurrence of leaks during installation. Each docking bay has an appropriate tanker already docked. Since the vasculoid contains a sufficient number of docking bays to accommodate peak metabolic loads, the preattached tankers can supply oxygen, glucose, and other nutrients, and accumulate wastes, in addition to performing instillation tasks (Section 4.13).

As originally envisioned, deployment would be initiated cardiocentrically as two primary segments imported into the future location of the right atrium and the left atrium. Deployment works outward from each chamber location, moving towards the distal capillary beds. From the right atrial entry point, the unfolding right atrial appliance segment has four "fingers" and simultaneously everts plates representing: (1) the superior vena cava; (2) the inferior vena cava; (3) the coronary sinus (which receives cardiac veins from heart tissue); and moves through and everts plates for the right atrial and ventricular chambers, finally creating (4) the pulmonary artery. The right atrial segment also everts plates to create all of the numerous Thebesian veins.[2087] From the left atrial entry point, the unfolding left atrial appliance segment has five "fingers" and simultaneously everts the plates representing: (1) the two left pulmonary veins (which frequently terminate by a common opening); (2) the two right pulmonary veins; and moves through and everts plates to create the left atrial and ventricular chambers, finally creating (3) the aorta. Additionally, a third vasculoid segment called the portal segment is inserted at an appropriate abdominal

---

[2086] Freitas RA Jr., Phoenix CJ. Vasculoid: A personal nanomedical appliance to replace human blood. J Evol Technol. 2002 Apr;11:1-139; Section 7.8 "Aggressive Installation Scenario"; http://www.jetpress.org/volume11/vasculoid.pdf.

[2087] These venules return blood from the myocardium without entering the venous current, and open directly into the right atrium; https://en.wikipedia.org/wiki/Smallest_cardiac_veins.

position in order to install plates representing the portal vein, which lies midway between the hepatic capillary beds and the intestinal capillary beds.

Advancing at 1 cm/sec (i.e., 2 cm/sec internal speed between the installed surface and the inverted tube), the vasculoid requires only 70 sec to plate out the maximum ~70-cm main arterial or venous course; the progression of the eversion may slow to ~10 micron/sec of travel, requiring another ~100 sec to complete all capillary plating. Human capillaries comprise ~95% of the surface area of the vascular system, so most of the appliance's plates are positioned during this final ~100 seconds. The power draw is ~150 watts if all 150 trillion plates were active throughout this process. Once the vasculoid has filled out the capillary plumbing, the arterial and venous branches are joined, detaching the internal fluid transfer channels running through the vasculoid lumen which are quickly retracted from the interior. The vasculoid now fills the print chamber, a fractal network of hollow diamondoid tubes with the tissue-facing underside of each basic plate exposed to the pure water environment, but still devoid of all biological material.

Next, shepherd nanorobots[2088] install patient-personalized cells and other biomaterials fabricated in the cell mill (Appendix D), starting with vascular endothelial cells which are emplaced as the first coating of biological material upon all water-exposed exterior vasculoid surfaces. Fibers and other connective materials are then laid down, building up the extracellular matrix (Section 4.12.3.3) as additional cells are emplaced, all according to the atomically precise map of the original body of the cryopreserved patient. Calciferous and other mineralized biomaterials are positionally deposited to establish the exact structure of the bony skeleton. Buildout begins along the body centerline roughly parallel to the aorta, filling in the deepest tissues first and progressing outward in a roughly cylindrical radial direction, leaving ingress and egress pathways available for mobile installation nanorobots until each tissue block under construction has been completely filled with cells and other essential biomaterial. Each overlong cell such as a muscle cell or a neuron with an extended axon can be carried into place and held in proper position by shepherd nanorobots as more normal cells and other biomaterials are installed around it.

One major benefit of scaffolded tissue printing is the possibility of massively parallel assembly operations,[2089] with nanorobots delivering and installing cells all throughout the vascular framework simultaneously. As a crude scaling analysis of basic cell emplacement operations, we assume that shepherd nanorobots must install $N_{bodycells} \sim 3.5 \times 10^{12}$ tissue cells to build a single replacement human body.[2090] We will assume that each shepherd nanorobot has a diameter of $D_{shep} = 2R_{shep} = 20$ μm and volume $V_{shep} \sim 8000$ μm^3, about the same size and volume as the biological cell that it must drag ~2 meters from the cell mill to an installation site somewhere in the print chamber, then return emptyhanded to the cell mill to receive its next load, a total transport distance of $x_{celltransportS} \sim 4$ robot-meters/cell at a transport speed of $v_{shep} \sim 1$ cm/sec, giving a transport time of $x_{celltransportS} / v_{shep} = 400$ sec. Spherical nanorobots with $R_{shep} = 10$ μm moving in 273 K (0 °C) water having absolute viscosity $\eta = 1.787 \times 10^{-3}$ Pa-sec require a drag

---

[2088] Freitas RA Jr. The Alzheimer Protocols: A Nanorobotic Cure for Alzheimer's Disease and Related Neurodegenerative Conditions. IMM Report No. 48, June 2016, 433 pp; Section 5.3.2.3, "Cell Insertion and Emplacement," pp. 327-332; http://www.imm.org/Reports/rep048.pdf.

[2089] A loosely analogous process has been pursued in conventional organ bioengineering:* "We decellularized rat, porcine and human kidneys by detergent perfusion, yielding acellular scaffolds with vascular, cortical and medullary architecture, a collecting system and ureters. To regenerate functional tissue, we seeded rat kidney scaffolds with epithelial and endothelial cells and perfused these cell-seeded constructs in a whole-organ bioreactor. The resulting grafts produced rudimentary urine *in vitro* when perfused through their intrinsic vascular bed. When transplanted in an orthotopic position in rat, the grafts were perfused by the recipient's circulation and produced urine through the ureteral conduit *in vivo*."
* Song JJ, Guyette JP, Gilpin SE, Gonzalez G, Vacanti JP, Ott HC. Regeneration and experimental orthotopic transplantation of a bioengineered kidney. Nat Med. 2013 May;19(5):646-51; https://www.ncbi.nlm.nih.gov/pmc/articles/PMC3650107/.

[2090] Freitas RA Jr. Nanomedicine, Volume I: Basic Capabilities, Landes Bioscience, Georgetown TX, 1999, Section 8.5.1, "Cytometrics"; http://www.nanomedicine.com/NMI/8.5.1.htm#p5.

power[2091] of $P_{ShepDrag} = 6\pi\ \eta\ R_{shep}\ v_{shep}^{2} = 34$ pW/nanorobot, which must be doubled to $P_{ShepDrag2} = 68$ pW/nanorobot because the robot is towing cargo of nearly equal size and viscous drag through the water. To avoid traffic congestion in the print chamber, we specify that the entire shepherd nanorobot population should not exceed $f_{shep} = 0.1\%$ of total human body (i.e., "workpiece") volume of $V_{body} = 0.06\ m^3$, hence total nanorobot volume is $V_{allshep} = f_{shep}\ V_{body} = 6 \times 10^{-5}\ m^3$, the maximum number of shepherds is $N_{shep} = V_{allshep} / V_{shep} = 7.5 \times 10^9$ nanorobots, and the nanorobot population requires a continuous power of $P_{allshep} = N_{shep}\ P_{shep} = 7.5$ watts if we generously allow P_{shep} (>> $P_{ShepDrag2}$) = 1000 pW/nanorobot. If each shepherd spends $\tau_{cellinstallS} = 1000$ robot-sec/cell after it reaches its designated installation site, properly installing the cell it carries into the growing tissue mass, then the whole-body cell installation time is $t_{cellinstallS} = N_{bodycells}\ (\tau_{cellinstallS} + x_{celltransportS} / v_{shep}) / N_{shep} \sim 2.3 \times 10^6$ sec (~27 days). If we assume as before (Section 5.2.3.3.1) that the installation of non-cellular biological materials adds $\tau_{noncellinstall} \sim 2.1 \times 10^6$ sec (~24 days) to the print job, and assuming that dealing with special cases such overlong cell placement adds another $f_{stp} \sim 10\%$ to cell installation time, then the total time to complete the 3D cell print job might be approximated as $t_{stp} \sim (1 + f_{stp})\ (\tau_{cellinstallS} + \tau_{noncellinstall}) \sim 4.8 \times 10^6$ sec (~**56 days**).

By the end of this process, a replacement whole-body has been reassembled around the vasculoid scaffolding in a pure water environment at 273 K (0 °C), with all cells manufactured lacking any water-leachable soluble molecules, metabolites, or ions. The vasculoid is left in place to allow the revival process to progress to the next steps, which include (A) patient warmup to 310 K (37 °C) and molecular instillation (Section 4.13), (B) vasculoid uninstallation and blood substitution (Section 4.14), and (C) patient wakeup (Section 4.15).

5.2.3.3.3 Nanorobot-Guided Embryonic Growth

An early proposal by Merkle[2092] for growing a replacement human brain by using nanorobots to guide embryonic growth and maturation processes might be workable but seems unlikely to reliably produce a close enough copy of the original brain to preserve memory and personality, and seems more technically challenging to achieve than the previous two methods because it relies upon controllably and reliably manipulating active biological entities that are inherently stochastic in their behavior (e.g., like "herding cats"). From the original proposal:

> "We know it is possible to make a human brain for this has been done by traditional methods for many thousands of years. If we were to adopt a restoration method that was as close as possible to the traditional technique for building a brain, we might use a 'guided growth' strategy. That is, in simple organisms the growth of every single cell and of every single synapse is determined genetically. 'All the cell divisions, deaths, and migrations that generate the embryonic, then the larval, and finally the adult forms of the roundworm *Caenorhabditis Elegans* have now been traced.'[2093] 'The embryonic lineage is highly invariant, as are the fates of the cells to which it gives rise.'[2094] The Appendix says: 'Parts List: *Caenorhabditis elegans* (Bristol) NEWLY

[2091] Freitas RA Jr. Nanomedicine, Volume I: Basic Capabilities, Landes Bioscience, Georgetown TX, 1999, Eqn. 9.74 in Section 9.4.2.4, "Force and Power Requirements"; http://www.nanomedicine.com/NMI/9.4.2.4.htm#p3.

[2092] Merkle RC. The molecular repair of the brain. Cryonics 1994 Jan;15(1) and Cryonics 1994 Apr;15(2); http://www.merkle.com/cryo/techFeas.html and https://www.alcor.org/library/molecular-repair-of-the-brain/.

[2093] Marx JL. *Caenorhabditis elegans*: getting to know you. Science 1984 Jul 6;225(4657):40-42; https://pubmed.ncbi.nlm.nih.gov/6729468/.

[2094] Sulston JE, Schierenberg E, White JG, Thomson JN. The embryonic cell lineage of the nematode *Caenorhabditis elegans*. Dev Biol. 1983 Nov;100(1):64-119; https://www.wormatlas.org/SulstonembCellLin_1983/SulstonembCellLin1983.html.

> HATCHED LARVA. This index was prepared by condensing a list of all cells in the adult animal, then adding comments and references. A complete listing is available on request to MRC, Cambridge.' The adult organism has 959 cells in its body, 302 of which are nerve cells.[2095]
>
> "Restoring a specific biological structure using this approach would require that we determine the total number and precise growth patterns of all the cells involved. The human brain has roughly 10^{12} nerve cells, plus perhaps ten times as many glial cells and other support cells. While simply encoding this complex a structure into the genome of a single embryo might prove to be overly complex, it would certainly be feasible to control critical cellular activities by the use of onboard nanocomputers. That is, each cell would be controlled by an onboard computer, and that computer would in turn have been programmed with a detailed description of the growth pattern and connections of that particular cell. While the cell would function normally in most respects, critical cellular activities, such as replication, motility, and synapse growth, would be under the direct control of the onboard computer. Thus, as in *C. elegans* but on a larger scale, the growth of the entire system would be "highly invariant." Once the correct final configuration had been achieved, the onboard nanocomputers would terminate their activities and be flushed from the system as waste. This approach might be criticized on the grounds that the resulting person was a 'mere duplicate,' and so 'self' had not been preserved. Certainly, precise atomic control of the structure would appear to be difficult to achieve using guided growth, for biological systems do not normally control the precise placement of individual molecules. While the same atoms could be used as in the original, it would seem difficult to guarantee that they would be in the same places."

It is difficult to estimate how long this process might take to produce a replacement body. In the normal natural process, the human body requires ~20 years to grow to full adult size from a single embryo. It may be possible to accelerate natural biological processes by employing several clever artifices of nanotechnology, biotechnology, or genetic engineering (Section 6.1.1), but even a ten-fold speed-up in a guided growth process would still require a ~2 year growth cycle.

5.2.3.4 Virtual 3D Bit Print (an "Upload")

Rather than printing a physical replacement of the cryopreserved patient's body, it would be possible to simply print the bits describing the person (whether at the atomic, molecular, or cellular level) into the memory of a computer that can emulate the operation of a physical body having that description, along with an emulation of some part of a real or artificial environment in which the emulated person would "live". This form of replacement printing may loosely be termed a "bit print" (instead of printing atoms), or, more commonly, an "upload".[2096]

This is the scan-to-WBE (Whole-Brain Emulation) scenario (Section 2.2.15),[2097] where the physical body is molecularly scanned, the repairs are computed, and then the repaired atomic-resolution body map is

---

[2095] Lewin R. Why is development so illogical? Science 1984 Jun 22;224(4655):1327-1329; https://www.jstor.org/stable/1692747?seq=1.

[2096] Randal A Koene. Uploading to Substrate-Independent Minds. The Transhumanist Reader, Mar 2013; https://www.researchgate.net/profile/Randal_Koene/publication/300463595_Uploading_to_Substrate-Independent_Minds/links/5ee452d092851ce9e7e04d4d/Uploading-to-Substrate-Independent-Minds.pdf. See also: https://en.wikipedia.org/wiki/Mind_uploading and https://carboncopies.org/.

[2097] Merkle RC. Revival of Alcor Patients. Cryonics 2018 May-Jun;39(3):10-19 and Cryonics 2018 Jul-Aug;39(4):10-15; https://www.alcor.org/library/revival-of-alcor-patients/.

uploaded into a computer and the cryopatient's WBE is activated in a virtual environment, producing a conscious patient without requiring physical body repair or physical reconstruction of any kind.

The concept sounds simple but there is an important difference from other print modalities that must be acknowledged. When one is performing an atomic print (Section 5.2.3.1), a molecular print (Section 5.2.3.2), or a cell print (Section 5.2.3.3), it is enough to simply duplicate the physical structure of the original body when fabricating the replacement body. That's because the laws of chemistry and physics will compel the replacement structures to behave exactly the same as the original structures when placed in the appropriate physical environment. For example, if you build a duplicate physical cell that is loaded with the same chemicals and biological structures as the original cell, the laws of chemistry will cause the duplicate cell to behave the same as the original cell. Chemicals in both cells will react in the same expected manner, producing the same expected reaction products, which will then lead to still more chemical reactions that are identical in both cells. However, if you merely copy the description of the original cell into a computer memory, it will be a static image that will not execute any of its normal biological functions. For biochemical reactions to appear as new bit streams inside the computer memory, the cell description must be copied into a software package that incorporates the relevant laws of physics and chemistry, and contains algorithms to apply those laws in a time-dependent manner to every atom (or bit) of the cell description. Such a software package may be called an **emulator**[2098] because it translates structure into function by faithfully duplicating the operation of the actual physical laws of the universe when applied to a given physical structure.

A few details of the design and operation of an emulator for a human brain have been discussed[2099] (and are well beyond the scope of this book), but a roadmap to such an emulator was first conceptually outlined in a 2007 Workshop[2100] in which the author participated. The Workshop participants compiled their best estimates of the memory and CPU requirements to computationally reproduce the performance of a human brain to various levels of emulation fidelity that are defined in the Workshop report – and summarized in **Table 15** below, assuming 64 bits/sec per FLOP for 64-bit words and one word per floating point operation. Estimated CPU requirements to emulate a realistic-seeming human body with all ~600 muscles actuatable and a "convincing" domiciliary environment for the emulated human brain/body combination were also provided by the Workshop, and this author has estimated (in **Table 15**) the cost per day of the

---

[2098] https://en.wikipedia.org/wiki/Emulator.

[2099] Koene RA. Fundamentals of Whole Brain Emulation: State, Transition and Update Representations. Intl J Machine Consciousness 2012;4:5-12; https://www.worldscientific.com/doi/abs/10.1142/S179384301240001X. Eth D, Foust JC, Whale B. The prospects of whole brain emulation within the next half-century. J Artif Gen Intell. 2013 Dec;4(3):130-152; https://content.sciendo.com/downloadpdf/journals/jagi/4/3/article-p130.pdf. Koene RA. Chapter 5. Mind Uploading. In: Blackford R, Broderick D, eds. Intelligence Unbound: The Future of Uploaded and Machine Minds, Wiley, 2014; https://onlinelibrary.wiley.com/doi/abs/10.1002/9781118736302.ch5. Hanson R. The Age of Em: Work, Love, and Life When Robots Rule the Earth. Oxford University Press, 2016. Serruya MD. Connecting the brain to itself through an emulation. Front Neurosci. 2017 Jun 30; https://www.frontiersin.org/articles/10.3389/fnins.2017.00373/full. See also https://en.wikipedia.org/wiki/Mind_uploading and https://en.wikipedia.org/wiki/Brain_simulation.

[2100] Sandberg A, Bostrom N. Whole Brain Emulation: A Roadmap. Technical Report #2008-3, Future of Humanity Institute, Oxford University, 2008; http://acikistihbarat.com/Dosyalar/science-brain-emulation-project-by-oxford-future-humanity-institute-acikistihbarat.pdf.

electricity needed to run each emulation, assuming the electricity is purchased at today's typical commercial rate of ~$0.10/KW-hr ($e_{\$}$ ~ 2.78 x 10^{-8} $/J; Appendix G) and the nanocomputer CPU is operated at LN2 temperatures which reduces the energy cost per processed bit to $E_{Landauer77K} \sim k_B T \ln(2)$ = 7.4 x 10^{-22} J/bit.

For example, a metabolome-level (Level 3) emulation would require (6.4 x 10^{26} bits/sec) / U_{nano} = **0.64 L** of diamondoid mechanical nanocomputers having a specific processing power U_{nano} ~ 10^{30} bit/sec-m^3 (Section 4.8.5), costing ~**$1100/day** to run the emulated person, or about ~$11/day in a future era when electricity is 100-fold cheaper (Appendix G). The required 8 x 10^{18} bits of memory storage data supporting a metabolome-level emulation of the individual patient could be distilled from a whole-body molecular-level data file containing $I_{MSVnowaterM}$ ~ 3.29 x 10^{27} bits, or from other sources.

Table 15. Estimated memory, CPU requirements, and cost to run an emulation of the human brain, body, and living environment, at the specified level of emulation fidelity[2101]

Emulation Fidelity Level	Memory Storage Requirements (bits)	CPU Demand Involving Floating Point Operations (bits/sec)	($/day)
Human Body (all muscles, excl. brain)	n/a	6.4 x 10^{15}	$1.1 x 10^{-8}
Environment (full sensory experience)	n/a	1.9 x 10^{16}	$3.4 x 10^{-8}
Human Brain:			
1-Spiking neural network	6 x 10^{16}	6.4 x 10^{19}	$1.1 x 10^{-4}
2-Electrophysiology	8 x 10^{16}	6.4 x 10^{23}	$1.1
3-Metabolome	8 x 10^{18}	6.4 x 10^{26}	$1100
4-Proteome	8 x 10^{19}	6.4 x 10^{27}	$11,000
5-States of protein complexes	8 x 10^{20}	6.4 x 10^{28}	$110,000
6-3D electron microscopy map[2102]	8 x 10^{21}	6.4 x 10^{31}	$110 x 10^{6}
7-Single molecules	3 x 10^{27}	6.4 x 10^{44}	$1.1 x 10^{21}

Which other sources? This raises an important implementation detail regarding uploads: What is a sufficient scanning resolution (and scan type) to support the creation and operation of an uploaded mind? Several alternatives can be distinguished:

(1) **Submicron Scan to WBE**. If ***future research*** determines that a purely structural description of the brain's connectome and synaptome down to ≥100 nm resolution is sufficient to initialize a WBE that can subsequently simulate the trafficking of much smaller molecules (e.g., neurotransmitters and metabolites) than the larger synaptic structures that dispense and absorb them, then the nondestructive scanning process described in Chapter 4 could be halted after obtaining the results of the submicron tissue scan (Section 4.7.1) and after compiling the 10^{16}-10^{20} bit whole-body neural connectome map (Section 4.8.1(5)) from that scan data. This would provide the information needed to create the WBE while also

---

[2101] Sandberg A, Bostrom N. Whole Brain Emulation: A Roadmap. Technical Report #2008-3, Future of Humanity Institute, Oxford University, 2008, p. 75, 78, and Tables 8 and 9; http://acikistihbarat.com/Dosyalar/science-brain-emulation-project-by-oxford-future-humanity-institute-acikistihbarat.pdf.

[2102] Fiala JC. Three-dimensional structure of synapses in the brain and on the web. Proc 2002 Intl Joint Conf on Neural Networks, IEEE Press, 2002, pp. 1-4; http://citeseerx.ist.psu.edu/viewdoc/download?doi=10.1.1.653.1423&rep=rep1&type=pdf.

allowing the cryopatient's almost-intact body to be returned to cryogenic storage for future reference or for subsequent additional processing.

(2) **Nanometric Scan to WBE.** The consensus of the 2007 WBE workshop participants was that a 5 nm x 5 nm x 50 nm neural scanning resolution would be needed to construct a human whole-brain emulation: "Synaptic spine necks and the thinnest axons can be on the order of 50 nm or smaller, requiring imaging on the order of the 5 nanometer scale to resolve them."[2103] This consensus presumed that a WBE requires emulation of neuron membrane states (ion channel types, properties, states), ion concentrations, currents, voltages and modulation states, along with concentrations of metabolites and neurotransmitters in compartments – which includes the spiking neural network (Level 1), electrophysiology (Level 2), and the metabolome (Level 3) in **Table 15**.[2104]

(2A) **Nanometric, Structural Only.** If a purely structural scan to ≥5 nm resolution will suffice not just to map the spiking network data but also to infer electrophysiologic and metabolomic processes in the brain, then it may be possible to create the WBE using only electron microscope scans at this resolution, perhaps collected from the cryopatient's solid brain tissue using a layer-by-layer destructive scan process that yields little or no chemical information.[2105] An electron microscope map of a cryopatient's body to $V_{evox} = (5\ nm)^3 = 125\ nm^3$/voxel resolution requires $(V_{MSV} / V_{evox})\ (I_{voxelBody} + I_{voxeltype}) = 3 \times 10^{25}$ bits, or $(V_{brain} / V_{evox})\ (I_{voxelBrain} + I_{voxeltype}) = 9 \times 10^{23}$ bits for just the brain.

(2B) **Nanometric, Structural and Chemical.** If chemical data is also required – whether to identify ambiguous structures or specific essential molecules, or to determine transcriptional activation states inside cells, or to determine if a synapse is excitatory or inhibitory (or other functions not anatomically visible), or to provide biochemical initialization data for the WBE – then preparing a WBE of a cryopreserved patient would absolutely require a molecular scan (Section 5.2.1 or Section 5.3.1), especially given that the examination will take place in the solid state. ***Future research*** must determine which of these two scanning modalities may suffice to create and operate a nanometric WBE.

Cryonicists differ in their acceptance of nonphysical instantiation in a computational substrate (uploading) as compared to some form of physical instantiation of their revived brain or body. Some "view the physical substrate on which their mind runs with philosophical indifference"[2106] while others retain philosophical worries about the survival of consciousness in uploads:[2107]

[2103] Sandberg A, Bostrom N. Whole Brain Emulation: A Roadmap. Technical Report #2008-3, Future of Humanity Institute, Oxford University, 2008, p. 14; http://acikistihbarat.com/Dosyalar/science-brain-emulation-project-by-oxford-future-humanity-institute-acikistihbarat.pdf.

[2104] Such a requirement need not conflict with our previous conclusion that knowledge of the instantaneous levels of neurotransmitter molecules at the time of cryopreservation is unnecessary to preserve personal identity (Section 2.1.3), as it may be presumed that these levels will be correctly reinitialized by the surviving synaptic structure upon resumption of metabolism.

[2105] Oregon Cryonics, "Future Repair Technologies: Connectome Scanning"; http://www.oregoncryo.com/futureTechnology.html.

[2106] Merkle RC. Revival of Alcor Patients. Cryonics 2018 May-Jun;39(3):10-19 and Cryonics 2018 Jul-Aug;39(4):10-15; https://www.alcor.org/library/revival-of-alcor-patients/. Koene R. Pattern Survival Versus Gene Survival. Cryonics 2019 Qtr 4;40(4):12-17; https://www.alcor.org/docs/cryonics-magazine-2019-04.pdf.

[2107] de Wolf A. Revival Scenarios. Cryonics 2018 May-Jun;39(3):5; https://www.alcor.org/docs/cryonics-magazine-2018-03.pdf.

> "Some cryonicists (including the 'godfather' of cryonics, Robert Ettinger) have expressed concerns[2108] that some of these proposals will not produce meaningful individual survival. In particular, it is argued that 'running' a complete simulation of the brain on a computer won't give rise to consciousness, let alone produce individual survival. Since it may be quite some time before technology is at a state to favor one position over the other, we need sound principles to make prudent decisions now. Most…may not be too concerned about the loss of identity-critical information in either cryopreservation option, but being wrong on the nature of consciousness could be fatal. If consciousness is substrate-dependent and/or destroying the original brain (during a scan) excludes personal survival, choosing a wrong revival method can produce certain death, despite having received an excellent cryopreservation."
>
> "Alexandre Erler introduces a new kind of 'wager' to make such decisions when faced with philosophical uncertainty concerning the nature of identity and consciousness.[2109] Erler simply asks the question what would be the prudent choice to make given that we cannot know with certainty (right now) which philosophical position is right. The short answer is that *in-situ* repair and revival of the preserved brain (or whole organism) will give rise to individual survival regardless of which philosophical view is correct. The conservative position on revival only claims that it would not be prudent to instruct the cryonics organization to discard the original brain and seek revival by 'running' that model on a computer….One complex question is whether it is currently possible to give informed consent for a revival scenario other than *in-situ* biological repair."

5.2.3.4.1 Upload from Revived Biological Intermediate (a "Live Transfer")

Another alternative is to revive the cryopatient in fully-repaired biological form with validated neural functionality and personal identity that is confirmed to be intact, then perform a transfer to a computational substrate or robot body as described conceptually by Moravec[2110] in his classic description of a "destructive" non-atomically-precise technological transmigration:

> "You've just been wheeled into the operating room. A robot brain surgeon is in attendance. By your side is a computer waiting to become a human equivalent, lacking only a program to run. Your skull, but not your brain, is anesthetized. You are fully conscious. The robot surgeon opens your brain case and places a hand on the brain's surface. This unusual hand bristles with microscopic machinery, and a cable connects it to the mobile computer at your side. Instruments in the hand scan the first few millimeters of brain surface. High-resolution magnetic resonance measurements build a three-dimensional chemical map, while arrays of magnetic and electric antennas collect signals that are rapidly unraveled to reveal, moment to moment, the pulses flashing among the neurons. These measurements, added to a comprehensive understanding of human neural architecture, allow the surgeon to write a program that models the behavior of the uppermost layer of the scanned brain tissue. This program is installed in a small portion of the waiting computer and activated. Measurements from the hand provide it with copies of the inputs that the original tissue is receiving. You and the surgeon check the accuracy of the simulation by

---

[2108] https://www.biostasis.com/can-you-build-a-locomotive-out-of-helium/.

[2109] Erler A. Brain Preservation and Personal Survival: The Importance of Promoting Cryonics-Specific Research. Cryonics 2017 Nov-Dec;38(6);20-23; https://www.alcor.org/docs/cryonics-magazine-2017-06.pdf.

[2110] Moravec H. Mind Children. Harvard University Press, 1988, pp.109-110; https://www.amazon.com/Mind-Children-Future-Robot-Intelligence/dp/0674576187/.

comparing the signals it produces with the corresponding original ones. They flash by very fast, but any discrepancies are highlighted on a display screen. The surgeon fine-tunes the simulation until the correspondence is nearly perfect."

"To further assure you of the simulation's correctness, you are given a pushbutton that allows you to momentarily 'test drive' the simulation, to compare it with the functioning of the original tissue. When you press it, arrays of electrodes in the surgeon's hand are activated. By precise injections of current and electromagnetic pulses, the electrodes can override the normal signaling activity of nearby neurons. They are programmed to inject the output of the simulation into those places where the simulated tissue signals other sites. As long as you press the button, a small part of your nervous system is being replaced by a computer simulation of itself. You press the button, release it, and press it again. You should experience no difference. As soon as you are satisfied, the simulation connection is established permanently. The brain tissue is now impotent – it receives inputs and reacts as before but its output is ignored. Microscopic manipulators on the hand's surface excise the cells in this superfluous tissue and pass them to an aspirator, where they are drawn away."

"The surgeon's hand sinks a fraction of a millimeter deeper into your brain, instantly compensating its measurements and signals for the changed position. The process is repeated for the next layer, and soon a second simulation resides in the computer, communicating with the first and with the remaining original brain tissue. Layer after layer the brain is simulated, then excavated. Eventually your skull is empty, and the surgeon's hand rests deep in your brainstem. Though you have not lost consciousness, or even your train of thought, your mind has been removed from the brain and transferred to a machine. In a final, disorienting step the surgeon lifts out his hand. Your suddenly abandoned body goes into spasms and dies. For a moment you experience only quiet and dark. Then, once again, you can open your eyes. Your perspective has shifted. The computer simulation has been disconnected from the cable leading to the surgeon's hand and reconnected to a shiny new body of the style, color, and material of your choice. Your metamorphosis is complete."

Nondestructive methods of non-atomically-precise scanning (Section 7.2.1.5) and uploading from a fully-repaired live biological form are also readily imagined using nanorobots,[2111] producing two "identical" individuals – the (revived) living biological cryopatient and the uploaded version of the cryopatient.

5.2.3.4.2 Physical Instantiation of Virtual Body (a "Download")

Presumably an upload with a virtual body can happily inhabit its virtual environment indefinitely, its operating software efficiently executing all necessary code instructions inside a solid block of computronium. However, from time to time the uploaded person may wish to interact with the actual physical universe that lies outside of its simulated virtual universe. To accomplish this, the upload may seek some form of physical instantiation that permits the desired direct physical interaction (a process called "downloading") by temporarily taking up residence in, or direct control of, one of several possible alternative substrates:

[2111] Martins NRB, Erlhagen W, Freitas RA Jr. Human connectome mapping and monitoring using neuronanorobots. J Evol Technol. 2016 Jan;26(1):1-24; https://jetpress.org/v26.1/martins.pdf. Martins NRB, Angelica A, Chakravarthy K, Svidinenko Y, Boehm FJ, Opris I, Lebedev MA, Swan M, Garan SA, Rosenfeld JV, Hogg T, Freitas RA Jr. Human Brain/Cloud Interface. Front Neurosci. 2019 Mar 29;13:112; https://www.ncbi.nlm.nih.gov/pmc/articles/PMC6450227/.

(1) **Computronium.** The upload, safely ensconced in the computronium operating environment, can remotely teleoperate a physical robot guided by data transmitted to the upload from the sensory organs of the robot via some convenient communications interface.

(2) **Robot brain.** The upload can copy an image of itself into a remote neuromorphic[2112] or *de novo* artificial robot brain, which then can partake of physical activities and experiences in a latency-free manner without the inconvenience of a light-speed communication time lag. The robot brain could reside in a carrier body with organic,[2113] artificial,[2114] or combined organic and inorganic[2115] components. Alternatively, rather than inhabiting a general-purpose "computronium" computer running emulation software, the upload could be transferred into a synthetic brain manufactured entirely using special-purpose artificial neurons (Section 5.2.2.3), encased in an appropriate carrier body.[2116]

(3) **Biological brain.** The upload could translate its data structures (algorithms, memories, etc.) into a biological brain supported by a biological body, possibly nonhuman, humanoid, or fully human (e.g., a copy of the patient's original biological body) in its construction. (The method for doing this may require detailed custom rewiring of the neural connectome of the brain and should be studied in ***future research*** by interested parties.) If the upload has been operating in the virtual world for awhile, it might have accumulated far too much algorithmic complexity and bulk data to be contained within a relatively low-capacity human brain. In this case, the resulting biological entity could incorporate only a stripped-down version of the original upload's full memory and personality. The biological entity containing the downloaded mind would contain only a selected mix of memories and algorithms representing but a subset of the whole uploaded mind, which would be consciously chosen by the original upload. This might be experienced by the download as partial or major amnesia.

Says brain emulation scientist Randal Koene[2117] of this latter approach: "I imagine that one avenue for biological revival of cryonics patients would be to produce an entirely new (young, healthy) body for the patient, and to also produce a brand-new biological brain for the patient. That brain would need to be grown/tuned so that its connectome and operations produce the same personal experience of being as before cryopreservation. It might be possible to carry out an upload to a whole brain emulation from the cryopreserved brain first, to ensure in that emulation that everything is working as desired, and to then use that to impose the right development/tuning on the fresh biological brain (i.e., to 'download' into that brain). To be honest, this is not something that I often carefully think about, because I don't regard the 'download' back to a biological brain as presenting any useful benefit that I would be personally interested in."

[2112] https://en.wikipedia.org/wiki/Neuromorphic_engineering.

[2113] e.g., a biological robot or "biot"; https://en.wikipedia.org/wiki/Rendezvous_with_Rama.

[2114] https://en.wikipedia.org/wiki/Robot.

[2115] https://en.wikipedia.org/wiki/Cyborg; https://en.wikipedia.org/wiki/Hybrot.

[2116] Abu-Hassan K, Taylor JD, Morris PG, Donati E, Bortolotto ZA, Indiveri G, Paton JFR, Nogaret A. Optimal solid state neurons. Nat Commun. 2019 Dec 3;10(1):5309; https://www.ncbi.nlm.nih.gov/pmc/articles/PMC6890780/. See also: https://techxplore.com/news/2019-12-world-artificial-neurons-chronic-diseases.html.

[2117] Weinstock N. Scholar Profile: Randal Koene. Cryonics 2019 Qtr 4;40(4):3-11; https://www.alcor.org/docs/cryonics-magazine-2019-04.pdf.

5.3 Molecular Reconstruction of the Original Body

For many cryonics patients it will be psychologically and philosophically important that the original body, and not a copy – not even an atomically precise copy – is the result of revival from cryopreservation. For such patients, a destructive scan is viewed as anathema or akin to death, and only a nondestructive scan will do. The simplest definition of "nondestructive" is "no part of the original was destroyed"; a dictionary definition is "no irreparable harm or damage was done".

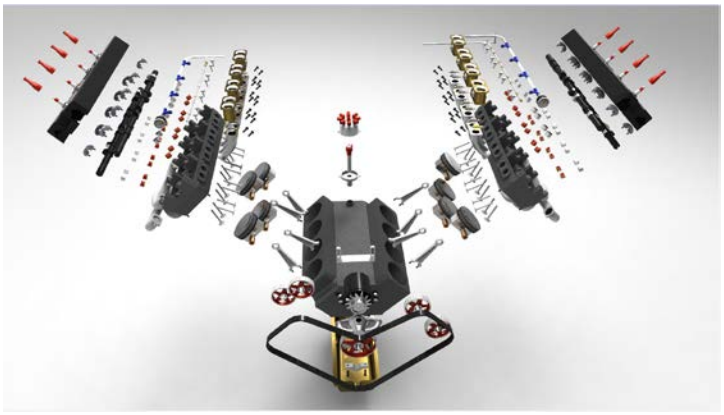

Imagine that we have a car that was assembled from ~30,000 separate parts.[2118] If we carefully disassemble the car into its component parts (image, right), being careful not to damage anything and keeping track of which parts fit where, then measure and record the names and dimensions of all 30,000 parts, then carefully reassemble the same 30,000 parts back into a completed car that is physically indistinguishable from the original with no parts missing, damaged, altered, or replaced, then we would assert that the car has been nondestructively scanned down to the scale of individual parts.

It should not matter if, when the individual parts are laid out on the garage floor, we additionally take each part into another room, one by one, and separate each part into its constituent molecules or atoms, record their element types and exact atomic positions within the part, then reassemble each part back into its initial structure with every molecule in its original position, using the original atoms in their original positions within each molecule, and with no atoms missing or replaced, then return the part to the same spot on the garage floor, before reassembling all the parts back into the original car. This second inspection process is exactly analogous to the previous scan to the level of individual parts, except that the "parts" are atoms instead of bolts and spark plugs. In this case we would still assert that the scan has been nondestructive because literally nothing has changed between the pre-scan car and the post-scan car, or between any pre-scan part and post-scan part, all the way down to the atoms.

It is true that even a parts scan is extremely invasive or intrusive[2119] – like a major surgery[2120] – and an atomic scan is as maximally invasive as it is physically possible to be. But a scan of this type, either to the

---

[2118] https://www.toyota.co.jp/en/kids/faq/d/01/04/.

[2119] Freitas RA Jr. Nanomedicine, Volume IIA: Biocompatibility, Landes Bioscience, Georgetown, TX, 2003; Chapter 15.6, "Nanorobot Volumetric Intrusiveness"; http://www.nanomedicine.com/NMIIA/15.6.htm.

[2120] https://en.wikipedia.org/wiki/Minimally_invasive_procedure.

parts level or to the molecular level, is nondestructive in the sense that nothing has physically changed as a result of the scan except for the acquisition of information.[2121]

In the context of revival from cryopreservation, we will define the ideal "nondestructive scan" to mean: (A) the original physical structure and all of its molecular bonding patterns are the same, before and after the scan; (B) the process uses a sequence of extremely thin scan slices, each representing, e.g., only 10^{-7} of total body volume, leaving 99.99999% of the body intact at any given time during the scan; and (C) all the same atoms and molecules are present, and in the same exact positions with the same chemical bonds, before and after the scan. As a practical matter there will inevitably be some minor errors in handling ~10^{25} separate nonwater molecules or >10^{27} individual atoms because no physical process is absolutely perfect. But at some reasonably low error rate, e.g., $p_{error} \sim 10^{-11}$ (the base-pair error rate for high-quality mammalian DNA replication)[2122] or better,[2123] the pre-scan and post-scan structures can be regarded as sufficiently "the same" with no observable functional differences and few observable structural differences, such that the scan process can be judged to be essentially "nondestructive".

This Section describes how a nondestructive molecular scan can be done (Section 5.3.1), how the initial scan file should be corrected in preparation for repair (Section 5.3.2), and finally how to repair the patient's original body using either cryogenic molecular exchange repair (Section 5.3.3.1) or fluidic molecular-informed cell repair (Section 5.3.3.2).

[2121] Is it possible to devise an atomically-precise scan that is both entirely nondestructive *and* noninvasive? We have already described a macrovascular scan process (Section 4.1) that provides a scan resolution as good as ~0.1 mm with only electromagnetic fields or acoustic waves allowed to enter the body. This can be considered "minimally invasive" but even this is not completely noninvasive. At the cost of allowing excavating nanorobots into the vasculature and deeper electromagnetic or acoustic irradiation of cryogenic tissues, we may achieve 1-10 μm of scan resolution using microvascular scans (Section 4.3) in a process that is a bit more invasive. Tolerating still more intrusion to allow the reversible installation of a whole-body vasculoid appliance (Section 4.6), we can perform submicron scans (Section 4.7) with a probable scan resolution of ~100 nm. Going still further, electron microscopy has demonstrated 1-10 nm resolution (Section 4.7.3), though the rate of positionally-uncontrolled irreversible destruction could possibly be high and the best scans of this type require samples only 10-40 nm thick, which implies a fairly high degree of invasiveness along with at least some destruction. ***Future research*** should examine and validate the apparent conclusion that higher scan resolution generally requires increased invasiveness but does not require irreversible destruction.

[2122] Fijalkowska IJ, Schaaper RM, Jonczyk P. DNA replication fidelity in *Escherichia coli*: a multi-DNA polymerase affair. FEMS Microbiol Rev. 2012 Nov;36(6):1105-21; https://www.ncbi.nlm.nih.gov/pmc/articles/PMC3391330/.

[2123] The error rate of mechanosynthetic operations depends on many factors including the repeatable precision of manipulator motions, the positional uncertainty of tooltip moieties that varies with the amplitude of molecular vibration as a function of temperature, the probability of radical poisoning that varies with the quality of the UHV vacuum, and so forth. One major factor in the reaction reliability is the energetic favorability $\Delta E_{transfer}$ of a transfer reaction (i.e., how "downhill" the reaction is) and the height of the energy barrier $\Delta E_{barrier}$ that blocks access to each unfavorable or pathological side reaction. Surveys of mechanosynthetic reactions* usually specify that reliable reactions should have a ΔE of at least 0.20-0.40 eV, which at LN2 temperatures implies an estimated probability of a failed mechanosynthetic reaction ranging from P_{fail} = **3 x 10^{-13}** (at ΔE = 0.20 eV) to P_{fail} = **5 x 10^{-26}** (at ΔE = 0.40 eV). The latter figure would be consistent with <100 errors after reactions involving all >10^{27} atoms in the entire human body.

* Freitas RA Jr., Merkle RC. A minimal toolset for positional diamond mechanosynthesis. J Comput Theor Nanosci. 2008;5:760-861; http://www.molecularassembler.com/Papers/MinToolset.pdf.

5.3.1 Nondestructive Molecular Scan

How might we perform a nondestructive molecular scan? In one simple concept, we carefully separate the molecules comprising the body of the cryopreserved patient, recording their exact positions and orientations at the time of removal – the equivalent of the parts-level scan of the car. Each removed molecule is then placed in a holder or box called a Lab Module (Section F.2) that performs either noninvasive chemohaptic analysis (Section F.1) or a more invasive analysis if necessary using subtractive mechanosynthesis (Section F.1.5(4)) followed by reassembly of the original molecule using the original atoms in their original positions. This completely characterizes the molecule at the atomic scale – equivalent to the atomic-level scan of the car parts described in Section 5.3. The individually-characterized original molecules are then reassembled, one by one, into the original tissue structure in the exact same positions and orientations as in the original cryopreserved body, completing the nondestructive (albeit highly invasive) molecular scan – a process somewhat reminiscent of the concept of the retractile cascade[2124] in the field of reversible computing.[2125] The scan may progress from feet to head, processing the entire body in a series of thin slices of biomaterial that are extracted from the left side, molecularly analyzed in Lab Modules, then replaced in the exact same order on the right side as suggested by the illustration at left.

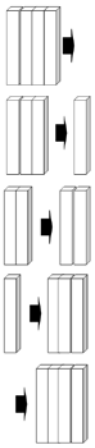

Several special cases must be dealt with. For example, the need to scan a few extended regions of noncovalently bonded ionic solids such as hydroxyapatite[2126] that are found in the teeth[2127] and bones[2128] of the human body will probably require positionally-controlled atomic-scale disassembly and reassembly of a small number of rigid structures, which in turn requires the use of subtractive and additive mechanosynthetic processes and further implies that such scans would most conveniently take place in a cryogenic UHV environment.[2129] Another special requirement is the need to lay down the first slice of transported and scanned tissue when no biomolecules have yet been laid down to anchor the initial structure onto the reassembling workpiece as the next molecules are emplaced (Section 5.2.3.1).[2130] It must also be noted that molecular reassembly from constituent atoms is not just time-reversed disassembly because additive mechanosynthetic reactions usually have pathological states that must be prevented by

---

[2124] In a retractile cascade, all inputs and all intermediate states leading to a result are retained during the course of a computation. After the computation is complete, the final result is copied to an output register, requiring the irreversible erasure of only enough bits in the output register to hold a copy of the final result, which need cost no more than $k_B T \ln(2)$ per erased bit. The computation is then reversed, step by step, culminating with the original inputs. Bennett CH. The Thermodynamics of Computation – a Review. Intl J Theor Phys. 1982;21(12):905-940; https://citeseerx.ist.psu.edu/viewdoc/download?doi=10.1.1.655.5610&rep=rep1&type=pdf. Hall JS. Nanocomputers and reversible logic. Nanotechnol. 1994;5:157-167; http://citeseerx.ist.psu.edu/viewdoc/download?doi=10.1.1.30.4090&rep=rep1&type=pdf.

[2125] https://en.wikipedia.org/wiki/Reversible_computing.

[2126] https://en.wikipedia.org/wiki/Hydroxyapatite.

[2127] https://en.wikipedia.org/wiki/Human_tooth#Parts.

[2128] https://en.wikipedia.org/wiki/Bone#Composition.

[2129] In principle, the molecular and ionic solid components of the body could be separated for scanning purposes and processed in different environments, then reassembled appropriately. This approach would seem to create unnecessary complications but should be further examined in ***future research***.

[2130] A ~1 nm sheet of synthetic organic material could be laid down as a sacrificial starter course, and there are many other possible alternatives.

careful design of tools, tool trajectories, and reaction sequences. ***Future research*** must identify all such special cases and propose methods for accommodating each of them.

Leaving aside these special cases, most biomolecules composing the cryopreserved human body are noncovalently bonded via relatively weak nonchemical bonds (typically involving van der Waals forces[2131] or hydrogen bonding[2132]) to neighboring biomolecules and thus can be separated and examined using the procedure previously described in Section 5.2.1 for destructive molecular scan, but with one major exception: molecules and atoms are not discarded but are retained. Complete positional and compositional information is recorded, enabling disassembled molecules to be reassembled from the original atoms in the same molecular positions as before, and enabling disassembled tissue to be reassembled with the original molecules in the same spatial positions and orientations as in the original tissue.

Performing a molecular scan in this new way will require additional nanomachinery to maintain a controlled inventory process and to perform mechanosynthetic molecular reassembly using inventoried atoms in the precise order needed to reconstruct the original molecules and tissues.

The first bit of additional nanomachinery is atomholders for the –OH and –H moieties that result from the abstraction of water molecules from the cryopreserved tissue as previously described in Section 5.2.1.1, and the infrastructure necessary to manipulate them. If: (1) each atomholder is a rectangular block of diamond measuring 1 nm x 1 nm x 10 nm for a volume of $V_{atomholder} = 10\ nm^3$,[2133] with the inventoried atom or moiety reversibly bonded to the 1 nm^2 apex; and (2) we must remove $N_{MSVwater} = 8.95 \times 10^{26}$ water molecules from the molecular scan volume (MSV) of a 70 kg cryopreserved human body (Section 5.2.1.3); and (3) we need two atomholders for each water molecule, one for the –OH and one for the –H; and (4) the body will be processed in a series of $n_{scanslices} = 10^7$ planar tissue slices; then we would need $V_{MSVatomholderW} = 2\ V_{atomholder}\ N_{MSVwater} / n_{scanslices} = 1.79\ cm^3$ of atomholders to simultaneously hold the atoms of all water molecules in one tissue slice in the MSV of the body.

[2131] https://en.wikipedia.org/wiki/Van_der_Waals_force.
[2132] https://en.wikipedia.org/wiki/Hydrogen_bond.

[2133] Each diamond 10 nm^3 atomholder has ~1760 carbon atoms. Writing a unique numerical identifier on each of the ~10^{20} atomholders in use requires ~ $\log_{10}(10^{20})/\log_{10}(2) \sim 67$ bits. Using 3 atoms/bit – possibly as surface bumps on the side of the atomholder block – requires ~200 atoms for the encoding.

The MSV also has an estimated $N_{MSVnonwaterA} \sim 1.92 \times 10^{27}$ nonwater atoms grouped into $N_{MSVnonwaterM} \sim 1.03 \times 10^{25}$ nonwater molecules (Section 5.2.2.1).[2134] To perform the molecular scan, each nonwater molecule is transferred to a microscale Lab Module (Section F.2) which has a volume of $V_{LabMod} = 1\ \mu m^3$, a peak power consumption of $P_{LabMod} = 100$ pW when operated at LN2 temperatures, and the ability to atomically scan a molecule presented to it in a processing time of $\tau_{LabMod} \sim 1$ sec using a 1 GFLOP ($I_{LC} = 64 \times 10^9$ bit/sec) onboard nanocomputer, allocating a plausible ($\tau_{LabMod}\ I_{LC}\ N_{MSVnonwaterM} / N_{MSVnonwaterA}$) ~ 0.34 gigabits for processing each atom in the molecule. This implies a need for $N_{Labslice} = N_{MSVnonwaterM} / n_{scanslices} \sim 1.03 \times 10^{18}$ Lab Modules with a nanomachinery volume of $V_{Labslice} = V_{LabMod}\ N_{Labslice} =$ **1.03 m^3** to process all the molecules in each tissue slice.

If the Lab Modules operate on an $f_{Labslice} = 10\%$ duty cycle to allow plenty of time for tissue transport and registration operations, then processing each tissue slice requires $\tau_{Labslice} \sim 10$ sec with a continuous power consumption of $P_{Labslice} = f_{Labslice}\ N_{Labslice}\ P_{LabMod} =$ **10.3 MW**,[2135] and the total scan time for an entire cryopreserved human body is $t_{LabScan} = n_{scanslices}\ \tau_{Labslice} = 1 \times 10^8$ sec (~**39 months** or ~1160 days). (A conceptual cooling system capable of extracting ~100 MW/liter of waste heat from macroscale volumes of nanomachinery at 273 K (0 °C) has been described in the literature.[2136]) Allocating one $V_{atomholder} = 10$ nm^3 atomholder per nonwater atom adds a negligible $V_{atomholder}\ N_{MSVnonwaterA} / n_{scanslices} \sim 1.92\ \mu m^3$ of nanomachinery volume to the ~1.03 m^3 total.

The incremental electricity cost is ($e_\$\ t_{LabScan}\ P_{Labslice}$) ~ $29 million to complete a nondestructive whole-body molecular scan at today's typical commercial electric rate of ~$0.10/KW-hr ($e_\$ \sim 2.78 \times 10^{-8}$ $/J;

[2134] Note that after water and inorganics, the most numerous molecules in human cells are lipids, primarily in the plasma membrane and the membranes of intracellular organelles. If there are $N_{celllipids} \sim 8.4 \times 10^{11}$ lipid molecules/cell (**Table 14** in Section 5.2.1.3) and $N_{bodycells} \sim 3.5 \times 10^{12}$ tissue cells in the human body,[*] then we must extract $N_{MSVlipids} = N_{celllipids}\ N_{bodycells} \sim 2.9 \times 10^{24}$ lipid molecules from the molecular scan volume (MSV) of a 70 kg cryopreserved human body, representing $N_{MSVlipids} / N_{MSVnonwaterM} \sim 28\%$ of all nonwater molecules. Extracting a single lipid molecule from a membrane requires only 12-70 pN for various lipids, membranes, and rates of extraction.[†] All lipid molecules possess a carbon chain backbone, so lipid molecules may be extracted one by one from a membrane by abstracting a single hydrogen atom that is covalently bonded to the carbon backbone, attaching a molecular tool that makes weak covalent bonds to the carbon radical created by the abstraction (e.g., a tool with a germanium radical tip), then mechanically pulling the lipid molecule out of the membrane. In this example, the Ge-C bond has a rupture strength of ~3640 pN,[‡] which is ~100 times stronger than necessary to extract the lipid molecule, and the Ge-C bond is readily disrupted by other means when it later becomes necessary to release the lipid molecule. ***Future research*** can identify alternative tooltip structures or mechanisms that can bond even more weakly to the lipid and thus more readily release the molecule at the appropriate time.

[*] Freitas RA Jr. Nanomedicine, Volume I: Basic Capabilities, Landes Bioscience, Georgetown TX, 1999, Section 8.5.1, "Cytometrics"; http://www.nanomedicine.com/NMI/8.5.1.htm#p5.

[†] Marrink SJ, Berger O, Tieleman P, Jähnig F. Adhesion forces of lipids in a phospholipid membrane studied by molecular dynamics simulations. Biophys J. 1998 Feb;74(2 Pt 1):931-43; https://www.cell.com/biophysj/pdf/S0006-3495(98)74016-0.pdf. Stetter FWS, Cwiklik L, Jungwirth P, Hugel T. Single lipid extraction: the anchoring strength of cholesterol in liquid-ordered and liquid-disordered phases. Biophys J. 2014 Sep 2;107(5):1167-1175; https://www.ncbi.nlm.nih.gov/pmc/articles/PMC4156670/.

[‡] Freitas RA Jr., Merkle RC. A minimal toolset for positional diamond mechanosynthesis. J Comput Theor Nanosci. 2008;5:760-861; http://www.molecularassembler.com/Papers/MinToolset.pdf.

[2135] The energy to break every covalent bond in the molecular scan volume (MSV) of the body may be approximated as (~2 bonds/atom) (~4.6×10^{27} atoms/MSV) (~600 zJ/bond) = 5.5×10^9 J/MSV, which if spread over a scan time of $t_{LabScan} \sim 10^8$ sec adds a negligible ~55 watts to the total power demand. Additionally, the sublimation enthalpy of ice at 77 K – the energy that must be added to a water molecule that's hydrogen-bonded to the cryogenic ice lattice surface in order to remove the molecule to the vapor phase – is about +0.51 eV or $E_{SEI} = 8.20 \times 10^{-20}$ J/molecule,[*] so the water separation energy for all MSV water molecules is $E_{SEIall} = N_{MSVwater}\ E_{SEI} = 7.34 \times 10^7$ J, adding a negligible $E_{SEIall} / t_{LabScan} \sim 0.7$ watt to total power demand.

[*] Feistel R, Wagner W. Sublimation pressure and sublimation enthalpy of H_2O ice Ih between 0 and 273.16 K. Geochim et Cosmochim Acta. 2007 Jan 1;71(1):36-45; http://www.personal.psu.edu/mrh318/Feistel-Wagner-GCA-2007.pdf.

[2136] Drexler KE. Nanosystems: Molecular Machinery, Manufacturing, and Computation, John Wiley & Sons, New York, 1992, Section 11.5.3 "Cooling capacity in a macroscopic volume", p. 332; https://www.amazon.com/dp/0471575186/.

Appendix G), over and above the ~$43 million electricity cost for a molecular print job (Section 5.2.3.2) for the 10^7 individual tissue slices, for a total nondestructive scan cost of ~**$72,000,000**.[2137] If early molecular manufacturing of atomically precise nanomachinery has an energy cost of $C_{mmE\$}$ ~ $100,000/kg,[2138] then building $V_{Labslice}$ ~ 1.03 m^3 of scanning nanomachinery could have an initial capital cost of up to $C_{mm\$} = C_{mmE\$} \rho_{normal} V_{Labslice}$ ~ $100 million assuming a nanofactory of normal density ρ_{normal} ~ 1000 kg/m^3, with this capital cost gradually declining by up to several orders of magnitude as the manufacturing technology matures and improves its energy efficiency.[2139]

As with destructive scans (Section 5.2.1.3), nondestructive scan time can be decreased by segmenting the patient body into multiple blocks that are scanned separately but in parallel. Reducing scan time by a factor of $(1/N_x)$ will require ~$(1.03\ N_x)$ m^3 of nanomachinery operating in parallel, along with equipment for segmenting the cryopreserved body into multiple blocks and then reassembling the blocks in the correct order. Capital costs for manufacturing the extra nanomachinery will increase linearly with N_x, but the total electricity cost for the faster multiblock scans should remain about the same as for the single-block scan. ***Future research*** should explore the range of plausible multiblock scenarios, but a value of N_x ~ 10 does not seem unreasonable.

While dividing the scan into ever smaller pieces generally reduces the scan time, the use of smaller pieces increases the total interfacial surface area of the pieces which might increase nondestructive scan time and scan complexity – the smaller the pieces, the more often the nanomanipulators will encounter a lengthy chain molecule that must be cut, properly recorded and terminated for chemical stability on both sides of the cut, then later both ends of the divided molecule must be located, unterminated, and rejoined to the proper partner. For example, extracellular matrix (ECM) incorporates a wealth of long molecules including collagen, elastin, large glycoproteins and proteoglycans, with mesh sizes ranging from 4-10 μm for fibronectins or laminins in ECM, 4-12 μm between adjacent collagen fibrils in skin and tendons, and 10-30 μm between adjacent fibrils in fibrous cartilage.[2140] Assuming an x_{grid} ~ 10 μm mean grid size for all cut-chain molecules, each side of each planar slice as described in Section 5.2.1.3 requires special handling for $N_{chaincut/1} \sim 2A_{cross} / x_{grid}^2 =$ **6.48×10^8** interface-crossing ECM molecules for the 1-slice scenario, and $N_{chaincut/15} \sim 30\ A_{cross} / x_{grid}^2 =$ **9.72×10^9** interface-crossing ECM molecules for the 15-slice scenario that requires ~1 year to complete. By contrast, the aggressive L_{cube} = 422 nm tissue nanocube scenario that is estimated to take a roughly similar time (~6 months) to complete as the 15-slice scenario involves creating $N_{cubes} = 1.8 \times 10^{16}$ tissue cubes requiring the excess cutting/rejoining of ~20,000 times more interface-crossing ECM molecules (i.e., $N_{chaincutCubes} = 6N_{cubes} (L_{cube} / x_{grid})^2 =$ **1.92×10^{14}**). If the spacing of interface-crossing long molecules is much closer than ECM, e.g., if x_{grid} ~ 1 μm or 0.1 μm, then the excess

---

[2137] It is estimated that the cost of commercial electricity might decline up to 100-fold in the era of widespread atomically-precise manufacturing using nanofactories (Appendix G), in which case the energy cost of the nondestructive scan might fall to only $720,000, whereupon other revival costs (e.g., human labor) might predominate.

[2138] Freitas RA Jr., Merkle RC. Kinematic Self-Replicating Machines, Landes Bioscience, Georgetown, TX, 2004; Fig. 4.42, "Physical device specifications for the Merkle-Freitas hydrocarbon molecular assembler"; http://www.molecularassembler.com/KSRM/Figures/4.42.JPG.

[2139] It is estimated that the cost of atomically-precise manufacturing using nanofactories might decline to as low as $1-1000/kg,* in which case the capital cost of a cubic meter of scanning nanomachinery might fall to only ~$1000-$1 million, whereupon other costs (e.g., human labor) might predominate.

* Freitas RA Jr., Merkle RC. Kinematic Self-Replicating Machines, Landes Bioscience, Georgetown, TX, 2004; Section 6.2.2, "Demonstration of Feasibility"; http://www.MolecularAssembler.com/KSRM/6.2.2.htm. Freitas RA Jr. Economic Impact of the Personal Nanofactory. Nanotechnology Perceptions: A Review of Ultraprecision Engineering and Nanotechnology 2006 May;2:111-126; http://www.rfreitas.com/Nano/NoninflationaryPN.pdf.

[2140] Freitas RA Jr. Nanomedicine, Volume I: Basic Capabilities, Landes Bioscience, Georgetown TX, 1999, Section 9.4.4.2, "ECM Brachiation"; http://www.nanomedicine.com/NMI/8.2.1.3.htm.

cutting/rejoining task would increase to 2 million or 200 million times more than the 15-slice scenario, respectively.

5.3.2 Initial and Corrected Scan Files

Similar to the case of the destructive molecular scan (Section 5.2.2.1), a nondestructive molecular scan (Section 5.3.1) will produce an initial scan file that includes the element identity and 3D positions (to ~20 pm precision) of the estimated $N_{MSVatoms} \sim 4.6 \times 10^{27}$ atoms occupying the molecular scan volume (MSV) of the average cryopreserved 70 kg human body. Unlike the outcome of a destructive scan in which the patient's physical body no longer exists, after a nondestructive scan the original body of the cryopreserved patient remains entirely intact. Nothing observable physically changes as a result of a nondestructive scan except for the acquisition of information.[2141]

The **nondestructive initial scan file** is essentially the same $I_{MSVatoms} \sim 5.4 \times 10^{29}$ bits as for a destructive scan, with a data handling requirement of $I_{MSVprocess} \sim 1.08 \times 10^{30}$ bits to acquire that data destructively (Section 5.2.2.1). There is additional data handling overhead to acquire the data nondestructively because we must individually sequester and track all individual molecules and many/most individual atoms, and we must specify reaction sequences for reassembling, using the original atoms, all original molecules that were temporarily disassembled during the nondestructive scan, using the same atoms in the same positions within the molecule.

Cryostasis revivals will occur in a future era of highly mature mechanosynthetic technology. By the time revivals are performed, libraries containing millions of validated mechanosynthetic reaction sequences will commonly exist, and sophisticated software packages will exist that can efficiently generate reliable new reaction sequences on the fly whenever needed. The additional data handling requirement for acquiring the nondestructive initial scan file can therefore be crudely estimated as follows:

(1) **Mechanosynthetic Tool Library.** If the full range of mechanosynthetic capability requires $n_{tooltypes} = 10^6$ distinct mechanosynthetic tooltypes, and if each tooltype includes $n_{tooltypeatoms} = 1000$ atoms per tooltype, and if each atom in each tooltype must be specified by element type [$i_{element} = \log_{10}(92 \text{ elements})/\log_{10}(2) = 7$ bits/atom] and by 3D position to 20 pm precision within a 2 meter apparatus [$i_{position} = 3\log_{10}(2 \text{ m} / 20 \text{ pm})/\log_{10}(2) = 110$ bits/atom], then the mechanosynthetic tool library requires $I_{toollib} = n_{tooltypes}\ n_{tooltypeatoms}\ (i_{element} + i_{position}) = 1.2 \times 10^{11}$ bits of storage.

(2) **Reaction Sequence Library.** If the full range of mechanosynthetic capability requires $n_{reactseqs} = 10^6$ distinct mechanosynthetic reaction sequences, and if each sequence includes $n_{reactsteps} = 100$ reaction steps, and if each reaction step in each sequence must be specified as using at least one of the $n_{tooltypes} = 10^6$ tooltypes [$i_{tooltypes} = \log_{10}(n_{tooltypes})/\log_{10}(2) = 20$ bits/step] and one round-trip trajectory from tooltip rack to workpiece and back to toolrack with the two endpoints specified in 3D to 20 pm precision within a 2 meter apparatus [$i_{toolpositions} = 6\log_{10}(2 \text{ m} / 20 \text{ pm})/\log_{10}(2) = 220$ bits/step], then the mechanosynthetic reaction sequence library requires $I_{seqlib} = n_{reactseqs}\ n_{reactsteps}\ (i_{tooltypes} + i_{toolpositions}) = 2.4 \times 10^{10}$ bits of storage. (This number increases by a factor of N if a specific path in space consisting of N intermediate steps between the two endpoints must be chosen, rather than merely specifying the two endpoints of tooltip motion.)

(3) **Post-Scan Reassembly.** In the worst-case scenario, all $N_{MSVatoms} \sim 4.6 \times 10^{27}$ atoms (Section 5.2.1.3) for all $N_{MSVmolecules} = N_{MSVwater} + N_{MSVnonwaterM} \sim 9.05 \times 10^{26}$ molecules in the MSV (Section 5.3.1) will require a mechanosynthetic reaction sequence to place each atom back into the molecule from which it

---

[2141] As noted elsewhere, a small amount of error must inevitably creep into any repetitive physical process, but the process should be designed to minimize that error to acceptably low levels.

came, thus reassembling the original molecule using the original atoms in their original positions within the molecule. During post-scan molecular reassembly, tissue is processed as $n_{scanslices} = 10^7$ isolated tissue slices (Section 5.3.1) so only the data required to process the atoms in each slice must be retained in memory at any given time. Processing each atom in the current tissue slice requires specifying (A) the unique identifier for the atom being added to a molecule [$i_{atom} = \log_{10}(N_{MSVatoms})/\log_{10}(2) = 92$ bits/atom], (B) the unique identifier for the molecule to which the atom is being added [$i_{molecule} = \log_{10}(N_{MSVmolecules})/\log_{10}(2) = 90$ bits/atom], (C) the unique identifier of the reaction sequence being used to add the named atom to the named molecule [$i_{seq} = \log_{10}(n_{reactseqs})/\log_{10}(2) = 20$ bits/atom], and (D) the bits that describe the details of the reaction sequence being executed by the nanomanipulators [$i_{reactseq} = I_{seqlib} / n_{reactseqs} = 24{,}000$ bits/atom]. Whole-body mechanosynthetic molecule assembly thus requires $I_{mechano} = (N_{MSVatoms} / n_{scanslices})(i_{atom} + i_{molecule} + i_{seq} + i_{reactseq}) =$ **1.1×10^{25} bits** of additional data handling, which includes $I_{toollib} + I_{seqlib} = 1.44 \times 10^{11}$ bits for the tool and reaction sequence libraries. Processing each tissue slice in $\tau_{Labslice} \sim 10$ sec implies a $I_{mechano} / \tau_{Labslice} =$ **1.1×10^{24} bits/sec** processing rate and a computational requirement of $I_{mechano} / \tau_{Labslice}\ U_{nano} \sim$ **1.1 cm^3** of diamondoid mechanical nanocomputers in addition to the computational requirements for a destructive molecular scan (Section 5.2.2.1).

The **nondestructive corrected scan file** should be of similar size as the destructive corrected scan file (Section 5.2.2.2), compiled in similar fashion as previously described from the initial file with similar computational requirements, and with similar imposed constraints allowing only lethal or near-lethal corrections to be made. Medical-related physical flaws such as the presence of a lethal tumor must be corrected in the original scan file by replacing the data representing the flawed tissue with data representing unflawed tissue. The ideal structure of the substitute unflawed tissue might be determined by analyzing the structure of the flawed tissue to determine the pathway by which the original tissue became flawed. For example, the current cell structure of a tumor can be analyzed to determine the likely identity and positions of the original normal cell(s) from which it sprang (image, left),[2142] and the growth path those cells most likely followed as they became cancerous and expanded to become a tumor. The results of this analysis can be supplemented with: (A) knowledge of the patient's own unique DNA, protein, and other molecular structures; (B) knowledge of the molecular structure of similar unflawed tissues in other places in the patient's body, as may be present elsewhere in the initial scan file; and (C) knowledge of the tissue ultrastructure and molecular signatures for generic unflawed human tissue of the type that has become flawed. ***Future research*** should investigate and develop algorithms for performing this kind of reconstructive analysis, along with the databases necessary to support such analysis. If the amount of replaced tissue represents only a small fraction (e.g., 1%) of total tissue mass, then the reconstructive analysis should add little to the previously-estimated computer memory and data processing mass, power, and time requirements for effecting revival.

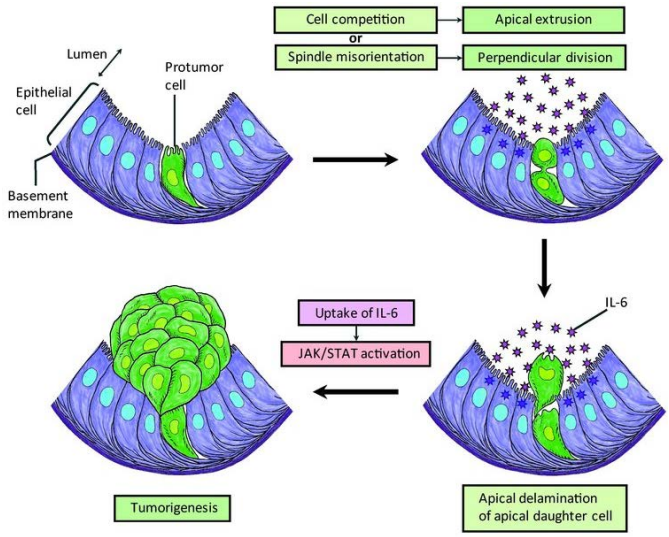

Besides medical-related physical flaws, additional biomolecular faults might have been injected into the data due to errors in the nondestructive molecular scanning process itself. ***Future research*** should

---

[2142] Tamori Y, Deng WM. Tissue-Intrinsic Tumor Hotspots: Terroir for Tumorigenesis. Trends Cancer. 2017 Apr;3(4):259-268; https://www.ncbi.nlm.nih.gov/pmc/articles/PMC5518481/.

investigate the feasibility, possible methods, and desirability of attempting appropriate error-correction procedures to correct scan-derived faults in the initial scan file data.

Finally, we recognize that even a perfectly repaired human body at cryogenic temperatures cannot simply be rewarmed to wakefulness but instead must be thawed following a specific procedure that preserves viability by avoiding the creation of new tissue damage. Accordingly, the initial scan file of the cryopreserved patient must be further corrected to enable the patient to survive rewarming without further damage. To accomplish this, additional cryoprotectant molecules must be inserted into the dataset at sufficient concentration and in the ideal pattern to forestall rewarming damage when the reassembled body is warmed above the glass transition temperature in an effort to awaken the patient, as previously described (Section 5.2.3.1(A)). The initial scan file must also be modified to create a description of a human body in full metabolic stasis, with all metabolic biochemicals removed from all tissues as described in Section 4.10.

5.3.3 Repair Original Patient Body

The original body of the cryopatient can be repaired using the nondestructive corrected scan file (Section 5.3.2) which includes comprehensive detailed information on the identity and position of every atom and molecule in the cryopreserved patient's original body, augmented with a few modifications designed to ensure a nondestructive warmup and successful revival process. Using nondestructive scan preserves all repair options.

This Section describes two distinct nondestructive repair protocols:

(1) **Cryogenic Molecular Exchange Repair** (Section 5.3.3.1), in which the atomically-precise data in the corrected scan file explicitly guides a nondestructive scan process wherein the body is reassembled in a manner that directly incorporates all necessary alterations at the molecular level; and

(2) **Fluidic Molecular-Informed Cell Repair** (Section 5.3.3.2), in which the patient is revived using the conventional cell repair protocols (Chapter 4) but the atomically-precise data in the corrected scan file is employed by nanorobots to perform desired alterations at a much finer feature resolution (e.g., 0.1-100 nm) than is possible using submicron scan data (Section 4.7) alone.

Alternatively, the patient's brain could be repaired by the nondestructive methods described in Section 5.3, after which the rest of the body could be repaired by these same methods or by the methods described in Chapter 4, or replaced using the methods described in Section 5.2.

5.3.3.1 Cryogenic Molecular Exchange Repair

To complete a molecular exchange repair of the cryopreserved patient's body, we perform a second nondestructive molecular scan almost exactly the same as the first nondestructive scan,[2143] but with one important difference.

[2143] It is not possible to perform both scan and reconstruction in one pass because the molecular scan is extremely localized (i.e., ranging from molecular surfaces to ~0.2 μm scan planes) but the reconstruction scan must take account of flawed structures and related debris fields that may span a cell width (i.e., ~20 μm) or even more distant structures in the case of neuron axons or muscle cells.

In the first nondestructive scan, as previously performed (Section 5.3.1), the patient was briefly separated into component molecules, then immediately reassembled using the same atoms and molecules, along an $L_{body} / n_{scanslices} \sim 200$ nm thick scan plane that was slowly swept through the body from feet to head, with the measured identities and positions of every molecule used as the guide for reassembling the original structure, taking human body length $L_{body} \sim 1.85$ m and $n_{scanslices} \sim 10^7$ planar tissue slices (Section 5.3.1).

In the second nondestructive scan, now performed here, the corrected data file (Section 5.3.2) is used as the guide for reassembly rather than real-time scan results. If, say, ~1% of the original tissue was determined to be flawed and was replaced in the initial scan file with a description of new unflawed tissue in the corrected scan file, then ~99% of the original molecules in the patient's body would be reassembled in exactly the same positions as before. Of the remaining ~1% of tissue that the reconstructive analysis (Section 5.3.2) determined should be different, two courses of action may be followed depending on the strictness of the patient's desire for fealty to their original substance:

(A) **Replace flawed tissue with non-native material.** The atoms and molecules representing the perhaps ~1% of tissue that is flawed can be discarded with new atoms and molecules imported from the cell mill (Appendix D) to take their place. In this case, the resulting repaired human body will consist of ~99% native (original) material and ~1% non-native material.[2144] The non-native material will have the exact same molecular structure as the inferred healthy tissue that existed before the flaw occurred – but it will be composed of different atoms and molecules than the original unflawed or flawed tissue.

(B) **Replace flawed tissue with native material.** The perhaps ~1% of tissue that is flawed can be reconstructed using atoms and molecules taken from the flawed tissue which, although flawed, is nonetheless native material. For example, the molecules comprising a tumor can be separated and reassembled in a slightly different way to fabricate healthy cells and tissues following the specifications of the corrected scan file. Any surplus atoms can be discarded without prejudice. A few non-native molecules might be imported in the case of excision or avulsion wounds where the original material is no longer present, but the number of such molecules should be very small. If molecules or cellular components of the original unflawed tissue can be discerned in modified form in the flawed tissue, those components might be used to reconstruct the original cells using some or even most of the original molecules. In the case of laceration injuries, virtually all of the original tissue might be present, mostly intact but spatially displaced, allowing almost all of the original atoms and molecules to be repositioned during the reassembly operation. The resulting human body could be ~99.99% (or better) of original atoms, molecules, or tissue material.[2145]

The end state of the molecular repair and reassembly process described in this Section is a fully restored and viable replacement human body in biochemical stasis resting at cryogenic temperatures that can be rapidly rewarmed to near 273 K (0 °C) in the reliquidified state, exactly the same as occurs by the completion of Section 4.12 during conventional cell repair, but in the present case with maximum molecular fidelity to the original cryopreserved body. As in the cryogenic 3D atomic print (Section 5.2.3.1) and cryogenic 3D molecular print (Section 5.2.3.2) scenarios, completion of revival from cryogenic molecular exchange repair then entails (A) installation of vasculoid (Section 4.6), (B) molecular extraction of the cryoprotectant (Section 4.10.1.7), (C) patient warmup to 310 K (37 °C) and molecular instillation (Section 4.13), (D) vasculoid uninstallation and blood substitution (Section 4.14), and (E)

[2144] The distinction between native and non-native material is valid as to source but is to some extent a philosophical question because present-day physics asserts that all atoms of a given element are physically indistinguishable from each other, and similarly with molecules of identical chirality – e.g., a molecule of L-alanine that is present in your body is believed to be physically indistinguishable from a molecule of L-alanine located anywhere else in the universe.

[2145] Since all atoms or molecules of a given type and state are physically indistinguishable at the quantum level according to present-day science, the maximal use of native atoms and molecules may represent a philosophical preference but is not a strictly medical necessity.

patient wakeup (Section 4.15). The details and validity of this protocol should be critically reviewed in ***future research***.

5.3.3.2 Fluidic Molecular-Informed Cell Repair

To complete a fluidic molecular-informed cell repair we would perform conventional cell repair as described in Chapter 4, but guided by a more precise repair plan that is informed by atomic resolution scans involving every molecule in the cryopreserved patient's body. This approach might be favored by patients who worry that some memory- or personality-relevant information resides in the sub-100 nm-resolution tissue structure, but who are unwilling to tolerate (or cannot afford) more than a single round of nondestructive scanning and molecular reassembly (Section 5.3.1). The atomically-precise data in the corrected scan file can be employed by nanorobots to guide desired alterations at a much finer feature resolution (e.g., 0.1-100 nm) – which could be relevant to some neural structures (Section 2.1.2) – than is possible using submicron scan data (Section 4.7) alone.

In this scenario, following bulk extraction (Section 5.1) and the nondestructive molecular scan (Section 5.3.1), a submicron scan (Section 4.7) can be readily extracted as a subset of the already-completed nondestructive molecular scan. The fluidic molecular-informed cell repair process then starts with installation of the vasculoid (Section 4.6) in the reassembled cryogenic tissue and compilation of a more precise whole-body repair plan (Section 4.8) using atomic-resolution scan data. This should be followed by warming (Section 4.9), molecular extraction (Section 4.10) and cell resealing (Section 4.11). Conventional cell and tissue repair using nanorobots (Section 4.12) can then proceed as before, but informed by a molecularly precise repair plan that permits tweaks to structures in the 0.1-100 nm subcellular size scale. Completion of revival from fluidic molecular-informed cell repair then entails (A) patient warmup to 310 K (37 °C) and molecular instillation (Section 4.13), (B) vasculoid uninstallation and blood substitution (Section 4.14), and (C) patient wakeup (Section 4.15). The details and validity of this protocol should be critically reviewed in ***future research***.

Repair times in this scenario should lie somewhere between those required for Conventional Cell Repair (Section 4.16) and those required for Nondestructive Molecular Exchange Repair (Section 5.3.3.1), but may vary widely depending on the protocol alternatives selected by the patient.

5.4 High-Speed Molecular Reconstruction

Other more advanced methods for molecular reconstruction of the repaired human body can be imagined that could, in principle, complete the work in much less time but which involve operational complexities that should be further examined in ***future research*** but are beyond the scope of this book. Here we take a quick look at just one of these ideas.

The concept of convergent assembly[2146] involves the manufacture of meter-sized objects (e.g., a human body) starting from building blocks whose size is measured in microns or nanometers. Convergent assembly is based on the idea that smaller parts can be assembled into larger parts, larger parts can be assembled into still larger parts, and so forth. In the conventional molecular manufacturing context, a finished assembly which is about 1 meter in size might be made from eight smaller subassemblies each

---

[2146] Freitas RA Jr., Merkle RC. Kinematic Self-Replicating Machines. Landes Bioscience, Georgetown, TX, 2004, Section 5.7 "Massively Parallel Molecular Manufacturing"; http://www.MolecularAssembler.com/KSRM/5.7.htm.

about 0.5 meters in size. The eight subassemblies could be assembled into a finished assembly by using one or more robotic arms (or other positional devices) in assembly modules depicted abstractly in the images below.[2147] Note that we are designating an "assembly module" by the size of its output port. The module size is larger – in this case, the 1.0 meter assembly module has a size of 2.0 meters. This additional size provides sufficient room to handle subassemblies and the final 1.0 meter assembly.

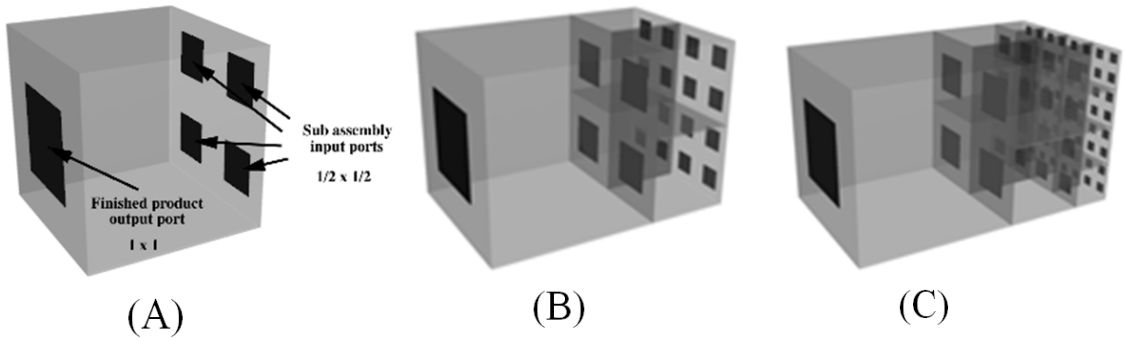

The first module at (A) is a single assembly module able to accept 8 cube-shaped subassemblies from the four input ports to the right, and which produces a cube-shaped finished assembly to the left through the single output port. If the output port has a size of one meter by one meter, each input port would have a size of 0.5 meters by 0.5 meters. The second module at (B) shows two stages of assembly starting with 64 sub-subassemblies each with a size of about 0.25 meters, producing 8 subassemblies with a size of about 0.5 meters, and producing a finished product with a size of about 1.0 meters. The third module at (C) shows three stages of convergent assembly producing a final product of ~1.0 meter in size from 512 sub-sub-subassemblies each of which is ~0.125 meters in size. We can continue adding stages to this process until the inputs to the first stage are as small as we might find convenient. For the purposes of general molecular manufacturing, it is usually easiest to assume that these initial inputs might be ~1 nm in size – essentially, bulk chemistry molecular inputs (image, right).

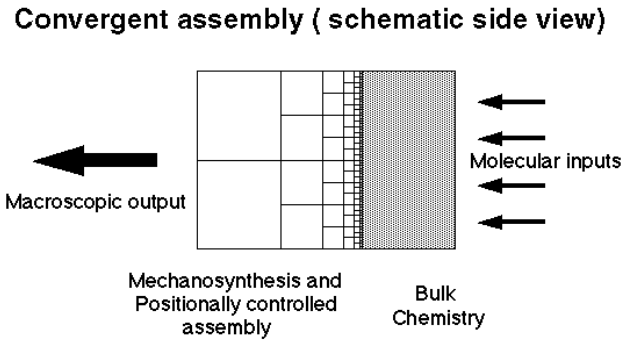

In the context of molecular reconstruction of a new replacement body (Section 5.2), we could imagine a cryogenic UHV convergent assembly device that accepts small blocks of frozen tissue and rapidly assembles them into larger blocks of frozen tissue, eventually resulting in a completely assembled replacement human body. The destructive molecular scan provides the atomically precise structural data which is compartmentalized into appropriately sized tissue blocks which are then fabricated in a nanofactory-type (Section 1.3.2) or a cell mill-type (Appendix D) manufacturing system, both of which are scaled to output ~1 kg/hour of product. If various practical difficulties could be overcome,[2148] a 70 kg

[2147] Merkle RC. Convergent assembly. Nanotechnology 1997;8:18-22; http://www.zyvex.com/nanotech/convergent.html.

[2148] For example, interfaces between adjacent blocks many be bridged by structures such as fibers whose separated termini must be precisely joined using covalent bonds, or by molecules that have been bisected with their termini passivated to avoid spontaneous reactivity and which now must be depassivated and precisely joined. Or some subassemblies may require blocks of different sizes, requiring ports of different sizes, or requiring more heterogeneous assembly sequences.

cryopatient could be convergently reassembled in **~70 hours** in fully repaired but cryogenic condition, then rewarmed as described in previous protocols.

In the context of molecular reconstruction of an original body (Section 5.3), the cryopatient could be segmented into blocks of appropriate size, after which the results of the preceding nondestructive molecular scan could be used to inform the repair of each individual tissue block that needs repair, whereupon the original body would be convergently reassembled in fully repaired but cryogenic condition, then rewarmed as described in previous protocols. In this case, the limiting factor is the speed of repair of the tissue blocks, which in turn will depend on the size and number of tissue blocks requiring repair. This process is conceptually similar to the "off-board repair" scenario described by Merkle (Section 2.2.9),[2149] who estimated that repairing a 1.4 kg human brain using ~10^9 dalton (2 x 10^{-18} kg, or ~100 million carbon atom) repair machines would demand ~1.8 x 10^{24} repair-machine-sec of work and burn ~10^{12} J of energy for the computational support, thus requiring ~14 kg of repair machines drawing ~4 MW of power to complete a brain reconstruction job in ~70 hours. Completing a 70 kg whole-body reconstruction job in $t_{fastreco}$ **~ 70 hours** would require ~700 kg of repair machines drawing $P_{fastreco}$ ~ 200 MW, costing $t_{fastreco}$ $P_{fastreco}$ $e_{\$}$ ~ $1,400,000 to complete the calculations assuming today's typical commercial electricity rate of ~$0.10/KW-hr ($e_{\$}$ ~ 2.78 x 10^{-8} $/J), which could be 10-100 times lower in the future (Appendix G).

The processes and challenges of cryostasis revival using convergent assembly following a molecular scan should be further explored in ***future research***.

5.5 Summary of Molecular Reconstruction

Table 16 lists the number of nanorobots or nanomanipulator devices and the estimated time required to complete each stage of the revival protocol using the molecular scan and reconstruction approach, for both whole-body (estimated from Sections 5.1, 5.2, and 5.3) and neuro (informal estimate) cryopreservation patients. While the task duration estimates are both reasonable and representative of the range of possibilities, all have large uncertainties and some are highly dependent upon the specific operational scenario and mission parameters chosen, and in some cases could vary from the stated figure by an order of magnitude or more.

[2149] Merkle RC. Molecular Repair of the Brain. Cryonics 1989 Oct;10(10):21-44; http://www.alcor.org/cryonics/cryonics8910.txt.

Table 16. Molecular reconstruction tasks and task durations for human cryopreservation revival using destructive and nondestructive molecular scan protocols

Molecular Reconstruction Cryopreservation Revival Task	Section Reference	Number of Nanorobots or Nano-manipulators	Task Duration (Whole-Body)	Task Duration (Neuro)
Macrovascular scan	5.1 [4.1]	---	>5 days	~1 day
Macrovascular excavation	5.1 [4.2]	2.97×10^9	17 days	~1 day
Microvascular scans	5.1 [4.3]	$\sim 3 \times 10^9$	~7 days	~1 day
Microvascular excavations				
Capillaries & crackface voids	5.1 [4.4.1]	2.3×10^9	17 days	~2 days
Organ & tissue surface perimeters	5.1 [4.4.2]	6×10^7	~0.5 day	~0.5 day
Extracellular ice	5.1 [4.4.3]	(variable)	(variable)	(variable)
Organ system excavations	5.1(5)	$\sim 3 \times 10^9$	~17.5 days	~2.5 days
Clear excavation debris	5.1 [4.5.1]	1×10^{10}	12 days	~0.5 day
---				
(DS) Cryogenic 3D Atomic Print:	5.2.3.1			
Destructive Molecular Scan	5.2.1.3	1.17×10^{15}	30 days	0.7 day
Create the corrected scan file	5.2.2.2	--- *	38 days	0.9 day
Create print file from corrected file	5.2.3.1	---	~38 days	~0.9 day
Cryogenic 3D Atomic Print	5.2.3.1	1.17×10^{15}	30 days	0.7 day
Re-attach vitreous slices	5.2.3.1	1.07×10^9	10 days	0.3 day
(DS) Cryogenic 3D Molecular Print:	5.2.3.2			
Destructive Molecular Scan	5.2.1.3	1.17×10^{15}	30 days	0.7 day
Create the corrected scan file	5.2.2.2	--- *	38 days	0.9 day
Create print file from corrected file	5.2.3.1	---	~38 days	~0.9 day
Create 3D molecular assembly file	5.2.3.2	--- †	24 days	~0.5 day
Cryogenic 3D Molecular Print	5.2.3.2	1.17×10^{15}	25 days	0.7 day
Re-attach vitreous slices	5.2.3.1	1.07×10^9	10 days	0.3 day
(DS) Planar Tissue Print:	5.2.3.3.1			
Destructive Molecular Scan	5.2.1.3	1.17×10^{15}	30 days	0.7 day
Create the corrected scan file	5.2.2.2	--- *	38 days	0.9 day
Create print file from corrected file	[5.2.3.1]	---	~38 days	~0.9 day
Create 3D cell assembly file	[5.2.3.2]	--- †	24 days	~0.5 day
Fluidic 3D Planar Tissue Print	5.2.3.3.1	800,000‡	75 days	~2 days
(DS) Scaffolded Tissue Print:	5.2.3.3.2			
Destructive Molecular Scan	5.2.1.3	1.17×10^{15}	30 days	0.7 day
Create the corrected scan file	5.2.2.2	--- *	38 days	0.9 day
Create print file from corrected file	[5.2.3.1]	---	~38 days	~0.9 day
Create 3D cell assembly file	[5.2.3.2]	--- †	24 days	~0.5 day
Fluidic 3D Scaffolded Tissue Print	5.2.3.3.2	7.5×10^9	56 days	~2 days
(NDS) Molecular Exchange Repair:	5.3.3.1			
Nondestructive Molecular Scan 1 (N_x=10)	5.3.1	1.03×10^{18} ⁋	116 days**	~3 days
Create the corrected scan file	5.3.2	--- *	38 days	0.9 day

Create print file from corrected file	[5.2.3.1]	---	~38 days	~0.9 day
Nondestructive Molecular Scan 2 (N_x=10)	[5.3.1]	1.03 x 10^{18} ⁋	116 days**	~3 days
---				
Warm printed body to 273 K	5.2.3.1(B):	9 x 10^{13}	0.1 day	0.1 day
Install arteriovenous vasculoid	[4.6.2]	1.5 x 10^{14}	0.04 day	~0.04 day
Molecular extraction - cryoprotectant	[4.10.1.7]	---	12 days	~12 days
Patient warmup & molec. instillation	5.2.3.1(A):			
Warm the patient to 310 K	[4.13.1]	---	0.04 day	~0.04 day
Instillation probe deployment	[4.10.1.9]	---	~1 day	~1 day
Instillation pumping	[4.13.2]	---	0.4 day	~0.4 day
Fluid check & perimeter cleanup	[4.13.3]	1 x 10^{12}	~1 day	~1 day
Instill storage nanorobots	[4.13.4]	3.5 x 10^{12}	0.4 day	~0.4 day
Uninstall vasculoid & finish repairs	5.2.3.1(A):			
Manufacture replacement blood	[4.14.1.2]	---	0.6 day	~0.6 day
Retract vasculoid	[4.14.2]	---	0.004 day	~0.004 day
Transfuse replacement blood	[4.14.4]	---	0.5 days	~0.5 day
TOTALS:				
Cryogenic 3D Atomic Print (Destructive Scan)			***237 days*** *(~7.9 months)*	***~27 days*** *(~0.9 month)*
Cryogenic 3D Molecular Print (Destructive Scan)			***256 days*** *(~8.5 months)*	***~28 days*** *(~0.9 month)*
Fluidic 3D Planar Tissue Print (Destructive Scan)			***296 days*** *(~9.9 months)*	***~29 days*** *(~0.9 month)*
Fluidic 3D Scaffolded Tissue Print (Destructive Scan)			***277 days*** *(~9.2 months)*	***~29 days*** *(~0.9 month)*
Cryogenic Molecular Exchange Repair (Non-Destructive Scan)			***399 days*** *(~13 months)*	***32 days*** *(~1.1 months)*
From Table 13 (Section 4.16)**:**				
Conventional Cell Repair			***512 days*** *(~17 months)*	***66 days*** *(~2.2 months)*
Conventional Cell Repair (whole-cell + high-power-density)			***244 days*** *(~8.1 months)*	***46 days*** *(~1.5 months)*

* 0.33 m^3 of nanomemory and 0.064 m^3 of nanocomputers
† 0.33 m^3 of nanomemory and 0.1 m^3 of nanocomputers
‡ 1 mm long, 0.3 mm wide cylindrical millimanipulators
⁋ microscale Lab Modules (Appendix F)
** processing the patient as $N_x \geq 10$ separate tissue blocks requires ≥10.3 m^3 of scanning nanomachinery (Section 5.3.1)
DS = Destructive Scan; NDS = Non-Destructive Scan

Table 16 suggests that molecular reconstruction may take the same or less time to complete as conventional cell repair. If molecular reconstruction always preserves more of the patient's original information, presumably better ensuring full recovery of memory and personality, then why would anyone choose conventional cell repair? There are several potentially good reasons:

(1) **Simpler is sooner.** While the nanorobotic systems and processes for conventional cell repair are far from simple, most are likely to be developed for conventional medical purposes and thus will be designed, tested, and generally available far sooner than the systems and processes necessary to achieve full molecular scanning and reconstruction. The technology required for molecular scanning and reconstruction is considerably more sophisticated, thus patients may have to wait longer in cryostasis to avail themselves of this technology. Time in the dewar is time spent at risk.[2150]

(2) **Reliability.** Cell repair, being a complex procedure but still simpler than molecular reconstruction, will be more reliable, at least in the early years. Error rates for mechanosynthetic disassembly and assembly of materials may initially be non-negligible, though declining over time, and more can go wrong unless everything is perfect when mole quantities of reactions are being undertaken. Molecular reconstruction attempts to get almost everything right, whereas conventional cell repair relies more on restoring biological systems to a state of biochemical functionality at which point biological systems may become self-repairing and self-correcting.

(3) **Close enough is good enough.** If the posited robustness of memory due to neural super-redundancy (Section 2.1.3) is confirmed, then even a comparatively imperfect means of revival may nonetheless preserve virtually all human memories and personal identity.

(4) **Philosophical concerns.** Molecular reconstruction at minimum requires patients to be disassembled into their constituent molecules or atoms at least once, and then reassembled precisely correctly. Practical molecular reconstruction also requires the patient to be processed in hundreds or even millions of slices, segments, or blocks, all of whose facing surfaces must be correctly and precisely mated at the molecular level during reassembly, in order to avoid unreasonable multi-decade processing times. Philosophically conservative patients may not be comfortable with this level of physical invasiveness, even when the intrusion is technically "nondestructive".

(5) **Mixed process.** Cost-conscious patients (or the organization that revives them) might rationally elect to restore the head using the more expensive molecular reconstruction and the body using the cheaper conventional cell repair, on the assumption that recovering the most valuable memory and personality attributes is most likely if the highest-fidelity revival technique is applied to the brain, whereas cell repair will suffice for the rest of the body (Section 6.1).

(6) **Revival expense.** An analysis of the cost of revival from cryopreservation, as summarized below in **Table 17**, suggests that molecular reconstruction may be 3-47 times more expensive than conventional cell repair assuming contemporary energy costs. However, much of this cost differential might disappear if the revival-era prices of commercial electricity (or comparable power sources) become at least 100-fold cheaper than today's rates (Appendix G).

[2150] A simple "cryonics calculator" (https://www.cryonicscalculator.com/) lets you "input the risk of cryonics disasters (storage facility fire, bankruptcy, etc) and the time frame for reanimation technology to develop, and outputs the overall odds of being successfully reanimated (repaired to youthful health by advanced medical technology)….for cryonics to work, the individual threats (fire, bankruptcy, etc) must be kept very low for long periods and the reanimation technology must be developed within one century, not many. While suspended you are vulnerable and even small threats may, over time, overwhelm the best of intentions. Taking the approach that 'once frozen you can wait many centuries for the technology to catch up' will almost surely fail. For…a cryonics proponent, there is an increased sense of urgency to make our cryonics organizations as stable as possible and to promote the advancement of suspension and reanimation technology."

Table 17. Estimated cost of revival from human cryopreservation in various scenarios for whole-body and neuro cases, for costly/cheap energy and manufacturing prices

Scenario	*Estimated Basic Cost of Revival*			
	Whole-Body, Costly Energy	**Neuro,* Costly Energy**	**Whole-Body, Cheap Energy†**	**Neuro,* Cheap Energy†**
Conventional Cell Repair, with whole-cell replacement and high-energy-density repair	$1,524,472	$338,061	$1,454,048	$286,930
Conventional Cell Repair	$2,174,370	$386,548	$2,103,820	$335,295
Cryogenic 3D Atomic Print	$10,643,176	$1,040,705	$1,518,445	$243,970
Cryogenic 3D Molecular Print	$15,619,585	$1,788,458	$1,614,827	$246,898
Fluidic 3D Planar Tissue Print	$15,716,600	$1,790,980	$1,711,750	$249,321
Fluidic 3D Scaffolded Tissue Print	$15,670,568	$1,790,986	$1,665,711	$249,321
Nondestructive Molecular Exchange Repair	$70,916,583	$5,020,013	$2,487,502	$271,720

* head repair only; does not include the cost of the replacement body or surgical reattachment (Chapter 6)
† assumes revival-era electricity costs are 100-fold cheaper than today ($0.001/KW-hr vs. $0.1/KW-hr)

Note that the estimates for neuro revival given in **Table 17** omit the additional costs of: (A) preparing a new replacement body that is biocompatible with, and appropriate to, the repaired neuro (head), and (B) surgically attaching the repaired replacement/original head to the new replacement body. These costs might run into the **$0.2-2 million** range (Section 6.1.4).

Table 17 shows the estimated range of raw revival costs, excluding any possible intellectual property (IP) related costs, government-imposed regulatory fees or taxes, or profitmaking by the reviving agency, as the sum of the following four classes of cost:

(A) **Computation**. This is the capital cost of fabricating the nanocomputers and nanomemory defined as [CPU mass (kg) + memory mass (kg)] x ($/kg) where the manufacturing cost per kg of nanomachinery is taken as $1000/kg at the revival-era high end to $1/kg at the revival-era low-end,[2151] plus the cost of the electricity to operate the computer hardware defined as (CPU power + memory power) x (calculation time) x ($/J) where the cost per joule of electricity ranges from 0.1 $/KW-hr as in the present-day era down to a low of 0.001 $/KW-hr in the revival era (Appendix G).

[2151] A previously published estimate for the electrical power cost of manufacturing for an entry-level first-generation nanofactory design is **$100,000/kg**.[*] However, it seems unlikely that cryonics revivals will be attempted using such primitive nanomachinery. It has been estimated that the cost of atomically-precise manufacturing using more mature later-generation nanofactories of the type that could support cryonics revivals may decline to the **$1/kg-$1000/kg** range.[†]

[*] Freitas RA Jr., Merkle RC. Kinematic Self-Replicating Machines, Landes Bioscience, Georgetown, TX, 2004; Fig. 4.42, "Physical device specifications for the Merkle-Freitas hydrocarbon molecular assembler"; http://www.molecularassembler.com/KSRM/Figures/4.42.JPG.

[†] Freitas RA Jr., Merkle RC. Kinematic Self-Replicating Machines, Landes Bioscience, Georgetown, TX, 2004; Section 6.2.2, "Demonstration of Feasibility"; http://www.MolecularAssembler.com/KSRM/6.2.2.htm. Freitas RA Jr. Economic Impact of the Personal Nanofactory. Nanotechnology Perceptions: A Review of Ultraprecision Engineering and Nanotechnology 2006 May;2:111-126; http://www.rfreitas.com/Nano/NoninflationaryPN.pdf.

(B) **Revival hardware**. This is the manufacturing and operating cost of nanorobots, taken as (# of nanorobots) x [($/kg) x (kg/nanorobot) + (watts/nanorobot) x (runtime) x ($/J)], plus the manufacturing and operating cost of other nanomachinery, taken as (mass of non-nanorobot nanomachinery) x [($/kg) + (watts/kg) x (runtime) x ($/J)].

(C) **Human labor**. This is the labor cost of the human personnel who are supervising and operating the revival nanomachinery, taken as (runtime) x ($100K/person-yr) x (5 operators).

(D) **Infrastructure**. This is the cost of the facility or clinic, including rent and utilities, where the revival procedure is conducted, which includes [($500/day rent) x (runtime)] + [($300/hr to run the MRI[2152] or alternative macroscale scanning machine) x (scanning runtime)].

Erring on the too-pessimistic side, this analysis assumes that all manufacturing costs to build the nanomachinery needed to do a single revival are borne by the recipient patient (i.e., all nanomachinery is single-use for that patient alone, and is never recycled). This artificially increases the apparent cost of revival because some or most of the nanomachinery can probably be recycled, reducing this cost.

Erring on the too-optimistic side, this analysis excludes from the direct costs to the patient any amortized share of the R&D costs needed to create the entire cryopreservation revival infrastructure. That is, we assume that some altruistic investor or organization has already built and paid for this infrastructure and is not recouping any of this expense from the patients that are revived). This artificially decreases the apparent cost of revival, because in the real world an investor would likely attempt to recapture at least some of this expense from the patient or from the organization that is responsible for the patient's revival, let alone extract a profit from the enterprise. Since there are so few cryopatients needing revival, these expenses will be amortized over a smaller customer base, increasing the allocated cost per customer. Additionally, the relatively small cryopatient population implies that significant economies of scale are unlikely.

Neither of these offsetting factors is readily quantifiable, so the present analysis simply assumes they have approximately equal impact on revival costs and essentially cancel each other out. ***Future research*** should more rigorously evaluate these factors to prepare more realistic cost estimates for cryostasis revival.

Key Technical Uncertainty. The key technical uncertainty underlying much of the molecular reconstruction approach is the speed of atom-by-atom molecular scanning (Section 5.2.1) and reconstruction (Section 5.2.3). In particular, the estimated scan rate is scaled to an assumed water molecular abstraction rate of $\mathfrak{A}_{water} \sim 10^6$ molecules/sec (Section 5.2.1.1) and a biomolecular abstraction rate of $\mathfrak{A}_{BiomolAtom} \sim 2 \times 10^6$ atoms/sec (Section 5.2.1.2), which in turn drive the assumed molecular reconstruction rate (e.g., Section 5.2.3.1). However, these $\sim 10^6$ sec^{-1} parameters represent the maximum mechanosynthetic processing rates postulated in the existing literature for mature molecular manufacturing systems operating under ideal conditions of ultra-high vacuum, cleanly-presented feedstock, and readily accessible workpieces – conditions that might not consistently apply to the body of a cryopreserved patient while it is being scanned or reconstructed. If these aggressive rates cannot be achieved and reality is perhaps ten-fold slower than optimistically assumed here, then the molecular reconstruction times estimated in **Table 16** and the costs estimated in **Table 17** might be an order of magnitude higher for all molecular reconstruction alternatives. Closer study of the scanning and reconstruction rates likely to be achieved in physically realizable molecular manufacturing systems applied to cryogenic biological workpieces is a suitable topic for ***future research***.

[2152] Yale University Magnetic Resonance Research Center, usage Charges, 1 Jul 2020; https://medicine.yale.edu/mrrc/users/charges/. Brigham and Women's Hospital, BWH Research Imaging Core Pricing, Nov 2020; https://www.brighamandwomens.org/radiology/research-imaging-core/pricing.

6. Replacement Bodies for Neuro Patients

About two-thirds of Alcor's current cryopreservation patients are "neuros". A neuro is a patient whose head (the "cephalon")[2153] has been surgically separated from the trunk of the body. While some may question the desirability of throwing away the brain's natural life support system,[2154] others have chosen this method of cryopreservation for any of several good reasons:

(1) **Cryopreservation Quality.** With current technology, it is possible to achieve a more thorough perfusion of cryoprotectant into the brain of an isolated cephalon than in a whole-body because (A) vascular access is more direct, (B) the perfusate used for isolated cephalon perfusion is less viscous and less dehydrating than the perfusate used for whole body perfusion so it can be perfused slightly faster with less toxicity accumulation, (C) pressure of draining veins is lower (zero) which reduces vessel leakage and cerebral edema, (D) venous cryoprotectant concentration can be separately monitored for each brain hemisphere, (E) arterial perfusion of brain hemispheres can be separately adjusted to compensate for asymmetric perfusion, and (F) perfusion time can be limited to what the brain requires to vitrify without over-perfusing or under-perfusing the brain because of perfusion being dictated by whole body venous cryoprotectant concentration instead of brain venous cryoprotectant concentration.[2155]

(2) **Cryopreservation Cost.** A neuro cryopreservation is 60% cheaper (e.g., $80K for neuro vs. $200K for whole-body at Alcor in 2021) and thus requires less-expensive insurance-based funding in all age categories.

(3) **Revival Speed and Cost.** A straight-frozen whole-body with lots of damage will require more effort to repair than just a cephalon with similar damage (for which a clean trunk can be grown), hence

---

[2153] **Cephalon** (from Greek *kephale*) refers to the head. **Encephalon** (from Greek *en* (in) + *kaphale*, or *enkephalos*) refers to inside the head, i.e., the brain. Thus **acephalic** means "without a head" and **anencephalic** (from Greek = *an* (not) + *enkephalos* (the brain)) means "without a brain".

[2154] The Shandong Yinfeng Life Science Research Institute, an organization that as of late 2020 had conducted 10 cryopreservation cases in China, "would only apply cryopreservation to entire bodies to keep the entire central nervous system intact. The company believes the whole body might be needed during a future resuscitation," according to Aaron Drake, Director of the Yinfeng Clinical Response Center and former Alcor Transport Coordinator. Shan Jie, Lu Yameng, Lin Xiaoyi, "China explores cryopreservation with leading technologies but doubts remain about widespread adoption of technology," Global Times, 21 Jan 2021; https://www.globaltimes.cn/page/202101/1213554.shtml.

[2155] Some cryonics researchers believe* that the *quality* case "for neuro perfusion is more qualified now. For example, the longer perfusion times for whole-body may favor stronger vitrification of the brain; the additional ingredient in the whole-body formulation may counteract ischemia/edema; the isolated neck perfusion method is more fragile and time-consuming, and without cannulating all four major vessels a patient with a compromised Circle of Willis may get compromised perfusion." Other researchers† believe the quality argument remains strong for neuro cases: "While…the magnitude of advantage is still an open question, the theoretical advantages are clear and best summarized by the simple fact that a neuro perfusion is by perfusate composition, perfusion control, and perfusion monitoring specifically focused on the brain. Properly-executed isolated cephalon perfusion is better for brain cryoprotectant perfusion for the same reason that in kidney cryopreservation experiments, the kidney is perfused as an isolated organ, not loaded with cryoprotectant by performing a whole body cryoprotectant perfusion and then removing the kidney." The *quality* argument would carry less weight in a future era where cryopreservations are fully reversible, i.e., true "suspended animation" (Section 7.1.6).

* Personal communication from Aschwin de Wolf to Robert Freitas, 21 Jul 2021.

† Personal communication from Brian Wowk to Robert Freitas, 30 Sep 2021.

neuros might hope to "get out of the dewar" quicker and cheaper, depending on the method and cost of producing the new trunk (Section 6.1).[2156]

(4) **Shipping Convenience.** In countries where there are no cryonics facilities, a practical reason for choosing neuro over full body cryopreservation is that shipping a head is simpler, quicker, and much less costly than doing so with a whole-body.[2157] Similarly, emergency evacuation from a cryonics storage facility in the event of natural disaster, legal problems,[2158] or other serious disturbance will be quicker with neuros because they are smaller and easier to handle than whole bodies.[2159]

(5) **Body Upgrade.** The replacement body to which the cephalon will be attached can be manufactured to be strong, youthful, and physically attractive.[2160]

Of course, when it comes time to revive a neuro patient their fully-repaired cephalon will require a new trunk or other artificial carrier to replace the functions of the missing body – e.g., physiological and nutrient support, communications, mobility, manipulation capabilities, and so forth. Section 6.1 describes three general approaches to this requirement – a grown biological body (Section 6.1.1), a nanofabricated biological body (Section 6.1.2), and a synthetic biological or robotic body (Section 6.1.3), along with crude estimates for the cost of each approach (Section 6.1.4). In all cases, the assumed preferred procedure is to warm a fully-repaired cryopatient cephalon to reliquidification temperature (~273 K) in full metabolic stasis, then to attach the replacement body and complete the revival process. ***Future research*** should assess the validity of this assumption by examining if there is any advantage in building an isolated

---

[2156] "In light of such wide-spread damage to the body during cryopreservation," says Alexander McLin, "it seems to me likely that future successful revival techniques will focus mainly on the brain, preferring to regrow the body instead of trying to repair cryogenic damage." Michael Darwin agrees: "The same conclusion was reached by a handful of cryonicists circa 1973-4. I was one of them. We thus decided that it was both wasteful and dangerous to haul our cryoinjured, aging and disease ravaged bodies across the decades or centuries for repair and rescue. Our solution was 'head only' cryonics (neuropreservation)." http://chronopause.com/chronopause.com/index.php/2012/02/14/the-effects-of-cryopreservation-on-the-cat-part-2/index.html#comment-3834. In 1988, Darwin described a revival scenario for a whole body patient that began by discarding the body below the neck while still at cryogenic temperature; https://www.alcor.org/library/resuscitation-a-speculative-scenario-for-recovery/.

[2157] Canatelli-Mallat M, Lascaray F, Entraigues-Abramson M, Portiansky EL, Blamaceda N, Morel GR, Goya RG. Cryopreservation of a Human Brain and Its Experimental Correlate in Rats. Rejuvenation Res. 2020 Dec;23(6):516-525; https://www.inibiolp.org.ar/Descargas/Publicaciones_Goya_PDF/CRYOPRESERVATION%20OF%20A%20HUMAN%20BRAIN%20AND%20ITS%20EXPERIMENTAL%20CORRELATE%20IN%20RATS.pdf.

[2158] Perry M. Our Finest Hours: Notes on the Dora Kent Crisis. Cryonics 1992 Sep-Oct-Nov; https://www.alcor.org/library/dora-kent-case/.

[2159] Increased portability may be viewed as a positive feature if a patient's head must be quickly hidden to thwart unlawful actions by overzealous government authorities, as in the Dora Kent case.[*] On the other hand, portability might be viewed as a flaw if the concern is theft by disgruntled employees of a cryonics organization.[†] Each cryonicist must make their own assessment of the relative importance of these risks.

[*] https://www.alcor.org/library/dora-kent-case/.

[†] https://www.the-sun.com/news/3637574/scorned-wife-raids-ex-husbands-lab/.

[2160] The neuro patient cannot know at the time of their cryopreservation what body replacement alternatives might be available at some future time of revival, so they may be given a new body that is not exactly to their liking – which they can then replace, in a second procedure, with a second body model more to their liking after reviewing the available possibilities and making a conscious choice. However, it might make more sense to be revived in one's original (repaired) body, and only then make the informed choice of a new body model with which to replace or upgrade the original – thus subjecting the patient to the psychological stress of dealing with a new body only once, instead of twice as in the former scenario. Such stress might be lessened if the new body is a genetic clone of the patient, but merely younger and healthier. In either circumstance, post-revival surgeries in the future nanomedical era should be quick and painless, requiring no lengthy period of incapacitation for "recovery" since all physical defects, including those resulting from the surgical process itself, can be simultaneously corrected by the same molecular surgical techniques.

cryogenic trunk, or if building a cryogenic replacement trunk and attaching it to a full-repaired cryogenic cephalon at cryogenic temperatures might risk additional damage to the cephalon as the recombined patient is warmed and revived. The relatively rare situation of a separately cryopreserved cephalon and trunk is briefly addressed in Section 6.2.

If the cryopreserved neuro chooses to be revived via a virtual 3D bit print, i.e., an upload (Section 5.2.3.4), the patient may require a virtual body for use in the virtual environment in which the upload resides.[2161] The design of such a replacement body is briefly discussed in Section 5.2.3.4 but is otherwise a suitable subject for ***future research***, as is a discussion of how and what to create for the virtual environment.

Whole-body patients unquestionably carry more personal information into the future than a neuro, but the significance of this extra information remains uncertain. ***Future research*** should address whether or not any significant parts of memory or personality reside outside of the cephalon. Neuro patients are assuming that there are no such parts (or that they can make do without them), but this assumption must be explicitly examined and verified in light of evidence that some extracephalonic aspects of personal identity may exist (Section 2.1.5). If extracephalonic information of value does exist, neuro patients might wish to revise their arrangements if they are concerned about whatever losses may occur.

Along these lines, O'Neal and de Wolf[2162] have presented a variation of "Merkle's Wager"[2163] that suggests whole-body cryopreservation may be the best choice for conservative cryonicists until more definitive data becomes available:

CRYONICS PAYOFF MATRIX	**Neuropreservation Is Sufficient**	**Neuropreservation Is Not Sufficient**
Neuropreservation	**Complete Survival**	**Incomplete Survival**
Whole-Body Cryopreservation	**Complete Survival**	**Complete Survival**

Brian Wowk counters that "[t]he extent to which body parts below the neck may be important to personal survival and identity is not unique to cryonics. It occurs in medicine today when body parts are lost or neurologically disconnected, especially for amputees, paraplegics, and quadriplegics, whose lives are drastically changed by their injuries, but not generally regarded as lost. Surgeon Robert White even developed the concept of whole body transplants for quadriplegics who would otherwise die from organ failure.[2164] Among many concerns about the surgery, the question of whether it would be life-saving if successful doesn't seem to be among them. Like loss of home or loss of family, loss of familiar life-long somatic attributes might be in the philosophical category of unacceptably difficult losses rather than loss of the person experiencing the pain of the loss. If loss of a body caused actual loss of the original person, then

---

[2161] For fictional treatment, see: Stephenson N. Fall; or, Dodge in Hell. William Morrow, 2019; https://en.wikipedia.org/wiki/Fall;_or,_Dodge_in_Hell. For nonfiction treatment, see: Hanson R. The Age of Em: Work, Love and Life when Robots Rule the Earth. Oxford University Press, 2016; https://en.wikipedia.org/wiki/The_Age_of_Em.

[2162] O'Neal MB, de Wolf A. The Case for Whole-Body. Cryonics 2014 Feb;35(2):16-21; https://www.alcor.org/library/case-for-whole-body/.

[2163] http://www.merkle.com/cryo/wager.html.

[2164] Lang M, Tsiang J, Moore NZ, Bain MD, Steinmetz MP. A Tribute to Dr Robert J. White. Neurosurgery. 2019 Aug 1;85(2):E366-E373; https://www.metrohealth.org/-/media/metrohealth/documents/neurosurgery/a-tribute-to-dr-robert-j-white.pdf.

the revived person would not feel loss because they would never have known anything different." That is, the revived person would perceive no loss, even if some loss had actually occurred.

Future research by neuropsychologists should also investigate whether or not the loss and subsequent replacement of one's physical body with something else might trigger heretofore relatively rare psychological conditions such as body integrity identity disorders[2165] in revived cryopreservation patients. Interestingly, even if the match and interface of the new biological body is only crude, the brain does appear to be amazingly plastic and adaptable. For instance, special eyeware equipment that completely inverts or left-right reverses vision can be adapted to in a small number of weeks, sometimes as little as 10 days.[2166]

Alcor has prepared an objective statement of the factors favoring either the neuro or whole-body cryopreservation options (Appendix N).

6.1 Fabricate and Attach Normothermic Replacement Body

The fully-repaired cephalon of a cryopreserved neuro patient must be united with a physical replacement body in order to resume its existence as a normal functioning biological human being. At least three general methods for obtaining a replacement body at normothermic[2167] temperatures have been identified:

(1) employ guided developmental processes to gestate and then grow an acephalic human body that is a genetic clone[2168] of the original patient (Section 6.1.1), to which the previously fully-repaired biological cephalon can readily be attached (Section 6.1.1.1); or similarly grow the trunk directly onto the cephalon, roughly in the manner of biological limb regeneration[2169] (Section 6.1.1.2); or simply attach the cephalon onto a donor trunk (Section 6.1.1.3).

(2) use genetic clone cells and related biological materials synthesized in a cell mill (Appendix D) to fabricate a new acephalic human body (Section 6.1.2), then attach the previously fully-repaired biological cephalon in a similar manner as before; or

---

[2165] Edwards MJ, Alonso-Canovas A, Schrag A, Bloem BR, Thompson PD, Bhatia K. Limb amputations in fixed dystonia: a form of body integrity identity disorder? Mov Disord. 2011 Jul;26(8):1410-4; https://www.ncbi.nlm.nih.gov/pmc/articles/PMC3664409/. Brugger P, Lenggenhager B. The bodily self and its disorders: neurological, psychological and social aspects. Curr Opin Neurol. 2014 Dec;27(6):644-52; https://www.zora.uzh.ch/100466/1/Brugger%20%20Lenggenhager%202014%20(ZORA).pdf. Tatu L, Bogousslavsky J. Phantom Sensations, Supernumerary Phantom Limbs and Apotemnophilia: Three Body Representation Disorders. Front Neurol Neurosci. 2018;41:14-22; https://pubmed.ncbi.nlm.nih.gov/29145179/. Gibson RB. Elective Impairment Minus Elective Disability: The Social Model of Disability and Body Integrity Identity Disorder. J Bioeth Inq. 2020 Mar;17(1):145-155; https://www.ncbi.nlm.nih.gov/pmc/articles/PMC7260267/. Garbarini F, Fossataro C, Pia L, Berti A. What pathological embodiment/disembodiment tell us about body representations. Neuropsychologia. 2020 Dec;149:107666; https://pubmed.ncbi.nlm.nih.gov/33130159/.

[2166] Marc Abrahams, "Experiments show we quickly adjust to seeing everything upside-down," The Guardian, 12 Nov 2012; https://www.theguardian.com/education/2012/nov/12/improbable-research-seeing-upside-down.

[2167] "normothermic" means "at normal human body temperature," i.e., 37 °C (310 K); https://www.merriam-webster.com/dictionary/normothermia.

[2168] In 2018 it was reported that about 70 countries had banned human cloning. https://en.wikipedia.org/wiki/Human_cloning#Current_law.

[2169] https://en.wikipedia.org/wiki/Regeneration_(biology).

(3) create a self-contained "head caddy" device that can keep the previously fully-repaired biological cephalon alive indefinitely, then attach the caddy to a robotic or other synthetic body to provide physical mobility for the cephalon (Section 6.1.3).

In those relatively rare cases[2170] where only the brain[2171] and not the skull has been cryopreserved, the replacement body must be anencephalic – including a skull but no brain – but can still be manufactured in the same manner as any one of the three methods as previously described.[2172]

6.1.1 Grown Acephalic Autologous Body

One method for making a new replacement body for a cryopreserved adult neuro is to create an acephalic (headless) autologous clone of the patient,[2173] growing it from an embryo to an adult body in a warm fluidic environment. The clone would incorporate a complete nervous system throughout the noncephalic regions of the body along with a full spinal column having enough structure to permit surgical attachment to the cryopreserved repaired cephalon of the neuro patient.

The growth process starts with the fabrication of a pre-fertilized ~100 μm diameter spherical human ovum in a cell mill (Appendix D), exhibiting the patient's original DNA code including all epigenetic modifications (to be determined by ***future research***) to ensure that the adult replacement body is an exact clone of the original body of the patient, lacking only the cephalon. The fabricated ovum is then placed

---

[2170] There were 11 **Alcor** brain-only cases as of 2021: https://www.alcor.org/library/complete-list-of-alcor-cryopreservations/case-report-a-1401/ (1993); A-1487 (1993); A-2510 (1998); https://www.alcor.org/docs/cryonics-magazine-1999-04.pdf, p. 34, "Patient B" (A-1215, 1999); A-2509 (2002); A-1194 (2002); A-2077 (2003); A-2264 (2006); https://www.alcor.org/docs/alcor-case-report-a-2699.pdf (2013); https://www.alcor.org/library/complete-list-of-alcor-cryopreservations/case-summary-a-2786/ (2014); https://www.alcor.org/complete-list-of-alcor-cryopreservations/case-summary-a-1468/ (2020). At least one brain-only case was prepared and shipped from Argentina to **Cryonics Institute** in Michigan: Canatelli-Mallat M, Lascaray F, Entraigues-Abramson M, Portiansky EL, Blamaceda N, Morel GR, Goya RG. Cryopreservation of a Human Brain and Its Experimental Correlate in Rats. Rejuvenation Res. 2020 Dec;23(6):516-525; https://www.inibiolp.org.ar/Descargas/Publicaciones_Goya_PDF/CRYOPRESERVATION%20OF%20A%20HUMAN%20BRAIN%20AND%20ITS%20EXPERIMENTAL%20CORRELATE%20IN%20RATS.pdf.

[2171] de Wolf A. The Case for Brain Cryopreservation. Cryonics 2014 Jan;35(1):5; https://www.alcor.org/docs/cryonics-magazine-2014-01.pdf. de Wolf C. Removal of the Brain for Human Cryopreservation. Cryonics 2014 Jan;35(1):6-95; https://www.alcor.org/docs/cryonics-magazine-2014-01.pdf.

[2172] Brian Wowk has observed (public email exchange, 3 May 1998) that brain preservation seems more "socially acceptable" than head preservation, yet heads are still done instead of brains because the removal process would further injure the brain. "I wouldn't trivialize the removal injury too much," writes Wowk. "The brain is not designed to exist outside of its zero-G bath of cerebrospinal fluid, and it can tear severely while being hand-held in open air. During the one brain-only case I was involved with, the corpus callosum tore on removal. I wouldn't want to be the nanotech engineer who has to figure out how to correctly match and re-attach all those millions of nerves. There are also logistical issues to be aware of. Cannulating (or sometimes even finding) blood vessels after the brain has been removed is difficult. In any reasonable brain preservation protocol, the brain would have to be perfused before removal from the body."

[2173] Shawlot W, Behringer RR. Requirement for Lim1 in head-organizer function. Nature. 1995 Mar 30;374(6521):425-30; https://www.ncbi.nlm.nih.gov/pubmed/7700351 (headless mice cloned). Shewmon DA, Capron AM, Peacock WJ, Schulman BL. The use of anencephalic infants as organ sources. A critique. JAMA. 1989 Mar 24-31;261(12):1773-81; https://www.ncbi.nlm.nih.gov/pubmed/2645454. Canadian Paediatric Society. Use of anencephalic newborns as organ donors. Paediatr Child Health. 2005 Jul;10(6):335-7; https://www.ncbi.nlm.nih.gov/pmc/articles/PMC2722973/.

inside an artificial uterus[2174] (image, right) or artificial womb[2175] in which the replacement body can be incubated from embryo to adult size. The design and operation of the artificial womb should be determined by ***future research***. Besides examining several thorny bioethical and legal issues – e.g., the acephalic clone would need to be "blind, deaf, unconscious, and unable to feel pain",[2176] and would have to be judged unworthy of legal personhood status[2177] – ***future research*** must also determine the means by which the developing embryo and fetus can be grown through all phases of tissue maturation in a strictly acephalic condition[2178] without disturbing any other growth processes such as proper spine formation, arteriovenous vascular formation, neck musculature, and the like. Bypasses for airflow, blood flow, lymph flow, and autonomic neural impulses must be mechanically or electrically provided at the neck stump by the artificial womb. Incubated acephalic clones must receive proper conditioning to avoid atrophy of the skeletal musculature and joints.

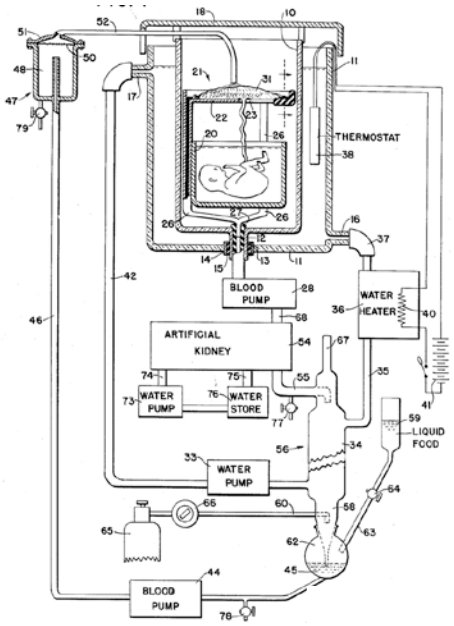

Assuming the cloned autologous ovum and the necessary incubation infrastructure are in place, how fast can an acephalic replacement human body[2179] be grown?

This question is one that should be addressed in ***future research***, but can initially be approached by considering the normal biological processes of human gestation and body growth. A single fertilized human ovum[2180] can grow from a single cell into perhaps $N_{bodycells} \sim 3.5 \times 10^{12}$ tissue cells (in the entire human body)[2181] during a gestation period of $t_{gestation} \sim 2.36 \times 10^{7}$ sec (~9 months or ~42 weeks). Assuming for computational simplicity that all cells are identical replicating cells and that each

---

[2174] Emanuel M. Greenberg. Artificial uterus. U.S Patent 2,723,660, 15 Nov 1955; https://patents.google.com/patent/US2723660A/en.

[2175] https://en.wikipedia.org/wiki/Artificial_womb. See also: https://en.wikipedia.org/wiki/Ectogenesis.

[2176] Anencephaly Information Page, National Institute of Neurological Disorders and Stroke, 27 Mar 2019; https://www.ninds.nih.gov/disorders/all-disorders/anencephaly-information-page.

[2177] Davis A. The status of anencephalic babies: should their bodies be used as donor banks? J Med Ethics 1988;14:150-153; https://jme.bmj.com/content/medethics/14/3/150.full.pdf. Gilman SJ. The use of anencephalic infants as an organ source: an on-going question. Elon Law Review 2012;4:71-92; https://www.elon.edu/u/law/wp-content/uploads/sites/996/2019/07/Elon_Law_Review_V4_No1_Gilman.pdf.

[2178] For a variety of medical and ethical reasons, it seems unlikely that growing an intact whole human body, from embryo to induced-comatose neonate or full adult, followed by decapitation and disposal of the never-conscious cloned cephalon, would ever be legally approved.

[2179] The discussion in this Section presumes that the cryopreserved patient was a full adult at the time of cryopreservation. If the neuro patient was pre-adult, then the cloned replacement body should match the age and physiological maturity of the cephalon. Similarly, a cryopreserved patient whose body differed significantly from the standard 70 kg might be provided a new body of the appropriate weight and size.

[2180] https://en.wikipedia.org/wiki/Egg_cell#Mammals_including_humans.

[2181] Freitas RA Jr. Nanomedicine, Volume I: Basic Capabilities, Landes Bioscience, Georgetown TX, 1999, Section 8.5.1, "Cytometrics"; http://www.nanomedicine.com/NMI/8.5.1.htm#p5.

new cell later splits with generational synchronicity into two daughter cells from ovum to birth, then there would be $\delta_{gestation} \sim \log_2(N_{bodycells} / 1\ ovum) = 41.7$ cell population doublings or generations in 9 months, giving an average cell doubling time of $\tau_{ovum} \sim t_{gestation} / \delta_{gestation} \sim 5.66 \times 10^5$ sec (~6.55 days or about **1 week**) over the entire course of the gestation.

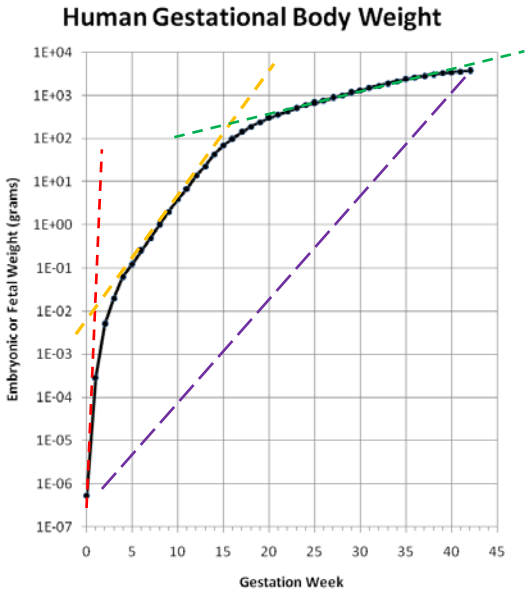

However, cell doubling time is not constant throughout gestation but rather starts out very fast and finishes very slow (see chart, left).[2182] Following fertilization, a single-cell human ovum of mass $m_{ovum} \sim 5.4 \times 10^{-10}$ kg[2183] splits into 2 cells after 30 hours, into 4 cells after another 15 hours, and into 16 cells after another 27 hours.[2184] After another 48 hours there are 70-100 cells, called a blastocyst, and the cells are dividing every 12-24 hours.[2185] The doubling rate of the embryo slows as the embryo becomes a fetus by the end of week 8, clocking in at $\tau_{8\text{-}14weeks} \sim 1$ week per doubling from week 8-14, the end of the first trimester. By the last week of gestation in week 42, body mass is only growing at $r_{42weeks} \sim$ 2.4%/week, a doubling time of ~29 weeks. Over the entire gestation period, the average doubling time is $\tau_{AvgGestDoubling} = t_{gestation} / \log_2(m_{neonatal} / m_{ovum}) \sim 722{,}000$ sec ~ 8.36 days, an average +71%/week rate (purple trendline in chart, above).

There are at least four theoretical scenarios if cell metabolism could be controlled and was the primary restrictive factor:

(1) **Normal Maturation Growth Rate.** Starting from a single fertilized ovum, it typically takes $t_{gestation} \sim 9$ months to grow to a neonatal weight of $m_{neonatal} = 3.685$ kg at birth (**purple** trendline),[2186] plus another $t_{postnatal} \sim 20$ years to reach 100% of male adult weight of $m_{body} \sim 70$ kg.[2187] (The normal human male reaches ~50% of full adult weight after 11 years, and ~75% of adult weight after ~14.4 years of growth after birth.[2188]) Relying only on unaltered natural biological maturation processes, a 70 kg acephalic adult male body could in principle be grown in $t_{gestation} + t_{postnatal} \sim 20.75$ years or ~**249 months**.

(2) **Neonatal Growth Rate** (**green** trendline in chart, above). If the $r_{24weeks} \sim 13.1\%$/week growth rate[2189] exhibited by a replacement body at the normal birth time 42 weeks after fertilization could somehow be induced to continue unabated at the same rate after week 42, then a 70 kg acephalic adult male

---

[2182] https://www.babycenter.com/pregnancy/your-body/growth-chart-fetal-length-and-weight-week-by-week_1290794.

[2183] Alternatively, the roughly spherical human ovum* measures $d_{ovum} \sim 100$ μm in diameter,† a volume of $V_{ovum} \sim (4\pi/3)(d_{ovum}/2)^3 = 5.24 \times 10^{-13}$ m^3; assuming a mean ovum density of $\rho_{ovum} \sim 1030$ kg/m^3, the mass of the ovum is $m_{ovum} \sim \rho_{ovum} V_{ovum} \sim 5.4 \times 10^{-10}$ kg.
* https://en.wikipedia.org/wiki/Egg_cell#Mammals_including_humans.
† "Eggs", in: Alberts B, Johnson A, Lewis J, Raff M, Roberts K, Walter P, eds. Molecular Biology of the Cell, 4th edition, Garland Science, New York, 2002; https://www.ncbi.nlm.nih.gov/books/NBK26842/.

[2184] https://web.archive.org/web/20200122235657/https://medlineplus.gov/ency/anatomyvideos/000025.htm.
[2185] https://www.sdfertility.com/blog/what-is-the-difference-between-a-day-3-and-a-day-5-embryo-transfer#.
[2186] https://www.babycenter.com/pregnancy/your-body/growth-chart-fetal-length-and-weight-week-by-week_1290794.
[2187] https://www.disabled-world.com/calculators-charts/height-weight-teens.php.
[2188] https://www.disabled-world.com/calculators-charts/height-weight-teens.php.

[2189] 190 gm in wk 18, 3685 gm in wk 42, 24 wks; $x = [\log_{10}(3685/190)]/24$; $r_{24weeks} \sim (100)[(10^x)-1] = 13.1\%$/week.

body could be grown in $t_{gestation} + \log(m_{body}/m_{neonatal}) / \log(1+r_{24weeks})$ = 65.9 weeks (i.e., ~1.3 years or ~**15 months**).

(3) **First Trimester Growth Rate** (**orange** trendline in chart, above). If we could induce the early fetal doubling time of $\tau_{trimester1}$ ~ 1 week (~100%/week) to continue after week 14 (the end of the first trimester, when fetal mass has reached $m_{14weeks}$ = 43 grams), then we could grow a 70 kg acephalic adult male body in $t_{gestation} + \tau_{trimester1} \log_2(m_{body}/m_{14weeks})$ = 24.7 weeks (i.e., ~0.48 years or ~**6 months**).

(4) **Embryonic Growth Rate** (**red** trendline in chart, above). If we could force the fertilized ovum to continuously replicate at its fastest $\tau_{embryonic}$ ~ 18 hour (12-24 hour) doubling rate all the way up to full adult mass, then we could grow a 70 kg acephalic adult male body in $\tau_{embryonic} \log_2(m_{body}/m_{ovum})$ ~ 2.39 x 10^6 sec (i.e., ~28 days or ~**1 month**).

Achieving the greatly reduced fabrication times described in the above scenarios (2), (3), and (4) will require alteration of the normal biological processes governing human body gestation and maturation.[2190] It is certainly possible to imagine interventions in cell biology that might force cell proliferation cycles to maintain the fastest possible pace.

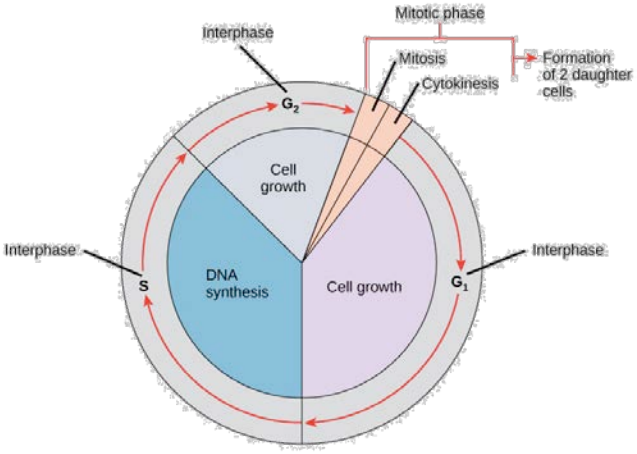

The standard cell cycle for adult proliferating cells includes four rigidly-controlled and sequentially-executed phases (image, right)[2191] which include: entry G1 phase (cell expands in size), S phase (DNA synthesis), G2 phase (resting), and final brief M phase (mitosis or cell division, only ~4% of total cycle duration). Cells not currently replicating are said to be in a quiescent G0 phase; cells may exit M phase into either G0 (to cease proliferating) or G1 (to resume proliferating). In adult organisms, many cell types (e.g., parenchymal cells of the liver and kidney, and glial (brain), retina, muscle (heart), and fibroblast cells) enter the G0 phase semi-permanently and can only be induced to resume dividing under very specific circumstances, while a few other cell types (e.g., bone marrow, epithelial cells, oral/intestinal mucosa, hair follicles) continue to divide throughout an organism's lifetime. The fraction of proliferating cells in a target organ or tissue varies greatly according to cytotype. For example, the observed growth fraction (the proportion of actively proliferating cells in G1/S/G2/M phase as a percentage of all viable cells of a given cytotype) is 0.4% for brain glial cells,[2192] 7.6% for oral mucosa,[2193] 9.8% for peripheral blood stem cells,[2194] 10-20%

[2190] The youngest Alcor cryopreservation patient at ~3 years old* and other non-adult patients would probably require a non-adult replacement trunk to be grown (or fabricated; Section 6.1.2), significantly reducing the maturation time and cost (Section 6.1.4) if they are neuro patients.
* https://www.thesun.co.uk/news/12673989/hope-frozen-netflix-cryogenically-froze-daughter-brain-einz-naovaratpong/

[2191] https://www.khanacademy.org/science/ap-biology/cell-communication-and-cell-cycle/cell-cycle/a/cell-cycle-phases.

[2192] Korr H, Schultze B, Maurer W. Autoradiographic investigations of glial proliferation in the brain of adult mice. II. Cycle time and mode of proliferation of neuroglia and endothelial cells. J Comp Neurol. 1975 Apr 15;160(4):477-90; https://pubmed.ncbi.nlm.nih.gov/1123464/.

[2193] Cox SC, Walker DM. Epithelial growth fraction and expression of p53 tumour suppressor gene in oral submucous fibrosis. Aust Dent J. 1996 Apr;41(2):91-96; https://europepmc.org/article/med/8670041.

for liver hepatocytes,[2195] 17.8% for bladder,[2196] ~40% for skin epidermis,[2197] and 44% for gut epithelium.[2198] Uninterrupted cell growth might be encouraged by (A) suppressing entry into G0,[2199] (B) reactivating quiescent cells,[2200] or (C) promoting the transition from G0 to G1[2201] thus forcing cells to proceed more rapidly from M phase to G1. Many promoters of cell proliferation are known,[2202] though

---

[2194] Takatoku M, Sellers S, Agricola BA, Metzger ME, Kato I, Donahue RE, Dunbar CE. Avoidance of stimulation improves engraftment of cultured and retrovirally transduced hematopoietic cells in primates. J Clin Invest. 2001 Aug;108(3):447-55; https://www.ncbi.nlm.nih.gov/pmc/articles/PMC209360/.

[2195] Post J, Huang CY, Hoffman J. The replication time and pattern of the liver cell in the growing rat. J Cell Biol. 1963 Jul;18(1):1-12; https://www.ncbi.nlm.nih.gov/pmc/articles/PMC2106283/.

[2196] Tsujihashi H, Nakanishi A, Matsuda H, Uejima S, Kurita T. Growth fraction of human bladder tumors. Urol Res. 1991;19(4):215-8; https://pubmed.ncbi.nlm.nih.gov/1926655/.

[2197] Heenen M, Galand P. The growth fraction of normal human epidermis. Dermatology. 1997;194(4):313-7; https://pubmed.ncbi.nlm.nih.gov/9252749/.

[2198] Przemioslo R, Wright NA, Elia G, Ciclitira PJ. Analysis of crypt cell proliferation in coeliac disease using MI-B1 antibody shows an increase in growth fraction. Gut. 1995 Jan;36(1):22-7; https://gut.bmj.com/content/gutjnl/36/1/22.full.pdf.

[2199] Rivard N, L'Allemain G, Bartek J, Pouysségur J. Abrogation of p27Kip1 by cDNA antisense suppresses quiescence (G0 state) in fibroblasts. J Biol Chem. 1996 Aug 2;271(31):18337-41; https://www.sciencedirect.com/science/article/pii/S0021925818319860. Weinberger M, Mesquita A, Caroll T, Marks L, Yang H, Zhang Z, Ludovico P, Burhans WC. Growth signaling promotes chronological aging in budding yeast by inducing superoxide anions that inhibit quiescence. Aging (Albany NY). 2010 Oct;2(10):709-26; https://www.ncbi.nlm.nih.gov/pmc/articles/PMC2993800/.

[2200] Tian Z, Zhao Q, Biswas S, Deng W. Methods of reactivation and reprogramming of neural stem cells for neural repair. Methods. 2018 Jan 15;133:3-20; https://pubmed.ncbi.nlm.nih.gov/28864354/.

[2201] Kimura I, Honda R, Okai H, Okabe M. Vascular endothelial growth factor promotes cell-cycle transition from G0 to G1 phase in subcultured endothelial cells of diabetic rat thoracic aorta. Jpn J Pharmacol. 2000 May;83(1):47-55; https://pubmed.ncbi.nlm.nih.gov/10887940/. Lataillade JJ, Clay D, Bourin P, Hérodin F, Dupuy C, Jasmin C, Le Bousse-Kerdilès MC. Stromal cell-derived factor 1 regulates primitive hematopoiesis by suppressing apoptosis and by promoting G(0)/G(1) transition in CD34(+) cells: evidence for an autocrine/paracrine mechanism. Blood. 2002 Feb 15;99(4):1117-29; https://pubmed.ncbi.nlm.nih.gov/11830456/. Ren S, Rollins BJ. Cyclin C/cdk3 promotes Rb-dependent G0 exit. Cell. 2004 Apr 16;117(2):239-51; https://pubmed.ncbi.nlm.nih.gov/15084261/. Li M, Zhou X, Mei J, Geng X, Zhou Y, Zhang W, Xu C. Study on the activity of the signaling pathways regulating hepatocytes from G0 phase into G1 phase during rat liver regeneration. Cell Mol Biol Lett. 2014 Jun;19(2):181-200; https://cmbl.biomedcentral.com/track/pdf/10.2478/s11658-014-0188-2?site=cmbl.biomedcentral.com. Matson JP, Cook JG. Cell cycle proliferation decisions: the impact of single cell analyses. FEBS J. 2017 Feb;284(3):362-375; https://www.ncbi.nlm.nih.gov/pmc/articles/PMC5296213/.

[2202] Li J, Zhang Z, Xiong L, Guo C, Jiang T, Zeng L, Li G, Wang J. SNHG1 lncRNA negatively regulates miR-199a-3p to enhance CDK7 expression and promote cell proliferation in prostate cancer. Biochem Biophys Res Commun. 2017 May 20;487(1):146-152; https://pubmed.ncbi.nlm.nih.gov/28400279/. Wakida T, Ikura M, Kuriya K, Ito S, Shiroiwa Y, Habu T, Kawamoto T, Okumura K, Ikura T, Furuya K. The CDK-PLK1 axis targets the DNA damage checkpoint sensor protein RAD9 to promote cell proliferation and tolerance to genotoxic stress. Elife. 2017 Dec 19;6:e29953; https://www.ncbi.nlm.nih.gov/pmc/articles/PMC5736350/. Xie S, Ge Q, Wang X, Sun X, Kang Y. Long non-coding RNA ZFAS1 sponges miR-484 to promote cell proliferation and invasion in colorectal cancer. Cell Cycle. 2018;17(2):154-161; https://www.ncbi.nlm.nih.gov/pmc/articles/PMC5884120/. Huang J, Ding Z, Luo Q, Xu W. Cancer cell-derived exosomes promote cell proliferation and inhibit cell apoptosis of both normal lung fibroblasts and non-small cell lung cancer cell through delivering alpha-smooth muscle actin. Am J Transl Res. 2019 Mar 15;11(3):1711-1723; https://www.ncbi.nlm.nih.gov/pmc/articles/pmid/30972195/. Liu BW, Wang TJ, Li LL, Zhang L, Liu YX, Feng JY, Wu Y, Xu FF, Zhang QS, Bao MZ, Zhang WY, Ye LH. Oncoprotein HBXIP induces PKM2 via transcription factor E2F1 to promote cell proliferation in ER-positive breast cancer. Acta Pharmacol Sin. 2019 Apr;40(4):530-538; https://www.ncbi.nlm.nih.gov/pmc/articles/PMC6462016/. Lyu Q, Jin L, Yang X, Zhang F. LncRNA MINCR activates Wnt/β-catenin signals to promote cell proliferation and migration in oral squamous cell carcinoma. Pathol Res Pract. 2019 May;215(5):924-930; https://pubmed.ncbi.nlm.nih.gov/30777615/.

almost always in the context of pathological cancer. ***Future research*** should investigate other possible means of accelerating the cell growth cycle.[2203]

However, there is evidence that the slowing of growth with increasing cell count during gestation is not driven primarily by restrictive cell biology but rather is a response to the logistics of nutrient supply, energy conservation between growth and maintenance tasks, and other systemic scaling issues. In particular, allometric scaling laws in biology[2204] suggest that replication time in biological systems follows a 1/4-power law function of replicator mass. This was confirmed by the author's study[2205] of biological replication time (τ_{repl}, in sec) as a function of replicator mass (M_{repl}, in kg) for biological replicators ranging in size from viruses, mitochondria and single-celled bacteria to protozoan and metazoan organisms including insects, birds, mammals and trees, which found that $\tau_{repl} \sim 1.78 \times 10^7 \ M_{repl}^{1/4}$ = **1.6 years** for M_{repl} = 70 kg. A similar $M^{1/4}$ law apparently also applies to exponential tumor growth rates.[2206] ***Future research*** should investigate these and other systemic scaling restrictions that may limit the maximum rate of biological growth of human replacement trunks.

Systemic scaling restrictions might be partially overcome using nanorobot-assisted biological growth. ***Future research*** should evaluate the feasibility of using a fleet of coordinated mobile shepherd nanorobots[2207] (Section 5.2.3.3.1) to more quickly reconfigure developing neural tendrils and axons, capillary networks, muscle and extracellular matrix fibers, and similar biological structures at a greater speed than natural motility processes normally allow. For example, the leading cells that extend capillary networks during angiogenesis have been observed to move through tissue at a speed of 0.2 ± 0.08 µm/min.[2208] Similarly, the filopodia-like processes of microglia cells extend and retract at 1-4 µm/min,

---

[2203] Kalejta RF, Shenk T. The human cytomegalovirus UL82 gene product (pp71) accelerates progression through the G1 phase of the cell cycle. J Virol. 2003 Mar;77(6):3451-9; https://www.ncbi.nlm.nih.gov/pmc/articles/PMC149542/. Huang DM, Hsiao JK, Chen YC, Chien LY, Yao M, Chen YK, Ko BS, Hsu SC, Tai LA, Cheng HY, Wang SW, Yang CS, Chen YC. The promotion of human mesenchymal stem cell proliferation by superparamagnetic iron oxide nanoparticles. Biomaterials. 2009 Aug;30(22):3645-51; https://pubmed.ncbi.nlm.nih.gov/19359036/. Wang Y, Qiu H, Hu W, Li S, Yu J. RPRD1B promotes tumor growth by accelerating the cell cycle in endometrial cancer. Oncol Rep. 2014 Mar;31(3):1389-95; https://pdfs.semanticscholar.org/80ee/cf577778b41d3b717f7afb917e55c544153a.pdf. Zhang L, Kang W, Lu X, Ma S, Dong L, Zou B. LncRNA CASC11 promoted gastric cancer cell proliferation, migration and invasion *in vitro* by regulating cell cycle pathway. Cell Cycle. 2018;17(15):1886-1900; https://www.ncbi.nlm.nih.gov/pmc/articles/PMC6152531/. Wang Q, He G, Hou M, Chen L, Chen S, Xu A, Fu Y. Cell Cycle Regulation by Alternative Polyadenylation of CCND1. Sci Rep. 2018 May 1;8(1):6824; https://www.ncbi.nlm.nih.gov/pmc/articles/PMC5931507/.

[2204] West GB, Brown JH, Enquist BJ. A general model for the origin of allometric scaling laws in biology. Science 1997 Apr 4;276(5309):122-126; http://citeseerx.ist.psu.edu/viewdoc/download?doi=10.1.1.205.3919&rep=rep1&type=pdf. West GB, Brown JH, Enquist BJ. The fourth dimension of life, fractal geometry, and allometric scaling of organisms. Science 1999 Jun 4;284(5420):1677-1679; http://citeseerx.ist.psu.edu/viewdoc/download?doi=10.1.1.590.3306&rep=rep1&type=pdf. West GB, Woodruff WH, Brown JH. Allometric scaling of metabolic rate from molecules and mitochondria to cells and mammals. Proc Natl Acad Sci. (USA) 2002 Feb 19;99(Suppl 1):2473-2478; https://www.pnas.org/content/pnas/99/suppl_1/2473.full.pdf.

[2205] Freitas RA Jr., Merkle RC. Kinematic Self-Replicating Machines, Landes Bioscience, Georgetown, TX, 2004; Section 5.2, "Replicator Time vs. Replicator Mass"; http://www.molecularassembler.com/KSRM/5.2.htm; Fig. 5.6, "The ¼-power law for replication time as a function of replicator mass"; http://www.molecularassembler.com/KSRM/Figures/5.6.JPG; and Appendix A, "Data for Replication Time and Replicator Mass"; http://www.molecularassembler.com/KSRM/AppA.htm.

[2206] Crean D, Jones E. Mathematical Models for Cancer Growth. 26 May 2011; https://chemoth.com/tumorgrowth.

[2207] Freitas RA Jr. The Alzheimer Protocols: A Nanorobotic Cure for Alzheimer's Disease and Related Neurodegenerative Conditions. IMM Report No. 48, June 2016, 433 pp; Section 5.3.2.3, "Cell Insertion and Emplacement," pp. 327-332; http://www.imm.org/Reports/rep048.pdf.

[2208] Farrukh A, Paez JI, delCampo A. 4D Biomaterials for Light-Guided Angiogenesis. Adv Funct Mater. 2018 Dec 17;29(6); https://onlinelibrary.wiley.com/doi/abs/10.1002/adfm.201807734.

while the cell bodies themselves move through tissue at only 0.02-0.03 µm/min.[2209] Natural biological gestational and maturation processes thus involve physical movement of microstructures through tissue at velocities ranging from **0.0003-0.07 µm/sec**. By comparison, shepherd nanorobots could easily tow neurons, axonal processes, or endothelial cells (building capillaries during vascular network construction) through tissue at a transit speed of at least **~1 µm/sec**,[2210] and tissue transit velocities up to ~100 µm/sec may be mechanically plausible and biocompatible.[2211] The activities of ~10^{12} nanorobots each burning ~100 pW of average power will collectively release only ~100 watts of additional waste heat. Nanorobots may eliminate at least some bottlenecks to maintaining faster growth by providing the ability to transport developing biological structures through tissue to their ultimate destinations at up to 1000-fold higher velocities than is available in purely natural systems.

Excess waste heat generation could be an additional constraint on the maximum rate of biological growth that should also be studied in ***future research***. The typically high metabolic rate of embryos is ~7 times greater than the maintenance rate and embryo growth typically costs $E_{embgrowth}$ ~ 1.2 MJ/kg,[2212] so maintaining the fastest embryonic growth rate ($\tau_{embryonic}$ ~ 64,800 sec/doubling) on a whole-body basis could generate significant incremental waste heat. For example, the last doubling of mass from m_{n-1} = 35 kg up to m_n = 70 kg) would add ($m_n - m_{n-1}$) ($E_{embgrowth}$) / ($\tau_{embryonic}$) ~ 648 watts of waste heat, more than 6 times the normal ~100 watt basal metabolic rate of an adult human body. Slowing the growth rate to that prevailing at the end of the first trimester (i.e., $\tau_{trimester1}$ ~ 1 week/doubling) could reduce waste heat generation to a more manageable ~100 watts, consistent with a ~**6 month** grow time for a 70 kg acephalic adult male human body.

We close this Section with a brief discussion of several possible approaches for the reunification of the biological body, including attaching the fully-repaired cephalon to a grown trunk (Section 6.1.1.1), growing the replacement trunk directly onto the repaired cephalon (Section 6.1.1.2), and attaching the repaired cephalon to a donor body (Section 6.1.1.3).

6.1.1.1 Cephalon Attached to Grown Trunk

Once the growth process is complete, the previously fully-repaired cephalon must be surgically attached to the new replacement acephalic human body. Conventionally, this might involve a surgical procedure akin to transplantation (the installation in a human body of an entire organ that was taken from another body)[2213] or replantation (the process of reattaching completely amputated or severed limbs or other body parts),[2214] typically making use of the techniques of microsurgery.[2215] Such surgeries traditionally cannot restore full function especially for large well-innervated body parts, of which the human head is probably the most difficult scenario.

[2209] Nimmerjahn A, Kirchhoff F, Helmchen F. Resting microglial cells are highly dynamic surveillants of brain parenchyma *in vivo*. Science. 2005 May 27;308(5726):1314-8; http://www.sciencemag.org/content/308/5726/1314.long.

[2210] Freitas RA Jr. The Alzheimer Protocols: A Nanorobotic Cure for Alzheimer's Disease and Related Neurodegenerative Conditions. IMM Report No. 48, June 2016, 433 pp; Section 5.3.2.3, "Cell Insertion and Emplacement," pp. 327-332; http://www.imm.org/Reports/rep048.pdf.

[2211] Freitas RA Jr. Nanomedicine, Volume I: Basic Capabilities, Landes Bioscience, Georgetown TX, 1999, Section 9.4.4.2, "ECM Brachiation"; http://www.nanomedicine.com/NMI/9.4.4.2.htm.

[2212] Vleck CM, Vleck D. Patterns of Metabolism and Growth in Avian Embryos. Amer Zoologist 1980 May;20(2):405-416; https://academic.oup.com/icb/article-pdf/20/2/405/6095790/20-2-405.pdf.

[2213] https://en.wikipedia.org/wiki/Organ_transplantation.
[2214] https://en.wikipedia.org/wiki/Replantation.
[2215] https://en.wikipedia.org/wiki/Microsurgery.

Surgical experimentation on head transplants[2216] (as distinct from brain transplants[2217]), involving the grafting of one organism's head onto the body of another, began in 1908 with the first attempt to transplant the head of one **dog** onto the body of another by Alexis Carrel and Charles Guthrie. The grafted head showed some reflexes but deteriorated quickly and was killed after a few hours.[2218]

In the mid-1950s, Vladimir Demikhov grafted a **dog**'s head and upper body onto the body of another (image, right),[2219] with an emphasis on providing blood supply to the donor head and not on grafting the nervous systems. One dog survived 29 days, with the transplanted head able to move and react to stimulus. Sano *et al.*[2220] also surgically produced a two-headed dog in 1964.

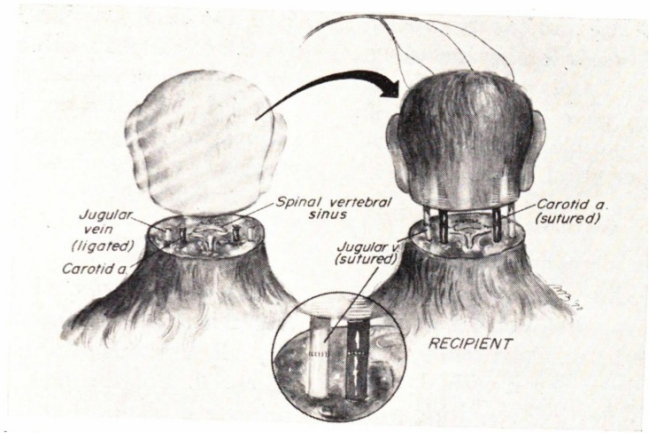

In 1970, Robert White performed the first cephalic exchange transplantation in a **primate** (image, left),[2221] employing direct suture of the carotid and jugular veins along with cervical laminectomy at the fourth through sixth cervical vertebrae, with partially successful results: "Three to four hours after surgery, each cephalon was able to chew, swallow food, track with eyes, and bite if orally stimulated. Moreover, through EEG monitoring, White demonstrated that these cephalons exhibited a characteristic awake pattern."[2222] White's experimental animals survived 6-36 hours.

[2216] https://en.wikipedia.org/wiki/Head_transplant.

[2217] https://en.wikipedia.org/wiki/Brain_transplant. See also: https://en.wikipedia.org/wiki/Spock's_Brain and https://en.wikipedia.org/wiki/The_Gamesters_of_Triskelion.

[2218] Lamba N, Holsgrove D, Broekman ML. The history of head transplantation: a review. Acta Neurochir (Wien). 2016 Dec;158(12):2239-2247; https://www.ncbi.nlm.nih.gov/pmc/articles/PMC5116034/.

[2219] Konstantinov IE. At the cutting edge of the impossible: a tribute to Vladimir P. Demikhov. Texas Hear Inst J. 2009;36(5):453-458; https://www.ncbi.nlm.nih.gov/pmc/articles/PMC2763473/. See also: Demikhov VP. Experimental Transplantation of Vital Organs. Consultant's Bureau Enterprises, Inc., 227 W 17th St, New York NY 10011, 1962, pp. 138-170; translated from the Russian by Basil Haigh.

[2220] Sano K, Terao H, Hayakawa I, Kamano S, Saito I. Experimental transplantation of the head – two headed dog. Neurol Med Chir (Tokyo). 1964;6:35-8; https://www.jstage.jst.go.jp/article/nmc1959/6/0/6_0_35/_article/-char/ja/.

[2221] White RJ, Wolin LR, Massopust LC Jr, Taslitz N, Verdura J. Primate cephalic transplantation: neurogenic separation, vascular association. Transplant Proc. 1971 Mar;3(1):602-4; https://pubmed.ncbi.nlm.nih.gov/4999463/. White RJ, Wolin LR, Massopust LC Jr, Taslitz N, Verdura J. Cephalic exchange transplantation in the monkey. Surgery. 1971 Jul;70(1):135-9; https://www.surgjournal.com/article/0039-6060(71)90099-7/fulltext. Lang M, Tsiang J, Moore NZ, Bain MD, Steinmetz MP. A Tribute to Dr Robert J. White. Neurosurgery. 2019 Aug 1;85(2):E366-E373; https://www.google.com/url?sa=i&url=https%3A%2F%2Fwww.metrohealth.org%2F-%2Fmedia%2Fmetrohealth%2Fdocuments%2Fneurosurgery%2Fa-tribute-to-dr-robert-j-white.pdf&psig=AOvVaw1Knq0VoV4Km78VuA3U9GqJ&ust=1617219570450000&source=images&cd=vfe&ved=0CAkQjhxqFwoTCPj57ark2O8CFQAAAAAdAAAAABAD. See also a video of White at: https://www.youtube.com/watch?v=8On7rktFZME.

In 2015, Xiao-Ping Ren grafted the head of one **mouse** onto the body of another using updated techniques (image, right).[2223] Ren's methods minimized trauma to the recipient, prevented development of ischemia, and allowed for intact brain function (with EEG recordings demonstrating normal brain activity), with over half the animals surviving >24 hours and the longest surviving 6 months.

Following Sergio Canavero's 2013 proposal for the first **human** head transplantation procedure,[2224] in 2017 Ren and Canavero successfully performed a cephalosomatic anastomosis procedure (a connection made surgically between adjacent blood vessels) using a human cadaver.[2225] In a 2017 interview earlier that year,[2226] Canavero embarrassingly claimed (without any foundation or connection to Alcor) that he planned to awaken patients frozen by the Alcor Life Extension Foundation: "We will try to bring the first of the company's patients back to life, not in 100 years. As soon as the first human head transplant has taken place, i.e., no later than 2018, we will be able to attempt to reawaken the first frozen head," said Canavero. "We are currently planning the world's first brain transplant, and I consider it realistic that we will be ready in three years at the latest." However, as of 2021 no successful head transplant had yet been performed on a live human subject,[2227] and the legal and ethical issues of body-head transplants were under active discussion (and controversy).[2228]

Far more advanced nanosurgical techniques and instrumentalities will be available by the time of the first cryonics revivals. In that future era, one possible reattachment protocol would start with a grown genetically-autologous acephalic replacement body prepared as described in Section 6.1.1. A vasculoid appliance (Section 4.6) would be installed throughout the vasculature of this warm replacement body, with appropriate interfaces to macroscale mechanical shunts for gases, liquids, and nerve impulses at the neck.

[2222] Lamba N, Holsgrove D, Broekman ML. The history of head transplantation: a review. Acta Neurochir (Wien). 2016 Dec;158(12):2239-2247; https://www.ncbi.nlm.nih.gov/pmc/articles/PMC5116034/.

[2223] Ren XP, Ye YJ, Li PW, Shen ZL, Han KC, Song Y. Head Transplantation in Mouse Model. CNS Neurosci Ther. 2015 Aug;21(8):615-8; https://www.ncbi.nlm.nih.gov/pmc/articles/PMC6495971/.

[2224] Canavero S. HEAVEN: The head anastomosis venture Project outline for the first human head transplantation with spinal linkage (GEMINI). Surg Neurol Int. 2013 Jun 13;4(Suppl 1):S335-42; https://www.ncbi.nlm.nih.gov/pmc/articles/PMC3821155/. Ren XP. The Age of Head Transplants. CNS Neurosci Ther. 2016 Apr;22(4):257-9; https://www.ncbi.nlm.nih.gov/pmc/articles/PMC6492870/.

[2225] Ren X, Li M, Zhao X, Liu Z, Ren S, Zhang Y, Zhang S, Canavero S. First cephalosomatic anastomosis in a human model. Surg Neurol Int. 2017 Nov 17;8:276; https://www.ncbi.nlm.nih.gov/pmc/articles/PMC5705925/.

[2226] Knapton S. Cryogenically frozen brains will be 'woken up' and transplanted in donor bodies within three years, says surgeon. The Telegraph, 27 Apr 2017; https://www.msn.com/en-in/news/techandscience/cryogenically-frozen-brains-will-be-woken-up-and-transplanted-in-donor-bodies-within-three-years-says-surgeon/ar-BBAr2O1.

[2227] Gkasdaris G, Birbilis T. First Human Head Transplantation: Surgically Challenging, Ethically Controversial and Historically Tempting – an Experimental Endeavor or a Scientific Landmark? Maedica (Bucur). 2019 Mar;14(1):5-11; https://www.ncbi.nlm.nih.gov/pmc/articles/PMC6511668/.

[2228] Furr A, Hardy MA, Barret JP, Barker JH. Surgical, ethical, and psychosocial considerations in human head transplantation. Int J Surg. 2017 May;41:190-195; https://www.ncbi.nlm.nih.gov/pmc/articles/PMC5490488. Ausman JI. Is it time to perform the first human head transplant? Comment on the CSA (CephaloSomatic Ansatomisis) paper by Ren, Canavero, and colleagues. Surg Neurol Int. 2018 Feb 13;9:28; https://www.ncbi.nlm.nih.gov/pmc/articles/PMC5820846/. Suskin ZD, Giordano JJ. Body-to-head transplant; a "caputal" crime? Examining the corpus of ethical and legal issues. Philos Ethics Humanit Med. 2018 Jul 13;13(1):10; https://www.ncbi.nlm.nih.gov/pmc/articles/PMC6045868/.

The vasculoid would then perform molecular extraction (Section 4.10) on the replacement body, placing it in a condition of comprehensive metabolic stasis as the body is simultaneously cooled to 273 K (0 °C) while maintaining a reliquidified state. Circulation and nerve conduction through the shunts are then terminated and the shunts are detached and removed as the vasculoid seals off all open vessels, muscle and nerve fibers, along with other exposed biological surfaces at the neck of the replacement body.

A second vasculoid appliance (Section 4.6) is installed throughout the vasculature of the fully-repaired but also non-metabolic cephalon of the cryopreserved neuro patient. The cephalon (whose temperature has now been raised to 273 K (0 °C) and is in the reliquidified state) and the replacement body are brought into physical proximity, allowing the two vasculoid systems to establish a single continuous vascular transport system using void-spanning components (Section 4.6.3) that keep exposed nonvascular biological surfaces a short distance apart. The opposing biological surfaces on head and body are slowly drawn together, using millimanipulators (Section 5.2.3.3.1) operated like segmentation nanomanipulators (Section 5.2.1.3) in reverse or using shepherd nanorobots (Section 5.2.3.3.2) employing manufactured cells and other biomaterials to align and adhere the two surfaces. The void-spanning components of the vasculoid are slowly retracted as the two biological surfaces properly mate. Any neural tissue mismatches between cephalon and trunk are identified, repaired, and resolved by cell repair nanorobots (Section 4.12.4).

With physical unification successfully accomplished, the revival process is completed by (A) patient warmup to 310 K (37 °C) and molecular instillation (Section 4.13), (B) vasculoid uninstallation and blood substitution (Section 4.14), and (C) patient wakeup (Section 4.15).

6.1.1.2 Trunk Grown onto Cephalon

Rather than growing an acephalic trunk and then attaching the repaired cephalon, many potential technical, ethical and legal difficulties might be eliminated if the trunk can be grown directly onto the fully-repaired normothermic cephalon.[2229] As proposed by Darwin[2230] in 1988 (Section 2.2.8): "The patient – an exposed pearly white brain floating within the womb of the revival unit – is now ready for the final phase of the revival process. On the surface of his brain a single cell begins to divide. Unlike the cancer which threatened the patient's life, the division of this cell is orderly and planned to restore life. A layer of dividing cells covers the restored but unconscious brain. The cells begin to differentiate, and slowly, like a newly conceived child, a body begins to take shape within the revival unit….Just a little over a year from the start of the revival procedure, the patient awakens in his hospital bed."

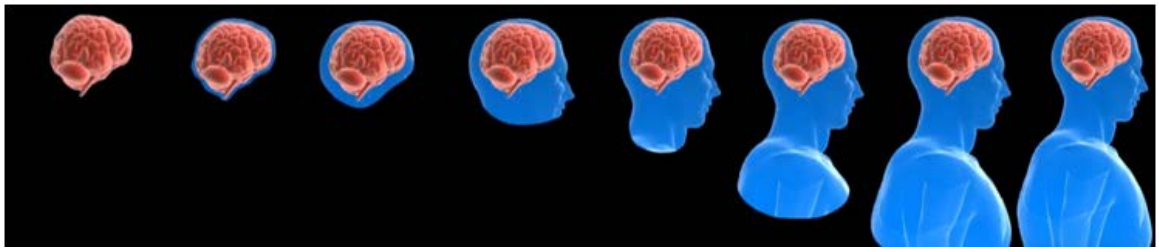

[2229] By 2021, scientists had induced optic cups (the structures that grow into the globe of the eye during embryonic development) to grow onto the side of small bits of brain tissue in organoids. Gabriel E, Albanna W, Pasquini G, *et al*. Human brain organoids assemble functionally integrated bilateral optic vesicles. bioRxiv; 2021; https://www.biorxiv.org/content/biorxiv/early/2021/03/30/2021.03.30.437506.full.pdf. See also https://www.eurekalert.org/news-releases/925127.

[2230] Darwin M. Resuscitation: A Speculative Scenario for Recovery. Cryonics 1988 Jul;9(7):33-37; https://www.alcor.org/library/resuscitation-a-speculative-scenario-for-recovery/.

Growing a replacement body around a repaired brain in less than year will require cells to maintain an ultrafast ~100%/week first-trimester growth rate (Section 6.1.1(3)), a rate that normally only prevails for ~10 weeks during natural human gestation, to progress from first cell to fully mature adult trunk in ~8.5 months.[2231] ***Future research*** as described in Section 6.1.1 should examine the feasibility of such high growth rates of body trunk mass and, if possible, estimate the maximum limits to macroscale biological growth rates.

According to a neuropreservation FAQ at Alcor:[2232] "In the future medicine will learn to master growth and development programs[2233] within the human body. Cells will be reprogrammed to heal severed spinal cords, regrow lost limbs, and even regenerate new organs. This kind of tissue regeneration already occurs naturally in children that lose fingertips, and in organs such as the liver. Extending these regenerative capabilities will be a matter of uncovering old programs that may still be dormant in our genes, and eventually writing new programs. In cases of severe injury, it is possible to imagine placing patients in a fluid support environment in which blood is artificially circulated to maintain life until vital organs are regenerated and all injuries healed. Such a healing process could theoretically start with just a brain. Programming a brain to regrow a new body may seem incredible, but nature already does things that are even more incredible. The body you have right now is the product of a growth program that started from a single cell."

As noted by Brian Wowk in a 2006 lecture:[2234] "According to the laws of physics, and principles of biology, there is no reason why it would not be possible to program cells on the surface of just even a brain, or even just one cell on the surface of a brain, to initiate a growth process that would eventually regrow a whole body around just a brain, if that's all that was able to be recovered from a victim of trauma. In case this seems fantastic, let me remind everyone that generation of whole bodies starting from a single cell is a technology already demonstrated in nature. This is not molecular nanotechnology. This is not anything exotic. The generation [and] production of tissue and organs is the normal business of biology that living things have been doing for hundreds of millions of years. It is just a matter of us learning to steer these processes in the direction of therapy and not just reproduction."

6.1.1.3 Cephalon Attached to Donor Trunk

Another alternative to growing an acephalic replacement trunk would be to acquire an adult donor trunk to which the fully-repaired cephalon could be attached. A donor trunk might appear to have several important advantages:

(1) **immediacy** (since the cryopreserved patient would not need to wait for time-consuming biological growth processes to slowly gestate and maturate an adult replacement body);

(2) **lower cost** (see below) than a grown (Section 6.1.1.1) or fabricated (Section 6.1.2) body trunk; and

(3) **surgical convenience**.

[2231] (~1 week/doubling)($\log_2$[(70,000 gm adult)/(5.4 x 10^{-7} gm embryo)]) ~ 36.9 weeks = 8.5 months.

[2232] https://www.alcor.org/library/neuropreservation-faq/#toggle-id-9.
[2233] https://web.archive.org/web/20030622221746/www.chrcrm.org/medal03.htm.
[2234] https://www.youtube.com/watch?v=kTo2MIacnM4&t=725s.

Body brokers[2235] in the U.S. commonly provide whole cadavers to medical schools and body farms[2236] for $3000-$10,000, though these specimens are not "fresh" but have suffered long periods of warm ischemic damage and have usually been thoroughly embalmed with formaldehyde. The retail price for a plastinated cadaver can run as much as $200,000.[2237] None of these sources provides a suitable trunk for a fully-repaired cephalon. One informal source[2238] estimated that the average market price of a fresh human dead body could be as much as **$550,000**, which is the sum of the independent value of the individual organs and other components. This price seems high, and confidential sources report that organizations exist which can provide "warm cadavers" immediately upon pronouncement of death on an as-available basis at a considerably lower cost.

However, donor trunks have numerous potential disadvantages, including:

(1) **serious damage** – bodies are normally donated after death,[2239] which means that any donor trunk to which the repaired cephalon must be attached will exhibit some pathological medical condition or physical trauma that was sufficiently serious to kill the donor (though probably correctable[2240] using nanorobotic medical techniques likely to be available in the future cryonics revival era);

(2) **increasing scarcity** – the advent of advanced nanorobotic medicine in the future cryonics revival era will leave fewer deaths due to natural medical causes or accidents, and the alleged higher pedagogical quality[2241] of computerized virtual dissection programs may reduce demand,[2242] causing the supply of medical cadavers to greatly diminish[2243] and the price of fresh cadavers to rise significantly;

(3) **biological incompatibility** – the need to resolve physiological and biochemical incompatibilities between the cephalon and the donor body, e.g., positions and sizes of nerves and blood vessels won't precisely match at the neck interface, proteins may lack histocompatibility requiring

---

[2235] Brian Grow, John Shiffman. "In the U.S. market for human bodies, almost anyone can dissect and sell the dead". Reuters, 24 Oct 2017; https://www.reuters.com/investigates/special-report/usa-bodies-brokers/.

[2236] https://en.wikipedia.org/wiki/Body_farm.
[2237] http://marketdesigner.blogspot.com/2013/03/cadavers-for-anatomy-classes.html.

[2238] Trace Dominguez, Tara Long, Laci Green. How much are your body parts worth? Seeker, 18 Aug 2014; https://www.seeker.com/how-much-are-your-body-parts-worth-1792475763.html.

[2239] https://en.wikipedia.org/wiki/Body_donation.

[2240] Lethal cancers or blocked blood vessels can be cleared from the body using microbivore-class nanorobots; blood clots in the brain causing lethal stroke will be eliminated when the injured cephalon is surgically detached from the otherwise healthy donor body; and physical trauma and the sequelae of aging can be corrected by various nanorobotic means.[*]
[*] Freitas RA Jr. Chapter 23. Comprehensive Nanorobotic Control of Human Morbidity and Aging. In: Fahy GM, West MD, Coles LS, Harris SB, eds, The Future of Aging: Pathways to Human Life Extension, Springer, New York, 2010, pp. 685-805; http://www.nanomedicine.com/Papers/Aging.pdf.

[2241] Gholipour B. Med School without cadavers? Sci Am. 2019 Oct;321(4):12-15; https://www.scientificamerican.com/article/med-school-without-cadavers/.

[2242] Simpson JS. An economical approach to teaching cadaver anatomy: A 10-year retrospective. Amer Biol Teacher 2014 Jan;76(1):42-46; https://online.ucpress.edu/abt/article/76/1/42/18626/An-Economical-Approach-to-Teaching-Cadaver. For example, Sectra virtual dissection tables cost $70,000 each; https://www.nationalgeographic.com/science/2018/12/digital-cadavers-are-replacing-real-ones-but-should-they-future-medicine/.

[2243] "The federal government does not monitor whole-body donations in the United States, but researchers estimate each year fewer than 20,000 Americans donate their bodies to medical research and training." https://www.nationalgeographic.com/news/2016/07/body-donation-cadavers-anatomy-medical-education/.

immunosuppression,[2244] or significant genetic differences may exist, though all these issues are probably correctable[2245] using nanorobotic medical techniques likely to be available in the future cryonics revival era;

(4) **identity conflicts** – possible psychological body-image conflicts that could affect personal identity, e.g., cephalon and donated trunk are of different race,[2246] gender,[2247] somatotype,[2248] body shape,[2249] or physical fitness,[2250] though all these issues are probably correctable[2251] using nanorobotic medical techniques likely to be available in the future cryonics revival era;

(5) **social problems** – possible social, privacy, or legal conflicts, e.g., between the patient and the family of the donor body analogous to the "reunion" issue in childhood adoption,[2252] or the unintended encouragement of illegal body harvesting by unscrupulous entrepreneurs if the potential financial gains for perpetrators are high enough;[2253] and

(6) **ethical problems** – the perception that saving the life of a cryonics patient requires the loss of someone else's life.

Given these many disadvantages, the Donor Trunk option is only included for completeness. The biological and nanomedical technology level necessary for recovering a brain or cephalon from a cryopreserved state would make possible much more elegant, healthy, biocompatible, and identity-compatible body replacement solutions than using a body from a different person.

6.1.2 Nanofabricated Acephalic Autologous Body

Rather than growing a replacement body in the conventional biological manner, a new acephalic body could be 3D printed[2254] from genetically autologous cells and biological materials fabricated in a cell mill

---

[2244] https://en.wikipedia.org/wiki/Immunosuppression.

[2245] Mismatched blood vessels can be topologically connected to each side using temporary vasculoid scaffolding that is then coated with new vascular endothelium manufactured in a cell mill; mismatched nerves can be rebuilt and reconnected using shepherd nanorobots to add neural connector cells fabricated in cell mills; genetic incompatibilities can be corrected by applying appropriate chromosome replacement therapy to all necessary cells in the trunk, using chromallocytes.

[2246] https://en.wikipedia.org/wiki/Race_(human_categorization).
[2247] https://en.wikipedia.org/wiki/Gender.
[2248] https://en.wikipedia.org/wiki/Somatotype_and_constitutional_psychology.
[2249] https://en.wikipedia.org/wiki/Body_shape.
[2250] https://en.wikipedia.org/wiki/Physical_fitness.

[2251] Chromallocytes can perform chromosome replacement therapy to reset all trunk cell genomes to a cephalon-matched race or gender; cosmetic nanorobots can remove fat deposits, and cell repair nanorobots can enlarge existing muscle cells or add new muscle cells fabricated in a cell mill.

[2252] https://en.wikipedia.org/wiki/Adoption#Reform_and_reunion_trends.
[2253] https://en.wikipedia.org/wiki/Burke_and_Hare_murders.

[2254] Juliet Childers. How Close are we to 3D Printing Bodies? Edgy, 14 Mar 2018; https://edgy.app/how-close-3d-printing-bodies. Caroline Haskins. 'Marie' Is the First Life-Sized, 3D-Printed Human Body. Motherboard Tech by Vice, 14 Dec 2018; https://www.vice.com/en_us/article/yw7kzv/marie-is-the-first-life-sized-3d-printed-human-body.

(Appendix D), possibly incorporating relatively primitive techniques borrowed from conventional tissue engineering,[2255] organ printing,[2256] or the manufacture of artificial tissues from synthetic cells.[2257]

The target body plan can be predicted by DNA phenotyping[2258] using genetic information available in the cryopreserved patient's genome (Section D.1.2.1), combined with dimensional measurements of the patient's head/body, knowledge of the patient's age and medical history, and nonmedical data such as old photographs, videos, or body scans for artistic or commemorative purposes, and possibly even functional specifications.[2259] This creates a target structure that can be converted to at least a cellular-resolution construction plan.

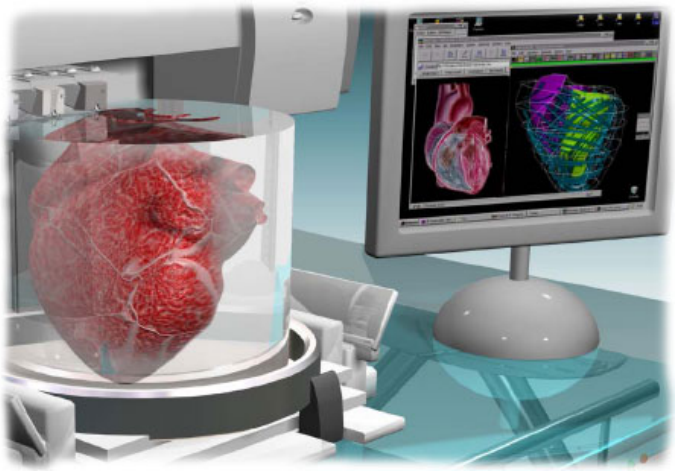

The now-well-defined target body structure can then be fabricated using either planar tissue printing[2260] (image, right; Section 5.2.3.3.1) or scaffolded tissue printing (Section 5.2.3.3.2) as previously described, with a likely print time on the order of ~**2 months**. The result is a new acephalic replacement trunk paused in metabolic stasis at 273 K (0 °C), ready for transplantation.

The nanofabricated acephalic replacement body and the fully-repaired cephalon are then combined and processed through patient wakeup as previously described in Section 6.1.1.1.

6.1.3 Head Caddy or Biocompatible Artificial Body

A third alternative is to host the fully-repaired cephalon of the cryopreserved neuro patient in a fully synthetic body or device. Such a machine could be fabricated from any desired combination of organic and inorganic materials, with the constraint that it must provide full life support functionality to keep the biological head alive and in physical control of the body indefinitely (assuming adequate energy and material resupply, and with proper maintenance).[2261]

[2255] https://en.wikipedia.org/wiki/Tissue_engineering.
[2256] https://en.wikipedia.org/wiki/Organ_printing.

[2257] Galanti A, Tortolero RM, Azad R, Cross S, Davis S, Gobbo P. A Floating Mould Technique for the Programmed Assembly of Protocells into Protocellular Materials Capable of Non-Equilibrium Biochemical Sensing. ChemRxiv; 2020 Nov 30; https://chemrxiv.org/ndownloader/articles/13373837/versions/1

[2258] https://en.wikipedia.org/wiki/DNA_phenotyping.

[2259] Kriegman S, Blackiston D, Levin M, Bongard J. A scalable pipeline for designing reconfigurable organisms. Proc Natl Acad Sci U S A. 2020 Jan 28;117(4):1853-1859; https://www.ncbi.nlm.nih.gov/pmc/articles/PMC6994979/.

[2260] https://en.wikipedia.org/wiki/Applications_of_3D_printing#Bio-printing.

[2261] LaRocco J, Li P, Ren X. Surgical evaluation of a full-body prosthetic. Ann Proc IEEE EMBS 2017; https://www.researchgate.net/profile/John_Larocco/publication/321485197_Surgical_Evaluation_of_a_Full-Body_Prosthetic/links/5a2468e40f7e9b71dd073e33/Surgical-Evaluation-of-a-Full-Body-Prosthetic.pdf.

A U.S. patent was actually issued for a primitive version of such a device (images, below) to inventor Chet Fleming in 1987.[2262] From the description in the patent:

> "This invention involves a device, referred to herein as a "cabinet," which provides physical and biochemical support for an animal's head which has been "discorporated" (i.e., severed from its body). This device can be used to supply a discorped head with oxygenated blood and nutrients, by means of tubes connected to arteries which pass through the neck. After circulating through the head, the deoxygenated blood returns to the cabinet by means of cannulae which are connected to veins that emerge from the neck. A series of processing components removes carbon dioxide and adds oxygen to the blood. If desired, waste products and other metabolites may be removed from the blood, and nutrients, therapeutic or experimental drugs, anti-coagulants, and other substances may be added to the blood. The replenished blood is returned to the discorped head via cannulae attached to arteries. The cabinet provides physical support for the head, by means of a collar around the neck, pins attached to one or more vertebrae, or similar mechanical means….it is possible that after this invention has been thoroughly tested on research animals, it might also be used on humans suffering from various terminal illnesses."

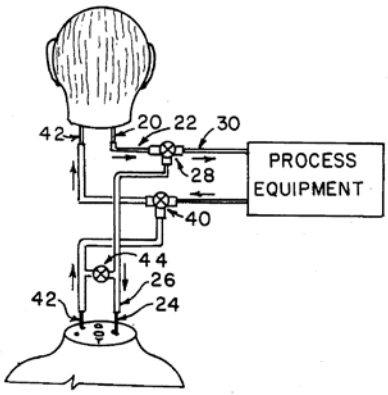

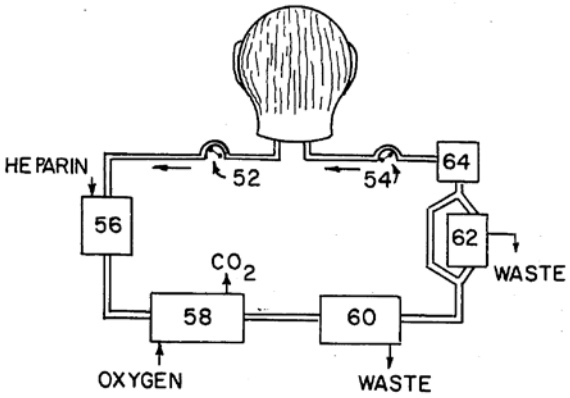

This concept of a "head caddy" has been only lightly explored in science fiction, ranging from the simplistic "head in a pan" concept[2263] to the more sophisticated "head on a robot body" concept exemplified by the crimefighter Robocop[2264] (image, far left) and the Star Trek Borg Queen[2265] (image, left). The first mention of the head caddy concept in science fiction may have occurred in 1931.[2266]

[2262] Chet Fleming. Device for Perfusing an Animal Head. U.S. Patent 4666425A, 19 May 1987; https://patents.google.com/patent/US4666425A/en. See also: Chet Fleming, If We Can Keep a Severed Head Alive, Polinym Press, 1988; https://www.amazon.ca/Keep-Severed-Alive-Discorporation-Patent/dp/0942287029.

[2263] https://en.wikipedia.org/wiki/The_Brain_That_Wouldn%27t_Die.

[2264] https://robotsupremacy.fandom.com/wiki/RoboCop_(2014); "community content is available under CC-BY-SA" (https://creativecommons.org/licenses/by-nc-sa/3.0/).

[2265] Image from http://www.tomspinadesigns.com/; http://www.tomspinadesigns.com/restoration/science-fiction-props/borg-queen-costume-restoration-display/.

[2266] "Bring him into my laboratory. I shall remove his brain and stimulate the cells into activity once more. We shall give him life again, transplanting his brain into the head of one of our machines." Neil Ronald Jones. The Jameson Satellite. Amazing Stories, Jul 1931; http://www.gutenberg.org/files/26906/26906-h/26906-h.htm.

No experiment has yet succeeded in maintaining a human brain, or parts of a human brain, alive after the death of the rest of the body, although isolated guinea pig brains have been kept alive, showing reaction to electrical stimuli, for ~8 hours using the apparatus shown below.[2267] Extracellular field potentials have been recorded from excised mouse brains up to 24 hours post-extraction,[2268] and isolated zebrafish brains have retained functionality for up to 7 days.[2269] A machine built using present-day technology that could supply all of the biomedical functions needed to keep a biological human brain or cephalon alive (e.g. providing blood flow, blood oxygenation, and nutrition)[2270] would likely be far larger than a human body – probably on the order of several cubic meters. However, the results of past scaling studies[2271] suggest that nanorobotic replacements for biological systems might be 1-3 orders of magnitude smaller in size while retaining similar functionality. A synthetic nanorobotic head caddy built using cryonics-revival-era atomically precise manufacturing can probably be far more compact, perhaps just a few liters in volume, estimated as follows:

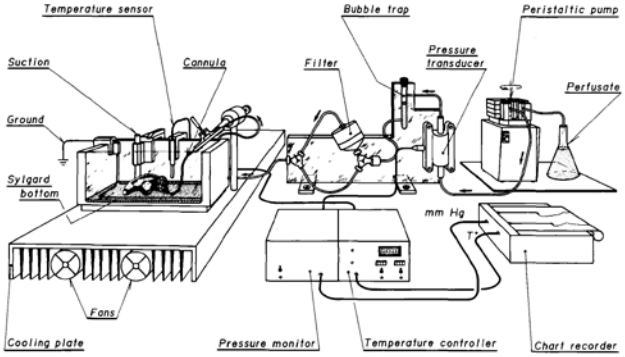

A simple scaling analysis of the head caddy starts with the observation that the P_{brain} ~ **20 watt** human brain has a basal metabolic energy density of (20 watts / 1400 cm^3) ~ 14,000 watts/m^3, eight times larger than the

[2267] Mühlethaler M, de Curtis M, Walton K, Llinás R. The isolated and perfused brain of the guinea-pig *in vitro*. Eur J Neurosci. 1993 Jul 1;5(7):915-26; https://pubmed.ncbi.nlm.nih.gov/8281302/. See also: Vrselja Z, Daniele SG, Silbereis J, Talpo F, Morozov YM, Sousa AMM, Tanaka BS, Skarica M, Pletikos M, Kaur N, Zhuang ZW, Liu Z, Alkawadri R, Sinusas AJ, Latham SR, Waxman SG, Sestan N. Restoration of brain circulation and cellular functions hours post-mortem. Nature. 2019 Apr;568(7752):336-343; https://www.ncbi.nlm.nih.gov/pmc/articles/pmid/30996318/.

[2268] von Bohlen und Halbach O. The isolated mammalian brain: an *in vivo* preparation suitable for pathway tracing. Eur J Neurosci. 1999 Mar;11(3):1096-1100; https://pubmed.ncbi.nlm.nih.gov/10103102/.

[2269] Tomizawa K, Kunieda J, Nakayasu H. *Ex vivo* culture of isolated zebrafish whole brain. J Neurosci Methods. 2001 May 30;107(1-2):31-8; https://pubmed.ncbi.nlm.nih.gov/11389939/.

[2270] Vrselja Z, Daniele SG, Silbereis J, Talpo F, Morozov YM, Sousa AMM, Tanaka BS, Skarica M, Pletikos M, Kaur N, Zhuang ZW, Liu Z, Alkawadri R, Sinusas AJ, Latham SR, Waxman SG, Sestan N. Restoration of brain circulation and cellular functions hours post-mortem. Nature. 2019 Apr;568(7752):336-343; https://www.ncbi.nlm.nih.gov/pmc/articles/PMC6844189/. See also: Regalado A. Researchers are keeping pig brains alive outside the body. MIT Technol Rev. 25 Apr 2018; https://www.technologyreview.com/2018/04/25/240742/researchers-are-keeping-pig-brains-alive-outside-the-body/. Shaer M. Scientists Are Giving Dead Brains New Life. What Could Go Wrong? The New York Times Mag. 2 Jul 2019; https://www.nytimes.com/2019/07/02/magazine/dead-pig-brains-reanimation.html.

[2271] Freitas RA Jr. Exploratory design in medical nanotechnology: a mechanical artificial red cell. Artif Cells Blood Substit Immobil Biotechnol. 1998 Jul;26(4):411-30; https://web.archive.org/web/20100420085137/http://www.foresight.org/Nanomedicine/Respirocytes.html. Freitas RA Jr. Clottocytes: Artificial Mechanical Platelets. Foresight Update 2000 Jun 30;41:9-11; https://web.archive.org/web/20060212200540/http://www.imm.org/Reports/Rep018.html. Freitas RA Jr. Microbivores: Artificial Mechanical Phagocytes using Digest and Discharge Protocol. J. Evol. Technol. 2005 Apr;14:55-106; http://www.jetpress.org/volume14/freitas.pdf.

(100 watts / 0.06 cm^3) ~ 1700 watts/m^3 energy density of the human body at its ~100 watt basal metabolic rate, hence energy and nutrient supply are the likely limiting resources. **Table 18** below gives the estimated molecular material requirements to keep an isolated biological cephalon alive, assuming that a supply of (20 watts/100 watts) = 20% of whole-body basal-activity material requirements will suffice for an isolated head ($m_{headreqs}$ ~ 9.5 x 10^{-6} kg/sec; **Table 18**). Nonmetabolic water is from skin loss (e.g., perspiration) on the cephalon, here conservatively assumed to be ~20% of the minimum whole-body rate of ~2 x 10^{20} molecules/sec.[2272]

A vasculoid appliance installed in the vasculature of the brain and other biological tissues in the cephalon would have a mass of up to M_{vasc} ~ 0.4 kg, a volume of up to V_{vasc} ~ 240 cm^3, and a power draw of P_{vasc} = **20 watts** assuming up to 20% of a whole-body vasculoid installation (**Table 5** in Section 4.6.1) and ~20% of whole-body vasculoid power[2273] at the basal metabolic level. This appliance-related mass, volume, and heat production resides entirely within the cephalon, providing sufficient nutrient transport capacity in place of the blood and lymph fluid flows that would otherwise be present.

Table 18. Maximum molecular nutrient transport requirements for an isolated biological cephalon, estimated as 20% of whole-body requirement[2274]

Molecular Component	Whole-Body Requirement (kg/sec)	Isolated Cephalon Requirement (kg/sec)
Glucose (metabolic)[2275]	9.6 x 10^{-6}	1.9 x 10^{-6}
Water (metabolic)	6.0 x 10^{-6}	1.2 x 10^{-6}
Water (nonmetabolic)	6.0 x 10^{-6}	1.2 x 10^{-6}
Carbon dioxide (metabolic)	1.4 x 10^{-5}	2.8 x 10^{-6}
Oxygen (metabolic)	1.1 x 10^{-5}	2.1 x 10^{-6}
Plasma proteins	8.1 x 10^{-7}	1.6 x 10^{-7}
Lipids	6.9 x 10^{-7}	1.4 x 10^{-7}
Other molecules	1.9 x 10^{-7}	3.8 x 10^{-8}
TOTAL	---	*9.5 x 10^{-6}*

The head caddy in which the cephalon is installed must supply (or remove) all of the materials listed in **Table 18** that are being transported by the vasculoid appliance. The plasma proteins, lipids, and other molecules can be fabricated from molecular feedstock using Fab Modules (Section D.1.1.2) similar to those employed in the cell mill (Appendix D). Fab Modules of mass M_{FM} = 2 x 10^{-18} kg, volume V_{FM} = 10^{-21} m^3,

---

[2272] Freitas RA Jr., Phoenix CJ. Vasculoid: A personal nanomedical appliance to replace human blood. J Evol Technol. 2002 Apr;11:1-139; Section 2.1.2 "Water"; http://www.jetpress.org/volume11/vasculoid.pdf.

[2273] Freitas RA Jr., Phoenix CJ. Vasculoid: A personal nanomedical appliance to replace human blood. J Evol Technol. 2002 Apr;11:1-139; Section 2.6 "Appliance Power Requirement"; http://www.jetpress.org/volume11/vasculoid.pdf.

[2274] Freitas RA Jr., Phoenix CJ. Vasculoid: A personal nanomedical appliance to replace human blood. J Evol Technol. 2002 Apr;11:1-139; Section 2.1 "Molecular Transport"; http://www.jetpress.org/volume11/vasculoid.pdf.

[2275] Whole body: [(100 watts) (0.180 kg/mole)] / [(65% efficiency) (4.77 x 10^{-18} J/glucose molecule) (6.022 x 10^{23} molecules/mole)] = 9.6 x 10^{-6} kg/sec glucose requirement for whole body at 100 watt basal rate. Cephalon: (20%) (9.6 x 10^{-6} kg/sec) = 1.9 x 10^{-6} kg/sec.

and power draw P_{FM} = 0.094 pW can manufacture R_{FM} = 7.6 x 10^{-21} kg/Module-sec of simple ~100 dalton organic molecules, which we will conservatively down-rate 10-fold to $R_{FMcaddy}$ ~ 7.6 x 10^{-22} kg/Module-sec to accommodate the production of ~1000 dalton essential-nutrient organic molecules. The synthesis of $m_{caddymols}$ = 3.38 x 10^{-7} kg/sec of plasma proteins, lipids, and other molecules thus requires N_{FMmols} = $m_{caddymols}$ / $R_{FMcaddy}$ = 4.4 x 10^{14} down-rated Fab Modules of total mass M_{FMmols} = N_{FMmols} M_{FM} = 0.0009 kg, volume V_{FMmols} = N_{FMmols} V_{FM} = 0.4 cm^3 and power draw P_{FMmols} = N_{FMmols} P_{FM} = **42 watts**. The feedstock for the Fab Modules is provided by Decomposition Modules of similar design, size, and power draw as the Fab Modules, doubling the aforementioned Fab Module estimate. Decomposition Modules recycle organic waste molecules transported out of the cephalon by breaking down waste molecules into the simplest molecular precursors suitable for use as feedstock for the Fab Modules using externally supplied energy.

The other four critical components can be provided almost entirely from internal recycling within the head caddy. From **Table 18**, the net result of metabolic energy processing is that $m_{oxyglucose}$ = 4 x 10^{-6} kg/sec of glucose and oxygen molecules are converted to an equal mass of waste carbon dioxide and water molecules with the production of useful biochemical energy. The resulting carbon dioxide and water can be mechanochemically recombined back into glucose and oxygen using externally supplied power according to $C_6H_{12}O_6 + 6O_2 \leftrightarrow 6CO_2 + 6H_2O$ + 2870 KJ/mole (4.77 x 10^{-18} J/glucose molecule) using $N_{FMoxyglucose}$ = $m_{oxyglucose}$ / R_{FM} = 5.3 x 10^{14} Fab Modules of total mass $M_{FMoxyglucose}$ = $N_{FMoxyglucose}$ M_{FM} = 0.001 kg, volume $V_{FMoxyglucose}$ = $N_{FMoxyglucose}$ V_{FM} = 0.5 cm^3 and a power draw of $P_{FMoxyglucose}$ = $N_{FMoxyglucose}$ P_{FM} = **50 watts**.

Nonmetabolic water losses ($m_{nonmetwater}$ = 1.2 x 10^{-6} kg/sec, $n_{watermolecules}$ = 4 x 10^{19} molecules/sec) through the exposed skin of the cephalon can be extracted from ambient air having a typical 0.5% water content by weight[2276] using $N_{waterrotors}$ = $n_{watermolecules}$ / $n_{waterrotors}$ = 4 x 10^{14} molecular sorting rotors (each V_{rotor} ~ 1372 nm^3/rotor, M_{rotor} ~ 2 x 10^{-21} kg/rotor, E_{rotor} ~ 20 zJ/molecule)[2277] with H_2O binding sites importing $n_{waterrotors}$ ~ 10^5 water molecules/rotor-sec, for a total sorting rotor mass of $M_{waterrotors}$ = M_{rotor} $N_{waterrotors}$ = 8 x 10^{-7} kg, volume $V_{waterrotors}$ = V_{rotor} $N_{waterrotors}$ = 5 x 10^{-10} m^3, and power draw $P_{waterrotors}$ = $n_{waterrotors}$ E_{rotor} $N_{waterrotors}$ = **0.8 watts**.

Prudence would dictate having at least one day's reserve inventory of all nutrients onboard the head caddy, amounting to $M_{storage}$ ~ $m_{headreqs}$ t_{day} ~ 0.82 kg or $V_{storage}$ ~ $M_{storage}$ / ρ_{water} ~ 0.82 liter of storage, for t_{day} = 86,400 sec/day. Additional masses can be included to account for inefficiencies, leaks, and wastage, but should not materially affect the above caddy mass and volume counts. ***Future research*** should evaluate the possible need for a supply of migratory or special-purpose biological cells (e.g., neutrophils, macrophages, lymphocytes, stem cells) to the fully-repaired brain or its surrounding tissues. If needed, such cells can be provided from internal stores periodically restocked from external cell mill production, onboard biological cell cloning facilities, or functionally-equivalent nanorobotic replacement devices. If the cephalon retains the vocal cords, a compressed-air handling system could be included to allow normal vocalization, but is really unnecessary because a voice can be perfectly synthesized electronically through a speaker on the caddy, with emitted sounds precisely matched to the lip and throat movements of the attached cephalon.

Finally, a self-contained caddy would need a refrigerator unit to remove the $P_{caddyactive}$ = P_{brain} + P_{vasc} + 2P_{FMmols} + $P_{FMoxyglucose}$ + $P_{waterrotors}$ ~ 175 watts of waste heat. Even assuming a relatively poor COP[2278] of

---

[2276] https://www.engineeringtoolbox.com/water-vapor-air-d_854.html.

[2277] Freitas RA Jr. Nanomedicine, Volume I: Basic Capabilities, Landes Bioscience, Georgetown, TX, 1999; Section 3.4.2, "Sorting Rotors"; http://www.nanomedicine.com/NMI/9.3.1.2.htm.

[2278] The coefficient of performance (COP) of a refrigerator is COP = Q/W, where Q = heat removed by the refrigerator and W = energy (work) required to operate the refrigerator; https://en.wikipedia.org/wiki/Coefficient_of_performance#Equation.

~2.75, typical of inefficient domestic refrigerators,[2279] the power requirement to operate the refrigerator is only $P_{caddyfridge} = P_{caddyactive} / COP \sim 65$ watts, giving a total power draw of $P_{caddy} = P_{caddyactive} + P_{caddyfridge} \sim 240$ watts for the head caddy including the refrigerator. Refrigerant fluid (e.g., hydrofluorocarbon or tetrafluoroethane) ranging from 30-185 gm or 0.1-0.2 liter in volume,[2280] circulating in condenser coils of typical total surface area ~0.1 m^2,[2281] can probably be packed into a $V_{caddyfridge} \sim 1$ liter refrigerator volume of mass $M_{caddyfridge} \sim 1$ kg, with the waste heat power $P_{caddyactive}$ carried off by pushing $V_{caddywater} = P_{caddyactive} / (C_{Vwater} \Delta T_{water}) = 2.5$ cm^3/sec of ice cold water past the refrigerator coils, taking heat capacity $C_{Vwater} = 1.93 \times 10^6$ J/m^3-K with an input-output coolant temperature differential of $\Delta T_{water} = 310$ K (human body temperature) – 273 K (ice water) = 37 K. The $P_{caddy} \sim$ **240 watt** head caddy has a total mass of $M_{caddy} \sim M_{vasc} + 2M_{FMmols} + M_{FMoxyglucose} + M_{waterrotors} + M_{storage} + M_{caddyfridge} \sim$ **2.22 kg** and a volume of $V_{caddy} \sim V_{vasc} + 2V_{FMmols} + V_{FMoxyglucose} + V_{waterrotors} + V_{storage} + V_{caddyfridge} \sim$ **2.06 liters**. The only external connections would be a supply hose carrying ice cold water to the caddy, a flush hose carrying body temperature water out of the caddy, and a power cord connecting the appliance to a battery, fuel cell, or electrical wall socket, all of which could in principle be replaced by additional onboard systems[2282] at the cost of a bit more mass and volume.

An isolated cephalon ensconced in a head caddy would retain all five primary senses of sight, hearing, taste, smell, and touch, and as previously noted can also retain the ability to speak. However, the lack of independent mobility would be disconcerting to many, a deficit that is readily cured by attaching the caddy-mounted cephalon to an appropriate robot body carrier (image, left)[2283] that could include arms, legs, or any other mechanical features desired by the patient. Neuroprosthetic[2284] signals could be routed from the cephalon through the caddy and into a powered exoskeleton body,[2285] allowing voluntary control of all its functions.

Of course, in the future cryostasis revival era the widespread availability of atomically-precise molecular manufacturing will make it possible to build designer biological super-bodies,[2286] nonbiological whole-body prosthetics,[2287] or synthetic bodies made of individual nanorobots like utility fog.[2288] The resulting

---

[2279] Taib MY, Aziz AA, Alias ABS. Performance Analysis Of A Domestic Refrigerator. National Conference in Mechanical Engineering Research and Postgraduate Students (1st NCMER 2010), 26-27 May 2010, FKM Conference Hall, UMP, Kuantan, Pahang, Malaysia, pp. 582-591 (2010); http://umpir.ump.edu.my/1593/1/59_NCMER_068.pdf.

[2280] https://homesteady.com/info-12170824-freon-capacity-refrigerator.html.

[2281] Subbaiah SR, Nagamani GV. Effect of Condenser Coil Diameter on Performance of a Domestic Refrigerator. Intl J Mag Eng Technol Mgmt Res. 2015 Dec;2(12):1391-1400; http://www.ijmetmr.com/oldecember2015/SRamaSubbaiah-GVNagamani-A-51.pdf.

[2282] For example, an air-cooled system (requiring no external water supply hoses, but adding a fan) would require $V_{caddyair} = P_{caddyactive} / (C_{Vair} \Delta T_{air}) = 3.7$ liters/sec of room temperature air flowing past the condenser coils, taking $C_{Vair} = 1.19 \times 10^3$ J/m^3-K for room-temperature air and $\Delta T_{air} = 40$ K.

[2283] https://www.popsci.com/john-brandon/article/2008-10/rent-robotic-suit-named-hal/.
[2284] https://en.wikipedia.org/wiki/Neuroprosthetics.
[2285] https://en.wikipedia.org/wiki/Powered_exoskeleton.
[2286] https://en.wikipedia.org/wiki/Transhuman.

[2287] https://www.kurzweilai.net/radical-body-design-primo-posthuman and https://devpost.com/software/whole-body-prosthetics.

robot body might appear much smoother in appearance (image, right)[2289] and variable in shape, with greater strength, flexibility, durability, and an ability to survive in a much wider range of operating environments, than a natural biological human body.

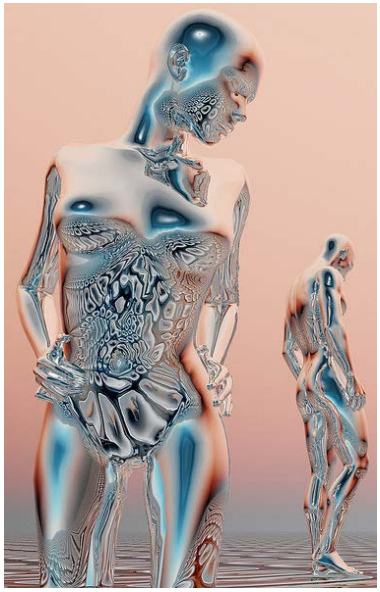

To a normal contemporary living person, existence as an isolated head attached to a life support machine is neither necessary for cryostasis revival nor particularly desirable. Future human-like bodies with enhanced capabilities are also not necessary for revival of cryopreserved neuro patients. However, artificial systems for cephalon life support may be an option that is available in the future, and chosen by some, because it is theoretically possible.

6.1.4 Cost of Replacement Body for Neuro Patients

Grown Acephalic Autologous Body (Section 6.1.1). One 2002 study[2290] of 253 geographically diverse U.S. hospitals found that the cost of a stay in an intensive care unit (ICU) varied depending on the intensity of care but ranged from $1500/day to $10,000/day due to equipment and supply, bed and board, nursing and other personnel, medications, and ventilation costs, but averaged $3968/day, or ~$5800/day in inflation-adjusted 2020 dollars, for long-term stays. Assuming the growth of an acephalic human body starting from an embryo requires equivalent levels of personnel and medical attentiveness to an artificial womb as an ICU facility, the cost would range from ($5800/day)(28 days) = **$162,400** at the embryonic growth rate (Section 6.1.1(4)) to ($5800/day)(173 days) = **$1,003,000** at the first trimester growth rate (Section 6.1.1(3)), ($5800/day)(1163 days) = **$6,745,000** at the neonatal growth rate (Section 6.1.1(2)), or ($5800/day)(7574 days) = **$43.9 million** at the normal 20.75-year maturation growth rate[2291] (Section 6.1.1(1)). These estimated costs may seem rather high, especially since medical procedures of all kinds should generally be much cheaper in the first decade or two of the nanorobot-rich future cryonics revival era – possibly as much as 10-100 times cheaper, assuming a high degree of automation. On the other hand, it also seems unlikely that cryonics revival procedures will achieve any significant economies of scale because, from an economics standpoint, cryonics should remain a tiny niche market with perhaps a few thousand cryopreserved patients worldwide needing this very specialized and aggressive medical service. The lack of a large market for revival procedures implies that costs may remain on the high side since outside capital will have little motivation to invest in its development and approval process. The burden of financing process development will fall to cryonics organizations, wealthy interested parties, or to side projects resourced by organizations with alternative funding sources.

[2288] https://en.wikipedia.org/wiki/Utility_fog.
[2289] https://mikepelletier.tumblr.com/post/64382878886.

[2290] Dasta JF, McLaughlin TP, Mody SH, Piech CT. Daily cost of an intensive care unit day: the contribution of mechanical ventilation. Crit Care Med. 2005 Jun;33(6):1266-71; https://pubmed.ncbi.nlm.nih.gov/15942342/.

[2291] Note that the option of employing a surrogate mother for $130K to carry the clone embryo for 9 months,[*] then employing a nursing home private-room equivalent for 20 years at $102.2K/yr[†] – a total cost of **$2.174 million** – is not available because the body must be grown in the acephalic state for the entire gestational and maturation period for legal and ethical reasons, which would require more specialized care.
[*] https://www.westcoastsurrogacy.com/surrogate-program-for-intended-parents/surrogate-mother-cost.
[†] https://health.usnews.com/best-nursing-homes/articles/how-to-pay-for-nursing-home-costs.

Nanofabricated Acephalic Autologous Body (Section 6.1.2). Building a nanofabricated body should have a cost very similar to the cost of whole-body conventional cell repair using replacement cells provided from a cell mill, or ~**$1.5 million** (**Table 17** in Section 5.5). It is difficult to imagine a sound rationale for employing a more expensive whole-body fabrication process such as atomic printing (Section 5.2.3.1), molecular printing (Section 5.2.3.2), or cryogenic molecular exchange repair (Section 5.3.3.1) when the pattern of the original trunk tissue is no longer available as a guide. The above estimate excludes the cost of reattaching the repaired cephalon to the nanomanufactured trunk, which may be in the **$2 million** range by current measures (**Table 19**, below),[2292] bringing the total cost of this option to $3.5 million. Once again, costs could fall by up to 10-100 fold in the early decades of the future nanorobot-rich cryonics revival era, as one might imagine the development of a vanity market for body-exchange surgery, just as the field of bionic reconstruction[2293] – where patients voluntarily amputate an existing subfunctional limb and replace it with a more functional prosthetic limb – began to emerge as soon as reasonably functional artificial substitutes became technically available.

Table 19. Estimated U.S. average 2020 transplant cost, per procedure[2294]

Transplant	Est. Billed Charges	Transplant	Est. Billed Charges
Single Organ/Tissue		Multiple Organs	
Pancreas	$408,800	Kidney-Pancreas	$713,800
Kidney	$442,500	Liver-Kidney	$1,355,100
Bone Marrow – Autologous	$471,600	Intestine with Other Organs	$1,662,900
Liver	$878,400	Other Multi-Organ	$2,185,800
Lung – Single	$929,600	Heart-Lung	$2,637,200
Bone Marrow – Allogenic	$1,071,700	Kidney-Heart	$2,644,600
Intestine	$1,240,000		
Lung – Double	$1,295,900		
Heart	$1,664,800		

Head Caddy and Biocompatible Artificial Body (Section 6.1.3). Top-of-the-line nonfunctional synthetic full-body medical cadavers sell for **$184,000**.[2295] A present-day advanced myoelectric-controlled prosthetic arm representing ~6% of acephalic body weight[2296] costs $20K-$100K,[2297] giving an acephalic

---

[2292] Other countries offer cheaper medical services. For example, "in the U.S. a heart surgery costs perhaps 20 or 30 times what it costs here [in the U.K.]," which would reduce the cost of reattaching the repaired cephalon to the nanomanufactured trunk from $2 million to only $100,000.
[*] Morris C. 'Production line' heart surgery. BBC News, Delhi, 2 Aug 2010; https://www.bbc.com/news/health-10837726.

[2293] Aman M, Festin C, Sporer ME, Gstoettner C, Prahm C, Bergmeister KD, Aszmann OC. Bionic reconstruction : Restoration of extremity function with osseointegrated and mind-controlled prostheses. Wien Klin Wochenschr. 2019 Dec;131(23-24):599-607; https://www.ncbi.nlm.nih.gov/pmc/articles/PMC6908564/.

[2294] Bentley TS, Ortner NJ. 2020 U.S. organ and tissue transplants: Cost estimates, discussion, and emerging issues. Millliman Research Report, Jan 2020; https://www.milliman.com/-/media/milliman/pdfs/articles/2020-us-organ-tissue-transplants.ashx.

[2295] https://www.atlasobscura.com/articles/syndaver-labs-synthetic-cadavers-tour.
[2296] https://exrx.net/Kinesiology/Segments.
[2297] https://health.costhelper.com/prosthetic-arms.html.

whole-body cost estimate of **$330,000-$1,700,000** assuming the functionality of the rest of the body could be replaced with technology of similar cost to the prosthetic arm,[2298] which seems optimistic. The lifelike humanoid robotic head and neck manufactured by Promobot[2299] ("the world's first android that looks just like a real person"; image, right) costs up to $50K and might represent ~9% of acephalic body weight,[2300] which could imply an acephalic whole-body cost estimate of **$560,000** if a larger whole-body model could be built. Presumably the proposed humanoid Tesla Bot[2301] would have a lower price point than that. But such devices would only mimic the kinematics and not the metabolic functions of a complete artificial replacement human body.

Single- and multiple-organ transplant costs in 2020 ranged from $400,000 to $2.6 million (**Table 19**). Simultaneously transplanting all major organs for a whole-body manufacture would probably cost at least **$10 million - $20 million** if it could have been done at all in 2020, a sum not inconsistent with the inflation-adjusted science fictional estimate[2302] of **$32 million** for the cost of major human whole-body rebuilds using the most advanced medical bionics[2303] technologies. Given likely cost reductions in the early decades of the future nanorobot-rich cryonics revival era, along with at least modest demand for artificial or augmented whole-body work in the general population (outside of the small-niche cryonics community), it seems plausible to expect that artificial body costs might fall by up to 10-100-fold into the **$0.2-2 million** price range.[2304] However this expectation should be validated in ***future research***.

[2298] Advanced prosthetic legs have similar costs; https://health.costhelper.com/prosthetic-legs.html.

[2299] https://www.cnbc.com/2019/10/31/human-like-androids-have-entered-the-workplace-and-may-take-your-job.html.
[2300] https://exrx.net/Kinesiology/Segments.
[2301] https://en.wikipedia.org/wiki/Tesla_Bot.

[2302] The fictional television USAF pilot Steve Austin had his entire body rebuilt with superhuman bionic gear,[*] reportedly costing $6 million in 1974, a sum equivalent to ~$31.9 million in inflation-adjusted 2020 dollars.
[*] https://en.wikipedia.org/wiki/The_Six_Million_Dollar_Man.

[2303] https://en.wikipedia.org/wiki/Bionics.

[2304] The manufacturing cost component of this overall price could be as low as $100-$100,000 for a 100 kg fully nanorobotic artificial body if the cost of atomically-precise fabrication eventually falls to the $1-$1000/kg range expected for more mature later-generation nanofactories of the type that could support cryonics revivals.[*] The remainder of the estimated price would be due to non-manufacturing costs.
[*] Freitas RA Jr., Merkle RC. Kinematic Self-Replicating Machines, Landes Bioscience, Georgetown, TX, 2004; Section 6.2.2, "Demonstration of Feasibility"; http://www.MolecularAssembler.com/KSRM/6.2.2.htm. Freitas RA Jr. Economic Impact of the Personal Nanofactory. Nanotechnology Perceptions: A Review of Ultraprecision Engineering and Nanotechnology 2006 May;2:111-126; http://www.rfreitas.com/Nano/NoninflationaryPN.pdf.

6.2 Separately Stored Cryopreserved Trunk

In a few rare cases, a cryopreserved patient's cephalon has been physically separated from the original body while both head and trunk are cryopreserved and stored individually.[2305] In Case A-1171 (1992),[2306] this occurred because of a gunshot wound to the head. In Case A-1876 (2002),[2307] the separation occurred because it was legal to immediately ship the cephalon but not the whole-body across state lines, and time was of the essence. In Case A-2063 (2004),[2308] the patient chose Alcor's "neuro-vitrification with whole-body cryoprotection" option, presumably to obtain the highest-quality cryopreservation for the brain while employing a less-expensive method for the trunk. And there may be one additional case of separated storage at Alcor.[2309]

Assuming that preservation of the original body along with the cephalon reflects the patient's preference and not mere happenstance, it could be inferred that such a patient does not desire a new replacement body (Section 5.2 or Section 6.1) but would prefer reattachment of his cephalon to the original trunk, restored either by conventional cell repair (Chapter 4) or by molecular reconstruction of the original body (Section 5.3). Cost-conscious patients (or the cost-conscious organization that revives them) might rationally elect to repair the head using the potentially more expensive molecular reconstruction process while repairing the body using the (presumably) less-expensive conventional cell repair – on the assumption that recovering the most valuable memory and personality attributes is most likely if the highest-fidelity revival technique is employed on the brain, whereas cell repair may suffice for the rest of the body.

In principle, a repaired cryogenic cephalon could be reattached to the unrepaired cryogenic trunk, followed by repair of the now-reunited whole-body using any of the techniques described in Chapter 4 or Chapter 5. On the positive side, such a course would ensure that all interface connections between head and trunk would be very well-matched because they both originate from the same patient. If the cephalon has already been repaired, subsequent repairs to the brain would be expected to be minimal aside from some minor rewarming damage that might develop during the revival process. Nevertheless, ***future research*** should analyze whether full molecular reconstruction of the trunk could negate much of the cost savings of the neuro option and end up costing slightly more than the whole-body option because of the extra work involved. Such extra cost might not outweigh the other major reason for choosing the neuro option (aside from the initial lower cost) – namely: the potential for a superior cryopreservation of the brain, because it is easier to get maximum concentration of cryoprotectant chemicals into a neuro patient than a whole-body patient during the perfusion phase of the cryopreservation process.[2310]

[2305] One Russian cryonicist has announced plans to maximize his chanced for survival by "storing half his brain in Russia and half elsewhere to hedge against a natural disaster"; Courtney Weaver, "Inside the weird world of cryonics," FT Magazine, 18 Dec 2015; https://www.ft.com/content/d634e198-a435-11e5-873f-68411a84f346.

[2306] https://www.alcor.org/library/complete-list-of-alcor-cryopreservations/case-report-a-1171/.
[2307] https://www.alcor.org/docs/alcor-case-report-a-1876.pdf.
[2308] https://www.alcor.org/docs/alcor-case-report-a-2063.pdf.

[2309] "Alcor's most famous patient, Major League baseball player Ted Williams, was cryopreserved after his death on 5 July 2002. Williams' body was separated from his head in a procedure called neuroseparation. The head was stored in a steel can filled with liquid nitrogen, while the body stands upright in a nine-foot tall cylindrical steel tank, also filled with liquid nitrogen." Cheryl Knight. A science without a deadline. E&T Engineering and Technology, 5 Nov 2008; https://eandt.theiet.org/content/articles/2008/11/a-science-without-a-deadline/.

[2310] Aschwin de Wolf refers to this option as "Brain-Optimized Whole-Body Cryopreservation", which in principle could allow a whole-body member to take advantage of hypothesized superior neuro-preservation, and even store the cephalon at Intermediate temperature Storage (ITS) temperatures (Section 7.1.2) in the future. This option (which one can privately arrange for at Alcor) potentially allows a person to "have it both ways" and thus could render much of the neuro vs. whole-body debate obsolete.

7. Alternatives, Validations, and Research Opportunities

We conclude this book with brief discussions of three important remaining considerations:

(1) the impact on revival of patients who have employed alternative (but not outrageous)[2311] means to enter biostasis (Section 7.1);

(2) methods of validating proposed methods of nanorobotic revival (Section 7.2); and

(3) proposals and recommendations for future research in the field of biostasis revival, and specifically for research into methods for revival from cryostasis (Section 7.3).

7.1 Alternative Pathways to (and from) Biostasis

In this Section we briefly examine the impact on revival of several alternative cryopreservation or biostasis scenarios.

Section 7.1.1 describes the case where the cryopatient receives no cryoprotectant of any kind (aka. "straight-freeze") or receives only incomplete perfusion of cryoprotectant, creating much additional damage that must be nanorobotically repaired.

One cryopreservative scenario that might create less damage is Intermediate Temperature Storage (Section 7.1.2). Xenon clathrates (Section 7.1.3) have been discussed as a possible alternative cryopreservative agent, along with persufflation using noble gases (Section 7.1.4), although no cryonics organization currently provides any of these services.

At the other end of the spectrum is chemical fixation (Section 7.1.5) or chemical preservation,[2312] which locks molecules in place and thus provides more secure stabilization during storage, but creates widespread chemical changes throughout the body that will likely require significant additional nanorobotic work to properly unlock the locked molecules during revival.

[2311] "Peat bogs," reports Mike Perry,[*] "have furnished surprising examples of preservation. One such location, a swampy pond near Windover, Florida, was excavated in the 1980s.[†] Remains of several individuals with recognizable if greatly shrunken brains were found. While there was much damage, definite cellular remnants could be seen on light and electron microscopic examination: axons; cerebellar purkinje cells in approximately their original spatial configurations and what appeared to be remnants of neurons. DNA was recovered, as well. The estimated age of this material was 7,000-8,000 years. The preservation, limited though it was, is all the more striking since it involved above-freezing storage under water, which normally results in rapid decomposition. Apparently the lack of oxygen and neutral pH in the water-soaked peat greatly slowed the normal processes of breakdown."

[*] Perry RM. The road less traveled: Alternatives to Cryonics. Cryonics 2007 Qtr 3;28(3):21-24; https://www.alcor.org/docs/cryonics-magazine-2007-03.pdf.

[†] Doran GH, Dickel DN, Ballinger WE Jr, Agee OF, Laipis PJ, Hauswirth WW. Anatomical, cellular and molecular analysis of 8,000-yr-old human brain tissue from the Windover archaeological site. Nature. 1986 Oct 30-Nov 5;323(6091):803-6; https://pubmed.ncbi.nlm.nih.gov/2430186/.

[2312] Olson CB. A possible cure for death. Med Hypotheses. 1988 May;26(1):77-84; https://web.archive.org/web/20100323035134/http://www.charlesolson.com/CBOCureForDeath.html.

Suspended animation by biological, chemical, hypothermic, or nanorobotic means is described in Section 7.1.6. The process is usually defined as being fully reversible, so revival from this form of biostasis requires only the normal reversal of metabolic arrest.

People can be "revived" from samples of their frozen DNA (Section 7.1.7), but little of their original personal identity will remain.

Finally, Section 7.1.8 describes the concept of whole-body backups – the use of cellular or molecular whole-body scans (or whole-brain scans) to allow the complete physical (or electronic) reconstruction of the patient in the event of a catastrophic disaster in which the original body is completely destroyed.

Most of these biostasis alternatives have received significantly less study than the traditional cryopreservation scenario, so their implementation details and the implications for revival are proper subjects for ***future research***.

7.1.1 Straight-Freeze and Poorly-Perfused Cryopreservation Patients

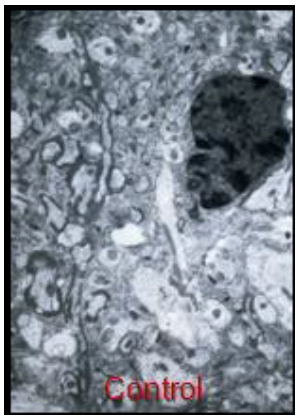

It has long been thought[2313] that cryopatients who are frozen without the infusion of any cryoprotectant, aka. a "straight-freeze", will suffer significant damage at the cellular level, along with ice formation.

For example,[2314] the image at left marked "Control" is a micrograph from the brain of a healthy anesthetized cat perfused with fixative and with no ischemia (e.g., heart still beating): "The fine architecture of the tissue is beautifully displayed and at 9K magnification it is possible to see intracellular organelles, such as the nuclei and mitochondria, as well the myelin sheathing, cell membranes and axoplasm."

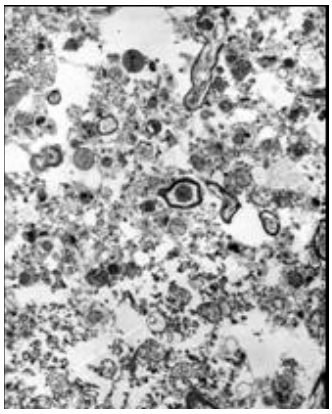

The image at right is from the same anatomical area of the brain of a different cat that was straight-frozen, then rewarmed. "Cell membranes are no longer visible and the field of view appears more like a tissue homogenate than a section of brain tissue." Tissue in this condition would be difficult to reconstruct using conventional cell repair (Chapter 4) because of the extensive fragmentation of cell components and the likely intermixing of those fragments amongst the remains of neighboring cells. Or, as one cryonicist notes:[2315] "For patients who have been straight-frozen, warming above freezing temperatures will immediately give

---

[2313] Completely unprotected tissues will experience massive mechanical damage* likely requiring extensive repairs.
* e.g., Lovelock JE, Smith AU. Studies in Golden Hamsters During Cooling To and Rewarming From Body Temperatures Below 0 degrees C. Part III: Biophysical Aspects and General Discussion. Proc R Soc Lond B Biol Sci. 1956 Jul 24;145(920):427-42; https://www.ncbi.nlm.nih.gov/pubmed/13359396; Fahy GM, Takahashi T, Crane AM. Histological cryoprotection of rat and rabbit brains. CryoLetters 1984;5:33-46

[2314] Darwin M. Cryonics: An Historical Failure Analysis. Part III: Dissociation of Researchers from the Clinical Environment. 2010; https://web.archive.org/web/20140906234205/http://cryoeuro.eu:8080/download/attachments/425990/Cryonics_Failure_Analysis_Part_3v5.4.pdf.

'mush' – just like thawing frozen strawberries. You will actually start to get 'mush' well below freezing temperatures because salt solutions turn liquid well below freezing temperature."

To avoid the "mush" kind of damage, such tissue must not be warmed but should be processed entirely at cryogenic temperatures. In these cases, as noted in Section 5.1, it may be useful to initially perform the scanning procedures described in Sections 4.1, 4.2, 4.3, 4.4, and 4.5 at LN2 temperatures, as this destroys no information and should permit a better assessment of the current physical state of the cryopreserved patient. If warming did occur, producing "mush," a molecular reconstruction (Chapter 5) would almost certainly be required, preceded by a molecular scan and a computationally intensive (and likely very costly) attempt to estimate the most likely diffusion paths of each fragment to help determine which fragments should be paired with other fragments, and in which orientation, like a 3D jigsaw puzzle.

Straight freezes may occur in cases where there is too much delay[2316] after arrest for vitrification perfusion protocols to be applied. Even when perfusion can be done, there can be an uneven distribution of the cryoprotectant so that some subvolumes of the brain are essentially just straight frozen. "Theoretically, cells freezing due to failed vitrification should freeze intracellularly due to supercooling and the absence of extracellular ice to translocate intracellular water and concentrate the [cryoprotective agents] inside the cells. Intracellular freezing results in vastly more damage than does conventional extracellular freezing with resultant vitrification of the intracellular milieu."[2317] To the extent that unwanted ice formation is localized in a few specific areas,[2318] ***future research*** should consider methods by which those blocks of tissue could be extracted from the body, separately processed via molecular reconstruction, and then returned to the body with full interfacial reintegration with existing tissue. On the other hand, if unwanted ice formation is ubiquitous throughout the brain or body, comprehensive molecular reconstruction (Chapter 5) will likely be required to restore patient viability. ***Future research*** should examine the nature and extent of various classes of "partial vitrification" scenarios, and determine the optimal approach for each scenario.

[2315] Best B. Cryonics: Introduction and Technical Challenges. In: Sames KH, ed. Applied Cryobiology – Human Biostasis. Ibidem-Verlag, Stuttgart, 2013, pp. 61-78; https://www.amazon.com/Applied-Cryobiology-Human-Biostasis-Klaus/dp/3838204581.

[2316] "The 5,200-year-old Tyrolean Ice Man discovered in a glacier in 1991," reports Mike Perry,[*] "is the oldest known frozen human mummy. Although frozen at high subzero-Celsius (non-cryogenic) temperature for most of the five millennia since his death, it is clear that some thawing and refreezing occurred, including an incident immediately following discovery. Despite the adverse circumstances, a 1998 study reports interesting findings for many parts of the anatomy, in which many details at the cellular level can be seen, albeit with substantial loss. In the brain there was preservation of the myelin sheaths of axons, even though the material of the axons and the neuron cell bodies were mostly obliterated.[†] Details of the myelin sheaths were discernible down to 10 nanometers, or about 65 carbon atom-diameters."

[*] Perry RM. The road less traveled: Alternatives to Cryonics. Cryonics 2007 Qtr 3;28(3):21-24; https://www.alcor.org/docs/cryonics-magazine-2007-03.pdf.

[†] Hess MW, Klima G, Pfaller K, Künzel KH, Gaber O. Histological investigations on the Tyrolean Ice Man. Am J Phys Anthropol. 1998 Aug;106(4):521-32; https://pubmed.ncbi.nlm.nih.gov/9712480/.

[2317] Darwin M. Cryonics: An Historical Failure Analysis. Part III: Dissociation of Researchers from the Clinical Environment. 2010; https://web.archive.org/web/20140906234205/http://cryoeuro.eu:8080/download/attachments/425990/Cryonics_Failure_Analysis_Part_3v5.4.pdf.

[2318] For example, during whole-body perfusion with M22, "significant portions of the body do not cryoprotect sufficiently to vitrify, mostly because things like fatty tissue and skeletal muscle are not well-vascularized." Staff of Cryonics magazine. Whole Body Cryopreservation Upgrade. Cryonics 2005 Nov/Dec;26(6):21; https://www.alcor.org/docs/cryonics-magazine-2005-06.pdf.

Advanced Neural Biosciences (ANB) has been working to carefully compare control (i.e., undamaged) and straight-frozen neural tissue to assess the degree and type of damage in a straight freeze scenario.[2319] At a 2019 cryonics symposium,[2320] Aschwin de Wolf, CEO of ANB, presented micrographs of brain tissue that was straight frozen and then thawed that "doesn't appear to have anywhere near as much damage as we might expect. The state of the tissue is worse than the same case for vitrification, but perhaps not as much worse as thought, and might lead to a lower-cost form of acceptable cryopreservation. More work [***future research***] is needed to assess this conjecture, but the findings are hopeful so far. He emphasized the point that freezing causes damage, but that by also lowering the temperature, identity-critical information may be preserved by inhibiting diffusion-based chemistry."

De Wolf has also introduced a deep learning algorithm that distinguishes the early stages of permanent cerebral ischemia from the late stages of permanent cerebral ischemia, trained on electron micrographs of the two damage states.[2321] Future versions of this algorithm – called "reconstructive connectomics" – might be able to computationally reconstruct the pre-ischemic state of the brain from the ischemic state, or to infer the non-frozen state from the frozen state (if there is freezing damage), providing an important tool to permit nanorobotic repair and revival of poorly-perfused cryopreservation patients.

Interestingly, post-mortem patients maintained for extended periods at temperatures slightly above freezing without ever being cryopreserved might sometimes retain enough neural features[2322] to permit at least some weak inference of identity-relevant structures that could be sufficient to recover some small percentage of personal identity, but such revivals are beyond the scope of this book.

7.1.2 Intermediate Temperature Storage

Liquid nitrogen provides an inexpensive, stable, and highly reliable storage environment for cryopreserved tissue at a temperature of -196 °C, but cooling to this very cold temperature causes cryopreserved tissues to fracture (Section 3.4.3). The presence of extensive fractures probably precludes recovery of the cryopatient

---

[2319] Phaedra C. Reconstructive Connectomics. Cryonics 2013 Jul;34(7):26-28; https://www.alcor.org/library/reconstructive-connectomics/.

[2320] Notes on the 1st Alcor New York Science Symposium. Cryonics 2020 Qtr I;41(1):32-35; https://www.alcor.org/docs/cryonics-magazine-2020-01.pdf.

[2321] de Wolf A, Phaedra C, Perry RM, Maire M. Ultrastructural Characterization of Prolonged Normothermic and Cold Cerebral Ischemia in the Adult Rat. Rejuvenation Res. 2020 Jun;23(3):193-206; https://pubmed.ncbi.nlm.nih.gov/31631775/.

[2322] Mike Perry reports* that "[t]he body of a woman was kept in a mortuary for 2 months at 3 °C with no fixation, then the brain was removed and fixed in a phosphate-buffered formaldehyde solution (4.5%) for 9 weeks. Subsequent examination† of the brain showed macroscopically visible surface deterioration; histologically, however, normal brain structures were preserved including all important cell types (neurons, astrocytes, oligodendrocytes, microglia), neuropil, axons, and myelin sheaths. From a cryonics standpoint the preservation was not good but, I would say, not negligible either." In another report,‡ electron micrographs of brain tissue subjected to 1 month of cold ischemia caused one observer to remark that he "would not have guessed that so much structure could remain after one month," causing the author to wonder: "If the damage of a straight freeze is a lot worse than the damage from moderate times of cold ischemia, cryoprotecting the brain (or both hemispheres separately) by soaking it in cryoprotectant could be a superior protocol for a select number of Alcor cases."

* Perry RM. The road less traveled: Alternatives to Cryonics. Cryonics 2007 Qtr 3;28(3):21-24; https://www.alcor.org/docs/cryonics-magazine-2007-03.pdf.

† Gelpi E, Preusser M, Bauer G, Budka H. Autopsy at 2 months after death: brain is satisfactorily preserved for neuropathology. Forensic Sci Int. 2007 May 24;168(2-3):177-82; https://pubmed.ncbi.nlm.nih.gov/16930897/.

‡ de Wolf A. Ultrastructural Signatures of Information-Theoretic Death. Cryonics 2013 Nov;34(11):5; https://www.alcor.org/docs/cryonics-magazine-2013-11.pdf.

by simple means such as rewarming and reperfusion (as in "suspended animation" approaches; Section 7.1.6) but doesn't compromise the neuroanatomical information preservation goals of cryonics because fractures can be stabilized (Section 4.6.3) and repaired (Section 4.9.2) by nanotechnological means. Nevertheless, it would be preferable to minimize the amount of additional damage imposed on the patient during the cryopreservation process in order to reduce the complexity, cost, and time required for revival.

In the proposed Intermediate Temperature Storage (ITS) for cryonics,[2323] patients thoroughly perfused with M22 cryoprotectant would be cooled to the glass transition temperature of T_g ~ -123 °C (150 K) and held near there, and not be cooled all the way to LN2 temperatures of -196 °C (77 K). At T_g, the patient has entered a rigid solid state like glass, effectively preventing molecular movement and ensuring biological preservation over long time periods, without cracking (image (a), below). Cooling much below T_g is what causes cracking (image (b), below) via differential contraction or other physical mechanisms.

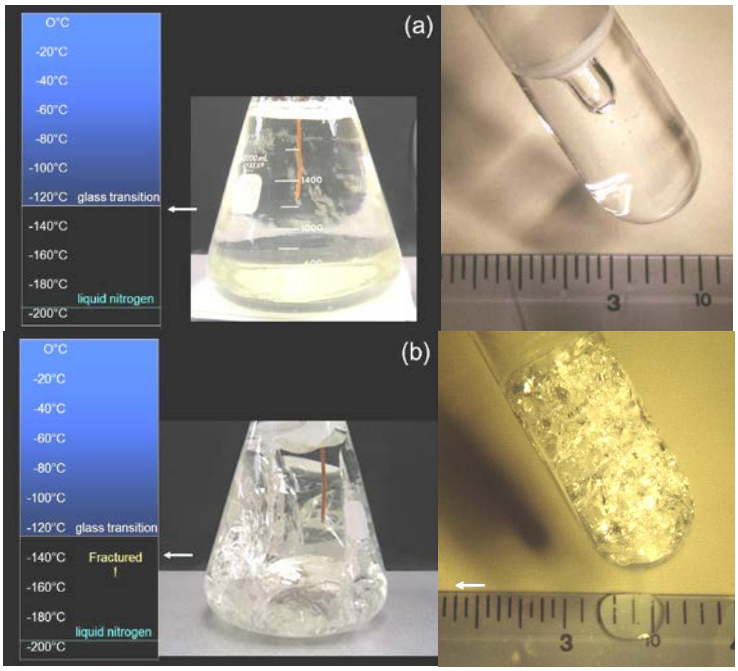

More recently, Brian Wowk has performed additional research on this issue and offers the following update on the prospects for ITS, with clear recommendations for ***future research***:[2324]

> "The most important finding was a product of the Whole Body Vitrification Project…[in which] whole adult pigs of the same mass as human cryonics patients were perfused with M22 vitrification solution. In some of those experiments, M22-perfused pigs were cooled and vitrified using circulated nitrogen gas at computer-controlled cold temperature….[W]e were then able to slowly rewarm the animals and perform detailed physical examination of organs looking for fractures. We determined from this research that the lowest temperature from which a whole animal could be cooled and subsequently rewarmed without any fractures is -130 °C. We were not able to cool/rewarm successfully from -135 °C without some fractures even when

---

[2323] Wowk B. Systems for intermediate temperature storage for fracture reduction and avoidance. Cryonics 2011 Qtr 3; https://www.alcor.org/library/systems-for-intermediate-temperature-storage-for-fracture-reduction-and-avoidance/.

[2324] Personal communications among Robert Freitas, Brian Wowk, Aschwin de Wolf, and others during 11-25 Sep 2019.

cooling/rewarming over weeks to minimize thermal stress. -130 °C is six degrees below the glass transition temperature of M22, so it's completely safe for long-term storage from the point of view of chemical changes. However I personally don't believe it's a safe temperature for cryonics patients because of a process called ice nucleation."

"We need more detailed DSC (differential scanning calorimetry) study of ice nucleation near and below the glass transition temperature…[as done in the past,[2325] which showed that]…nucleation occurs near, and apparently somewhat below, the glass transition temperature of vitrification solutions (-123 °C). [See chart in Section 4.9.1.] Some cryobiologists have privately expressed skepticism to me that nucleation can occur at all below T_g, [which] makes it even more important that this issue be studied carefully and thoroughly. It is of importance to both mainstream cryobiology (organ and tissue banking at intermediate temperatures) and especially cryonics storage at temperatures between liquid nitrogen (-196 °C) and the glass transition temperature (-123 °C). I find it disturbing as a matter of principle to store cryonics patients at a temperature at which we know change is occurring. I would therefore very much like to fully understand the nature of the nucleation process, especially to confirm that it is heterogeneous nucleation (catalyzed by surfaces), not homogeneous nucleation (happening wherever there are water molecules). If it's entirely heterogeneous, then it might exponentially trail off to an asymptotically limited amount of nucleation. Alternatively, if we can fit a physically plausible mathematical function to nucleation rate as a function of temperature, we might be able to calculate a temperature at which the nucleation rate is sufficiently negligible for us to be comfortable with it."

"[W]e don't currently understand the long-term safety of storage temperatures near the glass transition temperature very well. Until more research is done, we must be honest and say that we don't currently know how to cool and store cryonics patients at a safe temperature that reliably avoids fracturing. We know more than we used to, but complete fracture avoidance is still a science problem, not an engineering problem. All cryonics patients are going to fracture. Until the science problems are solved (if they can be solved), the merit of ITS is that cryonics patients will fracture less. ITS should not be regarded as a way to avoid fracturing in cryonics."

"Storing vitrified organs for transplant is a different story. Both the science and engineering problems of storing cryopreserved organs without fracturing, certainly kidneys, were solved many years ago by 21CM. We have ITS storage units at 21CM operating at -140 °C containing numerous rabbit kidneys that I regularly experiment on, and even some vitrified pig kidneys. I've cooled masses of solution the same mass as human kidneys to liquid nitrogen temperature (-196 °C) and back without fracturing. We've cooled a rabbit kidney to liquid nitrogen temperature and back without fracturing (we transplanted it without any bleeding). There are still academic questions to be answered about storing organs for transplant, but as a practical matter the specific problem of storing vitrified organs without fracturing for purposes of transplantation now looks easy."

At present no cryonics service provider offers or has offered ITS for whole-body cryopreservation,[2326] so the issue of revival from ITS cryopreservation is not of immediate concern. Revival from ITS would be a useful topic for ***future research*** if this situation changes.

[2325] Mehl PM. Nucleation and Crystal Growth in a Vitrification Solution Tested for Organ Cryopreservation by Vitrification. Cryobiology. 1993 Oct;30(5):509-518; https://pubmed.ncbi.nlm.nih.gov/11987991/. Wowk B, Fahy GM. Ice nucleation and growth in concentrated vitrification solutions. Cryobiology 2007;55(3):330; https://www.sciencedirect.com/science/article/abs/pii/S0011224007001708.

[2326] Alcor has a small number of neuro patients in an ITS unit, and the European Biostasis Foundation (EBF; https://ebf.foundation/) aims to offer whole-body storage in the next few years.

7.1.3 Clathrate Cryopreservation

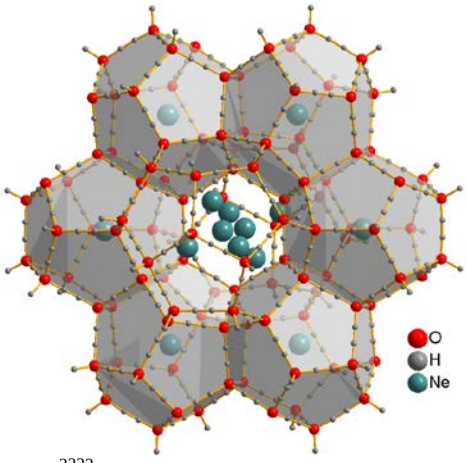

Clathrates[2327] have been proposed as an alternative to vitrification in human cryopreservation, due to the toxicity of present-day vitrification agents. Clathrate hydrates (image, right) are a class of solids in which gas molecules reside inside cages of hydrogen-bonded water molecules that are unstable when empty (collapsing into conventional ice crystal structure) but stabilized by the inclusion of a gas molecule inside them. Most low molecular weight gases such as O_2, N_2, CO_2, CH_4, H_2S, SF_6, Freon-23, Ne, Ar, Kr, and Xe will form a clathrate hydrate under some pressure-temperature conditions.[2328] Xenon is well-known as an anesthetic agent,[2329] possibly due to its high proclivity to form clathrate hydrate structures near synapses, impeding interneuronal transmission.[2330] Xenon is neuroprotective when administered before, during, or after ischemic or hypoxic insults,[2331] and can form clathrates at relatively low pressure.[2332]

After its use as a cryopreservative agent was first proposed in 1969,[2333] this possibility was studied *in vitro* by analyzing protein structure in the presence of xenon clathrate.[2334] Sheleg *et al.*[2335] report that "[p]reliminary tests of the cryostasis protocol (using a gaseous mixture of xenon-nitrogen-oxygen at +5 °C under high pressure) on *Planaria* showed xenon clathrate formation in the animal tissue and the reversibility of this procedure. Our results [on mouse heart tissue, at 6.8 atm Xe pressure] showed absence of mitochondrial swelling, rupture of inner and outer membranes, and leakage of mitochondrial matrix into the cytoplasm after applying the cryostasis protocol in comparing with freezing under high pressure of

---

[2327] https://en.wikipedia.org/wiki/Clathrate_compound.

[2328] Englezos P. Clathrate hydrates. Ind Eng Chem Res. 1993 Jul 1;32(7):1251-1274; https://pubs.acs.org/doi/pdf/10.1021/ie00019a001.

[2329] https://en.wikipedia.org/wiki/Xenon#Anesthesia.

[2330] Pauling L. A molecular theory of general anesthesia. Science. 1961 Jul 7;134(3471):15-21; https://authors.library.caltech.edu/62750/. Miller S. A theory of gaseous anesthetics. Proc Natl Acad Sci USA. 1961 Sep 15;47(9):1515–1524; https://www.ncbi.nlm.nih.gov/pmc/articles/PMC223167/.

[2331] https://en.wikipedia.org/wiki/Xenon#Neuroprotectant.

[2332] Ohgaki K, Sugahara T, Suzuki M, Jindai H. Phase behavior of xenon hydrate system. Fluid Phase Equilibria. 2000 Oct;175(1-2):1-6; https://www.sciencedirect.com/science/article/abs/pii/S0378381200003745.

[2333] Prehoda RW. Suspended Animation. Chilton Book Co., Philadelphia PA, 1969, pp. 81-86; https://www.amazon.com/dp/B0006CPDQI/.

[2334] Rodin VV, Isangalin FSH, Volkov VYA. Structure of protein solutions in a presence of xenon clathrate. Cryobiol CryoMed. 1984;14:3-7 (in Russian).

[2335] Sheleg S, Hixon H, Cohen B, Lowry D, Nedzved M. Cardiac mitochondrial membrane stability after deep hypothermia using a xenon clathrate cryostasis protocol - an electron microscopy study. Int J Clin Exp Pathol. 2008 Jan 1;1(5):440-7; https://www.ncbi.nlm.nih.gov/pmc/articles/PMC2480575/.

nitrogen. Intercellular freezing causes damage, not so much during the freezing process but rather in the course of thawing, during which re-crystallization can occur.[2336] Xenon clathrates are easily broken as the pressure drops, without intracellular water recrystallization (compared to damage after intracellular ice crystal formation)."

Relevant research on xenon clathrates continues,[2337] but Best[2338] notes that "[v]itrification and clathrate formation are incompatible approaches to cryopreservation. Clathrates are structures similar to ice, which means that vitrification would prevent clathrate formation at least as readily as it prevents ice formation. Although xenon clathrates may be useful for cryogenic temperature cryopreservation of small tissue samples, it cannot be applied to cryogenic organ cryopreservation or cryonics because of the mechanical damage caused by the large-volume clathrates."

At present no cryonics service provider offers or has offered clathrate-based cryopreservation, so the issue of revival from xenon clathrate hydrate cryopreservation is not of immediate concern.

7.1.4 Persufflation and Vascular Cryofluids

Persufflation is the process of passing cold gases through the vasculature instead of blood, most commonly for the purpose of extending the hypothermic preservation time of donor organs for transplantation,[2339] such as heart,[2340] liver,[2341] kidney,[2342] and pancreas.[2343] In particular, gaseous oxygen

---

[2336] Acker JP, McGann LE. Protective effect of intracellular ice during freezing? Cryobiology. 2003 Apr;46(2):197-202; https://pubmed.ncbi.nlm.nih.gov/12686211/.

[2337] Artyukhov VI, Pulver AY, Peregudov A, Artyuhov I. Can xenon in water inhibit ice growth? Molecular dynamics of phase transitions in water-Xe system. J Chem Phys. 2014 Jul 21;141(3):034503; http://citeseerx.ist.psu.edu/viewdoc/download?doi=10.1.1.766.6765&rep=rep1&type=pdf.

[2338] Best B. Viability, Cryoprotectant Toxicity and Chilling Injury in Cryonics. V. Clathrate Hydrates; https://www.benbest.com/cryonics/viable.html#clathrates.

[2339] Min CG, Papas KK. Recent developments in persufflation for organ preservation. Curr Opin Organ Transplant. 2018 Jun;23(3):330-335; https://pubmed.ncbi.nlm.nih.gov/29634496/.

[2340] Kunze S, Jeschkeit-Schubbert S, Dahnken S, Fischer JH, Herzig S. Endothelial function after prolonged coronary artery oxygen persufflation in a rabbit model of heart preservation. Interact Cardiovasc Thorac Surg. 2002 Sep;1(1):16-22; https://academic.oup.com/icvts/article/1/1/16/683296. Suszynski TM, Rizzari MD, Scott WE, Eckman PM, Fonger JD, John R, Chronos N, Tempelman LA, Sutherland DE, Papas KK. Persufflation (gaseous oxygen perfusion) as a method of heart preservation. J Cardiothorac Surg. 2013 Apr 22;8:105; https://www.ncbi.nlm.nih.gov/pmc/articles/PMC3639186/.

[2341] Treckmann J, Minor T, Saad S, Ozcelik A, Malagó M, Broelsch CE, Paul A. Retrograde oxygen persufflation preservation of human livers: a pilot study. Liver Transpl. 2008 Mar;14(3):358-64; https://pubmed.ncbi.nlm.nih.gov/18306377/. Gallinat A, Hoyer DP, Sotiropoulos G, Treckmann J, Benkoe T, Belker J, Saner F, Paul A, Minor T. Oxygen Persufflation in Liver Transplantation Results of a Randomized Controlled Trial. Bioengineering (Basel). 2019 Apr 27;6(2):35; https://www.ncbi.nlm.nih.gov/pmc/articles/PMC6630246/. Minor T, Lüer B, von Horn C, Paul A, Gallinat A. Effect of oxygen concentration in anterograde liver persufflation on high energy phosphates and graft function after ischemic preservation. Cryobiology. 2020 Feb 1;92:248-250; https://www.sciencedirect.com/science/article/pii/S0011224019305942.

[2342] Moláček J, Opatrný V, Matějka R, Baxa J, Třeška V. Retrograde Oxygen Persufflation of Kidney - Experiment on an Animal. In Vivo. 2016 11-12;30(6):801-805; https://iv.iiarjournals.org/content/30/6/801.full.pdf.

perfusion/persufflation can enhance organ preservation relative to static cold storage or hypothermic machine perfusion, since the lower viscosity of gases may help reach more regions of preserved organs and deliver more oxygen per gram of tissue.[2344]

In the context of cryopreservation,[2345] blood can be replaced with inert noble gases so that organs can cool more quickly and less antifreeze is needed. Since regions of tissue are separated by gas, small expansions do not accumulate, thereby protecting against shattering.[2346] Arigos Biomedical reportedly "recovered pig hearts from the 120 degrees below zero threshold," [2347] and a patent granted to that company[2348] states that performing the persufflation on a human body at hyperbaric pressures of 20-60 atm would help increase heat exchange rates.

At present no cryonics service provider offers or has offered persufflation-based whole-body cryopreservation,[2349] so the issue of revival from this form of cryopreservation is not of immediate concern.

A similar method for achieving rapid cooling is to circulate a chemically inert cryogen such as a chilled fluorocarbon liquid throughout the vascular system of a human patient, "controlling the temperature of the inert fluid which circulates through the vascular system, whereby the inert fluid functions as a heat exchange medium cooling or rewarming the organs, tissues, animals and whole humans internally and quickly. The cooling/rewarming rates of the internal cooling/rewarming method … are more than ten times faster than those that can be achieved by conventional external cooling/rewarming methods." [2350] Note that perfluorobutane[2351] has a liquid range of 145-271 K (-128 °C to -2 °C), which after cooling to near 145 K could be replaced with tetrafluoromethane[2352] with a liquid range of 89-145 K (-184 °C to -128 °C) to carry almost all the way to LN2 temperature.

[2343] Kelly AC, Smith KE, Purvis WG, Min CG, Weber CS, Cooksey AM, Hasilo C, Paraskevas S, Suszynski TM, Weegman BP, Anderson MJ, Camacho LE, Harland RC, Loudovaris T, Jandova J, Molano DS, Price ND, Georgiev IG, Scott WE 3rd, Manas DMD, Shaw JAM, O'Gorman D, Kin T, McCarthy FM, Szot GL, Posselt AM, Stock PG, Karatzas T, Shapiro AMJ, Lynch RM, Limesand SW, Papas KK. Oxygen Perfusion (Persufflation) of Human Pancreata Enhances Insulin Secretion and Attenuates Islet Proinflammatory Signaling. Transplantation. 2019 Jan;103(1):160-167; https://www.ncbi.nlm.nih.gov/pmc/articles/PMC6371803/.

[2344] Suszynski TM, Rizzari MD, Scott WE 3rd, Tempelman LA, Taylor MJ, Papas KK. Persufflation (or gaseous oxygen perfusion) as a method of organ preservation. Cryobiology. 2012 Jun;64(3):125-43; https://www.ncbi.nlm.nih.gov/pmc/articles/PMC3519283/.

[2345] https://en.wikipedia.org/wiki/Cryopreservation#Persufflation.

[2346] Linda Geddes. Heart of glass could be key to banking organs. New Scientist, 2013 Sep 11; https://www.newscientist.com/article/mg21929343-100-heart-of-glass-could-be-key-to-banking-organs/.

[2347] Matthew Flynn. We're closer than ever to freezing organs and making transplant waitlists a thing of the past. Boss Magazine, 10 Oct 2018; https://thebossmagazine.com/freezing-and-thawing-organs/.

[2348] Van Sickle S, Jones T. Method and apparatus for prevention of thermo-mechanical fracturing in vitrified tissue using rapid cooling and warming by persufflation. U.S. Patent 9,314,015, 19 Apr 2016; https://patentimages.storage.googleapis.com/b5/55/0f/ca634733c0b863/US9314015.pdf.

[2349] Arigos Biomedical allowed its patent to expire on 5 Oct 2020 (https://portal.uspto.gov/pair/PublicPair) and as of 2021 is apparently either in hibernation or no longer in business.

[2350] Wowk BG, Federowicz MG, Russell SR, Harris SB. A method for rapid cooling and warming of biological materials. International Patent Application WO1998019529A1, published 14 May 1998; https://patents.google.com/patent/WO1998019529A1.

[2351] https://en.wikipedia.org/wiki/Perfluorobutane.
[2352] https://en.wikipedia.org/wiki/Carbon_tetrafluoride.

7.1.5 Chemical Fixation

Chemical fixation has been proposed as a supplement or alternative to cryopreservation in the past.[2353] One cryonicist admits[2354] he is "not irrevocably wed to the idea of cryopreservation" and has expressed the opinion that he would "much prefer a preservation approach that has been validated over ~45 million years, such as the demonstrated preservation of cellular ultrastructure in glasses at ambient temperature, in the form of plant and animal tissues preserved in amber." As an example, images from a 2005 study[2355] examined the ultrastructure of plant cells that had been preserved for ~45 million years at essentially room temperature in Baltic amber. Amber is a tree-derived resin comprising macromolecules capable of polymerization under conditions of moderately elevated pressure and temperature,[2356] and conceivably serves a crudely analogous function in natural environments as glutaraldehyde fixation (described below).

The images at right, labeled "(a)" (above) and "(b)" (below), are transmission electron micrographs of ultrathin cross-sections of the amber cypress tissue. They suggest that a significant amount of structural information down to the 100 nm scale, and perhaps even smaller, has been preserved to some degree.

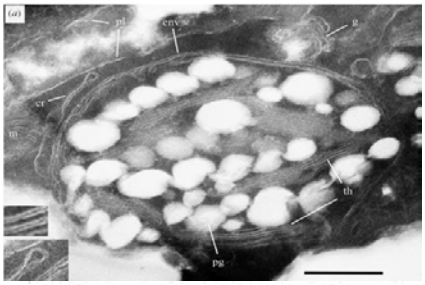

From the study authors' description of the images:

(a) **Scale bar 500 nm.** Section of a parenchyma cell with a chloroplast, the double membrane envelope (env), thylakoid membranes (th) and large plastoglobuli (pg), membranes of the endoplasmic reticulum (er), the golgi apparatus (g), the plasmalemma (pl) and part of a mitochondrion (m).

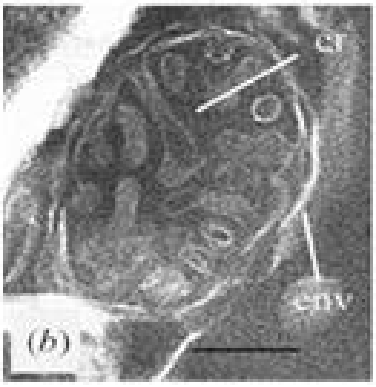

(b) **Scale bar 200 nm.** Cross-section of a mitochondrion with the outer envelope (env) and cristae (cr).

Chemical fixation[2357] (aka. embalming,[2358] or mummification[2359] in ancient times) is the modern version of this natural process.[2360]

[2353] Drexler KE. "Chapter 9. A Door to the Future. Methods of Biostasis," Engines of Creation, Doubleday, New York, 1986, pp. 133-134; https://web.archive.org/web/20060615004725/http://www.e-drexler.com/d/06/00/EOC/EOC_Chapter_9.html. Olson CB. A possible cure for death. Med Hypotheses. 1988 May;26(1):77-84; https://web.archive.org/web/20100323035134/http://www.charlesolson.com/CBOCureForDeath.html.

[2354] Michael Darwin. Cryonics, Nanotechnology and Transhumanism: Utopia Then and Now. Chronosphere, 19 Apr 2011; http://chronopause.com/chronopause.com/index.php/2011/04/19/cryonics-nanotechnology-and-transhumanism-utopia-then-and-now/index.html.

[2355] Koller B, Schmitt JM, Tischendorf G. Cellular fine structures and histochemical reactions in the tissue of a cypress twig preserved in Baltic amber. Proc Biol Sci. 2005 Jan 22;272(1559):121-6; https://www.ncbi.nlm.nih.gov/pmc/articles/PMC1634957/.

[2356] https://en.wikipedia.org/wiki/Amber.
[2357] https://en.wikipedia.org/wiki/Fixation_(histology).
[2358] https://en.wikipedia.org/wiki/Embalming.
[2359] https://en.wikipedia.org/wiki/Mummy.

Fixatives are comparatively large molecules that must diffuse into tissues to be effective. The diffusion rate may not be fast enough to prevent autolysis in brains subjected to as little as 10-15 minutes of ischemia.[2361] Also, stable preservation requires solidification which has traditionally required dehydrating the tissue with a nonaqueous solvent, then perfusing an epoxy resin with a plasticizer[2362] to catalyze a polymerization reaction.

Despite criticism that chemical fixation irreversibly destroys tissue viability and thus makes fixation unlikely ever to be accepted as a valid emergency procedure in critical care medicine,[2363] early advocates insisted that chemopreservation has several advantages over cryopreservation:[2364] "First, it is potentially cheaper, because it does away with the need for expensive long-term care. Chemopreserved patients would not require labor to keep them in the same condition, other than storage in a secure, designated area, unlike cryopreserved patients who are in continual danger of thawing. Cryopreserved patients require continual monitoring of liquid nitrogen levels and topping off with more liquid nitrogen, as well as special, expensive containers that can hold liquid nitrogen, and these containers need regular maintenance, repair, and replacement. Liquid nitrogen also presents hazards that require continual air monitoring and alarms. The basic techniques for chemopreserving a brain – fixation and polymer impregnation – would also not require the services of specially trained volunteers or professionals; they are routine techniques used in hospital pathology labs and departments of anatomy around the world….the cost of brain chemopreservation could be less than that of a typical funeral. [C]hemopreservation entirely avoids the danger of ice formation and fracturing, which in theory could destroy physical structures in the brain and cause irretrievable identity-critical information loss. While fixatives cause molecular changes in the brain, by crosslinking and denaturing proteins, cryoprotectants also cause chemical damage which must later be repaired."

Glutaraldehyde [HCO-$(CH_2)_3$-CHO] reacts rapidly and irreversibly with basic amino acid residues and is an efficient crosslinking agent for collagen (image, right).[2365] Crosslinking can occur through both of the -CHO groups and over variable distances. In aqueous solutions, glutaraldehyde is present largely

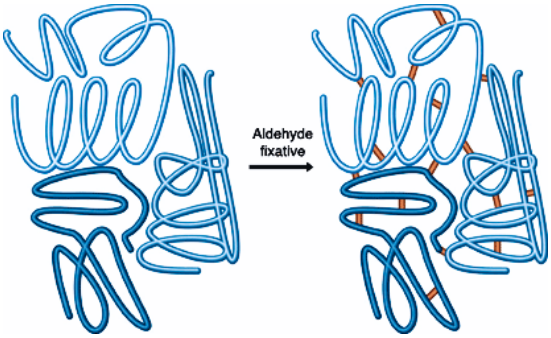

[2360] Anatomical brain collections (usually employing formaldehyde fixative) exist in major cities around the world, including Paris, Stockholm, Philadelphia, and Tokyo. Cornell University's Wilder Brain Collection contained 600-1200 brains at its peak.[*] The Moscow Brain Institute,[†] formerly known as the "pantheon of Brains," reportedly includes the preserved brains of Lenin, Stalin, Pavlov, and Tsiolkovsky – although Lenin's brain was apparently sectioned into 30,000 slices and a visitor in 2014 was told that "the brains of the gifted are located in a different building…we don't show them to the public."
[*] https://en.wikipedia.org/wiki/Wilder_Brain_Collection.
[†] Joy Neumeyer, "A Visit to Moscow's Brain Institute," 10 Apr 2014; https://www.vice.com/en/article/qbejbd/a-visit-to-moscows-brain-institute.

[2361] http://chronopause.com/chronopause.com/index.php/2012/02/14/the-effects-of-cryopreservation-on-the-cat-part-2/index.html#comment-3834.

[2362] https://en.wikipedia.org/wiki/Plastination.

[2363] de Wolf A. Chemical Brain Preservation and Human Suspended Animation. Cryonics 2013 Jan;34(1):17-25; https://www.alcor.org/library/chemical-brain-preservation/.

[2364] Greg Jordan. Biostasis through chemopreservation. Depressed Metabolism, 25 Feb 2008; https://www.biostasis.com/better-biostasis-through-chemosuspension/.

[2365] Noor Ullah, "Tissue fixation," 10 Oct 2018; https://www.slideshare.net/habibhasrat/tissue-fixation-histopathology.

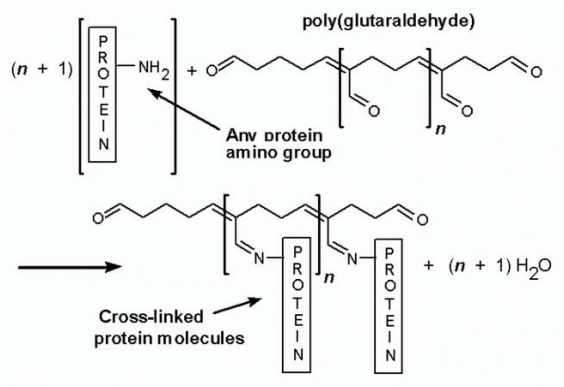

as polymers of variable size,[2366] with a free aldehyde group sticking out of the side of each unit of the polymer molecule as well as one at each end – all of these -CHO groups will combine with any protein nitrogens with which they come into contact, so there is enormous potential for cross-linking (image, left).[2367] The free aldehyde groups introduced by glutaraldehyde fixation cause non-specific binding of proteinaceous reagents, notably antibodies, and extensive cross-linking may also cause loss or severe reduction of most histochemically demonstrable enzymatic activities.[2368] Crosslinking fixatives also anchor soluble proteins to the cytoskeleton.

McIntyre and Fahy[2369] successfully performed the first **aldehyde-stabilized cryopreservation** (ASC) (aka. "vitrifixation") on rabbit and pig brains, winning the Large Mammal Brain Preservation Foundation Prize for their work[2370] after detailed technical evaluation of the results showed uniformly excellent structural preservation, including the connectome, under electron microscope examination.[2371] In ASC, the tissue is perfused with a glutaraldehyde-based chemical fixative[2372] that fixes proteins in place by covalent crosslinks. The relatively lengthy glutaraldehyde molecule deforms protein alpha helices, irreversibly bridges and links distant pairs of proteins, and even "glues up proteins' phosphorylation state."[2373] Perry reports[2374] that the "cross-linking causes specific changes which raise concerns, including denaturing of proteins, washing away of small molecules such as neurotransmitters, and fraying of the myelin sheaths that enclose nerve fibers," and mentions[2375] a possible additional concern about "defatting" during ASC.

[2366] Monsan P, Puzo G, Marzarguil H. Etude du mecanisme d'etablissement des liaisons glutaraldehyde-proteines. Biochimie 1975 Feb 14;57(11-12):1281-1292; https://www.sciencedirect.com/science/article/abs/pii/S0300908476805408.

[2367] Kiernan JA. Formaldehyde, Formalin, Paraformaldehyde And Glutaraldehyde: What They Are And What They Do. Microscopy Today 2000 Jan;8(1):8-13; https://publish.uwo.ca/~jkiernan/formglut.htm.

[2368] Sabatini DD, Bensch K, Barrnett RJ. Cytochemistry and electron microscopy. The preservation of cellular ultrastructure and enzymatic activity by aldehyde fixation. J Cell Biol. 1963 Apr 1;17(1):19-58; https://core.ac.uk/download/pdf/7808374.pdf.

[2369] McIntyre RL, Fahy GM. Aldehyde-stabilized cryopreservation. Cryobiology. 2015 Dec;71(3):448-58; https://www.sciencedirect.com/science/article/pii/S001122401500245X.

[2370] "Using a combination of ultrafast glutaraldehyde fixation and very low temperature storage, researchers have demonstrated for the first time…a way to preserve a brain's connectome (the 150 trillion synaptic connections presumed to encode all of a person's knowledge) for centuries-long storage in a large mammal….Extensive 3D electron microscopy alongside detailed evaluation by the BPF's judging committee was performed to verify the quality of connectome preservation following rewarming of the pig brain from cold storage." https://www.brainpreservation.org/large-mammal-announcement/.

[2371] https://www.brainpreservation.org/21cm-aldehyde-stabilized-cryopreservation-eval-page/.
[2372] https://en.wikipedia.org/wiki/Fixation_(histology)#Crosslinking_fixatives_%E2%80%93_aldehydes.
[2373] https://www.statnews.com/2019/01/30/nectome-brain-preservation-redemption/.

[2374] Perry RM. Viability versus Inferability: A Plea to Consider an Option of Fixative-Stabilized Cryopreservation. Cryonics 2018 Mar-Apr;39(2):24-34; https://www.alcor.org/docs/cryonics-magazine-2018-02.pdf.

[2375] "Typically, the process starts with an aldehyde-fixed specimen in aqueous solution. The specimen is placed in acetone, and successive changes of the bath remove water and fats. Finally the resin monomer is introduced, the remaining acetone is removed by vacuum, and induced catalysis yields the desired polymerization. Concerns have been raised about whether defatting would obliterate important brain information, though there does not appear to be strong evidence of this." [*]
[*] Perry RM. The road less traveled: Alternatives to Cryonics. Cryonics 2007 Qtr 3;28(3):21-24; https://www.alcor.org/docs/cryonics-magazine-2007-03.pdf.

However, another source[2376] claims that pH-based timing of the crosslinking activity during perfusion can produce a "uniform glutaraldehyde-based hydrogel" throughout a rat brain that evidences continued activity of key neuronal proteins associated with memory,[2377] supporting the proposition that "glutaraldehyde crosslinking is unlikely to dramatically change the structure of key proteins and molecules in the brain."

The extent of ASC-based molecular alterations should be closely examined in ***future research***. Since a fixed brain is still chemically active at normal (e.g., room) temperatures and can undergo chemical and morphological degradation over long storage times, in ASC the fixed brain must then be perfused with high concentrations of cryoprotectants to enable vitrification and is then cooled to cryogenic temperatures – "[f]ixation is also known to increase freezing damage if cryoprotectant penetration is inadequate, further adding to the risk of using fixation under non-ideal conditions that are common in cryonics."[2378]

Biological tissues of patients who have been cryopreserved using ASC may require significantly more data processing during molecular reconstruction to determine their original healthy state as compared to conventionally cryopreserved tissue. During a revival from ASC, the Digital Repair Algorithm (Section 5.2.2.2) must recognize, in addition to the many normal sources of damage, all cross-linking bonds caused by the introduction of glutaraldehyde (which can displace existing bonds), then correctly subtract their influence from the initial scan file, and then computationally reverse any steric distortions that were induced either by the physical intrusion of fixative molecules or by the formation of numerous unnatural covalent bonds during the fixation process.[2379] The amount of extra computation is presently unknown but could range from 2-10 times more than in the case of non-cross-linked conventional cryopreservations, depending on the exact manner of crosslinking, the number of molecules that are cross-linked, and the number of cross-links per molecule. The specific requirements and extent of these additional computations should be further investigated in ***future research***.

Once the corrected scan file has been created, the molecular reconstruction of the ASC cryopatient could proceed using any of the methods described in Section 5.2.3 or Section 5.3.3.

Ken Hayworth's Brain Preservation Foundation[2380] approves of the concept of ASC for brain preservation: "BPF is a nonprofit research organization, and our mission is to promote scientific research and services development of whole brain preservation for long-term static storage. This is presently very important for

---

[2376] https://www.brainpreservation.org/how-much-protein-structure-loss-is-there-following-glutaraldehyde-crosslinking/.

[2377] Murray E, Cho JH, Goodwin D, Ku T, Swaney J, Kim SY, Choi H, Park YG, Park JY, Hubbert A, McCue M, Vassallo S, Bakh N, Frosch MP, Wedeen VJ, Seung HS, Chung K. Simple, Scalable Proteomic Imaging for High-Dimensional Profiling of Intact Systems. Cell. 2015 Dec 3;163(6):1500-14; https://www.ncbi.nlm.nih.gov/pmc/articles/PMC5275966/.

[2378] "Groundbreaking Scientific Results," Cryonics 2016 Mar-Apr;37(2):17-20; https://www.alcor.org/docs/cryonics-magazine-2016-02.pdf.

[2379] According to the official Alcor response* to the ASC research: "While ASC produces clearer images than current methods of vitrification without fixation, it does so at the expense of being toxic to the biological machinery of life by wreaking havoc on a molecular scale. Chemical fixation results in chemical changes (the same as embalming) that are extreme and difficult to evaluate in the absence of at least residual viability. Certainly, fixation is likely to be much harder to reverse so as to restore biological viability as compared to vitrification without fixation. Fixation is also known to increase freezing damage if cryoprotectant penetration is inadequate, further adding to the risk of using fixation under non-ideal conditions that are common in cryonics. Another reason for lack of interest in pursuing this approach is that it is a research dead end on the road to developing reversible tissue preservation in the nearer future."

* More M. Alcor Position Statement on Brain Preservation Foundation Prize. Alcor blog, 12 Feb 2016; https://www.alcor.org/2016/02/alcor-position-statement-on-brain-preservation-foundation-prize/.

[2380] https://www.brainpreservation.org/.

scientific and medical brain banking and connectomics research. If useful information (memories, at least) is validated to be contained in preserved brains, by a minority neuroscience consensus on relevant structural preservation and computer emulation, we will also advocate for services development for the general public, as an end of life option….The BPF does not currently support the offering of ASC, or any other preservation method, to human patients, and will not endorse any particular preservation services company, now or in the future."

Oregon Cryonics[2381] has chemically preserved the brains of at least 5 human patients,[2382] starting in 2015.[2383] Nectome,[2384] a research company, was formed in 2018 to "develop biological preservation techniques to better preserve the physical traces of memory",[2385] especially by employing techniques of glutaraldehyde fixation,[2386] but generated some controversy in the popular press.[2387]

Perry argues[2388] that ***future research*** exploring ASC, or more generally the fixative-stabilized cryopreservation (FSC) alternative, is warranted: "FSC offers possible advantages ranging from more rapid stopping of deterioration after arrest (effectively reducing ischemic exposure) to just the apparently better preservation so far observed in the case of ASC. FSC tissue should not deteriorate quickly on thawing like its NFC [no-fixation cryopreservation] counterpart but could remain stable for extended periods of days or more at above-freezing temperatures….I think that there are good reasons to be confident that fixation would not be an impediment to biological revival….it is not necessary that…cryopreserved tissues be 'viable' by some present-day criterion, [but rather] that it be possible in the future to infer what the healthy state of the patient was from the remains that were preserved."

De Wolf notes[2389] that "[c]onventional cryo, conventional chemo, and a combination of the two are the three most widely discussed options for human biopreservation. Other hypothetical possibilities include (A) vitrification using agents with much higher glass transition temperatures that permit warmer storage such as at dry ice temperature, (B) polyvitrification, in which high molecular weight polymers are used to stabilize the patient near or at room temperature, and (C) the use of molecular nanorobots to induce reversible biostasis [i.e., "nanostasis"; Section 7.1.6.5]."

[2381] http://www.oregoncryo.com/.

[2382] Perry RM. A Visit to Oregon Cryonics. Cryonics 2018 Jul-Aug;39(5):30-33; https://www.alcor.org/docs/cryonics-magazine-2018-02.pdf.

[2383] Yount J. Woman's Brain Chemically Preserved by Oregon Cryonics; OC Now Offering Both Cryonics and Chemical Preservation Services. Long Life Magazine 2015 Qtr 2;47(2):10-12, 16-20; https://immortalistsociety.org/LongLifeV47-02.pdf.

[2384] https://nectome.com/.
[2385] https://nectome.com/about-us/.
[2386] https://nectome.com/the-case-for-glutaraldehyde-structural-encoding-and-preservation-of-long-term-memories/.

[2387] Regalado A. A startup is pitching a mind-uploading service that is "100 percent fatal". MIT Technol Rev. 2018 Mar 13; https://www.technologyreview.com/2018/03/13/144721/a-startup-is-pitching-a-mind-uploading-service-that-is-100-percent-fatal/. Letzter R. Brain-Uploading Company Has No Immediate Plans to Upload Brains. LiveScience 2018 Apr 3; https://www.livescience.com/62212-nectome-grant-mit-founder.html. Begley S. After ghoulish allegations, a brain-preservation company seeks redemption. Stat News, 2019 Jan 30; https://www.statnews.com/2019/01/30/nectome-brain-preservation-redemption/.

[2388] Perry RM. Viability versus Inferability: A Plea to Consider an Option of Fixative-Stabilized Cryopreservation. Cryonics 2018 Mar-Apr;39(2):24-34; https://www.alcor.org/docs/cryonics-magazine-2018-02.pdf.

[2389] de Wolf A. Human Biopreservation Options: Advantages and Limitations. Cryonics 2016 Mar-Apr;37(2):5; https://www.alcor.org/docs/cryonics-magazine-2016-02.pdf.

To enhance public confidence in current non-chemical cryonics practices at Alcor, Cryonics Institute, and other service providers, Perry[2390] suggests that ***future research*** should "[c]omplete the study to show that present cryopreservation methods preserve the brain's connection architecture as well or nearly as well as the aldehyde-stabilized cryopreservation that satisfied Ken Hayworth….This is not to suggest that the aldehyde-stabilized cryopreservation that Hayworth favors is necessarily a bad idea, but only that current practices that do not use this method at least are also preserving the brain's ultrastructure at comparable levels."

To this end, in 2021 Greg Fahy reported[2391] that "recent research has shown that it is possible to achieve excellent ultrastructural preservation of the neuropil of the brain after perfusion with the 9.45M vitrification solution, M22, without prior aldehyde fixation. M22 perfusion normally results in a reduction of brain mass by up to almost 50% due to exosmosis of water, which makes brain ultrastructure difficult to discern at the usual level of detail familiar to neurobiologists, raising the question as to whether essential anatomical details are preserved or not. This question has been answered in the case of rabbit brains[2392] by controlling the washout of M22 from the brain. Removing about half of the M22 reverses much of the dehydration caused by M22 introduction, and this allows visualization of uniformly intact neural processes and synapses, with clearly demonstrable presynaptic vesicles and postsynaptic densities. Opening the blood-brain barrier with sodium dodecylsulfate prior to introduction of M22 results in less dehydration during M22 washout and extremely normal-appearing ultrastructure. Completing M22 washout at a standardized rate results in ultrastructural damage caused by osmotic swelling, the opposite of osmotic shrinkage during M22 introduction, but this can be prevented using an osmolyte to counter the effect of retained intracellular M22 components during M22 washout. The ability to prevent swelling during M22 washout indicates that cell membranes are not only present but also retain their usual differential permeability to water and cryoprotectants."

"During M22 loading without pre-fixation, distortions of myelin sheaths can sometimes be seen, and separation between the neuropil and larger blood vessels can also sometimes be seen, but these do not represent significant information loss events. Further, humans may not experience these same distortions. Although it has not yet been possible to adequately evaluate the ultrastructure of human brains after partial washout of M22, it was recently possible to evaluate human brain histology and low and high magnification ultrastructure after perfusing slightly concentrated (102-105%) M22. The results showed uniformly preserved histological and ultrastructural integrity, without the myelin and vascular distortions seen in rabbits, although with typical dehydration. To observe ultrastructural detail despite the presence of significant dehydration, very high power electron microscopy (on the order of 20,000X magnification) was employed, and showed the persistence of intact neural processes and synapses despite the considerable shrinkage experienced."

7.1.6 Suspended Animation

Suspended animation, both in science[2393] and science fiction,[2394] refers to the halting of all metabolic and biological degradative processes in a human body, producing reversible human hibernation.[2395]

[2390] Perry RM. Cryonics and Public Skepticism: Meeting the Challenges to Our Credibility. Cryonics 2019 Qtr 4;40(4):24-37; https://www.alcor.org/docs/cryonics-magazine-2019-04.pdf.

[2391] Personal communication from Greg Fahy to Robert Freitas, 6 Oct 2021.

[2392] Fahy GM, Wowk BG, Vargas V, Hixon H, Graber S, Drake A, Thomson B, Roas R, Ge X, Olivos A, Harris SB, Coles LS. Ultrastructural Cryopreservation of the Mammalian Brain. In preparation, 2022.

[2393] https://en.wikipedia.org/wiki/Suspended_animation.

"Suspended animation is the temporary (short- or long-term) slowing or stopping of biological function so that physiological capabilities are preserved. It may be either hypometabolic or ametabolic in nature. It may be induced by … endogenous, natural or artificial biological, chemical or physical means. In its natural form it may be spontaneously reversible as in the case of species demonstrating hypometabolic states of hibernation or require technologically mediated revival when applied with therapeutic intent in the medical setting as in the case of deep hypothermic circulatory arrest."[2396]

Cryonicists sometimes assert that achieving human suspended animation should be the ultimate goal of cryonics organizations.[2397] Notes Aschwin de Wolf:[2398] "One silly premise of contemporary medicine that has got to go is the prevailing practice of abandoning people who can no longer be treated by today's technologies. What may appear irreversible now may be treatable in the future. But we want to place these patients in cryostasis in the most viable state. Ultimately our aim is widespread recognition for placing critically ill people in suspended animation until a cure for their disease is found. Instead of saying 'look how good the structure of this patient's brain looks', we should aim for a situation in which we can say 'this patient is in the same condition as when (s)he was admitted to us but now we have hundreds of years to think about a sensible treatment'." Along these lines, ***future research*** should seek pathways to achieving true suspended animation where minimal repairs are needed to the body, as this maximizes the likely percentage recovery of personal identity upon repair and revival.

In this Section we briefly review human hibernation (Section 7.1.6.1), chemical biostasis (Section 7.1.6.2), cryptobiosis (Section 7.1.6.3), hypothermic biostasis (Section 7.1.6.4), and nanostasis or warm biostasis (Section 7.1.6.5). Suspended animation is generally assumed to be fully reversible, so revival from suspended animation would only require the employment of conventional medical nanorobots to correct any pathology or trauma that might have caused the patient to be placed in suspension in the first place,[2399] followed by the normal reversal of whatever animation suspension process had been employed.

Note that patients in noncryogenic suspended animation may remain susceptible to microbial attack or parasitic invasion (or other physical misadventure), thus their inert bodies must be protected from these threats by various means (e.g., storage in a protective container, immersion in an inert or biostatic atmosphere, etc.).

[2394] https://en.wikipedia.org/wiki/Suspended_animation_in_fiction.

[2395] Nordeen CA, Martin SL. Engineering Human Stasis for Long-Duration Spaceflight. Physiology (Bethesda). 2019 Mar 1;34(2):101-111; https://journals.physiology.org/doi/pdf/10.1152/physiol.00046.2018.

[2396] https://en.wikipedia.org/wiki/Suspended_animation.

[2397] Donaldson T. Suspended Animation → Cryonics. Cryonics 1997 Qtr 4;18(4):39, 46; https://www.alcor.org/docs/cryonics-magazine-1997-04.pdf. More M. Maximizing Revival Probability: Preservation, Recording, Interpolation, and Reconstruction. Symposium on Resuscitation and Reintegration of Cryonics Patients, Portland OR, 12 May 2013; https://www.facebook.com/events/351957221581992/. de Wolf A. Cryonics Without Repair: Why Reversible Cryopreservation Matters. Cryonics 2013 Aug;34(8):11-13; https://www.alcor.org/docs/cryonics-magazine-2013-08.pdf. de Wolf A. Suspended Animation as a Research Goal and Case Benchmark. Cryonics 2015 Dec;36(12):5; https://www.alcor.org/docs/cryonics-magazine-2015-12.pdf.

[2398] de Wolf A. Killing Yourself to Live. Cryonics 2014 Jun;35(6):5; https://www.alcor.org/docs/cryonics-magazine-2014-06.pdf.

[2399] Freitas RA Jr. Chapter 23. Comprehensive Nanorobotic Control of Human Morbidity and Aging. In: Fahy GM, West MD, Coles LS, Harris SB, eds, The Future of Aging: Pathways to Human Life Extension, Springer, New York, 2010, pp. 685-805; http://www.nanomedicine.com/Papers/Aging.pdf.

7.1.6.1 Human Hibernation

Hibernation is generally defined as a state of metabolic depression with minimal physical activity, often accompanied by low body temperature, slow breathing, and slow heart rate.[2400] It occurs naturally in small primates,[2401] bears,[2402] ground squirrels[2403] and rodents. Obligate hibernators (squirrels, rodents, hedgehogs, monotremes and marsupials) spontaneously and annually enter hibernation regardless of ambient temperatures and food supply.[2404] Facultative hibernators (such as black-tailed prairie dogs) enter hibernation only when cold-stressed or food-deprived.[2405]

Hibernation in humans is being actively studied[2406] but has not yet been achieved.[2407] The primary focus of research for human hibernation is to reach a state of torpor, defined as a gradual physiological inhibition to reduce oxygen demand and obtain energy conservation by hypometabolic behaviors altering biochemical processes.[2408] There were early suggestions[2409] that "anti-metabolite" chemicals could be injected into the bloodstream of mammals, bringing biological processes to a halt: "[O]xygen utilization in blood could be stopped by anti-metabolites and then started again by appropriate antidotes, without injury to the animals involved. Probably several types of anti-metabolites would be required to reduce all the major activities pertinent to aging in cells, including anaerobic reactions using carbon dioxide in place of oxygen." In

---

[2400] https://en.wikipedia.org/wiki/Hibernation

[2401] Storey KB. The Gray Mouse Lemur: A Model for Studies of Primate Metabolic Rate Depression. Preface. Genomics Proteomics Bioinformatics. 2015 Apr;13(2):77-80; https://www.ncbi.nlm.nih.gov/pmc/articles/PMC4511782/. See also: https://en.wikipedia.org/wiki/Fat-tailed_dwarf_lemur#Hibernation.

[2402] https://en.wikipedia.org/wiki/Hibernation#Bears.

[2403] Andrews MT. Genes controlling the metabolic switch in hibernating mammals. Biochem Soc Trans. 2004 Dec;32(Pt 6):1021-4; https://pdfs.semanticscholar.org/578e/abf803a9c5b1527b45095fc4faadb6ccd030.pdf.

[2404] https://en.wikipedia.org/wiki/Hibernation#Obligate_hibernation.
[2405] https://en.wikipedia.org/wiki/Hibernation#Facultative_hibernation.

[2406] Lee CC. Is Human Hibernation Possible? Ann Rev Med. 2008 Feb;59:177-186; https://nature.berkeley.edu/garbelottoat/wp-content/uploads/lee2008-1.pdf. Pan M. Hibernation induction in non-hibernating species. Biosci Horizons 2018;11:hzy002; https://academic.oup.com/biohorizons/article/doi/10.1093/biohorizons/hzy002/4969915. Shi Z, Qin M, Huang L, Xu T, Chen Y, Hu Q, Peng S, Peng Z, Qu LN, Chen SG, Tuo QH, Liao DF, Wang XP, Wu RR, Yuan TF, Li YH, Liu XM. Human torpor: translating insights from nature into manned deep space expedition. Biol Rev Camb Philos Soc. 2020 Dec 14; https://www.researchgate.net/profile/Zhe-Shi/publication/347625129_Human_torpor_translating_insights_from_nature_into_manned_deep_space_expedition/links/5fe93920299bf14088504459/Human-torpor-translating-insights-from-nature-into-manned-deep-space-expedition.pdf. Soo E, Welch A, Marsh C, McKay DB. Molecular strategies used by hibernators: Potential therapeutic directions for ischemia reperfusion injury and preservation of human donor organs. Transplant Rev (Orlando). 2020 Jan;34(1):100512; https://www.ncbi.nlm.nih.gov/pmc/articles/PMC7141767/.

[2407] There is one recent unconfirmed report of possible natural hibernation in an extinct ice-age hominin species. Bartsiokas A, Arsuaga JL. Hibernation in hominins from Atapuerca, Spain half a million years ago. L'Anthropologie 2020 Dec;124(5):102797; https://www.sciencedirect.com/science/article/abs/pii/S0003552120300832.

[2408] https://en.wikipedia.org/wiki/Suspended_animation#Human_hibernation.

[2409] Cryonics of California, Feb 1967, pp. 13-15 (Cryonics Society of California newsletter); cited in: Perry RM. Cryonics Newsletters: Some Historical Highlights, Part 3, Cryonics Society of California. Cryonics 2018 Nov-Dec;39(6):20-36; https://www.alcor.org/docs/cryonics-magazine-2018-06.pdf.

modern medicine, antimetabolites[2410] are chemicals that inhibit the use of a particular metabolite that is a part of normal metabolism. "Such substances are often similar in structure to the metabolite that they interfere with, such as the antifolates that interfere with the use of folic acid; thus, competitive inhibition can occur, and the presence of antimetabolites can have toxic effects on cells, such as halting cell growth and cell division, so these compounds are used as chemotherapy[2411] for cancer." Unfortunately, there are tens of thousands of metabolites. Even if large numbers of different antimetabolites could be created and launched simultaneously, unless most metabolites could be inhibited at the same time with all chemicals producing similar and effective levels of inhibition, the result would likely be catastrophic.

Aschwin de Wolf[2412] ably summarized the state of induced hibernation research as of about a decade ago:

> "Producing a hibernating state in humans after cardiac arrest seems to be a formidable challenge considering the complex and multifactorial biochemical changes of hibernating animals during the hibernation cycle. Hibernators prepare for dormancy, or torpor, by increasing food intake and storage and by decreasing physical activity. Entrance into torpor is marked by lowering of the hypothalamic temperature setpoint, depression of metabolic activity, sequestering of leukocytes, and a decrease in body temperature. During torpor, heart rate and respirations are substantially reduced….Typical changes in metabolic rate can range from 80% to nearly 100% in cryptobiotic animals, whose metabolic activities come to a reversible standstill."
>
> "A number of general criteria apply to all animals that survive long-term hypometabolic suppression: (1) controlled global metabolic rate suppression, (2) storage and alternate energy metabolism and limited production of toxic end products, (3) triggering and signaling transduction mechanisms to coordinate metabolic pathways between cells and organs, (4) reorganization of metabolic priorities and energy expenditure, (5) coordinated up-and-down regulation of genes, and (6) enhanced defense mechanisms such as increased production of antioxidants and stabilization of macromolecules.[2413] Hibernating animals prevent hypothermia-induced injury by maintaining membrane potentials, decreasing blood clotting, and limiting energy expenditures to basic physiological necessities at the expense of protein synthesis, gene transcription, and cell division. Selective up-and-down regulation of regulatory enzymes and rapid arousal from torpor is achieved by reversible phosphorylation."
>
> "Because aspects of hypometabolism have been induced in some non-hibernating animals by injecting them with the plasma of hibernating animals, some researchers have speculated that a 'hibernation induction trigger' (HIT) may exist that controls entry into hibernation. If such a molecule (or number of molecules) exists, it is tempting to think that administration in humans can produce hibernation on demand. Practical applications would range from stabilization of cardiac arrest and stroke victims to long-term space flight. Current investigations into HIT-like substances indicate involvement of opioid receptors."

[2410] https://en.wikipedia.org/wiki/Antimetabolite.

[2411] Peters GJ, van der Wilt CL, van Moorsel CJ, Kroep JR, Bergman AM, Ackland SP. Basis for effective combination cancer chemotherapy with antimetabolites. Pharmacol Ther. 2000 Aug-Sep;87(2-3):227-53; https://pubmed.ncbi.nlm.nih.gov/11008002/.

[2412] de Wolf A. Depressed Metabolism. Cryonics 2007 Qtr 3;28(3):14-17; https://www.alcor.org/docs/cryonics-magazine-2007-03.pdf.

[2413] Storey KB, Storey JM. Tribute to P. L. Lutz: putting life on 'pause'--molecular regulation of hypometabolism. J Exp Biol. 2007 May;210(Pt 10):1700-14; https://jeb.biologists.org/content/jexbio/210/10/1700.full.pdf.

"The most promising HIT mimetic so far is the synthetic delta-opioid peptide DADLE ([D-Ala^2, D-Leu^5]-enkephalin).[2414] Administration of DADLE to a normothermic multiorgan block preparation was able to extend survival of organs to 46 hours, including the heart and liver.[2415] Using the same multiorgan block autoperfusion method, successful single canine lung transplantation after 24 to 33 hours was achieved when the lungs were preserved with woodchuck HIT-containing plasma.[2416] Hypothermic preservation time of the rat lung has been enhanced by adding DADLE to Euro-Collins solution.[2417] Improved function of hearts pretreated with HIT or DADLE after hypothermic storage [has] been reported for a number of non-hibernating species including rats, rabbits and swine." [2418]

"Although beneficial effects of DADLE have been reported in cortical neurons, investigations of DADLE as a neuroprotectant in global and forebrain ischemia have been limited to date. A 2006 study didn't find any improvement for pre-ischemic administration of DADLE in a forebrain ischemia rat model.[2419] In 2007 the Safar Center for Resuscitation Research reported that DADLE failed to improve neurological outcome in a deep hypothermic circulatory arrest rat model and even produced worse extracerebral organ injury for the highest dose administered (10 mg/kg). One explanation for these results is poor blood brain barrier (BBB) permeability of DADLE because of its unfavorable hydrophilicity and charge. A series of cyclic prodrugs of DADLE only improved BBB permeability in the presence of a P-glycoprotein inhibitor to prevent P-gP mediated efflux transporter activation. Bioconversion of the parent drug, however, was low.[2420] Alternatively, pre-ischemic cerebroventricular (ICV) administration of DADLE did confer neuroprotective benefits in a rat model of forebrain ischemia.[2421] As these results indicate, neuroprotective agents with high treatment potential do not necessarily have privileged access to the brain."

"Opioid receptor modulation in cerebral ischemia has proven to be a viable research direction but the results obtained with HIT-like substances do not seem to produce the multi-factorial and

---

[2414] https://en.wikipedia.org/wiki/DADLE.

[2415] Chien S, Oeltgen PR, Diana JN, Salley RK, Su TP. Extension of tissue survival time in multiorgan block preparation with a delta opioid DADLE ([D-Ala^2, D-Leu^5]-enkephalin). J Thorac Cardiovasc Surg. 1994 Mar;107(3):964-7; https://www.jtcvs.org/article/S0022-5223(94)70370-1/pdf.

[2416] Oeltgen PR, Horton ND, Bolling SF, Su TP. Extended lung preservation with the use of hibernation trigger factors. Ann Thorac Surg. 1996 May;61(5):1488-93; https://www.annalsthoracicsurgery.org/article/0003-4975(96)00108-7/pdf.

[2417] Wu G, Zhang F, Salley RK, Diana JN, Su TP, Chien S. delta Opioid extends hypothermic preservation time of the lung. J Thorac Cardiovasc Surg. 1996 Jan;111(1):259-67; https://www.sciencedirect.com/science/article/pii/S0022522396704245.

[2418] Sigg DC, Coles JA Jr, Gallagher WJ, Oeltgen PR, Iaizzo PA. Opioid preconditioning: myocardial function and energy metabolism. Ann Thorac Surg. 2001 Nov;72(5):1576-82; https://www.annalsthoracicsurgery.org/article/S0003-4975(01)03084-3/fulltext.

[2419] Iwata M, Inoue S, Kawaguchi M, Kurita N, Horiuchi T, Nakamura M, Konishi N, Furuya H. Delta opioid receptors stimulation with [D-Ala^2, D-Leu^5] enkephalin does not provide neuroprotection in the hippocampus in rats subjected to forebrain ischemia. Neurosci Lett. 2007 Mar 13;414(3):242-6; https://pubmed.ncbi.nlm.nih.gov/17207574/.

[2420] Ohe T, Sato M, Tanaka S, Fujino N, Hata M, Shibata Y, Kanatani A, Fukami T, Yamazaki M, Chiba M, Ishii Y. Effect of P-glycoprotein-mediated efflux on cerebrospinal fluid/plasma concentration ratio. Drug Metab Dispos. 2003 Oct;31(10):1251-4; https://pdfs.semanticscholar.org/2031/47add4b3dd9398bbd046851b7e7d6ec0e73a.pdf.

[2421] Su DS, Wang ZH, Zheng YJ, Zhao YH, Wang XR. Dose-dependent neuroprotection of delta opioid peptide [D-Ala2, D-Leu5] enkephalin in neuronal death and retarded behavior induced by forebrain ischemia in rats. Neurosci Lett. 2007 Aug 16;423(2):113-7; https://citeseerx.ist.psu.edu/viewdoc/download?doi=10.1.1.518.5438&rep=rep1&type=pdf.

> coordinated physiological effects of hypometabolism-mediated cytoprotection that can be observed in hibernating animals. Although induction of artificial hypometabolism in humans may be possible by pharmacologic modulation of conserved metabolic pathways with natural hibernators, it is doubtful that hibernation on demand will be possible anytime soon."

Research on the ability of DADLE[2422] and other means[2423] to induce hypometabolic stasis continues. Human hibernation, if it could be achieved, would require no special revival protocol involving systemic reparative activities, other than those conventional medical nanorobotic interventions which might be needed to reverse life-threatening medical pathologies that existed immediately prior to the induction of hibernation.

Hibernation does not seem to be a feasible useful approach in the case of a progressive worsening medical condition or serious trauma.

7.1.6.2 Chemical Biostasis

Chemically-induced biostasis is another possible approach to human hibernation. In some speculative or fictional writings, administration of a simple drug,[2424] inhalation of a special gas,[2425] eating a poisoned apple,[2426] or immersion in a favorite wine[2427] induces the state of suspended animation. Common anesthetic agents cause loss of consciousness but exhibit only minor effects on general body metabolism,[2428] though up to 50% suppression of local glucose metabolism in the brain does occur during

---

[2422] Colonna C, Dorati R, Conti B, Modena T, Biggiogera M, Spedito A, Genta I. Induction of an *in vitro* reversible hypometabolism through chitosan-based nanoparticles. J Microencapsul. 2011;28(4):229-39; https://pubmed.ncbi.nlm.nih.gov/21545314/.

[2423] Young JD, Taylor E. Meditation as a Voluntary Hypometabolic State of Biological Estivation. News Physiol Sci. 1998 Jun;13:149-153; https://pubmed.ncbi.nlm.nih.gov/11390779/. Liu S, Chen JF. Strategies for therapeutic hypometabothermia. J Exp Stroke Transl Med. 2012 Jan 1;5(1):31-42; https://www.ncbi.nlm.nih.gov/pmc/articles/PMC3811165/.

[2424] https://en.wikipedia.org/wiki/The_Sleeper_Awakes (novel, 1910); https://en.wikipedia.org/wiki/The_Man_Who_Awoke (novel, 1933); https://planetoftheapes.fandom.com/wiki/Icarus/Liberty_1 (film, 1968).

[2425] https://en.wikipedia.org/wiki/Buck_Rogers.
[2426] https://en.wikipedia.org/wiki/Snow_White.

[2427] From a 1773 personal letter* from Benjamin Franklin to Jacques Barbeu Dubourg: "I wish it were possible... [reference to experiments in which he revived flies drowned in Madeira wine]…to invent a method of embalming drowned persons, in such a manner that they might be recalled to life at any period, however distant; for having a very ardent desire to see and observe the state of America a hundred years hence, I should prefer to an ordinary death, being immersed with a few friends in a cask of Madeira, until that time, then to be recalled to life by the solar warmth of my dear country! But...in all probability, we live in a century too little advanced, and too near the infancy of science, to see such an art brought in our time to its perfection."
* Labaree LW, Bell WJ. Mr. Franklin: A Selection From His Personal Letters. Yale University Press, 1956, pp. 27-29; https://www.amazon.com/Mr-Franklin-Selection-Personal-Letters/dp/B003VZYTHQ/.

[2428] Carli F, Ramachandra V, Gandy J, Merritt H, Ford GC, Read M, Halliday D. Effect of general anaesthesia on whole body protein turnover in patients undergoing elective surgery. Br J Anaesth. 1990 Sep;65(3):373-9; https://pdfs.semanticscholar.org/50ef/3817f593b063d2cef15d45e8171705adbcca.pdf. Essén P, McNurlan MA, Wernerman J, Vinnars E, Garlick PJ. Uncomplicated surgery, but not general anesthesia, decreases muscle protein synthesis. Am J Physiol. 1992 Mar;262(3 Pt 1):E253-60; https://pubmed.ncbi.nlm.nih.gov/1550218/. Schricker T, Klubien K, Carli F. The independent effect of propofol anesthesia on whole body protein metabolism in humans. Anesthesiology. 1999 Jun;90(6):1636-42; https://pubs.asahq.org/anesthesiology/article/90/6/1636/38054.

anesthesia using halothane[2429] or propofol.[2430]

The inhalation administration of hydrogen sulfide[2431] or carbon monoxide – both known to be dangerous poisons at above-physiological levels – have been explored for inducing hypometabolism or hypoxia tolerance. One study found that mice who inhaled H_2S (80 ppm, 13 °C) for 6 hours entered a suspended-animation-like state, with metabolic rate reduced by 90% and body temperature falling to 15 °C; the effect was fully reversible when the mice were transferred into room air at room temperature.[2432] The effect could be confirmed in pigs[2433] but not in sheep,[2434] though the effect takes longer to manifest and is not as pronounced in large animals as in rodents. Infusion of soluble sodium sulfide salts such as hydrogen sulfide donor NaHS similarly reduces energy expenditure and temperature in rodent models.[2435] H_2S-based chemical hibernation is still being studied for possible use in human patients.[2436] Low-dose inhalation of carbon monoxide can also produce hypometabolism and hypoxia tolerance.[2437]

[2429] Alkire MT, Pomfrett CJ, Haier RJ, Gianzero MV, Chan CM, Jacobsen BP, Fallon JH. Functional brain imaging during anesthesia in humans: effects of halothane on global and regional cerebral glucose metabolism. Anesthesiology. 1999 Mar;90(3):701-9; https://pubs.asahq.org/anesthesiology/article/90/3/701/37843. Chen Y, Bao W, Liang X, Zhang J. Propofol Anesthesia Alters Spatial and Topologic Organization of Rat Brain Metabolism. Anesthesiology. 2019 Oct;131(4):850-865; https://pubs.asahq.org/anesthesiology/article/131/4/850/911.

[2430] Alkire MT, Haier RJ, Barker SJ, Shah NK, Wu JC, Kao YJ. Cerebral metabolism during propofol anesthesia in humans studied with positron emission tomography. Anesthesiology. 1995 Feb;82(2):393-403; https://pubs.asahq.org/anesthesiology/article/82/2/393/34837.

[2431] Wowk B. Is Hydrogen Sulfide the Secret to Suspended Animation? Cryonics 2005 Jul/Aug;26(4):20; https://www.alcor.org/docs/cryonics-magazine-2005-04.pdf.

[2432] Blackstone E, Morrison M, Roth MB. H_2S induces a suspended animation-like state in mice. Science. 2005 Apr 22;308(5721):518; http://li.mit.edu/Archive/Activities/PubFormat/Science/Brevia/Blackstone05.pdf.

[2433] Simon F, Giudici R, Duy CN, Schelzig H, Oter S, Gröger M, Wachter U, Vogt J, Speit G, Szabó C, Radermacher P, Calzia E. Hemodynamic and metabolic effects of hydrogen sulfide during porcine ischemia/reperfusion injury. Shock. 2008 Oct;30(4):359-64; https://pubmed.ncbi.nlm.nih.gov/18323742/.

[2434] Haouzi P, Notet V, Chenuel B, Chalon B, Sponne I, Ogier V, Bihain B. H_2S induced hypometabolism in mice is missing in sedated sheep. Respir Physiol Neurobiol. 2008 Jan 1;160(1):109-15; https://pubmed.ncbi.nlm.nih.gov/17980679/.

[2435] Aslami H, Pulskens WP, Kuipers MT, Bos AP, van Kuilenburg AB, Wanders RJ, Roelofsen J, Roelofs JJ, Kerindongo RP, Beurskens CJ, Schultz MJ, Kulik W, Weber NC, Juffermans NP. Hydrogen sulfide donor NaHS reduces organ injury in a rat model of pneumococcal pneumosepsis, associated with improved bio-energetic status. PLoS One. 2013 May 23;8(5):e63497; https://www.ncbi.nlm.nih.gov/pmc/articles/pmid/23717435/.

[2436] Wagner F, Asfar P, Calzia E, Radermacher P, Szabó C. Bench-to-bedside review: Hydrogen sulfide--the third gaseous transmitter: applications for critical care. Crit Care. 2009;13(3):213; https://www.ncbi.nlm.nih.gov/pmc/articles/pmid/19519960/. Asfar P, Calzia E, Radermacher P. Is pharmacological, H_2S-induced 'suspended animation' feasible in the ICU? Crit Care. 2014 Mar 18;18(2):215; https://www.ncbi.nlm.nih.gov/pmc/articles/pmid/25028804/. Merz T, Denoix N, Wepler M, Gäßler H, Messerer DAC, Hartmann C, Datzmann T, Radermacher P, McCook O. H_2S in acute lung injury: a therapeutic dead end(?). Intensive Care Med Exp. 2020 Dec 18;8(Suppl 1):33; https://www.ncbi.nlm.nih.gov/pmc/articles/pmid/33336306/.

[2437] Nystul TG, Roth MB. Carbon monoxide-induced suspended animation protects against hypoxic damage in *Caenorhabditis elegans*. Proc Natl Acad Sci U S A. 2004 Jun 15;101(24):9133-6; https://www.ncbi.nlm.nih.gov/pmc/articles/PMC428485/. Neto JS, Nakao A, Kimizuka K, Romanosky AJ, Stolz DB, Uchiyama T, Nalesnik MA, Otterbein LE, Murase N. Protection of transplant-induced renal ischemia-reperfusion injury with carbon monoxide. Am J Physiol Renal Physiol. 2004 Nov;287(5):F979-89; https://journals.physiology.org/doi/full/10.1152/ajprenal.00158.2004. Hartmann C, Nussbaum B, Calzia E, Radermacher P, Wepler M. Gaseous Mediators and Mitochondrial Function: The Future of Pharmacologically Induced Suspended Animation? Front Physiol. 2017 Sep 19;8:691; https://www.ncbi.nlm.nih.gov/pmc/articles/pmid/28974933/.

It has been pointed out[2438] that "only complete metabolic arrest constitutes real suspended animation. Such a state cannot be achieved in humans by the use of hydrogen sulfide (or its injectable derivatives) and requires either the use of extreme cold such as practiced through vitrification in cryonics or the use of advanced nanotechnology in warm biostasis (Section 7.1.6.5)."

7.1.6.3 Cryptobiosis

A few organisms are able to survive the slowing or halting of their metabolism in response to adverse external conditions, a process often called cryptobiosis[2439] (or occasionally "anabiosis"[2440]).

In anhydrobiosis,[2441] extreme desiccation halts metabolism survivably, most notably in seeds and plants, but also in many simple animal species including rotifers,[2442] tardigrades,[2443] brine shrimp and nematodes,[2444] and at least one insect species of chironomid.[2445] An 1862 novel[2446] explored the fictional idea of a human being who is preserved by desiccation at near freezing temperatures, and then returns to life. In 2020, researchers preserved nematodes in a suspended animation state of anhydrobiosis embedded in a solid blob of gallium metal (which melts at low temperature) for seven days, after which the worms were recovered alive.[2447]

In anoxybiosis,[2448] oxygen deprivation produces a seemingly inactive metabolic state that is survivable for months to decades in tardigrades, brine shrimp, copepods, nematodes, and sponge gemmules.

In chemobiosis and osmobiosis,[2449] tardigrades become immobile in response to high levels of environmental toxins. None of these are believed to be applicable to humans.

[2438] de Wolf A. The Purple Prose of Suspended Animation. Biostasis, 7 Dec 2008; https://www.biostasis.com/the-purple-prose-of-suspended-animation/.

[2439] https://en.wikipedia.org/wiki/Cryptobiosis.

[2440] This term has been used primarily by Russian authors. Soloviev M. From Anabiosis to Cryonics. Cryonics 1998 Qtr 3;19(3):21-26; https://www.alcor.org/docs/cryonics-magazine-1998-03.pdf.

[2441] https://en.wikipedia.org/wiki/Cryptobiosis#Anhydrobiosis.
[2442] https://en.wikipedia.org/wiki/Rotifer#Anhydrobiosis.
[2443] https://en.wikipedia.org/wiki/Tardigrade#Physiology.

[2444] Hibshman JD, Clegg JS, Goldstein B. Mechanisms of Desiccation Tolerance: Themes and Variations in Brine Shrimp, Roundworms, and Tardigrades. Front Physiol. 2020 Oct 23;11:592016; https://www.ncbi.nlm.nih.gov/pmc/articles/PMC7649794/.

[2445] https://en.wikipedia.org/wiki/Chironomidae#Anhydrobiosis_and_stress_resistance.

[2446] Edmond About. The Man With the Broken Ear. Ayer Co. Publisher, 1862; https://www.amazon.com/Broken-Science-Fiction-English-French/dp/0405062710. Reviewed in https://www.alcor.org/docs/cryonics-magazine-1994-04.pdf.

[2447] Contiliani DF, de Araújo Ribeiro Y, de Moraes VN, Pereira TC. *Panagrolaimus superbus* tolerates hypoxia within Gallium metal cage: implications for the understanding of the phenomenon of anhydrobiosis. J Nematol. 2020;52:1-6; https://www.ncbi.nlm.nih.gov/pmc/articles/pmid/32421263/.

[2448] https://en.wikipedia.org/wiki/Cryptobiosis#Anoxybiosis.

[2449] Møbjerg N, Halberg KA, Jørgensen A, Persson D, Bjørn M, Ramløv H, Kristensen RM. Survival in extreme environments - on the current knowledge of adaptations in tardigrades. Acta Physiol (Oxf). 2011 Jul;202(3):409-20; https://pubmed.ncbi.nlm.nih.gov/21251237/.

7.1.6.4 Hypothermic Biostasis

There are many reported cases of survival from accidental hypothermic cardiac arrest, defined as "cessation of circulation caused by hypothermia including ventricular fibrillation, ventricular tachycardia without pulse, pulseless electric activity and asystole…the presentation of severe [20-28 °C] and profound [<20 °C] accidental hypothermia is difficult to distinguish from clinical signs of death." A team of doctors at the University Hospital of North Norway (a country where accidents such as drowning in icy water are frequent) reported that 38% of hypothermic cardiac arrest patients survive resuscitation, the lowest temperature survived was 13.7 °C, and the longest time between cardiac arrest and the return of spontaneous circulation among survivors was 6.9 hours.[2450] (Note that shivering stops at about 30 °C, breathing at 25 °C, and the heart near 23 °C.) The record low temperature survival for a human dates back to 1955, when Suad Niazi at the University of Minnesota cooled a woman to only 9 °C in cardiac arrest for 45 minutes in an attempt to cure her cancer (she successfully recovered, but was not cured of cancer).[2451] Studies in large animals (e.g., pigs) have shown memory retention and absence of neurologic injury after 60 minutes at 10 °C,[2452] and recovery without neurologic abnormality in isolated cases after 3 hours of circulatory arrest at 0 °C.[2453] Brain activity is normally suspended (aka. "electrocerebral silence") at temperatures below 18 °C.[2454]
According to one research group:[2455] "Suspended animation is defined as the therapeutic induction of a state of tolerance to temporary complete systemic ischemia, i.e., protection-preservation of the whole organism during prolonged circulatory arrest (≥ 1 hr), followed by resuscitation to survival without brain

---

[2450] Hilmo J, Naesheim T, Gilbert M. Nobody is dead until warm and dead: prolonged resuscitation is warranted in arrested hypothermic victims also in remote areas – a retrospective study from northern Norway. Resuscitation. 2014 Sep;85(9):1204-11; https://core.ac.uk/download/pdf/82217869.pdf.

[2451] Niazi SA, Lewis FJ. Profound hypothermia in man; report of a case. Ann Surg. 1958 Feb;147(2):264-6; https://www.ncbi.nlm.nih.gov/pmc/articles/PMC1450560/pdf/annsurg01232-0140.pdf. Note that this was accomplished without cardiopulmonary bypass or blood substitutes, which is how induced deep hypothermic circulatory arrest (DHCA) is done today; https://en.wikipedia.org/wiki/Deep_hypothermic_circulatory_arrest.

[2452] Alam HB, Bowyer MW, Koustova E, Gushchin V, Anderson D, Stanton K, Kreishman P, Cryer CM, Hancock T, Rhee P. Learning and memory is preserved after induced asanguineous hyperkalemic hypothermic arrest in a swine model of traumatic exsanguination. Surgery. 2002 Aug;132(2):278-88; http://citeseerx.ist.psu.edu/viewdoc/download?doi=10.1.1.886.9931&rep=rep1&type=pdf.

[2453] Haneda K, Thomas R, Sands MP, Breazeale DG, Dillard DH. Whole body protection during three hours of total circulatory arrest: an experimental study. Cryobiology. 1986 Dec;23(6):483-94; https://pubmed.ncbi.nlm.nih.gov/3802887/.

[2454] Stecker MM, Cheung AT, Pochettino A, Kent GP, Patterson T, Weiss SJ, Bavaria JE. Deep hypothermic circulatory arrest: I. Effects of cooling on electroencephalogram and evoked potentials. Ann Thorac Surg. 2001 Jan;71(1):14-21; https://www.annalsthoracicsurgery.org/article/S0003-4975(00)01592-7/fulltext.

[2455] Bellamy R, Safar P, Tisherman SA, Basford R, Bruttig SP, Capone A, Dubick MA, Ernster L, Hattler BG Jr, Hochachka P, Klain M, Kochanek PM, Kofke WA, Lancaster JR, McGowan FX Jr, Oeltgen PR, Severinghaus JW, Taylor MJ, Zar H. Suspended animation for delayed resuscitation. Crit Care Med. 1996 Feb;24(2 Suppl):S24-47; https://pubmed.ncbi.nlm.nih.gov/8608704/. Safar P, Tisherman SA, Behringer W, Capone A, Prueckner S, Radovsky A, Stezoski WS, Woods RJ. Suspended animation for delayed resuscitation from prolonged cardiac arrest that is unresuscitable by standard cardiopulmonary-cerebral resuscitation. Crit Care Med. 2000 Nov;28(11 Suppl):N214-8; https://pubmed.ncbi.nlm.nih.gov/11098950/. Safar PJ, Tisherman SA. Suspended animation for delayed resuscitation. Curr Opin Anaesthesiol. 2002 Apr;15(2):203-10; https://pubmed.ncbi.nlm.nih.gov/17019202/. Nozari A, Safar P, Wu X, Stezoski WS, Henchir J, Kochanek P, Klain M, Radovsky A, Tisherman SA. Suspended animation can allow survival without brain damage after traumatic exsanguination cardiac arrest of 60 minutes in dogs. J Trauma. 2004 Dec;57(6):1266-75; https://pubmed.ncbi.nlm.nih.gov/15625460/.

damage. The objectives of suspended animation include: (a) helping to save victims of temporarily uncontrollable (internal) traumatic (e.g., combat casualties) or nontraumatic (e.g., ruptured aortic aneurysm) exsanguination, without severe brain trauma, by enabling evacuation and resuscitative surgery during circulatory arrest, followed by delayed resuscitation; (b) helping to save some nontraumatic cases of sudden death, seemingly unresuscitable before definite repair; and (c) enabling selected (elective) surgical procedures to be performed which are only feasible during a state of no blood flow." Induced hypothermia or deep hypothermic circulatory arrest (DHCA)[2456] has been employed in some open-heart surgeries as an alternative to heart-lung machines since the 1970s, but provides only a limited amount of time in which to operate and there is a risk of tissue and brain damage over prolonged periods.[2457]

Emergency Preservation and Resuscitation (EPR) [2458] "is an experimental medical procedure where an emergency department patient is cooled into suspended animation for an hour to prevent incipient death from ischemia, such as the blood loss following a shooting or stabbing. DHCA induces hypothermia to aid preplanned surgery, whereas EPR is an emergency procedure in cases where an emergency department patient is rapidly dying from blood loss and will not otherwise survive long enough for the patient's wounds to be stitched up. In EPR, blood is replaced by a saline solution,[2459] and the patient is cooled into a suspended state where metabolism is slowed and brain activity ceases."

Drug-induced hypothermia can alleviate brain damage in cerebrovascular disease, with the following categories of existing drugs providing some cooling effects: (1) dopamine receptor agonists, (2) cannabis, (3) opioid receptors, (4) vanilloid receptors, (5) vasopressins (potent neurotensin receptor agonists), (6) thyroid drugs, (7) adenosine drugs, and (8) purine drugs.[2460]

Induced hypothermia could also be useful in space travel, as it could lessen the resources needed to sustain the life of the astronaut while reducing the psychological stresses from prolonged confinement.[2461] Rats can be synthetically induced into a hibernation-like state of torpor, characterized by decreased metabolic rate, reduced body temperature, and modest protection from ionizing radiation.[2462]

[2456] https://en.wikipedia.org/wiki/Deep_hypothermic_circulatory_arrest.

[2457] Kheirbek T, Kochanek AR, Alam HB. Hypothermia in bleeding trauma: a friend or a foe? Scand J Trauma Resusc Emerg Med. 2009 Dec 23;17:65; https://www.ncbi.nlm.nih.gov/pmc/articles/pmid/20030810/.

[2458] https://en.wikipedia.org/wiki/Emergency_Preservation_and_Resuscitation.

[2459] Helen Thomson, "Exclusive: Humans placed in suspended animation for the first time," New Scientist, 20 Nov 2019; https://www.newscientist.com/article/2224004-exclusive-humans-placed-in-suspended-animation-for-the-first-time/.

[2460] Ma J, Wang Y, Wang Z, Li H, Wang Z, Chen G. Neuroprotective Effects of Drug-Induced Therapeutic Hypothermia in Central Nervous System Diseases. Curr Drug Targets. 2017;18(12):1392-1398; https://pubmed.ncbi.nlm.nih.gov/28595536/.

[2461] Bradford JE, Talk D. Torpor Inducing Transfer Habitat for Human Stasis to Mars. NASA/NIAC Study, SpaceWorks, 2014 Feb; https://www.nasa.gov/sites/default/files/files/NIAC_Torpor_Habitat_for_Human_Stasis.pdf. Bradford J. Advancing Torpor Inducing Transfer habitats for Human Stasis to Mars, 2016 May 13; https://www.nasa.gov/feature/advancing-torpor-inducing-transfer-habitats-for-human-stasis-to-mars/. Nordeen CA, Martin SL. Engineering Human Stasis for Long-Duration Spaceflight. Physiology (Bethesda). 2019 Mar 1;34(2):101-111; https://journals.physiology.org/doi/pdf/10.1152/physiol.00046.2018. Choukèr A, Bereiter-Hahn J, Singer D, Heldmaier G. Hibernating astronauts-science or fiction? Pflugers Arch. 2019 Jun;471(6):819-828; https://www.ncbi.nlm.nih.gov/pmc/articles/PMC6533228/.

[2462] Tinganelli W, Hitrec T, Romani F, Simoniello P, Squarcio F, Stanzani A, Piscitiello E, Marchesano V, Luppi M, Sioli M, Helm A, Compagnone G, Morganti AG, Amici R, Negrini M, Zoccoli A, Durante M, Cerri M. Hibernation and Radioprotection: Gene Expression in the Liver and Testicle of Rats Irradiated under Synthetic Torpor. Int J Mol Sci. 2019 Jan 16;20(2):352; https://www.ncbi.nlm.nih.gov/pmc/articles/pmid/30654467/.

7.1.6.5 Nanostasis (Warm Biostasis)

Nanorobots can be used to halt metabolism in normothermic patients via nanostasis or "warm biostasis" – an idea that most closely approaches the age-old dream of fast and fully-reversible suspended animation.

To accomplish this objective, nanorobotic instrumentalities will be used to execute the molecular extraction process as previously described in Section 4.10 on a living patient. From **Table 9** in Section 4.10.1.9, and excluding cryoprotectants (which would not be present in a patient who is not being prepared for cryostasis), establishing complete metabolic biostasis may require the extraction of ~3922 gm of metabolic chemicals, or V_{met} ~ 3922 cm^3 assuming normal density of these materials, representing V_{met} / V_{body} ~ 6.5% of body volume, using ~7.63 x 10^{18} sorting rotors.

Two nanostasis procedures are readily distinguished:

(A) **Vasculoid Nanostasis.** In vasculoid nanostasis, the suspension patient is anesthetized and then receives an arteriovenous and lymphovascular installation of a vasculoid appliance as described in detail elsewhere (Section 4.6.2).[2463] Installation is a ~7 hour procedure that starts with patient sedation and femoral artery cannulation, then injection with heparin and drugs including antibiotics and various chemical agents to depress cell activity. This is followed by 4 hours of vascular washout (including general anesthesia, respirocyte infusion, temporary cooldown to 7-17 ^oC to reduce oxygen demand, and cardioplegia[2464]), ~1 hour of vascular plating and ~0.3 hour of vascular defluidization, finishing with ~1.2 hours of appliance initialization and cold start. At this point the patient is sedated but normothermic and breathing, with all blood transport functions being handled by the vasculoid – whose installation has included a sufficient number of extraction plates (Section 4.6.5(3)) to perform the necessary molecular extractions to come. In the next step, extraction plates extend hairlike extraction probes into the patient's tissues and cells, deploy their sorting rotors and appropriate pipeage (Section 4.10.1.9), and operate the molecule-selective pumps, carrying the extracted materials back to the vasculoid for removal by vasculoid fleet tankers (Section 4.10). All metabolically relevant molecules are extracted from the patient in ~1 hour consuming ~20 watts of power (**Table 9**), placing the patient in complete metabolic stasis and a state of reversible suspended animation, leaving the vasculoid appliance installed but on standby. This condition of stasis can be maintained indefinitely without accumulation of biological damage at room or normal body temperature under proper storage conditions (see below).

To reverse the vasculoid suspension process and waken the patient, the vasculoid is reactivated and used to instill nonactivating molecules[2465] of thousands of different types into desired cytosolic locations throughout the patient's body at the desired concentrations, using the same or similar plumbing as before (Section 4.13.2); if diffusion-limited, this process could take ~10 hours to complete. The vasculoid also instills ~3.5 trillion storage nanorobots carrying activating molecules. Upon being released into the tissue, over the next ~1 hour each storage nanorobot migrates to its target cell, enters that cell and parks there, then awaits the command to release its multimolecular cargo either into the cytosol or into specific cytoplasmic subcompartments inside the cell (Section 4.13.4). Once all storage nanorobots are in place, the vasculoid is uninstalled and replaced with a transfused blood substitute (Section 4.14.2), and the nanorobots are globally

---

[2463] Freitas RA Jr., Phoenix CJ. Vasculoid: A personal nanomedical appliance to replace human blood. J Evol Technol. 2002 Apr;11:1-139; Section 7 "Hypothetical Vasculoid Installation Scenarios"; http://www.jetpress.org/volume11/vasculoid.pdf.

[2464] https://en.wikipedia.org/wiki/Cardioplegia.

[2465] "Nonactivating molecules" are molecules that cannot initiate, activate, or sustain any biochemical activity on their own in the absence of other molecules, called "activating molecules," that provide the necessary energy to drive biochemical reactions (e.g., oxygen, glucose, ATP) or provide specific substrates that can be acted upon by various enzymes; Section 4.13.2.

commanded via acoustic signal to release their cargoes of activating molecules and then exit the body by conventional means (Section 4.14.3). Possibly with the assistance of ACLS (Advanced Cardiac Life Support)[2466] or other conventional means of resuscitation,[2467] the patient's body is now metabolically active. The patient's blood substitute is exchanged for manufactured genetically autologous natural blood (Section 4.14.4), and a last course of nanorobots can be introduced to remove the remaining bloodborne anesthetic agents, causing the patient to awaken from suspension animation in a revival procedure that might require 12-24 hours to complete.

(B) **Nanorobotic Nanostasis.** For patients who might view the vasculoid approach as unduly invasive, an alternative procedure is to infuse a large fleet of mobile storage nanorobots throughout the tissues and cells of the patient's body, powered by external ultrasound. The robot fleet must incorporate V_{met} ~ 3900 cm^3 of onboard storage volume. Assuming onboard tankage represents about two-thirds of the loaded volume of the mobile storage nanorobots, the fully-loaded nanorobot fleet volume is ~6000 cm^3, close to the recommended maximum ~10% volumetric intrusiveness limit for medical nanorobots in human tissue.[2468] We assume that a fleet of storage nanorobots with reconfigurable metamorphic surfaces[2469] can be compacted to ~2000 cm^3 when empty, which will be their volume when they are transiting into or out of the body – representing, for example, a fleet of 50 trillion nanorobots each of volume $V_{storagebots}$ ~ $V_{chromstorage}$ = 40 μm^3, perhaps measuring ~3 μm in diameter and ~6 μm in length. The nanorobots are coated with sorting rotors[2470] having binding sites for up to ~25,000 critical metabolic molecules as identified in Section 4.10. About 15 μm^2, or ~21% of the 71 μm^2 nanorobot surface area, is covered with 152,600 sorting rotors (each with a 98 nm^2 outward-oriented face; Section 4.10.1), which provides the storage robot fleet with the 7.63 x 10^{18} sorting rotors that it needs to perform a molecular extraction in ~1 hour. The 1372 nm^3 of sorting rotors in each nanorobot occupy only 0.2 μm^3 or ~0.5% of unloaded nanorobot volume.

To enter nanorobotic suspended animation, the patient would be sedated and cannulated, and the nanorobot fleet would be slowly infused into tissues and cells. Intravascular infusion of ~2 liters of compacted empty nanorobots (that can expand to ~6 liters when full) suspended in ~2 liters of carrier fluid may require ~7 hours at an infusion rate of ~10 cm^3/minute. Once in their assigned locations inside tissues or cells, the individual storage nanorobots simultaneously pump all target molecules out of the extracellular (Appendix J) or cytosolic (Appendix I) spaces in which they are parked and into the robots' internal tankage volume, executing the molecular extraction process described in Section 4.10 and placing the patient into a state of

---

[2466] https://en.wikipedia.org/wiki/Advanced_cardiac_life_support.

[2467] Contemporary ACLS normally involves a whole algorithm of medications, equipment, and procedures for restarting the heart, including CPR. A technology capable of the metabolic stasis induction and reversal described here would probably not require anything as crude as contemporary ACLS, given that an uninjured and properly oxygenated heart tends to naturally start beating. Once nanodevices reestablish normal homeostatic biochemical conditions, everything should just work, naturally. Notes Brian Wowk:* "I've seen hypothermic human hearts stored on ice just start beating again when reperfused with fresh, warm oxygenated blood. Sometimes they fibrillate and need an external countershock to reestablish synchronous rhythm, but I suspect that's pathological and wouldn't happen with a fully healthy restored heart."
* Personal communication from Brian Wowk to Robert Freitas, 30 Sep 2021.

[2468] Freitas RA Jr. Nanomedicine, Volume IIA: Biocompatibility, Landes Bioscience, Georgetown, TX, 2003; Section 15.6.1, "Somatic Intrusiveness"; http://www.nanomedicine.com/NMIIA/15.6.1.htm.

[2469] Freitas RA Jr. Nanomedicine, Volume I: Basic Capabilities, Landes Bioscience, Georgetown, TX, 1999; Section 5.3, "Metamorphic Surfaces"; http://www.nanomedicine.com/NMI/5.3.htm.

[2470] For comparison, the original ~1 μm diameter respirocyte design* included 29,160 sorting rotors on the hull of each device.
* Freitas RA Jr. Exploratory design in medical nanotechnology: a mechanical artificial red cell. Artif Cells Blood Substit Immobil Biotechnol. 1998 Jul;26(4):411-30; https://www.tandfonline.com/doi/pdf/10.3109/10731199809117682. A longer version of this paper appears at:
https://web.archive.org/web/20100420085137/http://www.foresight.org/Nanomedicine/Respirocytes.html.

reversible suspended animation in ~1 hour or less. Revival is accomplished in similar time frames and power levels by reversing the intake, probably in a carefully staged progressive manner to redistribute all essential biochemicals to their original locations, then extracting the nanorobots from the body over a period of many hours using nanapheresis,[2471] or in under an hour using nanorobot washout (Appendix M), or over longer times via self-extraction through the kidneys or other excretory organs. Final revival might again be accompanied by ACLS or other conventional means of resuscitation.

While dormant in suspended animation using either of the two methods described above, the unconscious nanostatic patient remains susceptible to attack by bacteria and other external parasites, but microbivore-class nanorobots (Section 1.2.2) can thwart this invasion both internally and externally to the body using devices that are powered without using metabolically active chemicals (e.g., via acoustic power). If the nanostatic patient is not stored in an ideal inert environment (e.g., pure nitrogen) but is kept in an oxygen-rich environment (e.g., ambient air), storage nanorobots would need to remain active to continually extract any oxygen or other metabolically relevant molecules that might enter the body through the skin or elsewhere. The body should also be kept warm by external means since it will be generating no endogenous heat other than vasculoid or nanorobot thermal emissions. ***Future research*** can undertake a comprehensive nanorobot and mission design for the nanostasis application.

Writes Aschwin de Wolf:[2472] "[W]arm biostasis would not only produce a true *molecular* alternative to cryonics, it would also enable long-duration space travel and could be employed as a means to provide trauma care in emergency situations. These kind[s] of applications of molecular nanotechnology are extremely advanced and, as a result, literature, either fiction or non-fiction, about them is virtually non-existent." After researching for his 2008 posting on warm biostasis,[2473] de Wolf opined that "an advanced nanotechnology might be able to achieve suspended animation by arresting metabolism and stabilizing cells at a molecular level," noting that (A) Drexler briefly described a related form of "reversible biostasis" in 1986,[2474] (B) Freitas coined the term "warm biostasis" in 1999,[2475] and (C) Globus *et al.* hinted at the possibility in 2004.[2476]

[2471] Freitas RA Jr. Nanomedicine, Volume I: Basic Capabilities. Landes Bioscience, Georgetown, TX, 1999, Section 10.3.6, "Buoyancy Control and Nanapheresis"; http://www.nanomedicine.com/NMI/10.3.6.htm.

[2472] De Wolf A. Warm Biostasis Through Nanotechnology. Biostasis, 1 May 2008; https://www.biostasis.com/warm-biostasis-through-nanotechnology/.

[2473] Personal communication between Robert Freitas and Aschwin de Wolf, 3 Mar 2008.

[2474] "[I]magine that the blood stream carries simple molecular devices to tissues, where they enter the cells. There they block the molecular machinery of metabolism – in the brain and elsewhere – and tie structures together with stabilizing cross-links. Other molecular devices then move in, displacing water and packing themselves solidly around the molecules of the cell. These steps stop metabolism and preserve cell structures. Because cell repair machines will be used to reverse this process, it can cause moderate molecular damage and yet do no lasting harm….If a patient in this condition were turned over to a present-day physician ignorant of the capabilities of cell repair machines,…[s]eeing no signs of life, the physician would likely conclude that the patient was dead.…"*
* Drexler KE. Engines of Creation: The Coming Era of Nanotechnology. Anchor Press/Doubleday, New York, 1986, Chapter 7 "Engines of Healing"; https://web.archive.org/web/20180722191948/http://e-drexler.com/d/06/00/EOC/EOC_Chapter_7.html.

[2475] Freitas RA Jr. Nanomedicine, Volume I: Basic Capabilities, Landes Bioscience, Georgetown, TX, 1999, p. 32; Table 1.4, "Medical Challenges of Increasing Difficulty and Possible Approaches"; http://www.nanomedicine.com/NMI/Tables/1.4.jpg.

[2476] "An extremely advanced nanotechnology might use molecular manipulations of each cell to provide (a) better methods of slowing or suspending the metabolic activity of crew members and (b) better methods of restoring metabolic activity to a normal state. when the destination is reached."*
* Globus A, Bailey D, Han J, Jaffe R, Levit C, Merkle R, Srivastava D. NASA Applications of Molecular Nanotechnology. J Brit Interplanet Soc. 1998;51:145-152; https://www.nas.nasa.gov/assets/pdf/techreports/1997/nas-97-029.pdf.

This book (Section 7.1.6.5) has now presented a workable technical proposal for achieving whole-body nanostasis or whole-body warm biostasis, aka. true suspended animation.

7.1.7 Revival from Frozen Genetic Material

The woolly mammoth became extinct about 4000 years ago,[2477] but numerous frozen specimens[2478] have been found with their soft tissues in good enough condition to allow their DNA to be extracted and completely sequenced,[2479] and efforts are underway to clone the creature and thus resurrect a formerly extinct species.[2480] Similarly, studies of the extinct New Zealand moa show that the long-term mitochondrial DNA (nonenzymatic) decay rate gives a half-life of ~7200 years for storage temperatures around 0 °C and ~10^{66} years for storage in LN2 (Section 3.2.4). The complete genome for a Neanderthal female, a member of a race of humans that went extinct ~40,000 years ago,[2481] was first reported in 2013,[2482] and the study of fossil[2483] or ancient DNA[2484] – and species resurrection or de-extinction[2485] – is a thriving research field.

It would be theoretically possible to grow a high-fidelity clone from even the smallest sample of the remains of a human frozen in tundra or mountain ice for thousands of years. The clone would be a genetic twin[2486] of the original person but would possess little of the original's personal identity, making this form of revival far less desirable than other methods described in this book.

[2477] https://en.wikipedia.org/wiki/Woolly_mammoth#Extinction.
[2478] https://en.wikipedia.org/wiki/Woolly_mammoth#Frozen_specimens.

[2479] Palkopoulou E, Mallick S, Skoglund P, Enk J, Rohland N, Li H, Omrak A, Vartanyan S, Poinar H, Götherström A, Reich D, Dalén L. Complete genomes reveal signatures of demographic and genetic declines in the woolly mammoth. Curr Biol. 2015 May 18;25(10):1395-400; https://www.ncbi.nlm.nih.gov/pmc/articles/PMC4439331/.

[2480] https://en.wikipedia.org/wiki/Revival_of_the_woolly_mammoth.
[2481] https://en.wikipedia.org/wiki/Neanderthal_extinction.

[2482] Prüfer K, Racimo F, Patterson N, Jay F, Sankararaman S, Sawyer S, Heinze A, Renaud G, Sudmant PH, de Filippo C, Li H, Mallick S, Dannemann M, Fu Q, Kircher M, Kuhlwilm M, Lachmann M, Meyer M, Ongyerth M, Siebauer M, Theunert C, Tandon A, Moorjani P, Pickrell J, Mullikin JC, Vohr SH, Green RE, Hellmann I, Johnson PL, Blanche H, Cann H, Kitzman JO, Shendure J, Eichler EE, Lein ES, Bakken TE, Golovanova LV, Doronichev VB, Shunkov MV, Derevianko AP, Viola B, Slatkin M, Reich D, Kelso J, Pääbo S. The complete genome sequence of a Neanderthal from the Altai Mountains. Nature. 2014 Jan 2;505(7481):43-9; https://www.ncbi.nlm.nih.gov/pmc/articles/pmid/24352235/.

[2483] https://en.wikipedia.org/wiki/Archaeogenetics.
[2484] https://en.wikipedia.org/wiki/Ancient_DNA.

[2485] Sandrine Ceurstemont. Resurrecting nature: Extinct is not forever. New Scientist, 22 Feb 2017; https://www.newscientist.com/article/mg23331140-600-resurrecting-nature-extinct-is-not-forever/.

[2486] https://en.wikipedia.org/wiki/Twin_study.

7.1.8 Whole-Body Backups

Everyone is familiar with the concept of backing up computer files.[2487] In this process, at least one copy of all data that is considered to be worth saving is stored on a separate memory device such as a CD, flash drive, or disk drive. If the computer is stolen or destroyed, or if the original memory becomes corrupted, the original data can be copied over from the backup memory into the original or a replacement computer, and the user's functionality is fully restored. By analogy, if a human being suffers serious brain damage or physical destruction, the availability of a datafile (e.g., Section 4.8.5 or Section 5.2.2.1) that completely describes their original body and brain would allow the missing person to be reconstituted with mind and body fully intact.[2488]

Access to whole-body backups becomes increasingly important for cryonicists who expect to live extremely long lives in biological or physical bodies, since the probability of a fatal accident or misadventure rises with time. If all age-related causes of death and ill-health could be eliminated by medical nanorobotics and if the remaining non-medical causes of death are distributed randomly across all calendar ages, then the rate of death R_{mort} is constant over any increment of time. The number of survivors N(t) at time t, starting from an initial population N_{pop} at time t = 0, can be estimated, using the standard exponential formula for an interval-constant decay rate, as $N(t) = N_{pop} \exp(-R_{mort} t)$, where $R_{mort} \sim 5.75 \times 10^{-4}$ deaths/person-year at the turn of the 21st century (summing deaths from accidents, suicides, homicide, war, and executions),[2489] giving a median healthspan of $\tau_{half} \sim \ln(2) / R_{mort} \sim 1200$ years.[2490] In other

---

[2487] https://en.wikipedia.org/wiki/Backup.

[2488] Restoration of a living person from a catastrophic accident using a backup file prepared during their lifetime will not recover any memories that were gained after the last backup file was created. Similarly, while a cryopreserved patient who is revived will awaken with his surviving memories intact, subsequent restoration of this patient from their revival data files after some post-revival catastrophic mishap also will not recover any new memories gained since the revival unless the patient has submitted to another living brain scan. ***Future research*** should investigate whether living scans might be made illegal if courts determine that the scanning method "kills" or might "kill" a human patient who is subjected to the procedure while still alive, raising potential issues of homicide or suicide.

[2489] Freitas RA Jr. Chapter 23. Comprehensive Nanorobotic Control of Human Morbidity and Aging, Section 7.3 "Maximum Human Healthspan and the Hazard Function". In: Fahy GM, West MD, Coles LS, Harris SB, eds, The Future of Aging: Pathways to Human Life Extension, Springer, New York, 2010, pp. 685-805; http://www.nanomedicine.com/Papers/Aging.pdf.

[2490] It has sometimes been asserted that in most cases of death by accident or misadventure, the body should be recoverable soon thereafter using the advanced forms of nanotechnology that will already be available for cryostasis revival as described elsewhere in this book, so the span of time one might expect to live in an advanced nanotechnical society before irreversibly perishing by accident might range from **69,315 years**[*] to ~**100,000 years**.[†] Unfortunately, this conclusion is incorrect because it neglects the future efficacy of the other non-accident forms of death – suicide, homicide, war, and execution – all of which may be expected to be conducted in a manner highly likely to succeed in causing permanent death, using the same tools of advanced nanotechnology. Excluding accidents (3.62×10^{-4} deaths/person-year) only reduces the U.S. death rate (ca. 1999) from $R_{mort} \sim 5.75 \times 10^{-4}$ deaths/person-year to $R_{mort} \sim 2.13 \times 10^{-4}$ deaths/person-year, giving a revised accident-free median healthspan of $\tau_{half} \sim \ln(2) / R_{mort} \sim$ **3250 years**. (We might anticipate the existence of backups in many future cases of homicide and war deaths, but not in cases of suicide and execution deaths.) Further discussion of the likely prevalence or future existence of the practices of suicide, homicide, war and execution in an advanced nanotechnical society is beyond the scope of this book, as are potential new forms of death[‡] also enabled by advanced nanotechnology that are not yet included in today's death rates.

[*] Hixon H. Misadventure as a Cause of Death in a Long-Lived Population. Cryonics 1988 May;9(5):20-23; https://www.alcor.org/library/misadventure-as-a-cause-of-death/.

[†] Donaldson T. A Brief Scientific Introduction to Cryonics. 1976; https://www.alcor.org/library/a-brief-scientific-introduction-to-cryonics/.

words, after about a millennium of life, even a medically amortal human is likely to suffer a potentially life-terminating event. When this occurs, it would be highly desirable to have a backup that would allow you to resume living.

Cryonicists who expect to live long lives as uploads embedded in robot bodies or computronium are subject to similar failure modes in the embedding physical substrate (e.g., power outages, meteor strikes, political instability, sabotage, etc.), and should also find backups very useful to have – especially brain backups.

Ralph Merkle sees a potential future business opportunity for Alcor: "After Alcor has discharged its current mission, that of reviving its patients, it might find that it is well positioned to carry out a new mission: that of providing backup services to its members. Indeed, after reviving current members Alcor will already have the necessary backup data for many of its newly awakened members under the scenarios envisioned here. Offering backup services as a component of the revival and reintegration package for awakened patients seems both obvious and useful to the patient. It represents a new opportunity for Alcor that could be offered to future members. Of course, backup services can only be provided if, at a minimum, a scan of the patient's entire brain has been conducted at a sufficient resolution to support restoration." [2491]

A less satisfying version of this process, called "sideloading" in the 2010 science fiction novel[2492] where it was first described, involves creating a computational model of the brain (that will serve as the "backup") while the original modeled brain is still alive. The computational model starts with a generic human mind model and is then customized by interacting with the original until it can precisely mimic all observable outputs of the original living mind: "Sideloading is the process of training a neural network to mimic a particular organic brain, based on a rich set of non-intrusive scans of the brain in action….[Y]ou can expose the living brain to all kinds of stimuli – words, images, sounds, tastes, smells – and see how they bounce around inside the skull. And it doesn't really matter how little external behavior is evoked if you can watch the pattern of internal changes…"[2493]

A related concept called the "mindfile" involves creating a model of a person based solely on extant or purposely recorded non-neural information from which their personal identity can be inferred and simulated,[2494] aka. a "reconstructed facsimile".[2495] Something similar has already been achieved in the field

---

‡ e.g., Freitas RA Jr. Some Limits to Global Ecophagy by Biovorous Nanoreplicators, with Public Policy Recommendations. Zyvex Corp. report, April 2000; http://www.rfreitas.com/Nano/Ecophagy.htm. Freitas RA Jr. Molecular Manufacturing: Too Dangerous to Allow? Nanotechnology Perceptions: A Review of Ultraprecision Engineering and Nanotechnology. 2006 Mar;2:15-24; http://www.rfreitas.com/Nano/MMDangerous.pdf. Freitas RA Jr. What Price Freedom? Nanotechnology Perceptions: A Review of Ultraprecision Engineering and Nanotechnology. 2006 May;2:99-106; http://www.rfreitas.com/Nano/WhatPriceFreedom.pdf.

[2491] Merkle RC. Revival of Alcor Patients. Cryonics 2018 May-Jun;39(3):10-19 and Cryonics 2018 Jul-Aug;39(4):10-15; https://www.alcor.org/library/revival-of-alcor-patients/.

[2492] Greg Egan. Zendegi. Gollancz, 2010; https://en.wikipedia.org/wiki/Zendegi.

[2493] Two earlier stories by the same author similarly describe a neural implant called a "jewel" – a small computer inserted into the brain at birth that monitors its activity in order to learn how to mimic its behavior. By adulthood, the jewel's simulation is a near-perfect predictor of the brain's activity and the jewel is given control of the person's body while the now-redundant brain is discarded. Prior to the replacement, it could form a backup with its data copied to other locations. See "Learning to be Me" (Interzone #37, Jul 1990) and "Closer" (Eidolon #9, Winter 1992), in: Greg Egan. Axiomatic. HarperPrism, 1995; https://www.amazon.com/Axiomatic-Short-Stories-Science-Fiction/dp/1597805408/.

[2494] Rothblatt M. The Terasem Mind Uploading Experiment. Intl J Machine Consciousness 2012;4(1):141-158; https://terasemcentral.org/docs/Terasem_Mind_Uploading_Experiment_IJMC.pdf. See also the CyBeRev Project; https://www.cyberev.org/.

[2495] https://hpluspedia.org/wiki/Technological_resurrection#Reconstructed_facsimiles.

of genetics, wherein the genome of a man who died in 1827 has been partially pieced together from fragments of his DNA found in hundreds of his modern-day descendants.[2496]

Not everyone assumes there will come a time when every possible brain injury will be real-time reversible without a long time needed to figure out the repair and memory recovery approach. Malfunctions of nanomedical devices themselves might be a particularly vexing example, as would contrived examples such as criminal assaults using nanodevices that deliberately encrypted brain contents. As Thomas Donaldson wrote:[2497] "Fundamentally, cryonic suspension isn't about freezing people whose conditions are clearly just a matter of time until we find a technology to deal with them. It's about freezing people whom we don't know how to cure or even if a cure will be possible. Someday almost certainly we'll have better means to preserve people, too. Freezing is only our current best means. But cryonics is about preservation, the need for which will always remain."

7.2 Validation of Cryopreservation Revival Procedures

Cryopreservation revival protocols can be validated in a variety of animal models, including primates (Section 7.2.1). Positive results from these tests should provide sufficient technical validation to warrant approval of the revival of cryopreserved human patients using the same protocols.

Under certain circumstances it may be necessary or desirable to obtain human test data on the revival protocol before applying it to human patients. A procedure that employs human whole-brain emulations (Section 7.2.2) may suffice in such circumstances.

7.2.1 Animal Testing Should Suffice

Once we have devised an experimental cryopreservation revival protocol that we think will work, how do we test it to be sure?

The obvious answer: test it on animals.[2498]

[2496] Jagadeesan A, Gunnarsdóttir ED, Ebenesersdóttir SS, Guðmundsdóttir VB, Thordardottir EL, Einarsdóttir MS, Jónsson H, Dugoujon JM, Fortes-Lima C, Migot-Nabias F, Massougbodji A, Bellis G, Pereira L, Másson G, Kong A, Stefánsson K, Helgason A. Reconstructing an African haploid genome from the 18th century. Nat Genet. 2018 Feb;50(2):199-205; https://pubmed.ncbi.nlm.nih.gov/29335549/.

[2497] Donaldson T. Prospects of a Cure for "Death". Cryonics 1990 May;11(5):26-36; https://www.alcor.org/library/prospects-of-a-cure-for-death/.

[2498] https://en.wikipedia.org/wiki/Animal_testing.

7.2.1.1 Simple Memory

In 2015, Vita-More and Barranco[2499] conclusively established that *C. elegans* nematode worms (image, right) can survive cooldown to LN2 temperature and then be warmed back to normal temperature, with their memory of a trained behavior intact.[2500] Of course, the memories of a worm are not very complex. We need to revive more complex animals to increase our trust in the result, which is consistent with the possibility of successful revival. More specifically, the procedure should be performed on a series of trained animals, eventually including mammals, to strengthen the conclusion that an experimental revival procedure can preserve memory, personality, and personal identity.

In other words, ***future research*** should "[c]arry out studies to demonstrate post-cryopreservation survival with memories for more advanced creatures than *C. elegans*." [2501]

7.2.1.2 Complex Memory

We can start with rodents such as rats or mice that have learned complex tasks such as how to run a maze,[2502] and verify that, like the worms, these small mammals remember whatever they've been taught, demonstrating retention of complex memories after experiencing cryopreservation, followed by a revival procedure. Mice[2503] (image, right) are the most commonly used mammalian experimental animals in psychology laboratory research because they share a high degree of homology with humans, are small and inexpensive, have a widely varied diet, are easily maintained, and can reproduce quickly.

Specific regulations must be followed for legal laboratory mouse testing.[2504]

[2499] Vita-More N, Barranco D. Persistence of Long-Term Memory in Vitrified and Revived *Caenorhabditis elegans*. Rejuvenation Res. 2015 Oct;18(5):458-463; https://www.ncbi.nlm.nih.gov/pmc/articles/PMC4620520/.

[2500] Interestingly, a previous suggestive study had found preliminary evidence that frozen and revived *C. elegans* worms could remember their pre-freeze preference for warmer or cooler environments. Gerry Arthus. Cryonic Research: The Worms That Turned. Alcor New York News, No. 4, May 1992; http://www.cs.cmu.edu/afs/cs/user/tsf/Public-Mail/cryonics/archive/790.

[2501] Perry RM. Cryonics and Public Skepticism: Meeting the Challenges to Our Credibility. Cryonics 2019 Qtr 4;40(4):24-37; https://www.alcor.org/docs/cryonics-magazine-2019-04.pdf.

[2502] https://en.wikipedia.org/wiki/Maze#Mazes_in_psychology_experiments.

[2503] https://en.wikipedia.org/wiki/Laboratory_mouse, https://en.wikipedia.org/wiki/Mouse#Laboratory_mice. Image source: Aaron Logan; https://en.wikipedia.org/wiki/Laboratory_mouse#/media/File:Lightmatter_lab_mice.jpg.

[2504] Public Health Service. PHS Policy on Humane Care and Use of Laboratory Animals. NIH/Office of Laboratory Animal Welfare, 2015; https://olaw.nih.gov/policies-laws/phs-policy.htm.

7.2.1.3 Personality

We could then proceed to highly intelligent mammals such as dogs (household pets that are generally more eager to please humans than are cats) who have learned to recognize their owner[2505] or trainer and are readily taught a large number of tricks and word associations. For example, one border collie[2506] (representative image, at right) demonstrably knew the labels of over 200 different items, inferred the names of novel things by exclusion learning, and correctly retrieved those new items both immediately and four weeks after the initial exposure.[2507] Another border collie reputedly learned the names and could associate by verbal command over 1,000 words.[2508]

Dogs can read and react appropriately to human body language such as gesturing, pointing, and human voice commands. They can also pick up emotional cues. In one study,[2509] researchers showed 31 dogs photos of threatening, pleasant, and neutral faces to see how they reacted, and found that dogs have some skill at determining human emotion by looking at a person's eyes and mouth. Besides these tests of specific memories and abilities, long-time pet owners know that their canine companions can: (1) express empathy,[2510] deception,[2511] and imitation;[2512] (2) develop demonstrable personalities[2513] that reflect how they interact with owners,[2514]

[2505] A 1998 science fiction book* describes a revival test in which a golden retriever dog is cryopreserved and then reanimated, whereupon the pet exhibits recognition of her human owner and remembers a few complicated tricks that she'd been taught: "Some 50 minutes later at 1:47 a.m. Wendy stirred. Her first movements seemed lethargic, but I knew that was normal when coming out of general anesthesia. Then she wagged her tail, bounded from the cart, and leapt into my welcoming arms. Yes. Lord, yes! She knew me! At least she still knew me. And for just that instant, it was enough…."
* James Halperin. The First Immortal: A Novel of the Future. Del Rey Books, 1998, p. 337; http://www.cryonics.org/images/uploads/misc/firstimmortal.pdf.

[2506] https://en.wikipedia.org/wiki/Rico_(Border_Collie).
[2507] https://en.wikipedia.org/wiki/Dog#Intelligence.

[2508] Pilley J. Chaser: Unlocking the Genius of the Dog Who Knows a Thousand Words. Houghton Mifflin Harcourt, 2013; https://www.amazon.com/Chaser-Unlocking-Genius-Knows-Thousand/dp/0544334590.

[2509] Somppi S, Törnqvist H, Kujala MV, Hänninen L, Krause CM, Vainio O. Dogs Evaluate Threatening Facial Expressions by Their Biological Validity--Evidence from Gazing Patterns. PLoS One. 2016 Jan 13;11(1):e0143047; https://www.ncbi.nlm.nih.gov/pmc/articles/PMC4711950/.

[2510] Custance D, Mayer J. Empathic-like responding by domestic dogs (*Canis familiaris*) to distress in humans: an exploratory study. Anim Cogn. 2012 Sep;15(5):851-9; https://research.gold.ac.uk/7074/2/Custance_and_Mayer_draft_prior_to_publication.pdf. Albuquerque N, Guo K, Wilkinson A, Savalli C, Otta E, Mills D. Dogs recognize dog and human emotions. Biol Lett. 2016 Jan;12(1):20150883; https://www.ncbi.nlm.nih.gov/pmc/articles/PMC4785927/. Huber A, Barber ALA, Faragó T, Müller CA, Huber L. Investigating emotional contagion in dogs (*Canis familiaris*) to emotional sounds of humans and conspecifics. Anim Cogn. 2017 Jul;20(4):703-715; https://www.ncbi.nlm.nih.gov/pmc/articles/PMC5486498/.

[2511] Heberlein MTE, Manser MB, Turner DC. Deceptive-like behaviour in dogs (*Canis familiaris*). Anim Cogn. 2017 May;20(3):511-520; https://pubmed.ncbi.nlm.nih.gov/28251387/.

[2512] Fugazza C, Pogány Á, Miklósi Á. Do as I … Did! Long-term memory of imitative actions in dogs (*Canis familiaris*). Anim Cogn. 2016 Mar;19(2):263-9; https://pubmed.ncbi.nlm.nih.gov/26498155/.

friends, strangers, and other animals; and (3) display characteristic unique behaviors when confronted with challenges or during play.[2515] A dog that replicated its usual idiosyncratic behaviors after experiencing cryopreservation and experimental revival would provide good evidence that the animal's personality had survived intact.[2516] Again, specific regulations must be followed for legal laboratory dog testing.[2517]

7.2.1.4 Personal Identity

Perhaps the most important aspect of personal identity is self-consciousness – an awareness of the self as an entity distinct from the rest of the universe. At least in the view of some,[2518] self-awareness is a higher order of mentation than consciousness: "To be conscious is to think; to be self-aware is to realize you are a thinking being and to think about your thoughts." The standard method for examining self-awareness in animals is the mirror-mark test,[2519] first developed for chimpanzees.[2520] While the mirror-mark test does not work with every individual chimp, and there has been controversy over its interpretation, the basic result of attention to the affected body part seems to be well established.[2521] Likewise, mirror self-

---

[2513] Ilska J, Haskell MJ, Blott SC, Sánchez-Molano E, Polgar Z, Lofgren SE, Clements DN, Wiener P. Genetic Characterization of Dog Personality Traits. Genetics. 2017 Jun;206(2):1101-1111; https://www.ncbi.nlm.nih.gov/pmc/articles/pmid/28396505/. Wallis LJ, Szabó D, Kubinyi E. Cross-Sectional Age Differences in Canine Personality Traits; Influence of Breed, Sex, Previous Trauma, and Dog Obedience Tasks. Front Vet Sci. 2020 Jan 14;6:493; https://www.ncbi.nlm.nih.gov/pmc/articles/pmid/31993445/. See also: https://en.wikipedia.org/wiki/Dog_behavior#Personalities and https://iheartdogs.com/dogs-have-these-5-major-personality-types/.

[2514] Kubinyi E, Turcsán B, Miklósi A. Dog and owner demographic characteristics and dog personality trait associations. Behav Processes. 2009 Jul;81(3):392-401; http://etologia.elte.hu/file/publikaciok/2009/Kubinyietal_2009.pdf.

[2515] Cassie, my smartest-ever golden retriever, demonstrated a rudimentary understanding of momentum conservation in collision dynamics. When I would roll a tennis ball along the floor toward a wall, she would give chase but immediately head for the future position in the middle of the room that the ball would occupy after it had bounced off the wall at an angle equal to the angle of incidence, rather than simply chasing the ball directly along its rolling path as all my other dogs have done.

[2516] In the mid-1980s, bloodless deep hypothermia experiments were performed on 6 dogs, who, once revived, showed "no neurological or other deficits" and demonstrated full "preservation of memory and personality".[*] In one example,[†] a dog was anesthetized, her blood removed and substituted with a pumped and continuously oxygenated solution at 4.5 °C for 4.7 hours with no signs of life; once resanguinated and rewarmed, after some complications the dog recovered and "remembered her name and her tricks".[‡]

[*] https://www.alcor.org/library/alcors-pioneering-total-body-washout-experiments/.

[†] Darwin M. Bringing Dixie Back – A Research Diary. Cryonics 1985 Feb;6(2):6-15; https://www.alcor.org/docs/cryonics-magazine-1985-02.txt.

[‡] http://www.cryonet.org/cgi-bin/dsp.cgi?msg=26438.

[2517] https://en.wikipedia.org/wiki/Animal_testing#Dogs.

[2518] Jabr F. Self-Awareness with a Simple Brain. Sci Amer Mind 2012;23(5):28-29; https://www.scientificamerican.com/article/self-awareness-with-a-simple-brain/. See also: https://blogs.scientificamerican.com/brainwaves/does-self-awareness-require-a-complex-brain/.

[2519] https://en.wikipedia.org/wiki/Mirror_test.

[2520] Gallup GG Jr. Chimpanzees: self-recognition. Science. 1970 Jan 2;167(3914):86-7; http://radicalanthropologygroup.org/sites/default/files/pdf/class_text_023.pdf.

[2521] Heyes CM. Reflections on self-recognition in primates. Animal Behav 1994 Apr;47(4):909-919; https://www.sciencedirect.com/science/article/abs/pii/S0003347284711237. Gallup GG, Povinelli DJ, Suarez SD, Anderson JR, Lethmate J, Menzel EW. Further reflections on self-recognition in primates. Animal Behav 1995 Jun;50(6):1525-1532; https://www.danielpovinelli.com/s/Gallup-et-al-1995.pdf.

awareness has been demonstrated in elephants.[2522] Despite the difficulties of carrying out parallel studies with an animal that cannot use its limbs to touch most parts of its body, there are several demonstrations that dolphins also respond by inspection to a mark placed on their body.[2523] Researchers currently know of no evidence that dogs respond to their image in a mirror, following marking, in the same way that chimpanzees, dolphins, and humans do,[2524] but dogs do appear able to recognize their selves as unique individuals via smell.[2525]

A different way of measuring animal self-awareness is through "mental time travel" – the ability to project oneself into past events, through episodic memory, or into future events, through episodic future thought, or planning.[2526] While there are as yet no direct studies of episodic-like memory in chimpanzees or dolphins, planning and intention in chimpanzees has been investigated. For example, in the laboratory, chimpanzees will produce tools for future use,[2527] and will direct their travels with apparent forethought within a computerized maze[2528] or in their home range in the wild.[2529] Pigs have been reported[2530] to show episodic-like memory in time-estimation experiments[2531] and in modified what-where-when tests.[2532] The latter test, when applied to dogs, revealed an ability to "retrieve 'what' and 'where' information about seen (but now

---

[2522] Plotnik JM, de Waal FB, Reiss D. Self-recognition in an Asian elephant. Proc Natl Acad Sci U S A. 2006 Nov 7;103(45):17053-7; https://www.ncbi.nlm.nih.gov/pmc/articles/pmid/17075063/.

[2523] Marten K, Psarakos S. Using self-view television to distinguish between self-examination and social behavior in the bottlenose dolphin (*Tursiops truncatus*). Conscious Cogn. 1995 Jun;4(2):205-24; https://earthtrust.org/archive/delart.html. Reiss D, Marino L. Mirror self-recognition in the bottlenose dolphin: a case of cognitive convergence. Proc Natl Acad Sci U S A. 2001 May 8;98(10):5937-42; https://www.ncbi.nlm.nih.gov/pmc/articles/PMC33317/.

[2524] Lea SEG, Osthaus B. In what sense are dogs special? Canine cognition in comparative context. Learn Behav 2018 Dec;46:335–363; https://link.springer.com/article/10.3758/s13420-018-0349-7.

[2525] Gatti RC. Self-consciousness: Beyond the looking-glass and what dogs found there. Ethology Ecology & Evolution 2016;28(2):232–240; https://www.tandfonline.com/doi/abs/10.1080/03949370.2015.1102777?journalCode=teee20. See also: http://en.tsu.ru/news/dogs-have-self-awareness-it-was-confirmed-by-stsr-tests/.

[2526] Suddendorf T, Corballis MC. Mental time travel and the evolution of the human mind. Genet Soc Gen Psychol Monogr. 1997 May;123(2):133-67; https://pubmed.ncbi.nlm.nih.gov/9204544/.

[2527] Bräuer J, Call J. Apes produce tools for future use. Am J Primatol. 2015 Mar;77(3):254-63; https://www.eva.mpg.de/documents/Wiley-Blackwell/Braeuer_Apes_AmJPrim_2015_2070243.pdf.

[2528] Beran MJ, Parrish AE, Futch SE, Evans TA, Perdue BM. Looking ahead? Computerized maze task performance by chimpanzees (*Pan troglodytes*), rhesus monkeys (*Macaca mulatta*), capuchin monkeys (*Cebus apella*), and human children (*Homo sapiens*). J Comp Psychol. 2015 May;129(2):160-73; https://www.ncbi.nlm.nih.gov/pmc/articles/PMC4437918/.

[2529] Ban SD, Boesch C, Janmaat KR. Taï chimpanzees anticipate revisiting high-valued fruit trees from further distances. Anim Cogn. 2014 Nov;17(6):1353-64; https://www.eva.mpg.de/documents/Springer/Ban_Tai-chimpanzees_AnimCog_2014_2043138.pdf. Janmaat KR, Polansky L, Ban SD, Boesch C. Wild chimpanzees plan their breakfast time, type, and location. Proc Natl Acad Sci U S A. 2014 Nov 18;111(46):16343-8; https://www.ncbi.nlm.nih.gov/pmc/articles/PMC4246305/.

[2530] Kouwenberg AL, Walsh CJ, Morgan BE, Martin GM. Episodic-like memory in crossbred Yucatan minipigs (*Sus scrofa*). Appl Animal Behav Sci. 2009 Mar;117(3-4):165-172; https://www.sciencedirect.com/science/article/abs/pii/S0168159109000240.

[2531] Fuhrer N, Gygax L. From minutes to days-The ability of sows (*Sus scrofa*) to estimate time intervals. Behav Processes. 2017 Sep;142:146-155; https://pubmed.ncbi.nlm.nih.gov/28735073/.

[2532] Clayton NS, Dickinson A. Episodic-like memory during cache recovery by scrub jays. Nature. 1998 Sep 17;395(6699):272-4; http://www2.cs.arizona.edu/projects/wonac/papers/clayton-3.pdf.

invisible) items from incidental memory formed during a single past experience,"[2533] but this was considered an incomplete demonstration of episodic memory.

Chimpanzees and bonobos (image, right)[2534] have cognitive capacities superior to those of dogs in self-consciousness, although dogs do better than chimpanzees at using the behavior of other animals, especially a human, as a cue.[2535] The logical animal model for the final phase of cryopreservation revival testing is probably a primate, given their physiological similarities to humans and their clear demonstration of self-awareness.

Ideal animal subjects may be trained primates who have been taught language skills using sign language. For example, Koko,[2536] a gorilla, was able to understand ~1000 signs in ASL (American Sign Language)[2537] and ~2000 spoken English words after perhaps ~6 years of training. She "never understood grammar or symbolic speech, and did not display any cognition beyond that of a 2-3 year old human child,"[2538] but "understood nouns, verbs, and adjectives, including abstract concepts like 'good' and 'fake'...and scored between 70 and 90 on various IQ scales…"[2539] Kanzi,[2540] a bonobo, is believed to understand more human language (after perhaps ~8 years of training) than any other non-human animal in the world.[2541] When animals like these are revived from cryopreservation, they can be tested on their memory of words, their ability to perform trained tasks, and their characteristic behaviors to determine the persistence of memory and personality. More importantly, these primates could, in principle, be directly interrogated to obtain answers to questions about their internal mental state – such as "how do you feel?" and "who are you?" to test if their sense of self has survived the revival procedure. ***Future research*** should review existing knowledge of animal language ability and determine if such questions would provide useful information for determining the success or failure of an experimental revival procedure, and if so, exactly how this might be done.

Lawful access to primates for medical testing has become more problematic in recent years. Laboratory testing of non-human primates such as chimpanzees[2542] remains legal in the U.S. but is severely restricted: In 2014 Merck announced that the company would no longer use chimpanzees for research, joining 20 pharmaceutical companies and contract laboratories that had made the commitment.[2543] In 2015, the U.S.

[2533] Fujita K, Morisaki A, Takaoka A, Maeda T, Hori Y. Incidental memory in dogs (*Canis familiaris*): adaptive behavioral solution at an unexpected memory test. Anim Cogn. 2012 Nov;15(6):1055-63; https://core.ac.uk/download/pdf/39287490.pdf.

[2534] Image Credit: Bonobo by Natataek at English Wikivoyage CC BY-SA 3.0, via Wikimedia Commons.

[2535] Lea SEG, Osthaus B. In what sense are dogs special? Canine cognition in comparative context. Learn Behav 2018 Dec;46:335–363; https://link.springer.com/article/10.3758/s13420-018-0349-7.

[2536] https://en.wikipedia.org/wiki/Koko_(gorilla).
[2537] https://en.wikipedia.org/wiki/American_Sign_Language.

[2538] Ristau CA, Robbins D. Language in the Great Apes: A Critical Review. Adv in the Study of Behav. 1982;12:141-255; https://www.sciencedirect.com/science/article/pii/S0065345408600480. See also: https://en.wikipedia.org/wiki/Great_ape_language#Koko.

[2539] https://en.wikipedia.org/wiki/Koko_(gorilla).
[2540] https://en.wikipedia.org/wiki/Kanzi.
[2541] https://en.wikipedia.org/wiki/Great_ape_language.
[2542] https://en.wikipedia.org/wiki/Animal_testing_on_non-human_primates#Chimpanzees_in_the_United_States.

[2543] Pet Grocery Market 2020 - Challenges and Opportunities Under COVID-19 Pandemic. 24 Jun 2020; https://happyandpolly.com/blogs/news/pet-grocery-market-2020.

Fish and Wildlife Service designated both captive and wild chimpanzees as endangered,[2544] and NIH announced it would no longer support biomedical research on chimpanzees, would release its remaining 50 chimpanzees to sanctuaries,[2545] and would phase out NIH support for the remaining chimps supported, but not owned, by NIH.[2546] It was estimated the remaining non-government-owned 1,000 chimpanzees would be retired to sanctuaries around 2020.[2547] The 'endangered' designation "effectively end[ed] invasive experiments on chimpanzees" in the U.S.,[2548] and non-human primate testing has been outright banned in many countries.[2549] Bonobos are found in the African Congo and are also considered to be an endangered species.[2550] Primate research is still legal in many parts of the world[2551] but remains unpopular with animal rights activists.

7.2.1.5 Nanorobot- and WBE-Based Animal Validations

A cryopreservation and revival protocol could be performed on any of the aforementioned animal models and tested using conventional external monitors such as EEG and other scalp electrodes, whose readings of brain activity before and after the procedure could be compared, ideally delivering identical results in the case of an accurate repair and revival. Indwelling brain electrodes could be implanted into the test animals to collect more extensive and direct data from deeper inside the brain, allowing similar before/after comparisons. However, these primitive brain monitoring techniques that are available today will have far less relevance in the future era of cryonics revivals when we can place one or more neurobots[2552] (marked with a black arrow in the image at right)

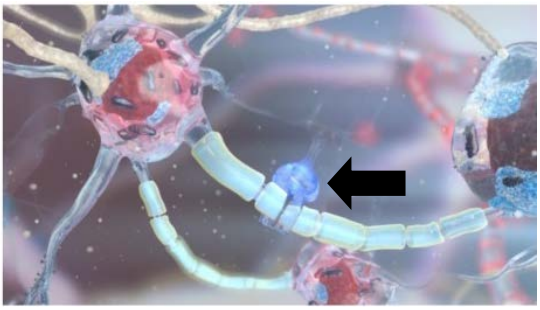

[2544] Grimm D. Research chimps to be listed as 'endangered'. Science Magazine, 12 Jun 2015; https://www.sciencemag.org/news/2015/06/research-chimps-be-listed-endangered. Endangered Species: Chimpanzee (*Pan troglodytes*). U.S. Fish and Wildlife Service, 19 Jun 2015; https://web.archive.org/web/20180123090709/https://www.fws.gov/endangered/what-we-do/chimpanzee.html.

[2545] NIH Will No Longer Support Biomedical Research on Chimpanzees. National Institutes of Health, 17 Nov 2015; https://www.nih.gov/about-nih/who-we-are/nih-director/statements/nih-will-no-longer-support-biomedical-research-chimpanzees.

[2546] Reardon S. NIH to retire all research chimpanzees. Nature News 2015 Nov 18; https://www.nature.com/news/nih-to-retire-all-research-chimpanzees-1.18817.

[2547] Pet Grocery Market 2020 - Challenges and Opportunities Under COVID-19 Pandemic. 24 Jun 2020; https://happyandpolly.com/blogs/news/pet-grocery-market-2020.

[2548] PETA. Chimpanzees in Laboratories. 2020; https://www.peta.org/issues/animals-used-for-experimentation/chimpanzees-laboratories/.

[2549] https://en.wikipedia.org/wiki/Animal_testing_on_non-human_primates#Legal_status; https://en.wikipedia.org/wiki/Countries_banning_non-human_ape_experimentation.

[2550] https://en.wikipedia.org/wiki/Bonobo#Conservation_status.

[2551] "Stolen from Paradise: The monkeys of St. Kitts & Nevis," ARFF, Aug 2015; http://arff.org/kitts.

[2552] Martins NRB, Erlhagen W, Freitas RA Jr. Human connectome mapping and monitoring using neuronanorobots. J Evol Technol. 2016 Jan;26(1):1-24; https://jetpress.org/v26.1/martins.pdf. Martins NRB, Angelica A, Chakravarthy K, Svidinenko Y, Boehm FJ, Opris I, Lebedev MA, Swan M, Garan SA, Rosenfeld JV, Hogg T, Freitas RA Jr. Human Brain/Cloud Interface. Front Neurosci. 2019 Mar 29;13:112; https://www.ncbi.nlm.nih.gov/pmc/articles/PMC6450227/.

inside each neuron of the brain of a test animal, allowing detailed whole-connectome before/after comparisons of their brain firing patterns. Data can be passed out of the brain to external computers using embedded fiber networks,[2553] circulating data-carrying nanorobots,[2554] time-stamped circulating polymer "ticker tapes"[2555] emitted by *in cyto* monitoring neurobots, or by other means. Nanorobots can also be used to directly inspect the physical structure of all neurons, dendrites, and synaptic connections inside the working brains of live subject animals, both before and after the cryopreservation/revival protocol is performed (to ensure a close match). Indeed, such measurements will undoubtedly be a major part of the research process that leads to the development of the cryonics revival protocol itself, a good subject for ***future research***. This development work may also require creating detailed models of the animal brain – up to and including a Whole-Brain Emulation or WBE (Section 5.2.3.4) – a technology that should be available by the time cryostasis revivals are attempted.

Merkle[2556] describes a WBE validation procedure that could be applied to test animals: "We could record every nerve impulse in the brain by embedding a sufficient number of neurobots….We could then record data from neurobots in the brain of an experimental animal before they were cryopreserved, cryopreserve them, revive them, and then record data from neurobots in the brain of the revived experimental animal, giving us two sets of neuronal data: 'before' and 'after'. Comparing the 'before' and 'after' data would let us tell if we had done a good job in cryopreserving and reviving the experimental animal."

"To spell this out in more detail, if we wish to evaluate a protocol for cryopreserving a biological experimental animal and reviving them as a biological experimental animal, we would: (1) use neurobots to monitor all nerve impulses in a test subject, (2) construct a 'before' WBE from the monitored nerve impulses, (3) cryopreserve the test subject while continuing to monitor their nerve impulses, (4) revive the test subject biologically, (5) use the neurobots to monitor all nerve impulses in the revived test subject, (6) construct an 'after' WBE from the second set of data produced by the neurobots, and then (7) compare the 'before' and 'after' WBEs and see if there are any significant differences. If there are significant differences, then the cryopreservation and revival technologies are regarded as 'not good enough'. If there are no significant differences, then the cryopreservation and revival technologies are regarded as 'good enough'….While we don't yet know whether passive collection of nerve impulse data is sufficient to allow correct inference of an individual's WBE, we'll need to determine the full set of synaptic connections even if passive collection is insufficient. To this end, we might need to inject signals into the nervous system, allowing us to interrogate the cellular circuits with a sufficient number of possible inputs to ensure that we have accurately determined all of the synaptic connections."

"Once we have constructed a WBE from the raw data gathered by the neurobots, then it would become possible to compare two such WBEs to each other in a meaningful way, as we expect that information like the connectome of a primate before and after they have been cryopreserved should remain the same. Changes in the WBEs would either be the result of damage caused by the cryopreservation-and-revival process, or would be the result of learning that took place between the 'before' and 'after' WBEs.

[2553] Freitas RA Jr. Nanomedicine, Volume I: Basic Capabilities, Landes Bioscience, Georgetown TX, 1999, Section 7.3.1, "Fiber Networks"; http://www.nanomedicine.com/NMI/7.3.1.htm.

[2554] Freitas RA Jr. Nanomedicine, Volume I: Basic Capabilities, Landes Bioscience, Georgetown TX, 1999, Section 7.3.2, "Mobile Networks"; http://www.nanomedicine.com/NMI/7.3.2.htm.

[2555] Marblestone AH, Zamft BM, Maguire YG, Shapiro MG, Cybulski TR, Glaser JI, Amodei D, Stranges PB, Kalhor R, Dalrymple DA, Seo D, Alon E, Maharbiz MM, Carmena JM, Rabaey JM, Boyden ES, Church GM, Kording KP. Physical principles for scalable neural recording. Front Comput Neurosci. 2013 Oct 21;7:137; https://www.ncbi.nlm.nih.gov/pmc/articles/PMC3807567/.

[2556] Merkle RC. Revival of Alcor Patients. Cryonics 2018 May-Jun;39(3):10-19 and Cryonics 2018 Jul-Aug;39(4):10-15; https://www.alcor.org/library/revival-of-alcor-patients/.

Assuming the neurobots remained in place during the cryopreservation, recording nerve impulses before and during the cryopreservation, and then later recording nerve impulses immediately following revival, there would be no loss of neuronal information. It should be possible to more directly compare the 'before' and 'after' WBEs with less concern about unaccounted-for changes that took place because of learning between the time the 'before' WBE was taken and the 'after' WBE was taken. The only unaccounted changes would then be those caused by damage due to the cryopreservation and revival process. [T]his protocol works for experimental animals...."

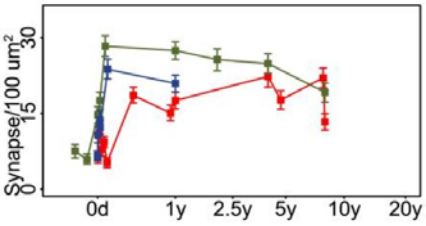

The larger great apes (chimps, orangutans, bonobos, gorillas) have 30%-40% as many neurons as a human brain,[2557] and human (red), chimp (blue), and rhesus macaque (green) neural tissues show similar adult synaptic number densities at 0.3-0.5 synapses/μm^3, varying slightly with age (chart, left).[2558] There are a few minor neuronal differences between humans and great apes. For example, prefrontal area 10 has greater spacing among cortical minicolumns in humans than in chimpanzees.[2559] The pyramidal neurons of humans have significantly longer and more branched dendritic arbors in all cortical regions than similar neurons in chimpanzees, and the human prefrontal cortex contains a greater proportion of dendrites, axons, synapses, glial cell processes, and microvasculature relative to the space occupied by neuronal and glial somata than in chimpanzees.[2560] Post-differentiation, cultured neurons show slightly different firing rates with time (chart, right).[2561] But these are all relatively minor differences in size, number, spatial distribution, and metabolic rate, not fundamental differences in kind that cell repair nanorobots would likely be able to handle in primates but unable to handle in humans. If we ever discover some exclusively-human neurocellular feature that absolutely must be repaired, nanorobots could practice and perfect these rare repair procedures on these specific human-unique features using brain tissue samples taken from fresh human cadavers.

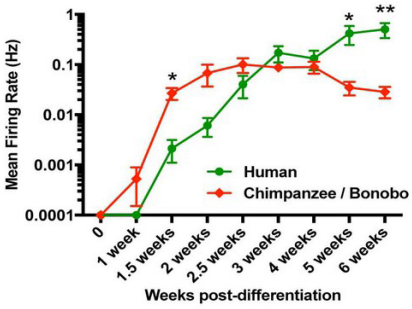

[2557] https://en.wikipedia.org/wiki/List_of_animals_by_number_of_neurons.

[2558] Liu X, Somel M, Tang L, Yan Z, Jiang X, Guo S, Yuan Y, He L, Oleksiak A, Zhang Y, Li N, Hu Y, Chen W, Qiu Z, Pääbo S, Khaitovich P. Extension of cortical synaptic development distinguishes humans from chimpanzees and macaques. Genome Res. 2012 Apr;22(4):611-22; https://www.ncbi.nlm.nih.gov/pmc/articles/PMC3317144/. Bianchi S, Stimpson CD, Duka T, Larsen MD, Janssen WG, Collins Z, Bauernfeind AL, Schapiro SJ, Baze WB, McArthur MJ, Hopkins WD, Wildman DE, Lipovich L, Kuzawa CW, Jacobs B, Hof PR, Sherwood CC. Synaptogenesis and development of pyramidal neuron dendritic morphology in the chimpanzee neocortex resembles humans. Proc Natl Acad Sci U S A. 2013 Jun 18;110 Suppl 2(Suppl 2):10395-401; https://www.ncbi.nlm.nih.gov/pmc/articles/PMC3690614/.

[2559] Semendeferi K, Teffer K, Buxhoeveden DP, Park MS, Bludau S, Amunts K, Travis K, Buckwalter J. Spatial organization of neurons in the frontal pole sets humans apart from great apes. Cereb Cortex. 2011 Jul;21(7):1485-97; https://academic.oup.com/cercor/article/21/7/1485/332179.

[2560] Bianchi S, Stimpson CD, Bauernfeind AL, Schapiro SJ, Baze WB, McArthur MJ, Bronson E, Hopkins WD, Semendeferi K, Jacobs B, Hof PR, Sherwood CC. Dendritic morphology of pyramidal neurons in the chimpanzee neocortex: regional specializations and comparison to humans. Cereb Cortex. 2013 Oct;23(10):2429-36; https://www.ncbi.nlm.nih.gov/pmc/articles/PMC3767963/.

[2561] Marchetto MC, Hrvoj-Mihic B, Kerman BE, Yu DX, Vadodaria KC, Linker SB, Narvaiza I, Santos R, Denli AM, Mendes AP, Oefner R, Cook J, McHenry L, Grasmick JM, Heard K, Fredlender C, Randolph-Moore L, Kshirsagar R, Xenitopoulos R, Chou G, Hah N, Muotri AR, Padmanabhan K, Semendeferi K, Gage FH. Species-specific maturation profiles of human, chimpanzee and bonobo neural cells. Elife. 2019 Feb 7;8:e37527; https://www.ncbi.nlm.nih.gov/pmc/articles/PMC6366899/.

If comparison of a before-cryopreservation WBE and an after-revival WBE of a large primate reveals no significant operating differences when placed in the same simulated environment, and if *in vivo* neurobot scans reveal no fundamental structural differences in the neurons, dendrites, synapses, and connectome of test primates before and after the revival procedure, then it is difficult to imagine how a human brain subjected to the same process would fare differently, given that the cytoarchitecture, cell type composition, and neurogenic gene expression programs of humans and chimpanzees are remarkably similar.[2562] Notes Aschwin de Wolf: "[T]he real issue...is...how closely an animal model tracks what happens in humans."[2563]

This confidence in animal models should extend even to the issue of "consciousness,"[2564] as evidenced by the 2012 Cambridge Declaration on Consciousness,[2565] signed by "a prominent international group of cognitive neuroscientists, neuropharmacologists, neurophysiologists, neuroanatomists and computational neuroscientists" that reads, in part: "Convergent evidence indicates that non-human animals have the neuroanatomical, neurochemical, and neurophysiological substrates of conscious states along with the capacity to exhibit intentional behaviors. Consequently, the weight of evidence indicates that humans are not unique in possessing the neurological substrates that generate consciousness."

These results lead to the tentative conclusion that **a successful primate validation of cryonics revival protocols should be sufficient evidence to warrant application of the same protocol to human cryopreservation patients**. This tentative conclusion should be vigorously explored by careful comparison of human and nonhuman primate neurological ultrastructure and brain cytoarchitecture, and should be validated, nuanced, or disproven in ***future research***.

7.2.2 Human WBE Testing

Requiring the testing of primate-validated procedures on live human subjects before applying them to existing cryopreservation patients could be medically, legally, and ethically fraught,[2566] and has been described by one writer as "ethically inappropriate to apply…to human test subjects".[2567] Science fiction provides proposals for testing cryonics procedures, e.g., on prison death-row inmates whose execution would be carried out, followed by cryopreservation and experimental revival, whereupon their sentences would be commuted and "their criminal proclivities…removed" in exchange for their voluntary

---

[2562] Mora-Bermúdez F, Badsha F, Kanton S, Camp JG, Vernot B, Köhler K, Voigt B, Okita K, Maricic T, He Z, Lachmann R, Pääbo S, Treutlein B, Huttner WB. Differences and similarities between human and chimpanzee neural progenitors during cerebral cortex development. Elife. 2016 Sep 26;5:e18683; https://www.ncbi.nlm.nih.gov/pmc/articles/PMC5110243/.

[2563] de Wolf A. How to Validate New Cryonics Technologies. Cryonics 2014 Aug;35(8):5; https://www.alcor.org/docs/cryonics-magazine-2014-08.pdf.

[2564] https://en.wikipedia.org/wiki/Consciousness.

[2565] http://fcmconference.org/img/CambridgeDeclarationOnConsciousness.pdf.

[2566] Farahany NA, Greely HT, Hyman S, Koch C, Grady C, Pașca SP, Sestan N, Arlotta P, Bernat JL, Ting J, Lunshof JE, Iyer EPR, Hyun I, Capestany BH, Church GM, Huang H, Song H. The ethics of experimenting with human brain tissue. Nature. 2018 Apr;556(7702):429-432; https://www.ncbi.nlm.nih.gov/pmc/articles/PMC6010307/. For example: "Any emerging technologies that could restore lost functionality to a person's brain could potentially undermine the diagnosis of brain death, because the cessation of brain function might no longer be permanent and irreversible."

[2567] Merkle RC. Revival of Alcor Patients. Cryonics 2018 May-Jun;39(3):10-19 and Cryonics 2018 Jul-Aug;39(4):10-15; https://www.alcor.org/library/revival-of-alcor-patients/.

participation.[2568] But experiments on prisoners can be problematic because of the difficulty in obtaining truly voluntary consent and because of the high probability of lawsuits if anything goes wrong.[2569]

Nevertheless, conservative cryonicists and identity purists might refuse to trust a revival procedure until it had first been tested on at least one live human being. A demonstration of successful animal testing of a revival protocol might also be unacceptable to a broader range of cryonicists if ***future research*** can identify at least one crucial identity-relevant neurological structure that is (A) found only in human brains but not in the brains of primates (even though chimps and bonobos share ~99.6% of human genes),[2570] and (B) sufficiently different from analogous biological structures that a nanorobotic repair procedure that has been proven to succeed on primate brains might somehow fail on human brains. In either case, some cryonicists might conclude that only live human testing will satisfy their concerns. Because live human testing can be ethically problematic, one possible solution may be human Whole-Brain Emulation (WBE) (Section 5.2.3.4) testing, as proposed by Ralph Merkle in 2018.[2571]

Merkle writes: "An obvious and rather awkward question is this: once we revive someone, how do we know we did it right?...One solution is to conduct some sort of test before a person is cryopreserved, then test them again after we revive them, and compare the results….We could record every nerve impulse in the brain by embedding a sufficient number of neurobots...a class of medical nanorobots [that could be located] on, in, or near nerve cells….The objective is to record all neuronal activity within the test subject's brain….[I]f we wish to evaluate a protocol for cryopreserving a biological experimental animal and reviving them as a biological experimental animal, we would: (1) use neurobots to monitor all nerve impulses in a test subject, (2) construct a 'before' WBE from the monitored nerve impulses, (3) cryopreserve the test subject while continuing to monitor their nerve impulses, (4) revive the test subject biologically, (5) use the neurobots to monitor all nerve impulses in the revived test subject, (6) construct an 'after' WBE from the second set of data produced by the neurobots, and then (7) compare the 'before' and 'after' WBEs and see if there are any significant differences. If there are significant differences, then the cryopreservation and revival technologies are regarded as 'not good enough.' If there are no significant differences, then the cryopreservation and revival technologies are regarded as 'good enough.'"

After proposing four general ethical principles applicable to the revival of cryonics patients, Merkle proposes "an ethically acceptable protocol for evaluating a revival protocol, an experimental scan technology, and an experimental scan-to-WBE algorithm on human volunteers:

[2568] e.g., James Halperin. The First Immortal: A Novel of the Future. Del Rey Books, 1998, p. 344; http://www.cryonics.org/images/uploads/misc/firstimmortal.pdf. "In February 2066, 171 former death-row prisoners who'd volunteered for biostasis experiments had become the first humans to be revived from cryonic suspension. These subjects had been frozen under perfect post-death conditions: Their executions had been scheduled. The first group of 71 prisoners, those whose offenses had been the most egregious, had all been revived as young, perfectly healthy partial amnesiacs. The second group of 100 was more fortunate. All but seven very early, nonvitrified subjects, were brought back with fully-preserved identity and memories. In spite of a half-hearted objection from the WCLU (formerly ACLU), their criminal proclivities were also simultaneously removed."

[2569] https://en.wikipedia.org/wiki/Experimentation_on_prisoners.

[2570] Gibbons A. Bonobos Join Chimps as Closest Human Relatives. Science Magazine News, 13 Jun 2012; https://www.sciencemag.org/news/2012/06/bonobos-join-chimps-closest-human-relatives.

[2571] Merkle RC. Revival of Alcor Patients. Cryonics 2018 May-Jun;39(3):10-19 and Cryonics 2018 Jul-Aug;39(4):10-15; https://www.alcor.org/library/revival-of-alcor-patients/.

1. Implant neurobots into a terminally ill human volunteer,[2572] after asking the volunteer for informed consent, using a successfully tested and validated protocol that complies with appropriate medical and ethical principles.

2. Cryopreserve the volunteer following their legal death using a cryopreservation protocol modeled after those actually used to cryopreserve Alcor patients.

3. Use the data obtained from the neurobots implanted in 1 to construct a WBE using a successfully tested and validated neurobot-to-WBE algorithm. Run the WBE in a suitable environment if that was part of the agreement with the terminally ill volunteer.

4. Carry out those parts of the revival protocol that take place at cryogenic temperatures.

5. Scan the cryopreserved brain produced by step 4 using the experimental scan technology.

6. If the purpose is to evaluate a biological revival protocol, then the scan in step 5 should either be a non-destructive scan or a destructive molecular scan. If it was a destructive molecular scan, rebuild an atomically precise duplicate of the cryopreserved brain that was destructively scanned using the scan data. Otherwise, simply continue.

7. Re-warm isolated one-cubic-millimeter samples of tissue from the cryopreserved volunteer to verify the re-warming phase of the protocol. This must be permitted by the informed consent obtained in step 1.

8. Construct a WBE from the scan data obtained in step 5, using the experimental algorithm. Do not run this WBE.

9. Compare the WBE from step 2 with the WBE from step 8.

10. Compute the percentage difference between the two WBEs. Subtract this percentage difference from 100 and call it the 'revival fidelity'. If there is no difference, we will have achieved 100% revival fidelity. A 100% revival fidelity is the best that can possibly be achieved."

Merkle concludes: "This is an ethically acceptable protocol which can be used to evaluate both a scan technology and a scan-to-WBE algorithm."

Future research should evaluate the feasibility of this approach. It is not yet clear whether it has any direct utility for cryonics patients who wish to initially return to active life as biological entities and not as uploads (Section 5.2.3.4), given our tentative conclusion (Section 7.2.1) regarding the sufficiency of animal testing. However, for cryonics patients wishing to initially return as uploads, the utility of developing a detailed human WBE approach is obvious.

Randal Koene has also asked the question of how we will know that a WBE has successfully reproduced the mind of a cryopreservation patient. According to a 2018 workshop report,[2573] "Koene proposed the

---

[2572] Cryonics revival will require the existence of an extremely mature medical nanorobotics technology in order to succeed. It is difficult to imagine what sorts of illnesses might remain medically "terminal" in this future cryonics-revival era when everything is nanomedically curable, other than cases of extreme brain damage where significant personal identity information has already been irretrievably lost (i.e., a shotgun blast to the head) in which case securing "informed consent" would be problematic at best.

[2573] Wiley K. From Brain Preservation to Reconstruction. Summary of the April 2018 Carboncopies workshop on whole brain emulation. Cryonics 2019 Qtr 1;40(1):37-39; https://www.alcor.org/docs/cryonics-magazine-2019-01.pdf.

concept of a neural fingerprint, some objective measurement of brain structure or function that distinctly identifies an individual, such that if a WBE exhibited the same fingerprint we could judge it to represent the same person who preceded the preservation. What sort of validation test or data would inform us on such matters? Koene proposed that in addition to neural modeling and neural circuit validation, we might also desire (or require) psychological behavioral validation by comparing the WBE's behavior to similar behavioral tests preceding the preservation process." Koene "also emphasized the importance of acknowledging model imprecision," thus agreeing that "no model is perfect." Just as molecular reconstruction (Chapter 5) will inevitably incorporate some very small number of reading and writing errors, so will any practical WBE include "variations between a model and its source data," with "tolerable model variances in terms of error or generalized noise and randomness".

7.3 Future Research Opportunities

Throughout this book, both in the main text and in the Appendices, we have highlighted 304 specific items of "***future research***" that should be pursued in order to establish the technical capabilities needed to ensure a successful nanorobotic-based revival from cryopreservation with maximum recovery of personal identity. For the reader's convenience, all such research items are listed in Appendix R in the order in which they appear in this book, linked to the Section in which they appear, and sequentially numbered for easy reference. The items vary widely in their urgency, importance, and level of difficulty to complete.

Further discussion should determine the best way to undertake this future research, including (1) prioritization of the research tasks, (2) allocation of the research tasks to those who may be the most competent and willing to perform them, (3) identifying individuals and organizations that should be recruited to perform the tasks, and (4) determining the likely source(s) of funding for this future research work. Many of these research topics seem to relate to better evaluations of Plan A/B parameters (e.g., time, cost, or algorithm complexity), while others relate to the tradeoffs in choosing Plan A or B, or to the overall feasibility of revival (e.g., what damage leads to information theoretic death), and we should determine the difficulty of answering these questions. Once the work is underway, we can better assess which specific nanorobotic capabilities should be developed and what additional biological or cryobiological basic data might need to be gathered – including identifying the kind of patient-specific data that will be unique to a particular procedure and accumulating general cryobiological data whose acquisition could be contracted out to research groups ahead of time.

Please note that virtually all of the listed research topics are specific to cryonics revival and do not include research aimed at the more generic development of mechanosynthesis, nanofactories, and medical nanorobots, as these objectives will be independently pursued elsewhere.

Why should we pursue this work now? Observes Mike Perry: "Projects like the above have something in common beyond furthering technology that might physically assist us in cryonics operations, whether at the preservation or at the revival end. That is, they are potentially *disruptive*, challenging mainstream attitudes at a deep level. It might be said that challenging attitudes in this way has importance at least comparable to the direct seeking of physical benefits. When attitudes change, progress accelerates due to a cascade effect: less opposition all around means existing research can proceed with less hindrance, researchers who might otherwise remain sidelined will join the effort, and more funding resources will become available. In this way rates of progress could vastly increase." [2574]

[2574] Perry RM. Cryonics and Public Skepticism: Meeting the Challenges to Our Credibility. Cryonics 2019 Qtr 4;40(4):24-37; https://www.alcor.org/docs/cryonics-magazine-2019-04.pdf.

Appendix A. Society for Cryobiology No Longer Openly Hostile to Cryonics

According to Mike Perry,[2575] on 15 Sep 1982 the professional Society for Cryobiology adopted revised bylaws that explicitly singled out cryonicists as targets for denial of, or expulsion from, membership in the Society.[2576]

Quoting from Section 2.04. Denial of Membership and Discipline of Members:[2577]

> "Upon a two-thirds vote of the Governors in office, the Board of Governors may refuse membership to applicants, or suspend or expel members (including both individual and institutional members), whose conduct is deemed detrimental to the Society, including applicants or members engaged in or who promote any practice or application which the Board of Governors deems incompatible with the ethical and scientific standards of the Society or as misrepresenting the science of cryobiology, **including any practice or application of freezing deceased persons in the anticipation of their reanimation**."

This provision remained in the bylaws for many years, but finally has been modified to remove the explicit, anti-cryonics content. In the latest version of the bylaws, whose adoption was announced 17 Jan 2018,[2578] the amended passage (now Section 3.04) reads:[2579]

> "Upon a two-thirds vote of the Governors in office, the Board of Governors may refuse membership to applicants, or suspend or expel members (including individual, institutional, corporate, or student members), whose conduct is deemed detrimental to the Society, including applicants or members engaged in or who promote any practice or application which the Board of Governors deems incompatible with the ethical and scientific standards of the Society or as misrepresenting the science of cryobiology."

However, the Society does still regard cryonics as lying outside the purview of their professional scientific focus, as indicated in their two-paragraph position statement[2580] on cryonics published later in the same year:

[2575] Perry RM. Society for Cryobiology No Longer Openly Hostile to Cryonics. Cryonics 2018 Sep-Oct;39(5):16; https://www.alcor.org/docs/cryonics-magazine-2018-05.pdf.

[2576] Darwin M. Cold War: The Conflict Between Cryonicists and Cryobiologists. Cryonics 1991 Jun;12(6):4-14, Cryonics 1991 Jul;12(7):2-8, and Cryonics 1991 Aug;12(8):5-7; https://www.alcor.org/Library/html/coldwar.html.

[2577] https://sc.memberclicks.net/assets/documents/bylaws.pdf.

[2578] Jason Acker. Bylaws Revision Complete. 17 Jan 2018; https://www.societyforcryobiology.org/index.php?option=com_dailyplanetblog&view=entry&year=2018&month=01&day=16&id=38:bylaws-revision-complete.

[2579] https://www.societyforcryobiology.org/assets/Bylaws_for_the_Society_for_Cryobiology_2017-12-20b.pdf.

[2580] "Cryonics," Society for Cryobiology Position Statement, Nov 2018; https://www.societyforcryobiology.org/assets/documents/Position_Statement_Cryonics_Nov_18.pdf.

"The Society for Cryobiology sometimes receives inquiries regarding its position on the practice of cryopreserving human cadavers or brains with the aim of eventual reanimation, known as cryonics."

"The Society recognizes and respects the freedom of individuals to hold and express their own opinions and to act, within lawful limits, according to their beliefs. Preferences regarding disposition of postmortem human bodies or brains are clearly a matter of personal choice and, therefore, inappropriate subjects of Society policy. The Society does, however, take the position that the knowledge necessary for the revival of live or dead whole mammals following cryopreservation does not currently exist and can come only from conscientious and patient research in cryobiology and medicine. In short, the act of preserving a body, head or brain after clinical death and storing it indefinitely on the chance that some future generation may restore it to life is an act of speculation or hope, not science, and as such is outside the purview of the Society for Cryobiology."

Appendix B. Cryopreservation in Science Fiction (1846-2021)

Revival from human cryopreservation has also been envisioned by numerous authors in fictional treatments including short stories, novels, movies, television, plays, and other media. The following is a representative (though perhaps not comprehensive) synopsized list of works, arranged in chronological order of first publication, that portray revival from accidental or purposeful cryopreservation or straight-freeze. Revival details are usually sketchy at best, and most entries describe scientifically implausible scenarios – especially the often-portrayed apparent speed and simplicity of revival (e.g., push a button, and in a few minutes the person wakes up).

* **1846 (short story): Hilda Silfverling. A Fantasy.**[2581] A woman condemned to death by beheading chooses an alternative means of execution, provided by a scientist who "had discovered a process of artificial cold, by which he could suspend animation in living creatures."

* **1887 (novel): The Frozen Pirate.**[2582] A French pirate, frozen for years in cold climes, is resuscitated briefly and tells the narrator the location of some buried treasure.

* **1889 (novel): 10,000 years in a Block of Ice.**[2583] A mad scientist attempts to impose accelerated evolution on the human race; awakening aeons later from suspended animation on ice, Monsieur Synthesis discovers a unified world-utopia peopled by small men who are descended from Chinese and Africans and can fly by the power of thought.

* **1899 (short story): A Thousand Deaths.**[2584] In Jack London's first published story, a man held captive on an island is subjected to fatal suffocation, then cold storage for 3 months while "not permitted to freeze or decay," then restoration to life by an experimental process.

* **1922 (movie): The Man from Beyond.**[2585] A man found frozen in arctic ice is brought back to life after 100 years of dormancy. First movie showing reanimation from the frozen state.

* **1929 (play): The Bedbug.**[2586] A young man in 1929 Soviet Russia is frozen in a basement on the day of his wedding. After 50 years, he is revived into a communist utopia, but cannot fit in and becomes a zoo exhibit, serving as an example of the vices of a past age to the citizens of the future.

* **1930 (short story): The Corpse That Lived.**[2587] A man dies in a plane crash in the year 2025 and is immersed in a bathtub of ice cubes, then returned to life by an electric pulse.

[2581] Lydia Maria Child. Hilda Silfverling. A Fantasy. Fact and Fiction: A Collection of Stories, C.S. Francis, 1846, pp. 205-240; https://web.archive.org/web/20120415091441/http://faculty.pittstate.edu/~knichols/hilda.html.

[2582] W. Clark Russell. The Frozen Pirate, 1887; http://www.sf-encyclopedia.com/entry/russell_w_clark.

[2583] Louis Boussenard. Dix mille ans dans un bloc de glace [translated in 1898 by John Paret as: 10,000 Years in a Block of Ice]. Journal des Voyages, 17 Aug – 26 Oct 1989; http://www.sf-encyclopedia.com/entry/boussenard_louis.

[2584] Jack London. A Thousand Deaths. The Black Cat, May 1899; https://en.wikisource.org/wiki/A_Thousand_Deaths.

[2585] https://en.wikipedia.org/wiki/The_Man_from_Beyond.

[2586] Vladimir Mayakovsky. The Bedbug. Molodaya Gvardia magazine, Nos. 3 and 4, 1929; reprinted as a book by Gosizdat, 1929; https://en.wikipedia.org/wiki/The_Bedbug. See English translation at https://briefly-ru.translate.goog/majakovskij/klop/?_x_tr_sl=ru&_x_tr_tl=en&_x_tr_hl=en-GB&_x_tr_pto=nui.

[2587] E.D. Skinner. The Corpse That Lived. Amazing Stories, Jan 1930, pp. 950-957.

* **1930 (novelette): The Ice Man.**[2588] Marcus Publius, frozen in Rome in 59 B.C., is defrosted in 1928 by a professor using an electric blanket.

* **1931 (short story): The Jameson Satellite.**[2589] This story, in which the subject has himself deliberately preserved in space after death (via a "straight-freeze"), has been credited with giving cryonics pioneer Robert Ettinger the seed of the idea of cryonics at the age of 12.[2590]

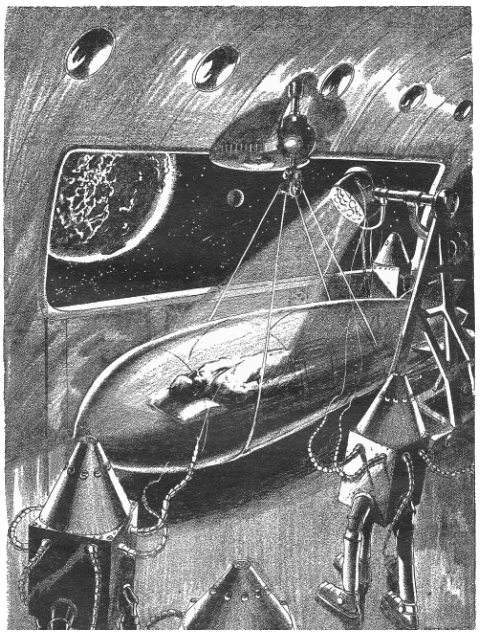

"The mammoths of the ancient world have been wonderfully preserved in the ice of Siberia. The cold, only a few miles out in space, will be far more intense than in the polar regions and its power of preserving the dead body would most probably be correspondingly increased. When the hero-scientist of this story knew he must die, he conceived a brilliant idea for the preservation of his body, the result of which even exceeded his expectations….He would have his body shot into space enclosed in a rocket to become a satellite of the earth..."[2591]

Millions of years later, alien robots visiting an Earth on which humanity has become extinct, discover Jameson's cryo-capsule floating in orbit, retrieve it (illustration, right),[2592] revive the man and install his brain in a robot body:

"He is dead!" pronounced one of the machine men after a long and careful examination of the corpse. "He has been like this for a long time."

"There are strange thought impressions left upon his mind," remarked another.

"Would you like to hear his story?" he asked.

"Yes!" came the concerted reply.

"You shall, then," was the ultimatum. "Bring him into my laboratory. I shall remove his brain and stimulate the cells into activity once more. We shall give him life again, transplanting his brain into the head of one of our machines."

* **1937 (short story): The Resurrection of Jimber-Jaw.**[2593] A cryogenicist-aviator flying over Siberia discovers the body of a cavemen frozen into a newly-uncovered glacier wall. The cryogenicist revives the man using transfusions and injections of drugs. The caveman proves to be intelligent, but after

---

[2588] William Withers Douglas. The Ice Man. Amazing Stories, Feb 1930, pp. 1020-1033.

[2589] Neil Ronald Jones. The Jameson Satellite. Amazing Stories, Jul 1931; http://www.gutenberg.org/files/26906/26906-h/26906-h.htm.

[2590] https://en.wikipedia.org/wiki/Robert_Ettinger#Roots_of_cryonics_in_science_fiction.

[2591] http://thenostalgialeague.com/olmag/jameson.html.

[2592] http://famous-and-forgotten-fiction.com/writings/jones/the-jameson-satellite/it-became-enveloped-in-a-haze-of-light.png.

[2593] Edgar Rice Burroughs. The Resurrection of Jimber-Jaw. Argosy Weekly, 20 Feb 1937; https://en.wikipedia.org/wiki/The_Resurrection_of_Jimber-Jaw.

realizing he doesn't fit in with current society, deliberately re-freezes himself in a meat locker with a note requesting that he not be thawed out again.

* **1938 (short story): Who Goes There?**[2594] Antarctic scientists discover a crashed alien spacecraft that has been buried in ice for 20 million years. The frozen alien pilot, who revives when the ice encasing him melts, can assume the shape, memories, and personality of any living thing it devours, while maintaining its original body mass for further reproduction. After killing many humans, the revived alien is finally destroyed by fire.

* **1940 (movie): The Man with Nine Lives.**[2595] Dr. Tim Mason is working on cryogenic treatment of chronic medical problems, continuing the work of the vanished Dr. Leon Kravaal, and visits Kravaal's home where he vanished 10 years before, along with the local sheriff and DA. Mason finds a hidden passage to a basement secret laboratory, where he discovers Kravaal and four others including the sheriff and DA frozen in suspended animation. Kravaal, who is revived, had been charged with murder by the sheriff for freezing a terminal cancer patient, so the doctor had placed them all on ice.

* **1948 (short story): The Penultimate Trump.**[2596] As an adult, the cryonics pioneer Robert Ettinger published a short story in which the explicit idea of cryopreservation of legally dead persons for future repair of medical causes of death is promulgated. A dying wealthy man funds his own cryopreservation, apparently only a "straight-freeze": "... just go to sleep in a nice refrigerator until people really know something about the body….We'll put the vault in Michigan...very safe country, geologically. We'll make the vault and the coolers of the very best, of course, granite and stainless steel and quartz that will never wear out.' According to the outline sketched that afternoon, the vault was to be safeguarded and the sleepers' interests looked after by the establishment of a Haworth Trust, with Garibaldi Jones the first Administrator. Only one person in each generation, the Administrator, would know all about the vault. Caches of treasure were to be tucked away in unlikely places, the key to their location securely hidden in H.D.'s mind. In course of time Harley D. Haworth was carefully laid away in his ice- cold 'coffin,' and those who read the obituaries did not suspect that he was the first of men to die a qualified death." The man is revived after 320 years, plus the "two years we've been working on you," by unspecified means.

* **1951 (movie): The Thing from Another World.**[2597] The first film version of the 1938 short story Who Goes There? (see description, above).

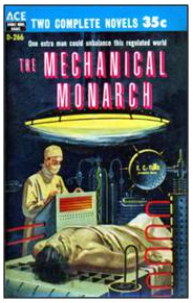

* **1953 (movie): The Beast from 20,000 Fathoms.**[2598] A dinosaur is frozen in Arctic ice until a nuclear test thaws it out and revitalizes it, freeing it to go on a rampage of destruction down the East Coast of the United States.

* **1954 (novel): Enterprise 2115 [**aka. **The Mechanical Monarch].**[2599] The first man sent into space "becomes marooned in the asteroid belt due to a malfunction

---

[2594] Don A. Stuart (John W. Campbell Jr.). Who Goes There? Astounding Science Fiction, Aug 1938; https://en.wikipedia.org/wiki/Who_Goes_There%3F.

[2595] Columbia Pictures Corporation; http://www.sf-encyclopedia.com/entry/man_with_nine_lives_the.

[2596] Robert Ettinger. The Penultimate Trump. Startling Stories, March 1948; https://archive.is/20120801065253/http://www.cryonics.org/Trump.html.

[2597] https://en.wikipedia.org/wiki/The_Thing_from_Another_World.
[2598] https://tvtropes.org/pmwiki/pmwiki.php/Film/TheBeastFromTwentyThousandFathoms.

[2599] Charles Grey (Edwin Charles Tubb). Enterprise 2115. Merit Books, London, 1954; later published in the U.S. as: E.C. Tubb, The Mechanical Monarch, Ace Books, NY, 1958; http://www.sf-encyclopedia.com/entry/tubb_e_c.

of his spacecraft that ends his life when the hull is breached. The spacecraft undergoes decompression; after which the astronaut orbits the cold far reaches of deep space for ~200 years, frozen and lifeless. Ultimately, he is discovered by an asteroid metal miner who transports him to medical facilities on Mars where he is subsequently repaired and resuscitated."[2600]

* **1957 (novel): The Door Into Summer.**[2601] A suspended animation technique called the Cold Sleep allows people to be quickly frozen and revived.

* **1960 (novel): He Owned the World.**[2602] A 20th century astronaut dies en route to the Moon and is preserved in the icy cold of space, then is revived 8000 years later in a process involving 11 years of transplant surgery and 5 years with wires in his body supplying neural stimuli electrically to his cells and organs, with new synthetic cells in his lungs and a new heart composed of a "graft of nylon and other materials of high tensile strength" that would last one thousand years.

* **1961 (novel): Second Ending.**[2603] A man awakes from cryo sleep post-World War III to discover that he's the last biological life form on a completely dead Earth, with just a bunch of moderately intelligent robots to keep him company; he then spends millions of years dipping in and out of cryo sleep while his robots work to restore the planet.

* **1963 (novelette): The Graveyard Heart.**[2604] A group of people spend a year in cryonic preservation, then come out of it for a single day to throw a huge party, then go back into stasis to repeat the cycle.

* **1964 (comics): Captain America.**[2605] Steve Rogers, aka. Captain America, believed lost at sea in 1945, was actually preserved in a block of arctic ice, which later melted. Steve's best friend Bucky Barnes also underwent cryonics several times in his life as a brainwashed assassin for the villainous group HYDRA.

* **1964 (movie): Frozen Alive.**[2606] A scientist experimenting with suspended animation decides to use himself as a test subject. Before he is frozen, his wife is killed, and he is suspected of her murder.

* **1964 (movie): The Evil of Frankenstein.**[2607] Frankenstein finds his original creation frozen inside a glacier and restores it to life.

[2600] http://chronopause.com/chronopause.com/index.php/2011/04/04/michael-g-darwin-a-biographical-precis/index.html.

[2601] Robert A. Heinlein. The Door Into Summer. Doubleday, 1957; https://en.wikipedia.org/wiki/The_Door_into_Summer. See also: https://amazingstories.com/2017/03/retro-review-robert-heinleins-door-summer/. Originally serialized in The Magazine of Fantasy and Science Fiction in Oct/Nov/Dec 1956.

[2602] Charles Eric Maine. He Owned the World. Avon Books, New York, 1960; https://www.amazon.com/Owned-World-Charles-Eric-Maine/dp/B00W52DII2.

[2603] James White. Second Ending, Ace Books, 1961; https://en.wikipedia.org/wiki/Second_Ending.

[2604] Roger Zelazny. The Graveyard Heart. 1963. Reprinted in The Door of His Face, 2001; https://www.amazon.com/Doors-His-Face-Lamps-Mouth/dp/0743413296/.

[2605] Stan Lee, Jack Kirby, Captain America Joins the Avengers, The Avengers 1964 Mar; Vol. 4; https://en.wikipedia.org/wiki/Captain_America#20th_century.

[2606] https://www.imdb.com/title/tt0058084/.

[2607] https://www.moriareviews.com/horror/evil-of-frankenstein-1964.htm.

* **1965 (TV): Lost in Space.**[2608] In the future year of 1997, a family of five board a saucer-shaped spacecraft to travel to Alpha Centauri as colonists. They are to be cryogenically frozen for the voyage in cylindrical chambers, then to be unfrozen when the spacecraft approaches its destination:[2609] "They will spend the five and a half years of their voyage frozen into a state of suspended animation, which will terminate automatically as the spacecraft enters the atmosphere of the new planet." The ship veers off course and the astronauts are awoken early.

* **1966 (TV): Adam Adamant Lives!**[2610] In 1902, Edwardian adventurer Adam Adamant is frozen alive in a block of ice by his arch-nemesis, the Face. In 1966, workmen discover him and he is revived, perfectly preserved but completely bewildered by his new environment.

* **1967 (novel): Death Is a Dream.**[2611] Three survivors from the twentieth century awake from suspended animation in post-nuclear London to find themselves unemployable, and unfit to live by virtue of their commitments to out-dated ideals.

* **1967 (novel): Notes from the Future.**[2612] A frozen sleeper awakens to 1991 where he is cured of leukemia and reflects somewhat heavily upon the nature of the world of 1991 he has come into, where immortality has become a possibility.

* **1967 (novel): Why Call Them Back From Heaven.**[2613] In 2148, mankind has decided to undertake cryogenic freezing of its elderly and hopelessly ill inhabitants, against the day when they might be resuscitated and cured.

* **1967 (novelette): This Mortal Mountain.**[2614] A party of mountain climbers ascending a forty-mile-high mountain on a colonized planet are impeded by holographic projections of glowing creatures generated by a computer programmed to prevent anyone from entering a cave in the mountain. Therein resides the last survivor of the first expedition to colonize the planet, who has been cryonically preserved to allow her to survive the disease that killed all the other colonists from the first expedition.

* **1967 (movie): In Like Flint.**[2615] Flint is placed in cryogenic suspension, but escapes.

* **1967 (TV): Space Seed (Star Trek).**[2616] In this original-series episode of Star Trek, 72 genetically-engineered superhumans are found – still alive in a state of suspended animation – in the "sleeper ship" Botany Bay that had been adrift in space for 200 years. Upon being reawakened, the

---

[2608] https://en.wikipedia.org/wiki/Lost_in_Space.

[2609] Lost in Space S01E01 The Reluctant Stowaway; https://www.youtube.com/watch?v=65f77cup2aM.

[2610] U.K. television series, 1966-67; http://www.sf-encyclopedia.com/entry/adam_adamant_lives.

[2611] E.C. Tubb. Death Is a Dream. Ace, 1967; https://www.amazon.com/Computer-War-Death-Dream-H-34/dp/B000OVAH4Y/.

[2612] Nikolai Amosov. Zapiski iz budushchego [translated in 1970 by George St. George as: Notes from the Future]. Nauka i Zhizn, 1967; http://www.sf-encyclopedia.com/entry/amosov_n.

[2613] Clifford D Simak. Why Call Them Back From Heaven? Doubleday/Ace, 1967; https://en.wikipedia.org/wiki/Why_Call_Them_Back_from_Heaven%3F.

[2614] Roger Zelazny. This Mortal Mountain, IF, Mar 1967. Reprinted in This Mortal Mountain, NESFA Press, Jul 2009, pp. 21-60; https://www.nesfa.org/book/this-mortal-mountain-2/.

[2615] https://en.wikipedia.org/wiki/In_Like_Flint.

[2616] https://en.wikipedia.org/wiki/Space_Seed.

superhumans attempt to take control of the Enterprise. This Star Trek episode ignited the author's first interest in cryonics at the age of 14. The official fan website Memory Alpha refers to "cryogenic chambers from the Botany Bay",[2617] and the faces of the sleepers appear white as if frozen. The original script reveals that on first approach to the Botany Bay, a crewman using bioscanners from the Enterprise reports detecting "heartbeats from over there…faint, and average only 4 beats per minute." To be consistent with cryostasis, this means the sleeper ship must have detected the approach of Enterprise and begun one or more anticipatory revivals, producing the faint heartbeats that Enterprise detected. The revival from suspension appears to have been fully automated and required no intravenous lines or any other direct physical links to the patient.

* **1967 (TV): The Tomb of the Cybermen (Doctor Who).**[2618] Dr. Who finds a vast underground chamber containing pods of frozen Cybermen, entombed in suspended animation. A control panel is activated, the ice begins to melt, and the Cybermen return to life.

* **1968 (novel): The Ice People.**[2619] Antarctic explorers discover a man and woman frozen in a chamber and revive them after a 900,000-year slumber.

* **1968 (novella): Wait It Out.**[2620] An astronaut marooned on Pluto exposes himself to the planet's extreme cold, intending to go into frozen sleep until rescue eventually comes, but suffers the torments of consciousness as each night's extreme cold makes his nervous system superconductive.

* **1968 (movie): 2001: A Space Odyssey.**[2621] In this science fiction classic, several of the astronauts aboard the interplanetary spacecraft Discovery are held unconscious in personal cryogenic[2622] hibernation pods.[2623] Life support for the hibernating astronauts is turned off when the HAL 9000 computer malfunctions, killing the astronauts before they can be revived.

* **1968 (movie): Planet of the Apes.**[2624] According to an authoritative fan website,[2625] the original mission of the spaceship that carried astronauts to the planet of the apes "was to journey to another star. After six months on the craft the crew placed themselves into a state of suspended animation using a special drug to keep them sedated, and confined themselves to stasis pods. It seems they planned to spend twelve months in suspended animation, a total of eighteen months on the ship. While they slept, the vessel was propelled two thousand years into the future…in a vehicle travelling near the speed of light. At some point in the journey, Lieutenant Stewart's stasis pod malfunctioned and an air leak caused her to die shortly after entering it….The ship splashed down into a stagnant salt lake about eleven months into the crew's

---

[2617] https://memory-alpha.fandom.com/wiki/Space_Seed_(episode)#Continuity_and_trivia.
[2618] https://tardis.fandom.com/wiki/The_Tomb_of_the_Cybermen_(TV_story).

[2619] Rene Barjavel. The Ice People. Les Presses de la Cite, 1968; https://en.wikipedia.org/wiki/The_Ice_People_(Barjavel_novel).

[2620] Larry Niven. Wait It Out. The Future Unbound Program Book, 1968; http://variety-sf.blogspot.com/2007/09/larry-nivens-wait-it-out-man-in-natural.html.

[2621] https://en.wikipedia.org/wiki/2001:_A_Space_Odyssey.

[2622] While the astronauts in the film don't appear to be frozen and are frequently referred to as "sleeping", the novel* accompanying the film explicitly mentions "three unconscious colleagues in the frozen peace of the Hibernaculum", implying a sub-zero hypothermic basis for the astronauts' suspended animation.
* Arthur C. Clarke. 2001: A Space Odyssey. Signet Books, New York, 1968; p. 91.

[2623] https://2001.fandom.com/wiki/Hibernation_pods.
[2624] https://en.wikipedia.org/wiki/Planet_of_the_Apes_(1968_film).
[2625] https://planetoftheapes.fandom.com/wiki/Icarus/Liberty_1.

stasis. Upon awakening, the remaining crew found the desiccated remains of Stewart's body in her pod." The entry for this well-known iconic film is included here only for completeness because the stasis pods shown in the movie appear to represent some form of chemically-induced hibernation (Section 7.1.6), *not* cryostasis.

* **1969 (novel): The Age of the Pussyfoot.**[2626] A man is revived from cryopreservation in the year 2527, by means undescribed, having been killed in a fire 500 years earlier. Thanks to his insurance, after the expenses of his revival are paid he still has a quarter of a million dollars, a fortune in his eyes. He thinks he can afford the luxuries of 26th century life, but soon discovers he has almost run out of money after just a few days.

* **1969 (novel): Bug Jack Barron.**[2627] The Foundation for Human Immortality is trying to get their Freezer Utility Bill through Congress, giving them a monopoly on "freezer contracts" that require a $500,000 payment for cryopreservation.

* **1969 (novel): Freezing Point.**[2628] The protagonist is incurably sick and is frozen until he can be cured. The world to which he awakens offers him ambivalent (and restricted) choices between an idle life (with death inevitable) and a life of drudgery (with access to spare parts).

* **1969 (novel): Ubik.**[2629] Cryonic technology allows recently deceased people to be maintained in a lengthy state of hibernation.

* **1969 (movie): Hibernatus.**[2630] A man frozen for 65 years is found in the ice of the North Pole by a scientific polar expedition and is brought back to life by unspecified methods – the man was exploring the pole in 1905, is now a 90-year-old young man, and has difficulty adjusting to the world of the future.

* **1969 (TV): Strange Paradise.**[2631] In the first story arc, a reclusive millionaire has his wife cryonically preserved after her death; several episodes featured fictional members of the "Cryonics Society".

* **1969 (TV): The Man Who Gambled with Life (The Saint).**[2632] A dying multi-millionaire has himself cryonically preserved.

* **1970 (novel): The Gods of Foxcroft.**[2633] A man and woman of the twentieth century are reborn from their cryogenic capsules by now highly sophisticated techniques.

[2626] Frederick Pohl. The Age of the Pussycat. Ballantine Books, 1969; https://en.wikipedia.org/wiki/The_Age_of_the_Pussyfoot. This story was first published as a serial in Galaxy Science Fiction in three parts, starting in October 1966, and was later published as a novel in 1969.

[2627] Norman Spinrad. Bug Jack Barron. Walker & Co., 1969; https://en.wikipedia.org/wiki/Bug_Jack_Barron.

[2628] Anders Bodelsen. Frysepunktet [translated in 1971 by Joan Tate as: Freezing Point]. Gyldendal, Copenhagen Denmark, 1969; http://www.sf-encyclopedia.com/entry/bodelsen_anders.

[2629] Philip K. Dick. Ubik. Doubleday, 1969; https://en.wikipedia.org/wiki/Ubik.

[2630] https://en.wikipedia.org/wiki/Hibernatus.
[2631] https://en.wikipedia.org/wiki/Strange_Paradise.
[2632] https://en.wikipedia.org/wiki/List_of_The_Saint_episodes#Series_6:_1968%E2%80%9369.

[2633] David Levy. The Gods of Foxcroft. Arbor House, 1970; https://www.amazon.com/Gods-Fox-Croft-David-Levy/dp/B000H7CKZY/.

* **1970 (TV): The Time of the Ice Box (Timeslip).**[2634] Volunteers testing a longevity drug are placed in "hibernation sleds" and kept cold outside of a secret lab in Antarctica.

* **1971 (novel): Absolute Zero.**[2635] A financier builds up a vast cryonics industry in an attempt to preserve his accidentally frozen dwarf parents.

* **1972 (short story): Ozmandias.**[2636] Five centuries after a nuclear holocaust, some people from the past who have been in cryogenic stasis wake up.

* **1973 (novella): The Defenseless Dead.**[2637] First use of "corpsicles" to refer to cryonics patients.

* **1973 (novel): Looking Backward from the Year 2000.**[2638] A multi-million dollar business mogul with only 6 months to live due to a bad heart turns to cold hibernation. He liquidates all of his assets, says good-bye to his love, buys priceless works of art and stores them in a secluded cave for hope of making a return on his investment, then goes into hibernation... awaking nearly thirty years later, by means unknown.

* **1973 (movie): Sleeper.**[2639] The owner of a health food store is cryogenically frozen in 1973 and defrosted 200 years later (on a conventional-looking operating table), awakening in an ineptly led police state. This is everyone's favorite cryonics comedy film.

* **1974 (novel): The Dream Millennium.**[2640] A medical doctor, captain of a sleeper ship built to colonize extrasolar worlds during its 1000-year voyage, spends almost all of his time in cryogenic hibernation, during which he dreams the entire lives of people and other creatures that lived and died on Earth in the past.

* **1975 (short story): Doing Lennon.**[2641] A wannabe rock star freezes himself with the hope of emerging, thawed, as the famous Beatle; no mention of how the revival was done.

* **1976 (novel): Doorways in the Sand.**[2642] Fred receives a generous stipend from his cryogenically-frozen uncle as long as he is a full-time student and has not received an academic degree,

---

[2634] https://en.wikipedia.org/wiki/Timeslip. See video of Episode 12 at https://www.youtube.com/watch?v=PFBCmjFeQI8.

[2635] Ernest Tidyman. Absolute Zero. The Dial Press, New York, 1971; http://www.sf-encyclopedia.com/entry/tidyman_ernest.

[2636] Terry Carr. Ozmandias. In: Ellison H, ed. Again, Dangerous Visions. Doubleday, 1972; https://www.amazon.com/Again-Dangerous-Visions-Original-Stories/dp/B0006C0GBA/.

[2637] Larry Niven. The Defenseless Dead. In Elwood R, ed. Ten Tomorrows. Fawcett Gold Medal Book, 1973; https://en.wikipedia.org/wiki/The_Defenseless_Dead.

[2638] Mack Reynolds. Looking Backward from the Year 2000. Ace Books, New York, 1973; https://www.amazon.com/Looking-Backward-Year-2000-Reynolds/dp/B00LDCSCIQ/.

[2639] https://en.wikipedia.org/wiki/Sleeper_(1973_film).

[2640] James White. The Dream Millennium. Michael Joseph, 1974; https://en.wikipedia.org/wiki/The_Dream_Millennium.

[2641] Gregory Benford. Doing Lennon. Analog Sci Fiction Sci Fact. 1975 Apr;95(4):152-163; https://www.publishersweekly.com/978-1-59606-686-1.

[2642] Roger Zelazny. Doorways in the Sand, Harper & Row, 1976; https://en.wikipedia.org/wiki/Doorways_in_the_Sand. First appeared in the Jun-Aug 1975 issues of Analog Sci Fiction Sci Fact.

which he has put off for 13 years by changing majors repeatedly. A cryonics scam, with 90% of a firm's "customers" disposed of to organ banks, is also featured in this book.[2643]

* **1976 (novel): A World Out of Time.**[2644] Jerome Branch Corbell has incurable cancer and is cryogenically frozen in the year 1970 in the faint hope of a future cure. His body is revived in 2190 by an oppressive, totalitarian global government called "The State" which gives no legal rights whatsoever to "corpsicles". His personality and memories are extracted (destroying his body in the process) and transferred into the body of a mindwiped criminal.

* **1977 (novel): Deep Freeze.**[2645] A wealthy man with a rare fatal disease has himself frozen (in 1978) until a cure came along (in 2008).

* **1978 (novel): The Far Arena.**[2646] A Roman gladiator, having offended the Emperor Domitian, is cast upon an ice floe where he freezes until resuscitated in the twentieth century.

* **1978 (movie): The Amazing Captain Nemo.**[2647] Two Navy officers on a diving exercise discover The Nautilus buried under a reef; inside, they find Captain Nemo in cryogenic suspension.

* **1979 (novel): The Forever Formula.**[2648] A teenager frozen for 180 years is revived, decides immortality is immoral, and thaws out a room full of cryonics patients, killing them.

* **1979 (movie): Parts: The Clonus Horror.**[2649] The Clonus Project is used by very powerful people such as politicians and industrial leaders to clone themselves; having reached maturity and peak physical fitness, the resulting clones are preserved in frozen suspended animation to serve as harvestable organ banks for future transplants.

* **1979 (movie): Alien.**[2650] The commercial space tug Nostromo is returning to Earth with its seven-member crew in stasis; there is an emergency, and the ship's computer awakens the crew. According to an authoritative fan website,[2651] the mechanics of stasis are never explicitly explored in the Alien franchise, although the novelization of Alien[2652] mentions that the process involves lowering the

---

[2643] http://www.sf-encyclopedia.com/entry/cryonics.

[2644] Larry Niven. A World Out of Time. Holt, Rinehart and Winston, 1976; https://en.wikipedia.org/wiki/A_World_Out_of_Time.

[2645] H. Walter Whyte. Deep Freeze. Manor Books, 1977; https://www.amazon.com/Deep-Freeze-H-Walter-Whyte/dp/0532125274.

[2646] Richard Ben Sapir. The Far Arena. Seaview Books, NY, 1978; http://www.sf-encyclopedia.com/entry/sapir_richard_ben; https://en.wikipedia.org/wiki/The_Far_Arena.

[2647] https://www.moriareviews.com/sciencefiction/amazing-captain-nemo-1978-return-of-captain-nemo.htm.

[2648] Frank Bonham. The Forever Formula. Scholastic Paperbacks, 1979; https://www.amazon.com/Forever-Formula-Frank-Bonham/dp/0590323059/.

[2649] http://www.sf-encyclopedia.com/entry/parts_the_clonus_horror.
[2650] https://en.wikipedia.org/wiki/Alien_(film).
[2651] https://avp.fandom.com/wiki/Stasis#Behind_the_Scenes.

[2652] Alan Dean Foster. Alien. Titan Books, 2014, p. 14; https://www.amazon.com/Alien-Official-Movie-Novelization-Foster/dp/B00SLSNE6U/.

body's core temperature considerably, and the novelization of the first sequel (Aliens)[2653] additionally states that hypersleep involves the use of drugs injected into the body. The entry for this well-known iconic film is included here for completeness because the stasis pods shown in the movie may not involve deeply hypothermic cryostasis.

* **1979 (TV): Buck Rogers in the 25th Century.**[2654] Due to a life-support malfunction, Buck is accidentally frozen for 504 years before his spacecraft is discovered adrift in the year 2491. The combination of gases that froze his body coincidentally comes close to the formula commonly used in the 25th century for cryopreservation, and his rescuers are able to revive him.

* **1980 (movie): The Empire Strikes Back (Star Wars).**[2655] Darth Vader encases Han Solo in a block of "carbonite".[2656] Solo is later revived in the sequel when a friend pushes a button on the carbonite block,[2657] activating a heater.

* **1982 (novel): Sleeping Beauty.**[2658] A newswoman's life is saved by cryonics, and she is the first successful revival.

* **1982 (movie): The Thing.**[2659] The second film version of the 1938 short story Who Goes There? (see description, above).

* **1983 (videogame): Suspended: A Cryogenic Nightmare.**[2660] The player character is a native of an offworld colony who has been selected by lottery to spend 500 years in cryogenic suspended animation. While the character is frozen in an underground complex, their subconscious mind is used to keep the colony's vital systems functioning.

* **1984 (movie): Iceman.**[2661] An anthropologist is brought to an arctic base when explorers discover the body of a prehistoric man who has been frozen for 40,000 years. After thawing the body to perform an autopsy, scientists first attempt – and succeed – to resuscitate the "iceman".

[2653] Alan Dean Foster. Aliens. Titan Books, 2014, p. 8; https://www.amazon.com/Aliens-Novelization-Alan-Dean-Foster/dp/178329017X.

[2654] https://en.wikipedia.org/wiki/Buck_Rogers_in_the_25th_Century_(TV_series).

[2655] https://en.wikipedia.org/wiki/The_Empire_Strikes_Back.

[2656] According to one description,[*] carbonite freezing "is based on the concept of cryonics, which involves freezing a living organism to keep it in suspended animation….the carbonite used in Star Wars might be a 'dry ice' with an opposite charge [or] a form of carbon dioxide mineral, which, like in cryonics, is kept at very low temperatures, to the point that there is no need for oxygen or blood-flow. This could keep living organisms and living tissue in suspended animation. While the freezing process as depicted in the films is realistic, reversing the same process by heating is more challenging and can be dangerous if heated too fast." Interestingly, in 2020 researchers preserved nematodes in a suspended animation state known as anhydrobiosis embedded in a solid blob of gallium metal (which melts at low temperature) for seven days, after which the worms were recovered alive.[†]

[*] https://en.wikipedia.org/wiki/Technology_in_Star_Wars#Carbonite_freezing.

[†] Contiliani DF, de Araújo Ribeiro Y, de Moraes VN, Pereira TC. *Panagrolaimus superbus* tolerates hypoxia within Gallium metal cage: implications for the understanding of the phenomenon of anhydrobiosis. J Nematol. 2020;52:1-6; https://www.ncbi.nlm.nih.gov/pmc/articles/pmid/32421263/.

[2657] https://live.staticflickr.com/5550/11303453375_9a885a90f2_b.jpg.

[2658] L.L. Greene. Sleeping Beauty. Signet, 1982; https://www.amazon.com/Sleeping-Beauty-L-Greene/dp/0451115481/.

[2659] https://en.wikipedia.org/wiki/The_Thing_(1982_film).

[2660] http://www.sf-encyclopedia.com/entry/suspended_a_cryogenic_nightmare.

[2661] https://en.wikipedia.org/wiki/Iceman_(1984_film).

* **1985 (movie): Wes Craven's Chiller.**[2662] A corporate executive dies and is cryonically preserved in the hopes that he can be revived. Ten years later, his storage tank malfunctions and begins to thaw, and he is rushed to a hospital. His mother arranges for surgeons there to perform a procedure that was not possible when he was originally frozen. The operation is a success and the man revives and returns home, but without his soul.

* **1985 (TV): Deep Freeze (Misfits of Science).**[2663] A cryopreserved subject from 1937, upon waking, is left simple-minded and with the power to freeze anything he touches, though vulnerable to warmer temperatures; he is kept cold in an ice cream truck.

* **1986 (novel): Fiasco.**[2664] Is a person who is cryopreserved for centuries and then revived with amnesia still the same person?

* **1986 (novel): Ralph's Journey.**[2665] Fictional life story of a car salesman who is cryopreserved in 1988 and revived in 2017.

* **1987-1990 (short stories): LifeQuest.**[2666] Cryonics fiction, written by cryonicists.

* **1987 (movie): The Return of Sherlock Holmes.**[2667] A hidden basement leads to a crude cryonics capsule in which a man is frozen in suspended animation. The man is revived and proves to be Sherlock Holmes, who is suffering from bubonic plague (from which he is quickly cured); Watson had helped devise the capsule to preserve Holmes until a cure was available.

* **1987 (movie): Order of the Black Eagle.**[2668] Duncan Jax must stop neo-Nazis from destroying communication satellites and awakening Hitler from a cryogenic sleep.

* **1987 (TV): The Big Thaw (Miami Vice).**[2669] The wife of a cryopreserved reggae singer wants his revival stopped so she can inherit his estate.

* **1988 (novel): Freeze.**[2670] "Enter a place where there is no death."

* **1988 (TV): The Neutral Zone (Star Trek).**[2671] The Enterprise-D discovers a derelict Earth satellite called the SS Birdseye[2672] with cryonically frozen humans aboard in "refrigeration pods" who died of causes they believed would be treatable in the future. Dr. Crusher, in reviving them, easily cures them

---

[2662] https://en.wikipedia.org/wiki/Wes_Craven's_Chiller.
[2663] https://en.wikipedia.org/wiki/Misfits_of_Science.

[2664] Stanislaw Lem. Fiasco. Fischer Verlag, 1986; https://en.wikipedia.org/wiki/Fiasco_(novel).

[2665] David Pizer. Ralph's Journey. Little Woofy Publishers, 1986; https://www.amazon.com/Ralphs-Journey-David-S-Pizer/dp/B004B04JF2/.

[2666] https://web.archive.org/web/20060328145643/http://www.lifepact.com/lifequestindex.htm.
[2667] http://www.sf-encyclopedia.com/entry/return_of_sherlock_holmes_the.
[2668] https://en.wikipedia.org/wiki/Order_of_the_Black_Eagle_(film).
[2669] https://www.imdb.com/title/tt0647118/.

[2670] William Raynor, G. Myles Wilder. Freeze. Critics Choice Paperbacks, 1988; https://www.amazon.com/Freeze-William-Raynor/dp/1555472443/.

[2671] https://en.wikipedia.org/wiki/The_Neutral_Zone_(Star_Trek:_The_Next_Generation).
[2672] https://memory-alpha.fandom.com/wiki/Cryonics_satellite.

of their illnesses. They have to cope with the culture shock of awakening in a distant future with the realization that everything they knew and had are now gone. "A lot has changed in the past three hundred years. People are no longer obsessed with the accumulation of things. We've eliminated hunger, want, the need for possessions. We've grown out of our infancy….The challenge, Mr. Offenhouse, is to improve yourself…to enrich yourself. Enjoy it."

* **1989 (novel): The Great Grave Robbery.**[2673] A detective investigates the theft of an artificial virus that allows cryogenically suspended people to be safely thawed, and is worth $100 million.

* **1989 (movie): The Chilling.**[2674] The bodies at a cryogenic center are defrosted by accident and turn into cannibalistic zombies.

* **1990 (novel): The Death of Sleep.**[2675] A woman keeps getting frozen during space accidents, and subsequently spends all of her time adjusting to new societies.

* **1990 (novel): The World at the End of Time.**[2676] A young man is cryopreserved and revived many times, and sees the rise and fall of various civilizations.

* **1990 (TV): The Good Human Bar (L.A. Law).**[2677] A lawyer's old law school girlfriend has an inoperable brain tumor and asks him to represent her suing the state for her constitutional right to be frozen alive.

* **1991 (novel): Heads.**[2678] A lunar corporation purchases 410 cryogenically frozen heads from Earth, then attempts to probe their minds.

* **1991 (movie): Late for Dinner.**[2679] On the run with a friend, a man discovers he has glomerulonephritis that will eventually kill him. A doctor has invented a procedure that can freeze a human being without killing him, and convinces the man to let the doctor freeze him and the friend until the man can be treated for kidney disease – maybe even get a new kidney – and to hide them from the police. Excited by the prospect of being cured, the man agrees, and assumes his unconscious friend will be okay with it. The doctor allows the man to think it's just like sleeping, and it will only be for a little while. The doctor sedates them and prepares the men for the cryogenic process. Twenty-nine years later, a truck crashes, destroying and flooding the cryogenic storage facility, and causing the tanks storing the two men to burst open. The man and his friend are revived after floating in electrified water.

[2673] John Minahan. The Great Grave Robbery. W.W. Norton & Company, 1989; https://www.publishersweekly.com/978-0-393-02721-1.

[2674] https://www.youtube.com/watch?v=kUUyzcOhYuM. See also https://www.imdb.com/title/tt0097059/.

[2675] Anne McCaffrey, Jody Lynn Nye. The Death of Sleep. Baen Books, 1990; https://en.wikipedia.org/wiki/The_Death_of_Sleep.

[2676] Frederik Pohl. The World at the End of Time. Del Rey Books, 1990; https://en.wikipedia.org/wiki/The_World_at_the_End_of_Time.

[2677] https://www.imdb.com/title/tt0624130/.

[2678] Greg Bear. Heads. St. Martins Press, 1991; https://www.amazon.com/Heads-Greg-Bear/dp/0312063679/. Previously serialized in Interzone Jul-Aug 1990.

[2679] https://en.wikipedia.org/wiki/Late_for_Dinner.

* **1992 (movie): Forever Young.**[2680] In 1939, when his girlfriend lapses into apparently terminal coma after being hit by a car, grief-stricken test pilot volunteers for a one-year experiment in cryonics conducted by his best friend. The friend dies, and the secret experiment sits unnoticed in a military warehouse until 1992, when two small boys accidentally open the cryonic chamber, play with its dials and controls, and accidentally activate the restoration process, whereupon the pilot revives, apparently still a sexy youngish man. Soon, however, it becomes clear that the pilot is aging very rapidly.[2681]

* **1992 (movie): Encino Man.**[2682] During the first ice age, a caveman attempts to make fire with his partner, but an earthquake causes a cave-in that buries the two of them. 10,000 years later, a California teenager is digging a pool in his backyard and comes across a chunk of ice that has the body of a man in it, following an earthquake. The ice block is left unattended in the garage where space heaters cause the ice to melt, releasing the caveman alive into the 20th century.

* **1992 (comics): Mr. Freeze.**[2683] A brilliant cryogenicist uses a freeze ray to put his cancer-stricken wife into suspended animation until a cure can be found.

* **1993 (novel): Chiller.**[2684] Describes a near-future development of cryonics technology under threat from a psychotic anti-freezer campaign conducted by a serial killer.

* **1993 (movie): Demolition Man.**[2685] A risk-taking police officer (John Spartan) with a reputation for causing destruction while carrying out his work fails to rescue hostages from an evil crime lord (Simon Phoenix), and in 1996 both men are sentenced to lengthy terms in the city's new "California Cryo-Penitentiary", a prison in which convicts are cryogenically frozen and exposed to subliminal rehabilitation techniques. The crime lord is thawed for a parole hearing in 2032 but escapes. Unable to deal with a criminal that dangerous, the authorities in that future time awaken the officer to help capture the crime lord again.

* **1994 (novel): Mirror Dance.**[2686] Miles Vorkosigan is killed by a needle-grenade and is frozen in a cryonic chamber on the spot, but the medic in charge becomes separated from the rest of the men while retreating under fire. The medic uses an automated shipping system to send the chamber to safety, but is killed before he can tell anyone what he did and where he sent it. The frozen Miles is later resuscitated, but his memory takes some time to return.

* **1994 (novel): Solis.**[2687] A man's brain is frozen in the 21st century and thawed 1000 years later.

* **1994 (novel): The Day After Tomorrow.**[2688] Bodies with the heads removed are being found in odd places all over Europe, and they seem to have been frozen to near absolute zero and then thawed.

[2680] https://en.wikipedia.org/wiki/Forever_Young_(1992_film).
[2681] http://www.sf-encyclopedia.com/entry/forever_young.
[2682] https://en.wikipedia.org/wiki/Encino_Man.
[2683] https://en.wikipedia.org/wiki/Mr._Freeze#Post-Crisis.

[2684] Sterling Blake (Gregory Benford). Chiller. Bantam Books, 1993; https://www.fantasticfiction.com/b/gregory-benford/chiller.htm.

[2685] https://en.wikipedia.org/wiki/Demolition_Man_(film)..
[2686] https://en.wikipedia.org/wiki/Mirror_Dance.

[2687] A.A. Attanasio. Solis. Easton Press, 1994; https://www.amazon.com/introd-Illustrated-coloured-frontispiece-Attanasio/dp/B000JD0I0K/. Reviewed in https://www.alcor.org/docs/cryonics-magazine-1995-02.pdf.

[2688] Allan Folsom. The Day After Tomorrow. Little, Brown, 1994; https://en.wikipedia.org/wiki/The_Day_After_Tomorrow_(novel). Reviewed in https://www.alcor.org/docs/cryonics-magazine-1995-02.pdf.

* **1994 (TV): Frosted Flakes (Picket Fences).**[2689] A boy dying of leukemia and his parents request a judge to allow them to cryonically freeze the boy before the illness destroys his body in the hope that a cure can be found and he can be revived.

* **1994 (TV): When We Dead Awaken (SeaQuest 2032).**[2690] Brody's Mom, who has been in cryofreeze for years, emerges and is targeted by someone trying to kill her for a crime she witnessed in the past.

* **1995 (novel): Gun, with Occasional Music.**[2691] A private detective story set in a future where criminals are placed in cryonic suspension.

* **1995 (novel): Host.**[2692] The girlfriend of a computer scientist is uploaded into a computer network just before her body is cryopreserved; the scientist accidently causes the girlfriend's physical body to be destroyed, and her upload becomes vengeful.

* **1995 (novel): Tech Heaven.**[2693] When Katie's husband, Tom, is not expected to survive injuries sustained in a helicopter crash, Katie insists that he be placed in cryonic suspension against the wishes of her family and the laws banning cryonics. Putting her faith in a science that hasn't been invented yet, Katie has Tom's body placed in cryonic suspension – frozen in liquid nitrogen against a time when advances in nanotechnology might heal his injuries and restore his life. Katie's life is taken over by the need to defend her husband's future and to shepherd into existence the controversial technologies that might let him live again.[2694] (The author provides a lengthy description of a hypothetical revival scenario at pp. 283-302.)

* **1995 (TV): The 37's (Star Trek).**[2695] On a distant planet, the crew of Voyager discovers a mineshaft leading to five cryostasis chambers, one of which includes 8 human bodies all from the 1930s, one of whom is Amelia Earhart who was abducted from Earth by aliens 434 years earlier. "When all the humans are removed from stasis, they wake up easily."

* **1996 (movie): Dead Fire.**[2696] The Earth of 2062 has been devastated and is uninhabitable; in orbit aboard the space station USS Legacy, soldiers tend a consignment of people kept in cryonic suspension.

* **1996 (TV): Cold Lazarus.**[2697] At a cryonics research institute in London in the 24th century, a group of scientists is working on reviving the mind of the 20th-century writer Daniel Feeld, whose head

---

[2689] https://www.imdb.com/title/tt0674696/. See also: Ryan D. Derek Ryan Reviews the recent Picket Fences episode focused on cryonics. Cryonics 1994 Qtr 3;15(3):24-26; https://www.alcor.org/docs/cryonics-magazine-1994-03.pdf.

[2690] https://www.imdb.com/title/tt0696961/.

[2691] Jonathan Lethem. Gun, with Occasional Music. Harcourt Brace & Co., 1995; https://en.wikipedia.org/wiki/Gun,_with_Occasional_Music.

[2692] Peter James. Host. Villard Books (Random House), 1995; https://www.amazon.com/Host-Peter-James/dp/0752837451/. Reviewed in https://www.alcor.org/docs/cryonics-magazine-1997-03.pdf.

[2693] Linda Nagata. Tech Heaven. Spectra, 1995; https://www.amazon.com/Tech-Heaven-Linda-Nagata/dp/0553569260/. Reviewed in https://www.alcor.org/docs/cryonics-magazine-1996-01.pdf.

[2694] https://www.amazon.com/Tech-Heaven-Nanotech-Succession-Linda-Nagata/dp/1937197018.
[2695] https://memory-alpha.fandom.com/wiki/The_37%27s_(episode).
[2696] https://www.moriareviews.com/sciencefiction/dead-fire-1996.htm.

was frozen after Feeld's death, funded by a media mogul who envisages making a fortune from broadcasting Feeld's memories on TV. As more of Feeld's thoughts and memories are unearthed, it becomes evident not only that Feeld's mind is conscious of its predicament, but also that Feeld is attempting to communicate with the scientists and is pleading to be allowed to die.

* **1997 (novel): Tomorrow and Tomorrow.**[2698] When his wife Ana is diagnosed with an unspecified incurable brain disorder, Drake exhausts every option attempting to cure her. Only then does he decide to have her body cryogenically stored, in the hope that future generations will discover an effective treatment. In case the future culture doesn't care about her plight, he has himself frozen as well. He is first awakened in the year 2512 but no cure for Ana yet exists. Drake is continually laid dormant and revived, progressively later into the future, all the way until the time of the Big Crunch.

* **1997 (novel): 3001: The Final Odyssey.**[2699] Frank Poole, murdered by the HAL 9000 computer in 2001: A Space Odyssey, was cryopreserved by his exposure to space. One millennium later, Poole's freeze-dried body is discovered in the Kuiper belt by a comet-collecting space tug named the Goliath, and revived. Poole is taken home to learn about Earth in the year 3001.

* **1997 (novel): A King of Infinite Space.**[2700] An obnoxious 1980s rich kid is killed in a car crash; his head is deep-frozen and he is revived into a cloned body centuries in the future, on an asteroid named for Jerry Garcia.

* **1997 (movie): Austin Powers: International Man of Mystery.**[2701] Austin and Dr. Evil are awakened after being cryogenically frozen for thirty years.

* **1997 (movie): Batman & Robin.**[2702] Mr. Freeze's wife is alive in cryogenic slumber.

* **1997 (movie): Open Your Eyes.**[2703] A man signs a contract with Life Extension, a company specializing in cryonics, to be cryogenically preserved and to experience extremely lucid and lifelike virtual reality dreams. He commits suicide at home shortly after signing the contract and is placed in cryonic suspension. From the midpoint of the movie onward, everything has been a dream, spliced retroactively into his actual life and replacing his true memories. At the end of the film, he decides to wake and be resurrected by committing suicide.

* **1997 (TV): Fair Trade (Star Trek).**[2704] A trading post in the Delta Quadrant visited by Voyager uses cryostatic suspension as a punishment – e.g., trafficking in illicit substances draws a sentence of fifty years of cryostatic imprisonment.

[2697] https://en.wikipedia.org/wiki/Cold_Lazarus.

[2698] Charles Sheffield. Tomorrow and Tomorrow. Bantam Spectra, 1997; https://en.wikipedia.org/wiki/Tomorrow_and_Tomorrow_(novel). Reviewed in https://www.alcor.org/docs/cryonics-magazine-1997-03.pdf.

[2699] Arthur C. Clarke. 3001: The Final Odyssey. Del Rey Books, 1997; https://en.wikipedia.org/wiki/3001:_The_Final_Odyssey.

[2700] Allen M. Steele. A King of Infinite Space, Harper Prism, 1997; https://www.amazon.com/King-Infinite-Space-Novel/dp/0061052868/.

[2701] https://en.wikipedia.org/wiki/Austin_Powers:_International_Man_of_Mystery.
[2702] https://en.wikipedia.org/wiki/Batman_%26_Robin_(film).
[2703] https://en.wikipedia.org/wiki/Open_Your_Eyes_(1997_film).
[2704] https://memory-alpha.fandom.com/wiki/Fair_Trade_(episode).

* **1998 (novel): Formerly Brandewyne.**[2705] A woman nearing middle age at the end of the millennium, tragically dies and is cryogenically frozen. Eighty years later she is cloned and given a second chance at life and love.

* **1998 (novel): The First Immortal.**[2706] The novel spans 200 years and gives a futuristic account of the first immortal human, who was born in 1925 and dies in 1988, then is re-animated after a cryonics procedure. The revival is briefly described on page 359: "An adult human body contains nearly a septillion (10^{24}) protein 'machines,' and each cell contains thousands of different kinds of molecules. Still, within 58 minutes, the army of 24 trillion nanomachines and nano-AIs had mapped the location of every molecule that comprised Benjamin Smith. Less than 141 minutes later, each broken or lost piece of protein had been repaired or replaced, and every molecule restored to its ideal position….He opened his eyes…."

* **1998 (TV): Lisa the Simpson (The Simpsons).**[2707] In this episode of the animated television comedy series "The Simpsons", an old man removes the ice cream from a freezer unit at a convenience store and climbs in, freezing himself while clutching an explanatory note in his hand[2708] that reads: "I have frozen myself so I may live to see the wonders of the future. Thaw me out when robot wives are cheap and effective." He later spontaneously defrosts and walks out of the store.

* **1999 (novel): A Deepness in the Sky.**[2709] An intelligent alien species lives on a planet orbiting an anomalous star dubbed OnOff because for 215 of every 250 years it is dormant, releasing almost no detectable energy. During this period, the planet freezes, the entire atmosphere condenses in solid form on its surface, and its fauna (and all members of the intelligent species) go into hibernation – a case of whole-planet reversible cryopreservation. The planet is visited by human explorers whose starships employ coldsleep technology to avoid aging while traveling between stars at sublight velocities.

* **1999 (novel): Love Me Tomorrow.**[2710] A one-time porno star is frozen in 1976 and comes back to life in 2000, still 32-years-old with an aging husband and grown children.

* **1999 (novel): The Centurion's Empire.**[2711] A Roman soldier dies in winter in the Alps and is frozen inside a glacier and preserved, after which he wakes up several times and goes into "sleep" again – courtesy of a whole centuries-old secret society that has found the secret of immortality by inventing a low-tech cryonic suspension, using only natural ice and drugs.

[2705] Jude Liebermann. Formerly Brandewyne. Independently published, 1998; https://www.amazon.com/Formerly-Brandewyne-Jude-Liebermann/dp/1973395835/. Reviewed in https://www.alcor.org/docs/cryonics-magazine-2001-02.pdf.

[2706] James L. Halperin. The First Immortal. Del Rey Books, 1998; http://www.cryonics.org/images/uploads/misc/firstimmortal.pdf.

[2707] https://en.wikipedia.org/wiki/Lisa_the_Simpson.

[2708] "S09E17 – Frostillicus"; https://www.youtube.com/watch?v=vgrTpew2iX8.

[2709] Vernor Vinge. A Deepness in the Sky. Tor Books, 1999; https://en.wikipedia.org/wiki/A_Deepness_in_the_Sky.

[2710] Robert H. Rimmer. Love Me Tomorrow. iUniverse, 1999; https://www.amazon.com/Love-Me-Tomorrow-Robert-Rimmer/dp/158348096X/.

[2711] Sean Mcmullen. The Centurion's Empire, Tor SF, 1999; https://www.amazon.com/Centurions-Empire-Sean-Mcmullen/dp/0812564758.

* **1999 (TV): Space Pilot 3000 (Futurama).**[2712] This pilot episode of the animated television comedy series Futurama[2713] focuses on the cryogenic freezing of the series protagonist, Philip J. Fry,[2714] and the events when he awakens 1,000 years in the future.

* **1999 (TV): The Last Train.**[2715] In this British miniseries, a random group of individuals on a train travelling between London and Sheffield are cryogenically frozen when the train crashes inside a tunnel and a canister of gas being carried by a passenger is released in their carriage. They unfreeze 52 years later to find the United Kingdom in ruins.

* **1999 (TV): Prehistoric Ice Man (South Park).**[2716] In this episode of the animated television comedy series South Park, Stan and Kyle discover a man frozen in ice inside a cave, then take the man to Dr. Mephesto who thaws the ice covering the man and discovers that he is alive and was frozen for only 32 months. Mephesto and all adults treat him as a prehistoric man and appear to be unable to understand him even though he speaks perfect English.

* **2000 (novel): Code Blue.**[2717] "The story largely concerns cryonics...as an 'ambulance' to the future where more advanced medical technology may make them well and young again."

* **2000 (novel): Project Resurrection.**[2718] In the year 2013, a group of scientists in Alaska's frozen Arctic are reanimating cryopreserved humans. They don't realize they are stealing the souls from the living, ripping through the barrier that lies between life and death.

* **2000 (novel): Rebirth of the Frozen Head in the Year 2240.**[2719] An eighty year old man is frozen in 1999 as a neuro and revived two centuries later.

*** 2000 (TV): The Cryonic Woman (Futurama).**[2720] Fry's old girlfriend from the year 2000 was also cryopreserved and is reawakened.

*** 2000 (TV): Looking Death in the Eye / Livia (Xena: Warrior Princess).**[2721] Xena and Gabrielle fake their own deaths only to be mistakenly entombed in an icy cave on Mount Aetna, where they are preserved for 25 years until an avalanche frees them.

[2712] https://en.wikipedia.org/wiki/Space_Pilot_3000.
[2713] https://en.wikipedia.org/wiki/Futurama.
[2714] https://images.fanpop.com/images/image_uploads/Fry-Gets-Frozen-futurama-605768_640_476.jpg.
[2715] https://en.wikipedia.org/wiki/The_Last_Train_(TV_series).
[2716] https://en.wikipedia.org/wiki/Prehistoric_Ice_Man.

[2717] Nancy Fisher. Code Blue. Onyx Fiction Penguin Putnam, 2000; https://www.amazon.com/Code-Blue-Nancy-Fisher/dp/0451197674/. Reviewed in https://www.alcor.org/docs/cryonics-magazine-2000-02.pdf.

[2718] Karen Duvall. Project Resurrection. Speculation Press, 2000; https://www.amazon.com/Project-Resurrection-Karen-Duvall/dp/0967197953/.

[2719] Morris Steinberg. Rebirth of the Frozen Head in the Year 2240. Xlibris, 2000; https://www.amazon.com/Rebirth-Frozen-Head-Year-2240/dp/0738825360/. Reviewed in https://www.alcor.org/docs/cryonics-magazine-2001-02.pdf.

[2720] https://en.wikipedia.org/wiki/The_Cryonic_Woman.

[2721] "Looking Death in the Eye" (#109, S5E19, 24 Apr 2000) and "Livia" (#110, S5E20, 1 May 2000); https://en.wikipedia.org/wiki/Xena:_Warrior_Princess_(season_5).

* **2001 (novel): Stasis.**[2722] Brad Harris, a political science major, is shocked to learn that his grandfather, James, declared clinically dead twenty years ago, has been revived from cryonic suspension. Stasis is the story of religious belief versus scientific reality and cryonics gone awry.

* **2001 (novel): The Precipice.**[2723] Many subjects have been cryonically preserved, but those who are revived have lost all their memories.

* **2001 (movie): Vanilla Sky.**[2724] A playboy's world comes apart at the seams following facial disfigurement in a discarded girlfriend's suicidal revenge car crash; a series of slippages in reality and identity are eventually explained as the result of cryonic suspension in a virtual reality.[2725] The life extension company uses cryonic suspension to save those with terminal illnesses until a cure can be found, keeping them in a lucid dream state to otherwise exercise their mind. (This film was a remake of the Spanish movie Open Your Eyes (1997); see above.)

* **2001 (movie): Jason X.**[2726] In this tenth installment of the "Friday the 13th" film series, Jason is cryogenically frozen for 445 years, until he is found and inadvertently awoken by a group of students in the year 2455, allowing him to stalk and kill them one by one aboard their spaceship.

* **2002 (novel): Waking Walt.**[2727] For nearly 40 years, the great entertainment genius has been in cryonic suspension, waiting to return when a cure for his lung cancer is found. Now, an experimental drug being tested looks like the answer, but a ruthless corporate raider launches a takeover attempt of The Disney Company, planning to sell off the company's assets to the highest bidders. But the Circle is still there, the small group of confidants who helped Walt escape death and who have been guarding him and his secret ever since.

* **2005 (TV): Let Sales Ring (Boston Legal).**[2728] Milton Bombay needs Denny and Shirley to help him be frozen so he can continue his legacy as a great lawyer in the future.

* **2006 (novel): I Was A Teenage Popsicle.**[2729] Floe Ryan was frozen – or "vitrified" – at sixteen. She and her parents had a rare disease, so it was their only choice until a cure was found. Now she's been thawed and it's ten years in the future – but she's still a teenager. A sequel novel[2730] was published in 2007.

* **2006 (movie): Idiocracy.**[2731] An American soldier takes part in a classified hibernation experiment, only to be accidentally frozen for too long and awaken 500 years later in a dystopian world

---

[2722] Kelly Steed, Colleen Elliott. Stasis. AmErica House, 2001; https://www.amazon.com/Stasis-Kelly-Steed/dp/1588512320/.

[2723] Ben Bova. The Precipice (The Asteroid Wars: 1). Tor Books, New York, 2001; https://en.wikipedia.org/wiki/The_Precipice_(Bova_novel).

[2724] https://en.wikipedia.org/wiki/Vanilla_Sky.
[2725] http://www.sf-encyclopedia.com/entry/vanilla_sky.
[2726] https://en.wikipedia.org/wiki/Jason_X.
[2727] https://www.amazon.com/Waking-Walt-Larry-Pontius/dp/059525425X/.
[2728] https://www.imdb.com/title/tt0530525/.

[2729] Bev Katz Rosenbaum. I Was a Teenage Popsicle. Berkley, 2006; https://www.amazon.com/Was-Teenage-Popsicle-Katz-Rosenbaum/dp/0425211800/. Reviewed in https://www.alcor.org/docs/cryonics-magazine-2009-04.pdf.

[2730] Bev Katz Rosenbaum. Beyond Cool. Berkley Trade, 2007; https://www.amazon.com/Beyond-Cool-Bev-Katz-Rosenbaum/dp/0425215636/. Reviewed in https://www.alcor.org/docs/cryonics-magazine-2009-04.pdf.

[2731] https://en.wikipedia.org/wiki/Idiocracy.

where dysgenics and commercialism have run rampant, leaving an entire human population of stupid people.

* **2006 (TV): Go God Go (South Park).**[2732] In this episode of the animated television comedy series South Park, Cartman can't wait three weeks until the Nintendo Wii console is released and attempts to enter cryonic suspension by burying himself in the snow at the top of Mount Elbert, whereupon he freezes to death, after which a freak avalanche buries his body. He remains frozen for over five centuries until being discovered and revived by members of the Unified Atheist League.

* **2007 (novel): Counting Heads.**[2733] Only Ellen, the heir to her mother's financial empire, is capable of saving Earth from complete domination plotted by the cynical, selfish, immortal rich, if she survives. Her cryonically frozen head is in the hands of her family's enemies. A ragtag ensemble of unlikely heroes join forces to rescue Ellen's head, all for their own purposes.[2734]

* **2007 (novel): 21st Century Kids.**[2735] Two kids are killed in a traffic accident in 2008 but are cryopreserved and revived 180 years later into an amazing high-tech world of the future.

* **2007 (novel): Tanner on Ice.**[2736] Evan is slipped a Mickey Finn and stuffed into a high-tech freezer in the basement of a house in Union City, New Jersey; he's found and awakened 25 years later when the then-current owner decides to have some renovation done.

* **2008 (novel): Immortal.**[2737] Novelist Bill Clem gives readers a chilling look at the science behind cryogenics in his sixth medical thriller.

* **2008 (novel): Long Life?**[2738] Rebecca Adler, a dedicated cryonicist, faces a murder charge for applying cryonics to a live person, despite claiming her alleged victim was willing and is only suspended in animation, not dead.

* **2009 (short story): Bridesicle.**[2739] Eighty years after her death in a car accident, Mira awakens in a "dating center". The patrons of the dating center are lonely men seeking wives, and dead women in cryogenic storage. A male patron can revive a female patron's head and interview her – and, if he doesn't like her, press a button to immediately return her to storage. As various suitors reject her and the years go

---

[2732] https://en.wikipedia.org/wiki/Go_God_Go.

[2733] David Marusek. Counting Heads. Tor Books, 2007; https://en.wikipedia.org/wiki/Counting_Heads.

[2734] https://www.amazon.com/Counting-Heads-David-Marusek/dp/0765317540/.

[2735] Shannon Vyff. 21st Century Kids. Warren Publishing, NC, 2007; https://www.amazon.com/Immortal-Bill-Clem/dp/097958082Xhttps://www.amazon.com/Century-CENTURY-Shannon-Mar-01-2007-Paperback/dp/B00AACI9C4/. Reviewed in https://www.alcor.org/docs/cryonics-magazine-2007-04.pdf.

[2736] Lawrence Block. Tanner on Ice, Harper, 2007; https://www.amazon.com/Tanner-Ice-Evan-Lawrence-Block/dp/0061283932/.

[2737] Bill Clem. Immortal. Vision Books, 2008; https://www.amazon.com/Immortal-Bill-Clem/dp/097958082X/.

[2738] Robert Begam. Long Life? A Courtroom Thriller. Journey into the Unknown World of Cryonics. Durban House, 2008; https://www.amazon.com/Long-Life-Journey-World-Cryonics/dp/0977986314/. See review by Mike Perry at https://www.alcor.org/docs/cryonics-magazine-2010-01.pdf.

[2739] Will McIntosh. Bridesicle. Asimov's Science Fiction 2009 Jan;32(1):40-50; https://scificats.files.wordpress.com/2011/04/bridesicle.pdf.

by, Mira's only chance to avoid being frozen forever is to convince a total stranger that she loves him enough that he should pay for her full revival – except that Mira is a lesbian who does not want to marry a man.

* **2009 (novel): Frozen in Time.**[2740] Ben and Rachel Carter's summer with their scientist uncle goes from dull to amazing when they discover an underground vault; hidden in a secret room within the vault are two children, Freddy and Polly, who have been kept in cryogenic suspension since 1956. One description[2741] of the abbreviated revival process in the book: "accidentally presses a button…and the bodies come to life".

* **2009 (novel): Lazarus Man: Resurrection.**[2742] Before Neil Jonathan Johnson was cryonically preserved in 2008, he didn't think he would ever be brought back to life. So when he is revived more than a century later, he's not ready for the world he encounters.

* **2009 (novel): The Unincorporated Man.**[2743] A successful industrialist is frozen in secret in the early twenty-first century, then discovered and resurrected in the 24th century where he is the only person who owns all existing shares of stock in himself.

* **2010 (novel): Cryoburn.**[2744] Miles Vorkosigan is investigating WhiteChrys, a major cryocorp, to which sick or dying people go to be frozen in hopes of one day being revived and cured. Evading kidnap, he escapes into the below-ground cryocombs where the frozen are stored. (This book is a sequel to the novel Mirror Dance (1994); see above.)

* **2010 (novel): Ice Hunt.**[2745] Ice Station Grendel is an abandoned Soviet research base until frozen creatures come to life.

* **2010 (novel): Laws of Time.**[2746] Along with his beloved wife, a powerful CEO embarks on a cryogenic journey to the future in the hopes that by freezing himself into hibernation, that it will be possible to skip through time until a point in the future where the true technology exists to travel in time, forwards and backwards.

* **2010 (novel): Star Pebble.**[2747] Cryonics is routine in space colonies orbiting the Earth.

[2740] Ali Sparkes. Frozen in Time. Oxford University Press, 2009; https://en.wikipedia.org/wiki/Frozen_in_Time_(novel). Reviewed in https://www.alcor.org/docs/cryonics-magazine-2014-04.pdf.

[2741] https://en.wikipedia.org/wiki/Frozen_in_Time_(novel).

[2742] Dennis Spaulding. Lazarus Man: Resurrection: The Life, Times, and Adventures of the First Cryonic Survivor. Xlibris, 2009; https://www.amazon.com/LAZARUS-MAN-RESURRECTION-Adventures-Survivor/dp/1441556877/.

[2743] Dani Kollin, Eytan Kollin. The Unincorporated Man. Tom Doherty Associates, 2009; https://en.wikipedia.org/wiki/The_Unincorporated_Man. Reviewed in https://www.alcor.org/docs/cryonics-magazine-2009-02.pdf.

[2744] Lois McMaster Bujold. Cryoburn. Baen Books, 2010; https://en.wikipedia.org/wiki/Cryoburn. Reviewed in https://www.alcor.org/docs/cryonics-magazine-2014-04.pdf.

[2745] James Rollins. Ice Hunt. Harper Illustrated, 2010; https://www.amazon.com/Ice-Hunt-James-Rollins/dp/0061965847/ and https://en.wikipedia.org/wiki/James_Rollins#Ice_Hunt_(2003).

[2746] Jeff Yee. Laws of Time. Lulu.com, 2010; https://www.amazon.com/Laws-Time-Jeff-Yee/dp/0557659213/.

[2747] Linda Chamberlain. Star Pebble. CreateSpace, 2010; https://www.amazon.com/Star-Pebble-Linda-Chamberlain/dp/1453798153.

* **2010 (novel): Thaw (Night Fall).**[2748] When the backup generators at the Institute for Cryogenic Experimentation fail during a power outage, the townsfolk learn that the bodies of 27 dangerous cult members who had been frozen for years are missing.

* **2010 (TV): A Christmas Carol (Doctor Who).**[2749] A planetary dictator keeps people stored in a cryogenics storeroom as "security" for loans.

* **2011 (novel): BioQuagmire.**[2750] A time is explored, several hundred years from now, when the clones of cryonicists frozen in the early 21st Century are empowered to make decisions about when their earlier twins are to be reanimated, and how this is to be done.

* **2011 (novel): Perdition's Gateway.**[2751] Cryonic researcher, Dr. Conner Brandt, has volunteered to die for one year. But his business executives, sensing enormous profit, and a dying billionaire desperate for a chance at life, don't want to wait that long before they use his research for themselves.

* **2011 (movie): The Thing.**[2752] The third film version of the 1938 short story Who Goes There? (see description, above), in which an alien body is found frozen in Antarctica and is excavated in a block of ice, which then thaws.

* **2011 (TV): Aurora.**[2753] A 20 year old woman is frozen and revived 20 years later, to fall in love with the son of her past love.

* **2011 (TV): Head Case (Castle).**[2754] Castle and Beckett investigate a crime scene that involves a large pool of blood, but no victim. The victim had a cryonics contract, triggered by an alarm which goes off when the victim's heart stops beating. Taking the bullet out would "kill" the corpse, so the severed head remains frozen at the cryogenics laboratory. When Ryan and Esposito find needles with the victim's brain matter on it, the head goes missing (to avoid autopsy).[2755]

* **2012 (novel): Extra Innings.**[2756] In the year 2092, Ted Williams, the greatest baseball hitter of all time, is brought back to life. Williams' cryopreserved head and brain are surgically attached to the body of a young tennis player who died in an accident.

[2748] Rick Jasper. Thaw (Night Fall). Darby Creek, 2010; https://www.amazon.com/Thaw-Night-Fall-Richard-Reece/dp/0761361618/. Reviewed in https://www.alcor.org/docs/cryonics-magazine-2014-04.pdf.

[2749] https://en.wikipedia.org/wiki/A_Christmas_Carol_(Doctor_Who).

[2750] Fred Chamberlain III, Linda L. Chamberlain. BioQuagmire. CreateSpace, 2011; https://www.amazon.com/BioQuagmire-Fred-Chamberlain-III/dp/1453816127/.

[2751] Terrance Drake. Perdition's Gateway. Cedar Fort, 2011; https://www.amazon.com/Perditions-Gateway-Terrance-Drake/dp/1599555077/.

[2752] https://en.wikipedia.org/wiki/The_Thing_(2011_film).

[2753] Aurora. 2011; https://www.telemundo.com/shows/aurora (a Spanish-based telenovela by Telemundo that deals with cryonics).

[2754] https://en.wikipedia.org/wiki/Castle_(season_4)#Episodes.
[2755] http://chronopause.com/chronopause.com/index.php/2011/10/06/cryonics-%e2%80%9ccastle%e2%80%9d/index.html.

[2756] Bruce E. Spitzer. Extra Innings. Bear Hill Media, 2012; https://www.amazon.com/Extra-Innings-greatest-Cryonics-brought/dp/0984956905/.

* **2012 (movie): Lockout.**[2757] A CIA agent wrongly accused of murder is sentenced to thirty years in cryogenic stasis at the orbiting prison M.S. One.

* **2013 (novel): Cryonic: A Zombie Novel.**[2758] A man is cryogenically frozen upon his death, then is reanimated in a future wrought with violence and despair.

* **2013 (movie): Ice Soldiers.**[2759] Scientists in the Canadian Arctic locate the bodies of three soldiers, created as genetic supermen and nearly invulnerable to damage and frozen since 1962; the three soldiers quickly revive and slaughter the entire complement of the base.

* **2013 (movie): Star Trek Into Darkness.**[2760] Enterprise is equipped with new torpedoes that turn out to contain cryonically-frozen genetically-enhanced human beings.

* **2014 (novel): Lockstep.**[2761] A teenager lost in space puts himself into cold sleep, then awakens to find himself the heir of a wealthy interplanetary dynasty.

* **2014 (novel): The Perfect Corpse.**[2762] A perfectly frozen body discovered in the Greenland ice sheet is resurrected in a fictional cryonics laboratory in Nevada.

* **2014 (novel): While We Run.**[2763] Tegan's no ordinary girl - she died in 2027, only to be frozen and brought back to life in Abdi's time, 100 years later.

* **2014 (movie): Interstellar.**[2764] While not explicitly noted in the movie, it appears that the hypersleep pods[2765] may employ a cryogenic-based suspended animation.

* **2015 (novel): Noggin.**[2766] A teenage boy dying of leukemia agrees to an experiment in which his head will be removed and cryopreserved, in hopes that someday he may be revived and given a new body. Unexpectedly, medical advances occur in only five years and he is revived with his head transplanted onto the body of another young man who died of a brain tumor. His girlfriend is now engaged to someone else, his parents threw out all his stuff…

[2757] https://www.moriareviews.com/sciencefiction/lockout-2012.htm.

[2758] Travis Bradberry. Cryonic: A Zombie Novel. Bruyere, 2013; https://www.amazon.com/Cryonic-Zombie-Novel-Travis-Bradberry/dp/0974320668.

[2759] https://www.moriareviews.com/sciencefiction/ice-soldiers-2013.htm.

[2760] https://en.wikipedia.org/wiki/Star_Trek_Into_Darkness.

[2761] Karl Schroeder. Lockstep. Tor Books, 2014; https://www.amazon.com/Lockstep-Novel-Karl-Schroeder/dp/0765337266/.

[2762] Giles Milton. The Perfect Corpse. Prospero Press, 2014; https://www.amazon.co.uk/The-Perfect-Corpse-Giles-Milton/dp/099289722X; also http://www.gilesmilton.com/fiction/perfect-corpse.

[2763] Karen Healey. While We Run. Little, Brown Books for Young Readers, 2014; https://www.amazon.com/While-We-Run-Karen-Healey/dp/031623382X/.

[2764] https://en.wikipedia.org/wiki/Interstellar_(film).

[2765] https://interstellarfilm.fandom.com/wiki/Hypersleep_Pod.

[2766] John Corey Whaley. Noggin. Atheneum Books for Young Readers, 2015; https://www.amazon.com/Noggin-John-Corey-Whaley/dp/1442458739/. Book review by Stephen Bridge: https://www.alcor.org/docs/cryonics-magazine-2016-04.pdf.

* **2015 (movie): Air.**[2767] The world has been devastated and key scientists are kept in cryogenic suspension in vast bunkers beneath ground.

* **2016 (novel): We are Legion (We are Bob).**[2768] Bob Johansson has just sold his software company and is looking forward to a life of leisure, but is killed crossing the street. Bob wakes up a century later to find that corpsicles have been declared to be without rights and he is now the property of the state. He has been uploaded into computer hardware and is slated to be the controlling AI in a self-replicating interstellar probe looking for habitable planets.

* **2016 (novel): Jesus Wept.**[2769] A 17-year-old girl is cryopreserved and brought back to life a century later. Suffering from an unexplained amnesia, she retains her sense of selfhood and remembers the skills she acquired in her pre-cryonics life, but has lost all episodic memories.

* **2016 (novel): Zero K.**[2770] A billionaire is inspired by the terminal illness of his wife to seek immortality for both of them through cryopreservation.

* **2016 (novel): Thawing A.C. Nielson.**[2771] A microbiologist is hired to discover a way to successfully revive famous people who have been in cryonic deep-freeze for years at the Chicago firm ExitStrategy.

* **2016 (movie): Realive.**[2772] A man with a terminal illness has his body frozen in cryostasis and becomes the first man to be resuscitated from cryonics seventy years later in the year 2084.

* **2016 (movie): Passengers.**[2773] Two people are awakened ninety years too early from induced hibernation on an interstellar spaceship that is transporting thousands of passengers in cryosleep pods.[2774]

* **2017 (comics): Aliens: Dead Orbit.**[2775] The crew of a space station comes upon a derelict ship; after a search, the crew finds a cryosleep chamber just beyond a damaged bulkhead where three remaining people are found. Upon attempting to revive the people, the frozen passengers experience seizures, after which alien "chestbursters" erupt from the passengers and escape the medbay.

[2767] https://www.moriareviews.com/sciencefiction/air-2015.htm.

[2768] Dennis E. Taylor. We are Legion (We are Bob). Worldbuilders Press (Ethan Ellenberg), 2016; https://www.amazon.com/We-Are-Legion-Bob-Bobiverse/dp/1680680587/.

[2769] Bridget Nash. Jesus Wept. CreateSpace Independent, 2016; https://www.amazon.com/Jesus-Wept-Bridget-Nash/dp/1539340554/.

[2770] Don DeLillo. Zero K. Scribner, 2016; https://www.amazon.com/Zero-K-Novel-Don-DeLillo/dp/1501138073/; also https://en.wikipedia.org/wiki/Zero_K_(novel).

[2771] Paul Carey. Thawing A.C. Nielson. White Tortoise Press, 2016; https://www.amazon.com/Thawing-C-Nielsen-Paul-Carey-ebook/dp/B01LOHEP7G/.

[2772] https://en.wikipedia.org/wiki/Realive.
[2773] https://en.wikipedia.org/wiki/Passengers_(2016_film).
[2774] https://medium.com/predict/the-truth-about-cryosleep-7d114ec22eb5.
[2775] https://avp.fandom.com/wiki/Aliens:_Dead_Orbit#Publisher.27s_Summary.

* **2017 (novel): Wake Me In The Future.**[2776] Over a thousand years have passed since his family mourned his death. But Richard Green is alive again, and desperate to find his wife. Is she among the thousands still waiting to be revived, or has he lost her forever?

* **2017 (novel): The Immortal Larrikin.**[2777] A man diagnosed with a terminal disease enters a contest to receive a free cryonic suspension, but his family is aghast at the prospect.

* **2017 (movie): What Happened to Monday.**[2778] Due to overpopulation, the Child Allocation Bureau has been instituted to enforce placing any extra children into cryosleep to be reawakened at a point in the future when the population has sufficiently dropped.

* **2018 (novel): Unfatally Dead: To Thaw or Not to Thaw?**[2779] An alternate history in which Walt Disney is cryopreserved; a contract provision requires a review, every five years, to assess whether enough medical advances would make reanimation feasible.

* **2018 (novel): Keep My Love Frozen in Time.**[2780] Set in Mumbai, an Indian woman opts for cryonic preservation, but her family is aghast.

* **2019 (novel): Thaw Walt.**[2781] An alternate history in which Walt Disney is revived from cryopreservation, and the social consequences that ensue.

* **2019 (novel): Fear of Missing Out.**[2782] A teenager whose terminal cancer has returned goes on a road trip to investigate the possibility of cryopreservation that would let her be frozen until the day when a cure is available.

* **2019 (novel): The End of Forever.**[2783] A 20th century business leader has been cryonically frozen for decades, and it's time for his reanimation.

* **2019 (novel): Reviving Emily.**[2784] Emily contracted a fatal virus and spent ten years in a cryostat, then became the first person to be reanimated.

[2776] Alex Oldham. Wake Me In The Future. Lulu.com, 2017; https://www.amazon.com/Wake-Me-Future-Alex-Oldham/dp/1447836650/.

[2777] Gary J. Burrett. The Immortal Larrikin. Zeus Publications, 2017; https://www.amazon.com/Immortal-Larrikin-ultimate-cryonic-adventure/dp/0648099873/.

[2778] https://www.moriareviews.com/sciencefiction/what-happened-to-monday-2017.htm.

[2779] Wayne R. Edmiston. Unfatally Dead: To Thaw or Not to Thaw? Wedmiston Publishing, 2018; https://www.amazon.com/Unfatally-Dead-Thaw-Not/dp/0999369806/.

[2780] Jayashree Srinath. Keep My Love Frozen in Time. White Falcon Publishing, 2018; https://www.amazon.com/Keep-My-Love-Frozen-Time/dp/9387193926/.

[2781] K. K. Trice. Thaw Walt. Trice Okrzynski, 2019; https://www.amazon.com/Thaw-Walt-K-K-Trice/dp/0578428334/.

[2782] Kate McGovern. Fear of Missing Out. Farrar, Straus and Giroux, 2019; https://www.amazon.com/Fear-Missing-Out-Kate-McGovern-ebook/dp/B07GVBTCM2/.

[2783] Allyn Radford. The End of Forever. MoshPit Publishing, 2019; https://www.amazon.com/End-Forever-Allyn-Radford/dp/1925959503/.

[2784] Becca Jameson. Reviving Emily. Becca Jameson Publishing, 2019; https://www.amazon.com/Reviving-Emily-Project-DEEP-Book-ebook/dp/B07Y239XXF/. (There are 6 successive books in Jameson's "Reviving" series.)

* **2019 (TV): In the Valley of the Shadows (Chicago Med).**[2785] A hospital patient with terminal cancer drinks a cocktail of drugs designed to end his own life so that his body can be placed in cryogenic suspended animation until there is a viable cure for his condition.

* **2020 (novel): Goddess in the Machine.**[2786] Andra is a teen girl who has was put into cryogenic stasis for 100 years to travel with her family to colonize a new planet. But she wakes up from a cryogenic sleep 1000 years later than she was supposed to and everyone thinks she's a goddess.

* **2020 (novel): An Awesome Journey.**[2787] High school sweethearts die at different times, are cryopreserved, then are revived 100 years later to resume their romance. The revival is explicitly described as follows: "We have to disassemble the entire brain, taking precise measurements of where every atom is. Then, we build a new, exact duplicate of the original brain using all new atoms, and restore the brain function, the cells, and the interconnections between the brain and the new body, which had to be cloned – built from some of your original adult stem cells. The most difficult part involves the stored information that represents memories. In earlier cases, the structures encoding memory were damaged and pushed around quite a bit by the cool-down process….But our reanimation-computer machines are now so good that when they come to an atom or cell whose location they can't be sure, they can fairly infer where it goes."

* **2020 (novel): Divergent Jason.**[2788] Nine-year-old Jason dreams of living forever and wants to try cryonics, but will his father let him?

* **2021 (novel): Cryopunk.**[2789] A retired MI6 agent dies in 2023 and is cryonically frozen, only to awake fifty years later to discover a despotic regime is using top-secret military strategies he helped theorize to terrorize the United Kingdom's people.

* **2021 (novel): The Beautiful Place.**[2790] A cryonics salesman engages in a quest for a dead man's frozen head.

* **2021 (movie): Oxygen.**[2791] A woman awakens in an airtight medical cryogenic unit, and discovers that she is trapped and that the unit's oxygen levels are falling rapidly. Suffering from memory loss, she does not remember who she is or how she got there.

[2785] "In the Valley of the Shadows," Chicago Med, Season 5, Episode 3; https://en.wikipedia.org/wiki/Chicago_Med_(season_5)#Episodes. Detailed synopsis: https://medium.com/harsh-light-news/chicago-med-s05-e03-in-the-valley-of-the-shadows-recap-f95bdb024e72.

[2786] Lora Beth Johnson. Goddess in the Machine. Razorbill, 2020; https://www.amazon.com/Goddess-Machine-Lora-Beth-Johnson/dp/1984835920/.

[2787] David Pizer. An Awesome Journey. BookBaby, 2020; https://www.amazon.com/Awesome-Journey-David-Pizer/dp/109831543X/. See also: https://www.anawesomejourneybook.org/.

[2788] Simon Sallyenjavi. Divergent Jason. Bezh Denmark, 2020; https://www.amazon.com/Divergent-Jason-Simon-Sallyenjavi/dp/879722555X/.

[2789] Stephen Willis. Cryopunk. Independently published, 2021; https://www.amazon.com/Cryopunk-Stephen-Willis/dp/B08XLGJQR4/.

[2790] Lee Gowan. The Beautiful Place. Thistledown Press, 2021; https://www.amazon.com/Beautiful-Place-Lee-Gowan/dp/177187208X/.

[2791] https://en.wikipedia.org/wiki/Oxygen_(2021_film).

Descriptions of several hundred additional instances of the cryonics and cryopreservation theme in science fiction may be found in other fictional works of anime and manga, Asian animation, comic books, comic strips, fan works, film animations, literature, live-action film, music, pinball, pro wrestling, puppet shows, radio, television, theatre, video games, visual novels, webcomics, websites, and Western animation.[2792] Several dozen "independently-published" or Kindle-only cryonics-related novels were mostly omitted but are available online or as eBooks.

[2792] https://tvtropes.org/pmwiki/pmwiki.php/Main/HumanPopsicle, https://tvtropes.org/pmwiki/pmwiki.php/Main/ColdSleepColdFuture, https://tvtropes.org/pmwiki/pmwiki.php/Main/CryonicsFailure, https://tvtropes.org/pmwiki/pmwiki.php/Main/CryoPrison, https://tvtropes.org/pmwiki/pmwiki.php/Main/SleeperStarship, and https://tvtropes.org/pmwiki/pmwiki.php/Main/HarmlessFreezing.

Appendix C. Early Nanorobotic Revival Concepts (G.M. Fahy, 1991)

During Aug-Sep 1991, Gregory Fahy sketched out several features of a nanorobotic-based fracture-stabilization and fracture-healing process; his previously unpublished notes and drawings are reproduced here with his kind permission.

Step 1: Identify all fractures via external scans

Step 2: Excavate CSF space

Step 3: Deploy CCA Crawlers [powered by solid state batteries]

CCA Crawlers are vehicles capable of deploying CCA's themselves as well as **CCA Reporting Stations (CCARSs)**. CCA Crawlers have onboard computers and crawler-to-crawler communications capability. Communications are achieved by sending impulses (mechanical) according to standard temporal code.

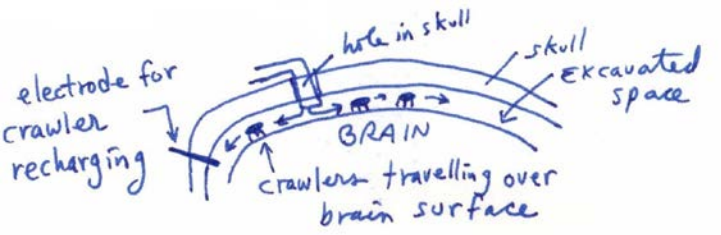

Step 4: Crawlers distribute themselves over the surface of the brain. Each crawler develops a model of its own region and sends this to adjacent crawlers, from which it receives contextual information as to the location of its local region within the brain's surface as a whole. This information is passed through the skull to external mainframes, which may display the results for any interested onlookers.

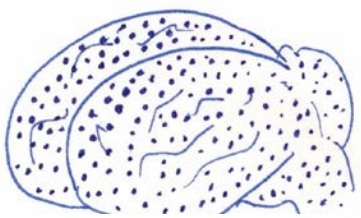

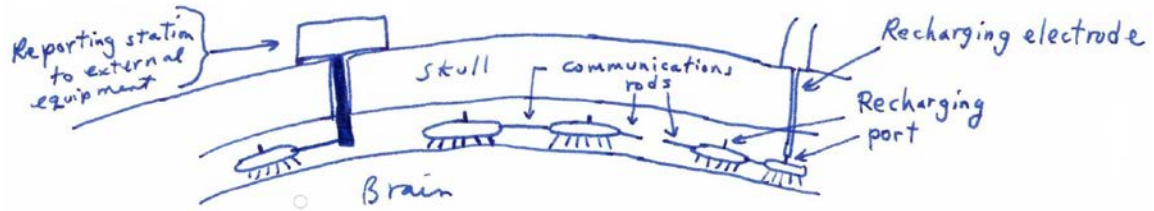

Step 5: Crawlers deploy CCAs and CCARSs, which proceed to analyze fractures.

CCAs are "Complementarity/Composition Analyzers". These are smaller mobile units that crawl into fractures. Their "feet" are connected to onboard computers that determine the width of the gap and therefore the shape of the fracture on a scale of about 40 Angstroms or so (less than the thickness of a cell membrane). Foot tip sensors determine surface composition on similar scale based on deformability, electrical conductivity, or whatever.

CCA Computer models each surface using both composition and distance from CCA body and from this model determines which points on FF1 are complementary to which points on FF2. (The amount of data is so vast and self-reinforcing that this is a relatively easy task, despite plastic deformations that create slight shape mismatches on the two surfaces.)

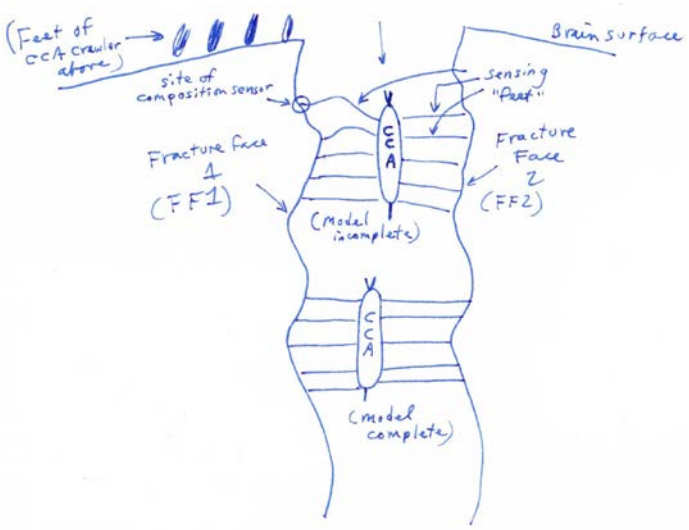

Like CCA Crawlers, the CCAs themselves are capable of inter-communication. CCAs come in more than one size, to handle fractures of different size.

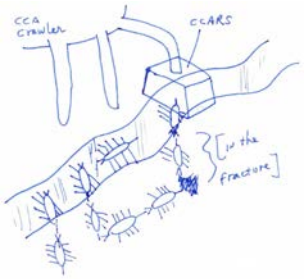

Working together, the CCAs model the entire fracture surface of each fracture, eventually depositing the information in the CCARSs, or CCA Reporting Stations. CCARSs in turn report to CCA Crawlers which in turn transmit information to external observers. Crawlers can deposit CCARSs and return to them later to collect and transmit the resulting data as needed.

Step 6: Wire base deposition: CCAs detect regions consisting of extracellular ice and glass and excavate pits using foot-tip digging tools ("molecular jackhammers"). Crawlers then pass wire bases to CCAs, which insert them into the excavated pits. (See more on "molecular jackhammers" below.) Wire bases protrude from or are recessed into the two different fracture faces.

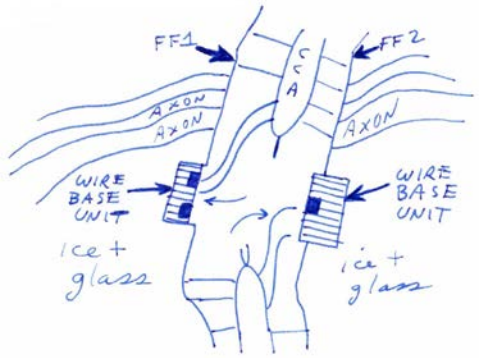

Step 7: The CCAs are withdrawn into the Crawlers and the Crawlers retreat to outside the skull. The CCARSs are left behind. **Evaporator Crawlers** are then deployed. The Evaporator Crawlers deploy evaporators, which emit metal atoms that coat and therefore form replicas of the fracture faces. Evaporators are deployed based on information tapped from the local CCARSs.

After evaporation step, the evaporators are withdrawn on the tethers and the Evaporator Crawlers are withdrawn.

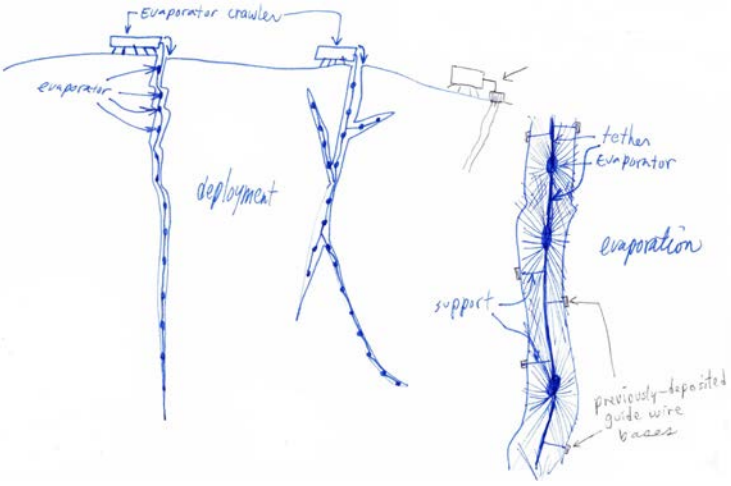

Step 8: The third wave of crawlers is now deployed. These are the **Wire Crawlers**. Because the mass of wire to be deployed is likely to exceed what can be contained in a single complement of crawlers, these crawlers have a special pass-off function permitting them to relay wires "hand-over –hand" to each other. Wire Crawlers deploy **Wire Placers (WPs)** [below, left].

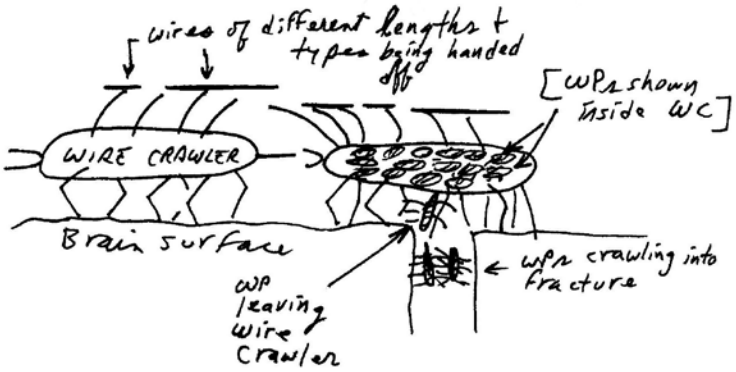

WPs travel in search of previously-deployed wire bases. These bases are easily found due to their distinctive size and shape, their existence as complementary depressions and elevations, and the presence of holes in the replicas over each wire base caused by withdrawal of the evaporator tether supports previously deployed onto them.

Detail of wire base recognition [below, right]

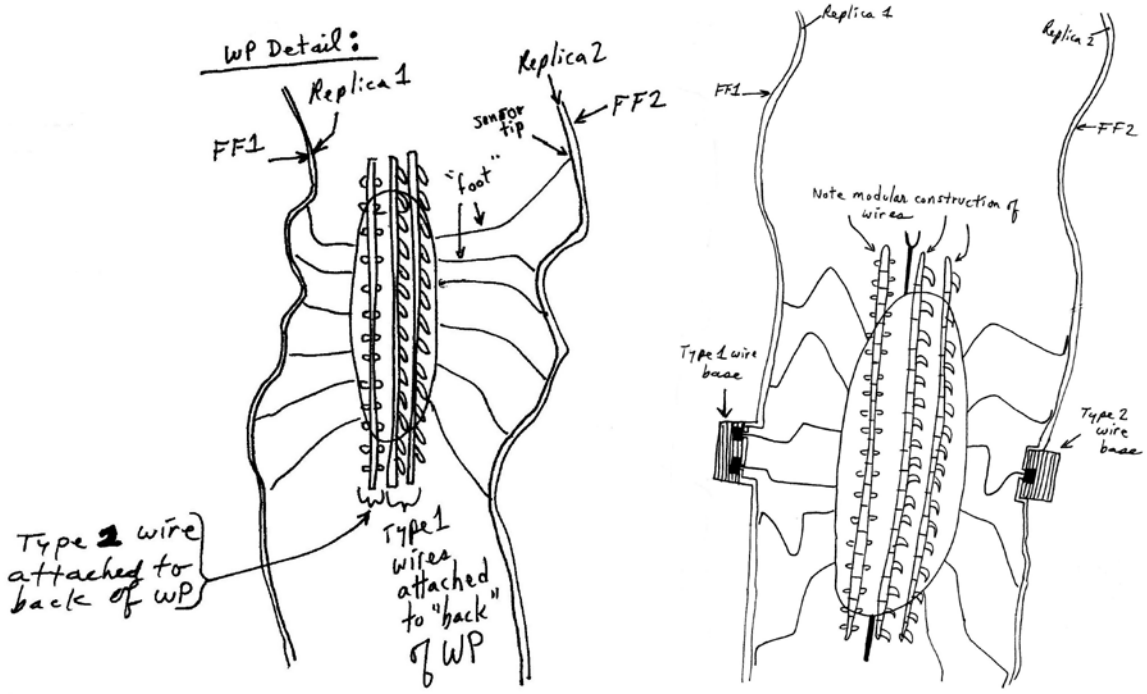

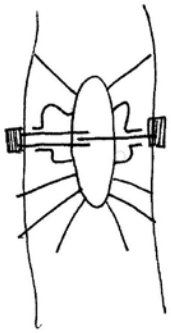

Step 9: WP now plugs wires into appropriate wire bases. Wires are adjusted in final length if necessary for best fit.

Step 10: All WPs retreat to Wire Crawlers, which in turn retreat.

Fracture Healing: Fracture healing takes place many steps after wire deployment. For clarity, however, fracture healing will be illustrated now to maintain continuity of presentation.

In the case of this fracture, the fracture faces have slipped after the fracture formed, leaving FF1 [Fracture Face 1] and FF2 [Fracture Face 2] out of register. The CCAs, however, have correctly deduced the proper sites of wire base deployment and the WPs have connected the bases correctly. The guide wires exert mechanical force on the replica faces as collective wholes, tending to force vertical relative motion of the faces as the tissue is warmed and softens. Furthermore, the guide wires exert traction on the faces in the horizontal direction as well, encouraging the faces to come together as the tissue thermally expands.

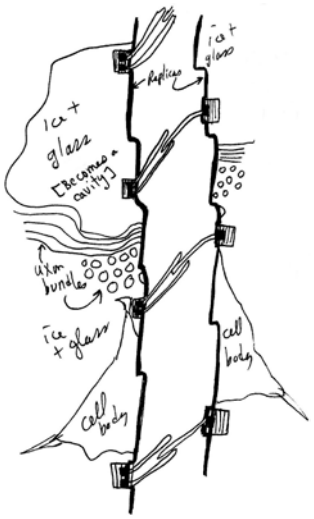

Detail of Guide Wire Action:

Position One: tractor arms on the Type 1 wires are fully extended to right, in contact with knobs on Type 2 wires.

Position Two: tractor arms have moved to the left, dragging Type 2 wire to the left along with its associated fracture face.

Position Three: lower tractor arms remain positioned to left, retaining Type 2 wire in position; upper tractor arms extend to attach to wire Type 2 next set of knobs.

Position Four: same as position one allowing cycle to repeat.

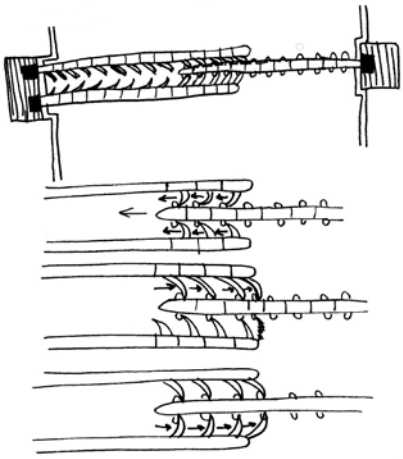

Situation #1: Wires intercalate fully.

This triggers wire disassembly. Disassembled parts are passed into cavities that once contained ice and glass on tissue sides (versus gap sides) of the replicas.

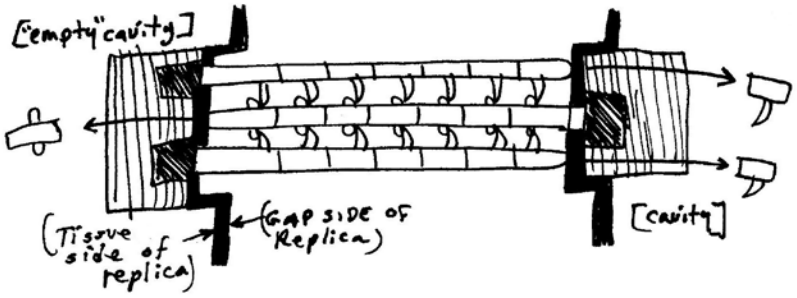

Situation #2: Termination of Wire Action/Completion of Gap Closure

Replicas of fracture faces come into contact as final Type 1 and Type 2 wire segments come into contact and all other segments have been discarded. Final wire segments maintain traction, thus locking fracture faces together.

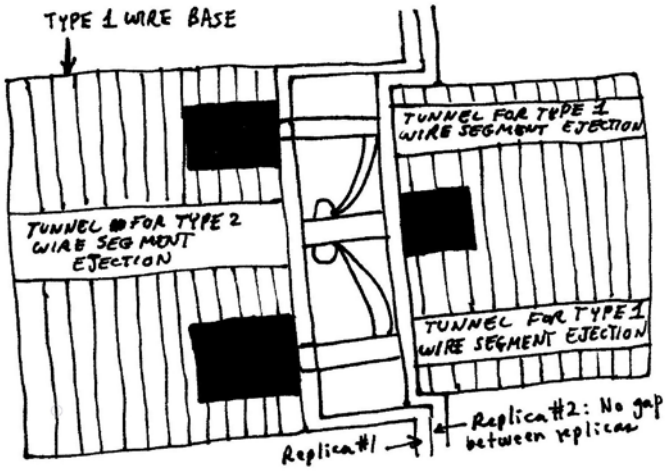

Fracture Healing Step #1: Registration of membrane-replica interfaces

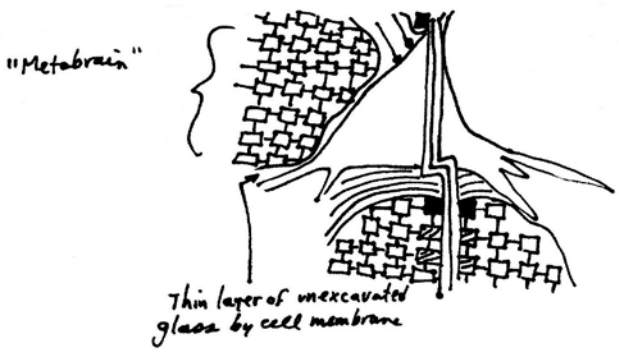

Having closed the fracture gap and therefore having brought corresponding tissue elements together with essentially molecular precision, replica material must be deleted to permit tissue structures to be fused. Replacement occurs first at membrane-replica interface.

"Metabrain" (extracellular communication and conveyance network) in the space formerly occupied by glass and ice [is indicated in the lower drawing]. The "Metabrain" detects the existence of a membrane-replica interface at the sites shown (■). (These interface sites were predicted based on data stored in the CCARSs previously "consulted", and are now confirmed.)

Fracture Healing Step #2: Membrane stabilization

Stabilization is accomplished by the physical presence of the "Metabrain", whose sensors sterically block egress of membrane elements adjacent to replica.

Detection of the membrane-replica interface at sensors A, B, and C triggers retraction of C and extension of B, flexing and breaking the replica at a point between B and C. For this to work, (a) C must be bonded to the replica, (b) B and C must be made of stronger material than the replica itself, and (c) the replica must be sufficiently brittle to break. Note: Use of evaporated metal atoms to create the replica is for convenience. More intelligent materials could be used if need be to ensure facile disassembly of the replica when this is desired.

Note: This is a 1-dimensional drawing of a 2-dimensional replica. Local replica breakdown will <u>not</u> cause replica faces to come apart.

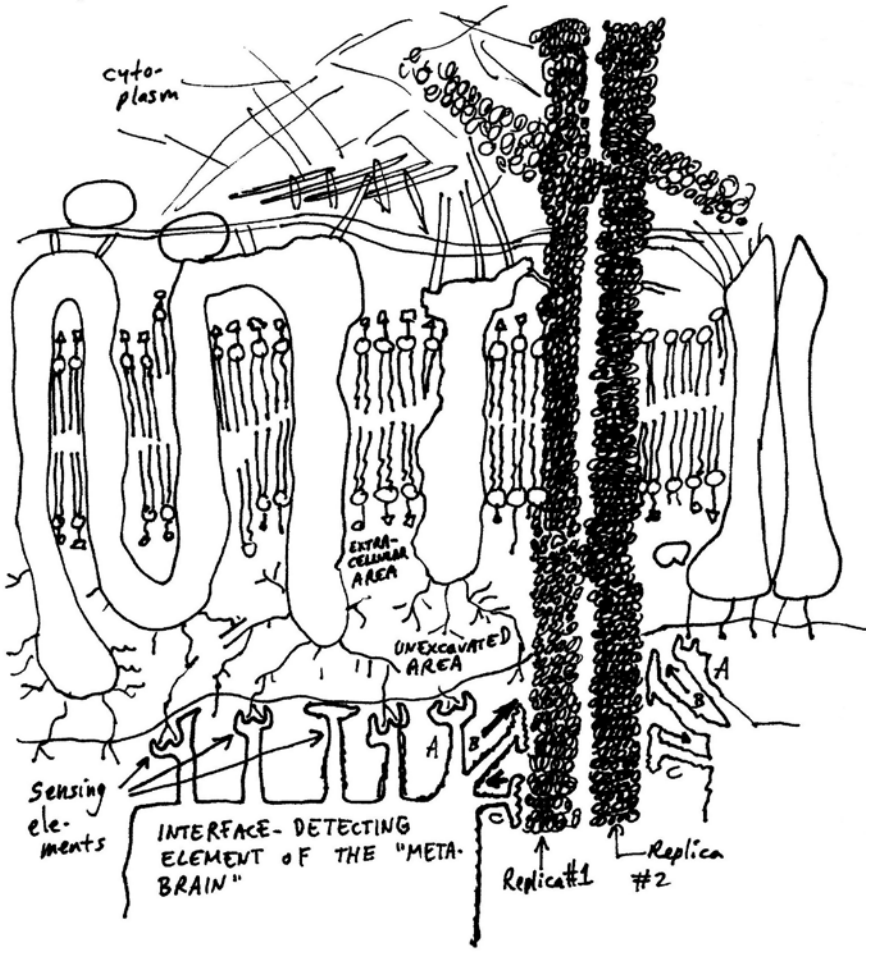

Fracture Healing Step #3:

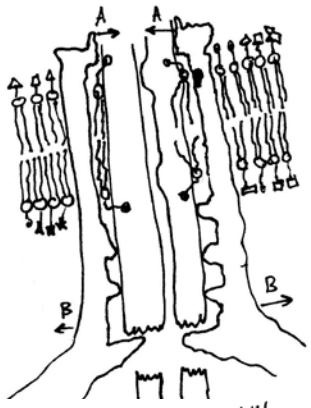

Sensor arms are extended through the thick but nevertheless liquid extracellular fluid and then through the membrane itself so as to separate the membrane from the replica. Lipids (and proteins, not shown) at the exact contact points with the replica will be partly buried in the replica and will have to be replaced later with identical elements. The nature of these "sacrificed" molecules may be detectable by the extended sensor arm.

When sensor tips at A sense completion of membrane penetration, replica grippers at B pull outward while sensor tips at A remain pushed inward so as to snap off the replica faces between A and B. Sensor arms A-B can now be withdrawn from the membrane to the level of B, creating a gap between naked membrane faces; the gap should spontaneously heal:

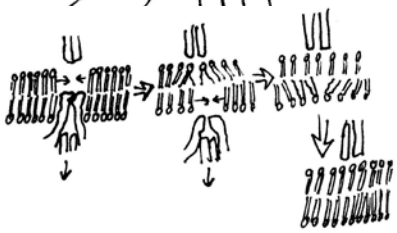

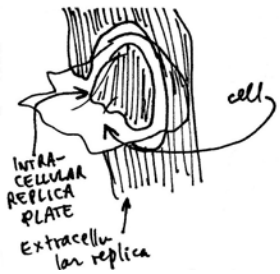

This process will tend to lead to membrane-bonded compartments, such as this cell, which are surrounded by a fracture plane that no longer touches them, and that contain a plate of intracellular replica. The intracellular plate is gradually removed and, eventually, the extracellular replicas are removed too, completing the job.

Detail of "Molecular Jackhammer": A tip to be attached to an appropriate effector arm / power supply for excavation of ice

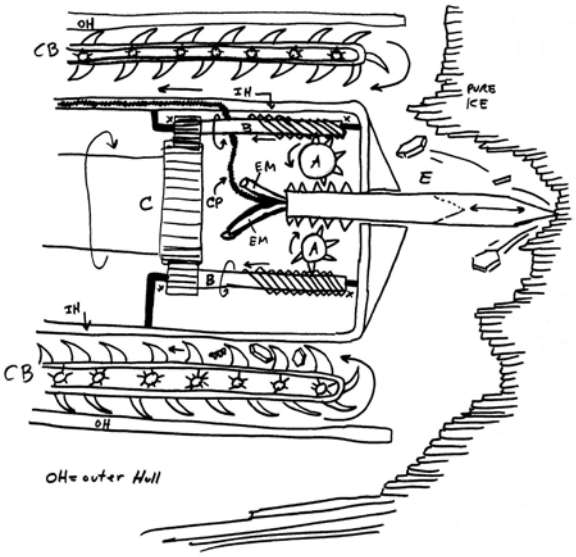

Excavator tip E is driven into ice front by gears A which in turn are driven by gears B at right angles to gears A. Gears A have complete set of teeth to engage gears B, but only incomplete teeth to engage E. Thus, when A disengages E, E is pulled back into unit by elastic molecules EM (which attach to inner hull IH at points which are out of the plane of view).

Gears B are driven by the master power gear C.

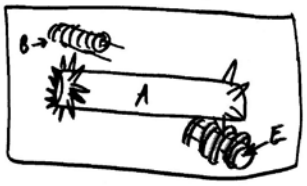

Gears B are supported by low-friction pivots at points X. Molecular conveyor belts CB remove dislodged pieces of ice. Excavation is controlled by tunneling current feedback via conductive polymer CP to CPU.

Appendix D. Cell Mills

The cell mill is a proposed molecular manufacturing system for fabricating whole human cells of several hundred different types[2793] in a viable but metabolically dormant state, personalized to a specific person (genetically), tissue destination, and activation state. This discussion is a major extension of previously published material by Freitas who first proposed the cell mill concept in 1999.[2794]

In operation, the cell mill is a desktop-style apparatus that accepts as input the consensus DNA sequence of a patient (whether living or cryopreserved), then manufactures human tissue cells or blood cells of any type in a convergent assembly process.[2795] Gross output of finished biological cells should approach $R_{CellMill} \sim 1$ kg/hr in finished quantity, roughly similar to the mature desktop nanofactory described elsewhere.[2796] Our conceptual design for a cell mill generically includes three working modules:

(1) **Biomolecule Synthesis Module** (Section D.1). All biomolecules, from the simplest organic compounds to long-chain proteins, are produced either by atomically precise molecular manufacturing or by conventional biological or biochemical techniques.

(2) **Cytocomponent Assembly Module** (Section D.2). Biomolecules are assembled into organelles, cytoskeleton fibers, and other cytological component structures, either using positionally controlled mechanical assembly or by using conventional biological or self-assembly techniques.

(3) **Cell Assembly Module** (Section D.3). Metabolically dormant but viable whole cells are assembled from organelles and other cytocomponents, and individual molecules as required, either using positionally controlled mechanical assembly or by using conventional biological or self-assembly techniques.

[2793] Freitas RA Jr. "Appendix C. Catalog of Distinct Cell Types in the Adult Human Body", Nanomedicine, Volume I: Basic Capabilities, Landes Bioscience, Georgetown, TX, 1999, pp. 393-395; http://www.nanomedicine.com/NMI/AppendixC.htm.

[2794] e.g., Freitas RA Jr. Nanomedicine, Volume I: Basic Capabilities, Landes Bioscience, Georgetown, TX, 1999, p. 32; Table 1.4, "Medical Challenges of Increasing Difficulty and Possible Approaches"; http://www.nanomedicine.com/NMI/Tables/1.4.jpg. Freitas RA Jr. Chapter 23. Comprehensive Nanorobotic Control of Human Morbidity and Aging. In: Fahy GM, West MD, Coles LS, Harris SB, eds, The Future of Aging: Pathways to Human Life Extension, Springer, New York, 2010; Section 23.6.3.5.2, "Tissue Printers, Cell Mills and Organ Mills"; pp. 744-747; http://www.nanomedicine.com/Papers/Aging.pdf. Freitas RA Jr. The Alzheimer Protocols: A Nanorobotic Cure for Alzheimer's Disease and Related Neurodegenerative Conditions. IMM Report No. 48, June 2016, 433 pp; Section 4.2.6, "Nanorobotic Cell Mills"; http://www.imm.org/Reports/rep048.pdf.

[2795] Merkle RC. Convergent assembly. Nanotechnology 1997;8:18-22; http://www.zyvex.com/nanotech/convergent.html. Freitas RA Jr., Merkle RC. Kinematic Self-Replicating Machines, Landes Bioscience, Georgetown, TX, 2004; Section 5.9.4, "Performance of Convergent Assembly Nanofactory Systems"; http://www.MolecularAssembler.com/KSRM/5.9.4.htm.

[2796] Drexler KE. Nanosystems: Molecular Machinery, Manufacturing, and Computation, John Wiley & Sons, New York, 1992, Section 14.4, "An exemplar manufacturing system architecture," pp. 421-427; https://www.amazon.com/dp/0471575186/.

D.1 Biomolecule Synthesis Module

All biomolecules, from the simplest organic compounds to long-chain proteins, may be produced either by atomically precise molecular manufacturing or by conventional biological or biochemical techniques. Most of the following discussion concentrates on the former approach.

Section D.1.1 describes the synthesis of generic organic molecules, using either the techniques of automated conventional chemical synthesis (Section D.1.1.1) or the techniques of molecular manufacturing (Section D.1.1.2).

Section D.1.2 describes the production of personalized organic molecules. The manufacturing process begins with the acquisition of the patient's consensus genomic sequence (Section D.1.2.1) – the patient-specific "clean" genome with all random mutations removed and corrected – which is obtained by selective genome sampling (Section D.1.2.1.1) followed by chromosome sequencing (Section D.1.2.1.2). With this data in hand, a DNA mill (Section D.1.2.2) can manufacture copies of the patient's fully-corrected chromosomes, suitably methylated to match the expression pattern and activation state of the particular cytotype under construction. The same data allows a protein mill (Section D.1.2.3) to fabricate proteins specific to the patient's unique biochemical signature, and related molecular mills can produce personalized carbohydrate-based and related organics equally well.

D.1.1 Generic Organic Molecules

The cell mill first needs to manufacture a large number of generic organic molecules shared by all humans. These can be produced either by the bulk methods of conventional chemical synthesis (Section D.1.1.1) or by the techniques of atomically precise manufacturing (Section D.1.1.2).

D.1.1.1 Conventional Manufacturing of Generic Organics

Many of the 10,000-100,000 different chemical substances found in human cells[2797] could be manufactured using conventional chemical synthesis techniques or by automated chemical synthesis microfactories, or could be purchased on the open market.

Conventional synthetic chemistry is a very labor-intensive task, often requiring the repeated installation and removal of protecting groups to prevent solution-phase reactions from occurring in one part of the molecule, while the chemist adds a new structure to some other part of the molecule that is unprotected. For larger-size molecules, this technique becomes cumbersome because there may be exponentially more sites where unwanted reactions can occur.

Automated synthesis machines for small organic molecules have been under serious development since at least the early 1990s.[2798] The synthesis of polymeric molecules using building blocks with well-defined

---

[2797] The Human Metabolome Database, HMDB Version 4.0; https://hmdb.ca/.

[2798] Sugawara T, Kato S, Okamoto S. Development of fully-automated synthesis systems. J Automat Chem. 1994;16(1):33-42; https://www.ncbi.nlm.nih.gov/pmc/articles/PMC2548029/pdf/JAMMC-16-033.pdf.

and chemically selective interfaces got an even earlier start, first automating the production of peptides (amino acid polymers),[2799] oligonucleotides (nucleic acid polymers),[2800] and oligosaccharides (carbohydrate polymers).[2801] Significant progress in the automated synthesis of nonpolymeric small organic molecules has awaited the development of techniques involving well-defined sets of organic building blocks with clean interfaces (image, right),[2802] and several commercial manufacturers of automated chemical synthesis equipment such as Chemspeed Technologies[2803] and Synple Chem[2804] are available.

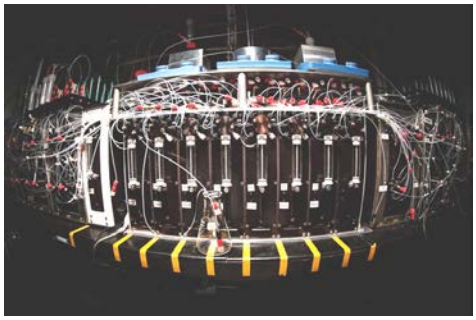

More recently, a research group at SRI International announced progress in synthesis automation on the way towards a "universal synthesizer" – an automated multistep chemical synthesizer called AutoSyn that "makes milligram-to-gram-scale amounts of virtually any drug-like small molecule in a matter of hours," so far demonstrated on ten known drugs. Of the FDA-approved small-molecule drugs for which they could compute a synthetic route, "87% are predicted to be synthesizable on AutoSyn."[2805] The process of "computing a synthetic route" has also greatly advanced with the development of algorithms for liquid-phase synthesis, e.g., by Synthia[2806] (formerly known as Chematica),[2807] a software package and database on 7 million chemicals connected by 86,000 chemical rules designed to combine long synthesis paths into shorter and more economical paths.

For a cell mill, many tens of thousands of distinct chemical species must be rapidly synthesized in order to build a living cell, and in differing amounts for each of the hundreds of possible cell types that might need to be manufactured. Despite much recent progress in miniaturizing automated chemical synthesis,[2808] nanorobotic biomolecule synthesis systems[2809] will be more compact, faster, and more productive than macroscale systems in achieving this objective, as illustrated in Section D.1.1.2 below.

[2799] Merrifield RB. Automated Synthesis of Peptides. Science 1965 Oct 8;150(3693):178-185; https://science.sciencemag.org/content/150/3693/178.

[2800] Caruthers MH. Gene synthesis machines: DNA chemistry and its uses. Science 1985 Oct 18;230(4723):281-285; https://science.sciencemag.org/content/230/4723/281.

[2801] Plante OJ, Palmacci ER, Seeberger PH. Automated Solid-Phase Synthesis of Oligosaccharides. Science 2001 Feb 23;291(5508):1523-1527; https://science.sciencemag.org/content/291/5508/1523.

[2802] Li J, Ballmer SG, Gillis EP, Fujii S, Schmidt MJ, Palazzolo AM, Lehmann JW, Morehouse GF, Burke MD. Synthesis of many different types of organic small molecules using one automated process. Science 2015 Mar 13;347:1221-6; http://www.sciencemag.org/content/347/6227/1221.full.pdf. See also https://news.illinois.edu/blog/view/6367/204395, the process machine illustrated in the image above.

[2803] https://www.chemspeed.com/.
[2804] http://synplechem.com/.

[2805] Collins N, Stout D, Lim JP, Malerich JP, White JD, Madrid PM, Latendresse M, Krieger D, Szeto J, Vu VA, Rucker K, Deleo M, Gorfu Y, Krummenacker M, Hokama LA, Karp P, Mallya S. Fully Automated Chemical Synthesis: Toward the Universal Synthesizer. Org Process Res Dev. 2020 Jun 23;24(10:2064-2077; https://pubs.acs.org/doi/abs/10.1021/acs.oprd.0c00143.

[2806] https://www.sigmaaldrich.com/chemistry/chemical-synthesis/synthesis-software.html.
[2807] https://en.wikipedia.org/wiki/Chematica.

[2808] Mattes DS, Jung N, Weber LK, Bräse S, Breitling F. Miniaturized and Automated Synthesis of Biomolecules-Overview and Perspectives. Adv Mater. 2019 Jun;31(26):e1806656; https://onlinelibrary.wiley.com/doi/pdf/10.1002/adma.201806656.

[2809] While we await the arrival of high-performance diamondoid molecular machine systems as envisioned in this book (Section 1.2), primitive low-capacity "enzyme nanofactory" systems* are being developed using DNA nanotechnology.

D.1.1.2 Molecular Manufacturing of Generic Organics

A fully automated system of atomically precise molecular manufacturing seems appropriate for the challenge of producing very small quantities of tens of thousands of specialty molecules to be used in fabricating cell structures and in populating the cytosol of manufactured human cells. As an example, we here provide a brief description of a hypothetical mechanosynthetic synthesis unit that could produce a simple organic molecule – ethyl alcohol or ethanol (C_2H_5OH) – along with tentative estimates of the mass and productivity of the nanomachinery necessary to accomplish this.[2810] It is believed that a similar set of molecular tools and reaction sequences can be devised for most simple organic molecules of interest, including hydrocarbons, carbohydrates, and other important biomolecules (e.g., amino acids) containing additional key elements such as nitrogen (N), sulfur (S), and phosphorus (P), whose study is a proper subject for ***future research***.

The **Generic Organic Synthesis Unit** builds molecules one at a time, usually on a surface via one or more tooltips that transfer reactive moieties from a source of small simple feedstock molecules (e.g., CH_4, H_2O) or surface-bound substituents (e.g., $–CH_3$, –OH, =O, –H) to the "workpiece" (i.e., the molecule that is being built). Atomically precise fabrication involves holding feedstock atoms or molecules, and a growing nanoscale workpiece, in the proper relative positions and orientations so that when they touch they will chemically bond in the desired manner. In this process, a mechanosynthetic tool is brought up to the surface of a workpiece. One or more transfer atoms are added to, or removed from, the workpiece by the tool. Then the tool is withdrawn and recharged. This process is repeated until the workpiece is completely fabricated to molecular precision with every atom in exactly the right place. Note that the transfer atoms are under positional control at all times to prevent unwanted side reactions from occurring. Side reactions are also prevented using proper reaction design so that the reaction energetics include energy barriers to avoid undesired pathological intermediate structures.

The mechanosynthetic fabrication of most organic molecules containing the three elements carbon (C), hydrogen (H), and oxygen (O) will generally require the ability to build and join together just five basic types of organic building blocks made from these elements, including:

(1) hydrocarbon chains, e.g., $–CH_2–CH_2–$;

(2) linear esters with a carbon chain interrupted by an oxygen atom, e.g., $–RCO_2R'–$, where R and R′ = a hydrocarbon chain;

(3) cyclic phenyl and phenylene groups, e.g., $–C_6H_5R$ and $–C_6H_4RR'$, where R and R′ = CH_3, OH, or other organic side group;

(4) cyclic lactones, e.g., $–O(C=O)(CH_2)_2(CHR)–$ or $–O(C=O)(CH_2)(CHR)(CHR')–$; and

(5) simple terminating groups, e.g., $–CH_3$, –OH, =O, –H, and –COOH.

It is asserted that any organic CHO molecule, including ethanol, can be built, atom by atom or group by group, by the sequential application of a surprisingly short list of mechanosynthetic tools. As few as 2 primary tools and 6 intermediate tool states ("•" indicates a radical site) may suffice for manufacturing ethanol and many similar organic molecules:

Primary #1: H abstraction "HAbst*" tool ($•CC–C_{10}H_{15}$) to remove an H atom;

---

[*] Chakraborty B, Weinhold E. DNA modification and visualization on an origami-based enzyme nano-factory. Nanoscale 2021; https://pubs.rsc.org/en/content/articlelanding/2021/nr/d0nr07618j#!divAbstract.

[2810] Freitas RA Jr. The Whiskey Machine: Nanofactory-Based Replication of Fine Spirits and Other Alcohol-Based Beverages. IMM Report No. 47, May 2016; Section 5.3.1, "Mechanosynthesis of Ethanol"; http://www.imm.org/Reports/rep047.pdf.

Primary #2: Ge radical "*GeRad" tool (•GeC_9H_{15}) for moiety transfer with weak bonding and for abstraction tool recharge reactions;

Intermediate #1: CH_3 transfer tool (CH_3–GeC_9H_{15}) to acquire a CH_3 group;
Intermediate #2: CH_2 donation tool (•CH_2–GeC_9H_{15}) to add a CH_2 group;
Intermediate #3: CH_3CH_2 donation tool (CH_3CH_2–GeC_9H_{15}) to add a CH_3CH_2 group;
Intermediate #4: OH donation tool (OH–GeC_9H_{15}) to add an OH group;
Intermediate #5: H donation tool (H–GeC_9H_{15}) to add an H atom; and
Intermediate #6: spent abstraction tool "HAbst-H" (H–CC–$C_{10}H_{15}$) needing recharge.

One possible minimal toolset for building linear, planar, branching, or cyclic organic molecules containing only the elements C (black), H (white), and O (red) is shown below, with the two primary tools at left (P1, P2) and six intermediate tool states at right (I1-I6). In this example, many tooltips also include Ge (yellow) atoms at the working apex or "bridgehead" position.[2811]

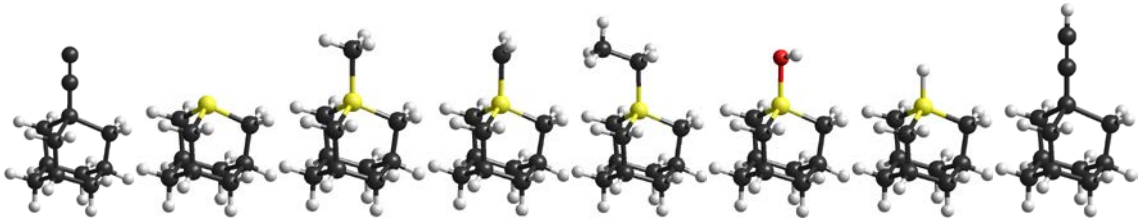

Each of these tooltips – all built on a single adamantane cage – is attached to a larger tool handle structure (not shown) that is mounted on a reagent device that is attached, in turn, to moving conveyor belt mechanisms (images, below).[2812] Note the "backing surfaces" in the mechanism illustrated at center, below – these may be used to apply large crushing forces to opposing moieties in constrained volumes to overcome reaction barriers if necessary.

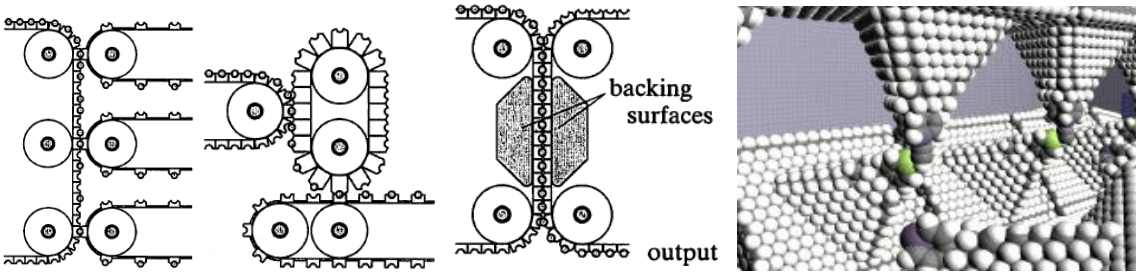

The following is a brief description of a hypothetical mechanosynthetic production line that could be used to build ethanol molecules in a cryogenic vacuum environment, using conveyor belts to move reactive molecules at high speed and to precisely control the location and nature of the interaction between these reactive molecules. The described chemistry is believed to be plausible but has not yet been computationally or experimentally validated. Nevertheless, even if this specific set of reaction sequences

---

[2811] Freitas RA Jr. The Whiskey Machine: Nanofactory-Based Replication of Fine Spirits and Other Alcohol-Based Beverages. IMM Report No. 47, May 2016; http://www.imm.org/Reports/rep047.pdf.

[2812] Adapted from: Drexler KE. Nanosystems: Molecular Machinery, Manufacturing, and Computation, Wiley, 1992, Figs. 13.7(b), 13.7(c), 13.7(d); https://www.amazon.com/dp/0471575186/.

and molecular tools proves flawed upon more detailed analysis, it seems highly likely that other reaction sequences and toolsets can be found that will provide a convenient path to the same result.

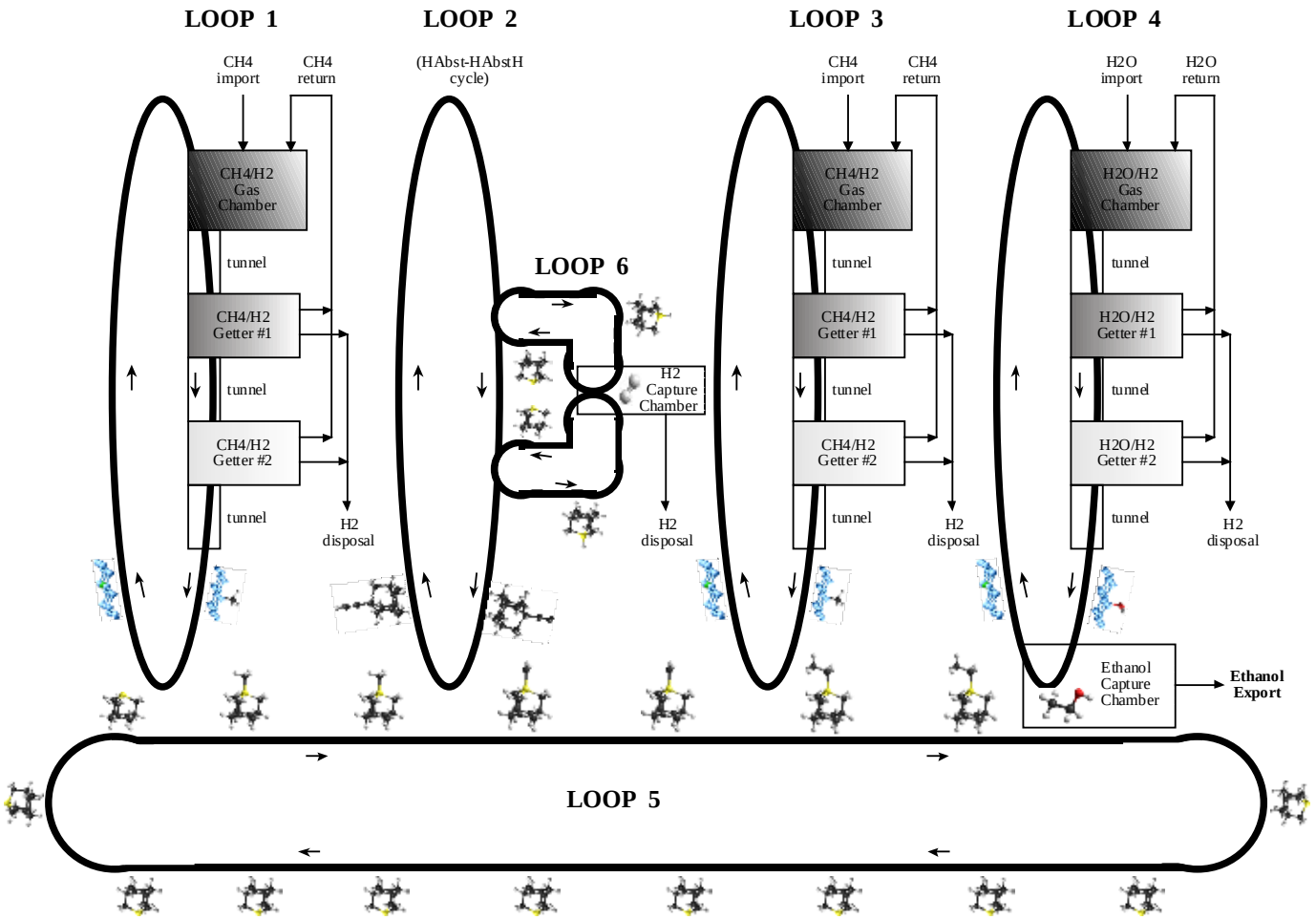

The above schematic of a hypothetical mechanosynthetic production line for ethanol molecules (black = C, white = H, yellow = Ge, red = O, blue = metal or Ge surface) has inputs of methane (CH_4) and water (H_2O) and outputs of ethanol (C_2H_5OH) and hydrogen gas (H_2). The production line consists of six interacting continuous or stepwise-moving conveyor loops as described below.

*** Loop 1: First methyl feedstock pickup.** A conveyor belt using carriers (image, right) having an outer coating of germanium (Ge)[2813], platinum (Pt)[2814], rhodium (Rh)[2815], or

[2813] A partially methylated germanium surface may provide a source of positionally controlled single-carbon feedstock. Such a surface can be prepared by thermal adsorption and reaction of CH_4 gas on Ge(100)* or by ion bombardment of clean Ge(111) at low substrate temperature (<470 K) using low-energy $\bullet CH_3$ ions, a strongly exoergic radical coupling reaction. After hydrocarbon CVD on Ge surfaces, absorption spectra indicate that bonding is mainly type sp^3 with CH, CH_2, and CH_3 bonds.† It may also be possible to prepare a CH_3-decorated Ge surface via conventional solution-phase chemical methylation,‡ since methylated germanium is found in the natural environment.

iridium (Ir)[2816] passes through a chamber containing methane gas molecules (CH_4). The coating surface strips one H off; the carrier is given enough residence time in the chamber to allow any H to migrate across the surface to recombine with another H on the surface, then to leave the surface as H_2 gas while remaining trapped in the chamber. This leaves a CH_3 bound to the Loop 1 carrier surface. The Loop 1 carriers then traverse a series of tunnels tight enough to prevent most stray CH_4 or H_2 molecules from following the carriers through the tunnel. At intervals the tunnels open up into small getter chambers equipped with sorting rotors (Section 4.10.1) having binding sites for CH_4 and H_2 to collect and remove any of these molecules that happen to slip through.

Cleared of any bound molecules other than the desired CH_3, the conveyor belt finally emerges into a vacuum where each carrier is brought into firm contact with carriers from another conveyor belt (Loop 5) whose carriers protrude a •GeRad tool. The CH_3 group hops from the Loop 1 carrier onto the •GeRad tool because this transfer is favored energetically, making a CH_3-GeRad intermediate on the Loop 5 carriers. The empty Ge-, Pt-, Rh- or Ir-coated carriers are returned to the starting point, re-entering the methane chamber ready for the next cycle without further processing.

*** Loop 2: Hydrogen abstraction from first methyl.** Each carrier that is attached to the Loop 2 conveyor belt protrudes an HAbst• tool and operates entirely in vacuum. The Loop 2 carriers are brought into firm contact with a CH_3 bound to a CH_3-GeRad intermediate in Loop 5, abstracting one of the H atoms from the bound CH_3 and leaving a •CH_2-GeRad intermediate bound to the carrier of System 5. The spent (hydrogenated) HAbst-H intermediates on the carriers of Loop 2 are brought into contact with a recharge subsystem (Loop 6) whereupon the excess H is removed and disposed of, after which the reclaimed and reactivated HAbst• tools resume the next cycle of Loop 2 operation without further processing.

---

[*] Murota J, Sakuraba M, Takehiro S. Atomically controlled processing for future Si-based devices. 2004 IEEE Workshop on Microelectronics and Electron Devices, Boise, ID, USA, 2004, pp. 31-34; https://ieeexplore.ieee.org/abstract/document/1297343.
[†] Franks J. Preparation and properties of diamondlike carbon films. J Vac Sci Technol A. 1989;7:2307; https://avs.scitation.org/doi/abs/10.1116/1.575933.
[‡] Sundermeyer W, Verbeek W. A Method for the Preparation of Methylmetal Compounds. Angew Chemie Intl Ed Engl. 1966 Jan;5(1):1-6; https://onlinelibrary.wiley.com/doi/abs/10.1002/anie.196600011; Mayer HP, Rapsomanikis S. Chemical methylation of germanium(II) in model aqueous solutions. Appl Organomet Chem. 1992 Apr;6(2):173-178; https://onlinelibrary.wiley.com/doi/abs/10.1002/aoc.590060210; Buriak JM. Organometallic chemistry on silicon and germanium surfaces. Chem Rev. 2002 May;102(5):1271-1308; http://www.gfmoorelab.com/uploads/4/2/3/1/42315775/buriak_chem_rev_2002.pdf.

[2814] Methane impinging on Pt(111) causes methyl to adsorb at 120 K.[*] On Pt(111) surface, the dissociative chemisorption of methane to CH_3 and H is downhill by 6.5 kcal/mole. Breaking the second C-H bond to form CH_2 adsorbed on the surface is 1.2 kcal/mole uphill; forming CH adsorbed is then downhill by 21.7 kcal/mole.[†]
[*] Papp C, Trankenschuh B, Streber R, Fuhrmann T, Denecke R, Steinruck HP. Influence of steps on the adsorption of methane on platinum surfaces. J Phys Chem C. 2007 Jan 18;111(5):2177-2184; https://pubs.acs.org/doi/abs/10.1021/jp066268f.
[†] Kua J, Goddard WA III. Chemisorption of Organics on Platinum. 2. Chemisorption of C_2H_x and CH_x on Pt(111). J Phys Chem B 1998 Nov 3;102(47):9492-9500; http://www.wag.caltech.edu/publications/sup/pdf/394.pdf.

[2815] Methane adsorbs dissociatively to the Rh(111) surface.[*]
[*] Mavrikakis M, Rempel J, Greeley J, Hansen LB, Norskov JK. Atomic and molecular adsorption on Rh(111). J Chem Phys. 2002 Oct 8;117(14):6737-6744; https://core.ac.uk/download/pdf/13727515.pdf.

[2816] Methane dissociatively adsorbs on Ir(111) surface.[*] It may be possible to start with ethylene which deposits on Ir surface as ethylidyne (C-CH_3) at 300 K. Abstraction of the CH_3 by GeRad may be possible because the C-C bond is apparently weak – the hydrocarbon decomposes at 500 K leaving only a C layer on the surface.[†]
[*] e.g., Henkelman G, Jónsson H. Theoretical Calculations of Dissociative Adsorption of CH_4 on an Ir(111) Surface. Phys Rev Lett. 2001 Jan 22;86(4):664-7; http://www.henkelmanlab.org/pubs/henkelman01_664.pdf.
[†] Kostov KL, Marinova TS. Ethylene adsorption on a clear iridium surface. Reaction Kinetics Catalysis Lett. 1986 Mar;32:141-146; https://link.springer.com/article/10.1007/BF02063463.

*** Loop 3: Second methyl feedstock pickup.** This conveyor belt system is exactly the same as Loop 1, and runs parallel to and in synchrony with it. Once the second -CH_3 group has been transferred (see Loop 5), the empty carriers are returned to the starting point, ready for the next cycle without further processing.

*** Loop 4: Hydroxyl feedstock pickup.** The Loop 4 conveyor belt system is almost the same as Loop 1, except that the feedstock attached to the carriers is an -OH group rather than a -CH_3 group (image, right). The bulk input is a chamber containing water (H_2O), which, like the methane, has had one H dissociatively removed, yielding in this case a migrating H and an –OH group bound to the carrier.[2817] Once the -OH group has been transferred, the empty carriers are returned to the starting point ready for the next cycle without further processing.

*** Loop 5: Build ethanol from two methyl groups and one hydroxyl group, then release.** Note that this is the previously-mentioned vacuum-residing conveyor belt system whose carriers initially protrude a •GeRad tool. A molecule of ethanol is assembled on each carrier as the Loop 5 belt encounters, in sequence, carriers from Loop 1, Loop 2, Loop 3, and Loop 4.

Encounter with Loop 1: When brought into contact with a Loop 1 carrier, a CH_3 group transfers from that carrier onto the Loop 5 •GeRad tool, making a CH_3-GeRad intermediate on the Loop 5 carrier. The empty Loop 1 carrier is returned to the starting point, ready for the next cycle without further processing.

Encounter with Loop 2: The CH_3-GeRad intermediate on the Loop 5 carrier is next brought into contact with an HAbst• tool on a Loop 2 carrier, which abstracts one of the H atoms from the bound CH_3 group, leaving a •CH_2-GeRad intermediate on the Loop 5 carrier.

Encounter with Loop 3: The •CH_2-GeRad intermediate on the Loop 5 carrier is next brought into contact with a Loop 3 carrier, whereupon a snap-on reaction occurs because there is an energetic preference for the CH_3 group on the Loop 3 carrier to be bonded to the C atom of the •CH_2-GeRad intermediate on the Loop 5 carrier rather than to the Ge or metal atom holding the CH_3 group onto the Loop 3 carrier. This leaves a CH_3CH_2-GeRad intermediate on the Loop 5 carrier. The empty Loop 3 carrier is returned to the starting point, ready for the next cycle without further processing.

Encounter with Loop 4: The CH_3CH_2–GeRad intermediate on the Loop 5 carrier is then pressed into contact with the OH-metal intermediate on the Loop 4 carrier inside an ethanol collection chamber.

[2817] A Cu(110) surface catalyzes water dissociation into H and OH under ambient conditions, and autocatalytic water dissociation is believed to be a general phenomenon on metal surfaces.[*] An $(IrO_2)_n$ (n=1-5) cluster when exposed to one H_2O molecule with 15.1 kcal/mole energy added can be driven uphill to form $IrO_2.H_2O$, which then exoergically transforms to $IrO(OH)_2$ which is downhill by -17.9 kcal/mole.[†] Oxygen-assisted water dissociation reaction (OWD: $H_2O + O \rightarrow 2OH$), based on a tunnel mechanism of H transfer, has activation energies much lower than those of water dissociation on clean metal (Pt, Cu, Ni, Rh) surfaces.[‡] OH groups rest stably on the Rh(111) surface with the H pointing away from the surface.[**]

[*] Andersson K, Ketteler G, Bluhm H, Yamamoto S, Ogasawara H, Pettersson LGM, Salmeron M, Nilsson A. Autocatalytic water dissociation on Cu(110) at near ambient conditions. J Am Chem Soc. 2008 Mar 5;130(9):2793-2797; https://escholarship.org/content/qt0zc1q9rv/qt0zc1q9rv.pdf.

[†] Zhou X, Yang J, Li C. Theoretical study of structure, stability, and the hydrolysis reactions of small iridium oxide nanoclusters. J Phys Chem A. 2012 Oct 11;116(40):9985-9995; https://pubmed.ncbi.nlm.nih.gov/22985267/.

[‡] German ED, Sheintuch M. Oxygen-Assisted Water Dissociation on Metal Surfaces: Kinetics and Quantum Effects. J Phys Chem C. 2011 Apr 29;115(20):10063-10072; https://pubs.acs.org/doi/abs/10.1021/jp200457h.

[**] Mavrikakis M, Rempel J, Greeley J, Hansen LB, Norskov JK. Atomic and molecular adsorption on Rh(111). J Chem Phys. 2002 Oct 8;117(14):6737-6744; https://core.ac.uk/download/pdf/13727515.pdf.

The hydroxyl group should have some energetic preference to be bonded to the Ge-bonded C atom of the CH_3CH_2–GeRad intermediate rather than to the metal atom holding the OH- group on the Loop 4 carrier,[2818] so a metal-Ge bond may form as the -OH group inserts into the Ge-C bond on the CH_3CH_2–GeRad intermediate on the Loop 5 carrier, creating a CH_3-CH_2-OH molecule of ethanol that is released into the ethanol collection chamber. The Loop 4 and Loop 5 carriers are then pulled apart, breaking the temporary bond between them. This leaves an empty carrier on Loop 4 and a •GeRad tool on Loop 5, both of which are returned to the starting point in their respective loops, ready for the next cycle without further processing.

*** Loop 6: HAbst-H tool recharge.** The recharge subsystem required for Loop 2 may involve two identical tracks and two pairs of specially configured •GeRad tools. In each pair, the first •GeRad tool alternately bonds and unbonds to the distal C atom of the ethynyl C_2 group on an HAbst-H intermediary on Loop 2, a process that can cycle endlessly. The second •GeRad tool of the pair approaches the excess H atom on the HAbst-H intermediary and abstracts it, making an H-GeRad intermediary on a Loop 6 carrier and restoring the active HAbst• tool on a Loop 2 carrier. The second pair of •GeRad tools performs the same operations on a second HAbst-H intermediary on Loop 2. The two H-GeRad intermediaries are then brought into forcible contact while parked inside a separate hydrogen capture chamber, creating a Ge-Ge bond between the two tools and releasing an H_2 gas molecule into the chamber which can be safely exhausted from the system. The two Loop 6 tools are then pulled apart, removed from the H_2 capture chamber, and returned to the starting point ready for the next recharge cycle without further processing. Alternatively, the H-GeRad intermediaries could be re-routed to a reaction sequence for building some molecule other than ethanol in which a hydrogen donation was required.

A similar process may be applied to build any CHO molecule of known structure and elemental composition. Many reaction sequences can be determined in advance and can be hard-coded. Production lines could use switchyards (image, left) to route carriers from one Loop to another Loop on the fly, essentially creating a reprogrammable production network. But in order to be able to handle any known molecule that is composed only of C, H, and O atoms and one or more of the five basic types of organic building blocks mentioned earlier, we will also need automated mechanosynthetic sequence generation to minimize or eliminate the human labor requirement. This seems achievable with ***future research***, given the relative structural simplicity of the molecular targets and the relatively small number of primary tools and core reactions that are likely to be needed (i.e., a relatively small "chemical alphabet" is required) to build organic molecules mechanosynthetically, functional group by functional group. Adding a few more elements such as nitrogen, sulfur, and phosphorus would raise the complexity level and increase the tooltype count – but probably tolerably so, while greatly extending the scope of manufacturable molecules to the full range of biologicals including amino acids, peptides, nucleic acids, proteins and DNA.

Quantitative Production. The 6-loop schema described above appears to fabricate individual molecules of ethanol fairly efficiently using only methane and water as the bulk inputs and generating

---

[2818] Since metal-oxygen and metal-germanium bond energy data were not readily available, we assumed for the purposes of this calculation that the OH group on Loop 4 is bonded to a GeRad. In this case, the reaction could be plausibly estimated to be exoergic because we are breaking one C-Ge bond (2.47 eV) and one (Loop 4) Ge-O bond (2.81 eV), total +5.28 eV, while creating one (Loop 4-Loop 5) Ge-Ge bond (1.95 eV) and one C-O bond (3.71 eV), total -5.66 eV, therefore the reaction appears energetically favored by **-0.38 eV**. However, this reaction has not been validated using quantum chemistry simulations. Sources: http://www.wiredchemist.com/chemistry/data/bond_energies_lengths.html and Jan Felix Binder, *Electronic and Structural Properties of the Ge/GeO2 Interface through Hybrid Functionals*, PhD Thesis, École Polytechnique Fédérale de Lausanne, 2012, p.30 and Fig. 3.9/p.37 (for estimate of Ge-O bond strength); http://infoscience.epfl.ch/record/176949/files/EPFL_TH5363.pdf.

hydrogen gas as the only waste product. Assuming that each conveyor belt/roller mechanism requires ~1 million carbon atoms,[2819] then six of these, along with infrastructure support including ~1 million atoms for the sorting rotor "getters" plus 5 million atoms for each of 11 chamber/getter boxes with tunnels and equipment housings, sums to 62 million carbon atoms. Adding in motors, controllers, and other hardware, each mechanosynthetic **Fab Module** incorporates perhaps $n_{C\text{-}FM}$ ~ 100 million carbon atoms of total mass $M_{FM} = m_C\ n_{C\text{-}FM} = 2 \times 10^{-18}$ kg (taking $m_C = 2 \times 10^{-26}$ kg/C atom). Each Fab Module may occupy a (100 nm)^3 cube having a volume V_{FM} ~ 0.001 micron^3, with about half of this volume occupied by machinery and the rest by empty space (vacuum).

While mechanosynthetic production lines are thought to be operable at MHz frequencies,[2820] to keep power consumption low we assume in the present example that each Fab Module will be operated at a frequency of only ν_{FM} = 0.1 MHz. This produces $r_{organics} = 10^5$ molecules/sec of organic (ethanol) molecules, representing a production rate of $R_{FM} = r_{organics}\ MW_{organics} / N_A = 7.6 \times 10^{-21}$ kg/sec of ethanol per Fab Module, taking molecular weight as $MW_{organics} \sim MW_{ethanol} = 0.046$ kg/mole, with Avogadro's number $N_A = 6.023 \times 10^{23}$ molecules/mole. Similar production rates should be achievable for other organic molecules of reasonable size, perhaps averaging ~0.090 kg/mole (~100 daltons), simply by adding a few more fabrication loops to Fab Module production lines.

For scaling purposes, we assume that the generic organic Fab Modules comprising the Generic Organic Synthesis Unit must produce near-absolute purity organic molecules similar to ethanol at a target production rate of $R_{FMB} = N_{FM}\ R_{FM} = 0.278$ gm/sec (~**1 kg/hr** ~ $R_{CellMill}$). This requires N_{FM} = 36,500 trillion Fab Modules having a volume of $V_{FMB} = N_{FM}\ V_{FM} =$ **36.5 cm^3** and a mass of $M_{FMB} = N_{FM}\ M_{FM}$ = 73 gm.

To estimate the power consumption for performing mechanosynthesis, we note that the standard enthalpy of formation for liquid ethanol is 470 zJ/molecule.[2821] With an efficient design, we should be able to closely approach this figure, but conservatively assuming ~50% energy efficiency implies a net energy dissipation of E_{diss} = 940 zJ/molecule.[2822] Adopting this estimate, the Fab Modules would produce generic organic molecules similar in size to ethanol at an energy cost of $E_{ethanol} = E_{diss}\ N_A / MW_{ethanol} = 12.3$ MJ/kg and the Fab Module Block would have a power draw of $P_{FMB} = R_{FMB}\ E_{diss}\ N_A / MW_{ethanol} = 3400$ W when operated at the $R_{FMB} = 0.278$ gm/sec ethanol production rate, with each Module drawing $P_{FM} = P_{FMB}/N_{FM} = 0.094$ pW. Power density for the Fab Modules would then be $P_{d\text{-}FMB} = P_{FMB} / V_{FMB} \sim 10^8$ W/m^3, well below the ~10^{10} W/m^3 power density estimated for molecular transport[2823] and significantly lower than the ~10^{11} W/m^3 power density estimated for the Lab Module Block of the Molecular Assay System (Section F.2.1).

[2819] Drexler KE. Nanosystems: Molecular Machinery, Manufacturing, and Computation, John Wiley & Sons, New York, 1992, Section 13.3.5; https://www.amazon.com/dp/0471575186/.

[2820] Drexler KE. Nanosystems: Molecular Machinery, Manufacturing, and Computation, John Wiley & Sons, New York, 1992, Table 14.4; https://www.amazon.com/dp/0471575186/.

[2821] http://en.wikipedia.org/wiki/Standard_enthalpy_change_of_formation_(data_table).

[2822] Even if we pessimistically assumed that all mechanosynthetic bond-breaking and bond-making events were completely dissipative, the energy cost would only be about 5.7-fold higher, around 5350 zJ/molecule for ethanol. This includes breaking a C-H bond (671 zJ) and making a C-Ge bond (391 zJ) at Loop 1, breaking a C-H bond (671 zJ) at Loop 2, breaking a C-H bond (671 zJ) and making a C-C bond (556 zJ) at Loop 3, breaking an O-H bond (753 zJ) and making a C-O bond (575 zJ) at Loop 4, breaking a C-Ge bond (391 zJ) at Loop 5, and breaking a C-H bond (671 zJ) at Loop 6.

[2823] Freitas RA Jr. Nanomedicine, Volume I: Basic Capabilities, Landes Bioscience, Georgetown TX, 1999, Section 6.5.6(A), "Power Analysis in Design: Molecular Transport"; http://www.nanomedicine.com/NMI/6.5.6.htm#p2.

D.1.2 Personalized Organic Molecules

Perhaps the most important task of the **first module** of the cell mill is to synthesize copies of the patient's own genetically autologous proteins and other relevant biomolecules, working from the patient's genome, possibly supplemented with samples of the patient's tissues.

To this end, a small representative set of microscopic physical samples of the cryopreserved patient's genome are obtained from noncritical tissues, allowing computational reconstruction of the individual's consensus genomic sequence (Section D.1.2.1).

Using this computed sequence, **DNA mills** can assemble patient-specific complete genome-length DNA strands for use in assembling manufactured cell nuclei (Section D.1.2.2).

After computationally translating the codons contained in the consensus genomic sequence, **protein mills** can assemble patient-specific proteins of all kinds found in the human body. Similar nanorobotic systems can assemble carbohydrate polymers or polysaccharides,[2824] glycoproteins,[2825] glycolipids,[2826] lipoproteins,[2827] nucleoproteins[2828] and the like with similar productivity (Section D.1.2.3).

D.1.2.1 Consensus Genomic Sequence

It is necessary to obtain the cryopreserved patient's consensus DNA sequence in order to manufacture biomolecules personalized to that patient. A consensus DNA sequence[2829] is the ordered list of nucleotide base pairs comprising a "clean" or "original" genome that results from sampling the entire set of chromosomes from at least 100 of the patient's cells and then compiling the most likely representative DNA sequence on which the majority of chromosomal samples agree, screening out all randomly occurring point mutations, viral insertions accumulated over a lifetime, read errors, and various other local genetic defects.

The patient's existing cellular chromosome set must be sampled and sequenced using a fast *ex vivo* DNA reading facility, first by securing representative physical samples of the patient's DNA (Section D.1.2.1.1) and then by rapidly sequencing the DNA samples in order to compile the consensus sequence (Section D.1.2.1.2).

[2824] https://en.wikipedia.org/wiki/Polysaccharide.
[2825] https://en.wikipedia.org/wiki/Glycoprotein.
[2826] https://en.wikipedia.org/wiki/Glycolipid.
[2827] https://en.wikipedia.org/wiki/Lipoprotein.
[2828] https://en.wikipedia.org/wiki/Nucleoprotein.

[2829] Freitas RA Jr. The Ideal Gene Delivery Vector: Chromallocytes, Cell Repair Nanorobots for Chromosome Replacement Therapy. J. Evol. Technol. 2007 Jun;16:1-97; http://jetpress.org/v16/freitas.pdf.

D.1.2.1.1 Genome Sampling

The first step in obtaining a patient's consensus genomic sequence is to secure samples of the patient's existing DNA.[2830] In the future nanomedical treatment environment in which cryonics revival will be practiced, templates for the standard human DNA sequences in each organ and for each cytotype (including organ- and age-specific[2831] epigenetic information such as methylation patterns) will be readily available. The task of the medical team is to ascertain how the patient's personal DNA – including the >1 million known single nucleotide polymorphisms (SNPs)[2832] and other structural and epigenetic variations – differs from standard sequences by directly sampling the patient's genome.

Genome acquisition would begin with the collection of at least 100 whole-cell samples taken from the patient's cryopreserved body. ***Future research*** should determine if these samples should be randomly collected throughout the body, or should be clustered in a specific location or organ where DNA damage is believed to be minimized. The removal of ~0.000001% of randomly-placed sampling cells should not disturb overall tissue or organ function in any way. It is already known that exposure to cryogenic conditions alone does not significantly damage DNA, since frozen egg[2833] and sperm[2834] cells retain viability after long-term storage in liquid nitrogen. ***Future research*** should verify that the base pair sequences and methylation patterns on chromosomes and DNA are not disturbed by the presence of the cryoprotectant chemicals used in cryopreservation.

After the sampled cells are warmed, thawed, and rehydrated, their DNA is extracted nondestructively and intact. The DNA collected from each set of 100 cell nuclei is sequenced (Section D.1.2.1.2) and compared. This yields a consensus sequence that should be identical to the original pristine fetal DNA such that all sequence information errors due to DNA damage accumulated during the patient's lifetime (e.g., due to aging) have been averaged out and eliminated. The statistical probability that a majority of 100 independent DNA samples of each cytotype will possess identical random single base pair errors at the exact same positions in the sequence is vanishingly small. Note that the consensus sequence for each chromosome will include one maternal- and one paternal-contributed set.

Systematic base pair errors and variations are more problematic. For example, all descendents of a reproducing cell that bears a retrovirus-modified sequence will retain the same sequence modifications, but this will be a known effect of the retrovirus and hence recognizable and correctable. Additional mixing may occur with recombination or transposons,[2835] but not identically in all or a majority of cells, hence is excludable. Some regions of the genome (e.g., hypervariable minisatellite DNA repeats at recombination

---

[2830] adapted from: Freitas RA Jr. The Ideal Gene Delivery Vector: Chromallocytes, Cell Repair Nanorobots for Chromosome Replacement Therapy. J. Evol. Technol. 2007 Jun;16:1-97; Section 4.1, "Genome Sampling and Modification"; http://jetpress.org/v16/freitas.pdf.

[2831] Horvath S. DNA methylation age of human tissues and cell types. Genome Biol. 2013;14(10):R115; https://www.ncbi.nlm.nih.gov/pmc/articles/PMC4015143/. Erratum: https://www.ncbi.nlm.nih.gov/pmc/articles/PMC4427927/.

[2832] Sachidanandam R, *et al.* International SNP Map Working Group. A map of human genome sequence variation containing 1.42 million single nucleotide polymorphisms. Nature 2001 Feb 15;409:928-933; http://repository.cshl.edu/id/eprint/29293/.

[2833] https://en.wikipedia.org/wiki/Oocyte_cryopreservation.
[2834] https://en.wikipedia.org/wiki/Semen_cryopreservation.
[2835] https://en.wikipedia.org/wiki/Transposable_element.

hotspots,[2836] hotspots at microRNA genes,[2837] and the hypermutating immunoglobulin variable region[2838] and proto-oncogenes[2839]) may be more susceptible to recombination or mutation[2840] than other regions and hence might accumulate similar types of errors preferentially in those locations.

To deal with such systematic errors, the consensus sequence should be compared to earlier genome sequencing scans that may be recorded in the patient's medical records, perhaps even from infancy, and these may be augmented by further sampling, either from the patient's quiescent stem cells[2841] (very low-activity cells likely to retain the most pristine copies of the "original" genome) or from the patient's undifferentiated white blood cell (WBC),[2842] hepatic,[2843] muscle,[2844] neural[2845] or other progenitor cells which have presumably undergone relatively fewer mutations and may be more abundant than stem cells, to the extent these can be found in a cryopreserved body. Comparing even a few of these should allow all errors other than those in the original fertilized egg cell to be detected and eliminated. Additionally, the unequal recombination of numerous (noncoding) minisatellite DNA regions (tandemly repeated 10-100 bp units typically representing <10% of mammalian genomes)[2846] can slightly adjust region lengths, making every individual genome distinct,[2847] but these systematic variations should be easily recognizable in the sequence data. Comparison to a few representative sample genomes from other organs of the patient might

---

[2836] Wahls WP, Moore PD. Recombination hotspot activity of hypervariable minisatellite DNA requires minisatellite DNA binding proteins. Somat Cell Mol Genet. 1998 Jan;24(1):41-51; https://www.ncbi.nlm.nih.gov/pmc/articles/PMC3151739/. Myers S, Bottolo L, Freeman C, McVean G, Donnelly P. A fine-scale map of recombination rates and hotspots across the human genome. Science. 2005 Oct 14;310(5746):321-324; https://pubmed.ncbi.nlm.nih.gov/16224025/.

[2837] Calin GA, Croce CM. MicroRNAs and chromosomal abnormalities in cancer cells. Oncogene. 2006 Oct 9;25(46):6202-6210; https://www.nature.com/articles/1209910.pdf?origin=ppub.

[2838] Woo CJ, Martin A, Scharff MD. Induction of somatic hypermutation is associated with modifications in immunoglobulin variable region chromatin. Immunity. 2003 Oct;19(4):479-489; https://core.ac.uk/download/pdf/82119720.pdf.

[2839] Pasqualucci L, Neumeister P, Goossens T, *et al*. Hypermutation of multiple proto-oncogenes in B-cell diffuse large-cell lymphomas. Nature. 2001 Jul 19;412(6844):341-346; https://pubmed.ncbi.nlm.nih.gov/11460166/.

[2840] Yauk C. Monitoring for induced heritable mutations in natural populations: application of minisatellite DNA screening. Mutat Res. 1998 Aug;411(1):1-10; https://macsphere.mcmaster.ca/bitstream/11375/6616/1/fulltext.pdf#page=52.

[2841] Young HE. Existence of reserve quiescent stem cells in adults, from amphibians to humans. Curr Top Microbiol Immunol. 2004;280:71-109; https://pubmed.ncbi.nlm.nih.gov/14594208/.

[2842] Pelayo R, Miyazaki K, Huang J, Garrett KP, Osmond DG, Kincade PW. Cell cycle quiescence of early lymphoid progenitors in adult bone marrow. Stem Cells. 2006 Dec;24(12):2703-2713; https://www.ncbi.nlm.nih.gov/pmc/articles/PMC1849950/.

[2843] Santoni-Rugiu E, Jelnes P, Thorgeirsson SS, Bisgaard HC. Progenitor cells in liver regeneration: molecular responses controlling their activation and expansion. APMIS 2005 Nov-Dec;113:876-902; https://onlinelibrary.wiley.com/doi/pdf/10.1111/j.1600-0463.2005.apm_386.x.

[2844] Relaix F. Skeletal muscle progenitor cells: from embryo to adult. Cell Mol Life Sci. 2006 Jun;63(11):1221-1225; https://search.proquest.com/openview/85523a50f0dcf5839e699ed12a52f27d/1?pq-origsite=gscholar&cbl=54068.

[2845] Klassen HJ, Imfeld KL, Kirov II, Tai L, Gage FH, Young MJ, Berman MA. Expression of cytokines by multipotent neural progenitor cells. Cytokine. 2003 May;22(3-4):101-106; https://pubmed.ncbi.nlm.nih.gov/12849709/.

[2846] Lewin B. Genes V, Oxford University Press, New York NY, 1995; https://www.amazon.com/dp/0198542879/.

[2847] Lewin B. Genes V, Oxford University Press, New York NY, 1995; https://www.amazon.com/dp/0198542879/.

be warranted to detect any possible epigenetic organ-specific asymmetric distribution patterns of post-mitotic old/new sister chromatid copies, as has been proposed by Armakolas and Klar.[2848]

Another complication is the discovery[2849] that in addition to single nucleotide polymorphisms, the genome of each person also has natural genetic "structural variations," including most importantly deletions, duplications and large-scale copy-number variants – collectively termed copy-number variants or copy-number polymorphisms[2850] – as well as insertions, inversions and translocations.[2851] There are 1,447 copy number variable regions (CNVRs) in the human genome,[2852] ranging in size from 960 bp to 3.4 Mb,[2853] with ~12% of the genome variable in copy number.[2854] These structural variants can comprise millions of nucleotides of heterogeneity within every genome, and possibly may contribute to human diversity and disease susceptibility.[2855] One initial mapping[2856] located 415,436 unique human insertion and deletion (INDEL) polymorphisms up to 9989 bp in length and split almost equally between insertions and deletions. The map identified five major classes of INDELs: (1) insertions and deletions of single-base pairs, (2) monomeric base pair expansions, (3) multi-base pair expansions of 2-15 bp repeat units, (4) transposon insertions, and (5) INDELs containing random DNA sequences. These INDELs are distributed throughout the human genome with an average density of one INDEL per 7.2 kb of DNA.[2857] Since all cells in a target organ of a given patient should share the same structural variants, the patient's uniquely variant genomic structure should be reconstructable during sequencing based on information provided by the genomic sampling procedure previously described.

Additional complications involve cell differences due to epigenetic gene regulation, most notably methylation (e.g., only ~10% of genes are activated at any given time). The eukaryotic genome is normally demethylated, then is re-methylated early in embryonic development via epigenetic reprogramming.[2858]

[2848] Armakolas A, Klar AJ. Cell type regulates selective segregation of mouse chromosome 7 DNA strands in mitosis. Science. 2006 Feb 24;311(5764):1146-1149; https://pubmed.ncbi.nlm.nih.gov/16497932/.

[2849] Tuzun E, Sharp AJ, Bailey JA, *et al*. Fine-scale structural variation of the human genome. Nat Genet. 2005 Jul;37(7):727-732; http://clavius.bc.edu/~marth/Download/Eichler-StructVar-FineStruct-NG-2003.pdf.

[2850] Sebat J, Lakshmi B, Troge J, *et al*. Large-scale copy number polymorphism in the human genome. Science. 2004 Jul 23;305(5683):525-528; https://pubmed.ncbi.nlm.nih.gov/15273396/.

[2851] Feuk L, Carson AR, Scherer SW. Structural variation in the human genome. Nat Rev Genet. 2006 Feb;7(2):85-97; http://psych.colorado.edu/~carey/pdffiles/cnv_feuk.pdf.

[2852] Redon R, *et al*. Global variation in copy number in the human genome. Nature. 2006 Nov 23;444(7118):444-54; https://www.ncbi.nlm.nih.gov/pmc/articles/PMC2669898/.

[2853] Komura D, Shen F, Ishikawa S, *et al*. Genome-wide detection of human copy number variations using high-density DNA oligonucleotide arrays. Genome Res. 2006 Dec;16(12):1575-1584; https://www.ncbi.nlm.nih.gov/pmc/articles/PMC1665641/.

[2854] Redon R, *et al*. Global variation in copy number in the human genome. Nature. 2006 Nov 23;444(7118):444-54; https://www.ncbi.nlm.nih.gov/pmc/articles/PMC2669898/.

[2855] Feuk L, Carson AR, Scherer SW. Structural variation in the human genome. Nat Rev Genet. 2006 Feb;7(2):85-97; http://psych.colorado.edu/~carey/pdffiles/cnv_feuk.pdf.

[2856] Mills RE, Luttig CT, Larkins CE, *et al*. An initial map of insertion and deletion (INDEL) variation in the human genome. Genome Res. 2006 Sep;16(9):1182-1190; https://www.ncbi.nlm.nih.gov/pmc/articles/pmc1557762/.

[2857] Mills RE, Luttig CT, Larkins CE, *et al*. An initial map of insertion and deletion (INDEL) variation in the human genome. Genome Res. 2006 Sep;16(9):1182-1190; https://www.ncbi.nlm.nih.gov/pmc/articles/pmc1557762/.

[2858] Haaf T. Methylation dynamics in the early mammalian embryo: implications of genome reprogramming defects for development. Curr Top Microbiol Immunol. 2006;310:13-22; https://pubmed.ncbi.nlm.nih.gov/16909904/.

After birth, differences in maternal care can induce differential methylation patterns in some promoter regions, influencing gene expression.[2859] It is now known that methylation correlates predictably with age in almost all organs, with methylation decreasing with age in about half of DNA sites and increasing with age in the other half.[2860] Genome-wide hypomethylation[2861] and hypermethylation[2862] may be implicated in cancer. An important special case is X-chromosome inactivation (XCI)[2863] in which the X-chromosome contributed from either maternal or paternal parent is silenced (becoming Barr bodies[2864]), leaving the other one active, in female mammalian cells. XCI for each cell is chosen randomly[2865] during embryogenesis and is presumed to be a permanent selection for all descendants of a cell. While X-linked transmembrane proteins such as the teneurins[2866] reside on the plasma membrane and thus may be antigenically visible, even in rare cases of extremely skewed XCI (e.g., 80% of cells favoring one parent,[2867] rather than the usual ~50%), the immune system recognizes both isoforms so a different assignment to any particular cell during molecular reconstruction should elicit no immune response. Nevertheless, a conservative protocol would ensure that any replacement genome will encode the parentally-correct XCI for each cell that is reconstructed. The XCI information may be acquired for each cell during initial whole-organ mapping by using chemical sensors to examine appropriate plasma membrane proteins such as teneurin and then to record whether the maternal or paternal variants are expressed in that cell.

The patient's genome can be repaired or modified during the replacement process, as described at length elsewhere,[2868] but this topic is beyond the scope of the present discussion.

[2859] Weaver IC, Cervoni N, Champagne FA, D'Alessio AC, Sharma S, Seckl JR, Dymov S, Szyf M, Meaney MJ. Epigenetic programming by maternal behavior. Nat Neurosci. 2004 Aug;7(8):847-854; https://pubmed.ncbi.nlm.nih.gov/15220929/.

[2860] Horvath S. DNA methylation age of human tissues and cell types. Genome Biol. 2013;14(10):R115; https://www.ncbi.nlm.nih.gov/pmc/articles/PMC4015143/. Erratum: https://www.ncbi.nlm.nih.gov/pmc/articles/PMC4427927/.

[2861] Chen RZ, Pettersson U, Beard C, Jackson-Grusby L, Jaenisch R. DNA hypomethylation leads to elevated mutation rates. Nature. 1998 Sep 3;395(6697):89-93; https://pubmed.ncbi.nlm.nih.gov/9738504/.

[2862] Nakayama M, Gonzalgo ML, Yegnasubramanian S, Lin X, De Marzo AM, Nelson WG. GSTP1 CpG island hypermethylation as a molecular biomarker for prostate cancer. J Cell Biochem. 2004 Feb 15;91(3):540-552; https://pubmed.ncbi.nlm.nih.gov/14755684/.

[2863] Chow JC, Yen Z, Ziesche SM, Brown CJ. Silencing of the mammalian X chromosome. Annu Rev Genomics Hum Genet. 2005;6:69-92; https://pubmed.ncbi.nlm.nih.gov/16124854/.

[2864] Anoop UR, Ramesh V, Balamurali PD, Nirima O, Premalatha B, Karthikshree VP. Role of Barr bodies obtained from oral smears in the determination of sex. Indian J Dent Res. 2004 Jan-Mar;15(1):5-7; https://pubmed.ncbi.nlm.nih.gov/15682788/.

[2865] Haig D. Self-imposed silence: parental antagonism and the evolution of X-chromosome inactivation. Evolution. 2006 Mar;60(3):440-447; https://haiggroup.oeb.harvard.edu/files/haig/files/haig-2006-evolution.pdf.

[2866] Tucker RP, Kenzelmann D, Trzebiatowska A, Chiquet-Ehrismann R. Teneurins: transmembrane proteins with fundamental roles in development. Int J Biochem Cell Biol. 2007;39(2):292-297; https://pubmed.ncbi.nlm.nih.gov/17095284/.

[2867] Ørstavik KH. Skewed X inactivation in healthy individuals and in different diseases. Acta Paediatr Suppl. 2006 Apr;95(451):24-29; https://pubmed.ncbi.nlm.nih.gov/16720461/.

[2868] Freitas RA Jr. The Ideal Gene Delivery Vector: Chromallocytes, Cell Repair Nanorobots for Chromosome Replacement Therapy. J. Evol. Technol. 2007 Jun;16:1-97; Section 4.1, "Genome Sampling and Modification"; http://jetpress.org/v16/freitas.pdf.

D.1.2.1.2 Chromosome Sequencing

A nanorobotic DNA sequencing facility[2869] could be extremely small, fast, and cheap. As early as 2002, J. Craig Venter had announced he was explicitly pursuing the goal of $1000/copy human whole-genome sequencing by 2012. In 2003 the J. Craig Venter Science Foundation offered a $500,000 prize for achieving this milestone, then announced in 2005 that it was seeking to raise the prize to $10 million.[2870] The NIH also solicited proposals for research leading to the $1000 genome.[2871] Noted Venter: "Once this threshold has been reached, it will be feasible for the majority of individuals to have their genome sequenced and encoded as part of their medical record." As shown in the chart below,[2872] by 2015 the goal of a $1000 human genome was reached, with raw sequencing costs falling to ~$10/gigabase of DNA.

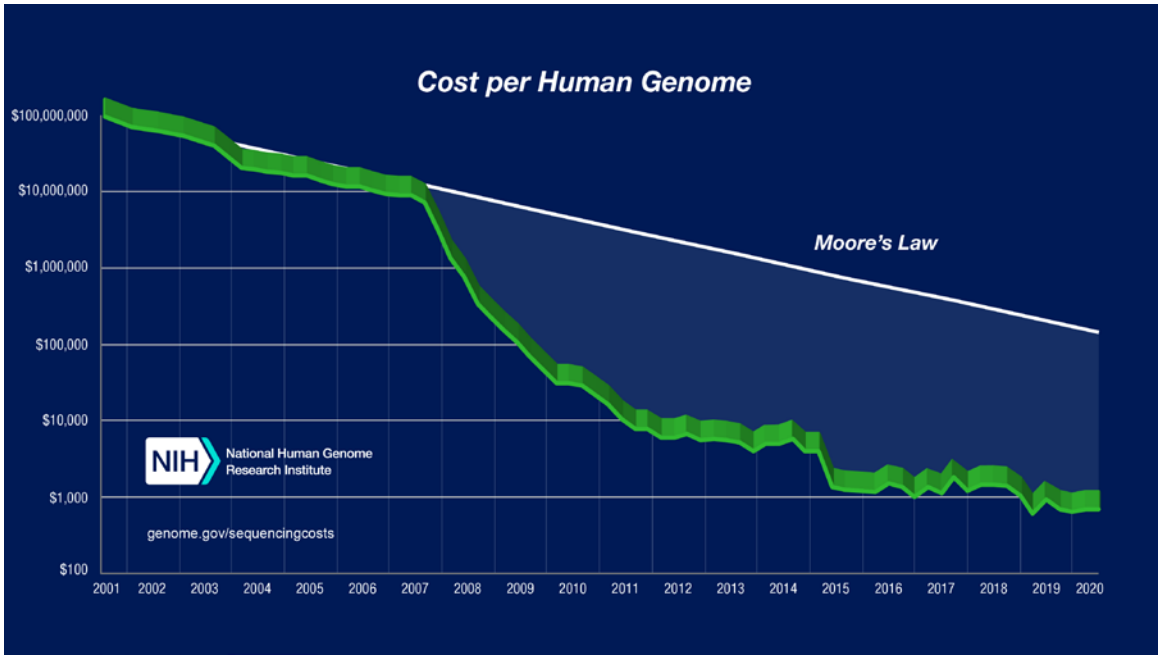

One of the foremost companies in automated genome sequencing is Illumina,[2873] whose industry-leading NovaSeq 6000 machine[2874] generated 20 billion base-pair reads in a single run and can read ~6 trillion

---

[2869] adapted from: Freitas RA Jr. The Ideal Gene Delivery Vector: Chromallocytes, Cell Repair Nanorobots for Chromosome Replacement Therapy. J. Evol. Technol. 2007 Jun;16:1-97; Section 4.2, "Chromosome Sequencing"; http://jetpress.org/v16/freitas.pdf.

[2870] K. Davies, "Venter Raises Stakes for $1,000 Genome Prize," Bio-IT World, 19 October 2005; http://www.bio-itworld.com/newsitems/2005/oct2005/10-19-05-news-genome-prize.

[2871] M. Anderson, "NIH offers $1000 genome grant," The Scientist 5(2004):20040223-05; http://www.the-scientist.com/news/20040223/05/.

[2872] National Human Genome Research Institute (NHGRI). DNA Sequencing Costs: Data (2020). https://www.genome.gov/about-genomics/fact-sheets/DNA-Sequencing-Costs-Data.

[2873] http://www.illumina.com/.

[2874] https://www.illumina.com/systems/sequencing-platforms/novaseq.html.

base-pairs per day[2875] ($R_{NovaSeq}$ = 6.93 x 10^7 bp/sec) with ~99.9% accuracy.[2876] According to the technical specifications,[2877] this amazingly compact machine (image, right) measured 165.6 cm x 80.0 cm x 94.5 cm ($V_{NovaSeq}$ = 1.25 m^3) with a mass of m_{NovSeq} = 481 kg and a peak power consumption of $P_{NovaSeq}$ = 2500 watts, yielding the following figures of merit for performance: ψ_V = 5.56 x 10^7 bp/m^3-sec, ψ_m = 1.44 x 10^5 bp/kg-sec, and ψ_P = 2.78 x 10^4 bp/watt-sec.

A competing DNA sequencing technology in 2020 was offered by Oxford Nanopore Technologies,[2878] in which electrophoresis is used to transport individual polynucleotide molecules through a nanopore measuring ~1 nm in diameter, bathed in an electrolyte solution, across which an electric field is applied. Passage of the molecule through the pore causes minute changes in the current passing through the pore that observably differ depending on which nucleotide base (A,G, C or T) is passing through the pore at the time. Oxford Nanopore sequencing[2879] systems are generally small in size. For example, Oxford offered the MinION system (image, left)[2880] incorporating 512 parallel nanopore channels that allowed sequencing at 20 billion base-pairs in 48 hours (R_{MinION} = 1.16 x 10^5 bp/sec) with a mass of 450 gm, dimensions 14 cm x 8 cm x 3 cm (336 cm^3), and power supplied through a 2.5 watt USB cable, yielding the following figures of merit for performance: ψ_V = 3.44 x 10^8 bp/m^3-sec, ψ_m = 2.57 x 10^5 bp/kg-sec, and ψ_P = 4.63 x 10^4 bp/watt-sec.

Mature nanomechanical sequencing systems should allow the speed of DNA reading to be improved by another 1-2 orders of magnitude beyond these diffusion-based methods, as illustrated by the following simple scaling analysis. We start by placing a whole-chromosome sample from a single cell in a small fluid-filled sorting chamber which is perhaps a few microns wide. Histones, other proteins, and attached mRNA strands are enzymatically removed and discarded, then the chromosomes are biochemically and mechanically separated into 46 haploid strands of dsDNA having a total duplex-DNA contour length of ~2 meters. A length measurement and a few other simple tests determine the chromosome number of every double strand. Each dsDNA duplex strand, ranging in length from 15.7-82.1 mm in contour length and suspended in an appropriate carrier fluid, is then transferred into a separate long

---

[2875] https://www.illumina.com/systems/sequencing-platforms.html.
[2876] https://en.wikipedia.org/wiki/Illumina,_Inc.#DNA_sequencing.

[2877] https://support.illumina.com/content/dam/illumina-support/documents/documentation/system_documentation/novaseq/novaseq-site-prep-guide-1000000019360-06.pdf.

[2878] http://nanoporetech.com/.
[2879] https://en.wikipedia.org/wiki/Nanopore_sequencing.
[2880] https://nanoporetech.com/products/minion.

narrow channel. The positionally-controlled end-effectors[2881] of two nanorobotic manipulator arms[2882] attach to either end of the dsDNA to establish orientation. The strand is cleaved in half at the center of the strand using a nuclease-like enzymatic end-effector mounted on a third positionally-controlled manipulator arm or sharp scanning probe tip,[2883] and the two cleaved ends are attached[2884] to another pair of manipulator arms to maintain the two strands in a known orientation. (Cleavage of individual chromosomes via femtolaser nanosurgery was first demonstrated experimentally in 1999.[2885]) Each half is transported under full positional control to a second pair of manipulator arms where the cleaving process is repeated. After 10 such cleavings, there would be a total of 1000 strand segments each of length 15.7-82.1 micron (47,000-245,000 bp) rigidly held by ~2000 manipulator arms. Each strand segment would then be mechanically scanned using an AFM-mounted tooltip that can chemotactically sense the size and orientation of the exposed nucleotide bases comprising each base pair, along with their methylation, thus fully sequencing the segment.[2886] Alternatively, dsDNA strands can be mechanically unzipped by applying as little as ~15 pN of force[2887] and it may be possible to partially infer single base-pair sequence by this

---

[2881] Freitas RA Jr. Nanomedicine, Volume I: Basic Capabilities, Landes Bioscience, Georgetown, TX, 1999; Section 9.3.2, "Nanoscale End-Effectors and Tool Tips"; http://www.nanomedicine.com/NMI/9.3.2.htm.

[2882] Freitas RA Jr. Nanomedicine, Volume I: Basic Capabilities, Landes Bioscience, Georgetown, TX, 1999; Section 9.3.1, "Nanoscale Manipulators"; http://www.nanomedicine.com/NMI/9.3.1.htm.

[2883] e.g., Iwabuchii S, Mori T, Ogawa K, Sato K, Saito M, Morita Y, Ushiki T, Tamiyaet E. Atomic force microscope-based dissection of human metaphase chromosomes and high resolutional imaging by carbon nanotube tip. Arch Histol Cytol. 2002 Dec;65(5):473-479; https://www.jstage.jst.go.jp/article/aohc/65/5/65_5_473/_pdf. Oberringer M, Englisch A, Heinz B, Gao H, Martin T, Hartmann U. Atomic force microscopy and scanning near-field optical microscopy studies on the characterization of human metaphase chromosomes. Eur Biophys J. 2003 Nov;32(7):620-627; https://pubmed.ncbi.nlm.nih.gov/14586520/. Fukushi D, Ushiki T. The structure of C-banded human metaphase chromosomes as observed by atomic force microscopy. Arch Histol Cytol. 2005;68(1):81-87; https://pubmed.ncbi.nlm.nih.gov/15827381/. An HJ, Guo YC, Zhang XD, Zhang Y, Hu J. Nanodissection of single- and double-stranded DNA by atomic force microscopy. J Nanosci Nanotechnol. 2005 Oct;5(10):1656-1659; https://pubmed.ncbi.nlm.nih.gov/16245523/. Hoshi O, Shigeno M, Ushiki T. Atomic force microscopy of native human metaphase chromosomes in a liquid. Arch Histol Cytol. 2006 Mar;69(1):73-78; https://www.jstage.jst.go.jp/article/aohc/69/1/69_1_73/_pdf.

[2884] Thalhammer S, Stark RW, Müller S, Wienberg J, Heckl WM. The atomic force microscope as a new microdissecting tool for the generation of genetic probes. J Struct Biol. 1997 Jul;119(2):232-237; http://citeseerx.ist.psu.edu/viewdoc/download?doi=10.1.1.12.6581&rep=rep1&type=pdf.

[2885] König K, Riemann I, Fischer P, Halbhuber KJ. Intracellular nanosurgery with near infrared femtosecond laser pulses. Cell Mol Biol (Noisy-le-grand). 1999 Mar;45(2):195-201; https://pubmed.ncbi.nlm.nih.gov/10230728/.

[2886] e.g., Kelson I, Nussinov S. A scheme for sequencing large DNA molecules by identifying local nuclear-induced effects. Proc Natl Acad Sci U S A. 1994 Jul 19;91(15):6963-6; https://www.ncbi.nlm.nih.gov/pmc/articles/PMC44318/. Seong GH, Niimi T, Yanagida Y, Kobatake E, Aizawa M. Single-molecular AFM probing of specific DNA sequencing using RecA-promoted homologous pairing and strand exchange. Anal Chem. 2000 Mar 15;72(6):1288-1293; https://pubmed.ncbi.nlm.nih.gov/10740872/. Voulgarakis NK, Redondo A, Bishop AR, Rasmussen KO. Sequencing DNA by dynamic force spectroscopy: limitations and prospects. Nano Lett. 2006 Jul;6(7):1483-1486; http://cnls.lanl.gov/External/voulgarakis_nano.pdf.

[2887] Cocco S, Monasson R, Marko JF. Unzipping dynamics of long DNAs. Phys Rev E Stat Nonlin Soft Matter Phys. 2002 Nov;66(5 Pt 1):051914; http://www.phys.ens.fr/~cocco/Art/21unzlongdna.pdf.

means because the force is base-pair dependent.[2888] (Contemporary scanning probe techniques are more commonly used to produce 3D ultrastructure images of chromatin strands with a minimum feature resolution of some tens of nanometers.[2889])

If: (1) initial sample preparation in the sorting chamber requires 10 seconds, (2) fluid transfer into the first channel occurs at ~10 mm/sec over a maximum 82.1 mm distance, (3) each subsequent positionally-controlled cleaving, attachment and transfer operation takes ~5 seconds, given that a manipulator end effector requires only 0.1 sec to be transported 100 microns at a conservative arm velocity of 1 mm/sec, and (4) the linear nucleotide sequencing of the final segment occurs at a conservative net scan rate of 1 micron/sec, then the total throughput time to mechanically sequence the longest chromosome would be ~**150 sec** (R_{nano} = 2.67 x 10^7 bp/sec). A contemporaneous scanning process could measure the methylation pattern of the dsDNA sample segments, matching these to the (by then) well-known human methylome[2890] for this cytotype and organ.

If: (1) the volume of each channel is ~1000 times the volume of the dsDNA segment placed within it, giving ~100,000 micron^3 of total channel volume for each haploid strand sequenced, and (2) each of the 2000 manipulator arms including all appurtenant structures averages ~1000 micron^3 in volume, giving ~2,000,000 micron^3 of total manipulator volume for each haploid strand sequenced, then the volume of channels and manipulators to process all 46 haploid chromosomes from a single cell sample, in parallel, is ~**0.1 mm^3**, weighing ~**0.0002 gm** assuming a net density about half that of diamond. The power demand for operating 2000 x 46 manipulator arms, assuming ~10 pW per micron-length manipulator, is **0.92 x 10^{-6} watts**, yielding the following figures of merit for performance: ψ_V = 2.67 x 10^{17} bp/m^3-sec, ψ_m = 1.33 x 10^{14} bp/kg-sec, and ψ_P = 2.90 x 10^{13} bp/watt-sec.

Comparison of the relative performance of the three systems in **Table 20** shows that the nanorobotic DNA sequencing system described above should provide productivity gains of about one billion-fold over the best present-day high-throughput gene sequencing technologies.

[2888] e.g., Sattin BD, Pelling AE, Goh MC. DNA base pair resolution by single molecule force spectroscopy. Nucleic Acids Res. 2004 Sep 14;32(16):4876-4883; https://www.ncbi.nlm.nih.gov/pmc/articles/pmid/15367697/. Singh N, Singh Y. Effect of genome sequence on the force-induced unzipping of a DNA molecule. Eur Phys J E Soft Matter. 2006 Feb;19(2):233-238; https://pubmed.ncbi.nlm.nih.gov/16505948/. Lee CH, Danilowicz C, Coljee VW, Prentiss M. Comparison of the measured phase diagrams in the force-temperature plane for the unzipping of two different natural DNA sequences. Eur Phys J E Soft Matter. 2006 Mar;19(3):339-344; https://pubmed.ncbi.nlm.nih.gov/16541209/. Baldazzi V, Cocco S, Marinari E, Monasson R. Inference of DNA sequences from mechanical unzipping: an ideal-case study. Phys Rev Lett. 2006 Mar 31;96(12):128102; http://www.phys.ens.fr/~cocco/Art/dnaseqprl.pdf.

[2889] e.g., Oberringer M, Englisch A, Heinz B, Gao H, Martin T, Hartmann U. Atomic force microscopy and scanning near-field optical microscopy studies on the characterization of human metaphase chromosomes. Eur Biophys J. 2003 Nov;32(7):620-627; https://pubmed.ncbi.nlm.nih.gov/14586520/. Fukushi D, Ushiki T. The structure of C-banded human metaphase chromosomes as observed by atomic force microscopy. Arch Histol Cytol. 2005;68(1):81-87; https://pubmed.ncbi.nlm.nih.gov/15827381/. An HJ, Guo YC, Zhang XD, Zhang Y, Hu J. Nanodissection of single- and double-stranded DNA by atomic force microscopy. J Nanosci Nanotechnol. 2005 Oct;5(10):1656-1659; https://pubmed.ncbi.nlm.nih.gov/16245523/. Hoshi O, Shigeno M, Ushiki T. Atomic force microscopy of native human metaphase chromosomes in a liquid. Arch Histol Cytol. 2006 Mar;69(1):73-78; https://www.jstage.jst.go.jp/article/aohc/69/1/69_1_73/_pdf.

[2890] e.g., Wilson IM, Davies JJ, Weber M, Brown CJ, Alvarez CE, MacAulay C, Schubeler D, Lam WL. Epigenomics: mapping the methylome. Cell Cycle. 2006 Jan;5(2):155-158; https://pubmed.ncbi.nlm.nih.gov/16397413/. Jeltsch A, Walter J, Reinhardt R, Platzer M. German human methylome project started. Cancer Res. 2006 Jul 15;66(14):7378; https://cancerres.aacrjournals.org/content/canres/66/14/7378.full.pdf. Schöb H, Grossniklaus U. The first high-resolution DNA "methylome". Cell. 2006 Sep 22;126(6):1025-1028; https://www.sciencedirect.com/science/article/pii/S0092867406011494.

Table 20. Figures of merit for DNA sequencing system productivity for three sequencing technologies

DNA Sequencing System	Raw System Seq. Rate R_{nano} (bp/sec)	Volumetric Productivity ψ_V (bp/m^3-sec)	Productivity Per Unit Mass Ψ_m (bp/kg-sec)	Productivity per Unit Power Consumption Ψ_p (bp/watt-sec)
NovaSeq 6000	6.93×10^7	5.56×10^7	1.44×10^5	2.78×10^4
MinION	1.16×10^5	3.44×10^8	2.57×10^5	4.63×10^4
Nano Sequencer	***2.67 x 10^7***	***2.67 x 10^{17}***	***1.33 x 10^{14}***	***2.90 x 10^{13}***

D.1.2.2 Manufacturing Personalized DNA

One of the most important biomolecules that a cell mill must produce is DNA for constructing chromosomes to be used in the nucleus of the manufactured cell. Each cell would require a duplicate copy of the patient's own DNA, suitably methylated to match the expression pattern (e.g., the "methylome," "transcriptome," etc.) and activation state of the particular cytotype under construction.

A large number of methods for artificial gene synthesis[2891] have been employed in molecular biology, generally involving a two step process in which short-chain polymers consisting of ~200 nucleotides called oligonucleotides are synthesized using the techniques of solid-phase DNA synthesis,[2892] after which these oligonucleotides are connected to each other in the proper sequence using various DNA assembly methods.[2893] Solid-phase oligonucleotide synthesis has been highly automated[2894] but remains expensive when product is ordered from a service. For example, a 100-base sequence of unmodified DNA cost $9,305/gm from Integrated DNA Technologies in 2021.[2895]

In 2020 there were several existing vendors for the equipment needed to perform high-throughput automated oligonucleotide synthesis. For example, the ÄKTA oligopilot plus lab scale oligonucleotide synthesizer (ÄKTA oligopilot plus 10; image, right)[2896] measured 0.48 m x 0.45 m x 0.61

[2891] https://en.wikipedia.org/wiki/Artificial_gene_synthesis.

[2892] "The occurrence of side reactions sets practical limits for the length of synthetic oligonucleotides (up to about 200 nucleotide residues) because the number of errors accumulates with the length of the oligonucleotide being synthesized." (https://en.wikipedia.org/wiki/Oligonucleotide_synthesis)

[2893] https://en.wikipedia.org/wiki/Artificial_gene_synthesis#DNA_assembly.

[2894] Anderson NG, Anderson NL, Taylor J, Goodman J. Large-scale oligonucleotide synthesizers. I. Basic principles and system design. Appl Biochem Biotechnol. 1995 Jul-Sep;54(1-3):19-42; https://pubmed.ncbi.nlm.nih.gov/7486979/. Lönnberg H. Synthesis of oligonucleotides on a soluble support. Beilstein J Org Chem. 2017 Jul 12;13:1368-1387; https://www.ncbi.nlm.nih.gov/pmc/articles/pmid/28781703/. Molina AG, Sanghvi YS. Liquid-Phase Oligonucleotide Synthesis: Past, Present, and Future Predictions. Curr Protoc Nucleic Acid Chem. 2019 Jun;77(1):e82; https://pubmed.ncbi.nlm.nih.gov/30920171/.

[2895] https://www.idtdna.com/pages/products/custom-dna-rna/large-scale-synthesis.

m ($V_{ÄKTA}$ = 0.132 m^3) in size with mass $m_{ÄKTA}$ = 63 kg and power draw $P_{ÄKTA}$ = 600 watts. It could reportly[2897] process 3 millimole batches of 25-mer oligonucleotides in 30 minutes, or $R_{ÄKTA}$ = 1 x 10^{18} oligos/sec ~ 25 x 10^{18} bp/sec (although with "some assembly required"), yielding the following figures of merit for performance: ψ_V = 1.90 x 10^{20} bp/m^3-sec, ψ_m = 3.98 x 10^{17} bp/kg-sec, and ψ_P = 4.18 x 10^{16} bp/watt-sec.

However, these simplistic figures of merit ignore the hardest and most time-consuming part of the synthesis problem – the rather substantial additional effort that would be required to string together millions of 25-mer oligos into a precisely-specified sequence to make ~200,000,000-mer human chromosomes using the rather cumbersome current techniques of DNA assembly.[2898] To calibrate the limitations of present-day technology, we note that the first complete genome of a simple microbial life form (*Mycoplasma genitalium*) with 485 protein-coding genes, containing a total of 582,970 base pairs, was assembled by Venter's group in 2008 from ~10,000 synthetic oligonucleotides each ~50 nucleotides in length in a laboratory experiment that was described as "a formidable technical challenge"[2899] and required "several years of work perfecting chemical assembly".[2900] Venter's group next created a synthetic *Mycoplasma mycoides* genome with 1,079,000 base pairs in 2010,[2901] and by 2019 a British team had "recoded" and synthesized an entire *E. coli* genome comprising ~4,000,000 base pairs[2902] – apparently the world record length for DNA assembly from synthetic oligos as of 2021. Genome-length DNA assembly operations remain a herculean task that involve many months and multiple personnel in well-equipped experimental laboratories, and are commonly referred to as "moonshot demonstrations."[2903] The assembly of a ~200,000,000 base-pair human-chromosome-length single strand of DNA from synthesized oligonucleotide fragments has not yet been accomplished and appears unlikely to be achieved by conventional chemosynthetic means for at least 5-10 more years, given the current pace of improvements.

Positionally-controlled molecular manufacturing of long-strand DNA would represent a fundamentally different and far more advanced process compared to present-day oligonucleotide hybridization and DNA

[2896] https://web.archive.org/web/20201021165225/https://www.cytivalifesciences.com/en/us/shop/molecular-biology/oligonucleotide-synthesis/instruments/akta-oligopilot-plus-oligonucleotide-synthesizer-p-05544. (This particular product was discontinued by the manufacturer in 2021.)

[2897] Sarah Goforth, "The Core of DNA Synthesis," The Scientist, 9 June 2002; https://www.the-scientist.com/technology-profile/the-core-of-dna-synthesis-53217.

[2898] https://en.wikipedia.org/wiki/Artificial_gene_synthesis#DNA_assembly.

[2899] Gibson DG, Benders GA, Andrews-Pfannkoch C, *et al*. Complete chemical synthesis, assembly, and cloning of a *Mycoplasma genitalium* genome. Science. 2008 Feb 29;319(5867):1215-1220; http://biol.wwu.edu/young/470/papers_2009/artificialchrompaper.pdf.

[2900] https://www.sciencedaily.com/releases/2008/01/080124175924.htm.

[2901] Hutchison CA 3rd, Chuang RY, Noskov VN, *et al*. Design and synthesis of a minimal bacterial genome. Science. 2016 Mar 25;351(6280):aad6253; http://www.cba.mit.edu/docs/papers/16.04.minimal.pdf.

[2902] Fredens J, Wang K, de la Torre D, Funke LFH, Robertson WE, Christova Y, Chia T, Schmied WH, Dunkelmann DL, Beránek V, Uttamapinant C, Llamazares AG, Elliott TS, Chin JW. Total synthesis of *Escherichia coli* with a recoded genome. Nature. 2019 May;569(7757):514-518; https://www.ncbi.nlm.nih.gov/pmc/articles/PMC7039709/.

[2903] Hughes RA, Ellington AD. Synthetic DNA Synthesis and Assembly: Putting the Synthetic in Synthetic Biology. Cold Spring Harb Perspect Biol. 2017 Jan 3;9(1):a023812; https://www.ncbi.nlm.nih.gov/pmc/articles/PMC5204324/.

assembly techniques, likely avoiding many current limitations such as high cost, low speed, and high error rate[2904] that produce unplanned process mutagenicity.

How fast could chromatin be manufactured in a nanorobotic-based DNA synthesizer? Scaling analyses for convergent-assembly-based desktop-sized nanofactories[2905] for manufacturing molecularly precise diamondoid products using positionally-controlled mechanosynthesis predict a start-to-finish throughput time of ~100 sec with productivity ratios of ~1 kg/hour of product per kg of nanofactory for a mature nanotechnology system.

Some biological comparisons are instructive. **Ribosomes** assemble proteins according to digitally encoded instructions using mechanochemically-driven positionally-controlled placement of amino acids *in vivo*.[2906] Analogously to the hypothesized nanofactory, ~1 kg of proteins can be assembled by ~1 kg of bacterial ribosomes in 270-710 sec,[2907] a productivity rate of **5-13 kg/hr of proteins per kg of ribosome**. Similarly, nonprocessive **DNA polymerase enzymes** can add $n_{polymerase} \sim 1$ nucleotide/sec to the growing DNA chain,[2908] which implies a DNA polymer production rate of $R_{polymerase} \sim 0.5\ m_{bp}\ n_{polymerase} \sim 5.45 \times 10^{-25}$ kg/sec = 1.96×10^{-21} kg/hour of DNA for each active polymerase molecule of mass $m_{polymerase} \sim 1.82 \times 10^{-22}$ kg,[2909] assuming ~650 daltons/base-pair for typical DNA[2910] or $m_{bp} \sim 1.09 \times 10^{-24}$ kg/bp. This gives a net enzyme productivity of **~11 kg/hr of DNA per kg of polymerase**, very similar to ribosome productivity for protein synthesis.

[2904] Carr PA, Park JS, Lee YJ, Yu T, Zhang S, Jacobson JM. Protein-mediated error correction for *de novo* DNA synthesis. Nucleic Acids Res. 2004 Nov 23;32(20):e162; https://www.ncbi.nlm.nih.gov/pmc/articles/pmid/15561997/. Binkowski BF, Richmond KE, Kaysen J, Sussman MR, Belshaw PJ. Correcting errors in synthetic DNA through consensus shuffling. Nucleic Acids Res. 2005 Mar 30;33(6):e55; https://www.ncbi.nlm.nih.gov/pmc/articles/pmid/15800206/. Fuhrmann M, Oertel W, Berthold P, Hegemann P. Removal of mismatched bases from synthetic genes by enzymatic mismatch cleavage. Nucleic Acids Res. 2005 Mar 30;33(6):e58; https://www.ncbi.nlm.nih.gov/pmc/articles/pmid/15800209/.

[2905] Drexler KE. Nanosystems: Molecular Machinery, Manufacturing, and Computation, John Wiley & Sons, New York, 1992, Section 14.4, "An exemplar manufacturing system architecture," pp. 421-427; https://www.amazon.com/dp/0471575186/. Merkle RC. Convergent assembly. Nanotechnology 1997;8:18-22; http://www.zyvex.com/nanotech/convergent.html. Freitas RA Jr., Merkle RC. Kinematic Self-Replicating Machines, Landes Bioscience, Georgetown, TX, 2004; Section 5.9.4, "Performance of Convergent Assembly Nanofactory Systems"; http://www.MolecularAssembler.com/KSRM/5.9.4.htm.

[2906] Nierhaus KH, Wilson DN, eds. Protein Synthesis and Ribosome Structure: Translating the Genome, John Wiley & Sons NY, 2004; https://www.amazon.com/dp/3527306382/.

[2907] Freitas RA Jr., Merkle RC. Kinematic Self-Replicating Machines, Landes Bioscience, Georgetown, TX, 2004; Section 4.2, "Ribosomes: Molecular Positional Assembly for Self-Replication"; http://www.MolecularAssembler.com/KSRM/4.2.htm.

[2908] Losick R, Watson JD, Baker TA, Bell S, Gann A, Levine MW. Molecular Biology of the Gene, 6th edition, Pearson/Benjamin Cummings, San Francisco CA, 2008; https://www.amazon.com/dp/B01JQ5RU9I/. However, much faster enzymatic rates have been reported. For example, processive DNA polymerase enzyme has been measured adding $n_{polymerase}$ = 749 nucleotides/sec in phage T4-infected *E. coli* cells during the period of exponential DNA increase at 37 °C; McCarthy D, Minner C, Bernstein H, Bernstein C. DNA elongation rates and growing point distributions of wild-type phage T4 and a DNA-delay amber mutant. *J Mol Biol*. 1976 Oct 5;106(4):963-981; https://pubmed.ncbi.nlm.nih.gov/789903/.

[2909] The polymerase I enzyme found in *E. coli* has a molecular weight of ~109,000 daltons ~ 1.82×10^{-22} kg at ~1.67×10^{-27} kg/dalton; http://www.worthington-biochem.com/DNAECI/default.html.

[2910] http://cels.uri.edu/gsc/cndna.html.

Biological mechanochemistry is found in DNA-related systems[2911] and the mechanochemistry of organic polymers using positionally-controlled scanning probe microscope tips has been demonstrated experimentally in a liquid solvent environment.[2912] Alternatively, DNA could be assembled as a rigid polymer structure at low temperature (e.g., 20-80 K) and in vacuum using mechanosynthetic tooltips similar to those envisioned for the fabrication of diamondoid structures under similar conditions.[2913] But rather than creating a detailed design for a nanorobotic DNA long-strand fabrication system (which is beyond the scope of this book but would be a suitable task for ***future research***), we shall assume that DNA and protein assembly times in mature nanofactories specialized for this purpose may be comparable to the assembly times required to manufacture diamondoid products, given that the making and breaking of predominantly C-C, C-H, C-N and related covalent bonds are involved in both cases.

DNA represents $f_{CellDNA}$ ~ 0.1% of cell mass (**Table 14**), so a cell mill manufacturing $R_{CellMill}$ ~ 1 kg/hr of cells must produce $R_{DNAMill} \sim f_{CellDNA}\ R_{CellMill}$ ~ 0.001 kg/hr of DNA to sustain the overall cell production rate, requiring a ~0.001 kg "DNA mill" if we assume that a ~1 kg mature nanofactory can produce ~1 kg/hr of atomically-precise molecular product. The required DNA production rate is $R_{DNAMillbp} \sim R_{DNAMill} / m_{bp}$ ~ 2.55 x 10^{17} bp/sec for a DNA mill having a volume of $V_{DNAmill} = f_{CellDNA}\ V_{mNF}$ ~ **50 cm^3**, mass $M_{DNAmill} = f_{CellDNA}\ M_{mNF}$ ~ **1 gm**, and power draw $P_{DNAmill} = f_{CellDNA}\ P_{mNF}$ ~ **1.3 watt**, extrapolated from published estimates[2914] that a mature nanofactory with a production rate of $R_{CellMill}$ ~ 1 kg/hr would have a mass of M_{mNF} ~ 1 kg, volume V_{mNF} ~ 0.05 m^3, and power draw P_{mNF} ~ 1300 watts. This yields the following figures of merit for DNA mill performance: ψ_V = 5.10 x 10^{21} bp/m^3-sec, ψ_m = 2.55 x 10^{20} bp/kg-sec, and ψ_P = 1.96 x 10^{17} bp/watt-sec. These figures exceed those of the ÄKTA system by only 25-fold, 641-fold, and 5-fold, respectively, but our nanorobotic DNA mill is producing genome-length DNA strands ready for methylation, histone-wrapping, and installation in cell nuclei – not beakers full of unconnected 25-mer oligos.

D.1.2.3 Manufacturing Personalized Proteins and Carbohydrates

The second most important biomolecules that a cell mill must produce are proteins that comprise most of the functional molecules and structural elements of the manufactured cell. Proteins can be made from amino acids prepared earlier in the Generic Organic Synthesis Unit (Section D.1.1.2) that are polymerized into a chain by enzymatically removing an H from the $-NH_2$ group at one end of an amino acid (the N-terminus), creating a radical site, and then joining it to a radical site at the other end of an amino acid that is created by removing the –OH from a –COOH group at the other end of another amino acid (the C-terminus). Peptides are short chains of 2-50 amino acids, with "oligopeptides" running 2-15 residues in length, "polypeptides" running up to 15-50 residues, and "proteins" generally having >50 residues.[2915]

[2911] Lionnet T, Dawid A, Bigot S, F.X. Barre FX, Saleh OA, Heslot F, Allemand JF, Bensimon D, Croquette V. DNA mechanics as a tool to probe helicase and translocase activity. Nucleic Acids Res. 2006;34(15):4232-4244; https://academic.oup.com/nar/article/34/15/4232/3111868.

[2912] Duwez AS, Cuenot S, Jérôme C, Gabriel S, Jerome R, Rapino S, Zerbetto F. Mechanochemistry: targeted delivery of single molecules. Nat Nanotechnol. 2006 Nov;1(2):122-125; http://citeseerx.ist.psu.edu/viewdoc/download?doi=10.1.1.188.9873&rep=rep1&type=pdf.

[2913] Freitas RA Jr., Merkle RC. A minimal toolset for positional diamond mechanosynthesis. J Comput Theor Nanosci. 2008;5:760-861; http://www.molecularassembler.com/Papers/MinToolset.pdf.

[2914] Drexler KE. Nanosystems: Molecular Machinery, Manufacturing, and Computation, John Wiley & Sons, New York, 1992, Section 14.4.4, "Mass and volume"; https://www.amazon.com/dp/0471575186/.

[2915] https://en.wikipedia.org/wiki/Peptide.

Solid-phase peptide synthesis (SPPS) is the classical method for preparing peptides in the lab,[2916] involving the rapid assembly of a peptide chain through successive reactions of amino acid derivatives on an insoluble porous support.[2917] SPPS is limited by reaction yields to peptides and proteins in the range of 70 amino acids; synthetic difficulty is again sequence dependent, with aggregation-prone sequences such as amyloids being especially difficult to make.[2918]

Longer lengths can be accessed by using ligation approaches such as native chemical ligation,[2919] where two shorter fully deprotected synthetic peptides can be joined together in solution – this method has prepared the 166-residue synthetic erythropoietin and the 203-residue HIV-1 protease proteins.[2920] An automated flow-based SPPS laboratory system has synthesized the single-domain 164-residue sortase protein in 6.5 hours, achieving a production rate of R_{SPPS} ~ 0.007 residues/sec, typically in milligram quantities.[2921]

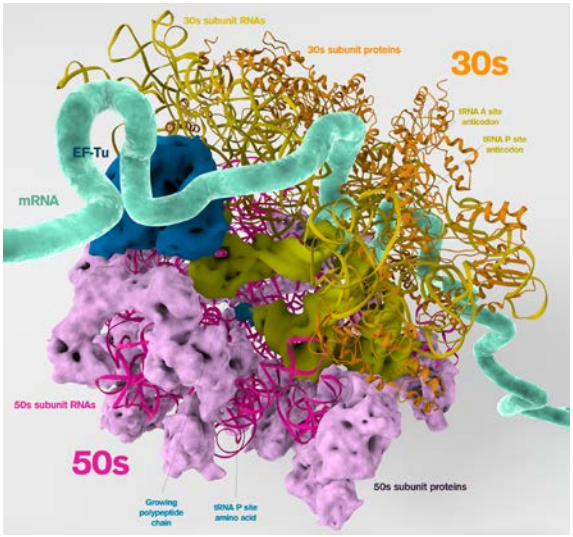

In biological systems, bacterial ribosomes (image, right)[2922] can assemble their own weight in protein in 270-710 sec,[2923] a production rate of ~0.001 kg/sec per kg of ribosomes or $\psi_m = 5 \times 10^{21}$ residues/kg-sec, given the $m_{residue}$ ~ 110 dalton average molecular weight of protein residues[2924] (amino acids having one water molecule removed). The volumetric production figure of merit for a bacterial ribosome[2925] with a volume of $V_{Ribosome}$ ~ $(20\ nm)^3 = 8000\ nm^3$ and a mass of $m_{Ribosome}$ ~ 4.2×10^{-21} kg per ribosome is

---

[2916] Merrifield RB. Solid Phase Peptide Synthesis. I. The Synthesis of a Tetrapeptide. J Am Chem Soc. 1963;85(14):2149-2154; https://pubs.acs.org/doi/pdf/10.1021/ja00897a025. Chan WC, White PD. Fmoc Solid Phase Peptide Synthesis: A Practical Approach. Oxford University Press, Oxford UK, 2000; https://www.amazon.com/Fmoc-Solid-Phase-Peptide-Synthesis/dp/0199637253/.

[2917] https://en.wikipedia.org/wiki/Peptide_synthesis#Solid-phase_synthesis.

[2918] Tickler AK, Clippingdale AB, Wade JD. Amyloid-beta as a "difficult sequence" in solid phase peptide synthesis. Protein Pept Lett. 2004 Aug;11(4):377-384; https://pubmed.ncbi.nlm.nih.gov/15327371/.

[2919] https://en.wikipedia.org/wiki/Native_chemical_ligation.
[2920] https://en.wikipedia.org/wiki/Native_chemical_ligation#Size_limitation.

[2921] Hartrampf N, Saebi A, Poskus M, Gates ZP, Callahan AJ, Cowfer AE, Hanna S, Antilla S, Schissel CK, Quartararo AJ, Ye X, Mijalis AJ, Simon MD, Loas A, Liu S, Jessen C, Nielsen TE, Pentelute BL. Synthesis of proteins by automated flow chemistry. Science 2020 May 29;368(6494):980-987; https://science.sciencemag.org/content/368/6494/980/tab-pdf.

[2922] https://3dciencia.com/blog/2011/02/bacterial-ribosome-internal-structure/.

[2923] Freitas RA Jr., Merkle RC. Kinematic Self-Replicating Machines, Landes Bioscience, Georgetown, TX, 2004; Section 4.2, "Ribosomes: Molecular Positional Assembly for Self-Replication"; http://www.MolecularAssembler.com/KSRM/4.2.htm.

[2924] The average molecular weight of amino acid residues was determined using a weighted mean approach that takes into account the relative proportion of each of the twenty amino acids present in proteins; https://www.promega.com/~/media/files/resources/technical%20references/amino%20acid%20abbreviations%20and%20molecular%20weights.pdf.

[2925] Freitas RA Jr., Merkle RC. Kinematic Self-Replicating Machines, Landes Bioscience, Georgetown, TX, 2004; Section 4.2, "Ribosomes: Molecular Positional Assembly for Self-Replication"; http://www.MolecularAssembler.com/KSRM/4.2.htm.

$\psi_V = (m_{Ribosome} / V_{Ribosome}) \psi_m = 2.6 \times 10^{24}$ residues/m^3-sec.

Each cell requires ~19 billion protein molecules comprising ~20% of total cell mass (**Table 14**), so a cell mill manufacturing $R_{CellMill}$ ~ 1 kg/hr of cells must produce $R_{ProteinMill}$ ~ 0.2 kg/hr (~3 x 10^{20} residues/sec) of protein mass to sustain the needed overall cell production rate. Conservatively adopting the ribosome productivity of only $\psi_m = 5 \times 10^{21}$ residues/kg-sec for the likely much more productive nanorobotic protein synthesis system to be designed in ***future research***,[2926] the resulting protein mill component would have a mass of $m_{ProteinMill} = R_{ProteinMill} / \psi_m$ ~ **60 gm** and a volume of $V_{ProteinMill} = m_{ProteinMill} / \rho_{ProteinMill}$ ~ **3000 cm^3** assuming the protein mill has a device density of $\rho_{ProteinMill}$ ~ 20 kg/m^3 (equivalent to ~3% solid diamond and ~97% vacuum by volume inside the device), the same as the DNA mill. Taking the operating power density of the protein mill as similar to that of the DNA mill (~26,000 W/m^3; Section D.1.2.2), the protein mill power draw is $P_{ProteinMill}$ ~ **78 watts**.

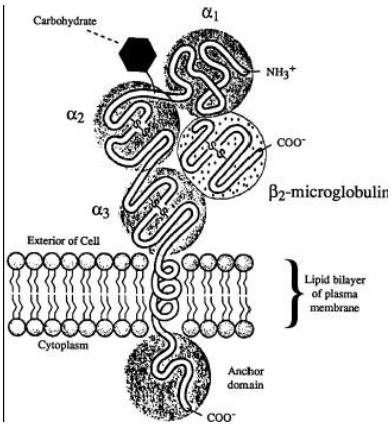

Besides providing the ability to replicate chromosomes in the cell mill, the genome DNA consensus sequence (Section D.1.2.1.1) makes it possible to build proteins, carbohydrates, glycoproteins, and other molecules that are customized to the particular biology of the cryopreserved patient. For example, glycoprotein molecules called the major histocompatibility complex (MHC)[2927] are embedded in the plasma membranes of all human cells and allow the immune system to distinguish self from non-self. MHC-I molecules (image, left) comprise up to ~1% of the protein content of the plasma membrane;[2928] MHC-II molecules (image, right) are less widely distributed, being found on glial cells in the brain and elsewhere; and MHC-III genes encode the 20 proteins that comprise the complement system. The residue sequences of MHC molecules are encoded in a 3.8 million base section of the genome and together create ~2 x 10^{14} fourteen-allele combinations, making the MHC protein set of every person essentially unique. Red cells contain no MHC molecules but instead include a set of 22 different blood group systems, 7 antigen collections, and 47 additional antigens not associated with any collection, which together allow ~10^{19} different combinations to be expressed.[2929] In addition, the plasma membranes of cells appear to be marked with protein antigens that identify the type of cell – for instance, platelets employ 5 separate alloantigen systems, and white cells and tissue cells bear other specific sets of

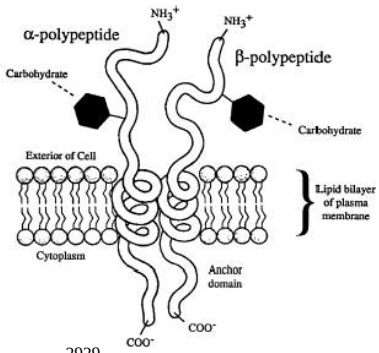

[2926] Ribosomes typically add 2-15 residues/sec to a growing protein chain; it would be plausible to expect that an efficient nanorobotic system could operate at ~1 MHz frequencies instead of the ~10 Hz frequency found in biology, possibly improving productivity over the performance of biological systems by up to 5 orders of magnitude using a nanorobotic system.

[2927] Freitas RA Jr. Nanomedicine, Volume I: Basic Capabilities, Landes Bioscience, Georgetown TX, 1999, Section 8.5.2.1, "Identification of Self"; http://www.nanomedicine.com/NMI/8.5.2.1.htm.

[2928] Becker WM, Deamer DW. The World of the Cell, Second Edition, Benjamin/Cummings Publishing Company, Redwood City CA, 1991; https://www.amazon.com/dp/0805308709/.

[2929] Freitas RA Jr. Nanomedicine, Volume I: Basic Capabilities, Landes Bioscience, Georgetown TX, 1999, Section 8.5.2.1, "Identification of Self"; http://www.nanomedicine.com/NMI/8.5.2.1.htm.

markers that are genetically determined.[2930] Knowledge of the patient's personal gene sequences allows the protein mill to stock cells with autologous proteins that the patient's immune system will recognize as self and that properly identify the variants of each cytotype that are the patient's own.

Multi-subunit proteins can be assembled under full positional control or may be allowed to self-assemble if ***future research*** deems this appropriate. More than 2 decades ago, functional copies of the human red cell **band 3 anion exchanger 1** (AE1, aka. Band 3, solute carrier family 4 member 1 (SLC4A1), or Band 3 anion transport protein), a proteinaceous transmembrane pump, was self-assembled from sets of 3, 4, or 5 complementary fragment subunits or "nanoparts" that were separately cloned in *Xenopus* oocytes.[2931]

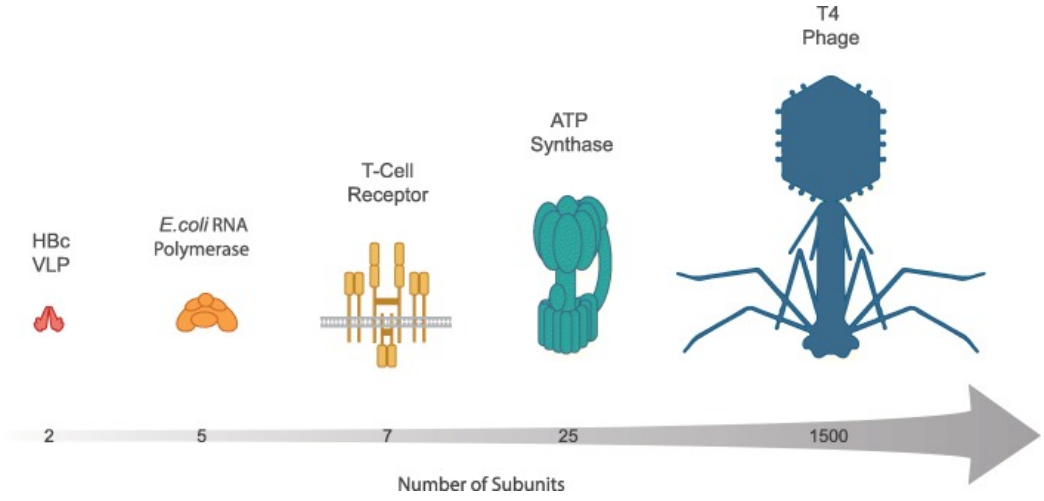

More recently, custom protein factories have been created using cell-free microfabricated bioreactors (which eliminates the maintenance of living systems inside the device) and are now being used to facilitate the on-demand production of therapeutic proteins for medicines and biopharmaceuticals.[2932] As reviewed by Tinafar *et al.* (image, above),[2933] the methods of cell-free synthesis have been used to produce increasingly intricate cytoprotein complexes including the hepatitis B core antigen HBc VLP,[2934] the *E. coli*

[2930] Freitas RA Jr. Nanomedicine, Volume I: Basic Capabilities, Landes Bioscience, Georgetown TX, 1999, Section 8.5.2.2, "Identification of Cell Type"; http://www.nanomedicine.com/NMI/8.5.2.2.htm.

[2931] Groves JD, Wang L, Tanner MJ. Functional reassembly of the anion transport domain of human red cell band 3 (AE1) from multiple and non-complementary fragments. FEBS Lett. 1998 Aug 21;433(3):223-7; http://www.sciencedirect.com/science/article/pii/S0014579398009090/pdf?md5=5a6fd338036616de263d878735192af6&pid=1-s2.0-S0014579398009090-main.pdf.

[2932] Ron Walli, "ORNL cell-free protein synthesis is potential lifesaver," Oak Ridge National Laboratory, 29 Dec 2015; https://www.ornl.gov/news/ornl-cell-free-protein-synthesis-potential-lifesaver.

[2933] Tinafar A, Jaenes K, Pardee K. Synthetic Biology Goes Cell-Free. BMC Biol. 2019 Aug 8;17(1):64; https://www.ncbi.nlm.nih.gov/pmc/articles/PMC6688370/.

[2934] Bundy BC, Franciszkowicz MJ, Swartz JR. *Escherichia coli*-based cell-free synthesis of virus-like particles. Biotechnol Bioeng. 2008;100(1):28-37; https://pubmed.ncbi.nlm.nih.gov/18023052/.

RNA polymerase,[2935] the human T-cell receptor,[2936] an ATP synthase,[2937] and finally the T4[2938] and T7[2939] phages (~1500 "nanoparts").

Automated systems using conventional chemical techniques to produce carbohydrate polymers, or oligosaccharides, while lagging well behind the technologies for synthesizing oligonucleotides (Section D.1.2.2) and oligopeptides (see above), also continue to progress.[2940] Nanorobot-based carbohydrate mills analogous to the previously-described DNA and protein mills should be able to produce both generic and personalized carbohydrate-based polymers much more quickly and efficiently than conventional synthetic techniques.

D.2 Cytocomponent Assembly Module

The cell mill concept relies on the assumption that the components of a cell are essentially modular, hence can be manufactured separately and later assembled into a complete working biological cell. The same assumption applies to the assembly of individual organelles and other basic components of cells, which can also be viewed as collections of modular components and thus can presumably be put together from basic nanoparts.

[2935] Asahara H, Chong S. *In vitro* genetic reconstruction of bacterial transcription initiation by coupled synthesis and detection of RNA polymerase holoenzyme. Nucleic Acids Res. 2010 Jul;38(13):e141; https://www.ncbi.nlm.nih.gov/pmc/articles/PMC2910072/..

[2936] Huppa JB, Ploegh HL. *In vitro* translation and assembly of a complete T cell receptor-CD3 complex. J Exp Med. 1997;186(3):393-403; https://www.ncbi.nlm.nih.gov/pmc/articles/pmid/9236191/.

[2937] Matthies D, Haberstock S, Joos F, Dötsch V, Vonck J, Bernhard F, *et al*. Cell-free expression and assembly of ATP synthase. J Mol Biol. 2011;413(3):593–603; https://www.ncbi.nlm.nih.gov/pubmed/21925509.

[2938] Rustad M, Eastlund A, Jardine P, Noireaux V. Cell-free TXTL synthesis of infectious bacteriophage T4 in a single test tube reaction. Synth Biol. 2018;3(1):1-7; http://noireauxlab.com/html%20pages/docs%20website/publications/Rustad%20et%20al%20-%202018.pdf.

[2939] Shin J, Jardine P, Noireaux V. Genome replication, synthesis, and assembly of the bacteriophage T7 in a single cell-free reaction. ACS Synth Biol. 2012 Sep 21;1(9):408-413; http://noireauxlab.com/html%20pages/docs%20website/publications/Shin%20et%20al%20-%202012.pdf. Rustad M, Eastlund A, Marshall R, Jardine P, Noireaux V. Synthesis of Infectious Bacteriophages in an *E. coli*-based Cell-free Expression System. J Vis Exp. 2017 Aug 17;(126):56144; https://www.ncbi.nlm.nih.gov/pmc/articles/PMC5614349/.

[2940] e.g., Plante OJ, Palmacci ER, Seeberger PH. Automated solid-phase synthesis of oligosaccharides. Science. 2001 Feb 23;291(5508):1523-1527; http://citeseerx.ist.psu.edu/viewdoc/download?doi=10.1.1.985.5831&rep=rep1&type=pdf. Seeberger PH. Automated oligosaccharide synthesis. Chem Soc Rev. 2008 Jan;37(1):19-28; https://pubs.rsc.org/en/content/articlehtml/2008/cs/b511197h. Panza M, Pistorio SG, Stine KJ, Demchenko AV. Automated Chemical Oligosaccharide Synthesis: Novel Approach to Traditional Challenges. Chem Rev. 2018 Sep 12;118(17):8105-8150; https://www.ncbi.nlm.nih.gov/pmc/articles/pmid/29953217/. Wen L, Edmunds G, Gibbons C, *et al*. Toward Automated Enzymatic Synthesis of Oligosaccharides. Chem Rev. 2018 Sep 12;118(17):8151-8187; https://pubmed.ncbi.nlm.nih.gov/30011195/. Zhang J, Chen C, Gadi MR, *et al*. Machine-Driven Enzymatic Oligosaccharide Synthesis by Using a Peptide Synthesizer. Angew Chem Int Ed Engl. 2018 Dec 17;57(51):16638-16642; https://www.ncbi.nlm.nih.gov/pmc/articles/pmid/30375138/. Joseph AA, Pardo-Vargas A, Seeberger PH. Total Synthesis of Polysaccharides by Automated Glycan Assembly. J Am Chem Soc. 2020 May 13;142(19):8561-8564; https://www.ncbi.nlm.nih.gov/pmc/articles/pmid/32338884/.

This Section briefly discusses the nanorobotic manufacture of cell membranes (Section D.2.1), six types of macromolecular organelles (Section D.2.2), five types of vesicular organelles (Section D.2.3), two types of membraneous organelles (Section D.2.4), and the cell nucleus (Section D.2.5).

D.2.1 Cell Membranes

The most prominent feature that all cells have in common, and which is also shared by many subcellular organelles, is the lipid membrane. For example, the plasma membrane which forms the boundary between the cell and its exterior environment consists of a bilayer[2941] of phospholipid molecules, each comprising a water-soluble (hydrophilic) phosphate head and a water-insoluble (hydrophobic) tail consisting of two fatty acid chains (e.g., long-chain hydrocarbon molecules). The phospholipid molecules readily self-assemble[2942] into solid micelles (with little interior space), hollow unilamellar liposomes,[2943] or large bilayer sheets (images, right),[2944] averaging ~8 nm thick.[2945] In the case of cells, the lipid bilayer sheet folds into a large spherical shell (image below, left) that provides a persistent barrier between a water-soluble interior space and the water-soluble exterior spaces, thus enabling both containment and separation.[2946]

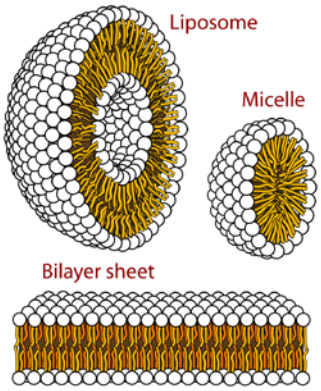

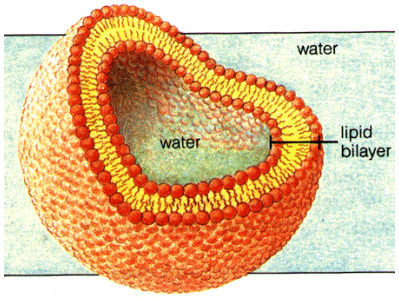

The several varieties of phospholipid molecules[2947] can be manufactured from phosphate ions, small nitrogen-containing molecules, and hydrocarbon chains prepared earlier in the Generic Organic Synthesis Unit (Section D.1.1.2). With these phospholipids in hand, the automated self-assembly of uniform 5-20 μm diameter spherical liposomes with lipid bilayers has been demonstrated experimentally in a controlled, robust, efficient and simple way using chip-based microfluidics.[2948] Biological-based phospholipids

[2941] https://en.wikipedia.org/wiki/Lipid_bilayer.

[2942] Marrink SJ, Lindahl E, Edholm O, Mark AE. Simulation of the spontaneous aggregation of phospholipids into bilayers. J Am Chem Soc. 2001 Sep 5;123(35):8638-9; http://compbio.chemistry.uq.edu.au/mediawiki/upload/5/5b/AM_01_07.pdf.

[2943] "A unilamellar liposome is a spherical chamber/vesicle, bounded by a single bilayer of an amphiphilic lipid or a mixture of such lipids, containing aqueous solution inside the chamber." https://en.wikipedia.org/wiki/Unilamellar_liposome.

[2944] Mariana Ruiz Villarreal: "Cross section of the different structures that phospholipids can take in a aqueous solution. The circles are the hydrophilic heads and the wavy lines are the fatty acyl side chains." https://en.wikipedia.org/wiki/Lipid_bilayer#/media/File:Phospholipids_aqueous_solution_structures.svg.

[2945] Freitas RA Jr., Nanomedicine, Volume I: Basic Capabilities, Landes Bioscience, Georgetown, TX, 1999, Table 8.17, "Approximate Quantification of the Components of a Typical 20-μm Human Tissue Cell"; http://www.nanomedicine.com/NMI/Tables/8.17.jpg.

[2946] https://en.wikipedia.org/wiki/Lipid_bilayer#Containment_and_separation.

[2947] https://en.wikipedia.org/wiki/Phospholipid#Main_phospholipids.

[2948] Deshpande S, Caspi Y, Meijering AE, Dekker C. Octanol-assisted liposome assembly on chip. Nat Commun. 2016 Jan 22;7:10447; http://www.ncbi.nlm.nih.gov/pmc/articles/PMC4735860/. Deshpande S, Birnie A, Dekker C. On-chip density-based purification of liposomes. Biomicrofluidics. 2017 May 8;11(3):034106; https://www.ncbi.nlm.nih.gov/pmc/articles/pmid/28529672/. Deshpande S, Dekker C. On-chip microfluidic production of cell-sized liposomes. Nat Protoc. 2018 May;13(5):856-874; https://pubmed.ncbi.nlm.nih.gov/29599442/.

are commonplace components of self-assembled conventional liposomes[2949] employed in a variety of medical therapeutics.[2950]

In a cell mill that employs positional assembly,[2951] the conceptual process of building a spherical plasma membrane of a precise and uniform size[2952] might begin with a hemispherical mould (image, left) with a perfect 20 μm diameter half-sphere indented into the surface. The surface of the mould is coated with embedded presentation semaphores[2953] having a staggered array of chemically inert alternating hydrophilic and hydrophobic ligands (image, right).[2954]

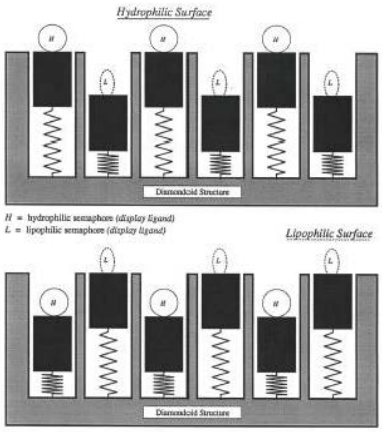

When the computer-controlled pistons extend the hydrophilic ligands and retract the hydrophobic ones (drive motors not shown), the surface will attract hydrophilic moieties such as the phosphate heads of phospholipid molecules, which when offered to the surface one by one will coat the interior surface of the cavity in a monolayer with their hydrophobic tails pointing outward towards the center of the sphere. Molecule-by-molecule placement of another monolayer of phospholipid molecules will bond to the first monolayer, hydrophobic tails to tails, with the hydrophilic heads now pointing toward the center, forming a hemispherical bilayer sheet. Additional work can now be done on this nascent plasma membrane, such as embedding integral proteins one by one or linking cytoskeletal elements to transmembrane proteins. When all interior work is completed, the first membrane hemisphere can be pressed mouth-to-mouth onto a second finished membrane hemisphere of equal size, causing the two miscible halves to join seamlessly into a sealed sphere. The presentation semaphores are now switched from hydrophilic to hydrophobic as the two moulds are pulled apart, repelling the phosphate heads in contact with the surface and freeing the completed spherical lipid bilayer plasma membrane. The entire process may be conducted either in an aqueous environment or under a humid inert gas such as argon or nitrogen.

Each biological cell or constituent membraneous organelle requires a slightly different combination of component protein, carbohydrate, and lipid molecules for its construction, as illustrated in **Table 21** below. All component molecules can be manufactured in the Generic Organic Synthesis Unit (Section D.1.1.2).

[2949] https://en.wikipedia.org/wiki/Liposome.

[2950] e.g., Riaz MK, Riaz MA, Zhang X, Lin C, Wong KH, Chen X, Zhang G, Lu A, Yang Z. Surface Functionalization and Targeting Strategies of Liposomes in Solid Tumor Therapy: A Review. Int J Mol Sci. 2018 Jan 9;19(1):195; https://www.ncbi.nlm.nih.gov/pmc/articles/PMC5796144/.

[2951] Tavares GD, de Oliveira MC, Vilela JMC, Andrade MS. Deposition of Lipid Bilayers with Atomic Force Microscopy. Microscopy and Microanalysis 2005 Dec;11(S03):44-47; https://search.proquest.com/openview/3ac85cd0fec1f75152e73ff9c4af01e4/1?pq-origsite=gscholar&cbl=33692.

[2952] Cells of nonspherical shapes will require nonspherical moulds; reconfigurable moulds also may be designed using structures similar to the pincushion sensor described elsewhere; Freitas RA Jr. Nanomedicine, Vol. I: Basic Capabilities, 1999; Sec. 3.5.7.4, "Pin Cushion Model"; http://www.nanomedicine.com/NMI/3.5.7.4.htm.

[2953] Freitas RA Jr. Nanomedicine, Volume I: Basic Capabilities, Landes Bioscience, Georgetown, TX, 1999; Section 5.3.6, "Presentation Semaphores"; http://www.nanomedicine.com/NMI/5.3.6.htm.

[2954] Freitas RA Jr. Nanomedicine, Volume I: Basic Capabilities, Landes Bioscience, Georgetown, TX, 1999; Figure 5.18; http://www.nanomedicine.com/NMI/Figures/5.18.jpg.

Table 21. Mass % biochemical composition of organelle and cell membranes.[2955]					
Type of Component Membrane Molecule	**Mitochondrion Inner / Outer Membranes**	**Endoplasmic Reticulum Membrane**	**Myelin Sheath**	**Liver Cell Plasma Membrane**	**Red Cell Plasma Membrane**
Lipid	~24% / ~48%	---	~81%	---	40%
Protein	~76% / ~52%	~50%	~19%	~50%	52%
Carbohydrate	---	---	---	---	8%
Lipid Class:					
Cholesterol	3%	6%	22%	17%	23%
Phospholipids					
Phosphatidylethanolamine	35%	17%	15%	7%	18%
Phosphatidylserine	2%	5%	9%	4%	7%
Phosphatidylcholine	39%	40%	10%	24%	17%
Sphingomyelin	0%	5%	8%	19%	18%
Glycolipids	trace	trace	28%	7%	3%
Other lipids	21%	27%	8%	22%	13%

Artificial self-assembling bilayer membranes such as polymersomes[2956] that can serve as the foundation for building synthetic living cells are also the subject of much recent research interest.

D.2.2 Macromolecular Organelles

Six well-known macromolecular organelles found in human cells must be manufactured in the cell mill, including:

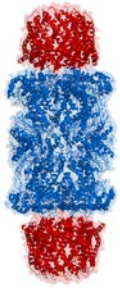

(1) **Proteasomes**[2957] are "protein complexes which degrade unneeded or damaged proteins by proteolysis." Proteasomes normally self-assemble with the assistance of four chaperone molecules.[2958] Proteasomes are ~11 nm in diameter with a typical volume of $V_{proteasome} \sim 3.4 \times 10^{-24}$ m^3 (**Table 10** in Section 4.12.2.3) and mass of

[2955] Freitas RA Jr. Nanomedicine, Volume I: Basic Capabilities, Landes Bioscience, Georgetown, TX, 1999; Table 8.18; http://www.nanomedicine.com/NMI/Tables/8.18.jpg.

[2956] Martino C, Kim SH, Horsfall L, Abbaspourrad A, Rosser SJ, Cooper J, Weitz DA. Protein expression, aggregation, and triggered release from polymersomes as artificial cell-like structures. Angew Chem Int Ed Engl. 2012 Jun 25;51(26):6416-6420; https://weitzlab.seas.harvard.edu/files/weitzlab/files/2012_angewchem_martino.pdf.

[2957] https://en.wikipedia.org/wiki/Proteasome.

[2958] Murata S, Yashiroda H, Tanaka K. Molecular mechanisms of proteasome assembly. Nat Rev Mol Cell Biol. 2009 Feb;10(2):104-115; https://pubmed.ncbi.nlm.nih.gov/19165213/. See also: https://en.wikipedia.org/wiki/Proteasome#Assembly.

$m_{proteasome}$ = 4.18 x 10^{-21} kg (~2.5 MDa),[2959] composed of $n_{ResidueProt} = m_{proteasome} / m_{residue}$ ~ 22,700 amino acid residues, assuming $m_{residue}$ ~ 110 dalton/residue (Section D.1.2.3). There are $n_{proteasome}$ ~ 10^7 proteasomes per typical V_{cell} ~ 8000 μm^3 tissue cell, representing $f_{proteasome} \sim n_{proteasome} V_{proteasome} / V_{cell}$ ~ 0.425 % of cell volume, so a cell mill manufacturing $R_{CellMill}$ ~ 1 kg/hr of cells must assemble $R_{ProtMill} \sim f_{proteasome} R_{CellMill}$ ~ 0.00425 kg/hr ($R_{ProtMillRes}$ ~ 6.4 x 10^{18} residues/sec) of proteasome mass to sustain the overall cell production rate.

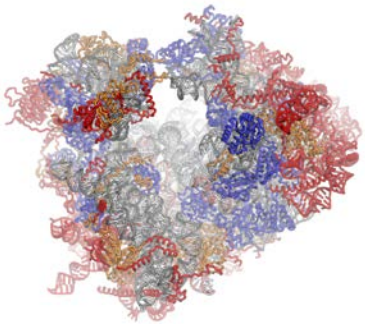

(2) **Ribosomes**[2960] are "macromolecular machines that perform biological protein synthesis (mRNA translation), and consist of two major components – the small and large ribosomal subunits – with each subunit including one or more ribosomal RNA (rRNA) molecules and many ribosomal proteins." For example, the 80S eukaryotic ribosome (image, right) has a 40S subunit with 1753 nucleotides and 33 r-proteins and a large 60S subunit with 3628 nucleotides and 46 r-proteins.[2961] Ribosomes use positionally-controlled solution-phase mechanochemistry to fabricate proteins from amino acid building blocks,[2962] a process that should be readily automated in a nanomechanical cell mill, although a small number of autologous proteins fabricated in this manner could then self-assemble into complete ribosomes, a simple way to make lots of copies of this organelle. The conventional reconstitution of ribosomes *in vitro* is well established,[2963] and steps toward the first artificial ribosome have also been reported.[2964]

Ribosomes are ~25 nm in diameter with a typical volume of $V_{ribosome}$ ~4 x 10^{-24} m^3 (**Table 10** in Section 4.12.2.3) and mass of $m_{ribosome}$ = 5.34 x 10^{-21} kg (~3.2 MDa). There are $n_{ribosome}$ ~ 10^7 ribosomes per typical V_{cell} ~ 8000 μm^3 tissue cell, representing $f_{ribosome} \sim n_{ribosome} V_{ribosome} / V_{cell}$ ~ 0.5 % of cell volume, so a cell mill manufacturing $R_{CellMill}$ ~ 1 kg/hr of cells must assemble $R_{RiboMill} \sim f_{ribosome} R_{CellMill}$ ~ 0.005 kg/hr of ribosome mass to sustain the overall cell production rate.

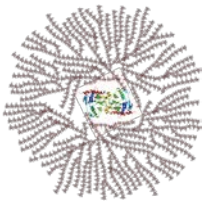

(3) **Glycogen granules**[2965] are a multibranched polysaccharide of glucose that serves as a form of energy storage in animals, and is the main storage form of glucose in the body. Granules self-assemble with the assistance of several enzymes in a process called glycogenesis.[2966] Glycogen granules or "glycosomes" are 10-40

[2959] Tanaka K. The proteasome: overview of structure and functions. Proc Jpn Acad Ser B Phys Biol Sci. 2009 Jan;85(1):12-36; https://www.ncbi.nlm.nih.gov/pmc/articles/PMC3524306/.

[2960] https://en.wikipedia.org/wiki/Ribosome.
[2961] https://en.wikipedia.org/wiki/Eukaryotic_ribosome_(80S).

[2962] Freitas RA Jr., Merkle RC. Kinematic Self-Replicating Machines. Landes Bioscience, Georgetown, TX, 2004, Section 4.2, "Ribosomes: Molecular Positional Assembly for Self-Replication," pp. 96-101; http://www.MolecularAssembler.com/KSRM/4.2.htm.

[2963] Nierhaus KH, Dohme F. Total reconstitution of functionally active 50S ribosomal subunits from *Escherichia coli*. Proc Natl Acad Sci U S A. 1974 Dec;71(12):4713-7; https://www.pnas.org/content/pnas/71/12/4713.full.pdf. Nierhaus KH. Reconstitution of ribosomes, in: Ribosomes and Protein Synthesis, A Practical Approach, Oxford University Press, 1990. Jewett MC, Fritz BR, Timmerman LE, Church GM: *In vitro* integration of ribosomal RNA synthesis, ribosome assembly, and translation. Mol Syst Biol 2013, 9:678; https://www.embopress.org/doi/pdf/10.1038/msb.2013.31.

[2964] Orelle C, Carlson ED, Szal T, Florin T, Jewett MC, Mankin AS. Protein synthesis by ribosomes with tethered subunits. Nature. 2015 Aug 6;524(7563):119-24; http://www.ncbi.nlm.nih.gov/pubmed/26222032.

[2965] https://en.wikipedia.org/wiki/Glycogen.
[2966] https://en.wikipedia.org/wiki/Glycogenesis.

nm in diameter with a typical volume of $V_{glycosome}$ ~1 x 10^{-23} m^3 (**Table 10** in Section 4.12.2.3) and mass of $m_{glycosome}$ = 1.6 x 10^{-20} kg.[2967] There are $n_{glycosome}$ ~ 10^5 glycosomes per typical V_{cell} ~ 8000 μm^3 tissue cell, representing $f_{glycosome}$ ~ $n_{glycosome}$ $V_{glycosome}$ / V_{cell} ~ 0.0125 % of cell volume, so a cell mill manufacturing $R_{CellMill}$ ~ 1 kg/hr of cells must assemble $R_{GlycoMill}$ ~ $f_{glycosome}$ $R_{CellMill}$ ~ 0.000125 kg/hr of glycosome mass to sustain the overall cell production rate.

(4) **Vaults**[2968] are "large ribonucleoprotein particles consisting primarily of proteins that have been implicated in a broad range of cellular functions including nuclear-cytoplasmic transport, mRNA localization, drug resistance, cell signaling, nuclear pore assembly, and innate immunity." Vaults self-assemble by linking and folding multiple joined copies of the major vault protein.[2969] Vaults are ~55 nm in diameter with a typical volume of V_{vault} ~5 x 10^{-23} m^3 (**Table 10** in Section 4.12.2.3) and mass of m_{vault} = 2.2 x 10^{-20} kg (~13 MDa). There are n_{vault} ~ 3000 vaults per typical V_{cell} ~ 8000 μm^3 tissue cell, representing f_{vault} ~ n_{vault} V_{vault} / V_{cell} ~ 1.9 x 10^{-5} of cell volume, so a cell mill manufacturing $R_{CellMill}$ ~ 1 kg/hr of cells must assemble $R_{VaultMill}$ ~ f_{vault} $R_{CellMill}$ ~ 1.9 x 10^{-5} kg/hr of vault mass to sustain the overall cell production rate.

(5) **Centrioles**[2970] are "cylindrical organelles (composed mainly of a protein called tubulin) whose main function as a bound pair is to produce the aster and mitotic spindle during cell division." Centrioles normally arise in association with an existing centriole, but under certain circumstances centrioles can self-assemble free of an existing centriole (*de novo* assembly).[2971] Two centrioles bound at nearly right angles (image, right) form the core of the centrosome,[2972] the main microtubulin organizing center during cell division. Centrioles are ~400 nm in diameter with a typical volume of $V_{centriole}$ ~7 x 10^{-21} m^3 (**Table 10** in Section 4.12.2.3) and mass of $m_{centriole}$ = 9.5 x 10^{-18} kg (assuming mean protein density ~1350 kg/m^3). There are $n_{centriole}$ ~ 2 centrioles per typical V_{cell} ~ 8000 μm^3 tissue cell, representing $f_{centriole}$ ~ $n_{centriole}$ $V_{centriole}$ / V_{cell} ~ 1.75 x 10^{-6} of cell volume, so a cell mill manufacturing $R_{CellMill}$ ~ 1 kg/hr of cells must assemble $R_{CentMill}$ ~ $f_{centriole}$ $R_{CellMill}$ ~ 1.75 x 10^{-6} kg/hr of centriole mass to sustain the overall cell production rate.

[2967] Prats C, Graham TE, Shearer J. The dynamic life of the glycogen granule. J Biol Chem. 2018 May 11;293(19):7089-7098; https://www.jbc.org/content/293/19/7089.full.pdf.

[2968] https://en.wikipedia.org/wiki/Vault_(organelle).

[2969] Muñoz-Juan A, Carreño A, Mendoza R, Corchero JL. Latest Advances in the Development of Eukaryotic Vaults as Targeted Drug Delivery Systems. Pharmaceutics. 2019 Jun 28;11(7):300; https://www.ncbi.nlm.nih.gov/pmc/articles/PMC6680493/.

[2970] https://en.wikipedia.org/wiki/Centriole.

[2971] Song MH, Miliaras NB, Peel N, O'Connell KF. Centrioles: some self-assembly required. Curr Opin Cell Biol. 2008 Dec;20(6):688-693; https://www.ncbi.nlm.nih.gov/pmc/articles/pmid/18840522/.

[2972] https://en.wikipedia.org/wiki/Centrosome.

(6) **Chromosomes**[2973] are "a DNA molecule that includes packaging proteins which, aided by chaperone proteins, bind to and condense the DNA molecule to prevent it from becoming an unmanageable tangle." The fabrication of a genome-length strand of pure DNA with a specified base-pair sequence has previously been described (Section D.1.2.2). Chromosomes are DNA strands wrapped around spool-shaped histone octamer[2974] molecules (image, right)[2975] that bind to DNA and serve as anchors around which the strands are wound, forming a DNA/protein complex called chromatin[2976] that when quadruply-folded (compacted) is 40,000 times shorter than an unpacked molecule (image, below).[2977] Each histone octamer wrapped with its 147-bp of spooled DNA is called a nucleosome.[2978]

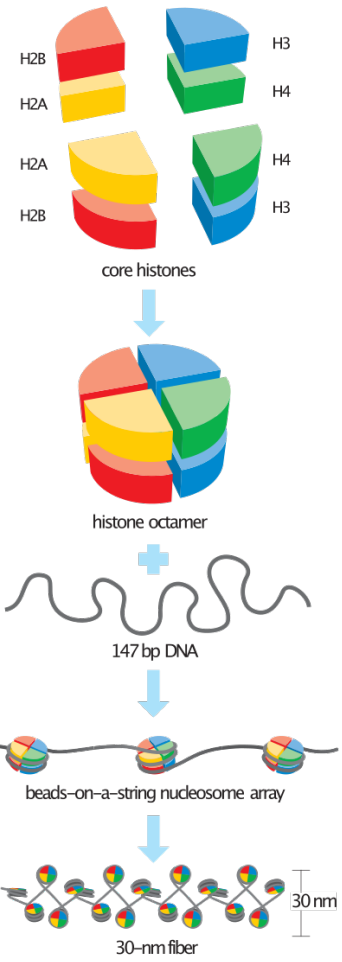

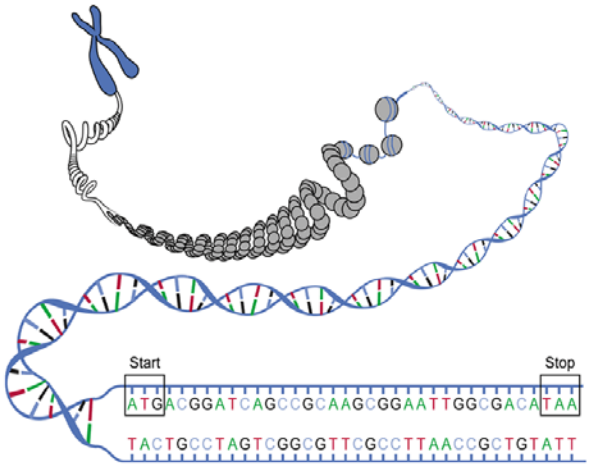

The manufactured genetic material destined for each manufactured cell will consist first of duplex dsDNA (ds = double-strand) which is assembled[2979] from two complementary strands of ssDNA (ss = single strand) that have been positionally fabricated base by base in a DNA mill (Section D.1.2.2). Using positionally

---

[2973] https://en.wikipedia.org/wiki/Chromosome.
[2974] https://en.wikipedia.org/wiki/Histone_octamer.

[2975] Image created by David O. Morgan from The Cell Cycle;
https://en.wikipedia.org/wiki/File:Basic_units_of_chromatin_structure.svg.

[2976] https://en.wikipedia.org/wiki/Chromatin.

[2977] Boston University School of Public Health, "Chromosomes Contain Our Genetic Code";
https://sphweb.bumc.bu.edu/otlt/MPH-Modules/PH/DNA-Genetics/DNA-Genetics2.html.

[2978] https://en.wikipedia.org/wiki/Nucleosome.

[2979] Cserpan I, Kalman M, Tjörnhammar ML, Simoncsits A. Conversion of single-stranded oligonucleotides into cloned duplexes and its consecutive application to short artificial genes. Acta Chem Scand. 1991 Mar;45(3):265-272;
https://pubmed.ncbi.nlm.nih.gov/1645560/.

controlled functionalized tooltips analogous to DNA methyltransferase enzymes,[2980] the dsDNA haploid strand is next partially methylated for the particular cell type, thus allowing the DNA, once installed in the manufactured nucleus (Section D.2.5), to express only the appropriate exons (at non-methylated sites) that are active in the cell type under construction. (Methylation involves the addition of methyl groups to deactivate expression of a given section of DNA.) The partially methylated strand is then wrapped around properly modified[2981] (possibly acetylated,[2982] methylated,[2983] phosphorylated,[2984] monoubiquitylated,[2985] or sumoylated[2986]) histones – normally incorporating post-translational modifications perhaps constituting a "histone code" that may be used by the cell to encrypt various chromatin conformations and gene expression states[2987] – after being joined with its homologue strand to make a diploid chromosome that is joined at the waist by a centromere.[2988] (***Future research*** should determine if alternative processes involving partial self-assembly of histones[2989] and other chromatin-associated proteins[2990] or "architectural proteins"[2991] onto positionally synthesized DNA can be equally reliable but more efficient.) The centromere is coded by a conserved relatively short repeating heterochromatin sequence and includes a small complex of associated proteins.[2992] Each completed 23-diploid-chromatid set of chromatin fibers

---

[2980] Pljevaljcic G, Schmidt F, Peschlow A, Weinhold E. Sequence-specific DNA labeling using methyltransferases. Methods Mol Biol. 2004;283:145-161; https://pubmed.ncbi.nlm.nih.gov/15197308/. Dalhoff C, Lukinavicius G, Klimasăuskas S, Weinhold E. Direct transfer of extended groups from synthetic cofactors by DNA methyltransferases. Nat Chem Biol. 2006 Jan;2(1):31-32; https://pure.mpg.de/rest/items/item_2630060_3/component/file_2630063/content. Bheemanaik S, Reddy YV, Rao DN. Structure, function and mechanism of exocyclic DNA methyltransferases. Biochem J. 2006 Oct 15;399(2):177-90; https://www.ncbi.nlm.nih.gov/pmc/articles/PMC1609917/.

[2981] LaVoie HA. Epigenetic control of ovarian function: the emerging role of histone modifications. Mol Cell Endocrinol. 2005 Nov 24;243(1-2):12-18; https://pubmed.ncbi.nlm.nih.gov/16219412/.

[2982] Clayton AL, Hazzalin CA, Mahadevan LC. Enhanced histone acetylation and transcription: a dynamic perspective. Mol Cell. 2006 Aug 4;23(3):289-296; https://www.cell.com/molecular-cell/pdf/S1097-2765(06)00432-1.pdf.

[2983] Torok MS, Grant PA. The generation and recognition of histone methylation. Results Probl Cell Differ. 2006;41:25-46; https://pubmed.ncbi.nlm.nih.gov/16909889/.

[2984] Wang Y, Fischle W, Cheung W, Jacobs S, Khorasanizadeh S, Allis CD. Beyond the double helix: writing and reading the histone code. Novartis Found Symp. 2004;259:3-17; https://pubmed.ncbi.nlm.nih.gov/15171244/.

[2985] Osley MA. H2B ubiquitylation: the end is in sight. Biochim Biophys Acta. 2004 Mar 15;1677(1-3):74-78; https://pubmed.ncbi.nlm.nih.gov/15020048/.

[2986] Nathan D, Ingvarsdottir K, Sterner DE, Bylebyl GR, Dokmanovic M, Dorsey JA, Whelan KA, Krsmanovic M, Lane WS, Meluh PB, Johnson ES, Berger SL. Histone sumoylation is a negative regulator in *Saccharomyces cerevisiae* and shows dynamic interplay with positive-acting histone modifications. Genes Dev. 2006 Apr 15;20(8):966-76; https://www.ncbi.nlm.nih.gov/pmc/articles/PMC1472304/.

[2987] Villar-Garea A, Imhof A. The analysis of histone modifications. Biochim Biophys Acta. 2006 Dec;1764(12):1932-1939; https://pubmed.ncbi.nlm.nih.gov/17015046/.

[2988] https://en.wikipedia.org/wiki/Centromere.

[2989] Fyodorov DV, Kadonaga JT. Dynamics of ATP-dependent chromatin assembly by ACF. Nature. 2002 Aug 22;418(6900):897-900; https://pubmed.ncbi.nlm.nih.gov/12192415/.

[2990] Hakimi MA, Bochar DA, Schmiesing JA, Dong Y, Barak OG, Speicher DW, Yokomori K, Shiekhattar R. A chromatin remodelling complex that loads cohesin onto human chromosomes. Nature. 2002 Aug 29;418(6901):994-998; https://pubmed.ncbi.nlm.nih.gov/12198550/.

[2991] https://en.wikipedia.org/wiki/Nuclear_organization#Architectural_proteins.

[2992] Foltz DR, Jansen LE, Black BE, Bailey AO, Yates JR 3rd, Cleveland DW. The human CENP-A centromeric nucleosome-associated complex. Nat Cell Biol. 2006 May;8(5):458-469; http://www.jansenlab.org/files/2006foltz.pdf.

would be fully condensed (e.g., by nondisruptive methods functionally similar to chemically-induced premature chromosome condensation)[2993] into compact supercoiled form,[2994] then stored for later use during the assembly of a manufactured nucleus (Section D.2.5).

The histone octamer is a squat cylinder ~11 nm in diameter and ~5.5 nm tall,[2995] giving a volume of $V_{histone}$ ~ 5.3 x 10^{-25} m^3 with a typical mass of $m_{histone}$ = 1.81 x 10^{-22} kg (~108,000 daltons) or $n_{ResidueHist}$ = 990 amino acid residues.[2996] There are $n_{histone}$ ~ 25 x 10^6 histone octamers per typical V_{cell} ~ 8000 μm^3 tissue cell, representing $f_{histone}$ ~ $n_{histone}$ $V_{histone}$ / V_{cell} ~ 0.166 % of cell volume, so a cell mill manufacturing $R_{CellMill}$ ~ 1 kg/hr of cells must assemble $R_{HistMill}$ ~ $f_{histone}$ $R_{CellMill}$ ~ 0.00166 kg/hr ($R_{HistMillRes}$ ~ 2.5 x 10^{18} residues/sec) of histone octamer mass to sustain the overall cell production rate.

For all six macromolecular organelles, the total manufacturing requirement is $R_{MacromolOrgs}$ = $R_{ProtMill}$ + $R_{RiboMill}$ + $R_{GlycoMill}$ + $R_{VaultMill}$ + $R_{CentMill}$ + $R_{HistMill}$ ~ 0.0111 kg/hr (or $R_{MacromolOrgsRes}$ ~ 1.67 x 10^{19} residues/sec) to sustain the overall cell production rate of $R_{CellMill}$ ~ 1 kg/hr. Again conservatively adopting the ribosome productivity of only ψ_m = 5 x 10^{21} residues/kg-sec for the nanorobotic protein synthesis system (Section D.1.2.3), the additional protein mill component would have a mass of $m_{ProteinMillMO}$ = $R_{MacromolOrgsRes}$ / ψ_m ~ **3 gm** and a volume of $V_{ProteinMillMO}$ = $m_{ProteinMill}$ / $\rho_{ProteinMill}$ ~ **170 cm^3** assuming the protein mill has a device density of $\rho_{ProteinMill}$ ~ 20 kg/m^3 (equivalent to ~3% solid diamond and ~97% vacuum by volume inside the device), the same as the DNA mill. Taking the operating power density of the protein mill as similar to that of the DNA mill (~26,000 W/m^3; Section D.1.2.2), the additional protein mill power draw is $P_{ProteinMillMO}$ ~ **4 watts**.

D.2.3 Vesicular Organelles

Five other organelles found in human cells consist of a vesicle or membrane that encloses metabolically active materials of various kinds. Each of these organelles consists of a phospholipid monolayer or bilayer membrane enclosing a roughly spherical or cylindrical space filled with lipids, digestive enzymes, material being transported, or, in the case of the mitochondrion, a system of internal membranes, ribosomes, granules, and DNA almost as complex as a complete living cell but much smaller, reflecting its ancient bacterial evolutionary origin.[2997] These vesicular organelles must be manufactured in the cell mill, and include:

[2993] Prasanna PG, Blakely WF. Premature chromosome condensation in human resting peripheral blood lymphocytes for chromosome aberration analysis using specific whole-chromosome DNA hybridization probes. Methods Mol Biol. 2005;291:49-57; https://pubmed.ncbi.nlm.nih.gov/15502211/.

[2994] Grigoryev SA, Bednar J, Woodcock CL. MENT, a heterochromatin protein that mediates higher order chromatin folding, is a new serpin family member. J Biol Chem. 1999 Feb 26;274(9):5626-5636; https://www.jbc.org/content/274/9/5626.full.pdf. Kimura K, Rybenkov VV, Crisona NJ, Hirano T, Cozzarelli NR. 13S condensin actively reconfigures DNA by introducing global positive writhe: implications for chromosome condensation. Cell. 1999 Jul 23;98(2):239-248; https://core.ac.uk/download/pdf/82504740.pdf.

[2995] Richmond TJ, Finch JT, Rushton B, Rhodes D, Klug A. Structure of the nucleosome core particle at 7 A resolution. Nature. 1984 Oct 11-17;311(5986):532-537; https://pubmed.ncbi.nlm.nih.gov/6482966/. Cutter AR, Hayes JJ. A brief review of nucleosome structure. FEBS Lett. 2015 Oct 7;589(20 Pt A):2914-22; https://www.ncbi.nlm.nih.gov/pmc/articles/PMC4598263/.

[2996] https://www.activemotif.com/catalog/details/31472/recombinant-histone-octamer-h3-3.

[2997] Sagan L. On the origin of mitosing cells. J Theor Biol. 1967 Mar;14(3):255-74; http://web.gps.caltech.edu/classes/ge246/endosymbiotictheory_marguli.pdf.

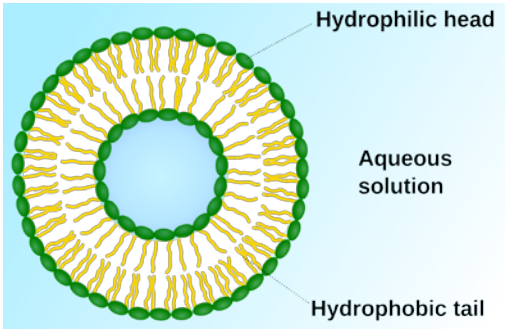

(1) **Transport vesicles**[2998] or **endosomes** are phospholipid membranes (**Table 21** in Section D.2.1) that form containers for protein transport that extrude from the endoplasmic reticulum and "are transported to the cis face of the Golgi apparatus, where they fuse with the Golgi membrane and empty their contents into the lumen," or which contain proteins destined for other organelles within the cell (e.g., lysosomes) or for extracellular release. A typical V_{cell} ~ 8000 μm^3 tissue cell might contain ~200,000 Golgi vesicles ~50 nm in diameter (each ~6.5 x 10^{-23} m^3 and ~7.3 x 10^{-20} kg, with shell volume ~4 x 10^{-23} m^3) and ~50,000 secretory vesicles ~0.1 μm in diameter (each ~4 x 10^{-21} m^3 and ~4.5 x 10^{-18} kg, with shell volume ~2 x 10^{-22} m^3).[2999] This gives a total vesicle volume of $V_{vesicle}$ = 2.2 x 10^{-16} m^3 and $M_{vesicle}$ = 2.5 x 10^{-13} kg per cell, representing $f_{vesicle}$ ~ $V_{vesicle}$ / V_{cell} ~ 2.75 % of cell volume, so a cell mill manufacturing $R_{CellMill}$ ~ 1 kg/hr of cells must assemble $R_{VesiMill}$ ~ $f_{vesicle}$ $R_{CellMill}$ ~ 0.0275 kg/hr of vesicle mass (roughly half protein, half lipid) to sustain the overall cell production rate.

Endosomes (membrane-bound intracellular compartments originating from the Golgi trans face containing molecules or ligands internalized from the plasma membrane that may be targeted to lysosomes for degradation) have been reconstituted *in vitro* from purified components.[3000]

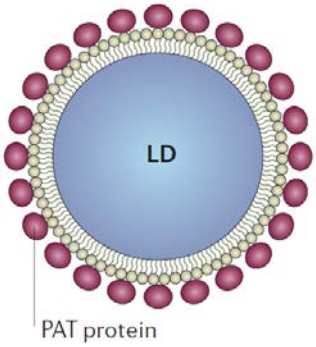

(2) **Lipid droplets**[3001] (aka. lipid bodies, oil bodies, or adiposomes) are "lipid-rich cellular organelles found largely in the adipose tissue that regulate the storage and hydrolysis of neutral lipids, and also serve as a reservoir for cholesterol and acyl-glycerols for membrane formation and maintenance." Lipid droplets have a neutral lipid core (triacylglycerols and cholesteryl esters) surrounded by a phospholipid monolayer 0.2-5 μm in diameter with a typical volume of $V_{droplet}$ ~ 10^{-19} m^3 and mass of $m_{droplet}$ = 8.5 x 10^{-17} kg.[3002] If there are $n_{droplet}$ ~ 100 lipid droplets per V_{cell} ~ 8000 μm^3 tissue cell, representing $f_{droplet}$ ~ $n_{droplet}$ $V_{droplet}$ / V_{cell} ~ 0.125 % of cell volume, then a cell mill manufacturing $R_{CellMill}$ ~ 1 kg/hr of cells must assemble $R_{DropMill}$ ~ $f_{droplet}$ $R_{CellMill}$ ~ 0.00125 kg/hr of lipid droplet mass to sustain the overall cell production rate.

(3) **Lysosomes**[3003] are roughly spherical vesicles containing ~50 hydrolytic enzymes that can degrade extracellular material internalized by endocytosis/phagocytosis, and can degrade and recycle

---

[2998] https://en.wikipedia.org/wiki/Golgi_apparatus#Vesicular_transport.

[2999] Freitas RA Jr., Nanomedicine, Volume I: Basic Capabilities, Landes Bioscience, Georgetown, TX, 1999, Table 8.17, "Approximate Quantification of the Components of a Typical 20-μm Human Tissue Cell"; http://www.nanomedicine.com/NMI/Tables/8.17.jpg.

[3000] Wollert T. Reconstituting multivesicular body biogenesis with purified components. Methods Cell Biol. 2012;108:73-92; http://www.ncbi.nlm.nih.gov/pubmed/22325598.

[3001] Image from: Martin S, Parton RG. Lipid droplets: a unified view of a dynamic organelle. Nat Rev Mol Cell Biol. 2006 May;7(5):373-378; https://pubmed.ncbi.nlm.nih.gov/16550215/. See also https://en.wikipedia.org/wiki/Lipid_droplet.

[3002] Freitas RA Jr., Nanomedicine, Volume I: Basic Capabilities, Landes Bioscience, Georgetown, TX, 1999, Table 8.17, "Approximate Quantification of the Components of a Typical 20-μm Human Tissue Cell"; http://www.nanomedicine.com/NMI/Tables/8.17.jpg.

[3003] https://en.wikipedia.org/wiki/Lysosome.

intracellular components that are delivered via autophagy.[3004] Lysosomes[3005] have a lipid bilayer membrane in which is embedded special transmembrane transport proteins that use ATP to pump H^+ into the organelle lumen to maintain internal pH at 5, along with special docking marker acceptor proteins that mark a lysosome as a target for fusion with specific transport vesicles in the cell.[3006] Lysosomes are ~0.5-1 μm in diameter with a typical volume of $V_{lysosome} \sim 3.1 \times 10^{-19}$ m^3 and mass $m_{lysosome} = 3.5 \times 10^{-16}$ kg.[3007] If there are $n_{lysosome} \sim 300$ lysosomes per typical $V_{cell} \sim 8000$ μm^3 tissue cell, representing $f_{lysosome} \sim n_{lysosome} V_{lysosome} / V_{cell} \sim 1.16$ % of cell volume, so a cell mill manufacturing $R_{CellMill} \sim$ 1 kg/hr of cells must assemble $R_{LysoMill} \sim f_{lysosome} R_{CellMill} \sim 0.0116$ kg/hr of lysosome mass to sustain the overall cell production rate.

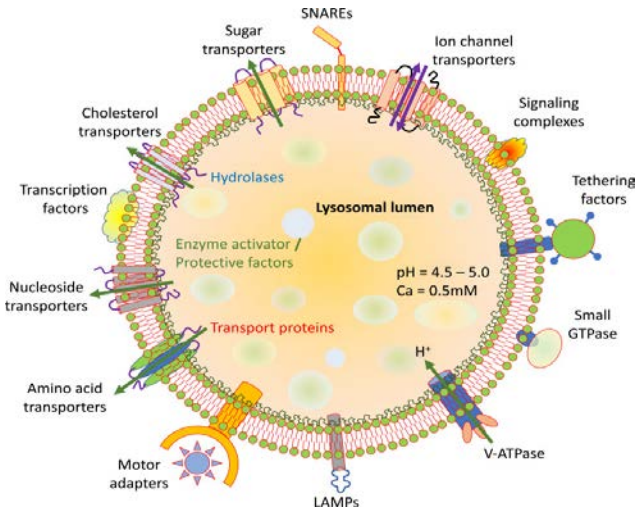

One of the first artificial lysosome "models" was reported in 1969.[3008] Lysosomal ion channel molecules have been successfully inserted into artificial membranes by conventional means.[3009]

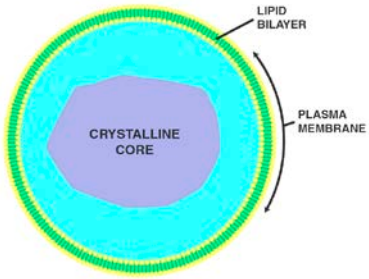

(4) **Peroxisomes**[3010] are cytoplasmic membrane-bounded oxidative organelles that "perform key roles in lipid metabolism and the conversion of reactive oxygen species." They "contain a variety of enzymes, which primarily function together to rid the cell of toxic substances, and in particular, hydrogen peroxide."[3011] Much like lysosomes, peroxisomes are ~0.5-1 μm in diameter with a typical

---

[3004] Wang F, Gómez-Sintes R, Boya P. Lysosomal membrane permeabilization and cell death. Traffic. 2018 Dec;19(12):918-931; https://onlinelibrary.wiley.com/doi/full/10.1111/tra.12613.

[3005] Image from: Allemailem KS, Almatroudi A, Alrumaihi F, Almatroodi SA, Alkurbi MO, Basfar GT, Rahmani AH, Khan AA. Novel Approaches of Dysregulating Lysosome Functions in Cancer Cells by Specific Drugs and Its Nanoformulations: A Smart Approach of Modern Therapeutics. Int J Nanomedicine. 2021 Jul 26;16:5065-5098; https://www.ncbi.nlm.nih.gov/pmc/articles/pmc8324981/.

[3006] Freitas RA Jr. Nanomedicine, Volume I: Basic Capabilities, Landes Bioscience, Georgetown, TX, 1999; Section 8.5.3.8, "Lysosomes and Proteasomes"; http://www.nanomedicine.com/NMI/5.3.6.htm.

[3007] Freitas RA Jr., Nanomedicine, Volume I: Basic Capabilities, Landes Bioscience, Georgetown, TX, 1999, Table 8.17, "Approximate Quantification of the Components of a Typical 20-μm Human Tissue Cell"; http://www.nanomedicine.com/NMI/Tables/8.17.jpg.

[3008] Sessa G, Weissman GJ. Formation of artificial lysosome *in vitro*. J Clin Invest. 1969 Jan 1;48(6):A76-A77. Sessa G, Weissmann G. Incorporation of lysozyme into liposomes. A model for structure-linked latency. J Biol Chem. 1970 Jul 10;245(13):3295-301; http://www.jbc.org/content/245/13/3295.long.

[3009] Venturi E, Sitsapesan R. Reconstitution of lysosomal ion channels into artificial membranes. Methods Cell Biol. 2015;126:217-36; http://www.ncbi.nlm.nih.gov/pubmed/25665448.

[3010] https://en.wikipedia.org/wiki/Peroxisome.
[3011] https://upload.wikimedia.org/wikipedia/commons/8/82/Peroxisome.jpg.

volume of $V_{peroxisome}$ ~ 3.1 x 10^{-19} m^3 and mass $m_{peroxisome}$ = 3.9 x 10^{-16} kg.[3012] If there are $n_{peroxisome}$ ~ 300 peroxisomes per typical V_{cell} ~ 8000 μm^3 tissue cell, representing $f_{peroxisome}$ ~ $n_{peroxisome}$ $V_{peroxisome}$ / V_{cell} ~ 1.16 % of cell volume, so a cell mill manufacturing $R_{CellMill}$ ~ 1 kg/hr of cells must assemble $R_{PeroxMill}$ ~ $f_{peroxisome}$ $R_{CellMill}$ ~ 0.0116 kg/hr of peroxisome mass to sustain the overall cell production rate. "Peroxisomes can be derived from the endoplasmic reticulum under certain experimental conditions and replicate by membrane growth and division out of pre-existing organelles."[3013]

(5) **Mitochondria**[3014] are double-membrane-bound organelles whose main function is to provide energy for the cell, most importantly by the production of the energy molecule ATP. Mitochondria are 0.5-1 μm wide and 2-3 μm long, with a typical volume of $V_{mitochondrion}$ ~ 1 x 10^{-18} m^3 and mass of $m_{mitochondrion}$ = 1.2 x 10^{-15} kg.[3015] There are $n_{mitochondrion}$ ~ 1000 mitochondria per typical V_{cell} ~ 8000 μm^3 tissue cell, representing $f_{mitochondrion}$ ~ $n_{mitochondrion}$ $V_{mitochondrion}$ / V_{cell} ~ 12.5 % of cell volume, so a cell mill manufacturing $R_{CellMill}$ ~ 1 kg/hr of cells must assemble $R_{MitoMill}$ ~ $f_{mitochondrion}$ $R_{CellMill}$ ~ 0.125 kg/hr of mitochondrial mass to sustain the overall cell production rate. A significant fraction of mitochondrial mass will consist of manufactured proteins such as enzymes (Section D.1.2.3), macromolecular organelles such as ribosomes and granules (Section D.2.2), and mitochondrial DNA in the form of a single 16 kilobase circular chromosome with 37 genes,[3016] requiring some special handling.

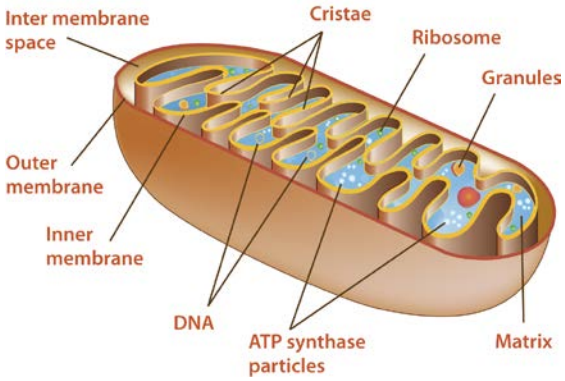

Organelle biogenesis in biological systems can occur by *de novo* synthesis from (1) a pre-existing membrane source, (2) fission,[3017] (3) fusion,[3018] and (4) decay, such as through partitioning during cell division or autophagy.[3019] For example, biogenesis of **mitochondria** (image, left) occurs by growth and

---

[3012] Freitas RA Jr., Nanomedicine, Volume I: Basic Capabilities, Landes Bioscience, Georgetown, TX, 1999, Table 8.17, "Approximate Quantification of the Components of a Typical 20-μm Human Tissue Cell"; http://www.nanomedicine.com/NMI/Tables/8.17.jpg.

[3013] Schrader M, Costello JL, Godinho LF, Azadi AS, Islinger M. Proliferation and fission of peroxisomes - An update. Biochim Biophys Acta. 2016 May;1863(5):971-983; https://www.sciencedirect.com/science/article/pii/S0167488915003365.

[3014] Image from: https://www.ck12.org/book/ck-12-biology-concepts/r6/section/2.25/. See also: https://en.wikipedia.org/wiki/Mitochondrion.

[3015] Freitas RA Jr., Nanomedicine, Volume I: Basic Capabilities, Landes Bioscience, Georgetown, TX, 1999, Table 8.17, "Approximate Quantification of the Components of a Typical 20-μm Human Tissue Cell"; http://www.nanomedicine.com/NMI/Tables/8.17.jpg.

[3016] Anderson S, Bankier AT, Barrell BG, de Bruijn MHL, Coulson AR, Drouin J, Eperon IC, Nierlich DP, Roe BA, Sanger F, Schreier PH, Smith AJH, Staden R, Young IG. Sequence and organization of the human mitochondrial genome. Nature. 1981 Apr 9;290(5806):457-465; https://pubmed.ncbi.nlm.nih.gov/7219534/. See also: https://en.wikipedia.org/wiki/Mitochondrial_DNA.

[3017] Lowe M, Barr FA. Inheritance and biogenesis of organelles in the secretory pathway. Nat Rev Mol Cell Biol. 2007 Jun;8(6):429-39; https://www.ncbi.nlm.nih.gov/pubmed/17505521/.

[3018] Denesvre C, Malhotra V. Membrane fusion in organelle biogenesis. Curr Opin Cell Biol. 1996 Aug;8(4):519-23; https://www.ncbi.nlm.nih.gov/pubmed/8791453/.

[3019] van der Vaart A, Mari M, Reggiori F. A picky eater: exploring the mechanisms of selective autophagy in human pathologies. Traffic. 2008 Mar;9(3):281-9;

division of pre-existing organelles,[3020] a process that could presumably be artificially accelerated using a bioreactor setup or by other means.[3021] The inventory of known proteins comprising all mammalian mitochondria (the full mitochondrial "parts list") is almost complete.[3022]

Mainstream research is also pursuing the possibility of artificial mitochondria. For example, the light-driven proton pump bacteriorhodopsin and the enzyme ATP synthase have successfully been co-reconstituted into small unilamellar vesicles[3023] and polymersomes.[3024] The energy from the reduction of oxygen might be usable for ATP production by replacing bacteriorhodopsin with ubiquinol bo_3 oxidase in small unilamellar vesicles[3025] and polymersomes[3026] – their co-reconstitution having been achieved in cell-sized giant unilamellar vesicles[3027] where ATP synthase has been shown to induce nonequilibrium membrane fluctuation.[3028]

Whether a biogenesis-type approach to manufacturing organelles is feasible or advisable is a matter for ***future research***, but the premise of this book is that positionally-controlled processes may serve as the

---

https://www.researchgate.net/profile/Fulvio_Reggiori/publication/5859063_A_picky_eater_exploring_the_mechanisms_of_selective_autophagy_in_human_pathologies/links/542408dc0cf238c6ea6e896e.pdf.

[3020] Valero T. Mitochondrial biogenesis: pharmacological approaches. Curr Pharm Des. 2014;20(35):5507-9; https://www.ncbi.nlm.nih.gov/pubmed/24606795.

[3021] Komen JC, Thorburn DR. Turn up the power - pharmacological activation of mitochondrial biogenesis in mouse models. Br J Pharmacol. 2014 Apr;171(8):1818-36; http://www.ncbi.nlm.nih.gov/pmc/articles/PMC3976607/. Thevis M, Schänzer W. Emerging drugs affecting skeletal muscle function and mitochondrial biogenesis - Potential implications for sports drug testing programs. Rapid Commun Mass Spectrom. 2016 Mar 15;30(5):635-51; http://www.ncbi.nlm.nih.gov/pubmed/26842585.

[3022] Calvo SE, Clauser KR, Mootha VK. MitoCarta2.0: an updated inventory of mammalian mitochondrial proteins. Nucleic Acids Res. 2016 Jan 4;44(D1):D1251-7; http://www.ncbi.nlm.nih.gov/pmc/articles/PMC4702768/.

[3023] Pitard B, Richard P, Duñach M, Girault G, Rigaud JL. ATP synthesis by the F_0F_1 ATP synthase from thermophilic *Bacillus* PS3 reconstituted into liposomes with bacteriorhodopsin. 1. Factors defining the optimal reconstitution of ATP synthases with bacteriorhodopsin. Eur J Biochem. 1996 Feb 1;235(3):769-778; https://febs.onlinelibrary.wiley.com/doi/epdf/10.1111/j.1432-1033.1996.00769.x.

[3024] Choi HJ, Montemagno CD. Artificial organelle: ATP synthesis from cellular mimetic polymersomes. Nano Lett. 2005 Dec;5(12):2538-2542; https://pubmed.ncbi.nlm.nih.gov/16351211/.

[3025] Nilsson T, Lundin CR, Nordlund G, Ädelroth P, von Ballmoos C, Brzezinski P. Lipid-mediated Protein-protein Interactions Modulate Respiration-driven ATP Synthesis. Sci Rep. 2016 Apr 11;6:24113; https://www.ncbi.nlm.nih.gov/pmc/articles/PMC4827085/. von Ballmoos C, Biner O, Nilsson T, Brzezinski P. Mimicking respiratory phosphorylation using purified enzymes. Biochim Biophys Acta. 2016 Apr;1857(4):321-331; https://core.ac.uk/download/pdf/33091349.pdf.

[3026] Otrin L, Marušič N, Bednarz C, *et al*. Toward Artificial Mitochondrion: Mimicking Oxidative Phosphorylation in Polymer and Hybrid Membranes. Nano Lett. 2017 Nov 8;17(11):6816-6821; https://pure.mpg.de/rest/items/item_2506715/component/file_2623632/content. Marušič N, Otrin L, Zhao Z, Lira RB, Kyrilis FL, Hamdi F, Kastritis PL, Vidaković-Koch T, Ivanov I, Sundmacher K, Dimova R. Constructing artificial respiratory chain in polymer compartments: Insights into the interplay between bo_3 oxidase and the membrane. Proc Natl Acad Sci U S A. 2020 Jun 30;117(26):15006-15017; https://www.ncbi.nlm.nih.gov/pmc/articles/PMC7334566/.

[3027] Biner O, Schick T, Müller Y, von Ballmoos C. Delivery of membrane proteins into small and giant unilamellar vesicles by charge-mediated fusion. FEBS Lett. 2016 Jul;590(14):2051-2062; https://febs.onlinelibrary.wiley.com/doi/pdf/10.1002/1873-3468.12233%4010.1002/%28ISSN%291873-3468%28CAT%29FreeEditorsChoiceArticles%28VI%29FECA.

[3028] Almendro-Vedia VG, Natale P, Mell M, Bonneau S, Monroy F, Joubert F, López-Montero I. Nonequilibrium fluctuations of lipid membranes by the rotating motor protein F_1F_0-ATP synthase. Proc Natl Acad Sci U S A. 2017 Oct 24;114(43):11291-11296; https://www.ncbi.nlm.nih.gov/pmc/articles/PMC5664490/.

foundation for most or all organelle assembly operations. To this end, assembling a $d_{organelle}$ = 1 μm diameter spherical vesicular organelle using nanorobot-mediated positionally-controlled processes might proceed in 4 steps:

(A) **Build Lipid Membrane.** A mould-based semaphore-assisted deposition of organelle phospholipid membranes is initiated for two matching hemispheres (Section D.2.1). A close-packed array of nanorobotic manipulator arms (Section 5.2.1.1) spaced at 100 nm intervals are employed to bond the lipid molecules onto the mould in a efficient pattern. Each nanomanipulator has H_{manip} = 100 nm of accessible horizontal space, a work area of $A_{manip} = H_{manip}^2 = 10^4$ nm^2, and a system volume (= mechanism + working volume) of $V_{manip} = H_{manip}^3 = 10^6$ nm^3. If nanomanipulator productivity $\mathfrak{D}_{mols} \sim \psi_V V_{manip}$ = 2600 molecules/manipulator-sec, taking $\psi_V = 2.6 \times 10^{24}$ molecules/m^3-sec on the conservative assumption that nanorobotic manipulators should have at least the same volumetric productivity as ribosomes in an aqueous operating environment,[3029] and given that there are $n_{lipidmols} \sim 2.5 \times 10^6$ lipid molecules/μm^2 in each layer of a plasma membrane lipid bilayer,[3030] then the hemispheric mould surface under each nanomanipulator in the array receives one complete lipid layer of $n_{lipidmols} A_{manip} \sim$ 25,000 lipid molecules in $t_{lipidlayer} \sim n_{lipidmols} A_{manip} / \mathfrak{D}_{mols} \sim$ 9.6 sec, dissipating $P_{manipulator} \sim$ 0.1 pW/manipulator while in continuous motion. A hemispheric mould for an organelle of diameter $d_{organelle}$ = 1 μm requires $n_{maniparray} \sim \pi d_{organelle}^2 / 2A_{manip} \sim$ 157 nanomanipulators consuming $n_{maniparray} P_{manipulator} \sim$ 157 pW of power, and needs $2t_{lipidlayer} \sim$ 19 sec to lay down a complete hemispheric lipid bilayer of $N_{bilayerlipids} = \pi d_{organelle}^2 n_{lipidmols} n_{maniparray} \sim 1.2 \times 10^9$ bilayer lipid molecules in that time.

(B) **Insert Membrane Proteins.** The same 157-arm manipulator array is next employed to embed transmembrane proteins into the lipid membrane and to attach integral and related proteins into the inward-facing surface of the membrane. The plasma membrane of a human tissue cell typically contains $n_{proteinmols}$ ~ 42,000 protein molecules/μm^2,[3031] so each manipulator in the array requires $t_{proteininsert} \sim n_{proteinmols} A_{manip} / \mathfrak{D}_{mols} \sim$ 0.16 sec to complete all protein insertion operations within its $A_{manip} = 10^4$ nm^2 workspace. The entire array of $n_{maniparray} \sim$ 157 manipulators can insert $N_{proteininsert} = (\pi/2) d_{organelle}^2 n_{proteinmols} n_{maniparray} \sim 10^7$ protein molecules in that time.

(C) **Build Internal Structure.** The internal structure of the organelle is built in place using the manipulator array. The solid volume of the $d_{organelle}$ = 1 μm diameter hemisphere under construction is $V_{hemisphere} = \pi d_{organelle}^3 / 12 =$ 0.262 μm^3. Taking the most conservative assumption, the entire hemispheric volume could be filled with covalently bonded $N_{hemisphericprotein} = \rho_{protein} V_{hemisphere} / m_{protein} \sim 4.2 \times 10^6$ protein molecules of average mass $m_{protein} \sim 8.4 \times 10^{-23}$ kg/molecule (~50,000 dalton protein molecules)[3032] and mean protein density $\rho_{protein} \sim$ 1350 kg/m^3 in a filling time of $t_{proteinbuild} \sim N_{hemisphericprotein} / n_{maniparray} \mathfrak{D}_{mols} \sim$ 10 sec using a single 157-manipulator array. Note that the internal structure of the mitochondrion has moderate complexity because of the presence of an internal highly invaginated membrane that produces

---

[3029] Ribosome volumetric productivity $\psi_V = 2.6 \times 10^{24}$ residues/m^3-sec when bonding amino acid molecules (each of which becomes a "residue") to proteins in an aqueous working environment (Section D.1.2.3).

[3030] Freitas RA Jr. Nanomedicine, Volume I: Basic Capabilities, Landes Bioscience, Georgetown, TX, 1999; Section 8.5.3.2, "Cell Membrane"; http://www.nanomedicine.com/NMI/8.5.3.2.htm.

[3031] Freitas RA Jr. Nanomedicine, Volume I: Basic Capabilities, Landes Bioscience, Georgetown, TX, 1999; Section 8.5.3.2, "Cell Membrane"; http://www.nanomedicine.com/NMI/8.5.3.2.htm.

[3032] Freitas RA Jr. Nanomedicine, Volume I: Basic Capabilities, Landes Bioscience, Georgetown, TX, 1999; Table 3.2; http://www.nanomedicine.com/NMI/Tables/3.2.jpg.

numerous small compartments or cristae that may change shape in response to local pH gradients and functional state;[3033] any necessary additional assembly steps should be determined in ***future research***.

(D) **Join and Release.** The two equal hemispheres are pressed together face to face, causing them to seamlessly join because of the inherent miscibility of the lipid bilayers along the equatorial perimeter of each face. After any further post-processing is completed,[3034] the finished vesicular organelle can be released from the moulds by switching the semaphores from hydrophilic to hydrophobic.

The total manufacturing requirement for all five vesicular organelles is $R_{VesicularOrgs} = R_{VesiMill} + R_{DropMill} + R_{LysoMill} + R_{PeroxMill} + R_{MitoMill} = 0.177$ kg/hr to sustain the overall cell production rate of $R_{CellMill} \sim 1$ kg/hr. The 157-manipulator array can lay down $m_{bilayerlipids} \sim m_{lipid}\ N_{bilayerlipids} \sim 1.4 \times 10^{-15}$ kg of bilayer lipid molecules in $2t_{lipidlayer} \sim 19$ sec, or $\psi_1 = m_{bilayerlipids} / 2t_{lipidlayer} \sim 7.4 \times 10^{-17}$ kg/array-sec; insert $m_{proteininsert} \sim m_{protein}\ N_{proteininsert} \sim 8.4 \times 10^{-16}$ kg of protein molecules in $t_{proteininsert} \sim 0.16$ sec, or $\psi_2 = m_{proteininsert} / t_{proteininsert} \sim 5.3 \times 10^{-15}$ kg/array-sec; and build out $m_{hemisphericprotein} \sim m_{protein}\ N_{hemisphericprotein} \sim 3.5 \times 10^{-16}$ kg of protein molecules in $t_{proteinbuild} \sim 10$ sec, or $\psi_3 = m_{hemisphericprotein} / t_{proteinbuild} \sim 3.5 \times 10^{-17}$ kg/array-sec, taking average lipid molecule mass as $m_{lipid} \sim 1.17 \times 10^{-24}$ kg/molecule (~700 daltons) and average protein molecule as $m_{protein} \sim 8.4 \times 10^{-23}$ kg/molecule (~50,000 daltons). Hence we require $N_{arrays} = (R_{VesicularOrgs} / \psi_1) + (R_{VesicularOrgs} / \psi_2) + (R_{VesicularOrgs} / \psi_3) \sim 2.1 \times 10^{12}$ arrays to deliver enough vesicular organelles to satisfy the required production rate of $R_{CellMill} \sim 1$ kg/hr of cells. These arrays have an estimated total volume of $V_{arrays} \sim n_{maniparray}\ V_{manip}\ N_{arrays} \sim 0.33$ cm^3.

If the solid volume of the mould structures, including all interior mechanisms, is some multiple α_{mould} of the volume of the organelles that are being manufactured, then a cubical mould enclosing a spherical organelle of diameter $d_{organelle} = 1$ μm would have a cubical edge length of $L_{cube} = (\pi\ \alpha_{mould} / 6)^{1/3}\ d_{organelle} = 1.26$ μm, taking $\alpha_{mould} = 3.8$.[3035] Since each array services one hemispherical mould having a solid volume of $0.5\ L_{cube}^3 \sim 1$ μm^3, the total solid volume of all moulds is $V_{VesOrgMoulds} = 0.5\ L_{cube}^3\ N_{arrays} = 2.1$ cm^3. Assuming a manipulator density of $\rho_{manip} \sim 100$ kg/m^3 (i.e., $\sim 10^{-19}$ kg / 10^6 nm^3) and a mould density approximating 10% of diamond at $\rho_{mould} \sim 350$ kg/m^3, then the vesicular organelle manufacturing equipment has a volume of $V_{CellMillVO} = V_{arrays} + V_{VesOrgMoulds} \sim$ **2.4 cm^3**, a mass of $m_{CellMillVO} = \rho_{manip}\ V_{arrays} + \rho_{mould}\ V_{VesOrgMoulds} \sim$ **0.768 gm**, and a power draw of $P_{CellMillVO} = n_{maniparray}\ N_{arrays}\ P_{manip} \sim$ **33 watts** for the manipulator arrays.

It might be necessary to introduce certain solutes or ions into the cytosol in order to prevent newly introduced vesicular organelles from shrinking, swelling, or bursting due to unwanted osmotic imbalances. Preventing this activity is especially important since new organelles may be introduced with internal inventories of enzymes and at least some reactive chemicals. This issue and its resolution are the proper subject of ***future research***.

[3033] Khalifat N, Puff N, Bonneau S, Fournier JB, Angelova MI. Membrane deformation under local pH gradient: mimicking mitochondrial cristae dynamics. Biophys J. 2008 Nov 15;95(10):4924-33; https://www.ncbi.nlm.nih.gov/pmc/articles/PMC2576396/.

[3034] For example, it may be deemed desirable to decorate the exterior surfaces of organelle membranes with protein or carbohydrate moieties (Section 4.12.2.7), or to insert sorting rotor probes through the outer membrane into the sealed interior of the organelle to extract or insert particular molecules of interest (Section 4.10.1.9). A list of all essential post-processing steps should be compiled, and the nanorobotic means for accomplishing all post-processing steps elucidated, in ***future research***.

[3035] By simple geometry, a cube of edge L with a hemispheric hole on one face of maximum radius R = L/2 has a cubical volume (including the hemispheric hole) equal to $L^3 / [(1/2)(4/3)\ \pi\ R^3] = 12 / \pi = 3.8$ times the volume of the hemispheric hole.

D.2.4 Membraneous Organelles

Two essential organelles found in human cells – the (1) Golgi apparatus and (2) endoplasmic reticulum – are essentially collections of membrane sheets arranged to form compartments through which a variety of packaged biochemicals can pass and be processed.

There organelles could be laboriously assembled fragment by fragment via positionally-controlled nanorobotic pick-and-place operations. However, the preliminary assessment is that under the correct conditions both membraneous organelles should largely self-assemble in place from simpler vesicular components. These components can be manufactured by the previously-described vesicular organelle cell mill (Section D.2.3), then be deployed by nanorobotic means to the correct intracellular positions for self-assembly. This supposition should be examined and critically re-assessed in ***future research***.

(1) The **Golgi apparatus**[3036] is "part of the endomembrane system in the cytoplasm [that] packages proteins into membrane-bound vesicles inside the cell before the vesicles are sent to their destination. The Golgi is of particular importance in processing proteins for secretion, containing a set of glycosylation enzymes that attach various sugar monomers to proteins as the proteins move through the apparatus."

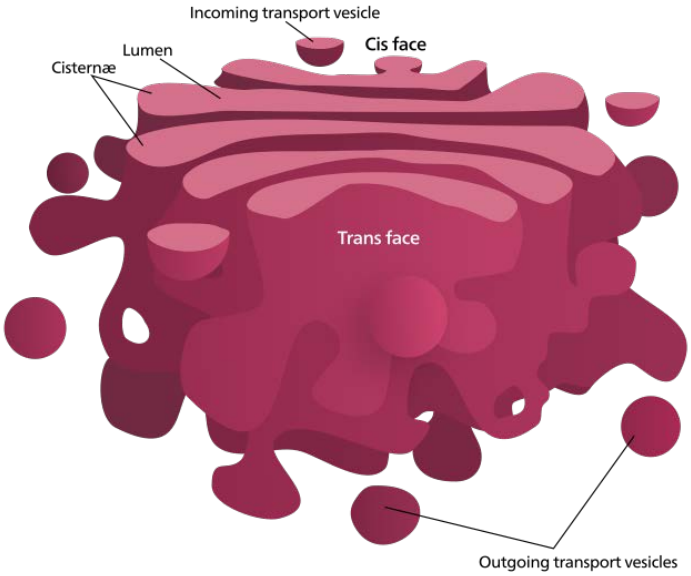

Mammalian cells typically contain 40-100 stacks of cisternae located near the cell nucleus close to the centrosome (Section D.2.2(5)), with each stack consisting of 4-8 cisternae or membrane-bounded compartments linked together via microtubule[3037] connections. Each cistern has a "cis" entry face that receives protein-containing vesicles migrating from the endoplasmic reticulum and a "trans" exit face from which vesicles containing proteins that have been chemically modified during their slow passage through the Golgi are released and slowly migrate to lysosomes, secretory vessels, or to the cell surface.

There is some confidence in the self-assembly approach because the Golgi body is known to disintegrate prior to cell mitosis and then reassemble with remarkable precision after cytokinesis,[3038] so deployment of manufactured Golgi material in the correct intracellular position after extraction of the original material

---

[3036] https://en.wikipedia.org/wiki/Golgi_apparatus.
[3037] https://en.wikipedia.org/wiki/Microtubule#Intracellular_organization.

[3038] Lowe M, Nakamura N, Warren G. Golgi division and membrane traffic. Trends Cell Biol. 1998 Jan;8(1):40-44; https://pubmed.ncbi.nlm.nih.gov/9695807/. Zaal KJM, Smith CL, Polishchuk RS, Altan N, Cole NB, Ellenberg J, Hirschberg K, Presley JF, Roberts TH, Siggia E, Phair RD, Lippincott-Schwartz J. Golgi membranes are absorbed into and reemerge from the ER during mitosis. Cell. 1999 Dec 10;99(6):589-601; https://core.ac.uk/download/pdf/82536976.pdf.

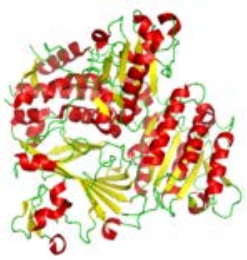

should result in self-assembly of a fully functional Golgi stack.[3039] In the most widely-accepted cisternal progression/maturation model of the self-assembling Golgi apparatus,[3040] coat protein II (COPII; image above, left)[3041]-coated vesicles fuse to form the first cis-cisterna of the Golgi stack, which progresses to become mature trans-Golgi network (TGN) cisternae as coat protein I (COPI; image, right)[3042]-coated vesicles continually recycle Golgi-specific proteins from older to younger cisternae (retrograde transport). Individual stacks have different assortments of enzymes that allow progressive processing of cargo proteins as they travel from the cis face to the trans face.[3043] Once matured, the TGN cisternae dissolve to become secretory vesicles. If this model is correct, then the cell mill need only manufacture the appropriate COPII- and COPI-coated vesicles (Section D.2.3(1)) that are normally produced in the endoplasmic reticulum, then progressively release these vesicles in the desired perinuclear location near the centrosome inside the manufactured cell, along with sufficient microtubular components, and the Golgi apparatus should spontaneously assemble as a viable intracellular organelle.

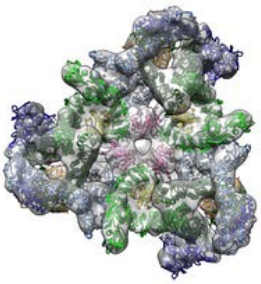

As an experimental example of this, Golgi stacks have been reassembled from isolated Golgi components (including random assortments of vesicles "▲", tubules ">", and cisternal remnants "→"; image, below left) to create a large reassembled Golgi stack (image, below right; scale bar = 0.5 μm).[3044]

A fully-assembled Golgi complex is several microns wide with a typical volume of $V_{Golgi} \sim 4.5 \times 10^{-16}$ m^3 and mass $m_{Golgi} = 4.9 \times 10^{-13}$ kg,[3045] representing $f_{Golgi} \sim V_{Golgi} / V_{cell} \sim 5.6$ % of the volume of a typical $V_{cell} \sim 8000$ μm^3 tissue cell, so a cell mill manufacturing $R_{CellMill} \sim 1$ kg/hr of cells must assemble $R_{GolgiMill} \sim f_{Golgi}\ R_{CellMill} \sim 0.056$ kg/hr of Golgi vesicles to sustain the overall cell production rate.

[3039] Rabouille C, Misteli T, Watson R, Warren G. Reassembly of Golgi stacks from mitotic Golgi fragments in a cell-free system. J Cell Biol. 1995 May;129(3):605-18; http://citeseerx.ist.psu.edu/viewdoc/download?doi=10.1.1.273.3233&rep=rep1&type=pdf. Puri S, Linstedt AD. Capacity of the golgi apparatus for biogenesis from the endoplasmic reticulum. Mol Biol Cell. 2003 Dec;14(12):5011-5018; https://www.ncbi.nlm.nih.gov/pmc/articles/PMC284802/. Kühnle J, Shillcock J, Mouritsen OG, Weiss M. A modeling approach to the self-assembly of the Golgi apparatus. Biophys J. 2010 Jun 16;98(12):2839-2847; https://www.ncbi.nlm.nih.gov/pmc/articles/PMC2884245/. Tachikawa M, Mochizuki A. Golgi apparatus self-organizes into the characteristic shape via postmitotic reassembly dynamics. Proc Natl Acad Sci U S A. 2017 May 16;114(20):5177-5182; https://www.ncbi.nlm.nih.gov/pmc/articles/PMC5441826/.

[3040] Glick BS, Luini A. Models for Golgi traffic: a critical assessment. Cold Spring Harb Perspect Biol. 2011 Nov 1;3(11):a005215; https://www.ncbi.nlm.nih.gov/pmc/articles/pmid/21875986/.

[3041] https://en.wikipedia.org/wiki/COPII.
[3042] https://en.wikipedia.org/wiki/COPI.

[3043] Day KJ, Staehelin LA, Glick BS. A three-stage model of Golgi structure and function. Histochem Cell Biol. 2013 Sep;140(3):239-249; https://www.ncbi.nlm.nih.gov/pmc/articles/pmid/23881164/. Alberts B., *et al*. Molecular Biology of the Cell, 6th Edition, W.W. Norton & Company, 2014; https://www.amazon.com/Molecular-Biology-Sixth-Bruce-Alberts/dp/0815344325/.

[3044] Rabouille C, Misteli T, Watson R, Warren G. Reassembly of Golgi stacks from mitotic Golgi fragments in a cell-free system. J Cell Biol. 1995 May;129(3):605-18; http://citeseerx.ist.psu.edu/viewdoc/download?doi=10.1.1.273.3233&rep=rep1&type=pdf.

[3045] Freitas RA Jr., Nanomedicine, Volume I: Basic Capabilities, Landes Bioscience, Georgetown, TX, 1999, Table 8.17, "Approximate Quantification of the Components of a Typical 20-μm Human Tissue Cell"; http://www.nanomedicine.com/NMI/Tables/8.17.jpg.

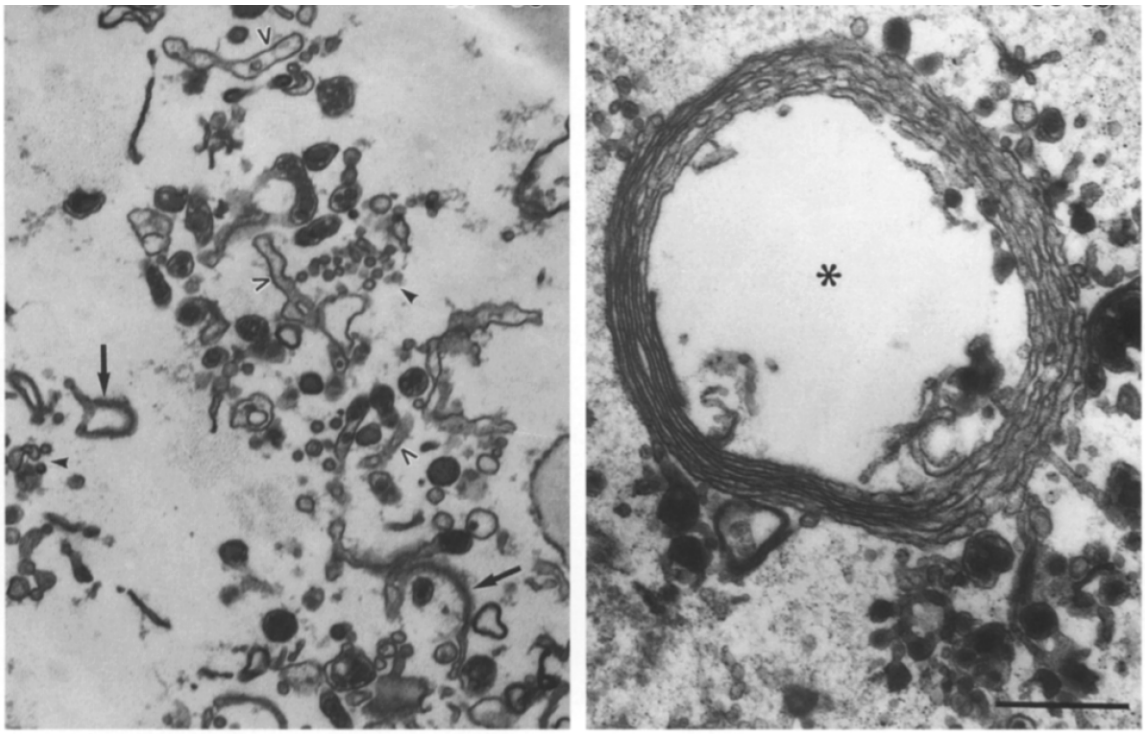

(2) The **endoplasmic reticulum**[3046] is "a type of organelle made up of two subunits – rough endoplasmic reticulum (RER)[3047] and smooth endoplasmic reticulum (SER)[3048] – [that] forms an interconnected network of flattened, membrane-enclosed sacs known as cisternae (in the RER), and tubular structures in the SER, [whose] membranes are continuous with the outer nuclear membrane. The two types of ER share many of the same proteins and engage in certain common activities such as the synthesis of certain lipids and cholesterol. Different types of cells contain different ratios of the two types of ER depending on the activities of the cell. The outer (cytosolic) face of the rough endoplasmic reticulum is studded with ribosomes that are the sites of protein synthesis. The

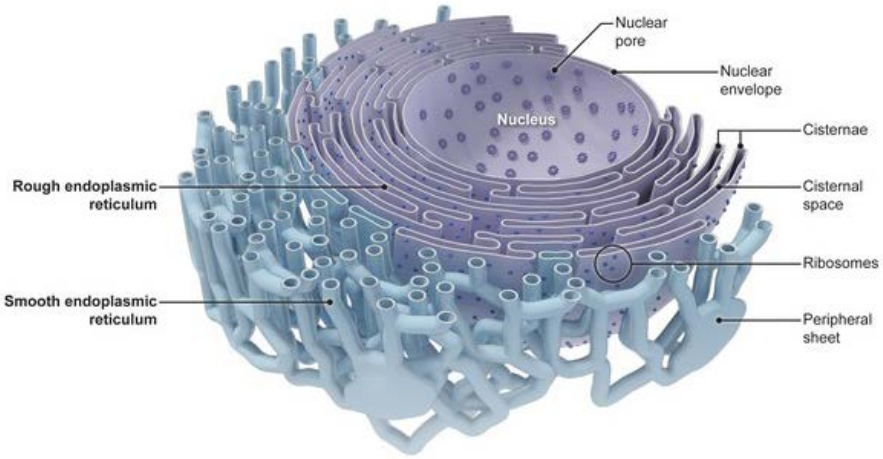

[3046] Image from: Goyal U, Blackstone C. Untangling the web: mechanisms underlying ER network formation. Biochim Biophys Acta. 2013 Nov;1833(11):2492-8; https://www.ncbi.nlm.nih.gov/pmc/articles/pmid/23602970/. See also:.https://en.wikipedia.org/wiki/Endoplasmic_reticulum.

[3047] https://en.wikipedia.org/wiki/Endoplasmic_reticulum#Rough_endoplasmic_reticulum.
[3048] https://en.wikipedia.org/wiki/Endoplasmic_reticulum#Smooth_endoplasmic_reticulum.

smooth endoplasmic reticulum lacks ribosomes and functions in lipid synthesis (but not metabolism), the production of steroid hormones, and detoxification."

Self-assembly of endoplasmic reticulum from manufactured material also appears likely,[3049] though coordination with nucleus manufacture (Section D.3.1) is essential and the viability and specific methodology of ER self-assembly processes must be tested and experimentally confirmed by ***future research***. Synthetic cells with multicompartment vesicles, nested vesicles, or "vesosomes" have been created (A) from spontaneous or induced endobudding of giant unilamellar vesicles,[3050] (B) from mimicking the natural process of endosymbiosis,[3051] or (C) by using capillary-based microfluidics devices.[3052] Multicompartment systems have been introduced into living cells where they have successfully performed enzymatic cascade reactions.[3053] Enzymes have been incorporated and operated inside polymersomes[3054] and vesicles,[3055] and complex enzyme cascades producing monoterpenes,[3056] isobutanol[3057] and polyhydroxybutyrate[3058] have been operated *in vitro* using glucose as feedstock. In another study, a synthetic pathway that captures and converts or "fixes" CO_2 required an *in vitro* metabolic network of 17 reactions established with enzymes originating from nine different organisms, including three engineered enzymes.[3059]

[3049] Ferencz CM, Guigas G, Veres A, Neumann B, Stemmann O, Weiss M. Shaping the endoplasmic reticulum *in vitro*. Biochim Biophys Acta. 2016 Sep;1858(9):2035-2040; https://www.sciencedirect.com/science/article/pii/S0005273616302127. Ferencz CM, Guigas G, Veres A, Neumann B, Stemmann O, Weiss M. *In Vitro* Reconstitution of the Endoplasmic Reticulum. Curr Protoc Cell Biol. 2017 Sep 1;76:11.22.1-11.22.16; https://pubmed.ncbi.nlm.nih.gov/28862340/. Li Q, Han X. Self-Assembled Rough Endoplasmic Reticulum-Like Proto-Organelles. iScience. 2018 Oct 26;8:138-147; https://www.ncbi.nlm.nih.gov/pmc/articles/PMC6180236/.

[3050] Okumura Y, Nakaya T, Namai H, Urita K. Giant vesicles with membranous microcompartments. Langmuir. 2011 Apr 5;27(7):3279-3282; https://pubmed.ncbi.nlm.nih.gov/21395271/.

[3051] Paleos CM, Pantos A. Molecular recognition and organizational and polyvalent effects in vesicles induce the formation of artificial multicompartment cells as model systems of eukaryotes. Acc Chem Res. 2014 May 20;47(5):1475-1482; https://pubmed.ncbi.nlm.nih.gov/24735049/.

[3052] Deng NN, Yelleswarapu M, Zheng L, Huck WT. Microfluidic Assembly of Monodisperse Vesosomes as Artificial Cell Models. J Am Chem Soc. 2017 Jan 18;139(2):587-590; https://pubs.acs.org/doi/full/10.1021/jacs.6b10977.

[3053] Godoy-Gallardo M, Labay C, Trikalitis VD, *et al*. Multicompartment Artificial Organelles Conducting Enzymatic Cascade Reactions inside Cells. ACS Appl Mater Interfaces. 2017 May 17;9(19):15907-15921; https://pubmed.ncbi.nlm.nih.gov/28117959/.

[3054] Peters RJ, Marguet M, Marais S, Fraaije MW, van Hest JC, Lecommandoux S. Cascade reactions in multicompartmentalized polymersomes. Angew Chem Int Ed Engl. 2014 Jan 3;53(1):146-150; https://core.ac.uk/download/pdf/19745137.pdf.

[3055] Elani Y, Law RV, Ces O. Vesicle-based artificial cells as chemical microreactors with spatially segregated reaction pathways. Nat Commun. 2014 Oct 29;5:5305; https://core.ac.uk/download/pdf/76995237.pdf.

[3056] Korman TP, Opgenorth PH, Bowie JU. A synthetic biochemistry platform for cell free production of monoterpenes from glucose. Nat Commun. 2017 May 24;8:15526; https://www.ncbi.nlm.nih.gov/pmc/articles/PMC5458089/.

[3057] Opgenorth PH, Korman TP, Iancu L, Bowie JU. A molecular rheostat maintains ATP levels to drive a synthetic biochemistry system. Nat Chem Biol. 2017 Sep;13(9):938-942; https://pubmed.ncbi.nlm.nih.gov/28671683/.

[3058] Opgenorth PH, Korman TP, Bowie JU. A synthetic biochemistry module for production of bio-based chemicals from glucose. Nat Chem Biol. 2016 Jun;12(6):393-395; https://pubmed.ncbi.nlm.nih.gov/27065234/.

[3059] Schwander T, Schada von Borzyskowski L, Burgener S, Cortina NS, Erb TJ. A synthetic pathway for the fixation of carbon dioxide *in vitro*. Science. 2016 Nov 18;354(6314):900-904; https://www.ncbi.nlm.nih.gov/pmc/articles/PMC5892708/.

A fully-assembled endoplasmic reticulum partly surrounds the nucleus and may have a typical volume of V_{ER} ~ 1.54 x 10^{-15} m^3 (including ~1120 μm^3 for rough ER and ~420 μm^3 for smooth ER)[3060] and mass m_{ER} ~ 1.7 x 10^{-12} kg, representing $f_{ER} \sim V_{ER} / V_{cell}$ ~ 19.3 % of the volume of a typical V_{cell} ~ 8000 μm^3 tissue cell, so a cell mill manufacturing $R_{CellMill}$ ~ 1 kg/hr of cells must assemble $R_{ERMill} \sim f_{ER}\ R_{CellMill}$ ~ 0.193 kg/hr of endoplasmic reticulum vesicles (plus any necessary supplementary ribosomes) to sustain the overall cell production rate.

The vesicles from which the Golgi and ER organelles may be self-assembled can be manufactured using the same specialty cell mill employed in the manufacture of vesicular organelles (Section D.2.3). The total manufacturing requirement for both membraneous organelles is $R_{MembraneousOrgs} = R_{GolgiMill} + R_{ERMill}$ = 0.249 kg/hr to sustain the overall cell production rate of $R_{CellMill}$ ~ 1 kg/hr, which implies that the membraneous organelle manufacturing equipment has a volume of $V_{CellMillMO} = (R_{MembraneousOrgs} / R_{VesicularOrgs})\ V_{CellMillVO}$ ~ **4.4 cm^3**, a mass of $m_{CellMillMO} = (R_{MembraneousOrgs} / R_{VesicularOrgs})\ m_{CellMillVO}$ ~ **10.4 gm**, and a power draw of $P_{CellMillMO} = (R_{MembraneousOrgs} / R_{VesicularOrgs})\ P_{CellMillVO}$ ~ **46 watts** for the manipulator arrays.

D.2.5 Cell Nucleus

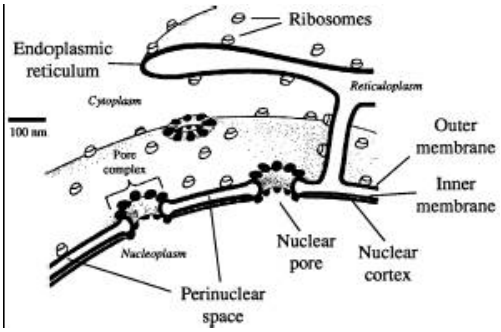

One of the largest organelles in the human cell is the cell nucleus,[3061] a vesicular organelle: "The main structures making up the nucleus are the nuclear envelope,[3062] a double membrane that encloses the entire organelle and isolates its contents from the cellular cytoplasm [image, right]; and the nuclear matrix (which includes the nuclear lamina[3063]), a network within the nucleus that adds mechanical support [image, below], much like the cytoskeleton supports the cell as a whole. The nuclear lamina (composed mostly of lamin proteins)[3064] forms an organized meshwork on the internal face of the envelope, while less organized support is provided on the cytosolic face of the envelope.[3065] Both systems provide structural support for the nuclear envelope and anchoring sites for chromosomes and nuclear pores. The contents of the nucleus are held in the nucleoplasm similar to the cytoplasm in the rest of the cell. The fluid component of this is termed the nucleosol, similar to the cytosol in the cytoplasm. Although the interior of the nucleus does not contain any membrane-bound subcompartments, its contents are not uniform, and a number of nuclear bodies exist, made up of unique proteins, RNA molecules,

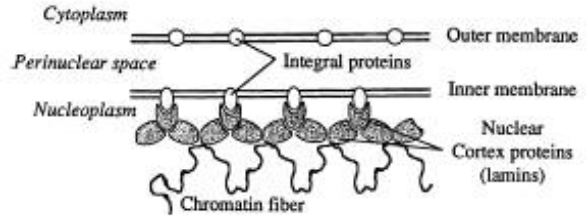

[3060] Freitas RA Jr., Nanomedicine, Volume I: Basic Capabilities, Landes Bioscience, Georgetown, TX, 1999, Table 8.17, "Approximate Quantification of the Components of a Typical 20-μm Human Tissue Cell"; http://www.nanomedicine.com/NMI/Tables/8.17.jpg.

[3061] https://en.wikipedia.org/wiki/Cell_nucleus.
[3062] https://en.wikipedia.org/wiki/Nuclear_envelope.
[3063] https://en.wikipedia.org/wiki/Nuclear_lamina.
[3064] https://en.wikipedia.org/wiki/Lamin.

[3065] Alberts B, Johnson A, Lewis J, Raff M, Roberts K, Walter P, eds. Chapter 4. Molecular Biology of the Cell, 4th edition, Garland Science, 2002, pp. 191-234; https://www.ncbi.nlm.nih.gov/books/NBK26842/.

and particular parts of the chromosomes."

The average nucleus of a V_{cell} ~ 8000 μm^3 tissue cell may be ~8 μm in spherical[3066] diameter with a typical volume of $V_{nucleus}$ ~ 2.68 x 10^{-16} m^3 and mass of $m_{nucleus}$ = 2.9 x 10^{-13} kg.[3067] While a few human cells are multinucleate (e.g., skeletal muscle cells[3068] and osteoclasts[3069]), most cells have just one nucleus representing $f_{nucleus}$ ~ $V_{nucleus}$ / V_{cell} ~ 3.4 % of cell volume, so a cell mill manufacturing $R_{CellMill}$ ~ 1 kg/hr of cells must assemble $R_{NuclMill}$ ~ $f_{nucleus}$ $R_{CellMill}$ ~ 0.034 kg/hr of cell nucleus mass to sustain the overall cell production rate. A 9-step nanorobotically-assisted positional assembly of a cell nucleus might proceed as follows:

(1) **Build outer membrane.** Manufacture a concave hemispherical lipid bilayer and insert the appropriate membrane proteins to create the outer membrane, in the same manner as previously described (Section D.2.3(A)-(B)) using a concave mould.

(2) **Build inner membrane.** Manufacture a convex hemispherical lipid bilayer and insert the appropriate membrane proteins to create the inner membrane, in the same manner as previously described (Section D.2.3(A)-(B)) but using a convex mould, and including all integral proteins that will create the perinuclear space when the two membranes are joined.

(3) **Combine inner and outer membranes.** Press the convex hemispherical membrane onto the concave hemispherical membrane, bonding the two membranes via the integral proteins and forming the perinuclear space.

(4) **Install nuclear pores.** Insert nuclear pore complexes[3070] through both membranes in an appropriate number density, which may range from 3-4 pores/μm^2 in some white cells up to 50 pores/μm^2 in oocytes,[3071] though a typical 20 μm tissue cell may have ~3000 pores in the ~200 μm^2 nuclear surface at a mean density of ~15 pores/μm^2.[3072] The human nuclear pore complex is a 1.84 x 10^{-19} kg (110 MDa) truncated conical structure ~100 nm wide (image, right)[3073] comprised of ~456 individual protein molecules of 34

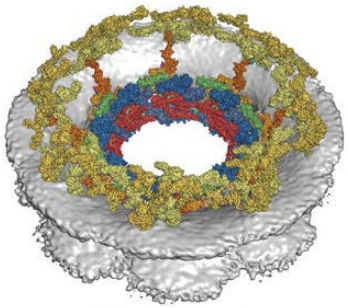

[3066] The nucleus of polymorphonuclear leukocytes is not spherical and normally has three lobes; https://en.wikipedia.org/wiki/Granulocyte.

[3067] Freitas RA Jr., Nanomedicine, Volume I: Basic Capabilities, Landes Bioscience, Georgetown, TX, 1999, Table 8.17, "Approximate Quantification of the Components of a Typical 20-μm Human Tissue Cell"; http://www.nanomedicine.com/NMI/Tables/8.17.jpg.

[3068] https://en.wikipedia.org/wiki/Skeletal_muscle.
[3069] https://en.wikipedia.org/wiki/Osteoclast#Structure.
[3070] https://en.wikipedia.org/wiki/Nuclear_pore.

[3071] Becker WM, Deamer DW. The World of the Cell, Second Edition, Benjamin/Cummings Publishing Company, Redwood City CA, 1991; https://www.amazon.com/dp/0805308709/.

[3072] Pokrywka N, Goldfarb D, Zillmann M, DeSilva A. The Transport of Macromolecules Across the Nuclear Envelope. In: Bittar EE, Bittar N, eds., Cellular Organelles, JAI Press, Greenwich CT, 1995, pp. 19-54; https://www.amazon.com/dp/044454657X/.

[3073] Lin DH, Hoelz A. The Structure of the Nuclear Pore Complex (An Update). Annu Rev Biochem. 2019 Jun 20;88:725-783; https://www.ncbi.nlm.nih.gov/pmc/articles/pmid/30883195/.

different types,[3074] and can be assembled in the same manner as the macromolecular organelles (Section D.2.2), initially omitting the cytoplasmic filaments which may be added later, prior to release of the finished nucleus.

(5) **Install nuclear cortex.** To the integral proteins previously installed in the inner membrane,[3075] attach on the nucleosolic face a 30-100 nm thick fibrillar network composed of lamins and nuclear lamin-associated membrane proteins[3076] that can be manufactured in the same manner as previously described (Section D.1.2.3).

(6) **Install chromosomes.** Attach chromatin molecules (Section D.2.2(6)) to the nuclear cortex. (Chromatin molecules have been directly manipulated inside cells using optical and magnetic tweezers,[3077] long before the advent of nanorobotics.)

(7) **Establish the nucleolus.** ***Future research*** should verify the presumption that when the newly manufactured cell is metabolically activated, the previously-installed chromatin will spontaneously self-arrange to form the nucleolus,[3078] the primary site of ribosome biogenesis[3079] in the cell. The nucleolus is composed of proteins, DNA, and RNA and forms around specific chromosomal regions called nucleolar organizing regions (NOR).[3080] Human NORs are located on the short arms of the acrocentric chromosomes 13, 14, 15, 21 and 22, in the genes RNR1, RNR2, RNR3, RNR4, and RNR5, respectively, that code for ribosomal RNA.[3081] Activating the nucleolus may require the prepositioning of RNA polymerase I,[3082] RNA polymerase III,[3083] and small nucleolar RNAs[3084] in the fibrillar center (FC), the protein fibrillarin[3085] in the dense fibrillar component (DFC), and the protein nucleophosmin[3086] in the granular component (GC) of the nucleolus. The nucleolus additionally enables "nucleolar detention" of a number of post-translational regulatory proteins[3087] which ***future research*** may determine must also be initially provided.

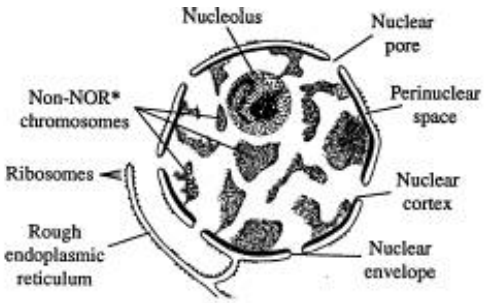

[3074] Lin DH, Stuwe T, Schilbach S, *et al*. Architecture of the symmetric core of the nuclear pore. Science. 2016 Apr 15;352(6283):aaf1015; https://www.ncbi.nlm.nih.gov/pmc/articles/pmid/27081075/.

[3075] https://en.wikipedia.org/wiki/Inner_nuclear_membrane_protein.
[3076] https://en.wikipedia.org/wiki/Nuclear_lamina#Structure_and_composition.

[3077] Kanger JS, Subramaniam V, van Driel R. Intracellular manipulation of chromatin using magnetic nanoparticles. Chromosome Res. 2008;16(3):511-22; https://www.researchgate.net/profile/Vinod_Subramaniam/publication/5392507_Intracellular_manipulation_of_chromatin_using_magnetic_nanoparticles/links/00b7d52e03fa9b3e22000000.pdf. Hong J, Purwar P, Cha M, Lee J. Spatial control of chromosomal location in a live cell with functionalized magnetic particles. Nanoscale. 2015 Dec 7;7(45):19110-7; http://www.ncbi.nlm.nih.gov/pubmed/26524004.

[3078] https://en.wikipedia.org/wiki/Nucleolus.
[3079] https://en.wikipedia.org/wiki/Ribosome_biogenesis#Eukaryotes.
[3080] https://en.wikipedia.org/wiki/Nucleolus_organizer_region.

[3081] McStay B. Nucleolar organizer regions: genomic 'dark matter' requiring illumination. Genes Dev. 2016 Jul 15;30(14):1598-1610; https://www.ncbi.nlm.nih.gov/pmc/articles/pmid/27474438/.

[3082] https://en.wikipedia.org/wiki/RNA_polymerase_I.
[3083] https://en.wikipedia.org/wiki/RNA_polymerase_III.
[3084] https://en.wikipedia.org/wiki/Small_nucleolar_RNA.
[3085] https://en.wikipedia.org/wiki/Fibrillarin.
[3086] https://en.wikipedia.org/wiki/NPM1.

(8) **Emplace nuclear bodies.** Besides the nucleolus, the cell nucleus normally contains a number of small nuclear bodies including 1-5 compact structures 0.1-2 μm in size called Cajal bodies,[3088] ~5 μm polymorphic interphase karyosomal association (PIKA) domains,[3089] PSE-binding transcription factor (PTF) domains,[3090] 25-50 nuclear speckles 20-25 nm in size,[3091] 10-30 paraspeckles 0.2-1 μm in size,[3092] and perichromatin fibrils.[3093] These proteins can be manufactured in the same manner as previously described (Section D.1.2.3) and installed in reasonable locations using a nanorobotic manipulator arm, if ***future research*** confirms that their installation in the nucleus of some or all cell types is essential for full cell viability and functionality.

(9) **Join and Release.** The two equal hemispheres representing opposite halves of the nucleus are pressed together face to face, causing them to seamlessly join because of the inherent miscibility of the lipid bilayers at the equatorial perimeter of each face (Section D.2.3(D)). After any further post-processing is completed,[3094] the finished cell nucleus can be released from the moulds by switching the presentation semaphores embedded in the mould surfaces from hydrophilic to hydrophobic.

The total manufacturing requirement for building a cell nucleus as a vesicular organelle is $R_{NuclMill} \sim 0.034$ kg/hr to sustain the overall cell production rate of $R_{CellMill} \sim 1$ kg/hr. Taking the same productivity metrics of $\psi_1 \sim 7.4 \times 10^{-17}$ kg/array-sec, $\psi_2 \sim 5.3 \times 10^{-15}$ kg/array-sec, and $\psi_3 \sim 3.5 \times 10^{-17}$ kg/array-sec as estimated for the other vesicular organelles (Section D.2.3), we require $N_{arraysCN} = (R_{CellMill} / \psi_1) + (R_{CellMill} / \psi_2) + (R_{CellMill} / \psi_3) \sim 4 \times 10^{11}$ arrays to deliver enough cell nucleus mass to satisfy the required production rate of $R_{CellMill} \sim 1$ kg/hr of cells. These arrays have an estimated total volume of $V_{arraysCN} \sim n_{maniparray} V_{manip} N_{arraysCN} \sim 0.063$ cm^3, taking $n_{maniparray} = 157$ manipulators/array and $V_{manip} = 10^6$ nm^3/manipulator as before.

If the solid volume of the mould structures, including all interior mechanisms, is the same multiple $\alpha_{mouldCN} \sim 3.8$ of the volume of the organelle that is being manufactured as before (Section D.2.3), then a cubical mould enclosing a spherical cell nucleus of diameter $d_{organelleCN} = 8$ μm would have a cubical edge length of $L_{cubeCN} = (\pi \alpha_{mouldCN} / 6)^{1/3} d_{organelleCN} \sim 10$ μm. Since each array services one hemispherical mould having a solid volume of $0.5 L_{cubeCN}^3 \sim 500$ μm^3, and since two separate moulds are required (i.e., one concave and

---

[3087] Audas TE, Jacob MD, Lee S. Immobilization of proteins in the nucleolus by ribosomal intergenic spacer noncoding RNA. Mol Cell. 2012 Jan 27;45(2):147-157; https://www.cell.com/molecular-cell/pdf/S1097-2765(11)00954-3.pdf.

[3088] https://en.wikipedia.org/wiki/Cajal_body.

[3089] Saunders WS, Cooke CA, Earnshaw WC. Compartmentalization within the nucleus: discovery of a novel subnuclear region. J Cell Biol. 1991 Nov;115(4):919-931; https://www.ncbi.nlm.nih.gov/pmc/articles/pmid/1955462/.

[3090] Pombo A, Cuello P, Schul W, Yoon JB, Roeder RG, Cook PR, Murphy S. Regional and temporal specialization in the nucleus: a transcriptionally-active nuclear domain rich in PTF, Oct1 and PIKA antigens associates with specific chromosomes early in the cell cycle. EMBO J. 1998 Mar 16;17(6):1768-78; https://www.ncbi.nlm.nih.gov/pmc/articles/pmid/9501098/.

[3091] Lamond AI, Spector DL. Nuclear speckles: a model for nuclear organelles. Nat Rev Mol Cell Biol. 2003 Aug;4(8):605-612; http://spectorlab.labsites.cshl.edu/wp-content/uploads/sites/14/2014/06/LamondSpector2003.pdf. See also: https://www.uniprot.org/locations/SL-0186.

[3092] https://en.wikipedia.org/wiki/Paraspeckle.

[3093] Matera AG, Terns RM, Terns MP. Non-coding RNAs: lessons from the small nuclear and small nucleolar RNAs. Nat Rev Mol Cell Biol. 2007 Mar;8(3):209-220; https://pubmed.ncbi.nlm.nih.gov/17318225/.

[3094] An example might include the attachment of cytoplasmic filaments on the cytosolic face of the nuclear pore complex. A list of all essential post-processing steps should be compiled, and the nanorobotic means for accomplishing all post-processing steps elucidated, in ***future research***.

one convex), the total solid volume of all moulds is $V_{NuclMoulds} = L_{cubeCN}^3 N_{arraysCN} \sim 400\ cm^3$. Assuming a manipulator density of $\rho_{manip} \sim 100\ kg/m^3$ (i.e., $\sim 10^{-19}\ kg / 10^6\ nm^3$) and a mould density approximating 10% of diamond at $\rho_{mould} \sim 350\ kg/m^3$, then the cell nucleus manufacturing equipment has a volume of $V_{CellMillCN} = V_{arraysCN} + V_{NuclMoulds} \sim$ **400 cm^3**, a mass of $m_{CellMillCN} = \rho_{manip} V_{arraysCN} + \rho_{mould} V_{NuclMoulds} \sim$ **140 gm**, and a power draw of $P_{CellMillCN} = n_{maniparray} N_{arraysCN} P_{manip} \sim$ **6 watts** for the manipulator arrays.

D.3 Cell Assembly Module

The foundational concept of a cell mill is the supposition that the components of a cell are essentially modular, hence can be manufactured separately and later assembled into a complete working biological cell. This "modularity" supposition seems plausible and has received at least some experimental support, but should be tested further in ***future research*** that attempts to reassemble living cells from even larger numbers of component parts than has been achieved to date (see below). Fully bottom-up methods of cell assembly from basic parts *in vitro* have been discussed for more than a decade by practitioners of the emerging field of synthetic biology (though mostly in the context of creating a viable "minimal cell" for research purposes),[3095] but all of these methods seem to rely upon the conventional principles of self-assembly which have inherent limitations that will no longer apply if the principles of positionally-controlled assembly are employed, as described below.

The exemplar cell mill would be a cytomanufacturing system crudely analogous to 3D printing[3096] but with full vertical integration. As long ago as 1970, an *Amoeba proteus* single-cell organism was physically reassembled from its major subcellular components – nucleus, cytoplasm, and cell membrane – taken from three different cells,[3097] demonstrating the physical capability of manually assembling living cells from more primitive parts. A viable 5-component cell reassembly was demonstrated four years later by Morowitz,[3098] who reported that "cell fractions from four different animals can be injected into the eviscerated ghost of a fifth amoeba, and a living functioning organism results." Mammalian cells have also

---

[3095] Forster AC, Church GM: Towards synthesis of a minimal cell. Mol Syst Biol 2006, 2:45; https://www.embopress.org/doi/pdf/10.1038/msb4100090. Liu AP, Fletcher DA. Biology under construction: *in vitro* reconstitution of cellular function. Nat Rev Mol Cell Biol. 2009 Sep;10(9):644-650; https://www.ncbi.nlm.nih.gov/pmc/articles/pmid/19672276/. Jewett MC, Forster AC: Update on designing and building minimal cells. Curr Opin Biotechnol 2010, 21:697-703; https://www.ncbi.nlm.nih.gov/pmc/articles/PMC2952674/. Caschera F, Noireaux V. Integration of biological parts toward the synthesis of a minimal cell. Curr Opin Chem Biol. 2014 Oct;22:85-91; http://www.noireauxlab.org/html%20pages/docs%20website/publications/Caschera%20and%20Noireaux%20-%202014%20COCB.pdf. Göpfrich K, Platzman I, Spatz JP. Mastering Complexity: Towards Bottom-up Construction of Multifunctional Eukaryotic Synthetic Cells. Trends Biotechnol. 2018 Sep;36(9):938-951; https://www.ncbi.nlm.nih.gov/pmc/articles/PMC6100601/. Schwille P, *et al*. MaxSynBio: Avenues Towards Creating Cells from the Bottom Up. Angew Chem Int Ed Engl. 2018;57(41):13382-13392; http://www.mpikg.mpg.de/rl/P/archive/445onl.pdf. Ganzinger KA, Schwille P. More from less - bottom-up reconstitution of cell biology. J Cell Sci. 2019 Feb 4;132(4):jcs227488; https://jcs.biologists.org/content/joces/132/4/jcs227488.full.pdf. Liu AP. The rise of bottom-up synthetic biology and cell-free biology. Phys Biol. 2019 May 7;16(4):040201; https://www.ncbi.nlm.nih.gov/pmc/articles/pmid/31018188/.

[3096] Mandrycky C, Wang Z, Kim K, Kim DH. 3D bioprinting for engineering complex tissues. Biotechnol Adv. 2016 Jul-Aug;34(4):422-434; https://www.ncbi.nlm.nih.gov/pmc/articles/PMC4879088/.

[3097] Jeon KW, Lorch IJ, Danielli JF. Reassembly of living cells from dissociated components. Science. 1970 Mar 20;167(3925):1626-7; http://science.sciencemag.org/content/sci/167/3925/1626.full.pdf.

[3098] Morowitz HJ. Manufacturing a living organism. Hospital Practice 1974 Nov; 9(11):210-215; https://www.tandfonline.com/doi/abs/10.1080/21548331.1974.11706459.

been assembled from separate nuclear and cytoplasmic parts,[3099] and intracellular organelles have been individually manipulated both directly[3100] and nanosurgically,[3101] a key capability that will be needed to assemble whole cells.

Early cell mills might make limited use of more traditional biotechnologies such as cloning, stem cells, tissue engineering, animal cell reactors,[3102] cell-like bioreactors,[3103] transdifferentiation[3104] and nuclear reprogramming.[3105] Lipid vesicles have been prepared containing polymerase enzymes that can synthesize RNA from externally added substrates, and the entire translation apparatus, including ribosomes, has been captured in vesicles.[3106] Relatively primitive methods have been demonstrated for the isolation and manipulation of individual organelles,[3107] and whole cells can be inspected, sorted,[3108] and transported by

---

[3099] Veomett G, Prescott DM, Shay J, Porter KR. Reconstruction of mammalian cells from nuclear and cytoplasmic components separated by treatment with cytochalasin B. Proc Natl Acad Sci U S A. 1974 May;71(5):1999-2002; http://www.ncbi.nlm.nih.gov/pmc/articles/PMC388372/pdf/pnas00058-0421.pdf. Veomett G, Prescott DM. Reconstruction of cultured mammalian cells from nuclear and cytoplasmic parts. Methods Cell Biol 1976;13:7-14; http://www.ncbi.nlm.nih.gov/pubmed/1263853.

[3100] Weber G, Greulich KO. Manipulation of cells, organelles, and genomes by laser microbeam and optical trap. Int Rev Cytol. 1992;133:1-41; http://www.ncbi.nlm.nih.gov/pubmed/1577585. Felgner H, Grolig F, Müller O, Schliwa M. *In vivo* manipulation of internal cell organelles. Methods Cell Biol. 1998;55:195-203; http://www.ncbi.nlm.nih.gov/pubmed/9352518. Bayoudh S, Mehta M, Rubinsztein-Dunlop H, Heckenberg NR, Critchley C. Micromanipulation of chloroplasts using optical tweezers. J Microsc. 2001 Aug;203(Pt 2):214-22; http://onlinelibrary.wiley.com/doi/10.1046/j.1365-2818.2001.00843.x/full. Sacconi L, Tolić-Nørrelykke IM, Stringari C, Antolini R, Pavone FS. Optical micromanipulations inside yeast cells. Appl Opt. 2005 Apr 10;44(11):2001-7; http://www.researchgate.net/profile/Francesco_Pavone/publication/7902546_Optical_micromanipulations_inside_yeast_cells/links/0c960520f4d61165f0000000.pdf. Maghelli N, Tolić-Nørrelykke IM. Optical trapping and laser ablation of microtubules in fission yeast. Methods Cell Biol. 2010;97:173-83; https://publications.mpi-cbg.de/Maghelli_2010_5020.pdf.

[3101] Freitas RA Jr. "Chapter 23. Comprehensive Nanorobotic Control of Human Morbidity and Aging," in Gregory M. Fahy, Michael D. West, L. Stephen Coles, and Steven B. Harris, eds, The Future of Aging: Pathways to Human Life Extension, Springer, New York, 2010, pp. 685-805; Section 6.4.2 "Cell nanosurgery"; http://www.nanomedicine.com/Papers/Aging.pdf.

[3102] Bliem R, Konopitzky K, Katinger H. Industrial animal cell reactor systems: aspects of selection and evaluation. Adv Biochem Eng Biotechnol 1991; 44:1-26; http://www.ncbi.nlm.nih.gov/pubmed/1781316. Nelson KL, Geyer S. Bioreactor and process design for large-scale mammalian cell culture manufacturing. Bioprocess Technol 1991; 13:112-143; http://www.ncbi.nlm.nih.gov/pubmed/1367130.

[3103] Noireaux V, Libchaber A. A vesicle bioreactor as a step toward an artificial cell assembly. Proc Natl Acad Sci U S A. 2004 Dec 21;101(51):17669-74; http://www.ncbi.nlm.nih.gov/pmc/articles/PMC539773/.

[3104] Collas P, Håkelien AM. Teaching cells new tricks. Trends Biotechnol 2003 Aug; 21:354-361; http://www.ncbi.nlm.nih.gov/pubmed/12902172.

[3105] Tada T. Nuclear reprogramming: an overview. Methods Mol Biol 2006; 348:227-236; http://www.ncbi.nlm.nih.gov/pubmed/16988383.

[3106] Deamer D. A giant step towards artificial life? Trends Biotechnol. 2005 Jul;23(7):336-8; http://www.pai.utexas.edu/faculty/isaxena/BIO320/A%20giant%20step%20towards%20artificial%20life%20-%202005.pdf.

[3107] Olson KJ, Ahmadzadeh H, Arriaga EA. Within the cell: analytical techniques for subcellular analysis. Anal Bioanal Chem. 2005 Jun;382(4):906-17; http://www.ncbi.nlm.nih.gov/pubmed/15928950. Satori CP, Kostal V, Arriaga EA. Review on recent advances in the analysis of isolated organelles. Anal Chim Acta. 2012 Nov 13;753:8-18; http://www.ncbi.nlm.nih.gov/pmc/articles/PMC3484375/.

[3108] Grover SC, Skirtach AG, Gauthier RC, Grover CP. Automated single-cell sorting system based on optical trapping. J Biomed Opt. 2001 Jan;6(1):14-22; http://www.ncbi.nlm.nih.gov/pubmed/11178576.

optical tweezers,[3109] microgrippers,[3110] or other conventional means[3111] to a collection area for export and further use.

But nanorobotic assembly of biological cells will require one or more micromanipulators that can reach across at least ~20 μm distances spanning the width of the typical tissue cell under construction, performing molecular and organelle pick-and-place operations while physically accessing the supply of premanufactured organelles and other needed cell building materials. For scaling purposes, if the size of the previously-described nanomanipulator (Section 5.2.1.1) was increased 100-fold in all three dimensions from 100 nm to x_{micro} = 10 μm in length and from 30 nm to 3 μm in cylindrical diameter, the resulting micromanipulator would have a 10^6-fold larger work volume of $V_{micromanip}$ = 1000 μm^3, along with a central transport channel ~1 μm in diameter which is wide enough to accommodate most but not all organelles. Maximum tip velocity would remain the same at v_{manip} ~ 1 cm/sec (Section 5.2.1.1). An arrangement of n_{micro} = 8 such manipulators arranged as two opposed sets of 2 x 2 manipulators would provide access to a 20 μm x 20 μm area from each side, roughly fulfilling the requirement of full access to a 20 μm x 20 μm x 20 μm tissue cell space. Power density scales inversely linearly with size,[3112] so the ~10^8 W/m^3 power density of the nanomanipulator (Section 5.2.1.1) reduces to ~10^6 W/m^3 for the micromanipulator, giving a power dissipation estimate of $P_{micromanip}$ ~ 1000 pW. (Note that since strength scales as the square of the linear dimension,[3113] the posited micromanipulator should be able to apply 10^6 times more force than the original nanomanipulator device if necessary.)

A description of one possible cell assembly process in Section D.3.1 is followed by a discussion of cell mill system scaling in Section D.3.2.

D.3.1 Cell Assembly Process

Presuming access to a sufficient inventory of premanufactured generic and personalized biomolecules (Section D.1), macromolecular organelles (Section D.2.2), vesicular organelles (Section D.2.3) including the nucleus (Section D.2.5), and membraneous organelles (Section D.2.4), the following is a general description of how the final assembly of a tissue cell might proceed:

(1) **Build plasma membrane.** Build a lipid bilayer plasma membrane on the inside surfaces of two 20 μm hemispheric moulds in the manner previously described (Section D.2.3(A)).

[3109] Zhang H, Liu KK. Optical tweezers for single cells. J R Soc Interface. 2008 Jul 6;5(24):671-90; http://www.ncbi.nlm.nih.gov/pmc/articles/PMC2408388/.

[3110] Kim K, Liu X, Zhang Y, Sun Y. Nanonewton force-controlled manipulation of biological cells using a monolithic MEMS microgripper with two-axis force feedback. J Micromech Microeng 2008 Apr 1;18(5):055013; http://amnl.mie.utoronto.ca/data/J35.pdf. Leong TG, Randall CL, Benson BR, Bassik N, Stern GM, Gracias DH. Tetherless thermobiochemically actuated microgrippers. Proc Natl Acad Sci U S A. 2009 Jan 20;106(3):703-8; http://www.ncbi.nlm.nih.gov/pmc/articles/PMC2630075/.

[3111] Gach PC, Wang Y, Phillips C, Sims CE, Allbritton NL. Isolation and manipulation of living adherent cells by micromolded magnetic rafts. Biomicrofluidics. 2011 Sep;5(3):32002-3200212; http://www.ncbi.nlm.nih.gov/pmc/articles/PMC3194786/.

[3112] Drexler KE. Nanosystems: Molecular Machinery, Manufacturing, and Computation, John Wiley & Sons, New York, 1992, Table 2.1; https://www.amazon.com/dp/0471575186/.

[3113] Drexler KE. Nanosystems: Molecular Machinery, Manufacturing, and Computation, John Wiley & Sons, New York, 1992, Section 2.3.2 and Table 2.1; https://www.amazon.com/dp/0471575186/.

(2) **Insert membrane proteins.** Insert integral proteins into the plasma membrane, including cytoskeletal components on the cytosolic wall, in an appropriate surface number density in the manner previously described (Section D.2.3(B)).

(3) **Assemble cell corpus.** Micromanipulators are employed to emplace organelles in appropriate locations and numbers (**Table 22**) in the growing corpus of the cell, in each of the two hemispheres. Placement of the manufactured nucleus (Section D.2.5) will be assigned to one of the two hemispheres, which will also determine the location of the attached membraneous endoplasmic reticulum (Section D.2.4(2)). Supportive cytoskeletal elements may be employed during assembly to provide positional and structural fixity of the organelles, and organelle installation should be closely coordinated with cytoskeletal emplacement (see Section D.3.1(4)). Determination of the optimum assembly sequence for all components in each hemisphere is a suitable topic for ***future research***.

Table 22. Number of organelles to be installed in a typical 8000 µm^3 tissue cell

Organelle	Approx. # per Cell	Section Reference	Organelle	Approx. # per Cell	Section Reference
Proteasomes	10^7	D.2.2(1)	Lysosomes	300	D.2.3(3)
Ribosomes	10^7	D.2.2(2)	Peroxisomes	300	D.2.3(4)
Glycosomes	10^5	D.2.2(3)	Mitochondria	1000	D.2.3(5)
Vaults	3000	D.2.2(4)	Golgi apparatus	1	D.2.4(1)
Centrioles	2	D.2.2(5)	Endo. reticulum	1	D.2.4(2)
Golgi vesicles	200,000	D.2.3(1)	Nucleus	1	D.2.5
Secretory vesicles	50,000	D.2.3(2)			
Lipid droplets	100	D.2.3(2)	***Total***	***20,354,705***	

(4) **Build out cytoskeleton.** Complete the installation of all remaining essential cytoskeletal features, which may include ~17 meters of cytoskeletal fibers and filaments inside each "typical" tissue cell representing ~11% of total cell volume (Section 4.12.2.4). Cytoskeleton elements have been directly manipulated inside cells using primitive optical and magnetic tweezers,[3114] but the availability of much stronger micromanipulators within the Cell Assembly Module that can reach into the growing cytoplasm and precisely position cytoskeletal components will provide much faster and more efficient assembly operations. The dynamic nature of some cytoskeletal components[3115] under physiological conditions may necessitate special procedures for cytoskeleton build-out that should be investigated in ***future research***.

Cytoskeletal emplacement should be closely coordinated with organelle installation (see Section D.3.1(3)). For example, α- and β-spectrin[3116] filaments joined to actin[3117] polymer microfilaments[3118] should first be installed on the cytosolic surface of the cell plasma membrane before the rest of the cytoplasm is laid down

---

[3114] Felgner H, Frank R, Schliwa M. Flexural rigidity of microtubules measured with the use of optical tweezers. J Cell Sci. 1996 Feb;109 (Pt 2):509-16; http://jcs.biologists.org/content/joces/109/2/509.full.pdf. de Vries AH, Krenn BE, van Driel R, Kanger JS. Micro magnetic tweezers for nanomanipulation inside live cells. Biophys J. 2005 Mar;88(3):2137-44; http://www.ncbi.nlm.nih.gov/pmc/articles/PMC1305265/.

[3115] e.g., https://en.wikipedia.org/wiki/Microtubule#Microtubule_dynamics.
[3116] https://en.wikipedia.org/wiki/Spectrin.
[3117] https://en.wikipedia.org/wiki/Actin.
[3118] https://en.wikipedia.org/wiki/Microfilament.

(Section D.3.1(2)), possibly with some assistance from self-assembly.[3119] Actin microfilaments are 5-7 nm in diameter and may run out to several microns in length. They represent ~59% of the total cytoskeletal length and 43% of total cytoskeletal volume (**Table 11** in Section 4.12.2.4) and are capable of self-assembly and disassembly in response to molecular cues via polymerization and depolymerization at a speed of 0.1-1 μm/sec.[3120]

Microfilaments should be initially be installed sparingly, serving as large-scale tensile elements to maintain overall cellular structural integrity and creating a 3D tensegrity[3121] structure in concert with much larger and more rigid microtubules[3122] which should be laid down in a sparse framework at the same time to serve as compressive elements. Microtubules are 25 nm diameter cylinders up to 25 μm in length, representing 42% of total cytoskeleton volume but only ~4% of total cytoskeletal fiber length (**Table 11** in Section 4.12.2.4). They can also self-assemble with a typical polymerization speed of ~0.06 μm/sec,[3123] with the speed of polymerization strongly force-dependent[3124] and biochemically controlled.[3125] Most microtubules in living cells have a half-life of 5-10 minutes with a few lasting for hours,[3126] but uncontrolled re- or de-polymerization will not be permitted within the Cell Assembly Module during cell construction where no GTP or ATP is available to energize polymerization activity.

After a coarse 3D fiber network is in place (with very large gaps), organelles can be attached to the skeletal framework via intermediate filaments,[3127] the most stable of the cytoskeletal elements as they are not subject to constant de-/re-polymerization. Intermediate fibers represent ~11% of skeletal volume and ~6% of total skeletal fiber length (**Table 11** in Section 4.12.2.4).

Once bound organelles are secured in their proper places, microfilaments and microtubules can be caused to self-assemble into the gaps via induced polymerization, filling out the bulk of the cytoskeleton network. For example, it has been demonstrated that a minimal system consisting of giant unilamellar vesicles and externally supplied microtubules and kinesin can produce membrane networks in the presence of ATP[3128]

[3119] Liu AP, Richmond DL, Maibaum L, Pronk S, Geissler PL, Fletcher DA. Membrane-induced bundling of actin filaments. Nat Phys. 2008 Aug 31;4:789-793; https://www.ncbi.nlm.nih.gov/pmc/articles/PMC2739388/. Carvalho K, Tsai FC, Lees E, Voituriez R, Koenderink GH, Sykes C. Cell-sized liposomes reveal how actomyosin cortical tension drives shape change. Proc Natl Acad Sci U S A. 2013 Oct 8;110(41):16456-61; https://www.ncbi.nlm.nih.gov/pmc/articles/PMC3799374/. Miyazaki M, Chiba M, Eguchi H, Ohki T, Ishiwata S. Cell-sized spherical confinement induces the spontaneous formation of contractile actomyosin rings *in vitro*. Nat Cell Biol. 2015 Apr;17(4):480-489; https://pubmed.ncbi.nlm.nih.gov/25799060/.

[3120] Maniotis AJ, Chen CS, Ingber DE. Demonstration of mechanical connections between integrins, cytoskeletal filaments, and nucleoplasm that stabilize nuclear structure. Proc Natl Acad Sci U S A. 1997 Feb 4;94(3):849-54; https://www.ncbi.nlm.nih.gov/pmc/articles/PMC19602/.

[3121] https://en.wikipedia.org/wiki/Tensegrity.
[3122] https://en.wikipedia.org/wiki/Microtubule.

[3123] Schulze E, Kirschner M. Microtubule dynamics in interphase cells. J Cell Biol. 1986 Mar;102(3):1020-31; https://core.ac.uk/download/pdf/186861731.pdf.

[3124] Janson ME, de Dood ME, Dogterom M. Dynamic instability of microtubules is regulated by force. J Cell Biol. 2003 Jun 23;161(6):1029-1034; https://www.ncbi.nlm.nih.gov/pmc/articles/pmid/12821641/.

[3125] Zwetsloot AJ, Tut G, Straube A. Measuring microtubule dynamics. Essays Biochem. 2018 Dec 7;62(6):725-735; https://www.ncbi.nlm.nih.gov/pmc/articles/PMC6281472/.

[3126] Infante AS, Stein MS, Zhai Y, Borisy GG, Gundersen GG. Detyrosinated (Glu) microtubules are stabilized by an ATP-sensitive plus-end cap. J Cell Sci. 2000 Nov;113 (Pt 22):3907-3919; https://jcs.biologists.org/content/joces/113/22/3907.full.pdf.

[3127] https://en.wikipedia.org/wiki/Intermediate_filament.
[3128] https://en.wikipedia.org/wiki/Adenosine_triphosphate.

and GTP[3129] without the aid of other proteins.[3130] Another example is the analogous GTPase enzyme dynamin,[3131] which self-assembles into spiral tubules in the absence of GTP and disassembles with the addition of GTP.[3132]

(5) **Join hemispheres.** After the cell corpus and cytoskeleton are fully assembled, the two equal hemispheres representing opposite halves of the manufactured cell are pressed together face to face, causing them to seamlessly join because of the inherent miscibility of the lipid bilayers at the equatorial perimeter of each face (Section D.2.3(D)). Any necessary post-processing work[3133] should also be completed during this stage.

(6) **Decorate and release.** Detach one external hemispheric mould by switching the presentation semaphores embedded in the mould surface from hydrophilic to hydrophobic, then decorate the exposed external face of the plasma membrane with glycocalyx[3134] and any other required external structures. The hemispheric mould is then reattached and the same process is repeated with the other external hemispheric mould. Once both hemispheres are completed, any final biochemical modifications to the cell may be made (e.g., extracting or injecting biomolecules to bring the cell to any state of activation or metabolic activity desired) after which the finished cell is released from the moulds and transported to inventory.

D.3.2 Cell Mill System Scaling

The required cell mass production rate of $R_{CellMill} \sim 1$ kg/hr of cells equates to a manufacturing rate of $N_{CellMill} = R_{CellMill} / m_{cell} = 1.17 \times 10^{11}$ cells/hr = 3.26×10^{7} cells/sec for the Cell Assembly Module, taking cell mass $m_{cell} = \rho_{cell} V_{cell} = 8.51 \times 10^{-12}$ kg/cell, cell density $\rho_{cell} = 1064$ kg/m^3, and cell volume $V_{cell} = 8000$ μm^3.

How many micromanipulators are needed in the Cell Assembly Module? If one micromanipulator can install one organelle by traversing a single round-trip armswing of maximum length $x_{RTarmswing} = 20$ μm, taking $n_{armorgs} = 1$ round-trip armswing per organelle, and if there are $n_{organelles} = 20{,}354{,}705$ organelles to be emplaced in each cell (**Table 22** in Section D.3.1), then the total armswing travel distance to place all organelles in one cell is $x_{organelles} = n_{organelles}\ n_{armorgs}\ x_{RTarmswing} = 407$ meters. The placement time for all organelles in one 8000 μm^3 cell using one micromanipulator is therefore $t_{organelles} = x_{organelles} / v_{manip} = 40{,}700$ sec, given the maximum micromanipulator arm velocity of $v_{manip} \sim 1$ cm/sec. This establishes a

---

[3129] https://en.wikipedia.org/wiki/Guanosine_triphosphate.

[3130] Leduc C, Campàs O, Zeldovich KB, Roux A, Jolimaitre P, Bourel-Bonnet L, Goud B, Joanny JF, Bassereau P, Prost J. Cooperative extraction of membrane nanotubes by molecular motors. Proc Natl Acad Sci U S A. 2004 Dec 7;101(49):17096-101; https://www.ncbi.nlm.nih.gov/pmc/articles/PMC535380/.

[3131] https://en.wikipedia.org/wiki/Dynamin.

[3132] Pucadyil TJ, Schmid SL. Real-time visualization of dynamin-catalyzed membrane fission and vesicle release. Cell. 2008 Dec 26;135(7):1263-75; https://www.ncbi.nlm.nih.gov/pmc/articles/PMC2673235/.

[3133] One example of such work is bonding cytoskeletal elements across the join plane between the two hemispheres, in whatever manner may be required, using membrane-inserted manipulators or nanorobots. It may also be desirable to insert sorting rotor probes through the plasma membrane into the cytosol to extract or insert particular molecules of interest (Section 4.10.1.9). All such essential post-processing steps should be enumerated, and the nanorobotic means elucidated, in ***future research***.

[3134] https://en.wikipedia.org/wiki/Glycocalyx.

per-cell micromanipulator work requirement of $r_{placement}$ = 40,700 micromanipulator-sec/cell, which implies that achieving the cell mass production rate of $R_{CellMill}$ ~ 1 kg/hr of cells will require the Cell Mill to operate, in parallel, $N_{micromanip} = r_{placement}\ N_{CellMill}$ = 1.33 x 10^{12} micromanipulators having a total mechanical volume of $V_{CellMillMM} = N_{micromanip}\ V_{micromanip}$ = 1330 cm^3, taking individual micromanipulator volume as $V_{micromanip}$ = 1000 μm^3. Assuming n_{micro} = 8 micromanipulators at each cell manufacturing site (Section D.3), the start-to-finish manufacturing time for a cell is $\tau_{cellthroughput} \sim t_{organelles} / n_{micro}$ ~ 1.41 hours.

There are two moulds for each cell manufacturing site, so the Cell Assembly Module requires $N_{CAMmoulds} = N_{micromanip} / (n_{micro} / 2)$ = 3.33 x 10^{11} moulds. If each mould is α_{mould} = 3.8 times the volume of the cell being manufactured, then each such mould is $V_{CAMM} = \alpha_{mould}\ V_{cell}$ = 30,400 μm^3 in volume, taking V_{cell} = 8000 μm^3, and the total volume of all cell moulds is $V_{CAMmoulds} = V_{CAMM}\ N_{CAMmoulds}$ = 10,100 cm^3.

The total volume of all micromanipulators and moulds in the Cell Assembly Module is $V_{MM} = V_{CellMillMM} + V_{CAMmoulds}$ = **11,430 cm^3**. Taking micromanipulator density as ρ_{manip} ~ 0.1 gm/cm^3 and mould density as ρ_{mould} ~ 0.35 gm/cm^3, the total mass of all micromanipulators and moulds in the Cell Assembly Module is $M_{MM} = \rho_{manip}\ V_{CellMillMM} + \rho_{mould}\ V_{CAMmoulds}$ = **3668 gm**. Power consumption for all Cell Assembly Module micromanipulators is $P_{MM} \sim N_{micromanip}\ P_{micromanip}$ ~ 1330 watts, taking $P_{micromanip}$ ~ 1000 pW for each micromanipulator.

If we add the volume, mass and power requirements for the preceding Biomolecule Synthesis Module (Section D.1) and the Cytocomponent Assembly Module (Section D.2), and if we add another ~85,000 cm^3 for support structures having a similar density as the micromanipulators, then the total volume of the Cell Mill is ~0.1 m^3 – a cubical box ~46 cm (~18 inches) on a side – with a total mass of ~12.5 kg and a total power draw of ~5 KW, as summarized in **Table 23** below.

Table 23. Summary of exemplar cell mill volume, mass, and power requirements

Nanorobotic Unit	Section Reference	Volume (cm^3)	Mass (gm)	Power (W)
Generic Organic Synthesis Unit	D.1.1.2	36.5	73	3400
Nano Sequencer	D.1.2.1.2	0.0001	0.0002	0.92 x 10^{-6}
DNA Mill	D.1.2.2	50	1	1.3
Protein Mill	D.1.2.3	3000	60	78
Macromolec. Organelle Protein Mill	D.2.2	170	3	4
Vesicular Organelle Mill	D.2.3	2.4	0.768	33
Membraneous Organelle Mill	D.2.4	4.4	10.4	46
Cell Nucleus Mill	D.2.5	400	140	6
Subtotals		*3663*	*288*	*3468*
Cell Assembly Unit	D.3	11,430	3668	1330
Active system subtotal		*15,093*	*3956*	*4798*
Unspecified support structures	D.3.2	~84,907	~8544	~202
Totals for Cell Mill		***100,000***	***12,500***	***5000***

Some biological cells, most notably muscle and neuron-related cells,[3135] will not be neatly spherical or cubical in shape as assumed throughout the present analysis but will possess long processes that extend well beyond the central cell body (images, right).

Procedures for assembling these and other nonstandard cell shapes are readily conceived but lie beyond the scope of this book and therefore must be left for ***future research***.

Specified blocks of extracellular matrix or ECM (Section 4.12.3.3) can be assembled by similar means, using methods that should also be detailed in ***future research***.

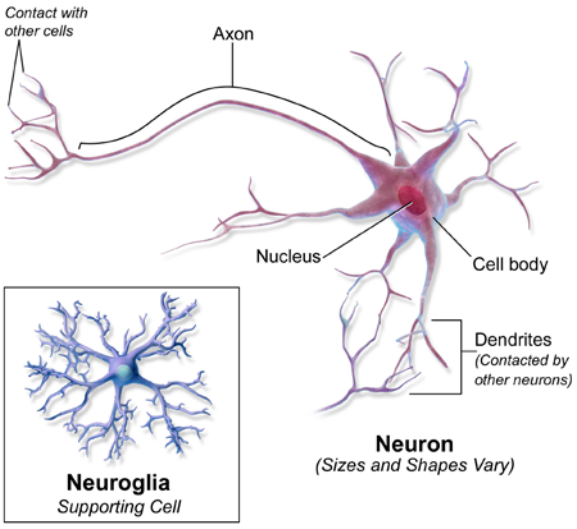

[3135] There are several hundred neuron types and subtypes in the entire human nervous system, as described at the NeuroMorpho database (http://neuromorpho.org/) and the "Neuroscience Lexicon" at http://neurolex.org/wiki/Category:Neuron.

Appendix E. Additional Plateable Tissue Surfaces

Appendix E. Additional surfaces that might be coated with vasculoid applications plates		
Tissue or Organ Surface	**Exterior Surface Area**	**Subtotals** (m^2)
Lung, interior[3136]		
Trachea	6786 mm^2	
Main bronchi	3649 mm^2	
Lobar bronchi	3051 mm^2	
Segmental bronchi	6638 mm^2	
Cartilaginous bronchi	54,208 mm^2	
Terminal bronchi	67,758 mm^2	
Muscled bronchioles	280,674 mm^2	
Terminal bronchiole	203,717 mm^2	
Respiratory bronchioles	1,560,839 mm^2	
Alveolar ducts	6,402,051 mm^2	
Alveolar sacs	5,403,382 mm^2	
Alveoli	60,695,570 mm^2	
Pleural membranes (exterior)	~1700 cm^2	
Subtotal		74.858
Alimentary system[3137]		
Salivary glands[3138]	~20 cm^2	
Oral and nasal cavities[3139]	~160 cm^2	
Esophagus	200 cm^2	
Stomach, int wall	~600 cm^2 (assumed spherical)	
Stomach, ext wall	~600 cm^2 (assumed spherical)	
Small intestine, int wall	3500 cm^2	
Small intestine, ext wall	3500 cm^2	
Small intestine villi[3140]	100,000 cm^2	

[3136] Surface area estimated as π x branch diameter x branch length x number of branches, using data from Table 8.7 in: Freitas RA Jr. Nanomedicine, Volume I: Basic Capabilities, Landes Bioscience, Georgetown TX, 1999, Table 8.7, "Approximate Quantification of the Human Bronchial System"; http://www.nanomedicine.com/NMI/Tables/8.7.jpg.

[3137] Freitas RA Jr. Nanomedicine, Volume I: Basic Capabilities, Landes Bioscience, Georgetown TX, 1999, Table 8.8, "Approximate Quantification of the Human Alimentary System"; http://www.nanomedicine.com/NMI/Tables/8.8.jpg.

[3138] Freitas RA Jr. Nanomedicine, Volume I: Basic Capabilities, Landes Bioscience, Georgetown, TX, 1999; Section 8.2.3, "Navigational Alimentography"; http://www.nanomedicine.com/NMI/8.2.3.htm.

[3139] Guyton AC. Anatomy and Physiology, Saunders College Publishing, New York, 1985. Freitas RA Jr. Nanomedicine, Volume I: Basic Capabilities, Landes Bioscience, Georgetown, TX, 1999; Section 8.2.2, "Navigational Bronchography"; http://www.nanomedicine.com/NMI/8.2.2.htm.

Large intestine, int wall	2000 cm^2	
Large intestine, ext wall	2000 cm^2	
Rectum, int wall	100 cm^2	
Rectum, ext wall	100 cm^2	
Subtotal		11.278
Epidermis (skin)		2.0
Kidney and Bladder		
Renal glomeruli[3141]	1.4 m^2	
Bladder, interior	305 cm^2	
Bladder, exterior	305 cm^2	
Subtotal		1.461
Abdominal peritoneum[3142]	~6000 cm^2	0.60
Ventricular system of the brain		
Subarachnoid space	~600 cm^2	
Brain ventricles	~200 cm^2	
Spinal subarachnoid space	~300 cm^2	
Subtotal		0.11
Heart (approx. as spherical)		
Interior surface	280 cm^2	
Exterior surface	280 cm^2	
Pericardium membrane[3143]	~300 cm^2	
Subtotal		0.086
Gall bladder		
Interior wall	227 cm^2	
Exterior wall	227 cm^2	
Subtotal		0.045
Lymphatic organs (external surfaces)		
Lymph nodes, ext surface	22,619 mm^2 (assumed spherical)	
Spleen, ext surface	13,685 mm^2 (assumed spherical)	
Thymus, ext surface	1521 mm^2 (assumed spherical)	
Subtotal		0.038
Synovial fluid capsules in joints[3144]	260 cm^2	0.026

[3140] Freitas RA Jr. Nanomedicine, Volume I: Basic Capabilities, Landes Bioscience, Georgetown, TX, 1999; Section 8.2.3, "Navigational Alimentography"; http://www.nanomedicine.com/NMI/8.2.3.htm.

[3141] Freitas RA Jr., Phoenix CJ. Vasculoid: A personal nanomedical appliance to replace human blood. J Evol Technol. 2002 Apr;11:1-139; Section 2.4.4.1 "Water Absorption and Elimination"; http://www.jetpress.org/volume11/vasculoid.pdf.

[3142] peritoneum surrounding the viscera in the abdomen; https://en.wikipedia.org/wiki/Peritoneum.

[3143] https://en.wikipedia.org/wiki/Pericardium.

[3144] assumed spherical, x 4: Freitas RA Jr. Nanomedicine, Volume I: Basic Capabilities, Landes Bioscience, Georgetown TX, 1999, Table 8.9, "Mass, Volume, and Scale Size of the Organs of the Human Body"; http://www.nanomedicine.com/NMI/Tables/8.9.jpg.

Aqueous humor of the eye (x2)		0.008
Other discrete organs (external surface)[3145]		
Liver	625 cm^2	
Cranium	590 cm^2	
Lungs x 2	1600 cm^2	
Kidneys x 2	200 cm^2	
Pancreas	50 cm^2	
Teeth x 32	150 cm^2	
Testes x 2	44 cm^2	
Uterus	50 cm^2	
Subtotal		0.331
TOTAL		**90.841**

[3145] assumed spherical: Freitas RA Jr. Nanomedicine, Volume I: Basic Capabilities, Landes Bioscience, Georgetown TX, 1999, Table 8.9, "Mass, Volume, and Scale Size of the Organs of the Human Body"; http://www.nanomedicine.com/NMI/Tables/8.9.jpg.

Appendix F. Chemohaptic Atomic Scanning and Identification

As slightly modified from a previously published discussion,[3146] this Appendix outlines one possible architecture for a Molecular Assay System that employs scanning probe-based **chemohaptic analysis** (Section F.1) to determine the positions and probable composition of all accessible atoms in molecules on a solid surface at cryogenic temperatures. This involves the use of Scanning Probe Microscopy (Section F.1.1), and Atomic Force Microscopy (AFM) in particular, to determine the structure (Section F.1.2) and element types (Section F.1.3) of the atoms and functional groups (Section F.1.4) of individual sample molecules, with a difficult cases requiring special procedures (Section F.1.5).

We describe an exemplar Molecular Assay System (Section F.2). The Molecular Assay System would be composed of a large number of individual microscale laboratory modules that are the minimum size necessary to perform the required single-molecule examinations (Section F.2.1). We then estimate the size and performance characteristics of a complete Molecular Assay System comprised of many such microscale laboratory modules (Section F.2.2).

Future research is required to add more detail to this architecture, to examine additional possible architectures, to extend the range of molecules that can be measured and typed using chemohaptic analysis, and to conduct technical trade studies among competing architectures to help choose the ideal final design for the Molecular Assay System.

F.1 Chemohaptic Analysis

Haptic perception[3147] is a generic process of recognizing objects through touch. The phrase is usually applied to a macroscale human sensory activity involving a combination of somatosensory perception of patterns on the skin surface (e.g., edges, curvature, and texture) and proprioception of hand position and conformation, but in the present context we are referring to an activity that takes place at the nanoscale. In particular, chemohaptic analysis is the process of inferring the chemical composition of a molecule by "touching" that molecule, after it is placed on some suitable surface, with the sharp tip of a scanning probe microscope such as the atomic force microscope (AFM) in its purest form. Chemohaptic analysis is the application of chemohaptics to the systematic identification of an unknown molecular structure. Today this field exists in only nascent form, though after the advent of nanofactories it will likely come into more common use for the rapid characterization of unknown organic molecules.

F.1.1 Scanning Probe Microscopy

It is useful first to review a bit of background on scanning probe microscopy (SPM) which is the key to understanding the basic process of chemohaptic analysis. In the following discussion, keep in mind that the diameters of individual atoms in covalently bonded molecules are approximately 76 pm for hydrogen, 146

[3146] Freitas RA Jr. The Whiskey Machine: Nanofactory-Based Replication of Fine Spirits and Other Alcohol-Based Beverages. IMM Report No. 47, May 2016; http://www.imm.org/Reports/rep047.pdf.

[3147] http://en.wikipedia.org/wiki/Haptic_perception.

pm for oxygen, 150 pm for nitrogen, and 154 pm for carbon,[3148] where 1 picometer (pm) = 0.01 Angstroms (Å) = 0.001 nanometers = 10^{-12} meter.

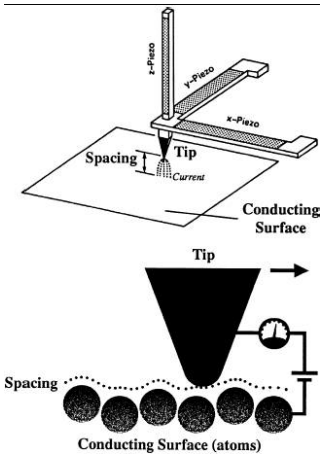

The first of the SPMs was the Scanning Tunneling Microscope (STM) developed in the late 1970s and early 1980s by Gerd Karl Binnig and Heinrich Rohrer at an IBM research lab in Zurich, Switzerland,[3149] earning these scientists the 1986 Nobel Prize in Physics. The STM was initially used as an imaging device, capable of resolving individual atoms by recording the quantum tunneling current that occurs when an extremely sharp conductive probe tip (usually tungsten, nickel, gold, or platinum-iridium) is brought to within about one atomic diameter of an atom, and then adjusting the position of the tip to maintain a constant current as the tip is scanned over a bumpy atomic surface (image, right). A height change as small as 100 pm can cause tunneling current to double. The tip is connected to an arm that is moved in three dimensions by stiff ceramic piezoelectric transducers that provide sub-nanometer positional control. If the tip is atomically sharp, then the tunneling current is effectively confined to a region within ~100 pm of the point on the surface directly beneath the tip, thus the record of tip adjustments generates an atomic-scale topographic map of the surface. STM tips can scan samples at ~KHz frequencies, although slower scans are used for very rough surfaces and in some modern STMs the sample is moved while the tip is held stationary. Perhaps most iconic is the classic 1989 picture of the IBM logo spelled out with 35 xenon atoms arranged on a nickel surface (image, right).[3150]

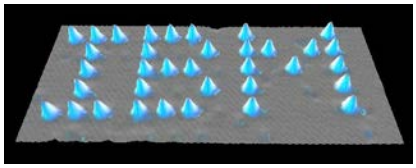

These atoms were imaged by an STM tip after lateral positioning of the individual atoms using the same tip.

A major limitation of the STM was that it only worked with conducting materials such as metals or semiconductors, but not with insulators or biological structures such as DNA.[3151] To remedy this situation, in 1986 Binnig, Quate and Gerber developed the Atomic Force Microscope (AFM),[3152] which is sensitive directly to the forces between the tip and the sample, rather than a tunneling current. An AFM (image, left) can operate in at least three modes. In "attractive" or non-

[3148] http://en.wikipedia.org/wiki/Atomic_radii_of_the_elements_(data_page).

[3149] Binnig G, Rohrer H. Scanning tunneling microscopy. Helv Phys Acta 1982;55:726-735. Binnig G, Rohrer H, Gerber C, Weibel E. Surface studies by scanning tunneling microscopy. Phys Rev Lett. 1982 Jul 5;49(1):57-61; https://www.sp.phy.cam.ac.uk/drp2/PhysRevLett.49.572Dscanning.pdf. Binnig G, Rohrer H. The Scanning Tunneling Microscope. Sci Am. 1985 Aug;253(2):50-56; http://www.grids.ac.uk/NWGrid/Seminar.20.3.07/WernerHofer_STM.pdf. Binnig G, Rohrer H. Scanning tunneling microscopy. IBM J Res Develop. 1986;30:355-369. Binnig G, Rohrer H. Scanning tunneling microscopy from birth to adolescence. Rev Modern Phys. 1987 Jul;59:615-625; https://link.aps.org/pdf/10.1103/RevModPhys.59.615.

[3150] Eigler DM, Schweizer EK. Positioning Single Atoms with a Scanning Tunnelling Microscope. Nature 1990 Apr 5;344:524-526; http://earl.wylie.solano.edu/nanotech/Eigler1990Paper.pdf.

[3151] Lee GU, Chrisey LA, Colton RJ. Direct Measurement of the Forces Between Complementary Strands of DNA. Science 1994 Nov 4;266:771-773; https://pubmed.ncbi.nlm.nih.gov/7973628/. Boland T, Ratner BD. Direct measurement of hydrogen bonding in DNA nucleotide bases by atomic force microscopy. Proc Natl Acad Sci USA 1995 Jun 6;92(12):5297-5301; https://www.pnas.org/content/pnas/92/12/5297.full.pdf.

[3152] Binnig G, Quate CF, Gerber C. Atomic Force Microscopy. Phys Rev Lett. 1986 Mar 3;56:930-933; http://www.geocities.ws/misnimisran/AFM07lec.pdf.

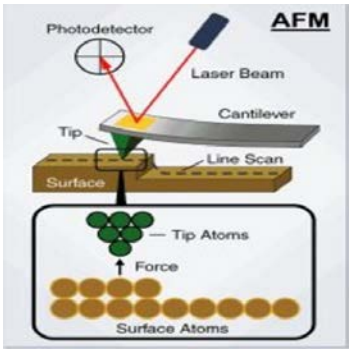

contact mode (NC-AFM or FM-AFM), the tip is held some tens of nanometers above the sample surface where it experiences the attractive combination of van der Waals, electrostatic, or magnetostatic forces. In "repulsive" or contact mode (C-AFM), the tip is pressed close enough to the surface for the tip and sample electron clouds to overlap, generating a repulsive electrostatic force of ~10 nN (nanonewtons), in operation much like the stylus riding a groove in an old record player. There is also intermittent-contact mode (IC-AFM), which is sometimes called "tapping" mode. In any of these modes, a topographic map of the surface is generated by recording the up-and-down motions of the cantilever arm as the tip is scanned. These motions may be measured either by the deflection of a light spot reflected from a mirrored surface on the cantilever (image, right) or by tiny changes in voltage generated by piezoelectric transducers attached to the moving cantilever arm. Typical laboratory AFM cantilevers have lengths of 100-400 microns, widths of 20-50 microns, and thicknesses between 0.4-3 microns. AFM tips may be positioned with ~10 pm precision, compressive loads as small as 1-10 pN of force are routinely measured,[3153] and the tips may even be operated in liquids.[3154]

SPM technology has also much improved over the last few decades, now regularly achieving resolutions of ~1 pm in the z direction (vertical) and ~10 pm in the xy (horizontal) plane, which is better than atomic resolution.

F.1.2 Structure Determination by AFM

The AFM is essentially a way to "touch" a molecule and to "feel" the shapes of the atoms comprising the molecule, while the molecule is resting on a surface. In 2009, researchers at IBM Zurich used an AFM in constant-height non-contact mode in ultra-high vacuum (UHV) at cryogenic temperatures (5 K) to scan an organic molecule that had been deposited either on a flat copper Cu(111) conductive surface, or on the same copper surface coated with a 2-monolayer thickness of insulating NaCl film.[3155] Scan forces ranged from 0-100 pN. The first organic molecule that was imaged was pentacene ($C_{22}H_{14}$), a linear polycyclic hydrocarbon consisting of five fused benzene rings with 22 carbon atoms.

In the images below, "E" shows an AFM tip consisting of gold atoms to which a single carbon monoxide (CO) molecule has been attached, making a very sharp tip hovering over a pentacene molecule viewed edge-on. "A" shows a ball-and-stick model of the pentacene molecule (gray = carbon, white = hydrogen) as it would lay flat on a surface. "C" is an actual scan image of a pentacene molecule resting on a copper Cu(111) surface, with all of its atoms clearly resolved. "D" is another scan image, again on Cu(111), with six atomically-resolved pentacene molecules in one image.

[3153] Weisenhorn AL, Hansma PK, Albrecht TR, Quate CF. Forces in atomic force microscopy in air and water. Appl Phys Lett. 1989;54(26):2651-2653; https://aip.scitation.org/doi/abs/10.1063/1.101024. Chen CJ. Introduction to Scanning Tunneling Microscopy, Oxford University Press, Cambridge, 1993. Wiesendanger R. Scanning Probe Microscopy and Spectroscopy: Methods and Applications, Cambridge University Press, Cambridge, MA, 1994.

[3154] Schaffer TE, Cleveland JP, Ohnesorge F, Walters DA, Hansma PK. Studies of vibrating atomic force microscope cantilevers in liquid. J Appl Phys. 1996 Oct 1;80(7):3622-3627; http://www.bioforce.uni-tuebingen.de/pubs/Schaffer_1996_JAP.pdf.

[3155] Gross L, Mohn F, Moll N, Liljeroth P, Meyer G. The chemical structure of a molecule resolved by atomic force microscopy. Science. 2009 Aug 28;325(5944):1110-1114; https://pubmed.ncbi.nlm.nih.gov/19713523/.

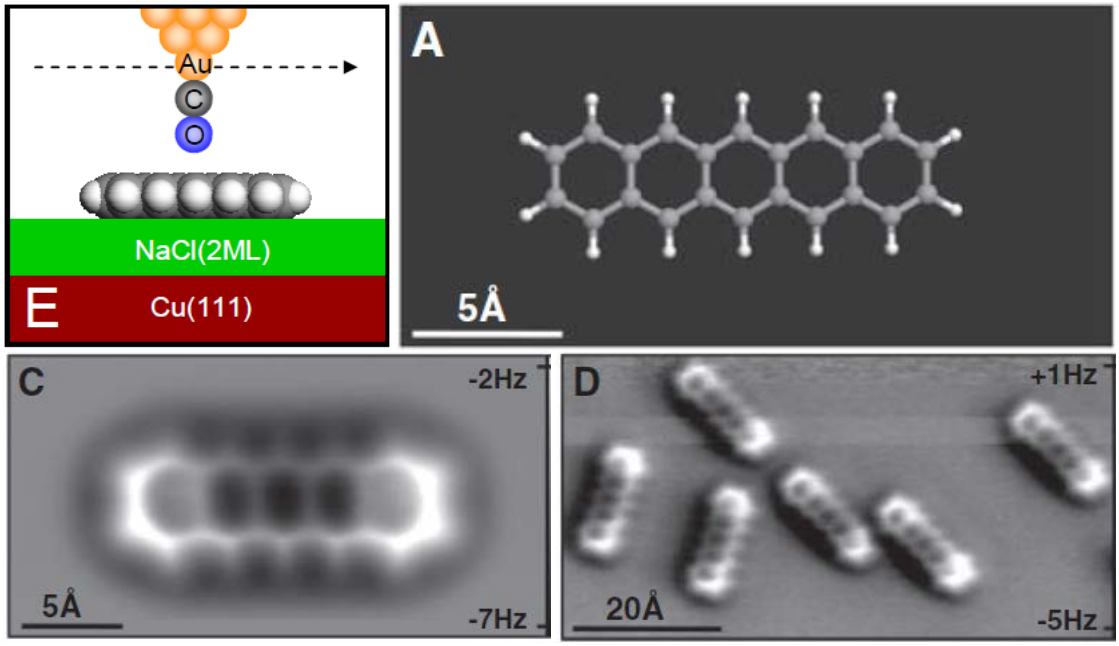

By 2014 the same Zurich group had imaged their largest molecule to date, a clover-shaped nanographene $C_{78}H_{36}$ molecule with 22 fused benzene rings.[3156]

In similar manner, the IBM team used their AFM to distinguish, by "touch" alone, the carbon atom "bond order" – that is, whether adjacent carbon atoms have single- (C–C), double- (C=C), or triple (C≡C) bonds – in various scanned individual organic molecules including polycyclic hydrocarbons and fullerenes.[3157] Along with the charge distribution within individual surface-bound molecules,[3158] the positioning of the sample molecule on the surface can be determined with very high precision using AFM, including the deposited molecule's lateral adsorption position to atomic resolution, its adsorption height differences to a precision of 3 pm, and the tilts of its molecular plane to within 0.2°.[3159]

In 2010, the IBM Zurich team used the same technique (i.e., the sample molecule is deposited on a Cu(111) surface and scanned by a CO-functionalized AFM tip) to determine the exact pattern of atomic connectivity in a natural organic molecule of previously undetermined structure, a metabolite called cephalandole A.[3160]

[3156] Schuler B, Collazos S, Gross L, Meyer G, Perez D, Guitián E, Peña D. From perylene to a 22-ring aromatic hydrocarbon in one-pot. Angew Chem Int Ed Engl. 2014 Aug 18;53(34):9004-9006; https://dominoweb.draco.res.ibm.com/reports/rz3875.pdf.

[3157] Gross L, Mohn F, Moll N, Schuler B, Criado A, Guitián E, Peña D, Gourdon A, Meyer G. Bond-Order Discrimination by Atomic Force Microscopy. Science 2012 Sep 14;337(6100):1326-9; https://pubmed.ncbi.nlm.nih.gov/22984067/.

[3158] Mohn F, Gross L, Moll N, Meyer G. Imaging the charge distribution within a single molecule. Nat Nanotechnol. 2012 Feb 26;7(4):227-31; https://pubmed.ncbi.nlm.nih.gov/22367099/.

[3159] Schuler B, Liu W, Tkatchenko A, Moll N, Meyer G, Mistry A, Fox D, Gross L. Adsorption geometry determination of single molecules by atomic force microscopy. Phys Rev Lett. 2013 Sep 6;111:106103; https://orbilu.uni.lu/bitstream/10993/25137/1/Adsorption%20geometry%20determination%20of%20single%20molecules%20by%20atomic%20force%20microscopy.pdf.

[3160] Gross L, Mohn F, Moll N, Meyer G, Ebel R, Abdel-Mageed WM, Jaspars M. Organic structure determination using atomic-resolution scanning probe microscopy. Nat Chem. 2010 Oct;2(10):821-825; https://pubmed.ncbi.nlm.nih.gov/20861896/.

By 2012, a larger collaboration of researchers[3161] used a combination of the same atomic resolution AFM, along with Density-Functional Theory (DFT) quantum chemistry structure calculations and computer-aided structure elucidation (CASE), to solve the structure (images at right) of the natural compound breitfussin A ($C_{16}H_{11}N_3O_2BrI$) as later validated independently using high-resolution mass spectrometry. Breitfussin A is a member of a chemical family of molecules that includes sterols, polyhalogenated monoterpenes, and anthracenone derivatives. (The white-dashed encircled region marks a non-intrinsic molecular feature.) Remarkably, AFM could be used to determine all the connection positions of the cyclic systems as well as those of the substituent groups (MeO, Br, and I) – information that is difficult to obtain with other techniques.

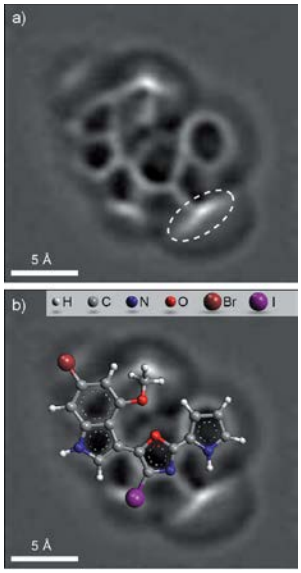

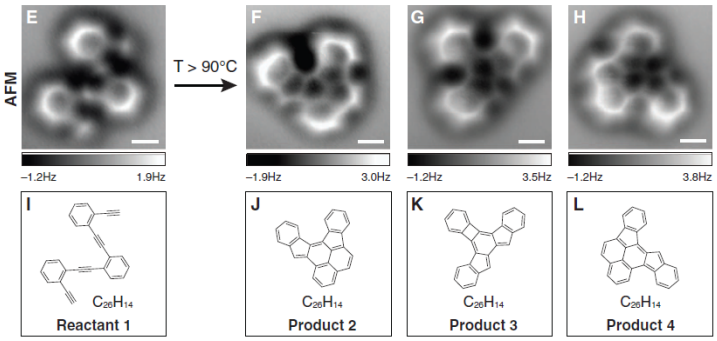

AFM is also regularly used to record the changes in chemical structure that occur as an individual molecule undergoes a complex reaction on a surface. For example, Crommie's group at U.C. Berkeley used a cryogenic UHV non-contact AFM to track the transformations of an individual molecule of 1,2-bis((2-ethynylphenyl)ethynyl)benzene on a silver Ag(100) surface as it underwent a series of cyclization processes (images above; scale bar = 3 Å).[3162] With the assistance of DFT-based quantum chemistry calculations, these bond-resolved single-molecule AFM images were sufficient to identify the structure of the original reactant and its successor product molecules.

F.1.3 Element Typing of Atoms by AFM

If we have the molecular formula – that is, if we know how many atoms of each element are present – then it is clearly possible to use AFM to infer the geometric structure and bonding pattern of an unknown molecule, provided it doesn't deviate too far from linear or planar form. But what if we don't have the molecular formula? Even then, in many cases, the sample molecule's geometric structure, its bond lengths and angles, the number of bonds per atom, and the measured bond order, may be enough to strongly infer, if not always unambiguously identify, the element type of a particular atom in an unknown organic molecule.

[3161] Hanssen KØ, Schuler B, Williams AJ, Demissie TB, Hansen E, Andersen JH, Svenson J, Blinov K, Repisky M, Mohn F, Meyer G, Svendsen JS, Ruud K, Elyashberg M, Gross L, Jaspars M, Isaksson J. A Combined Atomic Force Microscopy and Computational Approach for the Structural Elucidation of Breitfussin A and B: Highly Modified Halogenated Dipeptides from *Thuiaria breitfussi*. Angew Chem Int Ed. 2012 Dec 3;51(49):12238-41; https://pubmed.ncbi.nlm.nih.gov/23109225/.

[3162] de Oteyza DG, *et al*. Direct Imaging of Covalent Bond Structure in Single-Molecule Chemical Reactions. Science 2013 Jun 21;340:1434-7; https://scienceintheclassroom.org/sites/default/files/research-papers/science-2013-de_oteyza-1434-7.pdf.

In limited cases, cryogenic STM-based single-molecule inelastic electron tunneling spectroscopy can provide electron tunneling spectra that serve as fingerprints of the vibrational properties of adsorbed molecules (e.g., C-H and C-D stretch modes,[3163] ^{12}C-O and ^{13}C-O vibrational excitations,[3164] N-H stretching vibrations[3165]) and of the electronic properties of magnetic impurity atoms (e.g., Co-Au electronic resonance,[3166] Ce-Ag tunneling spectra anti-resonance[3167]), thereby allowing direct elemental identification of a particular atom. Non-destructive low-voltage EELS (Electron Energy-Loss Spectroscopy) single-atom spectroscopy has also correctly identified atoms of the elements Ca, La, Ce and Er,[3168] and other related methods have been disclosed.[3169]

Another convenient way to detect element type is via dynamic force microscopy (NC-AFM), which can image insulator, semiconductor and metal surfaces with true atomic resolution by detecting and precisely measuring the short-range forces that arise with the onset of chemical bonding between the apical tip atom and surface atoms. These forces depend sensitively upon the chemical identity of the atoms involved.

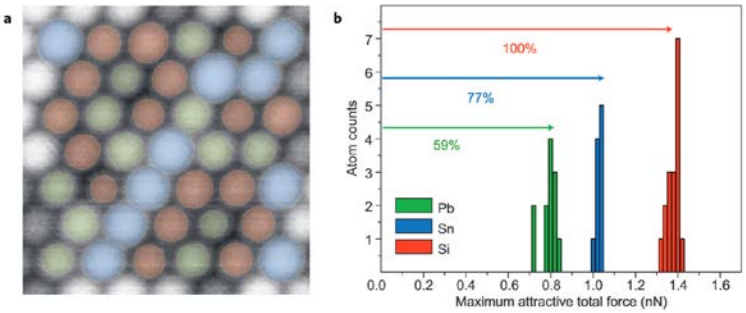

For example, Custance[3170] reported using room temperature chemical force measurements as the basis for atomic recognition by imaging a surface alloy containing equal proportions of Si, Sn, and Pb atoms on a silicon Si(111) substrate, and then successfully identifying the element types of all accessible surface atoms – even though these three elements exhibit very similar chemical properties and identical surface position preferences that render any discrimination attempt based on topographic measurements alone very difficult. In the images above, "a" (at left) shows an NC-AFM image of a surface alloy composed of Si, Sn and Pb atoms blended in equal proportions on a Si(111) substrate. The color coding (Pb = green, Sn = blue, Si = red) corresponds to the chemical species as

---

[3163] Stipe BC, Rezaei MA, Ho W. Single-Molecule Vibrational Spectroscopy and Microscopy. Science 1998 Jun 12;280(5370):1732-5; http://citeseerx.ist.psu.edu/viewdoc/download?doi=10.1.1.1024.9850&rep=rep1&type=pdf.

[3164] Heinrich AJ, Lutz CP, Gupta JA, Eigler DM. Molecular Cascades. Science 2002 Nov 15;298(5597):1381-7; http://citeseerx.ist.psu.edu/viewdoc/download?doi=10.1.1.454.2608&rep=rep1&type=pdf.

[3165] Pascual JI, Lorente N, Song Z, Conrad H, Rust HP. Selectivity in vibrationally mediated single-molecule chemistry. Nature 2003 May 29;423(6939):525-528; https://pubmed.ncbi.nlm.nih.gov/12774118/.

[3166] Madhavan V, Chen W, Jamneala T, Crommie MF, Wingreen NS. Tunneling into a Single Magnetic Atom: Spectroscopic Evidence of the Kondo Resonance. Science 1998 Apr 24;280:567-9; https://pubmed.ncbi.nlm.nih.gov/9554843/.

[3167] Li J, Schneider WD, Berndt R, Delley B. Kondo Scattering Observed at a Single Magnetic Impurity. Phys Rev Lett. 1998 Mar 30;80(13):2893-6; https://journals.aps.org/prl/abstract/10.1103/PhysRevLett.80.2893.

[3168] Suenaga K, Sato Y, Liu Z, *et al*. Visualizing and identifying single atoms using electron energy-loss spectroscopy with low accelerating voltage. Nat Chem. 2009 Aug;1(5):415-418; https://pubmed.ncbi.nlm.nih.gov/21378897/.

[3169] "Simultaneous topographic and elemental chemical and magnetic contrast in scanning tunneling microscopy," U.S. Patent App. 20140259235, http://www.freepatentsonline.com/y2014/0259235.html.

[3170] Sugimoto Y, Pou P, Abe M, Jelinek P, Perez R, Morita S, Custance O. Chemical identification of individual surface atoms by atomic force microscopy. Nature 2007 Mar 1;446(7131):64-7; https://www.osaka-u.ac.jp/migr/pdf/eng/research/annualreport/vol8/selection/pdf/vol8_24-26.pdf.

determined by room temperature force distance spectroscopy. Image "b" (at right) tabulates atom counts as a function of the maximum measured attractive force above the Pb, Sn and Si atoms. The three different elements can be clearly distinguished on the basis of their respective maximum forces.

F.1.4 Element Typing of Functional Groups by AFM

Besides element typing of specific atoms, we can also chemically recognize particular functional groups that consist of a small number of atoms (e.g., –OH, $-CH_3$, etc.). This may be accomplished using another variant of atomic force microscopy called **Chemical Force Microscopy** (CFM).[3171] Recall that with AFM, structural morphology is probed using simple tapping or contact modes that utilize van der Waals interactions between tip and sample to maintain a constant probe deflection amplitude (constant force mode) or maintain height while measuring tip deflection (constant height mode). But CFM, on the other hand, uses chemical interactions between functionalized probe tip and sample.

A typical contemporary laboratory setup might involve a gold-coated tip to which R-SH thiols[3172] have been attached using gold-thiol bonding, with the "R" being an organic functional group of interest such as –COOH or $-CH_3$. When the R-functionalized tip is brought close to a test molecule on a surface, the R-group experiences a chemical interaction with the sample, creating an identifiable force profile that enables the CFM to determine the chemical nature of the sample surface, irrespective of its specific morphology. Typically, CFM is limited by thermal vibrations within the cantilever holding the probe. This limits force measurement resolution to ~1 pN which is still very suitable considering that weak COOH/CH_3 interactions are ~20 pN per pair.[3173] One review paper[3174] described numerous CFM applications including titration-AFM to obtain the apparent *pKa* value at the surface, determination of adhesive forces and energy on a surface, finding a specific substance by measuring single intermolecular forces (e.g., host-guest interaction in a complex environment), detection of specific chemical groups, determining surface heterogeneity, and studies of surface chemical reactions on the nanoscale and in real time.

Initially developed by Charles Lieber at Harvard University in 1994, CFM (aka. chemical force spectroscopy[3175]) was originally demonstrated using hydrophobicity (i.e., repulsion from water) where polar molecules (e.g., COOH) tend to have the strongest binding to each other, followed by nonpolar molecules (e.g., CH_3-CH_3) bonding, and lastly a combination of the two being the weakest. Thus, a scan of a sample with a tip functionalized with a –COOH or a $-CH_3$ group can allow detection of the presence and location of either group on a sample surface.

[3171] http://en.wikipedia.org/wiki/Chemical_force_microscopy.
[3172] https://en.wikipedia.org/wiki/Thiol.

[3173] Frisbie CD, Rozsnyai LF, Noy A, Wrighton MS, Lieber CM. Functional Group Imaging by Chemical Force Microscopy. Science 1994 Sep 30;265(5181):2071-4; http://cmliris.harvard.edu/assets/science265_2071.pdf. Noy A, Frisbie CD, Rozsnyai LF, Wrighton MS, Lieber CM. Chemical Force Microscopy: Exploiting Chemically-Modified Tips to Quantify Adhesion, Friction, and Functional Group Distributions in Molecular Assemblies. J Am Chem Soc. 1995 Aug 1;117(30):7943-7951; https://cml.harvard.edu/assets/JACS_117_7943.pdf. Noy A, Vezenov DV, Lieber CM. Chemical Force Microscopy. Annu Rev Mater Sci. 1997 Aug;27:381-421; http://cmliris.harvard.edu/assets/annuRevMaterSci27_381.pdf.

[3174] Steffens C, Leite FL, Bueno CC, Manzoli A, Herrmann PS. Atomic force microscopy as a tool applied to nano/biosensors. Sensors (Basel). 2012;12(6):8278-300; https://www.ncbi.nlm.nih.gov/pmc/articles/PMC3436029/.

[3175] Noy A. Strength in numbers: probing and understanding intermolecular bonding with chemical force microscopy. Scanning 2008 Mar-Apr;30(2):96-105; https://onlinelibrary.wiley.com/doi/pdf/10.1002/sca.20082.

Other tip functionalizations will probably be needed to identify other common organic ligand groups such as $-NH_2$ (amine),[3176] –OH (hydroxyl),[3177] –SH (thiol),[3178] $-PO_4$ and $-PO_2H$ (phosphate),[3179] $-C_6H_5$ (phenyl),[3180] and the like, that might be present on an unknown organic molecule, and might incorporate Br or Xe at the tip.[3181] For example, Wong *et al.*[3182] in Lieber's group prepared nanotube tips by oxidation in air at 700 °C, burning off all but 2% of the original material and leaving the ends covered with carboxyl (COOH) groups whose chemistry is rich and well understood. Four different kinds of tips were created: (1) the original carboxyl tip, which is acidic; (2) an amine-terminated tip (made by forming an amide bond to one of the amine groups in ethylenediamine ($H_2NCH_2CH_2NH_2$)), which is basic; (3) a hydrocarbon-terminated tip (made by forming an amide bond to benzylamine ($C_6H_5CH_2NH_2$)), which is hydrophobic; and (4) a biotin-terminated tip (made by forming an amide bond to a biotin derivative), which shows specific binding to streptavidin. AFM contact forces between tips and selected samples varied in a deterministic manner and were shown to be sensitive to pH and to the chemical details of the sample surface in ways consistent with the tips' intended chemistry.

A biological implementation of CFM at the nanoscale level is the positionally-controlled unfolding of proteins using a functionalized tip and an adherent surface.[3183] Due to the increased contact area, the tip and the surface act as anchors holding protein bundles while they separate. As uncoiling ensues, the required force jumps in steps, indicating various stages of uncoiling such as: (1) separation into bundles, (2) bundle separation into domains of crystalline protein held together by van der Waals forces, and (3) linearization of the protein upon overcoming the secondary bonding. Information on the internal structures of these complex proteins and a better understanding of constituent interactions is provided with this method.

Similarly, the measured force required to peel a single-stranded DNA molecule away from a single-crystal graphite surface during retraction of an oligonucleotide-functionalized AFM tip differs for pyrimidine bases (e.g., 85.3 pN for thymine and 60.8 pN for cytosine), allowing their presence in a strand of DNA to

---

[3176] Hibino M, Nakano-Nishida T. Chemical force microscopy using functionalized ZnO whisker probe tips. J Nanosci Nanotechnol. 2014 Apr;14(4):3080-6; https://pubmed.ncbi.nlm.nih.gov/24734738/.

[3177] Ashby PD, Lieber CM. Ultra-sensitive imaging and interfacial analysis of patterned hydrophilic SAM surfaces using energy dissipation chemical force microscopy. J Am Chem Soc. 2005 May 11;127(18):6814-8; http://cmliris.harvard.edu/assets/JACS_127_6814.pdf.

[3178] Mandal T, Ward MD. Determination of specific binding interactions at L-cystine crystal surfaces with chemical force microscopy. J Am Chem Soc. 2013 Apr 17;135(15):5525-8; https://pubs.acs.org/doi/full/10.1021/ja401309d.

[3179] Wuttisela K, Triampo W, Triampo D. Chemical force mapping of phosphate and carbon on acid-modified tapioca starch surface. Int J Biol Macromol. 2009 Jan 1;44(1):86-91; https://pubmed.ncbi.nlm.nih.gov/19022283/. Kreller DI, Gibson G, vanLoon GW, Horton JH. Chemical force microscopy investigation of phosphate adsorption on the surfaces of iron(III) oxyhydroxide particles. J Colloid Interface Sci. 2002 Oct 15;254(2):205-13; https://pubmed.ncbi.nlm.nih.gov/12702389/.

[3180] Patete J, Petrofsky JM, Stepan J, Waheed A, Serafin JM. Hofmeister effect on the interfacial free energy of aliphatic and aromatic surfaces studied by chemical force microscopy. J Phys Chem B. 2009 Jan 15;113(2):583-8; https://pubmed.ncbi.nlm.nih.gov/19090670/.

[3181] Mohn F, Schuler B, Gross L, Meyer G. Different tips for high-resolution atomic force microscopy and scanning tunneling microscopy of single molecules. Appl Phys Lett. 2013;102:073109; https://aip.scitation.org/doi/abs/10.1063/1.4793200.

[3182] Wong SS, Joselvich E, Woolley AT, Cheung CL, Lieber CM. Covalently functionalized nanotubes as nanometer probes for chemistry and biology. Nature 1998 Jul 2;394(6688):52-55; http://cmliris.harvard.edu/assets/nature394_52.pdf.

[3183] Zlatanova J, Lindsay SM, Leuba SH. Single molecule force spectroscopy using the atomic force microscope. Prog Biophys Mol Biol. 2000;74(1-2):37-61; http://cbpmedia.cbp.pitt.edu/faculty/leuba/pdfs/ZlatanovaLindsayLeubaProgressBiophysMolBiol2001review.pdf.

be distinguished.[3184] AFM tips functionalized with specific single-strand DNA oligonucleotides (mixed multi-base strands) can discriminate between their biological binding partner and other molecules on a heterogeneous substrate.[3185] The partial sequencing of a single DNA molecule (i.e., the unambiguous identification of all guanines, as distinct from the other 3 bases) on a copper Cu(111) surface via high-resolution STM was first reported in 2009.[3186]

Functionalized AFM tips have been created to exploit the chemical forces involved in antibody-antigen recognition,[3187] protein-carbohydrate recognition,[3188] enzyme-ligand recognition,[3189] and charge-transfer complexes.[3190] A wide variety of methods for attaching biological molecules to AFM tips are known.[3191] Tips with embedded electrical charges can probe the electrostatic structure of sample organic molecules.[3192]

We can also use mechanosynthesis to build much sharper scanning probe tips such as the hydrogenated ethynyl on an adamantane handle (leftmost image at right), whose apical hydrogen atom (white) is smaller than the apical oxygen atom (red) of the IBM Zurich C-O tip (rightmost image at right) which is mounted on a single gold atom attached to a much larger and poorly characterized field of copper (green) atoms coating a standard silicon probe tip.

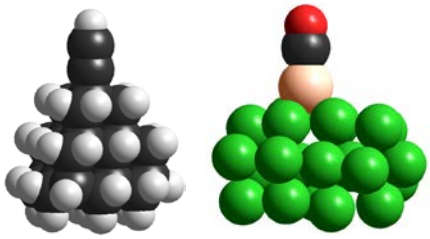

[3184] Manohar S, Mantz AR, Bancroft KE, Hui CY, Jagota A, Vezenov DV. Peeling single-stranded DNA from graphite surface to determine oligonucleotide binding energy by force spectroscopy. Nano Lett. 2008 Dec;8(12):4365-72; https://www.ncbi.nlm.nih.gov/pmc/articles/PMC2772178/.

[3185] Noy A, Vezenov DV, Kayyem JF, Meade TJ, Lieber CM. Stretching and breaking duplex DNA by chemical force microscopy. Chem Biol. 1997 Jul;4(7):519-27; https://cml.harvard.edu/assets/ChemBiol_1997_4_519-527_1997.pdf. Mazzola LT, Frank CW, Fodor SP, Mosher C, Lartius R, Henderson E. Discrimination of DNA hybridization using chemical force microscopy. Biophys J. 1999 Jun;76(6):2922-33; https://core.ac.uk/download/pdf/82483878.pdf.

[3186] Tanaka H, Kawai T. Partial sequencing of a single DNA molecule with a scanning tunnelling microscope. Nat Nanotechnol. 2009 Aug;4(8):518-522; https://www.osaka-u.ac.jp/en/research/annual-report/volume-11/Files/vol11pp24-27.pdf.

[3187] Hinterdorfer P, Baumgartner W, Gruber HJ, Schilcher K, Schindler H. Detection and localization of individual antibody-antigen recognition events by atomic force microscopy. Proc Natl Acad Sci USA 1996 Apr 16;93(8):3477-3481; https://www.pnas.org/content/pnas/93/8/3477.full.pdf.

[3188] For example, the measured rupture force between one molecule of mannose and the concanavalin A protein is 95 ± 10 pN. Zhang X, Yadavalli VK. Functionalized self-assembled monolayers for measuring single molecule lectin carbohydrate interactions. Anal Chim Acta. 2009 Sep 1;649(1):1-7; https://pubmed.ncbi.nlm.nih.gov/19664457/.

[3189] Fiorini M, McKendry R, Cooper MA, Rayment T, Abell C. Chemical force microscopy with active enzymes. Biophys J. 2001 May;80(5):2471-6; https://core.ac.uk/download/pdf/82215952.pdf.

[3190] Gil R, Fiaud JC, Poulin JC, Schulz E. Charge-transfer complexes interactions evidenced by chemical force microscopy. Chem Commun (Camb). 2003 Sep 7;2003(17):2234-5; https://pubs.rsc.org/en/content/articlelanding/2003/cc/b304829b/unauth#!divAbstract.

[3191] Barattin R, Voyer N. Chemical modifications of atomic force microscopy tips. Methods Mol Biol. 2011;736:457-83; https://pubmed.ncbi.nlm.nih.gov/21660744/.

[3192] Heinz WF, Hoh JH. Relative surface charge density mapping with the Atomic Force Microscope. Biophys J. 1999 Jan;76(1 Pt 1):528-538; https://core.ac.uk/download/pdf/82763832.pdf.

F.1.5 Chemohaptic Analysis of More Difficult Cases

Sample molecules that deviate significantly from linear or planar form will present additional difficulties. In these cases, at least four alternative approaches may be considered to obtain the full characterization information that we need.

(1) The scanning mechanism should include a procedure by which a molecule, once scanned and mapped, is physically rotated to a new position on the surface and then re-scanned. This procedure, which will bring new atoms and side groups into view, could be repeated multiple times as necessary until the data sets from all repeat tip scans can be matched up to yield a consistent picture of the molecular shape. The sample molecule could also be placed in a special jig to position it in a manner most conducive to useful data collection. The use of pattern-matching, based on our library of known molecular targets, could help here.

(2) A "pin-cushion" type receptor[3193] (see also brief description in Section 5.2.3.2) could be employed as a general-purpose molecular shape sensor.

(3) A hydrogen abstraction tool could be used to abstract any hydrogen present on the molecule, then a second tool of known configuration could be covalently bonded to the sample molecule at that position. The sample molecule is now securely held by a "hand" and can be translated, rotated, pushed, squeezed, stretched, or re-scanned at odd angles by a third tip acting as an examination tool to obtain any missing information about shape or composition.

(4) In the most difficult cases we can employ a protocol for progressive subtractive mechanosynthesis (Section 5.2.1.2) in which the sample molecule is disassembled group by group, or even atom by atom, with full re-scan after each disassembly step so that the original molecular structure can be inferred.

In ***future research***, mechanical tip-scanning techniques should be further conceptualized, extended, and developed to enable determination of both element identity and molecular geometry (including bond order) of all molecules of relevance to cryopreservation revival.

F.2 Molecular Assay System Scaling

In this Section, we describe an exemplar Molecular Assay System that is composed of a large number of individual microscale laboratory modules that are the minimum size necessary to perform the required single-molecule examinations (Section F.2.1). We then estimate the size and performance characteristics of a complete Molecular Assay System comprised of many such microscale laboratory modules (Section F.2.2).

[3193] Freitas RA Jr. Nanomedicine, Volume I: Basic Capabilities, Landes Bioscience, Georgetown TX, 1999, Section 3.5.7.4, "Pin Cushion Model"; http://www.nanomedicine.com/NMI/3.5.7.4.htm.

F.2.1 Minimum Size of Lab Module for Chemohaptic Analysis

A basic Lab Module for performing a chemohaptic analysis on one molecule at a time might include at least the following components and subsystems:

(1) a means to accept a single sample molecule to be tested into the apparatus;

(2) an examination surface upon which the sample molecule will be immobilized, prior to being tip-scanned;

(3) an evacuated (UHV) test chamber large enough to accommodate (a) the largest anticipated sample molecule, (b) the examination surface, and (c) the intrusion of all the tools that must work on the sample molecule;

(4) a large set of exchangeable probe tips with various functionalizations that serve different scanning purposes, and a means for storing these probe tips between uses;

(5) a means for extending, retracting, and exchanging probe tips, and a motorized means for performing the mechanical scanning process;

(6) a sensor system for measuring forces between scanning probe and sample molecule;

(7) a means for recording and transmitting the scanned force data;

(8) a local computer system to control Lab Module operations, analyze the raw data, and to modify the testing regimen on the fly in response to particular patterns detected in the data;

(9) specialized tools for manipulating the sample molecule;

(10) a set of mechanosynthetic tools for performing subtractive mechanosynthesis, if necessary, and a means for recharging spent tools; and

(11) a means for disposing of the sample molecule after the analysis is complete.

Table 24 compiles our best current estimates for atom count, mechanism volume, power consumption, and time budget to complete one analysis cycle for one sample molecule using a Lab Module consisting of appropriate sets of mechanisms and devices representing each of the aforementioned 11 categories of essential components and subsystems. Each subsystem component is accompanied by an explanatory footnote and some additional data.

Table 24. System parameters for a Lab Module that performs a single-molecule structural and elemental characterization.

Components or Subsystems	Carbon Atom Count *(millions)*	Volume *(nm^3)*	Maximum Power Consumption *(pW)*	Time Budget *(msec)*
(1) input one sample molecule[3194]	28.0	156,000		0.25
(2) exam table[3195]	1.8	10,000		
(3) UHV chamber[3196]	6,652.8	500,000,000		
(4) probe tips and tool rack[3197]	2.0	10,000		
(5) tip exchange & scanning the molecule[3198]	90.0	1,020,000	2	30.00
(6) force sensors[3199]	1.0	8,000	2	4.00
(7) data recording/process/transmission[3200]	3,000.0	20,000,000	6	400.00

[3194] (1): We'll assume a transfer arm that is 250 nm long and 625 nm^2 in cross-section, giving ~156,000 nm^3 and 28 million C atoms for this mechanism. Since it only operates twice or a small number of times during an examination cycle, the continuous power draw is negligible. If the sample molecule must be moved 250 nm at 1 mm/sec, the transfer time is 0.25 msec.

[3195] (2): The largest organic molecule or molecular fragment likely to be tested should be no more than a few nm in diameter, but we'll allocate 100 nm^2 for the examination surface, also assumed to be 10 nm thick. We'll also allocate 10 of these to accommodate the possibility of using different surfaces and with specialty jigs on these surfaces, giving a total ~10,000 nm^3 and 1.8 million C atoms for these surfaces.

[3196] (3): Assuming a 0.5 $micron^3$ cubic chamber with six 0.63 $micron^2$ walls that are 10 nm thick to support internal vacuum at ambient pressure, then we have 0.0378 $micron^3$ of solid diamond wall that incorporates 6.6528 billion C atoms. A chamber wall thickness of 10 nm should be more than sufficient because to avoid bursting, an analogous spherical pressure vessel wall thickness $t_{wall} \geq \Delta P\ R_{vessel} / 2\ \sigma_{wall} = 0.002$ nm, taking $\Delta P = 1$ atm $= 10^5$ N/m^2, $R_{vessel} = (3V_{vessel}/4\pi)^{1/3} = 492$ nm for $V_{vessel} = 0.5$ $micron^3$, and working stress $\sigma_{wall} \sim 10^{10}$ N/m^2 for diamond.*

* Freitas RA Jr. Nanomedicine, Volume I: Basic Capabilities, Landes Bioscience, Georgetown TX, 1999, Section 10.3.1, "Fluid Storage Tank Scaling"; http://www.nanomedicine.com/NMI/10.3.1.htm.

[3197] (4): We assume the Lab Module has 100 probe tips of various types, each tip having ~10,000 C atoms or ~50 nm^3 of volume. Allowing an equal volume for the tool rack to hold the 100 exchangeable probe tips we have a total of ~2 million C atoms and ~10,000 nm^3 of total volume for the probe tips.

[3198] (5): We allocate a $(100\ nm)^3$ volume of machinery that is 50% filled with diamondoid mechanical actuators, levers, gears, and so forth to drive the tip scan process and to enable tip changeout, and we'll use a linear dielectric drive motor that can produce 10 nN of force while consuming 2 pW of power in a ~2000 nm^3 volume at a power density of 10^{12} W/m^3. We also assume 10 redundant motors, operated one at a time but continuously. This gives a 1,020,000 nm^3 volume, 90 million C atoms, and ~2 pW power draw. If up to 100 exchangeable probe tips must be moved through a round-trip distance of 200 nm between tool rack and sample molecule at 1 mm/sec, then the total transfer time is (100 tips) (200 nm/tip) / (1 mm/sec) = 20 msec. Allowing 0.1 msec/tip for probe tip attachment and detachment at the tool rack adds another 10 msec to the time budget for this process.

[3199] (6): AFM tip scans typically measure up to 100 pN of force, but assuming we must accommodate forces up to ~10 nN from a tip that is scanning at a continuous speed of ~1 mm/sec, then a ~20 nm force sensor* has an 8000 nm^3 volume, ~1 million C atoms, and up to ~10 pW power draw if operated continuously. The smallest features are larger than 10 pm and the field of view for a single molecule is ~2 nm. If we raster scan along 2000 pm long lines with 10 pm separation between lines across the entire field of view using a tip moving at 1 mm/sec, then the tip travels 2000 pm x (2000 pm / 10 pm) = 400,000 pm (0.4 micron) per scan and each scan requires 0.4 msec to complete. A series of 10 tip-scans thus would require up to 4 msec.

* Freitas RA Jr. Nanomedicine, Volume I: Basic Capabilities, Landes Bioscience, Georgetown TX, 1999, Section 4.4.1, "Minimum Detectable Force"; http://www.nanomedicine.com/NMI/4.4.1.htm.

(8) computer[3201]	35,000.0	264,000,000	47	
(9) molecule manipulation tools[3202]	100.0	500,000	4	
(10) subtractive mechanosynthesis tools/operations[3203]	26.1	1,000,000	10	100.0
(11) disposal of sample molecule[3204]				0.25
Subtotals	44,901.7	786,704,000	71	534.50
Unallocated resources	15,098.3	213,296,000	29	465.50
TOTALS	**60,000.0**	**1,000,000,000**	**100**	**1,000.00**

F.2.2 Size and Performance of a Molecular Assay System

From **Table 24**, each diamondoid molecular machine-based Lab Module incorporates $n_{C\text{-}LM}$ = 60 billion carbon atoms of total mass $M_{LM} = m_C\ n_{C\text{-}LM} = 1.2 \times 10^{-15}$ kg (taking $m_C = 2 \times 10^{-26}$ kg/C atom), has a volume $V_{LM} = 1\ \mu m^3$, a power consumption up to $P_{LM} = 100$ pW in continuous operation, and requires $\tau_{LM} \sim 1$ sec/molecule in continuous operation to determine the molecular structure and element types of all atoms in an unknown molecule. A Molecular Assay System comprising $N_{LM} = 10^{10}$ Lab Modules, with a total volume of active nanomachinery of $V_{LMB} = N_{LM}\ V_{LM} = 10\ mm^3$ and an active nanomachinery mass of $M_{LMB} = N_{LM}\ M_{LM} = 0.012$ gram, can process $N_{LM} / \tau_{LM} =$ **10^{10} molecules/sec** with a maximum power consumption of $P_{LMB} = N_{LM}\ P_{LM} =$ **1 watt**. Power density is a quite reasonable $P_{d\text{-}LMB} = P_{LMB} / V_{LMB} =$

[3200] (7): Allocate another 10% of the computer memory budget from item (8) for this item: 0.02 micron^3, 3 billion C atoms, 6 pW power draw. A scanning tip moving at 1 mm/sec and recording 10 pm features will encounter 10^8 features/sec, implying 100 MHz operation – well within the anticipated ~GHz processing and transmission speeds of nanocomputers, nanoswitches, and other mature nanomechanical systems. Assuming 10 bits per feature, the data flow is 10^9 bits/sec during the 4 msec while the 10 tip-scans are in progress. If 100 computational operations must be performed on every bit to achieve molecular structure identification and element typing, then the total data processing time per 10 tip-scans is 400 msec.

[3201] (8): The Lab computer can be a 1 GFLOP ($I_{LC} = 64 \times 10^9$ bit/sec) mechanical nanocomputer occupying a volume of $I_{LC}/U_{nano} = 0.064$ micron^3, taking $U_{nano} = 10^{30}$ bits/sec-m^3 (Section 4.8.5), with an atom count of ~5 billion C atoms, mass ~10^{-16} kg, and a power draw of $I_{LC}\ E_{Landauer77K} = 47$ pW, taking $E_{Landauer77K} = 0.74$ zJ/bit for a nanocomputer operated at LN2 temperatures (Section 5.2.3.2), paired with 10^6 bits of fast-access (10^{10} bit/sec) mechanical memory and 10^9 bits of slow-access (10^9 bit/sec) spooled hydrofluorocarbon memory with a combined ~0.2 micron^3 volume and a ~30 billion C atom count.

[3202] (9): Assume 10 manipulators, each having 10 million C atoms and 50,000 nm^3 of displaced volume, but they're operated at most 2 at a time at a cost of 2 pW per manipulator. This yields a total of 500,000 nm^3, 100 million C atoms, and a 4 pW power draw, assuming continuous operation.

[3203] (10): A nanoscale fabricator might include 3 small mechanosynthetic manipulators and one large manipulator plus 20 toolheads and a toolrack, occupying 1,000,000 nm^3 of displaced volume with 26.1 million C atoms, burning ~10 pW of power when in continuous use. It could fabricate structures at the ~10 msec/atom rate if presentation of feedstock molecules is not a time-limiting factor, as would be the case during disassembly rather than fabrication where we are breaking bonds in a molecule at hand rather than making bonds between a workpiece and an imported moiety. Assuming ~10 C atoms for a "typical molecule", the disassembly portion of the analysis procedure, if needed to break the molecule down into haptically-readable pieces, could be done in ~100 msec. (The 10 scan times for 9 disassembly steps are already accounted for under item (6), above.)

[3204] (11): Mechanisms already included in (1); if the sample molecule or its remains must be moved 250 nm at 1 mm/sec, the transfer time is 0.25 msec.

10^8 W/m^3, well below the ~10^{10} W/m^3 power density estimated for molecular transport[3205] and the ~10^{12} W/m^3 power density estimated for mechanical computation.[3206] Spacing the Lab Modules with uniform separation throughout a **1 cm^3 housing** filled with cooling mechanisms and flowing cryogenic fluids reduces overall power density to ~10^6 W/m^3, roughly the same as an active mitochondrion.[3207]

Besides the requirement for cryogenic refrigeration, the Molecular Assay System must provide the large number of Lab Modules with access to infrastructure utilities including sample molecule preparation and distribution, electrical power distribution, a central computer providing process guidance and library functions, a materials distribution system for feedstock and waste, and a communications system linking all the Lab Modules to each other and to the external control interface. A complete system design is beyond the scope of this document – and may be a suitable topic for ***future research*** – but it appears that at least the sample molecule distribution system should have negligible mass and power draw.[3208]

[3205] Freitas RA Jr. Nanomedicine, Volume I: Basic Capabilities, Landes Bioscience, Georgetown TX, 1999, Section 6.5.6(A), "Power Analysis in Design. A. Molecular Transport"; http://www.nanomedicine.com/NMI/6.5.6.htm#A.

[3206] Freitas RA Jr. Nanomedicine, Volume I: Basic Capabilities, Landes Bioscience, Georgetown TX, 1999, Section 6.5.6(E), "Power Analysis in Design. E. Computation"; http://www.nanomedicine.com/NMI/6.5.6.htm#E.

[3207] Smith RE. Quantitative Relations Between Liver Mitochondria Metabolism and Total Body Weight in Mammals. Ann NY Acad Sci. 1956 Jan 31;62(17):403-422; https://www.cabdirect.org/cabdirect/abstract/19561404788. Nedergaard J, Cannon B. Chapter 10. Thermogenic Mitochondria, in: Ernster L, ed., Bioenergetics, Elsevier, New York, 1984, pp. 291-314; https://www.amazon.com/dp/0444805796/.

[3208] Freitas RA Jr. The Whiskey Machine: Nanofactory-Based Replication of Fine Spirits and Other Alcohol-Based Beverages. IMM Report No. 47, May 2016, pp. 94-96; Section 5.2.7, "Size and Performance of the Assay Unit"; http://www.imm.org/Reports/rep047.pdf.

Appendix G. Historical and Future Commercial Electricity Prices

The chart below compares the cost of commercial electricity in the U.S. in both nominal (actual dollar prices) and real (inflation-adjusted or constant-value dollars) during 1960-2011.[3209] The real price of electricity has been almost constant in real terms at **~$0.1/KW-hr** (2.78 x 10^{-8} $/J) for the last half-century.

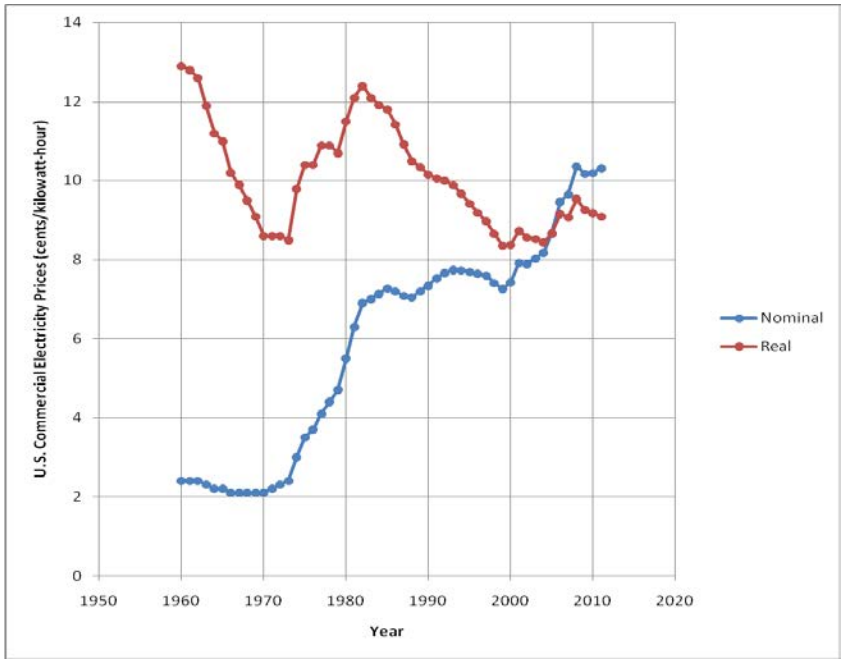

As noted elsewhere,[3210] we can consider a scenario for decentralized energy production that might exist in the future era when nanofactories exist and cryonics revivals are technologically feasible. In this forward scenario, solar energy would be captured by inexpensive nanofactory-made atomically-precise solar panels placed as ground cover over cheaply-priced vacant rural land, plausibly reducing the cost of commercial electricity about 100-fold down to **~$0.001/KW-hr**. This reduced cost of electricity is estimated as follows.

Taking average ground-level cloudless noontime optical-band solar intensity as 200 W/m^2,[3211] and correcting for day/night cycles (0.5), cloud cover (0.5), solar angle (0.5), and 50% conversion efficiency (0.5), the panels deliver ~50 KW/acre (12.5 W/m^2) or ~4.4 million KW-hr/acre over an assumed 10-year lifetime for the panels. Taking the average cost of vacant rural land as $500/acre,[3212] the carrying cost at

---

[3209] Table 8.10. Average Retail Prices of Electricity, 1960-2011 (Cents per Kilowatt-hour, Including Taxes). U.S. Energy Information Administration, Sep 2012; https://www.eia.gov/totalenergy/data/annual/showtext.php?t=ptb0810.

[3210] Freitas RA Jr. Economic Impact of the Personal Nanofactory. Nanotechnology Perceptions: A Review of Ultraprecision Engineering and Nanotechnology 2006 May;2:111-126; http://www.rfreitas.com/Nano/NoninflationaryPN.pdf.

[3211] Freitas RA Jr. Nanomedicine, Volume I: Basic Capabilities, Landes Bioscience, Georgetown, TX, 1999; Section 6.3.6, "Photonic Energy Conversion Processes"; http://www.nanomedicine.com/NMI/6.3.6.htm#p5.

[3212] U.S. rural farmland in 2004 ranged from $265/acre in NM to $10,200/acre in CT and RI; U.S. average is $1360/acre.[*] Canadian rural farmland in 2004 ranged from $350/acre in Saskatchewan to $3337/acre in Ontario,[†] with one writer reporting prices as low as $188/acre in southeastern Saskatchewan;[‡] Canadian average is $927/acre [48].† In 2005, relatively inaccessible virgin Brazilian timberlands were available for $18/acre in 10,000-acre parcels,[**] remote but water-accessible Brazilian grasslands could be bought for $200/acre in 200-acre parcels,[**] and cattle grazing property was for sale in remote Arizona for $125/acre in 20,000-acre parcels.[**]

[*] "Table 9-14. Farm real estate: Average value per acre of land and buildings, by State, Mar. 1, 1970 and Jan. 1, 2000-2004," Agriculture Statistics 2005, U.S. Department of Agriculture, p. IX-9; http://www.usda.gov/nass/pubs/agr05/05_ch9.pdf.

5% mortgage interest and a 1% property tax rate is $30/yr, or $300/acre for 10 years. Thin diamondoid solar panels with their support structures to cover 1 acre will have a total mass of ~2900 kg,[3213] costing $2900 if fabricated for $1/kg,[3214] bringing total cost over 10 years to $3200/acre and thus the cost of energy to ~$0.001/KW-hr. Cost is similar if the ground is first cleared by a bulldozer at $50-$150/hr plus move-in/out fees,[3215] allowing laying solar collectors on the ground without supports.

This analysis ignores any additional costs of local energy storage or transmission to a distant site. It also ignores the likelihood that environmental, regulatory and other government-imposed costs may offset at least some of the nominal cost reduction, due to restrictions or fees imposed to mitigate: (1) the possible death of covered vegetation due to sunlight deprivation (including both ecological impacts and the opportunity cost for foregone land uses); (2) the alteration of local weather patterns and watershed hydrodynamics including soil drainage, erosion, and water tables; (3) the destruction of natural "view easements" with solar collectors that may be aesthetically inconsistent with nature; (4) the interference with insect and bird navigation; and so forth. The arrival of this price reduction also might be somewhat delayed as most major new technologies start out expensive[3216] and then mature over time toward their ultimate cost-saving potential.

---

† "Table 2. Value per acre of farm land and buildings," Value of Farm Capital, Agriculture Economic Statistics, November 2005, Statistics Canada; http://www.statcan.ca/english/freepub/21-013-XIE/2005002/t002_en.htm.

‡ "Farmland Prices on the Prairies," Warren's Farm & Ranch Review, Spring 2001, pp. 14-15; http://www.warrensdirectory.com/pdf/2001/getting_intense.pdf.

** "Land for sale, Farms for sale, Rural property for sale," Rural Property Bulletin, 17 December 2005; http://www.landandfarm.com.

[3213] A solar-collector sheet of diamondoid material of dimension w = 67.1 m (edge length of 1 square acre), working strength $\sigma_w = 10^{10}$ N/m^2 (~0.2 times the failure strength of diamond*), and density $\rho_{diamond} = 3510$ kg/m^3 frontally impacted by a wind of density $\rho_{air} = 1.29$ kg/m^3 at STP traveling at maximum gust velocity v = 44.7 m/sec (100 mph) must have thickness $t > \rho_{air} w v^2/\sigma_w \sim 17$ microns to avoid tearing, giving a sheet of mass $M_{sheet} = \rho_{diamond} w^2 t = 270$ kg. Cylindrical diamond supporting columns (one at each corner) of length L = 10 m with Young's modulus $E_{diamond} = 1.05 \times 10^{12}$ N/m^2 must have radius $R > (4L^2 \rho_{air} w^2 v^2 / \pi^3 E_{diamond})^{1/4} = 7.7$ cm to avoid buckling† under a maximum whole-sheet 1200 metric ton wind load, giving total column mass $M_{columns} = 4 (\pi R^2 L \rho_{diamond}) = 2630$ kg, hence total installed diamond mass $M_{diamond} = M_{sheet} + M_{columns} = 2900$ kg. ($M_{diamond}$ is minimized using the largest possible sheet rather than multiple smaller sheets because $M_{columns} \sim w^{-1}$.) The above estimate ignores possible damage from seasonal snow loads, an additional 400 metric tons per foot of snow depth assuming a snow pack density of ~300 kg/m^3.‡

* http://www.nanomedicine.com/NMI/10.3.1.htm#p3.

† http://www.nanomedicine.com/NMI/9.3.1.2.htm#p2.

‡ "Snow Cover. Properties of Snow Cover: Snow Density," The Atlas of Canada, 18 April 2005; http://atlas.gc.ca/site/english/maps/environment/climate/snowcover/1.

[3214] Freitas RA Jr. Economic Impact of the Personal Nanofactory. Nanotechnology Perceptions: A Review of Ultraprecision Engineering and Nanotechnology 2006 May;2:111-126; http://www.rfreitas.com/Nano/NoninflationaryPN.pdf.

[3215] "Machinery Rental, Wisconsin, 2004," Wisconsin's 2004 Custom Rate Guide, Wisconsin Agricultural Statistics Service, p. 9; http://www.nass.usda.gov/wi/custom_rate_2004.pdf; "Summary Of EERA Rates, Bulldozers," California Interagency Emergency Hire Of Equipment Rental Rates, New Agreement Period: May 1, 2005 – April 30, 2008 , No. 29 April 2005, p. 3934-6; http://www.fire.ca.gov/php/fire_er_content/downloads/3934rev0405.pdf. See also: http://www.cityofmiddletown.com/Purchasing/Bids/2005-038.pdf.

[3216] e.g., NASA has posted* a commercial electricity price of $42.00/KW-hr on board the International Space Station.

* Kross JF. Trillions of pennies from heaven. Ad Astra 2020 Summer;32(3):32-37.

Appendix H. Binding Site Design

A binding site is a molecular-scale structure designed to selectively bind to a desired molecule of biological or medical interest. Binding sites can be used on a nanorobot's surface to detect or absorb molecules in biological fluids, to recognize biological or biochemical structures, or to transport selected molecules from the gaseous or liquid phase. Binding sites can be static (e.g., a receptor to measure one chemical) or dynamic (e.g., a programmable "pincushion" receptor,[3217] allowing significant receptor reconfiguration during operation; Section 5.2.3.2).

Biological organisms employ many binding sites to enable precise signaling and catalysis. These binding sites consist of proteins that fold into the shapes required to match the target molecule like a hand in a glove. While these binding sites obviously work in a fairly robust manner, the complexity of the folding process makes proteins difficult to design for novel applications. That is, even when the shape of a desired target molecule is known, it can be difficult to design a protein that will fold into a shape which results in the appropriate binding site that emerges in the tertiary or quaternary structure. In addition to the difficulty of predicting protein folding, the low stiffness of proteins limits their ability to maintain specific shapes in spite of external forces or other alterations in their operating environment such as temperature,[3218] pH, or changing solute concentration (e.g., salt). Proteins are also subject to degradation by proteases. These factors restrict the utility and longevity of protein-based binding sites in many applications.

The mechanical synthesis (i.e., mechanosynthesis) of covalently bonded structures of arbitrary shape enables the construction of a new class of molecular-scale binding sites. By placing each atom in a specified location, the final shape of the binding site can be designed directly. For example, the potential energy surface of the binding site can be designed to precisely complement just the target molecule and no other molecule likely to be found in the same environment. This design approach contrasts with the traditional indirect design of binding sites in biological molecules such as proteins, antibodies, aptamers and molecular imprinted polymers. For the most part, in 2021 it was not yet possible to rationally design novel biological molecules with specific desired functions. Instead, such molecules were typically screened from huge numbers of randomly generated variations.

The ability to define and build arbitrary structures through mechanosynthesis provides not only the ability to design binding sites without the complexities inherent in protein or oligonucleotide folding, but also to make binding sites out of materials not typically found in biological systems, such as diamond or diamond-like substances. The high stiffness of diamondoid materials can allow a binding site to maintain its shape and function despite challenging environmental conditions (e.g., temperature, pH, salts) that would denature a protein-based binding site. This is not to say that all synthetic binding sites must be made from diamondoid, and the concepts described herein certainly translate to other materials, but the inherent advantages of diamondoid substances make them an exemplary material on which to focus.

Moreover, stiff diamondoid structures can exert larger forces on bound molecules than proteins, allowing designs with improved signal-to-noise ratios due to the ability to mechanically activate the site or close it for a time, thereby allowing recently released molecules time to diffuse away rather than possibly rebinding to the site. Binding sites that are employed in sensors or pumps will usually include (1) a probe mechanism

---

[3217] Freitas RA Jr. Nanomedicine, Vol. I: Basic Capabilities, 1999; Sec. 3.5.7.4, "Pin Cushion Model"; http://www.nanomedicine.com/NMI/3.5.7.4.htm.

[3218] Revival operations take place at cryogenic or near-freezing temperatures, so trying to avoid the protein design problem by using a known protein binding site (taken from a cell membrane that functions well at normothermic human body temperature) may not work for nanorobots employed in cryostasis revival.

to determine whether the binding site is occupied or unoccupied and (2) an ejection mechanism that can force a bound molecule to be ejected from the binding site. Both functions can most easily be served by a thin rod that is inserted into the binding site, but other means (e.g., site flexure, charge manipulation) can also be used.

The main challenge in designing a binding site to be manufactured in an atomically-precise manner is finding a configuration of atoms whose shape and charge distribution provide both the required sensitivity (i.e., readily binds the desired molecule) and selectivity (i.e., does not bind other molecules). Typically, diffusion of the molecule to the site limits the binding rate, so the key design parameter for a binding site is how long it holds the bound molecule before thermal fluctuations release it. How well a binding site discriminates the target molecule from others depends both on the ratio of binding affinities for the molecules and on their concentrations.

A second challenge is to develop a general design methodology which would facilitate efficient design of binding sites for numerous target molecules. There are huge numbers of molecules of potential relevance to medicine, environmental monitoring, research and other fields. Due to the large number of potential target molecules, a design methodology for synthetic binding sites would ideally be amenable to extensive automation,[3219] and would include rules of thumb to restrict the nearly infinite design space that would otherwise have to be considered in the absence of such rules. Commercial and open source software such as AutoDock[3220] already permits at least computer-assisted binding site design.

A variety of generic binding site motifs have been described elsewhere in the literature[3221] and should be reviewed and explored in ***future research***. Binding sites for medical applications might initially include targets such as small molecules (see discussion below), monosaccharides, polysaccharides, amino acids, proteins, fatty acids, lipids, and various drugs.

The strength of the binding of the target molecule to the artificial receptor site can be designed to be sufficient to achieve high occupancy of all pockets (e.g., 99%) at the relatively low speeds of sorting rotor rotation (Section 4.10.1). The mechanical energy consumed to force the target molecule out of its binding site into the receiving chamber is delivered from the cam to the rods, but much of this energy can be returned with minimal losses to the cam on the source side by the compression of the rods during the binding of the target molecule to the receptor, a process that generates mechanical energy. In the medical context, artificial receptors are best designed for high affinity binding in the presence of a dominant background of quite different molecules. Analogies with antibodies suggest that a rotor with binding pockets of this type could deliver a product stream with impurity fractions up to 10^{-4} to 10^{-9} (i.e., 99.99% to

---

[3219] Salis HM, Mirsky EA, Voigt CA. Automated design of synthetic ribosome binding sites to control protein expression. Nat Biotechnol. 2009;27(10):946–950; https://www.ncbi.nlm.nih.gov/pmc/articles/PMC2782888/pdf/nihms145791.pdf. Jiménez J, Doerr S, Martínez-Rosell G, Rose AS, De Fabritiis G. DeepSite: protein-binding site predictor using 3D-convolutional neural networks. Bioinformatics. 2017;33(19):3036–3042; https://eclass.uoa.gr/modules/document/file.php/D464/Course%20Projects/deepsite.pdf. Khersonsky O, Lipsh R, Avizemer Z, *et al*. Automated Design of Efficient and Functionally Diverse Enzyme Repertoires. Mol Cell. 2018;72(1):178–186.e5; https://www.ncbi.nlm.nih.gov/pmc/articles/PMC6193528/pdf/emss-79915.pdf. Krivák R, Hoksza D. P2Rank: machine learning based tool for rapid and accurate prediction of ligand binding sites from protein structure. J Cheminform. 2018 Aug 14;10(1):39; https://www.ncbi.nlm.nih.gov/pmc/articles/PMC6091426/. Hossain A, Lopez E, Halper SM, Cetnar DP, Reis AC, Strickland D, Klavins E, Salis HM. Automated design of thousands of nonrepetitive parts for engineering stable genetic systems. Nat Biotechnol. 2020 Dec;38(12):1466-1475; https://pubmed.ncbi.nlm.nih.gov/32661437/.

[3220] http://autodock.scripps.edu/.

[3221] Freitas RA Jr. Nanomedicine, Vol. I: Basic Capabilities, 1999; Sec. 3.5.7, "Receptor Configurations"; http://www.nanomedicine.com/NMI/3.5.7.htm.

99.9999999% purity or better) depending on affinities, specificities, and the concentrations of the effectively competing ligands.[3222]

Much ***future research*** on binding site design remains to be done. An example of binding site design involving competing ligands was published in earlier work[3223] involving atmospheric carbon capture research, and is reproduced in Section H.1. Initial ideas for a few other medically relevant simple binding sites are described in Section H.2, and known binding sites for several cryoprotectant molecules are summarized in Section H3.

H.1 Binding Site Design for Carbon Dioxide Molecules

A detailed computational modeling and simulation effort will be required to create ideal selective binding site designs for **carbon dioxide** (CO_2) and also for possible alternative specific target atmospheric molecules of interest including NO_x, SO_x, CO, N_2, O_2, H_2O, H_2S, H_2, Ar, and other competing molecular species.

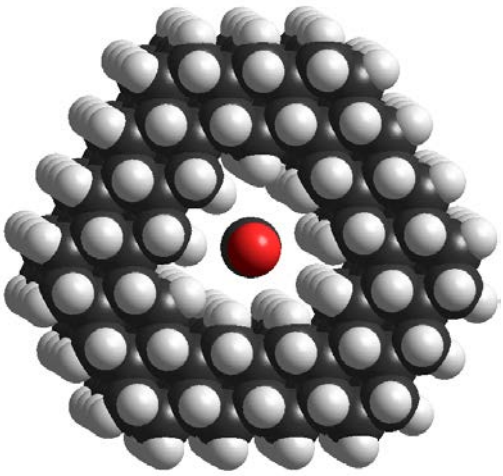

However, even an extremely simple binding site may be surprisingly effective. The figure at left[3224] is an example of a very simple 420-atom binding site (C = black, H = white, O = red) that does not employ strong covalent bonds between the site and the target molecule. To make this binding site, we took a thin sheet of hydrogen-terminated diamond with the C(111) lattice on the top and bottom horizontal faces, cut out a hexagonal perimeter with the C(100) lattice on all six vertical sides, punched a small hole in the center, and hydrogenated the inner walls of the pore, making a 420-atom ($C_{240}H_{180}$) all-hydrocarbon binding site. Such a structure could readily be nanofabricated as a solid block using a specific sequence of positionally-controlled tip-based mechanosynthetic reactions.[3225] A single CO_2 molecule (image, right) is shown nestled snugly inside the hydrogen-terminated pore, which employs only van der Waals attractions to provide the necessary binding interaction.

To assess the performance of our simple binding site for atmospheric carbon capture, we first list 38 major and trace atmospheric constituents typically found in non-urban air along with their fractional molar

---

[3222] Drexler KE. Nanosystems: Molecular Machinery, Manufacturing, and Computation. John Wiley & Sons, New York, 1992, Section 13.2.2(b); https://www.amazon.com/dp/0471575186/. Freitas RA Jr. Nanomedicine, Vol. I: Basic Capabilities, 1999; Section 3.5, "Molecular Receptor Engineering"; http://www.nanomedicine.com/NMI/3.5.htm.

[3223] Freitas RA Jr. The Nanofactory Solution to Global Climate Change: Atmospheric Carbon Capture. IMM Report No. 45, Dec 2015; Section 4.2, "Binding Site Design for Carbon Dioxide"; http://www.imm.org/Reports/rep045.pdf.

[3224] Design by Ralph C. Merkle; personal communication, 2015.

[3225] For mechanosynthesis theory work generally, see: Freitas RA Jr, Merkle RC. A Minimal Toolset for Positional Diamond Mechanosynthesis. J Comput Theor Nanosci. 2008 May;5:760-861; http://www.molecularassembler.com/Papers/MinToolset.pdf. For experimental mechanosynthesis work, see: Sugimoto Y, Pou P, Custance O, Jelinek P, Abe M, Perez R, Morita S. Complex Patterning by Vertical Interchange Atom Manipulation Using Atomic Force Microscopy. Science. 2008 Oct 17;322:413-417; http://www.sciencemag.org/content/322/5900/413.full.

concentration,[3226] then employ molecular mechanics methods using the AMBER99 force field[3227] (known to be highly parameterized for nonbonded interactions, using the computational tools of quantum chemistry) to estimate the binding energy (E_b) of the pore for each molecular species (**Table 25**, below). This is calculated as the difference between the total energy of the binding site with the molecule bound inside it and the sum of the total energies of the empty binding site and the isolated molecule. The fractional binding site occupancy of a molecular species, or $\exp(-E_b/k_BT)$ where $k_B = 8.625 \times 10^{-5}$ eV/molecule-K and ambient temperature T = 300 K (27 °C), is then multiplied by the fractional atmospheric molar concentration (f_{air}) of that molecule, then renormalized to obtain the percentage of each molecular species likely to pass through the binding site filtration mechanism in the first pass. Our simple binding site pore has very high affinity for CO_2 and even higher affinity for eight other molecules, but those other eight molecules are present in normal air at such low concentrations that the resulting gaseous filtrate is ~99% pure CO_2, with just ~1% of O_2 and N_2 and mere traces of everything else.[3228]

Filtrate purity will vary slightly with ambient environmental temperature (e.g., 99.26% CO_2 at 290 K / 17 °C, 98.49% CO_2 at 310 K / 37 °C). Note also that a single-stage filter of this type applied to flue gas from a coal-fired power plant would produce filtrate gas containing 52% CO_2 and 48% SO_2; applying a second stage of the same filters to the first-stage filtrate would extract essentially all of the SO_2, since the second-stage filtrate would be 99.6% SO_2 and 0.4% CO_2.

The 420-atom binding site design presented above is just one example of a wide range of possibilities. An

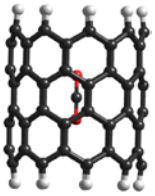

even simpler binding site based on the (9,0) carbon nanotube (image, left),[3229] similarly evaluated using AMBER, appears to prefer CO_2 (-0.73 eV) over SO_2 (-0.62 eV), with additional binding energies of -0.49 eV (O_2), -0.45 eV (CO), -0.35 eV (H_2O), -0.33 eV (N_2), and -0.06 eV (H_2). There is already widespread interest in using nanotubes for efficient CO_2 capture.[3230] An actual binding site that would be used in a molecular filter would necessarily be the result of an extensive design process – validated by higher-quality quantum chemistry simulations – that carefully balanced a large number of competing technical and operational requirements.

[3226] Killinger DK, Churnside JH, Rothman LS. Chapter 44. Atmospheric Optics. Bass M, Van Stryland EW, Williams DR, Wolfe WL, eds., Handbook of Optics, Volume I: Fundamentals, Techniques, and Design, Second Edition, McGraw-Hill, Inc., New York, 1994, pp. 44.1-44.50; https://www.amazon.com/Handbook-Optics-Fundamentals-Techniques-Design/dp/007047740X/. Weast RC, Handbook of Chemistry and Physics, 49th Edition, CRC, Cleveland OH, 1968; https://www.amazon.com/Crc-Handbook-Chemistry-Physics-49TH/dp/B0018NG0CU/.

[3227] Cornell WD, Cieplak P, Bayly CI, Gould IR, Merz KM Jr, Ferguson DM, Spellmeyer DC, Fox T, Caldwell JW, Kollman PA. A second generation force field for the simulation of proteins, nucleic acids, and organic molecules. J Am Chem Soc. 1995;117: 5179-5197; http://homepage.univie.ac.at/mario.barbatti/papers/method/amber_1995.pdf. Wang J, Cieplak P, Kollman PA. How well does a restrained electrostatic potential (RESP) model perform in calculating conformational energies of organic and biological molecules? J Comput Chem. 2000;21(12):1049-1074; http://banana.cnsm.csulb.edu/ffamber/pdfs/wang_amber99_2000jcc.pdf.

[3228] Freitas RA Jr. The Nanofactory Solution to Global Climate Change: Atmospheric Carbon Capture. IMM Report No. 45, Dec 2015; Section 4.2, "Binding Site Design for Carbon Dioxide"; http://www.imm.org/Reports/rep045.pdf..

[3229] Design by Ralph C. Merkle; personal communication, 2015.

[3230] Rahimi M, Babu DJ, Singh JK, YangY-B, Schneider JJ, Müller-Plathe F. Double-walled carbon nanotube array for CO_2 and SO_2 adsorption. J Chem Phys. 2015;143:124701; http://www.ncbi.nlm.nih.gov/pubmed/26429026.

Table 25. Gas molecule concentration in ambient U.S. dry atmosphere, their binding energy in a simple pore of a molecular filter, and their concentration in the resulting filtrate.

Atmospheric Molecular Component	Fractional Atmospheric Concentration (f_{air})	Amber99 Binding Energy of Molecular Component in Simple Binding Site (E_b)	% Concentration of Air Component in Gas Filtrate
Nitrogen (N_2)	7.80840×10^{-1}	-0.2521 eV	0.1386%
Oxygen (O_2)	2.09460×10^{-1}	-0.3336 eV	0.8665%
Water vapor (H_2O)	$\sim 1.00 \times 10^{-2}$	-0.2936 eV	0.0088%
Argon (Ar)	9.340×10^{-3}	-0.0586 eV	< 1 ppm
Carbon Dioxide (CO_2)	3.870×10^{-4}	-0.6190 eV	98.9341%
Neon (Ne)	1.818×10^{-5}	-0.1021 eV	< 1 ppm
Helium (He)	5.24×10^{-6}	-0.0535 eV	< 1 ppm
Methane (CH_4)	1.79×10^{-6}	-0.3210 eV	< 1 ppm
Krypton (Kr)	1.14×10^{-6}	-0.0904 eV	< 1 ppm
Hydrogen (H_2)	5.50×10^{-7}	-0.0461 eV	< 1 ppm
Nitrous Oxide (N_2O)	3.20×10^{-7}	-0.4611 eV	0.0002%
Carbon Monoxide (CO)	1.50×10^{-7}	-0.2999 eV	< 1 ppm
Xenon (Xe)	8.70×10^{-8}	-0.1028 eV	< 1 ppm
Ozone (O_3)	2.66×10^{-8}	-0.6287 eV	0.0099%
Formaldehyde (H_2CO)	2.4×10^{-9}	-0.5542 eV	0.0001%
Ethane (C_2H_6)	2.0×10^{-9}	-0.6816 eV	0.0058%
Hydrogen Chloride (HCl)	1.0×10^{-9}	-0.3833 eV	< 1 ppm
Methyl Chloride (CH_3Cl)	7.0×10^{-10}	-0.6842 eV	0.0022%
Carbonyl Sulfide (OCS)	6.0×10^{-10}	-0.7324 eV	0.0123%
Acetylene (C_2H_2)	3.0×10^{-10}	-0.5079 eV	< 1 ppm
Sulfur Dioxide (SO_2)	3.0×10^{-10}	-0.7650 eV	0.0216%
Nitric Oxide (NO)	3.0×10^{-10}	-0.3052 eV	< 1 ppm
Hydrogen Peroxide (H_2O_2)	2.0×10^{-10}	-0.4974 eV	< 1 ppm
Hydrogen Cyanide (HCN)	1.7×10^{-10}	-0.5523 eV	< 1 ppm
Nitric Acid (HNO_3)	5.0×10^{-11}	-0.4311 eV	< 1 ppm
Ammonia (NH_3)	5.0×10^{-11}	-0.1887 eV	< 1 ppm
Nitrogen Dioxide (NO_2)	2.3×10^{-11}	-0.5395 eV	< 1 ppm
Hypochlorous Acid (HOCl)	7.7×10^{-12}	-0.5970 eV	< 1 ppm
Hydrogen Iodide (HI)	3.0×10^{-12}	-0.4993 eV	< 1 ppm
Hydrogen Bromide (HBr)	1.7×10^{-12}	-0.4707 eV	< 1 ppm
Hydroxyl radical (OH^-)	4.4×10^{-14}	-0.3443 eV	< 1 ppm
Hydrogen Fluoride (HF)	1.0×10^{-14}	-0.2439 eV	< 1 ppm
Chlorine Monoxide (ClO)	1.0×10^{-14}	-0.6515 eV	< 1 ppm
Formic Acid (HCOOH)	1.0×10^{-14}	-0.7281 eV	< 1 ppm
Carbonyl Fluoride (COF_2)	1.0×10^{-14}	-0.3756 eV	< 1 ppm
Sulfur Hexafluoride (SF_6)	1.0×10^{-14}	0.3578 eV	< 1 ppm
Hydrogen Sulfide (H_2S)	1.0×10^{-14}	-0.3699 eV	< 1 ppm
Phosphine (PH_3)	1.0×10^{-20}	-0.4062 eV	< 1 ppm

Many proteins and enzymes have binding sites for carbon dioxide. For example, hemoglobin reversibly binds CO_2, forming carbamino hemoglobin. A zinc enzyme present in red blood cells, carbonic

anhydrase,[3231] catalyzes the hydration of dissolved carbon dioxide to bicarbonate ion, so this enzyme has receptors for both CO_2 and H_2O. The first step in chlorophyllic photosynthesis, in which CO_2 is added to a 5-carbon sugar, is catalyzed by ribulose biphosphate carboxylase, probably the world's most abundant enzyme because it accounts for more than half the soluble protein in every green leaf on Earth.[3232] (This enzyme effectively has two separate CO_2 binding sites, along with a third oxygenase site that binds O_2.[3233])

H.2 Binding Sites for Other Simple Molecules

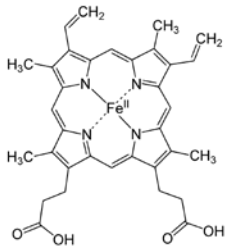

Oxygen (O_2) is reversibly bound by a variety of molecules. Oxygen transport pigments are often conjugated proteins, that is, proteins complexed with another organic molecule or with one or more metal atoms. Transport pigments contain metal atoms such as Cu^{++} or Fe^{++}, creating binding sites to which oxygen can reversibly attach. Besides hemoglobin (MW 68,000) and myoglobin (MW 17,000) in humans (the Fe^{++} site in heme reversibly binds O_2; image, right), other natural respiratory pigments include hemocyanin,[3234] a blue copper-based pigment found in molluscs and crustaceans (MW 1-7 million) and chlorocruorin,[3235] a green iron-based pigment found in marine polychaete worms (MW 3 million), both of which are only about 25% as efficient as oxygen carriers as hemoglobin;[3236] and hemerythrin,[3237] a purple iron-based pigment found in some molluscs and worms (MW 100,000), about 10% as efficient as hemoglobin.[3238] Artificial reversible oxygen-binding molecules have also been studied, including cobalt-based porphyrins such as coboglobin (a cobalt-based analog to hemoglobin) and cobaltodihistidine,[3239]

[3231] Devlin TM, ed. Textbook of Biochemistry with Clinical Correlations. John Wiley & Sons, New York, 1986; https://www.amazon.com/Textbook-Biochemistry-Clinical-Correlations-publication/dp/0471814628/.

[3232] Zubay G. Biochemistry, Second Edition. Macmillan, New York, 1988; https://www.amazon.com/Biochemistry-2ND-Geoffrey-Zubay/dp/B000O8QNJU/.

[3233] Stec B. Structural mechanism of RuBisCO activation by carbamylation of the active site lysine. Proc Natl Acad Sci U S A. 2012 Nov 13;109(46):18785-90; https://www.pnas.org/content/109/46/18785. Van Lun M, Hub JS, van der Spoel D, Andersson I. CO_2 and O_2 distribution in Rubisco suggests the small subunit functions as a CO_2 reservoir. J Am Chem Soc. 2014 Feb 26;136(8):3165-71; http://cmb.bio.uni-goettingen.de/pub/VanLun_JACS2014.pdf or https://biophys.uni-saarland.de/pub/VanLun_JACS2014.pdf.

[3234] https://en.wikipedia.org/wiki/Hemocyanin.
[3235] https://en.wikipedia.org/wiki/Chlorocruorin.

[3236] Wolvekamp HP. The evolution of oxygen transport. In: Macfarlane RG, Robb-Smith AHT, eds. Functions of the Blood. Academic Press, New York, 1961, pp. 1-72; https://www.amazon.com/dp/0124642500/.

[3237] https://en.wikipedia.org/wiki/Hemerythrin.

[3238] Mill PJ. Respiration in the Invertebrates. St. Martin's Press, New York, 1972; https://www.amazon.com/dp/0333137116/.

[3239] Michaelis L. Molecular oxygen as a ligand in metal porphyrins and other metal-complex compounds. Fed Proc 1948 Sep;7(3):509-514; https://pubmed.ncbi.nlm.nih.gov/18886080/. Hearon JZ, Burke D, Schade AL. Physicochemical studies of reversible and irreversible complexes of cobalt, histidine, and molecular oxygen. J Natl Cancer Inst 1949 Feb; 9(4):337-377; https://books.google.com/books?hl=en&lr=&id=BMPhx6DNFToC&oi=fnd&pg=PA337. Hoffman BM, Petering DH. Coboglobins: oxygen-carrying cobalt-reconstituted hemoglobin and myoglobin. Proc Natl Acad Sci U S A. 1970 Oct;67(2):637-43; https://www.ncbi.nlm.nih.gov/pmc/articles/pmid/4331717/. De Sanctis G, Falcioni G, Grelloni F, Desideri A, Polizio F, Giardina B, Ascoli F, Brunori M. Mini-myoglobin. Electron paramagnetic resonance and reversible oxygenation of the cobalt derivative. J Mol Biol. 1991 Dec 5;222(3):637-43; https://pubmed.ncbi.nlm.nih.gov/1660928/. Marden MC, Kiger L, Poyart C, Rashid AK, Kister J, Stetzkowski-Marden F, Caron G, Haque M, Moens L. Modulation of the oxygen affinity of cobalt-porphyrin by globin. FEBS Lett. 2000 Apr 28;472(2-3):221-4; https://core.ac.uk/download/pdf/81105789.pdf.

other metallic porphyrins,[3240] simple iron-indigo compounds,[3241] iridium complexes such as chloro-carbonyl-bis(triphenylphosphine)-iridium,[3242] a simple cobalt/ammonia complex,[3243] zeolite-bound divalent chromium,[3244] nonporphyrin lacunar iron complexes,[3245] and heme-linked NADPH oxidase.[3246] Unlike hemoglobin, hemocyanin, hemerythrin and coboglobin are not poisoned by carbon monoxide.

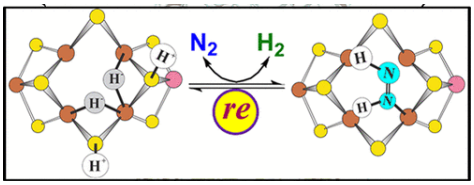

Binding sites for **nitrogen** (N_2) are also available for examination. Certain microorganisms, including the *Rhizobium* genera of bacteria found on leguminous plant roots, some free-living soil bacteria such as the *Azotobacter*, and a few species of blue-green algae such as *Cyanobacteria*, achieve biological fixation of atmospheric N_2 using an enzyme complex called nitrogenase.[3247] Nitrogenase is extremely labile in the presence of oxygen, but its nitrogen binding site (image above, left) has been examined extensively[3248] and might reward further study.

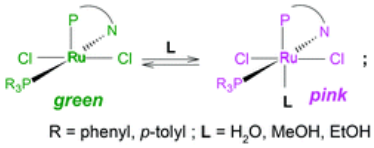

A few binding sites are also known for **water**. For example, helical transmembrane proteins acquire "buried water" in internal voids,[3249] a lithium-organic framework reversibly binds water,[3250] and the five-coordinate, square-pyramidal *trans*-$RuCl_2(P–N)(PPh_3)$ complex reversibly binds **water**, **methanol** and **ethanol** (image above,

---

[3240] Hearon JZ, Burke D, Schade AL. Physicochemical studies of reversible and irreversible complexes of cobalt, histidine, and molecular oxygen. J Natl Cancer Inst 1949 Feb; 9(4):337-377; https://books.google.com/books?hl=en&lr=&id=BMPhx6DNFToC&oi=fnd&pg=PA337. Falk JE. Porphyrins and Metalloporphyrins. Elsevier Publishing, New York, 1964; https://www.amazon.com/Porphyrins-Metalloporphyrins-Coordination-Chemistry-Laboratory/dp/0444402063/. Lapidot A, Irving CS. The electronic structure of coordinated oxygen. In: Hayaishi O, ed. Molecular Oxygen in Biology: Topics in Molecular Oxygen Research. American Elsevier, New York, 1974; https://www.amazon.com/Molecular-Oxygen-Biology-Topics-Research/dp/072044148X/.

[3241] Larkworthy LF. 783. Iron bisindigo, a compound reported to exhibit oxygen carrying properties. J Chem Soc. 1961:4025-4033; https://pubs.rsc.org/en/content/articlelanding/1961/jr/jr9610004025/unauth#!divAbstract.

[3242] Vaska L. Oxygen-Carrying Properties of a Simple Synthetic System. Science. 1963 May 17;140(3568):809-10; https://science.sciencemag.org/content/140/3568/809/tab-pdf. Vaska L, Chen LS, Senoff CV. Oxygen-carrying iridium complexes: kinetics, mechanism, and thermodynamics. Science. 1971 Nov 5;174(4009):587-9; https://science.sciencemag.org/content/174/4009/587/tab-pdf.

[3243] Hearon JZ, Burke D, Schade AL. Physicochemical studies of reversible and irreversible complexes of cobalt, histidine, and molecular oxygen. J Natl Cancer Inst 1949 Feb; 9(4):337-377; https://books.google.com/books?hl=en&lr=&id=BMPhx6DNFToC&oi=fnd&pg=PA337.

[3244] Kellerman R, Hutta PJ, Klier K. Reversible oxygen binding by divalent chromium (II) ion exchanged molecular sieve. J Amer Chem Soc 1974 Sep 1; 96(18):5946-5947; https://pubs.acs.org/doi/pdf/10.1021/ja00825a048.

[3245] Herron N, Cameron JH, Neer GL, Busch DH. A totally synthetic (nonporphyrin) iron(II) dioxygen carrier that is fully functional under ambient conditions. J Am Chem Soc. 1983 Jan 1; 105(2):298-301; https://pubs.acs.org/doi/pdf/10.1021/ja00340a029.

[3246] Youngson C, Nurse C, Yeger H, Cutz E. Oxygen sensing in airway chemoreceptors. Nature. 1993 Sep 9;365(6442):153-5; https://pubmed.ncbi.nlm.nih.gov/8371757/.

[3247] https://en.wikipedia.org/wiki/Nitrogenase.

[3248] Hoffman BM, Lukoyanov D, Yang ZY, Dean DR, Seefeldt LC. Mechanism of nitrogen fixation by nitrogenase: the next stage. Chem Rev. 2014 Apr 23;114(8):4041-62; https://www.ncbi.nlm.nih.gov/pmc/articles/PMC4012840/.

[3249] Renthal R. Buried water molecules in helical transmembrane proteins. Protein Sci. 2008 Feb;17(2):293-8; https://www.ncbi.nlm.nih.gov/pmc/articles/PMC2222723/.

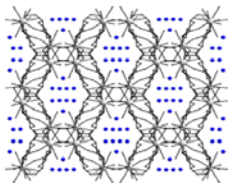

right);[3251] a similar ruthenium complex binds **carbon monoxide** (CO) and **ammonia** (NH_3).[3252] Various materials also form 3D networks that can reversibly bind crystallization **water** molecules (image, left).[3253] Many molecules bind water reversibly, including a wide variety of deliquescent crystals, efflorescent minerals, hydrophilic and polar amino acids, and numerous enzymes such as carbonic anhydrase, hydrolases and dehydratases,[3254] and binding sites for frozen water-ice also are known.[3255]

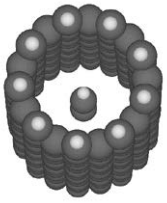

Simple binding sites for small hydrocarbon molecules such as **methane** (CH_4)[3256] and **acetylene** (C_2H_2)[3257] (image, left) have been reported in the literature, or have been computationally simulated.

Previous work has considered binding sites for **ethanol**.[3258] A computational modeling and simulation effort will be required to create highly-selective binding site designs for ethanol. A number of receptors for ethanol are already known in the biological literature. For example, the functioning of several proteins is altered by ethanol, including the Drosophila odorant-binding protein LUSH (image, right), human PKCα and human Glycine Receptor α1.

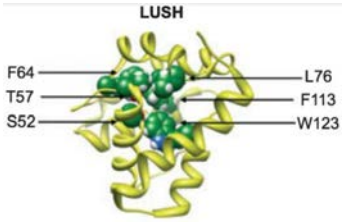

[3250] El Osta R, Frigoli M, Marrot J, Guillou N, Chevreau H, Walton RI, Millange F. A lithium-organic framework with coordinatively unsaturated metal sites that reversibly binds water. Chem Commun (Camb). 2012 Nov 7;48(86):10639-41; https://pubmed.ncbi.nlm.nih.gov/23001396/.

[3251] Ma ES, Patrick BO, James BR. Reversible binding of water, methanol, and ethanol to a five-coordinate ruthenium(II) complex. Dalton Trans. 2013 Mar 28;42(12):4291-8; https://pubmed.ncbi.nlm.nih.gov/23344393/.

[3252] Ma ES, Mudalige DC, James BR. Binding of CO and NH_3 at a five-coordinate Ru(II) centre in the solid state and in solution. Dalton Trans. 2013 Oct 7;42(37):13628-34; https://pubmed.ncbi.nlm.nih.gov/23900615/.

[3253] Zheng Y, Kustaryono D, Kerbellec N, Guillou O, Gérault Y, Le Dret F, Daiguebonne C. The lanthanide-containing cyclohexane-tri-carboxylate coordination polymers re-investigated," Inorganica Chimica Acta 2009 May 15;362(7):2123-2126; https://www.sciencedirect.com/science/article/abs/pii/S002016930800604X.

[3254] Devlin TM, ed. Textbook of Biochemistry with Clinical Correlations. John Wiley & Sons, New York, 1986; https://www.amazon.com/Textbook-Biochemistry-Clinical-Correlations-publication/dp/0471814628/.

[3255] Hudait A, Qiu Y, Odendahl N, Molinero V. Hydrogen-Bonding and Hydrophobic Groups Contribute Equally to the Binding of Hyperactive Antifreeze and Ice-Nucleating Proteins to Ice. J Am Chem Soc. 2019 May 15;141(19):7887-7898; https://par.nsf.gov/servlets/purl/10092995.

[3256] Nordlund P, Dalton H, Eklund H. The active site structure of methane monooxygenase is closely related to the binuclear iron center of ribonucleotide reductase. FEBS Lett. 1992 Aug 3;307(3):257-62; https://www.sciencedirect.com/science/article/pii/001457939280690I/pdf. Rana MK, Koh HS, Zuberi H, Siegel DJ. Methane Storage in Metal-Substituted Metal−Organic Frameworks: Thermodynamics, Usable Capacity, and the Impact of Enhanced Binding Sites. J Phys Chem C. 2014;118:2929-2942; http://www-personal.umich.edu/~djsiege/Energy_Storage_Lab/Publications_files/JPCC_CH4.pdf.

[3257] Merkle RC. Binding sites for use in a simple assembler. Nanotechnology 1997 Mar;8(1):23-28; http://www.zyvex.com/nanotech/bindingSites.html.

[3258] Freitas RA Jr. The Whiskey Machine: Nanofactory-Based Replication of Fine Spirits and Other Alcohol-Based Beverages. IMM Report No. 47, May 2016; Section 5.3.3, "Receptor-Based Purification of Ethanol and Water"; http://www.imm.org/Reports/rep047.pdf.

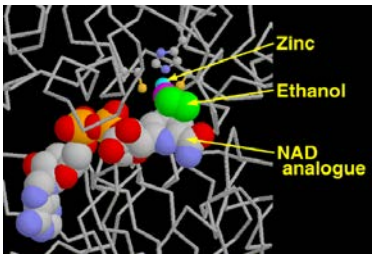

Coordination of ethanol in LUSH includes hydrogen bonding of S52 and T57 with the alcohol hydroxyl group and hydrophobic interactions of F64, L76, F113, and W123 with the alkyl chain.[3259] Ethanol binds directly to the receptors for acetylcholine, serotonin, and GABA, and to the NMDA receptors for glutamate.[3260] Ethanol also binds to the 9 amino-acid hydrophobic core of the alcohol dehydrogenase enzyme (image, left), although the site binds other alcohols besides ethanol.[3261] One researcher reports[3262] developing ultrasensitive ethanol receptors (USERs) by manipulating the Loop 2 (L2) structure of glycine receptors (GlyRs) and γ-amino butyric acid subtype-A receptors (GABAARs) which can significantly increase ethanol sensitivity of mutant receptors and can create ethanol receptors that respond to extremely low ethanol concentrations (≤ 1 mM or ≤46 mg/L) that would be too low to affect native receptors.

Binding sites for **glucose** are common in nature. For example, cellular energy metabolism starts with the conversion of the 6-carbon glucose to two 3-carbon fragments (pyruvate or lactate), the first step in glycolysis. This is catalyzed by the enzyme hexokinase,[3263] which has binding sites for both glucose[3264] and ADP. Another common cellular mechanism is the glucose transporter molecule, which carries glucose across cell membranes and contains several binding sites.[3265] Other glucose-binding proteins are found in the intestines,[3266] liver,[3267] kidney, adipose tissue, and elsewhere.

[3259] Howard RJ, Slesinger PA, Davies DL, Das J, Trudell JR, Harris RA. Alcohol-binding sites in distinct brain proteins: the quest for atomic level resolution. Alcohol Clin Exp Res. 2011 Sep;35(9):1561-73; https://www.ncbi.nlm.nih.gov/pmc/articles/PMC3201783/.

[3260] Murail S, Wallner B, Trudell JR, Bertaccini E, Lindahl E. Microsecond simulations indicate that ethanol binds between subunits and could stabilize an open-state model of a glycine receptor. Biophys J. 2011 Apr 6;100(7):1642-50; https://www.ncbi.nlm.nih.gov/pmc/articles/PMC3072665/.

[3261] http://www.chembio.uoguelph.ca/educmat/chm455/adh.ppt.

[3262] Karan Muchhala. Developing Ultrasensitive Ethanol Receptors (USERS) As Novel Tools for Alcohol Research: Optimizing Loop 2 Mutations in alpha1 GlyRs. PhD thesis, Univ. Southern California, 2013; http://gradworks.umi.com/15/51/1551520.html.

[3263] https://en.wikipedia.org/wiki/Hexokinase.

[3264] Mulichak AM, Wilson JE, Padmanabhan K, Garavito RM. The structure of mammalian hexokinase-1. Nat Struct Biol. 1998 Jul;5(7):555-60; https://pubmed.ncbi.nlm.nih.gov/9665168/.

[3265] Simpson IA, Cushman SW. Hormonal regulation of mammalian glucose transport. Annu Rev Biochem. 1986;55:1059-89; https://www.annualreviews.org/doi/abs/10.1146/annurev.bi.55.070186.005211. Baldwin SA, Lienhard GE. Purification and reconstitution of glucose transporter from human erythrocytes. Methods Enzymol 1989; 174:39-50; https://www.sciencedirect.com/science/article/pii/0076687989740088.

[3266] Zubay G. Biochemistry, Second Edition. Macmillan, New York, 1988; https://www.amazon.com/Biochemistry-2ND-Geoffrey-Zubay/dp/B000O8QNJU/.

[3267] Devlin TM, ed. Textbook of Biochemistry with Clinical Correlations. John Wiley & Sons, New York, 1986; https://www.amazon.com/Textbook-Biochemistry-Clinical-Correlations-publication/dp/0471814628/.

H.3 Binding Sites for Cryoprotectant Molecules

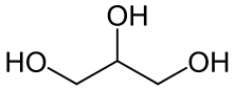

Binding sites are known for several cryoprotectant molecules. For example, the enzyme 3-dehydroquinate dehydratase (dehydroquinase or "MtDHQase") found in *Mycobacterium tuberculosis* has a binding site for **glycerol**, illustrated in the figure below.[3268] (Glycerol, or $C_3H_8O_3$, is a linear chain molecule; image, above). From the description of the figure in the paper: "The binding of glycerol to this pocket conserves most of the interactions formed by the guanidinium group of Arg19 and makes additional interactions with its three hydroxyl groups. The glycerol molecule bound to the active site flexible loop pocket forms direct hydrogen bonding interactions with the main-chain atoms of Asn12, Arg15, Arg18, and Arg19 and forms water-mediated hydrogen bonds with the side-chain atoms of Asn12 and Asp88 as well as with the main-chain atoms of Gly17, Arg18, Arg19, and Gly25. Hydrogen bond interactions are indicated with black dashed lines."

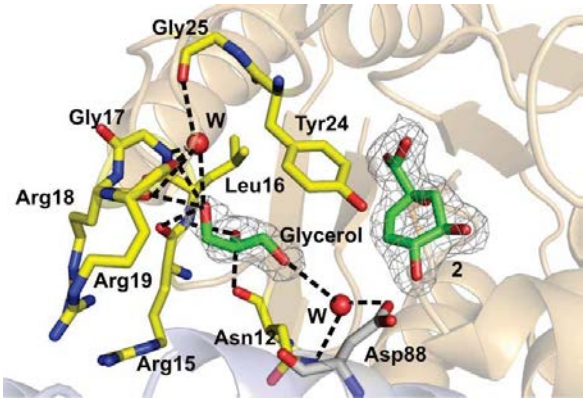

Glycerol dehydrogenase,[3269] glycerol kinase,[3270] and coenzyme B_{12}-dependent diol dehydratase[3271] have glycerol binding sites, and aquaglyceroporin[3272] also has a high affinity for glycerol.

The cryoprotectant molecule **dimethyl sulfoxide (DMSO)** (image, right) has a well-known binding site in a molybdenum-containing enzyme called DMSO reductase that is

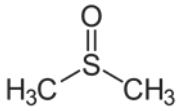

[3268] Dias MV, Snee WC, Bromfield KM, Payne RJ, Palaninathan SK, Ciulli A, Howard NI, Abell C, Sacchettini JC, Blundell TL. Structural investigation of inhibitor designs targeting 3-dehydroquinate dehydratase from the shikimate pathway of *Mycobacterium tuberculosis*. Biochem J. 2011 Jun 15;436(3):729-39; https://pdfs.semanticscholar.org/1caf/5c7423b314d21e979bfb7d8b7abedc52d856.pdf.

[3269] Ruzheinikov SN, Burke J, Sedelnikova S, Baker PJ, Taylor R, Bullough PA, Muir NM, Gore MG, Rice DW. Glycerol dehydrogenase. structure, specificity, and mechanism of a family III polyol dehydrogenase. Structure. 2001 Sep;9(9):789-802; https://www.cell.com/fulltext/S0969-2126(01)00645-1.

[3270] Yeh JI, Kettering R, Saxl R, Bourand A, Darbon E, Joly N, Briozzo P, Deutscher J. Structural characterizations of glycerol kinase: unraveling phosphorylation-induced long-range activation. Biochemistry. 2009 Jan 20;48(2):346-56; https://www.ncbi.nlm.nih.gov/pmc/articles/PMC3158585/.

[3271] Bilić L, Barić D, Banhatti RD, Smith DM, Kovačević B. Computational Study of Glycerol Binding within the Active Site of Coenzyme B12-Dependent Diol Dehydratase. J Phys Chem B. 2019 Jul 25;123(29):6178-6187; https://pubmed.ncbi.nlm.nih.gov/31251060/.

[3272] Rodriguez RA, Chan R, Liang H, Chen LY. Quantitative study of unsaturated transport of glycerol through aquaglyceroporin that has high affinity for glycerol. RSC Adv. 2020;10(56):34203-34214; https://www.ncbi.nlm.nih.gov/pmc/articles/PMC7494219/.

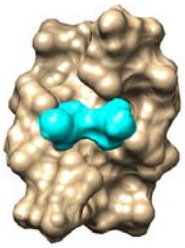

found exclusively in bacteria and archaea organisms;[3273] the crystal structure of this enzyme has been mapped to at least 1.9 Å resolution.[3274] A DMSO binding site has also been found in globular trimeric adiponectin,[3275] and DMSO has some unexpected binding affinity for Z-DNA (image, left, showing 2 docked DMSO molecules).[3276]

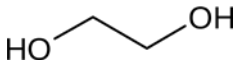

Finally, **ethylene glycol** (image, right) binds to "cryptic pockets" in proteins[3277] and to the active site of the PEPC (phosphoenolpyruvate carboxylase) enzyme,[3278] and has demonstrated at least weak binding affinity to an "indentation binding site" in a particular amorphous polymer.[3279] The ability to enzymatically metabolize ethylene glycol has been engineered into *E. coli* bacteria.[3280] Antibody-based binding sites for polyethylene glycol polymers have also been reported.[3281]

[3273] McEwan AG, Ridge JP, McDevitt CA, Hugenholtz P. The DMSO Reductase Family of Microbial Molybdenum Enzymes; Molecular Properties and Role in the Dissimilatory Reduction of Toxic Elements. Geomicrobiol J. 2002;19(1):3-21; https://www.tandfonline.com/doi/abs/10.1080/014904502317246138. See also: https://en.wikipedia.org/wiki/DMSO_reductase.

[3274] McAlpine AS, McEwan AG, Bailey S. The high resolution crystal structure of DMSO reductase in complex with DMSO. J Mol Biol. 1998 Jan 30;275(4):613-23; https://pubmed.ncbi.nlm.nih.gov/9466935/.

[3275] Yu D, Zhang C, Qin P, Cornish PV. Characterization of Dimethyl Sulfoxide Binding Sites on Globular Trimeric Adiponectin. Proc 10th IASTED International Conference on Biomedical Engineering (BioMed 2013), Feb 2013; https://pdfs.semanticscholar.org/aa17/c84a08033b727f39a63e5f02a53b592461ff.pdf.

[3276] Tunçer S, Gurbanov R, Sheraj I, Solel E, Esenturk O, Banerjee S. Low dose dimethyl sulfoxide driven gross molecular changes have the potential to interfere with various cellular processes. Sci Rep. 2018 Oct 4;8(1):14828; https://www.ncbi.nlm.nih.gov/pmc/articles/pmid/30287873/.

[3277] Bansia H, Mahanta P, Yennawar NH, Ramakumar S. Small Glycols Discover Cryptic Pockets on Proteins for Fragment-based Approaches. bioRxiv, 2 Aug 2020; https://www.biorxiv.org/content/10.1101/605121v2.full.

[3278] Schlieper D, Förster K, Paulus JK, Groth G. Resolving the activation site of positive regulators in plant phosphoenolpyruvate carboxylase. Mol Plant. 2014 Feb;7(2):437-40; https://www.cell.com/molecular-plant/pdf/S1674-2052(14)60299-9.pdf.

[3279] Chunsrivirot S, Trout BL. Free energy of binding of a small molecule to an amorphous polymer in a solvent. Langmuir. 2011 Jun 7;27(11):6910-9; https://pubmed.ncbi.nlm.nih.gov/21561080/..

[3280] Pandit AV, Harrison E, Mahadevan R. Engineering *Escherichia Coli* for the Utilization of Ethylene Glycol. Microbial Cell Factories 2021;20:22; https://microbialcellfactories.biomedcentral.com/articles/10.1186/s12934-021-01509-2.

[3281] Lee CC, Su YC, Ko TP, Lin LL, Yang CY, Chang SS, Roffler SR, Wang AH. Structural basis of polyethylene glycol recognition by antibody. J Biomed Sci. 2020 Jan 7;27(1):12; https://www.ncbi.nlm.nih.gov/pmc/articles/PMC6945545/.

Appendix I. Cell Metabolites

Appendix I. Number, volume, mass, and power draw of sorting rotors needed to extract cell metabolite molecular species from interstitial and intracellular fluid compartments in a human body to 1% of initial concentrations in ~1 hour

Molecular Species	Molec. Weight (g/mole)	Initial Conc. (mols/nm^3)	N_{fleet} (rotors)	V_{fleet} (cm^3)	M_{fleet} (gm)	Average P_{fleet} (W)
glutamate (the anion of glutamic acid)	147.3	5.07×10^{-2}	3.00×10^{17}	4.12×10^{-1}	6.00×10^{-1}	2.71×10^{-3}
glutathione	307.3	8.98×10^{-3}	1.24×10^{17}	1.70×10^{-1}	2.48×10^{-1}	2.65×10^{-2}
fructose-1,6-bisphosphate	340.1	7.92×10^{-3}	1.17×10^{17}	1.61×10^{-1}	2.34×10^{-1}	2.29×10^{-2}
ATP	507.2	5.07×10^{-3}	9.78×10^{16}	1.34×10^{-1}	1.96×10^{-1}	3.14×10^{-2}
UDP-N-acetyl-glucosamine	607.4	4.86×10^{-3}	9.90×10^{16}	1.36×10^{-1}	1.98×10^{-1}	3.16×10^{-2}
hexose-P	260.1	4.65×10^{-3}	8.07×10^{16}	1.11×10^{-1}	1.61×10^{-1}	3.22×10^{-2}
UTP	484.1	4.38×10^{-3}	8.88×10^{16}	1.22×10^{-1}	1.78×10^{-1}	3.28×10^{-2}
GTP	523.2	2.59×10^{-3}	6.58×10^{16}	9.03×10^{-2}	1.32×10^{-1}	3.54×10^{-2}
dTTP	482.2	2.43×10^{-3}	6.22×10^{16}	8.53×10^{-2}	1.24×10^{-1}	3.49×10^{-2}
aspartate	133.1	2.22×10^{-3}	4.50×10^{16}	6.17×10^{-2}	9.00×10^{-2}	3.59×10^{-2}
valine	117.2	2.11×10^{-3}	4.25×10^{16}	5.83×10^{-2}	8.50×10^{-2}	3.55×10^{-2}
glutamine	146.1	2.01×10^{-3}	4.32×10^{16}	5.93×10^{-2}	8.64×10^{-2}	3.61×10^{-2}
6-phospho-D-gluconate	276.1	2.01×10^{-3}	4.94×10^{16}	6.78×10^{-2}	9.88×10^{-2}	3.63×10^{-2}
CTP	483.2	1.43×10^{-3}	4.52×10^{16}	6.20×10^{-2}	9.04×10^{-2}	3.68×10^{-2}
NAD	663.4	1.37×10^{-3}	4.72×10^{16}	6.48×10^{-2}	9.44×10^{-2}	3.66×10^{-2}
alanine	89.1	1.32×10^{-3}	3.03×10^{16}	4.16×10^{-2}	6.06×10^{-2}	3.74×10^{-2}
UDP-glucose	566.3	1.32×10^{-3}	4.46×10^{16}	6.12×10^{-2}	8.92×10^{-2}	3.68×10^{-2}
glutathionedisulfide	612.6	1.27×10^{-3}	4.43×10^{16}	6.08×10^{-2}	8.86×10^{-2}	3.73×10^{-2}
uridine	244.2	1.11×10^{-3}	3.37×10^{16}	4.62×10^{-2}	6.74×10^{-2}	3.76×10^{-2}
citrate	192.1	1.06×10^{-3}	3.11×10^{16}	4.27×10^{-2}	6.22×10^{-2}	3.75×10^{-2}
UDP	404.2	9.51×10^{-4}	3.41×10^{16}	4.68×10^{-2}	6.82×10^{-2}	3.74×10^{-2}
malate	134.1	8.98×10^{-4}	2.61×10^{16}	3.58×10^{-2}	5.22×10^{-2}	3.70×10^{-2}
3-phosphoglycerate	186.1	7.92×10^{-4}	2.60×10^{16}	3.57×10^{-2}	5.20×10^{-2}	3.72×10^{-2}
glycerate	106.1	7.39×10^{-4}	2.21×10^{16}	3.03×10^{-2}	4.42×10^{-2}	3.60×10^{-2}
coenzyme-A	767.5	7.39×10^{-4}	3.36×10^{16}	4.61×10^{-2}	6.72×10^{-2}	3.68×10^{-2}
citruline	175.2	7.39×10^{-4}	2.46×10^{16}	3.38×10^{-2}	4.92×10^{-2}	3.64×10^{-2}
pentose-P	230.1	6.87×10^{-4}	2.49×10^{16}	3.42×10^{-2}	4.98×10^{-2}	3.57×10^{-2}
glucosamine-6-phosphate	259.2	6.34×10^{-4}	2.44×10^{16}	3.35×10^{-2}	4.88×10^{-2}	3.55×10^{-2}
acetylphosphate	138.0	5.81×10^{-4}	2.02×10^{16}	2.77×10^{-2}	4.04×10^{-2}	3.38×10^{-2}
gluconolactone	178.1	5.28×10^{-4}	2.02×10^{16}	2.77×10^{-2}	4.04×10^{-2}	3.33×10^{-2}
GDP	443.2	3.59×10^{-4}	1.94×10^{16}	2.66×10^{-2}	3.88×10^{-2}	2.81×10^{-2}
acetyl-CoA	809.6	3.22×10^{-4}	2.06×10^{16}	2.83×10^{-2}	4.12×10^{-2}	2.65×10^{-2}
carbamyl-aspartate	176.1	3.12×10^{-4}	1.47×10^{16}	2.02×10^{-2}	2.94×10^{-2}	2.63×10^{-2}
succinate	118.1	3.01×10^{-4}	1.32×10^{16}	1.81×10^{-2}	2.64×10^{-2}	2.55×10^{-2}
arginine	174.2	3.01×10^{-4}	1.43×10^{16}	1.96×10^{-2}	2.86×10^{-2}	2.53×10^{-2}
UDP-glucaronate	580.3	3.01×10^{-4}	1.84×10^{16}	2.52×10^{-2}	3.68×10^{-2}	2.53×10^{-2}
ADP	427.2	2.90×10^{-4}	1.69×10^{16}	2.32×10^{-2}	3.38×10^{-2}	2.49×10^{-2}
asparagine	132.1	2.69×10^{-4}	1.26×10^{16}	1.73×10^{-2}	2.52×10^{-2}	2.37×10^{-2}
2-ketoglutarate	146.1	2.32×10^{-4}	1.18×10^{16}	1.62×10^{-2}	2.36×10^{-2}	2.20×10^{-2}
lysine	146.2	2.11×10^{-4}	1.11×10^{16}	1.52×10^{-2}	2.22×10^{-2}	2.04×10^{-2}
proline	115.1	2.01×10^{-4}	1.03×10^{16}	1.41×10^{-2}	2.06×10^{-2}	2.03×10^{-2}
dTDP	402.2	2.01×10^{-4}	1.34×10^{16}	1.84×10^{-2}	2.68×10^{-2}	2.03×10^{-2}
dihydroxyacetone-phosphate	170.1	1.95×10^{-4}	1.10×10^{16}	1.51×10^{-2}	2.20×10^{-2}	1.99×10^{-2}
homocysteine	135.2	1.95×10^{-4}	1.05×10^{16}	1.44×10^{-2}	2.10×10^{-2}	2.01×10^{-2}
CMP	323.2	1.90×10^{-4}	1.24×10^{16}	1.70×10^{-2}	2.48×10^{-2}	1.97×10^{-2}
isoleucine+leucine	131.1	1.58×10^{-4}	9.20×10^{15}	1.26×10^{-2}	1.84×10^{-2}	1.76×10^{-2}
deoxyribose-5-P	214.1	1.58×10^{-4}	1.02×10^{16}	1.40×10^{-2}	2.04×10^{-2}	1.76×10^{-2}

AMP	347.2	1.48×10^{-4}	1.08×10^{16}	1.48×10^{-2}	2.16×10^{-2}	1.67×10^{-2}
inosine-monophosphate	348.2	1.43×10^{-4}	1.06×10^{16}	1.45×10^{-2}	2.12×10^{-2}	1.64×10^{-2}
PRPP	390.1	1.37×10^{-4}	1.06×10^{16}	1.45×10^{-2}	2.12×10^{-2}	1.60×10^{-2}
succinyl-CoA	867.6	1.21×10^{-4}	1.16×10^{16}	1.59×10^{-2}	2.32×10^{-2}	1.45×10^{-2}
inosine-triphosphate	508.2	1.06×10^{-4}	9.59×10^{15}	1.32×10^{-2}	1.92×10^{-2}	1.35×10^{-2}
guanine	151.1	1.00×10^{-4}	7.21×10^{15}	9.89×10^{-3}	1.44×10^{-2}	1.30×10^{-2}
S-adenosyl-L-methionine	398.4	9.51×10^{-5}	8.56×10^{15}	1.17×10^{-2}	1.71×10^{-2}	1.25×10^{-2}
phosphoenolpyruvate	168.0	9.51×10^{-5}	7.14×10^{15}	9.80×10^{-3}	1.43×10^{-2}	1.25×10^{-2}
threonine	119.1	9.51×10^{-5}	6.64×10^{15}	9.11×10^{-3}	1.33×10^{-2}	1.25×10^{-2}
FAD	785.5	8.98×10^{-5}	9.53×10^{15}	1.31×10^{-2}	1.91×10^{-2}	1.20×10^{-2}
methionine	149.2	7.39×10^{-5}	5.98×10^{15}	8.20×10^{-3}	1.20×10^{-2}	1.04×10^{-2}
2,3-dihydroxybenzoic acid	154.1	7.39×10^{-5}	6.03×10^{15}	8.27×10^{-3}	1.21×10^{-2}	1.05×10^{-2}
NADPH	744.4	6.34×10^{-5}	7.65×10^{15}	1.05×10^{-2}	1.53×10^{-2}	9.37×10^{-3}
fumarate	116.1	5.81×10^{-5}	4.91×10^{15}	6.74×10^{-3}	9.82×10^{-3}	8.76×10^{-3}
phenylpyruvate	164.2	4.75×10^{-5}	4.68×10^{15}	6.42×10^{-3}	9.36×10^{-3}	7.54×10^{-3}
NADH	663.4	4.38×10^{-5}	5.98×10^{15}	8.20×10^{-3}	1.20×10^{-2}	7.11×10^{-3}
N-acetylglucosamine-1P	221.1	4.33×10^{-5}	4.71×10^{15}	6.46×10^{-3}	9.42×10^{-3}	7.03×10^{-3}
serine	105.1	3.59×10^{-5}	3.60×10^{15}	4.94×10^{-3}	7.20×10^{-3}	6.09×10^{-3}
histidine	155.2	3.59×10^{-5}	3.91×10^{15}	5.36×10^{-3}	7.82×10^{-3}	6.10×10^{-3}
flavinmononucleotide	456.3	2.85×10^{-5}	4.27×10^{15}	5.86×10^{-3}	8.54×10^{-3}	5.11×10^{-3}
4-hydroxybenzoate	138.1	2.75×10^{-5}	3.25×10^{15}	4.46×10^{-3}	6.50×10^{-3}	4.97×10^{-3}
dGMP	347.2	2.69×10^{-5}	3.90×10^{15}	5.35×10^{-3}	7.80×10^{-3}	4.90×10^{-3}
glycerolphosphate	172.1	2.59×10^{-5}	3.28×10^{15}	4.50×10^{-3}	6.56×10^{-3}	4.72×10^{-3}
N-acetyl-ornithine	174.2	2.27×10^{-5}	3.04×10^{15}	4.17×10^{-3}	6.08×10^{-3}	4.26×10^{-3}
gluconate	196.2	2.22×10^{-5}	3.08×10^{15}	4.23×10^{-3}	6.16×10^{-3}	4.21×10^{-3}
malonyl-CoA	853.6	1.85×10^{-5}	3.76×10^{15}	5.16×10^{-3}	7.52×10^{-3}	3.64×10^{-3}
cyclic-AMP	329.2	1.85×10^{-5}	3.07×10^{15}	4.21×10^{-3}	6.14×10^{-3}	3.62×10^{-3}
dCTP	467.2	1.80×10^{-5}	3.25×10^{15}	4.46×10^{-3}	6.50×10^{-3}	3.54×10^{-3}
tyrosine	181.2	1.53×10^{-5}	2.42×10^{15}	3.32×10^{-3}	4.84×10^{-3}	3.11×10^{-3}
inosine-diphosphate	428.2	1.27×10^{-5}	2.59×10^{15}	3.55×10^{-3}	5.18×10^{-3}	2.68×10^{-3}
GMP	363.2	1.27×10^{-5}	2.50×10^{15}	3.43×10^{-3}	5.00×10^{-3}	2.67×10^{-3}
acetoacetyl-CoA	851.6	1.16×10^{-5}	2.84×10^{15}	3.90×10^{-3}	5.68×10^{-3}	2.50×10^{-3}
riboflavin	376.4	1.00×10^{-5}	2.19×10^{15}	3.00×10^{-3}	4.38×10^{-3}	2.21×10^{-3}
phenylalanine	165.2	9.51×10^{-6}	1.78×10^{15}	2.44×10^{-3}	3.56×10^{-3}	2.10×10^{-3}
aconitate	174.1	8.45×10^{-6}	1.68×10^{15}	2.30×10^{-3}	3.36×10^{-3}	1.92×10^{-3}
dATP	491.2	8.45×10^{-6}	2.09×10^{15}	2.87×10^{-3}	4.18×10^{-3}	1.92×10^{-3}
cytosine	111.1	7.39×10^{-6}	1.41×10^{15}	1.93×10^{-3}	2.82×10^{-3}	1.71×10^{-3}
shikimate	174.2	7.39×10^{-6}	1.55×10^{15}	2.13×10^{-3}	3.10×10^{-3}	1.72×10^{-3}
histidinol	141.2	6.87×10^{-6}	1.42×10^{15}	1.95×10^{-3}	2.84×10^{-3}	1.62×10^{-3}
tryptophan	204.2	6.34×10^{-6}	1.46×10^{15}	2.00×10^{-3}	2.92×10^{-3}	1.51×10^{-3}
dihydroorotate	158.1	6.34×10^{-6}	1.38×10^{15}	1.89×10^{-3}	2.76×10^{-3}	1.50×10^{-3}
quinolinate	167.1	6.34×10^{-6}	1.40×10^{15}	1.92×10^{-3}	2.80×10^{-3}	1.51×10^{-3}
ornithine	132.2	5.28×10^{-6}	1.19×10^{15}	1.63×10^{-3}	2.38×10^{-3}	1.28×10^{-3}
dAMP	331.2	4.65×10^{-6}	1.34×10^{15}	1.84×10^{-3}	2.68×10^{-3}	1.16×10^{-3}
adenosine-phosphosulfate	507.3	3.49×10^{-6}	1.23×10^{15}	1.69×10^{-3}	2.46×10^{-3}	9.03×10^{-4}
myo-inositol	180.2	3.01×10^{-6}	9.13×10^{14}	1.25×10^{-3}	1.83×10^{-3}	8.11×10^{-4}
propionyl-CoA	823.6	2.80×10^{-6}	1.20×10^{15}	1.65×10^{-3}	2.40×10^{-3}	7.59×10^{-4}
ADP-glucose	589.3	2.27×10^{-6}	9.88×10^{14}	1.36×10^{-3}	1.98×10^{-3}	6.37×10^{-4}
anthranilate	137.1	1.85×10^{-6}	6.44×10^{14}	8.84×10^{-4}	1.29×10^{-3}	5.34×10^{-4}
deoxyadenosine	251.2	1.48×10^{-6}	6.39×10^{14}	8.77×10^{-4}	1.28×10^{-3}	4.40×10^{-4}
cytidine	243.2	1.37×10^{-6}	6.07×10^{14}	8.33×10^{-4}	1.21×10^{-3}	4.12×10^{-4}
NADP+	744.4	1.11×10^{-6}	6.76×10^{14}	9.27×10^{-4}	1.35×10^{-3}	3.43×10^{-4}
guanosine	283.2	8.45×10^{-7}	4.70×10^{14}	6.45×10^{-4}	9.40×10^{-4}	2.71×10^{-4}
adenine	135.1	7.92×10^{-7}	3.88×10^{14}	5.32×10^{-4}	7.76×10^{-4}	2.56×10^{-4}
deoxyguanosine	267.2	2.75×10^{-7}	2.40×10^{14}	3.29×10^{-4}	4.80×10^{-4}	1.00×10^{-4}
adenosine	267.2	6.87×10^{-8}	1.12×10^{14}	1.54×10^{-4}	2.24×10^{-4}	2.88×10^{-5}
Average	*320.1*					
Subtotals			2.19×10^{18}	3.00	4.37	1.69

Missing metabolites (24) *	320.1	1×10^{-4}	2.01×10^{17}	0.28	0.40	0.31
Missing metabolites (308) *	320.1	1×10^{-5}	6.49×10^{17}	0.89	1.30	0.68
Missing metabolites (1898) *	320.1	1×10^{-6}	1.01×10^{18}	1.39	2.02	0.59
Missing metabolites (9898) *	320.1	1×10^{-7}	1.40×10^{18}	1.92	2.79	0.40
Subtotals (12,127 added metabolites)			3.26×10^{18}	4.47	6.51	1.98
TOTALS			**5.44×10^{18}**	**7.47**	**10.88**	**3.67**

* inferred to exist at these four concentration levels, using the procedure described in Section 4.10.1.3.

Appendix J. Blood Plasma Leakage Molecules

Appendix J. Number, volume, mass, and power draw of sorting rotors needed to extract leaked blood plasma molecular species from interstitial and intracellular fluid compartments in a human body to 1% of initial concentrations in ~1 hour

Molecular Species	Molec. Weight (g/mole)	Initial Conc. (mols/nm^3)	N_{fleet} (rotors)	V_{fleet} (cm^3)	M_{fleet} (gm)	Average P_{fleet} (W)
Fatty acids, total	200	1.67×10^{-3}	4.12×10^{16}	5.65×10^{-2}	8.24×10^{-2}	3.59×10^{-2}
Lipids, total	400	1.57×10^{-3}	4.61×10^{16}	6.32×10^{-2}	9.22×10^{-2}	3.65×10^{-2}
Ethanol	46	1.29×10^{-3}	2.59×10^{16}	3.55×10^{-2}	5.18×10^{-2}	3.66×10^{-2}
Urea	60	4.94×10^{-4}	1.54×10^{16}	2.11×10^{-2}	3.08×10^{-2}	3.21×10^{-2}
Cholesterol – LDLC	387	3.83×10^{-4}	1.96×10^{16}	2.69×10^{-2}	3.92×10^{-2}	2.90×10^{-2}
Acetate ($C_2H_3O^{2-}$)	59	3.77×10^{-4}	1.30×10^{16}	1.78×10^{-2}	2.60×10^{-2}	2.81×10^{-2}
Glucosamine	179	3.39×10^{-4}	1.55×10^{16}	2.13×10^{-2}	3.10×10^{-2}	2.74×10^{-2}
Choline, total	104	2.56×10^{-4}	1.17×10^{16}	1.61×10^{-2}	2.34×10^{-2}	2.36×10^{-2}
Triglycerides	885	2.51×10^{-4}	1.81×10^{16}	2.48×10^{-2}	3.62×10^{-2}	2.32×10^{-2}
Lecithin	758	2.20×10^{-4}	1.62×10^{16}	2.22×10^{-2}	3.24×10^{-2}	2.16×10^{-2}
L-Lactate (lactic acid)	89	1.65×10^{-4}	8.68×10^{15}	1.19×10^{-2}	1.74×10^{-2}	1.80×10^{-2}
Galactose (children)	180	8.22×10^{-5}	6.64×10^{15}	9.11×10^{-3}	1.33×10^{-2}	1.13×10^{-2}
Alanine	89	6.32×10^{-5}	4.89×10^{15}	6.71×10^{-3}	9.78×10^{-3}	9.35×10^{-3}
Furosemide glucuronide	507	5.85×10^{-5}	6.72×10^{15}	9.22×10^{-3}	1.34×10^{-2}	8.82×10^{-3}
Albumin	67,500	5.71×10^{-5}	1.85×10^{16}	2.54×10^{-2}	3.70×10^{-2}	8.66×10^{-3}
Glutamine	146	5.37×10^{-5}	4.92×10^{15}	6.75×10^{-3}	9.84×10^{-3}	8.29×10^{-3}
Glycine	75	5.33×10^{-5}	4.25×10^{15}	5.83×10^{-3}	8.50×10^{-3}	8.20×10^{-3}
Amino acids, total	110	3.70×10^{-5}	3.71×10^{15}	5.09×10^{-3}	7.42×10^{-3}	6.27×10^{-3}
Proline	115	3.67×10^{-5}	3.72×10^{15}	5.10×10^{-3}	7.44×10^{-3}	6.21×10^{-3}
Sphingomyelin	813	3.64×10^{-5}	5.59×10^{15}	7.67×10^{-3}	1.12×10^{-2}	6.19×10^{-3}
Fructose	180	3.29×10^{-5}	3.83×10^{15}	5.25×10^{-3}	7.66×10^{-3}	5.72×10^{-3}
Uric acid	168	3.17×10^{-5}	3.69×10^{15}	5.06×10^{-3}	7.38×10^{-3}	5.54×10^{-3}
Lysine	146	2.94×10^{-5}	3.42×10^{15}	4.69×10^{-3}	6.84×10^{-3}	5.21×10^{-3}
Leucine	131	2.94×10^{-5}	3.34×10^{15}	4.58×10^{-3}	6.68×10^{-3}	5.20×10^{-3}
Valine	117	2.65×10^{-5}	3.07×10^{15}	4.21×10^{-3}	6.14×10^{-3}	4.81×10^{-3}
Nitrogen (molecular)	28	2.57×10^{-5}	2.23×10^{15}	3.06×10^{-3}	4.46×10^{-3}	4.70×10^{-3}
Acetone	58	2.55×10^{-5}	2.59×10^{15}	3.55×10^{-3}	5.18×10^{-3}	4.68×10^{-3}
Isoleucine	131	2.37×10^{-5}	2.94×10^{15}	4.03×10^{-3}	5.88×10^{-3}	4.41×10^{-3}
Ketone bodies	110	2.02×10^{-5}	2.57×10^{15}	3.53×10^{-3}	5.14×10^{-3}	3.87×10^{-3}
Threonine	119	1.99×10^{-5}	2.59×10^{15}	3.55×10^{-3}	5.18×10^{-3}	3.83×10^{-3}
Histidine	155	1.81×10^{-5}	2.59×10^{15}	3.55×10^{-3}	5.18×10^{-3}	3.56×10^{-3}
Phenylalanine	165	1.79×10^{-5}	2.61×10^{15}	3.58×10^{-3}	5.22×10^{-3}	3.54×10^{-3}
β-Globulin	52,000	1.71×10^{-5}	8.50×10^{15}	1.17×10^{-2}	1.70×10^{-2}	3.42×10^{-3}
Cystine	240	1.54×10^{-5}	2.58×10^{15}	3.54×10^{-3}	5.16×10^{-3}	3.14×10^{-3}
Thiocyanate	58	1.53×10^{-5}	1.90×10^{15}	2.61×10^{-3}	3.80×10^{-3}	3.09×10^{-3}
Arginine	174	1.53×10^{-5}	2.40×10^{15}	3.29×10^{-3}	4.80×10^{-3}	3.11×10^{-3}
Glutamic acid	147	1.41×10^{-5}	2.20×10^{15}	3.02×10^{-3}	4.40×10^{-3}	2.90×10^{-3}
Serine	105	1.41×10^{-5}	2.05×10^{15}	2.81×10^{-3}	4.10×10^{-3}	2.90×10^{-3}
Glycerol, free	92	1.38×10^{-5}	1.97×10^{15}	2.70×10^{-3}	3.94×10^{-3}	2.85×10^{-3}
Taurine	125	1.24×10^{-5}	1.98×10^{15}	2.72×10^{-3}	3.96×10^{-3}	2.65×10^{-3}
Citric acid	192	1.23×10^{-5}	2.15×10^{15}	2.95×10^{-3}	4.30×10^{-3}	2.61×10^{-3}
Phospholipid	744	1.19×10^{-5}	2.81×10^{15}	3.86×10^{-3}	5.62×10^{-3}	2.56×10^{-3}
Cephalin	640	1.16×10^{-5}	2.67×10^{15}	3.66×10^{-3}	5.34×10^{-3}	2.49×10^{-3}
Mucopolysaccharides	15,000	1.11×10^{-5}	5.05×10^{15}	6.93×10^{-3}	1.01×10^{-2}	2.41×10^{-3}
Tryptophan	204	1.09×10^{-5}	2.02×10^{15}	2.77×10^{-3}	4.04×10^{-3}	2.36×10^{-3}
Tyrosine	181	1.02×10^{-5}	1.90×10^{15}	2.61×10^{-3}	3.80×10^{-3}	2.25×10^{-3}
Pyruvic acid (aka. pyruvate)	88	1.01×10^{-5}	1.62×10^{15}	2.22×10^{-3}	3.24×10^{-3}	2.22×10^{-3}

Creatinine	113	9.82×10^{-6}	1.68×10^{15}	2.30×10^{-3}	3.36×10^{-3}	2.17×10^{-3}
Pseudoglobulin I	150,000	9.38×10^{-6}	7.41×10^{15}	1.02×10^{-2}	1.48×10^{-2}	2.10×10^{-3}
Sulfates, inorganic (SO_4^{2-})	96	9.25×10^{-6}	1.56×10^{15}	2.14×10^{-3}	3.12×10^{-3}	2.05×10^{-3}
Immunoglobin G (IgG)	158,500	8.88×10^{-6}	7.25×10^{15}	9.95×10^{-3}	1.45×10^{-2}	2.01×10^{-3}
Ascorbic acid	176	8.41×10^{-6}	1.68×10^{15}	2.30×10^{-3}	3.36×10^{-3}	1.91×10^{-3}
γ-Globulin	153,100	8.23×10^{-6}	6.87×10^{15}	9.43×10^{-3}	1.37×10^{-2}	1.88×10^{-3}
α2-Globulin	93,000	7.97×10^{-6}	6.07×10^{15}	8.33×10^{-3}	1.21×10^{-2}	1.83×10^{-3}
Ornithine	132	7.84×10^{-6}	1.51×10^{15}	2.07×10^{-3}	3.02×10^{-3}	1.78×10^{-3}
Methionine	149	7.45×10^{-6}	1.51×10^{15}	2.07×10^{-3}	3.02×10^{-3}	1.74×10^{-3}
Phosphorated pentose	230	7.40×10^{-6}	1.64×10^{15}	2.25×10^{-3}	3.28×10^{-3}	1.71×10^{-3}
β-Hydroxybutyric acid	104	6.40×10^{-6}	1.27×10^{15}	1.74×10^{-3}	2.54×10^{-3}	1.50×10^{-3}
Bile acids	409	5.44×10^{-6}	1.54×10^{15}	2.11×10^{-3}	3.08×10^{-3}	1.32×10^{-3}
Creatine	131	5.25×10^{-6}	1.19×10^{15}	1.63×10^{-3}	2.38×10^{-3}	1.29×10^{-3}
Malic acid	134	4.97×10^{-6}	1.15×10^{15}	1.58×10^{-3}	2.30×10^{-3}	1.22×10^{-3}
Citrulline	175	4.23×10^{-6}	1.11×10^{15}	1.52×10^{-3}	2.22×10^{-3}	1.08×10^{-3}
Glucuronic acid	194	4.20×10^{-6}	1.13×10^{15}	1.55×10^{-3}	2.26×10^{-3}	1.07×10^{-3}
Transferrin	74,000	4.00×10^{-6}	3.83×10^{15}	5.25×10^{-3}	7.66×10^{-3}	1.03×10^{-3}
Pseudoglobulin II	150,000	3.95×10^{-6}	4.41×10^{15}	6.05×10^{-3}	8.82×10^{-3}	1.02×10^{-3}
α-Tocopherol	431	3.44×10^{-6}	1.18×10^{15}	1.62×10^{-3}	2.36×10^{-3}	8.95×10^{-4}
α1-Globulin	93,000	3.19×10^{-6}	3.50×10^{15}	4.80×10^{-3}	7.00×10^{-3}	8.47×10^{-4}
Succinic acid	118	3.14×10^{-6}	8.56×10^{14}	1.17×10^{-3}	1.71×10^{-3}	8.40×10^{-4}
Acetoacetate	102	3.12×10^{-6}	8.28×10^{14}	1.14×10^{-3}	1.66×10^{-3}	8.37×10^{-4}
Inositol	180	2.88×10^{-6}	8.88×10^{14}	1.22×10^{-3}	1.78×10^{-3}	7.80×10^{-4}
α-Antitrypsin	54,000	2.74×10^{-6}	2.86×10^{15}	3.92×10^{-3}	5.72×10^{-3}	7.50×10^{-4}
Glycoprotein, acid	42,000	2.65×10^{-6}	2.65×10^{15}	3.64×10^{-3}	5.30×10^{-3}	7.24×10^{-4}
Complement C4 binding protein	9,000	2.63×10^{-6}	1.91×10^{15}	2.62×10^{-3}	3.82×10^{-3}	7.19×10^{-4}
Aluminum	27	2.41×10^{-6}	5.38×10^{14}	7.38×10^{-4}	1.08×10^{-3}	6.72×10^{-4}
Iron	56	2.39×10^{-6}	6.22×10^{14}	8.53×10^{-4}	1.24×10^{-3}	6.66×10^{-4}
Nitric oxide	30	2.22×10^{-6}	5.23×10^{14}	7.18×10^{-4}	1.05×10^{-3}	6.25×10^{-4}
Ammonia	17	2.14×10^{-6}	4.54×10^{14}	6.23×10^{-4}	9.08×10^{-4}	6.04×10^{-4}
Haptoglobin	86,000	1.89×10^{-6}	2.52×10^{15}	3.46×10^{-3}	5.04×10^{-3}	5.43×10^{-4}
Copper	64	1.81×10^{-6}	5.41×10^{14}	7.42×10^{-4}	1.08×10^{-3}	5.24×10^{-4}
Immunoglobin A (IgA)	160,000	1.81×10^{-6}	2.79×10^{15}	3.83×10^{-3}	5.58×10^{-3}	5.21×10^{-4}
Fluoride	19	1.75×10^{-6}	4.13×10^{14}	5.67×10^{-4}	8.26×10^{-4}	5.10×10^{-4}
Zinc	65	1.70×10^{-6}	5.24×10^{14}	7.19×10^{-4}	1.05×10^{-3}	4.96×10^{-4}
Aspartic acid	133	1.67×10^{-6}	6.02×10^{14}	8.26×10^{-4}	1.20×10^{-3}	4.89×10^{-4}
Immunoglobin M (IgM)	150,000	1.48×10^{-6}	2.44×10^{15}	3.35×10^{-3}	4.88×10^{-3}	4.37×10^{-4}
α-Aminobutyric acid	103	1.44×10^{-6}	5.22×10^{14}	7.16×10^{-4}	1.04×10^{-3}	4.29×10^{-4}
Oxalate	128	1.39×10^{-6}	5.35×10^{14}	7.34×10^{-4}	1.07×10^{-3}	4.17×10^{-4}
Bilirubin	585	1.27×10^{-6}	6.95×10^{14}	9.54×10^{-4}	1.39×10^{-3}	3.84×10^{-4}
Indican	295	1.25×10^{-6}	5.99×10^{14}	8.22×10^{-4}	1.20×10^{-3}	3.81×10^{-4}
Pyramidine nucleotide	80	1.11×10^{-6}	4.25×10^{14}	5.83×10^{-4}	8.50×10^{-4}	3.43×10^{-4}
Nicotinic acid	123	9.03×10^{-7}	4.11×10^{14}	5.64×10^{-4}	8.22×10^{-4}	2.86×10^{-4}
Fibrinogen I	340,000	8.71×10^{-7}	2.11×10^{15}	2.89×10^{-3}	4.22×10^{-3}	2.76×10^{-4}
Corticosteroids (cortisone)	361	8.22×10^{-7}	4.86×10^{14}	6.67×10^{-4}	9.72×10^{-4}	2.64×10^{-4}
DHEA sulfate	369	7.32×10^{-7}	4.55×10^{14}	6.24×10^{-4}	9.10×10^{-4}	2.38×10^{-4}
Phytanic acid	313	7.11×10^{-7}	4.33×10^{14}	5.94×10^{-4}	8.66×10^{-4}	2.33×10^{-4}
Complement C3 (β1C globulin)	190,000	6.04×10^{-7}	1.50×10^{15}	2.06×10^{-3}	3.00×10^{-3}	2.01×10^{-4}
Hexosephosphate P	258	5.74×10^{-7}	3.66×10^{14}	5.02×10^{-4}	7.32×10^{-4}	1.92×10^{-4}
α2-Macroglobulin	820,000	4.88×10^{-7}	1.79×10^{15}	2.46×10^{-3}	3.58×10^{-3}	1.66×10^{-4}
Thyroxine-binding prealbumin	54,000	4.80×10^{-7}	1.00×10^{15}	1.37×10^{-3}	2.00×10^{-3}	1.63×10^{-4}
Complemt. Factor B C3 proactivator	75,000	4.44×10^{-7}	1.02×10^{15}	1.40×10^{-3}	2.04×10^{-3}	1.51×10^{-4}
Polysaccharides, total	250,000	3.88×10^{-7}	1.22×10^{15}	1.67×10^{-3}	2.44×10^{-3}	1.36×10^{-4}
β-Carotene	537	3.45×10^{-7}	3.16×10^{14}	4.34×10^{-4}	6.32×10^{-4}	1.23×10^{-4}
Ceruloplasmin	151,000	2.94×10^{-7}	9.30×10^{14}	1.28×10^{-3}	1.86×10^{-3}	1.07×10^{-4}
Manganese	55	2.56×10^{-7}	1.69×10^{14}	2.32×10^{-4}	3.38×10^{-4}	9.43×10^{-5}
Cholesterol - HDLC	270,000	2.47×10^{-7}	9.45×10^{14}	1.30×10^{-3}	1.89×10^{-3}	9.11×10^{-5}
RNA	18,000	2.47×10^{-7}	5.36×10^{14}	7.35×10^{-4}	1.07×10^{-3}	9.10×10^{-5}
Retinol	287	2.07×10^{-7}	2.07×10^{14}	2.84×10^{-4}	4.14×10^{-4}	7.78×10^{-5}
Lipoprotein (S, 12-20)	500,000	1.48×10^{-7}	7.92×10^{14}	1.09×10^{-3}	1.58×10^{-3}	5.77×10^{-5}
Complement C4 (β1E globulin)	190,000	1.44×10^{-7}	6.36×10^{14}	8.73×10^{-4}	1.27×10^{-3}	5.62×10^{-5}
δ-Aminolevulinic acid	131	1.30×10^{-7}	1.37×10^{14}	1.88×10^{-4}	2.74×10^{-4}	5.12×10^{-5}

Pantothenic acid	219	1.18×10^{-7}	1.44×10^{14}	1.98×10^{-4}	2.88×10^{-4}	4.71×10^{-5}
Prothrombin II	72,000	1.03×10^{-7}	4.25×10^{14}	5.83×10^{-4}	8.50×10^{-4}	4.15×10^{-5}
LK kininogen	65,000	9.63×10^{-8}	4.00×10^{14}	5.49×10^{-4}	8.00×10^{-4}	3.91×10^{-5}
Serotonin (5-hydroxytryptamine)	176	8.83×10^{-8}	1.18×10^{14}	1.62×10^{-4}	2.36×10^{-4}	3.62×10^{-5}
Iodine	127	8.46×10^{-8}	1.09×10^{14}	1.50×10^{-4}	2.18×10^{-4}	3.48×10^{-5}
Lysozyme (muramidase)	14,300	7.77×10^{-8}	2.59×10^{14}	3.55×10^{-4}	5.18×10^{-4}	3.23×10^{-5}
Complement C9	69,000	7.41×10^{-8}	3.47×10^{14}	4.76×10^{-4}	6.94×10^{-4}	3.09×10^{-5}
Tin	119	6.24×10^{-8}	9.32×10^{13}	1.28×10^{-4}	1.86×10^{-4}	2.65×10^{-5}
Prekallikrein	88,000	4.97×10^{-8}	2.89×10^{14}	3.97×10^{-4}	5.78×10^{-4}	2.15×10^{-5}
HMWK-kallikrein factor	120,000	4.88×10^{-8}	3.04×10^{14}	4.17×10^{-4}	6.08×10^{-4}	2.11×10^{-5}
Complement C7	110,000	4.71×10^{-8}	2.93×10^{14}	4.02×10^{-4}	5.86×10^{-4}	2.05×10^{-5}
Cortisol	363	4.70×10^{-8}	9.81×10^{13}	1.35×10^{-4}	1.96×10^{-4}	2.05×10^{-5}
Hemoglobin	65,000	4.56×10^{-8}	2.58×10^{14}	3.54×10^{-4}	5.16×10^{-4}	1.99×10^{-5}
Enzymes, total	100,000	4.44×10^{-8}	2.78×10^{14}	3.81×10^{-4}	5.56×10^{-4}	1.94×10^{-5}
Properdin	53,500	4.43×10^{-8}	2.44×10^{14}	3.35×10^{-4}	4.88×10^{-4}	1.94×10^{-5}
Fletcher factor	85,000	4.36×10^{-8}	2.66×10^{14}	3.65×10^{-4}	5.32×10^{-4}	1.91×10^{-5}
Acetylcholine	146	4.15×10^{-8}	8.00×10^{13}	1.10×10^{-4}	1.60×10^{-4}	1.83×10^{-5}
Mucoproteins	1,730,000	4.11×10^{-8}	4.77×10^{14}	6.54×10^{-4}	9.54×10^{-4}	1.81×10^{-5}
Complement C6	120,000	3.95×10^{-8}	2.69×10^{14}	3.69×10^{-4}	5.38×10^{-4}	1.74×10^{-5}
Pyridoxine	169	3.94×10^{-8}	7.99×10^{13}	1.10×10^{-4}	1.60×10^{-4}	1.74×10^{-5}
Androsterone	290	3.83×10^{-8}	8.58×10^{13}	1.18×10^{-4}	1.72×10^{-4}	1.70×10^{-5}
Complement C1r	80,118	3.51×10^{-8}	2.32×10^{14}	3.18×10^{-4}	4.64×10^{-4}	1.57×10^{-5}
Transcortin	55,700	3.32×10^{-8}	2.09×10^{14}	2.87×10^{-4}	4.18×10^{-4}	1.49×10^{-5}
Immunoglobulin D (IgD)	180,000	3.29×10^{-8}	2.63×10^{14}	3.61×10^{-4}	5.26×10^{-4}	1.48×10^{-5}
Complement C8	150,000	3.11×10^{-8}	2.45×10^{14}	3.36×10^{-4}	4.90×10^{-4}	1.40×10^{-5}
Complement C5 (β1F-globulin)	188,304	3.03×10^{-8}	2.53×10^{14}	3.47×10^{-4}	5.06×10^{-4}	1.37×10^{-5}
Cytochrome c	12,000	2.84×10^{-8}	1.42×10^{14}	1.95×10^{-4}	2.84×10^{-4}	1.29×10^{-5}
Lead	207	2.79×10^{-8}	7.13×10^{13}	9.78×10^{-5}	1.43×10^{-4}	1.27×10^{-5}
Hageman factor XII	80,000	2.69×10^{-8}	1.99×10^{14}	2.73×10^{-4}	3.98×10^{-4}	1.23×10^{-5}
Thiamine	265	2.51×10^{-8}	7.08×10^{13}	9.71×10^{-5}	1.42×10^{-4}	1.16×10^{-5}
Complement C2	140,000	1.80×10^{-8}	1.77×10^{14}	2.43×10^{-4}	3.54×10^{-4}	8.51×10^{-6}
Cyanide	26	1.71×10^{-8}	5.10×10^{13}	7.00×10^{-5}	1.02×10^{-4}	8.13×10^{-6}
β-2-microglobulin	11,000	1.62×10^{-8}	1.04×10^{14}	1.43×10^{-4}	2.08×10^{-4}	7.72×10^{-6}
Cocarboxylase	425	1.57×10^{-8}	6.32×10^{13}	8.67×10^{-5}	1.26×10^{-4}	7.51×10^{-6}
11-Deoxycortisol	347	1.50×10^{-8}	6.08×10^{13}	8.34×10^{-5}	1.22×10^{-4}	7.20×10^{-6}
Tissue thromboplastin III	4,960	1.49×10^{-8}	8.79×10^{13}	1.21×10^{-4}	1.76×10^{-4}	7.18×10^{-6}
25-hydroxyholecalciferol	401	1.48×10^{-8}	6.16×10^{13}	8.45×10^{-5}	1.23×10^{-4}	7.12×10^{-6}
Complement C1q	435,000	1.23×10^{-8}	1.78×10^{14}	2.44×10^{-4}	3.56×10^{-4}	5.98×10^{-6}
Flavine adenine dinucleotide	786	1.13×10^{-8}	6.10×10^{13}	8.37×10^{-5}	1.22×10^{-4}	5.57×10^{-6}
Bromide	80	9.27×10^{-9}	4.98×10^{13}	6.83×10^{-5}	9.96×10^{-5}	4.64×10^{-6}
Calciferol	397	7.65×10^{-9}	5.22×10^{13}	7.16×10^{-5}	1.04×10^{-4}	3.88×10^{-6}
Thyroid hormone	777	7.63×10^{-9}	5.47×10^{13}	7.50×10^{-5}	1.09×10^{-4}	3.87×10^{-6}
Riboflavin	376	7.28×10^{-9}	5.16×10^{13}	7.08×10^{-5}	1.03×10^{-4}	3.71×10^{-6}
Stuart factor X	59,000	6.28×10^{-9}	8.79×10^{13}	1.21×10^{-4}	1.76×10^{-4}	3.24×10^{-6}
Christmas factor IX	57,000	5.20×10^{-9}	8.03×10^{13}	1.10×10^{-4}	1.61×10^{-4}	2.72×10^{-6}
Dehydroepiandrosterone (DHEA)	288	5.14×10^{-9}	4.94×10^{13}	6.78×10^{-5}	9.88×10^{-5}	2.69×10^{-6}
C-reactive protein	120,000	5.06×10^{-9}	8.93×10^{13}	1.23×10^{-4}	1.79×10^{-4}	2.65×10^{-6}
Insulin-like growth factor I	7,649	4.84×10^{-9}	6.00×10^{13}	8.23×10^{-5}	1.20×10^{-4}	2.55×10^{-6}
Biotin	244	4.85×10^{-9}	4.92×10^{13}	6.75×10^{-5}	9.84×10^{-5}	2.55×10^{-6}
Corticosterone	347	4.28×10^{-9}	4.92×10^{13}	6.75×10^{-5}	9.84×10^{-5}	2.27×10^{-6}
Norepinephrine (noradrenalin)	169	3.72×10^{-9}	4.92×10^{13}	6.75×10^{-5}	9.84×10^{-5}	2.00×10^{-6}
Complement C1s (C1 esterase)	790,000	3.56×10^{-9}	1.03×10^{14}	1.41×10^{-4}	2.06×10^{-4}	1.92×10^{-6}
Folic acid	441	3.36×10^{-9}	4.92×10^{13}	6.75×10^{-5}	9.84×10^{-5}	1.81×10^{-6}
Folate	441	2.90×10^{-9}	4.92×10^{13}	6.75×10^{-5}	9.84×10^{-5}	1.59×10^{-6}
Progesterone	315	2.85×10^{-9}	4.92×10^{13}	6.75×10^{-5}	9.84×10^{-5}	1.56×10^{-6}
Proaccelerin V	330,000	2.69×10^{-9}	7.88×10^{13}	1.08×10^{-4}	1.58×10^{-4}	1.48×10^{-6}
Fibrin stabilizing factor XIII	320,000	2.31×10^{-9}	7.36×10^{13}	1.01×10^{-4}	1.47×10^{-4}	1.29×10^{-6}
Testosterone	288	2.25×10^{-9}	4.92×10^{13}	6.75×10^{-5}	9.84×10^{-5}	1.25×10^{-6}
Dihydrotestosterone (DHT)	290	2.04×10^{-9}	4.92×10^{13}	6.75×10^{-5}	9.84×10^{-5}	1.14×10^{-6}
Cyclic AMP	329	2.00×10^{-9}	4.92×10^{13}	6.75×10^{-5}	9.84×10^{-5}	1.12×10^{-6}
Plasma thromboplastin antecedent XI	160,000	1.85×10^{-9}	6.20×10^{13}	8.51×10^{-5}	1.24×10^{-4}	1.05×10^{-6}
Proconvertin VII	50,000	1.48×10^{-9}	5.26×10^{13}	7.22×10^{-5}	1.05×10^{-4}	8.49×10^{-7}

von Willebrand factor	500,000	1.04×10^{-9}	5.86×10^{13}	8.04×10^{-5}	1.17×10^{-4}	6.09×10^{-7}
Epinephrine (adrenalin)	183	1.01×10^{-9}	4.92×10^{13}	6.75×10^{-5}	9.84×10^{-5}	5.95×10^{-7}
Cyclic GMP	345	9.44×10^{-10}	4.92×10^{13}	6.75×10^{-5}	9.84×10^{-5}	5.58×10^{-7}
Androstenedione	286	7.76×10^{-10}	4.92×10^{13}	6.75×10^{-5}	9.84×10^{-5}	4.65×10^{-7}
Relaxin	21,043	7.04×10^{-10}	4.92×10^{13}	6.75×10^{-5}	9.84×10^{-5}	4.24×10^{-7}
17-Hydroxyprogesterone	331	6.72×10^{-10}	4.92×10^{13}	6.75×10^{-5}	9.84×10^{-5}	4.07×10^{-7}
Estriol (E_3)	288	5.14×10^{-10}	4.92×10^{13}	6.75×10^{-5}	9.84×10^{-5}	3.16×10^{-7}
Pregnenolone	317	4.68×10^{-10}	4.92×10^{13}	6.75×10^{-5}	9.84×10^{-5}	2.90×10^{-7}
Thyroxine-binding globulin (TBG)	54,000	4.66×10^{-10}	4.92×10^{13}	6.75×10^{-5}	9.84×10^{-5}	2.89×10^{-7}
24,25-dihydroxyholecalciferol	417	2.67×10^{-10}	4.92×10^{13}	6.75×10^{-5}	9.84×10^{-5}	1.71×10^{-7}
Chorionic gonadotropin	36,700	2.02×10^{-10}	4.92×10^{13}	6.75×10^{-5}	9.84×10^{-5}	1.32×10^{-7}
Erythropoietin	32,000	1.85×10^{-10}	4.92×10^{13}	6.75×10^{-5}	9.84×10^{-5}	1.22×10^{-7}
Immunoglobulin E (IgE)	200,000	1.85×10^{-10}	4.92×10^{13}	6.75×10^{-5}	9.84×10^{-5}	1.22×10^{-7}
Estradiol (E_2)	288	1.54×10^{-10}	4.92×10^{13}	6.75×10^{-5}	9.84×10^{-5}	1.02×10^{-7}
Prolactin	22,000	1.35×10^{-10}	4.92×10^{13}	6.75×10^{-5}	9.84×10^{-5}	9.01×10^{-8}
Platelet derived growth factor	33,500	1.11×10^{-10}	4.92×10^{13}	6.75×10^{-5}	9.84×10^{-5}	7.48×10^{-8}
C-peptide	3,020	9.81×10^{-11}	4.92×10^{13}	6.75×10^{-5}	9.84×10^{-5}	6.69×10^{-8}
Prostaglandin PGE	369	8.34×10^{-11}	4.92×10^{13}	6.75×10^{-5}	9.84×10^{-5}	5.74×10^{-8}
Dopamine	153	6.58×10^{-11}	4.92×10^{13}	6.75×10^{-5}	9.84×10^{-5}	4.59×10^{-8}
Aldosterone	360	6.17×10^{-11}	4.92×10^{13}	6.75×10^{-5}	9.84×10^{-5}	4.32×10^{-8}
Estrone (E_1)	270	5.51×10^{-11}	4.92×10^{13}	6.75×10^{-5}	9.84×10^{-5}	3.88×10^{-8}
Cobalamin	1,355	5.47×10^{-11}	4.92×10^{13}	6.75×10^{-5}	9.84×10^{-5}	3.85×10^{-8}
Somatotropin (growth hormone)	22,124	4.69×10^{-11}	4.92×10^{13}	6.75×10^{-5}	9.84×10^{-5}	3.33×10^{-8}
Ferritin	474,000	4.69×10^{-11}	4.92×10^{13}	6.75×10^{-5}	9.84×10^{-5}	3.33×10^{-8}
Prostaglandin PGF	355	3.26×10^{-11}	4.92×10^{13}	6.75×10^{-5}	9.84×10^{-5}	2.36×10^{-8}
Antihemophilic factor VIII	250,000	2.96×10^{-11}	4.92×10^{13}	6.75×10^{-5}	9.84×10^{-5}	2.16×10^{-8}
Prostate specific antigen (PSA)	34,000	2.83×10^{-11}	4.92×10^{13}	6.75×10^{-5}	9.84×10^{-5}	2.07×10^{-8}
Melatonin	232	2.27×10^{-11}	4.92×10^{13}	6.75×10^{-5}	9.84×10^{-5}	1.68×10^{-8}
α1-Fetoprotein	69,000	2.15×10^{-11}	4.92×10^{13}	6.75×10^{-5}	9.84×10^{-5}	1.59×10^{-8}
Thyrotropin-releasing hormone	362	1.23×10^{-11}	4.92×10^{13}	6.75×10^{-5}	9.84×10^{-5}	9.37×10^{-9}
Insulin	5,734	1.09×10^{-11}	4.92×10^{13}	6.75×10^{-5}	9.84×10^{-5}	8.35×10^{-9}
1,25-dihydroxyholecalciferol	417	8.00×10^{-12}	4.92×10^{13}	6.75×10^{-5}	9.84×10^{-5}	6.25×10^{-9}
Gastrin	2,098	7.06×10^{-12}	4.92×10^{13}	6.75×10^{-5}	9.84×10^{-5}	5.55×10^{-9}
Angiotensin I	1,031	6.32×10^{-12}	4.92×10^{13}	6.75×10^{-5}	9.84×10^{-5}	5.00×10^{-9}
Gastric inhibitory peptide	4,984	5.95×10^{-12}	4.92×10^{13}	6.75×10^{-5}	9.84×10^{-5}	4.72×10^{-9}
Thyroglobulin (Tg)	660,000	5.61×10^{-12}	4.92×10^{13}	6.75×10^{-5}	9.84×10^{-5}	4.46×10^{-9}
Nerve growth factor (NGF)	140,000	5.29×10^{-12}	4.92×10^{13}	6.75×10^{-5}	9.84×10^{-5}	4.22×10^{-9}
Gonadotropic releasing hormone	1,182	5.01×10^{-12}	4.92×10^{13}	6.75×10^{-5}	9.84×10^{-5}	4.01×10^{-9}
Bradykinin	1,060	4.89×10^{-12}	4.92×10^{13}	6.75×10^{-5}	9.84×10^{-5}	3.92×10^{-9}
Glucagon	2,485	4.47×10^{-12}	4.92×10^{13}	6.75×10^{-5}	9.84×10^{-5}	3.60×10^{-9}
Proinsulin	9,000	4.12×10^{-12}	4.92×10^{13}	6.75×10^{-5}	9.84×10^{-5}	3.32×10^{-9}
Pancreatic polypeptide	4,200	3.53×10^{-12}	4.92×10^{13}	6.75×10^{-5}	9.84×10^{-5}	2.87×10^{-9}
Oxytocin	1,007	3.53×10^{-12}	4.92×10^{13}	6.75×10^{-5}	9.84×10^{-5}	2.87×10^{-9}
Parathyroid hormone (PTH)	9,500	3.12×10^{-12}	4.92×10^{13}	6.75×10^{-5}	9.84×10^{-5}	2.55×10^{-9}
Cell-free DNA	106,920	2.36×10^{-12}	4.92×10^{13}	6.75×10^{-5}	9.84×10^{-5}	2.60×10^{-9}
Thyroxine (FT_4), free	777	2.29×10^{-12}	4.92×10^{13}	6.75×10^{-5}	9.84×10^{-5}	1.90×10^{-9}
Prostatic acid phosphatase	100,000	2.22×10^{-12}	4.92×10^{13}	6.75×10^{-5}	9.84×10^{-5}	1.85×10^{-9}
Calcitonin	3,455	2.14×10^{-12}	4.92×10^{13}	6.75×10^{-5}	9.84×10^{-5}	1.79×10^{-9}
Angiotensin II (Renin)	1,297	2.06×10^{-12}	4.92×10^{13}	6.75×10^{-5}	9.84×10^{-5}	1.72×10^{-9}
Adenocorticotrophic hormone	4,540	1.96×10^{-12}	4.92×10^{13}	6.75×10^{-5}	9.84×10^{-5}	1.64×10^{-9}
Cholecystokinin	3,931	1.14×10^{-12}	4.92×10^{13}	6.75×10^{-5}	9.84×10^{-5}	9.78×10^{-10}
Secretin	3,055	1.09×10^{-12}	4.92×10^{13}	6.75×10^{-5}	9.84×10^{-5}	9.39×10^{-10}
Carcinoembryonic antigen	180,000	1.03×10^{-12}	4.92×10^{13}	6.75×10^{-5}	9.84×10^{-5}	8.88×10^{-10}
MIP-1β	7,600	8.77×10^{-13}	4.92×10^{13}	6.75×10^{-5}	9.84×10^{-5}	7.63×10^{-10}
Free triiodothyronine	651	7.51×10^{-13}	4.92×10^{13}	6.75×10^{-5}	9.84×10^{-5}	6.58×10^{-10}
RANTES	7,800	6.65×10^{-13}	4.92×10^{13}	6.75×10^{-5}	9.84×10^{-5}	5.85×10^{-10}
Vasointestinal peptide (VIP)	3,327	3.56×10^{-13}	4.92×10^{13}	6.75×10^{-5}	9.84×10^{-5}	3.23×10^{-10}
Vasopressin	1,084	3.07×10^{-13}	4.92×10^{13}	6.75×10^{-5}	9.84×10^{-5}	2.80×10^{-10}
MIP-1α	7,800	2.18×10^{-13}	4.92×10^{13}	6.75×10^{-5}	9.84×10^{-5}	2.02×10^{-10}
Tumor Necrosis Factor (TNFα)	25,644	3.47×10^{-14}	4.92×10^{13}	6.75×10^{-5}	9.84×10^{-5}	3.46×10^{-11}
Epidermal growth factor (EGF)	29,000	2.55×10^{-14}	4.92×10^{13}	6.75×10^{-5}	9.84×10^{-5}	2.58×10^{-11}

Average	*58,138*					
Subtotals			4.76×10^{17}	0.65	0.95	0.53
Missing blood plasma chems (81) *	58,138	1×10^{-6}	1.28×10^{17}	0.18	0.26	0.025
Missing blood plasma chems (551) *	58,138	1×10^{-7}	2.20×10^{17}	0.30	0.44	0.022
Missing blood plasma chems (2361) *	58,138	1×10^{-8}	2.60×10^{17}	0.36	0.52	0.012
Missing blood plasma chems (9599) *	58,138	1×10^{-9}	4.82×10^{17}	0.66	0.96	0.006
Subtotals (12,591 added chemicals)			1.09×10^{18}	1.45	2.18	0.065
TOTALS			**1.57×10^{18}**	**2.15**	**3.13**	**0.59**

* inferred to exist at these four concentration levels, using the procedure described in Section 4.10.1.3.

Appendix K. Free Ions

Appendix K. Number, volume, mass, and power draw of sorting rotors needed to extract free ions from interstitial and intracellular fluid compartments in a human body to 1% of initial concentrations in ~1 hour

Ionic Species	Molec. Weight (g/mole)	Initial Conc. (mols/nm^3)	N_{fleet} (rotors)	V_{fleet} (cm^3)	M_{fleet} (gm)	Average P_{fleet} (W)
Intracellular (cytosolic)						
K^+	39.1	6.09×10^{-2}	2.53×10^{17}	3.47×10^{-1}	5.06×10^{-1}	7.19×10^{0}
HCO_3^-	61.0	5.26×10^{-3}	6.41×10^{16}	8.79×10^{-2}	1.28×10^{-1}	6.56×10^{-1}
Na^+	23.0	5.26×10^{-3}	5.22×10^{16}	7.16×10^{-2}	1.04×10^{-1}	6.55×10^{-1}
HPO_4^{2-}	96.0	2.19×10^{-3}	4.16×10^{16}	5.71×10^{-2}	8.32×10^{-2}	7.75×10^{-1}
Cl^-	35.5	1.75×10^{-3}	2.95×10^{16}	4.05×10^{-2}	5.90×10^{-2}	2.42×10^{-1}
Mg^{2+} (free)	24.3	3.50×10^{-4}	1.04×10^{16}	1.43×10^{-2}	2.08×10^{-2}	1.11×10^{-1}
Ca^{2+} (free)	40.1	4.38×10^{-8}	6.80×10^{13}	9.33×10^{-5}	1.36×10^{-4}	2.96×10^{-5}
H^+ (H_3O^+) @ pH = 7	1.0	4.38×10^{-8}	4.99×10^{13}	6.85×10^{-5}	9.98×10^{-5}	2.66×10^{-5}
Average	*40.0*					
Totals			**4.51×10^{17}**	**0.619**	**0.902**	**9.629**
Extracellular (interstitial)						
Na^+	23.0	2.38×10^{-2}	1.29×10^{17}	1.77×10^{-1}	2.58×10^{-1}	2.83×10^{0}
Cl^-	35.5	1.91×10^{-2}	1.23×10^{17}	1.69×10^{-1}	2.46×10^{-1}	2.24×10^{0}
HCO_3^-	61.0	4.76×10^{-3}	6.06×10^{16}	8.31×10^{-2}	1.21×10^{-1}	5.97×10^{-1}
HPO_4^{2-}	96.0	1.48×10^{-3}	3.29×10^{16}	4.51×10^{-2}	6.58×10^{-2}	3.87×10^{-1}
K^+	39.1	6.57×10^{-4}	1.67×10^{16}	2.29×10^{-2}	3.34×10^{-2}	1.13×10^{-1}
Ca^{2+} (free)	40.1	2.96×10^{-4}	1.04×10^{16}	1.43×10^{-2}	2.08×10^{-2}	9.50×10^{-2}
Mg^{2+} (free)	24.3	2.46×10^{-4}	8.42×10^{15}	1.16×10^{-2}	1.68×10^{-2}	8.16×10^{-2}
H^+ (H_3O^+) @ pH = 7	1.0	1.64×10^{-8}	4.32×10^{13}	5.93×10^{-5}	8.64×10^{-5}	1.06×10^{-5}
Average	*40.0*					
Totals			**3.81×10^{17}**	**0.523**	**0.762**	**6.344**

Appendix L. Cryoprotectants

Appendix L. Specifications of sorting rotors needed to extract M22[3282] cryoprotectants from interstitial and intracellular fluid compartments in a human body to 0.1% of initial concentrations in ~10^6 sec

Cryoprotectant Molecule or Cryonics Medication	Molec. Weight (g/mole)	Initial Conc. (mols/nm^3)	N_{fleet} (rotors)	V_{fleet} (cm^3)	M_{fleet} (gm)	Average P_{fleet} (W)
Cryoprotectant						
Dimethyl sulfoxide	78.1	1.03×10^{0}	5.51×10^{16}	7.56×10^{-2}	1.10×10^{-1}	1.43×10^{-1}
Formamide	45.0	1.03×10^{0}	4.91×10^{16}	6.74×10^{-2}	9.82×10^{-2}	1.43×10^{-1}
Ethylene glycol	62.1	9.80×10^{-1}	5.09×10^{16}	6.98×10^{-2}	1.02×10^{-1}	1.43×10^{-1}
N-methylformamide	59.1	1.83×10^{-1}	1.84×10^{16}	2.52×10^{-2}	3.68×10^{-2}	7.07×10^{-2}
3-Methoxy,1,2-propanediol	106.2	1.36×10^{-1}	1.74×10^{16}	2.39×10^{-2}	3.48×10^{-2}	5.83×10^{-2}
Polyvinyl pyrrolidone K12	5000.0	2.02×10^{-3}	3.13×10^{15}	4.29×10^{-3}	6.26×10^{-3}	2.10×10^{-3}
X-1000 ice blocker	2000.0	1.81×10^{-3}	2.41×10^{15}	3.31×10^{-3}	4.82×10^{-3}	1.90×10^{-3}
Z-1000 ice blocker	749.0	9.65×10^{-3}	5.37×10^{15}	7.37×10^{-3}	1.07×10^{-2}	7.87×10^{-3}
Carrier Solution						
Glucose	180.2	3.25×10^{-2}	8.25×10^{15}	1.13×10^{-2}	1.65×10^{-2}	2.08×10^{-2}
Mannitol	182.2	1.63×10^{-2}	5.45×10^{15}	7.48×10^{-3}	1.09×10^{-2}	1.20×10^{-2}
Lactose	342.3	1.63×10^{-2}	6.23×10^{15}	8.55×10^{-3}	1.25×10^{-2}	1.20×10^{-2}
KCl	74.6	1.02×10^{-2}	6.82×10^{15}	9.36×10^{-3}	1.36×10^{-2}	2.82×10^{-2}
K_2HPO_4	174.2	2.59×10^{-3}	3.58×10^{15}	4.91×10^{-3}	7.16×10^{-3}	8.16×10^{-3}
Reduced glutathione	307.3	1.81×10^{-3}	1.63×10^{15}	2.24×10^{-3}	3.26×10^{-3}	1.91×10^{-3}
Adenine HCl	171.6	3.58×10^{-4}	5.46×10^{14}	7.49×10^{-4}	1.09×10^{-3}	4.63×10^{-4}
$NaHCO_3$	84.0	3.61×10^{-3}	3.76×10^{15}	5.16×10^{-3}	7.52×10^{-3}	1.11×10^{-2}
Small Volume Medications						
Propofol	178.3	6.75×10^{-6}	5.08×10^{13}	6.97×10^{-5}	1.02×10^{-4}	1.26×10^{-5}
(Tri)Sodium citrate	258.1	4.67×10^{-4}	6.97×10^{14}	9.56×10^{-4}	1.39×10^{-3}	5.84×10^{-4}
Heparin	15000.0	4.01×10^{-8}	5.97×10^{12}	8.19×10^{-6}	1.19×10^{-5}	1.05×10^{-7}
Vasopressin	1084.2	4.17×10^{-10}	3.37×10^{11}	4.62×10^{-7}	6.74×10^{-7}	1.36×10^{-9}
Minocycline	457.5	2.63×10^{-6}	3.52×10^{13}	4.83×10^{-5}	7.04×10^{-5}	5.28×10^{-6}
SMT (S-methyl-isothiourea)	278.4	8.65×10^{-6}	6.47×10^{13}	8.88×10^{-5}	1.29×10^{-4}	1.58×10^{-5}
Streptokinase	47286.7	6.65×10^{-8}	1.02×10^{13}	1.40×10^{-5}	2.04×10^{-5}	1.67×10^{-7}
Large Volume Medications						
Decaglycerol	758.8	5.10×10^{-4}	9.23×10^{14}	1.27×10^{-3}	1.85×10^{-3}	6.34×10^{-4}
Tromethamine	121.1	7.21×10^{-4}	7.72×10^{14}	1.06×10^{-3}	1.54×10^{-3}	8.58×10^{-4}
Average (weighted)	*326.0*					
Totals			**2.41×10^{17}**	**0.330**	**0.180**	**0.667**

[3282] Fahy GM, Wowk B, Wu J, Phan J, Rasch C, Chang A, Zendejas E. Cryopreservation of organs by vitrification: perspectives and recent advances. Cryobiology. 2004 Apr;48(2):157-78; http://www.21cm.com/pdfs/cryopreservation_advances.pdf.

Appendix M. Nanorobot Extraction from the Body

Once a diagnostic or therapeutic mission is completed by bloodborne nanorobots, it is necessary to extract them from the circulation. Several possible methods have been described or conceived for early nanorobots, but here we will briefly compare just two of them – **nanapheresis** (centrifugal blood component separation) and **transfusion** (nanorobot washout).

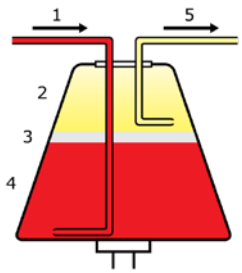

Nanapheresis. Active ballast control allows exfusion from the blood by early immotile nanorobots such as respirocytes that are incapable of removing themselves from the body. Blood to be cleared of nanorobots may be passed from the patient to a specialized centrifugation apparatus analogous to an apheresis[3283] circuit as in used in erythrocytapheresis,[3284] plateletpheresis,[3285] leukapheresis,[3286] plasmapheresis,[3287] and cytapheresis[3288] systems. In an apheresis system (image, left), whole blood enters the centrifuge (1) and separates into plasma (2), leukocytes (3), and erythrocytes (4); selected components are then drawn off (5).

In the concept of nanapheresis[3289] – originally proposed for use mainly in the early years of medical nanorobot implementation – acoustic transmitters would command passing nanorobots to establish neutral buoyancy. No other solid blood component can maintain exact neutral buoyancy, hence those other components precipitate outward during the gentle centrifugation and are drawn off and added back to filtered plasma on the other side of the apparatus. Meanwhile, after a period of centrifugation, the plasma, containing mostly suspended nanorobots but few other solids, is drawn off through a simple filter, removing the devices as residue. Plasma filtrate is then recombined with centrifuged solid components and returned undamaged to the patient's circulation.

It should be noted that absolute neutral buoyancy may not be strictly required – precise buoyancy control to some intermediate net density not shared by any other blood component may suffice to achieve efficient separation of nanorobots from the blood. The longer the robot is in the bloodstream, getting opsonized by natural adherent proteins, the more the overall device density may change, necessitating periodic alterations in the amount of onboard ballast to maintain good separation during each pass through the nanapheresis unit.

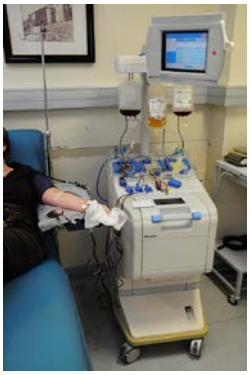

A conventional apheresis procedure takes at least 2-3 hours. In some cases, it is sufficient to place a needle in each arm. In other patients with small arm veins, it may be necessary to insert a catheter into the large veins under the collarbone or in other parts of the body. The process is not entirely comfortable. Nausea, cramps, and tingling in the fingers or around the mouth may be experienced, usually caused by the sodium citrate that is infused to prevent the clotting of blood that is exiting from the body. After the procedure (image, right), patients

---

[3283] https://en.wikipedia.org/wiki/Apheresis.
[3284] https://en.wikipedia.org/wiki/Erythrocytapheresis.
[3285] https://en.wikipedia.org/wiki/Plateletpheresis.
[3286] https://en.wikipedia.org/wiki/Leukapheresis.
[3287] https://en.wikipedia.org/wiki/Plasmapheresis.

[3288] Duvall D. Therapeutic cytapheresis: too many platelets, too many white blood cells. J Clin Apher. 2011;26(1):47-52; https://www.ncbi.nlm.nih.gov/pubmed/21312258.

[3289] Freitas RA Jr. Nanomedicine, Volume I: Basic Capabilities. Landes Bioscience, Georgetown, TX, 1999, Section 10.3.6, "Buoyancy Control and Nanapheresis"; http://www.nanomedicine.com/NMI/10.3.6.htm.

can feel cold, dizzy, lightheaded, or tired. Light anesthesia during and immediately after nanapheresis should alleviate most patient discomfort.

Courtesy of CaridianBCT

Let us next consider a simple mathematical blood filtration model for nanapheresis. The Spectra Optia Cell Separator (image, left) is a typical commercially available continuous-flow centrifugal apheresis system with a whole-blood processing rate of ~88 cm^3/minute and a plasma-removal efficiency of ~93%.[3290] We will assume that a comparable nanapheresis system could process a whole-blood volume of V_{aph} ~ 100 cm^3 in a cycle time of t_{pass} ~ 1 minute, with a nanorobot removal fraction during each cycle of f_{remove} ~ 90%-99%. After each ~1 minute processing time, it is assumed that the mostly-cleared blood is returned to, and thoroughly mixed with, the general circulation which includes 5400 cm^3 of blood volume.

Consider a nanomedical treatment protocol in which $N_{bot}(t_0)$ nanorobots are initially injected into the bloodstream of a patient with total blood volume V_{blood} ~ 5400 cm^3, after which nanapheresis is applied to the patient to extract the nanorobots down to a final target population of $N_{bot}(t_{final})$ in the circulation, making the simplifying assumptions that no nanorobots leave the circulation during the process and that the ratio of the whole-bloodstream nanorobot concentration before and after each nanapheresis cycle remains constant even down to the lowest concentrations.

The required process time to achieve the desired final nanorobot concentration in the blood is then $t_{final} = t_{pass} \log_{10}[c_{bot}(t_{final}) / c_{bot}(t_0)] / \log_{10}(\varepsilon)$, where the final nanorobot bloodstream concentration $c_{bot}(t_{final}) = N_{bot}(t_{final}) / V_{blood}$, the initial nanorobot bloodstream concentration $c_{bot}(t_0) = N_{bot}(t_0) / V_{blood}$, and the whole-bloodstream nanorobot concentration after one nanapheresis cycle divided by the whole-bloodstream nanorobot concentration before a cycle, aka. the net extraction ratio $\varepsilon = [N_{bot}(t_0) - (c_{bot}(t_0) V_{aph} f_{remove})] / [c_{bot}(t_0) V_{blood}]$.

The large chart below shows the model predictions for initial nanorobot injections of 50 million, 50 billion, and 50 trillion robots, along with the computed duration of nanapheresis that may be needed to reduce the circulating bloodstream nanorobot population to the indicated levels, assuming removal fractions (f_{remove}) of 0.50, 0.90, 0.99, and 0.999 per cycle through the apparatus. The model provides two main conclusions: (1) Increasing f_{remove} from 50% to 90% cuts filtration time almost in half for any target final concentration, but further improvements in f_{remove} don't significantly shorten filtration time; and (2) assuming f_{remove} ~ 100%, every ~2 hours of continuous filtration reduces bloodstream nanorobot concentration by almost tenfold (e.g., 2 hr → ~90% removal, 4 hr → ~99%, 6 hr → ~99.9%, etc.), given the parameters assumed here.

Transfusion (Nanorobot Washout). Spending 1-2 days to extract nanorobots from the bloodstream after a nanomedical procedure may be acceptable in the early years of nanorobot implementation but will be viewed as intolerably long in common medical practice. The key factor leading to slow filtration in nanapheresis is its requirement that small subvolumes of blood which have been cleared of robots are then returned to the general circulation and thoroughly mixed with the rest of the blood, effectively forcing the filtration system to filter the same subvolumes of blood over and over again. Nanorobot extraction would occur much faster if we could avoid this dilution effect by filtering each subvolume of blood only once, extracting virtually all nanorobots from the entire blood volume during one pass. Better yet, the fastest extraction of nanorobots from the blood would occur if we didn't bother to filter the blood at all before

---

[3290] Kim DK, Kim S, Jeong SH, Kim HO, Kim HJ. Therapeutic Plasma Exchange Using the Spectra Optia Cell Separator Compared With the COBE Spectra. Ann Lab Med. 2015 Sep;35(5):506-9; https://www.ncbi.nlm.nih.gov/pmc/articles/PMC4510503/.

returning it to the patient, but instead performed a whole-body blood transfusion that exchanged fresh nanorobot-free blood for all nanorobot-rich blood.

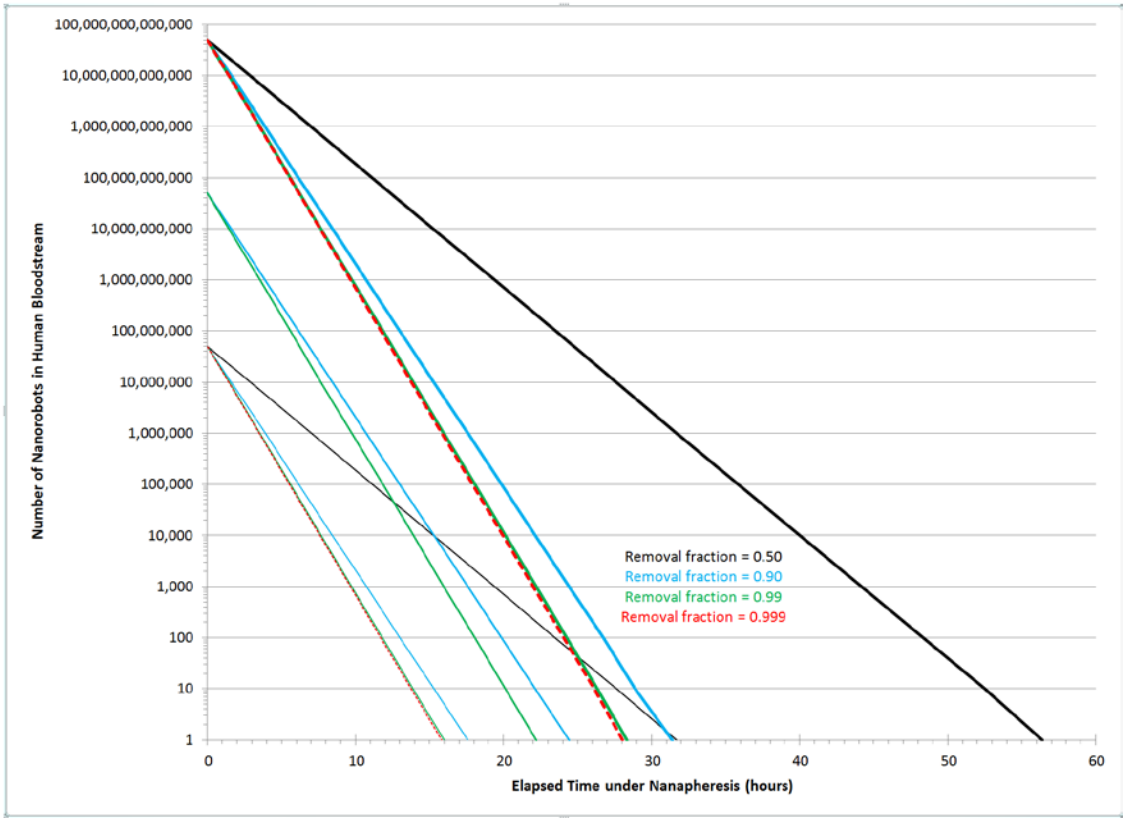

In a conventional exchange transfusion[3291] the patient's blood or blood components are slowly exchanged with other blood or blood products. According to one description: "The person's blood is slowly withdrawn (most often about 5 to 20 mL at a time, depending on the person's size and the severity of illness). An equal amount of fresh, prewarmed blood or plasma flows into the person's body. This cycle is repeated until the correct volume of blood has been replaced."[3292]

What we want is a much faster exchange of the entire blood volume. Therapeutic total body washouts have been successfully performed on living human patients at normothermic temperatures in special cases,[3293]

[3291] https://en.wikipedia.org/wiki/Exchange_transfusion.

[3292] "Exchange transfusion," MedlinePlus, 3 Dec 2020; https://web.archive.org/web/20201214033658/https://medlineplus.gov/ency/article/002923.htm.

[3293] Cline RE, Klebanoff G, Armstrong RG, Stanford W. Extracorporal circulation in hypothermia as used for total-body washout in stage IV hepatic coma. Ann Thorac Surg. 1973 Jul;16(1):44-51; https://www.annalsthoracicsurgery.org/article/S0003-4975(10)65811-0/pdf. Cooper GN Jr, Karlson KE, Clowes GH, Martin H, Randall HT. Total blood washout and exchange. A valuable tool in acute hepatic coma and Reye's syndrome. Am J Surg. 1977 Apr;133(4):522-30; https://pubmed.ncbi.nlm.nih.gov/848687/. Lee MC, Chang CH, Hsieh MJ. Use of a total wash-out method in an open heart operation. Ann Thorac Surg. 1989 Jan;47(1):57-8; https://www.annalsthoracicsurgery.org/article/0003-4975(89)90234-8/pdf.

and EPR[3294] replaces blood with ice-cold saline solution to extend life during emergency trauma surgery at 10-15 °C (Section 7.1.6.4). For decades, cryonicists have been performing washouts on patients in which all of the person's blood is removed and replaced with a special washout solution, using any of several available means including gravity-assisted blood substitution, blood substitution with embalmer's equipment (not used at Alcor), an air transportable perfusion circuit (preferred at Alcor), or professional extracorporeal perfusion equipment.[3295] The Alcor washout procedure consumes at least 20 liters of washout solution and may take up to an hour to complete.

In a nanorobot washout scenario, the initial perfusate might include pre-oxygenated fluorocarbons or some other convenient temporary blood substitute capable of sustaining human life. Liquid fluorocarbons selected for the preparation of injectable oxygen carriers are typically molecules of 8-10 carbon atoms with molecular weights in the 450-500 dalton range, dissolving 20-25 times more O_2 than water and delivering about the volume of oxygen to the tissues as an equal weight of hemoglobin. Rats breathing ~95% oxygen have survived total blood replacement with 20% fluosol solution,[3296] and baboons have survived a total exchange transfusion using 35% fluosol solution while breathing ~60% O_2.[3297] Because they are insoluble in water, fluorocarbons are administered in the form of emulsions of 0.1-0.2 μm droplets dispersed in a physiologic solution similar to fat emulsions routinely used for parenteral nutrition. Commercial preparations have been available for more than 40 years and have been administered to thousands of human coronary perfusion patients without life-threatening side effects.[3298]

After the patient's circulation has been flushed clear of bloodborne nanorobots, medical technicians would follow with a total exchange transfusion consisting of autologous blood of the patient's own serotype that could previously have been manufactured in a cell mill (Appendix D) and then made ready for infusion. Large solid blood elements (esp. red cells, white cells, and platelets) that appear in the drain perfusate during the transfusion are easily separated by size from the fluorocarbon droplets using external devices and could be returned to the patient's circulation with the need for remanufacture, continuing until minimal fluorocarbon appears in the drain fluid which indicates that the blood replacement process is complete. Since the fluorocarbon is transferred to lipid carriers in the blood (after opsonization and phagocytosis of the emulsion droplets) and released during passage through the pulmonary capillary bed, any remaining fluorocarbons will not be metabolized but would be excreted unchanged by exhalation as a vapor through the lungs over some period of hours.

Future research should further analyze, refine details, and extend the proposed nanorobot washout protocol for quickly removing nanorobots from the bloodstream.

[3294] https://en.wikipedia.org/wiki/Emergency_Preservation_and_Resuscitation.

[3295] De Wolf A, Platt C. Human Cryopreservation Procedures. Alcor Life Extension Foundation, 2020; "Chapter 16. Remote Blood Washout"; https://www.alcor.org/docs/cryopreservation-procedures-section-16-remote-washout.pdf.

[3296] Geyer RP. "Bloodless" rats through the use of artificial blood substitutes. Fed Proc. 1975 May;34(6):1499-1505; https://pubmed.ncbi.nlm.nih.gov/805063/. Hardy RN, Lowe KC, McNaughton DC. Acute responses during blood substitution in the conscious rat. J Physiol. 1983 May;338:451-61; https://www.ncbi.nlm.nih.gov/pmc/articles/pmid/6875966/. Lowe KC, McNaughton DC, Hardy RN. Changes in intravascular fluid composition following blood replacement with perfluorocarbon emulsion in the rat. Klin Wochenschr. 1985 Oct 1;63(19):1028-34; https://pubmed.ncbi.nlm.nih.gov/4068605/.

[3297] Gould SA, Sehgal LR, Rosen AL, Langdale LA, Sehgal HL, Krause L, Moss GS. Assessment of a 35% fluorocarbon emulsion. J Trauma. 1983 Aug;23(8):720-4; https://pubmed.ncbi.nlm.nih.gov/6887290/.

[3298] https://en.wikipedia.org/wiki/Blood_substitute#Perfluorocarbon_based.

Appendix N. Neuropreservation and Whole-Body Preservation Options

Alcor Life Extension Foundation ("Alcor") appreciates that members and prospective members need information when selecting a Neuropreservation ("N") or a Whole-Body ("WB") preservation option. There are pros and cons to each, and a decision as to which option to select can be quite personal. Alcor membership is almost evenly split between the two options. As of calendar year 2020, existing Alcor membership is 51% Neuro and 49% Whole-Body.

This document summarizes some information regarding N and WB options; however, Alcor encourages members and prospective members to avail themselves of the collection of in-depth articles in Alcor's library to make an informed decision (https://www.alcor.org/library/#neuro).

Members selecting the Neuropreservation option make observations such as, but not limited to:

- The nature of cryopreservation injury is such that there is effectively no difference in the technology level that will be required to revive N or WB patients. Both will require repairs at the tissue, cell, and molecular level, and tissue regeneration is implicitly possible with such technology.
- Brain preservation in WB patients may not be as good as N patients in some circumstances. Perfusion for N patients focuses on optimizing brain cryoprotection, including separate monitoring of venous cryoprotectant concentration from left and right brain hemispheres. The cryoprotectant concentration measured for WB patients is an average venous concentration from the whole body. A compromised circulatory system in WB patients may result in poorer perfusion, which can be corrected in bad cases by switching to carotid cannulation at the cost of time.
- The vitrification solution used for N patients is slightly less viscous so, all else being equal, perfusion of N patients can be completed in less time or lessen ice formation in the same perfusion time. N patients also get improved venous drainage due to lower venous pressure, which improves cryoprotectant perfusion.
- Although severing of the spinal cord is a direct loss of nerve connection information and motor memory, fine motor skills are believed to primarily be in the brain (cerebellum, motor cortex, dorsolateral striatum, and left parietal lobe). The brain also contains indirect information about the whole nervous system in the form of what feels familiar. Such memory could theoretically be used algorithmically to test candidate regenerated nervous systems before they are made. Even without such advanced techniques, brains have natural neuroplastic ability to adapt to new nerve connections.
- N patients can be moved across state lines without waiting for a permit, which can save many hours or even days.
- N allows some cremated remains for memorial services or family members to keep.
- N storage costs are significantly less than WB storage costs. Selecting the N option may enable people to fund above the minimum and allow for funding a trust.

Members selecting the Whole-Body option make observations such as, but not limited to:

- WB members may view their selection as the most conservative because their nervous system (including spinal cord), organs, endocrine glands, and microbiome will be preserved. WB members tend to believe that one's body is an integral part of who they are, revival may be smoother if one "wakes up" in his or her original body, they may not "feel" like themselves in a regenerated body, motor skills (walking, typing, playing musical instruments, athletics, etc.) won't have to be relearned, and the body may offer clues to assist with repair of the brain.
- The default surgical technique for WB perfusion entails a median sternotomy and cannulation of the heart, a mainstream medical perfusion technique that ensures perfusion of all healthy vessels leading to the head.
- The WB cryoprotectant contains an additional agent to reduce edema which may also mitigate cerebral edema in ischemic patients. This agent also produces a slightly stronger vitrification solution.

- For some WB members the choice of cryopreservation options is not just an individual preference because a controversial cryopreservation affects everyone. The aversion people feel to physically separating the body from the head produces a response that may make them more prone to object or engage in hostility. Some find it easier to enlist the support and cooperation of their family and friends when selecting WB cryopreservation.
- Some WB members are comforted by the fact that they have a "fall back" position in that WB members can switch to the less expensive N option should they experience an unexpected financial reversal at some point in their lifetime.
- Although cost and timing cannot be accurately predicted, at some time this century the quality of WB cryopreservation may become advanced enough that WB patients will require a lower level of technology for revival than N patients.
- Many WB members believe that practicing and perfecting WB human cryopreservation, contributes to the development of human suspended animation, which has applications beyond personal preservation.

The choice of Neuro or Whole-Body cryopreservation is a personal choice and, therefore, it is Alcor's policy not to make a recommendation to members and prospective members which option to choose. If a member or prospective member would like more in-depth information, Alcor recommends reading more about these cryopreservation options by using the link provided above.

Appendix R. List of Future Research Topics Supporting Cryostasis Revival

The following is an ordered listing of 304 specific "***future research***" topics, collected from the main text and Appendices of this book, that should be pursued to establish the technical capabilities needed to ensure a successful nanorobotic-based revival from cryostasis with maximum preservation of personal identity:

1. Find out more about the physical basis of memory in the brain, as it relates to personal identity. (Section 2.0)

2. Examine whether the exact number densities or spatial distributions of specific receptors or other molecular components within individual synapses are crucial to preserving long-term memory; and if so, whether this information can be adequately inferred solely from direct measurements of ≥100 nm features. (Section 2.1.2)

3. Confirm that synaptic cleft height variations have no significant role in LTM (Long Term Memory). (Section 2.1.2)

4. Are there any <100 nm-scale or molecular-scale structures that might need to be precisely scanned and precisely repaired in order to recover personal identity? (Section 2.1.2) Confirm if most or all surviving personal identity structures can be recovered using scans with ≥100 nm resolution for planning and executing the repairs. (Section 2.1.6) Modify or confirm the assertion that a minimum limit of 100 nm resolution for structural scan data is essential for preserving memory and personal identity. (Section 4.7)

5. Do we need detailed neurochemical information, including the transcriptional status of individual neurons, in addition to complete knowledge of brain ultrastructure to fully infer neural function? (Section 2.1.2)

6. What is the extent of structural variation from the norm in neurons and larger neural tissues, how do these variations affect personal identity (e.g., behavior, memories, etc.), and what are the effects of substituting structural norms for individual structures, especially in cases of damaged neurons or tissues where some original information has been lost? (Section 2.1.2)

7. Explore the extent of the robustness of long-term memory due to possible super-redundancy of neural data storage. (Section 2.1.3)

8. What is the upper bound of neuron attrition without loss of personal identity? (Section 2.1.3)

9. Ascertain the percentage of critical neuroreceptor occupancy or mean level of neuron functionality as a function of blood concentration or the degree of brain penetration of anesthetic agents, then use this information to generate an estimate of the fraction of neurons that must be quieted to eliminate episodic memory or consciousness, or to produce a given depth of sedation. (Section 2.1.3)

10. Match the neurological correlates of personal identity with the time course of ischemic damage to predict the approximate percentage of personal identity remaining after a given period of warm ischemia in past and current cryopreservation patients. (Section 2.1.3)

11. Demonstrate that the particular concentrations of neurotransmitters and other chemical messenger molecules that are present some time after cooldown are largely unrelated to live brain function, making it reasonable to assume that an accurately renovated connectome, once restored to functionality, will properly reconstitute all local metabolite and neurotransmitter concentrations to

the original levels that are appropriate for that individual in every neural compartment. (Section 2.1.4)

12. Examine the state of neurotransmitter concentrations in synapses after cessation of metabolism and brain activity during warm and cold ischemia. (Section 2.1.4)

13. Exactly which parts of the brain must be restored to capture personal identity? (Section 2.1.5)

14. Explore the degree to which it may be possible to (A) correct corrupted memories by altering connectomic and synaptic brain structures to replace missing memories that have been destroyed, (B) remove erroneous memories that are not real, or (C) edit memories that have become corrupted. (Section 2.1.5)

15. Resolve the question of whether personal identity may reside in any place other than the connectome and synaptome, and if so, to what level of significance. (Section 2.1.5)

16. Assess the possible importance of the "gut brain" and the spinal cord in human memory and personality. (Section 2.1.5)

17. Is it necessary to cryopreserve (and later revive and reimplant) a patient's original gut flora in order to fully recover their original personality? (Section 2.1.5)

18. How much information contained in the physical and informational artifacts with which we surround ourselves during life (e.g., our books, houses, cars, collectibles, pets, and computer files) contributes to our personal identity by forming a kind of external long-term memory? (Section 2.1.5)

19. Systematically review, from a cryonics perspective, the many subtleties involved in the precise philosophical definition of identity. (Section 2.1.5)

20. Repeat in greater detail our preliminary analysis of the impact of segmenting objects to be scanned into submicron cubes. (Section 2.2.9)

21. Show persistence of mammalian brain structure and functions post-mortem. (Section 3.2.7)

22. Determine if the fluid flow rates needed for tissue washout cycling during molecular extraction might risk removing larger molecular and biologically-derived structures. (Section 3.3.1)

23. Determine if there are any additional sources of potential freezing damage that have been overlooked in the present analysis. (Section 3.4)

24. Verify that microtubule depolymerization does not occur (A) during tissue cooling to below 4 °C or (B) when cryopreserved tissue is warmed from cryogenic temperatures up to just above the melting point (e.g., 4 °C) during reliquidification; or its significance when it does occur. (Section 3.4.1)

25. Specifically examine to what degree synaptic structures are damaged by freezing, or if there is little or no freezing damage at all. (Section 3.4.2)

26. Experimentally measure and quantify the number density, organ or tissue specificity (if any), the preferred propagation directions and patterns (if any), and exact lateral and length dimensions of fractures in blocks of frozen water-ice, frozen cryoprotectant and cryogenic vitrification solutions, and in cryopreserved human tissue, including specific organs and whole bodies. (Section 3.4.3)

27. Seek simple methods for reducing or eliminating cracking at cryogenic temperatures – such as thermal annealing or intermediate temperature storage – to reduce the severity (or entirely eliminate) this problem for future cryopatients. (Section 3.4.3)

28. Verify that quantum tunneling is not a problem for cryopreserved patients because (A) these are reactions mediated by free radicals that should not be present unless the tissue has been bombarded with electron beams or gamma rays, (B) most biological molecules susceptible to radical formation are present in only relatively low concentrations, and (C) the reaction rates from tunneling are expected to be negligible. (Section 3.5)

29. Verify that bloodstream and lymphatic vascular scans with feature resolution down to ~0.1 mm in cryopreserved tissues are already available, or are likely to become available in the not-too-distant future, or might become available in the future technological era of nanorobotically-enabled cryostasis revivals. (Section 4.1)

30. Explore whether it might be possible to detect magnetic resonance (MR) signal from hard-frozen tissue. (Section 4.1.1)

31. Explore whether it is possible to detect an MR signal from cryogenic-temperature vitrification solutions that might mostly fill the vasculature of a cryopreserved brain. (Section 4.1.1)

32. What resolution, contrast compensation, and maximum tolerable scan times are possible for computed tomography (CT) scans of cryopreserved tissue? (Section 4.1.2)

33. Can high image resolution be achieved in CT scans without the use of contrast agent, which would not be available in the case of cryopreserved patients? (Section 4.1.2)

34. Alcor has acquired numerous low-resolution NECT scans of cryopreserved patients' brains; these datasets should be computer-processed to extract vascular segmentation data or to compile a proper 3D vascular map. (Section 4.1.2)

35. Explore the potential imaging capabilities of ice-contacting ultrasound transducers, after verifying that ultrasound will not induce cracking in cryogenic, possibly highly mechanically stressed, frozen tissue. (Section 4.1.3)

36. Investigate other ultrasound-based scanning modalities for possible relevance in scanning cryopreserved tissue. (Section 4.1.3)

37. Consider whether thermoacoustic imaging or thermoacoustic computed tomography might work in cryopreserved tissue. (Section 4.1.3)

38. Consider whether terahertz tomography might work in cryopreserved tissue. (Section 4.1.4)

39. Measuring and modeling the exact volume changes of fully-patent liquid-filled blood vessels during the cryopreservation process would be a useful experimental project. (Section 4.2.1)

40. Determine the typical states of venous, lymphatic, and heart valves following cryopreservation. (Section 4.2.1)

41. Determine the typical states of precapillary sphincters following cryopreservation. (Section 4.2.1)

42. Perform a preliminary scaling study design for the excavation nanorobots and their mission requirements, that would permit more refined size, number, time, power, and thermal balance estimates. (Section 4.2.1)

43. Explore the possibility of alternative excavation scenarios, perhaps employing an upgraded variant of one of many catheter-based scanning modalities or using some form of vacuum sublimation system. (Section 4.2.1)

44. Investigate the best algorithms for estimating the number, size, and positions of missing or incomplete vasculature based on the available scanning data, wherever vascular maps are incomplete, to help guide exploratory excavation. (Section 4.2.2)

45. Design a GHz acoustic scanning system for whole-body cryogenic vascular mapping at microscale resolution. (Section 4.3.1)

46. Investigate the available contrast at higher frequencies near 30 THz for terahertz infrared imaging and determine if this contrast is sufficient to resolve cryopreservative-filled capillary vessels. (Section 4.3.2)

47. Identify or develop microscale emitters and receivers of THz radiation suitable for conveyance and use by nanorobots in order to make terahertz infrared imaging feasible. (Section 4.3.2)

48. Establish the performance and limitations of optical coherence tomography on cryopreserved human tissue at cryogenic temperatures. (Section 4.3.3)

49. Investigate the workability of confocal microscopy scanning methods on cryopreserved human tissue at cryogenic temperatures, and determine if operational optical emitting, masking, and receiving equipment can be reduced in size to microscopic dimensions to enable convenient deployment and use by medical nanorobots. (Section 4.3.4)

50. Explore the limits of high-resolution X-ray microtomography for resolving capillary tubes at the 2-5 μm size scale. (Section 4.3.5)

51. Examine in greater detail the extent and specifics of organ and tissue surface perimeter excavation requirements. (Section 4.4.2)

52. Ascertain where and how much extracellular ice is likely to be present in cryonics patients of early vs. modern vintage, using various cryoprotectants and different cryopreservation protocols. (Section 4.4.3)

53. Enumerate sensor-driven ice peel scenarios during reconditioning and mapping of exposed ice surfaces, especially the degree to which biological features should be exposed, and evaluate the technical tradeoffs involved. (Section 4.5.3)

54. Undertake a more thorough design of the vasculoid, specifically as optimized for cryostasis revival tasks. (Section 4.6.1)

55. Devise and simulate an efficient plating algorithm to allow vasculocytes to walk into the frozen vascular tunnels along the walls, carrying their vasculoid plate cargoes to a predetermined destination. (Section 4.6.2)

56. Develop additional strategies for cracks that are narrower than 1 μm if experimental work determines that such cracks exist in significant numbers, and create different plate designs for blood vessels and for crackfaces if necessary to accommodate the differences between these structures. (Section 4.6.3)

57. Devise a specific protocol for inserting new vasculoid plates into an existing plate array without breaking the watertight seal and without disrupting any directional tensioning that is being employed by the array. (Section 4.6.5(4))

58. Better define and perfect scan technologies that are theoretically capable of providing the required submicron data resolution. (Section 4.7)

59. Identify suitably efficient deployable microscale transmitters and receivers for ~40 GHz acoustic waves, establish efficient coupling mechanisms between these devices and vitrified or frozen water-ice at 77 K (-196 °C), determine actual attenuation coefficients in this ice for ~40 GHz acoustic waves, and assess which deployment scenario offers the most favorable technical tradeoffs. (Section 4.7.1)

60. Ascertain whether a HIRES optical lens or some other optical scanning methodology is sufficiently general to be applicable to scanning *in situ* cryopreserved tissue blocks. (Section 4.7.2)

61. Explore the potential applicability of NSOM methods to submicron cryopreserved tissue scanning. (Section 4.7.2)

62. Examine the tradeoff between scan intensity and the tolerable limits of biological damage during submicron scanning using electron microscopy, given the posited super-redundancy of neural storage data. (Section 4.7.3)

63. Explore the full range of scanning electron microscopy techniques for possible use in cryostasis revival. (Section 4.7.3)

64. Determine if a practical low-voltage electron-based scanning system can be defined and assess whether the use of ice boreholes can assist in reducing the required scan distances in ice. (Section 4.7.3.1)

65. Assess the viability and limitations of direct chemohaptic sensing to perform 100-nm resolution cryopreserved tissue scanning. (Section 4.7.4)

66. Assess the possibility of obtaining sub-100-nm scan information using direct chemohaptic sensing on cryopreserved tissue. (Section 4.7.4)

67. Investigate whether the whole-body maps described for the conventional cell repair approach can provide sufficient information to initialize a human brain emulation, and if so, what degree of personal identity might be expected to be recoverable in the absence of a full molecular scan. (Section 4.8)

68. Need to more precisely quantify the bits of data storage needed for the essential description of the human connectome. (Section 4.8.1(5))

69. Investigate and develop sophisticated computational neuroscience and neuroinformatics algorithms and software packages to enable cryonics repair in the presence of extensive damage. (Section 4.8.1)

70. In order to correctly simulate the stimulation and transmission of neural impulses in and through the modeled tissue, knowing only the physical structure of that tissue, validate that (A) sufficient computer power and simulation expertise will be available in a nanotechnological milieu advanced enough to permit cryostasis revivals, and that (B) this level of analysis will be needed for only a modest fraction of the tissue that is seriously damaged in any particular cryopreserved patient. (Section 4.8.2)

71. Create efficient maximum likelihood estimation algorithms, techniques, and software applicable to the problem of revival from cryopreservation. (Section 4.8.2)

72. Create or obtain databases containing high-resolution scans of actual human brains and bodies representing a variety of genders, races, nationalities, ages, and states of health, including computerized “typical”, “consensus”, “standard”, or “generic” human models based upon actual scan data. (Section 4.8.3)

73. Explore the possible application of automated jigsaw puzzle-solving to the processing of 3D images and models of cryopreserved neural tissue in particular, and to cryostasis revival in general. (Section 4.8.3)

74. Explore and create cryonics-related studies of cytoarchitectural brain maps. (Section 4.8.3)

75. More precisely define the computational processes to be employed in simulations (e.g., molecular dynamics, continuum models, etc.) of crackface fusion repairs, and to more accurately estimate the required computational effort. (Section 4.8.4)

76. Create “baseline” and “computationally-repaired” brain and body models, the metrics to be used for comparison of similarity, the standards of success to be applied, the design of the simulation algorithms to be employed, and the precise data storage and computational requirements for executing those algorithms. (Section 4.8.4)

77. Investigate the possible utility of quantum computers for performing the many calculations required for cryostasis revival. (Section 4.8.5)

78. Evaluate whether a four-fold decrease in biochemical reaction rates from using a lower reliquidification temperature is worth the trouble of workspace pressurization to ~2000 atm. (Section 4.9)

79. Review which nanorobot activities can be successfully performed while employing transit velocities as slow as 10 μm/sec in vitrified tissues, and consider the impact if any on revival mission design. (Section 4.9)

80. Improve initial crackface number and volume estimates using appropriate microhistological studies of a representative variety of animal tissues that have been cryogenically preserved using several relevant cryoprotectants, cooling rate profiles, terminal temperature targets, and storage conditions and durations. (Section 4.9)

81. Examine whether a pulsed warming regimen that hurries through both the ice nucleation temperature region (137-173 K) and the ice growth temperature region (193-217 K) during a transition from 77 K to 273 K can maximally suppress the formation of ice during prethaw. (Section 4.9.1)

82. Quantify the reliquidification temperature for various tissues, locations, and percentage tissue perfusion with cryoprotectant, and viscosity profile as a function of temperature in all cases. (Section 4.9.1)

83. Assess the severity of potential disruption of non-synaptic junctions between cells and the separation of capillaries from surrounding brain tissue, possibly causing localized tissue tearing and maceration, during the cryopreservation process, and the possible need for additional corrective measures. (Section 4.9.1)

84. Analyze and quantify the technical tradeoff between slower unwanted biochemical reaction rates with longer active biomolecule extraction times, and the reverse, and determine the optimum protocol for cryostasis revival. (Section 4.9.1)

85. Determine the tensile strength of *in situ* solid-state M22 at various subfreezing temperatures by direct experimental measurements. (Section 4.9.2)

86. Model the rate of vasculoid-mediated crackface rejoining (e.g., due to creep in the ice) as a function of applied force, shear rate, and temperature. (Section 4.9.2)

87. Develop a staggering scheme for vasculoid-mediated crackface rejoining that allows removing one plate one at a time during contraction of the microtube bridging capillaries. (Section 4.9.2)

88. Specify and explore alternative crackface void geometries other than V-cracks and slip-planes. (Section 4.9.2)

89. Explore the limitations, parameters, and possible procedures for performing whole-body molecular extractions faster than the default ~1 hour specification. (Section 4.10)

90. Determine the utility for cryostasis revival of identifying and recording exactly which molecules came from where during molecular extraction. (Section 4.10)

91. Determine the proper order in which molecules should be extracted from reliquidifying tissues so as to maintain continuous liquidity at the lowest possible temperatures while the patient thaws. (Section 4.10)

92. Examine the merits of molecular extraction versus tissue washout and make a recommendation favoring one or the other of them. Which kind of extraction (and its priorities) may be sufficient for metabolic stasis is an experimentally accessible question that could be researched now. (Section 4.10)

93. Determine whether a molecular extraction that takes ~1 hour to complete at ~273 K / 0 °C (producing the equivalent of ~3 minutes of normothermic ischemic damage) is sufficiently fast to avoid significant rewarming damage. (Section 4.10)

94. Determine the number and identity of key molecules that could be extracted at least an order of magnitude faster by varying the selection of sorting rotor binding sites and by other means, if molecular extraction must be completed faster than ~1 hour. (Section 4.10)

95. Determine which ions or solutes should be left in place at some minimum active concentration and not be maximally extracted, in order to prevent possible cellular structural deterioration or destabilization. (Section 4.10)

96. Assess the advisability or necessity of injecting a few specialized inhibitor molecules to reduce the risk of fast-spiking reperfusion injuries as cells are warmed enough to reliquidify. (Section 4.10)

97. Create designs (and automated design processes) for reversible binding sites with the necessary specificity and affinity for the numerous target molecules required to complete the molecular extraction task. (Section 4.10.1)

98. Model and quantify the effects of higher viscosity on molecular extraction operations at ~273 K (0 °C). (Section 4.10.1)

99. Determine the actual threshold concentrations of all biologically relevant free molecules below which no significant degradative biochemical reactions will occur. (Section 4.10.1)

100. Directly measure experimentally the intracellular concentration of ATP in human tissues as a function of time and temperature post-mortem, and in cryopreserved human tissues. (Section 4.10.1.2)

101. Validate the assumption that an ATP concentration as low as 28 nmol/L is sufficient to eliminate essentially all biological activity, so that no further ATP needs to be extracted from the cryopreserved tissue during the revival process. (Section 4.10.1.2)

102. Compile a comprehensive inventory of reactive intracellular metabolites, including molecular types and concentrations, that are present in post-mortem human tissue. (Section 4.10.1.3)

103. Compile a comprehensive inventory of reactive plasma components, including molecular types and concentrations, in post-mortem human blood plasma. (Section 4.10.1.3)

104. Validate or correct the assumption that a 100-fold decrement in the concentration of each of the cell metabolite or blood plasma reactive molecular species is sufficient dilution to effectively ensure complete biochemical stasis (i.e., negligible reaction rates) at ~273 K (0 ºC) temperatures over the timespans that may be required to complete all revival processes, perhaps on the order of ~10^6-10^7 sec (12-120 days). (Section 4.10.1.3)

105. Determine the priority sequence in which molecular species should be extracted in order to minimize the risk of biochemical reaction, chemical degradation, enzymatic synthesis, enzymatic decomposition, or biological activation. (Section 4.10.1.3)

106. Develop the technology of automated binding site design, so that highly selective binding sites for large numbers of target molecules can be generated quickly with a minimum of scarce human labor. (Section 4.10.1.3)

107. Perform a comprehensive literature search and experimental measurements if necessary to determine the correct free intracellular phosphate concentration. (Section 4.10.1.4)

108. Expand binding site designs to include additional relevant ion/water clusters. (Section 4.10.1.4)

109. Explore and identify the types and concentrations of all apoptotic signaling molecules, then include them in the molecular extraction protocol to be executed immediately following reliquidification of the cryopreserved patient's body. (Section 4.10.1.5)

110. Specify the pharmaceutical agents that might typically be found in a cryopreserved patient and their anticipated concentration ranges, evaluate the risk they might pose if they are not extracted, and create a ranked priority list for molecular extraction. (Section 4.10.1.6)

111. Since data is not readily available, for completeness we should accurately determine the NOAEL (no observed adverse effects limit) threshold for 3-methoxy,1,2-propanediol, a component of the cryoprotectant solution M22. (Section 4.10.1.7)

112. Ascertain whether the extraction of cryoprotectant chemicals can safely be postponed until later in the revival protocol, either after resealing major membrane compartments or after primary cell repair operations using nanorobots, which could allow nanorobot repair operations to start sooner or at slightly lower temperatures. (Section 4.10.1.7)

113. Determine if there are any chemicals or materials that could be added to the carrier solution of cryoprotectants used today that might assist in future scanning, re-warming, or repair efforts using one of the revival processes described in this book. (Section 4.10.1.7)

114. Acquire or compile a comprehensive list of all ~1300 enzymes and their concentrations in various human cells, both free and membrane-bound. (Section 4.10.1.8)

115. Investigate any possible residual activity from membrane-bound enzymes that are not extracted during molecular extraction, and might require special inhibition. (Section 4.10.1.8)

116. Investigate the nature and frequency of damage to organelles with compartmented enzymes in response to cryoinjury, and to what extent enzymes are freed from membranes suffering cryoinjury. (Section 4.10.1.8)

117. Determine the minimum possible number and identity of molecules that must be extracted to ensure complete metabolic stasis during the revival process described here. Reducing the number and mass of essential extractable molecules reduces the analysis, design, and operational complexity of the nanorobotic systems needed for a successful revival from cryostasis. (Section 4.10.1.9)

118. Design more efficient branched plumbing architectures than a cylindrical probe tipped with a sorting rotor cluster to be extended straight from the lower surface of the vasculoid to each service point in the human body. (Section 4.10.1.9)

119. Rather than molecular extraction, evaluate an alternative approach in which tissue solutes are washed out by injecting a bolus of fresh water, allowing dissolved solutes to leach into the injected bolus, and then pumping the bolus out again, removing some fraction of the solutes with each rinse cycle. (Section 4.10.2)

120. Design and analyze a less naïve plumbing architecture for tissue washout, as compared to the simple default design proposed in the text. (Section 4.10.2)

121. Estimate the fraction of cryopreserved tissue cell plasma membrane surface area that is damaged and in need of repair, ideally using direct physical measurements. (Section 4.11.1)

122. Undertake a more comprehensive analysis of the logistics of complete scan and repair operational cycles using estimates of achievable nanorobot scan and repair rates. (Section 4.11.1)

123. Experimentally measure the paths and rates of passive migration of nanoscale and microscale objects of irregular shape through cytosol and extracellular matrix as a function of temperature and viscosity. (Section 4.11.1)

124. Investigate the size, quantity, and character of cell debris items likely to be created during cryopreservation and subsequent thawing, as a function of tissue type and the extent of cryoprotectant perfusion in that tissue, in order to more accurately estimate nanorobotic debris-processing requirements. (Section 4.11.1)

125. Determine the preferred temperature for cell repair. (Section 4.11.3)

126. Determine the proper solute mix needed to maintain osmotic stability as water is imported to rehydrate cells during the earliest phase of cell repair. (Section 4.11.3)

127. Determine the size distribution and number density of extracellular microbodies including microvesicles, exosomes, and apoptotic bodies that may be found in the interstitial spaces of the tissues of normal cryopreserved patients, that are potential extraction targets after warming and reliquidification. (Section 4.12.1.1 and Section 4.10.1.8)

128. Determine if microbodies are likely to be distributed roughly uniformly throughout the human extracellular tissue volume or instead will have some nonuniform distribution that could allow a more focused and speedier extraction process. (Section 4.12.1.1)

129. Specify details of vesicle recognition, acquisition, and multiple round trips to and from the nearest vasculoid cellulock to deliver the captured vesicles for export, to achieve comprehensive microbody clearance. (Section 4.12.1.1)

130. Ascertain the precise number and location of tissue-trapped RBCs and platelets to be removed from a cryopreserved human body, and the ideal procedure for their removal. (Section 4.12.1.2)

131. Examine whether replacement of phagocytic cells in the brain, rather than repair, is a feasible repair alternative. (Section 4.12.1.3)

132. Determine which microbes must be removed and which (if any) can be ignored during the cryopreservation revival process. (Section 4.12.1.5)

133. Determine under what circumstances it may be more efficient to excise tumor masses using a nanocatheter or nanosyringe apparatus, rather than a microbivore fleet. (Section 4.12.1.6)

134. Investigate the feasibility and desirability of replacing entire cells with externally remanufactured whole cells sourced from a cell mill, the limitations and potential difficulties of such wholesale replacement, and the circumstances under which such replacement would be preferable or more efficient than component-level *in situ* repair. (Section 4.12.2)

135. Determine the correct protocol for repairing cells that are determined to be in various stages of apoptosis or growth cycle, and specify how this protocol will vary based on cell type and cell location. (Section 4.12.2.1)

136. Specify details of type, count, and cursory inspection of organelles for damage, making multiple round trips to and from the nearest vasculoid cellulock to deliver scavenged debris items for export, and reporting data that has been gathered out of the cell. (Section 4.12.2.1)

137. Determine the likely state(s) of a cell nucleus inside a cell that has first been cooled to LN2 temperatures (with or without cryoprotectants) after a period of warm ischemia and then rewarmed to icewater temperatures. (Section 4.12.2.2)

138. Examine the extent to which the chromatin state of individual neurons may differ from their neighbors in ways that might affect long-term memory, and determine the extent to which neural genomes may require special handling by chromallocytes if generic autologous genomic structures will not suffice. (Section 4.12.2.2)

139. Analyze and resolve the question of whether it might be necessary to add certain solutes or ions into the cytosol in order to prevent newly introduced vesicular organelles from shrinking, swelling, or bursting due to unwanted osmotic imbalances during intracellular organelle replacement – an important consideration because new organelles could be introduced with internal inventories of enzymes and at least some reactive chemicals. (Section 4.12.2.3(II) and Section D.2.3)

140. Test and experimentally confirm the viability of both Golgi and ER self-assembly processes intended to be used during nanorobotic cell repair operations. (Section 4.12.2.3(III))

141. Investigate and ascertain the additional resource overhead required for the detachment and reattachment of organelles to the cytoskeleton during an organelle replacement operation. (Section 4.12.2.3(III))

142. Determine if (or under what conditions) delaying infusion of lipid droplet and glycogen granule organelles is necessary to maintain biochemical stasis throughout the remainder of repair activities until it is time to re-energize the cell via full instillation of activating molecules. (Section 4.12.2.3(III))

143. Determine the exact extent of cytoskeletal damage caused by cryopreservation. (Section 4.12.2.4)

144. Compile a comprehensive list of undesirable molecules likely to bind to membrane receptors, requiring replacement of the whole receptor complex. (Section 4.12.2.5)

145. Establish the identity and generic number density of lipids and proteins for each particular cell type, so that missing amounts can be manufactured in a cell mill and inserted into a cell under repair. (Section 4.12.2.6)

146. Investigate possible strategies for expediting reconnecting new protein to the cytoskeleton by employing self-assembly or complementary surfaces to facilitate protein reattachment to the cytoskeleton or to peripheral proteins. (Section 4.12.2.6)

147. Investigate the extent to which carbohydrates in the plasma membrane might have suffered damage during cryopreservation. (Section 4.12.2.7)

148. Determine the level of effort required for glycocalyx editing by nanorobots performing cell repair. (Section 4.12.2.7)

149. Review the possible damage mechanisms (and needed repairs) for other cytosolic components, including racemized, oxidized, or otherwise modified structures, protein reaggregation, and the possible need to reverse glycerol-induced biochemical reactions. (Section 4.12.2.7)

150. Design a nanosyringe mechanism that could be inserted directly through the skin and steered to specific locations inside organs or tissues. (Section 4.12.2.8)

151. As a conceptual design exercise, analyze the whole-cell replacement option that could provide dramatically shorter repair times for neuron cells. (Section 4.12.2.8)

152. Quantify the exact nature and amount of damage to tissue ECM (extracellular matrix) that should be expected during warm ischemia, perfusion, and cryopreservation, by performing experiments to directly test and measure these effects. (Section 4.12.3.3)

153. Design nanorobots (called fibrobots) that can scan ECM fibers and perform all necessary ECM repairs. (Section 4.12.3.3)

154. Confirm and quantify the stripping of myelin from axons (including formation of gaps between the axon membrane and the myelin, unraveling of the myelin, and possible tearing of the axolemma resulting in loss of intra-axonal material) as a possible damage mechanism resulting from cryopreservation. (Section 4.12.4.1)

155. Comprehensively survey all key plasma membrane receptors employed in neural function and establish nominal membrane number density concentrations for each receptor type, for each cell type. (Section 4.12.4.2)

156. Identify and quantify situations where high release rates of nonactivating molecules during molecular instillation might cause damage by briefly creating localized concentrations of mixed molecules high enough to induce protein misfolding, molecular dehydration, enzyme poisoning, or other pathologies, if any, that could require more restrictive constraints on maximum release rates. (Section 4.13.2)

157. Determine if the presence of pharmaceutical-based general anesthetics in the cryopatient's body might mechanically distort neuronal lipid bilayer membranes, in turn affecting the process or reliability of plasma membrane repair. (Section 4.13.2)

158. Identify unwanted components that are present (to be removed) and desired components that are missing (to be restored) in a variety of bulk body fluids (lymph, synovial, CSF, etc.) during

molecular instillation, and their likely appearance or disappearance as a result of the cryopreservation process. (Section 4.13.3)

159. Enumerate the non-obvious "activating molecules" – chemical substances that can initiate, activate or sustain biochemical activity, perhaps including inhibitory metabolites that are normally present and needed to control the overactivity of other proteins or necessary protein cofactors – besides the more obvious ones (e.g., oxygen, glucose, ATP, etc.) involved in molecular instillation. (Section 4.13.4)

160. Critically examine the presumed preferability of introducing a temporary blood substitute before manufactured natural blood during the vasculoid uninstall procedure near the end of the revival process, and investigate the circumstances under which manufactured natural blood could be transfused without a temporary blood substitute precursor. (Section 4.14.1)

161. Enumerate the totality of the special biological functions performed by natural blood in order to ensure that nanorobots can be designed to supply all necessary functionality for a period of time sufficient to complete all revival tasks. (Section 4.14.1)

162. Determine the ideal mix of nanorobots, transport capabilities, and solutes to be dissolved in the carrier fluid of the temporary blood substitute that replaces the patency-preserving humid nitrogen gas that was insufflated into the total enclosed volume vacated by the vasculoid as the appliance was withdrawn during revival. (Section 4.14.1.1)

163. Verify the assumption that perfusion with cryoprotectants should only flush out the contents of the arteriovenous vasculature and not the contents of the lymphatic vasculature or the lymph nodes, so that the lymphocyte cell population of lymph nodes can remain intact and available for replication after cryopreservation. (Section 4.14.1.2)

164. Determine specific cytosolic release times, sequences, patterns, and organelle locations for each of the different "activating molecules" needed to initiate normal metabolism during revival. (Section 4.14.3)

165. Determine an appropriate post-repair revival protocol, possibly including the application of ACLS (Advanced Cardiac Life Support), medications, or electrical signals to stimulate the patient's heart to begin pumping and the lungs to begin normal respiration. (Section 4.14.3)

166. Determine if caution dictates first re-starting metabolism at temperatures just warm enough for spontaneous heartbeat, then monitoring the effects at the slower metabolic rate. (Section 4.14.3)

167. Decide the utility of restarting metabolism only in selected tissues or organs before it is restarted in others, if it is deemed useful to activate metabolism in stages. (Section 4.14.3)

168. Determine if some specific electrical or biochemical stimulus may be required to restart normal neural signal processing and other electrical activity in the brain. (Section 4.14.3)

169. Attempt to ascertain what cytometabolic complications might arise during metabolic restart procedures during revival. (Section 4.14.3)

170. Define an appropriate set of patient awakening protocols. (Section 4.15)

171. Design a test – perhaps a customized list of questions or tasks – that the patient could take to quantify exactly how much of their original memory and personality remains intact. (Section 4.15)

172. Define a process by which the revived patient can be re-integrated into society. (Section 4.15)

173. Determine the extent to which the nominal serial revival protocol using conventional cell repair can be temporally shortened or made more efficient. (Section 4.16)

174. Analyze whether neuro or whole-body repair procedures may be easier to parallelize. (Section 4.16)

175. Determine whether continuous vacuum pumping will be required throughout a molecular scan procedure, since the excavated cryopreserved body cannot be subjected to the customary high-temperature bakeout process to prevent outgassing but must be maintained at cryogenic temperatures for the duration. (Section 5.2.1)

176. Resolve the apparent discrepancy in reported ice sublimation rates in vacuum and normal air, perhaps including some study of the vacuum freeze-drying literature, other relevant literature sources, additional theoretical analyses, and direct experimental measurements if necessary. (Section 5.2.1)

177. Fully investigate the best tool for mechanosynthetic abstraction of water molecules from cryopreserved tissue. (Section 5.2.1.1)

178. Enumerate and quantify the ions and small molecules such as isolated amino acids, glucose, and the like that must be abstracted in order to disassemble cryopreserved tissue, and design and simulate molecular abstraction tools for all such targets. (Section 5.2.1.1)

179. Design, simulate, and test a whole set of useful reactions for the positionally controlled mechanosynthetic disassembly of organic molecules including proteins, carbohydrates, lipids, and others, as needed to disassemble cryopreserved tissue. (Section 5.2.1.2)

180. Pursue development of alternative recharge reaction sequences that may be required to restore to service exhausted HAbst-X tools bearing payloads other than hydrogen. (Section 5.2.1.2)

181. Assemble statistics of atom removal for proteins, carbohydrates and other polymeric biomolecules. (Section 5.2.1.2)

182. Determine the optimum subtractive mechanosynthesis protocols for performing a molecular scan on all types of biomolecules found in the human body, then design and simulate the specific mechanosynthetic tools needed to do it, while more accurately assessing the achievable biomolecule atom abstraction rate. (Section 5.2.1.2)

183. Examine possible mechanosynthetic tools, tool motions, and reaction sequences necessary for performing subtractive mechanosynthesis on more densely-bonded structures such as 3D cage molecules and sp^3-dense structures, with solid diamond structures representing the most extreme circumstance of this situation. (Section 5.2.1.2)

184. Examine the feasibility and relative efficiency of molecular rather than atomic disassembly of cryopreserved human tissue. (Section 5.2.1.2)

185. Formulate a more detailed estimate of the water and biomolecule clearance rates during a destructive whole-body mechanosynthetic molecular scan. (Section 5.2.1.3)

186. Investigate ideal geometries and the optimum degree of segmentation for destructive molecular scanning using a multiplicity of cross-sectional slices. (Section 5.2.1.3)

187. Examine the ideal methods and geometries for segmentation of the body of the cryopreserved patient for quick molecular scanning, including nanorobotically-enabled atomically fine cutting methods that preserve structural information across all matched cut planes. (Section 5.2.1.3)

188. Design the support sheet of atomically precise infrastructure that includes power supplies and mechanical actuators to drive the manipulator joints, tunnels and transport mechanisms to deliver tools and other materiel to and from the nanomanipulator tips, and provides sufficient structural rigidity to maintain the necessary positional registration as the support sheets are moved around in space and as the manipulators perform their various operations on cryogenic tissues. (Section 5.2.1.3)

189. Specify and design the atomically-imprecise macroscale supporting infrastructure (e.g., circulating coolant pumps and pipes, electrical power supplies, cryogenic vacuum systems, patient support crib, slice-handling mechanisms, etc.) for the atomically-precise molecular scanning equipment. (Section 5.2.1.3)

190. Verify that memory volume can be reduced using compactification that degrades data quality in specific acceptable ways in the initial scan file compiled during a molecular scan. (Section 5.2.2.1)

191. Develop algorithms to accurately infer the location of all water molecules in a compactified version of the initial scan file compiled during a molecular scan, when that location information has been deleted to save memory space. (Section 5.2.2.1)

192. Examine the technical merits and demerits of reducing data storage volume without sacrificing water or biomolecule detail data by allowing only one segment to be processed at a time in the initial scan file during molecular scan processing. (Section 5.2.2.1)

193. Can there exist a nonlethal mental defect – e.g., a case of moderate dementia that might preclude the possibility of informed consent if left uncorrected but would otherwise not affect the immediate viability of the patient's printed replacement body? (Section 5.2.2.2)

194. Examine the philosophical, legal, ethical, and technical aspects of a hypothetical procedure in which the scan file of a cryopreserved patient is repaired sufficiently to allow the generation of a computer-simulated conscious upload, whereupon the uploaded person is fully informed, educated, and then assents to additional procedures that will be applied to the replacement body (though not necessarily applied to the uploaded person). (Section 5.2.2.2)

195. Describe and design a Digital Repair Algorithm to compare observed structures detected in the initial scan file from a molecular scan with the structures of biological components whose state is considered healthy, normal, or ideal, then computationally transform the observed state into a normal state, in part by searching the entire initial scan file for pattern matches to the premises or conditions specified by all the rules, and then applying the limitations or actions prescribed by each rule in a predetermined priority order. (Section 5.2.2.2)

196. Improve the accuracy and reliability of the data processing cost estimates for compiling a corrected scan file, starting from an initial scan file from a whole-body molecular scan. (Section 5.2.2.2)

197. Examine feasible alternatives for converting the corrected scan file (produced by a molecular scan) to a synthetic conversion file in which all biological neurons are computationally replaced with artificial neurons of similar or smaller size, allowing biological structures in the patient's body to be replaced with artificial modules that mimic the original biological function of the patient's neural tissues. (Section 5.2.2.3)

198. Investigate the theoretical possibility of a general-purpose radical-free mechanochemistry that could remove the constraint of working in a UHV (ultra-high vacuum) environment from the atomic printing process. (Section 5.2.3.1)

199. Critically evaluate the assumption that an atomically-precise 3D-printed replacement body must be constructed in a cryogenic fabrication chamber under UHV, probably at ~10^{-12} atm pressure and LN2 temperatures. (Section 5.2.3.1)

200. Enumerate and quantify all sources of mechanosynthetic process error (e.g., the mechanical instability of tooltip placement mechanisms, metrological measurement errors, etc.) once simple mechanosynthetic systems of molecular manufacturing are in more widespread experimental use. (Section 5.2.3.1)

201. Critically review the validity and details of the "embedded cryoprotectants" protocol to prevent rewarming damage in 3D atomic-printed replacement bodies. (Section 5.2.3.1(A))

202. Undertake the technical and mission design of thermal generator nanorobots (thermocytes) to enable sufficiently fast and uniform whole-body warming. (Section 5.2.3.1(B))

203. Analyze the warming protocol, including determining (A) the minimum rapid-warming rate needed to avoid ice formation, (B) the warming power needed using thermophysical parameters for M22 solution rather than pure water, (C) the safe maximum heating rate and maximum tolerable uniform body-wide power density, and (D) the potential utility of a spatially patterned heating wave rather than simultaneous uniform nanorobot activation throughout the entire body. (Section 5.2.3.1(B))

204. Explore the ideal low-density distribution print pattern to minimize the buildup of mechanical stress and warmup fracturing, for the particular cryoprotectant compositions and concentrations chosen, during warming of 3D atomic-printed replacement bodies. (Section 5.2.3.1)

205. Define the appropriate molecular tools and procedures for handling two special circumstances that will occur repeatedly during an atomic print run: (A) how to initiate the fabrication of a new biomolecule when no atoms have yet been laid down to anchor the initial structure onto the workpiece as the next atoms are emplaced; and (B) how to pick and place water molecules onto the growing workpiece. (Section 5.2.3.1)

206. Parameterize the key variables and explore the optimum volume, geometry, and dimensions of the print slices for molecular print jobs, based on technical tradeoffs – e.g., weighing the benefits and demerits of replacing large print slices with vastly more numerous manufactured cubes 1 mm^3 or even 1 μm^3 in size. (Section 5.2.3.1 and Section 5.2.3.2)

207. Critically review the details and validity of the 3D atomic print protocol. (Section 5.2.3.1)

208. Develop specifications, software concepts and designs, and the computer hardware necessary to create and run the MASA code package, including at least a tenfold improvement in computational efficiency over the Sholomon algorithm. (Section 5.2.3.2)

209. Specify and design reversible binding sites, temporary jigs, and assembly procedures that are needed for the Biomolecule Synthesis Module of the cell mill, supporting molecular print jobs. (Section 5.2.3.2)

210. Critically review the details and validity of the 3D molecular print protocol. (Section 5.2.3.2)

211. Define the special mechanosynthetic tools, reaction sequences, and related procedures needed to fabricate extended regions of noncovalently bonded ionic solids such as hydroxyapatite that are found in the teeth (e.g., enamel, dentin, and cementum) and bones of the human body, for a cryogenic 3D molecular print job. (Section 5.2.3.2)

212. Examine reasonable estimates for molecule placement rates during 3D molecular print jobs. (Section 5.2.3.2)

213. Confirm that a fluidic 3D cell print can recreate a replacement body with sufficient fidelity to the (repaired) original patient as to preserve acceptable levels of patient memory and personal identity. (Section 5.2.3.3)

214. Can a cell mill reproduce the original molecular structure of fabricated cells to sufficient accuracy and completeness to preserve memory and personal identity? (Section 5.2.3.3)

215. Are biological printed structures stable enough over the course of a fluidic print job that may take many days or weeks to complete – e.g., might normal thermal agitation in 273 K (0 °C) water cause sufficient physical displacement of a precisely positioned synapse to reduce the fidelity or information content of a particular unit of memory? (Section 5.2.3.3)

216. Investigate non-water possibilities for the 3D cell print assembly fluid. (Section 5.2.3.3)

217. Examine the computational details by which a corrected scan file can be converted into a cell print file appropriate to planar tissue printing, scaffolded tissue printing, and nanorobot-guided organic growth. (Section 5.2.3.3)

218. Investigate the details of planar tissue printing, scaffolded tissue printing, and nanorobot-guided organic growth, and other possible fluidic 3D cell printing techniques, then perform a trade study to determine which method may produce the most desirable results with the greatest efficiency and lowest cost. (Section 5.2.3.3)

219. Define the appropriate size and shape of fragments of noncovalently bonded ionic solids such as hydroxyapatite that may be fabricated in a cell mill, and the bonding methods appropriate for joining these fragments into extended proteinaceous matrices as found in human teeth (e.g., enamel, dentin, and cementum) and bones, during a fluidic 3D cell print job. (Section 5.2.3.3)

220. Provide more complete details of the planar tissue based fluidic 3D cell printing process. (Section 5.2.3.3.1)

221. Enumerate the types and likely numbers of overlong cells, describe and parameterize the process of their emplacement using shepherd nanorobots, and estimate the size, number, run time and power consumption of the nanorobots required to complete the 3D cell print of the replacement body in concert with other Tissue Assembly Plate mechanisms and operations. (Section 5.2.3.3.1)

222. Examine the challenge of nanoscale and microscale fiber network assembly during planar tissue printing, and devise multiple technical strategies that can be compared in an engineering trade study to select the best alternative. (Section 5.2.3.3.1)

223. Provide more complete details of the scaffolded tissue based fluidic 3D cell printing process. (Section 5.2.3.3.2)

224. Confirm (or disprove) that a purely structural description of the brain's connectome and synaptome down to ≥100 nm resolution is sufficient to initialize a WBE that can subsequently simulate the trafficking of much smaller molecules (e.g., neurotransmitters and metabolites) than the larger synaptic structures that dispense and absorb them. (Section 5.2.3.4(1))

225. Determine which of two scanning modalities – nanometric structural only, or nanometric structural and chemical – will suffice to create and operate a WBE. (Section 5.2.3.4(2))

226. Analyze methods by which an upload could translate its data structures (algorithms, memories, etc.) into a biological brain supported by a biological body, possibly requiring detailed custom rewiring of the neural connectome of the brain. (Section 5.2.3.4.2)

227. Examine and validate the apparent conclusion that higher scan resolution generally requires increased invasiveness but does not require irreversible destruction. (Section 5.3)

228. Determine if the molecular and ionic solid components of the body should be separated for scanning purposes and processed in different environments, then reassembled appropriately, or if this just creates unnecessary complications. (Section 5.3.1)

229. Identify all special situations to be encountered in a nondestructive molecular scan (e.g., scanning ionic solids, initial anchoring at the start of a scan, etc.) and propose methods for accommodating each of them. (Section 5.3.1)

230. Identify alternative tooltip structures or mechanisms that can bond more weakly to a membrane lipid and thus may more readily release the molecule at the appropriate time. (Section 5.3.1)

231. Explore the range of reasonable multiblock scenarios for scanning and reassembly in a nondestructive molecular scan. (Section 5.3.1)

232. Investigate and develop algorithms for performing reconstructive analysis of flawed tissue, replacing it with a description of unflawed tissue, in a nondestructive molecular scan, along with the databases necessary to support such analysis. (Section 5.3.2)

233. Investigate the feasibility, possible methods, and desirability of attempting appropriate error-correction procedures to correct scan-derived faults in the initial scan file data. (Section 5.3.2)

234. Provide more complete details of the cryogenic molecular exchange repair of the original patient body. (Section 5.3.3.1)

235. Provide more complete details of the fluidic molecular-informed cell repair of the original patient body. (Section 5.3.3.2)

236. Review and assess more advanced methods for molecular reconstruction of the repaired human body that could in principle complete the work in much less time but which might involve various operational complexities. (Section 5.4)

237. Explore the processes and challenges of cryostasis revival using convergent assembly after a molecular scan. (Section 5.4)

238. More carefully evaluate cost factors including computation, revival hardware, human labor, and infrastructure, in order to prepare more realistic whole-procedure cost estimates for whole-body and neuro molecular reconstruction. (Section 5.5)

239. Perform a closer study of the scanning and reconstruction rates likely to be achieved in physically realizable molecular manufacturing systems on cryogenic biological workpieces. (Section 5.5)

240. When creating replacement bodies for neuro patients, assess the validity of an assumption – that the assumed preferred procedure is to warm a fully-repaired cephalon to reliquidification temperature (~273 K) in full metabolic stasis and then attach the replacement body to complete the revival process – by examining if there is any advantage in building an isolated cryogenic trunk, and if building a cryogenic replacement trunk and attaching it to a full-repaired cryogenic cephalon at cryogenic temperatures could risk additional damage to the cephalon as the recombined patient is warmed and revived. (Section 6.0)

241. Design a virtual replacement body for an uploaded person. (Section 6.0)

242. Assess whether any significant parts of memory or personality reside outside of the cephalon. (Section 6.0)

243. Investigate whether the loss and subsequent replacement of one's physical body with something else might trigger heretofore relatively rare psychological conditions such as body integrity identity disorders in revived cryopreservation patients. (Section 6.0)

244. Create or describe methods for determining all epigenetic modifications of the patient's original DNA code. (Section 6.1.1)

245. Investigate the design and operation of an artificial womb suitable for incubating a fabricated ovum from embryo to adult size. (Section 6.1.1)

246. Investigate the means by which the developing embryo and fetus can be grown through all phases of tissue maturation in a strictly acephalic condition without disturbing any other growth processes such as proper spine formation, arteriovenous vascular formation, neck musculature, and the like. (Section 6.1.1)

247. Determine how fast an acephalic replacement human body can be grown. (Section 6.1.1)

248. Investigate all possible means for accelerating the cell growth cycle. (Section 6.1.1)

249. Investigate all systemic scaling restrictions that may limit the maximum rate of biological growth of large organisms. (Section 6.1.1)

250. To partially overcome systemic scaling restrictions using nanorobot-assisted biological growth, evaluate the feasibility of using a fleet of coordinated mobile shepherd nanorobots to more quickly reconfigure developing neural tendrils and axons, capillary networks, muscle and extracellular matrix fibers, and similar biological structures at a greater speed than natural motility processes normally allow. (Section 6.1.1)

251. Determine if excess waste heat generation could be an additional constraint on the maximum rate of biological growth. (Section 6.1.1)

252. Examine the feasibility of high growth rates of body trunk mass and, if possible, estimate the maximum limits to macroscale biological growth rates. (Section 6.1.1.2)

253. Evaluate the possible need for a supply of migratory or special-purpose biological cells (e.g., neutrophils, macrophages, lymphocytes, stem cells) to the fully-repaired brain or its surrounding tissues residing in a head caddy or biocompatible artificial body. (Section 6.1.3)

254. Validate or refute the expectation that artificial body costs might fall by up to 10-100 fold from the present-day, given likely cost reductions in the early decades of the future nanorobot-rich cryostasis revival era along with at least modest demand for artificial or augmented whole-body work in the general population. (Section 6.1.4)

255. Analyze whether full molecular reconstruction of the trunk could negate much of the cost savings of the neuro option and end up costing slightly more than the whole-body option because of the extra work involved. (Section 6.2)

256. Review the implementation details and the implications for revival of alternative biostasis scenarios, most of which have received significantly less study than the traditional cryopreservation scenario. (Section 7.1)

257. Consider methods by which those blocks of tissue suffering unwanted ice formation could be extracted from the body, separately processed via molecular reconstruction, and then returned to the body with full interfacial reintegration with existing tissue. (Section 7.1.1)

258. Examine the nature and extent of various classes of "partial vitrification" scenarios, and determine the optimal procedure in each class. (Section 7.1.1)

259. Critically assess the conjecture that the state of "straight freeze" tissue is worse than the same case for vitrification, but perhaps might be not as much worse as generally thought. (Section 7.1.1)

260. More detailed DSC (differential scanning calorimetry) study of ice nucleation near and below the glass transition temperature is needed to fully understand the nature of the nucleation process, especially to confirm that nucleation is driven mainly by heterogeneous nucleation (catalyzed by surfaces) and not homogeneous nucleation (happening wherever there are water molecules). (Section 7.1.2)

261. Determine if we can fit a physically plausible mathematical function to nucleation rate as a function of temperature, whereupon we might be able to calculate a temperature at which the nucleation rate is sufficiently negligible that we might be comfortable ignoring it. (Section 7.1.2)

262. Devise protocols for revival from intermediate temperature storage (ITS) if any cryonics service provider ever offers ITS for whole-body cryopreservation. (Section 7.1.2)

263. Closely examine the extent of aldehyde-stabilized cryopreservation (ASC) based molecular alterations to cryopatient tissues. (Section 7.1.5)

264. Investigate the specific requirements and extent of additional computations required to determine the original healthy state as compared to conventionally cryopreserved tissue during molecular reconstruction of ASC-preserved tissues. (Section 7.1.5)

265. Explore more broadly the fixative-stabilized cryopreservation (FSC) alternatives to conventional vitrification cryopreservation. (Section 7.1.5)

266. Perform an experimental study to show that present cryopreservation methods preserve the brain's connection architecture as well or nearly as well as aldehyde-stabilized cryopreservation. (Section 7.1.5)

267. Seek pathways to achieving true suspended animation where minimal repairs to the body are needed, which would maximize the likely recovery of personal identity upon repair and revival. (Section 7.1.6)

268. Perform a more comprehensive nanorobot and mission design for the nanostasis application. (Section 7.1.6.5)

269. Investigate whether living scans might be made illegal if courts determine that the scanning method "kills" or might "kill" a human patient who is subjected to the procedure while still alive, raising potential issues of homicide or suicide. (Section 7.1.8)

270. Carry out studies to demonstrate post-cryopreservation survival with memories for more advanced animal species than *C. elegans*. (Section 7.2.1.1)

271. Review existing knowledge of animal language ability and determine if posing questions regarding internal mental states to animal subjects might provide useful information for determining the success or failure of an experimental cryostasis revival procedure, and if so, exactly how this might be done. (Section 7.2.1.4)

272. Direct measurements and inspection of the physical structure of all neurons, dendrites, and synaptic connections inside the working brains of live subject animals, both before and after the cryopreservation/revival protocol is performed, using nanorobots, will underlie a major part of the research process that leads to the development of the cryostasis revival protocol itself. (Section 7.2.1.5)

273. Validate, nuance, or disprove the tentative conclusion that a successful primate validation of cryonics revival protocols should provide sufficient evidence to warrant application of the same protocol to human cryopreservation patients, and should be vigorously explored by careful detailed comparisons of human and nonhuman primate neurological ultrastructure and brain cytoarchitecture. (Section 7.2.1.5)

274. Determine if it is possible to identify at least one crucial identity-relevant neurological structure that is found only in human brains but not in the brains of primates and is sufficiently different from analogous biological structures that a nanorobotic repair procedure that has been proven to succeed on primate brains might somehow fail to repair the structure in human brains. (Section 7.2.2)

275. Critically assess the feasibility of the proposed ethically acceptable protocol for evaluating a revival protocol involving an experimental scan technology and an experimental scan-to-WBE algorithm on human volunteers. (Section 7.2.2)

276. Devise a set of molecular tools and reaction sequences to mechanosynthetically fabricate most simple organic molecules of interest, including hydrocarbons, carbohydrates, and other important biomolecules (e.g., amino acids) containing additional key elements such as nitrogen (N), sulfur (S), and phosphorus (P). (Section D.1.1.2)

277. Investigate automated mechanosynthetic reaction sequence generation to minimize or eliminate the human labor requirement. (Section D.1.1.2)

278. Determine if a collection of at least 100 whole-cell samples taken from the patient's cryopreserved body should be randomly collected, or instead should be clustered in a specific location or organ where DNA damage is believed to be minimized. (Section D.1.2.1.1)

279. Verify that the base pair sequences and methylation patterns on chromosomes and DNA are not disturbed by the presence of the cryoprotectant chemicals used in cryopreservation. (Section D.1.2.1.1)

280. Create a detailed design for a nanorobotic DNA long-strand fabrication system. (Section D.1.2.2)

281. Design a nanorobotic protein synthesis system that is equally or more productive than ribosomes. (Section D.1.2.3)

282. Decide if it could be appropriate for multi-subunit proteins to be allowed to self-assemble, or if they should only be assembled under full positional control. (Section D.1.2.3)

283. Determine if alternative processes involving partial self-assembly of histones and other chromatin-associated proteins or "architectural proteins" onto positionally synthesized DNA can be equally reliable but more efficient as positionally fabricated systems. (Section D.2.2(6))

284. Determine whether a biogenesis-type approach to manufacturing organelles is feasible or advisable, as compared to positionally-controlled processes that may serve as the foundation for most organelle assembly operations. (Section D.2.3)

285. Specify or design any necessary additional mitochondrion assembly steps that might be required to complete the organelle, beyond those already described in the text. (Section D.2.3(C))

286. Compile a list of all essential post-processing steps in fabricating vesicular organelles – such as decorating the exterior surfaces of organelle membranes with protein or carbohydrate moieties, or inserting sorting rotor probes through the outer membrane into the sealed interior of the organelle to extract or insert particular molecules of interest – and elucidate the nanorobotic means for accomplishing these post-processing steps. (Section D.2.3(D))

287. Examine and critically re-assess the preliminary assessment that although membraneous organelles could be laboriously assembled fragment by fragment via positionally-controlled nanorobotic pick-and-place operations, under the correct conditions these organelles will largely self-assemble in place from proximately-emplaced simpler vesicular components that can be manufactured by a cell mill. (Section D.2.4)

288. The viability and specific methodology of endoplasmic reticulum (ER) self-assembly processes must be tested and experimentally confirmed. (Section D.2.4(2))

289. Verify the presumption that when a newly manufactured cell is metabolically activated, the previously-installed chromatin will self-arrange to form the nucleolus, the primary site of ribosome biogenesis in the cell. (Section D.2.5(7))

290. Determine if "nucleolar detention" of a number of post-translational regulatory proteins must be initially provided by the nucleolus. (Section D.2.5(7))

291. Confirm that the installation of "nuclear bodies" in the nucleus of some or all cell types is essential for full cell viability and functionality. (Section D.2.5(8))

292. Compile a list of all essential post-processing steps in fabricating a cell nucleus – such as attaching cytoplasmic filaments on the cytosolic face of the nuclear pore complex – and elucidate the nanorobotic means for accomplishing these post-processing steps. (Section D.2.5(9))

293. Test the supposition that the components of a cell are essentially modular, hence can be manufactured separately and later assembled into a complete working biological cell, by reassembling living cells from larger numbers of component parts than has been experimentally achieved to date (i.e., ~5). (Section D.3)

294. Determine the optimum assembly sequence for all components in each hemisphere during positional assembly of the cell corpus. (Section D.3.1)

295. Investigate the dynamic nature of some cytoskeletal components under physiological conditions that may necessitate special procedures for cytoskeleton build-out. (Section D.3.1)

296. Compile a list of all essential post-processing steps in a cell assembly process – such as bonding cytoskeletal elements across the join plane between the two hemispheres in whatever manner may be required using membrane-inserted manipulators or nanorobots, or inserting sorting rotor probes through the plasma membrane into the cytosol to extract or insert particular molecules of interest – and elucidate the nanorobotic means for accomplishing these post-processing steps. (Section D.3.1)

297. Devise procedures for assembling neurons with lengthy axons and other nonstandard cell shapes. (Section D.3.2)

298. Detail methods for assembling specified blocks of extracellular matrix in a cell mill. (Section D.3.2)

299. Add more detail to the Molecular Assay System architecture. (Section F.0)

300. Further conceptualize, extend, and develop mechanical tip-scanning techniques to enable determination of both element identity and molecular geometry (including bond order) of all molecules of relevance to cryopreservation revival. (Section F.1.5)

301. Devise a system design for the Molecular Assay System that provides the large number of Lab Modules with access to infrastructure utilities including sample molecule preparation and distribution, electrical power distribution, a central computer providing process guidance and library functions, a materials distribution system for feedstock and waste, and a communications system linking all the Lab Modules to each other and to the external control interface. (Section F.2.2)

302. Review and explore a variety of generic binding site motifs, which for medical applications might initially include targets such as small molecules, monosaccharides, polysaccharides, amino acids, proteins, fatty acids, lipids, and drugs; need more work on binding site design. (Section H.0)

303. Analyze, refine details, and extend the proposed nanorobot washout protocol for quickly removing nanorobots from the bloodstream. (Appendix M)

304. Identify tradeoffs among revival methods, both at a high level (i.e., Plan A or Plan B) and for the choices identified by these research questions (e.g., faster vs. more accurate vs. cheaper revival options) – this could be useful reference information for current Alcor members who wish to state their preferences among these tradeoffs by making them much more specific than the general conceptual questions available now.

Image Credits

Front Cover Art

Collage selected and arranged by Natasha Vita-More. Respirocyte design by Robert Freitas. Respirocyte image at lower left: Edrenaline / E-spaces, “Respirocytes Flowing Through a Blood Vessel” (1999), Philippe Van Nedervelde. Respirocyte image at lower right: “Four Respirocytes” (1999), Forrest Bishop.

1.1

Vitrified kidney: https://i1.wp.com/134.209.46.227/wp-content/uploads/2020/08/kidney.jpg?resize=350%2C263

1.2.1

Four Respirocytes: Forrest Bishop (1999); https://web.archive.org/web/20160325053612/https://foresight.org/Nanomedicine/Gallery/Captions/Image139.html.

Respirocyte Pumping Station Layout: Robert A. Freitas Jr., 1996; https://web.archive.org/web/20161228102818/http://www.foresight.org/Nanomedicine/Gallery/Captions/Image123.html.

Respirocyte Equatorial Cutaway: Robert A. Freitas Jr., 1996; https://web.archive.org/web/20210508220059/https://foresight.org/Nanomedicine/Gallery/Captions/Image124.html.

Respirocytes and Red Blood Cells, in Repose: Forrest Bishop (1999); https://web.archive.org/web/20210508220644/https://foresight.org/Nanomedicine/Gallery/Captions/Image140.html.

1.2.2

Microbivore hull: Forrest Bishop (1999); development image.

Microbivore: Forrest Bishop (1999); https://web.archive.org/web/20160827082558/https://foresight.org/Nanomedicine/Gallery/Captions/Image197.html.

Microbivore receptor array: Forrest Bishop (1999); development image.

Microbivore grapples on surface: Forrest Bishop (1999); development image.

Microbivore grapples motion study: Forrest Bishop (1999); development image.

Microbivore action sequence: Forrest Bishop (1999); from contract video.

Neutrophil Chasing Bacteria: https://embryology.med.unsw.edu.au/embryology/index.php/Movie_-_Neutrophil_chasing_bacteria.

1.2.3

Chromallocyte hull: Stimulacra (2006); development images.

Chromallocyte penetrating cell: E-Spaces (2009); from video presentation.

Chromallocyte penetrating nucleus: E-Spaces (2009); from video presentation.

Desktop sequencer: https://www.bioprocessonline.com/doc/fluidigm-biomark-system-helps-assure-the-0001.

Reclining patient: stock artwork.

Chromallocyte action sequence: E-Spaces (2009); from video presentation.

1.2.4

Vascular images: https://i.pinimg.com/474x/6d/6e/28/6d6e28839ae53d0410f19e295cc65cd0.jpg.

1.3.1

Carbon dimer donation to diamond surface: Image prepared by Freitas.

DCB6Ge-Xtip (left): Image prepared by Freitas.

Atomistic mechanosynthesis robot arm (right): Damian Allis’ website; https://www.somewhereville.com/nanotechnology-gallery/.

Diamond logical rod (left): Image prepared by Freitas.

Hydrocarbon bearing (center): Image prepared by Ralph Merkle.

Hydrocarbon universal joint (right): Image prepared by Ralph Merkle.

Four atomically precise molecular machines: Images from Nanorex (out of business); https://chem.beloit.edu/classes/nanotech/nanorex/index.html.

Mechanosynthetic production line: Burch & Drexler (2006), Lizardfire Nanofactory video; https://www.youtube.com/watch?v=zqyZ9bFl_qg.

1.3.2

Ultrasharp tips: Wu CC, Ou KL, Tseng CL. Fabrication and characterization of well-aligned and ultra-sharp silicon nanotip array. Nanoscale Res Lett. 2012 Feb 13;7(1):120; http://www.ncbi.nlm.nih.gov/pmc/articles/PMC3292956/.

Four nanofactory images: Burch & Drexler (2006), Lizardfire Nanofactory video; https://www.youtube.com/watch?v=zqyZ9bFl_qg.

Two desktop nanofactory images: Burch & Drexler (2006), Lizardfire Nanofactory video; https://www.youtube.com/watch?v=zqyZ9bFl_qg.

Convergent assembly nanofactory image: Burch & Drexler (2006), Lizardfire Nanofactory video; https://www.youtube.com/watch?v=zqyZ9bFl_qg.

2.1.2

Neuron schematic: https://neurosciencenews.com/calcium-neuron-memory-2270/.

Neuron on surface: Stern S, Debre E, Stritt C, Berger J, Posern G, Knöll B. A nuclear actin function regulates neuronal motility by serum response factor-dependent gene transcription. J Neurosci. 2009 Apr 8;29(14):4512-8; https://www.ncbi.nlm.nih.gov/pmc/articles/PMC6665722/.

Hippocampal dendrites and spines: Bourne JN, Harris KM. Balancing structure and function at hippocampal dendritic spines. Annu Rev Neurosci. 2008;31:47-67; http://www.ncbi.nlm.nih.gov/pmc/articles/PMC2561948/.

Two micrographs of synapses: https://synapseweb.clm.utexas.edu/structure-chemical-synapses.

Two remodeled dendrites: Darwin M. Does Personal Identity Survive Cryopreservation? Chronosphere, 23 Feb 2011; http://chronopause.com/chronopause.com/index.php/2011/02/23/does-personal-identity-survive-cryopreservation/.

Micrograph of dendritic spine growth in mouse brain: Yang G, Pan F, Gan WB. Stably maintained dendritic spines are associated with lifelong memories. Nature. 2009 Dec 17;462(7275):920-4; http://www.neuroscience.ubc.ca/CourseMat/Yang_et_al_2009.pdf.

Thin, mushroom, and stubby dendrites: https://en.wikipedia.org/wiki/Dendritic_spine.

Two schematics of a synapse: Freche D, Pannasch U, Rouach N, Holcman D. Synapse geometry and receptor dynamics modulate synaptic strength. PLoS One. 2011;6(10):e25122; https://www.ncbi.nlm.nih.gov/pmc/articles/PMC3184958/.

Multiple synapse shapes: Spacek J, Sorra Karin. Synapses of Stratum Radiatum. Figure 2: Variety of Synapse Morphologies. SynapseWeb, 2018 Mar 4; https://synapseweb.clm.utexas.edu/synapses-s-radiatum.

Small and large synapse size comparison: Bailey CH, Kandel ER, Harris KM. Structural Components of Synaptic Plasticity and Memory Consolidation. Cold Spring Harb Perspect Biol. 2015 Jul 1;7(7):a021758; https://www.ncbi.nlm.nih.gov/pmc/articles/PMC4484970/.

2.1.3

Gray matter volume vs. age: Courchesne E, Chisum HJ, Townsend J, Cowles A, Covington J, Egaas B, Harwood M, Hinds S, Press GA. Normal brain development and aging: quantitative analysis at *in vivo* MR imaging in healthy volunteers. Radiology. 2000 Sep;216(3):672-82; https://pubmed.ncbi.nlm.nih.gov/10966694/.

Levels of consciousness flowchart: "Continuum of Depth of Sedation: Definition of General Anesthesia and Levels of Sedation/Analgesia," American Society of Anesthesiologists, Oct 1999; https://www.asahq.org/standards-and-guidelines/continuum-of-depth-of-sedation-definition-of-general-anesthesia-and-levels-of-sedationanalgesia.

Cerebral metabolism suppression chart: Laureys S, Owen AM, Schiff ND. Brain function in coma, vegetative state, and related disorders. Lancet Neurol. 2004 Sep;3(9):537-46; https://orbi.uliege.be/bitstream/2268/2213/1/LAUREYS_S_2004_LancetNeurol_3_9_537.pdf.

2.2.2

Ettinger book cover: Ettinger RCW. The Prospect of Immortality. Doubleday, 1964; https://www.cryonics.org/images/uploads/misc/Prospect_Book.pdf.

2.2.4

Six anabolocyte images: Darwin M. The Anabolocyte: A Biological Approach to Repairing Cryoinjury. Life Extension Magazine, Jul/Aug 1977, pp. 80-83; http://www.alcor.org/Library/pdfs/anabolocyte.pdf

2.2.5

Man enveloped by chrysalis: Donaldson T. 24th Century Medicine. Analog Sci Fiction Sci Fact. 1988 Sep;108:64-80; http://www.alcor.org/Library/html/24thcenturymedicine.html.

2.2.7

Generic cell repair nanorobot: Wowk. B. Cell repair technology. Cryonics 1988 Jul;9(7):21-29; https://www.alcor.org/library/cell-repair-technology/.

Nanorobot working on a neuron: Wowk. B. Cell repair technology. Cryonics 1988 Jul;9(7):21-29; https://www.alcor.org/library/cell-repair-technology/.

2.2.8

Stock surgical image: Darwin M. Resuscitation: A Speculative Scenario for Recovery. Cryonics 1988 Jul;9(7):33-37; https://www.alcor.org/library/resuscitation-a-speculative-scenario-for-recovery/.

2.2.11

Two SCRAM images: Soloviov MV. SCRAM Reanimation. Cryonics 1996 Qtr 1;17(1):16-18; https://alcor.org/cryonics/cryonics1996-1.pdf.

2.2.14

Chromallocyte working on cell nucleus: Merkle RC, Freitas RA Jr. A Cryopreservation Revival Scenario using MNT. Cryonics 2008;29(4):6-8; http://www.alcor.org/cryonics/cryonics0804.pdf.

2.2.15

Generic futuristic scene: Merkle RC. Revival of Alcor Patients. Cryonics 2018 May-Jun;39(3):10-19 and Cryonics 2018 Jul-Aug;39(4):10-15; https://www.alcor.org/library/revival-of-alcor-patients/.

3.2

Ischemic damage schematic: Dirnagl U, Iadecola C, Moskowitz MA. Pathobiology of ischaemic stroke: an integrated view. Trends Neurosci. 1999 Oct;22(9):391–397; http://citeseerx.ist.psu.edu/viewdoc/download?doi=10.1.1.946.3210&rep=rep1&type=pdf.

3.2.5

Apoptosis schematic: Doyle KP, Simon RP, Stenzel-Poore MP. Mechanisms of ischemic brain damage. Neuropharmacology 2008 Sep;55(3):310-318; https://www.ncbi.nlm.nih.gov/pmc/articles/PMC2603601/.

3.2.7

Micrograph of warm ischemic rat brain: Phaedra C. Reconstructive Connectomics. Cryonics 2013 Jul;34(7):26-28; https://www.alcor.org/library/reconstructive-connectomics/.

3.3.1

Three CT scan images of shrunken brain: Linda Chamberlain. Alcor A-1990 Case Report. Cryonics, 2nd Quarter 2019, pp. 12-27; 27; https://www.alcor.org/cryonics/Cryonics2019-2.pdf.

3.4

Freezing process: Darwin M. Does Personal Identity Survive Cryopreservation? Chronosphere, 23 Feb 2011; http://chronopause.com/chronopause.com/index.php/2011/02/23/does-personal-identity-survive-cryopreservation/.

3.4.1

Schematic of synaptic activity: Voglis G, Tavernarakis N. The role of synaptic ion channels in synaptic plasticity. EMBO Rep. 2006 Nov;7(11):1104-1110; https://www.embopress.org/doi/full/10.1038/sj.embor.7400830.

Protein denaturation: Darwin M. Does Personal Identity Survive Cryopreservation? Chronosphere, 23 Feb 2011; http://chronopause.com/chronopause.com/index.php/2011/02/23/does-personal-identity-survive-cryopreservation/.

3.4.2

Myelinated neuron: https://en.wikipedia.org/wiki/Myelin#/media/File:Neuron.svg.

3.4.3

Graph of expansion coefficient vs. temperature: https://physics.stackexchange.com/questions/342707/coefficient-of-linear-expansion-of-ice.

Micrograph of cracking in frozen tissue: Rabin Y, Olson P, Taylor MJ, Steif PS, Julian TB, Wolmark N. Gross damage accumulation on frozen rabbit liver due to mechanical stress at cryogenic temperatures. Cryobiology. 1997 Jun;34(4):394-405; http://www.andrew.cmu.edu/user/yr25/RabinPublications/Rabin_Pub214.pdf.

Two flasks of cryoprotectant solution, before and after cooling; https://www.alcor.org/library/cryopreservation-and-fracturing/.

3.6

Reperfusion injury schematic: Best B. Ischemia and Reperfusion Injury in Cryonics. December 2003; https://www.benbest.com/cryonics/ischemia.html.

4.1.1

MRI machine: https://en.wikipedia.org/wiki/Magnetic_resonance_imaging#/media/File:Siemens_Magnetom_Aera_MRI_scanner.jpg.

Magnetic resonance angiogram: https://i.pinimg.com/originals/bc/34/75/bc3475d32161ad7f322051ac9cc03d52.png.

Graph of MRI signal with temperature: Daniel BL, Butts K, Block WF. Magnetic resonance imaging of frozen tissues: temperature-dependent MR signal characteristics and relevance for MR monitoring of cryosurgery. Magn Reson Med. 1999 Mar;41(3):627-30; https://onlinelibrary.wiley.com/doi/pdf/10.1002/(SICI)1522-2594(199903)41:3%3C627::AID-MRM28%3E3.0.CO;2-Q.

4.1.2

CT scan schematic: Brenner DJ, Hall EJ. Computed tomography--an increasing source of radiation exposure. N Engl J Med. 2007 Nov 29;357(22):2277-84; http://www.members.tripod.com/enotes/CT_radiation2007.pdf.

CT angiograph of the brain: Meijs M, Patel A, van de Leemput SC, Prokop M, van Dijk EJ, de Leeuw FE, Meijer FJA, van Ginneken B, Manniesing R. Robust Segmentation of the Full Cerebral Vasculature in 4D CT of Suspected Stroke Patients. Sci Rep. 2017 Nov 15;7(1):15622; https://www.ncbi.nlm.nih.gov/pmc/articles/PMC5688074/.

Synchrotron emitter: https://en.wikipedia.org/wiki/Synchrotron_radiation.

3D tomograph of fossilized embryo: Donoghue PC, Bengtson S, Dong XP, Gostling NJ, Huldtgren T, Cunningham JA, Yin C, Yue Z, Peng F, Stampanoni M. Synchrotron X-ray tomographic microscopy of fossil embryos. Nature. 2006 Aug 10;442(7103):680-683; https://seis.bristol.ac.uk/~jc1224/Publications/assets/Donoghue_et_al_2006b.pdf.

CT scan of cryopreserved human brain: "Post Cryopreservation CT Scan for Alcor Case A-2643," Cryonics, Mar 2014; 35(3):15-21; https://www.alcor.org/library/complete-list-of-alcor-cryopreservations/ct-scan-a-2643/.

4.1.3

Large-vessel ultrasound imaging: "eFLOW - New High-definition Blood Flow Imaging Mode," Hitachi Medical Systems, 2019; http://www.hitachi-medical-systems.eu/products-and-services/ultrasound/technologies/eflow.html.

Vascular sonograph with contrast microbubbles: Bob Yirka, "New way to use ultrasound allows for imaging live blood vessels with more clarity," Medical Xpress, 26 Nov 2015; https://medicalxpress.com/news/2015-11-ultrasound-imaging-blood-vessels-clarity.html.

Cryosurgery ultrasound schematic: Sheng L, Wang G, Li F, Luo J, Liu J. Ultrasound signal wavelet analysis to quantify the microstructures of normal and frozen tissues *in vitro*. Cryobiology. 2014 Feb;68(1):29-34; https://www.semanticscholar.org/paper/Ultrasound-signal-wavelet-analysis-to-quantify-the-Sheng-Wang/6e95a857572c53f3d9fe80bee6c1a6a82b2833ee.

Ultrasound transition zone on ice ball: Sheng L, Wang G, Li F, Luo J, Liu J. Ultrasound signal wavelet analysis to quantify the microstructures of normal and frozen tissues *in vitro*. Cryobiology. 2014 Feb;68(1):29-34; https://www.semanticscholar.org/paper/Ultrasound-signal-wavelet-analysis-to-quantify-the-Sheng-Wang/6e95a857572c53f3d9fe80bee6c1a6a82b2833ee.

Vibroacoustic scans of prostate tissue before and after freezing: Mitri FG, Davis BJ, Alizad A, Greenleaf JF, Wilson TM, Mynderse LA, Fatemi M. Prostate cryotherapy monitoring using vibroacoustography: preliminary results of an *ex vivo* study and technical feasibility. IEEE Trans Biomed Eng. 2008 Nov;55(11):2584-92; https://www.ncbi.nlm.nih.gov/pmc/articles/PMC2758914/.

Thermoacoustic CT of mouse brain vasculature: Kruger RA, Kiser WL, Reinecke DR, Kruger GA, Miller KD. Thermoacoustic molecular imaging of small animals. Mol Imaging. 2003 Apr;2(2):113-23; https://journals.sagepub.com/doi/pdf/10.1162/15353500200303109.

4.1.4

THz absorption of water during freezing: Ashworth PC, Zeitler JA, Pepper M, Wallace VP. Terahertz spectroscopy of biologically relevant liquids at low temperatures. 2006 Joint 31st International Conference on Infrared Millimeter Waves and 14th International Conference on Teraherz Electronics, 18-22 Sep 2006, Paper No. TueB6-2, p. 184; https://ieeexplore.ieee.org/document/4222126.

THz comparison of healthy and unhealthy tissue: Chen H, Lee WJ, Huang HY, Chiu CM, Tsai YF, Tseng TF, Lu JT, Lai WL, Sun CK. Performance of THz fiber-scanning near-field microscopy to diagnose breast tumors. Opt Express. 2011 Sep 26;19(20):19523-19531; https://www.osapublishing.org/viewmedia.cfm?uri=oe-19-20-19523&seq=0.

4.2.1

Utility fog nanorobot array: https://www.autogeny.org/Ufog.html.

Catheter-based vascular excavation: https://www.westernvascular.com/wp-content/uploads/2019/07/Atherectomy.png.

4.3

Arteriole and venule in capillary network: Sakai T, Hosoyamada Y. Are the precapillary sphincters and metarterioles universal components of the microcirculation? An historical review. J Physiol Sci. 2013 Sep;63(5):319-31; https://www.ncbi.nlm.nih.gov/pmc/articles/PMC3751330/. Or: https://doctorlib.info/physiology/physiology/17.html.

Arteriole and venule in lymphatic capillary network: http://www.differencebetween.net/science/difference-between-lymphatic-capillaries-and-blood-capillaries/.

Arteriovenous circulation in human body: Image provided by artist Gina "Nanogirl" Miller. Lymphatic circulation in human body: https://wiki.fed-space.com/images/thumb/7/78/Lymphatic_system.gif/300px-Lymphatic_system.gif.

4.4.2

Bowman's capsule in a renal glomerulus: https://en.wikipedia.org/wiki/Glomerular_basement_membrane.

4.5.1

Image from Erin McKenna under unsplash license: https://unsplash.com/photos/QjTUB3TMmLM.

4.5.2

Image from Tómas Rekstad under unsplash license: https://unsplash.com/photos/LjbaQRI3rnw.

4.5.4

Conga line: https://www.saccds.org/post/seventh-graders-form-blood-cell-conga-line-middle-school-quad.

4.6

Image of vasculoid tree in human body with magnifying glass on capillaries, provided by artist Gina Miller.

Enlarged image of the magnifying glass and plated vessels, provided by artist Gina Miller.

4.6.1

Mechanical ciliary transport: https://onlinelibrary.wiley.com/cms/asset/0a6e7ffe-d007-41e8-8c70-9e87168f1f57/adfm201706666-fig-0005-m.jpg

Image of vasculoid layout on vascular wall provided by artist Gina Miller.

4.6.3

Image of vasculoid bridging a crackface provided by artist Ping Lim, using electron micrograph of frozen brain tissue (courtesy of Advanced Neural Biosciences, Inc) with added fracture.

Ship in a bottle assembly: "Building a Ship in a Bottle. Step 8: Inserting the Bottom Half," leftmost image; https://www.instructables.com/Building-A-Ship-In-A-Bottle/.

4.7.3.2

Bacteriophage micrograph: Adrian M, Dubochet J, Lepault J, McDowall AW. Cryo-electron microscopy of viruses. Nature. 1984 Mar 1;308(5954):32-36; https://serval.unil.ch/resource/serval:BIB_BEC796503260.P001/REF.pdf.

4.7.3.4

Electron cryotomographic slice of synaptic body: Gan L, Jensen GJ. Electron tomography of cells. Q Rev Biophys. 2012;45(1):27-56; https://authors.library.caltech.edu/29858/1/Gan2012p17514Q_Rev_Biophys.pdf.

Electron cryotomographic slice of Golgi body: Gan L, Jensen GJ. Electron tomography of cells. Q Rev Biophys. 2012;45(1):27-56; https://authors.library.caltech.edu/29858/1/Gan2012p17514Q_Rev_Biophys.pdf.

4.8.1

Neural connectome map of brain: Gigandet X, Hagmann P, Kurant M, Cammoun L, Meuli R, Thiran JP. Estimating the confidence level of white matter connections obtained with MRI tractography. PLoS One. 2008;3(12):e4006; https://www.ncbi.nlm.nih.gov/pmc/articles/PMC2603475/.

4.8.3

Mouse whole-brain cellular-level wiring diagram: Oh SW, *et al*. A mesoscale connectome of the mouse brain. Nature. 2014 Apr 10;508(7495):207-14; https://www.ncbi.nlm.nih.gov/pmc/articles/PMC5102064/. Image: Allen Institute for Brain Science.

Macromolecular structural model of the *Mycoplasma genitalium* bacterium: From "Figure 1" in Maritan M, Autin L, Karr J, Covert MW, Olson AJ, Goodsell DS. Building Structural Models of a Whole Mycoplasma Cell. J Mol Biol. 2022 Jan 30;434(2):167351; https://www.sciencedirect.com/science/article/abs/pii/S002228362100588X.

4.9

Graph prepared by Freitas, using data from Brian Wowk at 21CM.

4.9.1

Ice nucleation and growth rate vs. temperature: Wowk B. Thermodynamic aspects of vitrification. Cryobiology 2010;60:11-22; http://www.21cm.com/pdfs/2010-Thermodynamics.pdf.

4.10.1

Classic sorting rotor schematic: Drexler KE. Nanosystems: Molecular Machinery, Manufacturing, and Computation, John Wiley & Sons, New York, 1992, Section 13.2.1(a) "Modulated receptors for selective transport: Basic concepts"; https://www.amazon.com/dp/0471575186/. Freitas RA Jr. Nanomedicine, Volume I: Basic Capabilities, Landes Bioscience, Georgetown, TX, 1999; Section 3.4.2, "Sorting Rotors"; http://www.nanomedicine.com/NMI/3.4.2.htm.

Revolver-style sorting rotor: Robert A. Freitas Jr., "The Nanofactory Solution to Global Climate Change: Atmospheric Carbon Capture," IMM Report No. 45, December 2015; http://www.imm.org/Reports/rep045.pdf.

Diffusion coefficient chart: chart drawn by Freitas; data from: Freitas RA Jr. Nanomedicine, Volume I: Basic Capabilities, Landes Bioscience, Georgetown, TX, 1999; Table 3.3; http://www.nanomedicine.com/NMI/Tables/3.3.jpg.

4.10.1.1

Oxygen content vs. temperature for water and seawater: Fondriest Environmental, Inc. "Dissolved Oxygen." Fundamentals of Environmental Measurements. 19 Nov 2013; https://www.fondriest.com/environmental-measurements/parameters/water-quality/dissolved-oxygen/.

4.10.1.2

Glucose molecule: https://en.wikipedia.org/wiki/Glucose.

ATP molecule: https://en.wikipedia.org/wiki/Adenosine_triphosphate.

4.10.1.3

Asteroid population vs. size: National Research Council. Defending Planet Earth: Near-Earth Object Surveys and Hazard Mitigation Strategies. National Academies Press, Washington DC, 2010, Table 2.4, p. 17; https://www.boulder.swri.edu/~bottke/Reprints/National_Academies_NEO_Report_Defending_Planet_Earth.pdf.

Number of molecules vs. cytosol concentration: chart by Freitas, data from Appendix I.

Number of molecules vs. plasma concentration: chart by Freitas, data from Appendix J.

4.10.1.7

Pie chart of M22 vitrification solution components: Wowk B. How cryoprotectants work. Cryonics, 3rd Qtr 2007, pp. 3-7; https://alcor.org/Library/pdfs/How-Cryoprotectants-Work.pdf.

4.10.1.8

Apoptotic cell and white cell: https://www.sciencedirect.com/topics/agricultural-and-biological-sciences/midwife-toad.

4.11.1

Lipid bilayer: https://www.thoughtco.com/phospholipids-373561.

4.12

Schematic of cell: Blausen.com staff (2014). "Medical gallery of Blausen Medical 2014". WikiJournal of Medicine **1** (2). DOI:10.15347/wjm/2014.010. Available at: https://en.wikipedia.org/wiki/Cell_(biology)#/media/File:Blausen_0208_CellAnatomy.png.

4.12.1.1

Exosomes, microvesicles, and apoptotic bodies: Chen Y, Li G, Liu ML. Microvesicles as Emerging Biomarkers and Therapeutic Targets in Cardiometabolic Diseases. Genomics Proteomics Bioinformatics. 2018 Feb;16(1):50-62; https://www.ncbi.nlm.nih.gov/pmc/articles/PMC6000161/.

4.12.1.2

Red cells: https://www.daviddarling.info/encyclopedia/E/erythrocyte.html.

Red cells with platelet: http://www.bioquicknews.com/node/5523.

4.12.1.3

Lymphocyte: https://en.wikipedia.org/wiki/Lymphocyte.
Macrophage: https://www.news-medical.net/life-sciences/What-is-a-Macrophage.aspx.

4.12.1.4
Types of bacteria: https://en.wikipedia.org/wiki/Bacteria#/media/File:Bacterial_morphology_diagram.svg.

4.12.1.5
Virus particle: https://en.wikipedia.org/wiki/Virus.
Collection of protozoa: https://www.daviddarling.info/encyclopedia/P/protozoan.html.

4.12.1.6
Cancer cell: https://www.nursingcenter.com/ncblog/july-2019/cancer-cells-vs-normal-cells.
Clumps of cancer cells: https://www.youtube.com/watch?v=R8klVTgjJSQ.
Microbivore: Microbivore: Forrest Bishop (1999); https://web.archive.org/web/20160827082558/https://foresight.org/Nanomedicine/Gallery/Captions/Image197.html.

4.12.2.2
Cell image on left: https://www.scienceabc.com/pure-sciences/what-is-the-function-of-the-nucleus.html.
Cell nucleus image on right: https://en.wikipedia.org/wiki/Nuclear_envelope#/media/File:Diagram_human_cell_nucleus.svg.
Chromallocyte working on cell nucleus: Merkle RC, Freitas RA Jr. A Cryopreservation Revival Scenario using MNT. Cryonics 2008;29(4):6-8; http://www.alcor.org/cryonics/cryonics0804.pdf.

4.12.2.3
(A) Proteasome: https://en.wikipedia.org/wiki/Proteasome.
(B) Ribosome: Noller HF. RNA structure: reading the ribosome. Science. 2005 Sep 2;309(5740):1508-14; http://rna-informatics.uga.edu/Readings/tertiary/2005-Noller-rRNA-SCI.pdf.
(C) Glycogen granule: https://en.wikipedia.org/wiki/Glycogen.
(D) Vault: https://en.wikipedia.org/wiki/Vault_(organelle).
(E) Centrioles: https://www.scienceabc.com/pure-sciences/centrioles-can-survive-without.html.
Half-cut mitochondrion: https://en.wikipedia.org/wiki/Mitochondrion.
Single stack of the Golgi apparatus (left): https://en.wikipedia.org/wiki/Golgi_apparatus.
Endoplasmic reticulum (right): https://elifesciences.org/articles/20468.

4.12.2.4
Cytoskeleton components: https://guidancecorner.com/cytoskeleton/.

4.12.2.5
Transmembrane receptor diagram (top): https://www.open.edu/openlearn/science-maths-technology/cell-signalling/content-section-1.3.
Transmembrane receptor diagram (bottom): https://www.researchgate.net/publication/265098999_II_A_Perspective_on_Endotoxemia/figures.

4.12.2.6
Plasma membrane with embedded proteins: https://www.khanacademy.org/science/high-school-biology/hs-cells/hs-the-cell-membrane/a/hs-the-cell-membrane-review.

4.12.2.7
Glycocalyx on lipid bilayer: https://pubs.rsc.org/en/content/articlelanding/2015/nr/c5nr01355k#!divAbstract.

4.12.2.8
Microneedle array: Gittard SD, Ovsianikov A, Chichkov BN, Doraiswamy A, Narayan RJ. Two-photon polymerization of microneedles for transdermal drug delivery. Expert Opin Drug Deliv. 2010 Apr;7(4):513-533; https://www.ncbi.nlm.nih.gov/pmc/articles/PMC2844933/.

4.12.3.3
Micrograph of extracellular matrix: "The Extracellular Matrix of Animals," Fig. 19-33, in: Alberts B, Johnson A, Lewis J, Raff M, Roberts K, Walter P, eds. Molecular Biology of the Cell, 4th edition, Garland Science, New York, 2002; https://www.ncbi.nlm.nih.gov/books/NBK26810/.
Schematic of extracellular matrix: Kular JK, Basu S, Sharma RI. The extracellular matrix: Structure, composition, age-related differences, tools for analysis and applications for tissue engineering. J Tiss Eng. 2014 Dec 21; 5; https://journals.sagepub.com/doi/full/10.1177/2041731414557112.

4.12.4.1
Axon: https://en.wikipedia.org/wiki/Axon.
Neuron cell body with myelin sheath: https://en.wikipedia.org/wiki/Axon#/media/File:Neuron_Cell_Body.png.
Myelin sheath: Myelinated neuron: https://en.wikipedia.org/wiki/Myelin#/media/File:Neuron.svg.

4.12.4.2
AMPA receptor: https://en.wikipedia.org/wiki/AMPA_receptor#/media/File:AMPA_receptor.png.

4.12.4.3

Healthy brain vs. Alzheimer's brain: https://adrcswwi.org/blog/what-is-dementia/.

Images of brains a different Alzheimer's stages: http://unionlosangeles.com/2012/09/21/pink-is-for-breast-cancer-purple-is-for-alzheimers-disease/.

4.14.1.1

Respirocytes and Red Blood Cells, in Repose: Forrest Bishop (1999); https://web.archive.org/web/20210508220644/https://foresight.org/Nanomedicine/Gallery/Captions/Image140.html.

4.14.2

Schematic of human heart: https://en.wikipedia.org/wiki/Atrium_(heart)#/media/File:Diagram_of_the_human_heart_(cropped).svg.

4.14.3

Sinoatrial mode in the heart: https://en.wikipedia.org/wiki/File:ConductionsystemoftheheartwithouttheHeart-en.svg.

5.2.1.1

Frozen feet: "Will we ever bring frozen corpses back to life?" Cosmos Magazine, 8 Jan 2017; https://cosmosmagazine.com/biology/will-we-ever-be-able-to-bring-cryogenically-frozen-corpses-back-to-life-a-cryobiologist-explains/. The rest of this composite image was assembled by Freitas.

Carbene water-abstraction tool: Image prepared by Freitas.

Water abstraction sequence: Images prepared by Freitas.

Telescoping nanorobot arm: Freitas RA Jr. Nanomedicine, Volume I: Basic Capabilities, Landes Bioscience, Georgetown TX, 1999, Fig. 9.8; http://www.nanomedicine.com/NMI/Figures/9.8.jpg. Adapted from: Drexler KE. Nanosystems: Molecular Machinery, Manufacturing, and Computation, John Wiley & Sons, New York, 1992, Section 13.4.1, "A bounded-continuum design for a stiff manipulator"; https://www.amazon.com/dp/0471575186/.

HAbst-H molecule: Image prepared by Freitas.

5.2.1.2

Glycine molecule: http://macromole.blogspot.com/2006/11/glycine.html.

Glycine peptide chain wrapped around a cylinder: Image prepared by Freitas.

Isolated glycine peptide molecule: Image prepared by Freitas.

Two ice excavation images: Images prepared by Freitas.

All tables of reaction sequences: Images prepared by Freitas.

HAbst recharge sequence: Images prepared by Freitas.

5.2.1.3

Sliced human: Image prepared by Freitas.

5.2.2.2

Closeup of myelin sheath molecule: Schulz G, Deyhle H, Bikis C, Bunk O, Muller B. Imaging the orientation of myelin sheaths in a non-stained histological slice of human brain. Precis Nanomed. 2020 Oct;3(4):656-665; https://precisionnanomedicine.com/article/17211-imaging-the-orientation-of-myelin-sheaths-in-a-non-stained-histology-slide-of-human-brain.

5.2.3.1

Dimer placement tool (X-bar) and positional uncertainty map: Peng J, Freitas RA Jr., Merkle RC, Von Ehr JR, Randall JN, Skidmore GD. Theoretical Analysis of Diamond Mechanosynthesis. Part III. Positional C_2 Deposition on Diamond C(110) Surface using Si/Ge/Sn-based Dimer Placement Tools. J Comput Theor Nanosci. 2006 Feb;3(1):28-41; http://www.molecularassembler.com/Papers/JCTNPengFeb06.pdf.

Critical cooling rate graph: Mullen SF, Fahy GM. Chapter 12. Fundamental aspects of vitrification as a method of reproductive cell, tissue and organ cryopreservation. In: Donnez J, Kim SS, eds. Principles and Practice of Fertility Preservation, Cambridge university Press, 2011, pp. 145-163.

Critical warming rate graph: Mullen SF, Fahy GM. Chapter 12. Fundamental aspects of vitrification as a method of reproductive cell, tissue and organ cryopreservation. In: Donnez J, Kim SS, eds. Principles and Practice of Fertility Preservation, Cambridge university Press, 2011, pp. 145-163.

Density vs. temperature for water and M22: Chart prepared by Freitas. M22 data provided by Brian Wowk.

5.2.3.2

Nanomechanical conveyor belt: Freitas RA Jr. Nanomedicine, Volume I: Basic Capabilities, Landes Bioscience, Georgetown TX, 1999, Fig. 3.9; http://www.nanomedicine.com/NMI/Figures/3.9.jpg. Adapted from: Drexler KE. Nanosystems: Molecular Machinery, Manufacturing, and Computation, John Wiley & Sons, New York, 1992, Section 13.3.1, "Reactive encounters using belt and roller systems"; https://www.amazon.com/dp/0471575186/.

Pincushion binding site: Freitas RA Jr. Nanomedicine, Volume I: Basic Capabilities, Landes Bioscience, Georgetown TX, 1999, Fig. 3.14; http://www.nanomedicine.com/NMI/Figures/3.9.jpg.

5.2.3.3.1

Tightly-packed neuropil of the brain: Kasthuri N, Hayworth KJ, Berger DR, Schalek RL, Conchello JA, Knowles-Barley S, Lee D, Vázquez-Reina A, Kaynig V, Jones TR, Roberts M, Morgan JL, Tapia JC, Seung HS, Roncal WG, Vogelstein JT, Burns R,

Sussman DL, Priebe CE, Pfister H, Lichtman JW. Saturated Reconstruction of a Volume of Neocortex. Cell. 2015 Jul 30;162(3):648-61; http://seunglab.org/wp-content/uploads/2015/09/saturatedreconstruction.pdf.

5.3

Exploded car engine: https://blender.stackexchange.com/questions/68434/explode-model.

5.3.1

Schematic of shifting blocks: Image prepared by Freitas.

5.3.2

Tumor growth in a small section of tissue: Tamori Y, Deng WM. Tissue-Intrinsic Tumor Hotspots: Terroir for Tumorigenesis. Trends Cancer. 2017 Apr;3(4):259-268; https://www.ncbi.nlm.nih.gov/pmc/articles/PMC5518481/.

5.4

Three convergent assembly boxes: Merkle RC. Convergent assembly. Nanotechnology 1997;8:18-22; http://www.zyvex.com/nanotech/convergent.html.

Convergent assembly schematic: Merkle RC. Convergent assembly. Nanotechnology 1997;8:18-22; http://www.zyvex.com/nanotech/convergent.html.

6.1

Brain dripping icicles: https://www.gograph.com/illustration/brain-freeze-gg65940568.html.

6.1.1

Patent drawing of artificial uterus: Emanuel M. Greenberg. Artificial uterus. U.S Patent 2,723,660, 15 Nov 1955; https://patents.google.com/patent/US2723660A/en.

Human gestational weight vs. time: Chart prepared by Freitas.

Cell cycle clock: https://www.khanacademy.org/science/ap-biology/cell-communication-and-cell-cycle/cell-cycle/a/cell-cycle-phases.

6.1.1.1

Two-headed dog: Konstantinov IE. At the cutting edge of the impossible: a tribute to Vladimir P. Demikhov. Texas Hear Inst J. 2009;36(5):453-458; https://www.ncbi.nlm.nih.gov/pmc/articles/PMC2763473/.

Monkey head transplant: Lang M, Tsiang J, Moore NZ, Bain MD, Steinmetz MP. A Tribute to Dr Robert J. White. Neurosurgery. 2019 Aug 1;85(2):E366-E373; https://www.google.com/url?sa=i&url=https%3A%2F%2Fwww.metrohealth.org%2F-%2Fmedia%2Fmetrohealth%2Fdocuments%2Fneurosurgery%2Fa-tribute-to-dr-robert-j-white.pdf&psig=AOvVaw1Knq0VoV4Km78VuA3U9GqJ&ust=1617219570450000&source=images&cd=vfe&ved=0CAkQjhxqFwoTCPj57ark2O8CFQAAAAAdAAAAABAD.

Two-headed mouse: Ren XP, Ye YJ, Li PW, Shen ZL, Han KC, Song Y. Head Transplantation in Mouse Model. CNS Neurosci Ther. 2015 Aug;21(8):615-8; https://www.ncbi.nlm.nih.gov/pmc/articles/PMC6495971/.

6.1.1.2

Body grown onto a brain; from Brian Wowk's talk at the 2006 Alcor conference: https://www.youtube.com/watch?v=kTo2MIacnM4&t=725s.

6.1.2

3D printing human organs: https://sites.google.com/a/ewg.k12.ri.us/medical-3d-printing/.

6.1.3

Two equipment drawings from the Fleming patent: Chet Fleming. Device for Perfusing an Animal Head. U.S. Patent 4666425A, 19 May 1987; https://patents.google.com/patent/US4666425A/en.

Robocop: https://www.slantmagazine.com/wp-content/uploads/2019/12/robocopbr.jpg.

Borg queen: Image from http://www.tomspinadesigns.com/; http://www.tomspinadesigns.com/restoration/science-fiction-props/borg-queen-costume-restoration-display/.

Isolated brain maintenance system: Mühlethaler M, de Curtis M, Walton K, Llinás R. The isolated and perfused brain of the guinea-pig *in vitro*. Eur J Neurosci. 1993 Jul 1;5(7):915-26. (To review the image, search the paper's title using Google Scholar, then upload the pdf from https://www.academia.edu/download/48866998/j.1460-9568.1993.tb00942.x20160915-6203-gb71zf.pdf.)

Headless kneeling robot body: https://www.popsci.com/john-brandon/article/2008-10/rent-robotic-suit-named-hal/.

Liquid metal torso: http://www.scienceandfilm.org/articles/2571/liquid-metal-terminator-genisys.

6.1.4

Human head and robot head: https://www.cnbc.com/2019/10/31/human-like-androids-have-entered-the-workplace-and-may-take-your-job.html.

7.1.1

Two micrographs of nonischemic and straight-frozen cat brain tissue: Darwin M. Cryonics: An Historical Failure Analysis. Part III: Dissociation of Researchers from the Clinical Environment. 2010; https://web.archive.org/web/20140906234205/http://cryoeuro.eu:8080/download/attachments/425990/Cryonics_Failure_Analysis_Part_3v5.4.pdf.

7.1.2

Flask and test tubes containing glassy and cracked M22 cryoprotectant: Wowk B. Systems for intermediate temperature storage for fracture reduction and avoidance. Cryonics 2011 Qtr 3; https://www.alcor.org/library/systems-for-intermediate-temperature-storage-for-fracture-reduction-and-avoidance/.

7.1.3

Clathrate molecule: https://en.wikipedia.org/wiki/Clathrate_compound#/media/File:Ne-water_clathrate.png.

7.1.5

Two images of cell structures preserved in amber: Koller B, Schmitt JM, Tischendorf G. Cellular fine structures and histochemical reactions in the tissue of a cypress twig preserved in Baltic amber. Proc Biol Sci. 2005 Jan 22;272(1559):121-6; https://www.ncbi.nlm.nih.gov/pmc/articles/PMC1634957/.

Aldehyde fixative cross-linking schematic: Noor Ullah, "Tissue fixation," 10 Oct 2018; https://www.slideshare.net/habibhasrat/tissue-fixation-histopathology.

Crosslinking chemistry diagram: Kiernan JA. Formaldehyde, Formalin, Paraformaldehyde And Glutaraldehyde: What They Are And What They Do. Microscopy Today 2000 Jan;8(1):8-13; https://publish.uwo.ca/~jkiernan/formglut.htm.

7.2.1.1

C. elegans nematode: https://phys.org/news/2019-05-scientists-worms.html.

7.2.1.2

White lab mice: https://en.wikipedia.org/wiki/Laboratory_mouse#/media/File:Lightmatter_lab_mice.jpg.

7.2.1.3

Border collie: https://canna-pet.com/breed/border-collie/.

7.2.1.4

Bonobo: https://sciworthy.com/do-nice-apes-finish-last-its-complicated/.

7.2.1.5

Nanorobots on neuron axon: Martins NRB, Angelica A, Chakravarthy K, Svidinenko Y, Boehm FJ, Opris I, Lebedev MA, Swan M, Garan SA, Rosenfeld JV, Hogg T, Freitas RA Jr. Human Brain/Cloud Interface. Front Neurosci. 2019 Mar 29;13:112; https://www.ncbi.nlm.nih.gov/pmc/articles/PMC6450227/.

Chart of synapse density vs. age: Liu X, Somel M, Tang L, Yan Z, Jiang X, Guo S, Yuan Y, He L, Oleksiak A, Zhang Y, Li N, Hu Y, Chen W, Qiu Z, Pääbo S, Khaitovich P. Extension of cortical synaptic development distinguishes humans from chimpanzees and macaques. Genome Res. 2012 Apr;22(4):611-22; https://www.ncbi.nlm.nih.gov/pmc/articles/PMC3317144/.

Chart of neural firing rate vs. age: Marchetto MC, Hrvoj-Mihic B, Kerman BE, Yu DX, Vadodaria KC, Linker SB, Narvaiza I, Santos R, Denli AM, Mendes AP, Oefner R, Cook J, McHenry L, Grasmick JM, Heard K, Fredlender C, Randolph-Moore L, Kshirsagar R, Xenitopoulos R, Chou G, Hah N, Muotri AR, Padmanabhan K, Semendeferi K, Gage FH. Species-specific maturation profiles of human, chimpanzee and bonobo neural cells. Elife. 2019 Feb 7;8:e37527; https://www.ncbi.nlm.nih.gov/pmc/articles/PMC6366899/.

B.

Jameson satellite: http://famous-and-forgotten-fiction.com/writings/jones/the-jameson-satellite/it-became-enveloped-in-a-haze-of-light.png.

Mechanical Monarch cover art: Charles Grey (Edwin Charles Tubb). Enterprise 2115. Merit Books, London, 1954; later published in the U.S. as: E.C. Tubb, The Mechanical Monarch, Ace Books, NY, 1958; http://www.sf-encyclopedia.com/entry/tubb_e_c.

D.1.1.1

Automated molecular synthesis machine: https://news.illinois.edu/view/6367/204395.

D.1.1.2

Tooltip molecules: Images prepared by Freitas.

Conveyor belt mechanisms (left): Adapted from: Drexler KE. Nanosystems: Molecular Machinery, Manufacturing, and Computation, Wiley, 1992, Figs. 13.7(b), 13.7(c), 13.7(d); https://www.amazon.com/dp/0471575186/.

Mechanosynthetic production line: Burch & Drexler (2006), Lizardfire Nanofactory video.

Multiloop molecular production line: Image prepared by Freitas.

Loop 1 methyl on surface: Mavrikakis M, Rempel J, Greeley J, Hansen LB, Norskov JK. Atomic and molecular adsorption on Rh(111). J Chem Phys. 2002 Oct 8;117(14):6737-6744; https://core.ac.uk/download/pdf/13727515.pdf.

Loop 4 hydroxyl on surface: Mavrikakis M, Rempel J, Greeley J, Hansen LB, Norskov JK. Atomic and molecular adsorption on Rh(111). J Chem Phys. 2002 Oct 8;117(14):6737-6744; https://core.ac.uk/download/pdf/13727515.pdf.

Switchyard: https://lehmanhill.blogspot.com/2010/05/b-29-turret-gun-gunsight.html.

D.1.2.1.2

Cost per human genome: National Human Genome Research Institute (NHGRI). DNA Sequencing Costs: Data (2020). https://www.genome.gov/about-genomics/fact-sheets/DNA-Sequencing-Costs-Data.

NovaSeq 6000 gene sequencing machine: https://uofuhealth.utah.edu/huntsman/shared-resources/gba/htg/illumina/novaseq.php.

MinION sequencer: https://product.statnano.com/product/11661/minion-sequencer.

D.1.2.2

AKTA oligopilot: https://ibook.antpedia.com/703/p/65387-p.html. (Product discontinued by manufacturer in 2021.)

D.1.2.3

Bacterial ribosome internal structure: https://3dciencia.com/blog/2011/02/bacterial-ribosome-internal-structure/.

MHC-I molecule embedded in plasma membrane (left): Freitas RA Jr. Nanomedicine, Volume I: Basic Capabilities, Landes Bioscience, Georgetown TX, 1999, Section 8.5.2.1, "Identification of Self"; http://www.nanomedicine.com/NMI/8.5.2.1.htm.

MHC-II molecule embedded in plasma membrane (top right): Freitas RA Jr. Nanomedicine, Volume I: Basic Capabilities, Landes Bioscience, Georgetown TX, 1999, Section 8.5.2.1, "Identification of Self"; http://www.nanomedicine.com/NMI/8.5.2.1.htm.

Progression of cell-free synthesis from VLP to T4: Tinafar A, Jaenes K, Pardee K. Synthetic Biology Goes Cell-Free. BMC Biol. 2019 Aug 8;17(1):64; https://www.ncbi.nlm.nih.gov/pmc/articles/PMC6688370/.

D.2.1

Liposome, micelle, and bilayer sheet: https://en.wikipedia.org/wiki/Lipid_bilayer#/media/File:Phospholipids_aqueous_solution_structures.svg.

Large spherical shell: https://web.archive.org/web/20190702230309/http://academic.brooklyn.cuny.edu/biology/bio4fv/page/lipos.gif.

Hemispherical mould: Similar to https://www.toolusa.com/products/tj9820-15?.

Presentation semaphores: Freitas RA Jr. Nanomedicine, Volume I: Basic Capabilities, Landes Bioscience, Georgetown, TX, 1999; Section 5.3.6, "Presentation Semaphores"; http://www.nanomedicine.com/NMI/5.3.6.htm.

D.2.2

Proteasomes: https://en.wikipedia.org/wiki/Proteasome.

80S eukaryotic ribosome: https://en.wikipedia.org/wiki/Eukaryotic_ribosome_(80S)#/media/File:80S_2XZM_4A17_4A19.png.

Glycogen granules: https://en.wikipedia.org/wiki/Glycogen#/media/File:Glycogen_structure.svg.

Vaults: https://en.wikipedia.org/wiki/Vault_(organelle).

Centrioles: https://www.scienceabc.com/pure-sciences/centrioles-can-survive-without.html.

Chromosomes (right side): https://commons.wikimedia.org/wiki/File:Basic_units_of_chromatin_structure.svg.

Chromosomes (bottom left): https://commons.wikimedia.org/wiki/File:DNA_ORF.png.

D.2.3

Transport vesicles: https://commons.wikimedia.org/wiki/File:Liposome_scheme-en.svg.

Lipid droplets: Martin S, Parton RG. Lipid droplets: a unified view of a dynamic organelle. Nat Rev Mol Cell Biol. 2006 May;7(5):373-378; https://pubmed.ncbi.nlm.nih.gov/16550215/.

Lysosomes: Allemailem KS, Almatroudi A, Alrumaihi F, Almatroodi SA, Alkurbi MO, Basfar GT, Rahmani AH, Khan AA. Novel Approaches of Dysregulating Lysosome Functions in Cancer Cells by Specific Drugs and Its Nanoformulations: A Smart Approach of Modern Therapeutics. Int J Nanomedicine. 2021 Jul 26;16:5065-5098; https://www.ncbi.nlm.nih.gov/pmc/articles/pmc8324981/.

Peroxisomes: https://upload.wikimedia.org/wikipedia/commons/8/82/Peroxisome.jpg.

Mitochondrion schematic: https://www.ck12.org/book/ck-12-biology-concepts/r6/section/2.25/.

D.2.4

Golgi apparatus: https://commons.wikimedia.org/wiki/File:Golgi_apparatus_(borderless_version)-en.svg.

Coat protein II (COPII, left): https://en.wikipedia.org/wiki/COPII#/media/File:COPIIprotein.png.

Coat protein I (COPI, right): https://en.wikipedia.org/wiki/COPI#/media/File:The_structure_of_the_COPI_triad.png.

Two Golgi complex micrographs: Rabouille C, Misteli T, Watson R, Warren G. Reassembly of Golgi stacks from mitotic Golgi fragments in a cell-free system. J Cell Biol. 1995 May;129(3):605-18; http://citeseerx.ist.psu.edu/viewdoc/download?doi=10.1.1.273.3233&rep=rep1&type=pdf.

Endoplasmic reticulum: https://elifesciences.org/articles/20468.

D.2.5

Outer nuclear membrane (top right): Freitas RA Jr., Nanomedicine, Volume I: Basic Capabilities, Landes Bioscience, Georgetown, TX, 1999, Figure 8.46; http://www.nanomedicine.com/NMI/Figures/8.46.jpg.

Inner nuclear membrane (bottom left): Freitas RA Jr., Nanomedicine, Volume I: Basic Capabilities, Landes Bioscience, Georgetown, TX, 1999, Figure 8.47; http://www.nanomedicine.com/NMI/Figures/8.47.jpg.

Nuclear pore: Lin DH, Hoelz A. The Structure of the Nuclear Pore Complex (An Update). Annu Rev Biochem. 2019 Jun 20;88:725-783; https://www.ncbi.nlm.nih.gov/pmc/articles/pmid/30883195/.

Nucleolus: Freitas RA Jr., Nanomedicine, Volume I: Basic Capabilities, Landes Bioscience, Georgetown, TX, 1999, Figure 8.47; http://www.nanomedicine.com/NMI/Figures/8.47.jpg.

D.3.2

Neuron and neuroglia: https://en.wikipedia.org/wiki/Nervous_tissue#/media/File:Blausen_0672_NeuralTissue.png.

F.1.1

Scanning tunneling microscope schematic: Freitas RA Jr., Nanomedicine, Volume I: Basic Capabilities, Landes Bioscience, Georgetown, TX, 1999, Figure 2.24; http://www.nanomedicine.com/NMI/Figures/2.24.jpg.

IBM: http://www-03.ibm.com/press/us/en/photo/28500.wss.

Atomic Force Microscope: (generic AFM image)

How the AFM works: (generic image)

F.1.2

Schematic of AuCO tip: http://www.vacuum-uk.org/pdfs/vs6/etvs/asweetman.pdf.

Three images of AuCO tip scanning a pentacene molecule: Gross L, Mohn F, Moll N, Liljeroth P, Meyer G. The chemical structure of a molecule resolved by atomic force microscopy. Science. 2009 Aug 28;325(5944):1110-1114; https://pubmed.ncbi.nlm.nih.gov/19713523/.

Two scan images of breitfussin A: Hanssen KØ, Schuler B, Williams AJ, Demissie TB, Hansen E, Andersen JH, Svenson J, Blinov K, Repisky M, Mohn F, Meyer G, Svendsen JS, Ruud K, Elyashberg M, Gross L, Jaspars M, Isaksson J. A Combined Atomic Force Microscopy and Computational Approach for the Structural Elucidation of Breitfussin A and B: Highly Modified Halogenated Dipeptides from *Thuiaria breitfussi*. Angew Chem Int Ed. 2012 Dec 3;51(49):12238-41; https://pubmed.ncbi.nlm.nih.gov/23109225/.

Four scan images of a cyclization: de Oteyza DG, *et al*. Direct Imaging of Covalent Bond Structure in Single-Molecule Chemical Reactions. Science 2013 Jun 21;340:1434-7; https://scienceintheclassroom.org/sites/default/files/research-papers/science-2013-de_oteyza-1434-7.pdf.

F.1.3

Two images of Si/Ge/Sn surface: Sugimoto Y, Pou P, Abe M, Jelinek P, Perez R, Morita S, Custance O. Chemical identification of individual surface atoms by atomic force microscopy. Nature 2007 Mar 1;446(7131):64-7; https://www.osaka-u.ac.jp/migr/pdf/eng/research/annualreport/vol8/selection/pdf/vol8_24-26.pdf.

F.1.4

Images of HAbstH and AuCO probe tips: Images prepared by Freitas.

G.

Electrical price chart: Image prepared by Freitas.

H.1

Diamondoid CO_2 binding site and CO_2 molecule: Images prepared by Freitas.

Carbon nanotube CO_2 binding site: Image prepared by Freitas.

H.2

Heme binding site for O_2: https://en.wikipedia.org/wiki/Heme#/media/File:Heme_b.svg.

Nitrogenase binding site for N_2: https://pubs.acs.org/doi/full/10.1021/cr400641x (illustration in Abstract)

Ruthenium-based binding site for water: Ma ES, Patrick BO, James BR. Reversible binding of water, methanol, and ethanol to a five-coordinate ruthenium(II) complex. Dalton Trans. 2013 Mar 28;42(12):4291-8; https://pubmed.ncbi.nlm.nih.gov/23344393/.

3D network water binding: Zheng Y, Kustaryono D, Kerbellec N, Guillou O, Gérault Y, Le Dret F, Daiguebonne C. The lanthanide-containing cyclohexane-tri-carboxylate coordination polymers re-investigated," Inorganica Chimica Acta 2009 May 15;362(7):2123-2126; https://www.sciencedirect.com/science/article/abs/pii/S002016930800604X.

Carbon nanotube binding site for acetylene: Image prepared by Freitas.

Binding site for ethanol (top right): Howard RJ, Slesinger PA, Davies DL, Das J, Trudell JR, Harris RA. Alcohol-binding sites in distinct brain proteins: the quest for atomic level resolution. Alcohol Clin Exp Res. 2011 Sep;35(9):1561-73; https://www.ncbi.nlm.nih.gov/pmc/articles/PMC3201783/.

Binding site for ethanol (bottom left): http://www.chembio.uoguelph.ca/educmat/chm455/adh.ppt.

H.3

Glycerol molecule: https://en.wikipedia.org/wiki/Glycerol.

Binding site for glycerol: Dias MV, Snee WC, Bromfield KM, Payne RJ, Palaninathan SK, Ciulli A, Howard NI, Abell C, Sacchettini JC, Blundell TL. Structural investigation of inhibitor designs targeting 3-dehydroquinate dehydratase from the shikimate pathway of *Mycobacterium tuberculosis*. Biochem J. 2011 Jun 15;436(3):729-39; https://pdfs.semanticscholar.org/1caf/5c7423b314d21e979bfb7d8b7abedc52d856.pdf.

Dimethyl sulfoxide molecule: https://en.wikipedia.org/wiki/Dimethyl_sulfoxide.

Z-DNA binding of DMSO: Tunçer S, Gurbanov R, Sheraj I, Solel E, Esenturk O, Banerjee S. Low dose dimethyl sulfoxide driven gross molecular changes have the potential to interfere with various cellular processes. Sci Rep. 2018 Oct 4;8(1):14828; https://www.ncbi.nlm.nih.gov/pmc/articles/pmid/30287873/.

Ethylene glycol molecule: https://en.wikipedia.org/wiki/Ethylene_glycol.

M.

Apheresis schematic: https://en.wikipedia.org/wiki/Apheresis#/media/File:Apheresis.svg.

Apheresis machine for blood filtration: https://cdn.kqed.org/wp-content/uploads/sites/27/2011/12/Apheresis_12022011Credit_ec-jpr_Flickr1.jpg.

Spectra Optia Cell Separator: https://www.terumobct.com/Spectra-Optia.

Filtration time chart: Image prepared by Freitas.

Cryostasis is an emergency medical procedure in which a human patient is placed in biological stasis at cryogenic temperatures. A cryopreserved patient can be maintained in this condition indefinitely without suffering additional degradation, but cannot yet be revived using currently available technology. This book presents the first comprehensive conceptual protocol for revival from human cryopreservation, using medical nanorobots. The revival methods presented in this book involve three stages: (1) collecting information from preserved structure, (2) computing how to fix damaged structure, and (3) implementing the repair procedure using nanorobots manufactured in a nanofactory – a system for atomically precise manufacturing that is now becoming visible on the technological horizon.

"Robert Freitas is an extraordinary thinker and author whose previous works have been transformational for our ability to visualize the extraordinary capabilities of future medical technology. In ***Cryostasis Revival***, he now puts his prodigious previous knowledge of nanomedicine to the task of envisioning methods for healing those whose injuries challenge even the ultimate limits of future medicine. His illuminating results and new insights will greatly inform debate over, and may even help to resolve, controversies that have persisted for decades."

– Gregory M. Fahy, Ph.D., Fellow, *Society for Cryobiology* & Executive Director, *21st Century Medicine, Inc.*

"***Cryostasis Revival*** is the most magnificent tour de force on cryonics ever done, with the signature flair, comprehensive coverage and authoritative style of Robert A. Freitas Jr. It describes all the issues involved in reviving cryopreserved patients: from the philosophical (what is "information theoretic death") to the practical (what damage actually takes place during a cryopreservation) to the technological (how to apply nanotechnology to restore a cryopreserved patient) and more. Nothing else even approaches such a complete and incisive treatment of this life-saving subject. ***Cryostasis Revival*** is the book to give anyone who's thinking about cryonics but 'isn't sure about the science'."

– Ralph C. Merkle, Ph.D., Senior Research Fellow, *Institute for Molecular Manufacturing*

"Future repair and revival of damaged cryopreserved tissue has been the subject of speculation for decades. This book by a nanomedicine expert examines the problem in detail far beyond anything ever written before. With more than 3000 references, it's both wide-ranging and intensely specific about diverse technical aspects of the problem. It will surely stimulate much discussion, and be an invaluable resource for thinkers about nanomedical cell repair for years to come."

– Brian Wowk, Ph.D., complex systems cryobiologist & Chief Technology Officer, *21st Century Medicine, Inc.*

"We now have considerable evidence that cryopreserved patients retain the physical structures encoding memory and personality. For most people, the difficulty lies in understanding how it could ever be possible to repair and revive patients. Leading nanomedicine expert Robert Freitas fills in that gap with admirable and remarkable depth. ***Cryostasis Revival*** provides an unparalleled clarification of pathways for researchers to explore in the quest to make human cryopreservation reversible."

– Max More, Ph.D., Ambassador, *Alcor Life Extension Foundation*